

This document was produced
by scanning the original publication.

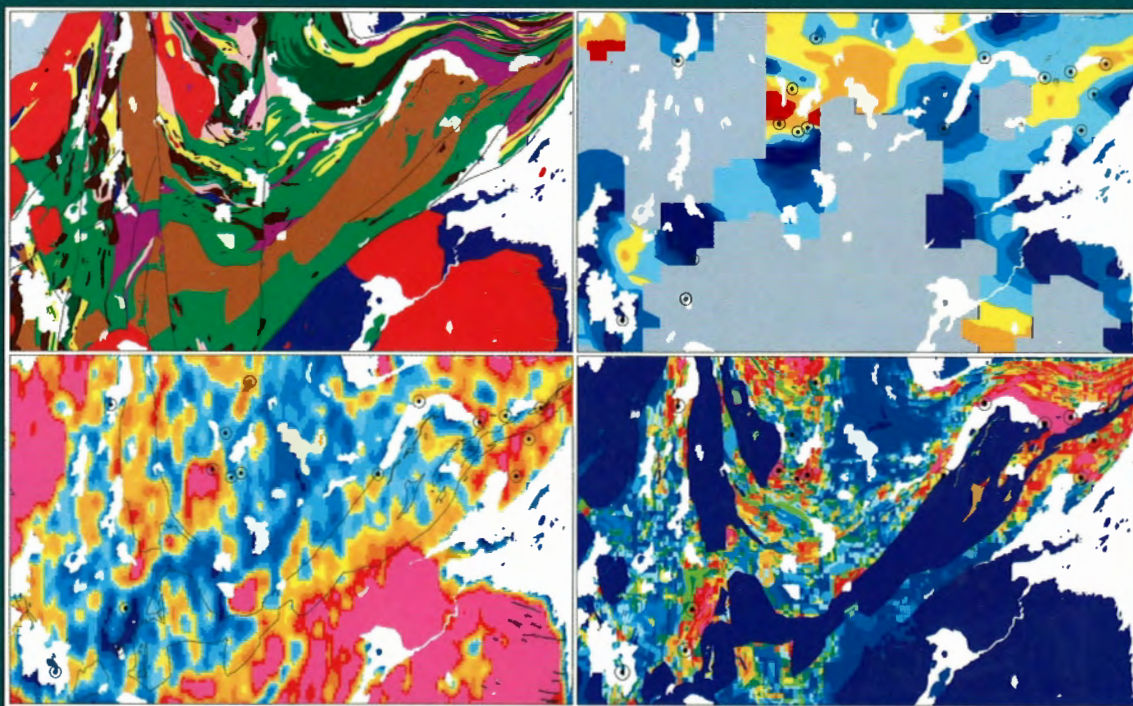
Ce document est le produit d'une
numérisation par balayage
de la publication originale.



GEOLOGICAL SURVEY OF CANADA
BULLETIN 426

EXTECH I: A MULTIDISCIPLINARY APPROACH TO MASSIVE SULPHIDE RESEARCH IN THE RUSTY LAKE-SNOW LAKE GREENSTONE BELTS, MANITOBA

Edited by
G.F. Bonham-Carter, A.G. Galley, and G.E.M. Hall



1996



Natural Resources Canada
Ressources naturelles Canada

Canada



**Geological Survey of Canada
Commission géologique du Canada**

Contribution to the 1989-1994 Rusty Lake-Snow Lake Mining Camps, Canada-Manitoba Exploration Science and Technology Initiative (EXTECH I).

**Manitoba Energy and Mines
Geological Services**



Contribution aux Mesures Canada-Manitoba relatives au Programme de science et technologie de l'exploration (EXTECH I) 1989-1994, camps miniers de Rusty Lake-Snow Lake.

Manitoba 

PARTNERSHIP // ASSOCIATION

**PARTNERSHIP AGREEMENT ON MINERAL
DEVELOPMENT 1990 - 1995**

**L'ENTENTE DE PARTENARIAT SUR
L'EXPLOITATION MINÉRALE 1990 - 1995**

Canada

Contribution to the Canada-Manitoba Partnership Agreement on Mineral Development (1990-1995), a subsidiary agreement under the Canada-Manitoba Economic and Regional Development Agreement/ Contribution à l'Entente de partenariat Canada-Manitoba sur l'exploitation minérale (1990-1995), entente auxiliaire négociée en vertu de l'Entente Canada-Manitoba de développement économique et régional.

GEOLOGICAL SURVEY OF CANADA
BULLETIN 426

**EXTECH I: A MULTIDISCIPLINARY APPROACH
TO MASSIVE SULPHIDE RESEARCH IN
THE RUSTY LAKE-SNOW LAKE
GREENSTONE BELTS, MANITOBA**

Edited by
G.F. Bonham-Carter, A.G. Galley, and G.E.M. Hall

1996

©Her Majesty the Queen in Right of Canada, 1996
Catalogue No. M42-426E
ISBN 0-660-16409-4

Available in Canada from

Geological Survey of Canada offices:

601 Booth Street
Ottawa, Ontario K1A 0E8

3303-33rd Street N.W.,
Calgary, Alberta T2L 2A7

100 West Pender Street
Vancouver, B.C. V6B 1R8

or from

Canada Communication Group — Publishing
Ottawa, Ontario K1A 0S9

and through authorized bookstore agents
and other bookstores

A deposit copy of this publication is also available for
reference in public libraries across Canada

Price subject to change without notice

Cover description

The cover illustration shows four maps from the GIS study of the Chisel Lake-Anderson Lake area. Upper left – geological map; upper right – copper values in till; lower left – airborne radiometric potassium; lower right – integrated mineral potential. See paper by Wright and Bonham-Carter.

Original manuscript received: 1995 – 10
Final version approved for publication: 1996 – 01

CONTENTS

| | |
|---------------------|---|
| Foreward | |
| J.M. Duke | 1 |

| | |
|--------------------------------------|---|
| Introduction | |
| W.B. Coker and A.G. Galley | 3 |

RUSTY LAKE SUBPROGRAM

GEOLOGY

| | |
|---|----|
| Stratigraphic and tectonic setting of the Paleoproterozoic Ruttan Cu-Zn VHMS deposit, Rusty Lake belt, Trans-Hudson Orogen | |
| D.E. Ames | 15 |

| | |
|--|----|
| Geology of the West Anomaly orebody, Ruttan volcanic-hosted massive sulphide deposit, Proterozoic Rusty Lake belt | |
| D.E. Ames and C. Taylor | 45 |

GEOCHEMISTRY

| | |
|--|----|
| Effects of acid mine effluent on sediment and water geochemistry, Ruttan Cu-Zn mine | |
| W.W. Shilts, W.B. Coker, and A.M. MacDonald | 77 |

SNOW LAKE SUBPROGRAM

GEOLOGY

| | |
|--|-----|
| Setting of Paleoproterozoic volcanic-hosted massive base metal sulphide deposits, Snow Lake | |
| A.H. Bailes and A.G. Galley | 105 |

GEOCHEMISTRY

| | |
|---|-----|
| Surficial geochemistry and response to volcanic-hosted massive sulphide mineralization in the Snow Lake region | |
| C.A. Kaszycki, E. Nielsen, and G. Gobert | 139 |

| | |
|---|-----|
| Application of phase selective and sequential extraction methodologies in surficial geochemistry | |
| C.A. Kaszycki and G.E.M. Hall | 155 |

| | |
|---|-----|
| Phase selective leaches for use in exploration geochemistry | |
| G.E.M. Hall, J.E. Vaive, R. Beer, and M. Hoashi | 169 |

| | |
|--|-----|
| Selective leaching of the labile organic component of humus and soils with sodium pyrophosphate solution G.E.M. Hall, J.E. Vaive, A.I. MacLaurin, and M. Hoashi | 201 |
| Readsorption of gold during the selective extraction of the 'soluble organic' phase of humus, soil, and sediment samples G.E.M. Hall, A.I. MacLaurin, and J.E. Vaive | 215 |
| The geochemistry of vegetation growing over the deeply buried Chisel North Zn-rich massive sulphide deposit, Snow Lake area M.A.F. Fedikow and C.E. Dunn | 225 |
| Results of a detailed infill lake-sediment survey in the Snow Lake area: evaluation and comparison of grab sample and short core data P.W.B. Friske and M.W. McCurdy | 257 |

GEOPHYSICS

| | |
|--|-----|
| Application of airborne multiparameter geophysical data (gamma ray, magnetometer, VLF-EM) to mapping and exploration in the Rusty Lake and Snow Lake areas R.B.K. Shives | 279 |
| Ground electromagnetic, magnetic, and VLF-EM surveys at four sites near Snow Lake A.K. Sinha and G.J. Palacky | 299 |
| Electrical properties of disseminated sulphide ore samples from Snow Lake T.J. Katsube, G.J. Palacky, D.F. Sangster, A.G. Galley, and N. Scromeda | 319 |
| Development of a borehole surveying probe using 3-component fluxgate magnetometers P.G. Killeen, C.J. Mwenifumbo, and G.R. Bernius | 331 |

GIS MODELLING

| | |
|---|-----|
| VHMS favourability mapping with GIS-based integration models, Chisel Lake-Anderson Lake area D.F. Wright and G.F. Bonham-Carter | 339 |
|---|-----|

EXTECH I PUBLICATIONS

| | |
|---|-----|
| List of other EXTECH I publications | 377 |
| Author Index | 402 |

FOREWORD

EXTECH was initiated in 1989 to promote the development of new approaches to base metal exploration. Canadian reserves of copper, lead, and zinc had decreased substantially during the 1980s and, in the absence of significant new discoveries, it seemed likely that production from some of Canada's established mining camps would begin to decline before the turn of the century. The decrease in reserves in large part reflected reduced expenditures on base metal exploration and a shift of the industry's priority to gold exploration. Many mining camps had been well explored using existing methods and the general consensus was that new discoveries would most likely come from innovative concepts and technologies.

EXTECH represents an integrated, multidisciplinary approach to mineral exploration research. It encourages synergies among specialists in the various fields of geology, geophysics, and geochemistry by focusing their efforts on understanding the occurrence of a specific deposit type in a specific mining camp. The nominal goal is to develop an integrated deposit model – that is, a model that incorporates not only the geological attributes but also the geophysical and geochemical signatures of the deposit type. In working towards this goal, the regional geoscience knowledge base is enhanced and specific technologies are developed.

This volume describes the results of the first EXTECH project which was implemented in the Snow Lake and Rusty Lake belts of Manitoba. This area was selected for a number of reasons. From the socio-economic standpoint, it represented a highly productive base metal district which urgently required the discovery of new reserves to forestall mine closures and the resulting loss of employment. From the scientific standpoint, it possessed the right combination of abundant outcrop, complex glacial stratigraphy, and well documented mineral occurrences for the multidisciplinary studies that were envisioned. From the operational standpoint, the project would build upon the excellent working relationships which already existed among the Geological Survey of Canada, the Manitoba Geological Services Branch, and the exploration companies active in the area.

AVANT-PROPOS

Le programme EXTECH a été créé en 1989 pour promouvoir l'élaboration de nouvelles méthodes d'exploration des métaux communs. Au cours des années quatre-vingts, les réserves canadiennes de cuivre, de plomb et de zinc avaient considérablement diminué et, faute de nouvelles découvertes importantes, il semblait que la production de certains camps miniers bien établis pourrait commencer à chuter avant la fin du siècle. La diminution des réserves était en grande partie attribuable à la réduction des fonds consacrés à l'exploration des métaux communs et à un changement de cap de la part des sociétés minières, qui s'étaient tournées vers la prospection de l'or. Cependant, on avait aussi l'impression que de nombreux camps miniers avaient été bien explorés selon les méthodes existantes et que, pour découvrir d'autres gisements, il faudrait probablement innover en matière de concepts et de technologies.

Le programme EXTECH se veut un exemple de recherche multidisciplinaire intégrée dans le domaine de l'exploration minière. Il encourage la synergie entre les spécialistes des divers aspects de la géologie, de la géophysique et de la géochimie, en focalisant leurs travaux sur la compréhension d'un type de gisement spécifique dans un camp minier particulier. L'objectif principal est d'élaborer un modèle géologique intégré, c'est-à-dire un modèle qui incorpore non seulement les caractéristiques géologiques du gisement à l'étude, mais également ses signatures géophysiques et géochimiques. Les travaux effectués pour atteindre cet objectif permettent d'améliorer la base de connaissances géoscientifiques régionales et de mettre au point des technologies adaptées.

Les résultats du premier volet du programme EXTECH (EXTECH I) sont l'objet du présent bulletin, lequel volet se concentrait sur les ceintures de Snow Lake et de Rusty Lake, au Manitoba. Cette région a été choisie pour les raisons suivantes. Du point de vue socio-économique, elle représentait un district de métaux communs hautement productif qui avait un urgent besoin de nouvelles réserves pour éviter des fermetures de mines et les pertes d'emploi qui s'ensuivent. Du point de vue scientifique, elle présentait la combinaison appropriée de caractéristiques (affleurements en grand nombre, stratigraphie glaciaire complexe et occurrences minérales ayant fait l'objet de travaux) pour les études multidisciplinaires prévues. Du point de vue opérationnel, EXTECH I partait du bon pied avec les excellentes relations de travail qui existaient déjà entre la Commission géologique du Canada, la Direction des services géologiques du Manitoba et les sociétés d'exploration actives dans la région.

This was in many respects a pilot project with both strengths and weaknesses. It was strongly multidisciplinary and benefitted from a significant degree of integration in both the planning and execution of the research. With the close integration of the efforts of the federal and provincial geological surveys, each side brought its particular expertise to bear on the problem. Although EXTECH I perhaps fell short of achieving all its goals, we believe that this volume contains many insights which could stimulate new approaches to massive sulphide exploration and contribute to the discovery of new resources.

*J.M. Duke
Director
Mineral Resources Division
Geological Survey of Canada
September 1995*

À maints égards, il s'agissait d'un projet pilote et, en rétrospective, il comportait à la fois des points forts et des points faibles. Fortement multidisciplinaire, il a bénéficié d'une intégration assez poussée quant à la planification et à l'exécution de la recherche. Les travaux des commissions géologiques fédérale et provinciale se sont en outre fait sous le signe de l'étroite collaboration, chaque partie fournissant sa propre expertise pour mener à bien le projet. Même si les objectifs d'EXTECH I n'ont pas tous été atteints, il semble que le présent bulletin contienne de nombreuses données nouvelles qui pourraient inciter à trouver des façons inédites d'explorer les sulfures massifs et ainsi contribuer à la découverte de ressources supplémentaires.

*J.M. Duke
Directeur
Division des ressources minérales
Commission géologique du Canada
septembre 1995*

Introduction

W.B Coker¹ and A.G. Galley²

Coker, W.B. and Galley, A.G., 1996: Introduction; in EXTECH I: A Multidisciplinary Approach to Massive Sulphide Research in the Rusty Lake-Snow Lake Greenstone Belts, Manitoba, (ed.) G.F. Bonham-Carter, A.G. Galley, and G.E.M. Hall; Geological Survey of Canada, Bulletin 426, p. 3-14.

The Exploration Science and Technology (EXTECH) program was initiated in 1989 in response to the significant decline in Canadian base metal reserves that had occurred in the preceding decade. The objective was to improve concepts and technologies applicable to exploration in established base metal camps; one means of achieving this was to foster a closer integration of the traditional disciplines of geology, geochemistry, and geophysics. Accordingly, a multidisciplinary team of geoscientists from the Geological Survey of Canada (GSC) and the Manitoba Geological Services Branch (MGSB) was assembled to undertake a comprehensive study of the Snow Lake and Rusty Lake volcanogenic massive sulphide districts of Manitoba.

The selection of these two Paleoproterozoic base metal mining districts for the first EXTECH project reflects the fact that the over 220 million tonnes of massive sulphide ore extracted from the two belts combined represents more contained base metal per square kilometre than any other tectonic province in Canada, and is the richest Paleoproterozoic domain in the world (Fig. 1). The identification of the controls responsible for the development of these base-metal-rich environments is clearly desirable. More specifically, the selection of the Snow Lake and Rusty Lake districts for the first EXTECH program was based on:

1. the need to identify new reserves in these districts because of mine closures and resultant loss of employment;
2. the already developed co-operation between the GSC, the MGSB, and mining and exploration companies in these areas;
3. a developed expertise for this region;
4. a pre-existing database to use as an effective framework, which included airborne geophysical data, surficial geology maps, detailed provincial bedrock maps, and mineral deposit inventory;
5. the presence of abundant outcrop and lakes, plus a complex Quaternary stratigraphy and ice-movement history; and
6. the presence of abundant sulphide deposits and occurrences, large alteration zones, and subvolcanic intrusions.

Le Programme de science et de technologie de l'exploration (EXTECH) a été créé en 1989 pour pallier à la forte diminution des réserves canadiennes de métaux communs qui a marqué les années quatre-vingts. Il avait pour objectif d'améliorer les concepts et les technologies applicables à l'exploration dans les camps bien établis de métaux communs et il était admis que l'un des moyens d'y parvenir était de viser une intégration plus étroite des disciplines classiques de la géologie, de la géochimie et de la géophysique. En conséquence, une équipe multidisciplinaire composée de géoscientifiques de la Commission géologique du Canada (CGC) et de la Direction des services géologiques du Manitoba a été mise sur pied pour entreprendre une étude globale des districts de Snow Lake et de Rusty Lake, districts de sulfures massifs volcanogènes du Manitoba.

Le choix de ces deux districts miniers du Paléoprotérozoïque pour le premier volet d'EXTECH découle du fait que plus de 220 millions de tonnes de sulfures massifs ont été extraits à partir des roches de ces deux ceintures, ce qui s'avère la concentration la plus élevée de métaux communs par kilomètre carré de toutes les provinces tectoniques canadiennes et fait de cette région le domaine paléoprotérozoïque le plus riche du monde (fig. 1). Il est donc nettement souhaitable d'identifier les métalotectes à l'origine de la formation de ces milieux riches en métaux communs. En particulier, le choix des districts de Snow Lake et de Rusty Lake pour le premier volet du programme EXTECH se fonde sur les critères suivants :

1. la nécessité de trouver de nouvelles réserves dans ces districts à cause de la fermeture de mines et des pertes d'emploi qui s'ensuivent;
2. la collaboration qui existe déjà entre la CGC, la Direction des services géologiques du Manitoba et les sociétés d'exploration actives dans ces districts;
3. l'expertise acquise dans cette région;
4. l'existence d'une base de données comme point de départ, dans laquelle sont intégrées des données géophysiques, des cartes des matériaux superficiels, des cartes provinciales détaillées du substratum rocheux et une liste des gîtes minéraux;
5. l'abondance des affleurements et des lacs, la complexité de la stratigraphie quaternaire et de la chronologie des mouvements glaciaires;
6. le grand nombre de gîtes et d'occurrences de sulfures, mais aussi la présence de vastes zones d'altération et de secteurs parsemés d'intrusions hypovolcaniques.

¹ BHP Minerals Canada Ltd., 33 Yonge Street, Suite 610, Toronto, Ontario M5E 1G4

² Geological Survey of Canada, 601 Booth Street, Ottawa, Ontario K1A 0E8

The choice of the Snow Lake and Rusty Lake mining districts for this EXTECH I program was also influenced by the concurrent initiation of LITHOPROBE and NATMAP projects in the area. This would allow the EXTECH I participants to take advantage of expertise that would not otherwise be available. The Rusty Lake district was included as it was a unique opportunity to define the depositional environment of Canada's fourth (tied with the Flin Flon Main mine) largest volcanogenic massive sulphide deposit. The GSC has been involved in the Snow Lake camp since the 1970s, and the federal and provincial surveys had already started a co-operative geological mapping program centred on the base metal deposits.

The five year project started in April 1989 in both the Snow Lake and Rusty Lake districts. The program had 13 projects divided into four main components: a) bedrock mapping and deposit modelling (4); b) geophysical methodology (4); c) geochemical methodology (4); and d) GIS-based data integration and computer modelling (1). The geological studies formed a base, or starting point, from which other projects were initiated (Fig. 2). The other focal point for the group was the GIS project through which all of the data collected were channelled for digital integration and regional-scale modelling.

The following papers are divided between the two sub-programs. The three projects completed in the Rusty Lake region involved bedrock geology, mineral deposit, and surficial geochemical studies. The remaining 13 papers describe research that took place in the Snow Lake mining camp, and include papers on bedrock geology, surficial geochemistry and associated methodologies, and geophysics. The volume includes a list of all publications related to the EXTECH I program.

La réalisation simultanée de projets dans le cadre du LITHOPROBE et du CARTNAT dans cette région a également influé sur le choix des districts miniers de Snow Lake et de Rusty Lake pour le premier volet du programme EXTECH. Les participants d'EXTECH pourraient ainsi avoir accès à une expertise qui, autrement, n'aurait pas été disponible. Le district de Rusty Lake a été inclus du fait qu'il offrait une occasion unique de définir le milieu de mise en place du quatrième gisement de sulfures massifs volcanogènes en importance au Canada (relié à la mine principale du district de Flin Flon). La CGC mène des travaux dans le camp de Snow Lake depuis les années soixante-dix et les commissions géologiques fédérale et provinciale y avaient déjà entrepris un programme conjoint de cartographie géologique centré sur les gîtes de métaux communs.

Le premier volet d'EXTECH a débuté en avril 1989 tant dans le district de Snow Lake que dans celui de Rusty Lake et s'est échelonné sur une période de cinq ans. Il comptait treize projets qui étaient divisés selon les quatre thèmes principaux suivants : a) la cartographie du substratum rocheux et la modélisation des gîtes (4); b) les méthodes géophysiques (4); c) les méthodes géochimiques (4); d) l'utilisation d'un SIG pour l'intégration des données et la modélisation informatique (1). Les études géologiques ont jeté la base des autres projets (fig. 2). L'autre point d'intérêt de ce volet a été l'utilisation d'un SIG pour intégrer toutes les données recueillies et produire des modèles régionaux.

Les articles qui suivent sont divisés selon qu'ils font partie du sous-programme de Rusty Lake ou de celui de Snow Lake. Les trois projets réalisés dans la région de Rusty Lake ont porté sur la géologie du substratum, la gîtologie et la géochimie des matériaux superficiels. Les treize autres articles décrivent les recherches menées dans le camp minier de Snow Lake et portent notamment sur la géologie du substratum, la géochimie des matériaux superficiels et les méthodes associées, de même que la géophysique. Le présent bulletin contient une liste de toutes les publications liées au programme EXTECH I.

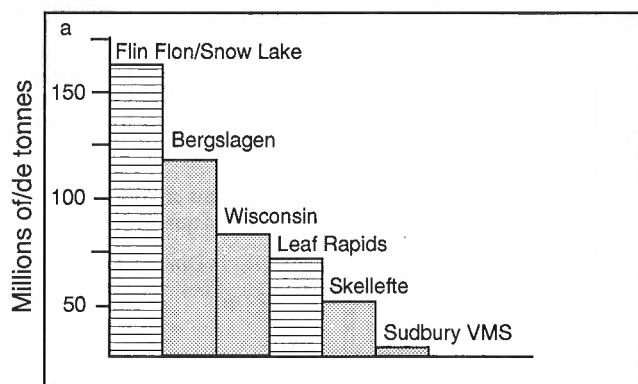


Figure 1. a) Histogram showing the developed tonnes of massive sulphide for the Flin Flon-Rusty Lake belts in comparison to other Paleoproterozoic terranes; **b)** The combined tonnage of the massive sulphide deposits of the Flin Flon-Rusty Lake belts in comparison to the world's larger mining districts.

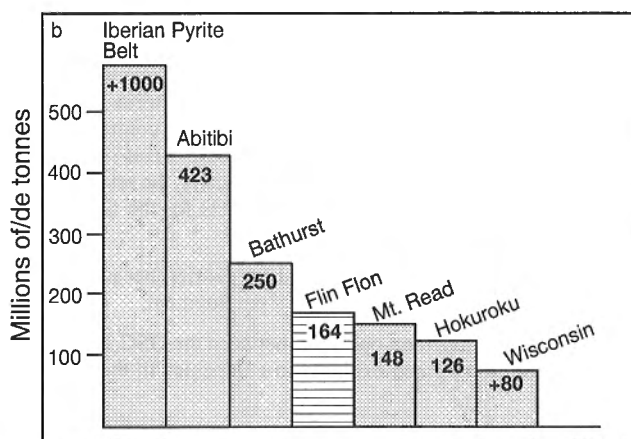


Figure 1. a) Histogramme montrant, à titre de comparaison, le nombre de tonnes de sulfures massifs extraits à partir des gisements sur le territoire des ceintures de Flin Flon et de Rusty Lake et sur celui d'autres domaines paléoprotérozoïques. **b)** Tonnage total des gisements de sulfures massifs des ceintures de Flin Flon et de Rusty Lake par rapport à celui des autres grands districts miniers du monde.

RUSTY LAKE SUBPROGRAM

Whereas most Precambrian massive sulphide districts are developed through a number of massive sulphide deposits, the Rusty Lake greenstone belt, to date, contains a single, 64 million tonne VMS deposit known as Ruttan. The other exception is, of course, the Archean Kidd-Munro belt, which hosts only the giant 145 million tonne Kidd Creek deposit. The Ruttan deposit is the fourth largest volcanogenic massive sulphide deposit in Canada, after Brunswick No. 12, Horne, and Kidd Creek. A deposit of this size usually lies at the far end of the deposit distribution curve in most massive sulphide camps, suggesting that other, albeit smaller, massive sulphide deposits should be present within the Rusty Lake belt. The main objective of the Ruttan bedrock mapping and deposit

SOUS-PROGRAMME DE RUSTY LAKE

Alors que la plupart des districts de sulfures massifs précambriens comptent plusieurs gîtes de sulfures massifs, la ceinture de roches vertes de Rusty Lake ne contient, à ce jour, qu'un seul gisement de sulfures massifs volcanogènes (SMV) de 64 millions de tonnes appelé Ruttan. Il existe une autre exception et c'est la ceinture archéenne de Kidd-Munro, qui renferme l'immense gisement de Kidd Creek (145 millions de tonnes). Le gisement de Ruttan est le quatrième gisement de sulfures massifs volcanogènes en importance au Canada, après ceux de Brunswick n° 12, de Horne et de Kidd Creek. Dans la plupart des camps de sulfures massifs, les gisements de cette taille se situent habituellement à l'extrémité de leur courbe de distribution, ce qui fait supposer que d'autres gisements de sulfures massifs, bien que plus petits, devraient exister dans la ceinture de Rusty Lake. Dans le cas du gisement de Ruttan, le projet de cartographie du substratum et de

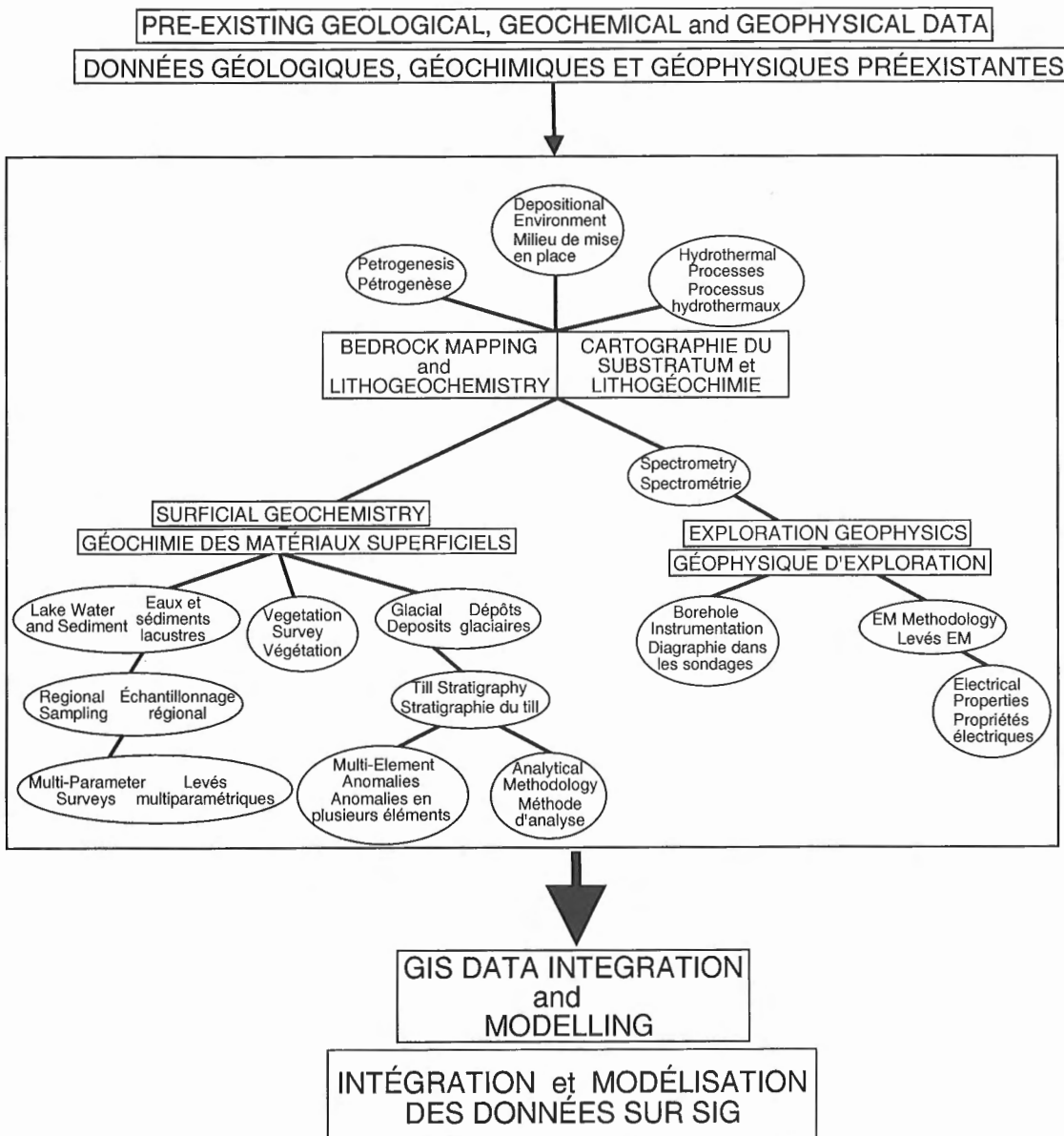


Figure 2. A schematic illustration of the multi-disciplinary nature of the EXTECH I program.

Figure 2. Schéma montrant le caractère multidisciplinaire du programme EXTECH I.

modelling project was to define the type of tectonic and depositional environment in which the Ruttan deposit formed, thereby fingerprinting a favourable volcanic domain for use as an exploration model in the remainder of the Rusty Lake belt.

The first paper of the volume by Doreen Ames is the documentation of the petrogenesis and depositional environment for the Ruttan deposit based on 1:5000 scale bedrock mapping of the Ruttan structural block. The detailed mapping resulted in a description of the proximal alteration facies about the deposit in light of pre-tectonic reconstruction, and the definition of the Ruttan horizon 900 m northeast of the deposit, where it is associated with a distinctive feldspar-rich alteration comparable to that found on the immediate periphery of several other VMS deposits of various ages. The most significant finding was the fact that the majority of the foot-wall strata are structurally emplaced from an arc terrane type (back arc) traditionally thought of as barren of economic VMS deposits. In light of the recent spate of lithogeochemical studies that have been used to define optimum VMS-hosting terranes, this study demonstrates that care must be taken in using strictly chemical discriminants in evaluating various structural blocks within a greenstone belt for VMS potential.

The second paper by Ames and Taylor gives a detailed description of the composition, morphology, and associated alteration of the 8.2 million tonne West Anomaly, the most recently developed lens in the Ruttan deposit. This study gives us another look at the characteristics of a giant massive sulphide deposit. That the deposit contains marginal metal grades does not detract from the fact that it is essential to understand the physical parameters necessary for the creation and preservation of such a giant, the nature of the metal-bearing fluids, and the reasons for the low base metal content. Like most giant massive sulphide deposits, Ames and Taylor have shown that it formed in a basin infilled with volcanoclastic material overlain by a thin rhyolite sequence that hosts the deposit itself. Whereas Kidd Creek, Flin Flon, and parts of the Horne deposit are covered by altered and mineralized volcanoclastic material, it appears that the Ruttan deposit formed near the top of a volcanoclastic sequence. It may be that the low base metal content is not a primary characteristic of the deposit, but rather a function of over-exposure at the seawater-rock interface where late-stage fluids "flushed" the mound of base metals.

The integration of exploration and environmental technology is becoming increasingly apparent as companies realize that the expertise gained by geoscientists for comprehending the hydrology and geochemistry of hydrothermal systems is essential in understanding lower temperature fluid reactions that concern environmental studies. An example is the third paper which documents a multi-parameter surficial geochemical study of the Ruttan tailings drainage system by Shilts et al. Using sonar profiling both as a guide to sediment collection strategy and as a tool in the interpretation of element anomalies, sediment (surface and core) and water samples were collected in Ruttan, Brehaut, Rusty, and Alto lakes. Anodic stripping voltametry was used for on-site analysis of waters down to low ppb levels of Zn, Cu, and Pb. At present, liming appears to control metal migration effectively so that, for example, concentrations of metals in Rusty Lake, downstream from Brehaut Lake, are equivalent to background for that lithology. A thorough understanding of the extreme variation in chemistry of the sediments, especially in Brehaut Lake, was predicated on

modélisation géologique visait principalement à définir le type de milieu tectonique et sédimentaire dans lequel la minéralisation s'est mise en place et ainsi faire ressortir un domaine volcanique qui pourrait être utilisé comme modèle d'exploration dans les autres parties de la ceinture de Rusty Lake.

Le premier article du bulletin, dont l'auteur est Doreen Ames, porte sur la définition de la pétrogenèse et du milieu de mise en place du gisement de Ruttan, à partir de travaux de cartographie à l'échelle de 1:5 000 du bloc structural de Ruttan. Ceux-ci ont permis de décrire, d'une part, le faciès d'altération proximal à la lumière d'une reconstruction pré-tectonique et, d'autre part, l'horizon de Ruttan là où il est associé à une altération distinctive riche en feldspaths (comparable à celle que l'on trouve à la périphérie de plusieurs autres gisements de SMV d'âges variés), c'est-à-dire à 900 m au nord-est du gisement. La conclusion la plus significative est que la majorité des couches de l'éponte inférieure ont été mises en place structuralement à partir d'un terrane d'arc, plus précisément d'arrière-arc, que l'on a toujours considéré comme dépourvu de gisements de SMV rentables. Avec en tête les nombreuses études lithogéochimiques réalisées récemment pour définir les terranes les plus susceptibles de contenir des SMV, l'auteur s'applique à démontrer qu'il faut prendre des précautions lorsqu'on n'utilise que des discriminants chimiques pour évaluer le potentiel en SMV des différents blocs structuraux dans une ceinture de roches vertes.

Le deuxième article par Ames et Taylor décrit en détail la composition, la morphologie et l'altération associée à l'amas minéralisé de West Anomaly de 8,2 millions de tonnes, soit la lentille du gisement de Ruttan dont la mise en valeur est la plus récente. Cette étude aborde d'un oeil différent les caractéristiques d'un immense gisement de sulfures massifs. Que le gisement recèle des teneurs marginales en métaux n'élimine pas le fait qu'il est essentiel de comprendre les paramètres physiques nécessaires pour créer et conserver un gisement aussi gigantesque, la nature des fluides minéralisateurs et les raisons pour lesquelles les teneurs en métaux communs sont faibles. Les auteurs démontrent que, comme la plupart des immenses gisements de sulfures massifs, celui de Ruttan s'est formé dans un bassin comblé de matériaux volcanoclastiques reposant sous une mince séquence de rhyolite dans laquelle est encaissée la minéralisation. Tandis que les gisements de Kidd Creek, de Flin Flon et de Horne (certaines parties) sont recouverts de matériaux volcanoclastiques altérés et minéralisés, il semble que celui de Ruttan se soit formé près du sommet d'une séquence volcanoclastique. Il se peut que la faible teneur en métaux communs ne soit pas une caractéristique primaire du gisement, mais plutôt le résultat d'une surexposition au niveau de l'interface eau de mer-roche, où les fluides tardifs auraient "évacué" l'amas de métaux communs.

L'intégration des techniques utilisées en exploration et en environnement est de plus en plus apparente depuis que les sociétés ont pris conscience que l'expertise acquise par les géoscientifiques pour comprendre l'hydrologie et la géochimie des systèmes hydrothermaux est essentielle pour reconstituer les réactions des fluides à des températures plus basses, un aspect important en environnement. Le troisième article de Shilts, Coker et MacDonald sur le gisement de Ruttan comprend un exemple illustrant ce fait. Il s'agit d'une étude géochimique multiparamétrique en surface visant le réseau de drainage des stériles de Ruttan. En se basant sur les profils obtenus par sonar pour orienter la stratégie d'échantillonnage des sédiments et pour faciliter l'interprétation des anomalies de certains éléments, on a prélevé des échantillons de sédiments (superficiels et carottes) et d'eau dans les lacs Ruttan, Brehaut, Rusty et Alto. On a eu recours au dosage voltamétrique par épuisement anodique pour l'analyse sur place des eaux jusqu'à des teneurs faibles en Zn, Cu et Pb, de l'ordre des ppb. À l'heure actuelle, le chaulage semble réduire efficacement la migration des métaux de telle façon que, par exemple, les concentrations de métaux dans le lac Rusty, en aval du lac Brehaut, soient équivalentes aux concentrations de fond de la lithologie du même nom. La connaissance approfondie des variations extrêmes dans la composition des sédiments, en particulier ceux

information derived from application of sonar profiling, phase-selective leaching, and scanning electron microscopy, in addition to "conventional" chemical analyses.

SNOW LAKE SUBPROGRAM

The Snow Lake mining district is considered ideal for a multi-disciplinary study as it is the source of at least 35 million tonnes of massive sulphide hosted by a well exposed, homoclinal sequence of volcanic strata. The strata are intruded by two large subvolcanic intrusive complexes, with both extrusive and intrusive suites affected by broad areas of synvolcanic hydrothermal alteration. The presence of abundant lakes and a complex Quaternary stratigraphy of variable thickness is ideal for surficial geological and geochemical studies, and the subcropping of several subeconomic sulphide occurrences is suitable for geophysical studies.

The first paper of this subprogram by Bailes and Galley is a description of the depositional environments of the area's seven past-producing VMS deposits. The study is based on detailed 1:5000 scale mapping of the Chisel Lake-Lost Lake-Ghost Lake and Anderson Lake-Stall Lake deposit-hosting strata and associated subvolcanic intrusions. The result is first of all a detailed physical and petrochemical description that, coupled with work by Stern et al. (in press), defines the evolution of an oceanic island arc sequence from the formation of a proto-arc through more evolved island arc cycles to rifting of the arc and creation of new seafloor. Questions are raised as to the possibility of bedding parallel tectonic discontinuities within the sequence that are still being addressed. The mapping program also defined the internal zonation within an intrusive complex hypothesized to be responsible for the generation of the Cu-rich deposits. This is important for allowing explorationists to evaluate the possibility of discovering VMS deposits quickly by recognizing certain characteristics of the subvolcanic suites. Lastly, three spatially distinct, regional-scale hydrothermal systems were defined, only two of which are associated with known massive sulphide deposits. The third zone may represent an immature phase of a broad-scale hydrothermal system.

The second part of the geology project was a study of the Chisel Lake-Chisel North Zn-Cu-Au-Ag-Pb massive sulphide mineralization (Galley et al., 1993). The results were a detailed mineralogical and lithogeochemical description of a carbonate-hosted VMS deposit, a type whose occurrence is so far restricted to other Paleoproterozoic camps such as Bergslagen (Sweden), Ladysmith-Rhineland (Wisconsin), and the VMS deposits of the Sudbury structure. The characteristics of the Chisel Lake orebodies and associated alteration suggest shallow-water (<1000 m) deposition. The recognition of shallow-water massive sulphide deposits is important as there appears to be a correlation between water depth of emplacement and the precious metal content of VMS systems, indicating that this deposit subtype may represent a transition between classic VMS and epithermal deposits.

The surficial geochemical program was specifically designed to develop new sampling and analytical methods utilizing media such as glacial till, humus, and vegetation. The glacial till project (by Kaszycki et al.) was carried out in a region that is not traditionally thought to be "friendly" to surficial geochemical exploration, due to the patchy nature of the glacial deposits and the presence of Quaternary lacustrine clay beds. The sampling program was established only after a thorough examination of the Quaternary stratigraphy and

du lac Brehaut, repose sur des informations tirées des profils sonar, de la lixiviation sélective des phases et de la microscopie électronique à balayage, sans oublier les «classiques» analyses chimiques.

SOUS-PROGRAMME DE SNOW LAKE

Le district minier de Snow Lake est considéré comme idéal pour mener une étude multidisciplinaire, étant donné qu'il recèle au moins 35 millions de tonnes de sulfures massifs encaissés dans une séquence de strates volcaniques monoclinales aux affleurements nombreux. Les strates sont recoupées par deux vastes complexes intrusifs hypovolcaniques, aux suites extrusives et intrusives présentant de grands secteurs d'altération hydrothermale synvolcanique. D'une part, la présence de nombreux lacs et d'une stratigraphie quaternaire complexe d'épaisseur variable est des plus appropriées pour les études géologiques et géochimiques en surface. D'autre part, l'affleurement au niveau de discordances de plusieurs occurrences subéconomiques de sulfures convient à la tenue d'études géophysiques.

Le premier article du sous-programme de Snow Lake, rédigé par Bailes et Galley, est une description des milieux de mise en place des sept gisements de SMV qui ont été exploités dans la région. L'étude se base sur la cartographie à l'échelle de 1:5 000 des strates minéralisées de Chisel Lake-Lost Lake-Ghost Lake et d'Anderson Lake-Stall Lake, de même que des intrusions hypovolcaniques associées. Le résultat est avant tout une description physique et pétrochimique qui, conjuguée aux travaux de Stern et al. (sous presse), établit l'évolution d'une séquence d'arc insulaire océanique allant de la formation d'un proto-arc qui se transforme en arc insulaire plus évolué pour aboutir à un rifting de l'arc et à la création de nouveau plancher océanique. Des questions sont soulevées quant à la possibilité qu'il existe des discontinuités tectoniques parallèles à la stratification au sein de la séquence. Les travaux de cartographie ont en outre permis d'établir la zonalité interne d'un complexe intrusif que l'on suppose être à l'origine de la formation des gisements cuprifères. Ce fait est important puisqu'il donne la chance au personnel des compagnies d'exploration d'évaluer la possibilité de découvrir rapidement des gisements de SMV sur la foi de certaines caractéristiques des suites hypovolcaniques. Enfin, on a défini trois systèmes hydrothermaux distincts d'échelle régionale, dont deux seulement sont associés à des gisements de sulfures massifs connus. Quant au troisième, il peut représenter une phase peu évoluée d'un système hydrothermal, mais à grande échelle.

La deuxième partie du sous-programme a porté sur l'étude de la minéralisation de sulfures massifs à Zn-Cu-Au-Ag-Pb de Chisel Lake-Chisel North (Galley et al., 1993). De cette étude découle une description minéralogique et lithogéochimique détaillée d'un gisement de SMV encaissé dans des roches carbonatées, type de gisement qui se limitait à ce jour à d'autres camps paléoprotérozoïques comme Bergslagen (Suède), Ladysmith-Rhineland (Wisconsin) et les gisements de SMV de la structure de Sudbury. Les caractéristiques des amas minéralisés de Chisel Lake et de l'altération associée indiquent une mise en place en eau peu profonde (~1 000 m). Il est important de distinguer les gisements de sulfures massifs mis en place en eau peu profonde, étant donné qu'il semble exister une corrélation entre la profondeur de l'eau et la teneur en métaux précieux des systèmes de SMV, indiquant que ce sous-type de gisement peut représenter une transition entre les gisements classiques de SMV et les gisements épithermaux.

Le levé géochimique des matériaux superficiels a été spécialement conçu pour élaborer de nouvelles méthodes d'échantillonnage et d'analyse de certains matériaux comme le till glaciaire, l'humus et la végétation. Le projet portant sur le till glaciaire (Kaszycki et al.) a été réalisé dans une région qui n'est pas habituellement considérée comme propice à la géochimie des matériaux superficiels, étant donné la nature clairssemée des dépôts glaciaires et la présence de couches d'argile lacustre datant du Quaternaire. Le programme d'échantillonnage n'a été établi qu'après un examen approfondi de la stratigraphie quaternaire et l'identification de trois

identification of three distinct till sheets. The success of the techniques used are reviewed by Kaszycki et al. in describing the three phases to the geochemical program. (1) Incorporating the knowledge acquired from the bedrock and mineral deposit studies on the mineralogy and chemistry of the VMS deposits and their associated alteration facies, till samples were analyzed by horizon and component. Multi-element plots revealed distinctive Cu-As-Hg anomalies, one of which sits directly over the Photo Lake Cu-Zn-Au deposit, found two years later by airborne EM. (2) Heavy mineral separates were then categorized by their aluminosilicate content in an attempt to define metamorphosed hydrothermal alteration zones. (3) Lithogeochemical alteration (i.e. alkali depletion and Fe-Mg enrichment) was employed to recognize material glacially transported from different alteration zones.

In surficial geochemical exploration for base metal deposits, the methods employed are only useful if an anomaly can be quantitatively assessed as a vector towards mineralization. Though the most common analytical method employed in geochemical exploration is based on determination of the "total" or near total element (e.g. dissolution of sediment or soil by aqua regia), it is usually the "labile" (free, noncrystalline) form of the element which is pertinent to the surface expression of a mineral deposit. Thus the geochemical pattern can be obscured by using a near total decomposition where that portion of an element bound in a silicate or sulphide phase is included. Renewed interest in the application of selective leaches was stimulated amongst the Canadian mining industry when, in 1990, major companies funded the demonstration of Russian methodologies designed to locate deeply buried mineral deposits. Two of the six methods presented by the team from Rudgeophysika, St Petersburg, are essentially selective leaches to extract metals bound in surface "scavenging" phases, that is, (a) in the humic and fulvic organic components of humus, and (b) in the amorphous Fe oxyhydroxide and Mn oxide "phase" of soil or till (Antropova et al., 1992). The Analytical Method Development Section of the GSC, under Hall's leadership, refined these two methods and went on to develop a sequential leach designed to identify and quantify four more phases which would be of use in the interpretation of surface geochemical anomalies. Three papers by Hall et al. describe these extractions, together with their advantages and limitations, and provide data on the precision and accuracy to be expected, using samples from the Snow Lake area and Canadian international reference standards. The cost-effective selective leaches developed were then applied in a study by Kaszycki and Hall to categorize surficial anomalies in the Chisel Lake area. The result was the differentiation between geochemical anomalies in humus, soil, and till associated with glacial dispersion, hydromorphic/biogenic remobilization, and anthropogenic contamination.

Completing the spectrum of surficial geochemical studies from glacial till through humus to vegetation is the study by Fedikow and Dunn on the sensitivity of northern tree species to the presence of deeply buried massive sulphide deposits. The premise is that certain elements will be transported towards the ground surface and incorporated into the living tissue of plants with an areally extensive root structure. Their choice of a study area overlies the Chisel North Zn-Cu deposit which lies 600 to 625 m below the ground surface. This careful study involved sampling of bark and twigs of three different species for a number of elements known to be anomalous within the massive sulphide mineralization. Ash

nappes de till distinctes. Les auteurs évaluent le succès des diverses techniques par l'intermédiaire d'une description du levé géochimique en trois étapes. 1) Les échantillons de till ont été analysés par horizon et par composante, sur considération des connaissances acquises par les études sur le substratum rocheux et les gîtes minéraux, notamment sur la minéralogie et la chimie des gisements de SMV et les faciès d'altération associés. Les diagrammes de plusieurs éléments ont révélé des anomalies distinctives de Cu-As-Hg, dont l'une se trouve directement à la verticale du gisement de Cu-Zn-Au de Photo Lake, découvert deux ans plus tard par levés EM aéroportés. 2) Les concentrés de minéraux lourds ont ensuite été classés selon leur teneur en aluminosilicates, afin de définir si possible les zones d'altération hydrothermale métamorphisées. 3) L'altération lithogéochimique (c'est-à-dire l'appauvrissement en alcalis et l'enrichissement en Fe-Mg) a servi à indiquer les matériaux ayant subi un transport glaciaire à partir de différentes zones d'altération.

En exploration, les levés géochimiques des matériaux superficiels visant à identifier des gisements de métaux communs ne sont valables que si une anomalie peut quantitativement servir de vecteur orienté vers la minéralisation. Même si la méthode d'analyse la plus courante en prospection géochimique repose sur la détermination de l'élément «total» ou quasi total (par ex. dissolution des sédiments ou du sol à l'eau régale), c'est habituellement la forme «labile» (libre, non cristalline) de l'élément qui est représentative de l'expression à la surface d'un gîte minéral. Par conséquent, la configuration géochimique peut être masquée par l'utilisation d'une décomposition quasi totale dans laquelle est incluse cette portion d'un élément lié dans une phase silicatée ou sulfurée. Le regain d'intérêt de l'industrie minière canadienne pour l'application de lixiviations sélectives date de 1990, lorsque d'importantes sociétés ont financé la démonstration de méthodes russes conçues pour localiser des gisements profondément enfouis. Deux des six méthodes présentées par l'équipe de *Rudgeophysika* de St-Petersbourg sont essentiellement des lixiviations sélectives servant à extraire les métaux liés dans des phases de «concentration» superficielles, c'est-à-dire a) dans les composantes humiques et fulviques de l'humus et b) dans les phases amorphes d'oxydes et d'hydroxydes de Fe de même que d'oxydes de Mn du sol ou du till (Antropova et al., 1992). Les scientifiques de la Section du développement des méthodes analytiques de la CGC, sous la direction de Hall, ont perfectionné ces deux méthodes et mis au point une lixiviation séquentielle pour identifier et quantifier quatre autres phases qui seraient utiles pour interpréter les anomalies géochimiques superficielles. Trois articles de Hall et al. décrivent ces méthodes, en soulignant leurs avantages et leurs limites, et présentent des données sur la précision et l'exactitude auxquelles on peut s'attendre, en utilisant des échantillons de la région du lac Snow et des étalons internationaux provenant du Canada. Les lixiviations sélectives rentables mises au point par Hall et ses collègues ont ensuite été appliquées dans le cadre d'une étude menée par Kaszycki et Hall visant à classer les anomalies superficielles dans la région du lac Chisel. Elle a eu pour résultat de différencier les anomalies géochimiques dans l'humus, le sol et le till associées à la dispersion glaciaire, à la remobilisation hydromorphe/biogène et à la contamination anthropique.

L'étude réalisée par Fedikow et Dunn sur la sensibilité de trois espèces d'arbres nordiques à la présence de gisements de sulfures massifs enfouis en profondeur complète l'éventail des levés géochimiques des matériaux superficiels, en l'occurrence le till glaciaire, l'humus et la végétation. Selon l'hypothèse sous-jacente à leurs travaux, certains éléments seront transportés vers la surface du sol et incorporés dans le tissu vivant des plantes dotées d'une structure radicale étendue. La zone d'étude qu'ils ont choisie couvre le gisement de Zn-Cu de Chisel North qui se trouve entre 600 m et 625 m de profondeur. Pour réaliser cette étude délicate, on a prélevé des échantillons d'écorce et de brindilles de trois espèces différentes d'arbres pour déterminer les teneurs en certains éléments qui sont considérées comme anormales dans l'amas de sulfures massifs. La normalisation de la

normalization was used to reduce effects of wind-blown contamination. The result was definition of a multi-element trace-element anomaly directly over the deposit.

A detailed lake sediment and water survey carried out by Friske and McCurdy resulted in the collection of samples at a density of 1 site per 4.3 km². In addition, short cores were collected from some lakes to aid in the interpretation of near-surface anomalies. Several anomalous base metal values were recognized in lakes directly south of known base metal occurrences and deposits indicating that bedrock mineralization has a strong influence over metal concentrations in the lakes. In most instances the near-surface anomalies were matched in the short cores by anomalies at depth, showing that the elevated values were caused by natural mineralized sources, not by mining contamination. In only three lakes, anomalies were caused by pollution from tailings. Other anomalies were recognized in lakes some distance from known mineralization, suggesting the presence of possibly untested bedrock base metal anomalies.

Four geophysical studies took place under the EXTECH I banner involving a broad range of data acquisition and analysis, from spectrometry through electromagnetics to magnetics. The spectrometry study by Shives et al. can be considered a cross between geophysics and geochemistry, as it involves the measurement of rock chemical properties in conjunction with VLF and total field and gradiometric magnetics. The objectives of the study were: (1) to ground-truth airborne anomalies with respect to mapped hydrothermal alteration, faulting, and differences in primary rock compositions; and, (2) to gather ground spectrometry data that would assist bedrock geologists in correlating units between stratigraphic sections and in differentiating various petrogenetic domains. The evaluation of airborne data resulted in the conclusion that the line spacing normally used for regional surveys was too coarse to define meaningful differences in either the volcanic stratigraphy or contained hydrothermal alteration zones. The airborne data were useful in differentiating subvolcanic from synkinematic plutons, a first order criterion for identifying potential VMS-hosting terranes. The ground surveys were successful in distinguishing among felsic volcanic formations, as well as identifying coeval extrusive-intrusive felsic suites. This is useful in correlating subvolcanic intrusive phases with potential VMS-hosting rhyolite complexes. This study shows that although bedrock geologists and explorationists have long used airborne magnetic data to assist in bedrock mapping, existing airborne spectrometry data have been under-utilized. The use of a hand-held spectrometer is also shown to be useful in differentiating and comparing felsic rock suites, a tool that is particularly useful in highly deformed terranes.

The next two geophysical studies on electromagnetic methods and electrical rock properties are interconnected, as the second was initiated due to the results of the first. The Sinha and Palacky study involved the re-evaluation of standard EM methodology on massive sulphide deposits in highly metamorphosed and deformed terranes. The study examined the problem of identifying the Snow Lake massive sulphide mineralization at detection levels expected for the size and composition of the orebodies. Four subeconomic occurrences (including the 13 million tonne Linda deposit) were tested using ground multi-frequency electromagnetic (HLEM), magnetic total field and gradiometer surveys. It became evident that the calculated conductivity values were very low in relation to similar sulphide mineralization in the Archean Superior Province. Sinha and Palacky made recommendations on how to increase the sensitivity of ground EM surveys

cendre a servi à réduire les effets de la contamination éolienne. Le résultat obtenu est la délimitation d'une anomalie en plusieurs éléments traces directement au-dessus du gisement.

Un levé détaillé des sédiments et des eaux lacustres a été réalisé par Friske et McCurdy; ils ont prélevé un échantillon au 4,3 km², mais aussi de courtes carottes dans certains lacs, afin de faciliter l'interprétation des anomalies proches de la surface. Plusieurs anomalies de métaux communs ont ainsi été observées dans les lacs situés directement au sud d'occurrences et de gisements connus de métaux communs, indiquant que la minéralisation du substratum rocheux influe beaucoup sur les concentrations de métaux dans les lacs. Dans la plupart des cas, les anomalies quasi superficielles dans les carottes courtes ont été corrélées à des anomalies profondes, ce qui signifie que les valeurs élevées sont dues à des sources minéralisées naturelles et non à une contamination minière. Il n'y a que trois lacs où les anomalies étaient associées à de la pollution par des stériles. D'autres anomalies ont été identifiées dans des lacs situés à une certaine distance d'une minéralisation connue, laissant croire à la présence probablement non vérifiée d'anomalies de métaux communs dans le substratum rocheux.

Quatre études géophysiques, dans le cadre desquelles on a acquis et analysé un large éventail de données (spectrométriques, électromagnétiques et magnétiques), ont été menées dans le cadre du programme EXTECH I. On peut considérer l'étude spectrométrique de Shives et al. comme un croisement entre la géophysique et la géochimie, puisqu'on y a mesuré les propriétés chimiques des roches en même temps que les très basses fréquences, le champ magnétique total et les gradients magnétiques. Cette étude avait pour objectif 1) de vérifier sur le terrain les anomalies identifiées lors des levés aéroportés en se concentrant sur les zones d'altération hydrothermale, les failles et les différences de composition des roches primaires figurées sur les cartes; 2) de rassembler les données spectrométriques acquises au sol qui pourraient aider les géologues à corréler les unités entre les coupes stratigraphiques et à différencier les divers domaines pétrogénétiques. L'évaluation des données recueillies par levés aéroportés indique que l'espacement des lignes de vol habituellement utilisé pour les travaux à l'échelle régionale était trop grand pour établir des différences significatives dans la stratigraphie volcanique ou les zones d'altération hydrothermale. Les données des levés aéroportés se sont avérées utiles pour différencier les plutons hypovolcaniques des plutons syncinématiques, ce qui constitue un critère de premier ordre pour identifier les terranes qui pourraient renfermer des SMV. Les levés terrestres ont permis d'identifier, d'une part, les formations volcaniques felsiques et, d'autre part, les suites felsiques intrusives et extrusives qui s'étaient mises en place en même temps. Ces données sont utiles pour corréler des phases intrusives hypovolcaniques à des complexes rhyolitiques susceptibles de renfermer des SMV. Il ressort de cette étude le fait suivant : même si les géologues et les prospecteurs ont depuis longtemps eu recours aux données des levés magnétiques aéroportés pour aider à établir la cartographie du substratum rocheux, les données des levés spectrométriques aéroportés ont, pour leur part, été sous-utilisées. Il est aussi démontré que le spectromètre portatif peut être utile pour différencier et comparer les suites de roches felsiques, ce qui en fait un outil particulièrement intéressant dans les terranes très déformés.

Les deux études géophysiques suivantes portant sur les méthodes électromagnétiques et les propriétés électriques des roches sont liées, puisque la seconde découle des résultats de la première. L'étude de Sinha et Palacky est une réévaluation de la méthode EM classique utilisée pour identifier des gisements de sulfures massifs dans les terranes fortement métamorphisés et déformés. Les scientifiques se sont penchés sur le problème d'identification des sulfures massifs de Snow Lake à des niveaux de détection prévus pour la taille et la composition des amas minéralisés. Ils ont tenté de détecter quatre occurrences subéconomiques (incluant le gisement de Linda de 13 millions de tonnes) à l'aide de levés électromagnétiques multi-fréquences (boucle horizontale), de levés du champ magnétique total et de levés gradiométriques, tous réalisés au sol. Il est devenu évident que les valeurs calculées de conductivité étaient très faibles comparativement à celles associées à des minéralisations de sulfures

over Snow Lake-type terranes, and also initiated a project to study the electrical properties of the Snow Lake massive sulphide deposits.

The electrical properties study by Katsube et al. analyzed specimens from a variety of types of Snow Lake base metal mineralization. The result showed an exponentially higher resistivity in comparison to other known massive sulphide camps which was thought to be caused by sulphide grain separation during amphibolite facies metamorphism.

The fourth study involved the development of borehole geophysical instrumentation. Killeen et al. describes the development of an oriented, 3-component borehole magnetometer. This instrument produces a continuous record of dip and azimuth of the borehole, and carries out a vector magnetic survey while traversing the borehole. The vector magnetics will allow for the detection of magnetically anomalous bodies in the vicinity of the drillhole. This is useful for two reasons: a) an anomalous magnetic field will result in the distortion of azimuth data as they are normally recorded in a drillhole, and b) it can detect the presence of Cu-rich mineralization which is commonly associated with massive pyrrhotite and disseminated to massive magnetite. Even if the drillhole is out of range of a magnetic field set up by a massive sulphide body, the associated metamorphosed alteration zones commonly contain disseminated magnetite and pyrrhotite. The changes in intensity of magnetization within the various alteration facies can therefore be used to direct drilling towards a potential orebody.

GIS DATA INTEGRATION AND MODELLING

Perhaps the most innovative aspect of the EXTECH I program was the work by Wright and Bonham-Carter demonstrating the power of Geographic Information Systems (GIS) for building a multi-layered exploration data set and combining the data to map mineral potential. Some of the early work on the EXTECH I data was published previously (e.g. Reddy et al., 1991; Reddy and Bonham-Carter, 1991; Reddy et al., 1992). GIS is a marvelous "electronic light table" for overlaying maps and searching for coincident anomalies, and for examining characteristics of individual localities by interactive query. It is also being increasingly recognized as a tool for decision support, and exploration decisions can be optimized by making use of *all* the data sets available by means of statistical and expert system models for data integration. Wright and Bonham-Carter show such models can be implemented, and produce a series of VMS potential (or favourability) maps. These maps show that all the known deposits occur in areas of elevated potential, as expected, and indicate several favourable zones where no deposits have been discovered. Recently, the Photo Lake deposit was discovered within one of these "hot spots", after the GIS study was complete. The discovery was made using airborne EM, without the benefit of the GIS map. Nevertheless, the GIS result bears out the value of the integrated approach, and the methods described in Wright and Bonham-Carter's paper are directly applicable to mineral exploration elsewhere.

semblables dans la Province archéenne du lac Supérieur. Sinha et Palacky ont fait des recommandations sur la façon d'accroître la sensibilité des levés EM terrestres dans les secteurs où s'observent des terranes qui s'apparentent à celui dans la région de Snow Lake; ils ont en outre entrepris un projet visant à analyser les propriétés électriques des gisements de sulfures massifs de Snow Lake.

Dans leur étude sur les propriétés électriques, Katsube et al. ont analysé des échantillons provenant de divers types de minéralisations de métaux communs dans la région de Snow Lake. Les résultats indiquent une résistivité exponentiellement plus élevée que dans d'autres camps de sulfures massifs, résistivité que l'on avait attribuée à la séparation des grains de sulfures durant le métamorphisme au faciès des amphibolites.

La quatrième étude porte sur la mise au point d'instruments de diagraphie géophysique. Killeen et al. décrivent la conception d'un magnétomètre orienté à trois composantes. Cet instrument produit un enregistrement continu du pendage et de l'azimut du trou de sondage et effectue une diagraphie magnétique vectorielle en descendant dans le trou. Les valeurs magnétiques vectorielles permettront de détecter les anomalies magnétiques correspondant à des amas minéralisés voisins du trou de sondage. Ces valeurs sont utiles pour deux raisons. a) Un champ magnétique anormal produira une distorsion des données azimutales, comme c'est normalement le cas dans une diagraphie de sondage. b) On peut détecter la présence d'une minéralisation cuprifère qui est habituellement associée à de la pyrrhotite massive et à de la magnétite disséminée à massive. Même si le trou de sondage est hors de la portée du champ magnétique créé par des sulfures massifs, les zones d'altération métamorphosées associées contiennent habituellement de la magnétite et de la pyrrhotite disséminées. Les changements d'intensité du caractère magnétique dans les différents faciès d'altération peuvent donc servir à diriger les forages vers un amas potentiellement minéralisé.

INTÉGRATION ET MODÉLISATION DES DONNÉES SUR SIG

L'aspect probablement le plus innovateur du premier volet du programme EXTECH est le projet de Wright et Bonham-Carter sur la capacité des systèmes d'information géographique à construire un ensemble de données d'exploration réparties sur plusieurs couches et à combiner les données afin de produire une carte du potentiel minéral. Quelques-uns des premiers travaux sur les données recueillies dans le cadre du programme EXTECH ont été publiés antérieurement par Reddy et al. (1991), Reddy et Bonham-Carter (1991) ainsi que Reddy et al. (1992). Les SIG sont, bien entendu, de puissantes «tables lumineuses» permettant de superposer des cartes et de déceler des anomalies qui se superposent, mais aussi de faire ressortir les caractéristiques d'une localité par le biais d'une consultation interactive. On considère de plus en plus les SIG comme un outil de décision; ainsi, dans le domaine de l'exploration, les décisions peuvent être optimisées en intégrant *tous* les ensembles de données disponibles dans des modèles statistiques et des modèles de système expert. Wright et Bonham-Carter montrent que de tels modèles peuvent être appliqués et aboutir à l'établissement d'une série de cartes du potentiel ou des «chances» de découvrir un gisement, dans le cas présent de SMV. Ces cartes montrent, comme prévu, que tous les gisements connus se concentrent dans des régions au potentiel élevé et indiquent plusieurs zones favorables où aucun gisement n'a été découvert. Le gisement de Photo Lake, découvert il y a peu de temps à l'aide de levés EM aéroportés, se trouve dans l'enceinte de l'un de ces «points chauds» identifié par le biais du SIG. Ainsi, les résultats obtenus grâce au SIG mettent en évidence la valeur de l'approche intégrée et les méthodes d'exploration minière décrites dans l'article de Wright et Bonham-Carter sont directement applicables ailleurs.

GIS as a focal point for an integrated project

The GIS study was a focal point through which the results of the various projects were integrated along with pre-existing data sets. The geological and mineral deposit research formed a starting point from which the other projects could define the various characteristics of a base metal camp that they would hope to identify and model geochemically and geophysically. The GIS group further directed data collection by pointing out gaps in the pre-existing data sets, and by identifying the relative importance of individual data layers as predictors of the known mineral deposits. From this starting point the projects and subprojects then can be arranged as shown in Figure 2. The collection of data sets and requirement for specialist information by the GIS group gave the project a constant focus.

GIS-based integration models

The success of the GIS work comes not simply from the application of a computational "black box", but from the careful development of a deposit model (and the subsequent exploration model) that guides the selection of data sets and the manipulation of these data sets to extract the spatial evidence that is critical for prediction. Wright and Bonham-Carter show that the statistical approach (such as weights of evidence, or logistic regression) is invaluable because it allows the spatial association between each data layer and the known deposits to be calculated objectively. On the other hand, the expert system approach (such as fuzzy logic or Dempster Shafer) is not bound by the *known* deposits, but makes use of exploration experience for assigning weights (in the form of "membership" or "belief" functions) to each data layer, and for formulating an "inference network" that attempts to mimic the thought processes of an experienced geologist in combining the data sources together. The result of applying a variety of different models, with different assumptions, is to produce a series of integrated "favourability" maps, and the degree of the differences between the maps is a measure of the sensitivity of the results to changes in assumptions and changes in the parameters. It is interesting that the three models applied here gave remarkably similar results, showing the robustness of the approach. Not only did the maps predict that the as yet undiscovered Photo Lake was in a highly favourable zone, but also that (1) the various data sources could be ranked according to predictive capability, and (2) both weights of evidence and Dempster Shafer methods allow maps showing uncertainty of prediction to be produced. These methods are valuable not just for target selection, but for formalizing an exploration model. This brings together the experts in different data types and leaves an "audit trail" so that others can repeat the modelling calculations and obtain the same answer. It also facilitates the explanation and justification of a particular decision to managers. It seems likely that GIS integration models will have a growing importance in the "toolbox" of the exploration industry.

EXTECH I: MULTI-DISCIPLINARY OR INTEGRATED?

At the completion of a project such as this, one must define objectively its successes and failures. One management objective was to involve the exploration industry in the design of the project to a greater extent than had been typical of

Le SIG : point central d'un projet intégré

L'étude sur le SIG a représenté un point central du premier volet d'EXTECH; les résultats des différents projets ont tous été intégrés à des ensembles de données préexistants. La recherche géologique et gîtologique a constitué l'assise du programme, à partir de laquelle il a été possible, dans le cadre des autres travaux, de définir les différentes caractéristiques d'un camp de métaux communs, le but étant d'identifier la minéralisation et de la modéliser à l'aide des méthodes géochimiques et géophysiques. Le groupe du SIG a orienté la collecte des données en signalant les vides à combler dans les ensembles de données et en établissant l'importance relative des couches de données pour identifier les gîtes minéraux connus. À partir de là, les projets et les sous-projets ont pu être disposés comme, par exemple, à la figure 2. L'intégration des ensembles de données et la nécessité qu'avait le groupe du SIG d'obtenir de l'information spécialisée ont donné une orientation constante au projet.

Modèles d'intégration sur SIG

Les résultats concluants dérivant de l'intégration des données sur un SIG ne sont pas simplement l'oeuvre de l'informatique, mais aussi de l'élaboration rigoureuse d'un modèle de gisement (et du modèle d'exploration qui en découle), lequel guide le choix des ensembles de données et la façon de les manipuler pour extraire l'information spatiale qui s'avère cruciale pour l'identification d'un gisement. Wright et Bonham-Carter montrent que la méthode statistique (comme le poids de la preuve ou la régression logistique) est un outil indispensable, étant donné qu'elle permet un calcul objectif de l'association spatiale entre chaque couche de données et les gisements connus. Par ailleurs, l'approche à l'aide d'un système expert (qui fait appel à la logique floue ou à la méthode de Dempster Shafer) ne repose pas sur les gisements *connus*, mais plutôt sur l'information acquise en cours d'exploration pour attribuer des poids (sous la forme d'«appartenance» des fonctions de «croyance») à chaque couche de données et pour bâtir un «réseau d'inférence» qui tente d'imiter les processus de pensée d'un géologue d'expérience; ainsi, toutes les données sont considérées. L'introduction de différents modèles, dont les hypothèses sous-jacentes varient, vise à produire une série de cartes intégrées du potentiel ou des «chances» de découvrir un gisement; l'importance des différences entre les cartes est une mesure de la sensibilité des résultats aux changements dans les hypothèses et dans les paramètres. Il est intéressant de noter que les trois modèles appliqués dans le cas présent ont donné des résultats remarquablement semblables, soulignant le bien-fondé de cette méthode. Les cartes ont non seulement fait ressortir que le gisement de Photo Lake non encore découvert était situé dans une zone très favorable, mais aussi 1) que les diverses sources de données pourraient être classées selon leur capacité de prédiction et 2) que tant le poids de la preuve que la méthode de Dempster Shafer permettent de produire des cartes montrant l'incertitude de la prédiction. Ces méthodes sont valables, d'une part, pour le choix des cibles et, d'autre part, pour valider un modèle. Ces travaux montrent aux spécialistes les différents types de données qui peuvent être utilisés et laissent une «méthode de vérification» qui permettra de répéter les calculs à la base d'un modèle et d'obtenir les mêmes résultats. L'explication et la justification d'une décision particulière aux gestionnaires s'en trouvent aussi facilitées. Il semble probable que les modèles d'intégration sur SIG joueront un rôle grandissant dans la «boîte à outils» des intervenants de l'industrie de l'exploration.

EXTECH I : MULTIDISCIPLINAIRE OU INTÉGRÉ ?

À la fin d'un programme comme celui-ci, il est essentiel de définir objectivement les résultats, qu'ils soient positifs ou négatifs. L'un des objectifs en matière de gestion était d'augmenter la participation de l'industrie de l'exploration à la conception du projet. On souhaitait atteindre un équilibre entre, d'une part, ce que les chercheurs considéraient être les directions

earlier survey projects. It was hoped that an appropriate balance would be achieved between what the researchers believed to be directions in which science can improve exploration strategy and the industry's pragmatic assessment of what scientific results could realistically be applied to exploration problems. We believe that the project was only partly successful in this respect because of some hesitancy to bridge the gap on the part of geoscientists in both government and industry at the outset. In the end, however, the project served to build mutual trust and understanding with the result that more recent co-operative projects such as the EXTECH II project in the Bathurst district of New Brunswick are achieving the desired degree of interaction.

As the GSC's first multidisciplinary mining camp study, EXTECH I was successful in acquiring critical new exploration data, and in developing several new methodologies. It was the first time that GSC and MGSB had attempted 1:5000 scale mapping of a mining camp, and the result was a much better understanding of the complexities of volcanogenic massive sulphide environments, of the hydrothermal systems spatially associated with these deposits, and the role of sub-volcanic intrusive complexes in generating these hydrothermal systems. It becomes evident though, that 1:20 000 scale mapping is the optimum scale for defining regional-scale relationships in a massive sulphide camp. Detailed till sampling resulted in the identification of meaningful multi-element discriminants, new analytical techniques (including speciation studies), and a chance to develop new discriminants centred on the mineralogical and chemical characteristics of metamorphosed hydrothermal alteration zones. Identification of deeply buried VMS deposits through vegetation geochemistry gives further proof of the release of tracer elements from deposits during deformation and metamorphism, and may develop into a powerful tool to be used in conjunction with phase-selective leaching and deep penetrating geophysics. Methodologies for identifying various sources of lake water and sediment anomalies, and for increasing our understanding of how metals can be cyclicly isolated and dispersed in these media will allow explorationists to better assess geochemical trace element anomalies, and help government and industry better forecast environmental impact from both natural and anthropogenic metal sources. Although airborne spectrometry was not shown to be a useful tool for identifying large-scale alteration systems, it can be used to identify K-poor subvolcanic intrusive complexes, whereas ground measurements can assist in correlating these intrusions with their extrusive equivalents. The results of the HLEM and electrical properties studies have alerted the exploration industry to the need of adjusting their methodologies for more sensitive detection of metamorphosed massive sulphide deposits.

This multi-disciplinary study can be considered integrated from two aspects. Firstly, the interaction of the group through planning sessions, semi-annual progress meetings, and ad-hoc discussions improved our collective knowledge as to the strengths and limitations of the individual disciplines. The gathering of the individual investigators into one field camp during the summer season was a further impetus to inter-group consulting and discussions. Politically these federal-provincial field camps helped cement co-operation between government surveys and minimized duplication. Secondly, the GIS study demonstrated how diverse data sources can be integrated, with the aid of a well-structured exploration model, to support the decision-making process.

dans lesquelles la science peut se diriger pour améliorer la stratégie d'exploration et, d'autre part, l'évaluation pragmatique de l'industrie des résultats scientifiques qui pourraient, de façon réaliste, être appliqués aux problèmes d'exploration. Sous ce rapport, le projet n'a été que partiellement concluant du fait que les géoscientifiques tant du gouvernement que de l'industrie ont manifesté, dès le départ, une certaine hésitation à combler l'écart. En dernier ressort, le projet a servi à établir une confiance mutuelle et à mené à une prise de conscience qui fait en sorte que les projets conjoints entrepris récemment, comme EXTECH II dans le district de Bathurst au Nouveau-Brunswick, réussissent à atteindre le niveau d'interaction souhaité.

À titre de première étude multidisciplinaire de la CGC dans un camp minier, EXTECH I a permis d'acquérir de nouvelles données d'exploration d'un intérêt crucial et d'élaborer plusieurs nouvelles méthodes. C'était la première fois que la CGC et la Direction des services géologiques du Manitoba tentaient de cartographier à l'échelle de 1:5 000 un camp minier. Le résultat est une connaissance plus approfondie de la complexité des milieux de mise en place des sulfures massifs volcanogènes, des systèmes hydrothermaux spatialement associés à ces gisements et du rôle des complexes intrusifs hypovolcaniques dans la formation de ces systèmes hydrothermaux. Il devient toutefois évident que la cartographie au 1:20 000 est la plus appropriée pour définir les relations d'échelle régionale dans un camp de sulfures massifs. L'échantillonnage détaillé des tills a permis d'identifier des discriminants significatifs composés de plusieurs éléments, d'élaborer de nouvelles techniques d'analyse (incluant les études sur les phases de certains éléments) et de trouver de nouveaux discriminants définis sur la base des caractéristiques minéralogiques et chimiques des zones d'altération hydrothermale métamorphisées. L'identification de gisements de SMV profondément enfouis par l'analyse géochimique de la végétation corrobore davantage le fait que des éléments traces sont libérés des gisements durant la déformation et le métamorphisme. Cette méthode pourrait devenir un outil puissant à utiliser de concert avec la lixiviation sélective des phases et les diagraphies géophysiques profondes. Les méthodes pour localiser les diverses sources des anomalies observées dans les eaux et les sédiments lacustres et pour mieux comprendre comment les métaux peuvent être cycliquement isolés et dispersés dans ces milieux aideront, d'une part, les géologues d'exploration à améliorer leur évaluation des anomalies d'éléments traces et, d'autre part, le gouvernement et l'industrie à mieux prévoir les répercussions environnementales des sources naturelles et anthropiques de métaux. Même si la spectrométrie aéroportée ne s'est pas avérée un outil utile pour localiser les systèmes d'altération à grande échelle, elle peut servir à localiser les complexes intrusifs hypovolcaniques faiblement potassiques; quant aux levés terrestres, ils peuvent faciliter la corrélation entre ces intrusions et leurs équivalents extrusifs. Les résultats des études sur les propriétés magnétiques (levés EM à boucle horizontale) et électriques ont fait en sorte que les intervenants de l'industrie de l'exploration ont pris conscience de la nécessité de modifier leurs méthodes pour mieux détecter les gisements de sulfures massifs métamorphisés.

Cette étude multidisciplinaire peut être considérée comme intégrée pour deux raisons. En premier lieu, les échanges au sein du groupe, par l'intermédiaire de séances de planification, de réunions semi-annuelles sur l'avancement des travaux et de discussions spéciales, ont accru la connaissance collective sur les points forts et les limites des disciplines individuelles. Il ressort que le regroupement des scientifiques dans un même camp durant la saison estivale a stimulé la consultation et les discussions au sein du groupe. Sur le plan politique, ces camps fédéraux-provinciaux ont favorisé la coopération entre les commissions géologiques des deux niveaux de gouvernement et ainsi minimiser le double emploi. Il est également à noter que l'utilisation du SIG a permis de démontrer comment on peut intégrer diverses sources de données, avec l'aide d'un modèle d'exploration bien structuré, pour appuyer le processus de prise de décisions.

The project came up short of being truly integrated, because the manuscripts within this volume are not products of co-operative authorships between disciplines, but rather a collection of papers whose common thread is that they took place in the same mining camps. Another missing factor was our inability to take better advantage of company data, especially in the field of airborne geophysics, and our failure in not formally involving individuals from the exploration industry in the research, experimentation, and documentation. This restricted our ability to evaluate the exploration methodologies used, and to evaluate the potential of such information as airborne EM data in further refining the GIS-generated favourability maps.

In the end we believe that our successes far outweighed the failures, and that EXTECH I not only generated new data, methodologies, and concepts, but also acted as a testing ground for a new generation of co-operative government-industry research geared to the needs of the mineral industry.

ACKNOWLEDGMENTS

The EXTECH I program was funded by the Geological Survey of Canada under the 1989-1994 Rusty Lake-Snow Lake Mining Camps Canada-Manitoba Exploration Science and Technology Initiative (EXTECH I), and by the Canada-Manitoba Partnership Agreement on Mineral Development (1990-1995).

REFERENCES

- Antropova, L.V., Goldberg, I.S., Voroshilov, N.A., and Ryss Ju.S.
1992: New methods of regional exploration for blind mineralization: application in the USSR; *Journal of Geochemical Exploration*, v. 43, p. 157-166.
- Galley, A.G., Bailes, A.H., and Kitzler, G.
1993: Geological setting and hydrothermal evolution of the Chisel Lake and North Chisel Zn-Pb-Ag-Au massive sulphide deposit, Snow Lake, Manitoba; *Exploration and Mining Geology*, v. 2, p. 271-295.
- Reddy, R.K.T. and Bonham-Carter, G.F.
1991: A decision-tree approach to mineral potential mapping in Snow Lake area, Manitoba; *Canadian Journal of Remote Sensing*, v. 17, p. 191-200.
- Reddy, R.K., Agterberg, F.P., and Bonham-Carter, G.F.
1991: Application of GIS-based logistic models to base-metal potential mapping in Snow Lake area, Manitoba; *Proceedings Canadian Conference on GIS*, Ottawa, Canada, March 18-22, 1991, p. 607-618.
- Reddy, R.K., Bonham-Carter, G.F., and Galley, A.G.
1992: Developing a geographic expert system for regional mapping of volcanogenic massive sulphide (VMS) deposit potential; *Nonrenewable Resources*, v. 1(2), p. 112-124.
- Stern, R.A., Syme, E.C., Bailes, A.H., and Lucas, S.B.
in press: Paleoproterozoic (1.90-1.86 Ga) arc volcanism in the Flin Flon Belt, Trans-Hudson Orogen, Canada, *Contributions to Mineralogy and Petrology*.

Contribution to the 1989-1994 Rusty Lake-Snow Lake Mining Camps, Canada-Manitoba Exploration Science and Technology Initiative (EXTECH I)

Le projet n'a pas connu de réelle intégration étant donné que les textes du présent volume ne sont pas les produits d'auteurs provenant de disciplines différentes, mais plutôt une collection d'articles dont le fil conducteur est de se rapporter aux mêmes camps miniers. Un autre facteur faisant défaut a été l'incapacité à tirer parti des données recueillies par les sociétés, surtout les données géophysiques de levés aéroportés, sans compter l'échec quant à demander officiellement à des scientifiques de l'industrie de participer à la recherche, l'expérimentation et la rédaction d'articles. Ces manques ont limité la capacité d'évaluer les méthodes d'exploration utilisées et l'utilité que pourraient avoir certaines données, comme celles des levés EM aéroportés, pour affiner les cartes du potentiel ou des «chances» de découvrir un gisement, produites à l'aide du SIG.

Pour conclure, il est espéré que les réussites ont de loin contrebalancé les échecs et qu'EXTECH I est non seulement à l'origine de nouvelles données, de méthodes innovatrices et de concepts différents, mais qu'il a également servi de banc d'essais pour une nouvelle génération de recherches menées conjointement par le gouvernement et l'industrie et axées sur les besoins de l'industrie minière.

REMERCIEMENTS

Le programme EXTECH I a été financé par la Commission géologique du Canada dans le cadre des Mesures Canada-Manitoba relatives au Programme de science et technologie de l'exploration dans les camps miniers de Rusty Lake et de Snow Lake (1989-1994) et de l'Entente de partenariat Canada-Manitoba sur l'exploitation minière (1990-1995).

Stratigraphic and tectonic setting of the Paleoproterozoic Ruttan Cu-Zn VHMS deposit, Rusty Lake belt, Trans-Hudson Orogen

D.E. Ames¹

Ames, D.E., 1996: Stratigraphic and tectonic setting of the Paleoproterozoic Ruttan Cu-Zn VHMS deposit, Rusty Lake belt, Trans-Hudson Orogen; in EXTECH I: A Multidisciplinary Approach to Massive Sulphide Research in the Rusty Lake-Snow Lake Greenstone Belts, Manitoba, (ed.) G.F. Bonham-Carter, A.G. Galley, and G.E.M. Hall; Geological Survey of Canada, Bulletin 426, p. 15-43.

Abstract: The depositional environment of the giant (64 Mt) Paleoproterozoic Ruttan Cu-Zn deposit in the Rusty Lake belt is constrained by new, detailed stratigraphic, structural, alteration, and lithotectonic data. A large component of the preserved footwall supracrustal sequence is ocean floor basalt that was deformed previous to juxtaposition with the tholeiitic island arc VMS hosting volcanic strata. Late intrusions and faulting have truncated much of the footwall strata, so that only a small portion of the original footwall strata remains. The Ruttan deposit is hosted in rhyolite near the top of synvolcanic fault-bounded basin-fill of dacitic to rhyolitic volcanoclastic strata that is capped by a thick formation of mafic volcanic turbidite. The presence of quartz-microcline-sericite \pm As and Au alteration and mineralization along the syn-depositional marginal faults to the basin, abundant large gas cavities in associated flow rocks and high Hg content of the Cu-Zn ore, suggests a shallow (<1000 m) water depositional environment.

Résumé : Le milieu de mise en place du gigantesque (64 Mt) gisement paléoprotérozoïque de Ruttan minéralisé en Cu-Zn (ceinture de Rusty Lake) est circonscrit par de nouvelles données sur la stratigraphie, le style structural, les altérations et le cadre lithotectonique. Une composante importante de la séquence supracrustale de l'éponte inférieure, qui a été conservée, est le basalte océanique; ce dernier a été déformé avant sa juxtaposition aux strates volcaniques de composition tholéiitique, mises en place dans un milieu d'arc insulaire et minéralisées en SMV. Des intrusions tardives et des failles recoupent la majorité des strates de l'éponte inférieure, de sorte qu'une petite partie seulement des couches originelles demeure. Le gisement de Ruttan est encaissé dans des rhyolites près du sommet d'un empilement de strates synvolcaniques de remplissage d'un bassin délimité par des failles, en l'occurrence un empilement de volcanoclastites dacitiques à rhyolitiques; ces dernières sont chapeautées d'une épaisse formation de turbidites volcaniques mafiques. L'altération en quartz-microcline-séricite et la minéralisation en \pm As-Au le long des failles marginales synsédimentaires du bassin, les abondantes cavités gazeuses dans les coulées associées et la forte teneur en mercure (Hg) du minerai de Cu-Zn témoignent d'un milieu de sédimentation en eau peu profonde (~1 000 m).

¹ Geological Survey of Canada, 601 Booth St., Ottawa, Ontario K1A 0E8

INTRODUCTION

The Ruttan Cu-Zn volcanic-hosted massive sulphide (VHMS) deposit is hosted by Paleoproterozoic metavolcanic rocks in the Rusty Lake belt, Trans Hudson Orogen (Fig. 1). It is situated 22 km east of the town of Leaf Rapids in north-central Manitoba and developed on a large 64 Mt volcanogenic massive sulphide (VMS) deposit, of which 57 Mt grading 1.27% Cu, 1.37% Zn, 0.56 g/t Au, 10.89 g/t Ag (A. Gottzman, pers. comm., 1993) is presently economic (Fig. 2, in pocket). The Rusty Lake belt to date contains only the large Ruttan base metal deposit with a small Zn occurrence (Fig. 2). Generally, VMS deposits occur in clusters and a felsic volcanic centre has a high probability of containing

several deposits (Sangster, 1980) although the Rusty Lake belt contains only one giant (>50 Mt) deposit. In terms of contained Cu and Zn metal, the Ruttan deposit is second to the Flin Flon mine at 1 676 800 and 3 990 345 tonnes respectively and contains twice as much metal as the Chisel deposit at 842 397 t, the two largest deposits in the Paleoproterozoic Flin Flon and Snow Lake mining camps respectively (Fig. 1), (data from Syme and Bailes, 1993; Galley et al., 1993).

A 1:5000 scale geological mapping program was initiated by the Geological Survey of Canada in 1990 to define the depositional environment of the Ruttan VMS deposit (Ames et al., 1990; Ames, 1991; Ames and Scoates, 1992), (Fig. 2). Prior to this study, knowledge of the composition, age, and structural setting of the Rusty Lake belt rocks was limited

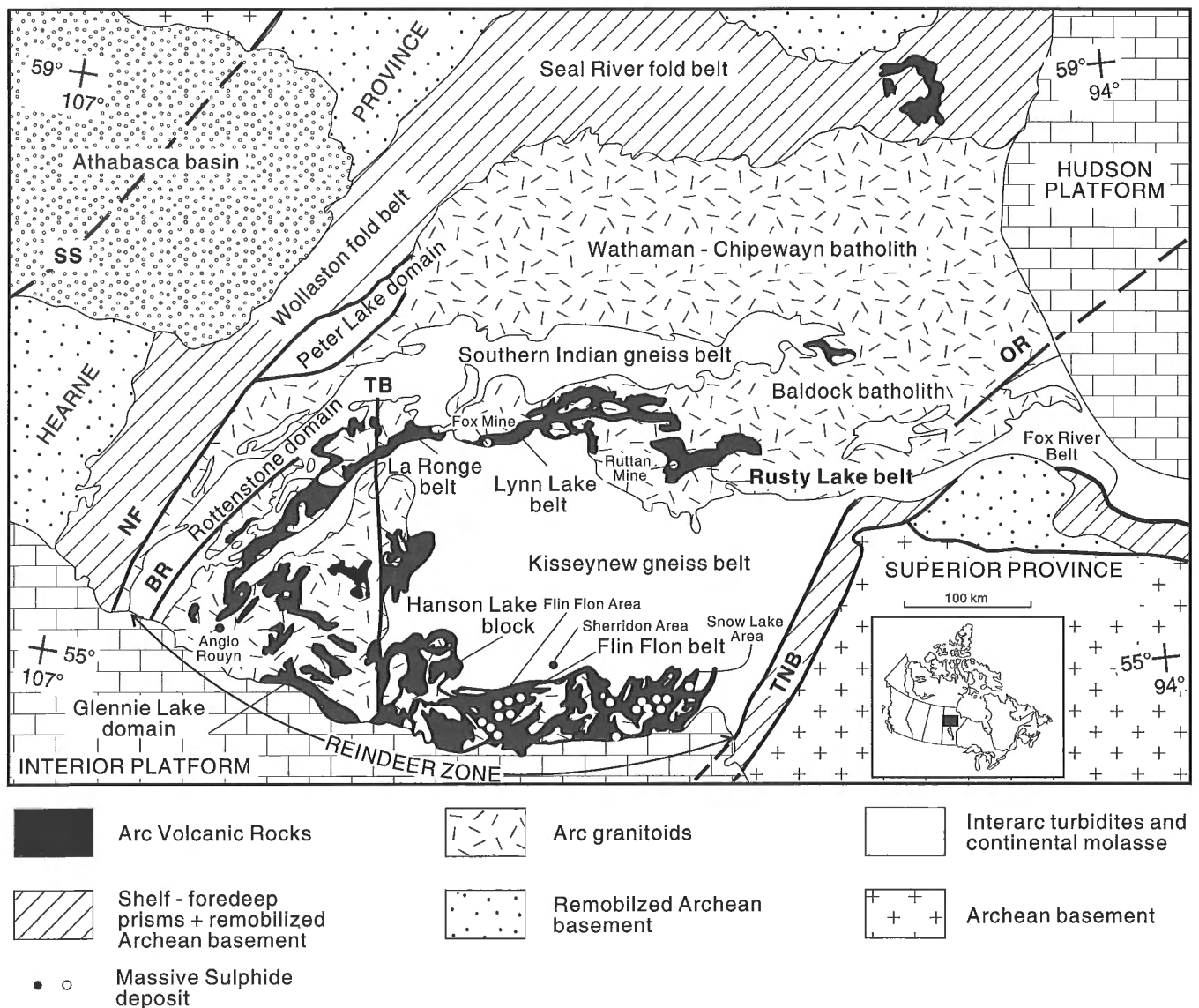


Figure 1. Lithotectonic domains of Early Proterozoic Trans-Hudson Orogen in northern Manitoba and Saskatchewan (after Hoffman, 1988). SS – Snowbird shear zone; NF – Needle Falls shear zone; BR – Birch Rapids shear zone; TB – Tabernor Fault; TNB – Thompson Nickel Belt; OR – Owl River shear zone.

(Baldwin et al., 1987). The purpose of this project is to provide data on the nature of the host rocks, volcanological features, alteration assemblages, structural-metamorphic and paleotectonic setting of the massive sulphide deposit. This paper provides information on the geology and geochemical signature of the Ruttan area stratigraphy and interprets the paleotectonic setting, whereas an accompanying paper (Ames and Taylor, 1996) describes the deposit-specific stratigraphy, alteration and mineral and bulk rock geochemistry of the Ruttan mine host rocks.

REGIONAL GEOLOGICAL SETTING

The Ruttan deposit is hosted by volcanic rocks of the 75 km long by 35 km wide, east-trending Rusty Lake belt which is within the Reindeer Zone of the Paleoproterozoic Trans-Hudson Orogen (Fig. 1, 2). The regional geology was initially described by Alcock (1921), Wright (1953), Burwash (1962), Milligan (1964), Pearce (1964), and, at the time of the mine discovery, Steeves and Lamb (1972). Parts of the belt were remapped by the Manitoba Mines Branch from 1978 to 1982, with the major part of the central Rusty Lake volcanic belt remapped at 1:20 000 scale by Baldwin (1982), the eastern part by Zwanzig (1982), and the region north and west of the Vol Fault by Bailes and Syme (1982). Detailed (1:10 000) volcanological observations of the Karsakuwigamak block were completed by Baldwin (1987).

The Rusty Lake belt is separated from the Lynn Lake Belt to the north by 10 km of plutonic rocks. Historically it was considered to be Archean (Stockwell, 1961) and part of the Lynn Lake-LaRonge belt. Recent U-Pb zircon geochronology of rhyolite flows within the Rusty Lake and Lynn Lake belts yielded an age 35 Ma younger for Rusty Lake belt rhyolite flows dated at 1878 ± 3 Ma (Baldwin et al., 1987; Baldwin, 1988). This age difference resulted in the Rusty Lake volcanic rocks being segregated from the Lynn Lake belt and renamed the Ruttan Group and a conglomerate of unknown age remained as part of the Sickie Group.

Subsequent subdivisions of the Rusty Lake belt were based on structurally bound stratigraphic sections encompassing four, fault-bounded structural blocks (Ruttan, Northern, Karsakuwigamak, and Eastern), with no apparent stratigraphic correlation between them (Baldwin, 1988). The present study reveals the complexities of the stratigraphy in the Ruttan Block, host to the large Ruttan massive sulphide deposit and cautions that previous subdivisions are simplified.

The Northern block is dominated by epiclastic units with minor iron-formation, the Ruttan and Eastern blocks by mafic volcanic strata and subordinate felsic volcanic and volcanoclastic units, and the Karsakuwigamak block by felsic volcanic flows and volcanoclastic rocks. Whereas the formations in the first three blocks represent submarine deposition, the rocks in the Karsakuwigamak Block are principally subaerial (Baldwin, 1987).

STRATIGRAPHIC SETTING

The Ruttan mine area is within the Ruttan structural block, and situated on the northern of two opposite-facing homoclinal sequences (Baldwin, 1988) separated by a granite pluton (Fig. 2, in pocket). Supracrustal rocks hosting the Ruttan deposit are bound on three sides by the Corner Lake pluton and Brehaut Lake pluton and are truncated by the Vol Fault to the north. The preserved stratigraphy near the Ruttan deposit forms a southeast-facing, southwest-tapering wedge, controlled by faults and plutons with a thickness varying from <1000 m to >280 m from the northeast to south of the mine site. The supracrustal stratigraphy is poorly exposed, with less than 20% exposure consisting of moss-covered outcrop. Recent 1:5000 mapping (Ames and Scoates, 1992) has made it possible to define the stratigraphic setting and lithotectonic domains present in the Ruttan mine area. Preliminary unit descriptions and characteristics may be found in Ames and Scoates (1992) and Ames and Taylor (1996).

The Ruttan strata are divided into footwall, host, and hangingwall successions (Fig. 2). The stratigraphic and structural footwall to the Ruttan deposit includes aphyric to pyroxene phyric effusive flows overlain by a mixed andesite-dacite-rhyolite sequence of dominantly volcanoclastic rocks with abundant lateral facies changes (Table 1). The host rocks to the Ruttan deposit are massive to fragmental rhyolite. In sharp contrast to the volcanic-dominated footwall and host strata, the hangingwall consists of turbiditic mafic to felsic wacke, siltstone, and conglomerate.

Footwall strata

Mill Pond formation

The stratigraphically lowest formation preserved in the Ruttan area is the Mill Pond formation, a >800 m thick sequence of massive to sparsely pillowed aphyric basalt. It is dominated by massive featureless aphyric basalt with trace, sparsely feldspar-phyric or hornblende-phyric basalt (Table 1, Fig. 2). The true thickness of the Mill Pond basalt is unknown as it is truncated in the west by the Brehaut Lake pluton, by the Vol Fault in the northeast and its upper contact is obscured by a zone of intense deformation and alteration – the Mill Pond shear zone. Primary volcanic features preserved include 1–3 mm amygdaloids, massive flows with flow top breccia, and rare pillowed flows with hyaloclastite. The pillowed flows outcrop in the deepest exposed units along the contact with the Brehaut Lake pluton at the mine site and to the northeast. Pillows are typically less than 0.5 m, with thin selvages less than 2 cm and epidote pods in the cores.

Actinolite composes 40–60% of the rock and also forms 2 mm porphyroblasts that are poikiloblastic grains enclosing quartz, titanite, opaque minerals, and monocrystalline 0.5 mm crystals. The granoblastic groundmass includes quartz and untwinned plagioclase plus trace amounts of disseminated sericite, titanite, calcite, chalcophyrite, and pyrrhotite. Feldspar-phyric flow units contain 35–40% feldspar phenocrysts and

Table 1. Stratigraphy of the Ruttan mine area.

| Mine area | Average thickness (m) | Principal lithology | Northeast | Average thickness (m) | Principal lithology |
|-------------------------------------|-----------------------|--|----------------------------------|-----------------------|---|
| Intrusive contact | | | | | |
| HANGINGWALL STRATA | | | | | |
| Powder Magazine formation | 150 | pebble and cobble paraconglomerate, minor orthoconglomerate | Powder Magazine formation | >350 | heterolithologic mafic volcanic breccia |
| | 100 | mafic wacke | | 60-250 | bedded mafic wacke |
| | 150 | thinly interbedded wacke mudstone, siltstone, minor dacite | | | |
| RUTTAN MINE SEQUENCE | | | | | |
| Conformable contact | | | Conformable contact | | |
| Upper felsic volcaniclastic unit | 10-50 | massive to bedded felsic quartz-bearing tuff, pebble breccia | Upper felsic volcaniclastic unit | 1.6 | quartz and feldspar bearing bedded felsic volcaniclastic |
| Conformable contact | | | Conformable contact | | |
| Mine rhyolite | 40 | massive sulphide and stringer mineralization chlorite schist | Massive rhyolite | 3-4 | massive rhyolite |
| | 20-30 | massive felsic rock | Lower felsic volcaniclastic unit | 3-4 | quartz bearing tuff |
| | | | Conformable contact | | |
| FOOTWALL STRATA | | | | | |
| | | | Trail formation | 25-100 | plagioclase phyric, massive to sparsely pillowed lava and related bedded volcaniclastic rocks |
| Conformable contact | | | Lateral changes | | |
| Mine dacite | >90 | homogeneous, massive to weakly layered volcaniclastic rock | Junction formation | 0-250 | massive dacitic volcaniclastic, minor aphyric and sparsely feldspar phyric, amygdaloidal basalt |
| Fault contact | | | Not exposed | | |
| Lower felsic volcaniclastic unit | >50 | thinly bedded felsic and subordinant mafic volcaniclastic | Vol formation | 250 | lateral facies changes; NE, series of 2m wide hornblende phyric massive flow rocks, SW heterolithologic mafic breccia |
| | | | Felsic tectonite | 0-110 | highly strained and altered felsic and mafic rocks |
| Fault contact: Mill Pond Shear Zone | | | Fault contact | | |
| Mill Pond formation | >0 | pillowed basalt | Mill Pond formation | >800 | massive, aphyric to sparsely feldspar phyric basalt, minor pillowed lava |

0-10% actinolite porphyroblasts after pyroxene. Interpillow material consists of chlorite, quartz and/or amphibole, and is locally sulphidic.

Vol formation

The 250 m thick Vol formation consists of an amphibole porphyroblastic basalt with amphibole pseudomorphous after pyroxene. The Vol formation is composed dominantly of narrow, 15 cm to 2 m wide massive pyroxene-phyric basaltic flows and/or sills with subordinate flows of feldspar-phyric, aphyric, and pyroxene-feldspar-phyric basalt. The massive flows grade to the southwest into pyroxene-phyric heterolithological mafic breccia. The lower contact is poorly exposed and partially obscured by dykes, intrusions, and alteration zones. The contact between the pyroxene-phyric basalt and the Trail basaltic andesite is sharp whereas the upper contact between the heterolithological breccia in the south and the Junction formation is unexposed.

The pyroxene-phyric basalt consists of 10-60% actinolite porphyroblasts, 0-40% feldspar porphyroblasts partially altered to epidote in a fine polycrystalline matrix of quartz and feldspar (10-30%) with trace amounts of biotite, titanite, sericite, pyrite, chalcopyrite, and calcite. Actinolite typically forms 1 mm monocrystalline and polycrystalline grains that reach a maximum size of 5 mm. Although no primary pyroxene is retained these porphyroblasts are pyroxene pseudomorphs. Plagioclase 1-2 mm, microphenocrysts, have been replaced by polygonal quartz, twinned feldspar, epidote, and minor actinolite.

Junction formation

The Junction formation is dominantly intermediate volcanoclastic strata with subordinate basalt flows and rare felsic volcanoclastic units. The Mine dacite (Ames and Taylor, 1996) and Junction formation intermediate volcanoclastic strata are separated by the North Wall shear zone. These units are interpreted to be equivalent due to their similar stratigraphic relationships, geochemical signature, and massive nature (Fig. 2). Extremely poor exposure of the sequence at the mine site, overprinting hydrothermal alteration, fault separation and lack of outcrop between the Mine dacite and poorly exposed Junction formation hinders an unequivocal correlation (Fig. 2). The lower and upper contacts of the Junction formation are not exposed at surface but the Mine dacite is bound by the North Wall shear zone at its base and is in sharp contact with the Mine rhyolite (Ames and Taylor, 1996).

The Junction intermediate volcanoclastic rocks are massive, poorly bedded, texturally inhomogeneous and interlayered with partially to pervasively silicified, sparsely feldspar-phyric and aphyric amygdaloidal basalt. Volcanoclastic rocks are massive to fragmental, containing 1 to 3 cm angular white felsic fragments, plus subrounded, black mafic fragments. Bleaching of the rock is common and produces inhomogeneities (Plate 1). The intermediate rocks are altered, well foliated, beige-brown weathering with 0-35% feldspar porphyroclasts in a matrix composed of 10-25% actinolite

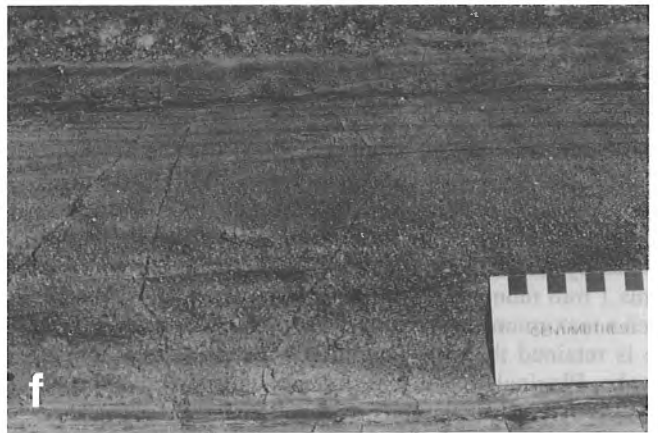
and/or biotite, 10-35% polycrystalline quartz, 10-60% plagioclase with trace amounts of titanite, garnet, epidote, calcite, and apatite. Microcline (5-10%) occurs in the matrix, as inclusions in actinolite, and in pressure shadows.

Trail formation

The Trail formation is a sequence of plagioclase-phyric volcanoclastic rocks and compositionally similar massive to rarely pillowed basaltic andesite lavas (Fig. 3; Plate 2). It outcrops along strike with the Junction formation and also overlies the pyroxene-phyric basalt in the north end of the map sheet (Fig. 2). The volcanoclastic rocks consist of a) heterolithological mafic breccia, b) poorly bedded lapilli tuff, and c) a well-bedded sequence of tuff and lapilli tuff that forms a series of lens-shaped deposits with a maximum thickness of 100 m (Fig. 3). The bedded and poorly bedded volcanoclastic rocks have a minimum strike length of 300 m (Fig. 3). The basaltic andesite lava unit forms a discontinuous lens, 100 m wide and 500 m long near the top of the pile. The upper flow surface is irregular (Plate 1) with a 50 cm wide discontinuous lens of finely bedded (millimetre to centimetre scale) mafic sediments deposited in depressions along the upper surface of the flows (Fig. 4). In some localities, the overlying Mine Sequence rhyolite is absent and here the contact between andesite and the hangingwall Powder Magazine formation wacke is sharp and silicified. Internal flow contacts are not exposed or have been affected by synvolcanic sills or alteration zones.

Heterolithological tuff-breccia with angular felsic fragments occurs at the base of the Trail formation (Fig. 3). Fragment types include scoreaceous mafic, feldspar-phyric epidotized mafic, angular light grey feldspar-bearing amygdaloidal volcanic, aphyric basalt, hornblende-phyric basalt, and angular feldspar-phyric felsic volcanic rocks. Many of the breccia layers are monolithic with cognate clasts.

In the southeast, the Trail formation consists of a series of lapilli-rich, fining-upward sequences, that are thinly bedded with reverse and normal size grading (Fig. 3). Coarse basal beds are up to 3 m thick and overlying finer grained beds are generally centimetres thick. The dominant clast types are clumps of feldspar or amygdales. Local discontinuous light grey, finely layered sediment may be ash. The volcanoclastic rocks contain 40% actinolite, 30% feldspar, and 0-10% amygdales, in a granoblastic matrix dominated by quartz with minor plagioclase (20-25%) and biotite (5-10%), trace zoisite, calcite, sericite, magnetite, chalcopyrite, and pyrite. Clasts consist of subrounded, 4 mm, glomeroporphyritic feldspar aggregates with recrystallized, polygonized, discontinuous, outer contacts. The recrystallized feldspar margins form diffuse boundaries with the matrix although the matrix is coarser than the polygonal rim. Intergranular contacts between plagioclase crystals are diffuse, serrated and the grains are poikilitic. Finer, 0.2 mm, sieve-textured grains have recrystallized edges that are intergrown with the matrix. Actinolite forms typically randomly oriented, 0.1-0.5 mm grains in the matrix, but also occurs with feldspar and quartz in relict mafic clasts. The amygdales are round with coarse monocrystalline



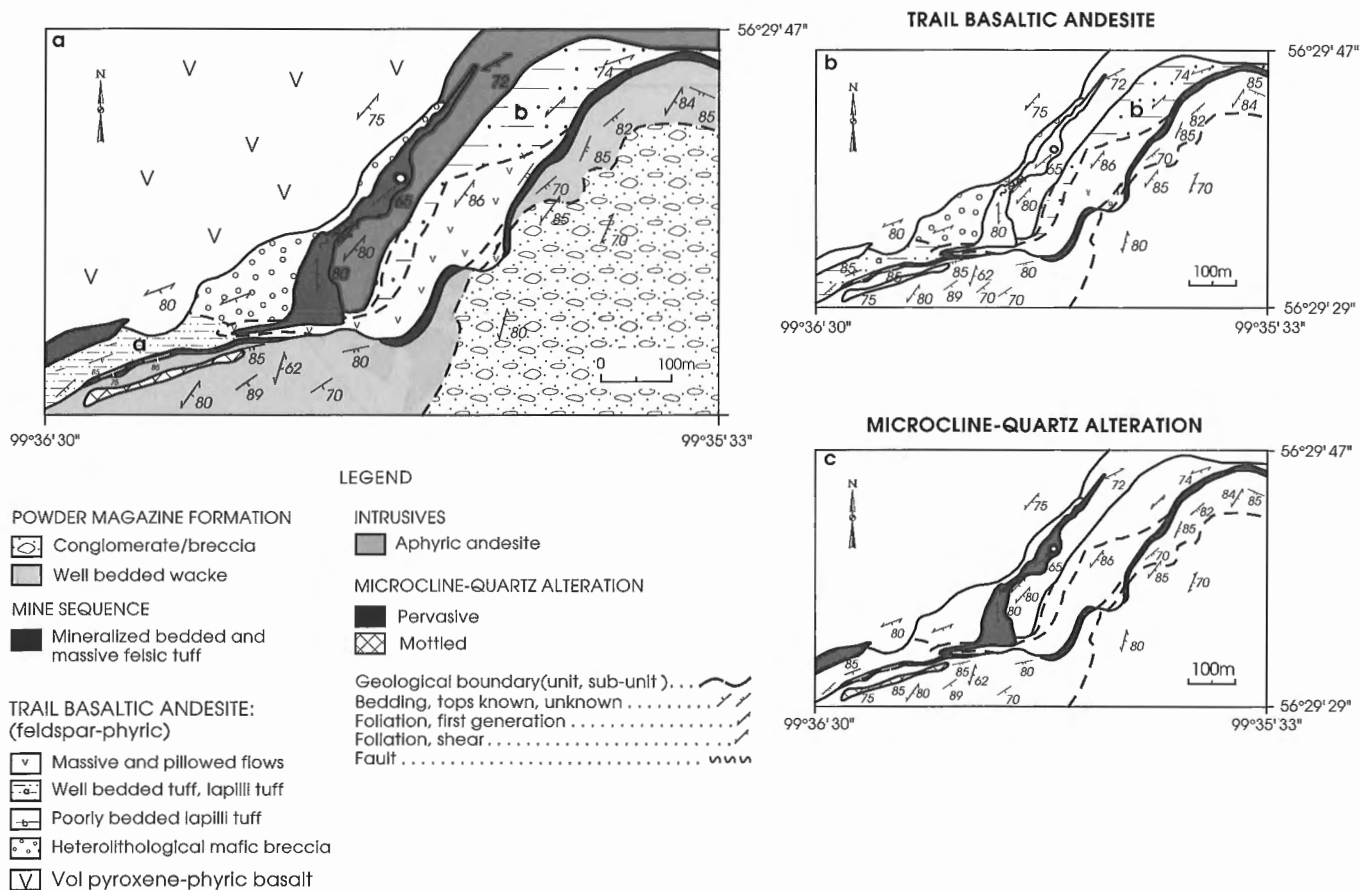


Figure 3. a) Detailed geological sketch of Ruttan extension area. b) Distribution of Trail basaltic andesite facies. c) Distribution of quartz-microcline alteration.

Plate 1

Host stratigraphy to Ruttan VHMS deposit

- a** – Pyroxene-phyric basalt, arc tholeiite sequence. Scale bar in centimetres. GSC 1995-183FFF
- b** – Plagioclase-phyric pillowed basaltic andesite of Trail formation, arc tholeiitic sequence. Scale bar in centimetres. GSC 1995-183MM
- c** – Well bedded lapilli tuff of Trail formation, arc tholeiite sequence. Pencil magnet at base of bed is 12.5 cm long. GSC 1995-183XX
- d** – Heterolithic lapilli-sized clasts in intermediate volcanoclastic rich of the Junction formation. Scale card is in centimetres. GSC 1995-183II
- e** – Fine grained gossanous felsic tuff at base of Ruttan extension rhyolite (top of photograph) intercalated with quartz-phyric massive rhyolite. Note crosscutting microcline alteration at 12.5 cm long magnet. GSC 1995-183QQ
- f** – Powder Magazine “Bouma” turbidite sequence indicates tops to southeast. Note normal grading at base of bed, parallel laminations, ripple cross laminations, faint parallel laminations and silt-rich top. Arc tholeiite signature. GSC 1995-183ZZ
- g** – Conformable irregular contact between Mine sequence rhyolite (left) underlain by Trail basaltic andesite (right). GSC 1995-183LL

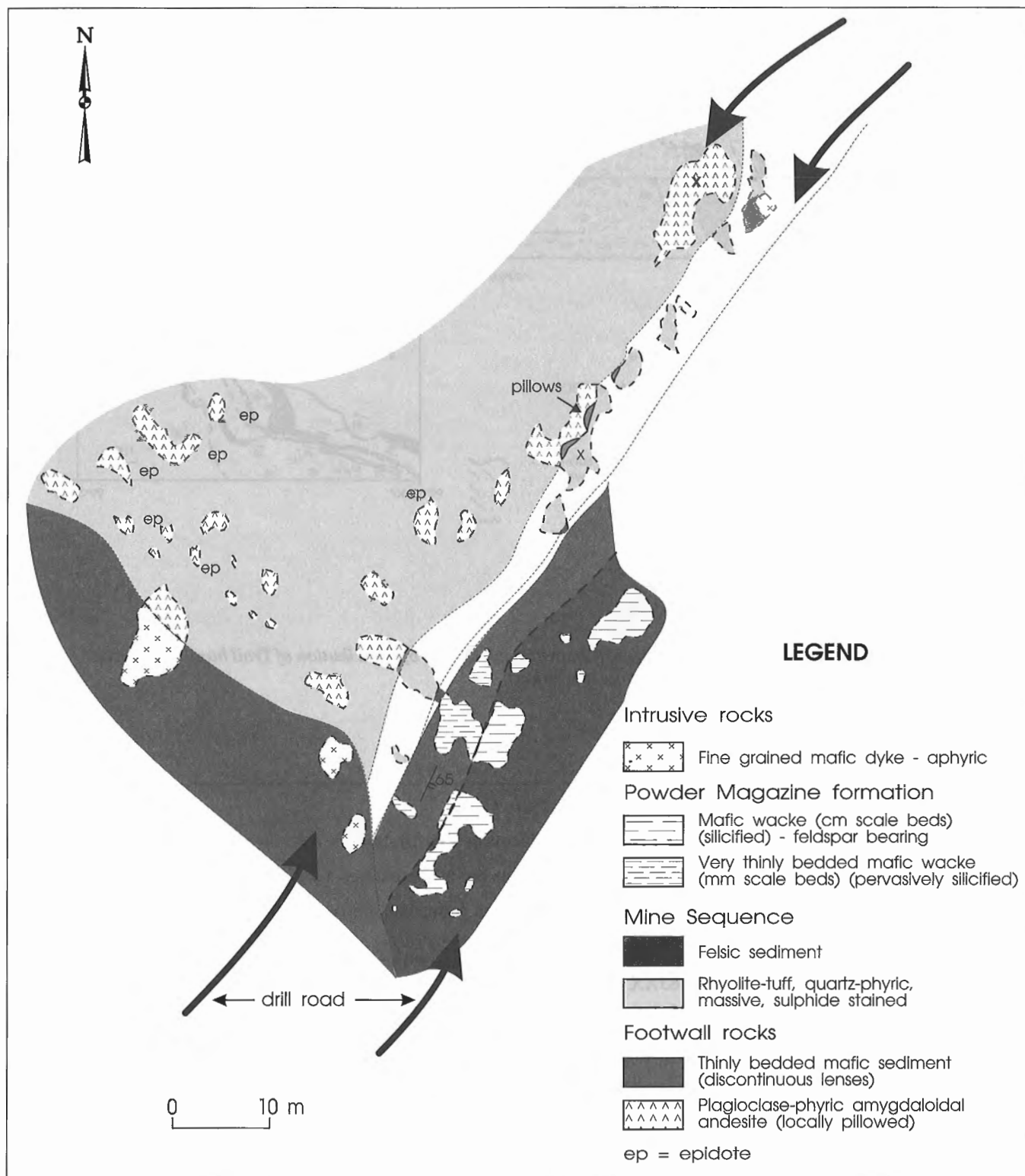


Figure 4. Detailed geological sketch of contact relationships of Mine sequence rhyolite, Ruttan extension.

quartz cores and rimmed by polygonized quartz. Attached to the amygdalae are irregular trails and indicate that they comprise a fragment.

Massive plagioclase-phyric andesite is distinct from the other lavas in the footwall sequence by the presence of abundant (30-50%) plagioclase phenocrysts and quartz filled amygdalae and sparse pyroxene phenocrysts (2%). The basaltic-andesites typically contain numerous epidote pods up to 40 cm across, 2 to 5 mm plagioclase phenocrysts and 2 to 15%, quartz filled amygdalae and gas cavities up to 2 cm in diameter. One exposure of pillowed basaltic-andesite was observed on the trail immediately below the Mine Sequence felsic tuff (Fig. 3, 4). The pillows are ovoid, amygdaloidal (4 mm in diameter), have selvages 2-4 cm wide, and contain 10 to 20 cm epidote cores. Plagioclase phenocrysts, 2-6 mm in diameter, are poikilitic and euhedral with minor recrystallization of the grain margins. Ragged, poikiloblastic, 1 mm, actinolite microphenocrysts are minor components (5%) and the recrystallized groundmass is an aggregate of 0.1 mm actinolite (30%), quartz and untwinned plagioclase (40%) with trace titanite, clinozoisite, pyrite, chalcopyrite, pyrrhotite, and ilmenite. Locally gas cavities reach 2.5 cm across although round, quartz-filled amygdalae are typically 4 mm. They contain a coarse monocrystalline core with a finer polygonal outer rim.

Ruttan Mine host strata

The host rocks to the Ruttan Cu-Zn orebodies consist of hydrothermally altered Mine dacite conformably overlain by a massive Mine rhyolite and associated mineralization and topped by an upper felsic volcanoclastic unit (Table 1, Fig. 2; Ames and Taylor, 1996). The lower felsic volcanoclastic unit below the Mine dacite is fault bounded and its relationship to ore unknown. The host package forms a cohesive sequence over 210 m thick and 2000 m in strike length at the mine that is in fault contact with the lower volcanic formations and is in conformable contact with the overlying Powder Magazine formation turbiditic wacke. The Ruttan Cu-Zn deposit consists of 8 ore zones grouped into the East Lenses, West Lenses, and the West Anomaly and hosted within the massive Mine rhyolite (Speakman et al., 1982; Ames and Taylor, 1996). The deposit is poorly exposed at surface but the deposit characteristics of the subsurface West Anomaly orebody are described in Ames and Taylor (1996).

The presence of shear zones and lack of outcrop between the mine site and the northeast make equivocal stratigraphic correlations impossible although similarities in composition, textures, and stratigraphic relationships exist (Fig. 2). A correlation may be made between the Lower felsic volcanoclastic rocks and Mine dacite, with the Junction formation volcanoclastic rocks due to similar compositional and stratigraphic subdivisions in the northeast (Fig. 2). Similarly a felsic bedded volcanoclastic sequence 700 m northeast of the open pit informally named the Ruttan extension area (Fig. 2, Table 1) is correlated with the Upper felsic volcanoclastic sequence in the mine, at the east edge of the open pit and near the Powder Magazines (Table 1, Fig. 2).

At the Ruttan extension, the rhyolite sequence is 7 to 10 m wide, sulphidic, steeply dipping, and laterally discontinuous (Fig. 2, 3). It is in conformable contact with the Trail

basaltic andesite and bedded mafic wacke of the Powder Magazine formation (Fig. 3). The rhyolite sequence consists of a 3-4 m wide base of quartz-phyric rhyolite tuff intercalated with minor mafic wacke overlain by 3-4 m of massive rhyolite and an upper 1.6 m normally graded sequence of felsic and mafic volcanoclastic rocks. The basal volcanoclastic rocks are rusty white weathering, finely bedded and quartz-phyric with 10-15%, 1 to 2 mm quartz and 5 to 10% garnet interlayered with minor, discontinuous, finely laminated mafic sediment. The proportion of biotite to actinolite is variable forming the different laminae. The massive rhyolite is rusty white weathering quartz phyric and aphyric and contains 5% magnetite, pyrite, pyrrhotite, sphalerite, and chalcopyrite. Subrounded, 2-5 mm quartz clasts and 0.6 mm feldspar porphyroblasts are surrounded by a polycrystalline matrix of 80-85% quartz, 10% feldspar, minor epidote, and trace sericite, biotite, garnet, calcite, pyrite, chalcopyrite, covellite, and pyrrhotite. Clasts are recognizable as finer felsic aggregates.

At the Ruttan extension (Fig. 3), the upper felsic volcanoclastic rocks are exposed over a 400 m strike length. Here the buff white weathering rhyolite tuff is interlayered with less than 5% mafic wacke, and is strongly altered to a microcline-quartz assemblage. The top is gradational with the overlying mafic wacke and consists of normally graded beds that are quartz- and feldspar-phyric with fine grained, white weathering, aphyric tops. Subrounded quartz clasts comprise <5%, 30-50% polygonal quartz, 20% plagioclase, up to 40% microcline alteration, 15% biotite, 5-10% sericite, clinozoisite and trace calcite, garnet, chlorite, pyrrhotite, pyrite, chalcopyrite and covellite. Where observed along the east shoulder of the open pit the upper felsic volcanoclastic rocks are 30 cm of very fine grained, sulphide stained, garnetiferous tuff that can be traced by drilling 300 m northeast to the headframe.

A microcline-rich rhyolite is intermittently present above the Vol formation (pyroxene-phyric basalt) and is within and above the Trail basaltic andesite. In the latter stratigraphic position the unit is 450 m long, thickening to the south from less than 10 m to over 100 m, forming a locally semiconformable to disconformable, dome-like body. This fine grained, aphyric rhyolite has a composition similar to the overlying Mine Sequence, but differs in that it contains abundant fracture-controlled microcline and quartz, sericite in vugs and arsenopyrite-gold veins. This rhyolite plug may be cogenetic with the overlying rhyolite sequence. The microcline and accompanying mineralization is believed to be a product of hydrothermal alteration, and is discussed later.

Hangingwall strata

Powder Magazine formation

The Powder Magazine formation is a >1 km thick mafic volcanic turbidite and debris flow sequence (Plate 1) that coarsens and becomes more felsic upwards (Speakman et al., 1982; Baldwin, 1982; Ames et al., 1990; Ames, 1991; Ames and Scoates, 1992). The upper contact is truncated by the Corner Lake pluton and its lower contact is conformable with the Ruttan Mine Sequence.

Immediately northeast of the open pit, the formation is a coarsening-upward sequence, with an up to 150 m thick, fine grained base of well-bedded volcanic wacke and siltstone intercalated with minor, thin, feldspar-hornblende-phyric mafic and dacite flows. The upper coarser grained strata form a unit greater than 100 m wide, composed of monolithic to heterolithological pebble and cobble breccia.

The fine grained lower part is typified by turbiditic sequences tens of centimetres in thickness, consisting of ABE and AE beds (Plate 1). Numerous stratigraphic facing indicators such as graded bedding, rip-up clasts, load casts, scour and flame structures indicate a southeast-younging direction, and a general transport direction from the northeast.

The upper unit is coarser grained, has thicker beds up to 20 m wide, and is composed of heterolithological breccia with minor monolithic and bilitic beds. These coarse grained strata were emplaced as mass flows that scour the underlying finer grained units truncating bedding contacts.

INTRUSIVE ROCKS

The strata hosting the Ruttan deposit are crosscut by several generations of sills and dykes, and is truncated to the east and west by the Corner Lake pluton and Brehaut Lake pluton, respectively (Ames and Scoates, 1992). All of the smaller intrusions postdate the footwall volcanic succession to the massive sulphide horizon. Gabbroic dykes intrude the Mill Pond basalt and diorite sills up to 250 m thick are observed at several stratigraphic intervals above the Mill Pond basalt; they occur as boudins within the massive sulphide lenses and are crosscut by younger plagioclase-phyric sills and dykes.

The Corner Lake pluton (unit 14, Fig. 2) is a zoned intrusion composed of diorite, quartz diorite, granodiorite, and a tonalitic core. The western border phase of this pluton in contact with the Powder Magazine formation is dominantly a medium grained hornblende diorite that locally contains xenoliths of bedded mafic wacke ranging from centimetre to block size. The Brehaut Lake pluton (unit 15, Fig. 2) is a high level intrusion that cuts the entire Ruttan mine stratigraphy and at its eastern contact is composed of tonalite, granodiorite, minor quartz diorite and granite. The border is dominated by an intrusion breccia phase with a granodiorite matrix and 60-70% angular xenoliths of aphyric basalt, mafic wacke, hornblende gabbro, diorite, hornblendite, and sulphidic and epidotized basalt of various sizes.

STRUCTURE AND METAMORPHISM

Low pressure-moderate temperature regional metamorphism at amphibolite grade in the Ruttan mine area was defined using alteration assemblages in the proximal alteration zone (Fig. 16 in Ames and Taylor, 1996). The entire map area is a southeast-facing succession that contains a penetrative fabric at 060°/85° (Baldwin, 1988; Ames, 1991; Ames and Scoates, 1992). The Mill Pond basalt sequence only, records an earlier fabric that is more northerly and shallower dipping

(025°/45°). The contact, between the Mill Pond basalt with the pyroxene-phyric basalt and diorite is a 50-75 m zone of mafic tectonite referred to as the Mill Pond shear zone. The Mill Pond shear zone removes part of the pyroxene-phyric basalt juxtaposing Mill Pond basalt against the Mine Sequence less than 300 m from the massive sulphide deposit. The majority of the footwall strata to the large Ruttan Cu-Zn VMS deposit has been structurally removed and displaced by the Brehaut Lake pluton.

The entire sequence is transected by a series of shear zones (Ames, 1991; Ames and Scoates, 1992; Ames and Taylor, 1996), the most notable of which are the Vol Fault, trending 110° separating the southeast-dipping, north-facing Northern block sequence from the southeast-facing Ruttan block sequence (Baldwin, 1988) and the North Wall shear zone (Fig. 2). The North Wall shear zone is a ductile, high angle reverse fault with south side up with an orientation of 070°/80° and a stretching lineation at 120°/80°. Minor down-facing Z-shaped folds in the Ruttan mine area and the ore lenses plunge parallel to the tectonic direction of the North Wall shear zone (Fig. 2). These reclined structures were either rotated into parallelism by the shear or are refolded folds. The lack of two foliations in the surrounding strata and the proximity of the rare folds to major shear zones suggest that they are not refolded folds but are related to the ductile shearing. The warping of the map scale pattern of units and the Mill Pond shear zone into the Vol Fault suggests a dextral sense of movement. The Mill Pond shear zone is interpreted as an earlier structure than either the Vol Fault or North Wall shear zone. It may have juxtaposed the mafic Mill Pond basalt that contains a previous recorded history of deformation with the dominantly felsic volcanoclastic sequence hosting the 64 Mt Ruttan deposit.

MAFIC VOLCANIC GEOCHEMISTRY

Mill Pond formation

The Mill Pond formation basalt contains 5.3-11.5 wt.% MgO, 44.4-50.6 wt.% SiO₂ (Table 2) and display an enrichment of TiO₂ with increasing FeO*/MgO (*total iron) and increasing Cr and Ni content with increasing MgO content (Fig. 5). Within the Mill Pond formation are two groups of basalt with slightly differing geochemistry. A high TiO₂ (1-1.62) and low MgO (5-7) group and a moderate TiO₂ (0.89-0.98), higher MgO (8-12) group. The high TiO₂ group dominates and consists of light grey green to medium green massive to sparsely pillowed basalt containing thin selvages and epidote domains. The moderate TiO₂ group occurs as a unit approximately 200 m wide within the high TiO₂ basalt. The moderate TiO₂ Mill Pond basalt units are dark greenish black and locally pale pistachio green due to local sparse epidotization. They are strongly deformed, with localized 4-6 mm black to dark green bands with irregular bulbous shapes that may represent pillow selvages. The basalt units are texturally heterogeneous, mottled, and contain 1-2 mm felsic inter-pillow material and quartz-carbonate-sulphide stringers.

Moderate TiO₂ Mill Pond basalt units have slightly convex rare earth element (REE) patterns that are slightly depleted at the light rare earth element (LREE) end and flat at the heavy rare earth element (HREE) end at about 20X chondrite (Fig. 6). The high TiO₂ Mill Pond basalt has a similar REE pattern but with depleted REE concentrations relative to the low TiO₂ group at approximately 12X chondrite with variability in geochemistry attributed to differentiation. The depletion in LREEs and flat HREE profile is similar to normalized-MidOcean Ridge Basalt (N-MORB) type suites in the Flin Flon Belt (Stern et al., 1995). The Mill Pond formation basalts have a sloping MORB-normalized trace element pattern that displays enrichment in large ion lithophile elements (such as K, Rb, Ba, Sr) (Fig. 7). The high field strength elements (Hf, Ti, Zr and Y), are slightly depleted relative to MORB and the Ni, Cr values are moderately depleted. The abundance of high field strength and LREE elements is similar to MORB.

The Mill Pond basalts plot on tectonic discriminant diagrams in the ocean floor basalt field, with minor overlap into the island arc basalt field or low K tholeiite field (Fig. 8, 9). The basalts in the Ruttan mine area can be distinguished between ocean floor and arc tholeiitic rocks based on their Mg/Ni ratios according to the criterion developed by Syme and Bailes (1993) for the Flin Flon area (Fig. 9).

Trail and Junction formations

The Junction formation basalt and Trail formation basaltic andesite differ from the Mill Pond formation basalts in that they have consistent TiO₂ abundances with increasing FeO*/MgO and contain low Ni and Cr values (Fig. 5). The Junction formation basalt contains 49-54 wt. % SiO₂ and 4-6 wt. % MgO whereas the Trail basaltic andesite has 53-58 wt. % SiO₂ and lower MgO at 2.1-4.2 wt. % (Table 2). The Trail basaltic andesite has a sloping REE pattern with an

Table 2. Mafic geochemistry.

| Formation | Mill Pond Basalt n=19 | Vol Basalt n=6 | Trail Bslt-and n=8 | Junction Basalt n=3 | SW Basalt n=2 |
|----------------------------------|--------------------------|-------------------|-----------------------|------------------------|------------------|
| SiO ₂ | 48.23 | 47.97 | 56.40 | 51.27 | 52.25 |
| TiO ₂ | 1.32 | 0.90 | 0.67 | 0.73 | 1.04 |
| Al ₂ O ₃ | 13.62 | 16.00 | 16.40 | 17.30 | 14.35 |
| Fe ₂ O ₃ T | 14.42 | 14.03 | 11.07 | 11.00 | 16.20 |
| Fe ₂ O ₃ | 3.33 | 4.00 | 2.44 | 2.03 | 4.50 |
| FeO | 9.99 | 9.03 | 7.76 | 8.07 | 10.55 |
| MnO | 0.22 | 0.24 | 0.18 | 0.19 | 0.32 |
| MgO | 7.25 | 6.28 | 3.37 | 5.06 | 3.41 |
| CaO | 11.72 | 11.92 | 7.76 | 10.07 | 8.23 |
| Na ₂ O | 1.79 | 1.87 | 2.92 | 2.83 | 1.50 |
| K ₂ O | 0.34 | 0.39 | 0.66 | 0.72 | 1.27 |
| H ₂ OT | 1.61 | 1.55 | 1.29 | 1.27 | 1.70 |
| CO ₂ T | 0.41 | 0.32 | 0.28 | 0.27 | 0.15 |
| P ₂ O ₅ | 0.10 | 0.11 | 0.11 | 0.15 | 0.19 |
| S | 0.06 | 0.05 | 0.02 | 0.01 | 0.03 |
| Ba | 49 | 103 | 284 | 172 | 280 |
| Au | | | 1020.0 | | |
| Hg | 3.7 | 2.5 | 1.8 | | |
| Ag | 3 | 40 | 1 | 1 | 1 |
| Be | 0.4 | 0.4 | 0.7 | 0.4 | 0.7 |
| Co | 50 | 45 | 25 | 31 | 26 |
| Cr | 110 | 101 | 30 | 91 | 5 |
| Cu | 54 | 58 | 102 | 9 | 17 |
| As | | | 4 | | |
| La | 5 | 5 | 5 | 5 | 5 |
| Nb | 5 | 5 | 5 | 5 | 5 |
| Ni | 69 | 42 | 20 | 30 | 5 |
| Pb | 15 | 13 | 13 | 10 | 10 |
| Rb | 10 | 11 | 13 | 19 | 18 |
| Sc | 45 | 36 | 17 | 34 | 42 |
| Sr | 139 | 258 | 303 | 397 | 170 |
| V | 324 | 280 | 233 | 227 | 140 |
| Y | 25 | 11 | 13 | 15 | 22 |
| Yb | 2.1 | 0.7 | 1.0 | 1.6 | 1.8 |
| Zn | 122 | 131 | 112 | 143 | 165 |
| Zr | 58 | 25 | 40 | 35 | 54 |

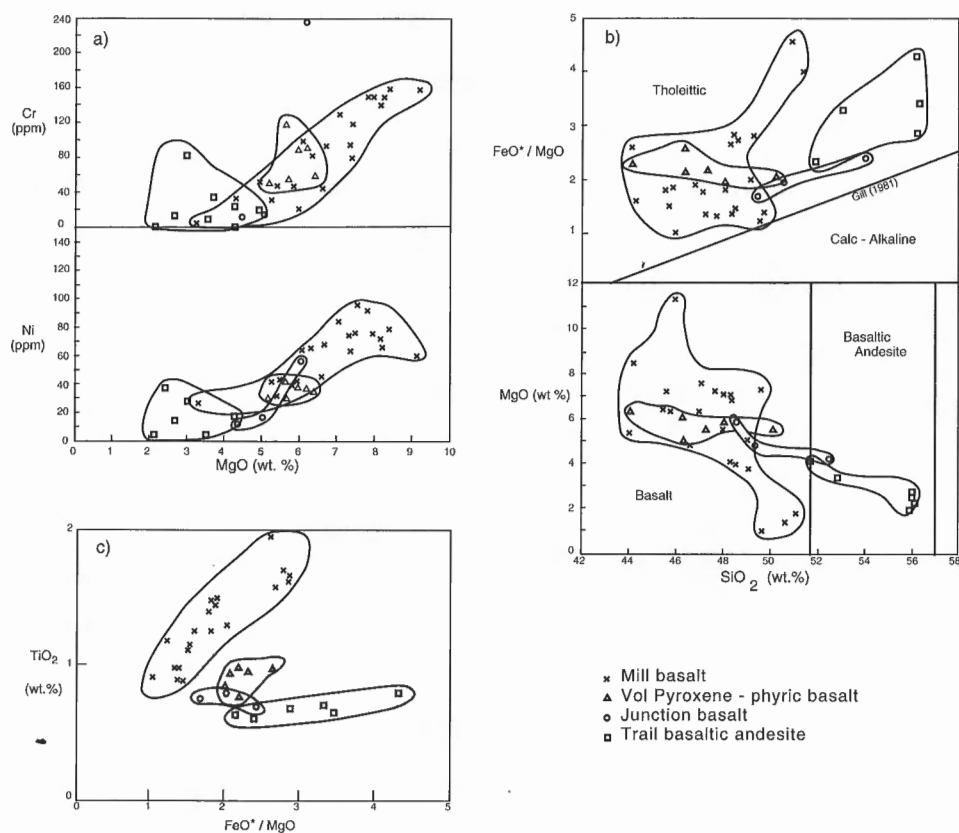
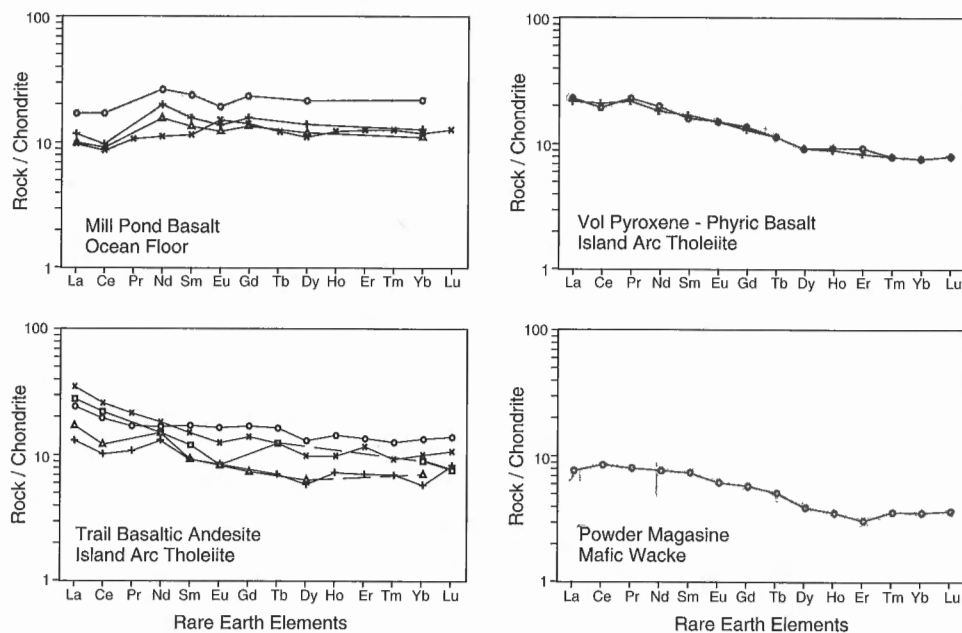


Figure 5.

Major and minor element geochemical characteristics of mafic volcanic rocks in study area. **a)** Cr and Ni vs. MgO plot for four mafic volcanic suites within Rusty Lake belt. **b)** FeO*/MgO and MgO vs. SiO₂ classification diagrams for mafic volcanic suites. Boundary between tholeiite and calcalkaline are from Gill (1981) and between basalt and basaltic andesite from LeMaitre (1989). **c)** TiO₂ vs. FeO*/MgO plot of mafic volcanic rocks in study area.

Figure 6.

Chondrite-normalized REE plots for mafic volcanic and mafic wacke strata in the Ruttan study area. Normalizing values are those of Sun and Nesbitt (1978); Pr, Tb and Tm values are from Haskin et al. (1968).



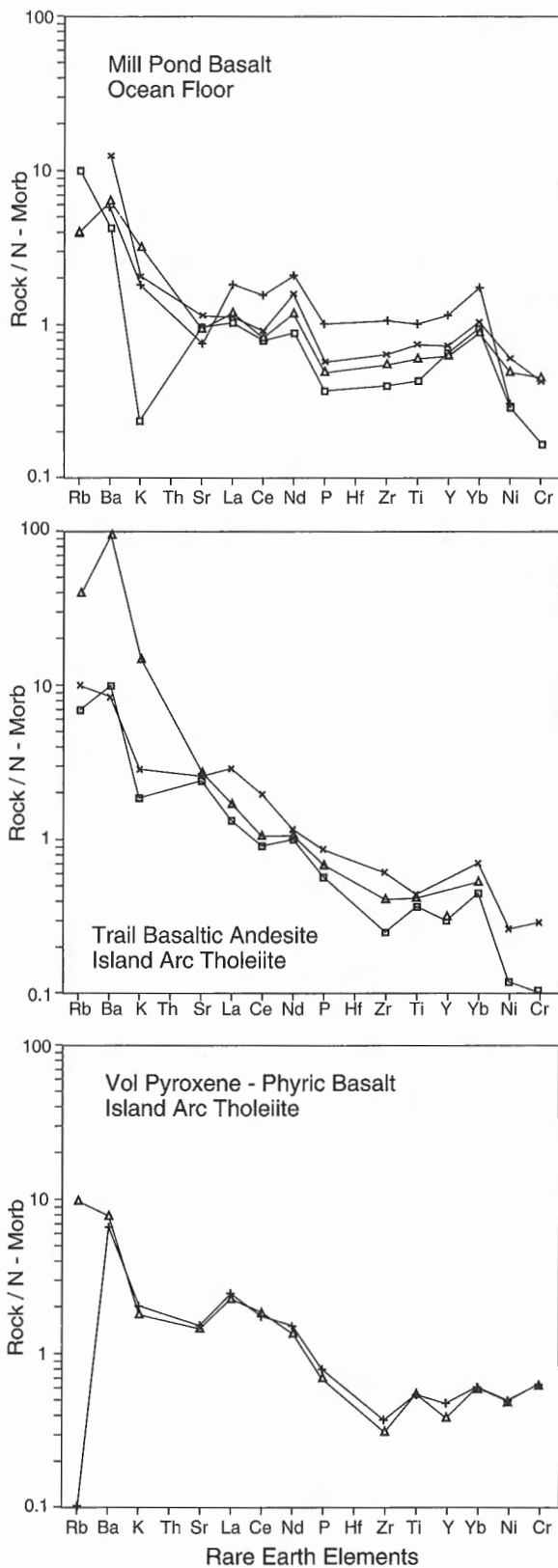


Figure 7. MORB-normalized incompatible element diagrams for mafic volcanic rocks in Ruttan study area. Normalizing values are from Wood et al. (1979) except Sm from Pearce et al. (1984) and Y and Cr from Saunders and Tarney (1984).

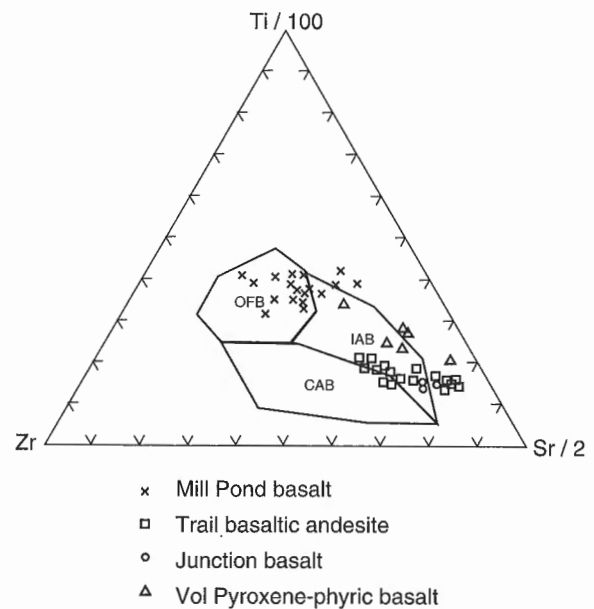


Figure 8. Tectonic-environment discriminant $Zr-Ti/100-Sr/2$ diagram (Pearce and Cann, 1973) for mafic volcanic rocks in Ruttan Study area. CAB – calc-alkaline basalt, OFB – ocean-floor basalt, IAB – island arc basalt.

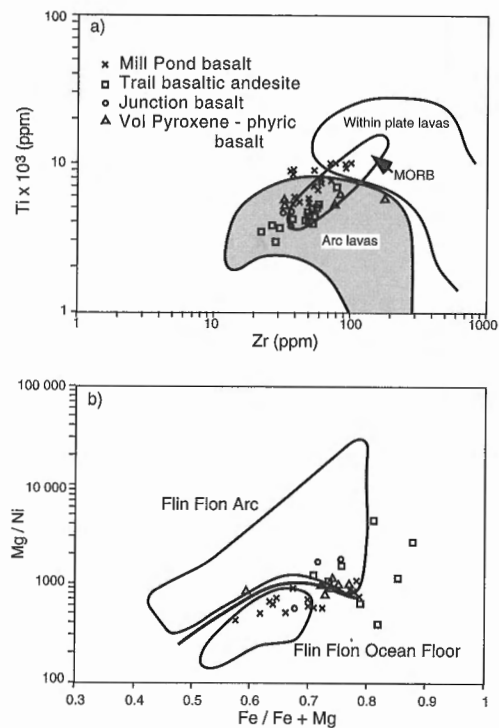


Figure 9. Major element tectonic discriminant diagrams for mafic volcanic rocks in Ruttan study area. **a)** $Ti \times 10^3$ vs. Zr plot with field boundaries from Pearce and Norry (1979). **b)** Mg/Ni vs. $Fe/Fe+Mg$ plot with Flin Flon Arc and Ocean Floor fields from Syme and Bailes (1993).

enrichment in LREEs and fairly flat HREE at a concentration of 10X chondrite (Fig. 6). N-MORB normalized trace element patterns for the Trail basaltic andesite are steep with a negative slope on the large ion lithophile elements (K, Rb, Ba Th, Sr) and a positive slope for the high field strength elements (Ti, Zr, Y) similar to subduction related magmas (Gill, 1981) (Fig. 7). On tectonic discriminant diagrams (Fig. 8, 9) these lavas plot in the island arc basalt field.

Vol formation

The Vol formation, pyroxene-phyric basalt outcrops between the ocean floor Mill Pond basalts and the arc tholeiitic Trail basaltic andesite (Fig. 2) and geochemically has similarities with both basalt types. The SiO_2 content is low (44-51 wt. %) and MgO ranges from 5.2-6.4 wt. % but can be distinguished based on TiO_2 vs. FeO^*/MgO (Table 1; Fig. 5) and Ni and Cr are in greater abundance than in the Trail basaltic andesite (Fig. 5). The REE profile shows a slight LREE enrichment and a gentle slope, with concentrations greater than 10X

chondrite (Fig. 6). Relative to MORB the large ion lithophile elements are enriched and the high field strength elements depleted (Fig. 7). The chemical affinity is more similar to the island arc assemblage represented by the Trail basaltic andesite (Fig. 8, 9).

Powder Magazine formation

Finely bedded mafic wackes produced by mass wasting in the immediate hangingwall of the Ruttan mine have a LREE-enriched chondrite-normalized signature similar to the arc tholeiite suites, although the total abundance of rare earth elements is less (Fig. 6).

PLUTONIC GEOCHEMISTRY

Preliminary major, trace, and REE data on the plutons in the Ruttan Cu-Zn mine area show a number of significant features (Fig. 10-12; Table 3). From major element and normative

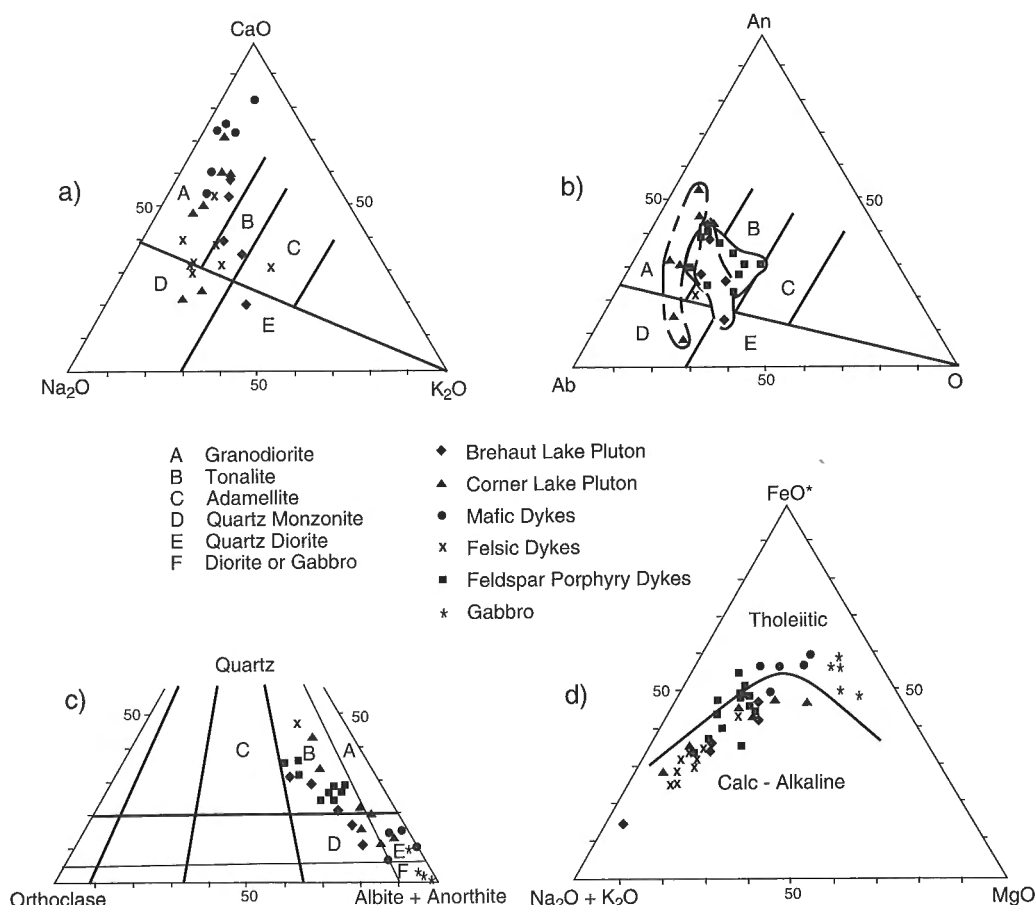


Figure 10. Major element and normative diagrams for plutonic rocks in Ruttan study area. **a)** CaO-Na₂O-K₂O plot with field boundaries from Glickson (1980). **b)** CIPW normative albite (Ab)-anorthite (An)-orthoclase (O) diagram after O'Connor (1965). **c)** Normative quartz-orthoclase-albite+anorthite diagram after Strekeisen (1973). **d)** AFM diagram after Irvine and Baragar (1971).

mineral diagrams (Fig. 10) the major rock types identified in the Corner Lake pluton lie dominantly within the tonalite and granodiorite fields with a trend toward the quartz monzonite and quartz diorite fields. The Brehaut Lake pluton phases plot in the tonalite, granodiorite, and granite fields. The plutons are sodic, with sodic to potassic ratios ranging from 1.1-1.9 and 2.3-4.5 for the Brehaut Lake pluton and Corner Lake pluton, respectively. Silica values for the former range from 56.8-73.1 wt. % and average 64.4% and for the latter from 55.5-74.3 wt. % and average 62.8% (Table 3).

Granodioritic compositions are displayed by intermediate feldspar-phyric dykes and sills, a quartz-feldspar porphyry dyke near the headframe crosscuts older quartz dioritic dykes (Fig. 10). Most intrusions belong to a calc-alkaline suite as displayed on the AFM diagram excluding the gabbroic dykes that intrude the Mill Pond ocean floor basalts and quartz diorite dykes (Fig 10).

Chondrite normalized rare earth element diagrams for the Corner Lake and Brehaut Lake plutons show similar abundances of REEs, a lack of an Eu anomaly and similar patterns

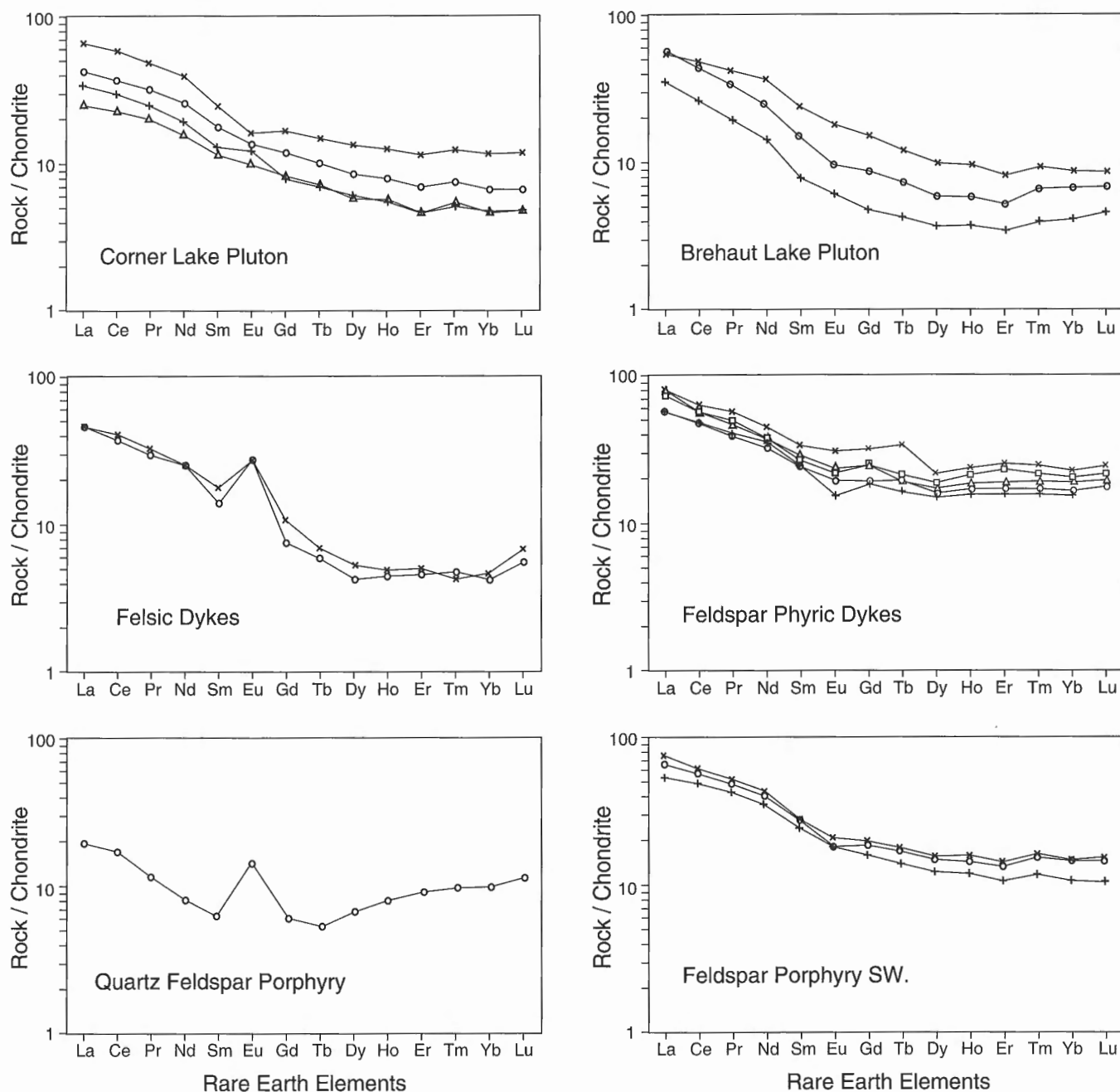


Figure 11. Chondrite-normalized REE patterns for plutons and dykes in Ruttan study area. Normalizing values are those of Sun and Nesbitt (1978); Pr, Tb and Tm values are from Haskin et al. (1968).

Table 3. Pluton geochemistry.

| Rock Sample | Brehaut Lake Pluton | | | | | Corner Lake Pluton | | | | | | |
|----------------------------------|---------------------|---------------|---------------|---------------|---------------|--------------------|---------------|---------------|---------------|---------------|---------------|---------------|
| | BLGD 91AV-552 | BLGD 91AV-553 | BLGD 91AV-555 | BLGD 91AV-556 | BLGT 91AV-551 | CLDI 91AV-527 | CLDI 91AV-528 | CLDI 91AV-530 | CLGD 91AV-523 | CLGT 91AV-526 | CLGD 91AV-529 | CLGT 91AV-524 |
| Location | 727 | 730 | 732 | 733 | 725 | 669 | 670 | 672 | 664 | 667 | 671 | 665 |
| Domain | | | | | | | | | | | | |
| SiO ₂ | 67.6 | 64.5 | 59.9 | 56.8 | 73.1 | 57.4 | 55.5 | 56.7 | 62.1 | 74.3 | 61.3 | 72.2 |
| TiO ₂ | 0.35 | 0.47 | 0.62 | 0.52 | 0.14 | 0.58 | 0.65 | 0.77 | 0.9 | 0.3 | 0.98 | 0.45 |
| Al ₂ O ₃ | 15.4 | 16.7 | 16.9 | 18.4 | 15 | 19.6 | 17.5 | 16.7 | 15.8 | 12.6 | 17 | 13.9 |
| Fe ₂ O ₃ T | 5 | 4.8 | 6.9 | 7.9 | 1.5 | 6.2 | 8.6 | 8.2 | 7.1 | 2.9 | 7.2 | 4.3 |
| Fe ₂ O ₃ | 1.8 | 1.4 | 2.2 | 2.8 | 0.4 | 1.2 | 2.5 | 2.5 | 2 | 0.7 | 3.1 | 1.3 |
| FeO | 2.9 | 3.1 | 4.2 | 4.6 | 1 | 4.5 | 5.5 | 5.1 | 4.6 | 2 | 3.7 | 2.7 |
| MnO | 0.09 | 0.08 | 0.12 | 0.17 | 0.03 | 0.09 | 0.13 | 0.14 | 0.12 | 0.04 | 0.12 | 0.07 |
| MgO | 1.56 | 1.8 | 2.84 | 2.86 | 0.29 | 2.72 | 4.7 | 3.26 | 2.15 | 0.6 | 1.44 | 0.7 |
| CaO | 3.52 | 4.31 | 6.08 | 7.48 | 2.03 | 7.76 | 9.03 | 6.9 | 5.65 | 1.71 | 5.17 | 2.22 |
| Na ₂ O | 3.4 | 4.1 | 3.5 | 3.5 | 4 | 3.7 | 2.9 | 3.1 | 4.2 | 4.4 | 4.6 | 4.4 |
| K ₂ O | 2.74 | 2.25 | 1.8 | 1.8 | 3.53 | 1.19 | 0.65 | 1.54 | 1.25 | 1.48 | 1.03 | 1.92 |
| H ₂ O ^T | 0.8 | 0.9 | 1.2 | 1.3 | 0.3 | 0.9 | 1.2 | 1.1 | 0.6 | 0.7 | 0.9 | 0.5 |
| CO ₂ T | | 0.2 | | | 0.1 | 0.4 | 0.2 | 0.3 | 0.2 | 0.6 | 0.2 | 0.2 |
| P ₂ O ₅ | 0.13 | 0.18 | 0.24 | 0.25 | 0.05 | 0.19 | 0.17 | 0.24 | 0.28 | 0.05 | 0.23 | 0.11 |
| S | 0.01 | 0.01 | 0.08 | 0.05 | 0.01 | 0.01 | 0.01 | 0.01 | 0.01 | 0.06 | 0.03 | 0.01 |
| Ba | 630 | 640 | 550 | 520 | 960 | 410 | 200 | 360 | 410 | 390 | 400 | 800 |
| Au | | | | | | | | | | | | |
| Hg | | | | | | | | | | | | |
| Ag | 1 | 1 | 1 | 1 | 1 | 1 | 1 | 2 | 3 | 1 | 1 | 1 |
| Be | 1 | 1.2 | 0.9 | 0.9 | 0.9 | 0.6 | 0.5 | 0.7 | 1.3 | 1.4 | 0.9 | 1.4 |
| Co | 13 | 15 | 23 | 19 | 3 | 22 | 32 | 27 | 19 | 7 | 13 | 8 |
| Cr | 5 | 13 | 18 | 5 | 5 | 30 | 26 | 26 | 16 | 5 | 5 | 5 |
| Cu | 13 | 18 | 20 | 18 | 5 | 13 | 40 | 19 | 24 | 38 | 21 | 5 |
| As | | | | | | | | | | | | |
| La | 13 | 15 | 15 | 14 | 10 | 5 | 5 | 13 | 22 | 23 | 11 | 21 |
| Nb | 5 | 5 | 5 | 5 | 5 | 5 | 5 | 5 | 5 | 5 | 5 | 5 |
| Ni | 5 | 10 | 13 | 5 | 5 | 30 | 58 | 25 | 12 | 5 | 5 | 5 |
| Pb | 22 | 24 | 10 | 10 | 28 | 10 | 10 | 28 | 21 | 10 | 26 | 20 |
| Rb | 57 | 56 | 35 | 42 | 58 | 20 | 10 | 37 | 21 | 20 | 25 | 31 |
| Sc | 7.1 | 7.7 | 13 | 14 | 1.6 | 13 | 21 | 19 | 17 | 7.2 | 17 | 8.2 |
| Sr | 330 | 780 | 740 | 740 | 410 | 640 | 500 | 530 | 450 | 300 | 580 | 350 |
| V | 36 | 46 | 96 | 81 | 3 | 73 | 150 | 110 | 52 | 3 | 20 | 5 |
| Y | 10 | 12 | 15 | 16 | 7 | 9 | 9 | 14 | 25 | 21 | 15 | 23 |
| Yb | 1.2 | 1.2 | 1.4 | 1.6 | 0.8 | 0.9 | 0.7 | 1.3 | 2.3 | 2.4 | 1.3 | 2.4 |
| Zn | 70 | 77 | 110 | 120 | 39 | 110 | 120 | 110 | 91 | 54 | 96 | 81 |
| Zr | 94 | 130 | 99 | 67 | 78 | 37 | 67 | 110 | 150 | 270 | 91 | 230 |

| Rock Sample | Diorite sills and dykes | | | | Mafic and felsic dykes | | | | | | | |
|----------------------------------|-------------------------|---------------|---------------|---------------|------------------------|---------------|---------------|---------------|---------------|---------------|------------------|------------------|
| | DIOR 91AV-443 | DIOR 91AV-535 | DIOR 91AV-585 | DIOR 91AV-589 | DYKE 91AV-392 | DYKE 91AV-422 | DYKE 91AV-431 | DYKE 91AV-459 | DYKE 91AV-546 | DYKE 91AV-565 | DYKE-MF 91AV-587 | DYKE-F 90AV-359A |
| Location | 1102 | 676 | 826 | DET | 380 | PM | LSFW | 1125 | 718 | 750 | DETAIL | 575 |
| Domain | SW | | | | | | SW | | | | | |
| SiO ₂ | 51.8 | 50.5 | 54 | 55.1 | 48.8 | 78.8 | 66.5 | 69.3 | 60.9 | 66.8 | 53 | 67.1 |
| TiO ₂ | 0.89 | 0.74 | 0.68 | 0.57 | 0.93 | 0.23 | 0.28 | 0.26 | 0.51 | 0.33 | 0.47 | 0.29 |
| Al ₂ O ₃ | 18.8 | 19.9 | 16.7 | 16.5 | 11.8 | 11.3 | 16.9 | 16 | 17.5 | 15.2 | 19 | 17.1 |
| Fe ₂ O ₃ T | 10.6 | 10.3 | 10.5 | 11.9 | 12.7 | 2.4 | 3.6 | 2.8 | 6.4 | 5.9 | 11.1 | 3.1 |
| Fe ₂ O ₃ | 3.2 | 2 | 1.9 | 2.5 | 2.1 | 0.6 | 0.5 | 0.5 | 1.6 | 1.2 | 2.3 | 0 |
| FeO | 6.7 | 7.5 | 7.7 | 8.5 | 9.5 | 1.6 | | 2.1 | 4.3 | 4.2 | 7.9 | 2.9 |
| MnO | 0.16 | 0.13 | 0.21 | 0.2 | 0.25 | 0.04 | 0.02 | 0.03 | 0.07 | 0.09 | 0.23 | 0.05 |
| MgO | 3.26 | 3.59 | 4.06 | 4.17 | 11.5 | 0.81 | 0.86 | 0.85 | 2.12 | 0.72 | 2.51 | 1.09 |
| CaO | 10.2 | 6.66 | 8.97 | 8.44 | 10.6 | 1.8 | 3.92 | 2.75 | 6.32 | 2.66 | 8.17 | 3.28 |
| Na ₂ O | 2.6 | 4.3 | 2.4 | 2.7 | 1 | 1.7 | 4.7 | 3.9 | 3.8 | 4.6 | 4.1 | 5 |
| K ₂ O | 1.2 | 1.24 | 0.58 | 0.2 | 1.1 | 2.17 | 1.05 | 2.86 | 1.51 | 1.57 | 0.9 | 1.66 |
| H ₂ O ^T | 1.3 | 1.9 | 1.3 | 1 | 2.4 | 0.9 | 0.9 | 0.8 | 0.8 | 0.8 | 1 | 1 |
| CO ₂ T | 0.1 | 0.2 | 0.1 | 0.1 | 0.3 | 0.1 | 0.5 | 0.2 | 0.2 | 0.3 | 0.1 | 0 |
| P ₂ O ₅ | 0.17 | 0.22 | 0.15 | 0.09 | 0.23 | 0.03 | 0.12 | 0.1 | 0.23 | 0.07 | 0.32 | 0.13 |
| S | 0.02 | 0.11 | 0.1 | 0.02 | 0.04 | 0 | 0.56 | 0.05 | 0.72 | 0.05 | 0.04 | 0.41 |
| Ba | 430 | 270 | 180 | 40 | 130 | 370 | 960 | 1100 | 650 | 420 | 320 | 1100 |
| Au | | | | 2.5 | | 1 | | | | | | |
| Hg | | | | 1 | | 1 | 13 | 1 | 1 | 1 | 1 | 1 |
| Ag | 1 | 1 | 1 | 0.3 | 0.3 | 0.3 | 1.6 | 1.1 | 1.1 | 0.8 | 2.3 | 1.8 |
| Be | 0.7 | 1.4 | 0.5 | | | | | | | | | |
| Co | 26 | 29 | 26 | 35 | 53 | 5 | 11 | 6 | 19 | 6 | 24 | 7 |
| Cr | 23 | 24 | 33 | 5 | 680 | 5 | 5 | 5 | 11 | 5 | 5 | 5 |
| Cu | 36 | 830 | 36 | 180 | 5 | 31 | 55 | 26 | 510 | 28 | 19 | 45 |
| As | | | | | | 10.83 | | | | | | |
| La | 5 | 5 | 5 | 5 | 10 | 17 | 5 | 5 | 22 | 15 | 5 | 11 |
| Nb | 5 | 5 | 5 | 5 | 5 | 0 | 5 | 5 | 5 | 5 | 5 | 0 |
| Ni | 18 | 27 | 20 | 17 | 200 | 5 | 5 | 5 | 5 | 5 | 5 | 5 |
| Pb | 10 | 21 | 29 | 26 | 10 | 10 | 10 | 10 | 23 | 10 | 32 | 10 |
| Rb | 24 | 21 | 10 | 10 | 28 | 58 | 26 | 33 | 38 | 37 | 12 | 30 |
| Sc | 27 | 19 | 31 | 38 | 26 | 5.9 | 4 | 3.4 | 11 | 10 | 8.4 | NA |
| Sr | 410 | 640 | 340 | 320 | 140 | 150 | 1500 | 980 | 690 | 220 | 580 | 1100 |
| V | 300 | 160 | 170 | 300 | 160 | 6 | 19 | 17 | 59 | 3 | 76 | 31 |
| Y | 16 | 14 | 16 | 9 | 16 | 26 | 9 | 6 | 17 | 26 | 15 | 8 |
| Yb | 1.4 | 1.3 | 1.6 | 0.7 | 1.2 | 3.4 | 0.8 | 0.3 | 1.7 | 3.8 | 1.6 | 0.8 |
| Zn | 93 | 88 | 110 | 110 | 150 | 57 | 36 | 64 | 60 | 65 | 120 | 58 |
| Zr | 41 | 10 | 47 | 20 | 87 | 140 | 160 | 94 | 160 | 63 | 49 | 130 |

| | Mafic and felsic dykes (cont.) | | Feldspar-phyric sills and dykes | | | | | | | | | |
|----------------------------------|-----------------------------------|---------------------|---------------------------------|-------------------|-------------------|-------------------|-------------------|-------------------|-------------------|--------------------|-------------------|-------------------|
| Rock Sample | DYKE-F 90AV-359B | DYKEFW 90AV-331A | FPOBP 90AV-167 | FPOBP 90AV-168 | FPOBP 90AV-169 | FPOBP 90AV-201 | FPOBP 90AV-202 | FPOBP 90AV-204 | FPOBP 90AV-224 | FPOBP 90AV-300A | FPOBP 90AV-368 | FPOBP 91AV-598 |
| Location | 575 | NDETAIL | R83-23 | R83-23 | R83-23 | 83 | 84 | 85 | 91 | PM160 | DATE | 1301 |
| Domain | | | | | | | | | | | | SW |
| SiO ₂ | 66.5 | 67.7 | 62.9 | 63.3 | 62 | 63.1 | 64.7 | 64 | 62.9 | 62.3 | 63.8 | 66.1 |
| TiO ₂ | 0.29 | 0.31 | 0.65 | 0.63 | 0.63 | 0.62 | 0.59 | 0.61 | 0.6 | 0.61 | 0.63 | 0.57 |
| Al ₂ O ₃ | 17 | 17.1 | 15.6 | 15.4 | 15.9 | 16 | 16.2 | 15.9 | 16.1 | 16 | 15.6 | 15.6 |
| Fe ₂ O ₃ T | 3.3 | 3.3 | 8.4 | 7.8 | 8.1 | 7.9 | 6.8 | 7.5 | 7.7 | 8.2 | 7.5 | 5.2 |
| Fe ₂ O ₃ | 0 | 1.1 | 2.2 | 2.8 | 2.5 | 2.2 | 1.9 | 1.9 | 2.4 | 2.1 | 2.2 | |
| FeO | 3.1 | 2 | 5.6 | 4.5 | 5 | 5.1 | 4.4 | 5 | 4.8 | 5.5 | 4.8 | |
| MnO | 0.04 | 0.05 | 0.09 | 0.08 | 0.08 | 0.11 | 0.09 | 0.12 | 0.12 | 0.09 | 0.11 | 0.08 |
| MgO | 1.04 | 1.13 | 2.41 | 2.45 | 1.25 | 1.83 | 1.88 | 2.07 | 1.7 | 2.51 | 1.91 | 0.71 |
| CaO | 3.3 | 3.65 | 4.49 | 4.15 | 6.7 | 3.64 | 4.08 | 3.68 | 5.66 | 4.7 | 5.16 | 4.23 |
| Na ₂ O | 5.1 | 4.6 | 3 | 3.2 | 3.2 | 3.8 | 3 | 3.5 | 3.2 | 3.2 | 3.1 | 3.8 |
| K ₂ O | 1.57 | 1.11 | 2.39 | 2.15 | 1.58 | 2.17 | 2.52 | 2.27 | 1.54 | 2.1 | 1.9 | 1.33 |
| H ₂ OT | 1.2 | 1 | 1.3 | 1.5 | 1.1 | 1.2 | 1.2 | 1.3 | 1.1 | 1.3 | 1 | |
| CO ₂ T | 0.3 | 0.3 | 0.1 | 0.1 | 0 | 0.2 | 0.1 | 0.1 | 0.1 | 0 | 0.1 | 0.1 |
| P ₂ O ₅ | 0.12 | 0.13 | 0.18 | 0.17 | 0.17 | 0.15 | 0.15 | 0.15 | 0.15 | 0.16 | 0.16 | 0.22 |
| S | 0.47 | 0.1 | 0.04 | 0 | 0.15 | 0.03 | 0.01 | 0.02 | 0 | 0 | 0.01 | 1.46 |
| Ba | 1100 | 1400 | 520 | 410 | 410 | 610 | 600 | 650 | 460 | 450 | 450 | 490 |
| Au | | | | | | | 2.5 | | 6 | | | |
| Hg | | | | | | | 1 | | 1 | | | |
| Ag | 1 | 1 | 1 | 1 | 2 | 1 | 1 | 1 | 1 | 1 | 1 | 1 |
| Be | 1.8 | 1.9 | 1.2 | 1.2 | 1.3 | 1.2 | 1.2 | 1.2 | 1.2 | 1.1 | 0.9 | 0.9 |
| Co | 6 | 5 | 15 | 14 | 13 | 12 | 11 | 12 | 16 | 12 | 13 | 15 |
| Cr | 5 | 5 | 5 | 5 | 5 | 10 | 5 | 10 | 5 | 5 | 5 | 5 |
| Cu | 42 | 34 | 53 | 5 | 42 | 25 | 5 | 5 | 17 | 5 | 12 | 32 |
| As | | | | | | | | | | | | |
| La | 5 | 5 | 14 | 13 | 14 | 18 | 13 | 13 | 13 | 14 | 12 | 16 |
| Nb | 0 | 5 | 11 | 5 | 13 | 5 | 10 | 5 | 12 | 5 | 0 | 5 |
| Ni | 5 | 5 | 5 | 12 | 5 | 5 | 5 | 5 | 5 | 5 | 5 | 5 |
| Pb | 10 | 10 | 10 | 10 | 10 | 10 | 10 | 10 | 10 | 10 | 10 | 10 |
| Rb | 36 | 21 | 50 | 47 | 37 | 42 | 66 | 56 | 32 | 42 | 45 | 10 |
| Sc | NA | NA | NA | NA | NA | NA | NA | NA | NA | NA | 18 | 17 |
| Sr | 1100 | 1400 | 190 | 280 | 180 | 180 | 160 | 220 | 240 | 250 | 230 | 370 |
| V | 31 | 29 | 76 | 71 | 72 | 76 | 73 | 73 | 75 | 72 | 63 | 7 |
| Y | 8 | 7 | 27 | 27 | 29 | 26 | 21 | 28 | 32 | 27 | 25 | 19 |
| Yb | 0.7 | 0.7 | 2.7 | 2.7 | 2.9 | 2.8 | 2.2 | 3.1 | 3.3 | 2.8 | 2.7 | 2 |
| Zn | 56 | 51 | 89 | 89 | 69 | 83 | 72 | 110 | 79 | 77 | 67 | 98 |
| Zr | 130 | 130 | 130 | 130 | 130 | 120 | 130 | 130 | 130 | 120 | 120 | 95 |

| | Feldspar-phyric sills and dykes (cont.) | | | | | | | | Gabbroic bodies | | |
|----------------------------------|---|-------------------|-------------------|-------------------|-------------------|-------------------|--------------------|-------------------|------------------|-------------------|-------------------|
| Rock Sample | FPOBP 91AV-603 | FPOBP 91AV-611 | FPOBP 91AV-613 | FPOBP 91AV-632 | FPOBP 91AV-640 | FPOBP 91AV-641 | FPOBP 90AV-300B | FPOBP 90AV-165 | GABB 91AV-404 | GABB 91AV-568A | GABB 91AV-568B |
| Location | 1331 | 1365 | 1365 | 91-1 | 91-2 | 91-2 | PM160 | R83-23 | 434 | 757 | 757 |
| Domain | SW | SW | SW | SW | SW | SW | | | | | |
| SiO ₂ | 62.8 | 63.5 | 63.9 | 53.5 | 52.9 | 67.7 | 62.4 | 63.9 | 49.3 | 49.8 | 49.6 |
| TiO ₂ | 0.55 | 0.7 | 0.58 | 0.82 | 0.74 | 0.59 | 0.6 | 0.6 | 0.8 | 1.19 | 1.21 |
| Al ₂ O ₃ | 16 | 15.4 | 16.1 | 17.8 | 16.9 | 16.7 | 15.4 | 15.5 | 18.2 | 13.7 | 14.1 |
| Fe ₂ O ₃ T | 8.3 | 8.5 | 7.1 | | | | 8.2 | 7.5 | 10.3 | 13.4 | 13.8 |
| Fe ₂ O ₃ | 3.7 | 2.8 | 2.1 | 9.98 | 10.2 | 2.59 | 2 | 2.2 | 1.5 | 2.2 | 3 |
| FeO | 4.1 | 5.1 | 4.5 | 5.8 | 6.3 | 1.8 | 5.6 | 4.8 | 7.9 | 10.1 | 9.7 |
| MnO | 0.27 | 0.22 | 0.15 | 0.19 | 0.21 | 0.07 | 0.09 | 0.1 | 0.16 | 0.21 | 0.22 |
| MgO | 0.93 | 1.11 | 1.55 | 3.11 | 3.69 | 0.63 | 2.46 | 2.23 | 6.71 | 6.62 | 7.01 |
| CaO | 6.4 | 5.84 | 5.38 | 9.36 | 8.73 | 4.45 | 4.89 | 4.9 | 11.8 | 11.6 | 11.6 |
| Na ₂ O | 2.7 | 1.8 | 3.3 | 2.96 | 2.88 | 4.14 | 3 | 3.1 | 2.4 | 1.7 | 2 |
| K ₂ O | 1.58 | 1.28 | 1.43 | 1.52 | 1.49 | 2.14 | 2.05 | 1.8 | 0.29 | 0.14 | 0.13 |
| H ₂ OT | 0.8 | 0.8 | 0.8 | 0.6 | 1.2 | 0.5 | 1.3 | 1.2 | 1.2 | 1.3 | 1.2 |
| CO ₂ T | 0.1 | 0.1 | 0.1 | 0.02 | 0.5 | 0.07 | 0.2 | 0.1 | 0.1 | 0.3 | 0.1 |
| P ₂ O ₅ | 0.22 | 0.2 | 0.23 | 0.21 | 0.18 | 0.23 | 0.15 | 0.16 | 0.08 | 0.08 | 0.09 |
| S | 0.05 | 0.06 | 0.07 | 0.19 | 0.08 | 0.05 | 0 | 0 | 0.06 | 0.01 | 0.01 |
| Ba | 430 | 480 | 510 | 743 | 342 | 854 | 440 | 450 | 40 | 15 | 50 |
| Au | | | | | | | | | | | |
| Hg | 6 | | | | | | | | | | |
| Ag | 1 | 1 | 1 | 0.25 | 0.5 | 0.25 | 1 | 1 | 1 | 9 | 1 |
| Be | 0.8 | 0.9 | 0.9 | NA | NA | NA | 1 | 1.1 | 0.3 | 0.3 | 0.3 |
| Co | 38 | 11 | 12 | 26 | 23 | 9 | 13 | 13 | 41 | 51 | 53 |
| Cr | 38 | 5 | 5 | 20 | 44 | 8 | 5 | 15 | 85 | 16 | 14 |
| Cu | 27 | 13 | 13 | 80.5 | 79 | 14.8 | 5 | 5 | 42 | 47 | 18 |
| As | | | | | | | | | | | |
| La | 12 | 18 | 21 | NA | NA | NA | 11 | 14 | 5 | 5 | 5 |
| Nb | 5 | 5 | 5 | 17 | 5 | 22 | 5 | 5 | 5 | 5 | 5 |
| Ni | 13 | 5 | 5 | 23 | 24 | 7 | 5 | 11 | 65 | 37 | 38 |
| Pb | 10 | 10 | 10 | 9 | 3 | 9 | 10 | 10 | 10 | 23 | 23 |
| Rb | 26 | 33 | 26 | 29 | 41 | 38 | 44 | 42 | 10 | 10 | 10 |
| Sc | 45 | 23 | 22 | NA | NA | NA | NA | NA | 33 | 41 | 45 |
| Sr | 310 | 230 | 300 | 440 | 375 | 378 | 230 | 210 | 230 | 160 | 160 |
| V | 150 | 6 | 6 | | | | 73 | 73 | 200 | 300 | 310 |
| Y | 22 | 25 | 26 | 18 | 27 | 42 | 24 | 26 | 10 | 20 | 21 |
| Yb | 2.9 | 2.6 | 2.7 | NA | NA | NA | 2.7 | 2.8 | 0.8 | 2 | 2.1 |
| Zn | 170 | 130 | 150 | 152 | 158 | 100 | 75 | 63 | 88 | 110 | 100 |
| Zr | 100 | 83 | 100 | 64 | 50 | 115 | 120 | 120 | 41 | 39 | 53 |

with moderately light rare earth enriched profiles with high field strength element depletion (Fig. 11). One significant difference is that the most felsic phase in the Brehaut Lake pluton is REE-depleted relative to the mafic components, whereas the opposite is shown by the most felsic phase in the Corner Lake pluton. Patterns are broadly similar between the mafic and felsic phases within each pluton, with a slight negative Eu anomaly in the Corner Lake pluton whose pattern can be related to fractional crystallization.

Chondrite normalized REE plots of feldspar-phyric dykes and sills northeast of the mine, at the mine site, and southwest of the mine all lie within a very tight field, with moderately sloping LREE-enriched profiles and a weak negative Eu

anomaly (Fig. 11). Felsic feldspar porphyritic dykes that intrude the Ruttan extension bedded felsic tuff, hornblende basalt, microcline altered felsic rocks and diorite dykes have a more pronounced negative slope and positive Eu anomaly. The quartz-feldspar porphyry in greater contrast has a bowed concave REE chondrite normalized profile with a positive Eu anomaly (Fig. 11).

Trace element geochemistry, combined with REE profiles of the Brehaut Lake and Corner Lake plutons indicate that the major plutons in the Ruttan mine area are volcanic arc granites (Fig. 12). These plutons are metaluminous (lack corundum), sodic, and are classified as medium-K calc-alkaline zoned plutons (Fig. 12). They can be further classified as I-type

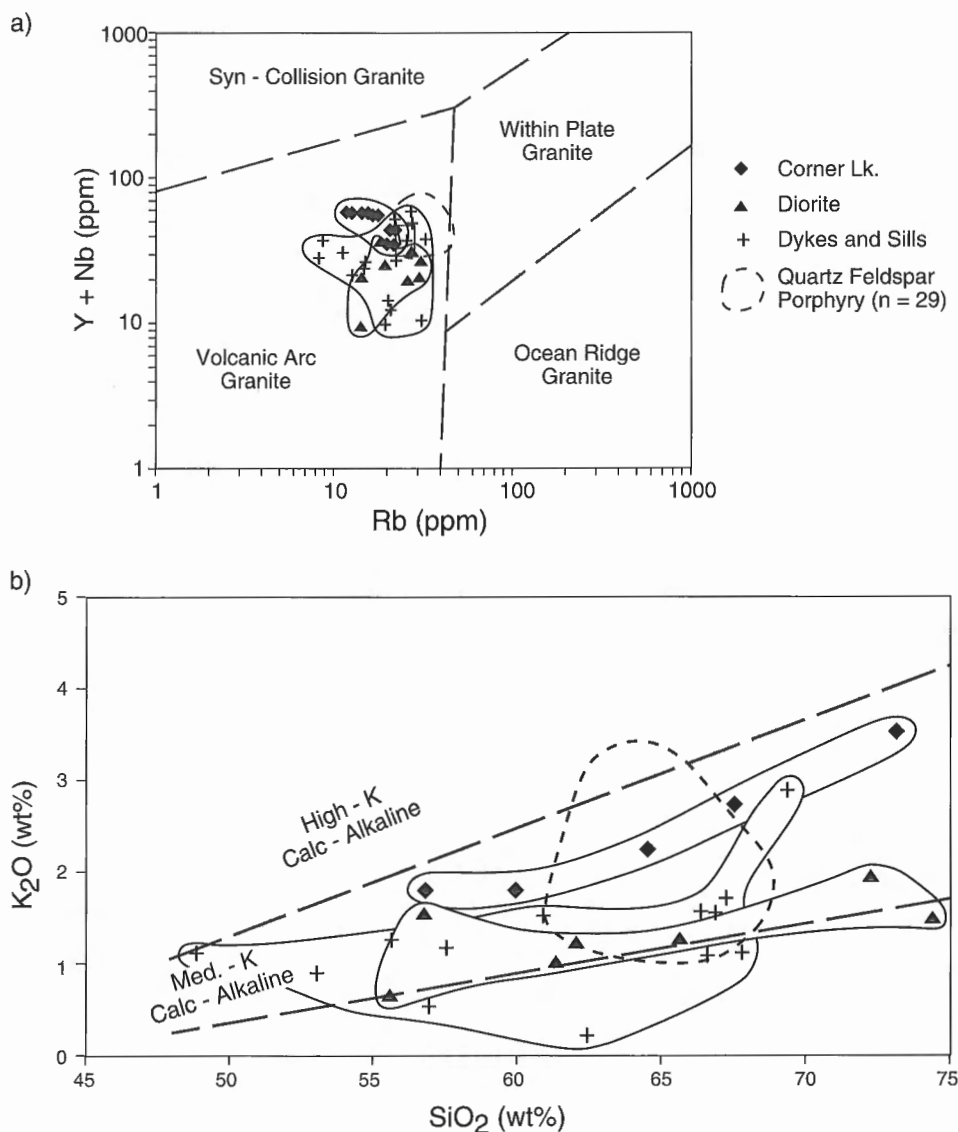


Figure 12. Tectonic-environment discriminant and major element plots for plutonic rocks in Ruttan study area. **a)** Y+Nb vs. Rb diagram after Pearce et al. (1984). **b)** K₂O vs. SiO₂ diagram for calc-alkaline rocks.

granitoids with an infracrustal source, and are probably subduction related with a small crustal component (Chappell and White, 1974; Chappell and Stevens, 1988).

HYDROTHERMAL ALTERATION

Variations in alteration types are categorized by variations in metamorphic mineral assemblages and morphologies (Fig. 2, in pocket). In general, they are divided morphologically into: a) semi-conformable alteration which includes epidote alteration, silica enrichment, amphibole and quartz-microcline alteration, and b) discordant alteration which includes Fe-Mg-sulphide, sericite, and microcline-quartz-sulphide alteration (Plates 2, 3, 4). The semi-conformable alteration is commonly controlled by zones of primary permeability, such as flow tops, or spatially associated with early diorite sills. The discordant alteration is restricted to the footwall stratigraphy in the Ruttan deposit. Dykes are affected by silica enrichment and epidote alteration. The later zoned plutons are unaffected by these alteration types.

Epidote alteration

Semi-conformable quartz-epidote-sulphide alteration occurs in the Mill Pond, Vol, and Trail formations, diorite sills, and is associated with a zone of silica enrichment in the hanging-wall. Epidote is patchy in the Mill Pond formation basalts and commonly concentrated within interpillow areas. Extensive epidote alteration in the Vol formation pyroxene-phyric basalts is ubiquitous and occurs as amoeboid domains up to 30 cm in diameter that comprise 5-15% of the outcrop. In the more massive parts of flows there are abundant laterally extensive, 3 to 5 cm wide epidote ribbons spaced at 10-20 cm that contain relict hornblende porphyroblasts. Minor sulphide occurs along schistosity as irregular sulphide stringers and fine disseminations in these epidote-altered basalts.

Intense epidote-carbonate alteration is present in the easternmost exposures of the Junction formation volcanoclastic rocks, with 40% epidote and 10% carbonate. Epidote alteration occurs in the Powder Magazine formation as open space fillings, particularly at the contact between the lower wacke-dominated and upper breccia-dominated components (Fig. 2). Diorite intrusions are variably epidote altered, containing 15 to 30%, 1 to 2 cm epidote pods.

Silica enrichment

Semi-conformable zones of silica enrichment are situated at various stratigraphic levels and locally are spatially controlled by either dykes and diorite sills or microcline-quartz alteration zones (Plate 2). Along the Mill Pond formation basalt and Vol formation pyroxene-phyric basalt (Fig. 2) contact are intense zones of patchy and fracture-controlled silicification. Fracture-controlled and patchy to pervasive silicification within the Trail formation basaltic andesite and Powder Magazine formation volcanoclastic strata is spatially associated with zones of microcline-quartz alteration (Fig. 3). The

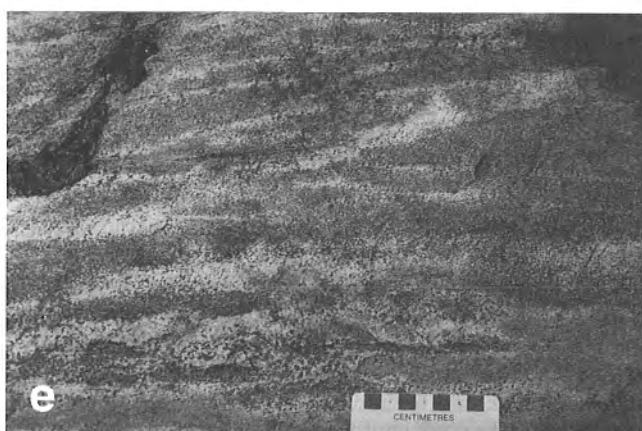
Powder Magazine formation also contains semi-conformable silicification zones along the wacke-breccia contact, the hangingwall contact of the bedded felsic volcanoclastic unit in the Ruttan Extension area and Junction area (Fig. 13), and along the margins of the epidotized diorite sills. Silicification of the hangingwall strata is lacking directly above the ore-bodies in the mine site. Amphibole blastesis is commonly associated with silicified beds in the Powder Magazine formation (Plate 2).

A wedge-shaped semi-conformable zone of silicification occurs along the Mill Pond basalt-Vol pyroxene basalt contact (Fig. 2) within a zone of anomalous high strain. It is texturally and compositionally heterogeneous with two millimetre to centimetre-wide basalt alternating with bleached white silicified bands producing a striped texture (Plate 2), bleached white patches also occur in a basaltic matrix producing a mottled texture. Adjacent to areas of pervasively altered basalt are zones with intense fracture-controlled alteration in massive basalt associated with weak epidote alteration. In the southern exposures are transitions from unaltered basalt through patchy silicified basalt to pervasively altered domains consisting of a white-weathering, bleached, quartz-feldspar-biotite-acicular amphibole-garnet-bearing rock. The silicified zones are dominated by polycrystalline aggregate of quartz and feldspar (40-65%), biotite (20-35%), actinolite (10-15, locally 30%), epidote (0-20%), garnet (2-10%), and trace amounts of titanite, pyrite, chalcopyrite, pyrrhotite, pyrite, magnetite, zircon, and calcite. The northernmost exposures have 10-45% feldspar porphyroblasts with recrystallized outer edges and minor fine grained microcline. Actinolite forms 1.6 mm poikiloblastic grains and fine matrix crystals similar to the 0.1 mm biotite grains. Garnet is up to 0.1 mm in diameter and poikiloblastic with quartz inclusions. Magnetite forms rims on, and partially replaces, pyrite.

Fracture-controlled silicification and patchy silicification of the Trail basaltic andesite produces a whitish-brown-weathering feldspar-bearing rock with 20% fine acicular amphibole needles that texturally is similar in appearance but chemically different to the Junction volcanoclastic rocks (Plate 2). Silicification in the Powder Magazine formation preferentially occurs along bedding planes with local discordant veins. The silicification and amphibole alteration is striped with black, 2-5 cm wide amphibole (60-80%), quartz (10-25%), and garnet (1-15%) bands alternating with bands 10-40 cm wide of bleached orangy, buff grey, sugary textured silicified wacke with minor acicular hornblende and garnet (Plate 2). Amphibole alteration, dominant in the hangingwall strata, occurs as bedding parallel ribbons, fractures oblique to bedding, thin rims on epidote pods, and irregular black clots (Plate 2).

Microcline Alteration

Microcline alteration is present in several localities, principally within the host strata to the Ruttan deposit. It occurs as fine grained disseminations within the silicified rocks along the Mill Pond and Vol formation contact, in the Junction formation volcanoclastic sequence, and as coarser (2-4 mm) grains within the Mine Sequence bedded felsic volcanoclastic



rocks north of the North Wall shear zone near the mine site and at the Ruttan extension. At the Ruttan extension a discontinuous, semiconformable zone of fracture-controlled and locally pervasive quartz-microcline alteration is present in the immediate hangingwall bedded mafic wacke (Plate 2f). The contacts with the surrounding stratigraphy are sharp, yet irregular, alteration fronts (Plate 3).

The most pervasive zone of microcline alteration occurs in the discordant rhyolite body that transects the Trail formation directly under the Mine Sequence in the Ruttan extension area (Fig. 2, 3). This spectacular, disconformable 425 m by 100 m rhyolite plug has extensive microcline-sericite-quartz alteration. Although the microcline-quartz alteration zone itself is not auriferous it contains an arsenopyrite-gold vein

(Au:Ag, 4:1). The pervasive alteration is characterized as orthogonal microcline veins and quartz stockwork with amoeboid microcline patches (Fig. 2, 4; Plate 3). The 2 cm wide orthogonal extensional veins weather in relief, contain 50-60%, 2 mm microcline porphyroblasts, and comprise 70% of the outcrop in the southern half of the main zone. The stockwork type is found dominantly in the northern half of the zone and contains a fine latticework of quartz-filled fractures (Plate 3). It is generally microcline poor with 5% amoeboid irregular microcline patches, contains minor garnet, magnetite and sulphide, and 10-15%, 2-4 cm vugs partially filled with coarse sericite (Fig. 3).

Garnet-amphibole alteration

The Junction formation dacitic volcanoclastic rocks contain crosscutting sulphide-amphibole fractures with bleached haloes and minor centimetre-sized chlorite-garnet patches and hornblende pods. Microcline-quartz alteration is transected by minor garnet-amphibole veins in the rhyolite plug in the Ruttan extension area. There is a small zone of chlorite schist at the base of the Powder Magazine formation immediately above the microcline-quartz felsic plug. The chlorite schist contains 30% amphibole, 20% garnet, and 10% magnetite. Disseminated garnet-amphibole alteration is also common with zones of silicification in the Powder Magazine formation.

Sericitization

Regionally, substantial sericite alteration is lacking except as coarse grained vug fillings in the microcline-quartz alteration zone. Trace sericite is present in the Junction formation, felsic volcanoclastic rocks. Sericitization occurs on the outer fringe of the ferromagnesian alteration pipe east of the open pit and in the West Anomaly (Ames and Taylor, 1996). Brown cordierite is characteristic of the sericite-rich assemblages in the footwall to the deposit.

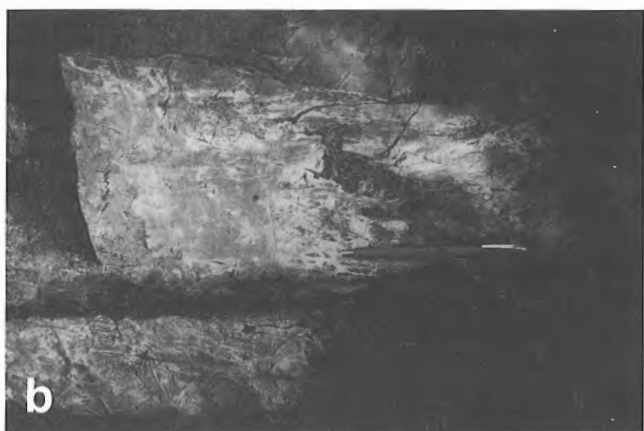
Ruttan Deposit Proximal Alteration

At the Ruttan Cu-Zn deposit there is a diversity of alteration assemblages which includes anthophyllite-garnet-chlorite schists associated with the West Anomaly orebody only, cordierite-chlorite±andalusite-biotite-garnet-staurolite-magnetite, staurolite-biotite-andalusite±chlorite-plagioclase, talc-chlorite-biotite and sericite-gahnite±sphalerite-biotite-galenite bearing schists (Fig. 2; Ames et al., 1990; Ames, 1991; Ames and Scoates, 1992; Ames and Taylor, 1996). Six centimetre euhedral plagioclase crystals were identified in hand specimen from the Ruttan deposit although feldspar alteration is not present in the studied 8.2 Mt West Anomaly orebody and associated Fe-Mg-rich anthophyllite-cordierite alteration zones (Ames and Taylor, 1996). In general, the West Anomaly contains cordierite-anthophyllite rocks and to the east cordierite-chlorite-biotite assemblages dominate. Alteration mineral chemistry, mineral assemblages, geochemistry and mass gains and losses are described for the 8.2 Mt West Anomaly orebody in Ames and Taylor (1996).

Plate 2

Textural and morphological features of silicification in the Ruttan mine area

- a** – Intense patchy silicification of amphibole porphyroblastic basalt. Note discontinuous variably bleached zones. Near contact between the Mill Pond basalt and pyroxene-phyric basalt. Scale card in centimetres. GSC 1995-183I
- b** – Moderate patchy silicification within heterolithological mafic breccia near contact between Mill Pond basalt and pyroxene-phyric basalt. Patchy silicification crosscut by amphibole-filled fracture with 1 cm silicified halo. GSC 1995-183EEE
- c** – Pervasive and fracture controlled silicification of plagioclase-phyric Trail basaltic andesite. Note less altered 1 cm domains in upper left. Immediately overlies a microcline-quartz alteration zone at contact between pyroxene-phyric basalt and Trail basaltic andesite. Pencil magnet is 12.5 cm long. GSC 1995-183R
- d** – Relict less-altered domains of plagioclase-phyric basaltic andesite of Trail formation within pervasively silicified zone. GSC 1995-183U
- e** – Patchy silicification within Junction volcanoclastic rocks. Note amphibole associated with silicification zones. GSC 1995-183F
- f** – Fracture-controlled silicification of hangingwall Powder Magazine mafic wacke immediately above microcline-quartz alteration zone at Ruttan extension. Dominant fracture set at 110° parallel to 12.5 cm pencil magnet is of similar orientation to microcline-quartz veins. GSC 1995-183Y
- g** – Bedding-controlled silicification common in hangingwall Powder Magazine mafic wacke. Note discontinuous beds partially replaced and associated amphibole porphyroblasts in silicified zones. GSC 1995-183L
- h** – Early bedding-controlled silicification deformed by minor Z-shaped folds in Powder Magazine formation. GSC 1995-183D



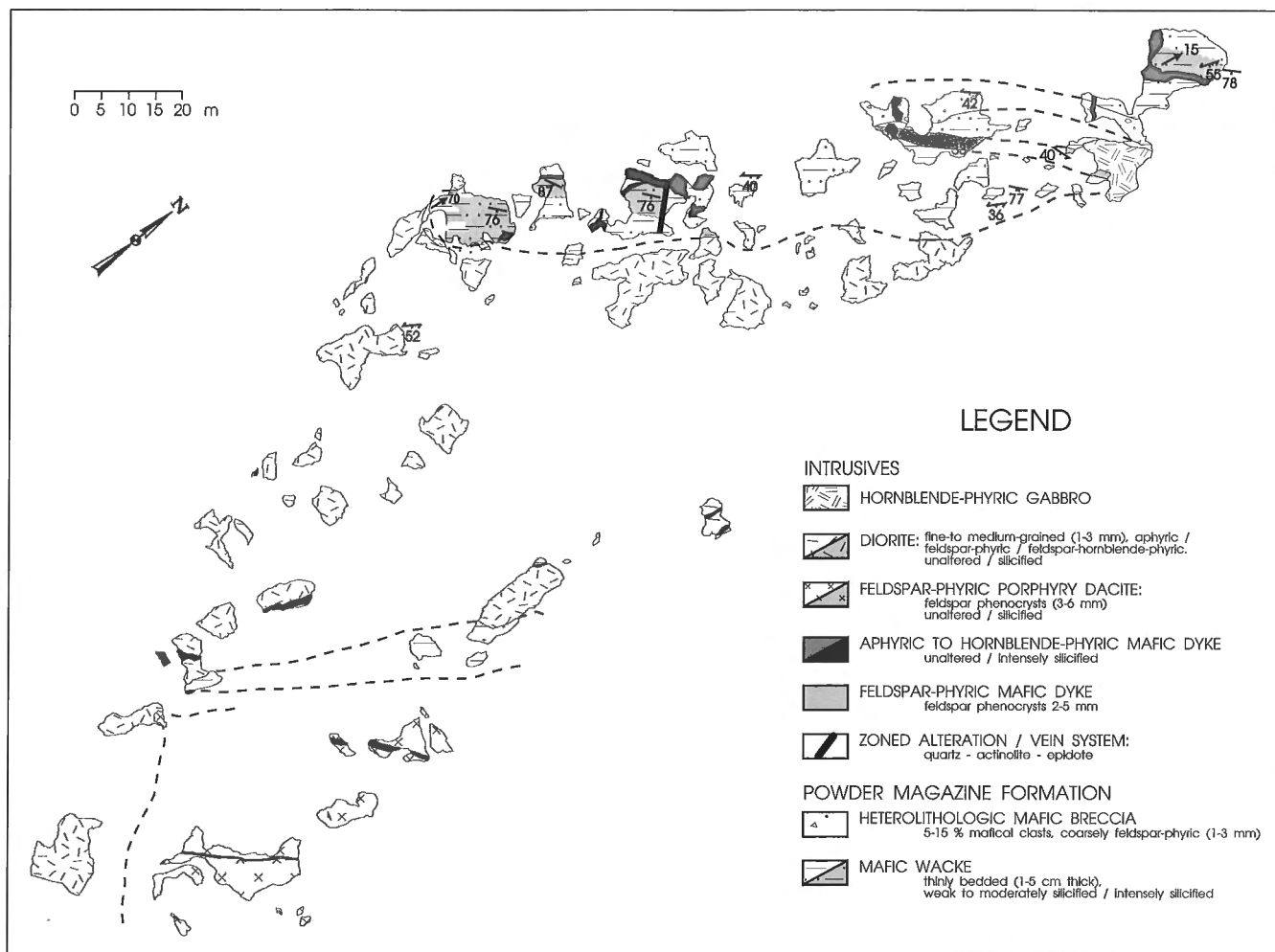


Figure 13. Map of alteration and stratigraphy in hangingwall Powder Magazine formation.

Plate 3

Textural characteristics of quartz-microcline alteration zone at the Ruttan extension

- a** – Diffuse replacement contact between microcline-quartz zone at top of photograph and aphyric andesite at bottom. Eastern contact of microcline-quartz alteration zone, scale card is in centimetres. GSC 1995-183A
- b** – Diffuse replacement contact between microcline alteration zone and Powder Magazine formation mafic wacke. Pencil magnet is 12.5 cm long. GSC 1995-183P
- c** – Intense vein-controlled microcline-quartz alteration. Microcline-quartz veins weather in relief and trend 110°. Canadian quarter for scale. GSC 1995-183N
- d** – Quartz stockwork type alteration in microcline-quartz zone. Note fine delicate lacey texture. Scale card in centimetres. GSC 1995-183S
- e** – Amoeboid patches of white-weathering microcline and vugs partially filled with coarse sericite. GSC 1995-183C
- f** – Deformed quartz veins within pervasive microcline-quartz alteration zone. GSC 1995-183E
- g** – Patchy relict amphibole in pervasive quartz-microcline-garnet-sericite alteration. GSC 1995-183O
- h** – Recessive-weathering discontinuous fractures partially filled with coarse sericite. GSC 1995-183CCC

The complexities of the spatial distribution of the alteration assemblages are shown from drillcore observations at the east side of the open pit (Fig. 2). Staurolite-biotite zones occur in the hangingwall within the upper felsic volcaniclastic rocks and below the chlorite-cordierite, talc or anthophyllite-cordierite zones in the Mine dacite unit. Alternating lensoid alteration zones, each 10-35 m wide, of chlorite-cordierite-biotite-andalusite-quartz-plagioclase schists and staurolite-biotite-andalusite-plagioclase-quartz schists comprise the immediate hangingwall stratigraphy with the southernmost chlorite-cordierite-biotite-andalusite schist enveloping an orebody



Plate 4

Mine proximal alteration zones

- a** – Staurolite-biotite-andalusite-plagioclase-quartz schist above the East Lense, east edge of open pit. GSC 1995-183KK
- b** – Proximal Fe-Mg alteration around the East Lense orebody, east edge of open pit. Chlorite-cordierite-biotite-andalusite schist. Note light cordierite porphyroblasts. GSC 1995-183FF

(Plate 4). At the top of the Mine Sequence are a series of narrow sericite-galena-sphalerite-gahnite zones less than 10 m from the contact between the altered rocks in the hangingwall to the ore and the overlying Powder Magazine mafic wacke.

There are extensive talc zones in the immediate footwall of the West and East lenses. These talc zones envelop, or occur within, the Cu-rich zones and may be situated at the base of stratigraphically higher zinc and copper orebodies. Typically between ore lenses are sericite-bearing schists. Below the East Lenses, talc zones extend 75 m into the footwall and are up to 35 m wide. The chalcopyrite-talc stringer zone is transposed parallel to the orebodies.

SUMMARY AND DISCUSSION

The stratigraphy surrounding the giant Ruttan Cu-Zn deposit records a complex history of tectonism, volcanism and sedimentation, hydrothermal alteration, and plutonism (Fig. 14, 15). The majority of the exposed footwall to the Ruttan deposit is an allochthonous sequence of ocean-floor basalts that has undergone an apparent previous tectonic history prior to accretion with the arc tholeiitic, dominantly felsic volcaniclastic sequence which hosts the Ruttan deposit (Fig. 14). The Mill Pond shear zone juxtaposes rocks with contrasting stratigraphy, geochemistry, and structural history, and may be interpreted as an early accretionary fault. Alternatively, the island arc sequence could have developed on top of an ocean floor sequence with deformation at the contact (Mill Pond shear zone), and contrasting recorded tectonic fabrics explained by differences in rheology. Medium-K calc-alkaline, zoned volcanic arc granitoid plutons in the Ruttan mine area intrude both the footwall and hangingwall stratigraphy. These intrusions are similar to those in the Flin Flon Belt interpreted as being related to successor arcs constructed on top of the Amisk accretionary collage (Lucas et al., in press). The Corner Lake pluton is less potassic than those from the Elbow Lake-Flin Flon Belt batholiths (Fig. 16) and other Precambrian syn-kinematic batholiths in general.

The lack of a subvolcanic pluton below the giant Ruttan base metal deposit is explained by a combination of structural dislocation and a syn-kinematic intrusion in the footwall strata. The Ruttan deposit lies 280 m from the western limit of the Rusty Lake belt defined by a late granitoid that intruded the footwall strata. In addition, the footwall strata have been displaced by a series of shear zones including the North Wall and Mill Pond shear zones and therefore only a small portion of the footwall stratigraphy is preserved. The original footwall to many giant VHMS deposits is truncated by tectonic structures (135 Mt, Kidd Creek deposit, Bleeker and Parrish, in press; 62.4 Mt, Flin Flon deposit, Koo and Mossman, 1975, and Bailes and Syme, 1989). This may be evidence that these large deposits form along or near deep crustal structures that were subsequently reactivated during tectonism.

In spite of the fact that only a small portion of the original footwall strata remains below the deposit some observations can be made with respect to the depositional environment in which the Ruttan deposit formed (Fig. 15). The thickening of the volcaniclastic pile from northeast to southwest below the

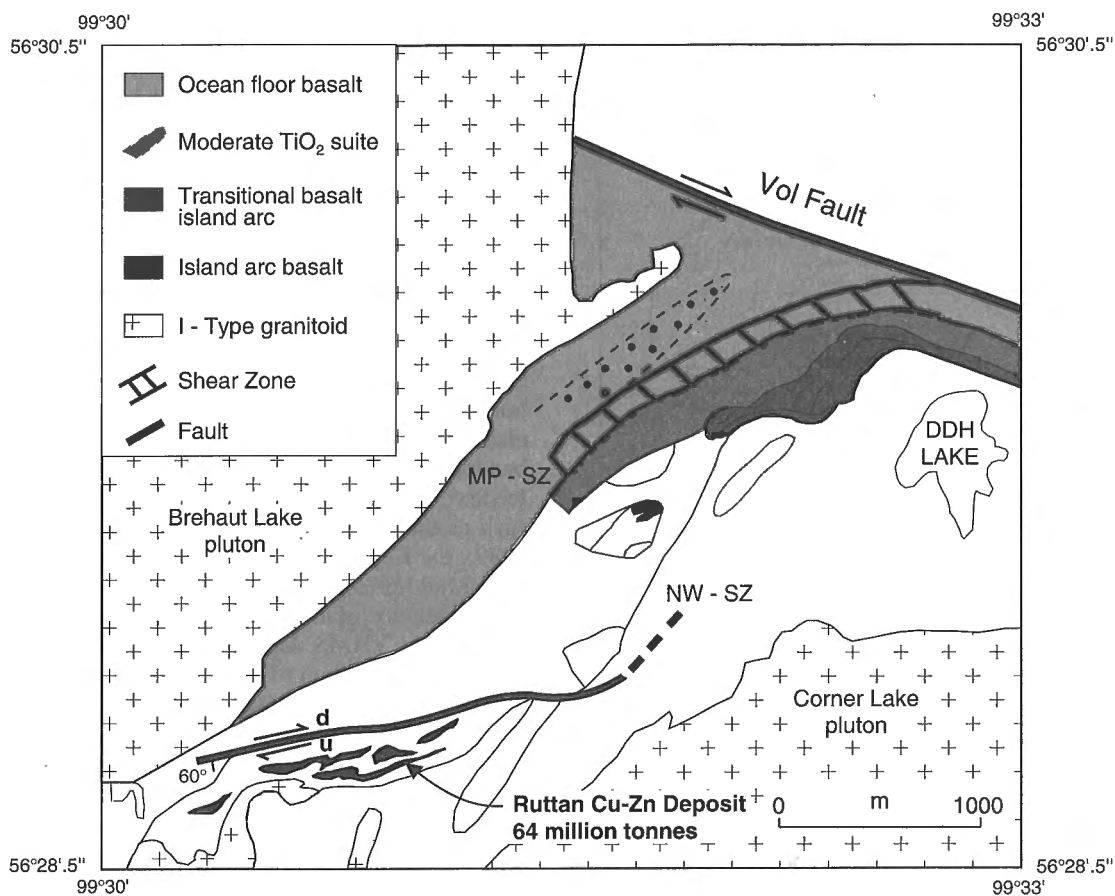


Figure 14. Map summarizing the main tectonic-environment and structural features in Ruttan study area. MP-SZ, Mill Pond shear zone; NW-SZ, North Wall shear zone.

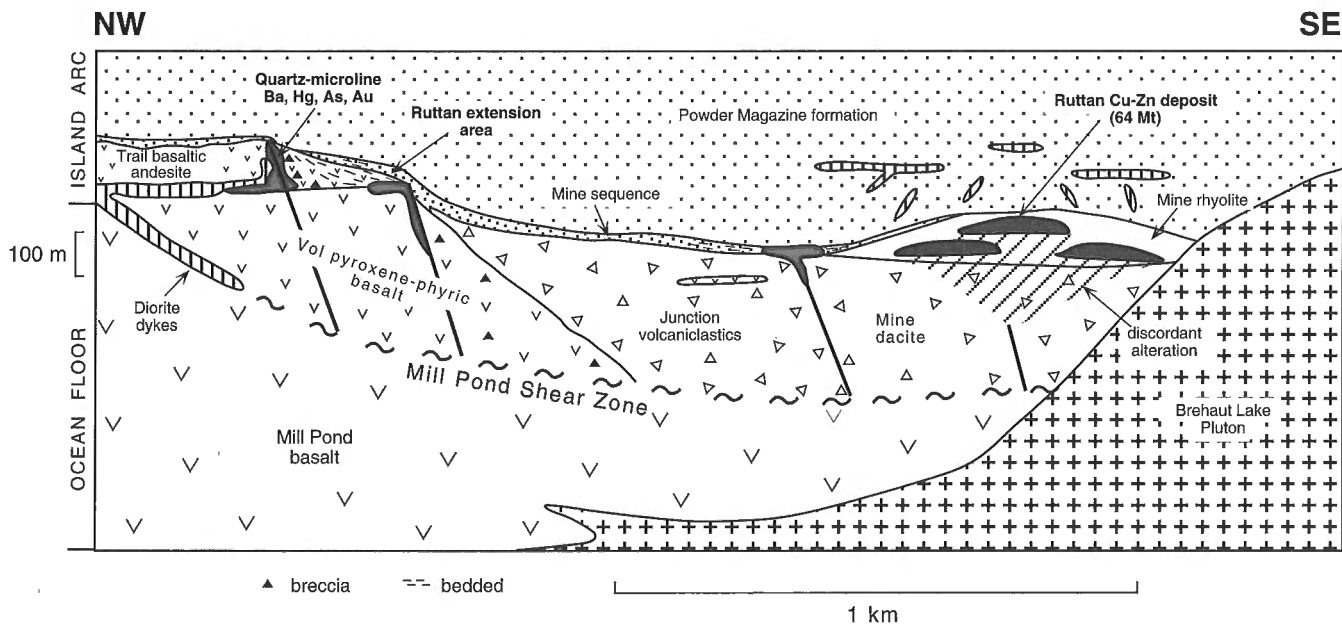


Figure 15. Schematic depositional setting for giant Ruttan massive sulphide deposit.

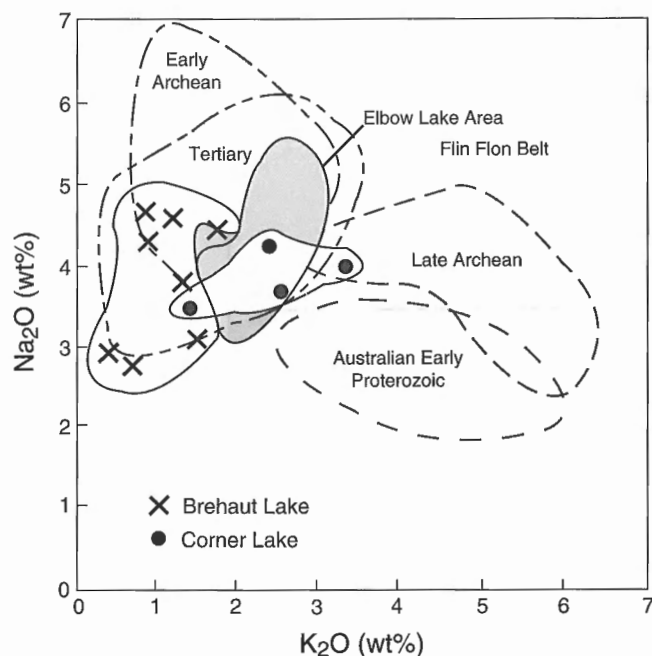


Figure 16. Na_2O vs. K_2O plot of Ruttan area major plutons in comparison with those in Flin Flon Belt and other I-type granites (fields from Whalen, 1992).

deposit, and the presence of a discordant rhyolite stock near where facies changes occur in the Vol and Trail formations from massive and pillowed flow to volcanoclastic deposition suggests that a fault-bounded basin fill hosted the Ruttan deposit (Fig. 15). This and facies changes in the footwall Vol and Trail formation strata indicate volcanoclastic transport from a constructional volcanic feature in the northeast, similar to the transport direction of the hangingwall Powder Magazine strata. Infilling of this basin initially by coarse heterolithic breccias containing fragments from the underlying volcanic flows may indicate proximal mass wasting from nearby growth faults presently occupied by dykes and microcline altered rhyolite plugs (Fig. 15). A single locality of clast-supported mafic breccia in the Powder Magazine formation in the Ruttan extension area suggests that these growth faults were still active during hangingwall deposition (Fig. 2).

Well-bedded Trail formation basaltic andesite in the southeastern exposures (Fig. 3) may represent local material shed off either the adjacent feldspar-phyric amygdaloidal andesite flow (Fig. 3) or a similar flow out of the section as clasts are composed of plagioclase-phyric basaltic andesite attached to 0.5 cm amygdaloids. Thus the Trail formation may represent a proximal volcanic facies. The presence of accessory angular rhyolite fragments in the Trail formation basaltic andesite suggests a felsic volcanic pile out of the section. The presence of abundant large gas cavities in the Trail formation flow and clastic rocks which require low pressures to enable robust vesiculation and centimetre-sized gas cavities in adjacent aphyric dykes are indicative of a shallow (<1000 m) water environment (Cas, 1992) as is the occurrence of quartz-microcline-sericite-arsenopyrite-gold mineralization

and alteration (discussed later). Although the Ruttan block is apparently separated by a major regional fault from the Karsakuwigamak block, the Ruttan mine host strata are situated only 6 km west of a large (8 km thick) subaerial felsic complex (Baldwin, 1988).

The volcanoclastic basal sequence of poorly bedded intermediate and felsic plagioclase-phyric volcanoclastic strata with minor tholeiitic basalt intercalations forms the footwall to the giant deposit. It is interesting to note that the giant Flin Flon, Horne, and Kidd Creek massive sulphide deposits are also hosted within relatively restricted, volcanoclastic-filled basins (Syme and Bailes, 1993; Kerr and Gibson, 1993; Bleeker et al., 1995). The massive sulphide is host within massive rhyolite overlying these dacitic volcanoclastic strata and is overlain by a thin (< 50 cm thick), well bedded, sulphidic, quartz-phyric and aphyric sequence of felsic volcanoclastic rocks analogous to "favourable horizons" such as the C Tuff at Noranda (Kalogeropoulos and Scott, 1989), the Key Tuffite at Matagami (Sharpe, 1968), and the Foot-Mud horizon at Snow Lake (Bailes and Galley, 1996). The association of the massive sulphide with massive rhyolite is typical of VHMS deposits (Franklin et al., 1981; Lydon, 1984). The formation of the deposit over a zone of focussed high heat flow is indicated by the high concentration of pre- and post-deposit intrusions in the immediate vicinity of the deposit such as quartz-feldspar porphyry, feldspar porphyry and diorite sills and dykes (Fig. 2, 15).

The hangingwall is marked by a pronounced change in depositional style to mass flow by turbiditic sedimentation, with transport from the northeast, that quickly buried the giant Ruttan deposit whereas volcanic flow rocks buried the giant Flin Flon, Horne, and Kidd Creek deposits. The lack of hydrothermal alteration in the hangingwall Powder Magazine formation immediately above the VMS deposit suggests that focussed hydrothermal discharge at the massive sulphide site had ceased. Silicification and Ba-microcline alteration of the hangingwall strata northeast of the deposit may be related to fluid discharge along footwall, syndepositional boundary faults located at the facies change from flow dominated sequences to volcanoclastic strata in the Ruttan extension area. These hangingwall alteration zones show an increase in radiogenic potassium (Shives, 1996) and thus detailed ground radiometric surveys in the Rusty Lake belt may define upflow zones.

Regional hydrothermal alteration within the Ruttan-hosting arc sequence is characterized by silicification, microcline, and epidote alteration. Silicification is prominent in volcanoclastic units above zones of intense quartz-microcline alteration at various stratigraphic levels and is controlled by zones of increased permeability along contacts and within volcanoclastic strata. The discordant and semi-concordant microcline-bearing plugs in the Ruttan extension area have similarities with adularia-sericite type epithermal deposits (Henley, 1986; Heald et al., 1987) in that: 1) the alteration occurs as open space filling, stockworks, vein networks and disseminations; 2) there is an enrichment in Ba, Au, and As; and 3) there is associated silicification, potash feldspar, and sericite alteration. The Ruttan Cu-Zn deposit is enriched in Hg and Ba (Speakman et al., 1982) and although there was a

significant accumulation of base metals, a large proportion of the deposit is pyritic and subeconomic to uneconomic. The empirical evidence of pervasive footwall alteration and abundant disseminated sulphide raises the possibility for boiling of hydrothermal fluids during ascent to seafloor (Henley, 1986; Large 1992) although the high metamorphic grade and complex tectonic history destroys any definitive evidence.

Similarly, the Que River Zn-Pb-Cu-Au deposit in the Mount Read volcanic unit is surrounded by an extensive low grade gold and microcline-bearing stringer zone although local high-grade sections are present (McGoldrick and Large, 1992). The microcline-bearing stringer mineralization is interpreted as forming from fluids of near-neutral pH that were less acidic and cooler than the fluid phase central to the massive sulphide deposit due to mixing of hydrothermal fluid with oxidized seawater in subaqueous volcanoclastic strata (McGoldrick and Large, 1992). The microcline-bearing zones at Ruttan may represent a fossil adularia-sericite-type volcanic-hosted epithermal deposit formed in very shallow water. These zones formed, possibly in proximity to a large felsic subaerial caldera (Karsakuwigamak block) either contemporaneously with the massive sulphide deposit in a shallow subaqueous setting or coincidentally as a later mineralizing episode.

The results of this study have broader implications in recording an evolutionary stage in the development of the Paleoproterozoic Trans-Hudson Orogen. A major component of the Rusty Lake belt is a thick (8 km) felsic subaerial caldera complex developed at 1878 Ma (Baldwin, 1987). This phase of felsic volcanism within the Rusty Lake belt is broadly coeval with magmatism within the adjacent Lynn Lake Belt (Baldwin et al., 1987) and lies within the age bracket of intra-oceanic accretion of the Flin Flon Belt juvenile arc assemblages (Gordon et al., 1990; Lucas et al., in press). Detailed regional stratigraphic, structural, geochronological, and Sm-Nd isotope studies of the Ruttan arc sequence, ocean floor sequence, and the subaerial Karsakuwigamak sequence would provide constraints on the formation of the Rusty Lake belt within the Trans-Hudson Orogen.

In light of this study, the base metal potential of the remainder of the Rusty Lake belt can be assessed using the paleotectonic geochemical constraints outlined above and with the detailed deposit characteristics, aid in more focussed exploration. The majority of the exposed mafic volcanic rocks below the deposit and indeed those at the mine site are MORB-type basalts. If, purely lithogeochemical sampling of the footwall strata were done and relied on exploration of island arc terranes only, the Ruttan deposit could be overlooked. Careful, structural and stratigraphic mapping combined with lithogeochemistry of the Eastern and southern Ruttan blocks may define favourable zones for base metal mineralization in the Rusty Lake belt. The subaerial Karsakuwigamak block may be prospective for epithermal gold exploration.

CONCLUSIONS

The large 64 Mt Ruttan Cu-Zn deposit formed in an oceanic island arc environment, and is hosted in an intermediate to felsic volcanoclastic pile localized within a fault-bounded basin. The massive sulphide lenses comprising the deposit are hosted within a felsic volcanoclastic formation that includes an areally extensive, sulphidic exhalite unit. The deposit-hosting basin-fill strata are conformably overlain by a thick sequence of mafic turbidite, indicating a major transition from a proximal to distal volcanic environment. The lack of hydrothermal alteration in the hangingwall mafic turbiditic sequence immediately above the Ruttan deposit suggests that the orebody was developed on the seafloor with hydrothermal activity waning prior to major mass wasting and burial of the ore bodies. Localized microcline alteration within discordant rhyolite plugs represents low sulphidation, adularia-sericite-type mineralization along the basin-bounding growth faults. The association of microcline-quartz comb textured veins, sericite and Ba-As±Hg and Au, scoreaceous fragments and abundant large gas cavities in host strata, and high Hg in the Ruttan deposit is suggestive of a shallow water depositional environment. Tectonic juxtaposition of ocean-floor basalt with the immediate footwall strata to the Ruttan deposit demands that large-scale lithogeochemical programs identifying VMS terranes should only be carried out in conjunction with careful bedrock mapping, as the tectonic terrane hosting the Ruttan deposit could easily be misidentified.

ACKNOWLEDGMENTS

The author would like to thank Hudsons Bay Mining and Smelting, particularly Andy Gottzman, Zabine Ramsden, Edgar Wright, and Linda Gutteridge for very open discussion, and access to the mine property and information. James Scoates is sincerely thanked for his insights, stimulating discussions and contributions to the regional mapping under less than perfect outcrop conditions. I'd also like to thank colleagues at the Geological Survey of Canada including Wouter Bleeker, Mark Hannington, Alan Galley, and Jim Franklin for discussions and Richard Lancaster, Dawn Russell and Kim Nguyen for drafting.

REFERENCES

- Alcock, F.J.
1921: Rat River route from Threepoint Lake to Southern Indian Lake, Manitoba; Geological Survey of Canada, Summary Report, 1920, Part C, p. 6-12.
- Ames, D.E.
1991: The Ruttan Cu-Zn deposit and depositional environment: an update; Manitoba Energy and Mines, Minerals Division, Report of Activities, p. 106-107.
- Ames, D.E. and Scoates, J.S.
1992: Geology, Preliminary map of the geological setting of the Ruttan Cu-Zn deposit, Rusty Lake Belt, Manitoba; Geological Survey of Canada, Open File 2571, scale 1:5000 and notes.

- Ames, D.E., Scoates, J.S., and Franklin, J.M.**
1990: Preliminary report on the geological setting of the Ruttan base metal deposit and associated hydrothermal alteration, Rusty Lake volcanic belt, Manitoba (NTS 64B/5); Manitoba Energy and Mines, Minerals Division, Report of Activities 1990, p. 178-186.
- Ames, D.E. and Taylor, C.**
1996: Geology of the West Anomaly orebody, Ruttan VHMS deposit, Paleoproterozoic Rusty Lake Belt, Manitoba; in *EXTECH I: a Multidisciplinary Approach to Massive Sulphide Research in the Rusty Lake-Snow Lake Greenstone Belts, Manitoba*, (ed.) G.F. Bonham-Carter, A.G. Galley, and G.E.M. Hall, Geological Survey of Canada, Bulletin 426, this volume.
- Bailes, A.H. and Galley, A.G.**
1996: Setting of Paleoproterozoic volcanic-hosted massive base metal sulfide deposits, Snow Lake, Manitoba; in *EXTECH I: A Multidisciplinary Approach to Massive Sulphide Research in the Rusty Lake-Snow Lake Greenstone Belts, Manitoba*, (ed.) G.F. Bonham-Carter, A.G. Galley, and G.E.M. Hall, Geological Survey of Canada, Bulletin 426, this volume.
- Bailes, A.H. and Syme, E.C.**
1982: Rusty Lake area; Manitoba Energy and Mines, Mineral Resources Division, Report of Field Activities, p. 15.
1989: Geology of the Flin Flon-White Lake area; Manitoba Energy and Mines, Geological Report GR 87-1, 313 p.
- Baldwin, D.A.**
1982: Mineral deposits in the Ruttan Lake, Karsakuwigamak Lake and Muskayk Lake areas, Manitoba (Parts of NTS 64B/5, 6, 11 and 12); Manitoba Department of Energy and Mines, Mineral Resources Division, Open File Report OF81-4, 59 p.
1987: Physical volcanology of the northwest segment of the Karsakuwigamak Block, Proterozoic Rusty Lake metavolcanic belt, Northern Manitoba; Ph.D. thesis, University of Manitoba, Winnipeg, Manitoba, 438 p.
1988: Geology of the southern part of the Rusty Lake volcanic belt; Manitoba Energy and Mines, Geological Report GR86-1, p. 1-90.
- Baldwin, D.A., Syme, E.C., Zwanzig, H.V., Gordon, T.M., Hunt, P.A., and Stevens, R.P.**
1987: U-Pb zircon ages from the Lynn Lake and Rusty Lake metavolcanic belts, Manitoba: two ages of Proterozoic magmatism; *Canadian Journal of Earth Sciences*, v. 24, p. 1053-1063.
- Bleeker, W., Parrish, R.R., and Kinsman, A.**
1995: The giant Kidd Creek VMS deposit: A new perspective; in *Precambrian '95*, Montreal, Canada; Program with Abstracts, p. 43.
- Bleeker, W. and Parrish, R.**
in press: Stratigraphy and U-Pb zircon geochronology of Kidd Creek: implications for the formation of giant VMS deposits and the tectonic history of the Abitibi greenstone belt; *Canadian Journal of Earth Sciences*.
- Burwash, R.A.**
1962: Geology of the Rusty lake area; Manitoba Mines Branch, Publication 60-3, 31 p.
- Cas, R.A.F.**
1992: Submarine volcanism: Eruption styles, products, and relevance to understanding the host rock successions to volcanic-hosted massive sulphide deposits; *Economic Geology*, v. 87, p. 511-541.
- Chappell, B.W. and Stephens, R.**
1988: Origin of infracrustal (I-type) granite magmas; *Transactions of the Royal Society of Edinburgh Earth Sciences*, v. 79, p. 71-86.
- Chappell, B.W. and White, A.J.R.**
1974: Two contrasting granite types; *Pacific Geology*, v. 8, p. 173-174.
- Franklin, J. M., Lydon, J.W., and Sangster, D.F.**
1981: Volcanic-associated massive sulfide deposits; *Economic Geology 75th Anniversary Volume*, p. 485-627.
- Galley, A.G., Bailes, A.H., and Kitzler, G.**
1993: Geological setting and hydrothermal evolution of the Chisel Lake and North Chisel Zn-Pb-Cu-Ag-Au massive sulfide deposits, Snow Lake, Manitoba; *Exploration and Mining Geology*, v. 2, no. 4, p. 271-295.
- Gill, J.B.**
1981: *Orogenic Andesites and Plate Tectonics*; Springer, New York, 390 p.
- Glickson, A.Y.**
1980: Precambrian sial-sima relations: evidence for earth expansion. *Tectonophysics*, v. 63, 193-234.
- Gordon, T.M., Hunt, P.A., Bailes, A.H., and Syme, E.C.**
1990: U-Pb ages from the Flin Flon and Kiseynew belts, Manitoba: chronology of crust formation at an Early Proterozoic accretionary margin; in *The Early Proterozoic Trans-Hudson Orogen of North America*; Geological Association of Canada, Special Paper 37, p. 177-200.
- Haskin, L.A., Haskin, M.A., Frey, F.A., and Wildeman, T.R.**
1968: Relative and absolute terrestrial abundances of the rare earths; in *Origin and Distribution of the Elements*, (ed.) L.H. Ahrens; Pergamon Press, New York, p. 889-912.
- Heald, P., Foley, N.K., and Hayba, D.O.**
1987: Comparative anatomy of volcanic-hosted epithermal deposits: acid-sulfate and adularia-sericite types; *Economic Geology*, v. 82, p. 1-26.
- Henley, R.W.**
1986: The geothermal framework for epithermal deposits; *Reviews in Economic Geology*, v. 2, p. 1-24.
- Hoffman, P.F.**
1988: United plates of America, the birth of a craton: Early Proterozoic assembly and growth of Laurentia; *Annual Review of Earth and Planetary Sciences*, v. 16, p. 543-603.
- Irvine, T.N. and Baragar, W.R.A.**
1971: A guide to the chemical classification of the common volcanic rocks; *Canadian Journal of Earth Sciences*, v. 8, 523-548.
- Kalogeropoulos, S.I. and Scott, S.D.**
1989: Mineralogy and geochemistry of an Archean tuffaceous exhalite: the Main Contact Tuff, Millenbach mine area, Noranda, Quebec; *Canadian Journal of Earth Sciences*, v. 26, p. 88-105.
- Kerr, D.J. and Gibson, H.L.**
1993: A comparison of the Home volcanogenic massive sulphide deposit and intracauldron deposits of the Mine Sequence, Noranda, Quebec; *Economic Geology*, v. 88, p. 1419-1442.
- Koo, J. and Mossman, D.J.**
1975: Origin and metamorphism of the Flin Flon stratabound Cu-Zn sulphide deposit, Saskatchewan and Manitoba; *Economic Geology*, v. 70, p. 48-62.
- Large, R.R.**
1992: Australian volcanic-hosted massive sulfide deposits: Features, style and genetic models; *Economic Geology*, v. 87, p. 471-510.
- LeMaitre, R.W.**
1989: A classification of igneous rocks and glossary of terms, recommendations of the International Union of Geological Sciences Subcommittee of the Systematics of Igneous Rocks; Blackwell Scientific Publications, Oxford, United Kingdom.
- Lucas, S.B., Stern, R.A., and Syme, E.C.**
in press: Flin Flon greenstone belt: Intraoceanic tectonics and the development of continental crust (1.92-1.84 Ga); *Geological Society of America Bulletin*.
- Lydon, J.W.**
1984: Ore deposit models #14: Volcanogenic massive sulphide deposits. Part 1: a descriptive model; *Geoscience Canada*, v. 11, p. 195-202.
- McGoldrick, P.J. and Large, R.R.**
1992: Geologic and geochemical controls on gold-rich stringer mineralization in the Que River deposit, Tasmania; *Economic Geology*, v. 87, p. 667-685.
- Milligan, G.C.**
1964: Geology of the Earp Lake area (West Half), Manitoba; Manitoba Mines Branch, Publication 61-2, p. 1-15.
- O'Connor, J.T.**
1965: A classification of quartz rich igneous rocks based on feldspar ratios; *United States Geological Survey, Professional Paper 525B*, p. 79-84.
- Pearce, J.A. and Cann, J.R.**
1973: Tectonic setting of basic volcanic rocks determined using trace element analysis; *Earth and Planetary Science Letters*, v. 19, p. 290-300.
- Pearce, J.A., Harris, N.B.W., and Tindle, A.G.**
1984: Trace element discrimination diagrams for the tectonic interpretation of granitic rocks; *Contributions to Mineralogy and Petrology*, v. 25, p. 956-983.
- Pearce, J.A. and Norry, M.A.**
1979: Petrogenetic implications of Ti, Zr, Y and Nb variations in volcanic rocks; *Contributions to Mineralogy and Petrology*, v. 69, p. 33-47.
- Pearse, G.**
1964: Geology of the Pemichigamau Lake area (East Half), Manitoba; Manitoba Mines Branch, Publication 61-3, p. 1-16.

Sangster, D.F.

- 1980: Quantitative characteristics of volcanogenic massive sulphide deposits 1. Metal content and size distribution of massive sulphide deposits in volcanic centres; Bulletin Canadian Institute of Mining and Metallurgy, Section B, v. 99, p. 21-42.

Saunders, A.D. and Tarney, J.

- 1984: Geochemical characteristics of basaltic volcanism within back-arc basins. In *Marginal Basin Geology*; (ed.) B.P. Kokelaar and M.R. Howells; Blackwell, Oxford, p. 59-76.

Sharpe, J.I.

- 1968: Géologie et gisements de sulfures de la région de Matagami, comté d'Abitibi-Est, Québec; Ministère des richesses naturelles du Québec, Rapport Géologique 137, 8 cartes, 122 p.

Shives, R.B.K.

- 1996: Application of airborne multiparameter geophysical data (gamma ray, magnetometer, VLF-EM) to mapping and exploration in Snow Lake and Rusty Lake areas; in *EXTECH I: A Multidisciplinary Approach to Massive Sulphide Research in the Rusty Lake-Snow Lake Greenstone Belts, Manitoba*, (ed.) G.F. Bonham-Carter, A.G. Galley, and G.E.M. Hall; Geological Survey of Canada, Bulletin 426, this volume.

Speakman, D.S., Chornoby, P.J., Haystead, B.C.W., and Holmes, G.F.

- 1982: Geology of the X Ruttan deposit, northern Manitoba; in *Precambrian Sulphide Deposits*, (ed.) R.W. Hutchison, C.D. Spence, and J.M. Franklin; Geological Association of Canada, Special Paper 25, p. 525-556.

Steeves, M.A. and Lamb, C.F.

- 1972: Issett-Opachuanau-Pemichigamau-Earp Lakes area; Manitoba Mines Branch, Publication 71-2F, p. 1-56.

Stern, R.A., Syme, E.C., and Lucas, S.B.

- 1995: Geochemistry of 1.9 Ga MORB- and OIB-like basalts from the Amisk collage, Flin Flon Belt, Canada: Evidence for an intra-oceanic origin; *Geochimica et Cosmochimica Acta*, v. 59, no. 15, p. 3131-3154.

Stockwell, C.H.

- 1961: Structural provinces, orogenies and time classification of rocks of the Canadian Precambrian Shield; in *Age Determinations by the Geological Survey of Canada, Report 2: Isotopic Ages*; Geological Survey of Canada, Paper 61-17, p. 108-118.

Streckeisen, A.L.

- 1973: Plutonic rocks: classification and nomenclature recommended by the IUGS Subcommission on the systematics of igneous rocks; *Geotimes*, v. 18, p. 26-30.

Sun, S.S. and Nesbitt, R.W.

- 1978: Petrogenesis of Archean ultrabasic and basic volcanics: Evidence from rare earth elements; *Contributions to Mineralogy and Petrology*, v. 65, p. 301-325.

Syme, E.C.

- 1990: Stratigraphy and geochemistry of the Lynn Lake and Flin Flon metavolcanic belts, Manitoba; Geological Association of Canada, Special Paper 37, p. 143-161.

Syme, E.C. and Bailes, A.H.

- 1993: Stratigraphic and tectonic setting of Early Proterozoic volcanogenic massive sulfide deposits, Flin Flon, Manitoba; *Economic Geology*, v. 88, p. 566-589.

Whalen, J.B.

- 1992: Elbow Lake project-Part B: granitoid rocks; in *Report of Activities 1992; Manitoba Energy and Mines, Minerals Division*, p. 47-51.

Wood, D.A., Joron, J.L., and Treuil, M.

- 1979: A re-appraisal of the use of trace elements to classify and discriminate between rock series erupted in different tectonic settings; *Earth and Planetary Science Letters*, v. 50, p. 326-336.

Wright, G.M.

- 1953: Uhlman Lake map-area, Manitoba; Geological Survey of Canada, Paper 53-12, 5 p.

Zwanzig, H.V.

- 1982: Rat River Channel area; in *Report of Field Activities 1982; Manitoba Department of Energy and Mines, Mineral Resources Division*, p. 11.

Contribution to the 1989-1994 Rusty Lake-Snow Lake Mining Camps, Canada-Manitoba Exploration Science and Technology Initiative (EXTECH I)

Geology of the West Anomaly orebody, Ruttan volcanic-hosted massive sulphide deposit, Proterozoic Rusty Lake belt

D.E. Ames¹ and C. Taylor²

Ames, D.E. and Taylor, C., 1996: Geology of the West Anomaly orebody, Ruttan volcanic-hosted massive sulphide deposit, Proterozoic Rusty Lake belt; in EXTECH I: A Multidisciplinary Approach to Massive Sulphide Research in the Rusty Lake-Snow Lake Greenstone Belts, Manitoba, (ed.) G.F. Bonham-Carter, A.G. Galley, and G.E.M. Hall; Geological Survey of Canada, Bulletin 426, p. 45-76.

Abstract: The 64 Mt Ruttan Zn-Cu deposit and contained 8.2 Mt West Anomaly orebody grading 1.49% Cu and 2.66% Zn, lies within Paleoproterozoic volcanic rocks in the Rusty Lake belt, Trans-Hudson Orogen. The deposit is located at the top of a felsic volcanoclastic sequence that overlies dacitic volcanoclastic rocks, which are laterally equivalent to arc tholeiitic andesitic lava flows and volcanoclastic debris. Mafic epiclastic strata form the hangingwall of the deposit. Polyphase faulting has resulted in juxtaposition of different lithogeochemical terranes and truncation of the footwall of the Ruttan massive sulphide deposit.

Mineral and bulk rock chemistry of proximal hydrothermal alteration constrains the metamorphic conditions and mass gains and losses in the system. Altered dacite and felsic volcanoclastic rocks metamorphosed to amphibolite facies consist of quartz-phlogopite-plagioclase (An₄₅)-andalusite-zincian staurolite-garnet schist in the former and quartz-cordierite-biotite-staurolite-garnet-andalusite-sillimanite zones with magnesian chlorite-anthophyllite±phlogopite-cordierite-anhydrite schists that envelop the orebody. Anthophyllite-bearing assemblages are unique to the West Anomaly orebody in the Ruttan mine. Silica flooding occurred immediately below the massive sulphide deposit in the stringer zone with more proximal Mg, Fe, Zn, Cu, and S enrichment and alkali depletion.

Subaqueous felsic volcanic and volcanoclastic packages with hydrothermally altered rocks within an arc tholeiitic terrane are prospective for VMS exploration in the Rusty Lake belt.

Résumé : Le gisement de Zn-Cu de Ruttan (64 millions de tonnes) et son amas minéralisé de West Anomaly (8,2 millions de tonnes), dont les teneurs en Cu et en Zn sont évaluées à 1,49 % et 2,66 % respectivement, sont encaissés dans des volcanites du Protérozoïque inférieur de la ceinture de Rusty Lake (orogène trans-hudsonien). Ce gisement se trouve au sommet d'une séquence volcanoclastique felsique qui recouvre des volcanoclastites dacitiques, lesquelles sont un équivalent latéral de coulées d'andésite tholéiitique d'arc insulaire et de débris volcanoclastiques. L'éponte supérieure du gisement est constituée de strates d'épiclastites mafiques. La formation de failles en plusieurs phases a provoqué la juxtaposition de terranes lithogéochimiques différents et le morcellement de l'éponte inférieure du gisement de sulfures massifs de Ruttan.

Les caractéristiques chimiques des minéraux et de la roche totale provenant des zones proximales d'altération hydrothermale permettent de déterminer les conditions métamorphiques ainsi que les gains et les pertes de masse du système. Les volcanoclastites dacitiques et felsiques, métamorphisées au faciès des

¹ Geological Survey of Canada, 601 Booth St., Ottawa, Ontario K1A 0E8

² Hudson Bay Mining and Smelting, Ruttan Mine, Leaf Rapids, Manitoba R0B 1W0

amphibolites, sont altérées respectivement en des schistes à quartz-phlogopite-plagioclase (An₄₅)-andalousite-staurotide zincifère-grenat et des schistes à chlorite magnésienne-anthophyllite± phlogopite-cordiérite-anhydrite, ces derniers enveloppant le gisement et présentant des zones à quartz-cordiérite-biotite-staurotide-grenat-andalousite-sillimanite. À la mine Ruttan, les assemblages à anthophyllite sont particuliers à l'amas minéralisé de West Anomaly. Une injection de silice est survenue immédiatement sous le gisement de sulfures massifs, dans la zone de minéralisation en filonnets; celle-ci est caractérisée, dans la portion plus proximale, par un enrichissement en Mg, Fe, Zn, Cu et S et un appauvrissement en alcalis.

Dans la ceinture de Rusty Lake, les ensembles de roches formées en milieu subaqueux (volcanites et volcanoclastites felsiques), qui comprennent des zones ayant subi une altération hydrothermale à l'intérieur d'un terrane tholéiitique d'arc, constituent de bonnes cibles d'exploration pour les sulfures massifs volcanogènes.

INTRODUCTION

The Ruttan deposit is one of two giant (>60 Mt) base metal deposits in the Trans-Hudson Orogen (Fig. 1) and in terms of tonnage is one of the largest volcanogenic massive sulphide (VMS) deposits in Canada after the Kidd Creek, Bathurst, and Flin Flon mines (McCutcheon, 1992; W. Bleeker, GSC Minerals Colloquium, abstract, 1994). As it is the only known base metal deposit in the entire Rusty Lake volcanic belt (Fig. 2), understanding the environment of deposition and the nature of hydrothermal alteration is of utmost importance to the explorationists in their search for new base metal resources in the region.

The objectives of the geological segment of the EXTECH study in the Ruttan area are to: 1. document the environment of deposition of the large base metal deposit; 2. define the ore horizon and determine its relationship to the regional stratigraphy; and 3. determine the mineralogical and chemical compositions of the host rocks, semi-conformable and dis-conformable alteration zones.

In this paper, the immediate mine stratigraphy and proximal hydrothermal alteration zones of the West Anomaly orebody are defined through field observations, petrography, and major oxide, trace element, and rare earth element (REE) analyses. The mine stratigraphy is compared with the stratigraphy in the Ruttan block (Ames and Scoates, 1992; Ames, 1996). Another paper (Ames, 1996) defines the regional geological and tectonic setting of the Ruttan mine based on 1:5000 mapping (Ames and Scoates, 1992).

HISTORY AND DEVELOPMENT

The Ruttan deposit contains 64 Mt to date, grading 1.35% Zn and 1.27% Cu. The discovery hole, drilled in 1969 was targeted on the basis of combined electromagnetic and magnetic surveys flown by Sheritt Gordon Mines Limited (Speakman et al., 1982). This large deposit has been owned and operated by Hudson Bay Mining and Smelting since 1987. Production commenced at 9000 t/day from an open pit in early 1973 and terminated in December 1980 at a depth of

210 m. Underground production utilizing open stope with delayed backfilling mining methods commenced in early 1979.

Three main orebodies are recognized; the East Lens, West Lens (or Main Mine) (Speakman et al., 1982), and the West Anomaly (Fig. 3, Ames and Scoates, 1992). The West, East, and West Anomaly ore lenses have a combined strike length of 1000 m and an average width of 40 m with individual lenses less than 350 m and 7-61 m wide. The strike length of the individual lenses decreases with depth. The East and West lenses are continuous from surface to the 800 mL with the East Lens open at depth below the 1000 mL. The West Anomaly was initially discovered based on a subsidiary EM and magnetic anomaly southwest of the main deposit in the 1970s. Subsequent drilling from the surface did not intersect adequate ore widths or grades, but later underground drilling resulted in the delineation of an economic orebody. The West Anomaly was accessed for diamond drilling by a drift west of the West Lens on the 660 mL (Fig. 3) in 1989 with initial ore production in August 1991 on the 740 mL. The orebody has been developed between the 590 m and 910 m levels at 570-890 m from the surface. The West Anomaly ore lens contains 8.2 Mt grading 1.49% Cu and 2.66% Zn with 941 800 t grading 1.48% Cu and 1.66% Zn mined as of November 1993. The West Anomaly to date contains 8.2 Mt of the 64 Mt in the entire Ruttan mine and is comparable in size to the Chisel Lake deposit in Snow Lake (7.17 Mt; Galley et al., 1993).

REGIONAL AND LOCAL GEOLOGY

The Paleoproterozoic Rusty Lake belt forms a 75 km long by 35 km wide, east-trending belt within the juvenile core of the Trans-Hudson Orogen (Fig. 1, 2) (Baldwin et al., 1987; Hoffman, 1988; Gordon et al., 1990; Ames and Scoates, 1992). The Rusty Lake belt consists of a number of supra-crustal segments separated by synvolcanic to synkinematic intrusions ranging from granite through quartz monzonite and granodiorite to gabbro. The central part of the belt was divided by Baldwin (1988) into four, fault-bounded structural blocks (Ruttan, Northern, Karsakuwigamak and Eastern) that apparently have opposing facing directions and

no stratigraphic correlation (Fig. 2). The Ruttan block is bound to the north by the Vol Fault, an east-trending structure separating rocks with opposing stratigraphic sequences and interpreted as a late structure (Ames, 1996), to the south and west by plutonic rocks and to the east by a structure that separates an extensive subaerial rhyolite sequence of the Karsakuwigamak block (Baldwin, 1987) from the submarine volcanic rocks of the Ruttan block. The only age date in the belt is subaerial rhyolite volcanism at 1878 ± 3 Ma within the Karsakuwigamak block (Baldwin et al., 1987; Baldwin, 1988) but the age of the volcanic rocks in the Ruttan block is unknown.

Field, petrological, and chemical evidence based on mapping by the senior author in 1990 and 1991 suggests that much of the mafic footwall to the deposit has been either structurally

juxtaposed along a pre-Vol Fault, the Mill Pond shear zone, joining oceanic floor basalts with island arc basalt or the ore hosting island arc developed on ocean floor (Ames, 1996). The geometry of faults and the close proximity of the deposit (250 m) to the Brehaut Lake pluton that defines the edge of the greenstone belt has obliterated most of the primary footwall and any possible synvolcanic heat source for the Ruttan VMS deposit. The preserved host stratigraphy of the Ruttan deposit is a southwest-facing and tapering wedge, controlled by faults and plutons, with an apparent thickness of <1000 m in the northeast to >280 m in the south at the mine site (Fig. 4 in Ames, 1996). The deposit is located in massive rhyolite near the top of a basin-fill sequence composed of felsic, dacitic, and trace mafic volcanoclastic rocks which are lateral to, and intermixed with, arc tholeiitic basaltic lava flows and

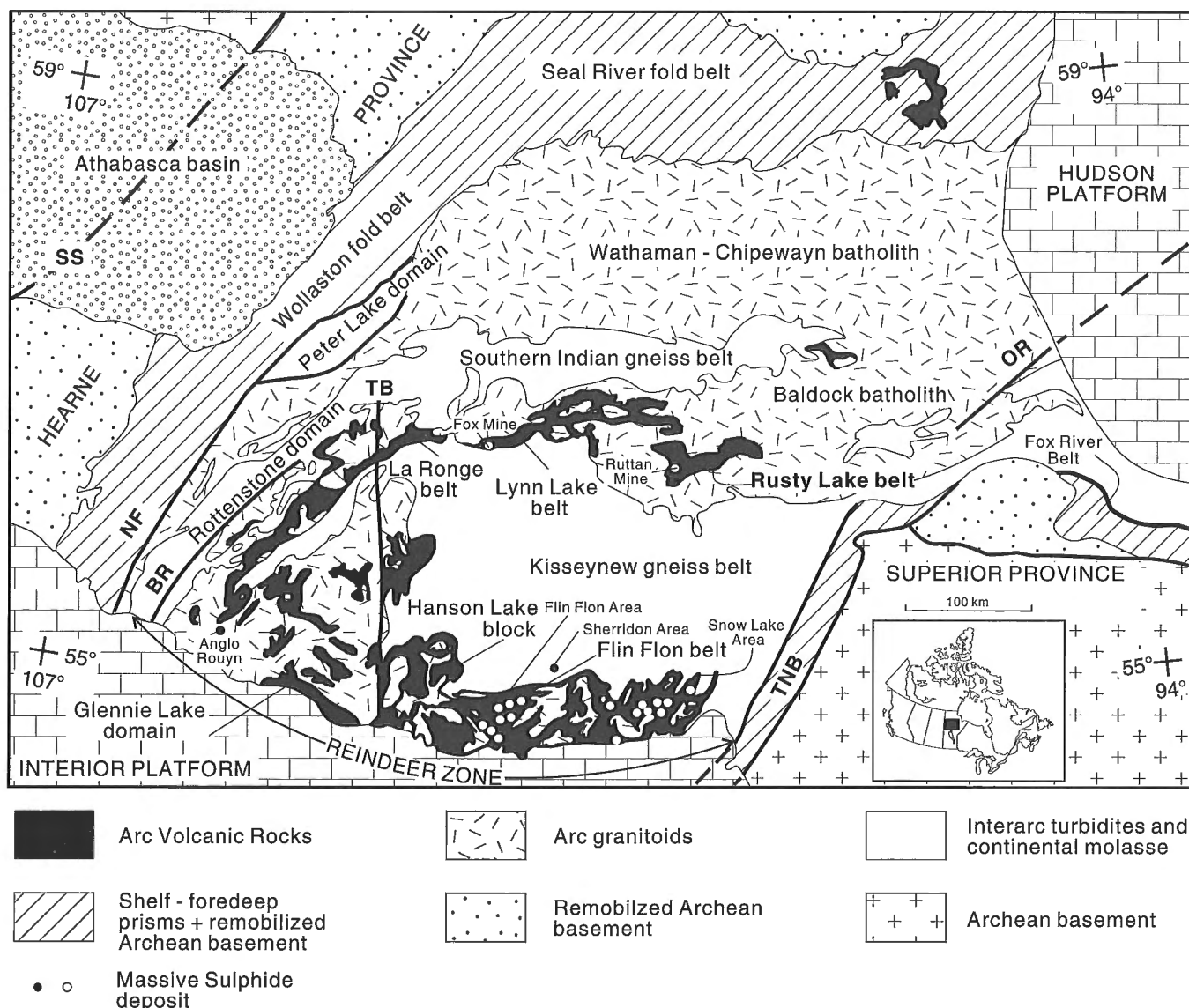


Figure 1. Lithotectonic domains of Early Proterozoic Trans-Hudson orogen in northern Manitoba and Saskatchewan (after Hoffman, 1988). SS – Snowbird shear zone; NF – Needle Falls shear zone; BR – Bird Rapids shear zone; TB – Tabbarnor Fault; TNB – Thompson Nickel belt; OR – Owl River shear zone.

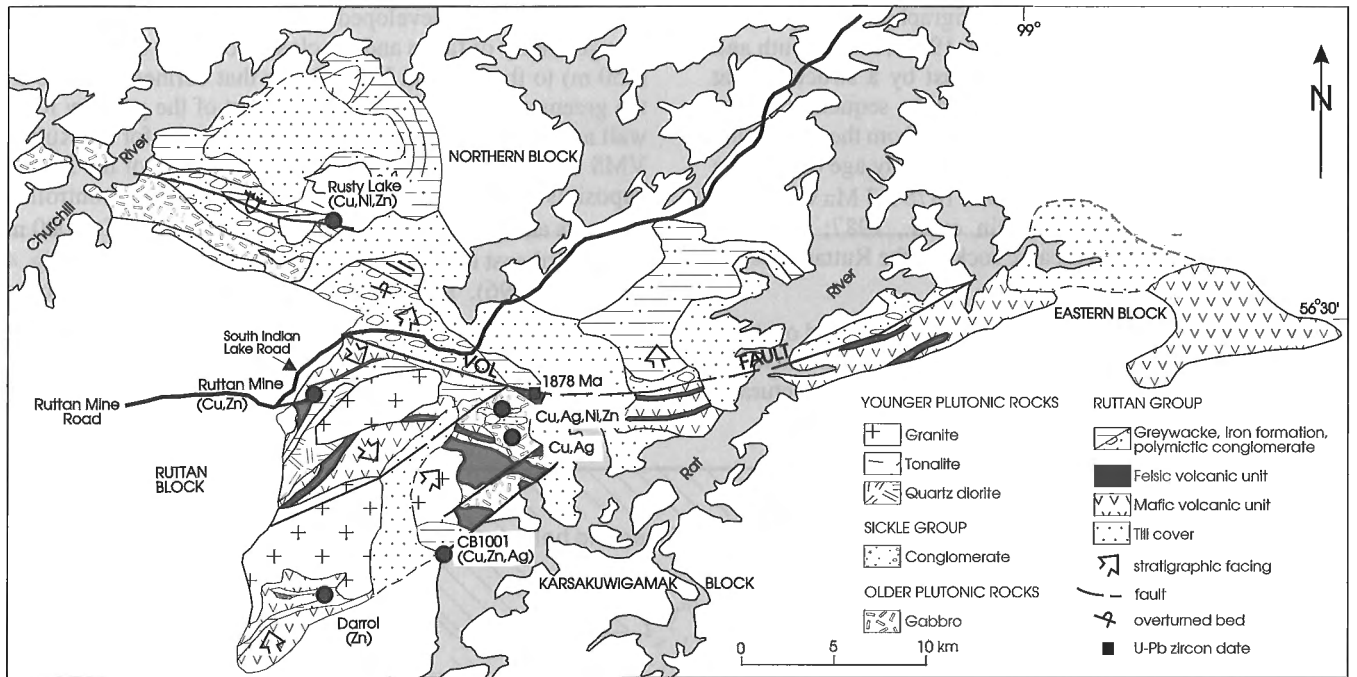


Figure 2. Generalized geology, mineral occurrence, and Ruttan mine locations in Rusty Lake belt, northern Manitoba.

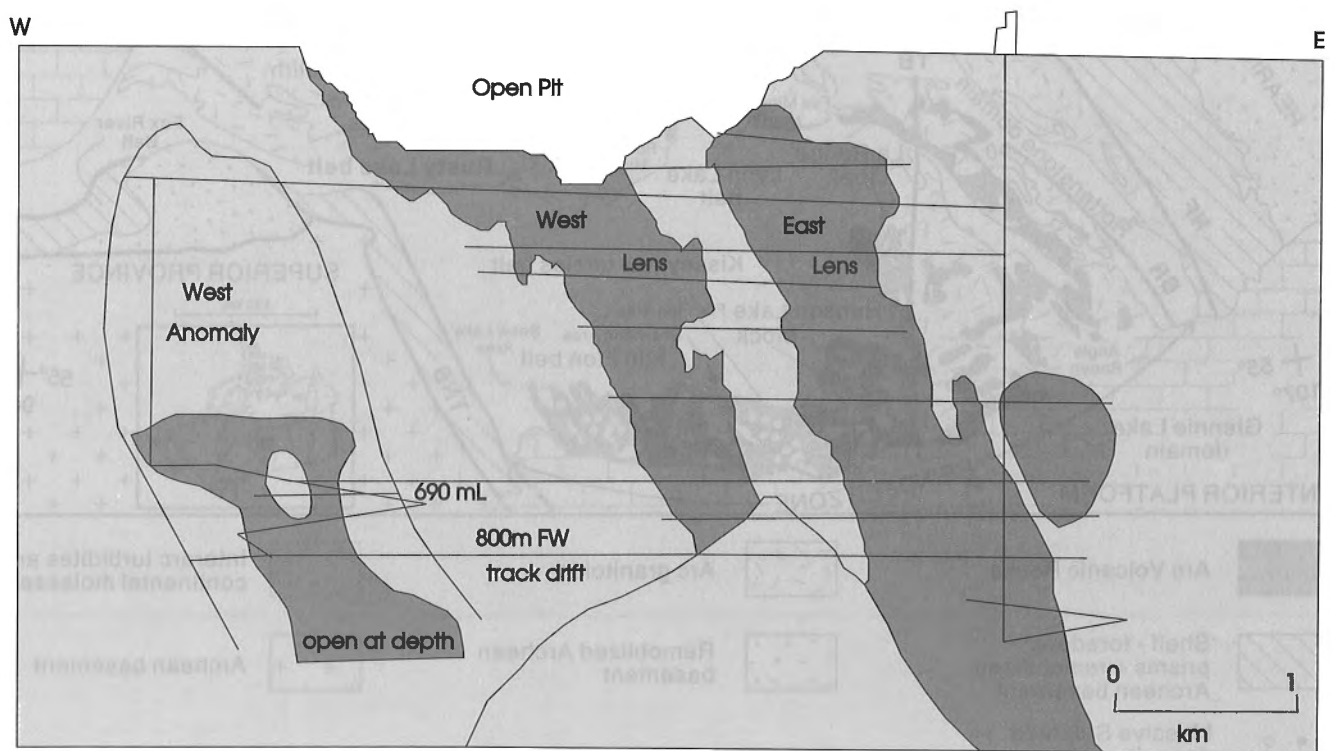


Figure 3. Longitudinal section of three southeast-plunging orebodies hosting Ruttan Cu-Zn ore.

related volcanoclastic deposits that outcrop to the northeast (Table 1) (Ames et al., 1990; Ames and Scoates, 1992; Ames, 1996) (see Fig. 3, Ames, 1996). Mafic epiclastic rocks of the Powder Magazine formation form the hangingwall rocks to the Ruttan deposit (Speakman et al., 1982; Baldwin, 1988; Ames et al., 1990).

Feldspar porphyry dykes and sills chemically similar to the dacitic volcanoclastic rocks intrude the arc tholeiitic package. The strata have been intruded by mafic and felsic dykes, as well as, the Corner Lake and the Brehaut Lake plutons (Ames, 1996).

WEST ANOMALY DEPOSIT GEOLOGY

The West Anomaly ore lens is situated at the western extremity of the mine with a host stratigraphy comparable to that of the rest of the Ruttan deposit (Fig. 4). The fragmental units were subdivided using the classification scheme modelled after Fisher (1966). The classification terms are strictly descriptive as primary volcanic features have been obscured by alteration and recrystallized during metamorphism in the mine area. The host rocks to the Ruttan deposit are altered to various degrees with few representative least altered

Table 1. Table of formations within Ruttan mine area.

| Mine area | Average thickness (m) | Principal lithology | Northeast unit | Average thickness (m) | Principal lithology |
|-----------------------------|-----------------------|--|-------------------------|-----------------------|--|
| Intrusive contact | | | | | |
| Powder Magazine | 150 | pebble and cobble paraconglomerate, minor orthoconglomerate | Powder Magazine | >350 | heterolithological mafic volcanic breccia |
| | 100 | mafic wacke | | 60-250 | bedded mafic wacke |
| | 150 | thinly interbedded wacke mudstone, siltstone, minor dacite | | | |
| Conformable contact | | | Conformable contact | | |
| Upper felsic volcanoclastic | 10-50 | massive to bedded felsic quartz-bearing tuff, pebble breccia | Ruttan extension | 1.6 | quartz- and feldspar-bearing bedded felsic volcanoclastic rocks |
| Conformable contact | | | Conformable contact | | |
| Mine rhyolite | 40 | massive sulphide and stringer mineralization | Ruttan extension | 3-4 | massive rhyolite |
| | 20-30 | chlorite schist massive felsic rock | | 3-4 | quartz-bearing tuff |
| | | | Conformable contact | | |
| | | | Trail basaltic andesite | 25-100 | plagioclase phyrlic, massive to sparsely pillowed lava and related bedded volcanoclastic rocks |
| Conformable contact | | | Lateral changes | | |
| Mine dacite | >90 | homogeneous, massive to weakly layered volcanoclastic rock | Junction dacite | massive dacitic 0-250 | volcanoclastic, minor aphyric and sparsely feldspar phyrlic, amygdaloidal basalt |
| Fault contact | | | Not exposed | | |
| Lower felsic volcanoclastic | >50 | thinly bedded felsic and subordinant mafic volcanoclastic | Hornblende basalt | 250 | lateral facies changes; NE, series of 2m wide hornblende phyrlic massive flow rocks, SW heterolithological mafic breccia |
| | | | Felsic volcanoclastic | 0-110 | highly strained and altered felsic and mafic rocks |
| Fault contact | | | Fault contact | | |
| Mill Pond basalt | >0 | pillowed basalt | Mill Pond basalt | >800 | massive, aphyric to sparsely feldspar phyrlic basalt, minor pillowed lava |

examples. The footwall rocks consist of bedded felsic volcani-clastic rocks in fault contact with overlying massive altered dacite which is in turn overlain by intensely altered massive rhyolite that contains the massive sulphide lenses. The ore lens is normally zoned with a chalcopyrite-pyrrhotite rich base and a sphalerite-pyrite rich top and is enveloped by a

chlorite-talc schist. The immediate hangingwall strata consist of variably altered quartz-phyric, layered felsic tuff and tuff breccia which are conformably overlain by volcanic mafic wacke and conglomerate of the Powder Magazine formation (Table 1) (Fig. 4).

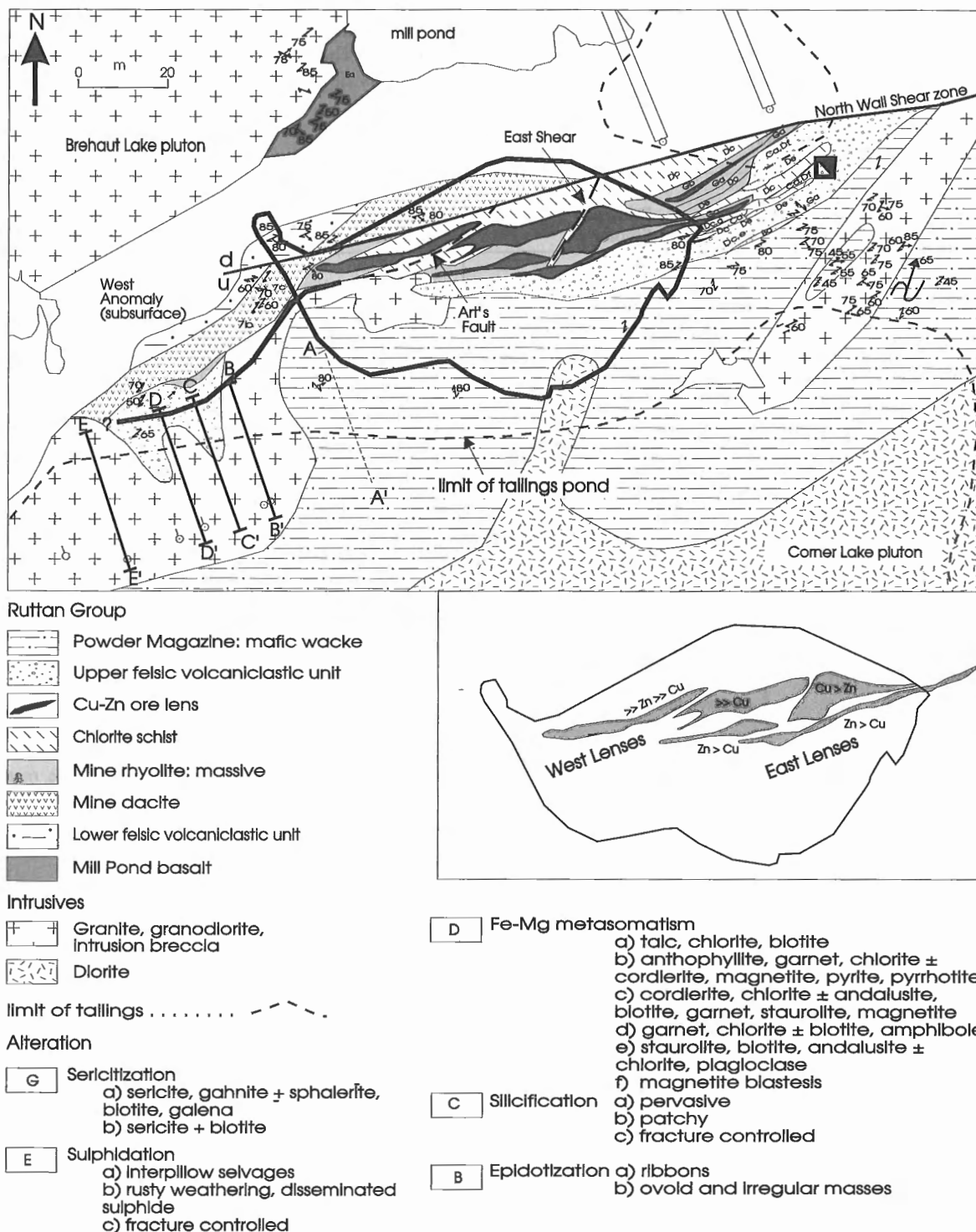


Figure 4. Simplified surficial geology of Ruttan mine (after Ames and Scoates, 1992). Lines of sections shown (e.g. A-A', B-B').

Lower felsic volcanoclastic rocks

The Lower felsic volcanoclastic unit is a poorly exposed, fault-bounded sequence. Northeast of the mine site, the Mill Pond formation basalt is in fault contact with the Vol formation (Fig. 4; Ames, 1996) and it is inferred that the lower contact, between the Mill Pond basalt and Lower felsic volcanoclastic rocks in the mine area, is also structural. The upper contact is represented both at depth in the West Anomaly and along the northwestern edge of the open pit, by the North Wall shear zone – a high angle reverse fault (Fig. 4).

The Lower felsic volcanoclastic rocks are thinly bedded (0.1 to 1 m) and interlayered with minor mafic tuff/sediment. Approximately 20% of the unit in the West Anomaly area is

cut by 0.5 to 2 m mafic and granitoid dykes. The tuff is typically unaltered, consisting of 65% polycrystalline plagioclase and quartz and 35% biotite. Minor zones are composed of quartz and plagioclase (50%), biotite (10%), hornblende (15%), and trace chlorite, magnetite, and pyrite.

Mine dacite

South of the North Wall shear zone is a lensoid package of hydrothermally altered dacitic volcanoclastic rocks whose upper contact is generally sharp but, locally it grades into the Mine rhyolite. In drill core the contact is commonly masked by mafic dykes and/or quartz veins. At depth the exposed

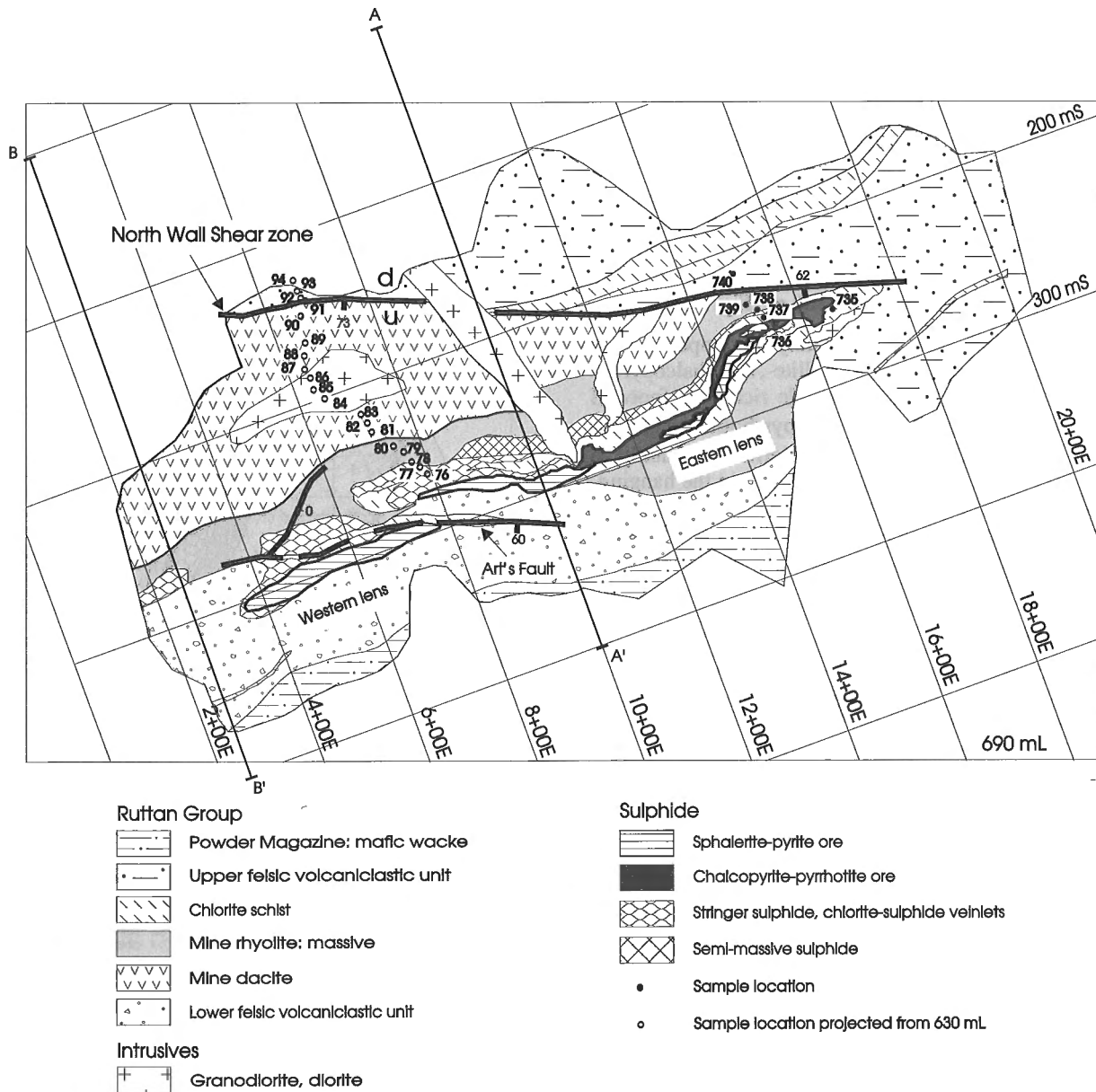


Figure 5. Geology of 8.2 Mt West Anomaly orebody on 690 m level. Sample locations marked by filled dots; from level 690 mL and open dots represent sample locations projected onto this plane from level 630.

sequence is approximately 90 m wide (Fig. 5, 7; A-A') and thickens westward due to the geometry of the North Wall shear zone and geological contacts (Fig. 4, 5, 7).

The massive to weakly layered dacite is typically a lapilli tuff that weathers pale greenish-grey and contains poorly defined, elongate ($R=2:1$; R =aspect ratio of length:width) felsic clasts. Least altered dacite west of the mine (Fig. 7; D-D') is composed of fine grained (<0.5 mm) 30% quartz, 40-50% plagioclase, 15% 0.5 mm biotite, and 5% (2 mm) poikilitic garnet. Trace amounts of retrogressive chlorite are associated with garnet porphyroblasts.

Mine rhyolite

The Mine rhyolite occurs stratigraphically above the dacitic volcanoclastic rocks and hosts the massive sulphide lenses. In the West Anomaly, rhyolite contacts are sharp with the sulphide lenses and chlorite schist. A massive basal sequence contains 30-60% quartz, 5-35% chlorite, 5-20% biotite, 0-30% cordierite±garnet, trace pyrite, pyrrhotite, and magnetite. It also contains disseminated sulphides and small 1-100 cm chlorite-sulphide stringers. Toward the deposit the rhyolite is brecciated and crosscut by 1-30 cm chlorite-pyrrhotite-chalcopryrite stringers. The stringer zone consists of 40-80%, 0.1 to 2 m, rounded quartzite blocks in a sulphidic matrix. It is exposed on 690 mL subparallel to the po-cpy massive sulphide as a pod 100 m x <10 m x 300 m (Fig. 5, 6).

A chloritic schist partially to totally envelopes the ore zones. Its base is cordierite-, anthophyllite-, and chalcopryrite-bearing whereas the hangingwall is talc rich. The footwall chlorite schist contains <60% pyrite, pyrrhotite, magnetite with <5% chalcopryrite and trace sphalerite dominantly in stringers. Sphalerite is more abundant, ~5% in the hangingwall, with total disseminated sulfide content less than 40%. Anhydrite occurs as vug-like open space fillings with feldspar crystals in the chlorite schist and is intergrown with the ore.

Mineralization

The West Anomaly comprises three orebodies: (1) the Western lens (Zn), (2) the Eastern lens (Cu-Zn), and (3) the Hangingwall South lens (Cu-Zn) (Fig. 4, 5, 6). Two of the lenses are west of the section in Figure 6. The lowermost Eastern lens has a maximum true thickness of 30 m, is elongate east-northeast (070°) with a strike length of 350 m and plunge of 500 m. The Eastern lens is comparable in true thickness and plunge length but the strike length is shorter at 150 m. The Western and Eastern lenses are probably the same orebody displaced by the Art's Fault (Fig. 4). The Hangingwall South lens is still being delineated and is not described further (Fig. 6).

Stringer sulphide

The stringer mineralization can be divided into two spatially distinctive types: (1) rhyolite-hosted stringer and (2) chlorite schist-hosted stringer. The rhyolite-hosted stringer mineralization is located below both the Western and Eastern lenses with a zone of most intense stringer development at the west

limit of the Eastern lens (Fig. 5). The stringer dimension at the Eastern lens is less than that of the massive sulphide, and has a strike length of 30 m, a maximum thickness of 15 m and is elongate along plunge 175 m. The Western lens stringer zone is more extensive, with dimensions of 110 m strike length, 25 m wide and >330 m depth. The upper contact is gradational into the massive sulphide. The rhyolite-hosted stringer zone typically comprises 20-40% sulphide stringers within an altered rhyolite host but in the most intense stringer zone adjacent to the ore 70-80% of the zone is sulphide stringers. The stringers are 0.5 to 30 cm wide and contain 50-90% iron sulphides with a pyrite to pyrrhotite ratio of 1:>1, 0.5 to 50% chalcopryrite, <10% chlorite, <5% anhydrite and rare sphalerite. Rhyolite fragments are 10 cm to 2 m, angular to subrounded, and massive to weakly foliated. They are bleached, weakly chloritized, and may contain andalusite or anhydrite.

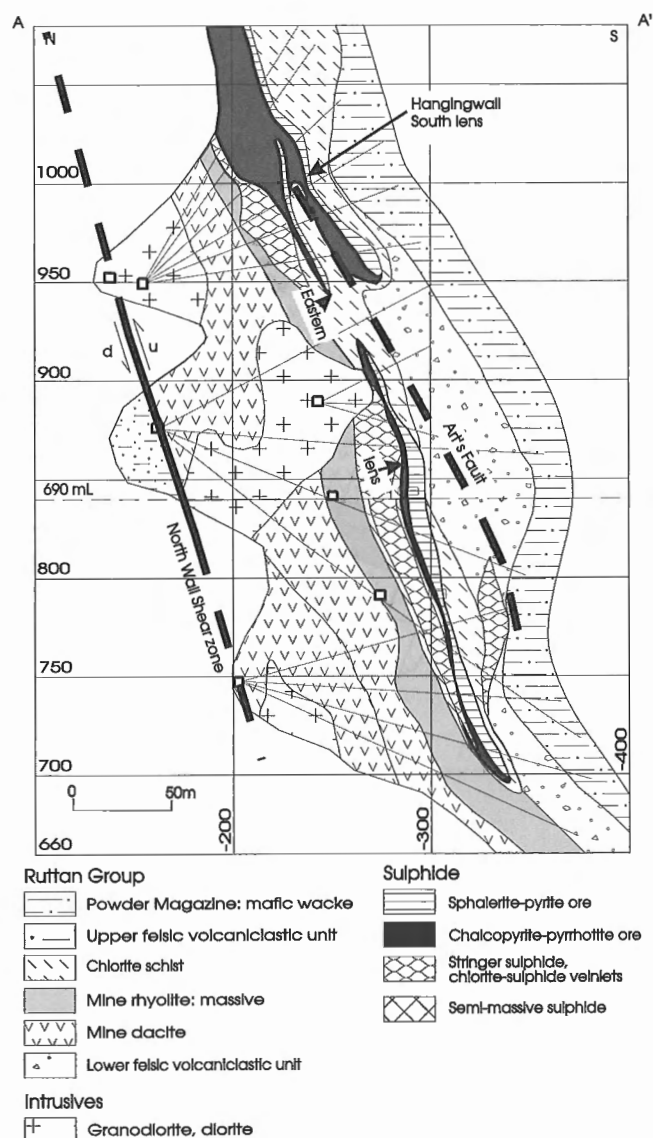


Figure 6. Geology of section 10 +00 E (A-A'; Fig. 5) across the Eastern lens of the West Anomaly.

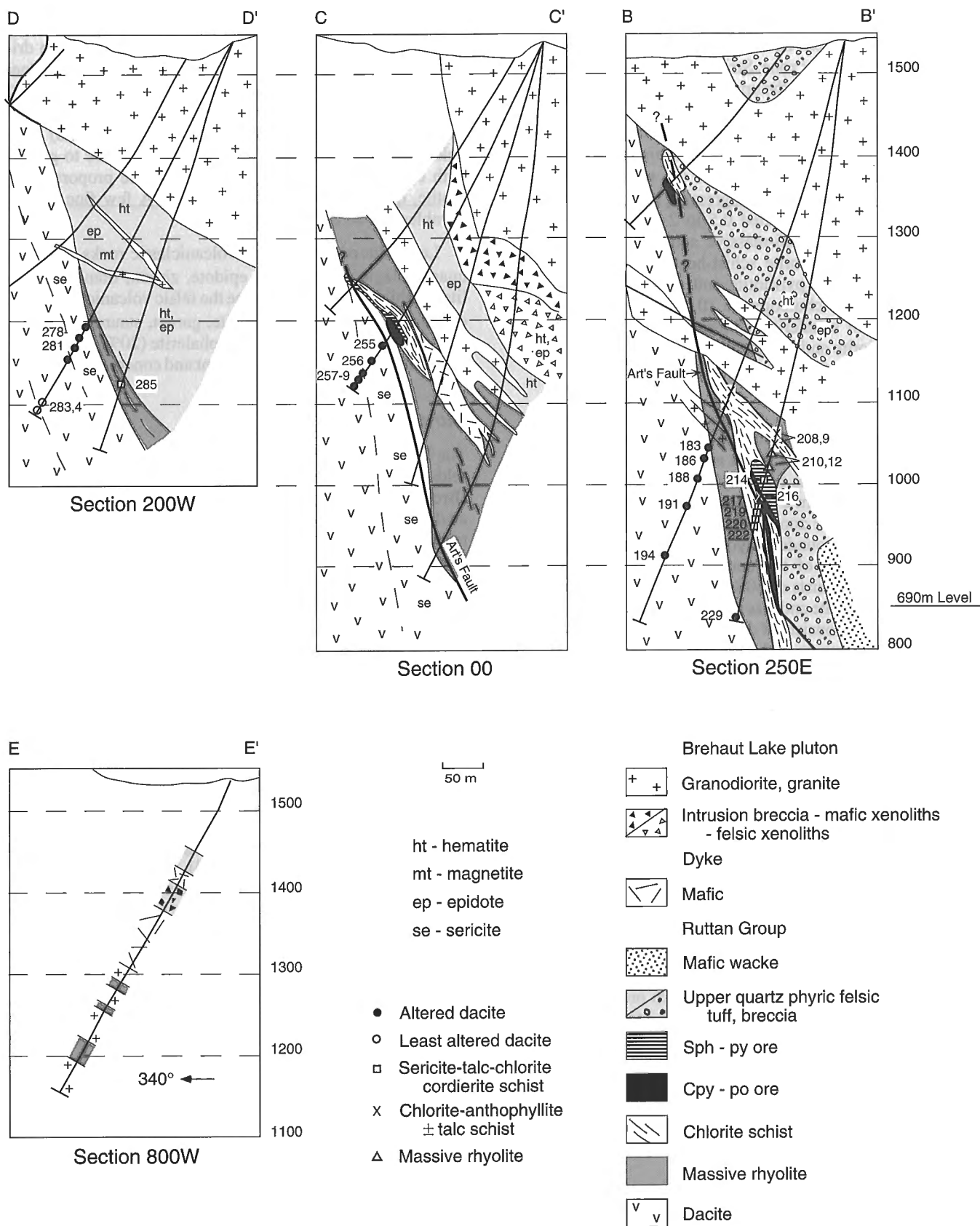


Figure 7. Sections displaying lateral variations in stratigraphy up to 1050 m west (E-E') of West Anomaly orebody (B-B'). Location of cross-sections shown in Figures 4 and 5. Sample locations noted.

The chlorite schist-hosted stringer mineralization is a tabular, laterally extensive zone, 1 to 10 m thick, that underlies most of the Eastern lens and is spatially exclusive of the rhyolite-hosted stringer zone. Stringers extend into the underlying altered rhyolite and the upper contact is gradational with the massive sulphide. There is a progression from chlorite schist, through sulphidic chlorite schist into massive sulphide. Distal to the massive ore the chlorite schist-hosted stringer consists of a chlorite schist with 1-2 cm sulphide pods and <10% disseminated sulphide progressing into a zone of chlorite schist with interconnected 0.5 to 2 cm wide, sulphide stringers and finally semi-massive sulphide with 1-30 cm chlorite pods. The chlorite schist-hosted stringers contain subequal amounts of pyrrhotite and pyrite with total iron sulphide (5-80%), chalcopyrite (0.5 to 30%), anhydrite (1-5%), and rare sphalerite. Chlorite is the most common silicate with biotite and talc locally abundant.

Cu-rich massive sulphide

Copper-rich massive ore is situated stratigraphically above the Mine rhyolite and chlorite schist and occurs only at the base of the Western lens. It is typically <10 m thick but thickness can change rapidly from 2 to 20 m due to deformation. At the basal 2-3 m, there are zones, less than 10 m in strike length, with 1 cm to 2 m rounded rhyolite and chloritic fragments which are remnants of the underlying stringer zone. The copper-rich ore consists of 60% pyrite, 30% pyrrhotite with 0.5 to 6% chalcopyrite and less than 1% sphalerite. Locally up to 20% of the ore consists of disseminated and massive magnetite. Magnetite occurs in the Eastern lens ore within 100 m of the North Wall shear as randomly oriented stringers. The silicate mineralogy is dominated by chlorite with only trace biotite or talc. Up to 5% anhydrite is intergrown with the ore. Although the ore is weakly to moderately foliated, boudinaged blocks of mafic dyke and granite are present.

Zn-rich massive sulphide

Zinc-rich ore within the Eastern lens occurs stratigraphically above the copper-rich ore as several pencil shaped zones 1 to 20 m thick, and having lengths of 30 to 85 m and extending >250 m in section (Fig. 6). The Western lens is predominantly zinc-bearing ore (Zn:Cu, 10:1). These Zn-rich massive sulphide lenses are dominated by 60-90% iron sulphides with a ratio of pyrite to pyrrhotite at 10:1. This contrasts with the pyrite to pyrrhotite ratio of the copper-rich ore which is 2:1. The modal amount of sphalerite varies from 3 to 30%, averages 10%, and chalcopyrite ranges from 0.5 to 6% with an average of 2%. The gangue is composed of <20% quartz, <10% chlorite, 2-10% anhydrite, trace biotite and talc. The ore is weakly to moderately foliated and has 0.5 to 5 cm thick bands containing >50% sphalerite alternating with pyrite-rich bands.

Upper felsic volcanoclastic rocks

The immediate hangingwall strata to the orebody consist of massive to bedded felsic volcanoclastic rocks that are typically quartz-phyric tuff to pebble breccia. The apparent width is variable from 10-50 m thick and the upper contact is sharp,

but locally obscured by silicification. A raft of the moderately altered, garnetiferous quartz-phyric felsic volcanoclastic rocks outcrop west of the open pit (Fig. 4, 7; B-B'). In drill core (Fig. 7) the sequence generally consists of a fine grained aphanitic base followed by, a fragmental unit with 15%, 2-6 mm felsic- and biotite-rich fragments and overlain by thinly laminated to thinly bedded (10 cm to 2-3 cm) felsic volcanoclastic rocks. Individual beds are massive to graded, with compositional banding due to variable proportions of biotite, quartz, feldspar, and actinolite. A few fine grained hornblende beds are present.

Least altered upper felsic volcanoclastic rocks consist of quartz, plagioclase, biotite, epidote, zircon, titanite±actinolite. Within 50 m of the ore zone the felsic volcanoclastic rocks contain quartz, biotite, ±sericite, garnet, staurolite, andalusite, and sillimanite. Pyrite and sphalerite (20%) are disseminated and occur as minor discordant and concordant stringers.

Intrusions

The Ruttan mine area has been intruded by early mafic and feldspar porphyry sills and dykes and a later granodiorite (Brehaut Lake pluton). Early mafic dykes and sills are foliated, boudinaged, and altered. The Brehaut Lake pluton contains randomly oriented and foliated xenoliths of the Mill Pond basalts and is undeformed at the northern end and deformed to the south (Ames, 1996). Dating of this pluton would bracket the last deformation event. Mafic dykes composed of hornblende, plagioclase±biotite, pyrrhotite and pyrite transect all supracrustal rocks.

WEST ANOMALY STRUCTURE

Strata within the northern Ruttan block generally strike 040° with minor, short strike length, east-striking fold limbs (Ames and Scoates, 1992; Ames, 1996). Bedding and structural facing are both south-southeast and the Ruttan mine is situated within a more easterly trending domain (Fig 4). In the immediate Ruttan mine area (Fig. 4), there is a minor flexure in the strike of bedding, from west to east, 055° to 070° and back to 055°. Structural measurements from surface outcrops are dominated by the western and eastern limbs of the flexure (Fig. 8a). The penetrative fabric is subparallel to bedding and is axial planar to minor Z-shaped F₁ folds in outcrop. This foliation has been gently folded about a northwest-trending axis at 116°/66° (Fig. 8b). The mineral stretching lineations and folds show a minor scatter about 125°/80°. Anomalous fold measurements are from rafted felsic volcanoclastic rocks within the Brehaut Lake pluton on the western edge of the open pit (see Fig. 7; B-B'). The coincidence of mineral lineation trend and plunge of minor folds and ore lenses was documented in the Ruttan Main mine (Speakman et al., 1982). The lower hemisphere, equal area projection of the poles to the foliation at depth in the West Anomaly show that the primary foliation has been folded about an axial trace trending 114° similar to that at surface, although the plunge is shallower (44°) at depth than at surface (66°) (Fig. 8c, d).

Shear zones within the Ruttan mine play a major role in controlling the present shape and distribution of ore lenses. Strata within the Ruttan mine, have been affected by a major shear zone, the North Wall shear and associated splay faults, Art's Fault and the East Fault (Speakman et al., 1982). Shear zones delineated through drill core and underground workings at depth in the West Anomaly project onto the North Wall shear at surface and Art's Fault on level 320. The North

Wall shear is a high angle reverse fault with south side up (Ames, 1991; Ames and Scoates, 1992) striking generally $070^{\circ}/70^{\circ}$ that contains a mineral stretch lineation $130^{\circ}/75^{\circ}$. On a local scale the foliation is transposed into the shear zone in a dextral manner. Similarly, the Eastern lens warps into the North Wall shear in a dextral sense within 40 m of the shear zone in plan view (Fig. 5) and is duplicated by Art's Fault up plunge as shown in Figure 6. Observations of Art's Fault in

RUTTAN MINE DOMAINS

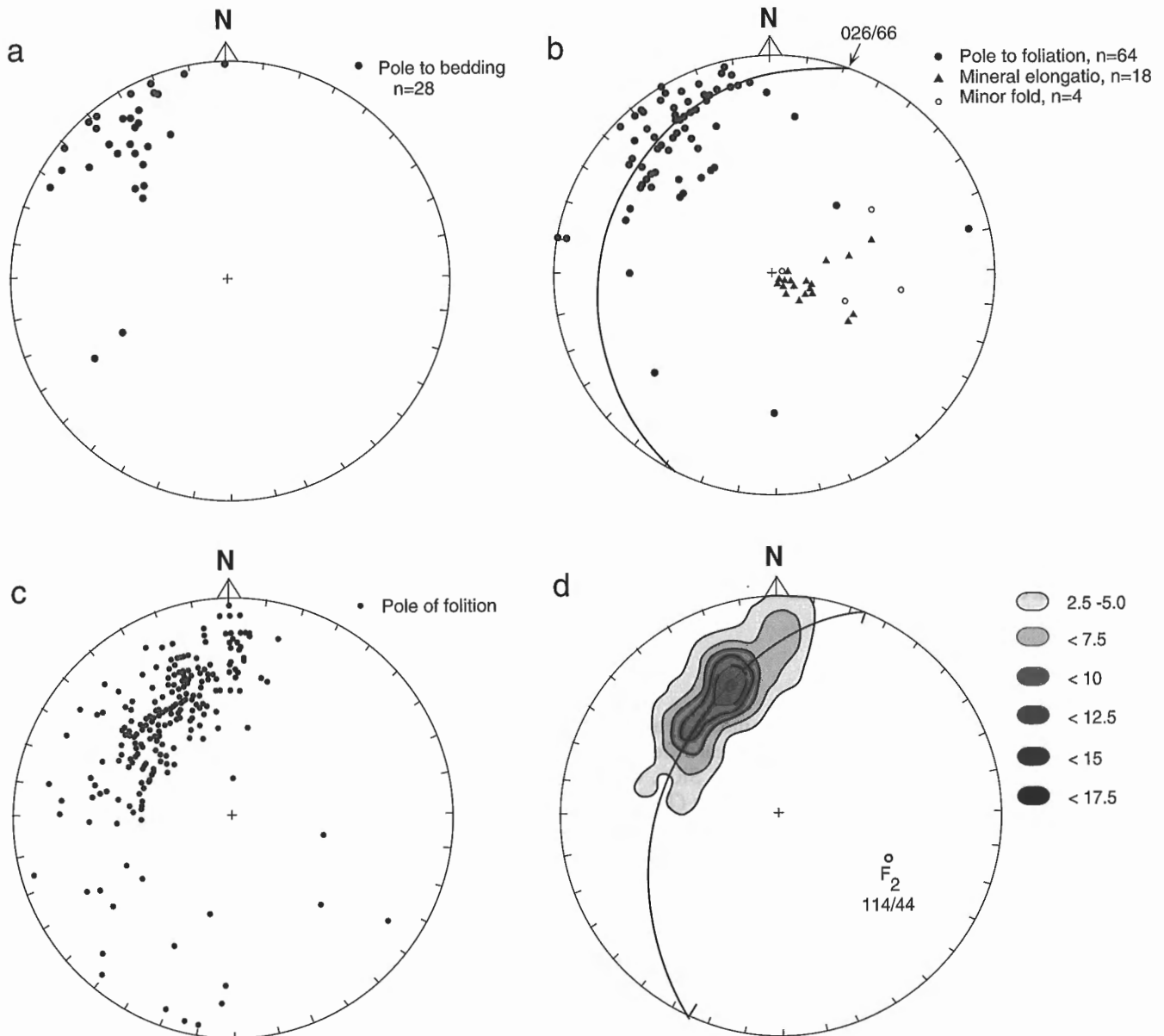


Figure 8. Lower hemisphere, equal area projection of poles to: a) surficial bedding measurements in Ruttan mine domain; b) foliation from Ruttan mine domain; c) foliation measurements from West Anomaly at depth; and d) contoured poles to foliation measurements in West Anomaly. Mineral stretching lineations and minor folds are also plotted in Figure 8b. Primary foliation has been folded about axis at $114^{\circ}/44^{\circ}$. F_2 fold axis, plunge of ore zones, and mineral lineations are coincident.

drillcore reveal fractured cubic pyrite grains, crenulated anthophyllite and biotite and, to the west, crenulated sericite. This suggests a post-penetrative (F_1) cleavage development of the shear zones.

GEOCHEMICAL METHODOLOGY

Ninety-three samples were collected for analyses to classify the volcanic rocks and to determine, the geological environment of the West Anomaly and the extent of metasomatism. Eighty were analyzed at the Geological Survey of Canada laboratories whereas 13 samples were analyzed in other laboratories. Hidden standards were included to compare the precision of different laboratories. The methods used include inductively coupled plasma (ICP-ES), atomic absorption spectrometry (AAS), combustion and wet chemical methods. REE analyses were determined by ICP-MS at Memorial University and at the Geological Survey of Canada (samples 250, 170, 171, 292 and 284).

GEOCHEMISTRY OF LEAST ALTERED MINE STRATIGRAPHY

Dacite geochemistry

Sixteen massive dacite samples from four diamond-drill holes in sections A-A' to D-D' and six additional samples from 630 mL were collected (Fig. 5, 6, 7), which included two least altered dacite (Table 2). The least altered dacite plots in a field on a TiO_2/Zr bivariate plot (Fig. 9) and a $Ti/10, Zr, Y*3$ ternary diagram (Fig. 10a) that overlaps with least altered Junction dacitic rocks and dacitic rocks that outcrop south of the mine site. On a chondrite normalized REE plot the mine dacite shows a slight LREE enrichment ($La_n/Yb_n = 3$), fairly flat HREE at concentrations 20X chondrite and a pronounced negative Eu anomaly (Fig. 11a).

Felsic geochemistry

The Lower felsic volcanoclastic rocks show a moderate amount of chemical variability due to modal mineralogical differences in beds but generally contain 69.2-73.5 wt. % SiO_2 , 0.25-0.4 wt. % TiO_2 , 120-150 ppm Zr, and 8% alkalis (Table 2). Three samples were collected from the 630 mL of the West Anomaly and one on the northwestern edge of the open pit. The Lower felsic volcanoclastic strata lie in a distinct field relative to the dacitic strata on a $Ti/10, Zr, Y*3$ diagram (Fig. 10b) even though the REE profiles are similar in pattern and concentration to the Mine dacite (Fig. 11b). The La_n/Yb_n ratio of the Lower felsic volcanoclastic rocks is slightly higher at 4.3.

In general, the Upper felsic volcanoclastic rocks are more silica-rich than the Lower felsic volcanoclastic rocks although the Upper felsic rocks contain minor dacitic beds. Seven samples were collected from drillholes and on surface west of the open pit. The average rhyolite bed and dacite bed analyses are listed in Table 2. In samples from sections C-C', D-D', and E-E', SiO_2 ranges from 72.4-75.9 wt. %, TiO_2 0.19-0.34

wt. %, Zr 120-170 ppm, and total alkalis <7 wt. % in the felsic beds. The field of the Upper volcanoclastic rocks overlaps with the Mine dacite and the Lower felsic volcanoclastic rocks on a $Ti/10, Zr, Y*3$ ternary diagram (Fig. 10b). The REE profile of the Upper felsic rocks has a gentler LREE enriched

Table 2. Average analytical results of least altered rock types in West Anomaly, Ruttan mine area.

| | Dacite n=2 | LFV n=4 | UFV-r n=5 | UFV-d n=2 | MR-rex n=10 |
|------------|---------------|------------|--------------|--------------|----------------|
| SiO_2 | 68.15 | 71.45 | 73.36 | 66.9 | 71.42 |
| TiO_2 | 0.43 | 0.3575 | 0.314 | 0.56 | 0.34 |
| Al_2O_3 | 14.05 | 13.5 | 12.3 | 14.35 | 12.38 |
| Fe_2O_3T | 6.5 | 4.875 | 4.84 | 6.75 | 6.14 |
| Fe_2O_3 | 1.3 | 0.95 | 0.76 | 1.3 | 2.70 |
| FeO | 4.7 | 3.525 | 2.66 | 4.9 | 2.82 |
| MnO | 0.145 | 0.09 | 0.088 | 0.105 | 0.08 |
| MgO | 2.265 | 1.515 | 1.612 | 1.94 | 1.01 |
| CaO | 3.075 | 3.1775 | 2.504 | 4.08 | 3.26 |
| Na_2O | 2.3 | 3 | 1.76 | 2.8 | 1.81 |
| K_2O | 2.14 | 1.4425 | 1.952 | 1.77 | 1.88 |
| H_2OT | 0.95 | 1.05 | 0.86 | 1 | 1.20 |
| CO_2T | 0.05 | 0.025 | 0.02 | 0.2 | 0.32 |
| P_2O_5 | 0.13 | 0.1075 | 0.076 | 0.135 | 0.08 |
| S | 0.04 | 0.12 | 0.492 | 0.17 | 0.779 |
| Ba | 515 | 510 | 698 | 355 | 725 |
| Be | 1.15 | 1.125 | 0.78 | 0.8 | 0.83 |
| Co | 10.5 | 10.75 | 8.4 | 11.5 | 6.9 |
| Cr | 5.5 | 0 | 2 | 5 | 123.3 |
| Cu | 89 | 44.75 | 44.6 | 32.5 | 3.616 |
| La | 14 | 16 | 15.2 | 12.5 | 15.7 |
| Nb | 10 | 7.5 | 403.6 | 6.5 | 4.7 |
| Ni | 999 | 0 | 402.6 | 9.5 | 7.6 |
| Pb | 0 | 0 | 19.4 | 17 | 11 |
| Rb | 47.5 | 38.5 | 48 | 36 | 35.5 |
| Sc | 16.5 | 14.5 | 11.72 | 18 | 12.08 |
| Sr | 245 | 287.5 | 182 | 265 | 163.4 |
| V | 10.5 | 8.25 | 208.6 | 30.5 | 28.4 |
| Y | 25.5 | 25.75 | 34.4 | 30 | 27.7 |
| Yb | 2.65 | 2.9 | 3.7 | 3.45 | 3.53 |
| Zn | 72 | 71 | 145 | 135 | 124 |
| Zr | 120 | 130 | 144 | 125 | 138.8 |

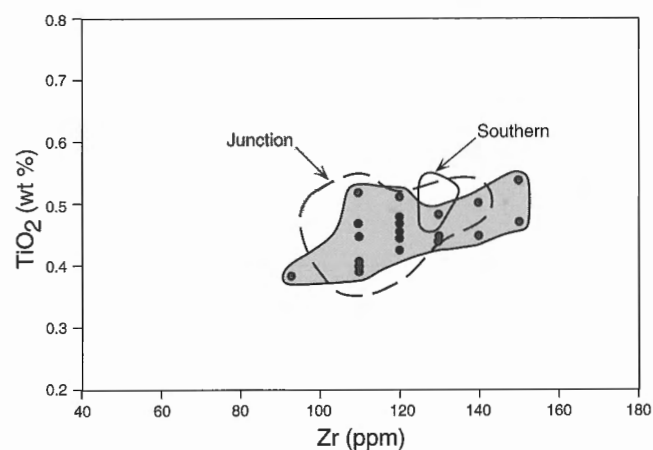


Figure 9. Bivariate TiO_2 vs. Zr plot of Mine dacite (shaded) compared with Junction dacite and Southern dacite.

slope than the footwall felsic rocks, a flat HREE pattern ($La_n/Yb_n=2.3$), and a pronounced negative Eu anomaly (Fig. 11c).

ALTERATION MINERALOGY

A summary of representative alteration assemblages observed petrographically are listed in Table 3.

Mine dacite

Mineralogy

The altered dacite consists of quartz, plagioclase, biotite, andalusite, staurolite±garnet, cordierite, sillimanite, and trace pyrite, pyrrhotite, magnetite, chalcopyrite, rutile, zircon, and apatite. It

is crosscut by 1 cm to 1 m wide, chlorite-garnet-sulphide stringers. The dacite below the Eastern and Western lenses consists of a fine grained (0.1-0.5 mm) quartz/feldspar matrix with 15% 0.2-1 mm biotite, 20-25% 1-2 mm poikilitic staurolite, and rare andalusite, garnet, and cordierite porphyroblasts. Trace amounts of sillimanite, pyrite, pyrrhotite, magnetite, chalcopyrite, rutile, zircon, and apatite are present. Ragged skeletal porphyroblasts of andalusite commonly occur as cores within cordierite porphyroblasts. The footwall dacite is crosscut by 1 cm to 1 m wide, chlorite-garnet-sulphide stringers. At section D-D' (Fig. 7) the mineralogy of the dacite changes to a dominantly quartzose matrix with 20-25% biotite, 10-15% staurolite, 5% andalusite,

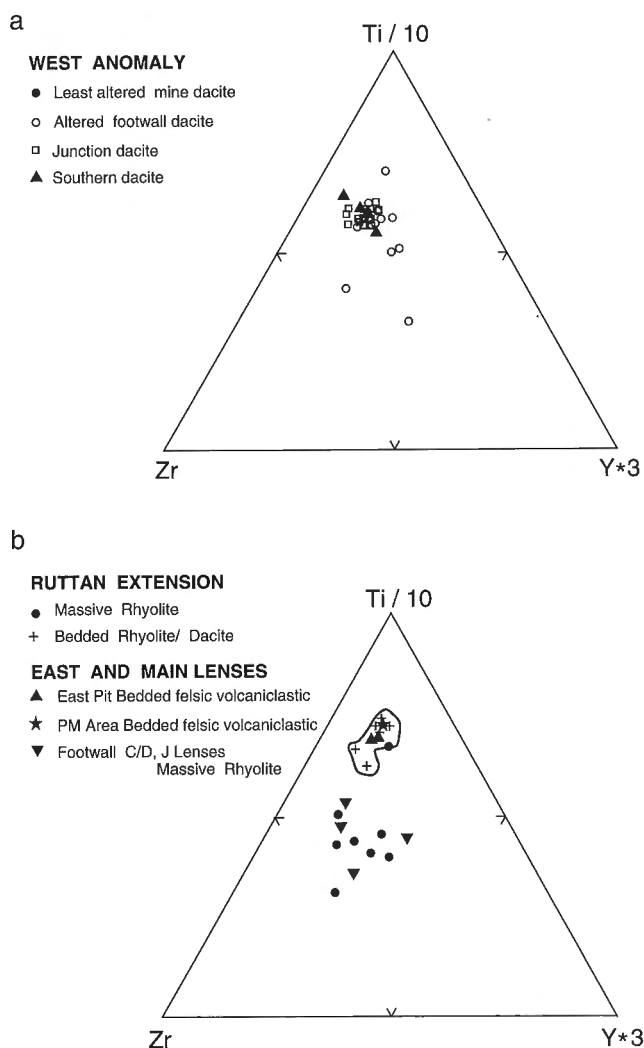


Figure 10. Ternary diagram (Ti/10, Zr, Y*3) of **a**) Mine dacite in relation to Junction and Southern dacite from regional data (Ames, 1996), and **b**) massive and bedded rhyolites in Ruttan mine and those in Ruttan extension. Massive and bedded units lie in distinct fields with those in mine environment and Ruttan extension overlapping.

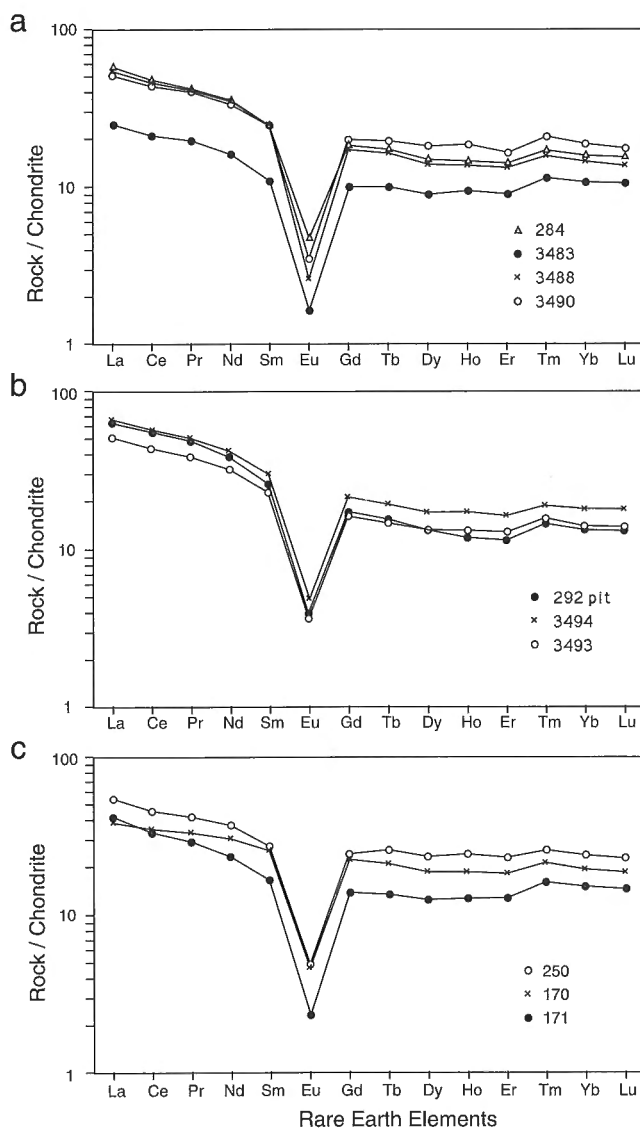


Figure 11. Chondrite-normalized REE profiles of **a**) Mine dacite in West Anomaly, **b**) Lower felsic volcaniclastic rocks, and **c**) Upper (hangingwall) quartz-phyric felsic volcanoclastic rocks in West Anomaly. Normalizing values are those of Sun and Nesbitt (1978); Pr, Tb and Tm values are from Haskin et al. (1968).

20-25% cordierite, 10-15% sericite, and <3% garnet. Sericite (<4 mm) crosscuts biotite, grows around staurolite, and locally is associated with retrograde chlorite.

Mine rhyolite

Footwall to massive sulphide deposit

Close to the dacite contact, the assemblage is 40% quartz, 30% cordierite, 10% biotite, 5% staurolite, 2-5% garnet, <15% pyrite, and magnetite. The Mine rhyolite below the chlorite schist consists of a fine grained 50-60% quartzose matrix with 20% talc, 10% chlorite, pyrrhotite, chalcopyrite, and pyrite. Pyrite cubes overprint pyrrhotite. Along the

western fringe of the ore lens the Mine rhyolite becomes sericitic as described below. In section D-D' (Fig. 7) the Mine rhyolite consists of 20-25% cordierite, 25% biotite, 40% quartz, and trace andalusite, sericite and garnet.

Rhyolite-hosted stringer zone

At the top of the stringer zone are areas of semi-massive sulphide that consist of 30% fine grained (1 mm) polycrystalline quartz, 30% cubic pyrite, 15% gahnite, 5% pyrrhotite and chalcopyrite, and trace chlorite and biotite. Pyrite and sphalerite are associated as are chalcopyrite-pyrrhotite and gahnite-pyrrhotite. At the base of the stringer zone, stringers

Table 3. Representative mineral assemblages of alteration zones in West Anomaly.

| | Qz | Pg | Mu | Bi | Si | An | St | Cd | Gt | Oa | Ta | Ac | Gh | Cl | Py | Po | Sph | Cpy | Mt | Ilm | Rt | Acc |
|--|----|----|----|----|----|----|----|----|----|----|----|----|----|----|----|----|-----|-----|----|-----|----|-----|
| MINE DACITE | | | | | | | | | | | | | | | | | | | | | | |
| 90av257 | o | | o | o | | o | | o | | | | | | s | | | | | | | | |
| 258 | o | | | o | o | o | o | o | | | | | | s | | | | | | | | |
| 259 | o | | | o | | | o | o | | | | | | | | | | | | | o | |
| 279 | o | | | o | o | | o | | o | | | | | | | | | | | | | |
| 280 | o | | | o | | o | | o | | | | | | s | | | | | | | | |
| 281 | o | | | o | o | | o | o | | | | | | | | | | | | | | |
| 285 | o | | | o | o | o | | o | o | | | | | | | | | | | | | |
| 89av007 | | | | | | | | | | | | | | | | | | | | | | |
| 011 | | * | | o | o | o | * | o | | | | | | | | | | | | | | |
| MINE RHYOLITE | | | | | | | | | | | | | | | | | | | | | | |
| Least altered | | | | | | | | | | | | | | | | | | | | | | |
| 90av221 | o | o | o | o | | | | | | | | | | | o | | | o | | | | |
| 251 | o | | o | o | o | | | | | | | | | s | o | o | | o | | | | |
| 252 | o | | s | o | | | o | | o | | | | | s | | | | | | | | |
| Intensely altered | | | | | | | | | | | | | | | | | | | | | | |
| 91av744 | | o | | o | | | o | o | | | | | | s | o | o | o | o | | | | |
| 745 | | | | o | | | | o | o | o | | o | | o | | o | o | o | | | | ap |
| 90av210 | o | o | o | | | | | | | | | | | | | | | | | | | |
| 212 | | o | o | | o | | | | | | | | | | | o | o | o | | | | |
| Rhyolite-hosted stringer | | | | | | | | | | | | | | | | | | | | | | |
| 91av741 | o | | | o | | | | o | | | | | o | o | o | o | o | o | | | | |
| Chlorite-anthophyllite schist | | | | | | | | | | | | | | | | | | | | | | |
| 91av742 | | | | | | | | o | | o | | | | | o | o | o | o | | | | zi |
| 90av254 | o | | | o | | | | o | | o | | | | | | o | | o | o | | | ap |
| 89av010 | o | | | * | | | | * | | * | | | | * | | | | | o | o | | |
| 022 | | | | * | | | | * | | * | | | | * | | | | | o | | | ap |
| Chlorite schist | | | | | | | | | | | | | | | | | | | | | | |
| 91av737 | | | | o | | | o | | | | | | | o | | o | o | o | | | | ti |
| 90av217 | o | o | o | o | o | | | o | | | o | | | | | | | | | | | |
| 219 | o | | | | | | | o | | | o | | | | o | | | | | | | |
| 220 | | o | | | | | | | | | | | o | | | | | | | | | |
| 89av019 | | * | | * | | | o | | | | | | * | * | | | o | | | | | |
| o present Qz - quartz Bi - biotite St - staurolite Oa - orthoamphibole | | | | | | | | | | | | | | | | | | | | | | |
| * probed Pg - plagioclase Si - sillimanite Cd - cordierite Ta - talc | | | | | | | | | | | | | | | | | | | | | | |
| s secondary Mu - muscovite An - andalusite Gt - garnet Ac - actinolite | | | | | | | | | | | | | | | | | | | | | | |
| Gh - gahnite Cl - chlorite Py - pyrite Po - pyrrhotite | | | | | | | | | | | | | | | | | | | | | | |
| Sph - sphalerite Cpy - chalcopyrite Mt - magnetite Ilm - ilmenite | | | | | | | | | | | | | | | | | | | | | | |
| Rt - rutile Acc - accessories ap - apatite zi - zircon | | | | | | | | | | | | | | | | | | | | | | |
| ti - titanite | | | | | | | | | | | | | | | | | | | | | | |

that extend into the Mine rhyolite consist of 70% cordierite, 10-15% anthophyllite, 10% chlorite, trace apatite, biotite, and garnet, and pyrrhotite, chalcopyrite and rare sphalerite.

Chlorite schist

Chlorite-anthophyllite schist surrounding the Eastern lens consists of 35% chlorite, 40% biotite, \pm 10% anthophyllite with magnetite, anhydrite, and chalcopyrite, \pm 10% staurolite, titanite with pyrrhotite, chalcopyrite, sphalerite. Anhydrite occurs as large porphyroblasts with quartz, feldspar, chalcopyrite, and magnetite inclusions. Feldspar occurs as large (>2 cm) euhedra. West of the Western lens along section B-B' (Fig. 7) the chlorite schist contains 20-25% anthophyllite, 25% chlorite, and 5-10 % feldspar that is partially to totally replaced by 15% sericite and 30% combined honey coloured (low Fe) sphalerite and pyrite. Minor chalcopyrite occurs as inclusions in pyrite and anthophyllite porphyroblasts. Locally the schist is dominated by biotite-anthophyllite-cordierite. Chlorite-anthophyllite schist also occurs as discontinuous pods and stringers within the Mine rhyolite with 40% 2 mm anthophyllite, 30% cordierite, trace andalusite with 10% sphalerite, 15% pyrite, and 5% chalcopyrite along foliation planes. Pyrite occurs as cubic overgrowths that are interpreted as metamorphic and as fine anhedral grains associated with sphalerite and pyrrhotite. Anthophyllite is common in the West Anomaly but the

Table 4. Microprobe analyses of cordierite.

| | 89-22 n=1 | 89-10 Avg. | SD n=6 |
|--------------------------------|--------------|---------------|-----------|
| SiO ₂ | 49.4 | 49.49 | 0.23 |
| Al ₂ O ₃ | 33.35 | 33 | 0.26 |
| TiO ₂ | 0.02 | 0.01 | 0.01 |
| Fe ₂ O ₃ | 0 | 0 | 0 |
| MgO | 11.13 | 10.6 | 0.08 |
| FeO | 0 | 0 | 0 |
| MnO | 0.13 | 0.1 | 0.02 |
| Na ₂ O | 0.26 | 0.21 | 0.01 |
| CaO | 0.01 | 0.01 | 0.01 |
| K ₂ O | 0 | 0.01 | 0.02 |
| TOTAL | 94.3 | 93.43 | 0.21 |
| FORMULA (BASIS 18 OXYGENS) | | | |
| Si | 5.089 | 5.136 | 0.02 |
| Al | 0.911 | 0.864 | 0.02 |
| | 6 | 6 | 0 |
| Al | 3.138 | 3.173 | 0.013 |
| Ti | 0.001 | 0.001 | 0.001 |
| Fe ⁺³ | 0 | 0 | 0 |
| | 3.139 | 3.174 | 0.012 |
| Mg | 1.709 | 1.64 | 0.012 |
| Fe ⁺² | 0 | 0 | 0 |
| Mn | 0.011 | 0.009 | 0.002 |
| Na | 0.052 | 0.043 | 0.003 |
| Ca | 0.001 | 0.001 | 0.001 |
| K | 0 | 0.001 | 0.002 |
| | 1.773 | 1.694 | 0.014 |

chlorite schists in the West and East lenses in the Ruttan mine are void of anthophyllite and are typically composed of chlorite, andalusite, cordierite, garnet \pm biotite (Speakman et al., 1982).

Sericite schist

Enveloping the ore on the western fringe of the Western lens is a sericite schist. The schist consists of a 10-15% quartz-plagioclase matrix, with 25% sillimanite, 35% sericite, and 25% chalcopyrite-pyrrhotite-sphalerite stringers, and minor arsenopyrite, marcasite, and cubic pyrite.

In the immediate footwall to uneconomic mineralization are sericitic zones that lie along the projected Art's Fault. These consist of 15-60% sericite, 25-40% cordierite, biotite in a quartz, pyrite matrix \pm plagioclase, sillimanite, talc, garnet, andalusite, and chlorite.

Table 5. Microprobe analyses of anthophyllite.

| | 89-10 AVERAGE n=6 | SD | 89-22 AVERAGE n=5 | SD |
|--------------------------------|-------------------------|-------|-------------------------|-------|
| SiO ₂ | 53.32 | 0.47 | 53.37 | 0.66 |
| Al ₂ O ₃ | 2.67 | 0.64 | 3.22 | 0.85 |
| TiO ₂ | 0.05 | 0.03 | 0.05 | 0.01 |
| Cr ₂ O ₃ | 0.01 | 0.01 | 0.02 | 0.02 |
| Fe ₂ O ₃ | 0.00 | 0.22 | 0 | 0.59 |
| FeO | 20.72 | 0.70 | 19.92 | 0.57 |
| MnO | 0.51 | 0.05 | 1.13 | 0.27 |
| MgO | 19.17 | 0.32 | 19.68 | 0.36 |
| CaO | 0.17 | 0.01 | 0.22 | 0.04 |
| Na ₂ O | 0.28 | 0.11 | 0.38 | 0.12 |
| K ₂ O | 0.01 | 0.01 | 0.01 | 0.01 |
| TOTAL | 96.91 | 1.03 | 98.00 | 0.35 |
| FORMULA (BASIS 23 OXYGENS) | | | | |
| Si | 7.751 | 0.086 | 7.667 | 0.085 |
| Al | 0.249 | 0.086 | 0.333 | 0.085 |
| | 8.000 | 0.000 | 8.000 | 0.000 |
| Al | 0.208 | 0.049 | 0.213 | 0.076 |
| Ti | 0.005 | 0.003 | 0.006 | 0.001 |
| Cr | 0.001 | 0.001 | 0.002 | 0.002 |
| Fe ⁺³ | 0.000 | 0.024 | 0 | 0.064 |
| Fe ⁺² | 2.519 | 0.076 | 2.393 | 0.062 |
| Mn | 0.062 | 0.007 | 0.138 | 0.034 |
| Mg | 4.153 | 0.063 | 4.214 | 0.074 |
| Ca | 0.027 | 0.002 | 0.033 | 0.006 |
| Na | 0.025 | 0.026 | 0.001 | 0.014 |
| | 7.000 | 0.011 | 7.000 | 0.000 |
| Na | 0.053 | 0.044 | 0.106 | 0.038 |
| K | 0.002 | 0.001 | 0.002 | 0.002 |
| | 0.055 | 0.045 | 0.108 | 0.038 |
| Fm | 0.378 | 0.010 | 0.362 | 0.007 |

Metamorphism and mineral chemistry

Mineral analyses were determined on a CAMEBAX electron microprobe with wavelength dispersion spectrometers at the Geological Survey of Canada. The mineral assemblages associated with the probed minerals are listed in Table 3. Stable assemblages in the cordierite-anthophyllite schists include cordierite-anthophyllite-biotite-chlorite-magnetite± ilmenite, pyrite, pyrrhotite, chalcopyrite of which cordierite, anthophyllite, chlorite and biotite were probed (Tables 4-7). Staurolite and plagioclase from an aluminous alteration

assemblage were analyzed (Tables 8-9). Chlorite, plagioclase, and gahnite were analyzed from the intensely altered rhyolite (Tables 6, 9, 10).

The chemical composition of the chlorite within the cordierite-anthophyllite schists and the intensely altered rhyolite form a tight cluster on the sheridanite to ripidolite border on an Fe/Fe+Mg vs. Si (Hey, 1954) diagram (Fig. 12).

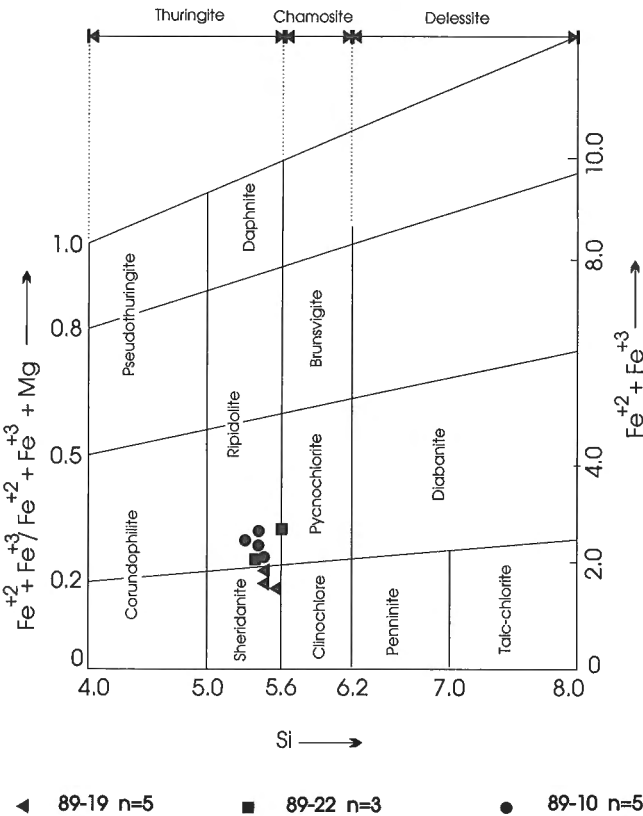


Figure 12. Chlorite compositions within West Anomaly alteration zones (after Hey, 1954).

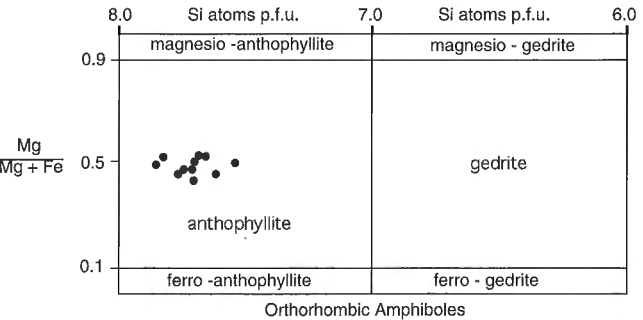


Figure 13. Orthorhombic amphibole classification diagram (Leake, 1978).

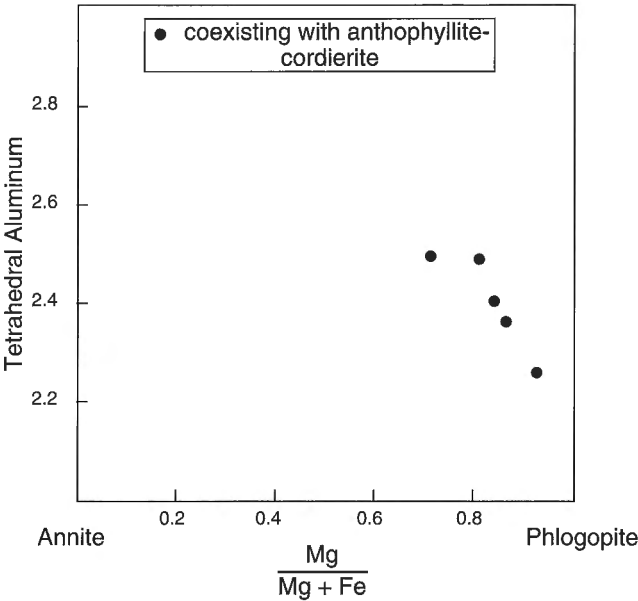


Figure 14. Classification of biotite species in West Anomaly strata.

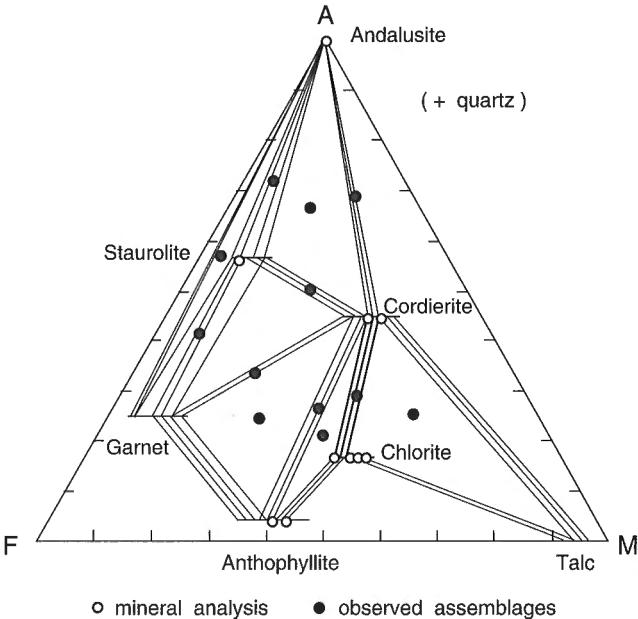


Figure 15. AFM diagram of stable assemblages in West Anomaly alteration zones displaying observed and analyzed assemblages.

These cordierite-chlorite-anthophyllite schists contain Mg-rich chlorites; the orthoamphiboles are anthophyllite proper (Fig. 13) and the coexisting biotite is phlogopite-rich (Fig. 14).

Feldspar compositions within the Junction volcanoclastic rocks distal to the deposit are anorthite-rich (An_{45}) whereas in the intensely altered rhyolite and in the staurolite-andalusite-bearing dacite the feldspars are more sodic (An_{18} and An_{25} , respectively).

The stable assemblages observed in the West Anomaly alteration zones can be shown in an AFM diagram (Fig. 15). The diagram is based on the probed mineral analyses reported except for garnet and talc and, the observed mineral assemblages have been shown. A typical almandine garnet composition was assumed. Tielines are schematic yet constrained by the mineral compositions. Based on the mineral compatibilities the assemblages observed in the West Anomaly area suggest a pressure less than 4 kbars and temperature between 525 and 600°C, using the PT grid of Carmichael (Fig. 16) (Davidson et al., 1990).

Table 6. Microprobe analyses of chlorite.

| | 89-22 | | 89-10 | | 89-19 | |
|--------------------------------|----------------|-------|----------------|-------|----------------|-------|
| | Average n=3 | SD | Average n=5 | SD | Average n=5 | SD |
| SiO ₂ | 27.22 | 0.83 | 26.42 | 0.28 | 27.06 | 35 |
| Al ₂ O ₃ | 22.06 | 0.45 | 22.09 | 0.31 | 21.36 | 0.41 |
| TiO ₂ | 0.07 | 0.06 | 0.07 | 0.01 | 0.1 | 0.03 |
| Cr ₂ O ₃ | 0.03 | 0.02 | 0.01 | 0.01 | 0 | 0.01 |
| FeO | 16.15 | 0.34 | 16.15 | 0.71 | 14.18 | 0.86 |
| MnO | 0.19 | 0.01 | 0.05 | 0.04 | 0.15 | 0.06 |
| MgO | 21.65 | 0.74 | 21.35 | 0.42 | | |
| CaO | 0.01 | 0.01 | 0.01 | 0.01 | 0.02 | 0.01 |
| Na ₂ O | 0.02 | 0.02 | 0.01 | 0.01 | 0.01 | 0.01 |
| K ₂ O | 0.35 | 0.61 | 0.01 | 0.01 | 0.02 | 0.02 |
| F | 0.16 | 0.09 | 0.16 | 0.06 | 0.11 | 0.05 |
| Cl | 0.02 | 0.01 | 0.02 | 0.01 | 0.01 | 0.01 |
| TOTAL | 87.93 | 0.84 | 86.35 | 1.26 | 86.43 | 1.75 |
| TOT-O | 87.86 | 0.81 | 86.28 | 1.26 | 86.38 | 1.77 |
| FORMULA (BASIS 28 OXYGENS) | | | | | | |
| Si | 5.452 | 0.144 | 5.383 | 0.046 | 5.452 | 0.033 |
| Al | 2.548 | 0.144 | 2.617 | 0.046 | 2.548 | 0.033 |
| | 8.000 | 0 | 8.000 | 0 | 8.000 | 0 |
| Al | 2.661 | 0.027 | 2.688 | 0.034 | 2.525 | 0.048 |
| Ti | 0.011 | 0.008 | 0.011 | 0.002 | 0.015 | 0.004 |
| Cr | 0.004 | 0.003 | 0.002 | 0.002 | 0.001 | 0.001 |
| Fe | 2.705 | 0.042 | 2.753 | 0.105 | 2.39 | 0.106 |
| Mn | 0.032 | 0.002 | 0.009 | 0.006 | 0.026 | 0.01 |
| Mg | 6.466 | 0.247 | 6.485 | 0.083 | 7.031 | 0.056 |
| Ca | 0.003 | 0.002 | 0.002 | 0.003 | 0.003 | 0.002 |
| Na | 0.008 | 0.008 | 0.004 | 0.006 | 0.006 | 0.004 |
| K | 0.089 | 0.153 | 0.002 | 0.002 | 0.004 | 0.004 |
| | 11.979 | 0.014 | 11.956 | 0.036 | 12.001 | 0.032 |
| F | 0.101 | 0.059 | 0.100 | 0.04 | 0.071 | 0.031 |
| Cl | 0.006 | 0.004 | 0.007 | 0.004 | 0.003 | 0.002 |
| | 0.107 | 0.063 | 0.107 | 0.044 | 0.074 | 0.032 |

ALTERATION GEOCHEMISTRY

Gross geochemical trends associated with hydrothermal alteration at the Ruttan mine are shown on an unfolded FCAK tetrahedron ((Na₂O+CaO), (FeO+MgO), K₂O and Al₂O₃ on the apices) for the two main protoliths in the footwall rocks (Fig 17a, b). The FeO+MgO apice represents mainly chlorite (lesser anthophyllite, cordierite), CaO+Na₂O is unique for feldspar and K is dominantly sericite. Al₂O₃ represents the least mobile component during most alteration events. Each alteration type is shown relative to the field defined by the least altered parent which was selected by petrographic (lack of alteration minerals) and chemical means described in detail below. The gross chemical changes of the Mine dacite relative to the regional least altered Junction dacitic volcanoclastic

Table 7. Microprobe analyses of biotite.

| | 89-22 | 89-19 | 89-10 | SD |
|--------------------------------|-------|-------|----------------|-------|
| | n=1 | n=1 | n=4 Average | |
| SiO ₂ | 37.99 | 39.35 | 38.82 | 0.38 |
| Al ₂ O ₃ | 16.98 | 14.77 | 16.67 | 0.42 |
| TiO ₂ | 1.01 | 0.92 | 0.95 | 0.03 |
| Cr ₂ O ₃ | 0.00 | 0.05 | 0.02 | 0.02 |
| FeO | 12.01 | 12.14 | 12.21 | 0.97 |
| NiO | 0.00 | 0.00 | 0.00 | 0.00 |
| MnO | 0.07 | 0.10 | 0.06 | 0.03 |
| MgO | 16.92 | 18.22 | 16.93 | 0.14 |
| CaO | 0.00 | 0.02 | 0.02 | 0.02 |
| BaO | 0.17 | 0.26 | 0.25 | 0.05 |
| Na ₂ O | 0.44 | 0.37 | 0.37 | 0.09 |
| K ₂ O | 7.55 | 7.88 | 7.91 | 0.14 |
| F | 0.81 | 1.01 | 1.02 | 0.05 |
| Cl | 0.05 | 0.03 | 0.03 | 0.01 |
| TOTAL | 94.00 | 95.12 | 95.26 | 0.54 |
| TOT-O | 93.65 | 94.69 | 94.82 | 0.52 |
| FORMULA (BASIS 22 OXYGENS) | | | | |
| Si | 5.641 | 5.803 | 5.709 | 0.058 |
| Al | 2.359 | 2.197 | 2.291 | 0.058 |
| Ti | 0.000 | 0.000 | 0.000 | 0.000 |
| | 8.000 | 8.000 | 8.000 | 0.000 |
| Al | 0.613 | 0.371 | 0.599 | 0.053 |
| Ti | 0.112 | 0.102 | 0.105 | 0.003 |
| Cr | 0.000 | 0.006 | 0.002 | 0.002 |
| Fe | 1.492 | 1.497 | 1.501 | 0.120 |
| Ni | 0.000 | 0.000 | 0.000 | 0.000 |
| Mn | 0.008 | 0.012 | 0.007 | 0.004 |
| Mg | 3.745 | 4.005 | 3.713 | 0.031 |
| | 5.970 | 5.993 | 5.927 | 0.045 |
| Ca | 0.000 | 0.003 | 0.003 | 0.002 |
| Ba | 0.010 | 0.015 | 0.014 | 0.003 |
| Na | 0.126 | 0.106 | 0.107 | 0.026 |
| K | 1.430 | 1.484 | 1.485 | 0.024 |
| | 1.566 | 1.608 | 1.609 | 0.022 |
| F | 0.380 | 0.473 | 0.475 | 0.024 |
| Cl | 0.013 | 0.009 | 0.008 | 0.003 |
| | 0.393 | 0.482 | 0.483 | 0.022 |

rocks are reflected in a relative enrichment in FeO and MgO, a marked depletion in alkalis ($\text{Na}_2\text{O} + \text{CaO}$), and minor variable change in K_2O . Mineralogically the chemical changes are manifested by the presence of biotite, staurolite, and andalusite in the altered rocks (Fig. 17).

In contrast, altered rhyolite immediately beneath the deposit shows a significant increase in the chloritic component accompanied by an obliteration of the feldspathic component. These results compare favourably with the alteration pipe beneath the Mattagami Lake deposit (Riverin and Hodgson, 1980). This inexpensive major element technique for determining the alteration intensity readily displays the gross chemical changes during metasomatism but specific element mobility is not identified.

Mass balance methodology

One approach used to examine the chemical aspects of alteration is to first determine the mass gain and loss of components during metasomatism and then relate the element mobility to mineralogy. Elemental mass gains and losses during metasomatism can be calculated by comparing less altered and altered rocks but the selection of the unaltered protolith of the alteration zone is critical. The principles of

mass balance were established by Akella (1966) and Gresens (1967). Grant (1986) developed the isocon (equal concentration) plot based on concepts introduced by Gresens (1967) which enables only one altered sample (altered concentrations for each element/oxide) to be plotted against an unaltered parent sample. Isocon diagrams are difficult and cumbersome to compare multiple altered samples as each altered sample is shown on a single isocon plot. To overcome this Huston (1993) developed an arbitrary scaling factor for each element.

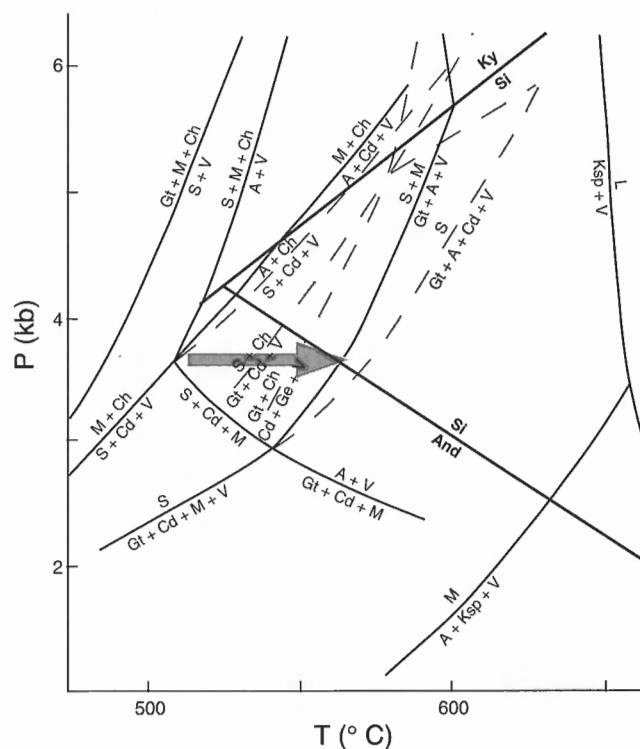


Figure 16. *P-T* petrogenetic grid for part of $\text{K}_2\text{O}-\text{Na}_2\text{O}-\text{FeO}-\text{MgO}-\text{Al}_2\text{O}_3-\text{SiO}_2-\text{H}_2\text{O}$ system (Davidson *et al.*, 1990) with field of the West Anomaly alteration assemblages denoted by arrow. A – aluminosilicate, And – andalusite, Cd – cordierite, Ch – chlorite, Gt – garnet, Ge – gedrite, Ksp – K-feldspar, Ky – kyanite, L – granitic liquid, M – muscovite, S – staurolite, Si – sillimanite, V – vapour.

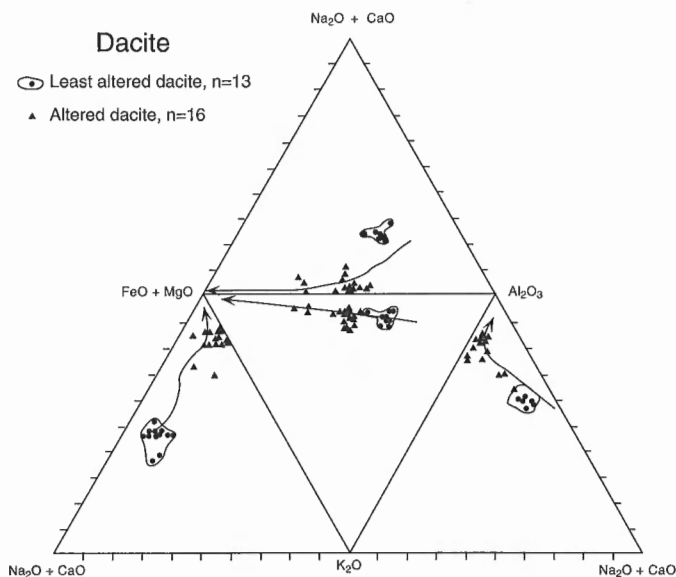


Figure 17a. Unfolded FCAK tetrahedron showing progression from least altered dacite (Junction dacite; analyses in Ames, 1996) to altered dacite in the footwall to the West Anomaly.

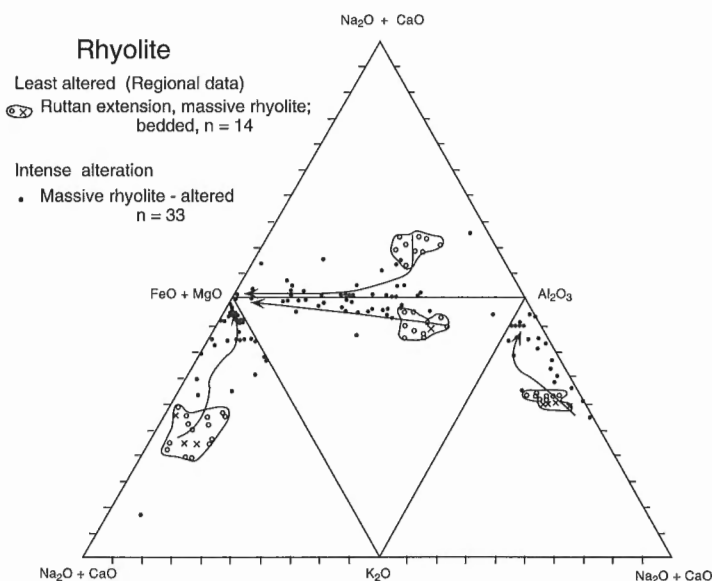


Figure 17b. Unfolded tetrahedron showing the progressive alteration with least altered (Ruttan extension) massive rhyolite and altered rhyolite in West Anomaly.

The scaling factors (1-19) are selected by sequencing elements with large mass gains before those with small to large mass losses (Fig. 18a), with immobile elements dispersed throughout.

The chemical changes produced by alteration were determined using Huston's (1993) modification of Grant (1986) graphical isocon method. The equations for determining the scaling factor, the net mass change relative to the least altered parent rock, the relative density change of the altered rock, volume changes, relative and absolute mass changes are well explained in Huston (1993). The presence of polyphase moderate to intense deformation in the alteration zones and coarse grained metamorphic minerals, at the Ruttan mine negate the common inference that the final density change between the altered rock and unaltered rock is due to the hydrothermal event that formed the alteration zones. Therefore no assumptions have been made about the volume change during calculation of the relative mass changes.

Dacite geochemistry

The parent least altered rock for the dacite was selected through petrographic and geochemical observations and is defined by an average of two samples (Table 2). The two samples are lateral equivalents of the altered Mine dacite west of the deposit. Internal variations within the least altered parent could add tremendous error limits on the calculated mass changes, however, the dacites within the Ruttan area are

Table 8. Staurolite microprobe analyses.

| | 89-11 Average n=7 | SD |
|--------------------------------|-------------------------|-------|
| SiO ₂ | 27.17 | 0.16 |
| Al ₂ O ₃ | 53.13 | 0.54 |
| TiO ₂ | 0.47 | 0.05 |
| Fe ₂ O ₃ | 0.00 | 0.00 |
| Cr ₂ O ₃ | 0.01 | 0.01 |
| FeO | 0.00 | 0.00 |
| MnO | 0.35 | 0.03 |
| MgO | 2.26 | 0.30 |
| ZnO | 2.71 | 0.17 |
| TOTAL | 86.10 | 0.33 |
| FORMULA (BASIS 23 OXYGENS) | | |
| Si | 4.041 | 0.030 |
| | 4.041 | 0.030 |
| Al | 9.313 | 0.074 |
| Ti | 0.053 | 0.006 |
| Fe ⁺³ | 0.000 | 0.000 |
| Cr | 0.001 | 0.002 |
| | 9.367 | 0.073 |
| Fe+2 | 0.000 | 0.000 |
| Mn | 0.044 | 0.004 |
| Mg | 0.501 | 0.066 |
| Zn | 0.297 | 0.018 |
| | 0.842 | 0.065 |

relatively homogeneous (Fig. 9, Table 2). The altered Mine dacite plots in a field on a TiO₂/Zr bivariate plot (Fig. 9) and a Ti/10, Zr, Y*3 ternary diagram (Fig. 10a) that overlaps with least altered Mine dacite, Junction dacitic rocks and dacitic rocks that outcrop south of the mine site (chemical data in Ames, 1996) suggesting that the elements Ti, Zr, and Y are some of the least mobile elements during alteration and that the regional dacite samples chosen represent the parent rock composition.

Lateral changes in mass gains and losses were determined by comparing the average parent rock with altered samples in each cross-section from the West Anomaly (section A-A') to 1 km west of the ore lens (B-B', C-C', D-D'; Fig. 6, 7; Table 11). The slope of the best fit isocon was determined by taking the mean of the ratio of the concentration of the immobile elements Ti, Zr, and Al in all altered dacite samples

Table 9. Microprobe analyses of plagioclase.

| | 89-19 Average n=5 | SD | 89-11 Average n=3 | SD |
|--------------------------------|-------------------------|-------|-------------------------|-------|
| SiO ₂ | 62.69 | 0.52 | 60.38 | 1.10 |
| Al ₂ O ₃ | 24.49 | 0.27 | 25.54 | 0.52 |
| Na ₂ O | 8.64 | 0.14 | 7.73 | 0.46 |
| CaO | 3.58 | 0.12 | 4.57 | 0.49 |
| K ₂ O | 0.06 | 0.01 | 0.04 | 0.01 |
| BaO | 0.02 | 0.03 | 0.00 | 0.00 |
| SrO | 0.00 | 0.00 | 0.00 | 0.00 |
| FeO | 0.05 | 0.04 | 0.04 | 0.02 |
| TOTAL | 99.53 | 0.70 | 99.30 | 0.55 |
| FORMULA (BASIS 32 OXYGENS) | | | | |
| Si | 11.085 | 0.028 | 10.833 | 0.124 |
| Al | 5.104 | 0.030 | 5.401 | 0.146 |
| | 16.189 | 0.017 | 16.234 | 0.022 |
| Na | 2.963 | 0.068 | 2.688 | 0.142 |
| Ca | 0.678 | 0.022 | 0.878 | 0.100 |
| K | 0.013 | 0.002 | 0.010 | 0.002 |
| Ba | 0.001 | 0.002 | 0.000 | 0.000 |
| Sr | 0.000 | 0.000 | 0.000 | 0.000 |
| | 3.655 | 0.064 | 3.576 | 0.042 |
| Fe | 0.007 | 0.006 | 0.006 | 0.004 |
| | 0.007 | 0.006 | 0.006 | 0.004 |
| WT. % END MEMBERS | | | | |
| Ab | 73.12 | 1.21 | 65.39 | 3.89 |
| An | 17.75 | 0.61 | 22.66 | 2.43 |
| Or | 0.34 | 0.04 | 0.26 | 0.05 |
| Ba | 0.04 | 0.06 | 0.00 | 0.00 |
| Sr | 0.00 | 0.00 | 0.00 | 0.00 |
| TOTAL | 91.25 | 0.99 | 88.30 | 1.44 |
| MOL.% END MEMBERS | | | | |
| Ab | 81.07 | 0.67 | 75.17 | 3.09 |
| An | 18.55 | 0.69 | 24.55 | 3.07 |
| Or | 0.36 | 0.05 | 0.28 | 0.06 |
| Ba | 0.03 | 0.05 | 0.00 | 0.00 |
| Sr | 0.00 | 0.00 | 0.00 | 0.00 |

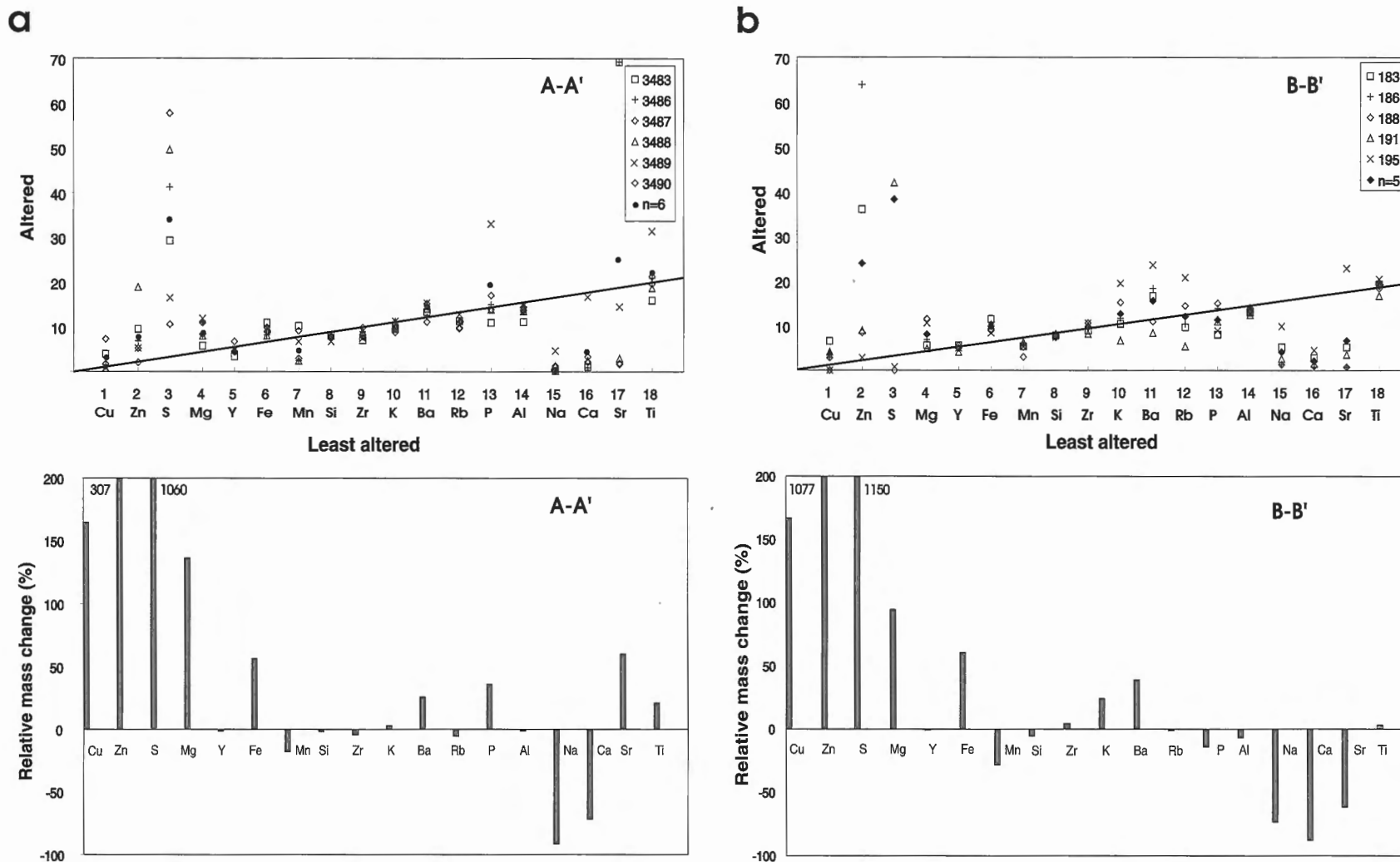


Figure 18. Isocon diagrams and histograms illustrating relative mass changes in altered dacite from West Anomaly: **a)** altered dacite from section A-A' (Fig. 4, 5, 6), **b)** altered dacite from section B-B' (Fig. 4, 5, 6), **c)** altered dacite from section C-C' (Fig. 4, 6), and **d)** altered dacite from section D-D' (Fig. 4, 6). Solid line represents best fit isocon.

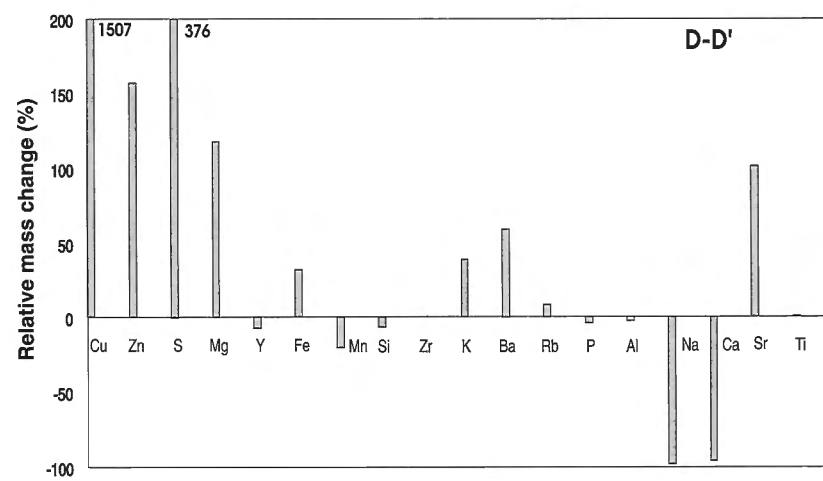
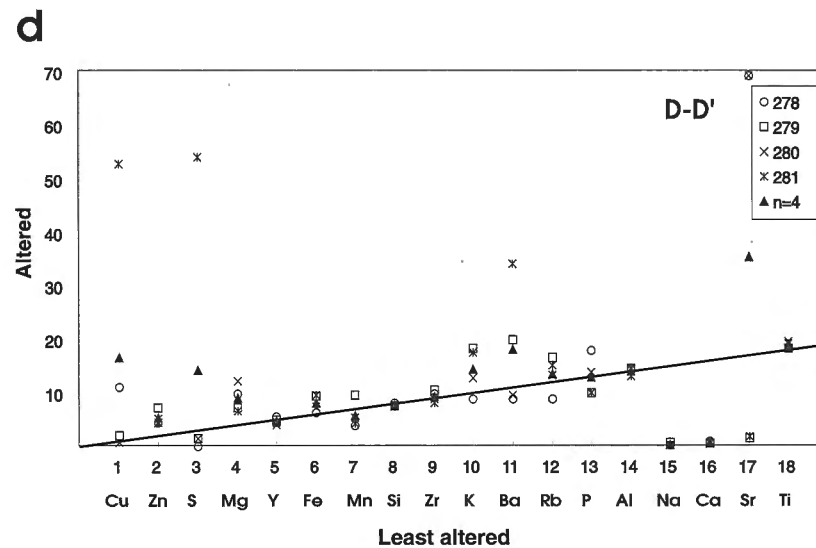
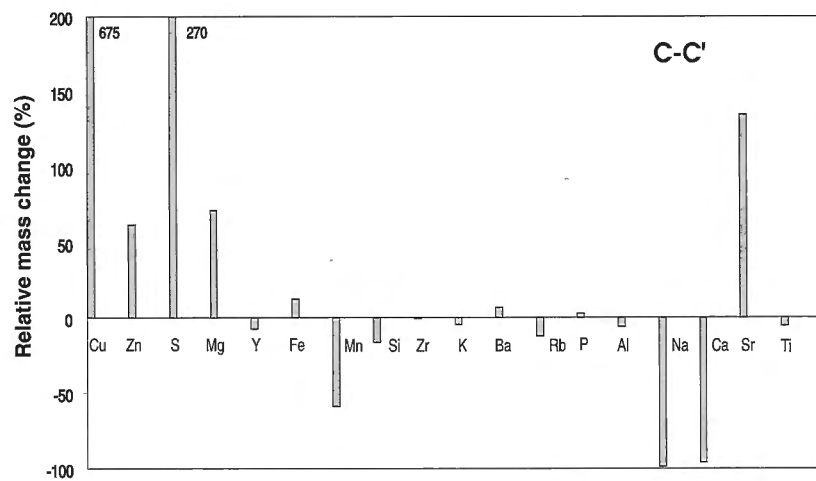
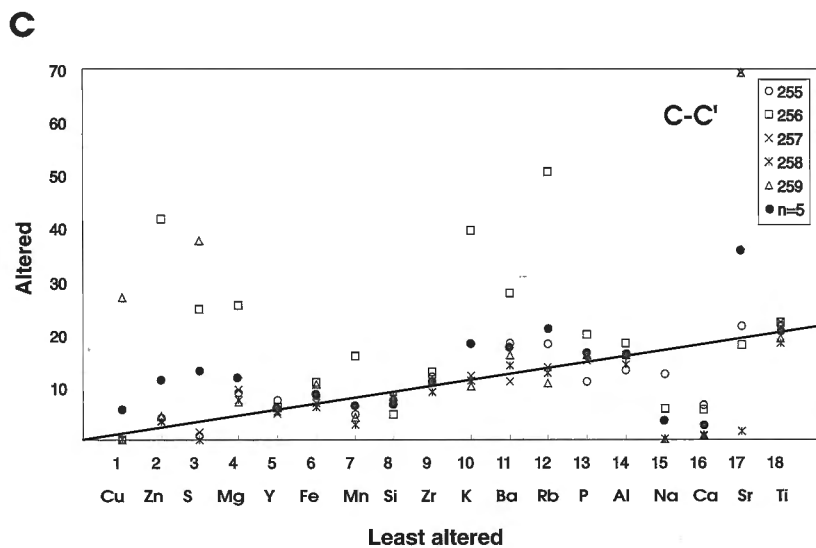


Figure 18. (cont.)

per section with the concentrations in the least altered parent. The slope of these isocons was used to estimate the relative mass changes in each section (Fig. 18, Table 12).

Isocon analyses of the dacite (Fig. 18; Table 12) immediately below the Western lens on the 630 mL and from sections B to D progressing away from known mineralization show similar element mobility trends except for rocks in the section most distal from the deposit (section D). There is a slight increase in K distal to the deposit. The altered dacites show consistent relative additions of Ba, Mg, S, Zn, and Cu; Fe is constant in section C (Fig. 18c) but is generally enriched in

the altered dacitic rocks. Consistent major losses of Ca and Na are displayed on all transects through the altered dacite (Fig. 18; Table 12). Si is generally unchanged but one erratic analysis in Figure 18c shows a minor loss that is not considered significant.

Rhyolite geochemistry

All rhyolite samples selected underground and in drillhole in the Ruttan mine are altered (Table 13). The Main Mine rhyolite sampled in the footwall of the C/D and J lenses as

Table 10. Microprobe analyses of gahnite.

| | 2 | 3 | 4 | 5 | Average | SD |
|--------------------------------|--------|--------|--------|--------|---------|-------|
| Al ₂ O ₃ | 56.79 | 56.79 | 58.10 | 57.16 | 57.21 | 0.62 |
| Cr ₂ O ₃ | 0.00 | 0.00 | 0.00 | 0.00 | 0.00 | 0.00 |
| Fe ₂ O ₃ | 1.17 | 0.67 | 0.63 | 0.80 | 0.80 | 0.25 |
| V ₂ O ₃ | 0.00 | 0.00 | 0.00 | 0.00 | 0.00 | 0.00 |
| TiO ₂ | 0.00 | 0.00 | 0.00 | 0.00 | 0.00 | 0.00 |
| FeO | 5.82 | 6.13 | 6.00 | 6.21 | 6.05 | 0.17 |
| MgO | 2.79 | 2.53 | 3.53 | 2.90 | 2.94 | 0.42 |
| MnO | 0.09 | 0.10 | 0.16 | 0.00 | 0.09 | 0.07 |
| ZnO | 33.58 | 33.50 | 32.63 | 33.14 | 33.21 | 0.43 |
| NiO | 0.00 | 0.00 | 0.00 | 0.00 | 0.00 | 0.00 |
| TOTAL | 100.24 | 99.72 | 101.05 | 100.21 | 100.30 | 0.55 |
| FORMULA (BASIS 32 OXYGENS) | | | | | | |
| Al | 15.794 | 15.880 | 15.888 | 15.859 | 15.856 | 0.043 |
| Cr | 0.000 | 0.000 | 0.000 | 0.000 | 0.000 | 0.000 |
| Fe ³⁺ | 0.207 | 0.120 | 0.109 | 0.141 | 0.141 | 0.044 |
| V | 0.000 | 0.000 | 0.000 | 0.000 | 0.000 | 0.000 |
| Ti | 0.000 | 0.000 | 0.000 | 0.000 | 0.000 | 0.000 |
| | 16.001 | 16.000 | 15.997 | 16.000 | 15.997 | 0.002 |
| Fe ²⁺ | 1.148 | 1.216 | 1.164 | 1.223 | 1.191 | 0.037 |
| Mg | 0.981 | 1.164 | 1.219 | 0.895 | 1.029 | 0.137 |
| Mn | 0.017 | 0.021 | 0.031 | 0.031 | 0.017 | 0.013 |
| Zn | 5.852 | 5.868 | 5.590 | 5.590 | 5.767 | 0.128 |
| Ni | 0.000 | 0.000 | 0.000 | 0.000 | 0.000 | 0.000 |
| | 7.998 | 8.000 | 8.004 | 8.000 | 8.004 | 0.003 |
| WT. % END MEMBERS | | | | | | |
| spinel | 9.72 | 8.86 | 12.35 | 10.14 | 10.26 | 1.48 |
| hercynite | 13.89 | 14.71 | 14.40 | 14.90 | 14.51 | 0.44 |
| gahnite | 74.71 | 74.90 | 72.96 | 74.00 | 74.12 | 0.88 |
| galaxite | 0.20 | 0.25 | 0.38 | 0.00 | 0.21 | 0.16 |
| magnesiofersite | 0.18 | 0.09 | 0.12 | 0.13 | 0.13 | 0.04 |
| magnetite | 0.24 | 0.15 | 0.13 | 0.18 | 0.17 | 0.05 |
| franklinite | 1.29 | 0.74 | 0.66 | 0.87 | 0.87 | 0.28 |
| TOTAL | 100.24 | 99.72 | 101.00 | 100.20 | 100.26 | 0.53 |
| MOL. % END MEMBERS | | | | | | |
| spinel | 12.11 | 11.10 | 15.13 | 12.60 | 12.74 | 1.71 |
| hercynite | 14.17 | 15.09 | 14.44 | 15.15 | 14.75 | 0.48 |
| gahnite | 72.22 | 72.80 | 69.36 | 71.37 | 71.42 | 1.50 |
| galaxite | 0.21 | 0.26 | 0.38 | 0.00 | 0.21 | 0.16 |
| magnesiofersite | 0.16 | 0.08 | 0.10 | 0.11 | 0.11 | 0.03 |
| magnetite | 0.19 | 0.11 | 0.10 | 0.13 | 0.13 | 0.04 |
| franklinite | 0.95 | 0.55 | 0.48 | 0.63 | 0.64 | 0.21 |

Table 11. Average analytical results of altered Mine dacite, West Anomaly area.

| | A-A' n=6 | B-B' n=5 | C-C' n=5 | D-D' n=4 |
|----------------------------------|-------------|-------------|-------------|-------------|
| SiO ₂ | 65.57 | 65.58 | 60.74 | 66.30 |
| TiO ₂ | 0.51 | 0.45 | 0.50 | 0.45 |
| Al ₂ O ₃ | 13.58 | 13.36 | 15.66 | 14.25 |
| Fe ₂ O ₃ T | 9.98 | 10.64 | 9.28 | 8.90 |
| Fe ₂ O ₃ | 1.78 | 3.14 | 2.34 | 1.95 |
| FeO | 7.37 | 4.52 | 6.26 | 6.25 |
| MnO | 0.12 | 0.11 | 0.13 | 0.12 |
| MgO | 5.25 | 4.49 | 6.62 | 5.13 |
| CaO | 0.86 | 0.39 | 0.56 | 0.12 |
| Na ₂ O | 0.20 | 0.62 | 0.58 | 0.05 |
| K ₂ O | 2.16 | 2.71 | 3.91 | 3.08 |
| H ₂ OT | 1.93 | 1.58 | 2.02 | 2.15 |
| CO ₂ T | 0.05 | 0.00 | 0.02 | 0.03 |
| P ₂ O ₅ | 0.17 | 0.11 | 0.16 | 0.13 |
| | 0.46 | 0.51 | 0.17 | 0.19 |
| S | | | | |
| Ba | 635 | 728 | 818 | 853 |
| Be | 0.6 | 0.5 | 0.5 | 0.5 |
| Co | 22 | 17 | 15 | 13 |
| Cr | 15 | 5 | 5 | 0 |
| Cu | 231 | 242 | 485 | 1488 |
| La | 13 | 16 | 22 | 16 |
| Nb | 9 | 8 | 4 | 508 |
| Ni | 10 | 5 | 1 | 999 |
| Pb | 0 | 59 | 11 | 0 |
| Rb | 44 | 48 | 84 | 54 |
| Sc | 18 | 18 | 18 | 16 |
| Sr | 384 | 95 | 518 | 512 |
| V | 24 | 13 | 14 | 10 |
| Y | 25 | 26 | 31 | 25 |
| Yb | 2.6 | 2.7 | 3.1 | 2.6 |
| Zn | 287 | 864 | 412 | 193 |
| Zr | 112 | 128 | 150 | 125 |

Table 13. Average analytical results of altered rhyolite, West Anomaly.

| Locn Sample_N | MMR n=4 | RHS n=2 | LAR n=5 | QTZ n=8 | CANT n=7 | CDSETA n=7 |
|----------------------------------|------------|------------|------------|------------|-------------|---------------|
| SiO ₂ | 79.6 | 63.3 | 71.24 | 52.70 | 47.97 | 50.01 |
| TiO ₂ | 0.19 | 0.095 | 0.344 | 0.44 | 0.23 | 0.55 |
| Al ₂ O ₃ | 7 | 4.13 | 13.26 | 15.04 | 13.18 | 16.94 |
| Fe ₂ O ₃ T | 7.05 | 19.9 | 5.78 | 16.65 | 15.04 | 12.66 |
| Fe ₂ O ₃ | 2.325 | 0 | 1.82 | 0.00 | 0.76 | 0.30 |
| FeO | 4.25 | 0 | 2.54 | 0.00 | 1.83 | 1.70 |
| MnO | 0.0425 | 0.02 | 0.046 | 0.16 | 0.13 | 0.09 |
| MgO | 3.835 | 0.585 | 3.118 | 6.55 | 13.06 | 9.59 |
| CaO | 0.24 | 0.555 | 1.686 | 1.85 | 3.32 | 1.95 |
| Na ₂ O | 0.225 | 0.35 | 1.466 | 0.48 | 0.94 | 0.58 |
| K ₂ O | 0.575 | 0.115 | 1.428 | 1.60 | 1.31 | 1.58 |
| H ₂ OT | 1.775 | 0 | 0.86 | 0.00 | 1.87 | 1.49 |
| CO ₂ T | 0.075 | 0.05 | 0.04 | 0.05 | 0.07 | 0.03 |
| P ₂ O ₅ | 0.04 | 0.05 | 0.098 | 0.15 | 0.05 | 0.13 |
| S | 0.3675 | 11.3 | 1.048 | 3.72 | 3.73 | 4.54 |
| Ba | 130 | 30 | 538 | 346.88 | 287.14 | 377.14 |
| Be | 0.3 | 0.6 | 0.82 | 0.58 | 0.90 | 0.76 |
| Co | 10.5 | 63.5 | 12.4 | 39.25 | 14.14 | 14.29 |
| Cr | 5 | 11 | 3 | 34.88 | 146.71 | 18.00 |
| Cu | 119.5 | 4100 | 192 | 5550.00 | 2337.57 | 1967.00 |
| La | 14.25 | 2.5 | 10.6 | 8.63 | 16.14 | 14.71 |
| Nb | 5.75 | 2.5 | 603 | 5.63 | 7.86 | 10.43 |
| Ni | 5 | 2.5 | 600.4 | 14.00 | 23.57 | 156.71 |
| Pb | 10 | 65 | 17.6 | 11.38 | 50.00 | 61.00 |
| Rb | 13 | 5 | 33 | 29.88 | 27.57 | 16.57 |
| Sc | 7.625 | 2.6 | 12.34 | 18.75 | 7.57 | 11.71 |
| Sr | 34.25 | 48.5 | 457.8 | 318.13 | 241.43 | 225.71 |
| V | 11.25 | 501 | 19 | 41.50 | 176.14 | 24.29 |
| Y | 19 | 6.5 | 24.8 | 24.25 | 39.57 | 24.29 |
| Yb | 2 | 0.15 | 2.72 | 2.53 | 4.50 | 2.56 |
| Zn | 73.25 | 10500 | 128.8 | 3982.50 | 1725.71 | 515.71 |
| Zr | 84.5 | 47 | 114.4 | 101.75 | 145.29 | 165.71 |

Table 12. Lateral compositional changes in altered Mine dacite from 0 to 1050 m west of mine.

| | A-A' | B-B' | C-C' | D-D' |
|--|---------------|-------------|------------|----------------|
| Gains | | | | |
| Major | Mg,Fe,S,Cu,Zn | Fe,S,Cu,Zn | S,Cu,Zn | Mg,S,Cu,Zn, Sr |
| Minor | P,Ba,Sr | Mg,K,Ba | Mg,Ba | Fe,K,Ba |
| Least Change | | | | |
| | Ti,Zr,Al,Y | Ti,Al,Zr,Y, | Ti,Al,Zr,Y | Ti,Al,Y,Zr |
| | Si,K,Rb | Si,Rb | Fe,Rb,K,P | Si,P,Rb |
| Losses | | | | |
| Minor | — | Mn | Si | Mn |
| Major | Ca,Na | Ca,Na,Sr | Mn,Ca,Na | Ca,Na |
| Erratic | | | | |
| | Mn | P | Sr | — |
| Major gains >100, moderate gains <100, major losses 50-100, minor losses <50. Ca*= | | | | |

least altered representatives contain up to 84.3 wt. % SiO₂ and contain low concentrations of alkali elements reflecting silicification and feldspar destruction. The high field strength elements (Ti, Zr, and Y) were relatively immobile during weak hydrothermal alteration and were used to compare the weakly altered mine rhyolite with the regional Ruttan extension rhyolite (Fig. 10b) (Ames, 1996). Bedded felsic volcaniclastic rocks and massive rhyolite define distinct fields irrespective of sample location (Fig. 10b). The mine and Ruttan extension, massive rhyolite compositions coincide, but other rhyolites within the Karsakuwigamak and Northern blocks are chemically distinct (Ames, unpublished data). Bedded volcaniclastic rocks from the Ruttan extension are chemically and texturally similar to the hangingwall Upper felsic volcaniclastic rocks in the Ruttan mine. Therefore, the massive rhyolite from regional mapping in the Ruttan extension area is considered to be the best candidate for the least altered equivalent to the Mine rhyolite.

An average of ten analyses of the Ruttan extension massive rhyolite was used as the parent rhyolite in the mass balance calculations (Table 2). Elements commonly used as immobile elements during mass balance calculations include Ti, Zr, Al, Nb and Y (MacLean and Kranidiotis, 1987; MacLean, 1990; Elliot-Meadows and Appleyard, 1991). Ti and Zr do not have consistent ratios throughout the alteration zones in the altered rhyolite implying either mobility or cryptic variable parent compositions. Due to the intense alteration, macroscopic evidence of volcaniclastic deposition has been obliterated but the possibility of variable Ti and Zr content due to reworking cannot be overruled. Al₂O₃ was assumed to be immobile due to its experimentally determined low Al solubility (Sokolova and Khodakovskiy, 1977). Using Grant's graphical representation modified by Huston (1993) the slope of the isocon can be determined for each alteration type and the corresponding mass changes. The

average mass change was determined for each alteration type; however, the variations can readily be observed on the isocon diagrams (Fig. 19). Table 14 summarizes the chemical changes in the alteration zones within the Ruttan mine.

Mine Rhyolite

Increasing intensity of alteration in the West Anomaly is shown in Figure 19. Titanium is the only element consistently least mobile that lies on the isocon defined by constant Al. Although Ti, Y, and Zr are immobile in weakly altered zones, during intense alteration it appears that Zr shows some mobility and within the stringer zone minor Y is lost. Locally, in the weakly altered zones, Si or Mn are immobile.

a) Weakly altered rhyolite (Main Mine and West Anomaly)

Isocon analysis (Fig. 19a) indicates that the Main Mine rhyolite underwent major gains in Mg and Fe and major losses in Ca, Na, and Ba. Minor enrichments in Si and Cu and depletions in K and Sr are observed. Weakly altered rhyolite sampled distal to the West Anomaly ore lens, shows similar trends: major enrichment of Mg, minor enrichment of Cu, major loss of Ca, and minor loss of K and Ba (Fig. 19b). Sodium is more erratic as a group and may reflect a mixture of variably (least to weakly) altered samples.

The major influx of Mg and the shallow isocon slope (0.57) of the Main Mine rhyolite suggest that the distal footwall to the deposit underwent a major mass gain associated with magnesium metasomatism. In contrast, the isocon slope of the weakly altered rhyolite, laterally distal to the ore approximates one (1.07), indicating no significant mass change during alteration.

Table 14. Compositional changes of alteration types surrounding West Anomaly orebody.

| | Main Mine Wk. Alt. rhyolite | West Anomaly Wk. Alt. rhyolite | Int. alt. rhyolite | Rhyolite- hosted stringer | Chl-anth±ta schist | Chl-cd±ta schist |
|---|-----------------------------------|--------------------------------------|-----------------------|---------------------------------|-----------------------|---------------------|
| Gains | | | | | | |
| Major | Mg,Fe | Mg | Mg,Fe,S,Cu,Zn | Si,Fe,S,Cu,Zn | Mg,Fe,Cu,Zn | Mg,Cu,Zn |
| Minor | Si,Cu | Cu | Mn | Mg,P | Y | — |
| Least Change | Al,Ti,Y, Zr,Mn,Zn | Al,Ti,Si, Y,Zr | Ti,Al,Y | Zr,Ti,Al | Al,Zr | Al |
| Losses | | | | | | |
| Minor | K,Sr | Mn,K,Ba | Si,K,Rb,Sr,Zr | Y,Ca,Na,Mn | K,P,Rb,Si,Ti | Mn,K,Sr,Y |
| Major | Ca,Na,Ba | Ca | Ca,Na,Ba | K,Ba,Rb | Na,Ba | Si,Na,Ba,Rb |
| Erratic | S,P,Rb | S,Na,P, Rb,Sr | P | Sr | Mn,Ca,S, Sr | Ti,Fe,Ca,P, S,Zr |
| Major gains >100, moderate gains <100, major losses 50-100, minor losses <50. | | | | | | |

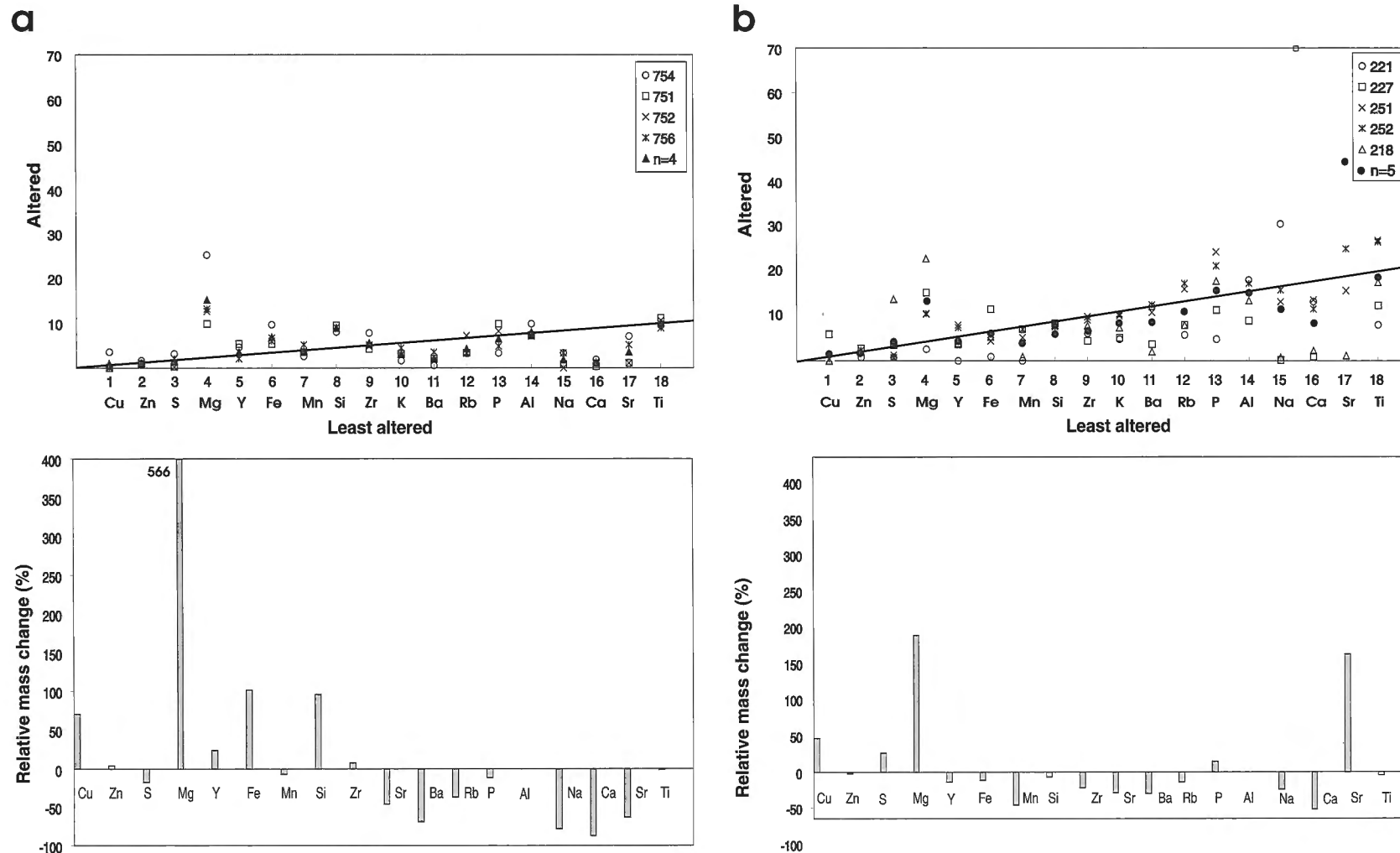


Figure 19. Isocon diagrams and histograms illustrating relative mass changes in altered rhyolite from West Anomaly and Main Mine: **a)** weakly altered Main Mine rhyolite, **b)** weakly altered West Anomaly rhyolite, **c)** intensely altered West Anomaly rhyolite, **d)** rhyolite-hosted stringer alteration in West Anomaly. **e)** West Anomaly chlorite-anthophyllite schist, and **f)** West Anomaly sericite-chlorite-cordierite schist.

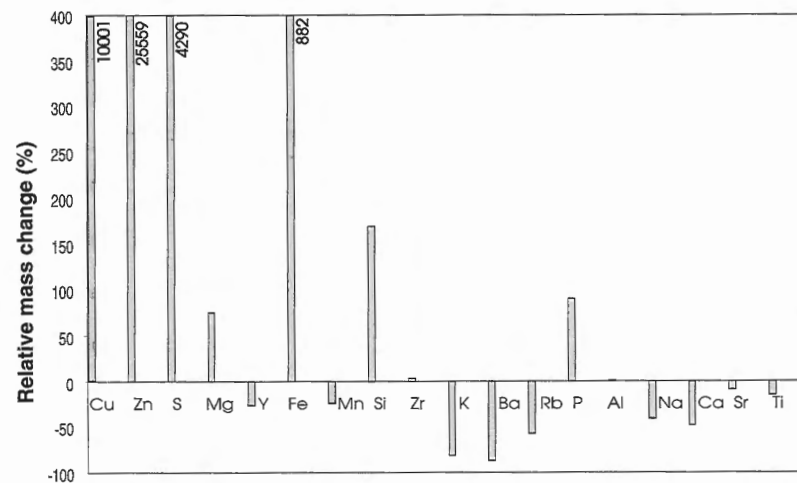
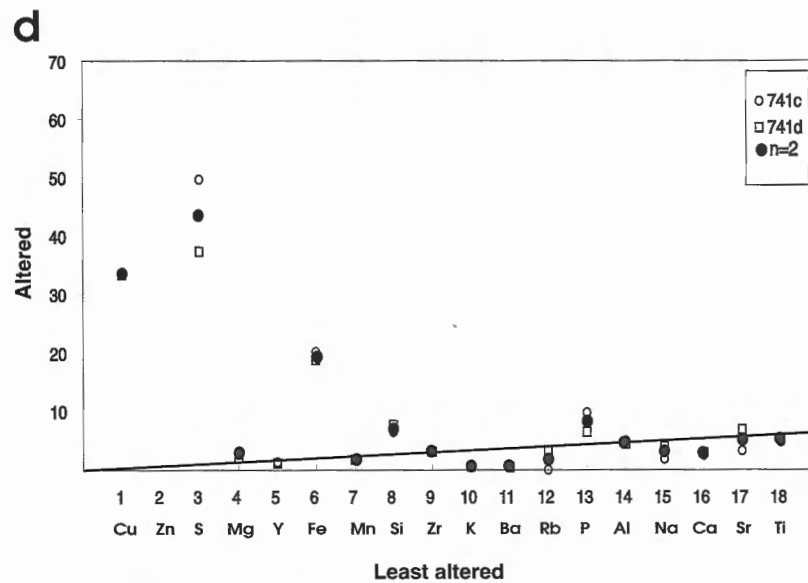
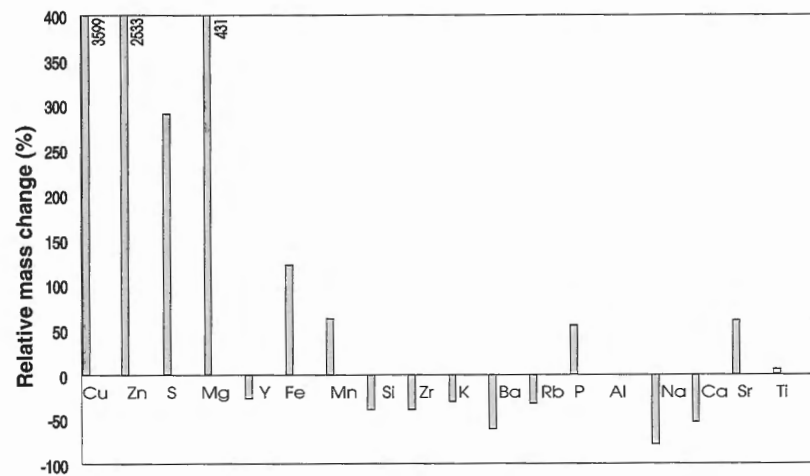
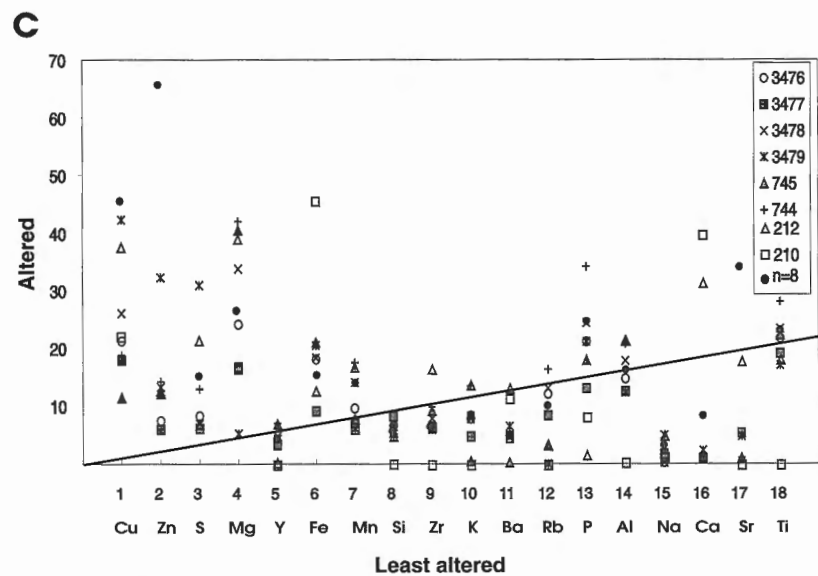


Figure 19. (cont.)

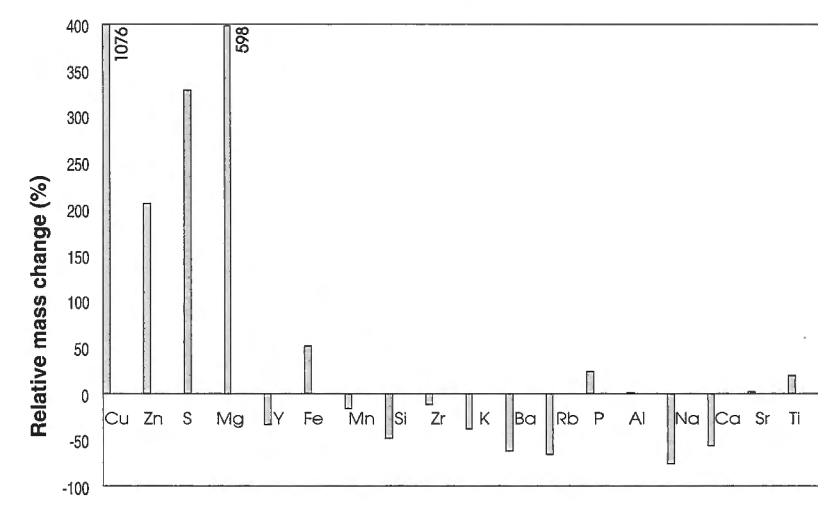
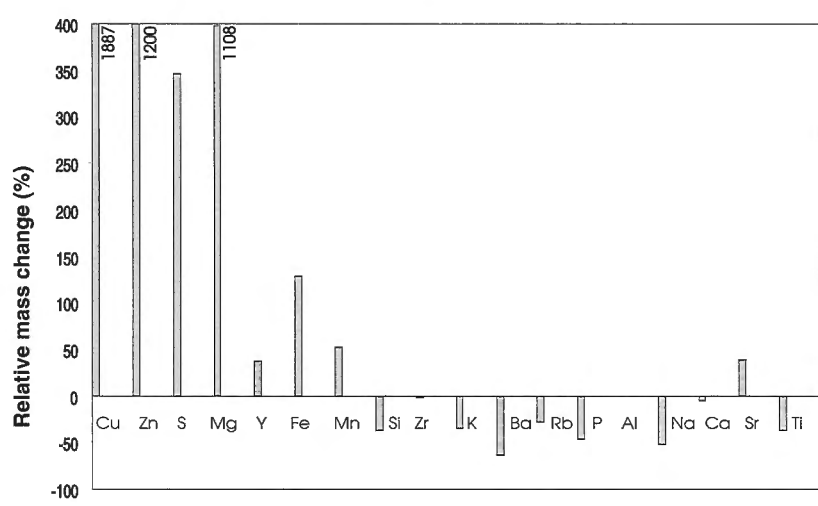
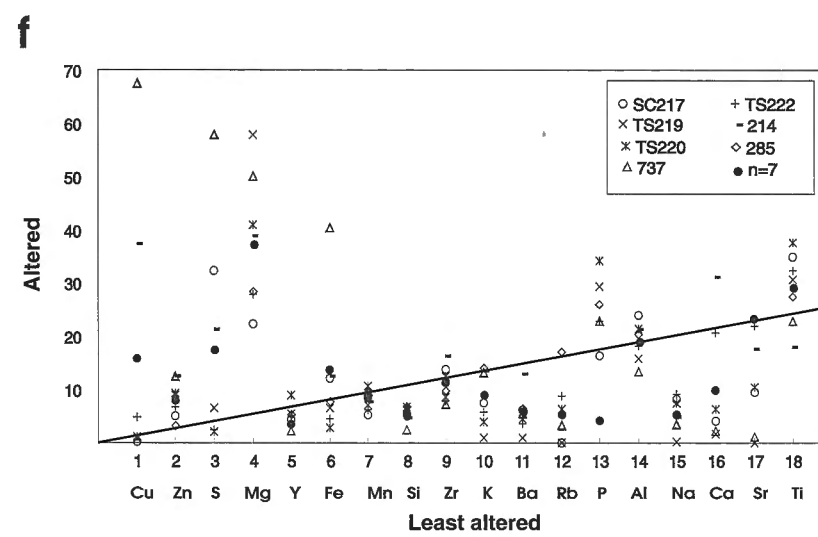
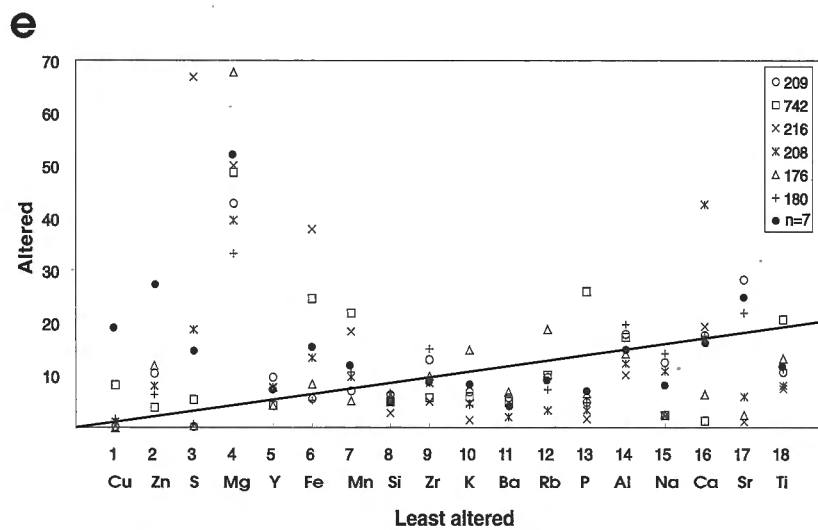


Figure 19. (cont.)

b) Intensely altered

The footwall to the Cu-Zn West Anomaly ore lens had a significant addition of Mg, Fe, S, Cu, and Zn and depletion in Ca, Na, Ba and Si, K, Rb, Sr (Fig. 19c, Table 14). Distal from the ore lens, the Al ratios of the parent and altered samples vary from 0.88-1.27 ($n=4$) but, in close proximity to the ore the slope significantly changes to 1.48-1.52 ($n=3$). This may reflect an average mass loss due to silica depletion and alteration of Na- and Ca-bearing minerals. The relative additions are reflected in the mineralogy: chlorite, talc, chalcopyrite, sphalerite, pyrrhotite, and pyrite.

c) Rhyolite-hosted stringer zone

The altered rhyolite between the pyrrhotite-chalcopyrite-chloritic stringers was analyzed. In contrast to the preceding alteration types, Mg has not been added in significant amounts (Fig. 19d). Isocon analyses show a major enrichment in Si, Fe, S, Cu, and Zn and only minor enrichment in Mg and P. K, Ba, Rb, Mn, Ca, Na (Ca-48%, Na 41% loss) have had large relative losses. The major silica addition and slope of the isocon (0.33) suggest that silica flooding occurred immediately below the massive sulphide orebody. This may be partially due to a pressure decrease accompanying formation of the sulphide stringers.

d) Chlorite schist

Ti was mobile at the time of formation of the most intensely altered chlorite schist. The chlorite-anthophyllite±talc schist has major additions of Mg, Zn, Cu, and Fe and depletions in Na, Ba, Si(37%), K, P, Rb, and Ti (Fig. 19e; Table 14). These reflect only overall trends since the chlorite schist has undergone multiple strain and hydrothermal events. Mobile elements important in the formation of these zones are Mg (extreme enrichment) and Si (major depletion).

e) Sericite schist

The sericite-cordierite±talc schist occurs dominantly in the footwall to the Art's Fault in the West Anomaly area and isocon analysis suggests major enrichments in Mg, Cu, and Zn and major depletions of Na, Si, Ba, and Rb with a minor loss of Mn, K, Sr, and Y (Fig. 19f). Fe is generally lost in the sericite schist in contrast to the major addition in the chlorite-anthophyllite schist zones. The sericite-cordierite±talc schist has relatively less sulphide than the chlorite-anthophyllite schist which is shown by the lower Fe and Zn additions. The compositional variability in the sericite-cordierite±talc schist is reflected in the large number of elements that behave erratically. The erratic behaviour of Ca and S can be related to the patchy distribution of anhydrite within the schists enveloping the ore lenses.

DISCUSSION

Tectonic and depositional environments

The tectonic and depositional environments of Paleoproterozoic volcanogenic massive sulphide deposits within Manitoba and Saskatchewan have been documented most extensively in the Flin Flon-Snow Lake Belt (Bailes and Syme, 1989; Syme and Bailes, 1993; Galley et al., 1993). Amisk mafic volcanic rocks were divided into arc tholeiite, back arc/ocean floor, and ocean island suites based on geochemical characteristics (Syme, 1990) with the largest deposits (Flin Flon, Trout Lake, Chisel Lake, and Stall Lake) located in an arc assemblage (Syme and Bailes, 1993). Protoarc environments contain deposits of less than 1.3 Mt (Syme and Bailes, 1993). The Flin Flon and Ruttan deposits, both developed in an arc tholeiitic assemblage (Ames and Scoates, 1992; Syme and Bailes, 1993; Ames, 1996), are an order of magnitude larger than the other deposits in the belt (62.4 Mt and 64 Mt respectively) and yet the Flin Flon belt contains 24 present and past producers and the Rusty Lake belt only the large Ruttan mine. It is therefore important that the geochemical characteristics of the volcanic rocks be documented and their tectonic environment defined in the Rusty Lake belt (Ames, 1996).

The Ruttan VMS deposit occurs near the top of a thick sequence of felsic volcanoclastic rocks overlying a mixed sequence of dacitic and andesitic volcanoclastic rocks and associated distal andesitic lava. It occurs near a major stratigraphic interval with overlying well bedded volcanogenic mafic wacke, siltstone, and conglomerate. Speakman et al. (1982) suggested that the Mine rhyolite may be the silicified equivalent of the altered footwall volcanoclastics (altered Mine dacite) and that Al and Ti were lost during alteration. Although this study suggests minor Ti and Zr mobility in the formation of the chlorite schist, the mine stratigraphy of a massive dacitic volcanoclastic unit overlain by felsic rocks is duplicated northeast of the mine site within a relatively unaltered stratigraphic package (Ames, 1996). Although the primary volcanological features of the Mine rhyolite have been obscured by hydrothermal alteration, the concentrations of TiO_2 (0.18 wt. %), Zr (120 ppm) and Al_2O_3 (8.7 wt. %) in the less altered units are typical of felsic volcanic rocks and not silicified dacite.

Magmatism and faulting have removed much of the footwall stratigraphy in the Ruttan mine area. Faulting either juxtaposed ocean floor basalt with ore hosting arc volcanic rocks or an island arc sequence developed on top of the ocean floor sequence and the shearing at the contact and multiple foliations in the Mill Pond formation would therefore be insignificant (Ames, 1996). A thin wedge of ore hosting stratigraphy is preserved in which the Upper felsic volcanoclastic unit is laterally continuous providing an excellent marker horizon.

The Fox mine in the Lynn Lake Belt, hosted by felsic volcanoclastic rocks, contains <12 Mt grading 1.82% Cu and 1.78% Zn. It is also structurally complex with much of the ore

environment displaced (Olsen, 1987). Both of these deposits are fault bounded, located at the extremity of their respective greenstone belts and were deposited in a similar setting. The style of deformation in the West Anomaly of the Ruttan mine is dominated by high angle reverse faults which have duplicated, offset, and affected the morphology of the ore zones.

The metal zonation at the Ruttan deposit is typical of VMS deposits with a Cu-Fe-rich base and Zn-Fe-Pb-Ag-bearing top. Attributes of the Ruttan deposit that differ with the classic model of subaqueous VMS deposition are: 1) the presence of stockwork-type and orthogonal veins of microcline alteration distal and proximal to the deposit (Ames et al., 1990; Ames and Scoates, 1992); 2) the high Hg content of the ores (Speakman et al., 1982); and 3) the presence of anhydrite and carbonate within the ore lenses and in the hangingwall chlorite schist. A shallow water environment (<1000 m) for deposition of the Ruttan deposit was inferred based on the combined presence of abundant large vesicles in proximal volcanic strata, microcline alteration, and the dominance of volcanoclastic rocks (Ames, 1996).

Alteration

The proximal alteration zones in the West Anomaly formed and recrystallized during a complex series of events ranging from early hydrothermal alteration to amphibolite grade metamorphism and polyphase deformation. Alteration zones exhibit the same grade of metamorphism and contain the same fabrics as observed in the surrounding Ruttan Group strata; these features suggest synvolcanic formation. The intensity of alteration is greater in the footwall than in the hangingwall of the deposit. Hydrothermal alteration minerals formed at low temperatures have been recrystallized during higher temperature metamorphic conditions; this coarsened and changed the primary mineralogy of the alteration zones. In complexly folded terranes, the competency contrast among felsic rocks, alteration zones, and orebodies concentrates the deformation in local high strain zones. The formation of phyllosilicates – Mg-smectites, illite-smectite during hydrothermal conditions (Alt and Jiang, 1991; Ames et al., 1993; Percival and Ames, 1993) – results in the formation of higher grade schists during tectonism and metamorphism.

Various measures of alteration intensity of areas surrounding massive sulphide deposits provide initial targets for exploration. The most commonly identified metasomatic changes such as Na and Ca depletion, Mg and Fe addition, and variable K are observed in the Ruttan deposit. The most outstanding alteration effect is the loss of sodium and calcium. There are similar metasomatic trends in the West Anomaly strata shown on an FCAK ($\text{FeO}+\text{MgO}$, $\text{CaO}+\text{Na}_2\text{O}$, Al_2O_3 , K_2O) flattened tetrahedron (Fig. 17) as those noted in the Millenbach deposit, Quebec (Riverin and Hodgson, 1980). Geochemical indices useful for targetting massive sulphide deposits include: Hashimoto's alteration index $((\text{K}_2\text{O}+\text{MgO})/(\text{K}_2\text{O}+\text{Na}_2\text{O}+\text{CaO}+\text{MgO}))\times 100$ (Bubar and Heslop, 1985); the Hughes (1973) diagram to monitor spili-zation and the development of keratophyres ($\text{Na}_2\text{O}+\text{K}_2\text{O}$) versus $(\text{K}_2\text{O}/\text{K}_2\text{O}+\text{Na}_2\text{O})\times 100$; and an alkali depletion Pearce Element ratio (Medeisky and Stanley, 1993) and

numerous other immobile element bivariate plots (e.g. Beswick and Soucie, 1978; Finlow-Bates and Stumpfl, 1981; Barrett and MacLean, 1991).

West Anomaly chlorite schist zones differ from those in the West and East lenses in that anthophyllite is a common constituent. In the East massive sulphide lens, cordierite-chlorite alteration zones occur mainly in the footwall (Ames et al., 1990) and, in the Main Mine, the chlorite schist consists of chlorite-biotite-quartz-cordierite±garnet, talc, tremolite (Speakman et al., 1982). The alteration in the West Anomaly is more magnesian and less potassic than that in the rest of the Ruttan mine. At the top of the East lens there are narrow sericite-galena-sphalerite-gahnite zones situated within 10 m of the contact of the overlying turbiditic volcanoclastic Powder Magazine formation (Ames et al., 1990). Structural complexities make it difficult to reconstruct the primary position of individual sulphide lenses within the Ruttan deposit. However, the West Anomaly on the western extremity of the deposit, correlates best with the lower ore lenses at the base of the Main Mine ore lenses (West Lens, Fig. 4). The intense magnesium metasomatism in the West Anomaly ore zone may be explained by the entrainment of fresh seawater along the margins of the sulphide mound as observed in ancient (Roberts and Reardon, 1978) and modern (Ames et al., 1993) deposits.

Chlorite schist zones are common proximal alteration types underlying massive sulphide deposits. They may be pipe-shaped in the classical sense (Franklin, 1986) or irregular broadly discordant tabular zones that lie subparallel to the base metal lenses as at Ruttan, the Jerome deposits in Arizona (Anderson and Nash, 1972), and some Australian VMS deposits (Large, 1992). The position of the chlorite schist surrounding the West Anomaly ore lenses may represent one Mg-rich layer that has been duplicated by folding or two Mg-rich zones developed above and below the massive sulphide lens. Evidence to support the latter interpretation is: 1) the consistent metal zoning from a Cu-rich base to a Zn-rich top in the intervening sulphide lens and 2) the change in mineralogy in the basal chlorite schist from 60% combined pyrrhotite, pyrite, and magnetite with 5% chalcopyrite-rich stringers and trace sphalerite to a chlorite schist above the orebody with lesser total combined sulphide (40%) and an increase in the sphalerite content (5%).

The geochemistry of the chlorite schists in the West Anomaly is similar to other VMS-related chlorite schist zones in that Mg, Fe, S, and Cu are gained and K, Ca, Sr, and Na are lost (Riverin and Hodgson, 1980; Elliot-Meadows and Appleyard, 1991). In contrast, Huston (1993) showed a significant gain in silica in the formation of the chlorite schist at the Balcooma deposit, Australia.

The presence of anhydrite in ancient massive sulphide deposits is thought to be rare (Lydon, 1988) although all of the Paleoproterozoic Snow Lake deposits contain anhydrite in association with calcite (Anderson Mine, Walford and Franklin, 1982; Chisel Lake, Stall and Osborne Lake mines, J. Kitzler, Hudson Bay Exploration and Development, pers. comm., 1991) and has been reported in Western Australian VMS deposits (Reynolds et al., 1975). Most Archean massive

sulphides lack anhydrite but it is present at the Geco deposit, Manitouwadge (Franklin, pers. comm., 1990). Anhydrite is a common constituent in modern seafloor massive sulphide occurrences in caps and chimneys (Bischoff, 1969; Koski et al., 1988; Ames et al., 1993; Turner et al., 1993) and forms part of the sekko ore in Kuroko-type deposits (Shikazono et al., 1983). In both of these situations, anhydrite is formed by subsurface mixing of seawater and hydrothermal fluid above 130°C (Hattori and Muehlenbachs, 1980; Haymon and Kasner, 1981; Styr et al., 1981; Shikazono et al., 1983).

Anhydrite occurs within the gangue of zinc-copper zones and as vug infillings near the top of the East Lens (Ames et al., 1990), in the West Anomaly in the Zn-rich ore and hanging-wall chlorite schist. Speakman et al. (1982) also noted the high concentrations of carbonate and sulphate in the chlorite schist zones, particularly towards the hanging wall of the Main mine, West Lens (Fig. 4). Although the anhydrite is mainly present in the upper Zn-rich zones and in capping chlorite schists, rare anhydrite veins occur in the footwall rocks. The association of anhydrite at the top of the Ruttan deposit in stratigraphically higher, zinc-bearing zones and zones of intense magnesium metasomatism indicates that the anhydrite formed through mixing of S-bearing hydrothermal fluid and entrained Mg-Ca rich seawater.

EXPLORATION IMPLICATIONS AND CONCLUSIONS

The large Ruttan volcanogenic massive sulphide deposit occurs in a thick sequence of felsic volcanoclastic rocks associated with arc tholeiitic assemblages, at a major stratigraphic break. The mineralogical and chemical classification of the least altered and proximal altered rock types in the Ruttan mine stratigraphy will assist in locating other prospective VMS areas. The Upper felsic volcanoclastic unit is a laterally continuous significant marker horizon. Environments similar to that of the Ruttan mine should be assessed in the remainder of the greenstone belt, based on the new geochemical and geological data. The Ruttan deposit is surrounded by a zone of Fe, Cu, Zn, and S enrichment and Ca and Na depletion. Mg enrichment is more local and generally associated with chlorite schist and intensely altered rhyolite. Silicification without magnesium enrichment is localized in the rhyolite-hosted stringer zone. Immobile elements in the distal alteration include Ti, Al, Zr, Y, Si, and Rb whereas only Al is considered immobile within the intensely altered rhyolite and chloritic schist. Lithogeochemistry of altered rocks limits the initial target area and provides exploration guides to mineralization.

The en échelon distribution of orebodies and thickening of ore zones are largely controlled by high angle reverse faulting although Z-shaped minor folds are common. Primary stacking of the orebodies in several hydrothermal sites and zone refining also occurred as the geochemistry and mineralogy of the various orebodies change with stratigraphic height. The large size of the Ruttan deposit also suggests multiple primary sites of sulphide deposition. Stretching lineations and

fold axis plunge subparallel to the plunge of the orebodies should aid mine explorationists in extending the life of the mine.

ACKNOWLEDGMENTS

We would like to thank Hudsons Bay Mining and Smelting for property and data access and J.M. Franklin and I.R. Jonasson for enthusiastic discussions. Z. Ramsden shared his vast knowledge of the Ruttan mine, after years of careful observations. The efforts of R. Lancaster and E. (Hillary) McEwen in drafting the figures are much appreciated. This manuscript benefitted from the review by and discussions with, E. Froese.

REFERENCES

- Akella, J.
1966: Calculation of material transport in some metasomatic processes; *Neues Jahrbuch furr Mineralogie, Abhandlung*, v. 104, no. 3, p. 316-329.
- Alt, J.C. and Jiang, Wei-The
1991: Hydrothermally precipitated mixed-layer illite-smectite in recent massive sulphide deposits from the sea floor; *Geology*, v. 19, p. 570-573.
- Ames, D.E.
1991: The Ruttan Cu-Zn deposit and depositional environment: an update; in *Report of Activities 1991*; Manitoba Energy and Mines, Minerals Division, p. 106-107.
- 1996: Stratigraphic and tectonic setting of the Paleoproterozoic Ruttan Cu-Zn VHMS deposit, Rusty Lake belt, Trans Hudson Orogen; in *EXTECH I: A Multidisciplinary Approach to Massive Sulphide Research in the Rusty Lake-Snow Lake Greenstone Belts*, Manitoba, (ed.) G.F. Bonham-Carter, A.G. Galley, and G.E.M. Hall; Geological Survey of Canada, Bulletin 426 (this volume).
- Ames, D.E. and Scoates, J.S.
1992: Geology, Preliminary map of the geological setting of the Ruttan Cu-Zn deposit, Rusty Lake belt, Manitoba; Geological Survey of Canada, Open File 2571, scale 1:5000 and notes.
- Ames, D.E., Franklin, J.M., and Hannington, M.D.
1993: Mineralogy and geochemistry of active and inactive chimneys and massive sulphide, Middle Valley, northern Juan de Fuca Ridge: an evolving hydrothermal system; *Canadian Mineralogist*, v. 31, p. 997-1024.
- Ames, D.E., Scoates, J.S., and Franklin, J.M.
1990: Preliminary report on the geological setting of the Ruttan base metal deposit and associated hydrothermal alteration, Rusty Lake volcanic belt, Manitoba (NTS 64B/5); in *Report of Activities 1990*; Manitoba Energy and Mines, Minerals Division, p. 178-186.
- Anderson, C.A. and Nash, J.T.
1972: Geology of the massive sulphide deposits at Jerome, Arizona – a Reinterpretation; *Economic Geology*, v. 67, p. 845-863.
- Bailes, A.H. and Syme, E.C.
1989: Geology of the Flin Flon-White Lake area; Manitoba Energy and Mines, Geological Report GR 87-1, 313 p.
- Baldwin, D.A.
1987: Physical volcanology of the northwest segment of the Karsakuwigamak Block, Proterozoic Rusty Lake metavolcanic belt, Northern Manitoba; Ph.D. thesis, University of Manitoba, Winnipeg, Manitoba, 438 p.
- 1988: Geology of the southern part of the Rusty Lake volcanic belt; Manitoba Energy and Mines, Geological Report GR86-1, p. 1-90.
- Baldwin, D.A., Syme, E.C., Zwanzig, H.V., Gordon, T.M., Hunt, P.A., and Stevens, R.P.
1987: U-Pb zircon ages from the Lynn Lake and Rusty Lake metavolcanic belts, Manitoba: two ages of Proterozoic magmatism; *Canadian Journal of Earth Sciences*, v. 24, p. 1053-1063.

- Barrett, T.J. and MacLean, W.H.**
1991: Chemical, mass, and oxygen isotope changes during extreme hydrothermal alteration of an Archean rhyolite, Noranda, Quebec; *Economic Geology*, v. 86, p. 406-414.
- Beswick, A.E. and Soucie, G.**
1978: A correction procedure for metasomatism in an Archean greenstone belt; *Precambrian Research*, v. 6, p. 235-248.
- Bischoff, J.L.**
1969: Red Sea geothermal brine deposits: Their mineralogy, chemistry and genesis; in *Hot Brines and Recent Heavy Metal Deposits in the Red Sea*, (ed.) E.T. Degens and R.A. Ross; Springer-Verlag, New York, p. 368-401.
- Bubar, D.S. and Heslop, J.B.**
1985: Geology of the Gondor volcanogenic massive sulphide deposit, Slave Province, N.W.T.; Canadian Institute of Mining and Metallurgy Bulletin, v. 78, no. 876, p. 52-60.
- Davidson, A., Carmichael, D.M., and Pattison, D.R.M.**
1990: Metamorphism and geodynamics of the southwestern Grenville Province, Ontario; International Union of Geological Sciences, International Geological Correlation Program (IGCP) Projects 235/304, Field Trip #1 Guidebook, 123 p.
- Elliot-Meadows, S.R. and Appleyard, E.C.**
1991: The alteration geochemistry and petrology of the Lar Cu-Zn Deposit, Lynn Lake area, Manitoba, Canada; *Economic Geology*, v. 86, p. 486-505.
- Finlow-Bates, T. and Stumpfl, E.F.**
1981: The behaviour of so-called immobile elements in hydrothermally altered rocks associated with volcanogenic submarine-exhalative ore deposits; *Mineralium Deposita*, v.16, p. 319-328.
- Fisher, R.V.**
1966: Rocks composed of volcanic fragments and their classification; *Earth Science Reviews*, v. 1, p. 287-298.
- Franklin, J.M.**
1986: Volcanogenic massive sulphide deposits-an update; in *Geology and Genesis of Mineral Deposits in Ireland*, (ed.) C.J. Andrew, R.W.A. Crowe, S. Finlay, W.M. Pennell, and J.F. Pyne; Irish Association for Economic Geology, v. 70, p. 63-79.
- Galley, A.G., Bailes, A.H., and Kitzler, G.**
1993: Geological setting and hydrothermal evolution of the Chisel Lake and North Chisel Zn-Pb-Cu-Ag-Au massive sulphide deposits, Snow Lake, Manitoba; *Exploration Mining Geology*, v. 2, no. 4, p. 271-295.
- Gordon, T.M., Hunt, P.A., Bailes, A.H., and Syme, E.C.**
1990: U-Pb ages from the Flin Flon and Kiseeynew belts, Manitoba: chronology of crust formation at an Early Proterozoic accretionary margin; in *The Early Proterozoic Trans-Hudson Orogen of North America*, (ed.) J.F. Lewry and M.R. Stauffer; Geological Association of Canada, Special Paper 37, p. 177-200.
- Grant, J.A.**
1986: The isocon diagram – a simple solution to Gresens' equation for metasomatic alteration; *Economic Geology*, v. 81, p. 1976-1982.
- Gresens, R.L.**
1967: Composition – volume relationships of metasomatism; *Chemical Geology*, v. 2, p. 47-65.
- Haskin, L.A., Haskin, M.A., Frey, F.A., and Wildeman, T.R.**
1968: Relative and absolute terrestrial abundances of the rare earths; in *Origin and Distribution of the Elements*, (ed.) L.H. Ahrens; Pergamon Press, New York, p. 889-912.
- Hattori, K. and Muehlenbachs, K.**
1980: Marine hydrothermal alteration at a Kuroko ore deposit, Kosaka, Japan; *Contributions to Mineralogy and Petrology*, v. 74, p. 285-292.
- Haymon, R.M. and Kastner, M.**
1981: Hot spring deposits on the East Pacific Rise at 21°N: preliminary description of mineralogy and genesis; *Earth and Planetary Science Letters*, v. 53, p. 363-381.
- Hey, M.H.**
1954: A new review of the chlorites; *Mineralogical Magazine*, v. 30, p. 277-292.
- Hoffman, P.F.**
1988: United plates of America, the birth of a craton: Early Proterozoic assembly and growth of Laurentia; *Annual Review of Earth and Planetary Sciences*, v. 16, p. 543-603.
- Hughes, C.J.**
1973: Spilites, keratophyres and the igneous spectrum; *Geological Magazine*, v. 109, p. 513-527.
- Huston, D.L.**
1993: The effect of alteration and metamorphism on the wall rocks to the Balcooma and Dry River South volcanic-hosted massive sulphide deposits, Queensland, Australia; *Journal of Geochemical Exploration*, v. 48, p. 277-307.
- Koski, R.A., Shanks, W.C. III, Bohrsen, W.A., and Oscarson, R.L.**
1988: The composition of massive sulphide deposits from the sediment covered floor of Escanaba Trough, Gorda Ridge: Implications for depositional processes; *Canadian Mineralogist*, v. 26, p. 655-673.
- Large, R.R.**
1992: Australian volcanic-hosted massive sulphide deposits: Features, styles and genetic models; *Economic Geology*, v. 87, p. 471-510.
- Leake, B.E.**
1978: Nomenclature of amphiboles; *American Mineralogist*, v. 63, p. 1023-1053.
- Lydon, J.W.**
1988: Volcanogenic massive sulphide deposits Part 2: Genetic models. *Geoscience Canada*, v. 15, p. 43-65.
- MacLean, W.H.**
1990: Mass change calculations in altered rock series; *Mineralium Deposita*, v. 25, p. 44-49.
- MacLean, W.H. and Kranidiotis, P.**
1987: Immobile elements as monitors of mass transfer in hydrothermal alteration: Phelps Dodge massive sulphide deposit, Matagami, Quebec; *Economic Geology*, v. 82, p. 951-962.
- McCutcheon, S.R.**
1992: Base-metal deposits of the Bathurst-Newcastle district: characteristics and depositional models; *Exploration Mining Geology*, v. 1, no. 2, p. 105-120.
- Mediesky, H.E. and Stanley, C.R.**
1993: Identifying metasomatic zones associated with volcanic-hosted massive sulphide deposits using Pearce element ratio analysis. The Gangué, Geological Association of Canada-Mineral Deposits Division Newsletter, Jan. 1993, p. 5-7.
- Olsen, P.E.**
1987: The stratigraphy, structural geology and geochemistry of the Fox Lake massive sulphide deposit; M.Sc. thesis, University of Manitoba, Winnipeg, Manitoba, 163 p.
- Percival, J.B. and Ames, D.E.**
1993: Clay mineralogy of active hydrothermal chimneys and an associated mound, Middle Valley, northern Juan de Fuca ridge; *Canadian Mineralogist*, v. 31, p. 957-971.
- Reynolds, D.G., Brook, W.A., Marshall, A.E., and Allchurch, P.D.**
1975: Volcanogenic copper-zinc deposits in Pilbara and Yilgarn Archean blocks; in *I. Metals*, (ed.) C.L. Knight; Australasian Institute of Mining and Metallurgy, Monograph 5, p. 185-194.
- Riverin, G. and Hodgson, C.J.**
1980: Wall-rock alteration at the Millenbach Cu-Zn mine, Noranda, Quebec; *Economic Geology*, v. 75, p. 424-444.
- Roberts, R.G. and Reardon, E.J.**
1978: Alteration and ore-forming processes at Mattagami Lake Mine, Quebec; *Canadian Journal of Earth Sciences*, v. 15, p. 1-21.
- Shikazono, N., Holland, H.D., and Quirk, R.F.**
1983: Anhydrite in Kuroko deposits: mode of occurrence and depositional mechanisms; *Economic Geology Monograph 5*, p. 329-344.
- Sokolova, N.T. and Khodakovskiy, I.L.**
1977: The mobility of aluminum in hydrothermal solutions; *Geochemistry International*, v. 14, no. 3, p. 105-112.
- Speakman, D.S., Chornoby, P.J., Haystead, B.C.W., and Holmes, G.F.**
1982: Geology of the X Ruttan deposit, northern Manitoba; in *Precambrian Sulphide Deposits*, (ed.) R.W. Hutchison, C.D. Spence, and J.M. Franklin; Geological Association of Canada, Special Paper 25, p. 525-556.
- Styrt, M.M., Brackmann, A.J., Holland, H.D., Clark, B.C., Pisutha-Arnond, V., Eldridge, C.S., and Ohmoto, H.**
1981: The mineralogy and the isotopic composition of sulfur in hydrothermal sulfide/sulfate deposits on the East Pacific Rise, 21°N latitude; *Earth and Planetary Science Letters*, v. 53, p. 382-390.
- Sun, S.S. and Nesbitt, R.W.**
1978: Petrogenesis of Archean ultrabasic and basic volcanics: evidence from rare earth elements; *Contributions to Mineralogy and Petrology*, v. 65, p. 301-325.
- Syme, E.C.**
1990: Stratigraphy and geochemistry of the Lynn Lake and Flin Flon metavolcanic belts, Manitoba; Geological Association of Canada, Special Paper 37, p. 143-161.

Syme, E.C. and Bailes, A.H.

- 1993: Stratigraphic and tectonic setting of Early Proterozoic volcanogenic massive sulphide deposits, Flin Flon, Manitoba; *Economic Geology*, v. 88, p. 566-589.

Turner, R.J.W., Ames, D.E., Franklin, J.M., Goodfellow, W.D., Leitch, C.H.B., and Hoy, T.

- 1993: Character of active hydrothermal mounds and nearby altered hemipelagic sediments in the hydrothermal areas of Middle Valley, northern Juan de Fuca ridge: Data on shallow cores; *Canadian Mineralogist*, v. 31, p. 973-995.

Walford, P.C. and Franklin, J.M.

- 1982: The Anderson Lake mine, Snow Lake, Manitoba; in *Precambrian Sulphide Deposits*, (ed.) R.W. Hutchison, C.D. Spence, and J.M. Franklin; Geological Association of Canada, Special Paper 25, p. 481-524.

Contribution to the 1989-1994 Rusty Lake-Snow Lake Mining Camps, Canada-Manitoba Exploration Science and Technology Initiative (EXTECH I)

Effects of acid mine effluent on sediment and water geochemistry, Ruttan Cu-Zn mine

W.W. Shilts¹, W.B. Coker², and A.M. MacDonald³

Shilts, W.W., Coker, W.B., and MacDonald, A.M., 1996: Effects of acid mine effluent on sediment and water geochemistry, Ruttan Cu-Zn mine; in EXTECH I: A Multidisciplinary Approach to Massive Sulphide Research in the Rusty Lake-Snow Lake Greenstone Belts, Manitoba, (ed.) G.F. Bonham-Carter, A.G. Galley, and G.E.M. Hall; Geological Survey of Canada, Bulletin 426, p. 77-103.

Abstract: Waters were collected from the surface and bottom of four lakes as well as from the Churchill River and approximately 20 small ponds beside the Leaf Rapids-Ruttan mine-South Indian Lake road to determine geochemical variations related to tailings and waste rock disposal from the Ruttan Cu-Zn VHMS deposit. Using sonar profiling as a guide, grab samples and cores of sediments were also collected in Ruttan, Brehaut, Rusty, and Alto lakes to investigate the geochemical and sedimentological effects of liming the acid (pH 2.5) outflow from Ruttan Lake. Preliminary results indicate that metals anthropogenically enriched in Ruttan Lake (Zn, Cd, and Hg in particular) are scavenged and precipitated at the inflow end of Brehaut Lake as a result of adding lime solutions to the Vermilion River, midway through the 500 m reach that connects Ruttan Lake and Brehaut Lake. Zn in Ruttan Lake water (up to 17 ppm) is precipitated in the limey sediment. Zn is not enriched in waters of Rusty Lake, the next lake downstream from Brehaut Lake. Rusty Lake has Zn concentrations comparable to background water from Alto Lake (<10 ppb Zn). At present, liming appears to be controlling metal migration effectively, but a body of Zn-Cd-Hg-rich carbonate precipitate occupies the south end of Brehaut Lake which, without liming, would be receiving water of pH 2.5 from Ruttan Lake, resulting in a remobilization of metals. The related study also showed that Zn concentrations are elevated in water in contact with waste rock used to upgrade sections of the Leaf Rapids-South Indian Lake and Brehaut Lake roads.

Résumé : Des échantillons d'eau ont été recueillis à la surface et au fond de quatre lacs ainsi que dans le fleuve Churchill et dans une vingtaine d'étangs situés le long de la route qui relie Leaf Rapids à la mine Ruttan et à South Indian Lake; le but était de déterminer les variations géochimiques liées à l'accumulation des résidus miniers et des stériles provenant du gisement de Cu-Zn (sulfures massifs volcanogène) de Ruttan. De plus, des échantillons de sédiments lacustres ont été prélevés à la benne et au carottier dans les lacs Ruttan, Brehaut, Rusty et Alto, en se servant de profils établis par sonar; cette fois-ci, l'échantillonnage avait pour objectif d'étudier les effets géochimiques et sédimentologiques du chaulage des écoulements acides (pH = 2,5) du lac Ruttan. Les résultats préliminaires montrent que les métaux d'origine anthropique présents dans le lac Ruttan (zinc, cadmium et mercure en particulier) sont entraînés et précipités au niveau de l'affluent du lac Brehaut, à la suite de l'ajout de solutions de chaux dans la rivière Vermilion, à mi-chemin entre le lac Ruttan et le lac Brehaut qui sont à 500 m l'un de l'autre. Le zinc présent dans l'eau du lac Ruttan (jusqu'à 17 ppm) est précipité dans les sédiments calcaires. Sa teneur n'augmente pas dans les eaux du premier lac en aval du lac Brehaut. Le lac Rusty présente des concentrations de zinc comparables à celles de fond mesurées dans le lac Alto (<10 ppb). Le chaulage semble limiter efficacement la migration des métaux, mais on observe à l'extrémité sud du lac Brehaut une masse de précipité de carbonates riche en zinc, en cadmium et en mercure qui, à défaut de chaulage, recevrait des eaux à un pH de 2,5 provenant du lac Ruttan. Cela se traduirait par une remobilisation des métaux. Une étude connexe a également permis de constater que les teneurs en zinc sont élevées dans les eaux en contact avec les débris rocheux utilisés pour la réfection de portions de la route qui relie Leaf Rapids à South Indian Lake, ainsi que de la route d'accès au lac Brehaut.

¹ Illinois State Geological Survey, Illinois Department of Natural Resources, 615 Peabody Drive, Champaign, Illinois, 61820 U.S.A.

² BHP Minerals Canada Ltd., 33 Yonge Street, Suite 610, Toronto, Ontario M5E 1G4

³ Geological Survey of Canada, 601 Booth St., Ottawa, Ontario K1A 0E8

INTRODUCTION

As part of the first Exploration Science and Technology (EXTECH) Initiative, a detailed geochemical study was undertaken in lakes and drainage systems around the Ruttan copper-zinc mine in northern Manitoba (Ames, 1996).

The main objectives of the study were to establish the geochemical effects of mine tailings on sedimentation and sediment and water chemistry in the surrounding area and to understand the nature of the carbonate precipitate in Brehaut Lake that is forming as a result of the liming of waste water outflow from Ruttan Lake.

Previous environmental studies focused primarily on the effects of the mine on water quality and on the biological community (Munro and Ruggles, 1978; Green and Beck, 1992). In this study, water samples, sediment grab samples, and sediment cores were collected from lakes and drainage channels in the area surrounding the mine. Samples were subjected to total chemical analysis, sequential extractions, and scanning electron microscope analysis. Sonar profiles were done to determine sediment thickness and facies for both Alto Lake and Brehaut Lake.

GENERAL DESCRIPTION OF STUDY AREA

The Ruttan mine is located in northern Manitoba, approximately 24 km east of Leaf Rapids and 750 km northwest of Winnipeg (see Ames, 1996). The surrounding rolling to hilly terrain, typical of the Canadian Shield, is covered by northern coniferous forests with numerous lakes and ponds.

Ruttan Lake is a small lake with a $<1 \text{ km}^2$ surface area. Its discharge water flows into Brehaut Lake which has a surface area of about 3.3 km^2 and which had an average natural depth of 3.4 m before it was raised about 2 m by the installation of a concrete weir on the northwestern arm of the lake. Discharges from the Brehaut Lake weir flow into the Vermilion River, which enters Rusty Lake about 8 km downstream. Rusty Lake has a surface area of approximately 15 km^2 and is less than 4 m deep at its deepest (Munro and Ruggles, 1978). Water from Rusty Lake re-enters the Vermilion River and flows downstream approximately 12 km before entering the Churchill River.

Ruttan Lake is part of the tailings confinement area at the Ruttan mine. It has also been artificially raised by about 2 m through installation of a concrete weir midway along the 500 m-long reach of the Vermilion River linking Ruttan Lake and Brehaut Lake. The tailings, which form a substantial delta in Ruttan Lake, have caused a radical lowering of its pH and an increase in the concentration of metals in its water. To counteract this, a lime slurry is piped into the waterway at the weir about 250 m upstream from the inlet into Brehaut Lake. The result is the formation of a thick, metal-rich, lime precipitate at the south end of Brehaut Lake.

GEOLOGY

Bedrock geology

The geological setting, both regional and local, of the Ruttan mine is described by Ames (1996). Brehaut Lake and Alto Lake lie in granitic and granodioritic terrane, whereas Rusty Lake lies in a complex of metavolcanic, metasedimentary, and acidic igneous rocks.

The geology of the Ruttan orebody, and the nature of the mineralization within the orebody, are thoroughly described in Ames (1996).

Surficial geology

The surficial geology of the area has been mapped by Kaszycki and Way Nee (1989) and by Klassen (1986) (Fig. 1). The study area lies on the Southern Indian Bedrock Plateau which consists mostly of drift-veneered bedrock hills

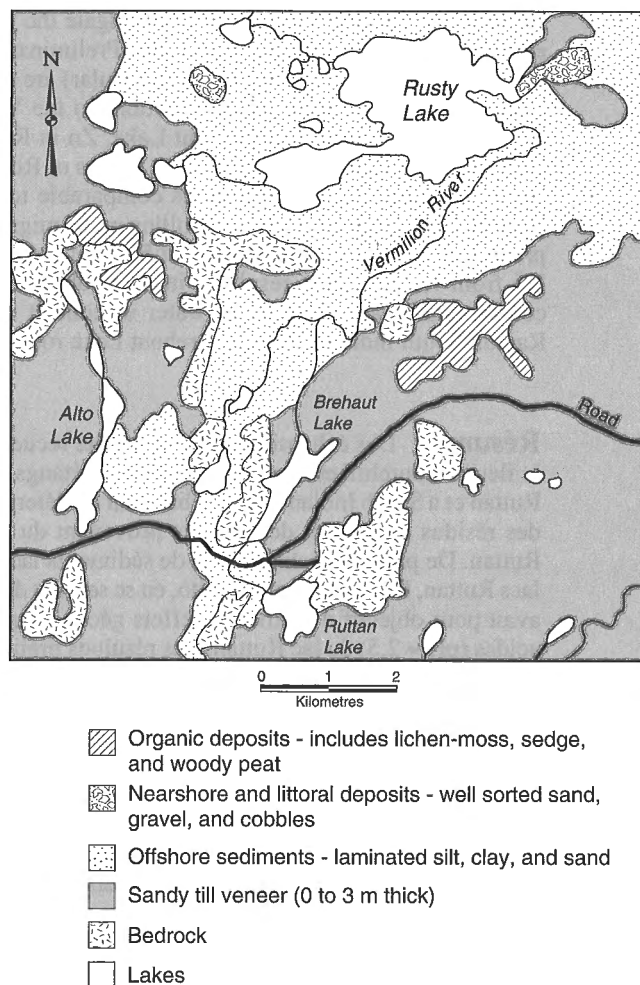


Figure 1. Generalized surficial geology of study area (simplified from Kaszycki and Way Nee (1989)).

and knobs with intervening low areas of organic terrain. The organic deposits overlie laminated clays of Glacial Lake Agassiz; the clays form a 2 to 5 m-thick cover over much of the area. The lake clays drape bedrock or sandy till, the latter representing the last of at least five glacial events to affect the area.

DESCRIPTION OF THE RUTTAN MINE

History

Sheritt Gordon Mines Ltd. staked the area which was to become the Ruttan orebody in August 1968 on the basis of combined airborne magnetic and input electromagnetic surveys conducted earlier that year (Speakman et al., 1982). During the late sixties and early seventies, the milling plant and the townsite of Leaf Rapids were constructed. Glacial overburden and waste rock overlying the deposit were removed during the development of the open pit, and used to upgrade the road between the Ruttan mine and Leaf Rapids. The mine opened in April 1973. In 1987, ownership of the deposit was transferred to Hudson Bay Mining and Smelting Company Limited. The remaining life of the mine is not known.

Table 1. Composition of lime solution added to water exiting Ruttan Lake (Dishaw, pers. comm., 1993).

| COMPOUND | CONCENTRATION |
|--|---------------|
| total CaO | 95.7 % |
| available CaO | 92.3 % |
| acid insolubles | 1.7 % |
| R ₂ O ₃ ** | 1.0 % |
| MgO | 0.7 % |
| total S | 0.045 % |
| Fe ₂ O ₃ | 0.16 % |
| heavy metals | <0.5 ppm |
| * Available CaO is the reactive lime | |
| ** R is a variable in metal oxides e.g. Al in Al ₂ O ₃ | |

Ore processing

The 64 Mt comprising the ore lenses of the entire Ruttan massive sulphide orebody has an average grade of 1.27% Cu and 1.35% Zn (Ames, 1996). Milling transforms the ore into a concentrate grading 50-52% Zn and 26-28% Cu (Green and Beck, 1992). The ore goes through a basic process of crushing, grinding, selective flotation, and de-watering of the slurry. Sodium amyl xanthate is used as a collector in the Zn and Cu flotation processes (Dishaw, pers. comm., 1993). The xanthate adsorbs onto the surfaces of the Cu and Zn particles, making flotation possible. Copper sulphate is added in the Zn flotation process so that the Zn will adsorb onto the collector satisfactorily. In order for the reagents to work, the pH must be modified from neutral to 11 or 12; to accomplish this, approximately 2.0 kg lime is added to every metric tonne of mined ore during processing. Eighty per cent of the water used during the processing is reused (Dishaw, pers. comm., 1993).

Waste water remediation

In spite of the addition of lime during the milling process, by 1976 the pH of water exiting Brehaut Lake had fallen noticeably from natural levels, indicating that the entire Vermilion River system downstream from the Ruttan mine was being contaminated rapidly and that the Churchill River, of which the Vermilion River is a tributary, could be in jeopardy. To counteract the acidification and the enhanced metal mobility resulting from it, various schemes to add lime to the effluent from the mine site were tried, culminating in the construction in 1989 of a concrete weir about 200 m downstream from the original outlet of Ruttan Lake. At the weir, lime is added continuously during the summer months, and the flow from Ruttan Lake is cut off in October by closing the weir. At that time Brehaut Lake is full and Ruttan Lake is at a low water stage. Over the winter, Ruttan Lake fills with waste water from the mine. Thus, the transfer of aqueous mine wastes from Ruttan Lake to Brehaut Lake is cyclical, the drainage link functioning only during the 6-month warm season when lime can be added effectively.

Table 2. Limits on metal concentrations (mg/L) and total suspended matter set by Manitoba Department of Mines, Natural Resources and Environment under Clean Environment Commission Order No. 858VO.

| Parameter | Maximum Concentration "dissolved" in water (mg/L) | Maximum Concentration in suspended sediment ¹ (mg/L) |
|---|--|--|
| Total Arsenic | 0.5 | 0.75 |
| Total Copper | 0.3 | 0.45 |
| Total Lead | 0.2 | 0.3 |
| Total Nickel | 0.5 | 0.75 |
| Total Zinc | 0.5 | 0.75 |
| Total Suspended Matter | 25.0 | 37.5 |
| - pH must be greater than 6.0 in a water sample and 5.5 in a sediment grab. | | |
| ¹ expressed as equivalent concentration in water | | |

When lime is added at the weir, it is introduced at the rate of 2.5 kg/metric tonne of ore mined. Daily mining rates have varied between 5000 to 9000 t. Table 1 gives the average composition of the lime solution presently added to the runoff.

Limits on pH and the concentration of metals released from the Brehaut Lake outlet weir are set by the Manitoba Department of Mines, Natural Resources and Environment (MDMNRE). These limits, which are summarized in Table 2,

are from the Clean Environment Commission (CEC) Order No. 858VO. Dissolved metal concentrations and pH are monitored at the weir structure at the outlet of Brehaut Lake.

The impacts on downstream waterways caused by mining at Ruttan Lake were assessed by MDMNRE in 1991. Except for Zn, metal concentrations in Brehaut Lake discharges were constantly within the limits set by CEC Order No. 858VO. Zn periodically exceeded the limit, with the greatest number of exceedances between 1987 and 1990. In Rusty Lake there

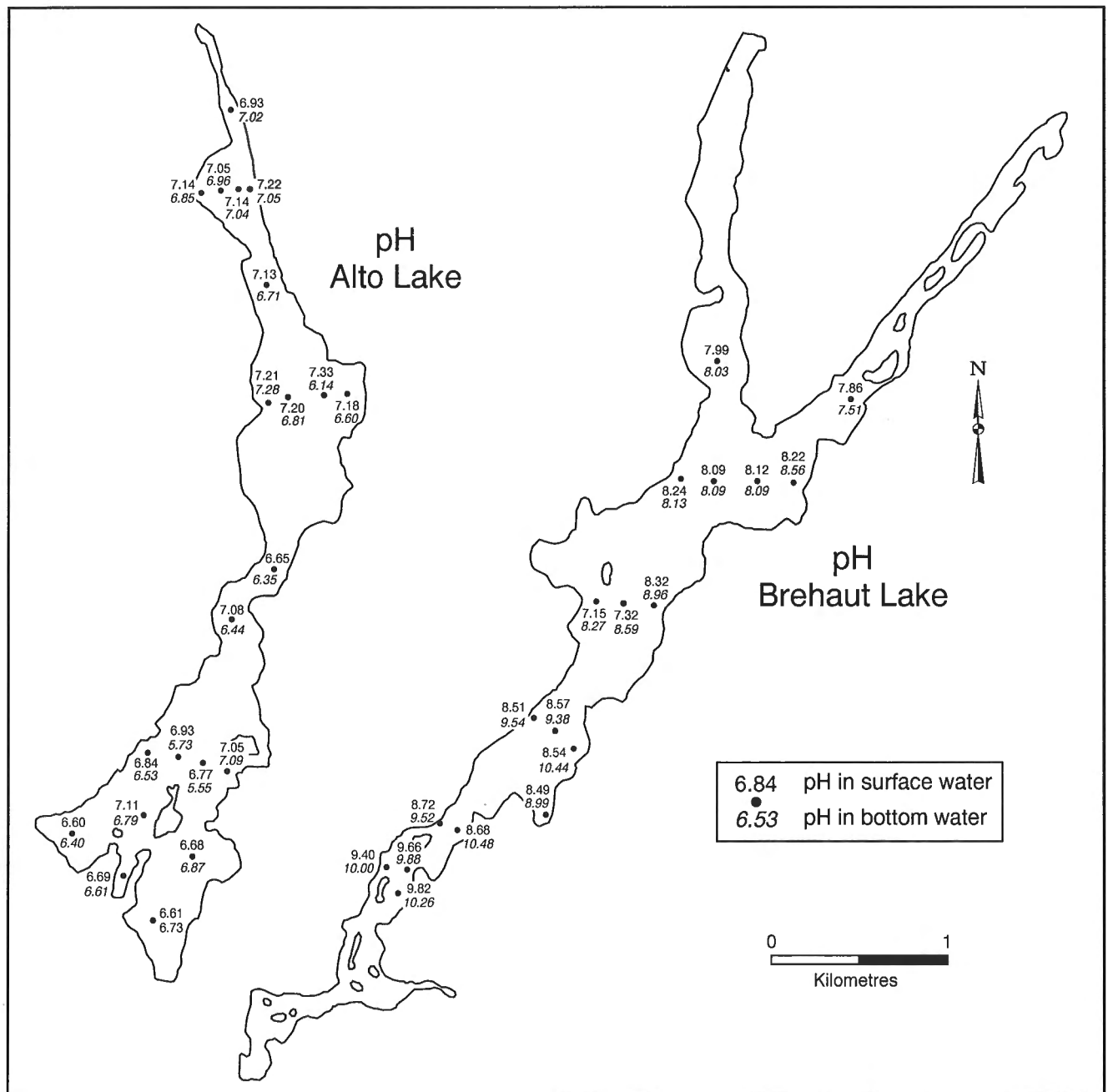


Figure 2. Location of lake sampling sites (1990), with surface and bottom water pH values, for Alto Lake and Brehaut Lake.

were significant increases in conductivity and Ca concentrations in 1974-1990 and 1976-1984 respectively. Concentrations of metals at the outlet of Brehaut Lake and in Rusty Lake were analyzed statistically to determine if parameters such as pH and metal concentration had increased or decreased over time. It was found that over time the water at the outfall of Brehaut Lake had a reduction in its pH and a significant increase in its conductivity, total solids, dissolved solids, Ca, Mg, hardness, sulphate, Cu, and Zn. Elevated Zn concentrations occurred occasionally at both the inlet and outlet of Rusty Lake. There was no evidence that the Ruttan mine had any influence upon water quality downstream of the confluence of the Vermilion and Churchill rivers.

SAMPLE COLLECTION METHODOLOGIES

Water samples

During the summer of 1990, water samples were collected from Brehaut Lake and Alto Lake (Fig. 2). In the summer of 1991, further water samples were collected from Rusty Lake, Ruttan Lake, Alto Lake, Brehaut Lake, the Vermilion River, and the Churchill River; samples were also collected from flooded depressions and drainages along the Leaf Rapids-Ruttan mine-South Indian Lake road (Fig. 3).

Bottles were triple rinsed at each site with water from the site. Lake water samples were collected in the rinsed bottles from near the surface (0.5-1.0 m depth) and from the lake bottom about 0.2 to 0.5 m above the sediment-water interface, using a Van Dorn sampler. All waters were filtered (0.45 µm) and acidified (to 0.4% in Ultrex HNO₃) for cation determination within 24 h.

The water samples collected on a transect from Leaf Rapids to the outlet of Issett Lake were taken from small pools formed where drainage was partially blocked by the road, in streams, and in the water of Issett Lake, itself. Care was taken

to avoid any influence of local sources of chemical input, such as galvanized culverts or heavy aquatic plant or algal growth. The weather was extremely hot when this sampling was done, daytime temperatures sometimes reaching 36°C, such that these waters were probably much warmer than normal.

Samples collected in 1990 were analyzed, at base camp, for "dissolved" (<0.45 µm) concentrations of Zn, Cd, Cu, and Pb using anodic stripping voltametry (ASV) (Hall and Vaive, 1992). Determination of pH was done the same day that the samples were collected. Samples collected in 1991 were analyzed for pH and for dissolved Zn, Cu, Ni, Pb, Cd, Mn, and Fe after being shipped to Ottawa. Metal concentrations were determined using a combination of atomic absorption spectrometry (flame and graphite furnace AAS) and ASV (Hall and Vaive, 1992).

Sediment grab samples

During the summer of 1990, grab samples were collected from Brehaut Lake and Alto Lake (Fig. 2). The following summer, sediment cores and additional grab samples were collected from Ruttan Lake, Brehaut Lake, Alto Lake, Rusty Lake, and from the Churchill River at the confluence with the Vermilion River (Fig. 3).

Lake sediment grab samples were collected using an Ekman Dredge. They were placed in paper bags and dried at air temperature before shipment to Ottawa. The dried, disaggregated, sieved samples were analyzed by Bondar-Clegg and Company, Ltd., using the extractions and techniques described in Table 3.

Sonar profiles

Before sampling in Brehaut Lake and Alto Lake, detailed subbottom acoustic profile (SAP) (Sonar) surveys were carried out on both lakes. The surveys provided a detailed map

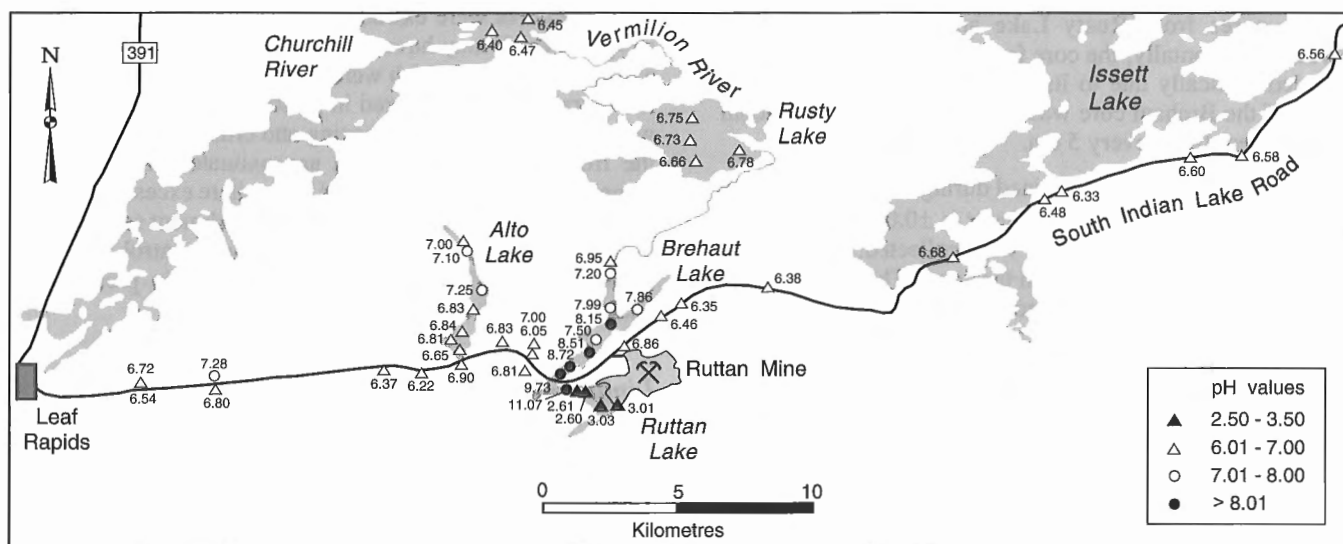


Figure 3. Location of regional lake, stream and pond sampling sites (1990 and 1991), with surface water pH values.

Table 3. Analyses and extractions performed on 1990 and 1991 sediment grab samples.

| Element | Year | Method | Extraction |
|-------------------------|------|------------------------|----------------------------|
| Mn, Fe, Co, Ni, Cu, Zn, | 1990 | AAS | HCl-HNO ₃ (1:3) |
| Ag, Cd, Pb | 1991 | | |
| Hg | 1990 | Cold Vapour AAS | HNO ₃ -HCl |
| | 1991 | | |
| As | 1990 | Hydride Generation AAS | HCl-HNO ₃ (3:1) |
| Loss-on-Ignition | 1990 | Gravimetric | |
| | 1991 | | |

of bathymetry and bottom sediment facies on which the sampling plan was based. In addition to providing information on the areal distribution of sediments, it was possible to determine the thickness and stratigraphy of sediments and the distribution of gas within them. The system used was a Raytheon RTT 1000, operating at frequencies of 200 kHz and 7 kHz. Navigation was by eye, and traverses were run from headland to headland. This preliminary survey was useful, because it was found, as discussed later, that both natural and anthropogenic metal concentrations varied strongly according to the sediment facies sampled.

Lake sediment cores

During the summer of 1991, lake sediment cores were collected from Ruttan Lake, Brehaut Lake, and Rusty Lake using a Brown Corer. This corer, which operates on the same principle as a Livingston Corer, is pushed into the sediment manually using metal poles. In the south part of Brehaut Lake the water with suspended or flocculated sediment grades downward into consolidated sediment, making it difficult to estimate a depth for the sediment-water-interface. This problem was not encountered elsewhere in Brehaut Lake, Ruttan Lake, or Rusty Lake. The cores were refrigerated as soon as possible after collection and remained refrigerated at 4°C, until extrusion in Ottawa.

The cores from Rusty Lake and Ruttan Lake were extruded horizontally; the core from Brehaut Lake had to be extruded vertically due to its high water content. The first 20 cm of the Brehaut core was sampled together, additional samples were taken every 5 cm.

Pore water pH was determined during extrusion. Though the margin of error for the pH meter is ± 0.05 , the cores did not remain stationary after they were collected, and the pore water may have migrated within the cores. Therefore, the pH measurements may be of limited value.

X-radiographs were used to determine structure in the cores, such as laminations, before extrusion.

SEQUENTIAL LEACH METHODOLOGIES

Description of the method

Sequential extractions consist of a series of chemical leaches applied to a soil or sediment sample. Each succeeding extraction is more intense and attacks a different phase in the sample.

Sequential extractions can be used to identify the main binding sites of trace elements, estimate biological availability of metal pollutants, evaluate sedimentary diagenetic effects on metal mobility, and estimate the remobilization of metals under changing environmental conditions. In environmental studies, trace metal species identification can be more informative than total element concentrations because the biogeochemical and ecotoxicological significance of a given pollutant is a function of the chemical form or species of the element present (Batley, 1989).

The sequential extraction procedure (Hall et al., 1996) was designed to extract metal preferentially from the following phases: (1) adsorbed, exchanged, and in carbonate minerals, (2) hydrous iron and manganese oxides, (3) crystalline iron oxides, (4) sulphides, and (5) silicates and other resistate minerals.

Sediments from Ruttan Lake, Brehaut Lake, and Rusty Lake were probably deposited under anoxic conditions; however, the cores were extruded and analyzed in atmospheric oxygen, which may have driven diagenetic reactions. After extrusion, samples which were to be examined using sequential extractions, were stored in plastic freezer bags. Samples were homogenized by squeezing and crushing the sample in the freezer bags, after which approximately 1.5 g of wet sample was put into a centrifuge tube where excess water was removed by centrifuging. Twenty-two sediment samples (including two repeats, one blank, and two control reference standards (LKSD-4, TILL-2; Lynch, 1990, in press) were analyzed in each of two runs.

Limitations of the method

Direct determination of the sediment component with which a metal is associated is not always possible, due to the great variety of solid phases that can bind a metal and the low metal concentrations involved (Rapin et al., 1986). As noted above, sample pretreatment and the presence/absence of atmospheric oxygen during treatment can affect the partitioning of trace metals within the lake sediment samples.

Although the cores were stored in a refrigerator at 4°C before extrusion, no storage method completely preserves the initial metal partitioning of sediments; short-term wet storage (2-4°C) is considered acceptable (Rapin et al., 1986).

The cores were analyzed under toxic conditions. The samples in the first run were transferred from freezer bags to test tubes the day before analysis began. The samples in the second run were kept in centrifuge tubes for about two to six days before analysis (transfer from freezer bags was done over a period of a week).

Rapin et al. (1986) made the following points concerning anoxic sediments extracted under toxic conditions:

1. generally it is not possible to predict the consequences of exposure to oxygen during extraction;
2. some of the amorphous sulphide will be extracted before the sulphide extraction, possibly due to oxidation (i.e. in the carbonate and hydrous iron and manganese extraction); and
3. Fe, which was originally in exchangeable form or bound in (or adsorbed onto) carbonates, is actually extracted with the hydrous iron and manganese oxides.

Accuracy and precision

In each run, two reference control standards (LKSD-4 and TILL-2), prepared and accredited by the GSC (Lynch, 1990, in press), were analyzed. A comparison of the selective leach data obtained for these controls in this work with those presented by Hall et al. (1996) is excellent. Comparison of the element concentrations summed over the five selective leaches with the accepted total values for these samples shows that losses of elements through the various manipulations of the sequential extraction are minimal (<10%) (Macdonald, 1993). Relative standard deviation values for the elements extracted from the five phases were typically in the range 5-12% at concentrations 10% greater than the detection limits. Precision for sediment samples from Brehaut Lake tended to be higher (worse) than that for those from either Rusty Lake or Ruttan Lake, probably a reflection of the higher water content of this core and the greater sampling variability therefore encountered (MacDonald, 1993).

PHYSICAL AND CHEMICAL CHARACTERISTICS OF THE LAKES STUDIED

Brehaut Lake and Alto Lake share no common drainage. They are similar in size, shape, orientation, and bathymetry, but significant anthropogenic changes have altered many of the natural physical and chemical parameters controlling the sedimentation and the chemistry of the sediments and waters in Brehaut Lake (Fig. 2, 3).

Sonar surveys show Alto Lake to have a steep shoreface descending to a flat bottom at about 4 m depth (Fig. 4). Alto Lake is an elongated, structurally controlled bedrock depres-

sion, draped with acoustically laminated Lake Agassiz inorganic silty clay which reaches thicknesses of more than 10 m in some bedrock basins. Depressions remaining in this silty-clay substrate are filled to the general level of Alto Lake's flat floor by an average of 3 m of acoustically 'clear' gyttja, an organic sediment with gelatin-like consistency which constitutes the modern, post-Lake Agassiz sedimentary fill (Fig. 5). Within this organic unit, dense concentrations of gas bubbles form an acoustic mask that generally lies near the sediment-water interface in most of Alto Lake except for a small area in the north part of Alto Lake where it lies more than 1 m below the sediment-water interface (Fig. 6). Similar gas concentrations, analyzed in physically comparable lakes on the Canadian Shield near Ottawa, were largely composed of methane and nitrogen, with lesser amounts of CO₂ and traces of other organic gasses (Edwards and Klassen, 1984).

The bathymetry (Fig. 7) and sediment facies (Fig. 8) of Brehaut Lake, as determined by the sonar surveys (examples shown in Fig. 9), are similar to those of Alto Lake, except that no deep depressions scar the 4-6 m deep bottom plain (Fig. 7).

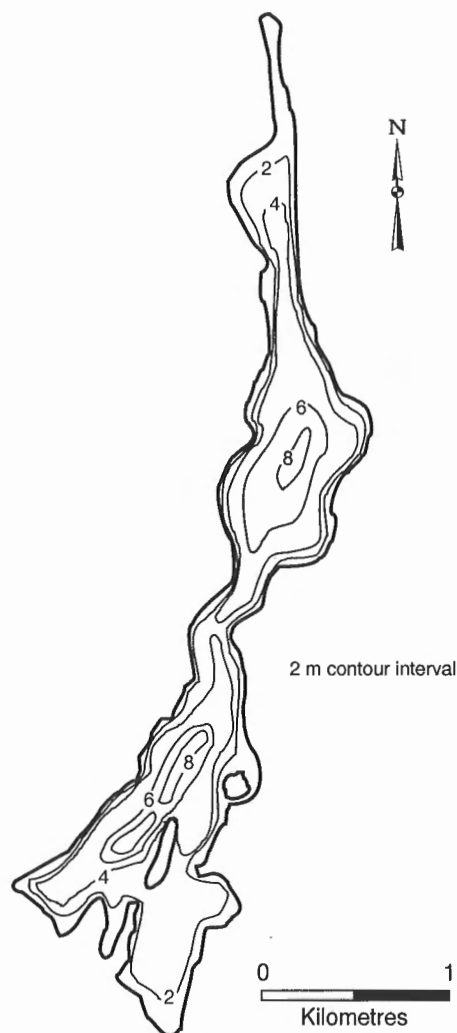


Figure 4. Bathymetry of Alto Lake.

Long arms of shallow water, clogged with the debris of dead vegetation, extend north and south of the original lake as a result of flooding caused by construction of the weir at the lake's outlet into the Vermilion River. The southernmost part of the lake is almost completely filled by a white precipitate caused by liming at the weir between Ruttan Lake and Brehaut Lake. Like Alto Lake, gyttja fills depressions in the Lake Agassiz clay that drapes the slopes and bottom of the northeast-trending bedrock depression of Brehaut Lake (Fig. 8, 9). Much of the original lake's bottom in and near the arm from which the Vermilion River originally exited, has little or no gyttja cover and consists of inorganic Lake Agassiz silty clay. Gas occurs throughout the area of gyttja fill in the original lake, but unlike that in Alto Lake, the surface of the acoustic mask formed by the gas is 1-2 m below the sediment-water interface (Fig. 10).

Sonar surveys were not carried out on Ruttan Lake and Rusty Lake, but sampling, inspection of airphotos, and previous reports indicate that they have a fairly simple bathymetry and sediment fill. Rusty Lake is a broad, shallow depression on the Glacial Lake Agassiz clay plain. Where

cored, water was less than 3 m deep, a depth probably characteristic of the whole lake. Cores indicated that, typically, a rather thin (<1 m) modern sediment unit (gyttja) overlies inorganic Lake Agassiz clay. Without sonar surveys, however, this generalization cannot be confirmed.

Ruttan Lake has been extensively modified from its original form by damming and deposition of tailings and waste rock into its eastern side (Fig. 11). Originally, it was a shallow lake in the last stages of infill by peat accumulation onshore. The mosses and woody plants of that peat rim are now drowned and constitute the bottom of the nearshore parts of the lake, except for the eastern side. Today, sediment in the central basin consists of 2-10 cm of sand-sized sulphide particles lying on a peaty or gyttja substrate; a delta, largely composed of sand-sized sulphide particles, is prograding into

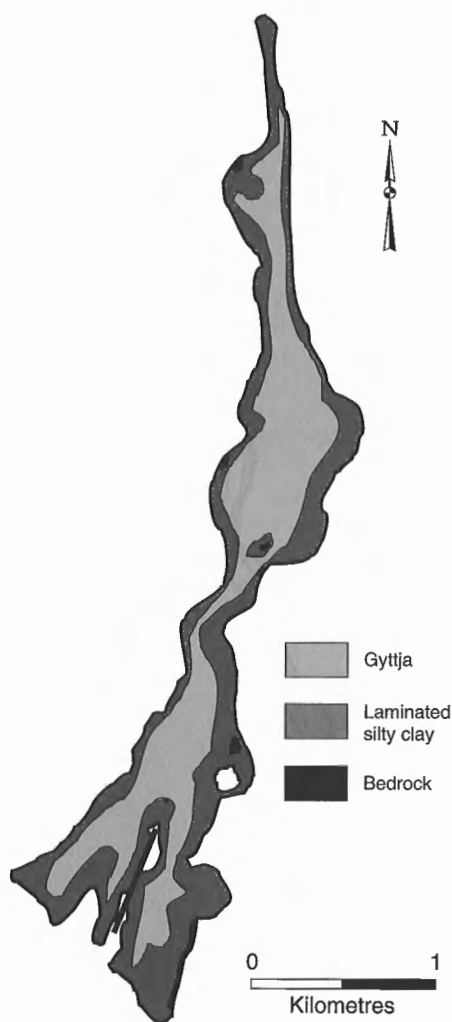


Figure 5. Sediment facies of Alto Lake.

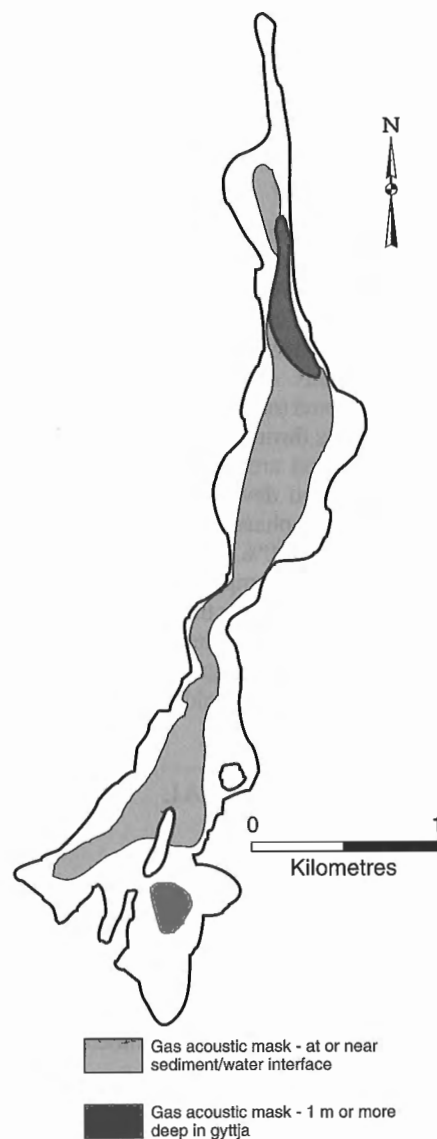


Figure 6. Gas distribution in Alto Lake.

the eastern part of the lake through a breach in a 5-10 m high dyke of waste rock, apparently originally built to contain the tailings.

The nature of the roadbed between the town of Leaf Rapids and the Ruttan mine is strikingly different from that between the mine and Issett Lake (Fig. 3). The Leaf Rapids-Ruttan mine segment is almost totally constructed of "waste rock" from the mine site and contains trace sulphides. The road's unpaved surface is disturbed by traffic much of which comprises heavy trucks carrying supplies to the mine and concentrate from the mine, as well as private vehicles transporting personnel between Leaf Rapids and the Ruttan mine. On dry days, significant amounts of dust are generated from the road surface.

The road east of the Ruttan mine, going to South Indian Lake (Fig. 3), is composed of glacial gravel, presumably taken from pits on the large glaciofluvial complex in the Leaf Rapids area. Although this road can also generate dust, it is not as heavily travelled as the western segment. It is likely that all water bodies within a few hundred metres of the road receive substantial amounts of dust in the snow-free months.

SEDIMENTATION AND SEDIMENTS

In the sediment sampling program, four main types of lake sediment were encountered, two of anthropogenic origin and two naturally occurring. The natural sediments occurring below wave base and away from inlet stream deltas are an inorganic grey, laminated silty clay deposited in Glacial Lake Agassiz and a younger, gel-like organic sediment referred to as 'gyttja' (Coker et al., 1979). Loss-on-ignition (LOI) analyses yield values between 2% to 9% for Lake Agassiz clays and 15% to 28% for gyttja. Coker and Nichol (1975) stated that LOI/2.4 yields an approximate figure for the carbon (C) content of organic lake sediment (gyttja) samples from similar Canadian Shield lakes. The 2-9% values for the Lake Agassiz sediments are thought to reflect largely H₂O and OH losses from clays that contain little or no organic carbon.

The anthropogenic components comprise: (1) the aforementioned white precipitate, being deposited in the south end of Brehaut Lake, caused by liming of the outflow from Ruttan Lake; and, (2) the clastic, sulphide-rich sand being sedimented directly into Ruttan Lake. Loss-on-ignition for the lime precipitate is more than 30%, and probably reflects loss

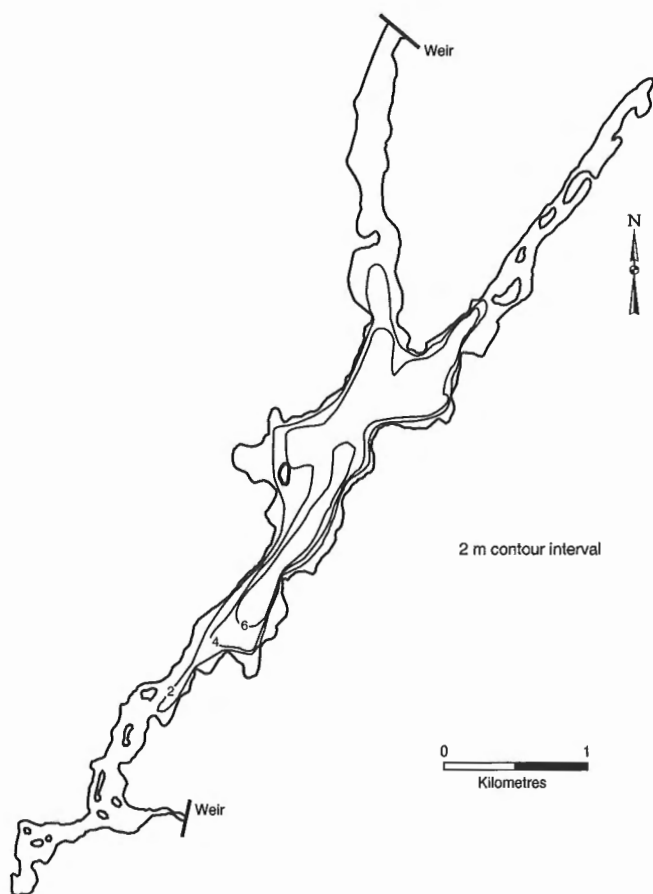


Figure 7. Bathymetry of Brehaut Lake.

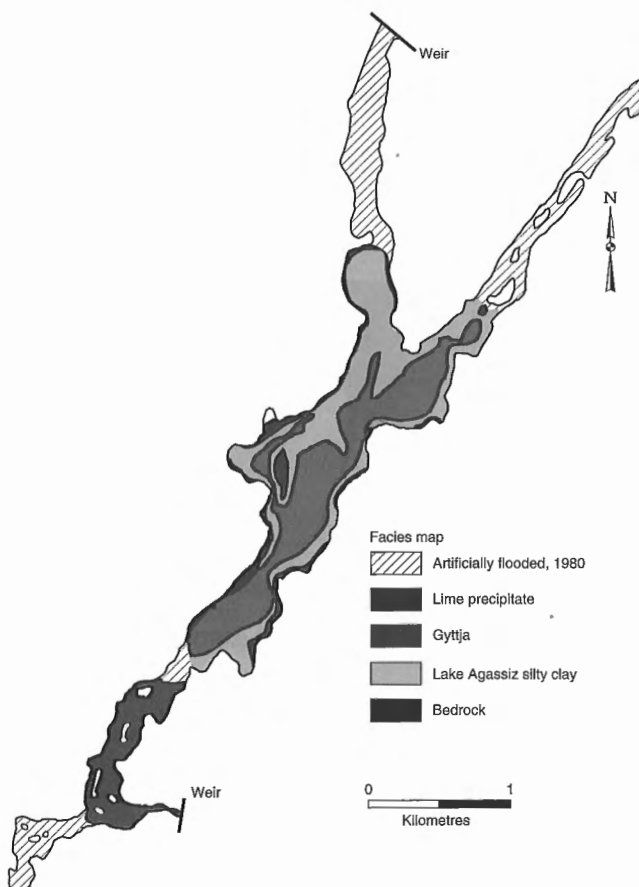


Figure 8. Sediment facies of Brehaut Lake.

¹ Glacial "clay", as used in this report, actually consists of varying proportions of silt- and clay-sized mineral fragments, mostly finer than 63 µm. Laminations in Lake Agassiz "clays" are due to cyclical changes in flux of silt-sized particles to deposition sites. Cycles can be related to a number of glacial and nonglacial processes, but are generally related to annual, seasonal climatic fluctuations.

of H_2O , OH , and other components from the mineralogically complex and largely artificial sediment (J.D. Adshead, unpublished report, 1991). The precipitate appears to contain very little organic carbon.

COMPOSITION OF LAKE SEDIMENTS

Four components of lake sediments are typically considered as having high potential for scavenging through adsorption or exchange reactions with cations in solution in lake water: clay (phyllosilicates finer than about $4\ \mu m$),

organic matter, secondary Fe oxides/hydroxides, and secondary Mn oxides/hydroxides. Glacial clays¹ tend to be dominated by well-crystallized, physically abraded phyllosilicate (micas, chlorites, clay minerals) debris created by glacial erosion of fresh bedrock surfaces, and thus tend to have relatively low cation exchange capacity. For this reason, glacial rock flour, which is deposited as glaciolacustrine clay such as that deposited in Glacial Lake Agassiz, has limited exchange capacity compared to organic sediments, secondary oxides, or clays formed by chemical weathering processes. This is clearly shown by the pattern of metal concentrations in Alto Lake. Samples of Lake Agassiz clay have distinctly lower concentrations of metal than those from the organic facies, which have a relatively higher adsorption potential.

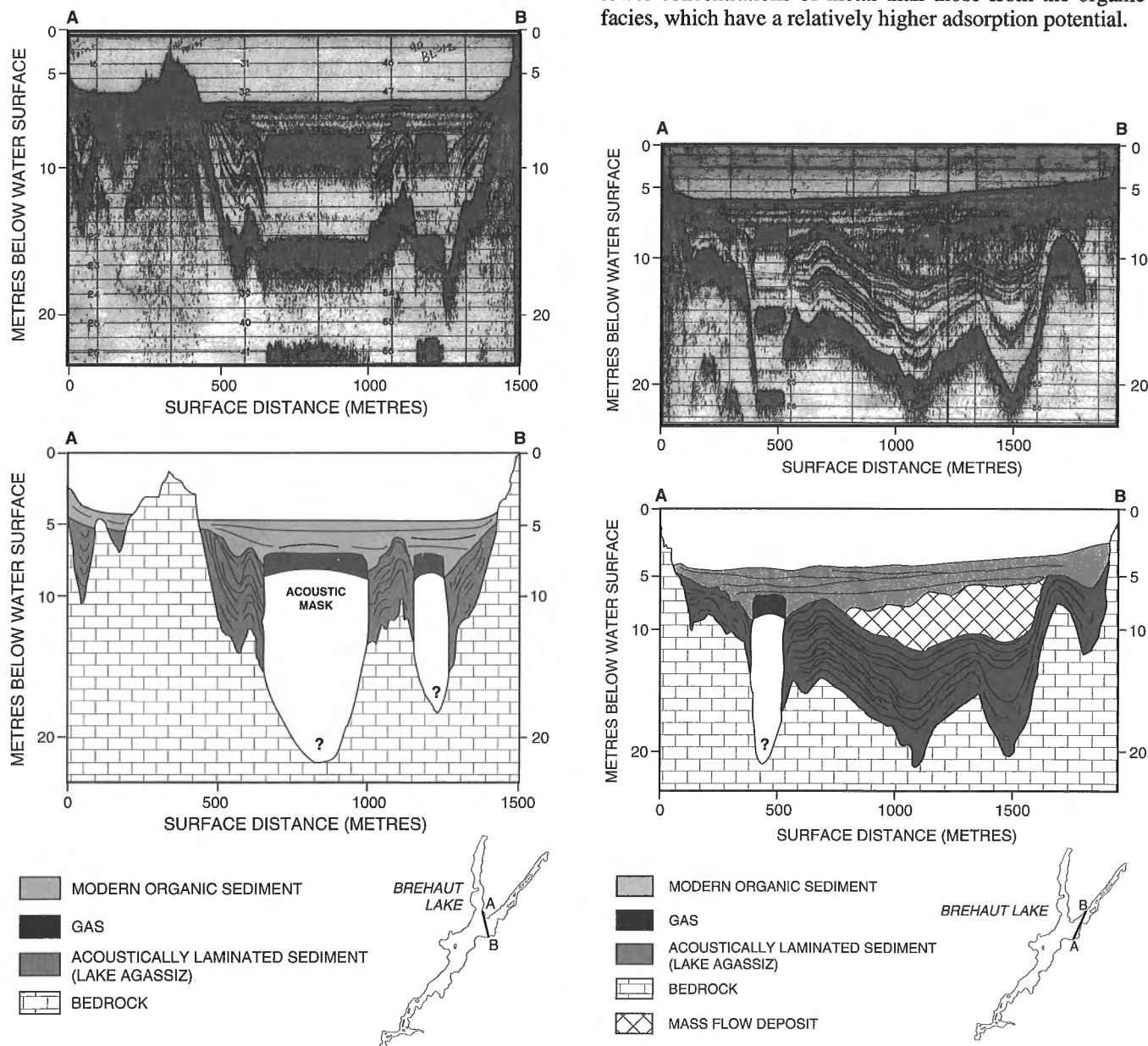


Figure 9. Examples (A, B) of two sonar profiles (interpreted) from Brehaut Lake.

In Alto Lake, the geochemistry of bottom sediments is represented by two distinct populations that are clearly related to the natural sediment facies, as determined by the subbottom acoustic profile surveys, and to LOI, which is a reflection of the two facies (Fig. 5, 12). In Brehaut Lake (Fig. 8, 12) and Ruttan Lake (Fig. 11), the geochemistry of bottom sediments is likewise influenced strongly by natural sediment facies, but anthropogenically formed sediments, sulphide sand, and lime precipitate form additional geochemical populations.

In Brehaut Lake, the same two natural sediment facies (Fig. 8, 12) are present, outside of the area of lime precipitation, and likewise have significantly different geochemical character. However, in Brehaut Lake concentrations of cations from metals mined at the Ruttan mine are an order of magnitude higher than those in Alto Lake due to water with high concentrations of dissolved metal entering Brehaut Lake from Ruttan Lake. In addition, the south end of Brehaut Lake is filled with an artificial lime precipitate which has highly elevated metal concentrations. The surfaces of all sediment samples collected from Brehaut Lake are discoloured by red and black oxide/hydroxide precipitates probably related to the high dissolved Fe and Mn concentrations produced by oxidation of sulphide tailings in and adjacent to Ruttan Lake.

WATER pH

A limited suite of geochemical parameters was determined for bottom and surface waters at 21 sites in Alto Lake and at 18 sites in Brehaut Lake. Surface water samples were also collected in the outlet stream above and below the liming station at the weir between Ruttan Lake and Brehaut Lake, at four sites each on Ruttan Lake and Rusty Lake, at three sites near the junction of the Vermilion River and Churchill River, and at 20 sites along the Leaf Rapids-Ruttan mine-South Indian Lake road (Fig. 3).

Except in Brehaut Lake and Ruttan Lake, pH of these water samples (Fig. 3), collected in the summers of 1990 and 1991, ranged from 6.3 to just over 7.2, averaging 6.7 ($n = 35$). In Ruttan Lake, pH ranged from 2.6 at the outlet to 3.0, the acidity probably being caused by oxidation of sulphides in the tailings on land or in shallow water. Sulphide grains sampled from the deepest part of Ruttan Lake appeared fresh and unoxidized.

In Brehaut Lake (Fig. 2), pH of surface and bottom waters is distinctly alkaline as a result of the liming of its inflow. At the liming site itself, pH of water on the upstream side of the weir is 2.5 or lower whereas, water immediately downstream is greater than 11.0. The lowest pH in Brehaut Lake was 7.2, recorded at its outlet weir in 1990 (Fig. 3); pH of surface water declines in a regular manner from over 9.0 at the inlet to 7.2 at the outlet. In the southern half of Brehaut Lake, pH of bottom water is significantly higher than that of surface water, possibly indicating that cooler, more dense, lime-laden water is following the bottom as a density underflow, preferentially settling in the deeper southern basin of the lake. North of that basin, pH of bottom and surface waters is virtually the same.

In Alto Lake (Fig. 2), for comparison, surface waters are near neutral throughout the lake (range 6.6-7.3), but the bottom waters in the deep north and south basins are significantly more acidic than surface waters (5.5-6.1).

METALS IN SEDIMENTS AND WATER

Iron

The effect of sediment facies on Fe concentration can be seen clearly in Alto Lake where surface samples² of gyttja average 3.44% Fe ($n = 16$) and Lake Agassiz clay samples average 1.46% Fe ($n = 7$) (Fig. 13). In comparison, Fe concentrations in Brehaut Lake, with its visibly iron-stained bottom and high Fe input from oxidizing sulphides in and around Ruttan Lake, are difficult to characterize either by sediment facies or by a simple average (Fig. 13). This is probably because heavy, visible Fe precipitates are found at the sediment-water interface, regardless of facies or location in the lake, so that the homogenization process associated with subsampling mixes surface Fe concentrates with iron-poor lower sediment.

² Surface samples are actually sediment homogenized from the upper 10-15 cm of the sediment column.

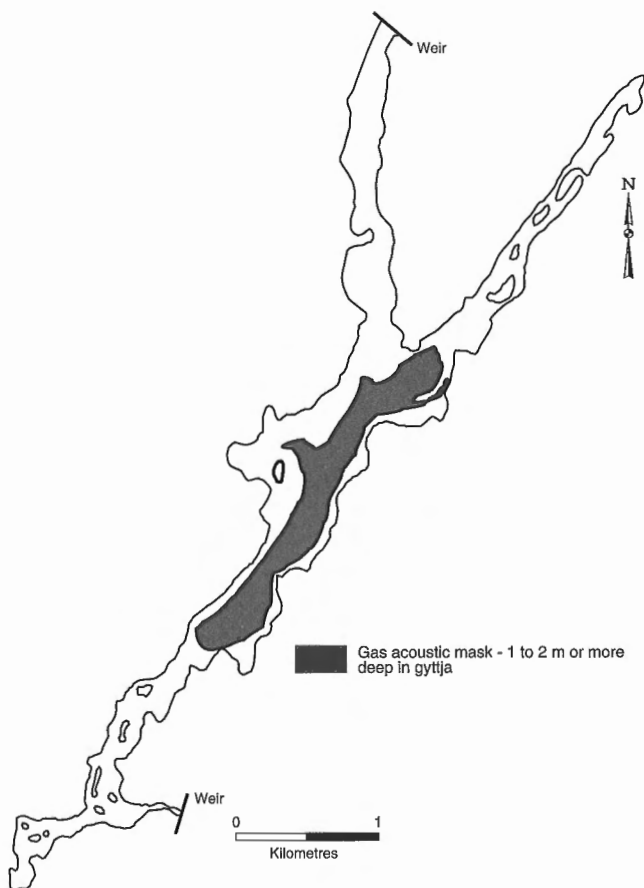


Figure 10. Gas distribution in Brehaut Lake.

The exceptions are four samples, three from Lake Agassiz clays at the north end of the lake (1.5-2.5% Fe) and one at the south end (2.6% Fe), beneath a surface layer of iron-rich limey precipitate (9.4% and 7.3% Fe). Samples from the rest of the lake, regardless of facies, exceed 3.7% Fe and range from 5.1 to 9.4% Fe in the lime precipitate. The cation scavenging potential for these iron oxides/hydroxides is probably considerable.

Manganese

Like Fe, Mn is clearly partitioned between the two sediment facies in Alto Lake, gyttja averaging 778 ppm Mn ($n = 16$) and Lake Agassiz clay averaging 347 ppm Mn ($n = 7$) (Fig. 14). In Brehaut Lake partitioning exists, but its pattern is confounded by the homogenization process, as for Fe. Mn concentrations in gyttja are significantly lower than in Alto Lake, ranging from about 300 ppm to 500 ppm, but the lime precipitate has Mn concentrations in the thousands of ppm (1860-7560 ppm) (Fig. 14). The clay facies at the north end of the lake has Mn concentrations below 200 ppm.

The reason for the low Mn concentrations in surface sediments in Brehaut Lake compared to Alto Lake and other unaltered lakes is not known, but samples collected from the bottom of the Churchill River at the mouth of the Vermilion River consisted of a dense concentration of Mn nodules apparently precipitated on the bare till surface of an artificially

flooded segment of the river. Possibly the early acid drainage that passed through Brehaut Lake during the first seven years of operation of Ruttan mine leached Mn from the sediment-water interface to be transported in solution and precipitated on the calcareous till substrate on the bottom of the Churchill River.

Zinc

Zn and Cu are the most important metals in the Ruttan mine's ore, and as such, contribute substantially to the metal that is leaching into the Vermilion River system. Zn concentrations in the sediments of Alto Lake are strongly related to bottom sediment type, the inorganic Lake Agassiz sediments averaging half (58 ppm Zn; $n = 7$) the concentration levels of the organic-rich modern lake sediments (122 ppm Zn; $n = 16$) (Fig. 15). Over most of the lake, surface waters are below or near the detection limit of 1.5 ppb Zn as are bottom waters in all but the deepest basins (Fig. 16). In the northernmost, 1 km-long arm, however, Zn in bottom and surface waters reaches concentrations in the 30 ppb range, as high as those in contaminated waters of Brehaut Lake to the east. The cause of these high concentrations is not immediately apparent; there is no known geological reason for the enrichment, but similar Zn enrichment was noted in waters of remote Cook Lake (near Snow Lake, Manitoba) near its north shore, where Zn-bearing massive sulphide mineralization is known to out crop on the lake bottom. If Zn is entering the lake from

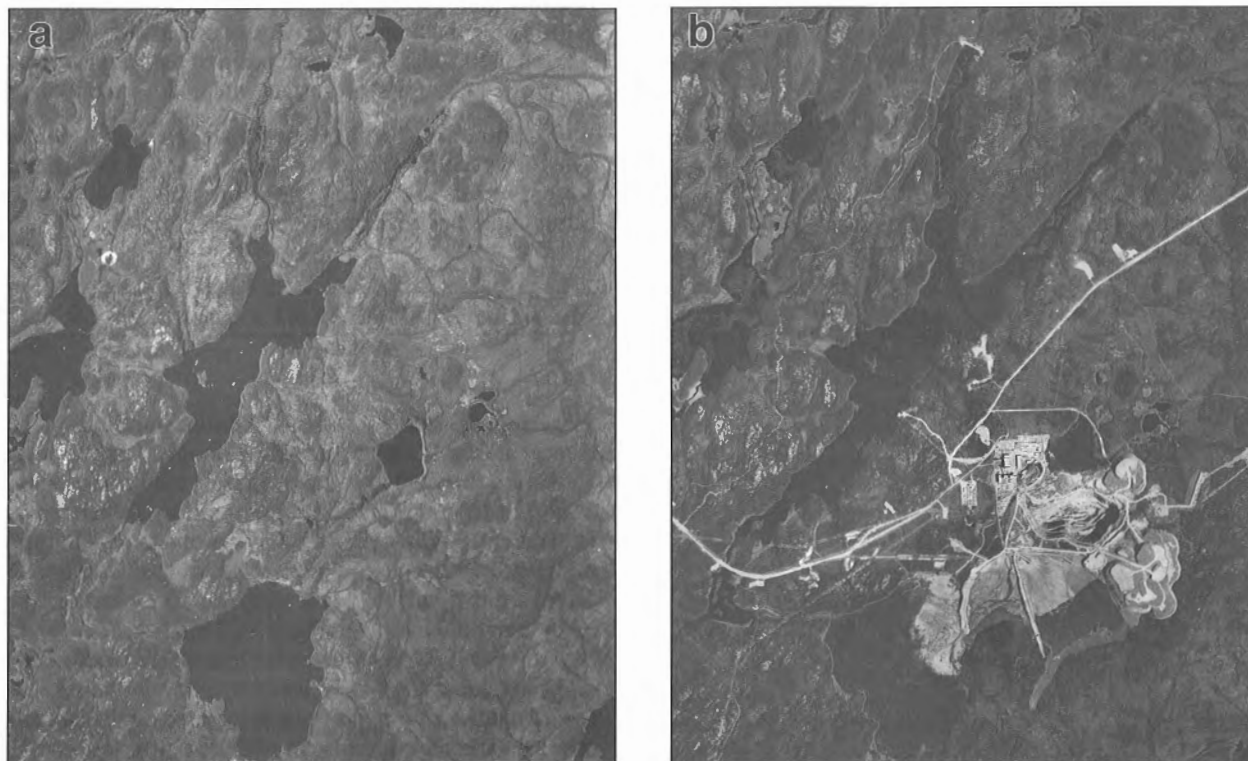


Figure 11. Air photographs comparing **a)** pre-mining (1958) and **b)** mining (1977) settings of Ruttan Lake and Brehaut Lake.

drainage reacting with waste rock or windblown dust from ore-truck traffic on the road at the south end of the lake, the area of enrichment should be in the southern bays, which show only slight enrichment.

Water in Ruttan Lake has pH levels ranging from 2.6 to 3.0 (Fig. 3) and contains 16.2-18.6 ppm Zn in solution (Fig. 17). The sulphide-rich sediments in Ruttan Lake itself contain about 6800 ppm Zn, where sampled. Immediately downstream from the liming weir between Ruttan Lake and Brehaut Lake, Zn concentrations in the alkaline waters drop to 2.2-3.6 ppb (Fig. 17), a radical decrease related to

complexing of Zn and other cations common to the ore within the various phases that comprise the carbonate precipitate that is deposited where the water draining from Ruttan Lake enters Brehaut Lake. In the less alkaline waters in the northern half of Brehaut Lake, Zn concentrations range from 20.8 to 40.3 ppb in surface waters and from 27.3 to 59.3 ppb in bottom waters (Fig. 16).

Sediments in Brehaut Lake have Zn concentrations well above those in nearby "pristine" lakes, but as in Alto Lake, observed Zn concentrations are related to the two naturally occurring sediment types as well as to the anthropogenic

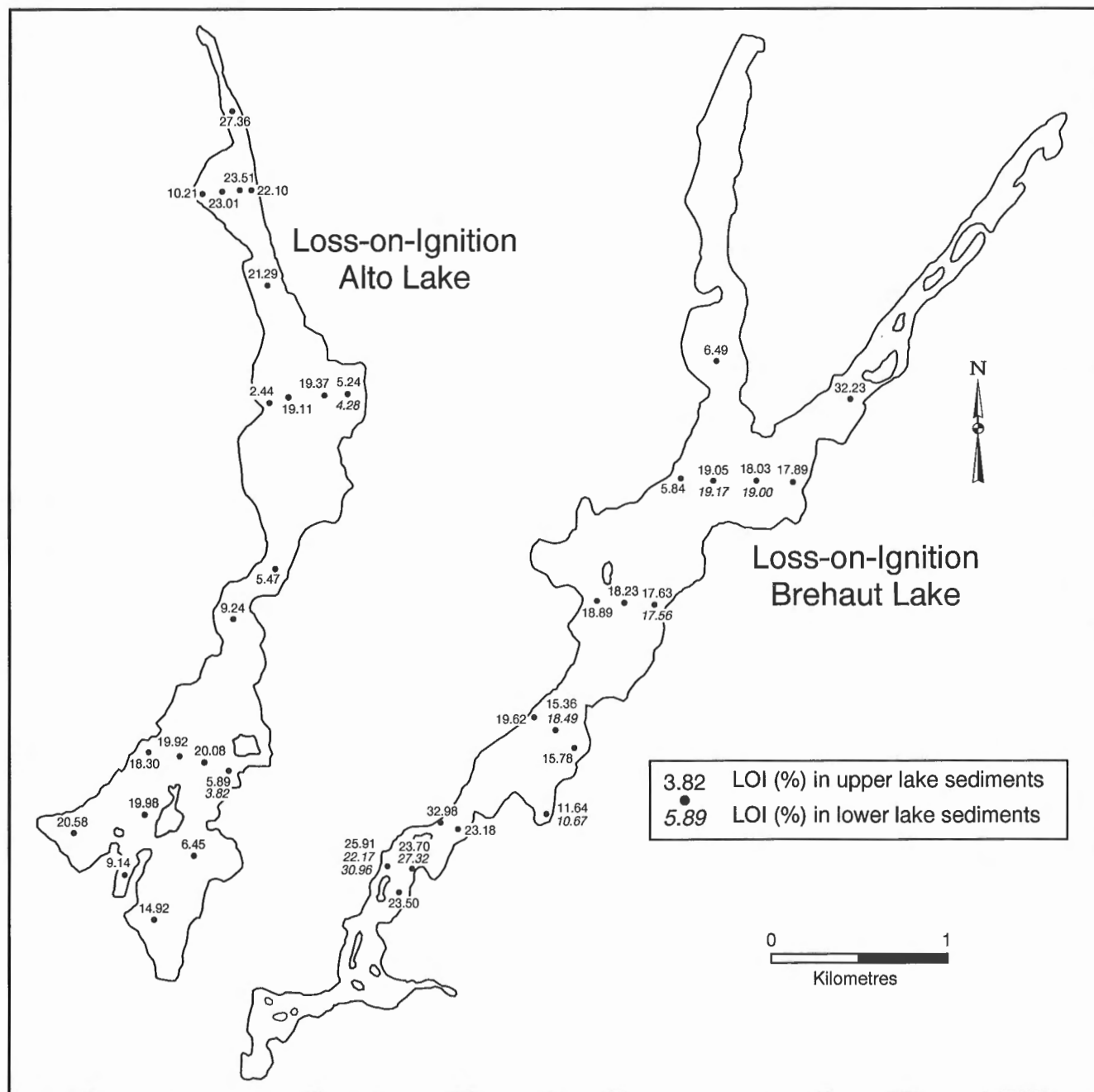


Figure 12. Loss-on-ignition (%) for sediments in Alto Lake and Brehaut Lake.

sediment (Fig. 15). Zn concentrations in the anthropogenic precipitate at the south end of Brehaut Lake range from 0.9 to about 4.7%. Organic sediment north of the area covered by the precipitate is substantially contaminated with Zn concentrations in the thousands of ppm, even in the northernmost basin. Lake Agassiz clay samples have less Zn than the organic facies, but they still average hundreds of ppm.

Organic sediment from the stream channel of the Vermillion River, just downstream from the weir that dams Brehaut Lake, contains 240 ppm Zn.

In Rusty Lake, about 6-8 km down the Vermillion River from Brehaut Lake, Zn concentrations in water are below detection limit (0.5 ppb) except near the inflow of the Vermillion River (9.7 ppb) (Fig. 17). Zn concentrations in the

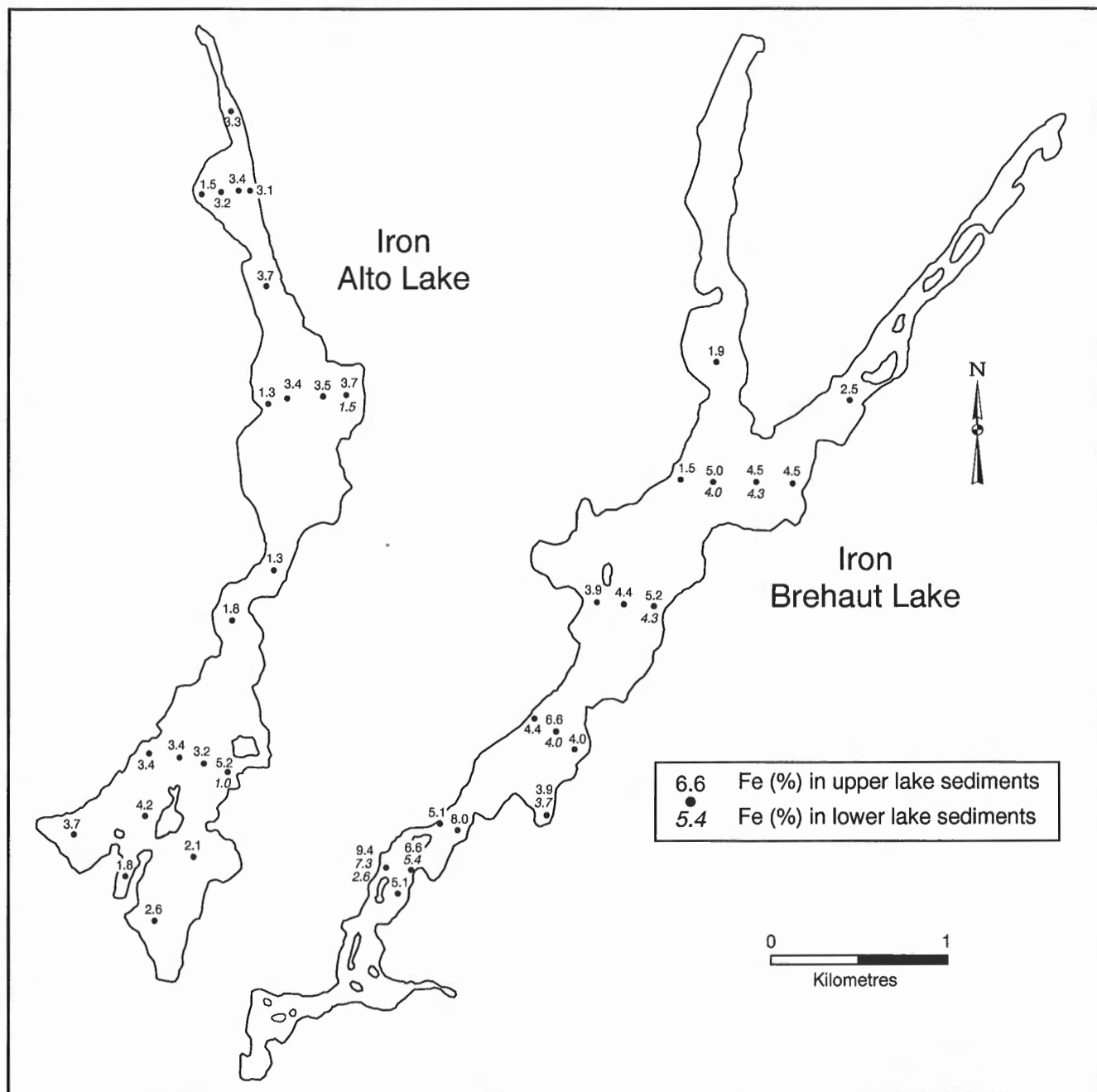


Figure 13. Iron content (%) of sediments in Alto Lake and Brehaut Lake.

organic sediments of Rusty Lake (241-363 ppm) are, however, comparable to those in the north end of Brehaut Lake (Fig. 15), about three times the regional background.

The regional pattern of Zn in waters reveals how extensive the anthropogenic effects associated with mining and ore haulage can be. As expected, the excessively high levels of

dissolved Zn in Ruttan Lake waters are effectively mitigated by liming, so that concentrations of the metal in Brehaut Lake are reduced by 1000-fold and those in Rusty Lake are further reduced by a factor of 10 to below detection limits (Fig. 17). This confirms the effectiveness of the mitigation procedures put in place in the late 1980s. However, high dissolved Zn concentrations in pools and drainages beside the highway,

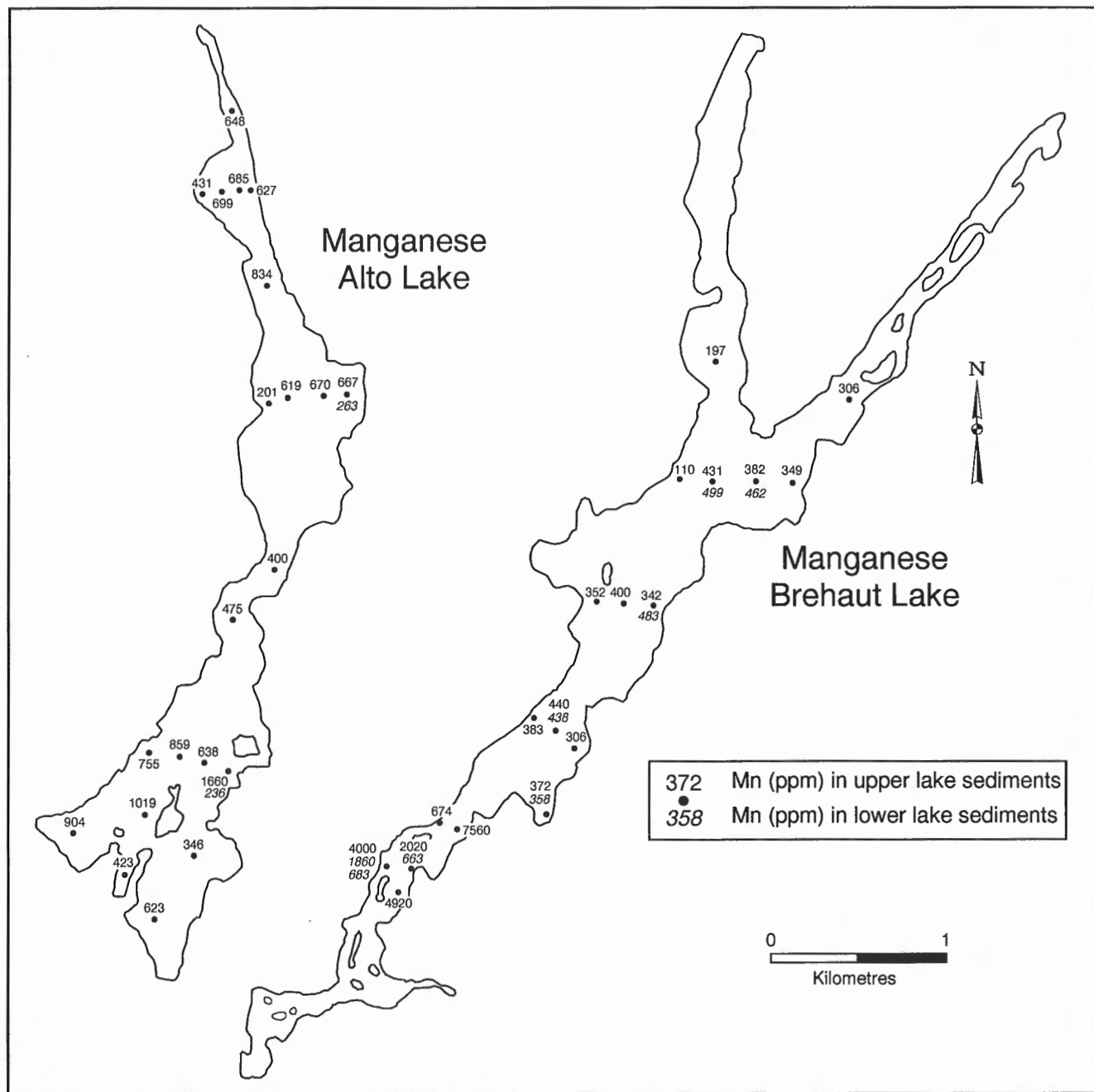


Figure 14. Manganese content (ppm) of sediments in Alto Lake and Brehaut Lake.

composed of waste rock, between the Ruttan mine and Leaf Rapids, suggest that highway dust, dust from blowing ore concentrate into trucks (probably negligible), and direct reaction of drainage water with materials of which the road is built are impacting local drainage over a wide area (Fig. 17).

Copper

Cu is the other main constituent of the ore at the Ruttan mine and is redistributed through leaching of tailings throughout Ruttan Lake. Using Alto Lake as a model for natural regional Cu distribution in lake sediments, Cu in Brehaut Lake can be seen to be enhanced by a factor of 10 times in natural sediments and up to 40 times in the lime precipitate at its southern end (Fig. 18).

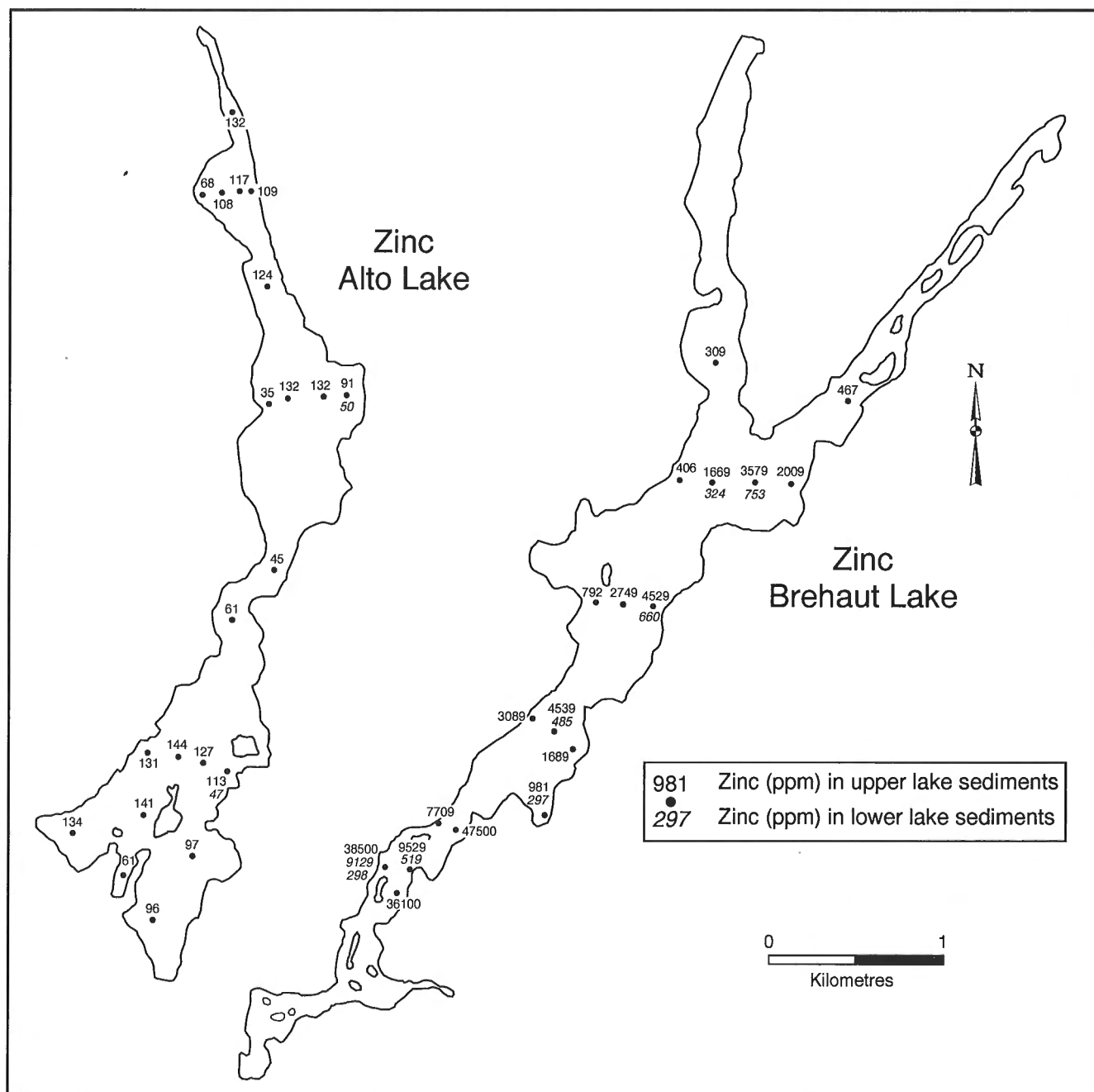


Figure 15. Zinc content (ppm) of sediments in Alto Lake and Brehaut Lake.

The map displays two lakes, Zinc Alto Lake and Zinc Brehaut Lake, with various sampling points marked by dots. Each dot is accompanied by a numerical value representing zinc concentration in ppb. A legend box in the lower right corner specifies that values less than 1.5 represent zinc in surface water, while values of 2.8 or greater represent zinc in bottom water. A north arrow is located to the right of the lakes, and a scale bar at the bottom right indicates a distance of 1 kilometre.

Zinc Alto Lake

Zinc Brehaut Lake

Legend:

- <1.5 zinc (ppb) in surface water
- 2.8 zinc (ppb) in bottom water

Scale: 0 to 1 Kilometres

Figure 16. Zinc content (ppb) of surface and bottom waters in Alto Lake and Brehaut Lake.

0.5 ppb. However, waters sampled beside the Leaf Rapids-Ruttan Mine road have Cu concentrations ranging from about 2 ppb to 33 ppb. Water beside the road beyond Ruttan mine in most cases contains <0.5 ppb Cu.

Near Leaf Rapids, water was sampled immediately upstream and downstream of a drainage crossing the road where the road is composed of oxidizing, sulphide-bearing waste rock. It contained <0.5 ppb Cu upstream and 2.9 ppb Cu downstream, suggesting that leaching of road materials, and not dust, is the main source of contamination at that site.

Accessory metals

Several other cations have been determined in the water and sediments from the Leaf Rapids-Ruttan mine region. The principal accessory metals in the ore at the Ruttan mine are Pb, Cd, and Hg, all potentially noxious or toxic to the natural biological community and to humans.

Lead

Pb is also an important trace component in the ore of the Ruttan mine. The highest natural concentrations of Pb occur in the organic sediments of Alto Lake (13-21 ppm), whereas lower (7-11 ppm) natural concentrations of Pb occur in the Lake Agassiz clays of Alto Lake (Fig. 19). In the tailings-polluted bottom sediment of Ruttan Lake, Pb (166-186 ppm) is enriched about 10 times or more over the average natural Pb values of the organic sediments within Alto Lake. However, it should be noted that Pb concentrations in pre-mining sediments at the base of a core taken from Ruttan Lake are only in the order of 8-10 ppm. Concentrations up to 264 ppm Pb have been measured from the lime precipitate in Brehaut Lake, and Pb in surface organic sediments throughout the rest of the lake is enriched anywhere from 3 to 10 times (46 to 177 ppm) above background. Pb, like Cd and

Hg, is reduced to near background concentrations in the outlet arm of Brehaut Lake (Fig. 19) and is found in background concentrations in Rusty Lake (16-18 ppm).

Cadmium

Cd is commonly associated with Zn ores, substituting readily in various Zn-bearing mineral phases. If the Cd concentrations (<0.2 to 0.3 ppm) in the sediments of Alto Lake are indicative of the natural Cd concentrations in nearby lakes, Cd concentrations would have been at or slightly above the 0.2 ppm detection limit of the analytical method. A grab sample containing sand-sized sulphide tailings from Ruttan Lake yielded 20.2 ppm Cd, a 100-fold enrichment above the sediments of Alto Lake. A short core from the west side of the Ruttan Lake basin had near background values (0.4-0.7 ppm) of Cd in the natural sediment at the core's base, rising to 16 ppm Cd in the tailings-contaminated surface sediment. In Brehaut Lake, Cd levels range from 20.9 to 54.2 ppm in the lime precipitate at its southernmost end and from 0.9 to 12.2 ppm in the organic surface sediments elsewhere in the lake. There is an obvious decline of Cd northward in the lake and the clayey facies have, as for other metals, far less Cd than the gyttja. Cadmium levels (0.3 to 0.8 ppm) in organic samples from Rusty Lake are 3 to 15 times lower than in Brehaut sediments, but in some cases are still up to three times higher than the background concentrations in Alto Lake. Manganese nodules from the bottom of the Churchill River are noticeably enriched in Cd (3.0 ppm), suggesting that they have formed since the mine opened in 1973. Cd concentrations in most regional water samples are below the 0.2 ppb Cd detection limit, but surface waters in Ruttan Lake, upstream from the liming weir, have concentrations between 20-37 ppb Cd. Detectable Cd also was found in some water over the lime precipitate in Brehaut Lake (0.8 ppb) and in a pool of Fe-stained water beside the Leaf Rapids-Ruttan mine road (1.5 ppb).

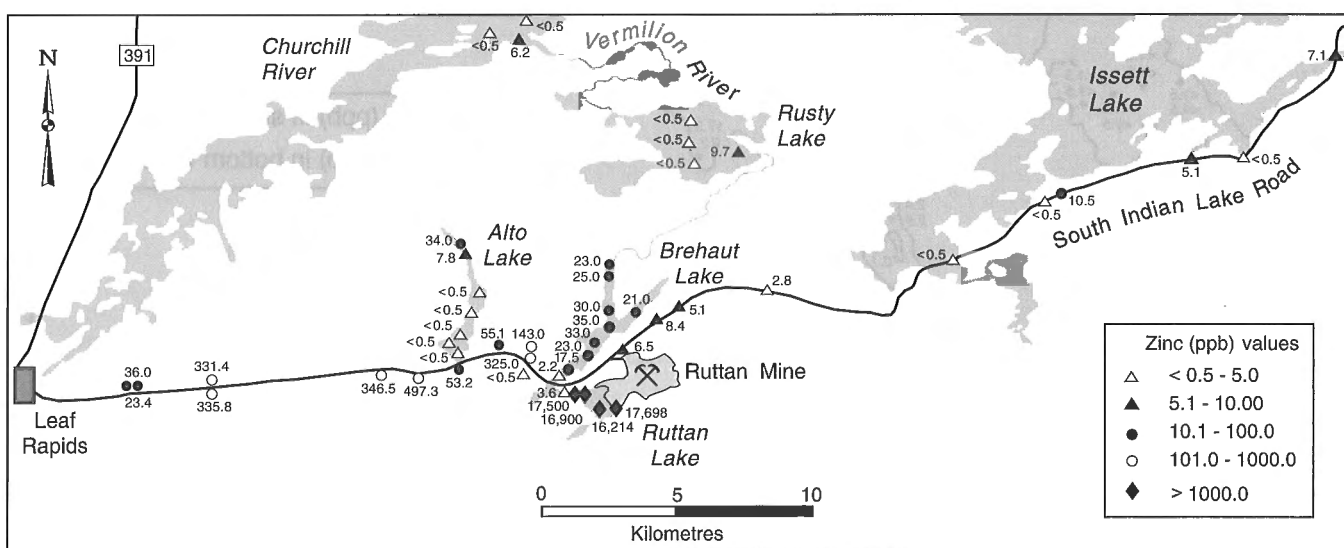


Figure 17. Zinc content (ppb) of surface waters throughout region

Mercury

Hg is an important accessory element in the ore at the Ruttan mine and is highly concentrated in the tailings-polluted surface sediments of Ruttan Lake (2473 ppb). Background concentrations in Alto Lake range from 16 to 88 ppb, substantially less than the sediment concentrations in Brehaut Lake. It is important to recognize, however, that although Hg

concentrations in Brehaut Lake range from 333 to 1206 ppb in the lime precipitate and from 104 to 282 ppb in organic sediments elsewhere in the lake, concentrations in sediments (54 to 67 ppb) in the outflow arm of Brehaut Lake are well within the natural distribution of Hg as indicated by sediments from Alto Lake. Sediments from Rusty Lake likewise reflect “normal” Hg concentrations (60-76 ppb).

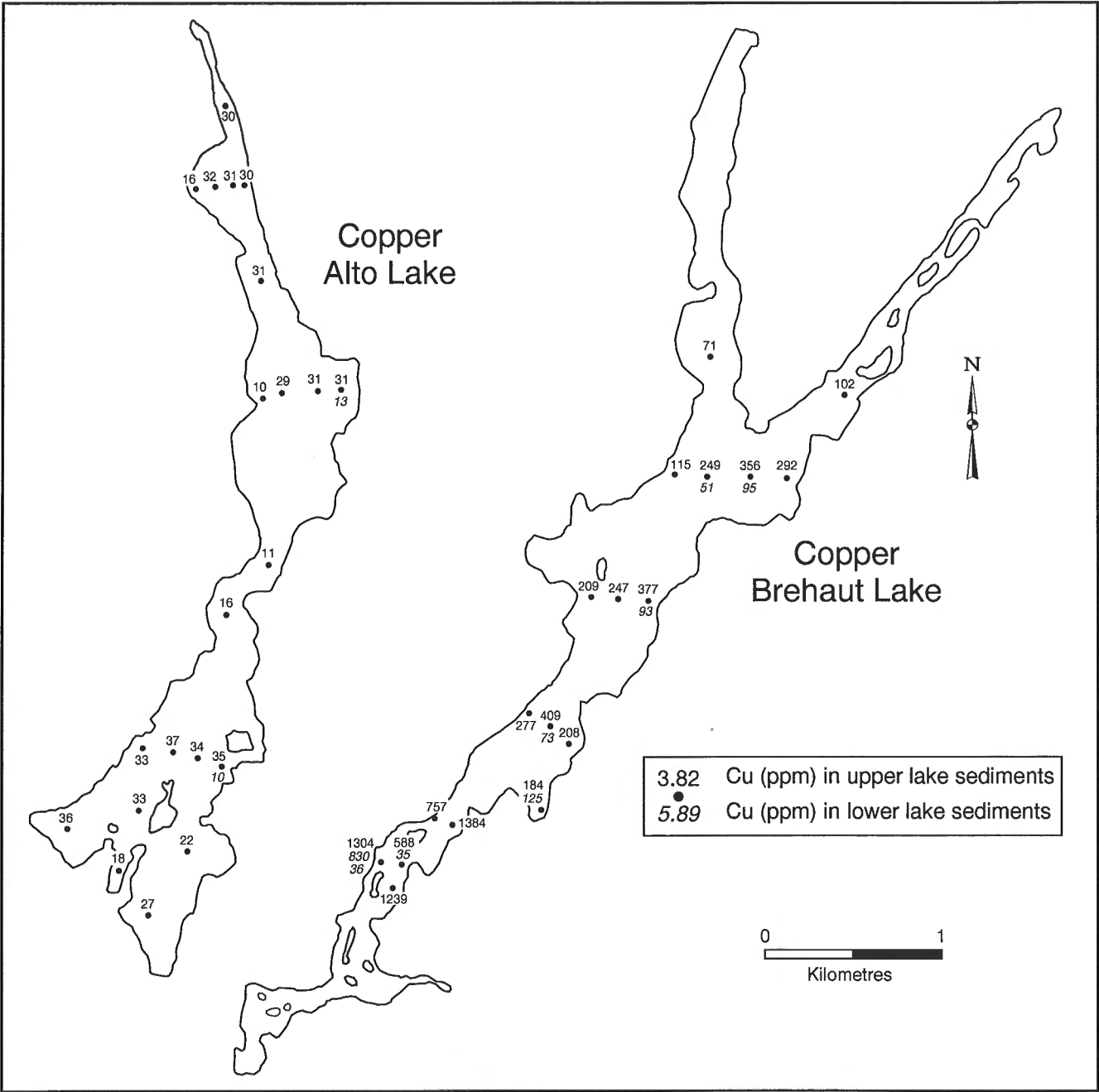


Figure 18. Copper content (ppm) of sediments in Alto Lake and Brehaut Lake.

Silver

Ag is usually found in base metal deposits in trace amounts, and concentrations of 6-9 ppm Ag in tailings-contaminated sediments from Ruttan Lake confirm its importance. Within Brehaut Lake, Ag is found in the lime precipitate ranging from

0.9 to 3.5 ppm, whereas elsewhere in the lake Ag concentrations, above the 0.1 ppm analytical detection limit, range from 0.2 to 0.9 ppm. In the organic sediments in the outlet arm of Brehaut Lake, in Rusty Lake, and in Alto Lake, Ag concentrations fall below the detection limit of 0.1 ppm.

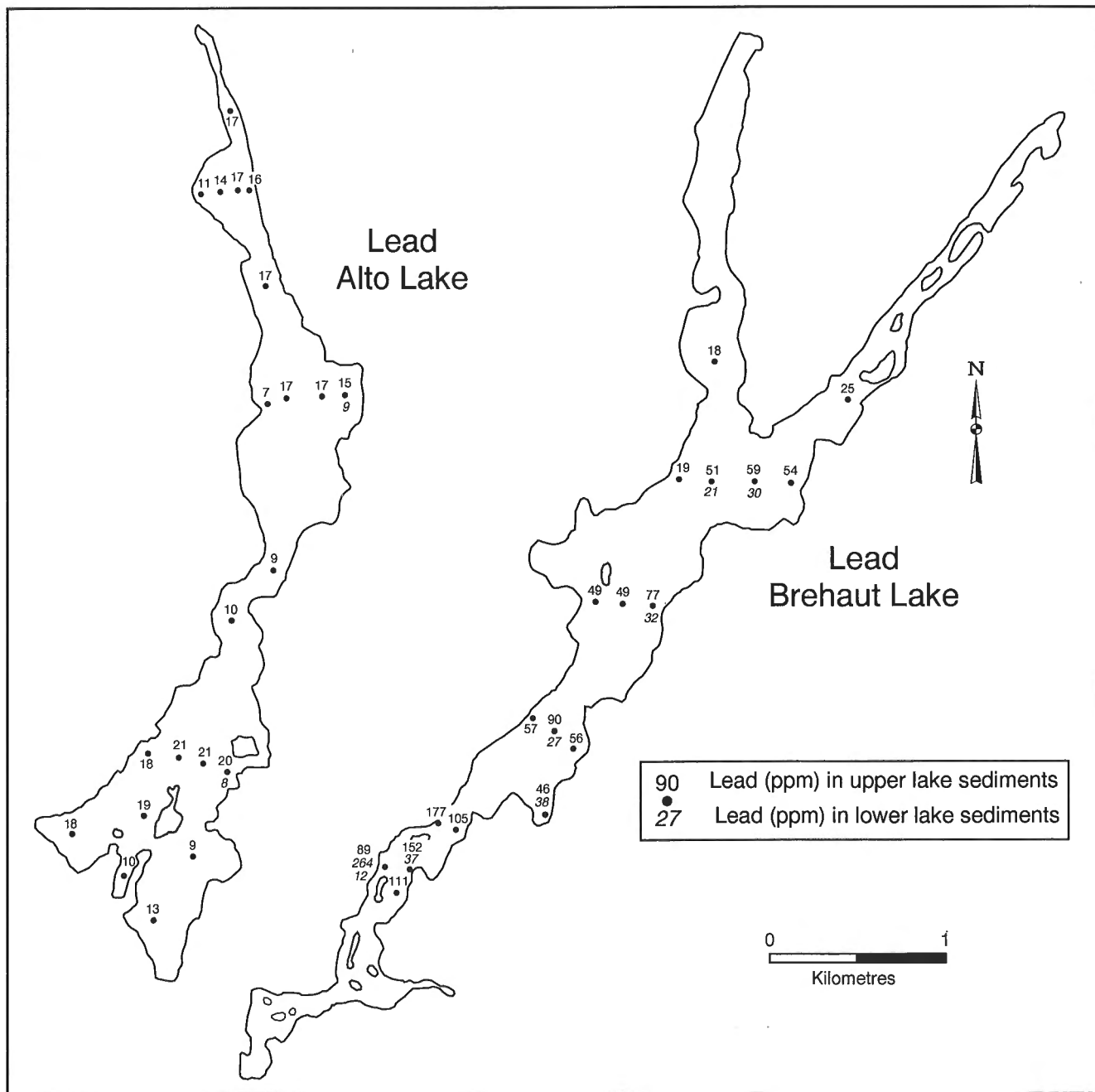


Figure 19. Lead content (ppm) of sediments in Alto Lake and Brehaut Lake.

Arsenic

As, like Ag and Hg, sometimes is an important subordinate cation in base metal deposits, particularly those rich in Au. In Alto Lake, As ranges from 1-3 ppm in bottom sediments of all facies. In Brehaut Lake, As exceeds Alto Lake sediment concentrations by as much as three times in the most contaminated sediments (3-9 ppm), but even the highest As concentration (9 ppm) in Brehaut Lake is within normal background ranges for Canadian Shield lakes.

Cobalt

In the most highly impacted sediments of Ruttan Lake, concentrations of 77-97 ppm Co have been measured. Pre-mining organic sediments in a core from Ruttan Lake contained only 14-16 ppm Co, concentrations similar to those in Alto Lake, which range from 14 to 21 ppm for organic sediment and from 5 to 9 ppm for Lake Agassiz clay. Except for Co concentrations of 33 to 187 ppm in the lime precipitate, other sediments in Brehaut Lake have Co concentrations (7-27 ppm) similar to those in Alto Lake. Rusty Lake sediments have similar low Co concentrations (17-18 ppm), but the single analysis of manganese nodules from the bottom of the Churchill River yielded 136 ppm Co. Co is typically enriched in manganese nodules regardless of the environment in which they are formed.

Nickel

Ni is actually less concentrated in the impacted sediments (24-42 ppm) of Ruttan Lake than in its pre-mining sediments (46-48 ppm). Organic sediments in Alto Lake contain from 20 to 47 ppm Ni and those in Rusty Lake from 53 to 57 ppm Ni. Nevertheless, the lime precipitate in Brehaut Lake is enriched in Ni, containing up to 238 ppm Ni. Sediments elsewhere in Brehaut Lake have Ni concentrations (15-47 ppm) similar to those in similar facies in Alto Lake. The manganese concretions in the Churchill River contain 125 ppm Ni, an enrichment similar to that for Co and typical of manganese concretions elsewhere.

CORING AND SEQUENTIAL EXTRACTION RESULTS

Ruttan Lake cores

Characteristics of the core extruded on site

Samples were analyzed from a core which was collected from Ruttan Lake's central basin and extruded on site (Fig. 20). The interface between the tailings and the brown organic gel (gyttja) occurs transitionally between 10 and 20 cm from the top of the core.

Concentrations of Pb, Zn, Co, Cd, Ag, and Fe decrease with depth, whereas Ni and Mn increase with depth (Fig. 20). Upwardly decreasing total Mn profiles may result from the removal of Mn from the top sediment layers due to acidic

conditions (Carignan and Nriagu, 1985). The concentration of Cu varies in the top 20 cm of the core from 174 ppm at 5 cm, to 941 ppm at 15 cm; Cu then decreases downward through the remainder of the core.

Characteristics of the core extruded in laboratory

A second core (Fig. 21) was collected from Ruttan Lake on the side of the central basin. An X-radiograph of the core showed no obvious structures or changes in the nature of the sediment. The core is mainly organic and contains fragments of plant matter, roots, and pieces of wood which increase in concentration toward its bottom. There is little to no evidence of sludge/tailings because the core was collected at the edge of the basin. The pH of the sediment increases from 3.1 at the top to 5.0 at the bottom of the core, and water just above the core has a pH of 2.6.

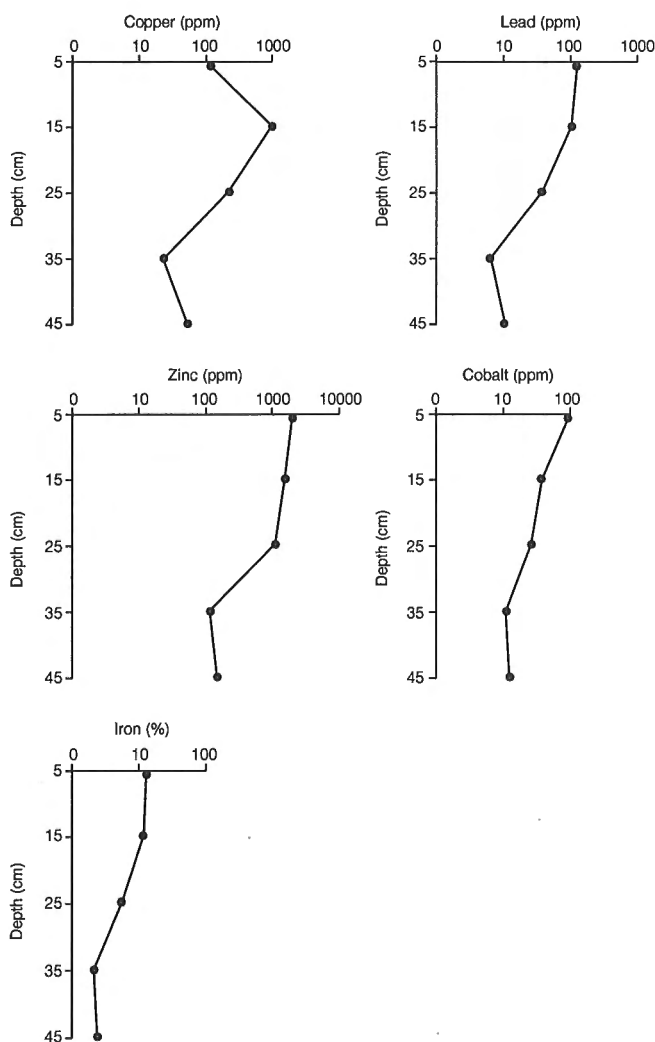


Figure 20. Vertical distributions of total concentrations of Cu (ppm), Pb (ppm), Zn (ppm), Co (ppm), and Fe (%) in sediment of core from central basin of Ruttan Lake.

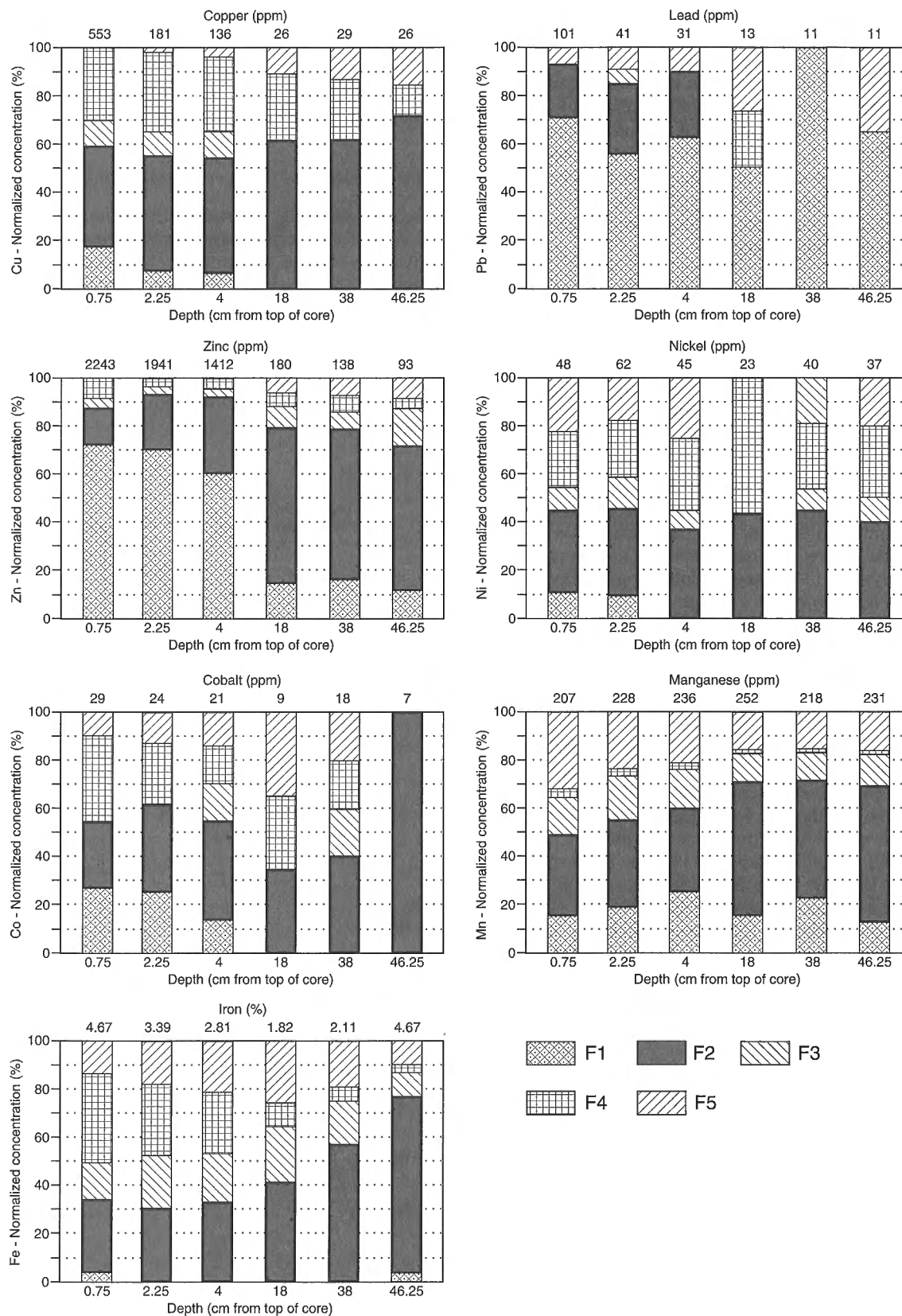


Figure 21. Sequential extraction data for Cu (ppm), Pb (ppm), Zn (ppm), Ni (ppm), Co (ppm), Mn (ppm), and Fe (%) for sediment of core from Ruttan Lake. F1 – adsorbed and exchanged carbonate phase; F2 – hydrous iron and manganese phase; F3 – crystalline iron oxides; F4 – sulphide phase; F5 – silicates and residual oxides phase. Numbers at top of bars indicate total metal concentrations.

The top of the core is rust-coloured; the bottom end is light brown. The sides and the bottom had a blood-red staining. This could be due to bacteria reacting with the plastic core shell (R. McNeely, pers. comm., 1993).

Sequential extractions

The total concentrations of Cu, Pb, Zn, Ni, and Co generally decrease, some quite rapidly, with depth in the top half of the core (Fig. 21). Except for Zn and Fe, the aforementioned metals tend to show little to no variation in concentration in the bottom half of the core. The concentration of Fe decreases from the top down to 18 cm, and then begins to increase. This downward decrease, followed by an increase in Fe concentration is similar to that seen in the core extruded on site. The pattern of Mn concentration shows no discernable trend.

Pb, Fe, Ni, Co, and Mn have lower concentrations in the bottom of the core than those found in the lower parts of the core collected in Rusty Lake (Fig. 23). Often the concentrations are so low at the bottom of the core that it negates interpretation of the selective leach data.

Mn, Zn, and Pb are associated with the carbonate phase throughout the length of the core. The relative amount of Zn associated with the carbonate phase decreases significantly in the deeper half of the core which corresponds to similar decrease in the total content of Zn in the core. The relative amounts of Mn and Pb associated with the carbonate phase show no pattern or trend with depth in the core. A significant portion of Zn, Ni, and Cu along with the Mn and Fe are variably tied up in either the hydrous iron and manganese oxide phase, the crystalline iron oxide phase, or the sulphide phase.

In the bottom half of the core, Cu and Mn have similar phase configurations to those from the Rusty Lake core (Fig. 23).

Brehaut Lake core

Characteristics of the cored sediments

The core from Brehaut Lake was taken approximately 200 m downstream from the liming station. The majority of sediment in the core was deposited within the last 17 years as a result of the liming process. Horizontal laminations at approximately 34 and 68 cm from the top of the core are visible on X-radiographs and confirm that the core is undisturbed, at least below 34 cm. From top to bottom, the core graded from a liquid to a slurry and then to a solid. At about 75 cm from the top, samples were dry enough to form clumps. The bottommost sample had no free liquid present.

The pH of the sediment ranged from 6.8 at the bottom to 9.0 at the top of the core. The water decanted from the core's surface had a pH of 8.3. Surface lake water collected where the core was taken had a pH of 8.7.

The colour of the core changed with depth. At the top it was a reddish brown, at about 35 cm down, a black substance, possibly sulphides, produced a marbled effect in the samples. About 90% of the sample from the 70-75 cm interval was composed of this black material. Below 75 cm, samples were brown and contained plant fragments. This material probably represents the organic surface of the subaerially exposed, pre-mining alluvial plain of the Vermilion River, flooded when the level of Brehaut Lake was raised by construction of the weir at its outlet.

Sequential extractions

Except for Fe, all metal concentrations tend in general terms to decrease from the top of the core down to approximately 70 cm (Fig. 22). An interface occurs around 75 cm. When the core was extruded, it was noticed that around this point the sediment became tacky and had a higher percentage of black matter than the sediment above it. All metal concentrations drop substantially below 73 cm. Sediment below 73 cm is natural, pre-mining organic detritus, and the metal concentrations in it are typical of those of pre-mining sediment in Ruttan Lake and in background sediment in Alto Lake. This suggests that any migration of metals or metal-rich solutions that may have taken place as a result of diagenetic processes in the limy sediment was confined to the artificial sediment and that metal was not circulated downward into older sediment or its pore waters in any significant amount.

In the top 70 cm of the core, the majority of all metals determined are tied up in the carbonate phase (Fig. 22). With increasing depth, all of the metals that were bound up with the carbonates at the top of the core become increasingly, to a varied degree, adsorbed onto the hydrous manganese and iron oxides. Pb, Cu, and Fe show a higher affinity for this phase than does Zn, but this may be an analytical artifact of the extremely high Zn concentrations in the precipitate. The metal adsorption selectivity order on hydrous iron oxide is: $Pb > Zn > Ni = Cd$ (Smith, 1991). An analysis of a sample of the lime sludge shows the presence of aluminum oxides (5%) and magnesium oxides (17%) (J.D. Adshead, unpublished report, 1991). It is not known where or if metals bound in these oxides are released.

Rusty Lake core

Characteristics of the cored sediments

The only visible structures in the Rusty Lake core are horizontal 'partings' in the bottom half of the core. The Rusty Lake core was a uniform grey-brown colour. A sharp contact about 20 cm below the top of the core separates upper organic sediments from more clayey sediments. Roots were seen in the clayey sediment at a depth of 44 cm from the top of the core. Spherical black objects (about 2 mm in diameter) were scattered through the bottom part of the core.

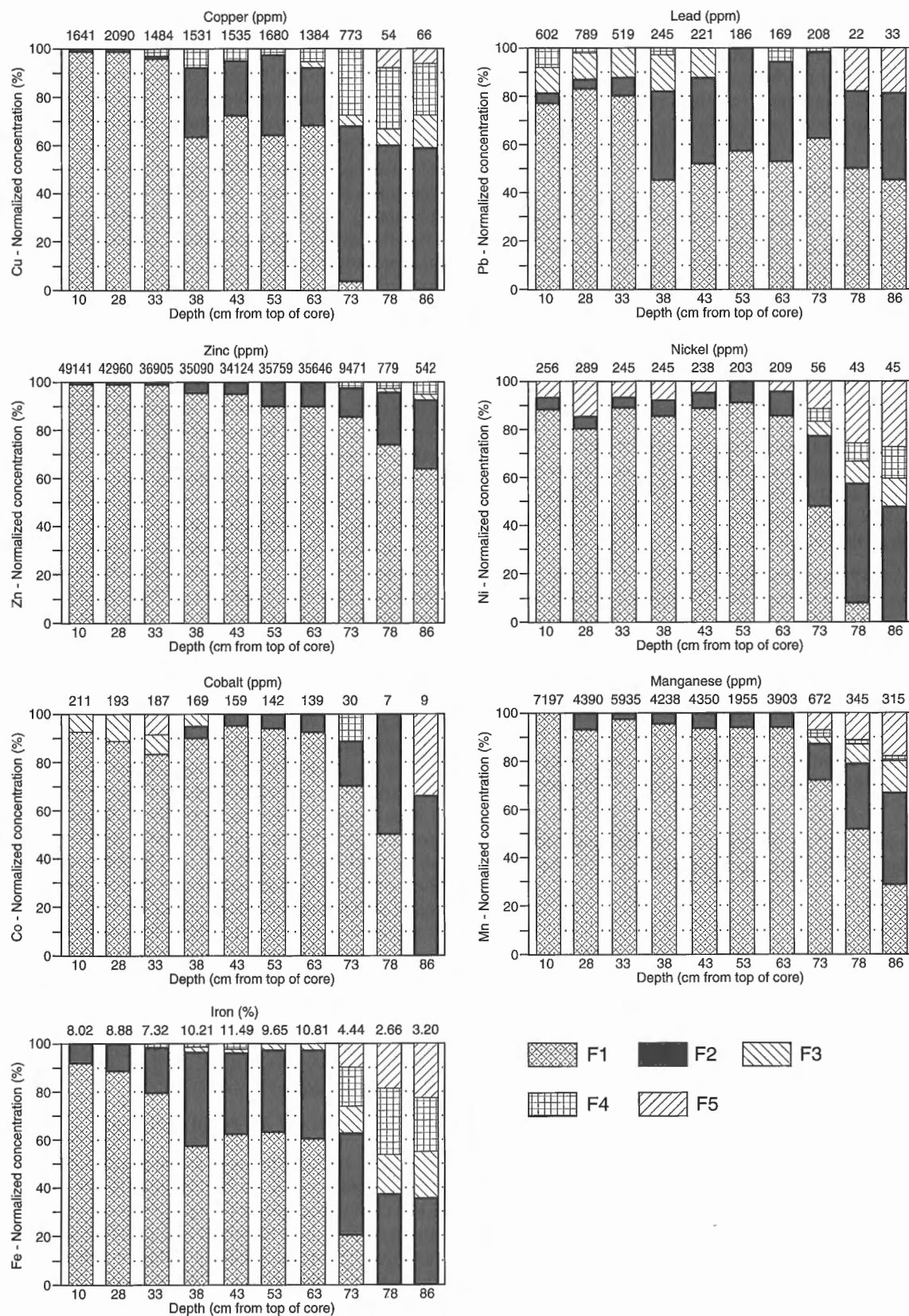


Figure 22. Sequential extraction data for Zn (ppm), Cu (ppm), Pb (ppm), Ni (ppm), Co (ppm), Mn (ppm), and Fe (%) for sediment of core from Brehaut Lake. F1 – adsorbed and exchanged carbonate phase; F2 – hydrous iron and manganese phase; F3 – crystalline iron oxides; F4 – sulphide phase; F5 – silicates and residual oxides phase. Numbers at top of bars indicate total metal concentrations.

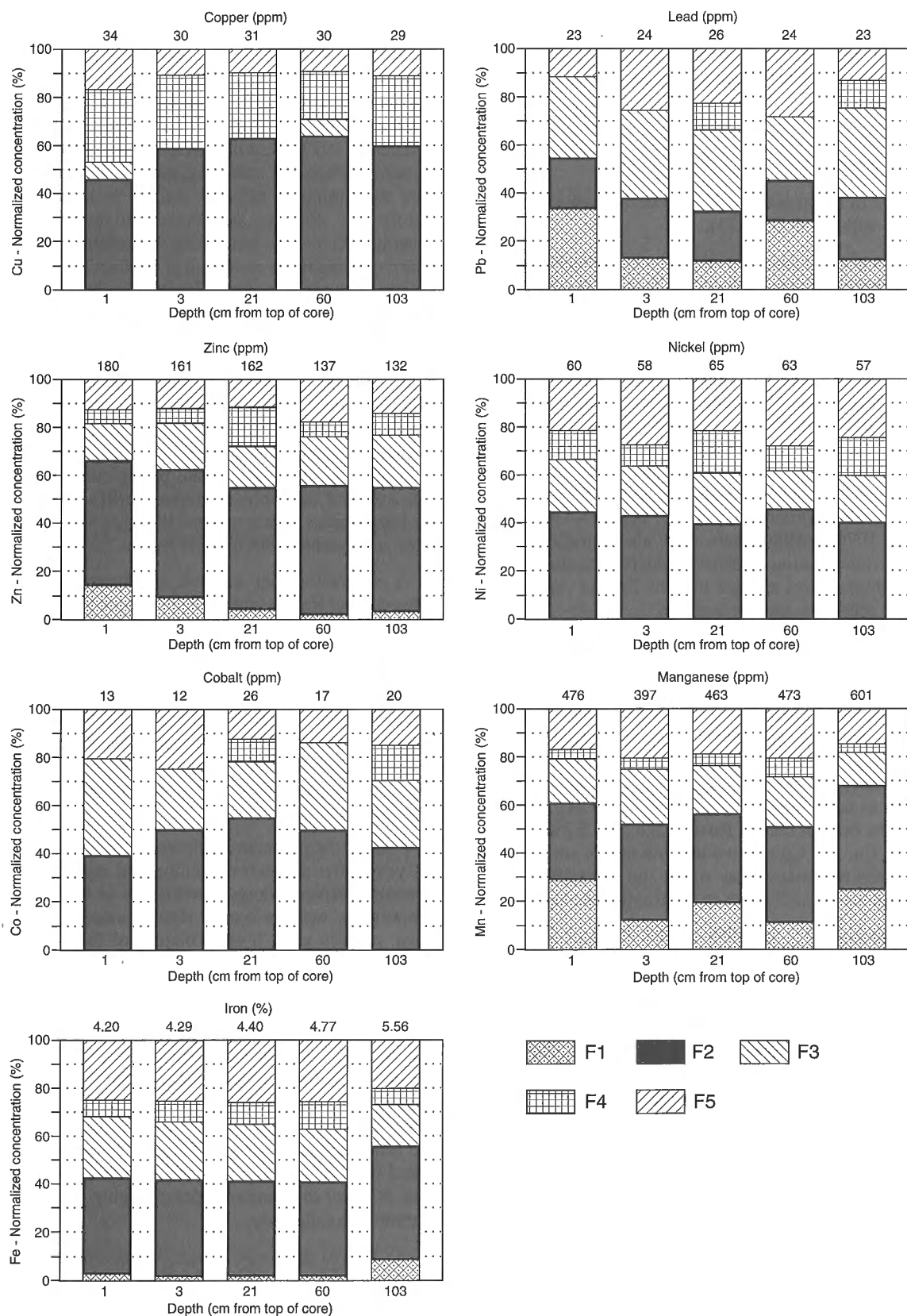


Figure 23. Sequential extraction data for Cu (ppm), Pb (ppm), Zn (ppm), Ni (ppm), Co (ppm), Mn (ppm), and Fe (%) for sediment of core from the edge of Rusty Lake. F1 – adsorbed and exchanged carbonate phase; F2 – hydrous iron and manganese phase; F3 – crystalline iron oxides; F4 – sulphide phase; F5 – silicates and residual oxides phase. Numbers at top of bars indicate total metal concentrations.

Sediment pH ranged from 3.8 at the top to 5.8 at the bottom of the core. The lake water above where the core was taken has a pH of about 6.8.

Sequential extractions

The percentage of metal associated with each phase changes less than 20% with depth (Fig. 23).

Zn shows a gradual decrease in total concentration from the top (180 ppm) of the core to the bottom (132 ppm). Accompanying this decrease is a corresponding decrease in the percentage of Zn extracted from the carbonate phases. Possible explanations are: (1) Zn is moving up the sediment column and the carbonate is related to decaying organic matter, or it may originate in part in the calcareous Lake Agassiz clays that underlie the modern organic sediment; (2) the Zn and the carbonate are products of the mining and liming operations; or (3) any combination of the first two. There were several exceedances of the Zn limit in Rusty Lake, as specified by CEC Order No. 858VO, between 1987 and 1990. During 1976 to 1984, there were also significant increases in Ca concentrations in Rusty Lake (Green and Beck, 1992). Both observations suggest that the Zn and carbonate relationship is related to mining activity.

Fe increases in concentration with depth. Possibly it is moving down through the sediment column. Fe concentrations are more than double those found in the pre-mining sediments in Ruttan Lake. In addition to Fe, concentrations of Ni, Co, Pb, and Mn in the natural pre-mining sediment at the bottom of the Ruttan Lake core (Fig. 20) are lower than those in the Rusty Lake core. For example, the average Fe concentration in the bottom half of the Ruttan Lake core is 2.9% and in the bottom half of Rusty Lake core 5.2%. Most of the Zn, Ni, Cu, and Co are tied up with the Fe and Mn in the hydrous iron and manganese oxide and crystalline iron phases throughout the sediments in the Rusty Lake core.

Approximately 15% to 30% of the Pb and Mn are adsorbed onto or bound up in the carbonate phase throughout the Rusty Lake core. The carbonate in the Rusty Lake core may originate in part in the calcareous Lake Agassiz clays that underlie the modern organic sediment. Several coring attempts were necessary to obtain a core with a substantial thickness of organic sediment. Most cores penetrated <10 cm of organic surface sediment lying on grey, presumably calcareous Glacial Lake Agassiz laminated clay. Both till and glaciolacustrine clay in this area are calcareous below their weathered surface and constitute a potential source of carbonate through weathering and erosion.

CONCLUSIONS

This study, as suspected, has shown that the sediments and waters of Brehaut Lake are severely impacted by metals left in the tailings produced by mining and ore processing at the Ruttan mine. The impacts are much more subdued but

detectable in Rusty Lake and perhaps in manganese nodules on the bottom of the Churchill River near its confluence with the Vermilion River. It is not known whether the impacts observed in the north part of Brehaut Lake and in Rusty Lake predate the 1977 debut of liming effluent from Ruttan Lake. Certainly, when the sampling was carried out in 1990 and 1991 the liming of effluent seemed to have restricted the mobility of Zn, Cu, and associated metals through the Vermilion River system, causing substantial amounts of metal to be deposited in the south end of Brehaut Lake. It is doubtful that the large amount of metal currently chemically contained in the area of lime precipitation in Brehaut Lake would remain immobile should the liming stop and the very acid effluent from Ruttan Lake be allowed to attack the body of precipitated metal. In fact, it is probable that a 'spike' of intense metal pollution would pass through the lower Vermilion River and into the Churchill River as several years of metal accumulation were released in a short time. The soluble nature of the Zn-bearing components of the precipitate, as identified by J.D. Adshead (unpublished report, 1991) and by sequential leaching studies herein suggest that they not be permitted to come into contact with low pH waters.

A conclusion that was not anticipated is that the road between Leaf Rapids and the Ruttan mine, composed substantially of waste rock from the mine, is, itself, a source of metal pollution to waters that rest against or flow through it. The road has spread low-level effects of the mining across a large swath of terrain. Beyond the mine, the road to the northeast is built of glacial gravels and has had little or no detectable impact on waters that contact it. The extent to which the low-level pollution of the waste-rock portion of the road affects drainage downstream, is not known and bears further consideration.

Finally, the procedure followed here, even though carried out years after the start of mining and impacts on the lower Vermilion River, allows conclusions to be made that have temporal as well as spatial significance. For instance, the sonar surveys yield a clear picture of the stratigraphy and modern depositional patterns of the bottoms of the lakes surveyed, something that grid sampling or single cores could not provide adequately. The extreme variation in bottom chemistry, particularly in Brehaut Lake, would not be easily understood without a clear idea of the stratigraphy and configuration of Lake Agassiz clays and younger gyttja. The sequential leaching and SEM studies (J.D. Adshead, unpublished report, 1991) give details of the mineral phases, natural and artificial, implicated in the sequestering of Zn and associated metals; they yield, in addition, indications of metals' susceptibility to solution under changing pH conditions and to their bioavailability.

As part of the study design, we carried out comparative sampling and surveying of adjacent lakes from different drainage basins, but with similar bathymetry, bedrock and surficial geology on shore, and similar sediment configuration and stratigraphy. This comparative study was absolutely necessary to establish geochemical norms for water and various sediment facies of lakes in the region.

ACKNOWLEDGMENTS

We gratefully acknowledge Hudson Bay Mining and Smelting, and in particular staff at the Ruttan mine, for their help, co-operation, and logistical support throughout this project. Staff of the Analytical Method Development Labs (GSC), under the direction of Gwendy Hall, are thanked for their diligent efforts in carrying out the sequential extraction analyses on the lake sediment cores.

REFERENCES

- Ames, D.E.**
1996: Stratigraphic and tectonic setting of the Paleoproterozoic Ruttan Cu-Zn VHMS deposit, Rusty Lake belt, Trans-Hudson Orogen; in *EXTECH I: A Multidisciplinary Approach to Massive Sulphide Research in the Rusty Lake-Snow Lake Greenstone Belts, Manitoba*, (ed.) G.F. Bonham-Carter, A.G. Galley, and G.E.M. Hall; Geological Survey of Canada, Bulletin 426 (this volume).
- Batley, G.E.**
1989: Trace Element Speciation: Analytical Methods and Problems; CRC Press, Boca Raton, 350 p.
- Carignan, R. and Nriagu, J.O.**
1985: Trace metal deposition and mobility in sediments of two lakes near Sudbury, Ontario; *Geochemica et Cosmochimica Acta*, v. 49, p. 1753-1764.
- Coker, W.B. and Nichol, I.**
1975: The relation of lake sediment geochemistry to mineralization in the northwestern Ontario region of the Canadian Shield; *Economic Geology*, v. 71(5), p. 955-963.
- Coker, W.B., Hornbrook, E.H.W., and Cameron, E.M.**
1979: Lake sediment geochemistry applied to mineral exploration; in *Geophysics and Geochemistry in the Search for Metallic Ores*, (ed.) P.J. Hood; Geological Survey of Canada, Economic Geology Report 31, p. 435-477.
- Edwards, T. and Klassen, R.A.**
1984: Preliminary isotopic and chemical characterization of natural gas in sediments of Lac Harrington, Quebec and Golden Lakes, Ontario; in *Current Research, Part B*; Geological Survey of Canada, Paper 84-1B, p. 237-243.
- Green, D.J. and Beck, A.E.**
1992: Assessments of impacts from the Ruttan mine site upon downstream waterways; Manitoba Department of the Environment, Water Quality Management Report No. 92-8, 156 p.
- Hall, G.E.M., Vaive, J.E., Beer, R., and Hoashi, M.**
1996: Phase selective leaches for use in exploration geochemistry; in *EXTECH I: A Multidisciplinary Approach to Massive Sulphide Research in the Rusty Lake-Snow Lake Greenstone Belts, Manitoba*, (ed.) G.F. Bonham-Carter, A.G. Galley, and G.E.M. Hall; Geological Survey of Canada, Bulletin 426 (this volume).
- Hall, G.E.M. and Vaive, J.E.**
1992: Application of a field portable anodic stripping voltammeter to the analysis of sulphide selective leaches and waters; *Chemical Geology*, v. 97, p. 292-306.
- Kaszycki, C.A. and Way Nee, V.J.**
1989: Surficial geology, Uhlman Lake, Manitoba (64B); Geological Survey of Canada, Map 1758A.
- Klassen, R.W.**
1986: Surficial geology of north-central Manitoba; Geological Survey of Canada, Memoir 419, 57 p. and 2 maps.
- Lynch, J.J.**
1990: Provisional elemental values for eight new geochemical lake sediment and stream sediment reference materials LKSD-1, LKSD-2, LKSD-3, LKSD-4, STSD-1, STSD-2, STSD-3 and STSD-4; *Geostandards Newsletter*, v. 14(1), p. 153-167.
- in press: Provisional elemental values for four new geochemical soil and till reference materials TILL-1, TILL-2, TILL-3 and TILL-4; *Geostandards Newsletter*.
- MacDonald, A.M.**
1993: Geochemical study of the Ruttan Mine, Manitoba; BSc. thesis, Queen's University, Kingston, Ontario, 109 p.
- Munro, D. and Ruggles, R.**
1978: A preliminary water pollution study in the vicinity of the Sherritt Gordon Ruttan Lake Mine and mill operation in 1977-78; Environment Canada, Environment Protection Service, Water Pollution Control Section MS Report No. EPS MS-MW-78-10.
- Rapin, F., Tessier, A., Campbell, P.G.C., and Carignan, R.**
1986: Potential artifacts in the determination of metal partitioning in sediments by a sequential extraction process; *Environmental Science and Technology*, v. 20(8), p. 836-840.
- Smith, K.S.**
1991: Water/sediment partitioning of trace elements in a stream receiving acid-mine drainage; in *Proceedings, Second International Conference on Abatement of Acidic Drainage, 1991*; Mine Environment Neutral Drainage Program, Report 5.6.1., v. 3, p. 437-450.
- Speakman, D.S., Chornoby, P.J., Haystead, B.C.W., and Holmes, G.F.**
1982: Geology of the Ruttan Deposit, northern Manitoba; in *Precambrian Sulphide Deposits*, (ed.) R.W. Hutchison, C.D. Spence, and J.M. Franklin, Geological Association of Canada, Special Paper 25, p. 525-556.

Contribution to the 1989-1994 Rusty Lake-Snow Lake Mining Camps, Canada-Manitoba Exploration Science and Technology Initiative (EXTECH I)

Setting of Paleoproterozoic volcanic-hosted massive base metal sulphide deposits, Snow Lake

A.H. Bailes¹ and A.G. Galley²

Bailes, A.H. and Galley, A.G., 1996: Setting of Paleoproterozoic volcanic-hosted massive base metal sulphide deposits, Snow Lake; in EXTECH I: A Multidisciplinary Approach to Massive Sulphide Research in the Rusty Lake-Snow Lake Greenstone Belts, Manitoba, (ed.) G.F. Bonham-Carter, A.G. Galley, and G.E.M. Hall; Geological Survey of Canada, Bulletin 426, p. 105-138.

Abstract: Two discrete volcanic-hosted massive sulphide (VHMS) mineralizing events, one Cu-rich and the other Zn-rich, are recognized in the oceanic arc sequence at Snow Lake, Manitoba. Cu-rich deposits occur in volcanic rocks accumulated in a primitive, possibly forearc or protoarc, arc tectonic setting. Zn-rich deposits exist in a stratigraphically higher sequence formed in an evolved, more mature arc tectonic setting. Rhyolite flow complexes and geochemically similar subvolcanic tonalite plutons are spatially associated with both Cu- and Zn-rich deposits at Snow Lake. A separate genesis for the felsic and mafic parental magmas is likely as rhyolite flows and subvolcanic tonalite intrusions share similar ϵ_{Nd} values that are distinctly higher than those of associated mafic flows.

Volcanic-hosted massive sulphide deposits typically occur stratigraphically above the subvolcanic tonalite plutons within rhyolite flow complexes and associated regionally extensive semiconcordant zones of altered supracrustal rocks. Altered rocks are interpreted to be a product of pluton generated, seawater-dominated hydrothermal activity. Discordant, planar zones of highly altered rocks in the footwall to volcanic-hosted massive-sulphide deposits are interpreted to be the trace of hydrothermally modified synvolcanic faults.

Our work indicates that exploration activity at Snow Lake could be targeted into the most prospective terrains by: 1) choosing volcanic rocks with arc geochemical signature, 2) picking areas with known subvolcanic intrusions, 3) emphasizing terranes with large zones of hydrothermally altered rocks, 4) concentrating on rhyolite flow complexes, and 5) targeting of crosscutting alteration zones.

Résumé : Dans la séquence d'arc océanique de la région de Snow Lake, au Manitoba, on distingue deux épisodes de minéralisation en sulfures massifs volcanogènes, l'un cuprifère et l'autre zincifère. Les gisements cuprifères sont encaissés dans des volcanites accumulées dans un milieu tectonique à un stade d'évolution précoce, probablement d'avant-arc ou de proto-arc. Les gisements zincifères s'observent dans une séquence stratigraphiquement plus haute, formée dans un milieu tectonique à un stade d'évolution plus avancé, donc d'arc plus mature. Les complexes de coulée rhyolitique et les plutons hypovolcaniques de tonalite géochimiquement semblables sont spatialement associés aux gisements tant cuprifères que zincifères de la région de Snow Lake. Il semble que les magmas parentaux felsiques et mafiques aient une origine distincte, étant donné que les coulées de rhyolite et les intrusions hypovolcaniques de tonalite ont des valeurs de ϵ_{Nd} semblables qui sont nettement plus élevées que celles des coulées mafiques associées.

¹ Manitoba Energy and Mines, Suite 360, 1395 Ellice Ave., Winnipeg, Manitoba R3G 3P2

² Geological Survey of Canada, 601 Booth St., Ottawa, Ontario K1A 0E8

Dans la stratigraphie, les gisements de sulfures massifs volcanogènes sont typiquement situés au-dessus des plutons hypovolcaniques de tonalite. Ils s'observent au sein des complexes de coulée rhyolitique et des zones semi-concordantes associées, qui sont d'étendue régionale et composées de roches supracrustales altérées. Les roches altérées sont interprétées comme le produit d'une activité hydrothermale d'origine plutonique où domine l'eau de mer. Les zones planaires discordantes de roches très altérées dans l'éponte inférieure des gisements de sulfures massifs volcanogènes sont interprétées comme le témoignage de failles synvolcaniques modifiées par l'activité hydrothermale.

Les présents travaux indiquent que l'exploration dans la région de Snow Lake pourrait être orientée vers les terrains les plus prometteurs en ciblant 1) les volcanites dont la signature géochimique est celle d'un milieu d'arc, 2) les secteurs où il y a des intrusions hypovolcaniques, 3) les terrains caractérisés par de vastes zones de roches altérées par des fluides hydrothermaux, 4) les complexes de coulée rhyolitique et 5) les endroits où les zones d'altération se recoupent.

INTRODUCTION

The Snow Lake area contains 11 producing and past-producing base metal mines, and accounts for production plus reserves of 25.4 Mt (Table 1). It is located at the east end of the Paleoproterozoic Flin Flon metavolcanic belt in northern Manitoba and Saskatchewan (Fig. 1 and 2). At 109.5 Mt of contained base metal sulphide ore, the Flin Flon Belt is one

of the most productive base metal regions in Canada (Syme and Bailes, 1993), and the most productive Paleoproterozoic greenstone belt in the world (Franklin et al., 1995).

Snow Lake area polymetallic base metal massive sulphide deposits are noteworthy in that their host volcanic rocks are well exposed in cross-section, from a series of underlying subvolcanic intrusions, through hydrothermally altered volcanic rocks to the overlying massive sulphide deposits. This represents a unique opportunity to investigate factors that

Table 1. Metal grades in volcanic-hosted massive sulphide.

| Deposit | District | Status | Cu % | Zn % | Cu:Zn | Au g/t | Ag g/t | Au:Ag | Prod.+Res. (tonnes) |
|----------------------|----------|--------|------|-------|-------|--------|--------|-------|---------------------|
| Flin Flon | Flin | CL | 2.19 | 4.2 | 0.52 | 2.6 | 41.5 | 0.06 | 62 446 734 |
| Trout Lake | Flin | OP | 2.11 | 4.79 | 0.44 | 1.41 | 15.43 | 0.09 | 10 180 608 |
| Chisel Lake | Snow | CL | 0.6 | 10.94 | 0.05 | | | | 7 299 816 |
| Stall Lake | Snow | CL | 4.39 | 0.5 | 8.78 | | | | 7 000 000 |
| Osborne Lake | Snow | CL | 3.14 | 1.52 | 2.07 | | | | 3 380 061 |
| Anderson Lake | Snow | CL | 3.41 | 0.10 | 34.10 | | | | 3 189 601 |
| Callinan | Flin | OP | 1.43 | 3.7 | 0.39 | 1.68 | 20.57 | 0.08 | 2 800 000 |
| Spruce Point | Snow | CL | 2.36 | 2.8 | 0.84 | 2.0 | 25.0 | 0.08 | 1 931 000 |
| Schist Lake | Flin | CL | 4.21 | 7.00 | 0.60 | 1.4 | 37.0 | 0.04 | 1 877 813 |
| Centennial | Flin | CL | 1.41 | 2.48 | 0.57 | 0.05 | 0.59 | 0.08 | 1 624 550 |
| Westarm | Flin | CL | 3.34 | 1.25 | 2.67 | | | | 1 579 403 |
| Coronation | Sask | CL | 4.25 | 0.30 | 14.17 | 1.87 | 4.68 | 0.40 | 1 282 088 |
| Dickstone | Snow | CL | 2.47 | 3.13 | 0.79 | | | | 1 083 590 |
| Chisel pit | Snow | CL | 0.23 | 10 | 0.03 | 2.74 | 54.86 | 0.05 | 1 140 000 |
| White Lake | Flin | CL | 1.97 | 4.63 | 0.43 | | | | 849 598 |
| Rod No. 2 | Snow | CL | 6.63 | 2.9 | 2.30 | | | | 810 440 |
| Photo Lake | Snow | OP | 5.6 | 6.2 | 0.9 | 5.1 | 20 | 0.26 | 660 000 |
| Ghost Lake/Lost Lake | Snow | CL | 1.34 | 8.87 | 0.15 | | | | 605 690 |
| Cuprus | Flin | CL | 3.24 | 6.42 | 0.50 | 1.37 | 28.69 | 0.05 | 462 002 |
| Flexar | Sask | CL | 3.75 | 0.47 | 7.98 | | | | 305 940 |
| Birch | Sask | CL | 6.15 | | | | | | 278 825 |
| North Star | Flin | CL | 6.11 | | | | | | 241 643 |
| Mandy | Flin | CL | 5.63 | 13.95 | 0.40 | | | | 123 116 |
| Don Jon | Flin | CL | 3.07 | | | | | | 79 313 |
| Rod No. 1 | Snow | CL | 5.00 | 4.5 | 1.11 | | | | 22 675 |

District: Flin = Flin Flon; Snow = Snow Lake; Sask = Amisk Lake, Saskatchewan
Status: OP = present producer; CL = past producer
Grades quoted are production grades
Deposit size includes production plus reserves
Sources of grade and tonnage information: Bamburak, 1990; Thomas, 1990; Hudson Bay Exploration and Development data, 1995

control massive sulphide deposition. In this paper we describe and discuss the setting of and controls on the Snow Lake volcanic-hosted massive sulphide deposits.

Regional geology

The Paleoproterozoic Flin Flon belt is a collage of 1.92-1.88 Ga tectonostratigraphic assemblages juxtaposed during a period of 1.88-1.87 Ga intra-oceanic accretion and subsequent 1.84-1.78 Ga terminal collision of bounding Archean cratons (Lucas et al., in press). The volcanic rocks include oceanic arc, ocean floor-back arc, oceanic island, oceanic plateau, and older crustal assemblages (Syme and Bailes, 1993, Stern et al., 1995, in press). Oceanic arc assemblages include tholeiite, calc-alkaline, and rare shoshonite and boninite suites (Stern et al., 1995), almost identical to those forming in modern intra-oceanic arcs (e.g. Gill, 1981).

Volcanic-hosted base metal massive sulphide deposits in the Flin Flon Belt occur preferentially in oceanic island arc rocks that were extruded between 1.91 and 1.88 Ga (Machado and David, 1992; Syme and Bailes, 1993; David et al., 1993; Stern et al., 1993, 1995). Two volcanic-hosted massive sulphide-hosting oceanic island arc segments, one near the town of Flin Flon and one at Snow Lake, occur in the Manitoba portion of the Flin Flon Belt (Fig. 2). They are separated by an extensive, northeast-trending collage of 1904 Ma (Stern et al., 1994) ocean floor (MORB-like) back arc basalt flows and associated gabbro and ultramafic rocks (Stern et al., in press), with no associated volcanic-hosted massive sulphide deposits (Fig. 2). Lithological, geochemical, and isotopic criteria, for example the higher overall ϵ_{Nd} of mafic flows in the Snow Lake segment relative to those at Flin Flon (Stern et al., 1993), suggest that these oceanic island arc segments may represent unrelated, structurally juxtaposed terranes (Stern et al., 1995; Lucas et al., in press).

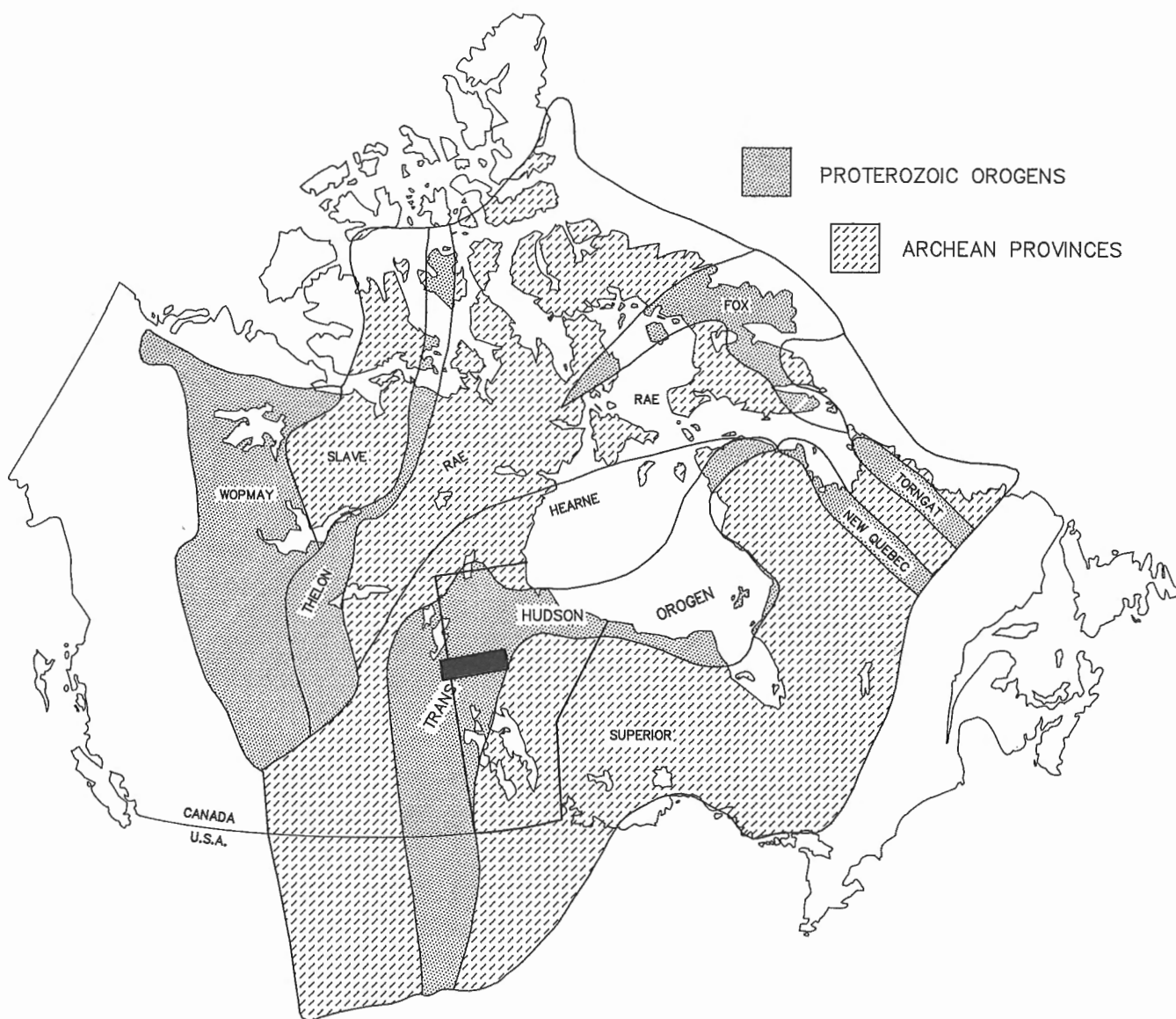


Figure 1. Location of Flin Flon Belt (filled rectangle) in Trans-Hudson Orogen (after Hoffman, 1988).

Accretion of intra-oceanic volcanic rocks (1.88-1.87 Ga) is followed by 1.87-1.83 Ga intrusion of isotopically juvenile calc-alkaline plutons, and eruption of volcanic equivalents (only rarely preserved). Lucas et al. (1994) and Stern et al. (1994) interpret these rocks to be successor arc(s) and basins developed on the older, accreted, oceanic volcanic rocks. The Snow Lake area is dominated by ca. 1.84-1.83 Ga fold-thrust style tectonics (Connors and Ansdell, 1994) that is atypical of central and western portions of the Flin Flon Belt. This difference in tectonic style may reflect the fact that the entire Snow Lake segment is a south-verging, allochthonous, imbricate zone that was thrust ca. 1.84 Ga (Lucas et al., 1993; Syme et al., 1995; Lucas et al., in press) over the previously amalgamated collage of oceanic and arc rocks to the west (Fig. 2).

Setting of Snow Lake area volcanic-hosted massive sulphide deposits

An 84 km² area directly south of the town of Snow Lake (shown in Fig. 3) contains eight of the area's eleven producing and past-producing base metal mines, plus numerous sub-economic base metal occurrences. Host rocks for Snow Lake massive sulphide deposits (Fig. 3 and 4) comprise a ca. 1.89 Ga bimodal mafic-felsic volcanic sequence intruded by two large, subvolcanic tonalite intrusive complexes (Bailes et

al., 1991; David et al., 1993). We divide the volcanic rocks into five depositional phases, based on groupings of strata that display either distinct geochemical signatures or geological attributes, or a combination of both (Fig. 4b).

Mafic volcanic rocks consist mainly of basalt (45-53 wt.% SiO₂) and basaltic andesite (53-57 wt.% SiO₂) flows and related breccias (Fig. 4b). Those belonging to phases 2 to 4 include significantly more volcanoclastic rocks than either phases 1 or 5. Mafic flows and volcanoclastic rocks of phases 1 to 4 display classic oceanic arc tholeiite geochemical characteristics whereas phase 5 mafic flows show ocean floor-back arc affinities (Stern et al., 1995). Geochemical signatures of phase 1 mafic flows are typical of magmas formed in a primitive forearc tectonic setting whereas those of phases 2-4 are similar to mafic magmas formed in an evolved arc setting (Stern et al., 1995).

Dacite (62-70 wt.% SiO₂) and rhyolite (70-80 wt.% SiO₂) are volumetrically less extensive than mafic flows and volcanoclastic rocks but are important as most of the significant volcanic-hosted massive sulphide deposits at Snow Lake are hosted by felsic extrusive complexes. Cu-rich deposits are associated with phase 1 rhyolite complexes in the primitive arc (e.g., Stall Lake, Anderson Lake, Rod) and Zn-rich deposits are affiliated with phase 3 dacite volcanoclastic rocks

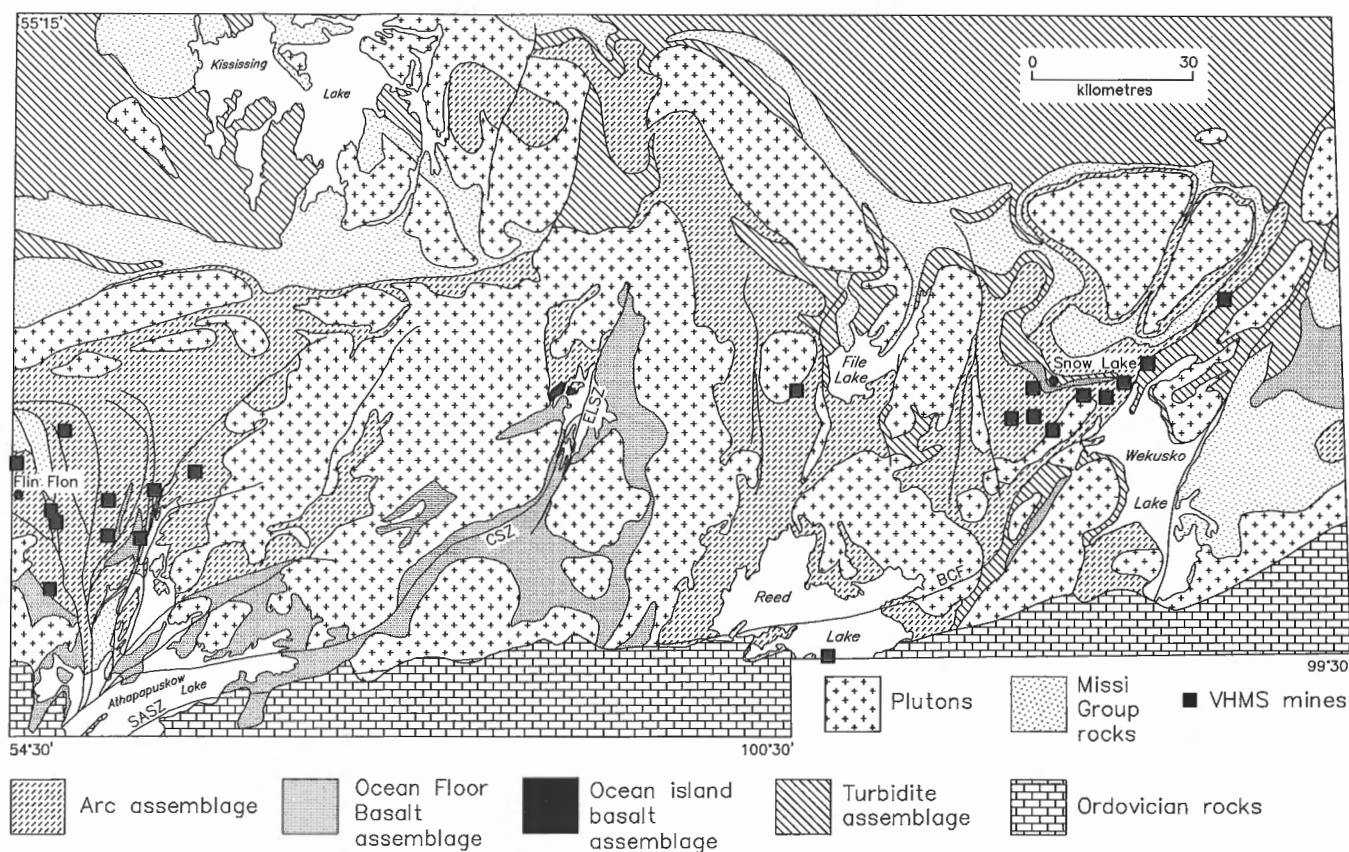


Figure 2. Simplified geological map of Flin Flon Belt. Base metal mines (past and current producers), shown by bold squares, occur in arc volcanic rocks near towns of Flin Flon and Snow Lake. SASZ – South Athapapaskow shear zone; CSZ – Cranberry shear zone; ELSZ – Elbow Lake shear zone; BCF – Berry Creek Fault.

and rhyolite flows in the evolved arc (e.g., Chisel Lake, Ghost Lake, Lost Lake) (Fig. 3 and 4). The recently discovered Photo Lake Cu-rich deposit is contained wholly within rhyolite flows (Fig. 3).

Thick accumulations of heterolithological mafic breccia are not directly related to volcanic-hosted massive sulphide deposits at Snow Lake, but we speculate that these highly permeable units may have played an important role in the

hydrology of hydrothermal systems integral to the genesis of Zn-rich deposits at Chisel Lake. The heterolithological mafic breccias include minor amounts of felsic volcanic debris.

Most of the volcanic rocks in the Snow Lake area were deposited in a shallow to moderately deep marine environment. Some of the pyroclastic rocks may have been erupted subaerially and then deposited under water. Blocks of subvolcanic tonalite in mafic heterolithological breccias indicate the presence of primary topographic relief sufficient for portions

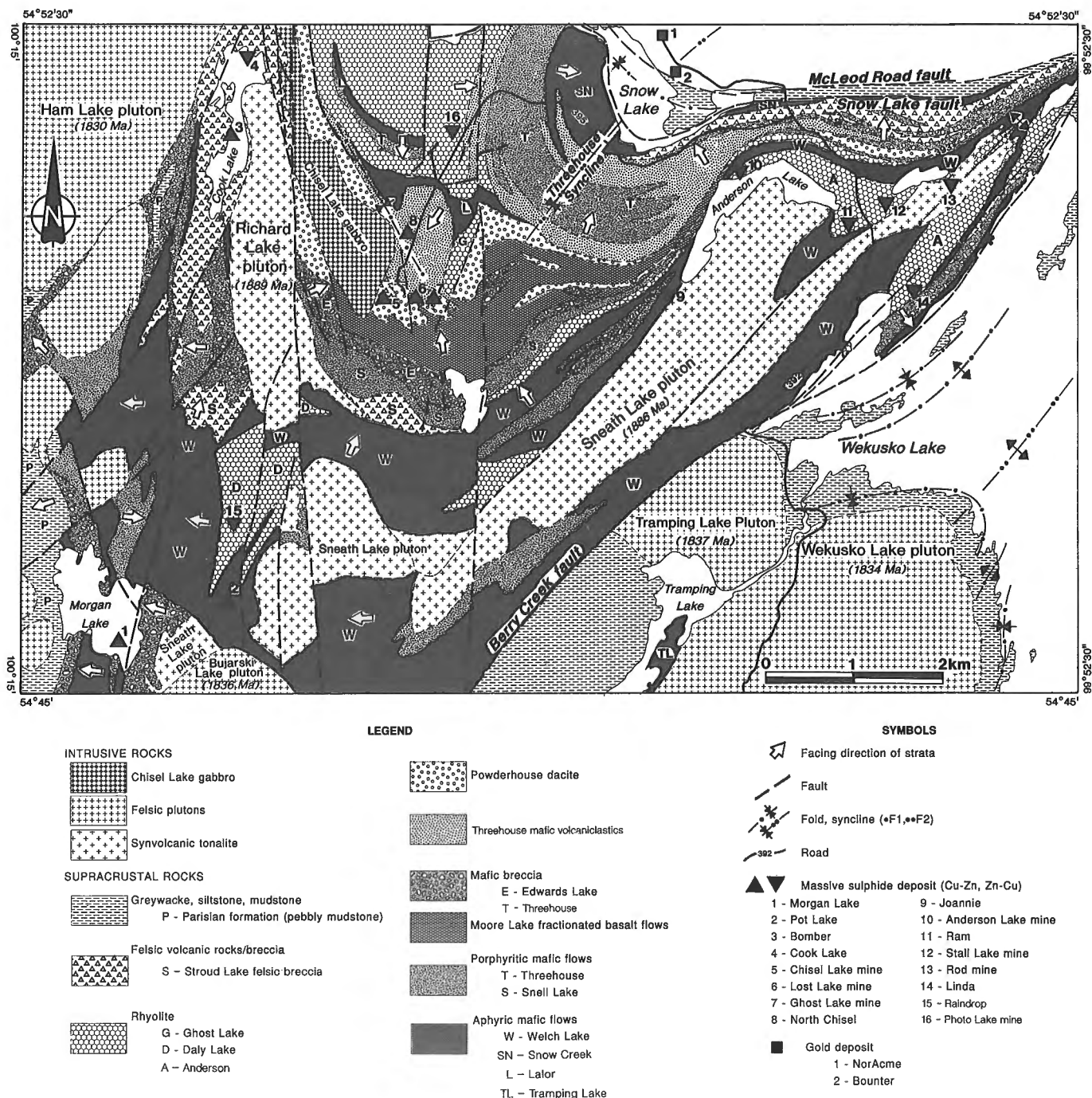


Figure 3. Simplified geology of Snow Lake area. Bold triangles mark location of massive sulphide deposits.

of the subvolcanic intrusions to be unroofed and eroded. An angular unconformity at the base of phase 4 (Bailes and Simms, 1994) attests to topographic relief and local subaerial erosion during deposition of the volcanic succession at Snow Lake.

Megascopically altered rocks (Fig. 5a and 5b), occur in broad, semiconformable zones, and affect up to 25% of the rocks at Snow Lake. These zones are evidence that large portions of the volcanic succession at Snow Lake were

affected by circulatory hydrothermal fluid flow. This geothermal activity is most logically interpreted to have been caused by emplacement of two large subvolcanic tonalite intrusions (Bailes et al., 1991). Base metal deposits at Snow Lake are generally considered to be products of this geothermal activity and, thus, to be genetically related to the subvolcanic tonalite bodies (Walford and Franklin, 1982; Bailes, 1987b; Galley et al., 1990).

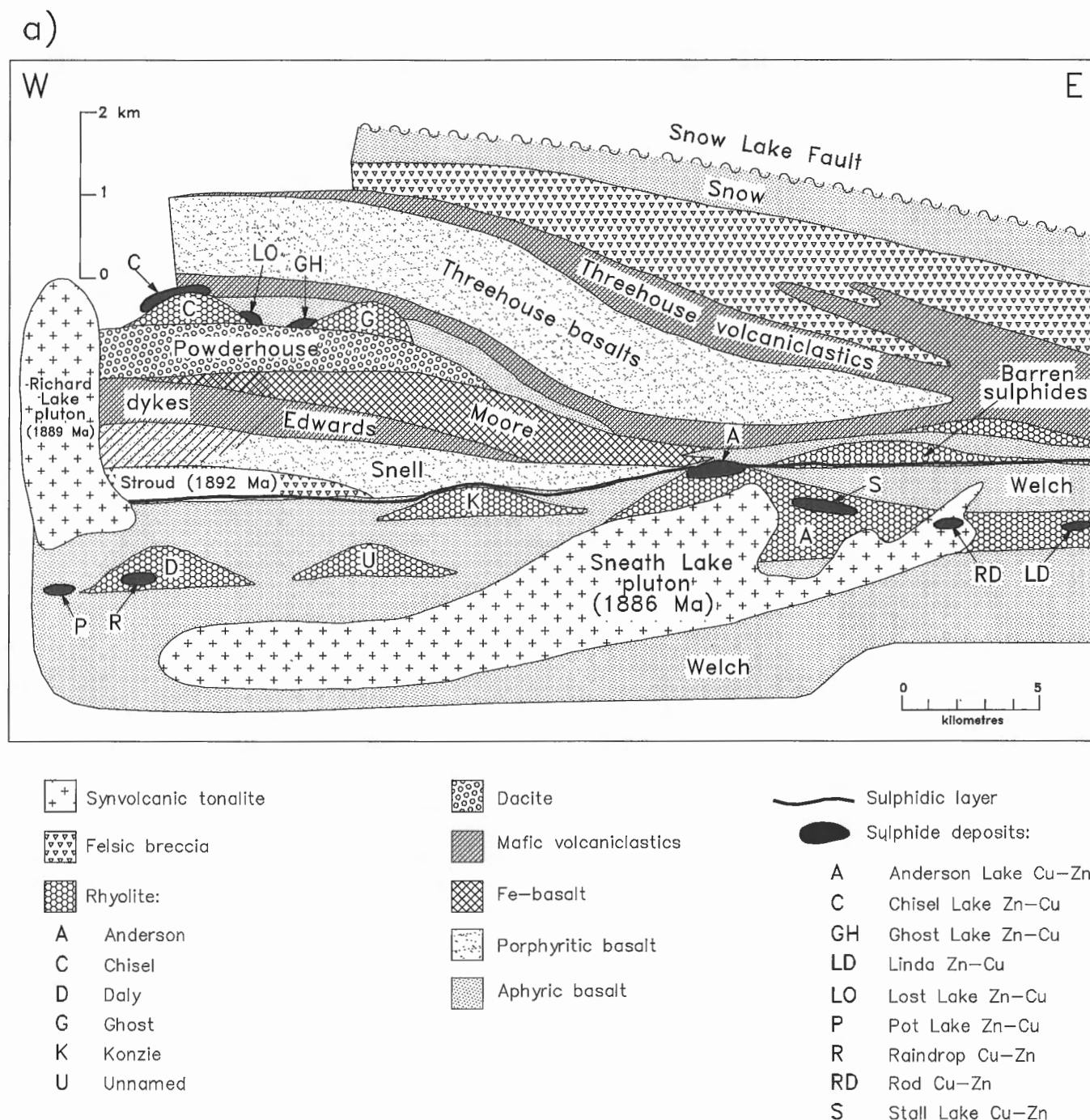


Figure 4. a) Schematic geological cross-section showing massive sulphide-hosting volcanic rocks at Snow Lake, b) five "phases" of volcanism, and c) tectonic setting in which volcanic rocks were extruded.

b)

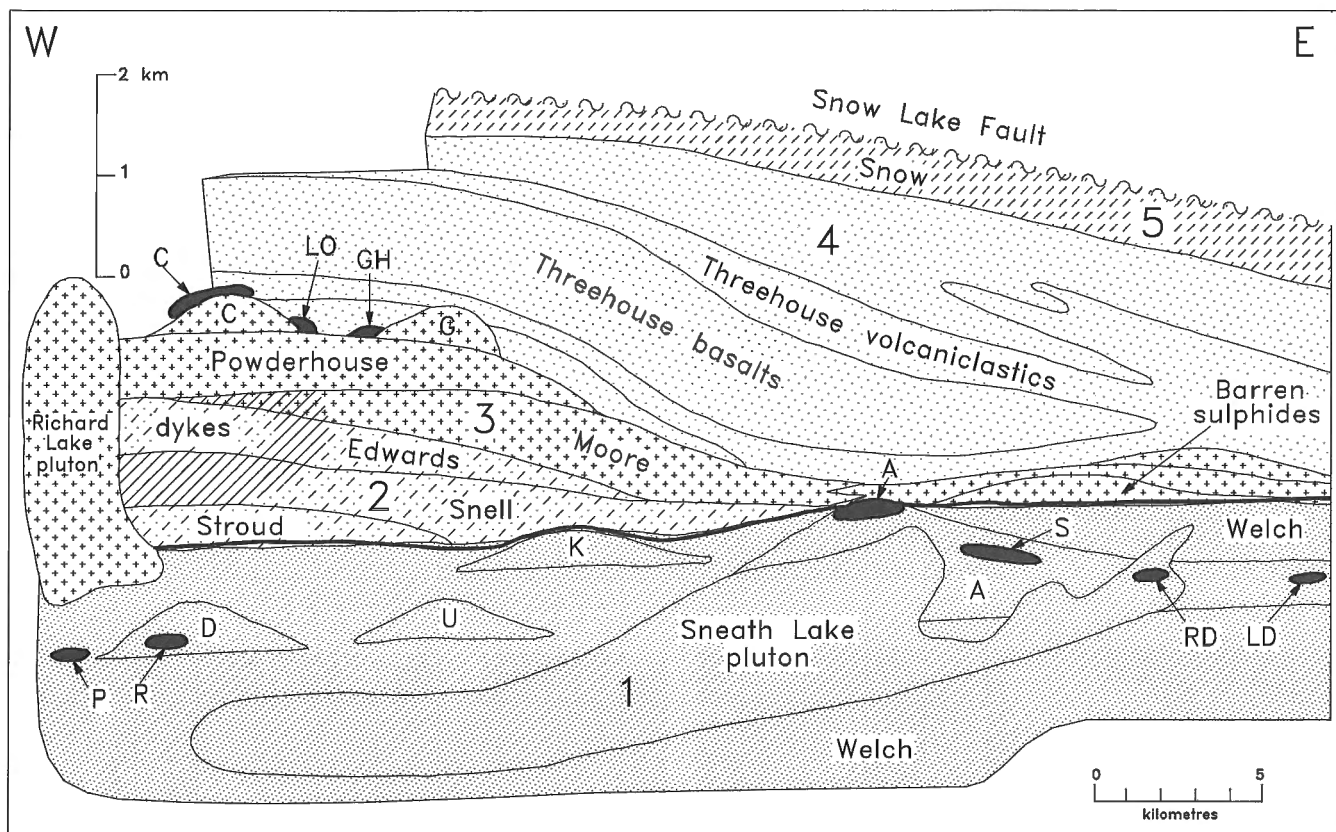


Figure 4b.

c)

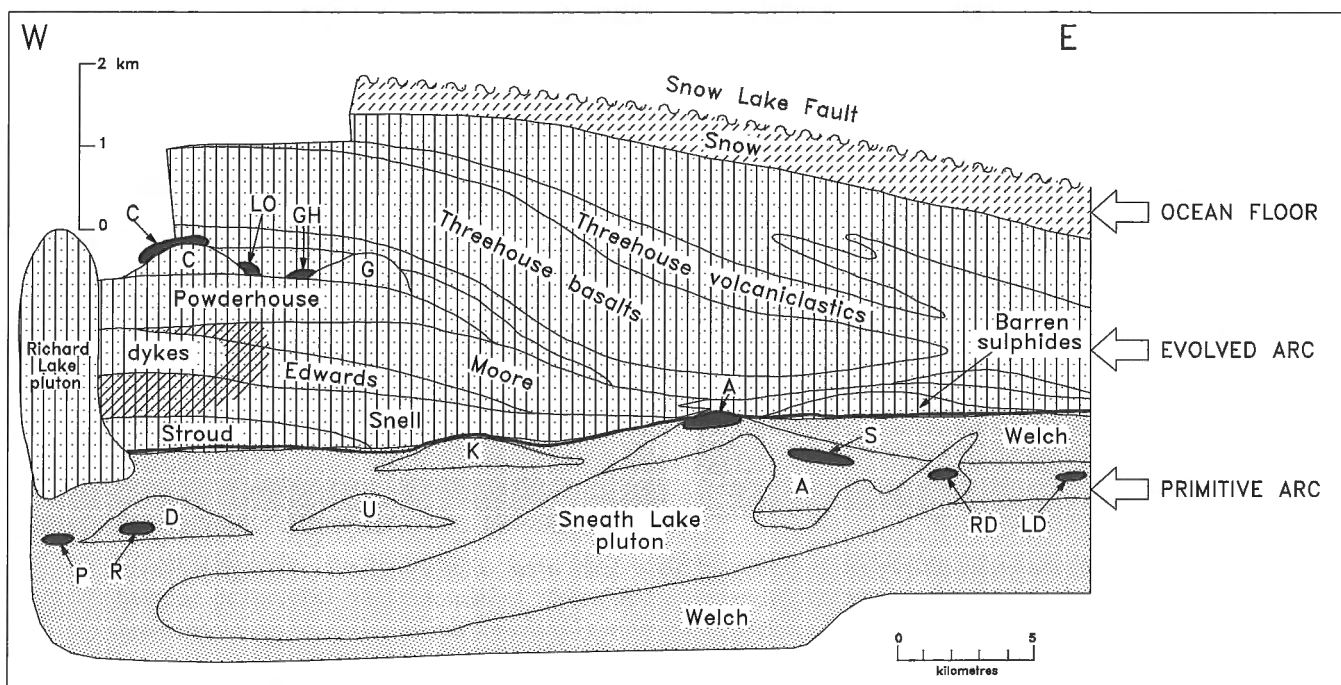


Figure 4c.

Four folding events and a peak regional metamorphic event coincident with the second folding episode are recognized in the Snow Lake area rocks (Kraus and Williams, 1993; Connors and Ansdell, 1994). A titanite age from a sample in the Anderson felsic complex dates the peak regional metamorphism at 1810 Ma (Machado and David, 1992), and indicates that this metamorphism postdated volcanism and hydrothermal activity by 80 million years. Mineral assemblages, formed during peak regional metamorphism, grade south to north from greenschist to middle almandine-amphibolite facies. Most massive sulphide deposits and associated hydrothermally altered rocks are coarsely recrystallized to lower to middle amandine amphibolite facies mineral assemblages. This recrystallization enhances ability to recognize altered rocks, because even weakly altered lithologies are characterized by distinctive metamorphic mineral assemblages.

Two major episodes of deposition of base metal-rich massive sulphides are recognized at Snow Lake: 1) Cu-rich deposits within the phase 1 Anderson and Daly rhyolite

complexes in the primitive arc succession, and 2) Zn-rich deposits at the top of phase 3 associated with evolved arc rhyolite flows (Fig. 4). Each sulphide mineralizing event is clearly related to a distinct episode of hydrothermal alteration. The interplay between massive sulphide deposition and hydrothermal activity is described in the following sections. Other volcanic-hosted massive sulphide deposits shown on Figure 3 (Morgan Lake, Bomber, North Cook, Photo Lake) are of uncertain stratigraphic affinity to the main mineralizing episodes. The Morgan Lake Zn-rich deposit is most similar in setting and composition with the Chisel Lake area Zn-rich deposits at the top of phase 3. The Bomber, North Cook, and Photo Lake deposits are tentatively interpreted to be associated with a third mineralizing event (Bailes and Simms, 1994) that is not discussed in this paper. A base metal-poor episode of sulphide deposition, the Foot-Mud unit, is briefly discussed in the section dealing with hanging wall alteration to the Anderson Lake area Cu-rich deposits.

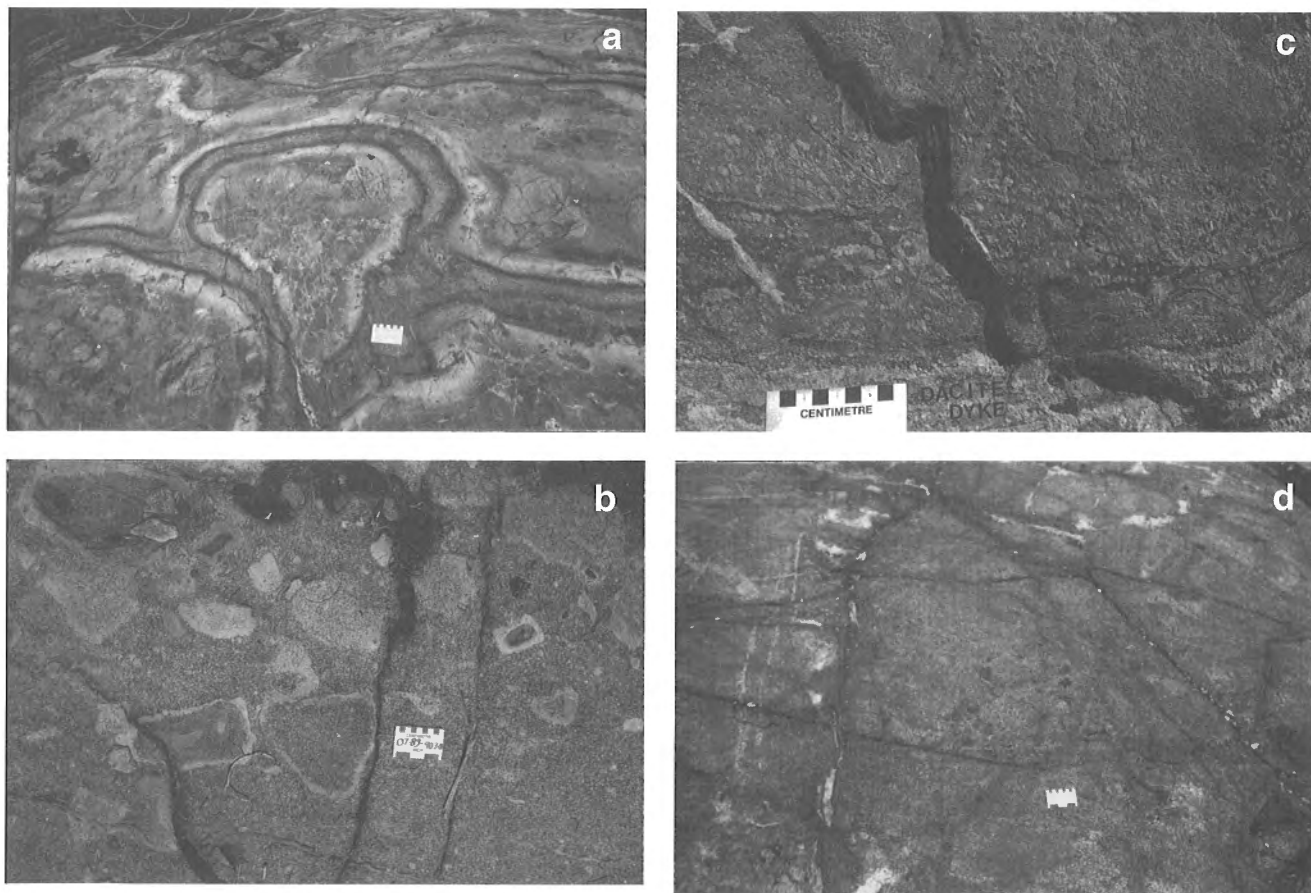


Figure 5. Hydrothermally altered rocks typical of Snow Lake area: *a)* silicified pillow margins, Welch formation basalt, *b)* silicified rims on fragments in Edwards formation mafic breccia, *c)* mottled silicification in Edwards formation mafic wacke adjacent to synvolcanic dacite dyke, and *d)* chlorite- and staurolite-rich altered fractures in Sneath Lake tonalite.

PRIMITIVE ARC-HOSTED Cu-RICH DEPOSITS

Introduction

Cu-rich volcanic-hosted massive sulphide deposits in the primitive arc bimodal basalt-rhyolite sequence are spatially associated with the rhyolite flow complexes (Fig. 3 and 4). The Anderson rhyolite is host to three economic Cu-rich deposits (Anderson Lake, Stall Lake, and Rod) that originally contained 10.1 Mt with an average grade of 4.15% Cu and 0.53% Zn. It also hosts the uneconomic 13 Mt Linda deposit grading 0.3% Cu and 0.79% Zn, and two subeconomic, stockwork-type zones (Joannie and Ram). The primitive arc Daly Lake rhyolite hosts the subeconomic Cu-rich Raindrop occurrence and is in close proximity to the Pot Lake deposit. The Unamed rhyolite, which lies geographically between the Daly and Anderson rhyolites, contains minor Cu-rich volcanic-hosted massive sulphide-type mineralization (G. Kitsler, Hudson Bay Exploration and Development, pers. comm., 1995).

In this section we describe the geological setting of the Anderson rhyolite-hosted deposits (Anderson Lake, Stall Lake, Rod, and Linda) as an example of the nature of primitive arc-hosted mineralization at Snow Lake. The Anderson Lake, Stall Lake, and Rod deposits occur on the north limb of a major east-northeast-trending fold, the Anderson Bay anticline, and the Linda deposit occurs on the south limb (Fig. 6). Deformation has structurally thinned host units and elongated individual sulphide deposits into prolate lenses that plunge parallel to regional stretching lineations.

Stratigraphic footwall

Phase 1 volcanic rocks

Welch basalt

Aphyric to minor porphyritic subaqueous Welch basalt flows are present both in the footwall and hanging wall to the massive sulphide deposits at Anderson Lake. Footwall portions of the Welch basalt are poorly preserved to the south of Anderson Lake, due to intrusion by the Sneath Lake pluton (Fig. 6), but to the west form an up to 3000 m thick unit (Fig. 7) truncated to the south by the Berry Creek fault and capped to the north by the Foot-Mud sulphidic sediments. Welch mafic flows are primitive arc tholeiites (Stern et al., 1995) that display a crude upward change from basalt to andesite, and are intercalated with minor lenses of pillow fragment breccia, heterolithological mafic breccia, and porphyritic high-Mg flows. The high-Mg porphyritic flows geochemically resemble Ca-boninites (Stern et al., 1995) that occur in forearc, or protoarc settings in modern arcs (Crawford et al., 1987).

Anderson rhyolite

This 1 x 12 km rhyolite body is the largest of several felsic extrusive complexes that occur in the upper 1 km of the Welch basalts (Fig. 6 and 7). Near the Stall Lake deposit, the basal 750 m of the Anderson rhyolite is aphyric and massive, and

is overlain to the north by 100 m of quartz-phyric and 150 m of quartz megacrystic varieties. The original character of the Anderson rhyolite is obscured by intrusion of the Sneath Lake pluton, by large areas of hydrothermal alteration, by tight folding about the Anderson Bay anticline (Fig. 6), and by recrystallization to lower almandine-amphibolite facies mineral assemblages during regional metamorphism. Recrystallized lithologies are composed of fine grained granoblastic mosaics of quartz, feldspar, and biotite, with varying amounts of amphibole, garnet, sericite, chlorite, staurolite, and kyanite that increase in amount with degree of hydrothermal alteration.

Primitive arc phase 1 rhyolites, including that at Anderson Lake, have similar rare-earth element and ϵ_{Nd} values as do the underlying Sneath Lake tonalite complex and are, for this reason, interpreted as an extrusive equivalent. Primitive arc rhyolites and tonalites display higher ϵ_{Nd} values (+3.7) than the Welch basalt (+3.0) indicating that they are not directly related to the Welch basalt by fractionation of the same parent magma (Stern et al., 1992).

Sneath Lake pluton

This sill-like, semiconformable 1.5 x 22 km complex displays many of the features expected of a high level subvolcanic intrusion: absence of a metamorphic halo, multiple phases, bodies of intrusion breccia, textural variation, porphyritic character, internal alteration (including disseminated chalcopyrite) and overprinting by kinematic and metamorphic events. A synvolcanic age is supported by a U-Pb zircon age of 1886 ± 17/-9 Ma for the quartz megacrystic tonalite (Bailes et al., 1991) and 1892 ± 4 Ma for overlying phase 2 Stroud felsic breccia (Machado and David, 1992). Fragments of the distinctive Sneath Lake quartz megacrystic tonalite in overlying phase 1 and 2 volcanogenic breccia units is conclusive evidence that the intrusion is synvolcanic.

The Sneath Lake pluton is composed of at least seven texturally distinct tonalite bodies separated by intrusive contacts. The largest individual body, located south of Anderson Lake, is 1.5 x 5 km, semiconformable, and composed of quartz megacrystic tonalite (Fig. 3 and 6). From west to east this body cuts up section, at a shallow angle, through approximately 1 km of phase 1 volcanic stratigraphy, rising to within 0.3 km of the top of phase 1 volcanic rocks at its eastern end (Fig. 7). A quartz-feldspar porphyry phase of the Sneath Lake tonalite, previously interpreted to be extrusive (Coats et al., 1970; Studer, 1982; Walford and Franklin, 1982; Zaleski, 1989), completely envelops the Rod volcanic-hosted massive sulphide deposit, and intrudes hanging wall portions of the Welch basalt. This suggests a range in age of the different phases of the Sneath Lake tonalite, with some postdating massive sulphide deposition.

Footwall alteration zone

Various types and intensities of alteration affect almost all of the Anderson rhyolite, portions of the underlying Welch basalt, as well as the upper portion of the underlying Sneath

Lake tonalite. Many of the more highly altered rocks are soft, preferentially eroded, and poorly exposed. Diamond drilling by Hudson Bay Exploration and Development Co. Ltd. (HBED) has demonstrated that the shape of Anderson Lake is largely due to an extensive domain of highly altered lithologies under the lake (Walford and Franklin, 1982; Hudson Bay Exploration and Development, pers. comm., 1992). The

Anderson Lake alteration system has three main components: a broad zone of weak alteration that affects most of the Anderson rhyolite; a large, semiconformable zone of moderate to strong alteration centered in the top of the Sneath Lake pluton and in directly overlying strata; and discordant zones of strongly altered rocks.

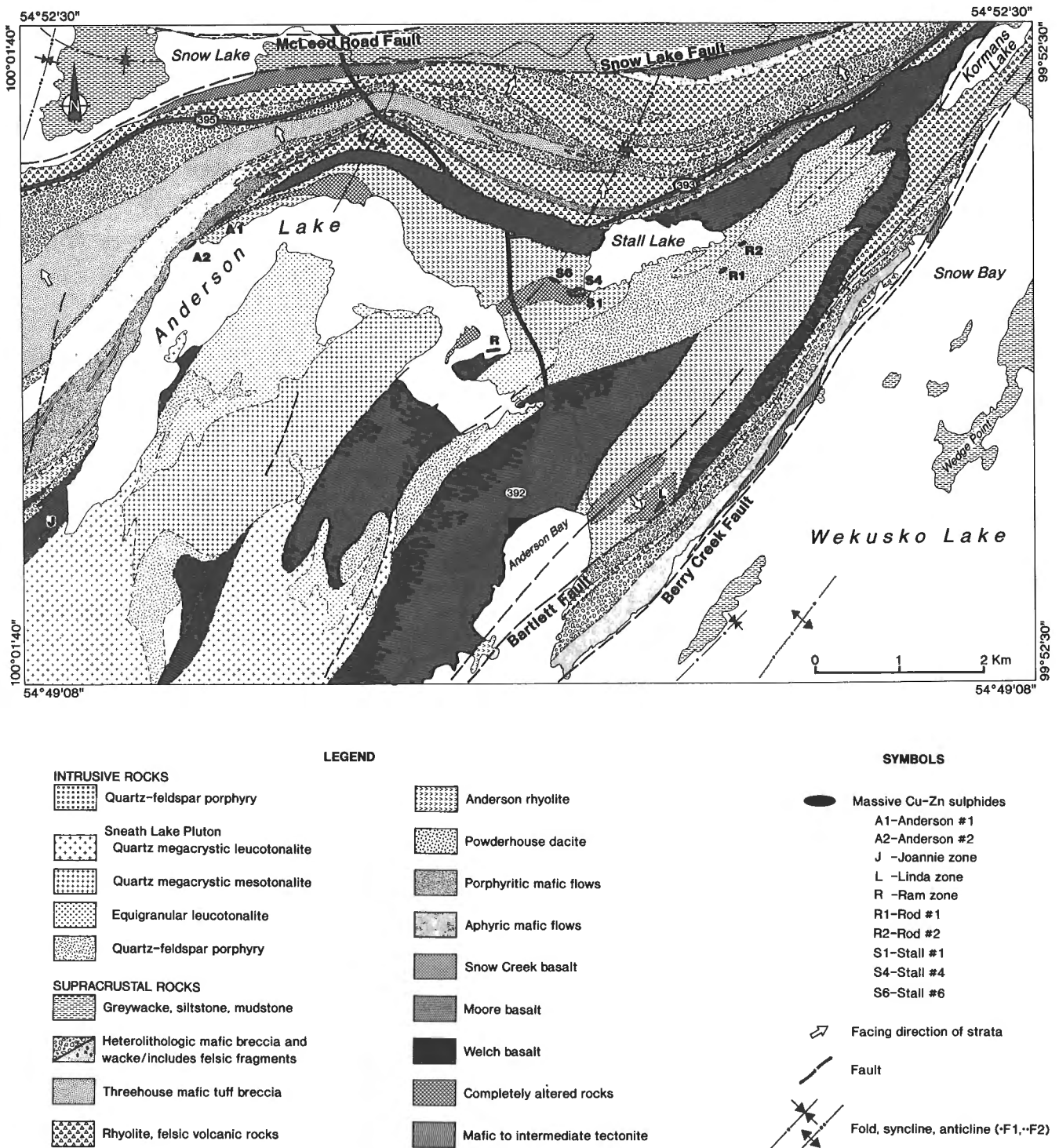


Figure 6. Simplified geology of Anderson Lake area.

The broad domain of weak, pervasive alteration that affects virtually all of the Anderson rhyolite complex is characterized by quartz-biotite-staurolite-garnet metamorphic mineral assemblages. The altered rocks contain distinctive 1-5% staurolite porphyroblasts and patchy, 1-5 cm bleached domains overgrown by actinolite porphyroblasts. The amount and size of staurolite porphyroblasts gradually increases towards discordant alteration zones. The altered rhyolites display a patchy depletion in Na (Walford and Franklin, 1982) that, according to studies by Mottl and Holland (1978) and Riverin and Hodgson (1980), can be interpreted as a product of interaction of the rhyolite with a Na-depleted hydrothermal fluid at high fluid/rock ratios.

The large semiconformable zone of moderately to strongly altered rocks under Anderson Lake is 150-700 m in width and approximately 5 km long. It is generally widest and most intense stratigraphically above the mesotonalite phase of the Sneath Lake pluton, between the Anderson Lake and Stall Lake mine sites, but has been identified in drill core and in surface exposures from the Joannie zone in the west to Stall Lake in the east (Fig. 6). Although the semiconformable alteration mainly affected the Anderson rhyolite, it has also affected the upper 300 m of the Sneath Lake pluton and parts of the Welch basalt southeast of the Anderson Lake mine. The semiconformable alteration consists of a broad zone of chlorite-rich rocks containing varying amounts of coarse grained biotite, staurolite, amphibole, garnet, magnetite, and kyanite. Down section the semiconformable zone displays increasing chlorite and staurolite contents. Chlorite-rich alteration also affects the upper part of much of the Sneath Lake pluton, with remnant, 2 cm quartz megacrysts the only evidence of the tonalite precursor. Chlorite-rich altered rocks in the semiconformable zone are generally characterized by abundant porphyroblasts of biotite, staurolite, and kyanite.

A more areally restricted zone of semiconformable alteration is present in the footwall stratigraphy to the Linda deposit (Zaleski, 1989; Zaleski et al., 1991). This 150 m thick and over 450 m long "distal zone" occurs 150-200 m below the massive sulphide body, and consists of a core of Na-Ca depletion composed of staurolite-rich gneiss surrounded by an envelope of calc-silicate alteration characterized by abundant plagioclase, epidote and amphibole.

Discordant zones of completely altered rocks, referred to colloquially as "pipes" by Sangster (1972), transect the Anderson rhyolite in the immediate footwall to the Anderson Lake, Stall Lake, and Linda deposits. These zones are characterized by chlorite- and sericite-rich rocks containing varying concentrations of staurolite, garnet, biotite, magnetite, and kyanite. A general observation for the Anderson Lake and Stall Lake discordant zones is that their lower parts and cores are chlorite-rich, with sericite-rich envelopes surrounding their upper margins. At Anderson Lake the discordant zone has a core of chlorite-biotite-kyanite schist and an irregular margin of muscovite-kyanite schist (Walford and Franklin, 1982). At Stall Lake it is composed largely of chlorite-staurolite schist with subordinate sericite-kyanite schist (Fig. 8; Studer, 1982). At the Linda deposit the discordant alteration zone is more diffuse than at either Anderson

Lake or Stall Lake and is dominated by sericite, typically with a core of muscovite-staurolite-gahnite and a periphery of muscovite-garnet-staurolite (Zaleski et al., 1991). The Anderson Lake and Stall Lake discordant zones contain disseminated blebs, veinlets, and stockworks of sulphide minerals, mainly pyrite, within 10 to 20 m of the main sulphide lenses, as well as local areas of anhydrite-, carbonate- and anthophyllite-rich domains in proximity to the ore bodies.

The Anderson Lake discordant alteration zone is over 2 km long and 300 m wide and the Stall Lake zone is 1 km by 100 m; both originate near the mesotonalite phase of the Sneath Lake pluton (Fig. 6 and 7b). At both Anderson Lake and Stall Lake the discordant zones terminate up-section at the massive sulphide deposits, with only minor, metres-wide zones of intensely altered rocks immediately above the sulphide lenses. The planar morphology of both the Anderson Lake and Stall Lake discordant alteration zones suggests that they may have been fault- or fracture-controlled channelways for discharging hydrothermal fluids involved in formation of the sulphide lenses. The acute angle of the footwall alteration zone to primary layering at Anderson Lake and Stall Lake has been attributed by Walford and Franklin (1982) to tectonic flattening. However, because this does not explain the similar shallow angle to primary layering of the footwall alteration zone beneath the much less deformed Raindrop deposit in the Daly rhyolite (Hodges and Manojlovic, 1993), we suggest that the shallow orientation to primary layering may be as much a product of primary orientation as it is of subsequent tectonic flattening.

The Rod deposit only has a small zone of intensely altered, chlorite- and staurolite-rich rocks directly adjacent to the ore lens. We interpret these rocks to be the remnants of an originally much larger footwall alteration zone that has been largely obliterated by intrusion of a late phase of the Sneath Lake tonalite (see description of the Rod deposit below). The Joannie and Ram sulphide occurrences are postulated to be discordant stockwork zones defining proximal, discordant alteration zones (Fedikow et al., 1989; this study).

The Stall Lake and Linda deposits both display stacked massive sulphide ore lenses, attached by disconformable alteration zones (Studer, 1982; Zaleski et al., 1991). This stacking of massive sulphide lenses is a characteristic of "Noranda" type deposits where it has been interpreted by Knuckey et al. (1982) as evidence for long-lived hydrothermal activity coeval with continued plutonism and extrusion of felsic flows, an interpretation that we embrace for phase 1 volcanic-hosted massive sulphide deposits at Anderson Lake.

Massive sulphide deposits

Stall Lake deposit

The Stall Lake deposit, discovered in 1963 and mining discontinued in 1994, is the largest Cu-rich orebody in the Snow Lake area at 7 Mt, grading 4.39% Cu and 0.5% Zn (Table 1). It is described in considerable detail by Studer (1982) and a summary of his observations follow.

The Stall Lake orebody consists of four large and a number of smaller massive sulphide lenses. The main massive sulphide lenses consist of coarse grained pyrrhotite with lesser pyrite and chalcopyrite. They commonly contain massive magnetite and anhydrite along footwall contacts. Hanging wall contacts of the ore are sharp but footwall contacts are generally gradational. Disseminated stockwork and vein breccia ore were prominent only at the west end of the No. 4 orebody, where it was associated with a discordant chlorite-rich alteration zone. The deposit has an average Cu-Zn ratio (Cu/Cu+Zn) of 90, with sections of the No. 1 and No. 4 lenses

consistently containing in excess of 10% Cu. The west sides of ore lenses grade higher in Cu. For example, portions of the ore zone in contact with the footwall sulphide stockwork on the west side of the No. 4 lens are richer in Cu by a factor of two. Such Cu-rich zones are also Au-rich, with some intersections of massive sulphide and vein stockwork from No. 4 lens grading up to 32 g/t Au (Studer, 1982).

Main ore lenses at Stall Lake occur at the contact between the lower aphyric and middle quartz phyrlic members of the Anderson rhyolite, whereas smaller lenses lie

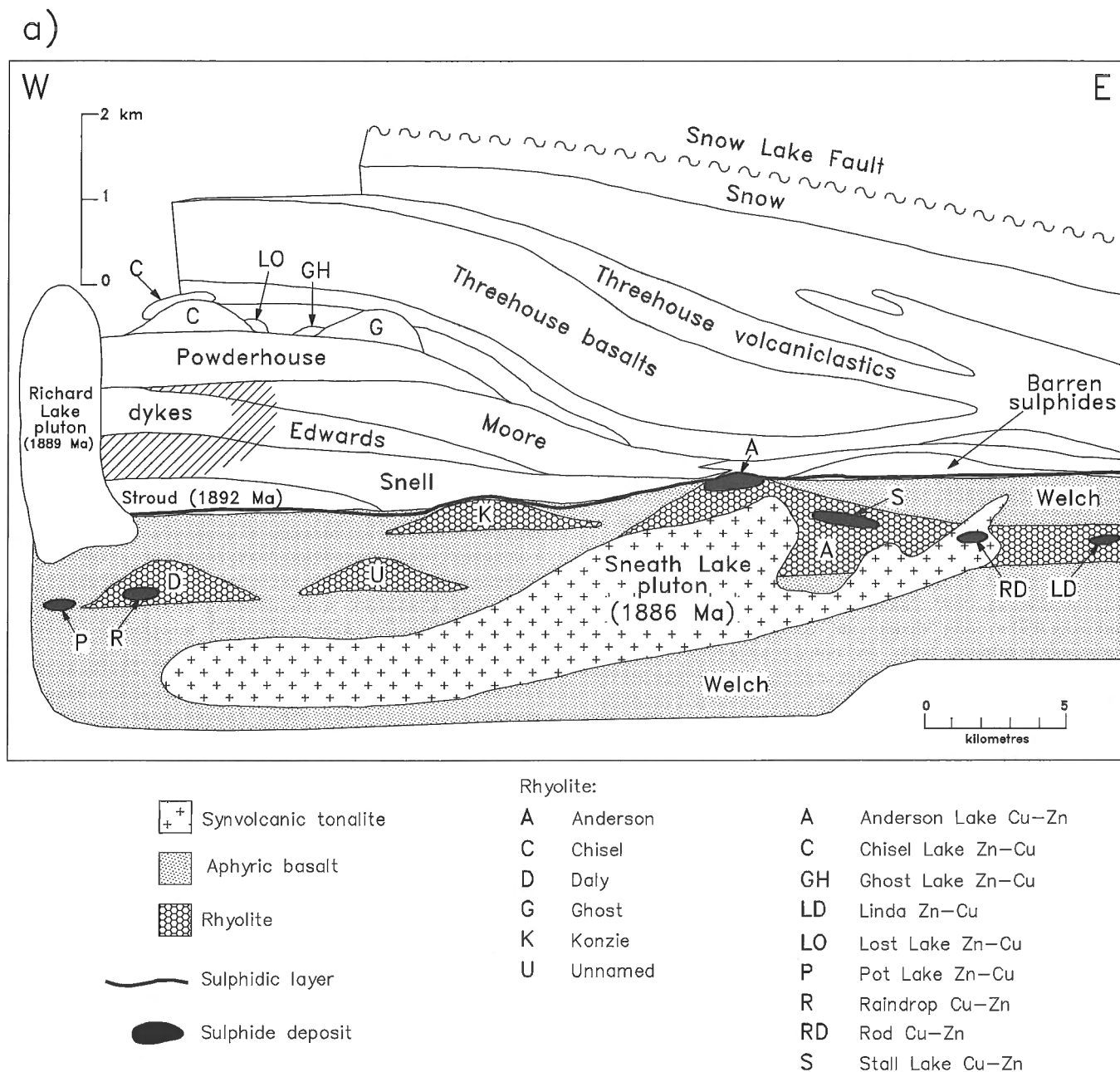


Figure 7. Schematic geological cross-section of phase 1 (primitive arc) volcanic rocks with location of associated Cu-rich massive sulphide deposits: a) geological units, b) distribution of hydrothermally altered rocks.

stratigraphically within the overlying quartz-phyric flow unit. The ore lenses strike 105° and dip 45°N, and together extend from surface to about 1450 m along a plunge of 45° at an azimuth of 015°. The largest individual sulphide lens, the No. 4 ore zone, has a down-plunge length of 950 m, with an average strike length of 91 m and a width up to 40 m. The sulphide lenses define a series of connected synclines and anticlines with long axes of individual lenses parallel to the north- northeast-trending elongation lineations.

Anderson Lake deposit

The Anderson Lake deposit, discovered in 1963 and mined out in 1988, consists of two sulphide lenses (Fig. 6), 350 m apart. Only the eastern body was mined and it contained 3.2 Mt grading 3.41% Cu and 0.10% Zn (Table 1). This deposit, with an average Cu-Zn ratio (Cu/Cu+Zn) of 97, is the most Cu-rich of the Anderson Lake area deposits. It is conformable with the volcanic host rocks, strikes 065° and dips 60°N, and plunges 65°NE. It has a strike length of 150 m, a maximum width of 10 m, and a down-plunge length of 1220 m (Fig. 9). It is composed largely of pyrite, chalcopyrite, and pyrrhotite, with minor sphalerite. The Cu grade of the sulphide zone decreases from stratigraphic footwall to hanging wall.

The stratigraphic/structural hanging wall to the sulphide lens consists of 4 m of muscovite schist, 5 m of muscovite-bearing partly altered quartz phyric felsic rocks, and a 1-3 m cap of barren sulphidic sediments ("Foot-Mud horizon"). The footwall consists of up to 50 m of sparsely quartz-phyric altered rhyolite followed down section by 300 m of aphyric rhyolite. This suggests that the Anderson Lake sulphide body occurs at a slightly higher stratigraphic position than the main sulphide bodies at the Stall Lake mine as they occur along the contact between aphyric and quartz-phyric rhyolite.

Rod deposit

The Rod deposit consists of two elongate, strongly deformed sulphide lenses (Fig. 6 and 10). The small Rod No. 1 lens was discovered in 1957 whereas the somewhat larger Rod No. 2 lens was located down-plunge in 1969 (Table 1). The Rod deposits are described in detail by Coats et al. (1970) and portions of their description are summarized in this section.

The Rod No. 1 orebody contained 22 675 t averaging 5% Cu and 4.5% Zn, and was mined between 1962 and 1964. This prolate sulphide lens has an aspect ratio of 24:14:1 and varies from 0.5 to 8 m in thickness, with a strike length up to 68 m, and a down-plunge length of 120 m. It strikes west-southwest and dips 40 to 45°NW, and plunges 32° at an azimuth of 28°.

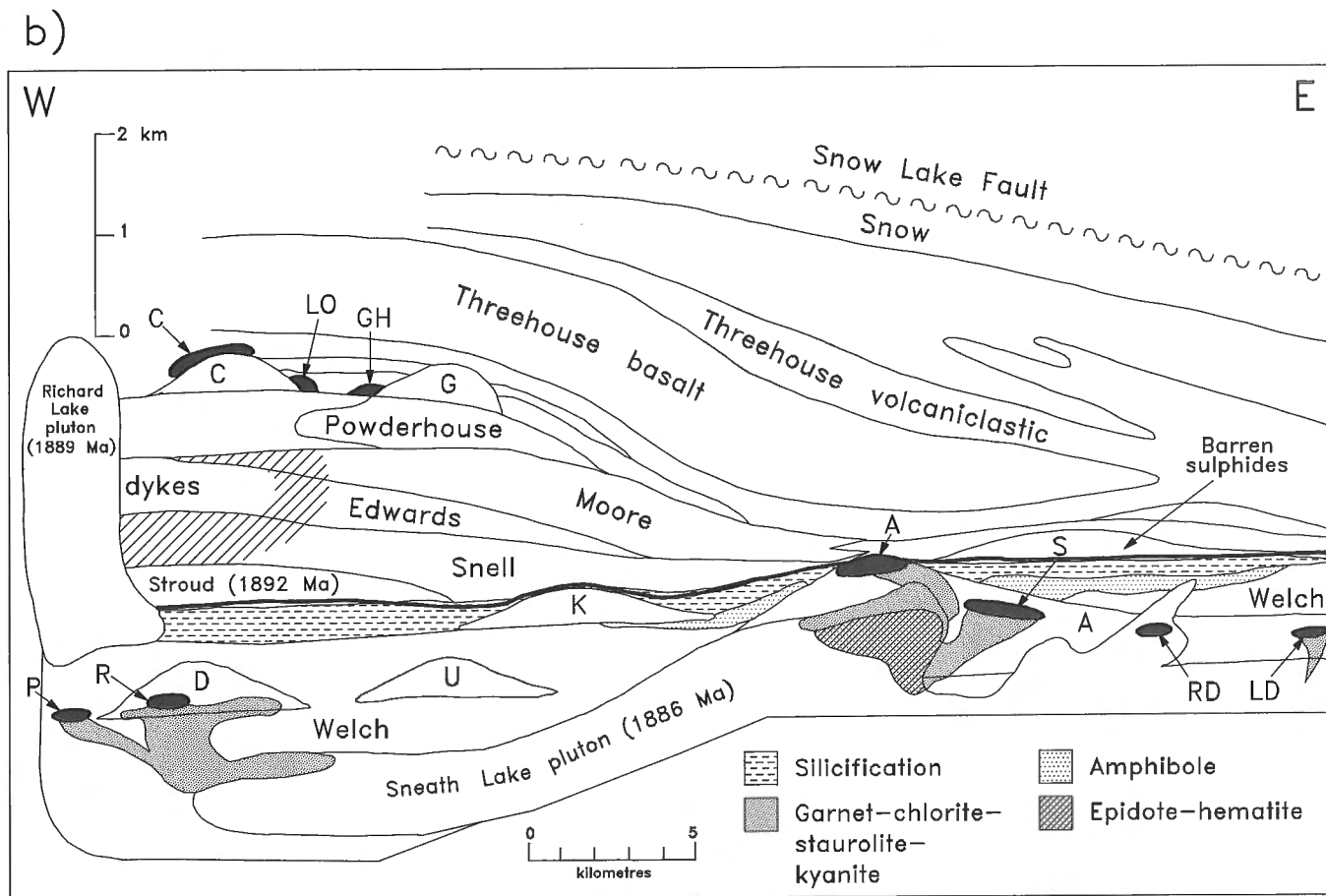


Figure 7b.

The ore has knife-edge hanging wall and footwall contacts. It contains wall rock fragments, including quartz porphyritic Sneath Lake tonalite, that are believed to have been incorporated during deformation of the sulphide lens.

The Rod No. 2 ore body, mined from 1984 to 1991, contained 810 440 t grading 6.63% Cu and 2.9% Zn (G. Kitzler, Hudson Bay Exploration and Development, pers. comm., 1993) with the combined No. 1 and 2 orebodies having a composite Cu-Zn ratio (Cu/Cu+Zn) of 69. The Rod No. 2 ore body has an aspect ratio of 180:14:1 and averages 3.5 m in thickness, 50 m in strike length, and 625 m in down-plunge length. It strikes west-southwest, dips 55°NW, and plunges 25° to 35° at azimuth 45° (shallowing at depth). The ore is tectonically banded, full of foliated wall rock fragments, and consists of coarsely recrystallized chalcopyrite and pyrrhotite locally containing abundant 5 to 10 mm porphyroblasts of arsenopyrite. Many ore zone contacts are faults and the ore itself is complexly deformed and tectonically remobilized (Hudson Bay Exploration and Development staff, pers. comm., 1991). The presence of tectonic breccias, strong tectonic banding and local interfolial folding of the massive sulphides, and extreme rodding of the sulphide lenses indicates a higher degree of deformation than is displayed by the Anderson Lake and Stall Lake deposits to the

west. This is probably due to proximity of the deposit to the axial trace of the east-northeast-trending Anderson Bay anticline (Fig. 3).

The host rock for both of the Rod deposit ore lenses is a fine grained felsic rock with 5 mm quartz phenocrysts. Although Coats et al. (1970) consider this to be a pyroclastic rock, recent mapping by Bailes and Galley (1994) demonstrates that it is more likely a younger and crosscutting quartz porphyry phase of the subvolcanic Sneath Lake pluton (Fig. 6). Narrow, 1 to 2 m zones of staurolite-sericite schist, that locally occur adjacent to the sulphide ore body, are interpreted to be remnants of altered host supracrustal rocks that were left adjacent to the ore zone after intrusion of the Sneath Lake pluton. Coats et al. (1970) suggested that fracture-controlled carbonate, which is abundant in the vicinity of the Rod deposit, was produced by synvolcanic alteration but we interpret this as a late feature associated with subsequent deformation.

Linda deposit

The 13 Mt Linda massive sulphide deposit is the largest in the Snow Lake area. It is pyrite-rich with 0.30% Cu, 0.79% Zn, and an unusual Cu-Zn ratio (Cu/Cu+Zn) of 27 for a phase 1-hosted primitive arc deposit. The Linda deposit and host rocks are described in detail by Zaleski (1989) and Zaleski et al. (1991), and most of the following information is excerpted from these sources.

The Linda deposit occurs on the south limb of the Anderson Bay antiform (Fig. 3 and 6) within the quartz-megacrystic upper unit of the Anderson felsic extrusive complex. Footwall alteration associated with the Linda deposit lies northwest of the deposit, in the structural hanging wall, a configuration that requires stratigraphy to face down and to the southeast (Fig. 11). The host felsic rocks are in possible fault contact with heterolithic mafic breccias to the southeast (Bailes and Galley, 1994).

The Linda deposit consists of a series of stacked massive sulphide lenses, one large and three small, with the largest lens stratigraphically highest in the sequence. It consists of granular pyrite (60-90%) and granoblastic calcite (10-40%), with disseminated magnetite and pyrrhotite, and minor sphalerite and chalcopyrite. Minor barren enclaves and veins of calcite cut the pyrite-rich ore.

The main sulphide lens is elongate, with an aspect ratio of at least 30:2:1, plunging 30° at an azimuth of 030°. Elongation of clasts, mineral lineations, and mineral aggregates in host volcanic rocks are indistinguishable from the orientation of the sulphide lens. The lineations are considered by Zaleski (1989) to be related to the same deformation event that produced the Anderson Bay antiform.

Stratigraphic hanging wall

At Stall Lake, the massive sulphide-hosting Anderson rhyolite is overlain by up to 300 m of phase 1 Welch basalt. This basalt thins to the west, disappearing from the section 300 m before the Anderson Lake sulphide deposit. The Welch mafic

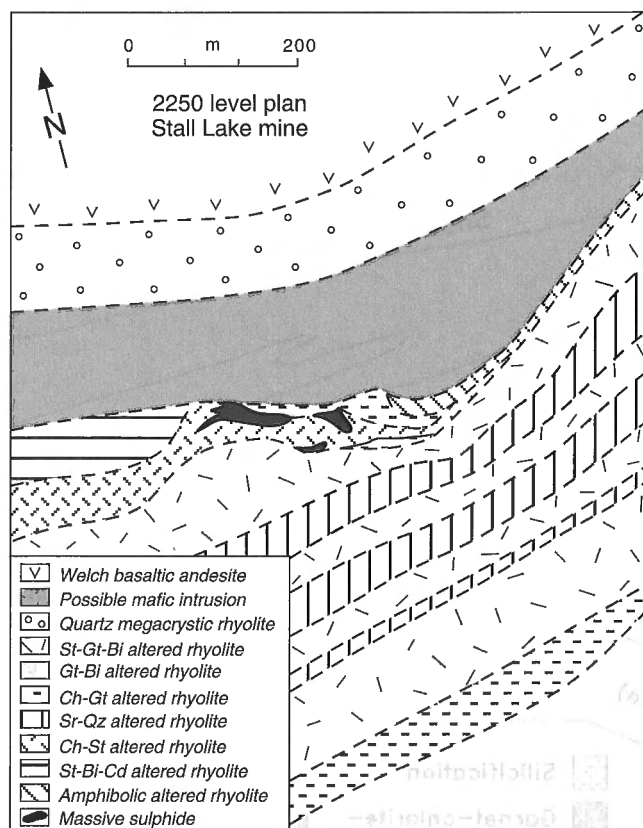


Figure 8. 2250 Level plan, Stall Lake mine (modified from Studer, 1982) St – staurolite; Gt – garnet; Bi – biotite; Ch – chlorite, Cd – cordierite; Qz – quartz.

flows are capped by 2 to 3 m of sulphidic sediments, locally termed the "Foot-Mud horizon". The sulphidic sediments, which contain disseminated pyrite and pyrrhotite, have been traced by drilling and geophysics for over 20 km. Although low in base metal content, they represent a significant episode of sulphide deposition in the Snow Lake region. The Foot-Mud unit is overlain to the north by up to 1 km of intermixed, coarse mafic and felsic volcanoclastics, with some contained mafic flows.

Hanging wall semiconformable alteration

Welch basalt and related mafic flows in the hanging wall to the Anderson rhyolite complex contain two zones of semiconformable alteration (Fig. 7b). One is an over 7 km long zone that is characterized by amphibole blastesis and the other is an over 20 km long zone of albitization/silicification that is prominent in the upper 0.5 km of the Welch basalt.

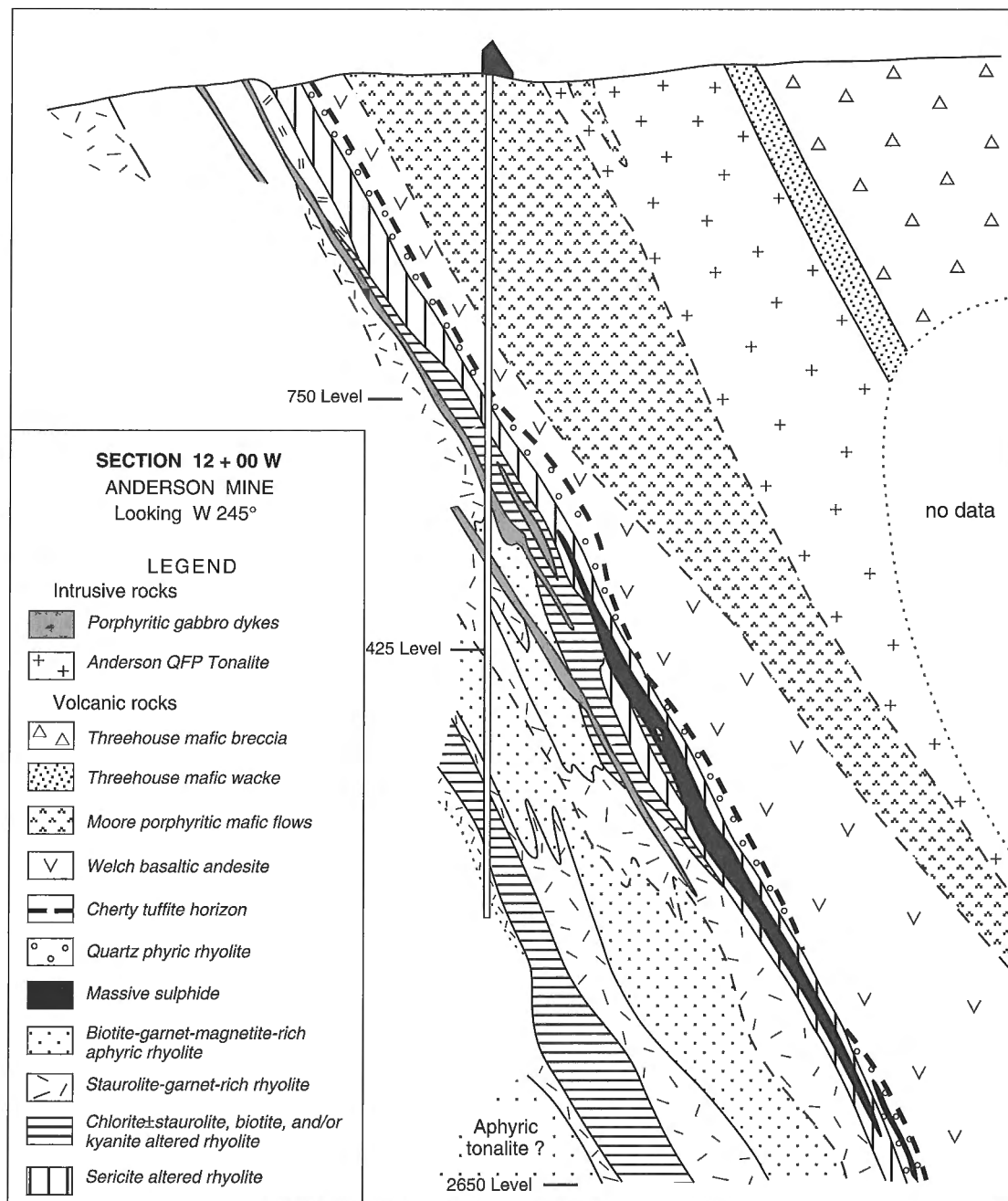


Figure 9. Cross-section (12+00W), Anderson Lake mine, looking west (modified from Walford and Franklin, 1982).

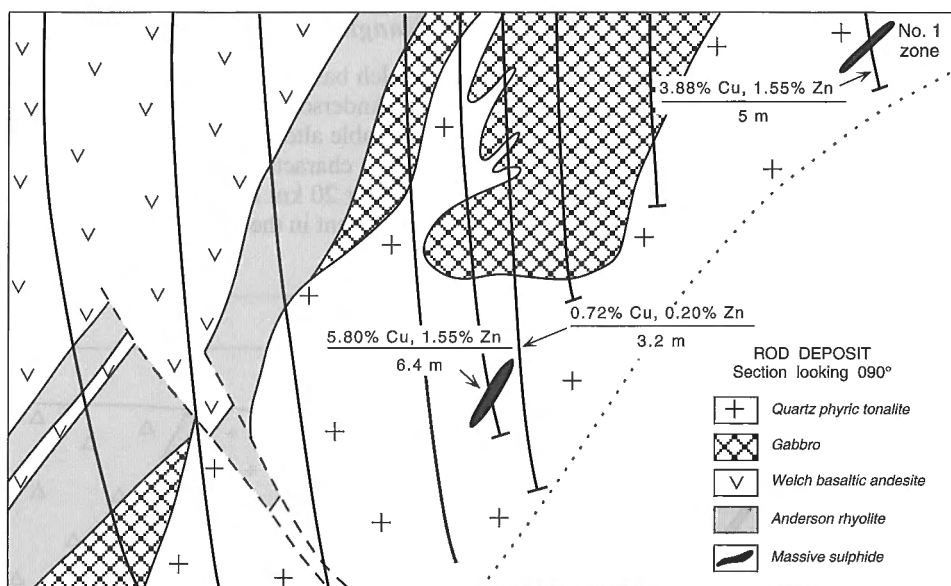


Figure 10. Longitudinal section of Rod deposit, looking south (modified from Coats *et al.*, 1970).

The zone of amphibole blastesis occurs consists of up to 70% coarse grained amphibole with associated intermittent concentrations of Fe-carbonate and disseminated pyrrhotite and chalcopyrite. The alteration overlies the Joannic occurrence in the west and extends for 7 km with varying intensity to the stratigraphic hanging wall of the Linda deposit. This unusual alteration type does not display large net mass gains or losses of major elements relative to less altered equivalents. Its spatial association with a discontinuous zone of mylonite along the northwest shore of Anderson Lake has raised the possibility that it may represent an altered and metamorphosed syn- F_1 fault zone.

The 0.5 by over 20 km semiconformable albitization/silicification zone at the top of the Welch basalt directly underlies the Foot-Mud sulphidic sediments (Fig. 7b). The albitization/silicification is not related to the prominent foot-wall alteration associated with phase 1 Cu-rich volcanic-hosted massive sulphide deposits. Rather it overlies these deposits and represents either a separate hydrothermal event or a waning stage of the mineralizing hydrothermal activity. The alteration involved a gain in Si and Na and losses in Mg, Fe, Mn, and Zn (Skirrow, 1987). The close temporal and spatial relationship between this semiconformable alteration zone and the directly overlying Foot-Mud unit suggests that geothermal activity responsible for the alteration zone also produced the barren sulphidic sediments. Skirrow and Franklin (1994) interpret the albitization/silicification as a product of interaction of diffuse, near-seafloor hydrothermal discharge with hot lava flows. Gibson (1989) suggested a similar genesis for the silicified Upper Amulet Formation and overlying C contact tuff of the Cental Volcanic Complex at Noranda, Quebec. Gibson (1989) has postulated that the Amulet silicification zone played a major role in forming volcanic-hosted massive sulphide deposits at Noranda by self sealing the hydrothermal system leading to production of

evolved base metal-rich fluids. The apparent absence of any economically significant base metal mineralization in the Foot-Mud sulphidic sediments suggests that the underlying semiconformable albitization/silicification zone did not self-seal a hot hydrothermal system and generate evolved base metal rich fluids.

Summary

Volcanic-hosted massive sulphide deposits in the primitive arc sequence are comparable in a number of respects to the "Noranda-type" deposits of Morton and Franklin (1987). They are Cu-rich (Cu/Cu+Zn ratios range from 27 to 98), occur in a bimodal basalt-rhyolite package, are hosted within isolated subaqueous rhyolite flow complexes, consist of multiple (stacked) lenses with extensive discordant chlorite-rich discordant alteration zones, and are underlain by a large felsic subvolcanic intrusive complex.

The integral role played by the subvolcanic Flavrian pluton in generating Noranda volcanic-hosted massive sulphide deposits is paralleled at Anderson Lake by the Sneath Lake intrusive complex. This is apparent from the coeval nature of the Sneath Lake tonalite and ore-hosting rhyolite flows, the increase in intensity of alteration of the host rocks with proximity to the pluton, and the steady increase in the Cu-Zn ratio (Cu/Cu+Zn) of the volcanic-hosted massive sulphide deposits from 27 at Linda to 97 at Anderson Lake as distance to the pluton decreases. We interpret this increase in Cu-Zn ratio of the sulphide deposits as a product of high Cu values coincident with higher temperature, pluton-proximal portions of the regional synvolcanic hydrothermal system. The presence of molybdenum and high Cu-Au values at Anderson Lake may also indicate a stronger magmatic component to the hydrothermal fluid responsible for the generation of this deposit. The high concentration of pyrite and, carbonate and

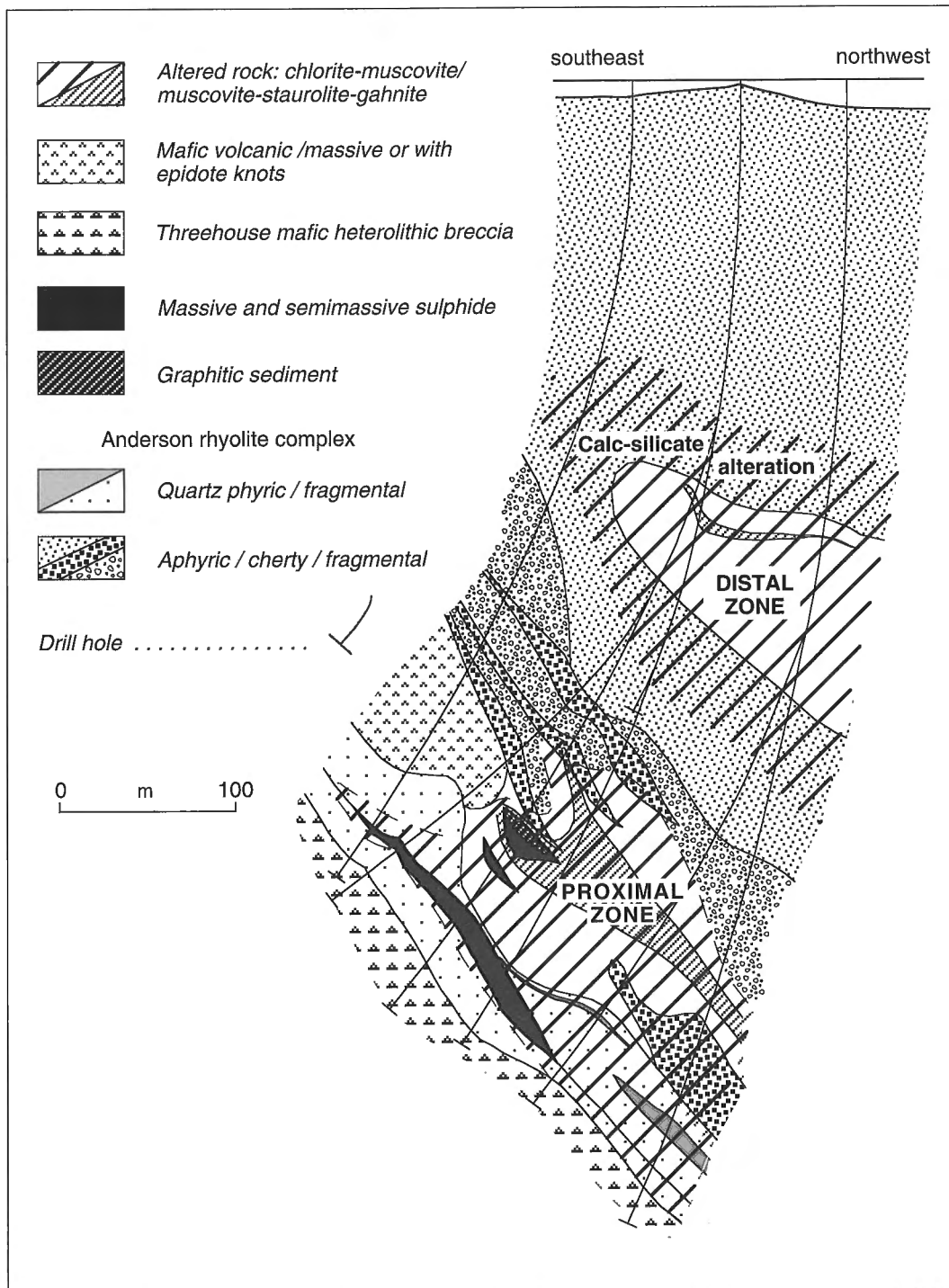


Figure 11. Subsurface geology of Linda deposit in cross-section looking southwest (modified from Zaleski, 1989).

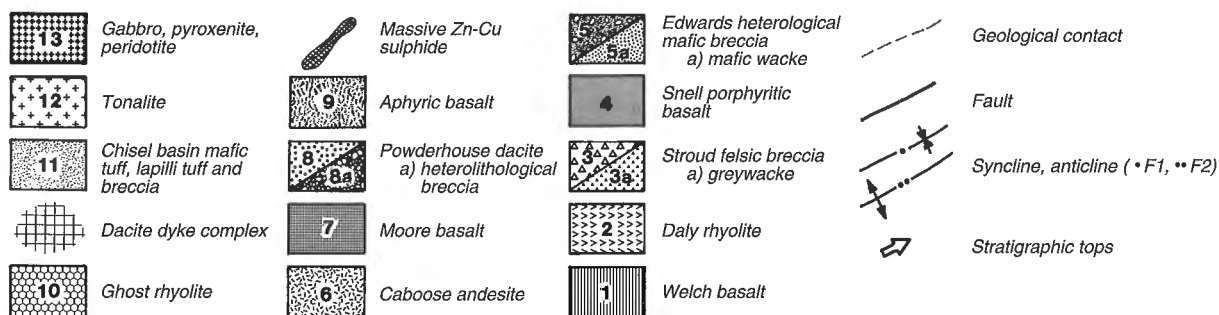
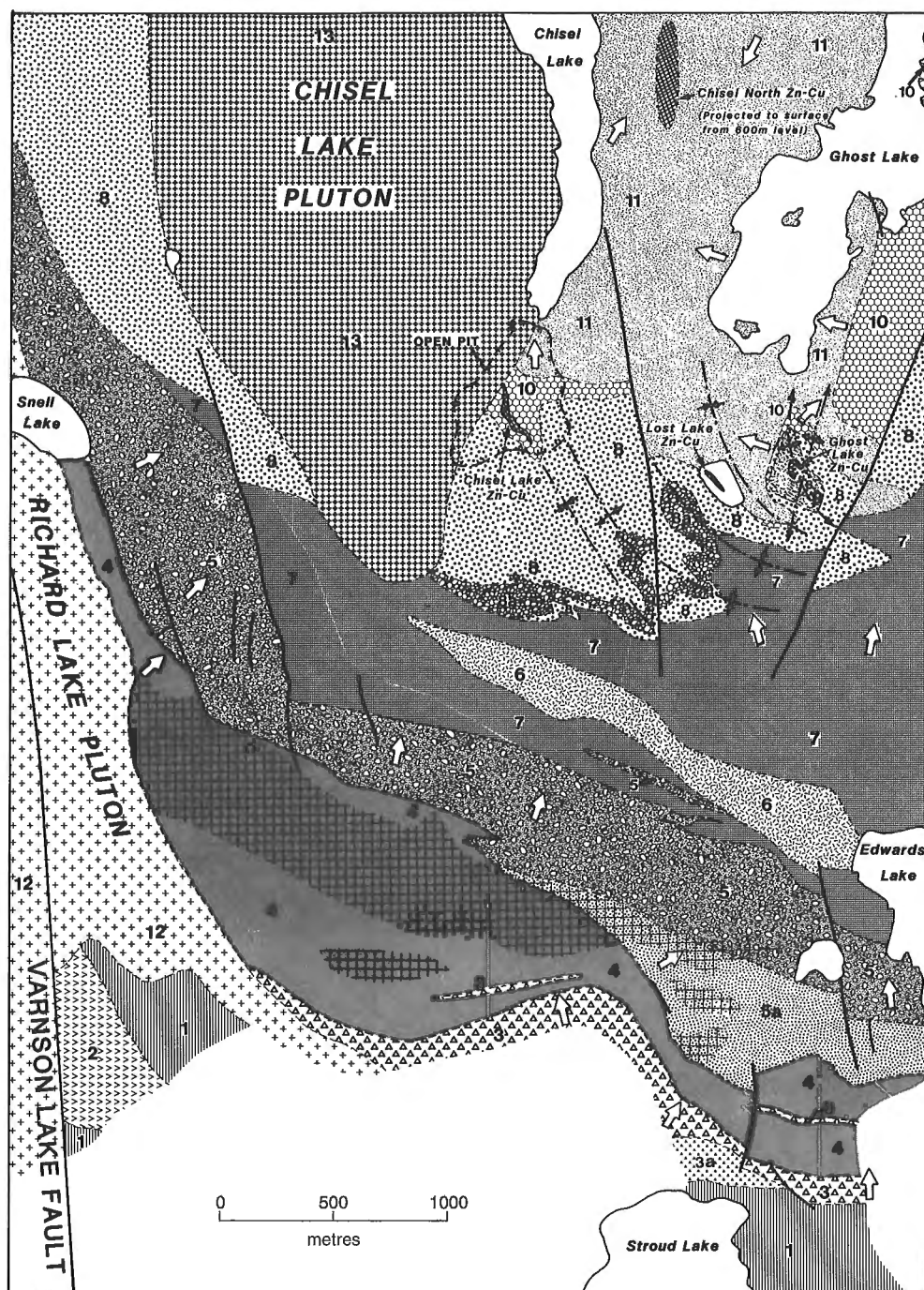


Figure 12. Simplified geology of Chisel Lake area.

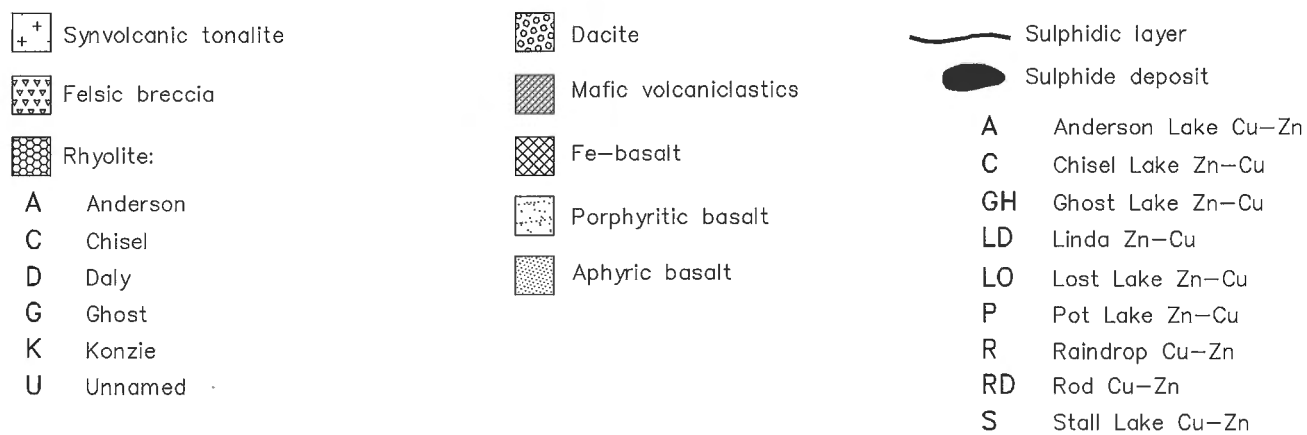
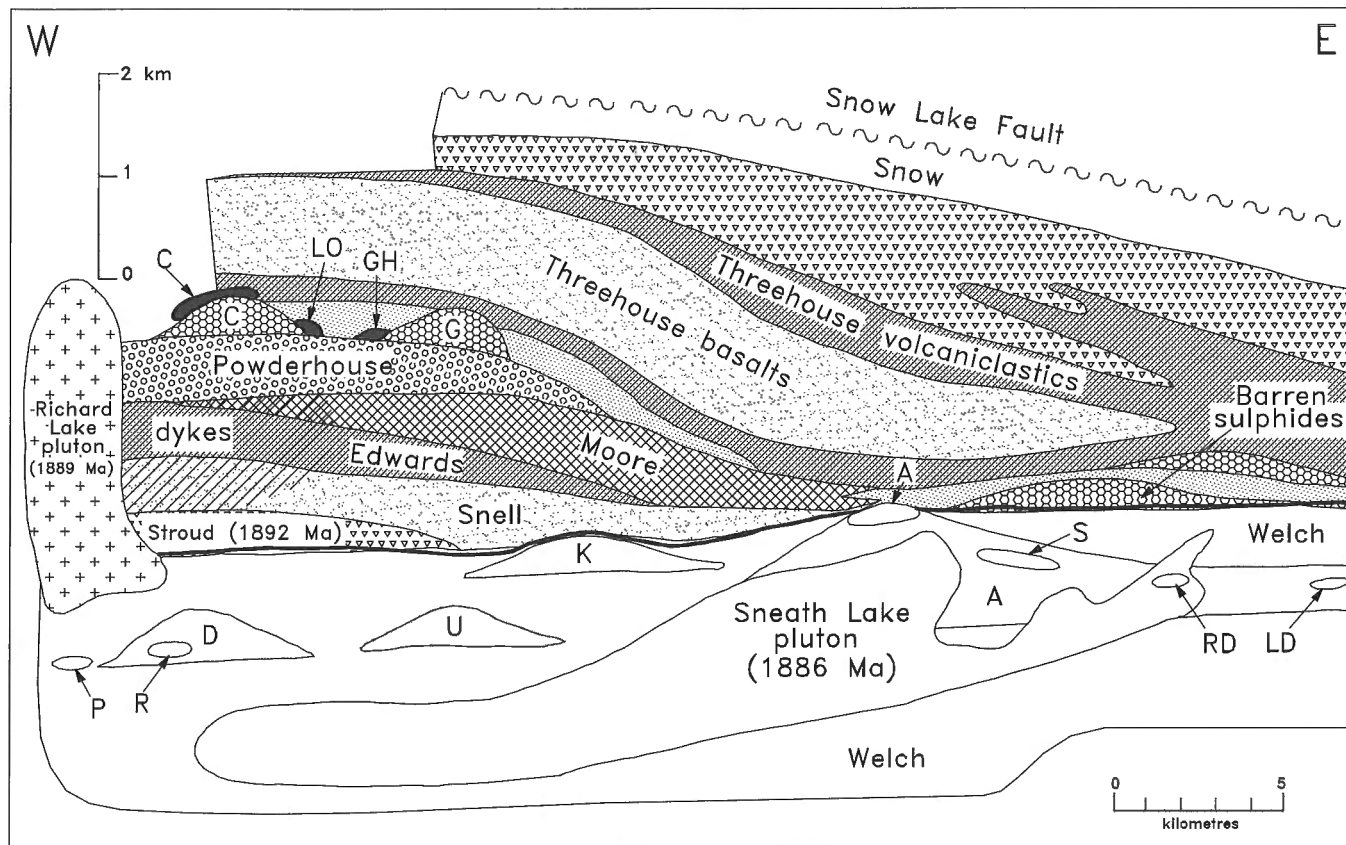


Figure 13. Schematic geological cross-section of phases 2-4 (evolved arc) volcanic rocks with location of associated Zn-rich massive sulphide deposits: **a)** geological units, **b)** distribution of hydrothermally altered rocks.

low base metal values at the Linda deposit may indicate that a high sulphur, low temperature, moderate pH fluid was responsible for formation of the deposit near the periphery of the pluton-generated regional hydrothermal system.

EVOLVED ARC-HOSTED Zn-RICH DEPOSITS

Introduction

The evolved arc hosts a second episode of base metal sulphide deposition in the Snow Lake area. It consists of four known Zn-rich massive sulphide deposits (Fig. 3, 4, 12, and 13) of which three (Chisel Lake, Lost Lake, and Ghost Lake) have been mined for a total of 7.8 Mt (production plus reserves) grading 0.42% Cu and 10.06% Zn. The fourth deposit (North Chisel), which has been drilled off but is unmined, contains 2.6 Mt grading 0.23% Cu and 8.9% Zn; it occurs 300 m down-plunge from the Chisel Lake deposit at a depth of 600-800 m. All four deposits occur in the same stratigraphic interval. The stratigraphic affinity of a recently discovered Cu-Au rich volcanic-hosted massive sulphide deposit at Photo Lake (Bailes and Simms, 1994), 4 km north of the Chisel Lake area deposits, is uncertain and is not discussed in this paper.

All of the Chisel Lake area massive sulphide deposits occur along the contact between phase 3 volcanic rocks and overlying formations. The Chisel Lake deposit is associated with a rhyolite flow complex (Chisel rhyolite), whereas the

other deposits occur at the same stratigraphic position at the top of the Powderhouse dacite. A 1 to 2 m thick sulphide-chert unit with up to several per cent Zn and Ag occurs at the top of the Chisel rhyolite and has been traced continuously along strike from the Chisel Lake to the Chisel North deposits (Galley et al., 1993).

The Chisel Lake area massive sulphide deposits are located along a linear alteration zone that is interpreted by Galley et al. (1993) to be the expression of a synvolcanic fault. The deposits are underlain by an extensive system of synvolcanic dykes that are spatially associated with hydrothermally altered rocks. As demonstrated below, the synvolcanic dykes display the same strongly fractionated and LREE geochemical signature as do the ore-hosting phase 3 volcanic cycle.

Stratigraphic footwall

A >4.5 km thick, essentially homoclinal, north-facing stratigraphic footwall section to the Chisel Lake area massive sulphide deposits is well exposed south of Chisel Lake (Fig. 3, 12, and 13). This steeply to moderately north-dipping section consists of 2.5 km of phase 1 volcanic rocks and intrusions (previously discussed in description of rocks hosting the phase 1 Cu-rich Anderson Lake area massive sulphide deposits), 1 km of phase 2 rocks (Stroud, Snell, and Edwards formations), and 1 km of phase 3 (Moore, Powderhouse, and Ghost formations).

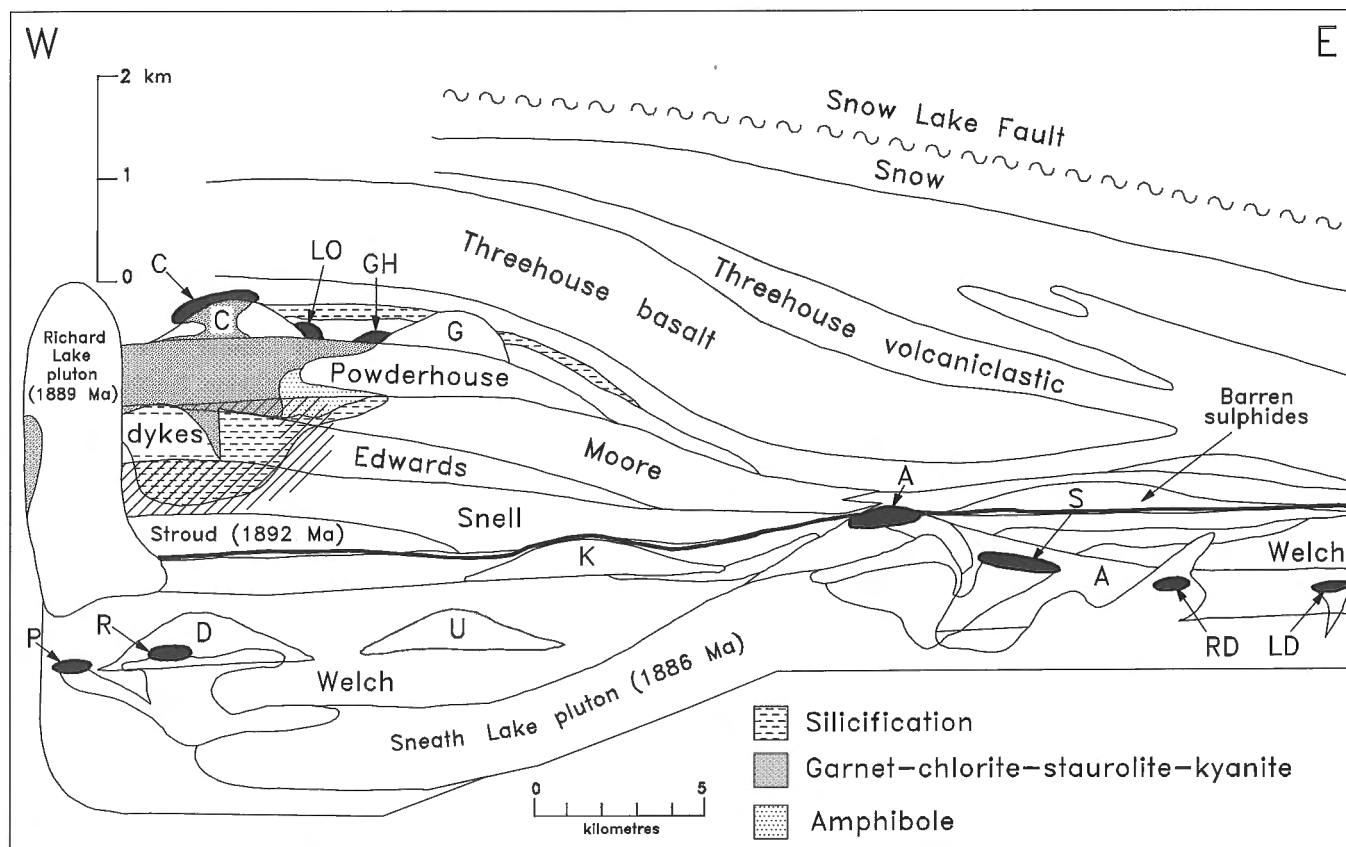


Figure 13b.

Phase 2 volcanic rocks

Phase 2 volcanic rocks are a loosely affiliated sequence of largely volcanoclastic rocks that occur between the phases 1 and 3. The volcanoclastic rocks include both felsic (Stroud) and mafic (Edwards) units that were derived by mass wasting of a source terrane located to the west. The volcanoclastic units are intercalated with basalts (Snell) that are derived from a geochemically distinctive, evolved arc magma source unlike the one that supplied the primitive arc basalts (Welch) of phase 1.

Stroud felsic breccia

This 0-400 m thick unit consists of well bedded heterolithological to monolithological felsic breccia and wacke, locally intercalated with sulphide-bearing intermediate to mafic volcanic wacke. Felsic breccia beds are organized in a manner consistent with deposition by subaqueous debris flows (Cas and Wright, 1984). Most of this unit lies directly upon phase 1 primitive arc volcanic rocks, although rare beds of this felsic breccia occur higher in the section intercalated with the Snell basalt.

Snell basalt

Up to 500 m of porphyritic mafic flows overlie and are locally intercalated with the Stroud felsic volcanoclastic rocks. These mafic flows are interpreted to have accumulated rapidly from a different magma source than the underlying phase 1 Welch basalt. They display the lowest ϵ_{Nd} values of any mafic flows in the Flin Flon Belt, a feature interpreted by Stern et al. (1992, 1994) to be a consequence of interaction with much older, possibly Archean, lithosphere. The presence of inherited Archean zircons in the Stroud felsic breccia (Machado and David, 1992; David et al., in press) is consistent with this interpretation. Intercalation of Snell mafic flows with Stroud felsic breccias suggests that magma extrusion was contemporaneous with uplift and erosion of felsic complexes.

Edwards heterolithological mafic wacke and breccia

This unit is up to 500 m thick, is upward-coarsening, and consists of fine grained, thin bedded mafic volcanoclastic sediments overlain by a sequence of coarse, thick bedded mafic breccias. East of Edwards Lake the heterolithological mafic breccias are separated from the underlying mafic volcanic wackes by a rapidly gradational boundary. The boundary is marked by an increase in heterogeneity of clast population, in addition to the abrupt increase in maximum clast dimensions (Skirrow, 1987). Organization of breccia beds is consistent with deposition by subaqueous debris flow deposits (Bailes, 1987a; Skirrow, 1987). A local source for the mafic breccias is supported by the presence of very thick beds.

Phase 3 volcanic rocks

Phase 3 rocks consist of a comagmatic mafic to felsic sequence: Moore basalt, Powderhouse dacite, and Ghost rhyolite. This sequence is chemically distinctive and characterized by high incompatible element and elevated light REE abundances. Zinc-rich base metal deposits at Chisel Lake occur at the top of this volcanic cycle, typically associated with Ghost rhyolite flow complexes. Stern et al. (1995) suggest that high HFSE (high field strength element) and light REE abundances of the Moore basalt may indicate involvement of an enriched mantle source component in generation of phase 3 magmas.

The Chisel Lake area is underlain by a swarm of phase 3 dacite sills and dykes that are recognized by their high incompatible and light REE abundances. The dyke swarm is spatially associated with areas of hydrothermally altered rocks indicating that the dykes played a significant role in generating or focusing hydrothermal solutions. The subvolcanic Richard Lake tonalite pluton, with a U-Pb zircon age of $1889 \pm 6/-5$ Ma (Bailes et al., 1991), cuts across the phase 3 dyke swarm and attendant altered rocks, but still may be part of the phase 3 magmatic event as it displays the characteristic phase 3 high incompatible and light REE geochemical signature.

Moore basalt

This unit is up to 1000 m thick and displays lateral variations in thickness and in flow facies (Fig. 13). Where thickest, 3 km east of Chisel Lake, this unit consists mainly of pillowed basalt. At Chisel Lake the Moore formation is less than 350 m thick and is composed of a less proximal mixture of pillowed flows, amoeboid pillow breccia, and pillow fragment breccia. To the east the Moore formation disappears from the section before Anderson Lake. Moore pillowed flows are characterized by abundant vesicles, including many 2-3 cm long radial pipe vesicles, suggesting a moderately shallow water environment of extrusion.

Powderhouse dacite

A 100-250 m thick unit of Powderhouse dacite tuff and lapilli tuff overlies the Moore basalt, and forms the immediate stratigraphic footwall to the Ghost Lake, Lost Lake, Chisel North, and part of the Chisel Lake Zn-rich massive sulphide deposits. Amygdaloidal Powderhouse dacite flows are also locally intercalated with the Moore basalt. A prominent, footwall dacite dyke complex is chemically identical to and clearly a feeder system to Powderhouse volcanism.

Powderhouse dacite is characterized by 5-15%, 0.5-2 mm tablet-shaped plagioclase phenocrysts and glomerocrysts, and, more rarely, quartz phenocrysts. The dacite tuff is generally massive, featureless, only rarely displays fragments, and is only occasionally well bedded. Heterolithological, coarse debris flow breccia, composed of mixed felsic and mafic detritus, forms an up to 30 m thick unit near the base of the Powderhouse dacite. Well bedded dacite wacke forms a unit up to 20 m thick at the top of the Powderhouse formation.

Ghost rhyolite

Local, domal complexes of massive rhyolite and lobehyaloclastite rhyolite flows up to 100 m thick, overlie the Powderhouse dacite. The rhyolite bodies include aphyric and sparsely quartz- and plagioclase-phyric varieties. The Zn-rich massive sulphide deposits occur either in direct association with (Chisel Lake) or along strike from (Lost Lake, Ghost Lake, Chisel North) the rhyolite complexes. A 1-2 m thick, sulphide-chert-wacke unit directly overlies the rhyolite flows and forms an apron about and connects the massive sulphide deposits.

The Ghost Lake rhyolite displays the elevated light REE pattern typical of phase 3 volcanic rocks. The ϵ_{Nd} value of the Ghost Lake rhyolite (+3.3) is higher than that of the underlying Powderhouse dacite (+2.6 to 3.05) but identical to that of the Richard Lake tonalite (+3.35) (Stern et al., 1992).

Subvolcanic intrusions

A large number of phase 3 subvolcanic intrusions are present in the footwall stratigraphy to the Chisel Lake massive sulphide deposits. They commonly form up to 35% of the Chisel Lake footwall, and were possibly part of a vent facies, or eruptive centre (Williams and McBirney, 1979). The intrusions include a small, layered mafic-ultramafic sill, a quartz-plagioclase porphyritic stock, dykes ranging in composition from peridotite through diorite to dacite, and a large tonalite pluton (Richard Lake). Crosscutting relationships between dyke sets suggest that intrusion was contemporaneous from several magma sources. Many of the intrusions have geochemical characteristics similar to overlying supracrustal volcanic units. Dyke margins in volcanoclastic strata are commonly amoeboid, and this suggests that they were intruded into unconsolidated, water-saturated detritus.

Many of the subvolcanic intrusions were probably involved in generating and sustaining hydrothermal activity that is now recorded by altered rocks spatially associated with the intrusions. Of these a dacite sill/dyke swarm west of Edwards Lake and the Richard Lake pluton (Fig. 12 and 13) were the most significant, and the most likely to have focused hydrothermal activity in the Chisel Lake area. The dacite intrusions are similar in composition to the Powderhouse dacite formation that forms the immediate footwall to the Chisel Lake area massive sulphide deposits. This sill/dyke swarm occurs near the base of a semiconformable alteration zone in the Chisel Lake footwall; individual dykes are demonstrably the heat source that focused alteration of adjacent Snell basalts and Edwards Lake wackes and breccias (Fig. 5c; Skirrow and Franklin, 1994).

The Richard Lake pluton is a multi-phase intrusion composed of quartz porphyritic to aphyric tonalite. A U-Pb zircon age of 1886 Ma demonstrates its synvolcanic character. However it intrudes and therefore postdates the dacite sill/dyke swarm and related alteration. The Richard Lake tonalite is geochemically and isotopically identical to the Ghost Lake and Chisel Lake rhyolite that are associated with the Chisel Lake area Zn-rich massive sulphide deposits.

Footwall alteration

Rocks in the stratigraphic footwall to the Chisel Lake area Zn-rich massive sulphide deposits are extensively altered. The alteration includes a semiconformable zone, largely confined to volcanoclastic units, and a disconformable zone, located in the Powderhouse dacite directly below the deposits. The relationship between the semiconformable and disconformable zones of alteration is uncertain, but south of the Chisel Lake deposit the two alteration zones appear to merge.

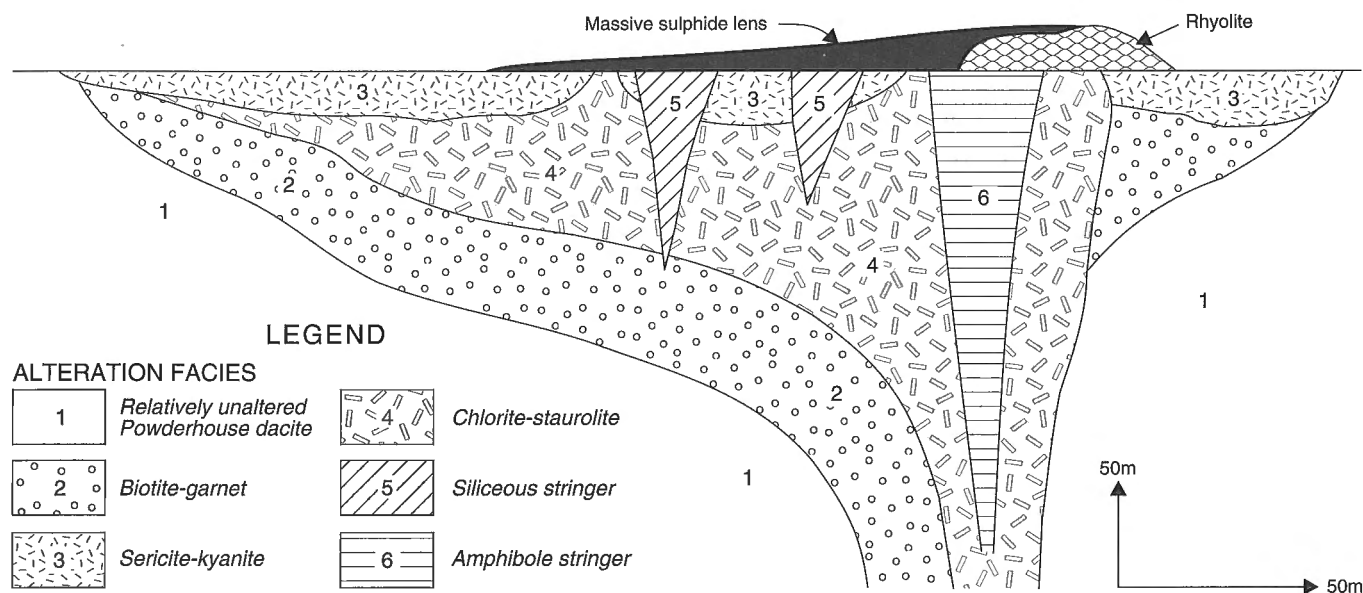


Figure 14. Schematic cross-section showing distribution of disconformable alteration facies in the footwall of Chisel Lake deposit. (from Galley et al., 1994)

The semiconformable alteration zone, which is dominated by silicification, is 0.5 to 1 km wide and over 5 km long and occurs 1 to 2 km below the Chisel Lake area massive sulphide deposits. It has two prominent associations: 1) localization in fragmental units, specifically the Edwards Lake heterolithological mafic volcanoclastics and, to a lesser extent, the Moore mafic breccias, and 2) spatial association with a prominent synvolcanic dyke complex. Alteration involved gains in Si, Na, and Ca, and losses in total Fe, Cu, and Zn (Galley et al., 1993; Skirrow and Franklin, 1994). The alteration is clearly related to dyke emplacement as silicification commonly occurs as zones parallel to dyke margins (Fig. 5c). Other forms of silicification, such as mottled varieties with random distribution, alteration of margins of fragments (Fig. 5b), and alteration of matrix between fragments are less clearly related to dyke emplacement, but they do coincide with large concentrations of synvolcanic dykes.

The disconformable alteration zone is tulip-shaped in cross-section (Fig. 14), is characterized by several overlapping alteration facies, and is interpreted to be due to localized hydrothermal discharge along a synvolcanic fault (Galley et al., 1993). The various alteration facies, all derived from a dacite protolith, are easily recognized by characteristic metamorphic mineral assemblages that were formed during subsequent almandine-amphibolite metamorphic recrystallization. They consist of three broad zones (biotite-garnet, chlorite-staurolite, and sericite-kyanite), forming an apron under the sulphide deposit and two crosscutting facies, siliceous stockwork and amphibole stockwork (Fig. 14). The biotite-garnet, chlorite-staurolite, and sericite-kyanite zones represent progressively more altered dacite interpreted to have formed in a broad hydrothermal field through diffuse upflow. Sulphide-bearing, crosscutting siliceous- and amphibole-stockwork zones are interpreted to be the products of more focused hydrothermal discharge that produced the directly overlying sulphide deposits (Galley et al., 1993). A tremolite-rich skarn directly overlies a Cu-Fe rich sulphide stockwork zone at the Chisel Lake deposit. The disconformable alteration zone displays elevated concentrations of Fe, Mg, Ca, Zn, Pb, Ag, and Au relative to "unaltered" dacite, and an overall decrease in Na and Sr (Galley et al., 1993).

Skirrow and Franklin (1994) suggest, and we concur, that the Edwards Lake formation was probably a hydrothermal aquifer that was modified by intrusion of the phase 3 synvolcanic dykes. Intrusion of the dykes probably raised the temperature of silica-rich hydrothermal fluids in the aquifer above 380°C causing them to precipitate silica (Kennedy, 1950). Dyke emplacement likely restricted upward movement of the hydrothermal fluids, similar to the "gable trapping" mechanism described by Lydon and Jamieson (1984) in the Troodos ophiolite complex, and may have produced evolved, metal-rich solutions. In this interpretation the disconformable zone of Mg-Fe enrichment below the Zn-rich massive sulphide deposits at Chisel Lake represents a product of fault-controlled discharge of these evolved, metalliferous solutions onto the paleoseafloor to produce the overlying massive sulphide deposits. This interpretation requires that the two alteration zones be connected. The semiconformable and disconformable zones are close to each other south of the Chisel Lake

mine site, but are separated by 400 m with no outcrop. A deep drill hole in this area of no outcrop follows indicates that they are connected as it follows the disconformable alteration down to the projected continuation of the semiconformable zone (Hudson Bay Exploration and Development, pers. comm., 1989).

Massive sulphide deposits

The Chisel Lake, Ghost Lake, Lost Lake, and Chisel North Zn-rich massive sulphide deposits clearly form at or close to the same stratigraphic interval. The two largest deposits, Chisel Lake and Chisel North, are connected along strike by a 1 to 2 m thick sulphidic, siliceous exhalite. Both the Chisel Lake and Chisel North deposits comprise a series of ore lenses that originally formed a more or less continuous sulphide sheet over 2000 m long and 200 m wide, with a gap of 300 m between the Chisel Lake and North Chisel deposits. Although this elongate sulphide sheet parallels the linear alteration "keel", presumed to be the expression of a synvolcanic fault, it occurs 100 m west rather than directly above this feature. The sulphide deposits and host strata are affected by at least two folding events with individual sulphide ore lenses constituting rootless F_1 fold hinges and boudinaged fold limbs. The Ghost Lake and Lost Lake deposits are small, Pb-rich, satellite deposits near the Chisel Lake mine, and were simply accessed by a separate decline rather than from the main Chisel Lake mine workings.

Chisel Lake deposit

The Chisel Lake deposit, discovered in 1956, is the largest Zn-rich ore body in the Snow Lake area at 7.5 Mt, grading 0.32% Cu, 10.1% Zn, 56 g/t Ag, and 2.2 g/t Au (Syme and Bailes, 1993; Table 1). The deposit is described in detail by Martin (1966) and Galley et al. (1993). It consists of seven structurally stacked massive sulphide lenses that strike north-northwest, dip northeast at 65°, and together plunge 45° at an azimuth of 020°. Most ore lenses consist of S-asymmetrical rootless folds with an average amplitude of 50 m. These folded ore lenses are truncated to the west by the late kinematic Chisel Lake gabbroic pluton.

Structurally thickened sulphide lenses in the Chisel Lake deposit average 12 m but are locally up to 40 m thick. They consist of crudely interlayered sphalerite-pyrite and sphalerite, plus minor amounts of chalcopyrite, pyrrhotite, galena, and arsenopyrite, with traces of lead-arsenic sulphides, tellurides, and native Au, Ag, Bi, and As (Galley et al., 1993). Some ore lenses locally consist of several metres of near-solid sphalerite grading up to 35% Zn. Carbonate, mainly dolomite, occurs in the sulphide ore as lenses, wispy bands and patches, and near the top as matrix to the sulphides. Carbonate-rich zones and associated tremolite skarn are locally present along the stratigraphic base of the massive sulphide deposit. They typically contain disseminated sulphides, mainly arsenopyrite with lesser amounts of galena, sphalerite, chalcopyrite, pyrrhotite, and bornite. The stratigraphic hanging wall contact of the massive sulphide lens with overlying mafic wacke locally consists of over 1.5 m of coarse grained, euhedral galena in a

siliceous argillite matrix. Individual orebodies display a consistent metal zonation, with Cu-Fe-rich stratigraphic bases, and Zn-Fe-Pb-rich tops (Galley et al., 1993).

Zones of disseminated and vein-controlled sulphide mineralization occur locally in the stratigraphic footwall to the massive sulphide horizon. They include sphalerite-pyrite veins, crosscutting siliceous brecciated rhyolite, and chalcopryrite veins, associated with chlorite-biotite-hornblende (or amphibole stringa) zones (Fig. 14). Tectonically remobilized veins of sulphide are also present both in the stratigraphic footwall and hanging wall.

Chisel North deposit

The North Chisel deposit was discovered in 1987 during exploration drilling 1.5 km north of the original Chisel Lake discovery (Fig. 15). The new deposit, which occurs at the same stratigraphic position, contains in excess of 2.58 Mt of 8.9% Zn, 0.22% Cu, 0.4% Pb, 23.3 g/t Ag, and 2.54 g/t Au (Galley et al., 1993). Chisel North, not currently in production, consists of a single, asymmetrically folded lens, 300 m long that plunges 10-20° at an azimuth of 020°. The sulphide mineralization occurs 300 m down-plunge from the Chisel Lake deposit. The attenuated limb of the folded sulphide lens is below ore grade, and for mining purposes the deposit consists of two discrete bodies.

Chisel North differs from the original Chisel Lake deposit in that it consists of up to 20 m of silicate-dolomite-rich semimassive sulphides rather than massive sulphide ore as at Chisel Lake. The semimassive ore contains thin massive sulphide layers which are characterized by interstitial dolomite or by thin bands of fine grained tremolite-rich siliceous material. The main sulphide minerals are sphalerite and pyrite, but in addition, the Chisel North deposit contains pyrrhotite-rich layers concentrated near the hanging wall contact.

The Chisel North deposit directly overlies altered Powderhouse formation dacite, but unlike the original Chisel Lake deposit, is not directly associated with rhyolite. It occurs 100 m west of a "keel" of altered rocks that is interpreted to be the expression of an altered synvolcanic fault. The southern one-third of the deposit is overlain by the same mafic wackes (Threehouse) that directly overlie the Chisel Lake deposit, but the northern two-thirds has a different hanging wall succession, which includes overlying heterolithological breccia, aphyric mafic flows and a rhyolite complex.

Lost Lake and Ghost Lake deposits

The Lost Lake and Ghost Lake deposits occur 900 and 1100 m, respectively, east of the Chisel Lake orebody. Between 1972 and their closure in 1988 they produced 590 233 t grading 8.6% Zn, 1.33% Cu, 32.61 g/t Ag, and 3.83 g/t Au (G. Kitzler, pers. comm., 1993). There are no published descriptions of either deposit.

The Lost Lake and Ghost Lake deposits occur at the same stratigraphic position as the main Chisel Lake sulphide lens. All three deposits occur directly atop the Powderhouse dacite, with the Chisel Lake and Ghost Lake deposits associated with rhyolite flow complexes. The Chisel Lake and Lost Lake deposits are directly overlain by turbidity current deposited mafic wackes, whereas the Ghost Lake deposit is overlain by a 100 m thick basalt flow and then the mafic volcanoclastic unit.

Stratigraphic hanging wall

The stratigraphic hanging wall to the Chisel Lake massive sulphide deposit consists (in ascending order) of 1 to 2 m of sulphide-bearing cherty sediments that grade upwards into approximately 50 m of well bedded, mafic turbidite wacke, and several hundred metres of poorly bedded, scoria-rich mafic tuff-breccia and heterolithological mafic breccia.

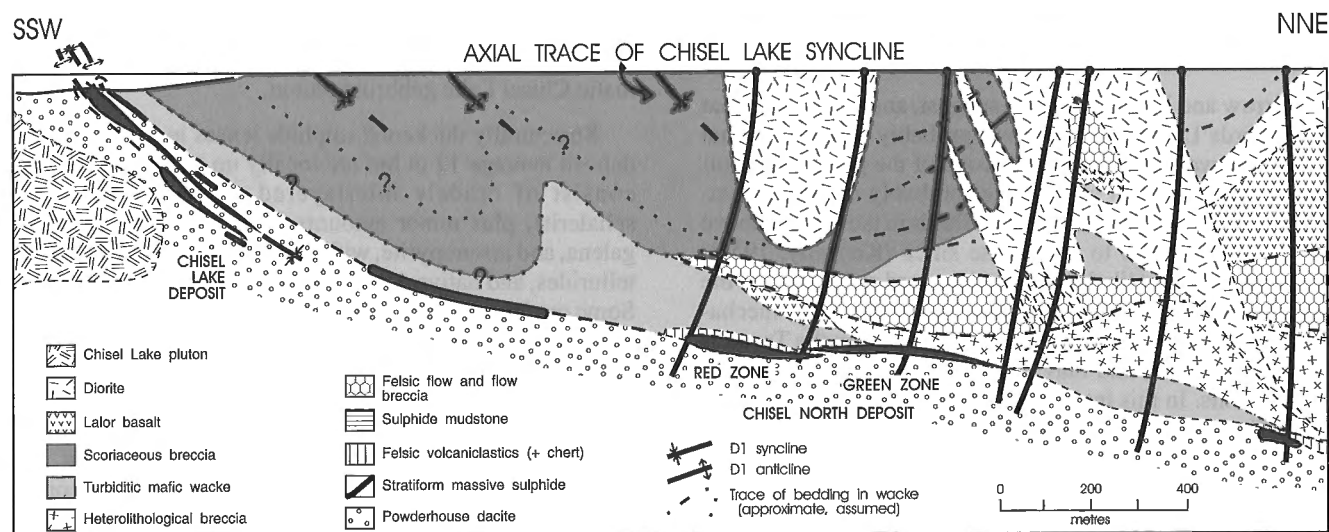


Figure 15. Cross-section illustrating the relationship between the Chisel Lake and Chisel North Zn-rich massive sulphide deposits from Galley et al. (1993). Note the along strike variation in hanging wall stratigraphy.

Contacts between these units, all part of the phase 4 Threehouse formation, are structurally intact and rapidly gradational. The Threehouse mafic volcanoclastics at Chisel Lake most likely accumulated in a topographic depression or basin, shed from an adjacent shallow water to subaerial mafic edifice.

The simple hanging wall stratigraphy at Chisel Lake breaks down at a regional scale and is replaced by a more complex hanging wall succession including a variety of heterolithological breccia units, mafic flows, rhyolite flows, and rhyolite breccia, in addition to the usual Threehouse mafic wacke and breccia. This is apparent above the northern two-thirds of the Chisel North massive sulphide deposit where the hanging wall succession includes heterolithological breccia, basalt flows, and rhyolite flows not present to the south (Fig. 11). In the past this has been attributed to facies variations in postore stratigraphy but the recent identification of an unconformable contact at the base of the Threehouse formation (Bailes and Simms, 1994) suggests that some of the postore units north of Chisel Lake may predate Threehouse formation rocks. Thus, the heterolithological breccia, aphyric mafic flows and rhyolite complex above the northern two-thirds of the Chisel North deposit may be the "intact" hanging wall, with these rocks eroded at the "Threehouse" unconformity above deposits to the south, such as Chisel Lake and Lost Lake.

Summary

Volcanic-hosted massive sulphide deposits in the evolved arc sequence are radically different from deposits in the primitive arc succession. Besides the obvious Zn- versus

Cu-rich character they differ in stratigraphic setting, massive sulphide morphology, and associated metamorphosed alteration mineral assemblages. For example the host rocks are part of an evolved arc terrane, are characterized by abundant volcanoclastic rocks, and are lithologically diverse compared to the simple bimodal (basalt-rhyolite) flow-dominated sequence in the primitive arc. In addition, the evolved arc volcanic-hosted massive sulphide deposits are laterally continuous sheets with broad, diffuse, sericite- and carbonate-rich disconformable alteration zones compared to the discrete sulphide lenses and well defined chlorite-rich pipes of primitive arc volcanic-hosted massive sulphide deposits.

The primitive arc volcanic-hosted massive sulphide deposits at Chisel Lake share some of the features of the Archean "Mattabi-type" deposits of Morton and Franklin (1987), but are more comparable to other Paleoproterozoic volcanic-associated such as the Ladysmith-Rhinelander deposits in Wisconsin (DeMatties, 1994) and some of the Bergslagen district volcanic-hosted massive sulphide deposits in Sweden (Lundstrom and Papunen, 1986). This group of deposits are characterized by thick footwall sequences of felsic volcanoclastic rocks, by layered pyrite-sphalerite-chalcopryrite-galena orebodies, by interlayered carbonate-rich sedimentary units and by associated skarns. Analogous to the Chisel Lake area deposits they are characterized by Cu-Zn ratios ($\text{Cu}/\text{Cu}+\text{Zn}$) <10, by high Ag and, rarely, by high Au values. They also share the sericite-pyrite-aluminosilicate-rich discordant alteration zones cored by more discrete chlorite-chalcopryrite-pyrrhotite alteration noted in the Chisel Lake deposit by Galley et al. (1993).

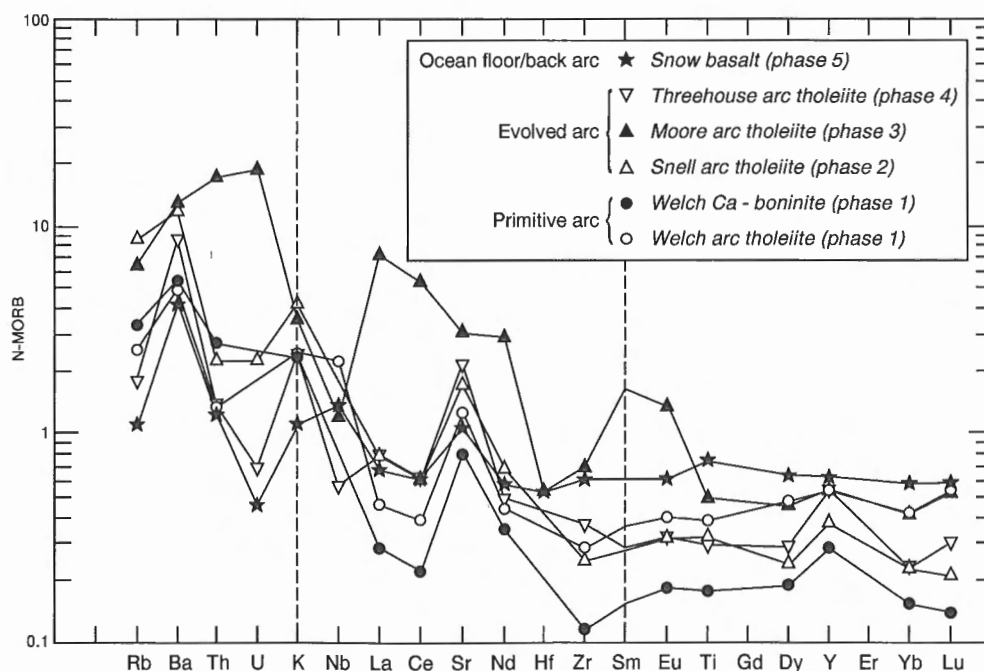


Figure 16. MORB-normalized trace element patterns for average basalt units at Snow Lake.

GEOCHEMISTRY

Geochemistry of mafic and intermediate rocks

Major element, trace element, REE, and Nd isotopic compositions show that mafic to intermediate metavolcanic rocks in the Flin Flon Belt formed in variety of tectonic settings (Syme, 1990; Syme and Bailes, 1993; Stern et al., 1995). This permits determination of the tectonic setting of massive sulphide deposits (Syme and Bailes, 1993) and allows exploration to be focused on those tectonic settings with greatest volcanic-hosted massive sulphide potential. Eighty-three whole rock and trace element geochemical analyses, fifty-five REE analyses, and fifteen Nd isotopic analyses have been obtained from least-altered mafic and intermediate volcanic rocks at Snow Lake.

The main units of mafic flows at Snow Lake each display unique geochemical attributes that serve not only to distinguish among them but also to demonstrate that they are not simply episodic extrusions of fractionated material from a single magmatic source. On the basis of their geochemistry the mafic flows appear to have formed in three separate tectonic environments (Stern et al., 1995): primitive forearc (phase 1: Welch), evolved arc (phase 2-4: Snell, Moore, Anderson, Threehouse) and back arc/ocean floor (phase 5: Snow Creek and Tramping) (Figures 4b and 4c).

Phase 1 Welch mafic flows, interpreted to have formed in the primitive fore-arc environment, have high contents of large ion lithophile (LIL: e.g. Rb, Ba, Th, Sr) elements, low

contents of high field strength (HFS: e.g. Hf, Ti, Zr, Y) elements and very low Ni and Cr relative to N-MORB (Fig. 16). These features are characteristic of subduction-related magmas (Gill, 1981; Tarney et al., 1981) formed within oceanic arc tectonic settings. The particularly low La/Yb ratios, and low Th, Ti, and Zr contents (Fig. 16, 17, 18) are characteristic of primitive arc basalts. This primitive arc genesis for Welch mafic flows is further supported by their intercalation with high-Ca boninites (Stern et al., 1995), a rock type currently found only in the fore-arc regions of primitive Cenozoic island arcs. In the Flin Flon Belt, high Ca-boninites are unique to the Welch basalts at Snow Lake.

Although phase 2-4 mafic flows display the same "decoupling" of large ion lithophile and high field strength elements as do phase 1 flows, they are different in a number of other geochemical attributes. For example, many of the evolved arc basalts are LREE enriched (Fig. 17) and most have higher overall contents of Th, P_2O_5 , and Zr. This implies that phase 2-4 mafic flows had a different magmatic evolution than those of the underlying phase 1 basalts. This conclusion is substantiated by the lower ϵ_{Nd} values of 0 to 2.7 for phase 2-4 mafic flows compared to values near 3 for phase 1 mafic flows (Fig. 19). Stern et al. (1995) interpret the lower ϵ_{Nd} of phase 2-4 basalts to be a consequence of intracrustal contamination or, less likely, a contaminated mantle source. Intracrustal contamination during phase 2-4 magma genesis is supported by the presence of an inherited zircon population between 2650 and 2824 Ma in the 1892 Ma phase 2 and 3 felsic volcanic rocks (Machado and David, 1992; David et al., in press).

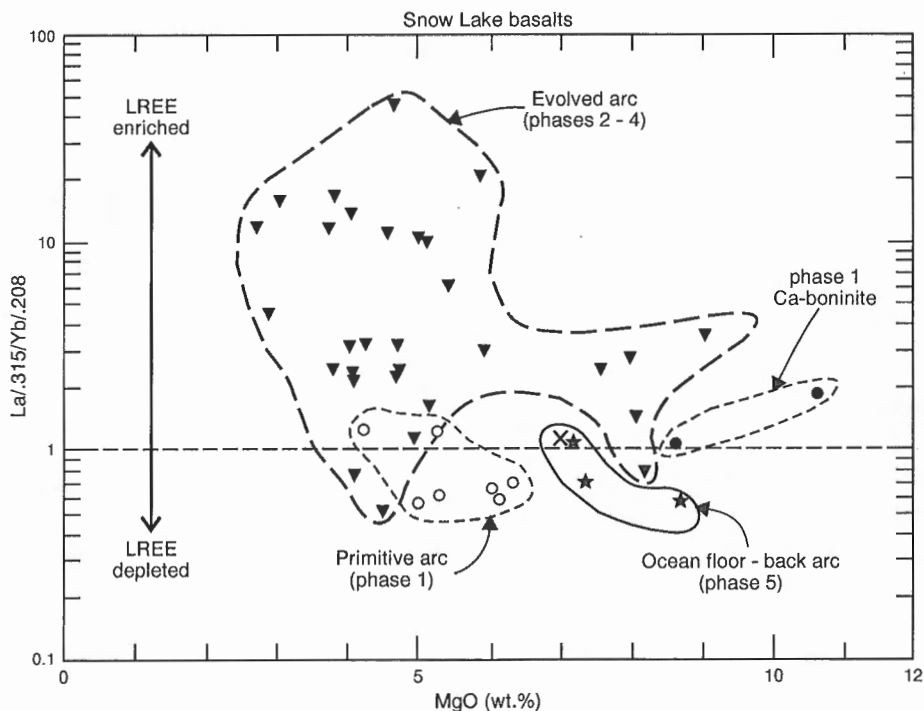


Figure 17. Snow Lake basalts on diagram of La/Yb (normalized) versus MgO (wt.%) (after Stern et al., 1995).

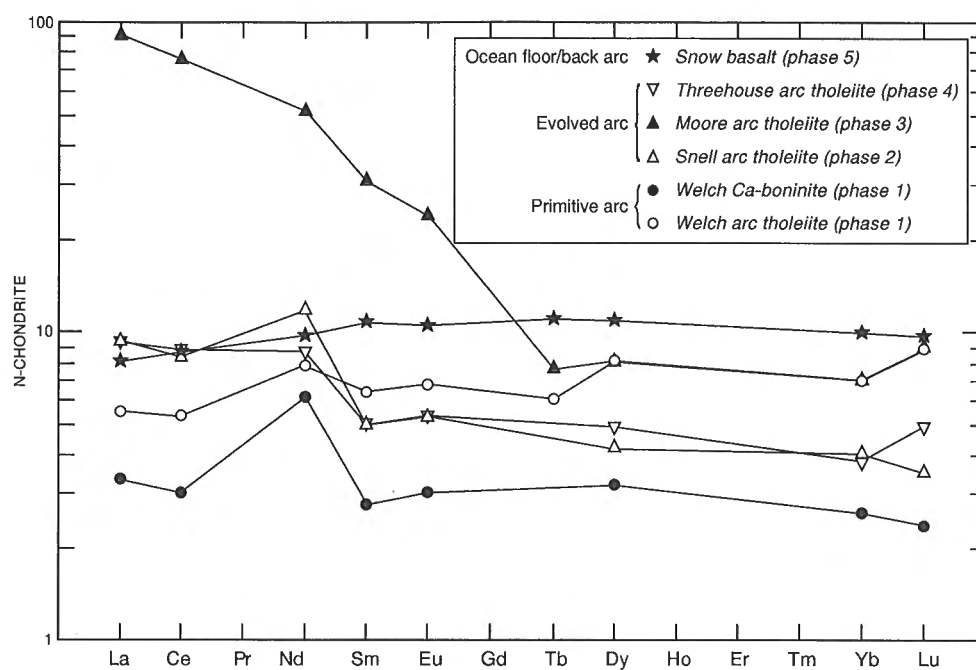


Figure 18. Chondrite normalized REE plots of Snow Lake basalts and basaltic andesites.

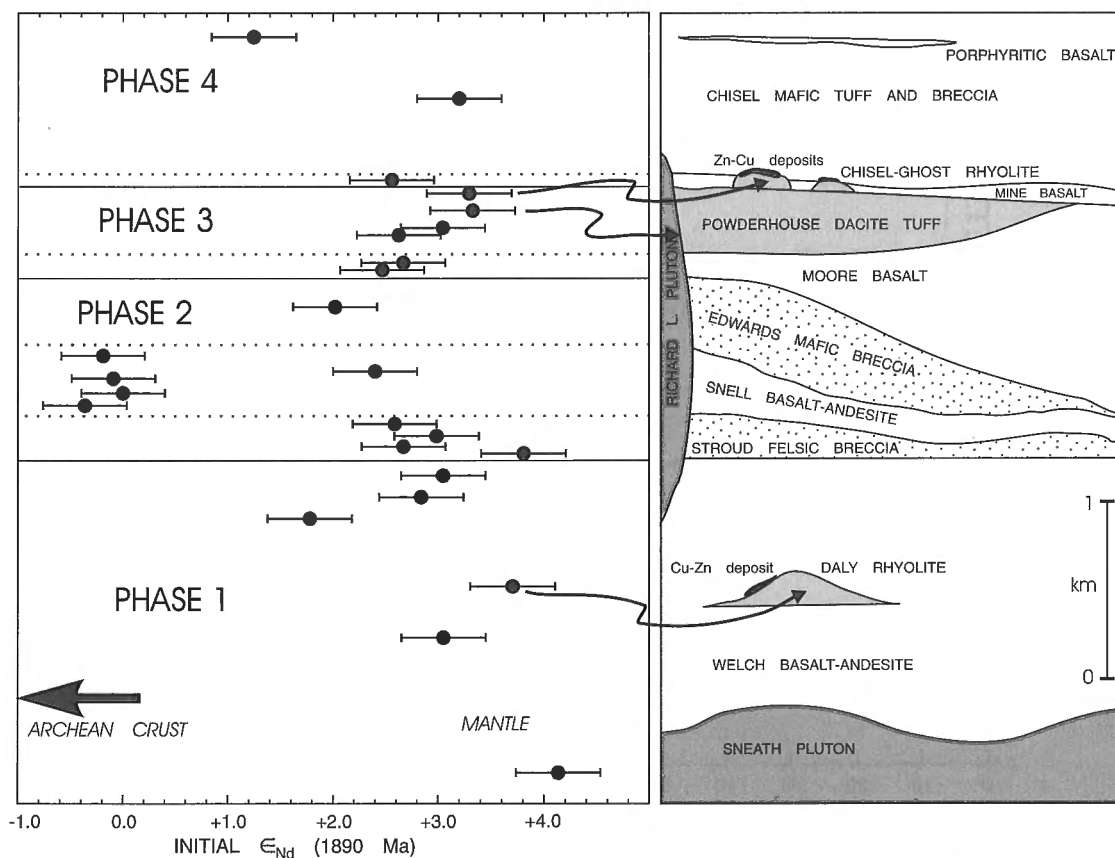


Figure 19. Isotopic and geological stratigraphy of Chisel Lake section at Snow Lake (after Stern et al., 1992).

Geochemical features displayed by phase 2-4 mafic flows are characteristic of the more complex conditions present in an evolved arc terrane where older crustal fragments or previously formed arc segments diversify arc magma genesis.

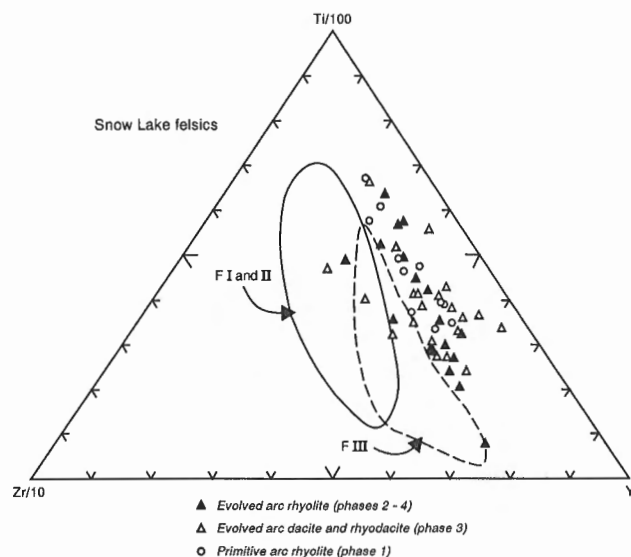


Figure 20. Snow Lake rhyolites plotted on $(Zr/10)-(Ti/100)-Y$ projections from Lesher et al. (1985) for discriminating between barren (FI + FII) and ore-associated (FIII) Archean rhyolites.

Phase 5 Snow Creek formation basalts have flat REE patterns and do not show the “decoupling” of large ion lithophile and high field strength elements typical of arc basalts. They are similar to the back arc/ocean floor basalts that are prominent in the Athapuskow and Elbow lakes area in more westerly portions of the Flin Flon Belt (Syme and Bailes, 1993; Stern et al., in press).

The distinctly different geochemistry of mafic flows of phase 1, phases 2-4, and phase 5 indicates that these rocks formed in disparate tectonic settings and suggests that either profound changes in the volcanism took place in the evolving Snow Lake volcanic terrane or, possibly, that these volcanic rocks of diverse origin were tectonically juxtaposed. Since the volcanic sequence at Snow Lake is apparently conformable the implication of the latter is that juxtaposition may have occurred along thrusts. Thrust faults, most notably the McLeod Road thrust (Russell, 1957; Froese and Moore, 1980), have been previously identified in the Snow Lake area but only recently postulated to affect the volcanic sequence itself (Bailes, 1993; Syme et al., 1995).

Geochemistry of felsic rocks

The close association between felsic volcanic rocks and base metal massive sulphide deposits in Precambrian terranes in Canada has prompted interest in rhyolite geochemistry as a predictor of their potential to host ore (Campbell et al., 1982). Lesher et al. (1985) and Barrie et al. (1993) suggest a number of discriminants that distinguish ore-hosting from barren

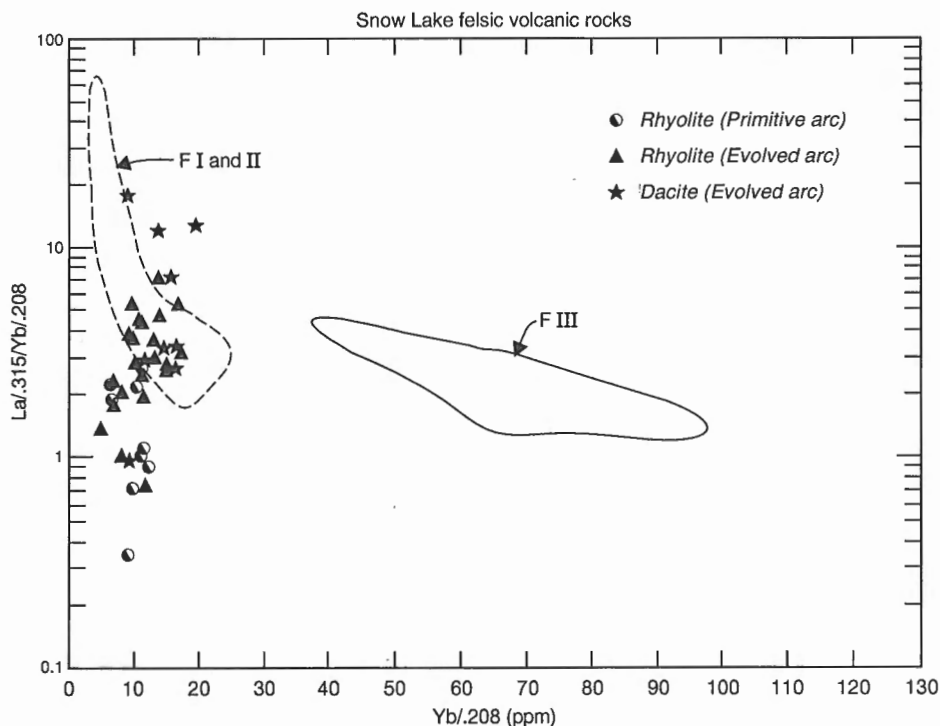


Figure 21. $[Yb]_n$ vs. $[La]_n/[Yb]_n$ plot comparing Snow Lake area felsic meta-volcanic rocks to Abitibi belt barren (FI + FII) and ore-hosting (FIII) rhyolites of Lesher et al. (1985).

Archean rhyolites of the Superior Province. However, these discriminants do not appear applicable to the Paleoproterozoic rhyolites from the Snow Lake area, as ore-hosting varieties plot with barren Archean rhyolites (Fig. 20 and 21). This is because magmas in the Flin Flon Belt are depleted in REEs and high field strength elements (Zr, Y, and Ti), elements that are used extensively in the discriminant diagrams developed by Leshner et al. (1985). Stern et al. (1995, in press) suggest

that this depletion is a consequence of production of magmas in the Flin Flon Belt from depleted mantle that had been previously involved in extensive back-arc magmatism. Ore-hosting rhyolites at Snow Lake also do not display an Eu depletion anomaly suggesting that even this criteria (Leshner et al., 1985) for identifying ore-hosting rhyolites may not be useful in Paleoproterozoic Flin Flon Belt rocks. Obviously

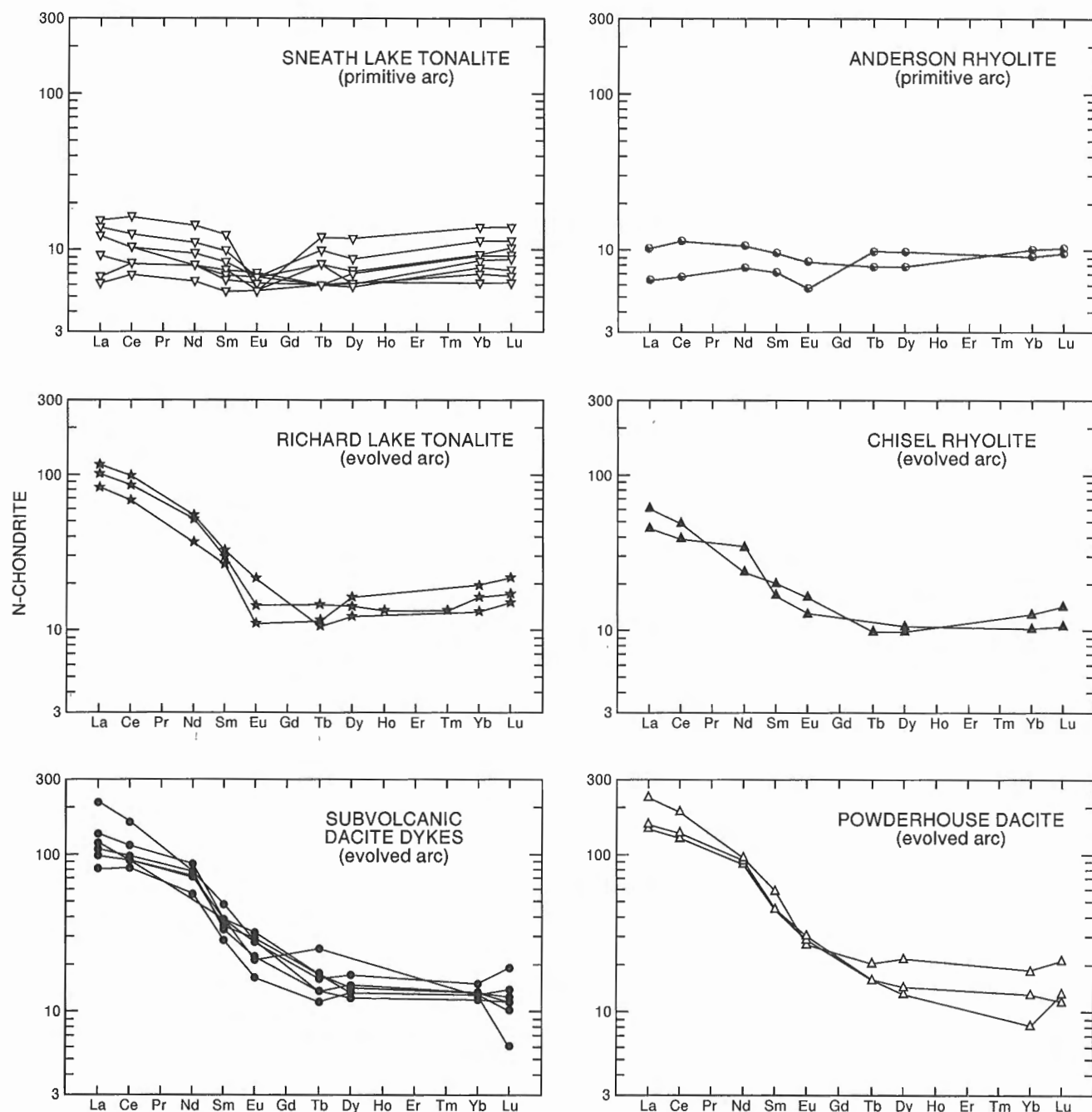


Figure 22. Chondrite-normalized REE plots of ore-hosting Anderson and Chisel rhyolites compared to synvolcanic Sneath Lake and Richard Lake tonalites. Also shown are Powderhouse dacite and related synvolcanic dacite dykes from footwall succession to Chisel Lake area Zn-rich volcanic-hosted massive sulphide deposits.

the discriminants proposed by Leshner et al. (1985) must be used with caution in volcanic belts of the Paleoproterozoic Trans-Hudson Orogen.

Geochemical similarities between felsic volcanic rocks at Snow Lake and the stratigraphically underlying tonalites of the Sneath Lake and Richard Lake subvolcanic intrusive complexes suggest that the extrusive felsic rocks are derived directly from near surface magma chambers. For example the phase 1 rhyolites and the Sneath Lake pluton share flat REE profiles at 10 times chondrite, and the phase 3 rhyolites have sloped REE profiles with elevated LREE contents similar to the associated Richard Lake pluton (Fig. 22). The rhyolites and associated tonalite plutons also share similar ϵ_{Nd} contents (Stern et al., 1992). Higher ϵ_{Nd} values for the rhyolites than the associated mafic flows (e.g. Welch basalt and Daly rhyolite, Fig. 19) preclude rhyolites from simply forming by fractionation of the same magma that produced the mafic flows. The direct genetic relationship between felsic volcanic rocks and underlying intrusions is also displayed by the phase 3 Powderhouse dacite which is geochemically indistinguishable from a prominent footwall dacite dyke swarm.

The low ϵ_{Nd} contents of the ore-hosting rhyolites and associated subvolcanic tonalite intrusive complexes makes them the most isotopically juvenile members of the Snow Lake sequence. The implication is that geochemically primitive, mantle-derived felsic magmas may be important for the generation of base metal mineralization in the Snow Lake area (Stern et al., 1992).

DISCUSSION

Role of subvolcanic intrusions in massive sulphide generation

A number of subvolcanic intrusions are clearly related to alteration events, with the Sneath Lake tonalite pluton, the Richard Lake tonalite pluton and the Edwards Lake area dacite dyke complex the most significant. The traditional view of these intrusions is that they are the "heat engine" that drove the hydrothermal system, which in turn was responsible for alteration of the overlying rocks and for deposition of the base metal massive sulphide deposits themselves (Walford and Franklin, 1982). The association of the massive sulphide deposits with rhyolite flows and synvolcanic faults can be viewed as a consequence of the intrusion-derived rhyolite flows using the same zone of weakness as the mineralizing hydrothermal fluids to reach the paleoseafloor.

The Sneath Lake intrusive complex, 22 km long and 2 km wide, and estimated to have been over 1.2×10^{12} t in size, was emplaced at a depth of 0.3 to 2 km below the paleoseafloor. The pluton must have been a major subvolcanic heat source, but has no thermal contact aureole, which strongly suggests that cooling of the pluton occurred by convection of seawater in the overlying volcanic rocks. Cathles (1983) suggests that a 1.5×10^{11} t igneous mass, smaller than the Sneath Lake intrusion, would have been sufficient to drive the hydrothermal system that produced all the known Kuroko base metal mineralization in the Hokuroko basin of Japan. Thus

we attribute the considerable alteration above the Sneath Lake body to geothermal-hydrothermal activity necessitated by shallow emplacement of the intrusion.

Portions of the Sneath Lake intrusion are affected by considerable alteration, at least some of which, is due to postcrystallization collapse of the geothermal-hydrothermal system into still hot, fractured portions of the intrusive complex (Fig. 5d). The most prominently altered part of the multiphase Sneath Lake pluton is a mesotonalite body that coincidentally contains an order of magnitude more Cu than other phases of the pluton. The mesotonalite is characterized by large areas affected by fracture-controlled epidote and hematite alteration and by more pervasive areas of epidotization and silicification. This alteration may have played a role in generating Cu-rich hydrothermal fluids. The discordant alteration "pipes" that progress up stratigraphy to the Stall Lake and Anderson Lake massive sulphide deposits are "rooted" along the margins of the altered mesotonalite body.

Similar to Sneath Lake tonalite, the Richard Lake tonalite body, 7.3 km by 1.6 km, and estimated to have been over 1.1×10^{11} t in size, is large enough to have driven a prominent geothermal system. This pluton, which is not as altered as the Sneath Lake intrusion, varies from porphyritic in the south to fine grained and equigranular in the north. It has no discernible contact metamorphic halo, suggesting that cooling occurred through convection of seawater above the body. A possible manifestation of this geothermal system is an over 500 m wide sheath of alteration that surrounds the intrusion on its east, north, and west sides. All of the major base metal massive sulphide deposits in the Chisel Lake area are adjacent to this envelope of altered rocks. However, the exact relationship of the Richard Lake body to this alteration zone is complicated by the fact that, in some localities, phases of it clearly cut the altered rocks. Nevertheless, most heat calculations suggest that the formation of massive sulphide deposits, such as those at Chisel Lake, require a heat source of the order of magnitude of the Richard Lake intrusion.

The exact role of a prominent dacite sill/dyke complex west of Edwards Lake is uncertain, but it is clearly involved in hydrothermal activity. Although probably not capable of generating a prominent geothermal-hydrothermal system on its own, this intrusive complex has clearly modified and focused existing geothermal-hydrothermal activity. Rocks adjacent to the dacite dykes have been extensively silicified and epidotized, a feature that Skirrow and Franklin (1994) attribute to a temperature increase above 380°C adjacent to the dykes. They suggest that dacite dyke emplacement prompted already existing silica-rich hydrothermal fluids to precipitate silica, due to a temperature increase and resultant decrease in silica solubility (Kennedy, 1950). In addition to causing local temperature increase, emplacement of the dykes may also have played an important role in producing evolved metal-rich hydrothermal fluids by restricting fluid movement in a manner similar to the "gable trapping" mechanism described by Lydon and Jamieson (1984) in the Troodos ophiolite complex. The clear involvement of the dacite dykes in geothermal-hydrothermal activity and their role as the feeder system for the Powderhouse dacite, a unit that forms the immediate stratigraphic footwall to the Chisel Lake area

massive sulphide deposits, demonstrates without doubt that they were involved in the hydrothermal-mineralizing event that produced the Chisel Lake area Zn-rich massive sulphide deposits.

Controls on distribution of massive sulphide deposits

A number of empirical controls that appear to influence the location of base metal massive sulphide deposits at Snow Lake are evident from this study. They are similar to controls on distribution of volcanic-hosted massive sulphide deposits in many Precambrian and Phanerozoic volcanic belts (Lydon, 1984, 1988) and elsewhere in the Flin Flon Belt (Syme and Bailes, 1993). These controls provide a method to focus exploration on most prospective portions of the belt. In order from regional to local, discriminators are: 1) affiliation with volcanic rocks with oceanic arc geochemical signature, 2) proximity to synvolcanic dyke swarms and tonalite plutons, 3) association with areally extensive semiconformable zones of hydrothermally altered rocks, 4) occurrence within or adjacent to rhyolite flow complexes, and 5) proximity to synvolcanic faults.

The association of base metal massive sulphide deposits in the Flin Flon Belt with 1904 Ma to 1885 Ma arc tholeiite volcanic rocks has been well established in recent years (Syme, 1990; Syme and Bailes, 1993; Lucas et al., 1994; Stern et al., 1995). Volcanic sequences belonging to the arc assemblage can be separated from basalt flow-dominated ocean floor-back arc sequences as they typically contain abundant volcanoclastic and felsic units not normally present in the ocean floor-back arc successions. Geochemically, the arc tholeiite mafic flows can be separated from the ocean floor-back arc types by more abundant large ion lithophile elements, moderate to strongly depleted high field strength elements and by strongly depleted Ni and Cr. In the absence of extensive trace element data, a higher Mg/Ni ratio can be used to discriminate between arc tholeiite and ocean floor-back arc assemblages (Syme and Bailes, 1993).

The association of volcanic-hosted massive sulphide deposits with island arc volcanism is not unique to the Paleoproterozoic Flin Flon Belt. For example, in Cambrian and Ordovician rocks of the Dunnage zone of Newfoundland, Swinden (1991) observed that island arc assemblages are "by far the most prolific hosts for volcanogenic massive sulphide deposits" and "many if not most of the back arc sequences are barren". Although the arc sequences of the Flin Flon Belt are more prolific hosts for base metal massive sulphide deposits than the back arc-ocean floor successions, this is unlikely to be universally applicable to other Precambrian volcanic terranes. For example, Barrie et al. (1993) showed that, by tonnage, over 50% of the polymetallic volcanic-hosted massive sulphide deposits in the Archean Abitibi belt are hosted within thickened oceanic rift suites and 35% occur within rifted island arcs.

Snow Lake massive sulphide deposits occur in the stratigraphic hanging wall of two major subvolcanic tonalite intrusions: the primitive arc-hosted Cu-rich deposits above the Sneath Lake intrusive complex and the evolved arc-hosted Zn-rich deposits about the Richard Lake tonalite complex.

These intrusions are geochemically similar to overlying ore-hosting rhyolite complexes, which suggests a close genetic relationship between the tonalites, rhyolites, and massive sulphide deposits. In the Chisel Lake area a prominent subvolcanic dacite dyke complex occurs in the footwall to the Zn-rich massive sulphide deposits; this dyke complex is intimately associated with synvolcanic hydrothermal alteration and, perhaps, with ore-forming processes, as was discussed in the previous section.

The ore-hosting volcanic strata at Snow Lake are characterized by volumetrically extensive zones of metamorphosed altered rocks. These zones are interpreted to result from large-scale convection of hydrothermal fluids and resultant fluid-rock interaction above cooling subvolcanic intrusions. Locally, the subvolcanic intrusions are also altered, either reflecting alteration of early phases by hydrothermal activity generated by subsequent phases or collapse of the circulatory hydrothermal system into the intrusive complex as the intrusion cooled. At Snow Lake, three regionally extensive alteration systems are recognized, two of them clearly related to base metal sulphide mineralization; the other is associated with a base metal-poor sulphidic sediment. We consider terranes that contain altered supracrustal rocks together with altered subvolcanic tonalite bodies to be favourable terranes to target for base metal exploration.

The spatial association of massive sulphide deposits with felsic flows is a recurring theme in all major base metal volcanic-hosted massive sulphide districts regardless of age (Franklin et al., 1981; Ohmoto and Takahashi, 1983; Lydon, 1984, 1988). At Snow Lake the association of base metal sulphide deposits with rhyolite flow complexes is clear. All of the Cu-rich deposits in the primitive arc are contained in rhyolite complexes and all the Zn-rich deposits in evolved arc rocks are contained in or along the same stratigraphic horizon as rhyolite bodies. In addition the Snow Lake area volcanic-hosted massive sulphide deposits are much more closely affiliated with subaqueously deposited rhyolite domes and flow complexes than they are with units of felsic volcanoclastic rocks.

Synvolcanic faults have long been recognized as important in the genesis of base metal massive sulphide deposits (Hodgson and Lydon, 1977; Lydon and Galley, 1986; Gibson and Watkinson, 1990; Morton et al., 1990). Focusing of hydrothermal fluids by synvolcanic faults, as is hypothesized for ancient deposits, is supported by observations in many modern sulphide-forming environments (Rona and Clague, 1989; Zierenberg et al., 1993; Goodfellow and Franklin, 1993). At Snow Lake massive sulphide deposits clearly occur above synvolcanic faults. These faults are recognized by their strong alteration by through-going hydrothermal fluids during formation of the overlying base metal deposits. At Anderson Lake the altered, regionally metamorphosed faults are represented by planar, crosscutting, up to 2 km long zones of chlorite-biotite-kyanite, muscovite-kyanite, and chlorite-staurolite-garnet schists that terminate abruptly up-section at the massive sulphide deposits. At Chisel Lake the synvolcanic fault is expressed as a >2 km long by >300 m deep "keel" of chlorite-staurolite rich rocks below the Zn-rich deposits. Recognition of synvolcanic faults is currently restricted to areas,

such as Snow Lake, where detailed mapping has identified abrupt stratigraphic facies changes or narrow discordant zones of alteration. Regional-scale stable isotope studies, which can detect isotopic shifts due to fluid-rock interaction, offer another method of delineating hydrothermal upflow zones, as areas with anomalous stable isotopes form larger targets than do the faults (Cathles, 1993).

SUMMARY

Polymetallic base metal deposits in the island arc sequence at Snow Lake occur in two settings: Cu-rich volcanic-hosted massive sulphide deposits (at Anderson Lake) deposited in a primitive forearc-protoarc setting and Zn-rich volcanic-hosted massive sulphide deposits (at Chisel Lake) in an evolved arc setting. Volcanic-hosted massive sulphide deposits in both tectono-magmatic sequences are associated with large subvolcanic tonalite intrusive complexes of similar geochemical character as the host supracrustal rocks.

Volcanic-hosted massive sulphide deposits in both the primitive forearc and evolved arc settings occur in rhyolite flow complexes. The ore-hosting rhyolite flows are geochemically similar to underlying subvolcanic tonalite plutons. For example both rhyolite and tonalite share similar ϵ_{Nd} contents that are higher than those of associated mafic flows (Stern et al., 1992). This is significant as it precludes formation of the rhyolite and tonalite magmas by fractionation of the same magma that produced the mafic flows. The low ϵ_{Nd} contents of the ore-hosting rhyolites and associated tonalite plutons identifies them as the most isotopically primitive members of the Snow Lake sequence.

The spatial association of base metal deposits with rhyolite bodies is not unique to the Snow Lake area. In fact the widespread association of volcanic-hosted massive sulphide deposits with rhyolites has prompted use of rhyolite geochemistry as a screening technique to predict their potential to host ore. Although this technique has proven valuable in the Archean Superior Province of Canada (Leshner et al., 1985), the derived discriminants do not appear to be applicable to Paleoproterozoic rhyolites at Snow Lake. Stern et al. (1994) suggest that magmas in the Flin Flon Belt, including those at Snow Lake, were produced by melting of depleted mantle that had previously been involved in back-arc magmatism. This process has yielded volcanic products depleted in REEs and high field strength elements, elements that are used extensively in discriminant diagrams developed by Leshner et al. (1985). The implication is that discriminants developed in one area are not necessarily universal in applicability.

Extensive zones of altered supracrustal rocks occur stratigraphically above the subvolcanic intrusive complexes and below the volcanic-hosted massive sulphide deposits at Snow Lake. The altered rocks are interpreted to be the products of geothermal-hydrothermal activity generated by near surface cooling of the subvolcanic tonalite intrusions. The subvolcanic tonalite bodies are large enough, according to calculations by Cathles (1983) for the Kuroko area, to activate subsurface seawater geothermal systems capable of generating the Snow Lake area volcanic-hosted massive sulphide

deposits. Because rocks in the Snow Lake area are well exposed from the subvolcanic plutons up to the volcanic-hosted massive sulphide deposits, they represent an excellent opportunity to study the nature of the subvolcanic plutons and overlying fossil hydrothermal systems. Further work in the Snow Lake area will focus on the interrelationship between the subvolcanic plutons, hydrothermally altered rocks, and the overlying volcanic-hosted massive sulphide deposits.

ACKNOWLEDGMENTS

Ric Syme (MSG), Karen Fierreira (MSG), and Mark Hannington (GSC) are thanked for their constructive reviews which have added to the quality of this manuscript. Bonnie Lenton (MSG) and Kim Nguyen (GSC) are responsible for the computer drafting of the illustrations. We would also thank Gerry Kitzler of Hudson Bay Exploration and Development for his advice and support during this project.

REFERENCES

- Bailes, A.H.
 1987a: Chisel-Morgan Lakes Project, Manitoba; in Report of Activities, 1987, Manitoba Energy and Mines, Minerals Division, p. 70-79.
 1987b: Silicification, Fe-Mg metasomatism and synvolcanic plutonism, Snow Lake, Manitoba; Geological Association of Canada-Mineralogical Association of Canada, Joint Annual Meeting, Saskatoon, Saskatchewan, Program with Abstracts, v. 12, p. 22.
 1993: Snow Lake mapping projects (NTS 63K/16SE and 63J/13SW); in Report of Activities, 1993, Manitoba Energy and Mines, Geological Services, p. 93-95.
- Bailes, A.H. and Galley, A.G.
 1994: Geology of the Anderson-Stall volcanic-hosted massive sulphide area, Snow Lake, Manitoba; Geological Survey of Canada, Open File 2772, map with marginal notes, scale 1:10 000.
- Bailes, A.H. and Simms, D.
 1994: Implications of an unconformity at the base of the Threehouse formation, Snow Lake, Manitoba (NTS 63K/16); in Report of Activities, 1994, Manitoba Energy and Mines, Geological Services, p. 85-88.
- Bailes, A.H., Hunt, P.A., and Gordon, T.M.
 1991: U-Pb zircon dating of possible synvolcanic plutons in the Flin Flon belt at Snow Lake, Manitoba; in Radiogenic Age and Isotopic Studies: Report 4, Geological Survey of Canada, Paper 90-2, p. 35-43.
- Bamburak, J.D.,
 1990: Metallic mines and mineral deposits of Manitoba; Manitoba Energy and Mines, Geological Services, Open File Report OF90-2, 105 p.
- Barrie, C.T., Ludden, J.N., and Green, A.H.
 1993: Geochemistry of volcanic rocks associated with Cu-Zn and Ni-Cu deposits in the Abitibi Subprovince; Economic Geology, v. 88, p. 1341-1358.
- Campbell, I.H., Coad, P., Franklin, J.M., Gorton, M.P., Scott, S.D., Sowa, J., and Thurston, P.C.
 1982: Rare earth elements in volcanic rocks associated with Cu-Zn massive sulphide mineralization: a preliminary report; Canadian Journal of Earth Sciences, v. 9, p. 619-623.
- Cas, R.A.F. and Wright, J.V.
 1984: Volcanic Successions, Modern and Ancient; Allen Unwin, London, 528 p.
- Cathles, L.M.
 1983: An analysis of the hydrothermal system responsible for massive sulphide deposition in the Hokuroku basin of Japan; Economic Geology Monograph 5, p. 439-487.
 1993: Oxygen isotope alteration in the Noranda mining district, Abitibi greenstone belt, Quebec; Economic Geology, v. 88, p. 1483-1511.

- Coats, C.J.A., Clark, L.A., Buchan, R., and Brummer, J.J.**
1970: Geology of the copper-zinc deposits of Stall Lake Mines Ltd., Snow Lake area, N. Manitoba; *Economic Geology*, v. 65, p. 970-984.
- Connors, K.A. and Ansdell, K.M.**
1994: Transition between the Flin Flon and Kiseynew domains of the Trans-Hudson Orogen, File Lake-Limestone Point Lake area, northern Manitoba; in *Current Research 1994-C*, Geological Survey of Canada, p. 183-192.
- Crawford, A.J., Falloon, T.J., and Eggins, S.**
1987: The origin of island arc high alumina basalts; *Contributions to Mineralogy and Petrology*, v. 37, p. 1-13.
- David, J., Bailes, A.H., and Machado, N.**
in press: Evolution of the Snow Lake portion of the Paleoproterozoic Flin Flon and Kiseynew Belts, Trans Hudson Orogen, Manitoba, Canada; *Precambrian Research*.
- David, J., Machado, N., and Bailes, A.H.**
1993: U-Pb geochronology of the Proterozoic Flin Flon Belt, Snow Lake, Manitoba; Geological Association of Canada-Mineralogical Association of Canada, Edmonton, Alberta, Program with Abstracts, v. 17, p. A-22.
- DeMatties, T.A.**
1994: Early Proterozoic volcanogenic massive sulfide deposits in Wisconsin: an overview; *Economic Geology*, v. 89, p. 1122-1151.
- Fedikow, M.A.F., Ostry, G., Ferreira, K.J., and Galley, A.G.**
1989: Mineral deposits and occurrences in the File Lake area, NTS 63K/16; Manitoba Energy and Mines, Mineral Deposits Series, Report No. 5, p. 75-78.
- Franklin, J.M., Barrie, T., and Hannington, M.**
1995: Volcanic-associated massive sulphide deposits through time; in *Precambrian '95*, International Conference on Tectonics and Metallogeny of Early/Mid Precambrian Orogenic Belts, Program with Abstracts, p. 315.
- Franklin, J.M., Lydon, J.W., and Sangster, D.F.**
1981: Volcanic-associated massive sulphide deposits; *Economic Geology, Seventy-fifth Anniversary Volume 1905-1980*, (ed.) B.J. Skinner; p. 485-627.
- Froese, E. and Moore, J.M.**
1980: Metamorphism in the Snow Lake area, Manitoba; *Geological Survey of Canada, Paper 78-27*, 16 p.
- Galley, A.G., Bailes, A.H., and Kitzler, G.**
1993: Geological setting and hydrothermal evolution of the Chisel Lake and North Chisel Zn-Pb-Ag-Au massive sulphide deposit, Snow Lake, Manitoba; *Exploration and Mining Geology*, v. 2, p. 271-295.
- Galley, A.G., Bailes, A.H., Syme, E.C., Bleeker, W., Macek, J.J., and Gordon, T.M.**
1990: Geology and ore deposits of the Paleoproterozoic Flin Flon and Thompson belts, Manitoba; *Fieldtrip Guidebook, The International Association on the Genesis of Ore Deposits: 8th Symposium*, Ottawa, Ontario, 1990, 136 p.
- Gibson, H.L.**
1989: The Mine Sequence of the Central Noranda Volcanic Complex: geology, alteration, massive sulphide deposits and volcanological reconstruction; PhD. thesis, Carleton University, Ottawa, Ontario, 715 p.
- Gibson, H.L. and Watkinson, D.H.**
1990: Volcanogenic massive sulfide deposits of the Noranda Cauldron and Shield Volcano, Quebec; in *The Northwestern Québec Polymetallic Belt*, (ed.) M. Rive, P. Verplaest, Y. Gagnon, J.M. Lulin, G. Riverin, and A. Simard; The Canadian Institute of Mining and Metallurgy, Special Volume 43, p. 119-132.
- Gill, J.B.**
1981: *Orogenic Andesites and Plate Tectonics*. Springer-Verlag, Berlin, 390 p.
- Goodfellow, W.D. and Franklin, J.M.**
1993: Geology, mineralogy and chemistry of sediment-hosted clastic massive sulphides in shallow cores, Middle Valley, Northern Juan de Fuca Ridge; *Economic Geology*, v. 88, no. 8, p. 2037-2069.
- Hodges, D.J. and Manojlovic, P.M.**
1993: Application of lithochemistry to exploration for deep VMS deposits in high grade metamorphic rocks, Snow Lake, Manitoba; *Journal of Geochemical Exploration*, v. 48, p. 201-224.
- Hodgson, C.J. and Lydon, J.W.**
1977: Geological setting of volcanogenic massive sulphide deposits and active hydrothermal systems: some implications for exploration; *Canadian Mining and Metallurgy Bulletin*, v. 95, p. 106.
- Hoffman, P.F.**
1988: United Plates of America, the birth of a craton: Early Proterozoic assembly and growth of Proto-Laurentia; *Annual Review of Earth and Planetary Sciences*, v. 16, p. 543-603.
- Kennedy, G.C.**
1950: A portion of the system silica-water; *Economic Geology*, v. 45, p. 629-653.
- Knuckey, M.J., Comba, C.D.A., and Riverin, G.**
1982: Structure, metal zoning and alteration at the Millenbach deposit, Noranda, Quebec; Geological Association of Canada, Special Paper 25, p. 255-296.
- Kraus, J. and Williams, P.F.**
1993: Tectonometamorphic development of the Eastern segment of the Flin Flon-Snow Lake greenstone belt, Trans-Hudson Orogen, Manitoba; Geological Association of Canada-Mineralogical Association of Canada, Edmonton, Alberta, Program with Abstracts, p. A 54.
- Leshner, C.M., Goodwin, A.M., Campbell, I.H., and Gorton, M.P.**
1985: Trace element geochemistry of ore-associated and barren felsic metavolcanic rocks in the Superior Province, Canada; *Canadian Journal of Earth Sciences*, v. 23, p. 222-237.
- Lucas, S.B., Green, A., Hajnal, Z., White, D., Lewry, J., Ashton, K., Weber, W., and Clowes, R.**
1993: Deep seismic profile across a Proterozoic collision zone: surprises at depth; *Nature*, v. 363, p. 339-342.
- Lucas, S.B., Stern, R.A., and Syme, E.C.**
in press: Flin Flon Greenstone Belt: intraoceanic tectonics and the development of continental crust (1.92-1.84 Ga); *Geological Society of America Bulletin*.
- Lucas, S.B., Stern, R.A., Syme, E.C., and Thomas, D.J.**
1994: Early tectonic history of the Flin Flon belt and its significance for the structural setting and regional distribution of VMS deposits (abstract); in *1994 Program, Manitoba Mining and Minerals Convention*, Winnipeg, Manitoba, p. 24.
- Lundstrom, I. and Papunen, H. (ed.)**
1986: Mineral deposits of southwestern Finland and the Bergslagen Province, Sweden; 7th International Association on the Genesis of Ore-Deposits Symposium and Nordkalott Meeting, Excursion guide no. 3, *Sveriges Geologiska Undersökning Ca 61*, p. 1-43.
- Lydon, J.W.**
1984: Volcanogenic massive sulphide deposits Part 1: a descriptive model; *Geoscience Canada*, v. 11, p. 195-202.
1988: Volcanogenic massive sulphide deposits Part 2: genetic models; *Geoscience Canada*, v. 15, p. 43-65.
- Lydon, J.W. and Galley, A.**
1986: The chemical and mineralogical zonation of the Mathiati alteration pipe, Cyprus, and its genetic significance; in *Metallogeny of basic and ultrabasic rocks*, (ed.) M.J. Gallagher, R.A. Ixer, C.R. Neary, and H.M. Prichard; Institute of Mining and Metallurgy, p. 49-68.
- Lydon, J.W. and Jamieson, H.E.**
1984: The generation of ore-forming hydrothermal solutions in the Troodos Ophiolite Complex: some hydrodynamic and mineralogical considerations; in *Current Research, Part A*; Geological Survey of Canada, Paper 84-1A, p. 617-625.
- Machado, N. and David, J.**
1992: Geochronology of the Reindeer-Superior transition zone and of the Snow Lake area: preliminary results; in *Lithoprobe Trans-Hudson Orogen Transect Workshop No. 2*, Report No. 26, p. 40-42.
- Martin, P.L.**
1966: Structural analysis of the Chisel Lake orebody; *Canadian Institute of Mining and Metallurgy Bulletin*, v. 69, p. 208-214.
- Morton, R.L. and Franklin, J.M.**
1987: Two-fold classification of Archean volcanic-associated massive sulphide deposits; *Economic Geology*, v. 82, p. 1057-1063.
- Morton, M.L., Hudak, G.J., Walker, J.S., and Franklin, J.M.**
1990: Physical volcanology and hydrothermal alteration of the Sturgeon Lake caldera complex; in *Mineral Deposits in the Western Superior Province, Ontario*, (ed.) J.M. Franklin, B.R. Schnieders, and E.R. Koopman; Geological Survey of Canada, Open File 2164, p. 74-94.
- Mottl, M.J. and Holland, H.D.**
1978: Chemical exchange during hydrothermal alteration of basalt and seawater; *Geochimica et Cosmochimica Acta*, v. 33, p. 1103-1115.

- Ohmoto, H. and Takahashi, T.**
1983: Geological setting of the Kuroko deposits, Japan: Part III. Submarine calderas and Kuroko genesis; *Economic Geology Monograph* 5, p. 39-54.
- Riverin, G. and Hodgson, C.J.**
1980: Wall-rock alteration at the Millenbach Cu-Zn mine, Noranda, Quebec; *Economic Geology*, v. 75, p. 424-444.
- Rona, P.A. and Clague, D.A.**
1989: Geologic controls of hydrothermal discharge on the northern Gorda Ridge; *Geology*, v. 17, p. 1097-1101.
- Russell, G.A.**
1957: Structural studies of the Snow Lake-Herb Lake area; Manitoba Mines and Natural Resources, Mines Branch, Publication 55-3, 33 p.
- Skirrow, R.G.**
1987: Silicification in a lower semiconformable alteration zone near the Chisel Lake Zn-Cu massive sulphide deposit, Manitoba; MSc. thesis, Carleton University, Ottawa, Ontario, 171 p.
- Skirrow, R.G. and Franklin, J.M.**
1994: Silicification and metal leaching in subconcordant alteration zones beneath the Chisel Lake massive sulphide deposit, Snow Lake, Manitoba; *Economic Geology*, v. 89, no. 1, p. 31-50.
- Stern, R.A., Lucas, S.B., Syme, E.C., Bailes, A.H., Thomas, D.J., Leclaire, A.D., and Hulbert, L.**
1993: Geochronological studies in the Flin Flon Domain, NATMAP Shield Margin Project area: results for 1992-1993; in *Radiogenic Age and Isotopic Studies: Report 7*, Geological Survey of Canada, Paper 93-2, p. 59-70.
- Stern, R.A., Lucas, S.B., Syme, E.C., Thomas, D.J., and Reilly, B.A.**
1994: Geochronological constraints on the early tectonic history of the Flin Flon belt, Flin Flon-Amisk Lake area (abstract); in 1994 Program, Manitoba Mining and Minerals Convention, Winnipeg, Manitoba, p. 29.
- Stern, R.A., Syme, E.C., Bailes, A.H., Galley, A.G., Thomas, D.J., and Lucas, S.B.**
1992: Nd-isotopic stratigraphy of the Early Proterozoic Amisk Group metavolcanic rocks from the Flin Flon belt; in *Radiogenic Age and Isotopic Studies: Report 5*, Geological Survey of Canada, Paper 92-2, p. 73-84.
- Stern, R.A., Syme, E.C., Bailes, A.H., and Lucas, S.B.**
1995: Paleoproterozoic (1.90-1.86 Ga) arc volcanism in the Flin Flon Belt, Trans-Hudson Orogen, Canada; *Contributions to Mineralogy and Petrology*, v. 119, p. 117-141.
- Stern, R.A., Syme, E.C., and Lucas, S.B.**
in press: MORB- and OIB-like volcanism in the Flin Flon Belt, Canada: tapping heterogeneties in the 1.9 Ga sub-oceanic mantle; *Geochemica et Cosmochimica Acta*.
- Studer, R.D.**
1982: Geology of the Stall Lake copper deposit, Snow Lake, Manitoba; *Canadian Institute of Mining and Metallurgy Bulletin*, v. 75, p. 66-72.
- Swinden, H.S.**
1991: Paleotectonic settings of volcanogenic massive sulphide deposits in the Dunnage Zone, Newfoundland Appalachians; *Canadian Institute of Mining and Metallurgy Bulletin*, v. 83, p. 59-69.
- Syme, E.C.**
1990: Stratigraphy and geochemistry of the Lynn Lake and Flin Flon metavolcanic belts, Manitoba; in *The Early Proterozoic Trans-Hudson Orogen of North America* (ed.) J.F. Lewry and M.R. Stauffer; Geological Association of Canada, Special Paper 37, p. 143-161.
- Syme, E.C. and Bailes, A.H.**
1993: Stratigraphy and tectonic setting of Early Proterozoic volcanogenic massive sulphide deposits, Flin Flon, Manitoba; *Economic Geology*, v. 88, p. 566-589.
- Syme, E.C., Bailes, A.H., and Lucas, S.B.**
1995: G-10: Geology of the Reed Lake area (parts of 63K/9, 63K/10); in *Manitoba Energy and Mines, Report of Field Activities 1995*, p. 42-60.
- Tarney, J., Saunders, A.D., Matthey, D.P., Wood, D.A., and Marsh, N.G.**
1981: Geochemical aspects of back-arc spreading in the Scotia Sea and Western Pacific; *Philosophical Transactions of the Royal Society of London*, v. A300, p. 263-285.
- Thomas, D.J.**
1990: New perspectives on the Amisk Group and regional metallogeny, Douglas Lake-Phantom Lake area, northern Saskatchewan; *Saskatchewan Geological Survey, Saskatchewan Energy and Mines Miscellaneous Report* 90-4, p. 13-20.
- Walford, P.C. and Franklin, J.M.**
1982: The Anderson Lake Mine, Snow Lake, Manitoba; in *Precambrian Sulphide Deposits*, (ed.) R.W. Hutchinson, C.D. Spence, and J.M. Franklin; Geological Association of Canada, Special Paper 25, p. 481-523.
- Williams, H. and McBirney, A.R.**
1979: *Volcanology*; Freeman, Cooper and Co., San Francisco, 397 p.
- Zaleski, E.**
1989: Metamorphism, structure and petrogenesis of the Linda massive sulphide deposit, Snow Lake, Manitoba, Canada; PhD. thesis, University of Manitoba, Winnipeg, Manitoba, 344 p.
- Zaleski, E., Froese, E., and Gordon, T.M.**
1991: Metamorphic petrology of Fe-Zn-Mg-Al alteration at the Linda volcanogenic massive sulphide deposit, Snow Lake, Manitoba; *Canadian Mineralogist*, v. 29, p. 995-1017.
- Zierenberg, R.A., Koski, R.A., Morton, J.L., Bouse, R.M., and Shanks, W.C.**
1993: Genesis of massive sulphide deposits on a sediment-covered spreading centre, Escanaba Trough, Southern Gorda Ridge; *Economic Geology*, v. 88, p. 2069-2098.

Contribution to the 1989-1994 Rusty Lake-Snow Lake Mining Camps, Canada-Manitoba Exploration Science and Technology Initiative (EXTECH I)

Surficial geochemistry and response to volcanic-hosted massive sulphide mineralization in the Snow Lake region

C.A. Kaszycki¹, E. Nielsen², and Gilles Gobert³

Kaszycki, C.A., Nielsen, E., and Gobert, G., 1996: Surficial geochemistry and response to volcanic-hosted massive sulphide mineralization in the Snow Lake region; in EXTECH I: A Multidisciplinary Approach to Massive Sulphide Research in the Rusty Lake-Snow Lake Greenstone Belts, Manitoba, (ed.) G.F. Bonham-Carter, A.G. Galley, and G.E.M. Hall, Geological Survey of Canada, Bulletin 426, p. 139-154.

Abstract: A primary objective of the till geochemistry program was to develop new approaches for the identification of volcanic-hosted massive sulphide deposits (VHMS) and associated alteration zones. In the Chisel Lake area, detailed multi-media sampling was designed to evaluate the geochemical response of various soil horizons and sample media (C- and B-horizon till, humus), sample size fractions thereof, and different analytical methods. The geochemical expression of mineralization was found to vary dramatically with sample type and soil horizon, ranging from patterns that reflect glacial transport and erosion (C-horizon till), to hydromorphic and biogenic dispersion (B-horizon till and humus), and anthropogenic contamination (humus).

At the regional scale, the most pronounced geochemical trend occurs in the area southwest of the town of Snow Lake and northeast of the Chisel Lake mine. In this region, a multi-element Cu, Hg, Pb, As, Au, and Sn anomaly occurs immediately north of the Chisel Lake mine and extends northward to the south shore of Snow Lake, encompassing the recently developed Photo Lake deposit. High ratios of Cu/Zn in C-horizon till samples were found to closely reflect those felsic horizons that host Cu-rich volcanic-hosted massive sulphide deposits (Anderson, Rod, and Stall). Conversely, high ratios of Zn/Cu in C-horizon till samples were found to closely reflect Zn-rich mineralization at the Chisel Lake/Lost Lake/Ghost Lake deposits and also, somewhat surprisingly, at the Cu-rich Linda 2 deposit.

Résumé : Le programme de géochimie des tills a pour principal objectif d'élaborer de nouvelles façons de déceler les gisements de sulfures massifs volcanogènes et les zones d'altération associées. Dans la région du lac Chisel, une campagne d'échantillonnage détaillé de plusieurs milieux a été planifiée afin d'évaluer, d'une part, la réponse géochimique de divers horizons pédologiques et milieux (till d'horizon B et C, humus) de même que des fractions granulométriques des échantillons et, d'autre part, différentes méthodes d'analyse. L'expression géochimique de la minéralisation varie considérablement selon le type d'échantillon et l'horizon du sol; certaines configurations reflétaient un transport et une érosion glaciaire (till d'horizon C), d'autres une dispersion hydromorphe et biogène (till d'horizon B et humus) ou même une contamination anthropique (humus).

À l'échelle régionale, la tendance géochimique la plus prononcée s'observe dans la région au sud-ouest de la ville de Snow Lake et au nord-est de la mine Chisel Lake. Dans cette région, une anomalie en plusieurs éléments, soit en Cu, Hg, Pb, As, Au et Sn, est signalée juste au nord de la mine Chisel Lake et se prolonge vers le nord jusqu'à la rive sud du lac Snow, ce qui englobe le territoire du gisement récemment découvert de Photo Lake. Les rapports Cu/Zn élevés dans les échantillons de till d'horizon C correspondent à ceux des horizons felsiques où se trouvent les sulfures massifs volcanogènes riches en cuivre (Anderson, Rod et Stall). Par ailleurs, les rapports Zn/Cu élevés dans les échantillons de till d'horizon C sont associés aux gisements zincifères de Chisel Lake, de Lost Lake et de Ghost Lake et, fait surprenant, au gisement cuprifère de Linda 2.

¹ Ontario Geological Survey, Ministry of Northern Development and Mines, 933 Ramsey Lake Road, Sudbury, Ontario P3E 6B5

² Manitoba Energy and Mines, 1395 Ellice Ave., Winnipeg, Manitoba R3G 3P2

³ R.R. #2, P.O. Box 16, Portage la Prairie, Manitoba R1N 3A2

INTRODUCTION

A primary objective of the till geochemistry program of the Exploration Technology Working Group (EXTECH) was to develop new approaches for the identification of volcanic-hosted massive sulphide deposits (VHMS) and associated alteration zones. This joint program included a regional sampling component carried out by the Manitoba Department of Energy and Mines and detailed case studies carried out by the Geological Survey of Canada. The regional sampling program was designed to help identify large scale geochemical trends that may indicate potential base metal mineralization. Detailed sampling was carried out in the vicinity of known deposits in an effort to map the scale and form of glacial dispersal associated with volcanic-hosted massive sulphide deposits and to evaluate sample media and analytical techniques best suited for identification of base metal mineralization. Multi-element geochemical trends observed in case studies were then used to guide interpretation of regional data. In addition to till sampling, detailed studies of Quaternary stratigraphy, and ice flow history were carried out in order to identify the depositional and erosional controls on till composition within the region.

Regional setting

The study area comprises two 1:50 000 NTS scale maps sheets, NTS 63K/16 and NTS 63J/13, roughly centred on the town of Snow Lake in northwestern Manitoba (Fig. 1). It is located at the eastern end of the Flin Flon metavolcanic belt and is bounded by the Kiseynew Gneiss Belt to the north and Paleozoic terrane to the south. Mineralization in the Snow Lake area occurs within thick sequences of subaqueous volcanic rocks, associated mainly with felsic flows. Two distinct mineralizing events are recognized; one Cu-rich, and the other Zn-rich. Both Cu-rich and Zn-rich deposits are spatially associated with rhyolite flow complexes and subvolcanic tonalite intrusions (Bailes and Galley, 1996). In this

area, a regional sampling survey was carried out over both 1:50 000 NTS map sheets. Detailed studies were carried out in the Chisel Lake area, in the vicinity of the Chisel Lake, Ghost Lake, and Lost Lake mines and the North Chisel deposit, as well as in the vicinity of the Linda 2 deposit on Wekusko Lake (Fig. 1).

METHODOLOGY

Field methods

Regional sampling was restricted to areas of easy access along roads, powerlines, and lakeshores between File Lake and Morton Lake to the west and the Osborne Lake mine to the east (Fig. 1). Table 1 summarizes the field methods used in both regional and detailed studies. In the regional survey, the distribution and density of sample sites is quite variable, ranging from 1 sample per kilometre in areas of easy access to 1 per several kilometres in remote parts of the region. Samples of C-horizon till were collected from hand-dug pits averaging 1 m in depth. C-horizon material is defined in this study as the soil horizon underlying the zone of maximum B-horizon development, characterized by a brownish grey to olive-grey colour, and exhibiting little to no mottling with reddish brown to orange ferric oxide. In this 'upper' C-horizon, sulphide minerals have generally been oxidized and carbonate may or may not have been leached by surface weathering processes. In 1991, humus samples were collected at each site, in addition to C-horizon samples. An attempt was made to collect humus from the organic layer directly overlying the C-horizon sample to ensure comparable results.

In detailed surveys, sample spacing averaged approximately 1 per 200 m. At each site, samples of B-horizon glacial till (soil), C-horizon glacial till (parent material), and humus were collected in an effort to evaluate and compare the geochemical response of various sample media.

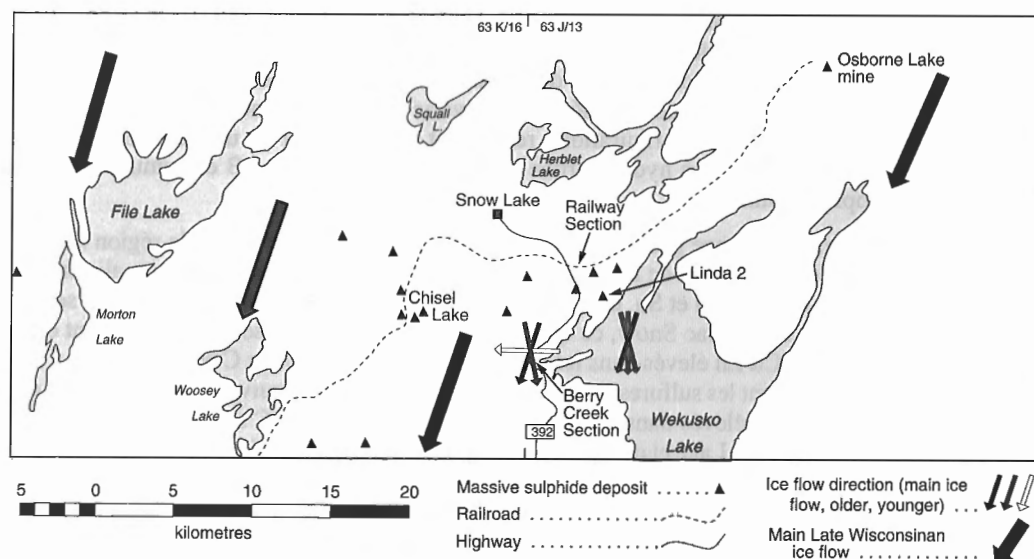


Figure 1. Major mineral deposits and ice flow directions in the Snow Lake study area.

Analytical methods

Several different fractions of each sediment type have been analyzed by a variety of analytical methods. Subsplittings of the <2 µm and <63 µm size-fractions were extracted from both B-horizon and C-horizon till and analyzed using conventional geochemical techniques (Table 2). The heavy mineral fraction of C-horizon till samples was also extracted and analyzed for visible gold (VG). The less than 177 µm fraction (80-mesh) of humus samples was analyzed using aqua regia decomposition and ICP emission spectrometry (ICP-ES).

In addition to conventional analytical methods, samples were also analyzed by sequential extraction techniques designed to identify the residence sites of trace metals within the various sample media. These specialized analytical methods were developed as part of the EXTECH program and are presented in detail in accompanying papers (Hall et al., 1996; Kaszycki and Hall, 1996). Sequential extraction was carried out on the <2 µm sized fraction of B- and C-horizon tills. Humus samples were analyzed for metals held in the soluble organic fraction (humic and fulvic components). In addition, the insoluble organic residue was analyzed using the sequential extraction scheme.

QUATERNARY GEOLOGY

In addition to till sampling, detailed striation mapping and stratigraphic profiling was undertaken in order to decipher the erosional record of regional ice flow and associated depositional history. Regional aspects of the Quaternary geology of Snow Lake and adjacent areas have been summarized by Kaszycki (1986, 1989), McMartin (1994) and Nielsen (1992). Most of the Snow Lake study area is characterized by a relatively simple depositional sequence consisting of thin till (<3 m) overlying bedrock. In low lying areas, till may be capped by a thin to moderate thickness (<1 m to 3-4 m) of laminated silt and clay deposited in glacial Lake Agassiz. In general, till is characterized by a sandy to sandy-silty matrix and contains little to no carbonate. Clast content is variable and clast composition predominantly reflects local bedrock lithologies.

A calcareous till was observed in fresh roadcut exposures along Highway 392, extending from the Paleozoic contact (just south of the field area) northward to Snow Lake. Calcareous till was also observed at several sites along the western shore of Wekusko Lake. This till exhibits a silty to sandy-silty matrix, with variable carbonate content.

Table 1. Sampling strategies for regional and detailed studies.

| SCALE | AREA | SAMPLE SPACING | SAMPLING MEDIA |
|----------|---|---|--|
| Regional | NTS 63K/16 NTS 63J/13 | variable from 1 per km up to 1 per several km | C-horizon till, Humus (1991 only) (total 254 sample sites) |
| Detailed | Chisel Lake and North Chisel Linda 2 Ruttan | ~ 1 per 200 m (total 66 sample sites) ~ 1 per 100 - 200 m (total 59 sample sites) ~ 1 per 200 m (total 19 sample sites) | C- and B-horizon till, Humus C- and B-horizon till, Humus C- and B-horizon till, Humus |

Table 2. Analytical scheme for various sample media.

| SAMPLE MEDIA | SIZE FRACTION | ANALYSIS |
|--|---|--|
| C-horizon till | heavy minerals <2 µm (clay fraction) | Visible gold, point count *AAS (10 elements) + Hg, As (HG-AAS) *ICP-ES (31 element suite) Sequential Extraction (7 element suite) |
| | < 63 µm (silt & clay fraction) | INAA (Au + 34 element suite) *ICP-ES (31 element suite) |
| B-horizon till | < 2 µm (clay fraction) | *AAS (10 elements), Hg, As (HG-AAS) *ICP-ES (31 element suite) Sequential Extraction (7 element suite) |
| | <63 µm (silt & clay fraction) | INAA (Au + 34 element suite) *ICP-ES (31 element suite) |
| Humus | <177 µm fraction soluble organic fraction insoluble organic residue | *ICP-ES (31 element suite) Na ₄ P ₂ O ₇ leach (7 element suite) Sequential Extraction (7 element suite) |
| * aqua regia leach AAS – Atomic absorption spectrometry HG – Hydride generation ICP-ES – Inductively coupled plasma emission spectrometry | | |

Regional ice flow

Striation mapping revealed the occurrence of several ice flow events that both predate and postdate the strong southwesterly ice flow toward 210° associated with Main Late Wisconsinan glaciation (Fig. 1). Striations predating Main Late Wisconsinan ice flow range from due south to southeast and have been observed at several localities on Wekusko Lake. Striations postdating the 210° Main Late Wisconsinan ice flow have been observed in borrow pits along the road west of Wekusko Lake. Two separate late glacial ice flows have been recorded, one trending to the southeast at 160° and another trending to the west-southwest ranging from 250–270°. The relative ages of these late glacial flows could not be determined; however, they appear to have had little impact on observed patterns of glacial dispersal.

Stratigraphy

The sedimentary sequence at three sites was studied in detail, in order to identify the depositional sequence associated with the late glacial events observed in the striation record. At all three sites, till containing calcareous Paleozoic debris was encountered. At one site (Railway Section, Fig. 1), till fabric data suggest that calcareous till was emplaced by westward to west-southwestward flowing ice, indicating that at least some calcareous till was deposited during late glacial westward ice flow. Westward flowing ice could easily have transported Paleozoic debris into the Snow Lake region from the northern extension of the Paleozoic-Precambrian contact in the Ponton area, 45 km to the east, or from local unmapped Paleozoic outliers.

DETAILED TILL GEOCHEMISTRY OF THE CHISEL LAKE AREA

Detailed sampling was carried out in the vicinity of known mineral deposits in the Chisel Lake area in an effort to map the scale and form of glacial dispersal associated with volcanic-hosted massive sulphide deposits and to evaluate sample media and analytical techniques best suited to identification of this style of mineralization. Results of these studies have been used to guide interpretation of regional data.

Samples were collected from 66 sites, extending from approximately 400 m north of the Chisel North deposit to approximately 4 km south of the Chisel Lake, Ghost Lake, and Lost Lake deposits (Fig. 2). At most sites, samples of B-horizon glacial till (soil), C-horizon glacial till (parent material), and humus were collected in order to evaluate and compare the geochemical response of various sample media. In general, samples of C-horizon till reflect primary glacial erosion and transport of underlying bedrock. B-horizon till samples have been subjected to secondary chemical processes in the near-surface weathering environment and as a result may be enriched or depleted in base metals relative to the underlying C-horizon. Humus reflects a combination of surficial geochemical, biogeochemical, and atmospheric processes. Different size fractions of B- and C-horizon till were analyzed to evaluate the optimal geochemical response within a given sample media.

C-horizon till

Geochemical trends for Zn and Cu in C-horizon till, in both the <2 µm and <63 µm size fractions, are presented in Figures 3 and 4, respectively. In general, patterns for both elements, in both size fractions, exhibit a well defined south-southwesterly dispersal fan, parallel to ice flow. Highest concentrations are localized over the ore zones, and decrease systematically in the down-ice direction. The contrast between background and anomalous concentrations is greatest in the <2 µm size fraction, resulting in large, high contrast anomalies, extending up to 1 km southwest of Ghost and Lost lakes. The lower contrast tails of these trains, can be resolved up to 2 km in the down-ice direction. Geochemical signatures within the <63 µm size fraction tend to be more localized over the ore zone. High contrast anomalies extent only a few

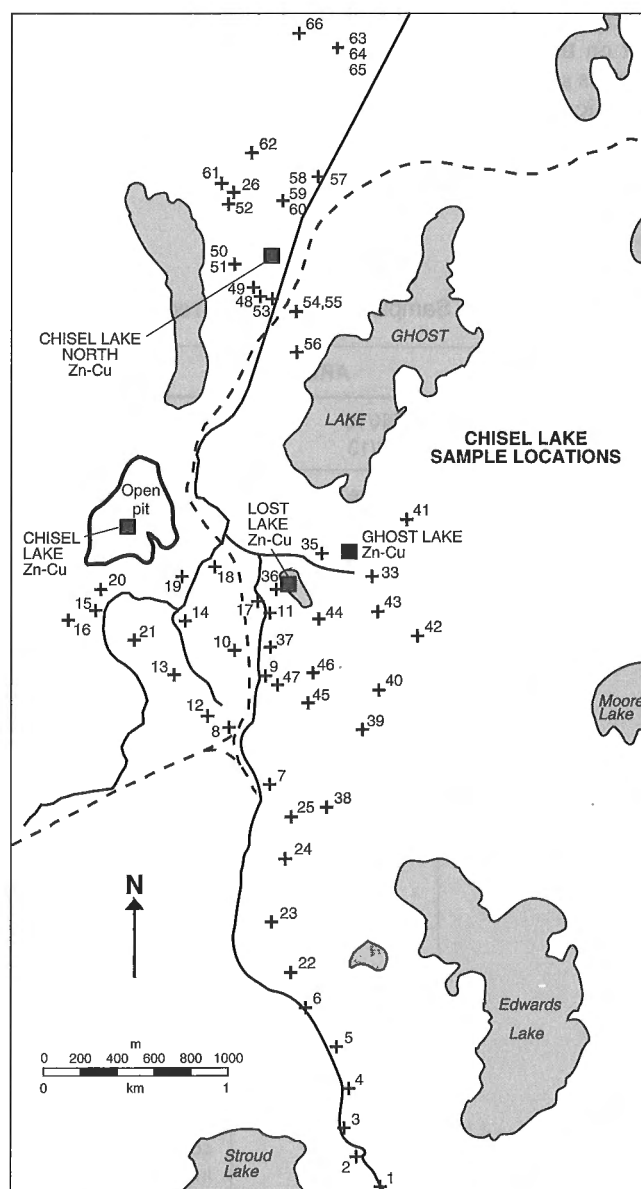


Figure 2. Sample location plan for the Chisel Lake area detailed survey.

hundred metres down-ice from the source area. In some instances, the tails of these trains can be traced for up to a kilometre down-ice from source; however, the contrast with background concentration is very low. In a regional sampling program, where the tail of a train is likely to be intersected at one or two sample sites, this low contrast geochemical response is difficult to resolve.

The contrast in geochemical response between size fractions reflects the residence sites of indicator metals within the till. Results of phase selective sequential extractions on the $<2\ \mu\text{m}$ size fraction indicate that base metals are equally concentrated within sulphide, crystalline oxide, and amorphous

hydroxide mineral phases (Hall et al., 1996; Kaszycki and Hall, 1996). Both the residual silicate phase and the adsorbed/exchangeable phase are notably depleted in metals. The more well-defined anomalies observed in the $<2\ \mu\text{m}$ size fraction reflect a dominant phyllosilicate mineralogy typical of this size fraction. Unfortunately, using this extraction scheme it is not clear at which stage in the process phyllosilicates are dissolved. It is likely that most, if not all, phyllosilicate is dissolved prior to extraction of the residual silicate phase, and contributes to the geochemical signature of the oxide and sulphide phases. In contrast, the silt size fraction ($2\text{--}63\ \mu\text{m}$) is dominated by silt-sized silicate minerals (quartz and feldspar) that are barren of base metals, resulting in a subdued geochemical signature.

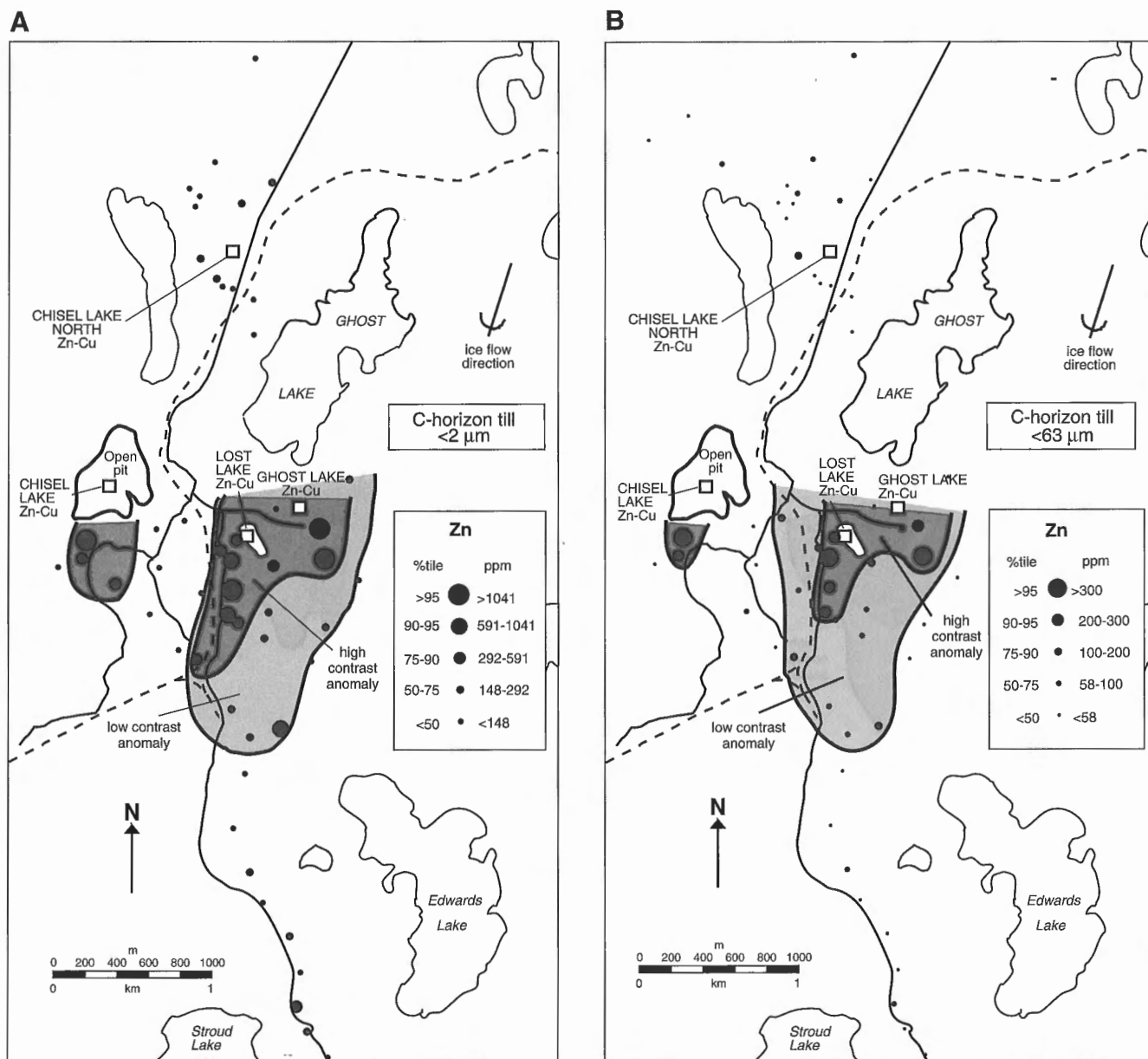


Figure 3. Patterns of glacial dispersal as illustrated by Zn in A) the $<2\ \mu\text{m}$ size fraction and B) the $<63\ \mu\text{m}$

B-horizon till

The dispersal trends for Cu, As, and Zn in the <2 µm size fraction of B-horizon till samples are presented in Figure 5. Geochemical patterns for Cu and As (Fig. 5A, B) are similar to those observed for these elements in C-horizon till, reflecting glacial dispersal to the southwest. In general, these anomalies are irregular in shape and are more restricted in down-ice extent than those observed in C-horizon till, possibly reflecting leaching of metals in the near-surface weathering environment. Summary statistics and site by site comparison of element concentrations in both B- and C-horizon till samples indicate that most elements are depleted in the B-horizon relative to the underlying C-horizon. Detailed weathering profiles in till observed throughout

northwestern Manitoba (Fig. 6; Kaszycki, unpub. data, 1990) supports this conclusion. These observations suggest that the degree of postglacial soil development has been insufficient to produce a classical podzolic B-horizon, characterized by an increase in clay content, Fe- and Mn-hydroxides and associated illuviated metals (Fig. 6B). Rather than an increase in metal content in the B-horizon, soils in northern Manitoba are generally depleted of metals in this horizon relative to underlying parent material (C-horizon). In instances where the parent material is calcareous, carbonate leached from the B-horizon is reprecipitated in the upper C-horizon (Fig. 6A). Metals that are insoluble under alkaline conditions (Zn and Cu) also precipitate, resulting in metal-enrichment within this zone. Where parent material is noncalcareous and neutral to slightly acidic conditions persist throughout the soil profile,

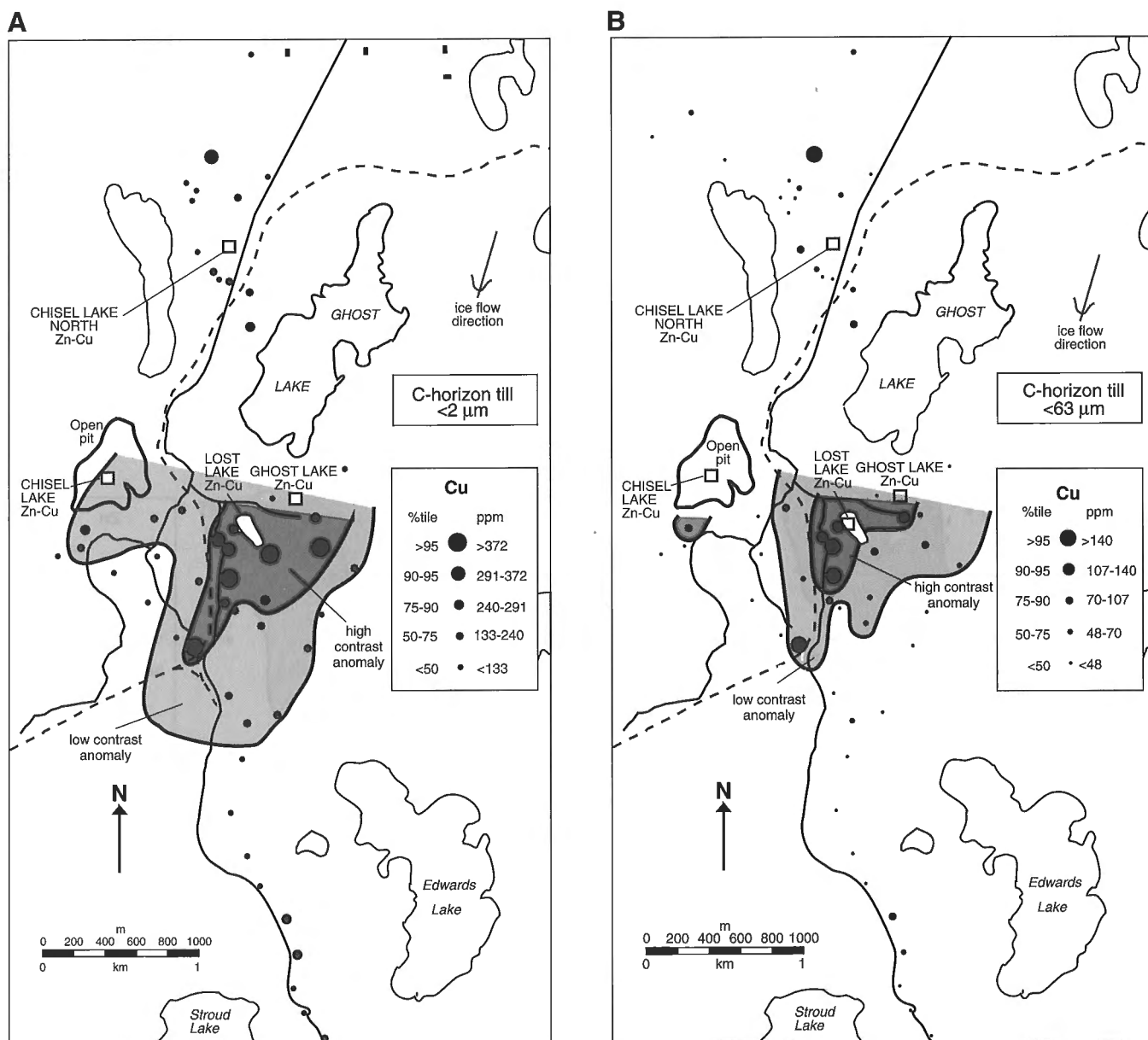


Figure 4. Patterns of glacial dispersal as illustrated by Cu in A) the <2 µm size fraction and B) the <63 µm size fraction of C-horizon till samples in the Chisel Lake area.

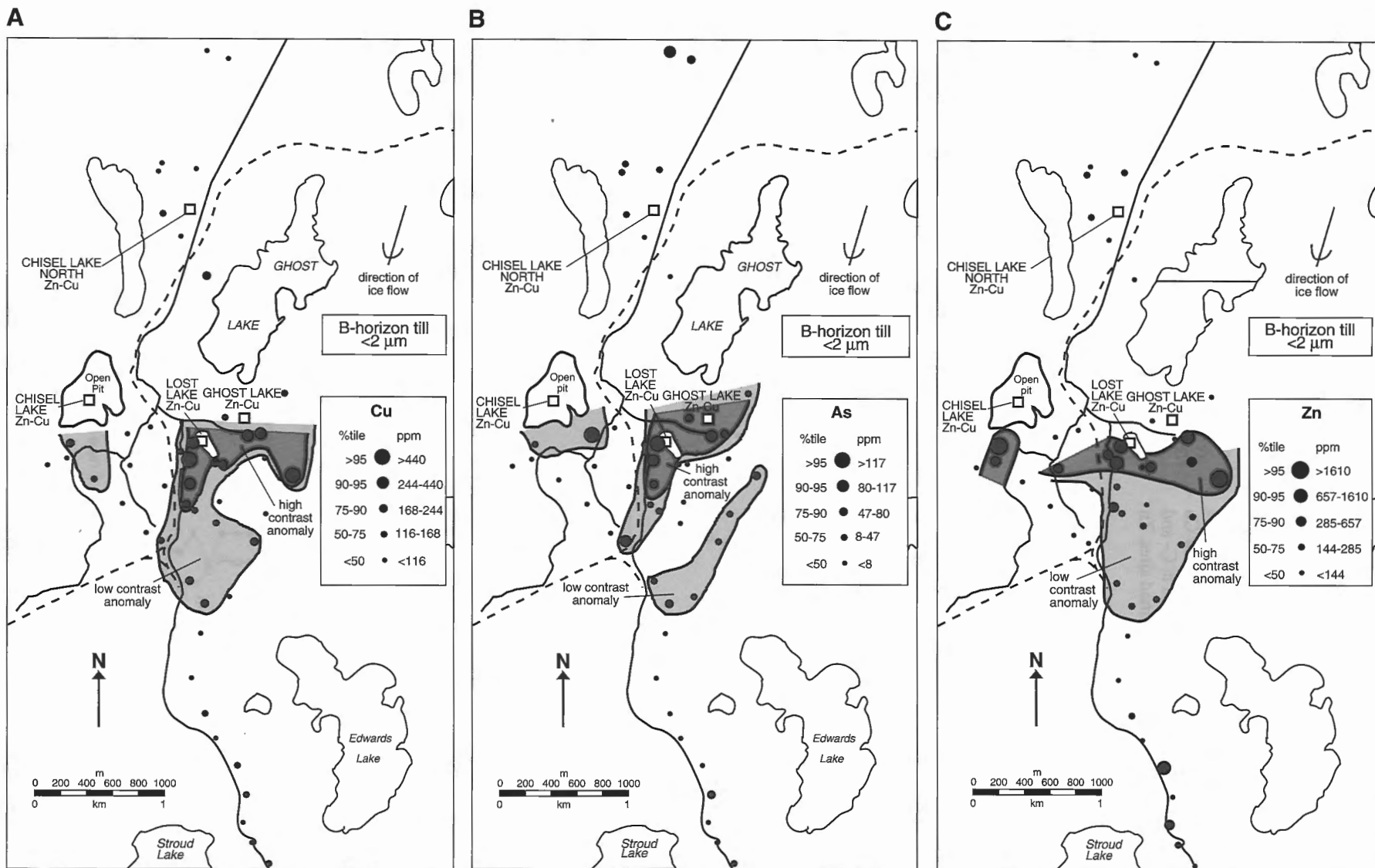


Figure 5. Geochemical anomalies for A) Cu, B) As and C) Zn as expressed in the <2 μm size fraction of B-horizon till. Geochemical trends reflect the combined effects of primary glacial erosion and transport of ore materials and secondary redistribution in the near-surface weathering environment.

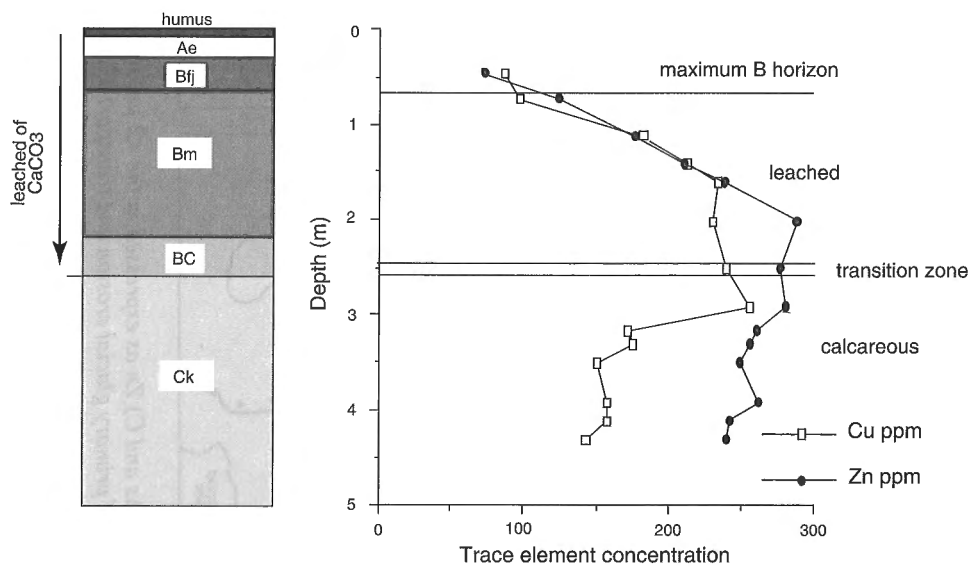
metals such as Cu and Zn remain in solution and are transported to the water table. In either case, metal concentrations in the zone of maximum B-horizon development are depleted with respect to parent material, resulting in suppressed B-horizon anomalies.

In contrast to Cu and As, Zn exhibits a markedly different distribution. Elevated Zn concentrations are localized over the ore zone; however the high contrast anomaly trends east-west rather than northeast-southwest as observed for Cu and As (Fig. 5C). Comparison of Zn concentrations in C- and B-horizon tills reveals that, at several poorly drained sites, Zn

(and to a lesser extent Cu) is more highly concentrated in the B-horizon than the underlying C-horizon. Sequential extraction of these samples indicates that most of this metal resides in the adsorbed/exchangeable phase and the amorphous Fe- and Mn-hydroxide mineral phase, a pattern consistent with a hydromorphic anomaly. A more poorly defined low contrast anomaly extends up to 1 km down-ice from the source area, consistent with trends observed in C-horizon material. These relationships suggest that the geochemical response in B-horizon till is a complex function of both primary lithological controls and secondary surface weathering processes.

A

WEATHERING PROFILE IN CALCAREOUS TILL



B

WEATHERING PROFILE IN SHIELD TILL

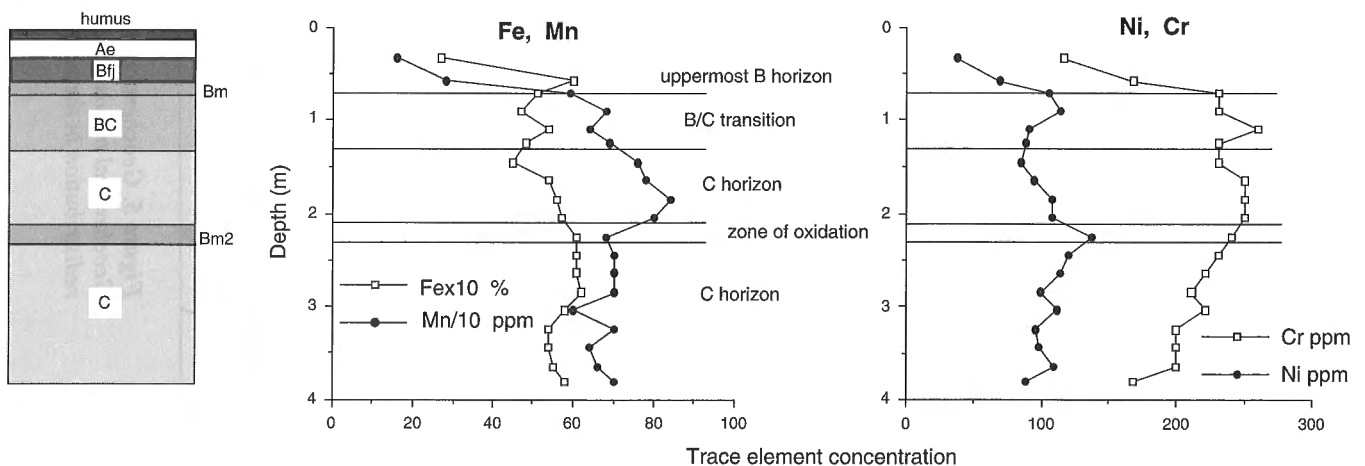


Figure 6. Surface weathering profiles in glacial till derived from A) calcareous Paleozoic debris, and B) noncalcareous shield lithologies.

As a general rule, geochemical anomalies within B-horizon till are limited in areal extent and exhibit patterns that may reflect one or a number of glacial and surface weathering processes. The geochemical expression of surface weathering processes is dependent upon in situ pH and redox conditions and the relative solubility of various elements under these conditions. As a result, element behaviour is not predictable and resulting geochemical patterns may vary from element to element under different surface weathering conditions.

Humus

Geochemical trends for Cu and Zn in humus are summarized for each element reporting as: A) "total" in <177 μm fraction; B) bound in the "soluble" organic phase; and C) remaining in the insoluble organic residue (Fig. 7, 8). Geochemical patterns vary dramatically for each element and for the individual organic phases analyzed. Copper in the <177 μm fraction exhibits an amoeboid shaped anomaly, centred on the ore zone and with a pronounced south-southwesterly elongation extending approximately 1 km in the down-ice direction (Fig. 7). Two fingers of elevated Cu concentration also extend in a southeasterly direction. The major portion of this anomaly is mimicked by an anomaly in both the soluble organic phase and the insoluble organic residue. The pronounced southwesterly trend of these anomalies is parallel to ice flow and mimics that of underlying till. This suggests that Cu is effectively absorbed by roots and recycled upward from underlying B- and C-horizons. A low contrast anomaly in the insoluble residue phase mimics the southeasterly trending fingers of high Cu content observed in the <177 μm fraction.

This southeasterly trend is even more pronounced for Zn (Fig. 8). Zinc anomalies in the <177 μm fraction ("total") are centred on the ore zone but define a pronounced southeasterly trending geochemical dispersion fan. The anomaly in the soluble organic phase trends east-west across the ore zone, similar to the pattern observed for B-horizon till, suggesting that Zn has been absorbed and recycled upward by surface vegetation. Elevated Zn concentration within the insoluble organic residue exhibits a well defined southeasterly orientation, perpendicular to ice flow. Sequential extraction analyses performed on the insoluble organic residue indicate that Zn is concentrated within a mineral phase dominated by sulphides and refractory organic matter. The presence of Zn in sulphide within humus samples suggests a particulate origin, likely in the form of mine dust from tailings piles and open pit operations. The southeasterly trend of this anomaly is parallel to prevailing wind direction. It is concluded that the extensive southeast-trending anomaly observed in the <177 μm fraction primarily reflects airborne contamination from mining operations. The muted southeasterly response observed for Cu likely reflects the relative abundance of Cu versus Zn in the ore itself. In the Chisel Lake area, all ores are Zn-rich, containing up to 20 times more Zn than Cu (Bailes and Galley, 1996).

In general, observed geochemical trends in humus indicate that trace metals are recycled upward from underlying B- and C-horizon tills into the overlying vegetation. Anomalies tend to mimic those observed in underlying glacial sediments,

except in areas where airborne contamination is prevalent. Humus generally is useful in bedrock dominated terrain or in areas where till is geochemically anomalous.

SURFICIAL GEOCHEMISTRY OF THE SNOW LAKE AREA

Based on the results of multi-media orientation studies in the Chisel Lake area, interpretations of regional geochemical trends have been derived from analysis of the <2 μm size fraction of C-horizon till samples. The geochemical signature of this material produces well-defined anomalies related to lithological composition of the till. Orientation studies also indicate that humus anomalies tend to mimic those of underlying till. Comparisons of regional till and humus data are also presented (Fig. 9, 10).

Regional till geochemistry

Regional C-horizon till data have been interpreted at two different scales: 1) a regional scale, including data from all samples collected from within the study area (exclusive of detailed sample sites); and 2) an intermediate scale including data from all samples collected within a subarea containing the main past and present volcanic-hosted massive sulphide-producing deposits (inclusive of detailed sample sites).

At the regional scale, the most pronounced geochemical trend occurs in the area southwest of the town of Snow Lake and northeast of the Chisel Lake mine. In this region, a multi-element Cu, Hg, Pb, As, Au, and Sb anomaly occurs immediately north of the Chisel Lake mine and extends northward to the south shore of Snow Lake, encompassing the recently developed Photo Lake deposit. In this area, the regional distribution of Cu exhibits a pronounced anomaly associated with felsic volcanic lithologies (Fig. 9A). Elevated Cu concentrations can be traced eastward, following the trend of felsic volcanic lithologies, which host Cu-rich mineralization at the Rod 1, 2, Stall Lake and Anderson Lake mines. Anomalous concentrations of Cu are also associated with mafic intrusions along the northeast arm of Herblet Lake. At several sites along the shore of Woosey Lake, elevated Cu concentrations appear to be associated with mafic volcanics in that area.

In contrast, Zn concentrations are elevated south of Chisel Lake, reflecting Zn-rich mineralization in this area (Fig. 10A). Anomalous Zn concentrations occur in association with Cu and Pb in the Woosey Lake area. Uniformly high concentrations of Zn along the west shore of Wekusko Lake coincide with carbonate-rich till in this area, likely reflecting an increase in background concentration associated with calcareous Paleozoic debris. Similar relationships have been observed elsewhere in northwestern Manitoba (Kaszycki, 1989).

Regional patterns of Cu and Zn have also been evaluated at an intermediate scale, defined by a subarea containing the main past and present volcanic-hosted massive sulphide deposits within the region. This region corresponds to the area of 1:20 000 scale bedrock mapping described by Bailes and

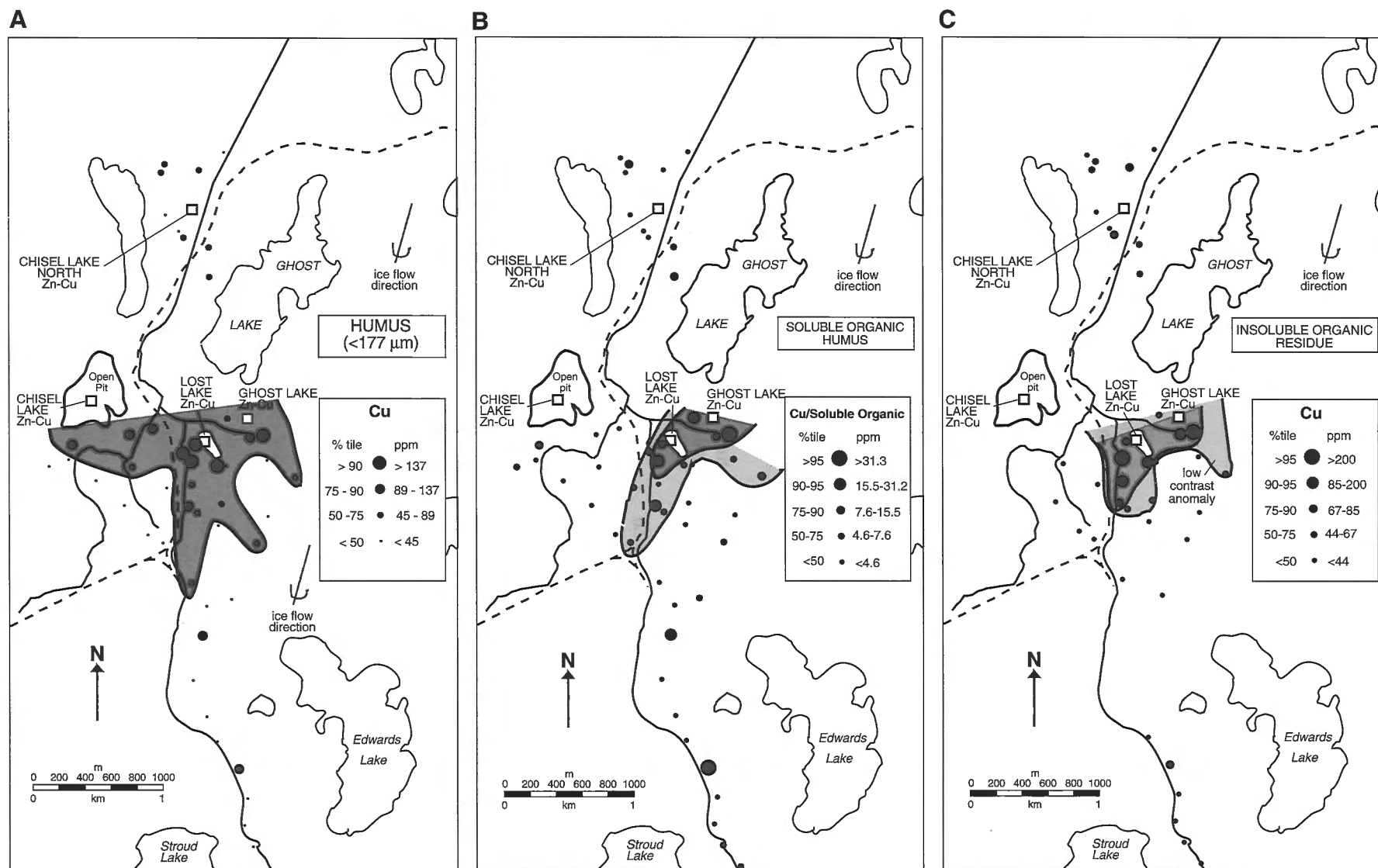


Figure 7. Distribution of Cu in humus within the Chisel Lake study area. Various fractions analyzed produce geochemical patterns reflecting biological redistribution of metal in the surface environment (A and B) and the impact of airborne contamination on humus geochemistry (C).

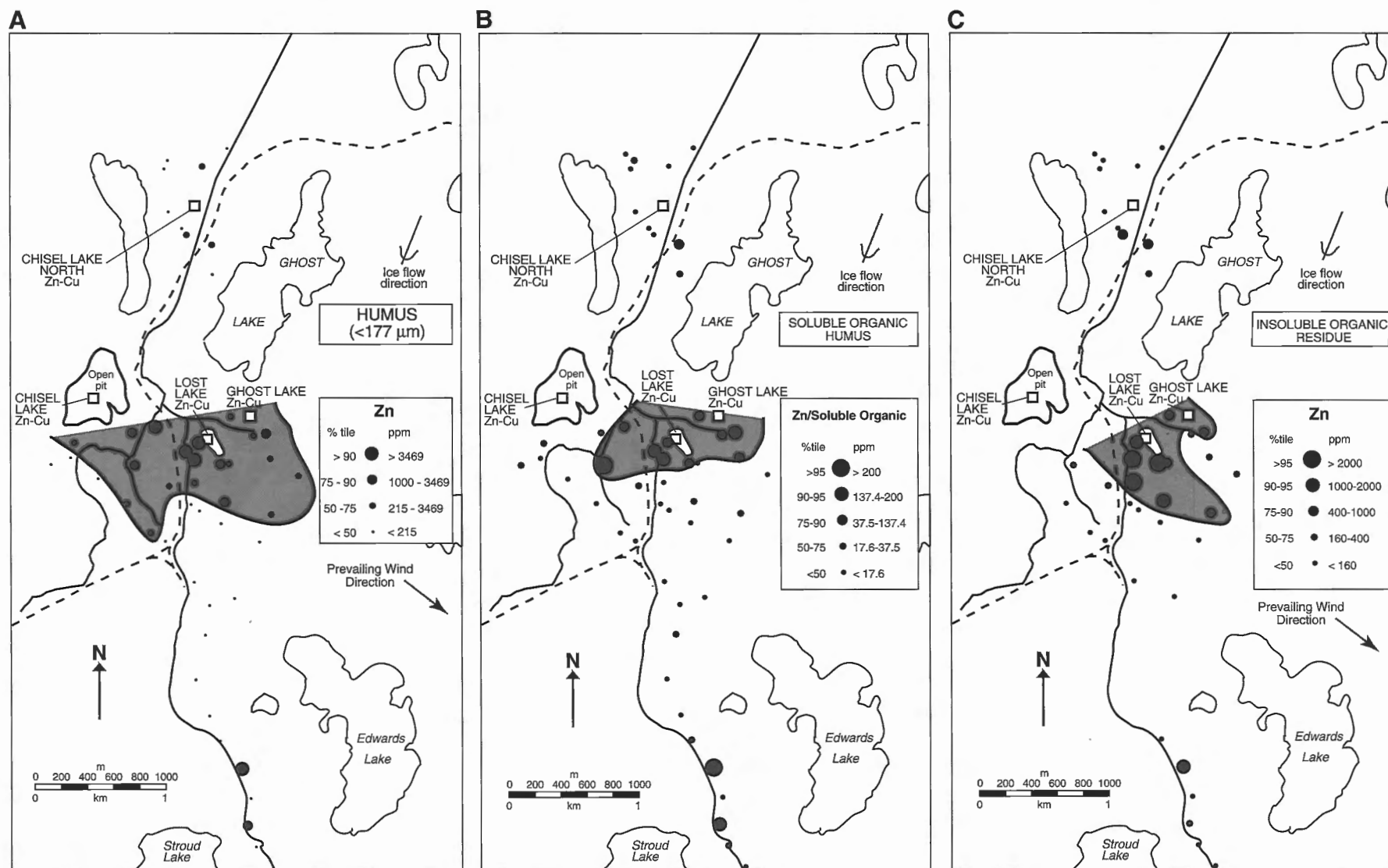


Figure 8. Distribution of Zn in humus within the Chisel Lake study area. Various fractions analyzed produce geochemical patterns reflecting biogenic redistribution of metal in the surface environment (B) and the impact of airborne contamination on humus geochemistry (A and C).

Galley (1996) and used as the basis for mineral potential modelling (Wright and Bonham-Carter, 1996). In an effort to differentiate the geochemical signature of Cu-rich versus Zn-rich deposits, the ratio of Cu/Zn and Zn/Cu concentrations within the <2 μm size fraction of C-horizon till were plotted

(Fig. 11). The distribution of high ratios of Cu/Zn in C-horizon till samples clearly defines the transition from Zn-rich till south of Chisel Lake to Cu-enriched till to the north. Cu-enriched till can be traced eastward from the area north of Chisel Lake, encompassing the Photo Lake deposit,

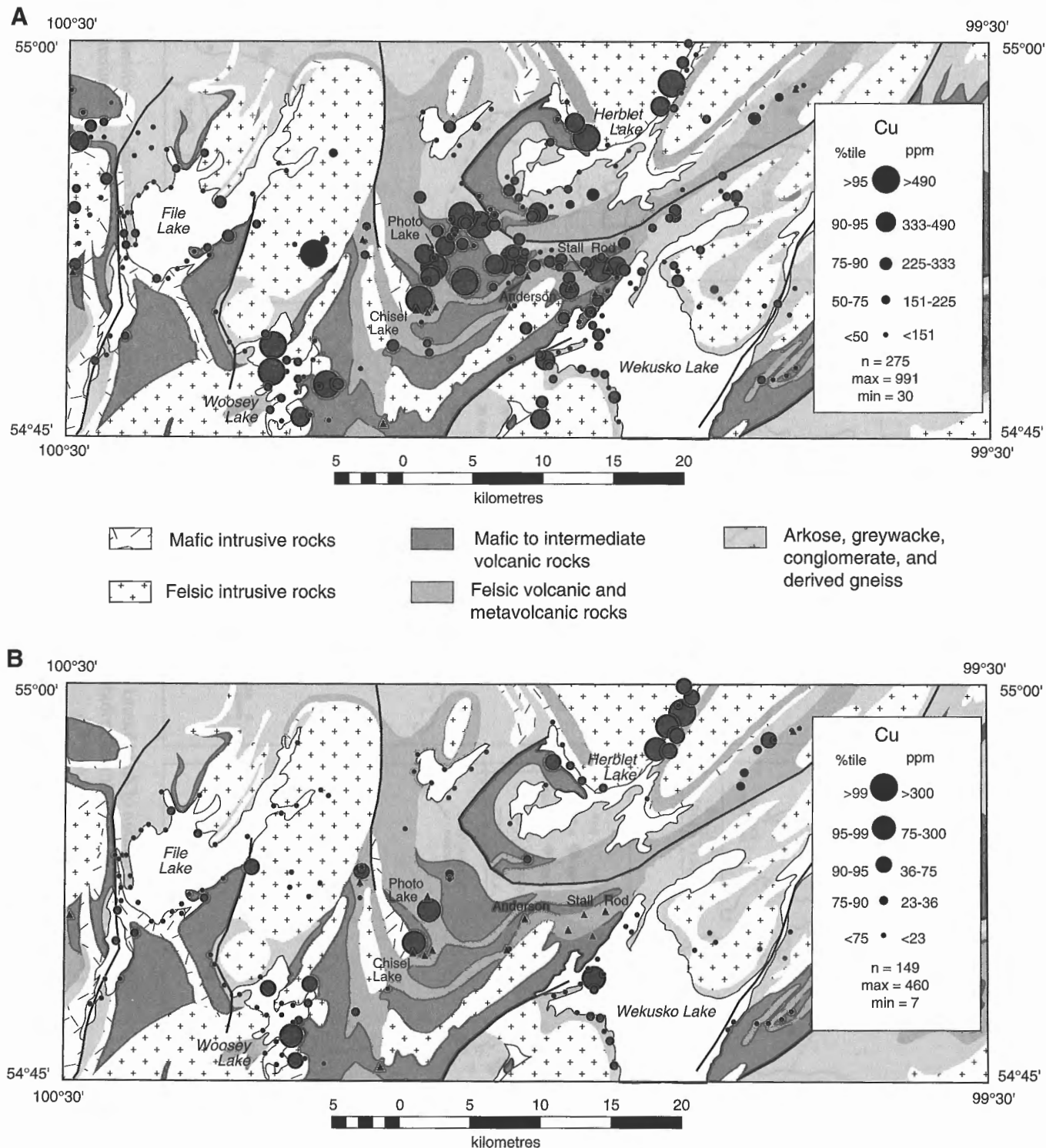


Figure 9. Regional distribution of Cu in A) the <2 μm size fraction of C-horizon till and B) <177 μm mesh fraction of humus.

along the strike of felsic volcanic rocks hosting Cu-rich deposits at the Anderson Lake, Rod 1, 2 and Stall Lake mines (Fig. 11A). Cu-enrichment is observed in samples collected over both felsic and mafic volcanic rocks throughout this area. In contrast, Zn-enriched till dominates the geochemical signature of the Zn-rich Chisel Lake, Ghost Lake, and Lost Lake

deposits. Zinc also appears to dominate the geochemical signature of the Linda 2 deposit. Although the Linda deposit is thought to be stratigraphically associated with Cu-rich mineralization (Bailes and Galley, 1996), sulphide mineralization at this site is slightly enriched in Zn, with 0.79% Zn and 0.30% Cu (Fig. 11B).

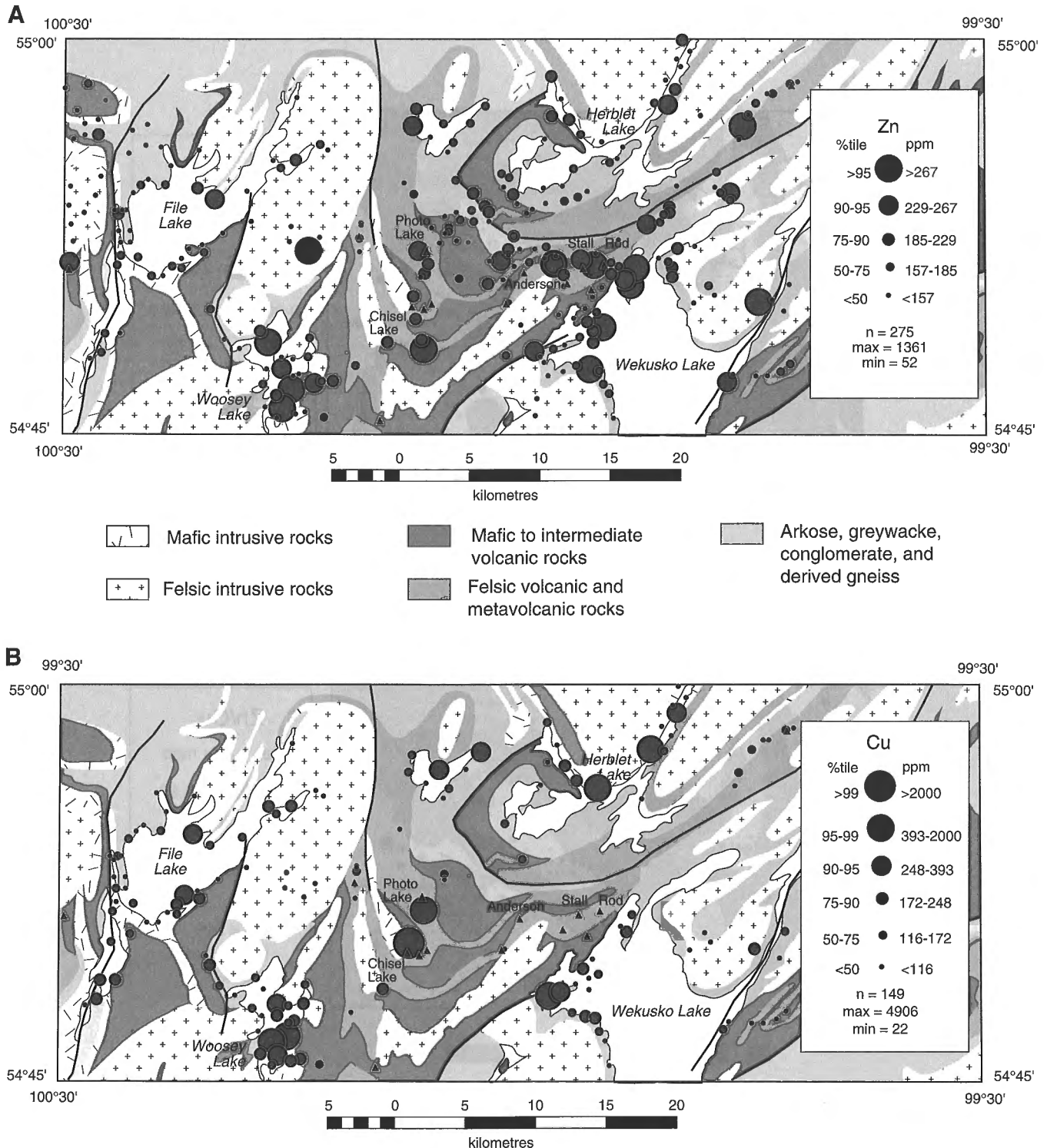


Figure 10. Regional distribution of Zn in A) <2 μm size fraction of C-horizon till and B) <177 μm fraction of humus.

Arsenic also exhibits large concentrations north of Chisel Lake (Fig. 12A), similar to Hg, Cu, and Pb. However, highest As concentrations are found further north in the Tern Lake area, where Cu concentrations are low. Attention was first focused on the Tern Lake area in 1990, when a clearly defined multi-element Au, visible gold, As, and Hg anomaly was identified that extends from Tern Lake, southwestward to the Chisel Lake area. This trend is best developed for As (Fig. 12A), and appears to form, at least in part, a dispersal train extending southwestward about 5 km from its source

near Tern Lake. Arsenic concentrations near the head of the train range up to 950 ppm, decreasing systematically to the southwest. The trends for Au and visible gold are less well developed (Fig. 12B), although both exhibit clearly defined anomalies in the Tern Lake area, where Au in the <63 μm size fraction reaches 78 ppb, and visible gold in the heavies reaches 286 grains of which 233 were pristine. A site at the head of the train was resampled in 1991 and returned a grain count of 604 grains of which 468 were pristine. It was thought that the association between Au and As reflects a zone of

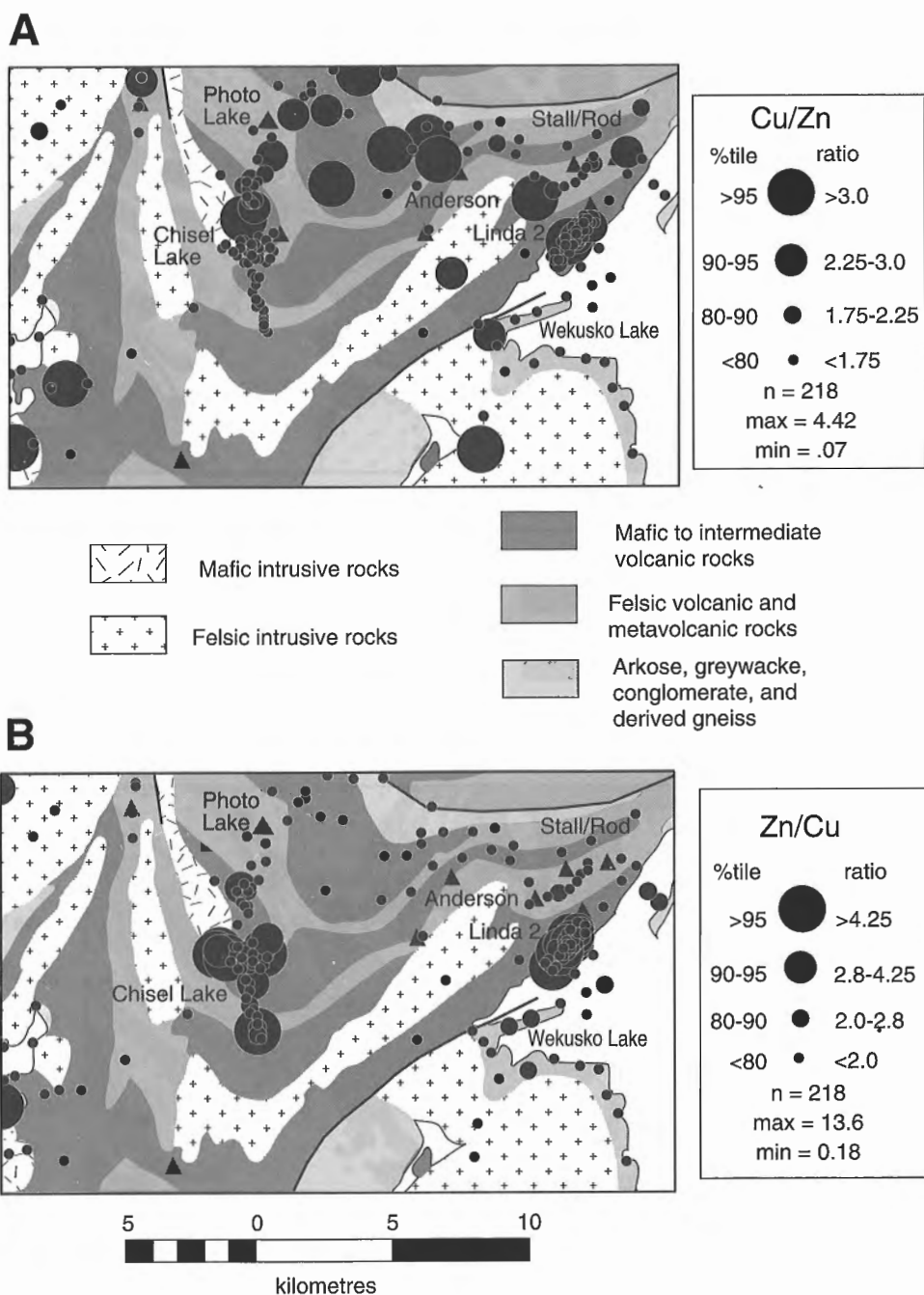


Figure 11. Regional variations in the relative proportions of Cu and Zn in the vicinity of past-producing deposits in the Chisel Lake area and along the Anderson Lake- Rod 1, 2-Stall Lake horizon; A) regional distribution of Cu/Zn; B) regional distribution of Zn/Cu.

strong alteration associated with fault-hosted mineralization, similar to that observed within the Nor-Acme and other Au deposits in the town of Snow Lake. The recent discovery of the Cu-Au Photo Lake deposit to the south however, may indicate that high Au concentrations within this area are related to base metal mineralization.

Regional humus geochemistry

The regional distribution of Cu and Zn in the $<177\ \mu\text{m}$ fraction of humus is presented in Figures 9B and 10B. Because humus was collected only in the 1991 regional sampling program, the sample distribution is not directly comparable with that of

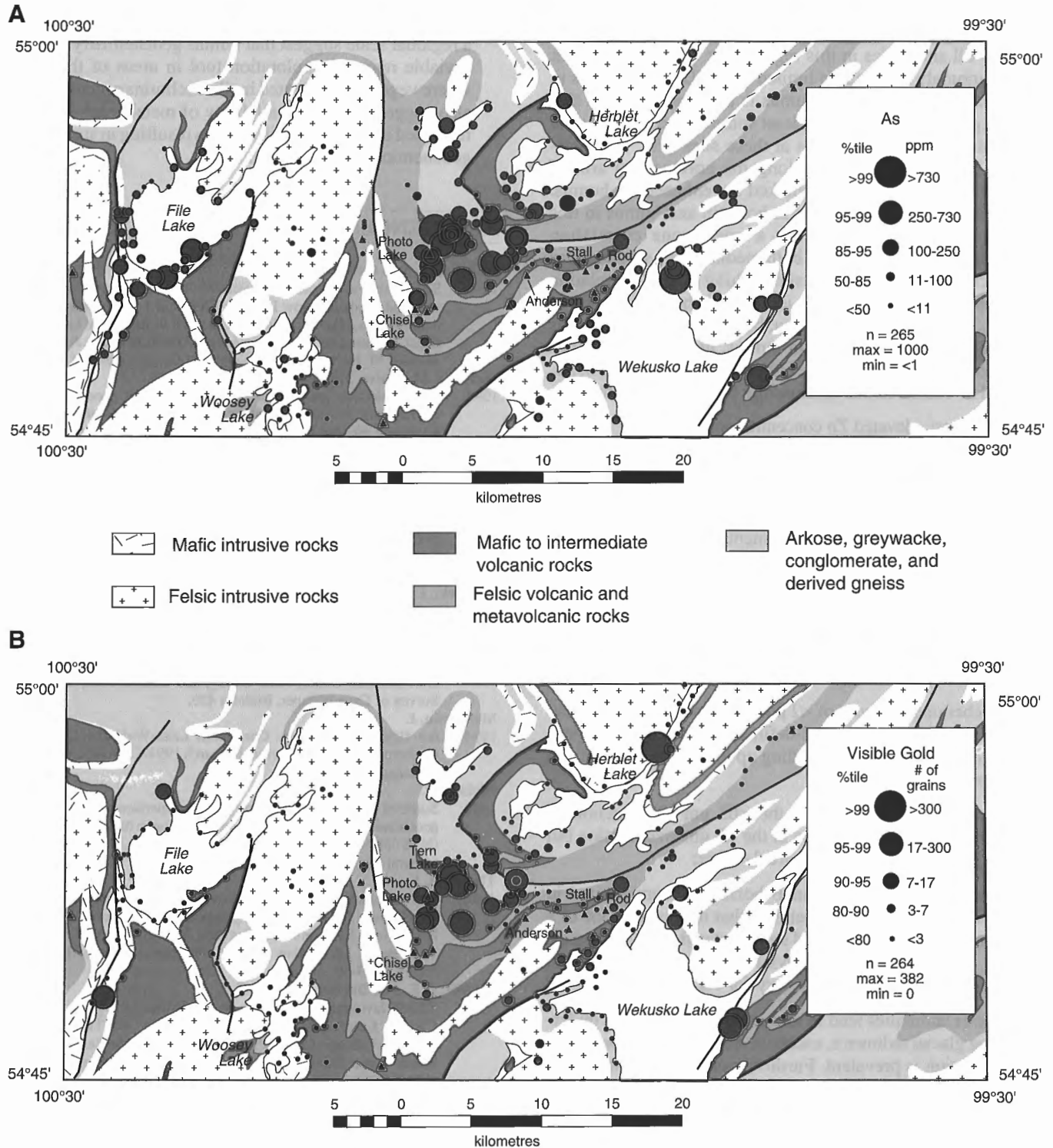


Figure 12. Regional distribution of A) As in the $<2\ \mu\text{m}$ size fraction of C-horizon till; and B) visible gold (VG) grains extracted from the heavy mineral fraction of C-horizon till.

C-horizon till. The 1990 sampling program focused on areas of road access in the central part of the map area, coinciding with the occurrence of the main past and present volcanic-hosted massive sulphide-producing deposits in the region. Consequently, humus data are limited in these areas.

In general, there is a good correlation between anomalies in humus and those identified in C-horizon till (Fig. 9 and 10). Anomalous concentrations of Cu in humus occur at two sites immediately north of Chisel Lake, corresponding with well defined till anomalies in this region (Fig. 9). The definition of this anomaly in humus is limited by the lack of samples in this area. Unlike till, Zn in humus is also anomalous in this region, possibly suggesting at least some element of airborne contamination from road dust at these sites (Fig. 10). Elsewhere, Cu anomalies in till along the northeastern arm of Herblet Lake are not only mimicked but enhanced in humus. Likewise, Zn anomalies occur in both till and humus in this region. Although there is not a one-to-one correlation between anomalous samples, both media define similar areas of enrichment. Several other sites exhibit a good correlation between anomalies observed in till and those observed in humus. In the Woosey Lake area, both Cu and Zn anomalies observed in till are repeated in humus, as are Zn anomalies observed in the File Lake area. Other elements such as Pb, As, Hg, and Sb exhibit similar relationships between till and humus.

In contrast, elevated Zn concentration in till along the west shore of Wekusko Lake are not observed well in humus (Fig. 10). These till anomalies are thought to represent elevated background concentration associated with carbonate till in this area. The subdued response in humus may indicate that Zn is less bio-available in calcareous environments (Thornton, 1986).

CONCLUSIONS AND RECOMMENDATIONS

Detailed examination of the geochemical signature of surficial sediments in the Snow Lake area indicates:

1. geochemical analysis of <2 µm size fraction of C-horizon till produces large, well-defined and predictable geochemical anomalies, extending up to 2 km down-ice from source;
2. geochemical anomalies in the <63 µm size fraction of C-horizon till mimic those in the <2 µm size fraction but are limited in contrast and areal extent;
3. geochemical anomalies in B-horizon till are limited in areal extent and exhibit patterns that may reflect one or a combination of glacial and surface weathering processes. As a result, element behaviour is not predictable and geochemical patterns may vary for each element;
4. humus anomalies tend to mimic those observed in underlying glacial sediments, except in areas where airborne contamination is prevalent. Further, more rigorous statistical analysis is required to firmly establish these relationships;
5. a multi-element Cu, Hg, Pb, As, Au, and Sb anomaly occurs north of Chisel Lake, encompassing the Photo Lake deposit. The Cu-Au association observed in till in this area, is consistent with known mineralization;

6. the ratio of Zn/Cu and Cu/Zn clearly distinguishes between volcanic assemblages hosting Cu-rich mineralization and those characterized by Zn-rich deposits;
7. numerous multiple and single sample multi-element anomalies such as those along the northeast arm of Herblet Lake and along the shore of Woosey Lake remain to be investigated;
8. observed correlation between humus and till anomalies on a regional scale suggest that humus geochemistry may be a viable regional exploration tool in areas of thin drift where vegetation is rooted in till. Preliminary conclusions also suggest that bio-availability of metals may be more restricted in alkaline environments resulting in suppressed geochemical responses in humus.

REFERENCES

- Bailes, A.H. And Galley, A.G.**
1996: Setting of Paleoproterozoic volcanic-hosted massive base metal sulphide deposits, Snow Lake; in EXTECH I: A Multidisciplinary Approach to Massive Sulphide Research in the Rusty Lake-Snow Lake Greenstone Belts, Manitoba, (ed.) G.F. Bonham-Carter, A.G. Galley, and G.E.M. Hall, Geological Survey of Canada, Bulletin 426.
- Hall, G.E.M., Vaive, J.E., Beer, R., and Hoashi, M.**
1996: Phase selective leaches for use in exploration geochemistry; in EXTECH I: A Multidisciplinary Approach to Massive Sulphide Research in the Rusty Lake-Snow Lake Greenstone Belts, Manitoba, (ed.) G.F. Bonham-Carter, A.G. Galley, and G.E.M. Hall, Geological Survey of Canada, Bulletin 426.
- Kaszycki, C.A.**
1986: Surficial geology and till geochemistry, Lynn Lake-Leaf Rapids region, Manitoba; in Current Research, Part B, Geological Survey of Canada, Paper 86-1B, p. 245-256.
1989: Surficial geology and till composition, northwest Manitoba; Geological Survey of Canada, Open File 2118, 48 p.
- Kaszycki, C.A. And Hall, G.E.M.**
1996: Application of phase selective and sequential extraction methodologies in surficial geochemistry; in EXTECH I: A Multidisciplinary Approach to Massive Sulphide Research in the Rusty Lake-Snow Lake Greenstone Belts, Manitoba, (ed.) G.F. Bonham-Carter, A.G. Galley, and G.E.M. Hall, Geological Survey of Canada Paper, Bulletin 426.
- McMartin, I.**
1994: Ice flow events in the Cormorant Lake-Wekusko Lake area, northern Manitoba; in Current Research 1994-C; Geological Survey of Canada, p. 175-182.
- Nielsen, E.**
1992: Surficial geology mapping and glacial dispersion studies as aids to geochemical exploration and mineral tracing in the Elbow Lake area (NTS 63K/15); in Report of Activities, Manitoba Energy and Mines, Mineral Division, 1992, p. 52-55.
- Thornton, I.**
1986: Soil and plant factors that influence element availability and uptake: implications for geochemical prospecting; in Mineral Exploration Biological Systems and Organic Matter, (ed.) D. Carlisle, W.L. Berry, I.R. Kadan, and J.R. Watterson; Prentice-Hall, New Jersey, p. 47-59.
- Wright, D.F. And Bonham-Carter, G.F.**
1996: VHMS favourability mapping with GIS-based integration models, Chisel Lake-Anderson Lake area; in EXTECH I: A Multidisciplinary Approach to Massive Sulphide Research in the Rusty Lake-Snow Lake Greenstone Belts, Manitoba, (ed.) G.F. Bonham-Carter, A.G. Galley, and G.E.M. Hall, Geological Survey of Canada, Bulletin 426.

Contribution to the 1989-1994 Rusty Lake-Snow Lake Mining Camps, Canada-Manitoba Exploration Science and Technology Initiative (EXTECH I)

Application of phase selective and sequential extraction methodologies in surficial geochemistry

C.A. Kaszycki¹ and G.E.M. Hall²

Kaszycki, C.A. and Hall, G.E.M., 1996: *Application of phase selective and sequential extraction methodologies in surficial geochemistry; in EXTECH I: A Multidisciplinary Approach to Massive Sulphide Research in the Rusty Lake-Snow Lake Greenstone Belts, Manitoba, (ed.) G.F. Bonham-Carter, A.G. Galley, and G.E.M. Hall; Geological Survey of Canada, Bulletin 426, p. 155-168.*

Abstract: Phase selective and sequential extraction techniques have been used to identify the residence sites of metals in a variety of surficial materials and to characterize different types of surficial geochemical anomalies. Based on analysis of C-horizon till, B-horizon till, and humus samples collected at each of approximately 65 sites in the Chisel Lake area, three different types of geochemical anomalies have been characterized. Firstly, *mineralogenic* anomalies, created by glacial erosion and transport are typified by uniformly high concentrations of Zn, Cu, Fe, and Mn in all crystalline mineral phases of the B- and C-horizon tills, except exchangeable metals and carbonate. Secondly, *hydromorphic/biogeochemical* anomalies are characterized by elevated concentrations of Zn, Cu, Fe, and Mn within the exchangeable metal and Fe/Mn hydrous oxide phases of B-horizon till and "insoluble organic" residue of humus. These metals are also highly concentrated within the soluble organic phase of humus. Thirdly, *surface contamination* is reflected in anomalous concentrations of Zn in the sulphide phase within the insoluble organic residue of humus. The presence of sulphide within this phase suggests airborne contamination related to mine dust from tailings and open pit mining operations.

Résumé : Les techniques de lixiviation sélective et séquentielle des phases ont été utilisées pour localiser les sites de séjour des métaux dans divers matériaux superficiels et pour caractériser différents types d'anomalies géochimiques superficielles. Trois différents types d'anomalies géochimiques ont été identifiés sur la base de l'analyse d'échantillons de till d'horizon C, de till d'horizon B et d'humus prélevés à chacun des 65 sites de la région du lac Chisel. Il y a d'abord les anomalies *minéralogiques* découlant de l'érosion et du transport glaciaire, qui sont représentées par des concentrations uniformément élevées de Zn, Cu, Fe et Mn dans toutes les phases minérales cristallines des tills des horizons B et C, à l'exception de la phase métallique à cations échangeables et de la phase des carbonates. Il y a ensuite les anomalies *hydromorphes/biogéochimiques* qui sont caractérisées par des concentrations élevées de Zn, Cu, Fe et Mn dans la phase métallique à cations échangeables et la phase des oxydes hydratés de fer et de manganèse du till d'horizon B et les résidus de «matières organiques insolubles» de l'humus. Ces métaux sont en outre très concentrés dans la phase organique soluble de l'humus. Quant à la *contamination superficielle*, elle se traduit par des concentrations anormales de zinc dans la phase sulfurée des résidus de matières organiques insolubles de l'humus. La présence de sulfures dans cette phase incite à supposer une contamination aérienne liée aux poussières produites par les résidus miniers et les mines à ciel ouvert.

¹ Ontario Geological Survey, Ministry of Northern Development and Mines, 933 Ramsey Lake Road, Sudbury, Ontario P3E 6B5

² Geological Survey of Canada, 601 Booth St., Ottawa, Ontario K1A 0E8

INTRODUCTION

One of the primary objectives of the till geochemistry program of the Exploration Technology Working Group (EXTECH) was to develop new analytical approaches for the identification of volcanic-hosted massive sulphide deposits. Part of this program involved the development of a series of phase selective extractions that can assist in refining the geochemical signature of base metal mineralization in different surficial media. A second objective of this work was to develop a comprehensive sequential extraction scheme, designed to identify the residence sites of metals within surficial materials. The identification of the main binding sites of trace metals not only enhances our understanding of near surface geochemical processes but also enables the discrimination of various sources of metal in the environment (e.g., atmospheric deposition, hydromorphic transport, glacial dispersal), and the estimation of potential element mobility, including bioavailability. This discussion will focus primarily on the application of sequential extraction methodologies in a surficial geochemistry study of volcanic-hosted massive sulphide mineralization in the Chisel Lake area, northwestern Manitoba.

Regional setting

The EXTECH study area encompasses two 1:50 000 NTS scale map sheets: NTS 63K/16 and NTS 63J/13, roughly centred on the town of Snow Lake in northwestern Manitoba (Fig. 1). It is located at the eastern end of the Flin Flon metavolcanic belt, bounded by the Kisseynew Gneiss Belt to the north. Contact with Paleozoic rocks marks the southern

boundary of the study area. Mineralization in the Snow Lake area occurs within thick sequences of subaqueous volcanic rocks, associated mainly with felsic flows. Two distinct mineralizing events are recognized; one Cu-rich and the other Zn-rich. Both Cu-rich and Zn-rich deposits are spatially associated with rhyolite flow complexes and subvolcanic tonalite intrusions (Bailes and Galley, 1996).

The Chisel Lake study area encompasses a suite of four Zn-rich deposits including the Chisel Lake, Lost Lake, and Ghost Lake mines and the North Chisel deposit (Fig. 2A). All four deposits occur at the same stratigraphic interval, marked by the contact between felsic volcanic rocks (Ghost rhyolite and Powderhouse dacite) and overlying formations. Mineralization in this area is characterized by a high ratio of Zn:Cu (>10). The Chisel Lake deposit also contains significant amounts of Au (>2.0 g/t) (Bailes and Galley, 1996).

Quaternary geology of the Chisel Lake study area is characterized by a relatively simple depositional sequence consisting of thin till (<3 m) overlying bedrock. In low-lying areas, till may be capped by a thin to moderate thickness (<1 m to 3-4 m) of laminated silt and clay deposited in glacial Lake Agassiz. In general, till is characterized by a sandy to sandy-silty matrix and contains little to no carbonate. Clast content is variable and clast composition predominantly reflects local bedrock lithologies.

Regionally, a complex ice flow history can be recognized based on patterns of crosscutting striae observed at several sites (Fig. 1). The main regional ice flow event associated with Main Late Wisconsinian glaciation trends to the south-southwest (Kaszycki, 1989; Nielsen, 1992; McMartin, 1994). This is preceded by an earlier ice flow to the southeast and is followed by late glacial ice flows to the west and to the

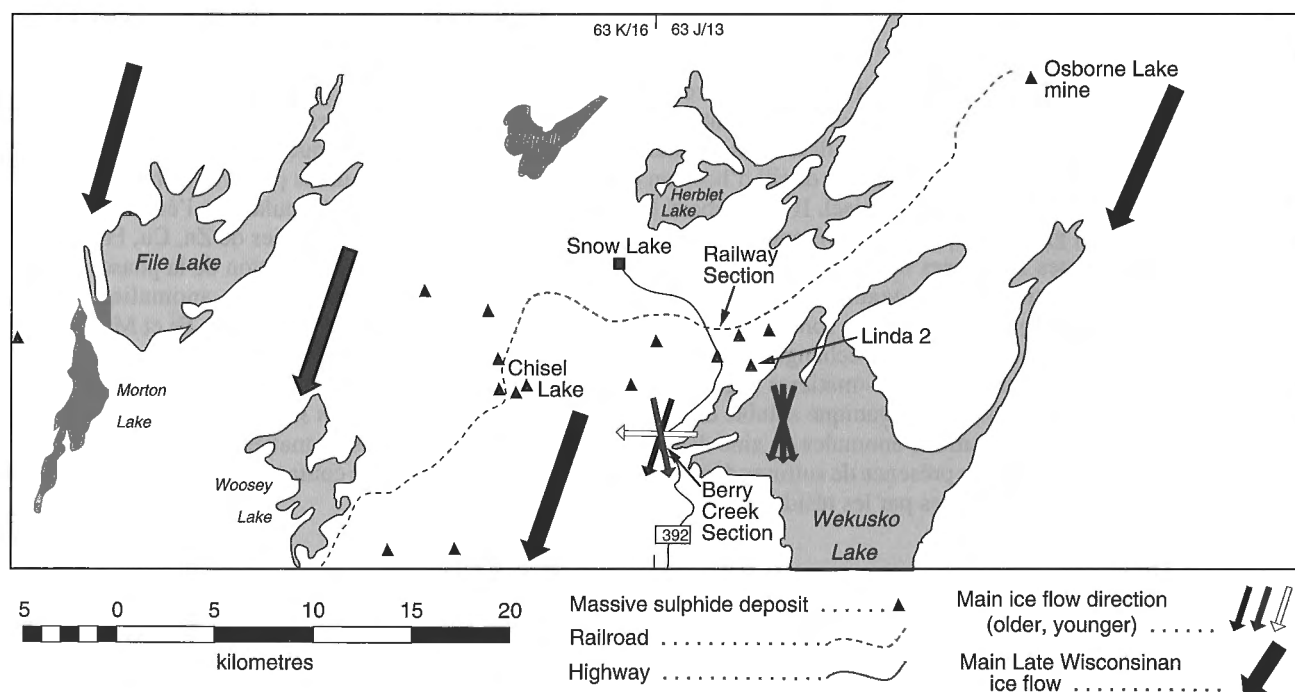


Figure 1. Mineral deposits and major ice flow directions in the Snow Lake study area.

southeast. In the Chisel Lake area, only the regional south-southwesterly ice flow event could be recognized in the striation record. It is unlikely that earlier or later ice flow events had a significant impact on glacial dispersal in this region (Kaszycki et al., 1996).

Vegetation in the area is characterized by a typical boreal forest assemblage, including black spruce, jack pine, birch, poplar, alder, and labrador tea. Soils are generally poorly developed, ranging from immature podzols to groundwater podzols and peat bogs. These soil types are typical of those developed in coarse grained acidic parent materials in cool

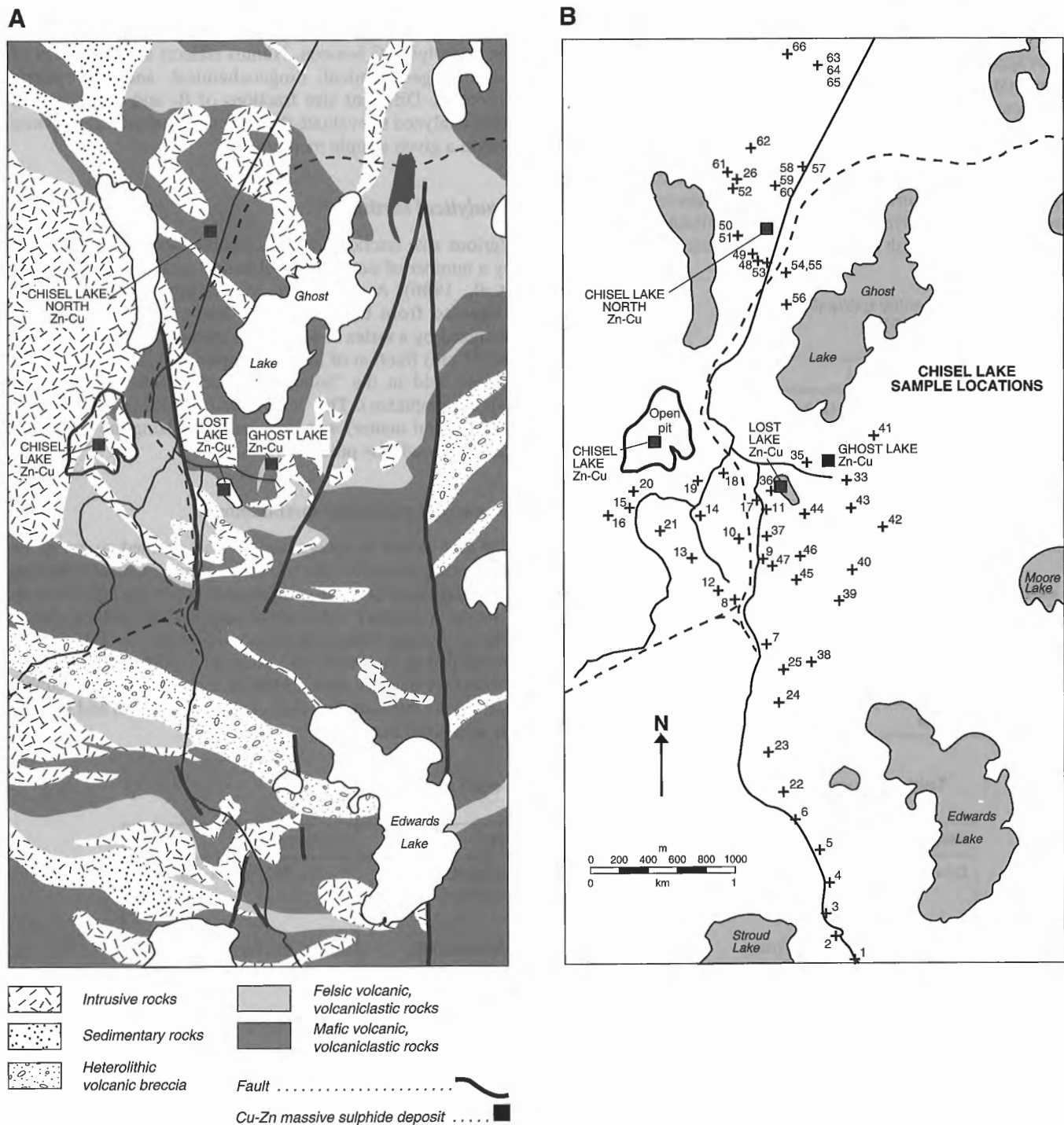


Figure 2. The Chisel Lake study area; A) bedrock geology, and B) sample site locations.

temperate climatic zones (Brady, 1974). Podzols and podzolic soils are characterized by a subsurface zone of accumulation of organic matter, and aluminum oxide with or without iron oxide.

METHODOLOGY

Field methods

The Chisel Lake study consists of 66 sample sites, extending from approximately 400 m north of the Chisel North deposit, to approximately 4 km south of the Chisel Lake, Ghost Lake, and Lost Lake deposits (Fig. 2B). At most sites, samples of C-horizon till, B-horizon till and humus were collected from hand-dug pits averaging 1 m in depth. C-horizon material is defined in this study as the soil horizon underlying the zone of maximum B-horizon development, characterized by a brownish grey to olive-grey colour, and exhibiting little to no mottling with reddish brown to orange ferric oxide. In this

Table 1. Sequential extraction scheme (after Hall et al. 1996).

| Extractant | Phase dissolved |
|---|---|
| 1M NaO Ac.HoAc pH 5 | Carbonates, adsorbed and exchangeable metals (AEC) |
| 0.25M NH ₂ OH.HCl in 0.25M HCl | Amorphous oxyhydrates of Fe and Mn |
| 1M NH ₂ OH.HCl in 25% HoAc | Crystalline Fe oxides (e.g. haematite, goethite, magnetite, maghemite, lepidocrocite) |
| KClO ₃ /HCl for 0.5 h, followed by 4M HNO ₃ at 90°C | Sulphides, organic matter |
| HF/HClO ₄ /HNO ₃ /HCl | Silicates, residual crystalline fraction |
| Ac.HoAc = acetate | |

'upper' C-horizon, sulphide minerals have generally been oxidized and carbonate may or may not have been leached by surface weathering processes. An attempt was made to collect humus from the organic layer directly overlying the C-horizon sample to ensure comparable results.

In general, samples of C-horizon till reflect primary glacial erosion and transport of underlying bedrock. B-horizon till samples have been subjected to secondary chemical processes in the near-surface weathering environment and as a result may be enriched or depleted in base metals relative to the underlying C horizon. Humus reflects a combination of surficial geochemical, biogeochemical, and atmospheric processes. Different size fractions of B- and C-horizon till were analyzed to evaluate the optimal geochemical response within a given sample medium.

Analytical methods

Various size fractions of each sample media were analyzed by a number of standard geochemical techniques (Kaszycki et al., 1996). A subsplit of the <2 µm size fraction was extracted from both B- and C-horizon till samples and analyzed by a series of sequential extractions. The <80 mesh (<177 µm) fraction of humus samples was first analyzed for metals held in the "soluble organic" fraction (humic and fulvic complexes). The "insoluble organic" residue (humin and mineral matter) was then analyzed using the sequential extraction scheme presented below.

Sequential extraction methodology

For this initial investigation, it was decided to focus on attempting to resolve the residence sites of metals reflecting secondary near-surface geochemical processes and those reflecting a primary lithological response to mineralization. The sequential extraction scheme illustrated in Table 1 was developed by Hall et al. (*this volume*) as part of the EXTECH project. A detailed description of methodology and quality control are presented by Hall et al. (*this volume*) and will not be addressed here.

Table 2. Summary of trace element data reported for each sample site.

| Sample media | Fraction | Mineral phase analyzed | Elements |
|----------------|-----------------------------|--|------------------------------------|
| C-horizon till | <2 µm (clay) | AEC, amorphous oxide/hydroxide, crystalline Fe oxide, sulphide/organics, silicate/residual oxide | Cu, Zn, Pb, Fe, Mn, Co, Ni |
| B-horizon till | <2 µm (clay) | AEC, amorphous oxide/hydroxide, crystalline Fe oxide, sulphide/organics, silicate/residual oxide | Cu, Zn, Pb, Fe, Mn, Co, Ni |
| Humus | "soluble organics" | | Cu, Zn, Pb, Fe, Mn, Co, Ni, C, LOI |
| | "insoluble organic" residue | AEC, amorphous oxide/hydroxide, crystalline Fe oxide, sulphide/organics, silicate/residual oxide | Cu, Zn, Pb, Fe, Mn, Co, Ni |

It was hypothesized that secondary concentration or depletion of elements in the near-surface environment should be reflected in the adsorbed/exchangeable cation phase and the hydrous Fe- and Mn-oxide phase (referred to as "labile" phases), and perhaps to some degree in the crystalline Fe oxide phase of surface sediments. Current theory suggests that the geochemical response to mineralization in the labile phases should be enhanced by adsorption and coprecipitation of metals associated with secondary oxides, hydroxides, and other weathering products (Antropova et al., 1992). A primary, lithologically-controlled response to mineralization should be reflected in the geochemistry of at least a portion of the crystalline Fe oxide phase (e.g., magnetite), the sulphide/organic phase and the silicate/residual oxide phase. It must be appreciated that results obtained by sequential extraction procedures are "operationally-defined" and absolute selectivity is not assumed. For example, any "soluble organic" component of B-horizon till will report to the amorphous Fe/Mn oxide phase, unless extracted earlier using pyrophosphate solution.

The relative contribution of metals from phyllosilicate minerals, a third mineral phase reflecting mineralization, has not been assessed. It is felt that at least some, if not all

phyllosilicate minerals, are attacked fairly early in the extraction sequence, likely contributing to element concentrations reporting to the first two labile phases of the scheme (Table 1). Trace element concentration of phyllosilicate minerals should reflect to some degree geochemical patterns related to alteration associated with volcanic-hosted massive sulphide deposits (chloritization and sericitization). Further work assessing residue mineralogy following each extraction is required to determine the relative contribution of phyllosilicate minerals reporting to the various mineral phases analyzed.

RESULTS

Table 2 summarizes the trace element data reported for each sample site. Total concentrations represent the sum of element concentrations determined for each of the five individual extractions. Because of the large number of analyses per site (134) it was most efficient to summarize the data in graphical form to identify systematic relationships in element concentrations between mineral phases and sample media. Figure 3 illustrates the graphical presentation used to interpret data in

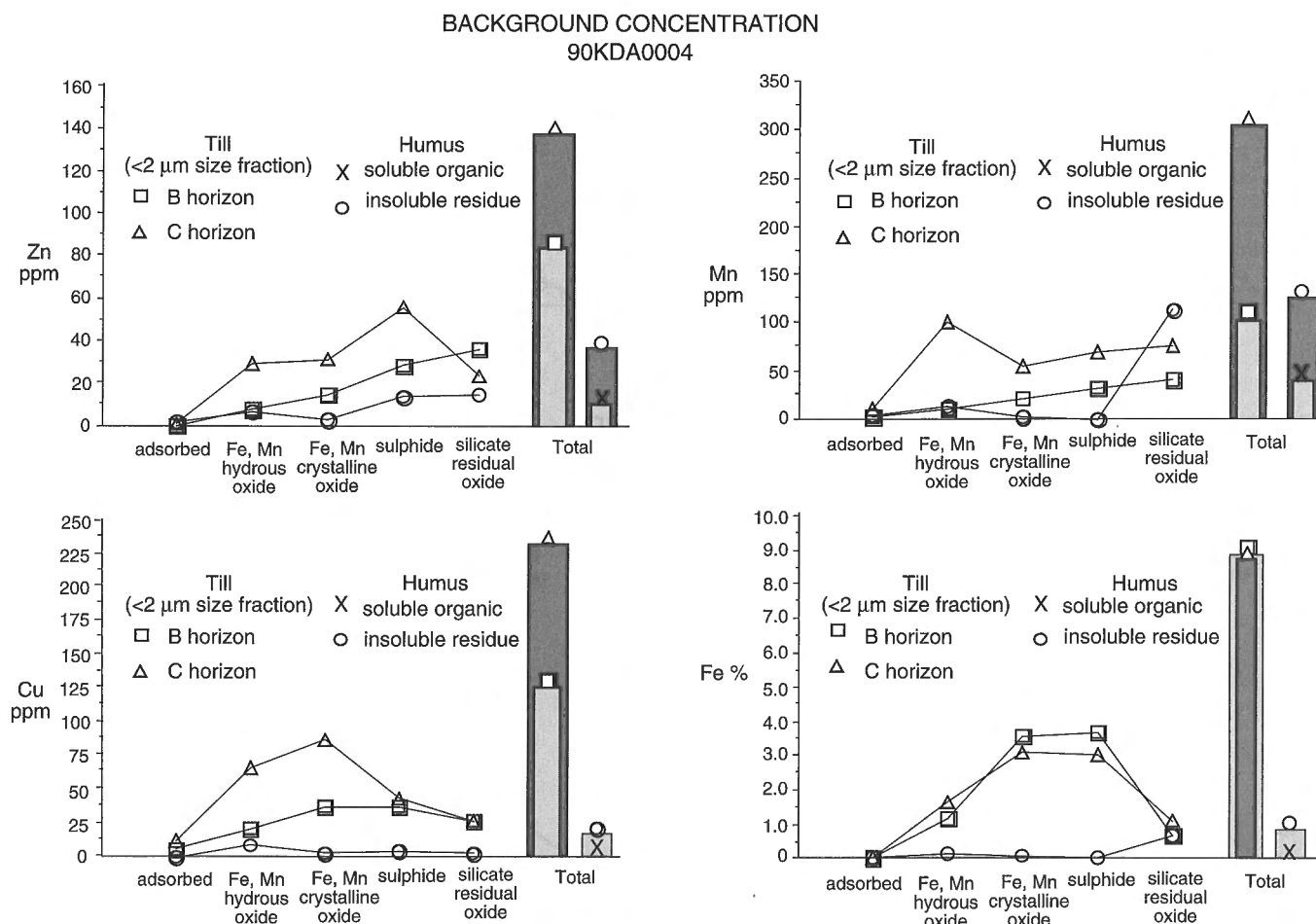


Figure 3. Background concentrations of Zn, Cu, Mn, and Fe for each mineral phase and sample media analyzed. Bar graphs represent the relationship between total (summed) metal concentrations in B- and C-horizon till, and soluble and insoluble organic fractions of humus.

this study. Element concentrations are graphed against mineral phase for each of the three media studied. This enables immediate visual identification of trends within a given sample and between sample media at each site. Bar graphs illustrate the relationship between total (summed) metal concentrations in B- and C-horizon till, and soluble and insoluble organic fractions of humus. Similar graphs were constructed for each of the 66 sites sampled, and consistent patterns and trends amongst sample sites were identified. Zinc exhibits the most consistent and readily identified trends from site to site. This reflects the high concentrations of Zn in all surface media, typical of the response to mineralization in this area (Kaszycki et al., 1996). In addition, Zn is very mobile in the near surface environment, enabling patterns related to secondary near-surface geochemical processes to be identified. Typically, Cu exhibits similar but more subdued

responses than Zn, reflecting their relative mobility and abundance in the mineralized environment. The trends exhibited by Fe and Mn are not always consistent with those observed for Cu and Zn. This may reflect a more significant contribution of Fe and Mn from phyllosilicates.

Background element concentrations

The distributions of Zn, Cu, Mn, and Fe at a site representative of background conditions are presented in Figure 3. In this region, background concentrations reflect primary glacial erosion and transport of nonmineralized bedrock. The soluble organic fraction of humus is significantly depleted in Zn, Cu, Mn, and Fe relative to underlying B- and C-horizon till, suggesting very little secondary hydromorphic or biogenic dispersion.

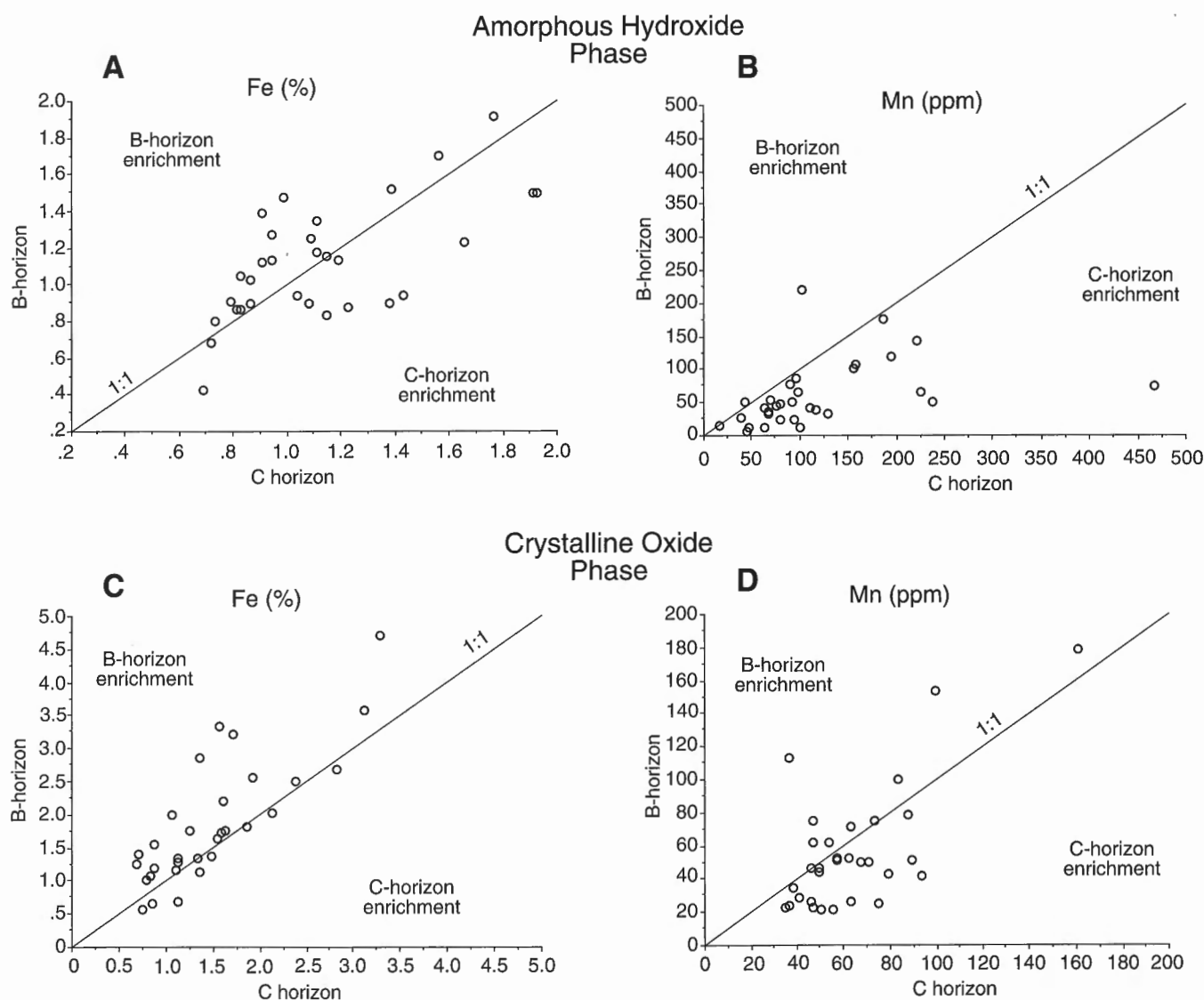


Figure 4. Fe and Mn concentrations in the amorphous hydroxide and crystalline oxide phases of B-horizon versus C-horizon till. Line represents 1:1 relationship.

Adsorbed, exchangeable, carbonate phases (AEC)

Concentrations of Zn, Cu, Mn, and Fe in the AEC phase are very low in all media. This is somewhat unexpected considering all analyses were performed on the $<2\ \mu\text{m}$ (clay) size fraction of these samples. Previous studies comparing the trace element concentration of the $<2\ \mu\text{m}$ size fraction and heavy mineral fraction of till have suggested that trace elements, liberated as sulphide minerals are oxidized from the heavy mineral fraction, and adsorbed onto exchange sites in the clay fraction (Shilts, 1976). In contrast, observed relationships in the Chisel Lake area suggest that very little metal is held at exchange sites. This may reflect more acidic surface conditions at Chisel Lake. Here, till is noncalcareous and trace metals released by oxidation of sulphides likely remain in solution and are transported out of the system. Alternatively, trace elements released by weathering of sulphides may

coprecipitate with amorphous hydrous oxides, rather than occupy exchange sites on oxide surfaces (Plant and Raiswell, 1983).

Amorphous Fe/Mn hydroxide and crystalline Fe oxide phases

In general, C-horizon till is enriched in Zn, Cu, and Mn in the hydrous and to a lesser extent crystalline oxide phases. At site 4 (Fig. 3), Mn reporting to the hydrous oxide phase is significantly enriched in the C-horizon, whereas Fe is more evenly distributed between the two. Scatter plots of Fe and Mn concentrations in B-horizon versus C-horizon tills illustrate these relationships for the entire Chisel Lake study area (Fig. 4). Iron is enriched in the B-horizon in the crystalline oxide phase, reflecting formation of secondary crystalline

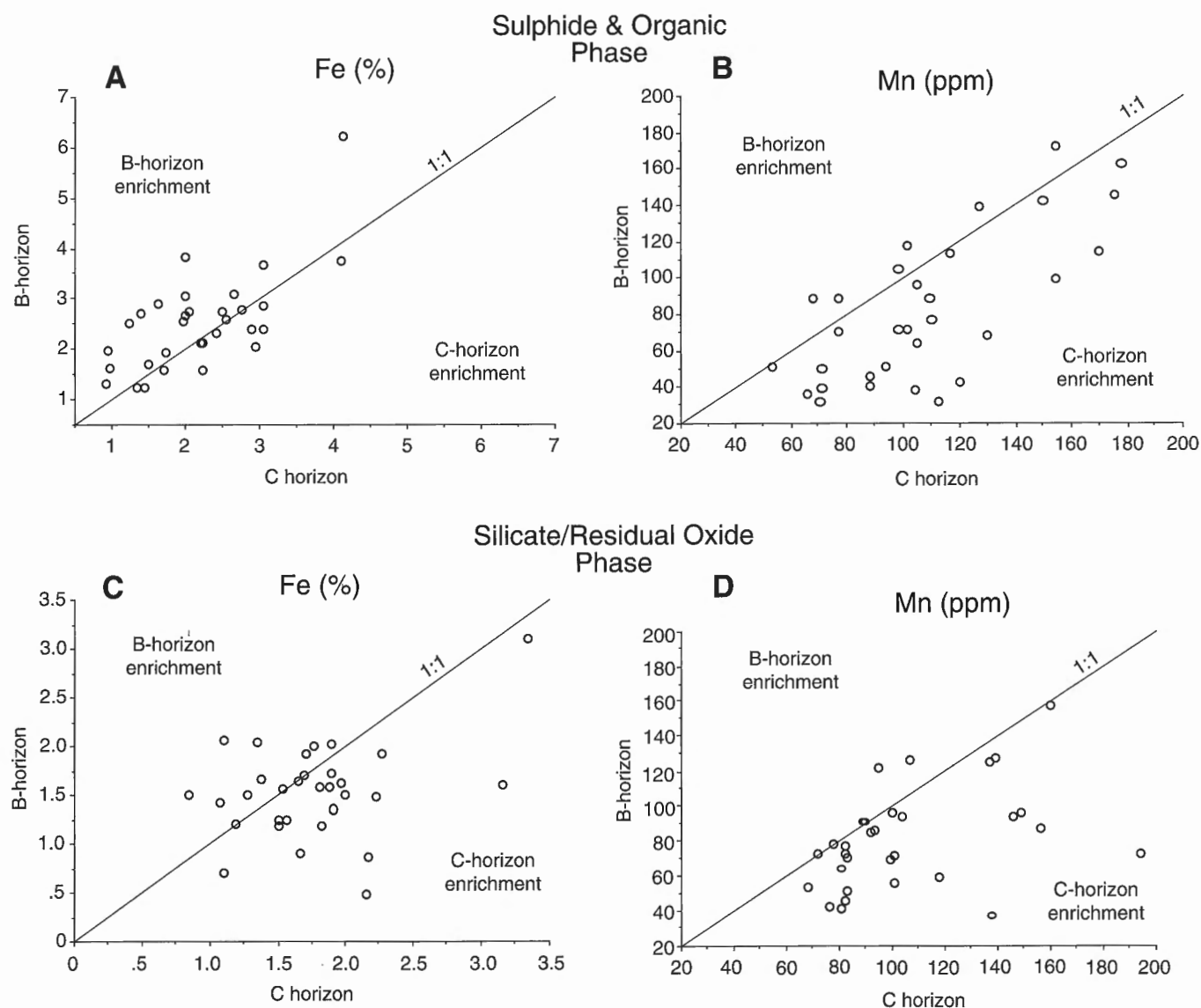


Figure 5. Fe and Mn concentrations in the sulphide/organic and silicate/residual oxide phases of B-horizon versus C-horizon till. Line represents 1:1 relationship.

oxides such as goethite and lepidocrocite (Fig. 4C). This trend is less well developed in the hydrous oxide phase with Fe-enrichment occurring in only 50% of B-horizon samples (Fig. 4A). Manganese in both the hydrous and crystalline oxide phases is depleted in the B-horizon (Fig. 4B, D), particularly in the former phase. These relationships suggest that, in general, the formation of hydrous oxides in B-horizon soils plays a minor role in concentrating trace elements in this area, supporting the interpretation that most element concentrations reflect primary lithological controls on till geochemistry. Manganese enrichment in the hydrous oxide phase of C-horizon till may reflect hydroxide formation associated with oxidation of sulphides (Plant and Raiswell, 1983). In addition, under acidic conditions, Mn and Cu are principally associated with organic complexes (Sposito, 1983). Depletion of these and other metals in the B horizon of podzolic soils in Tasmania (Baker, 1986) and Colorado (Curtin and King, 1986) has been attributed to organic complexing and transport of metals through the soil system. Baker (1986) confirms these observations experimentally and suggests that humic and fulvic acids may be the single most important

factor controlling metal mobility in the near-surface environment, allowing for transport of metals typically considered immobile as inorganic species.

Sulphide/organic and silicate/residual oxide phases

In the sulphide/organic phase, Fe once again exhibits a tendency toward enrichment in the B horizon. Conversely, Mn in this horizon is significantly depleted (Fig. 5A, B). The fact that this step in the extraction scheme is selective for sulphide and organics may suggest that elevated Fe concentrations in the B-horizon are associated with finely disseminated (non-labile) organic matter rather than sulphide. It is highly unlikely that any sulphide would have survived oxidation in the near-surface weathering environment. Heavy mineral concentrates extracted from C-horizon till did not contain any identifiable sulphide material, suggesting that even in the less severely oxidizing C-horizon environment sulphide minerals have been destroyed. Associated depletion of Mn in the B horizon suggests that Mn is mobile in this environment,

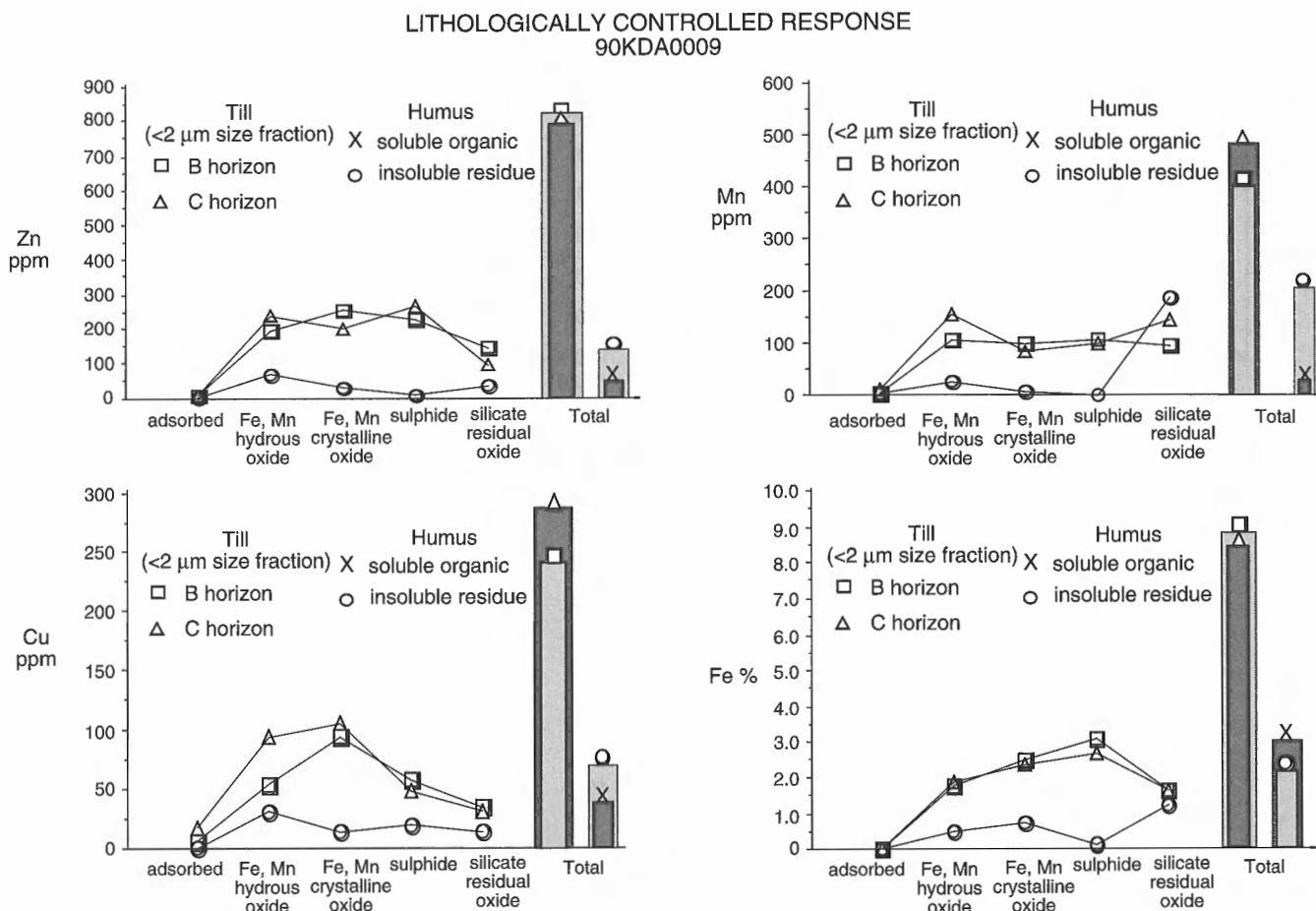


Figure 6. Geochemical signature of a primary lithologically controlled response to mineralization. Concentrations of Zn, Cu, Mn, and Fe are plotted against mineral phase for each of the three sample media analyzed. Bar graphs represent the relationship between total (summed) metal concentrations in B- and C-horizon till, and soluble and insoluble organic fractions of humus.

possibly moving through the soil system as chelates of humic and/or fulvic acids (Sposito, 1983). This interpretation is supported by the fact that Mn is depleted, to some degree, in all mineral phases of B-horizon till.

Primary lithologically controlled response to mineralization

Anomalous trace element relationships reflecting primary glacial erosion and transport (glacial dispersal) of mineralized bedrock are presented in Figure 6. At these sites, the distribution of trace metals reporting to various mineral phases are similar to those observed in background samples, with the exception that total abundances of Zn and Cu reflect mineralization. As before, little or no metal reports to the AEC phase, indicating no secondary accumulation. In general, Zn, Cu, Mn, and Fe are equally distributed among all mineral phases. Equivalent concentrations between B- and C-horizon samples also suggest little secondary accumulation. Elevated

concentrations of Cu and Mn in the hydrous oxide phase of C-horizon till again suggest oxidation of sulphides and coprecipitation of hydrous oxides metals in the C horizon.

Secondary accumulation in the near-surface environment

A geochemical signature interpreted to represent secondary accumulation of metal in the near-surface environment is present in Figure 7. At site 5, this type of anomaly is characterized by:

- anomalous concentrations of Zn in the soluble organic fraction of humus (4607 ppm);
- elevated concentrations of Zn and Mn in the AEC phase of B-horizon till and insoluble organic fraction of humus;
- elevated concentrations of Zn, Mn, and Fe in the hydrous oxide phase of B-horizon till;

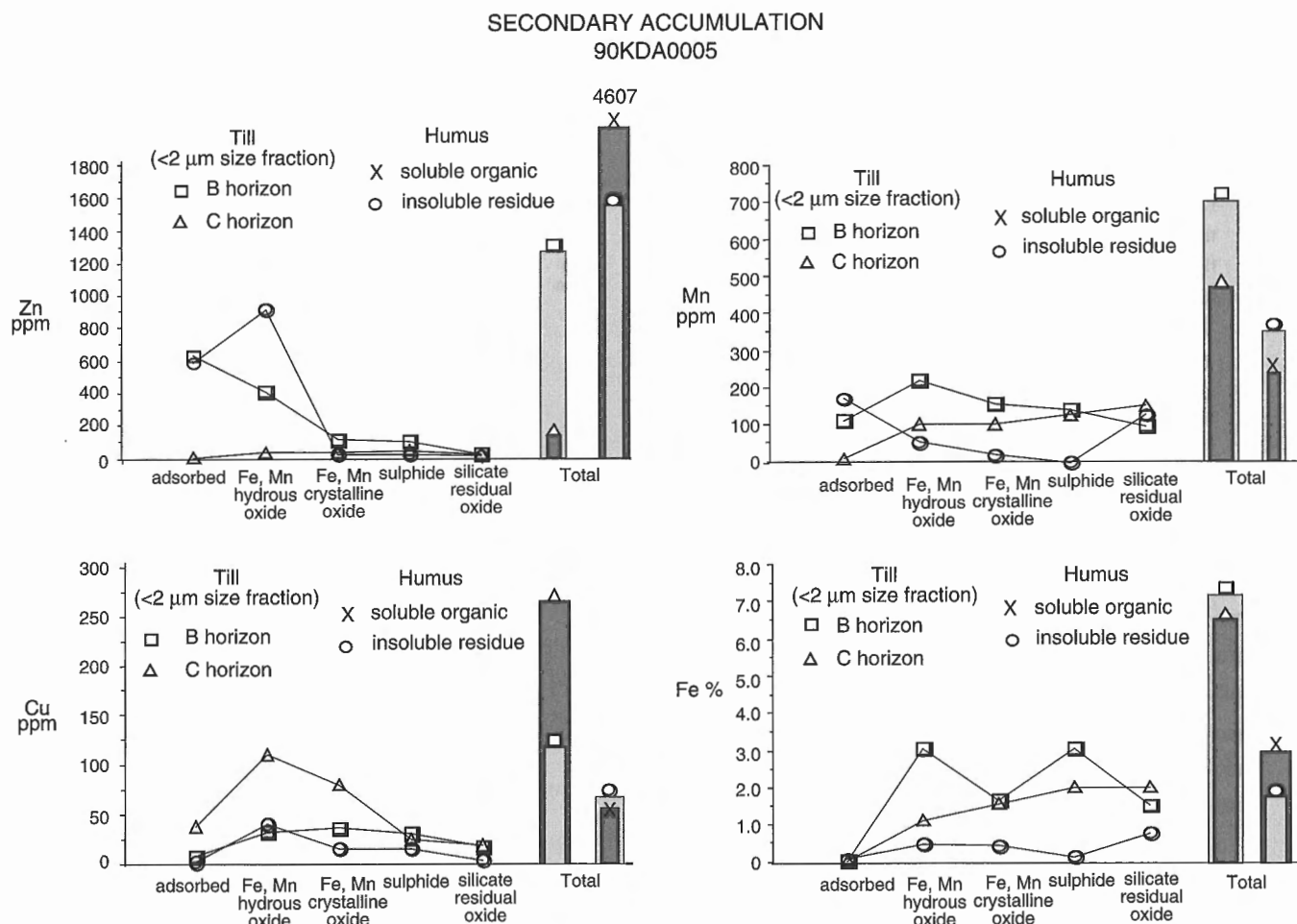


Figure 7. Geochemical signature of secondary metal accumulation in the near-surface environment. Concentrations of Zn, Cu, Mn, and Fe are plotted against mineral phase for each of the three sample media analyzed. Bar graphs represent the relationship between total (summed) metal concentrations in B- and C-horizon till, and soluble and insoluble organic fractions of humus.

- d) elevated concentrations of Cu and Zn in the hydrous oxide phase of insoluble organic fraction of humus;
- e) elevated concentrations of Cu in the AEC and hydrous oxide phases of C-horizon till.

These sites tend to occupy more poorly drained positions in the landscape and are characterized by poorly developed B horizons and thicker more well developed humic horizons.

Adsorbed and exchangeable cations (AEC)

In contrast to element relationships observed for background concentrations and primary responses to mineralization, secondary anomalies are characterized by pronounced accumulations of metals in all labile mineral phases. Anomalous concentrations of Zn in the soluble organic fraction suggest that Zn is effectively being fixed by organic compounds, specifically humic and fulvic acids generated by decay within the humus horizon. Zinc and manganese concentrations are also elevated in the AEC phase of B-horizon till, likely indicating translocation of metal from the humus horizon as chelates of humic and fulvic acid. Cation-exchange from

metal-enriched soil solutions in contact with clay minerals and amorphous hydroxides would enhance metal concentration in this phase.

Amorphous hydroxides and crystalline oxides

At site 90KDA0005 (Fig. 7), Cu is concentrated in the labile phases of C-horizon till, while Zn, Fe, and Mn are concentrated in the labile phases of B-horizon till. This partitioning of metals between soil horizons may reflect:

- a) preferred scavenging of Zn by amorphous Fe, Mn hydroxides in the B horizon. In general, Cu is thought to be more readily scavenged by Fe hydroxides than Zn (Levinson, 1980). In the presence of humic and fulvic acids however, Cu may remain in solution, while Zn is coprecipitated with Fe and Mn hydroxides (Sposito, 1983).
- b) enrichment of Cu in the C horizon. Precipitation of Cu may result from increased pH ($\text{pH} > 5$), as acid soil waters are neutralized by interactions with soil solids. Alternatively, Cu may be coprecipitated with hydroxides formed as a result of oxidation of sulphides, as observed in C-horizon till associated with lithologically controlled anomalies.

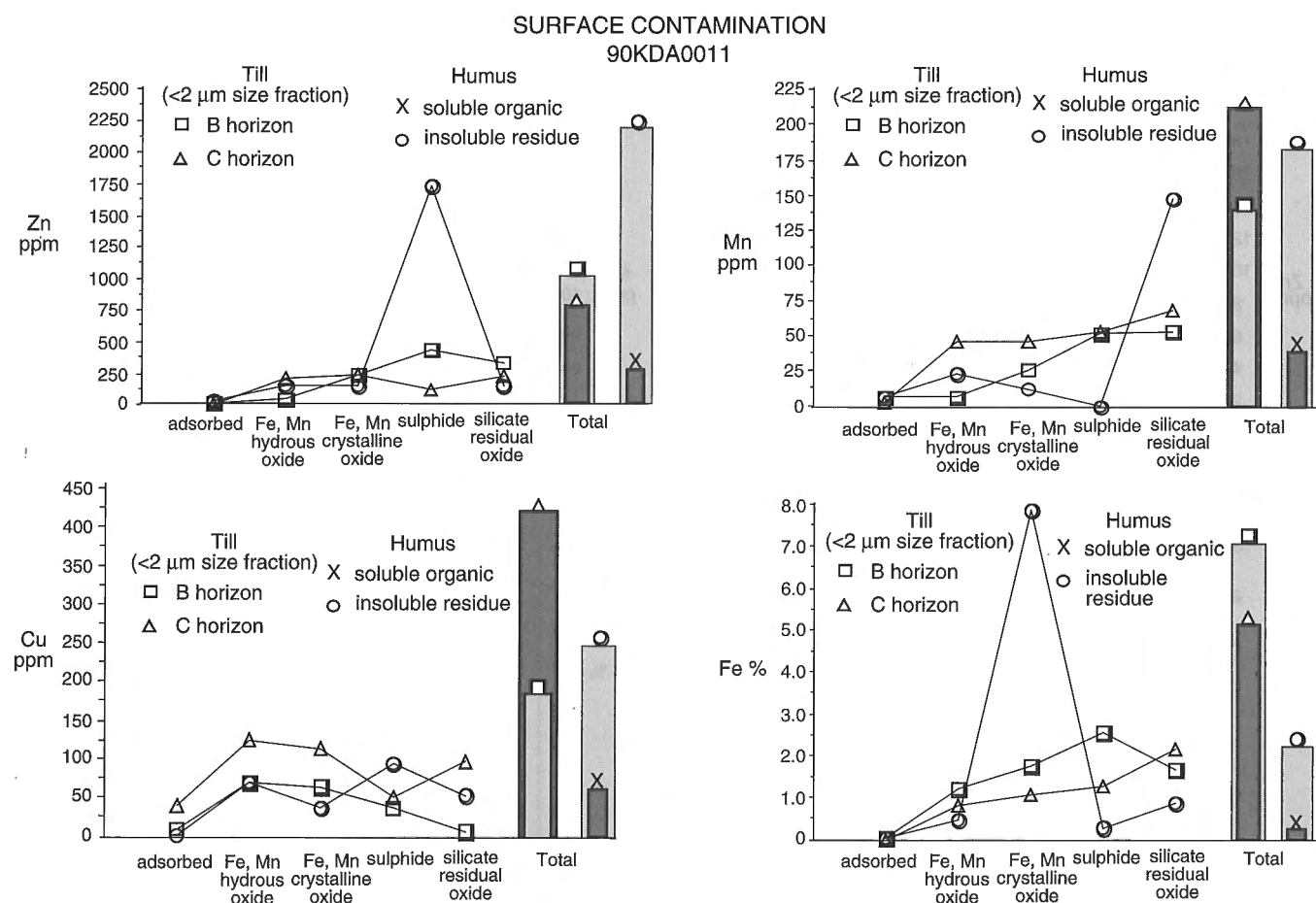


Figure 8. Geochemical signature of surface contamination. Concentrations of Zn, Cu, Mn, and Fe are plotted against mineral phase for each of the three sample media analyzed. Bar graphs represent the relationship between total (summed) metal concentrations in B- and C-horizon till, and soluble and insoluble organic fractions of humus.

Five other sites have been identified as exhibiting characteristics of secondary accumulation based on elevated concentrations of Zn in the labile phases of B-horizon till and insoluble organic fraction of humus. Not all these sites exhibit the same inter-relationships among Fe, Cu, and Mn as observed at site 5. Further work is required to characterize secondary accumulation of trace metals in all mineral phases and sample media.

Surface contamination

Surface contamination anomalies are characterized by anomalous concentrations of various trace elements in the insoluble organic fraction of humus (Fig. 8). These include:

- anomalous concentration of Zn in the sulphide phase;
- elevated concentration of Mn in the silicate phase; and
- anomalous concentration of Fe in the crystalline oxide phase.

Anomalous concentrations of these metals likely reflect airborne contamination related to mine dust from tailings piles and open operation at the nearby mines. At site 90KDA0011, Zn and Cu are also uniformly high throughout all phases of B- and C-horizon till except for the AEC phase. This suggests that the element concentrations in till reflect glacial dispersal, and that leaching of the surface contamination in humus in a downward direction is minimal.

DISTRIBUTION OF ANOMALIES

Element distributions at each site were classified according to anomaly type, as describe above. At some sites, trace element concentrations reflect the combined effect of two or more dispersion mechanisms. An attempt was made to resolve individual components of complex anomalies. In an effort to establish a geographic context for each type of anomaly, the distribution of anomaly types was mapped to provide an interpretive context for anomaly definition.

Glacial dispersal

Figure 9 illustrates the distribution of sample sites exhibiting characteristics attributed to glacial erosion and transport of mineralized debris. No attempt was made to scale relative concentrations from one site to another (see Kaszycki et al., 1996). Sample sites classified as glacial dispersal anomalies are clustered immediately south of the Ghost Lake-Lost Lake horizon and the Chisel Lake open pit. These anomalies extend approximately 1 km to the south-southwest of the deposits, parallel to the direction of glacial ice flow. This distribution confirms the interpretation of these anomalies as reflecting primary lithological till composition produced by glacial erosion and transport of mineralized debris.

Surface contamination

Sample sites with geochemistry reflecting surface contamination are clustered immediately south of the Ghost Lake-Lost Lake horizon and the Chisel Lake open pit (Fig. 10). In contrast to glacial dispersal anomalies however, the distribution of surface contamination anomalies trends toward the southeast, perpendicular to ice flow but parallel to prevailing wind direction. This corroborates the interpretation that

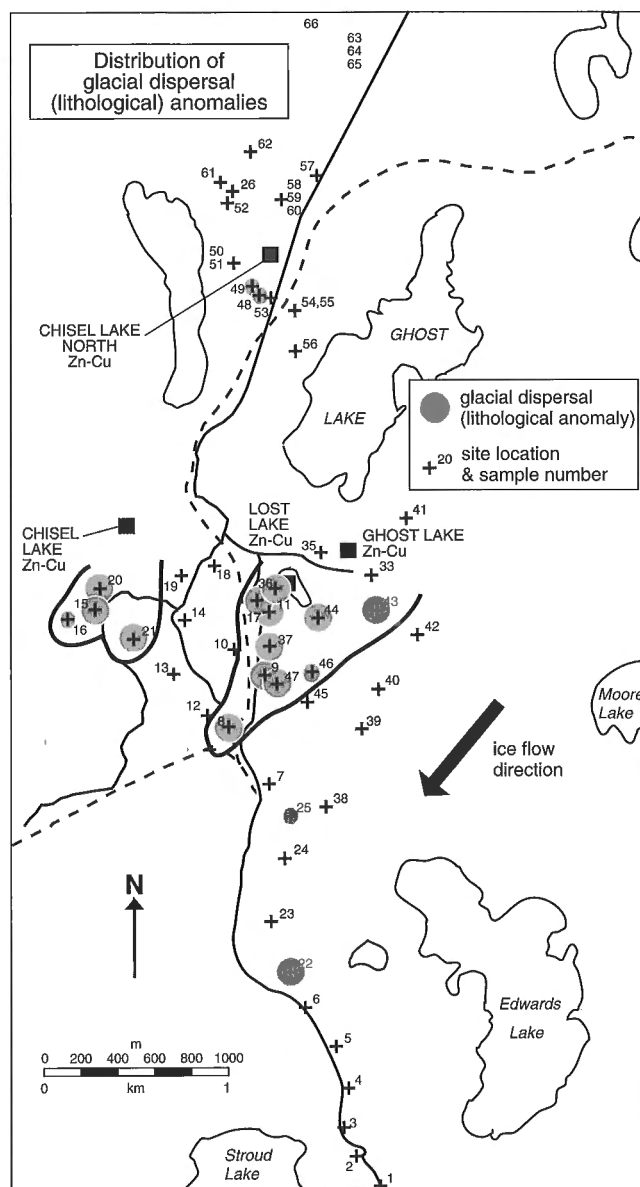


Figure 9. Distribution of lithologically controlled geochemical anomalies reflecting mineralization. Anomalies are clustered over the mineralized horizon and extend south-southwestward parallel to ice flow (glacial dispersal).

anomalous concentrations of Zn in the sulphide phase of the insoluble fraction of humus represent contributions from tailings dust and open pit mining operations. The concentration of Cu within the sulphide phase of humus exhibits only a slightly elevated concentration. This may reflect the relative concentrations of Zn and Cu within the ore itself, with a ratio of Zn:Cu ranging up to 20:1 (Bailes and Galley, 1996).

Anomalies reflecting secondary accumulation

The distribution of sites reflecting secondary accumulation of metals in the near-surface environment is sporadic (Fig. 11). Four sites are located over the ore zone and trend roughly east

following the strike of the ore horizon. The two remaining sites are located near the southern edge of the study area and are not related to mineralization. This sporadic distribution of secondary anomalies reflects the site-specific nature of near-surface geochemical processes particularly in an area of disrupted and discontinuous near-surface groundwater flow. Conditions favouring secondary accumulation of metals in the near-surface environment may exist for only brief periods of time throughout the course of a sampling season, and as such their geochemical response may be ephemeral in nature (Baker, 1986). Resolution of these anomaly types is therefore dependent on very site-specific factors that are not consistent from site to site. At most sites, B-horizon soil is depleted in

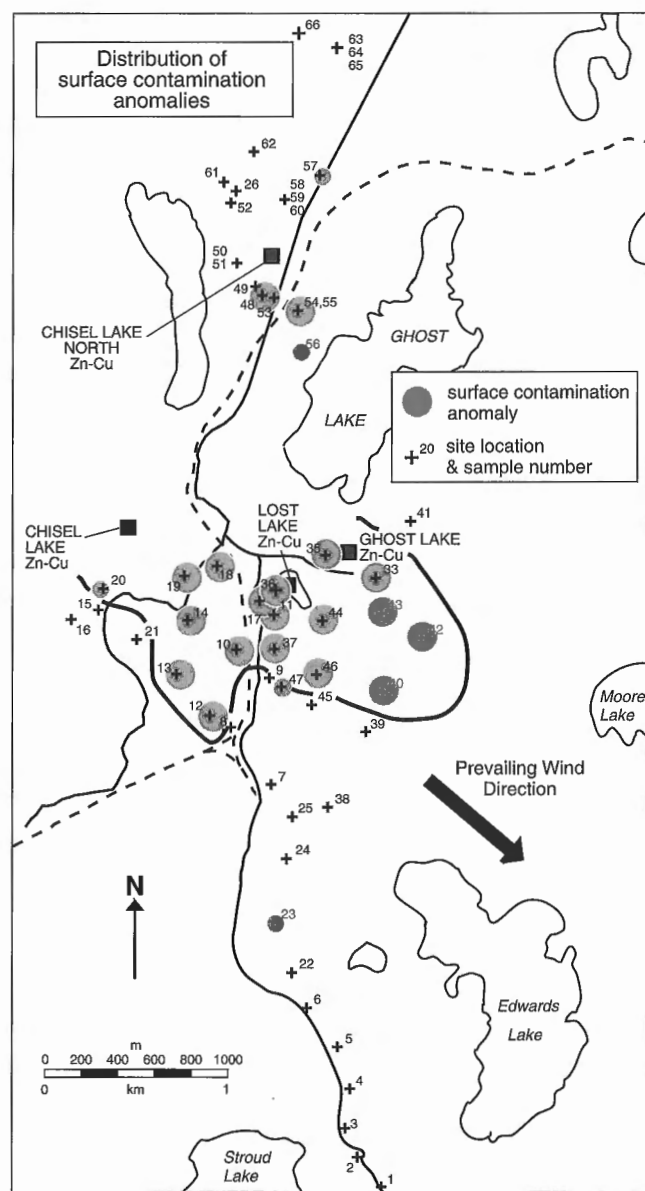


Figure 10. Distribution of surface contamination anomalies. These are clustered near the ore zone, but extend to the southeast, parallel to prevailing wind direction.

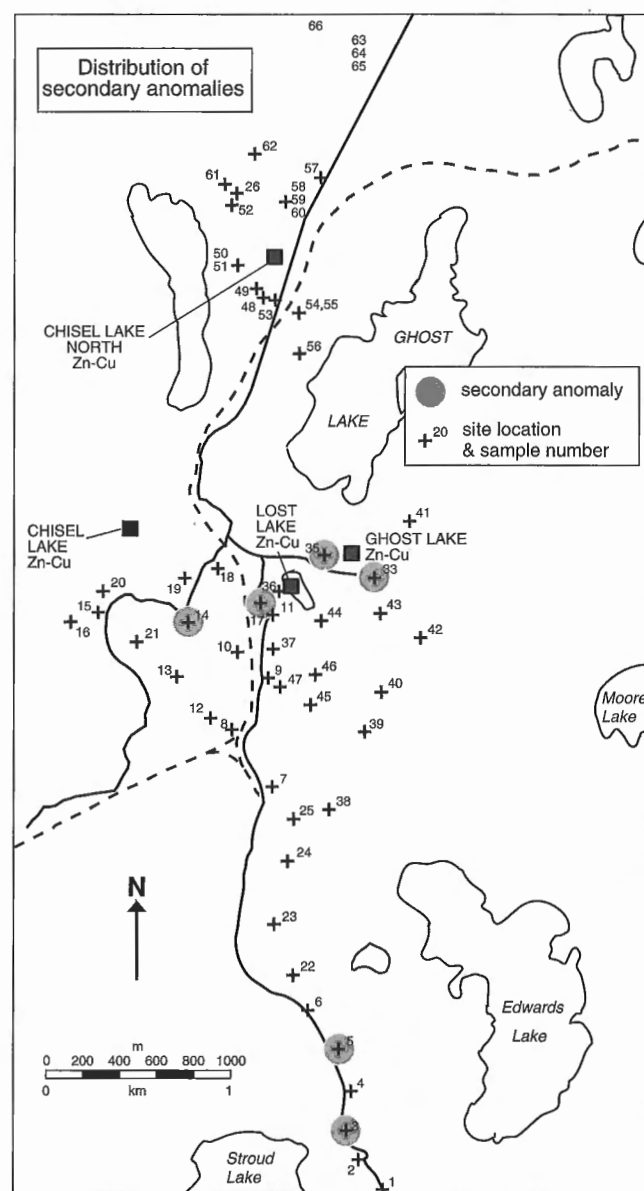


Figure 11. Distribution of anomalies reflecting secondary accumulation in the near-surface environment. These are sporadically distributed reflecting site-specific nature of near-surface geochemical processes.

trace metals rather than enriched, suggesting that the geochemical response to mineralization will not likely be enhanced in B-horizon samples (Kaszycki et al., 1996). Similar relationships have been observed in B-horizon soils in Colorado and Idaho (Curtin and King, 1986).

CONCLUSIONS AND RECOMMENDATIONS

1. Background concentrations of Zn, Cu, Fe, and Mn in most mineral phases reflect the primary mineralogical composition of B- and C-horizon till. Very little secondary metal accumulation has occurred as evidenced by very low concentrations of all elements in the soluble organic phase of humus and the AEC phase of B- and C-horizon till.
2. In general, Fe is enriched in the crystalline oxide phase of B-horizon till, while Mn is enriched in the amorphous hydroxide phase of C-horizon till. These relationships suggest that the formation of hydrous oxides plays a minor role in concentrating metals in the near-surface environment in this area. Enrichment of Mn in this mineral phase in the C-horizon likely reflects oxidation of sulphides and precipitation of hydroxides.
3. Organic complexes appear to play a major role in mobilizing trace metals throughout the soil profile, resulting in depletion of most metals in B-horizon till relative to C-horizon material.
4. Sites which do exhibit evidence of secondary accumulation of hydroxides and metals in the B horizon are rare and are characterized by elevated concentrations of metals in the soluble organic phase of humus and AEC and hydroxide phases of B-horizon till. These relationships likely reflect organic complexing in humus, transport of metals within organic compounds into underlying soil horizons, and cation-exchange from metal-enriched soil solutions in contact with clay minerals and hydroxides in the B horizon.
5. Surface contamination is recognized by elevated concentrations of Zn in the sulphide phase of the insoluble organic residue of humus. Coincident anomalies occur in the crystalline oxide phase for Fe and the silicate/residual oxide phase for Mn. The distribution of these anomalies exhibits a pronounced southeasterly trend parallel to prevailing winds suggesting airborne particulate contamination related to mine dust from tailings piles and open pit operations at nearby mines.
6. The observed relationships among element concentration, residence sites, and sample media (soil horizon) can be explained in terms of documented soil-forming processes, suggesting that the specificity of extractions for the various mineral phases is very good. However, further work assessing the residue mineralogy following each extraction is required to determine the relative contribution of phyllosilicate minerals reporting to the various phases analyzed.

7. Subsequent studies should also include a field evaluation of soil pH and Eh, to provide a better framework for interpretation of geochemical process. Studies should also be expanded to include sequential extraction studies in various types of surficial environment (e.g. alkaline, reducing, etc.).
8. Concurrent biogeochemical studies would augment discussion of the role of biological cycling of metals through the soil profile. Analysis of soil water chemistry particularly with respect to humic compounds would assist in defining the role of humic and fulvic acids in mobilizing and transporting metals out of the soil system.
9. Results of this study suggest that B-horizon samples do not produce enhanced geochemical anomalies that can be easily related to mineralization in this area. In general, the distribution of B-horizon anomalies is sporadic reflecting site-specific soil conditions that may vary throughout the course of a sampling season.

REFERENCES

- Antropova, L.V., Goldberg, I.S., Voroshilov, N.A., and Ryss, Ju.S.**
1992: New methods of regional exploration for blind mineralization: application in the USSR; *Journal of Geochemical Exploration*, v. 43, p. 157-166.
- Bailes, A.H. and Galley, A.G.**
1996: Setting of Paleoproterozoic volcanic-hosted massive base metal sulphide deposits, Snow Lake; in *EXTECH I: A Multidisciplinary Approach to Massive Sulphide Research in the Rusty Lake-Snow Lake Greenstone Belts, Manitoba*, (ed.) G.F. Bonham-Carter, A.G. Galley, and G.E.M. Hall; Geological Survey of Canada, Bulletin 426.
- Baker, W.E.**
1986: Humic substances and their role in the solubilization and transport of metals; in *Mineral Exploration Biological Systems and Organic Matter*, (ed.) D. Carlisle, W.L. Berry, I.R. Kaplan, and J.K. Watterson; Prentice-Hall, New Jersey, p. 377-407.
- Brady, N.C.**
1974: *The Nature and Properties of Soils*; 8th edition, MacMillan Publishing Co. Inc., New York, 639 p.
- Curtin, G.C. and King, H.D.**
1986: Utility of mull in geochemical exploration; in *Mineral Exploration Biological Systems and Organic Matter*, (ed.) D. Carlisle, W.L. Berry, I.R. Kaplan, and J.R. Watterson; Prentice-Hall, New Jersey, p. 356-376.
- Hall, G.E.M., Vaive, Beer, R., and Hoashi, M.**
1996: Phase selective leaches for use in exploration geochemistry; in *EXTECH I: A Multidisciplinary Approach to Massive Sulphide Research in the Rusty Lake-Snow Lake Greenstone Belts, Manitoba*, (ed.) G.F. Bonham-Carter, A.G. Galley, and G.E.M. Hall; Geological Survey of Canada, Bulletin 426.
- Kaszycki, C.A.**
1989: Surficial geology and till composition, northwestern Manitoba; Geological Survey of Canada, Open File Report 2118, 48 p.
- Kaszycki, C.A., Nielsen, E., and Gobert, G.**
1996: Surficial geochemistry and response to volcanic-hosted massive sulphide mineralization in the Snow Lake region; in *EXTECH I: A Multidisciplinary Approach to Massive Sulphide Research in the Rusty Lake-Snow Lake Greenstone Belts, Manitoba*, (ed.) G.F. Bonham-Carter, A.G. Galley, and G.E.M. Hall; Geological Survey of Canada, Bulletin 426.
- Levinson, A.A.**
1980: *Introduction to Exploration Geochemistry*; second edition, Applied Publishing Ltd., Wilmette, Illinois, 924 p.

McMartin, I.

- 1994: Ice flow events in the Cormorant Lake-Wekusko Lake area, northern Manitoba; in *Current Research 1994-C*; Geological Survey of Canada, p. 175-182.

Nielsen, E.

- 1992: Surficial geology mapping and glacial dispersion studies as aids to geochemical exploration and mineral tracing in the Elbow Lake area (NTS 63K/15); in *Report of Activities, Manitoba Energy and Mines, Mineral Division*, p. 52-55.

Plant, J.A. and Raiswell, R.

- 1983: Principles of environmental geochemistry; in *Applied Environmental Geochemistry*, (ed.) I. Thornton; Academic Press, Geology Series, New York, p. 1-39.

Shilts, W.W.

- 1976: Glacial till and mineral exploration; in *Glacial Till – an Inter-Disciplinary Study*, (ed.) R.F. Leggett; Royal Society of Canada, Special Publication, No. 12, p. 205-224.

Sposito, G.

- 1983: The chemical forms of trace metals in soils; in *Applied Environmental Geochemistry*, (ed.) I. Thornton; Academic Press, Geology Series, New York, p. 123-170.

Contribution to the 1989-1994 Rusty Lake-Snow Lake Mining Camps, Canada-Manitoba Exploration Science and Technology Initiative (EXTECH I)

Phase selective leaches for use in exploration geochemistry

G.E.M. Hall¹, J.E. Vaive¹, R. Beer, and M. Hoashi

Hall, G.E.M., Vaive, J.E., Beer, R., and Hoashi, M., 1996: Phase selective leaches for use in exploration geochemistry; in EXTECH I: A Multidisciplinary Approach to Massive Sulphide Research in the Rusty Lake-Snow Lake Greenstone Belts, Manitoba, (ed.) G.F. Bonham-Carter, A.G. Galley, and G.E.M. Hall; Geological Survey of Canada, Bulletin 426, p. 169-200.

Abstract: This paper describes the development and evaluation of a sequential extraction scheme for application to soils, tills, and surficial sediments to elucidate the form(s) in which an element is held and hence to provide information as to its genesis. The operationally defined phases selected for extraction have been assigned the following categories: adsorbed/exchangeable/carbonate, 'AEC'; amorphous Fe oxyhydroxide, 'am Fe ox'; crystalline Fe oxide, 'cry Fe ox'; sulphides and organics; and residual, mainly silicates. Particular attention has been paid to the specificity of the hydroxylamine reagent, 0.25 M $\text{NH}_2\text{OH}\cdot\text{HCl}$ in 0.25 M HCl, for extraction of the 'am Fe ox' phase, well recognized for its scavenging properties of trace metals in the surficial environment. A decrease in the acid strength to 0.05 M HCl in this leach lessens the solubility of sphalerite and galena to <1% but a major portion of the humate and fulvate component in a sediment is dissolved, regardless of HCl concentration.

Other reagents used in this scheme comprise: 1 M CH_3COONa for 'AEC'; 1 M $\text{NH}_2\text{OH}\cdot\text{HCl}$ in 25% CH_3COOH for 'cry Fe ox'; KClO_3/HCl followed by HNO_3 for sulphides and organics; and finally $\text{HF}\cdot\text{HClO}_4\text{-HNO}_3\text{-HCl}$ for the residual minerals. Typical long-term precision values are provided in the data obtained by replicate application of these five leaches to the international standard reference materials TILL-1, TILL-2, TILL-3, TILL-4, and LKSD-4, for the elements Zn, Cu, Pb, Ni, Co, Mn, and Fe.

Résumé : Dans le présent article, il est question de la conception et de l'évaluation d'une technique de lixiviation séquentielle applicable aux sols, aux tills et aux matériaux superficiels; le but consiste à élucider la (les) forme(s) sous laquelle (lesquelles) un élément est capté et, ainsi, avoir de l'information sur sa genèse. Les phases à extraire ont été définies en fonction des opérations et classées dans les catégories suivantes : métaux à cations échangeables, métaux adsorbés et métaux coprécipités avec les carbonates (adsorbed/exchangeable/carbonate, «AEC»); oxydes et hydroxydes de fer amorphes («am Fe ox»); oxydes de fer cristallins («cry Fe ox»); sulfures et matières organiques; phases résiduelles, surtout des silicates. On a porté une attention particulière à la spécificité du réactif hydroxylamine ($\text{NH}_2\text{OH}\cdot\text{HCl}$ 0,25 M dans HCl 0,25 M) pour l'extraction de la phase «am Fe ox», bien connue pour ses propriétés de captage des métaux traces dans les milieux de surface. Une diminution de la concentration du HCl à 0,05 M dans le lixiviat a pour effet de réduire la solubilité de la sphalérite et de la galène à ~1 %; cependant, une partie importante de l'humat et du fulvat dans les sédiments est dissoute, quelle que soit la concentration du HCl.

D'autres réactifs ont été utilisés. Ce sont les suivants : CH_3COONa à 1 M («AEC»); $\text{NH}_2\text{OH}\cdot\text{HCl}$ à 1 M dans 25 % de CH_3COOH («cry Fe ox»); KClO_3/HCl suivi de HNO_3 (sulfures et matières organiques); et enfin $\text{HF}\cdot\text{HClO}_4\text{-HNO}_3\text{-HCl}$ (minéraux résiduels). Des valeurs représentatives de précision à long terme sont tirées des données obtenues par l'application répétée des cinq lixiviations susmentionnées aux étalons internationaux TILL-1, TILL-2, TILL-3, TILL-4 et LKSD-4, quant aux éléments Zn, Cu, Pb, Ni, Co, Mn et Fe.

¹ Geological Survey of Canada, 601 Booth St., Ottawa, Ontario K1A 0E8

INTRODUCTION

During the early 1990s there was renewed interest in North America amongst the mining industry in the use of selective leaches in geochemical exploration for deeply buried deposits. This had been stimulated by the reported success of the Russians in their own country (Antropova et al., 1992) and by demonstration of their methodologies in Canada (Ryss et al., 1990; Hamilton et al., 1992). As part of the analytical component of the EXTECH I program, to develop new methods of exploration for volcanogenic massive sulphide deposits, the Analytical Method Development Section of the Geological Survey of Canada (GSC) initiated research into designing a cost-effective sequential extraction scheme for application to soils and sediments. Two leaches in this sequence were developed to mimic the action of two Soviet methods: 'MPF', the acronym used to describe the leach employed to dissolve specifically 'soluble' metal-organic complexes; and 'TMGM', the procedure to selectively leach from the matrix those elements adsorbed by amorphous Fe and Mn oxyhydroxides. These two leaches are designed to release elements which have been fixed or 'scavenged' by reactive sites at surface, the premise being that ore or pathfinder elements are transported to surface by various mechanisms (e.g., as gaseous molecules) from the source below. While particular attention was paid to refining these two leaches to dissolve the 'surface-active' phases of a soil, the objective of the project was to establish a comprehensive scheme for identification and quantification of elements bound in both labile and nonlabile forms in different phases typical of geochemical media.

The use of selective dissolution techniques in exploration geochemistry up to 1984 has been summarized by Chao (1984); a more recent compilation of the relevant literature, pertaining more to speciation in sediments, can be found in a book chapter by Kersten and Forstner (1989). The identification of the main binding sites of trace metals not only helps in the understanding of geochemical processes but also allows one to predict the potential for remobilization, to determine the bioavailability of an element, and to discriminate between sources (e.g. atmospheric deposition vs. hydromorphic transport vs. clastic dispersion). The measurement of speciation is a much more challenging task than the determination of the total content. A sequential extraction scheme consists of a series of successive chemical treatments of a sample, each being more drastic in action or of a different nature than the previous one. The order in which the extractants are used is critical and may well depend upon sample type and overall composition. It must be recognized that the results obtained are 'operationally defined', i.e. selectivity is not 100% and is dependent upon such factors as the chemicals employed, the time and nature of contact, sample to volume ratio, etc. Clearly, results will also be predicated on the grain size fraction chosen for analysis and whether coarser grains have been made finer by ball-milling, thus increasing exposure to attack. Some of the more common schemes are listed in Table 1. Selective leaching for metals bound to humates and fulvates (equivalent to 'MPF') is the subject of a separate paper by Hall et al. (1996).

The water-soluble fraction of a soil or sediment is the first to be brought into solution in any sequential scheme. This fraction is usually negligible, except in areas where evaporites are present. Exchangeable metals, those held through electrostatic attraction on exchange sites on the surface and interface of negatively charged complexes of soils, also generally constitute a small proportion and can be replaced by neutral salts such as MgCl_2 or ammonium acetate, $\text{CH}_3\text{COONH}_4$. We decided to group exchangeable and adsorbed metals with those coprecipitated with carbonates and to extract this component ('AEC') with sodium acetate, CH_3COONa , buffered at pH 5. Also extracted together, in the next step, are the hydrous oxides of Mn and Fe, the well known 'sinks' in the surficial environment for heavy metals. Scavenging by these secondary oxides, present as coatings on mineral surfaces or as fine discrete particles, may occur by any or a combination of the following mechanisms: coprecipitation; adsorption; surface complex formation; ion exchange; and penetration of the lattice. These mechanisms and their interrelations have been discussed by Chao and Theobald (1976); clearly, predominant forms will depend upon the element in question and the physicochemical conditions prevailing. It is well known that the scavenging capacity of Mn oxides for heavy metals is greater than that of Fe and this can be explained in part by the very complex mineralogical structure of these oxides. Manganese exists in several oxidation states, it forms non-stoichiometric oxides with variable valency states and its higher oxides exist in several crystalline or pseudocrystalline forms. On the other hand, Fe forms relatively few crystalline oxyhydroxides (including hematite, goethite, lepidocrocite, maghemite, magnetite). Amorphous Fe oxyhydroxide ($\text{Fe}(\text{OH})_3 \cdot n\text{H}_2\text{O}$) is chemically more reactive than the other forms and it is on this basis that they are separated. Both Fe and Mn form mixed oxides, owing to their similar chemical properties and ionic radii. The relative importance of Fe and Mn oxides as scavengers will depend upon such conditions as existing pH-Eh values, degree of oxide crystallinity, their abundances and presence of organic matter; it is impossible to generalize. Therefore, we decided to group the extraction of Mn oxides together with that of amorphous Fe oxyhydroxides, rather than differentiate the two as most schemes in Table 1 have done. Chao and Zhou (1983) compared the specificity of the following reagents in the extraction of amorphous Fe oxyhydroxides from soils and sediments: Tamm's reagent, 0.175 M ammonium oxalate ($(\text{NH}_4)_2\text{C}_2\text{O}_4$) in oxalic acid, in the dark; HCl at different concentrations and temperature; 3% oxalic acid at 100°C; 0.25 M $\text{NH}_2\text{OH} \cdot \text{HCl}$ in 25% CH_3COOH at 70°C; and 0.25 M hydroxylamine hydrochloride, $\text{NH}_2\text{OH} \cdot \text{HCl}$, in 0.25 M HCl at 70°C. Their results confirmed others' work in that Tamm's reagent (at a pH of 3.2) in the dark was selective only in the absence of magnetite and organic complexes, and for this reason, it was rejected here. Magnetite is known to contain a host of trace metals (Overstreet et al., 1978). Although extraction of the amorphous Fe oxides in 1 M HCl for 30 min at room temperature seemed to be specific and dissolved <1% of the hematite, goethite, and magnetite minerals tested, this attack may well bring into solution clays, amorphous allophanic materials, and some sulphides. Progressive increase in both the concentration of the reducing agent, hydroxylamine hydrochloride,

and acidity can be used to selectively dissolve Mn oxides, amorphous Fe oxyhydroxides, and finally crystalline Fe oxides. Chao and Zhou's study demonstrated that, after about 30-60 min in 0.25 M $\text{NH}_2\text{OH}\cdot\text{HCl}$ /0.25 M HCl at 70°C, further dissolution of the two amorphous Fe oxides was minimal while <1% of the crystalline Fe oxides were dissolved except one magnetite (about 2%). They concluded that this was the optimum, most selective extraction but reduced the temperature to 50°C to minimize the degree of dissolution of the crystalline Fe oxides below 1% total Fe. We chose this extraction for the amorphous Fe oxyhydroxide phase, operating at an intermediate temperature of 60°C as there seemed to be continued dissolution with time of their synthetic amorphous Fe at the lower temperature (i.e. plateau of the per cent extracted-time curve was not very sharp). Evidence for the increased efficiency of extraction with fresh hydroxylamine hydrochloride solution added to the sample has been shown and discussed by Kersten and Forstner (1989). Therefore, replicate extraction of each of the first three leaches in our sequence was thought necessary to carry out and evaluate.

The citrate-dithionite buffer ('DCB') extraction has been used often to dissolve crystalline Fe oxides (see Table 1) but we eliminated it for several reasons. Firstly, disproportionation of dithionite leads to the formation of sulphides which can precipitate and adsorb trace elements. Secondly, the degree of dissolution of hematite and goethite is far from 100% if grinding is not invoked, while Fe-rich layer silicates may dissolve easily. Finally, this reagent is highly contaminated, requiring cation exchange techniques to clean it sufficiently. Dissolution of crystalline Fe oxides with Tamm's reagent under UV irradiation was thought cumbersome to set up for high volume application. We decided to employ hydroxylamine hydrochloride under stronger reducing conditions, after the method originally designed by Chester and Hughes (1967) for the partitioning of trace elements in pelagic sediments. This extractant comprises 1 M $\text{NH}_2\text{OH}\cdot\text{HCl}$ in 25% CH_3COOH and is carried out at 90°C. In the frequently employed sequential scheme first published by Tessier et al. (1979), a weaker solution of 0.04 M $\text{NH}_2\text{OH}\cdot\text{HCl}$ in 25% CH_3COOH at 96°C is used to extract metals bound to Fe-Mn oxides; differentiation between amorphous and crystalline forms of Fe oxides is not made.

Metals bound to organic matter and sulphides are next in the sequence of most selective extraction schemes, assuming that these forms have not been previously dissolved to any significant degree. The type of action on the sample changes from reducing to oxidizing and the results of a study of different attacks on sulphide minerals by Chao and Sanzalone (1977) are pertinent here. They compared the efficiency of the following reagents in the dissolution of nine sulphide minerals: aqua regia; 4 M HNO_3 ; H_2O_2 -ascorbic acid; oxalic acid; KClO_3 and HCl; and KClO_3 and HCl followed by 4 M HNO_3 with gentle boiling. Only with the last reagent mixture were all the sulphides completely dissolved. Attack of silicates along edges, corners, and surfaces was suggested to be likely but of little concern if the element of interest was not a major constituent of the silicate structure. Finally, the common mixed acid attack comprising HCl - HF - HClO_4 - HNO_3 was used in our scheme to dissolve silicates and resistant mineral

species from the residue. In some cases where refractory primary minerals such as tourmaline, beryl, chromite, and sphenes are present, a small residue still persists.

Flame atomic absorption spectrometry (FAAS) was the primary analytical technique initially employed to evaluate the figures of merit associated with the sequential extraction scheme. Later, inductively coupled plasma emission spectrometry (ICP-ES) was used to expand the number of elements determined and eventually the more sensitive technique of ICP mass spectrometry (ICP-MS) was investigated as a further tool but those results will be reported separately later. During the development stages, the extraction scheme was applied to various standard reference materials (SRM) and eventually to soils and tills collected in the Snow Lake area of northern Manitoba under the EXTECH I program. Not included in this investigation is the effect of storage (temperature, humidity) or drying (air, oven) on sample integrity. These factors, as well as exposure to air during extraction, are particularly important in the analysis of *anoxic* samples. For example, Kersten and Forstner (1989) compared the phase distribution of Fe and Cd in anoxic sediment extracted (a) immediately upon collection, under an inert gas atmosphere and (b) after oven drying and exposure to air. Oxidation of the sediment caused the Cd to be shifted (about 50%) from the sulphide phase to the more labile exchangeable and reducible fractions. The partitioning of Fe amongst the carbonate and exchangeable phases moved to the reducible fraction upon exposure of the sample to air. Soils, tills, and humus collected under the EXTECH project were already aerated and low temperature drying was used in their preparation.

METHOD DEVELOPMENT

All reagents used in this project were Baker (Phillipsburg, New Jersey, U.S.A.) 'analysed reagent' grade. Standard solutions employed for calibration in the measurement techniques of AAS and ICP-MS were purchased from Seastar Chemicals (Sidney, British Columbia). Distilled deionized water was used throughout. Most of the leaches were performed in 'Falcon' polypropylene centrifuge tubes (Becton Dickinson and Co., Lincoln Park, New Jersey, U.S.A.) and the Teflon centrifuge tubes employed in the later stages of the procedure were purchased from Nalgene Co. (Rochester, New York, U.S.A.). The CH_3COONa extractant solution was first cleaned of trace elements by passing it through a column of Chelex 100 resin (50-100 mesh). A Perkin-Elmer Model 3030, in the air-acetylene mode, was employed for measurement by AAS and ICP-MS analysis was carried out with a Fisons VG PlasmaQuad 2+. Interferences in both techniques were negated in the usual manner (Viets and O'Leary, 1992; Hall, 1992) and calibration solutions were prepared by spiking, with known quantities of analytes, 'blank' solutions of the particular extractants.

Two standard reference materials, LKSD-4 and TILL-2, previously described by Lynch (1990) were used to study the effects of changing various procedural parameters. These SRMs form part of a series (LKSD-1 to LKSD-4, STSD-1 to STSD-4, TILL-1 to TILL-4) produced by the GSC and

Table 1. Common sequential extraction techniques.

available from CANMET under the Canadian Certified Reference Materials Project (CCRMP). Other CCRMP SRMs employed include: CCu-1, a Cu concentrate (mainly chalcopyrite); CPb-1, a Pb floatation concentrate (73% galena); CZn-1, a Zn concentrate (84% sphalerite); and SU-1, a Ni-Cu-Co sulphide ore (1.2% Ni). A second series of sulphides-chalcopyrite (S-CuFeS₂), pyrite (S-FeS₂), and sphalerite (S-ZnS) – were prepared in-house and have been described previously (Hall et al., 1988). Two in-house till samples, DS-A (a peridotite sill from Dundonald, Timmins, Ontario) and SB-B (from Sissons Brook, New Brunswick), were also used in method development. All these control samples were sieved to a fineness of at least 74 μ m, in contrast to many of the samples tested which were sieved to only <177 μ m (80 mesh).

Leach times were chosen based on the observations that there was no further change in the amount of element being extracted and that the reproducibility of results was acceptable. A second application of each of the first three leaches was carried out to see if there was a significant amount of element extracted further with fresh reagent solution. Other than the concentration of HCl used in the extraction of the amorphous Fe oxyhydroxide phase (discussed below), the reagent concentrations were not investigated. TILL-2 was employed to study the effect of shaking frequency during each extraction. The sequential scheme employed is shown schematically in Figure 1.

Sequential extraction procedure

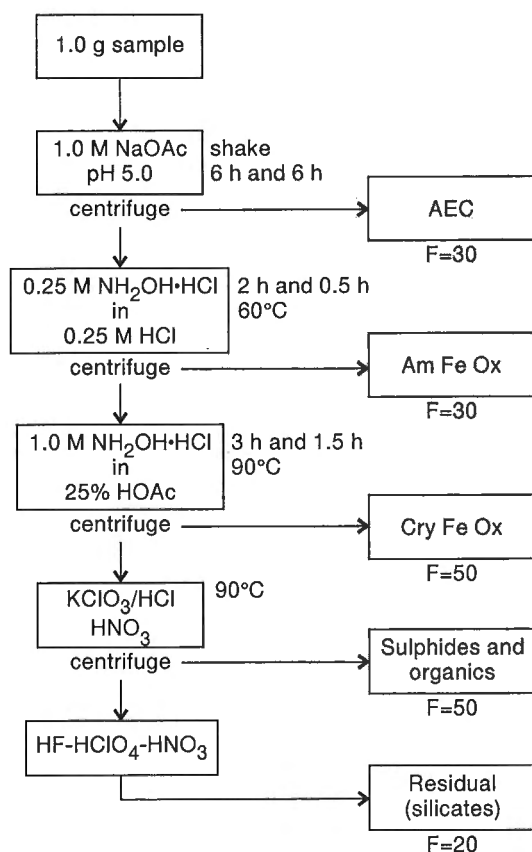


Figure 1. Schematic of sequential extraction procedure. 'F' is dilution factor prior to analysis.

Proposed sequential leach procedure

AEC (adsorbed/exchangeable/carbonate) phase

1. To 1 g of sample in a 50 mL screw-cap centrifuge tube, add 20 mL of 1.0 M CH₃COONa (at pH 5) and cap.
2. Vortex contents for 5-10 s and place in a horizontal shaker for 6 h.
3. Centrifuge for 10 min at 2800 rpm and decant supernatant into a labelled test-tube. Rinse residue with 5 mL of water, vortex, and repeat centrifuge; do this twice and add supernatant rinses to the test-tube. Make up to the 30.0 mL mark and analyze.
4. Carry out a second 20 mL 1 M CH₃COONa leach of the residue, repeating steps 2 and 3.

Am Fe ox (amorphous Fe oxyhydroxide)

5. To the residue from step 4, add 20 mL of 0.25 M NH₂OH·HCl in 0.25 M HCl, cap and vortex for 5-10 s.
6. Place in a water bath at 60°C for 2 h with cap loosened. Every 30 min, cap tightly and vortex the contents.
7. Centrifuge for 10 min and decant supernatant into a labelled test-tube. Rinse residue with 5 mL of water, vortex, and repeat centrifuge; do this twice and add supernatant rinses to the test-tube. Make up to the 30.0 mL mark and analyze.
8. Carry out a second 0.25 M NH₂OH·HCl leach of the residue but heat for only 30 min.

Cry Fe ox (crystalline Fe oxide)

9. To the residue from step 8, add 30 mL of 1.0 M NH₂OH·HCl in 25% CH₃COOH, cap, and vortex for 5-10 s.
10. Place in a water bath at 90°C for 3 h with caps on tightly. Vortex contents every 20 min.
11. Centrifuge for 10 min and decant supernatant into a labelled test-tube. Rinse residue with 10 mL of 25% CH₃COOH, water, vortex, and repeat centrifuge; do this twice and add supernatant rinses to the test-tube. Make up to the 50.0 mL mark and analyze.
12. Carry out a second 1.0 M NH₂OH·HCl leach of the residue but heat for only 1.5 h.

Sulphides and organics

13. To the residue from step 12, add 750 mg of KClO₃ and 5 mL of 12 M HCl. Cap and vortex (care, may froth). Add a further 10 mL of HCl, cap, and vortex.
14. After 30 min, add 15 mL of water, cap, vortex, and centrifuge for 10 min. Decant supernatant into a labelled test-tube.
15. To the residue, add 10 mL of 4 M HNO₃, cap, and vortex. Place in a water bath at 90°C for 20 min. After digestion, transfer all contents to a Teflon pressure tube.

16. Vortex and centrifuge for 10 min. Decant supernatant into the previous labelled test-tube, in effect mixing the KClO_3/HCl extractant with this HNO_3 leachate.
17. Rinse the residue with 5 mL of water, vortex, and repeat centrifuge; do this twice and add supernatant rinses to the test-tube. Make up to 50.0 mL and analyze.

Silicates and residual oxides

18. To the residue, add 2 mL of 16 M HNO_3 and place in a dry heating block on a hot plate at 200°C . Heat to about 0.5 mL volume.
19. After cooling, add 2 mL of 12 M HCl and heat for 20 min at 90°C in the water bath.
20. After cooling, add 10 mL of the acid mixture (all concentrated) – HF (5 mL)/ HClO_4 (3 mL)/ HNO_3 (2 mL) – and cap tightly. Heat for 1 h at 90°C in the water bath.
21. Transfer the contents to a Teflon beaker, rinsing with water for complete transfer. Evaporate at about 70°C overnight and raise the heat to about 120°C in the last stage to achieve incipient dryness.
22. Add 1 mL of HCl and 3 mL of HNO_3 and swirl contents. Add 3 mL of water and warm gently for 5–10 min. Transfer the contents to a calibrated test-tube, rinsing with water. Make up to 20.0 mL and analyze.

RESULTS AND DISCUSSION

Sequential leach

Table 2 shows the effect of frequency of shaking (i.e. mixing sample and reagent with a vortex mixer) with the amount of Zn, Cu, Ni, Mn, and Fe extracted from TILL-2 by the 1.0 M $\text{NH}_2\text{OH}\cdot\text{HCl}$ leach for quantification of the 'cry Fe ox' phase. Slightly higher concentrations were found when mixing at least every 10–20 min and thus a frequency of 20 min was chosen. Similar data were obtained for the 0.25 M $\text{NH}_2\text{OH}\cdot\text{HCl}$ for the 'am Fe ox' phase except that results for 10, 20, and 30 min intervals were identical and thus the 30 min frequency was chosen. Results of the sequential extraction scheme applied to eight 1 g samples of TILL-2 and to five of LKSD-4 over a 1.5 year period by different analysts are given in Table 3. Results for each of the first three leaches (AEC, am Fe ox, and cry Fe ox) represent the sum of the two individual extractions. Also shown in Table 3 are mean results for TILL-2 where four 0.5 g subsamples have been taken instead of the usual 1 g weight (i.e. halving the sample-to-reagent volume ratio). These mean results do not differ significantly from those using the 1 g weight, therefore indicating that saturation has not been reached and readsorption is minimal. The precision associated with the 0.5 g TILL-2 data is superior to that obtained for the 1 g set shown here and is due to the fact that these four samples were processed together and not over an extended period. Clearly, nearness to the method's detection limit dominates the reproducibility of results. For example, values for relative standard deviation (RSD) rise

above 20% for Pb, Ni, and Co at levels below about 5 ppm. However, at concentrations at least a decade above detection limits, RSDs are generally in the range 5–12% which is excellent considering the number of manipulations involved. In the absence of certified values for particular phase concentrations of elements in these SRMs, the only estimation of accuracy available to us is to compare the summed elemental concentrations with the recommended values provided by Lynch (1990, J.J. Lynch, pers. comm., 1995). These two values agree within two standard deviations, with the exceptions of Pb and Fe in TILL-2 which appear to be slightly low, using both the 0.5 g and 1 g sampling weights.

During the early development stages of the sequential leach procedure, six control samples were used to study the effect of multiple applications of the individual leaches. The controls used were the TILL series (-1 to -4), DB-A and SB-B, all described earlier. These samples were taken in triplicate (1 g subsamples) through the sequential procedure, but this time three rather than two applications of the 6 h CH_3COONa leach (steps 1–3, for the 'AEC' phase) were carried out and a second 30 min attack by 0.25 M $\text{NH}_2\text{OH}\cdot\text{HCl}$ in 0.25 M HCl (step 8, for the 'am Fe ox' phase) was included. The protocols were also different in that the frequency of shaking sample and leach solution was less than that finally adopted and the temperature of the 'cry Fe ox' phase digestion was 85°C rather than 90°C (step 10). These results, together with those obtained by *direct* $\text{HF}\text{--}\text{HClO}_4\text{--}\text{HNO}_3$ digestion (i.e. steps 18–22) of a second suite of these controls in triplicate, are presented in Tables 4–9 for Zn, Cu, Ni, Co, Mn, and Fe, respectively. With a few exceptions where data are close to detection levels (e.g. Cu in DS-A and Zn in TILL-4), the summation of the leach results agrees very well with the 'total' value obtained by the HF digestion, indicating that there is minimal loss of analyte through the numerous steps of the procedure. However, comparison of these results for TILL-2 with those shown in Table 3 obtained using the later protocols is somewhat surprising. As expected, results for the first phase, 'AEC', in Tables 4–9 are higher than in Table 3 because of the additional leach performed; this amount would otherwise have reported to the 'am Fe ox' phase. However, most notable is the sharp decrease in amounts extracted in the 'cry Fe ox' digestion, offset by increases in the concentrations found in the sulphide and silicate phases (Tables 4–9). For example, under the initial operating conditions used to produce the data in Table 9, the concentrations of Fe extracted from TILL-2 representing the 'cry Fe ox', sulphide, and silicate phases are 1.07%, 0.77%, and 0.78%, respectively. The equivalent amounts of Fe found using the final recommended procedure are 1.49%, 0.41%, and 0.58%, respectively. Similar behaviour is observed for the other elements. These differences are not caused by additional leaches performed for the first two phases but largely by the higher temperature applied (90°C vs. 85°C) in the 'cry Fe ox' phase digestion. These data serve to document the dramatic differences in results which occur in sequential extractions when experimental conditions are altered. Note the excellent precision shown by the majority of results in Tables 4–9, significantly superior to the corresponding figures in Table 3 which pertain to long term rather than short term precision.

Table 2. Effect of frequency of mixing on the amount of Zn, Cu, Ni, Mn and Fe extracted from the crystalline Fe oxide phase of TILL-2 using 1.0 M NH₂OH·HCl in 25% CH₃COOH.

| Frequency | Zn (ppm) | Cu (ppm) | Ni (ppm) | Mn (ppm) | Fe (%) |
|-----------|----------|----------|----------|----------|--------|
| 10 min | 46 | 48 | 15 | 125 | 1.50 |
| 20 min | 45 | 47 | 15 | 124 | 1.48 |
| 30 min | 44 | 45 | 15 | 119 | 1.40 |
| 40 min | 43 | 43 | 14 | 115 | 1.38 |
| 50 min | 42 | 43 | 13 | 112 | 1.33 |
| 60 min | 42 | 42 | 13 | 108 | 1.21 |

Table 3. Mean and standard deviation values in ppm for Zn, Cu, Pb, Ni, Co, Mn, and Fe in five phases of controls TILL-2 (n = 8) and LKSD-4 (n = 5). First TILL-2 data refers to 0.5 g testing (n = 4).

| Element | PHASE | | | | | | |
|------------------------|------------------|-------------|-------------|------------|------------|--------------|----------------------|
| | AEC ² | am Fe ox | cry Fe ox | sulphides | silicates | total | recom'd ³ |
| Zn-TILL-2 | 3.0 ± 0.1 | 31.2 ± 0.2 | 46.3 ± 0.2 | 14.5 ± 0.5 | 23.8 ± 0.3 | 119 ± 2 | |
| Zn-TILL-2 | 3.0 ± 0.3 | 34.1 ± 1.0 | 44.9 ± 1.4 | 13.8 ± 2.0 | 24.0 ± 2.0 | 120 ± 3 | 130 ± 8 |
| Zn-LKSD-4 ¹ | 9.8 ± 1.8 | 64.4 ± 5.1 | 16.2 ± 1.5 | 9.6 ± 0.5 | 14.8 ± 3.5 | 191 ± 10 | 194 ± 19 |
| Cu-TILL-2 | 12.5 ± 0.5 | 52.4 ± 1.0 | 49.2 ± 0.9 | 9.9 ± 0.5 | 22.5 ± 0.5 | 147 ± 1 | |
| Cu-TILL-2 | 12.2 ± 0.9 | 56.1 ± 1.9 | 46.6 ± 1.3 | 8.3 ± 2.2 | 22.4 ± 2.0 | 146 ± 3 | 150 ± 10 |
| Cu-LKSD-4 ¹ | <1 | 6.8 ± 0.4 | 4.6 ± 0.9 | 11.4 ± 3.0 | 2 ± 0.4 | 32.2 ± 2.4 | 31 ± 4 |
| Pb-TILL-2 | 3.9 ± 0.7 | 11.0 ± 0.3 | <1 | <1 | 7.9 ± 0.4 | 22.8 ± 0.6 | |
| Pb-TILL-2 | 4.8 ± 0.8 | 10.2 ± 0.4 | <1 | <1 | 8.0 ± 0.7 | 22.8 ± 1.4 | 31 ± 3 |
| Pb-LKSD-4 ¹ | 4.6 ± 0.8 | 16.0 ± 1.2 | <1 | <1 | 6.2 ± 3.3 | 84 ± 10 | 91 ± 6 |
| Ni-TILL-2 | <1 | 3.5 ± 0.5 | 13.4 ± 0.5 | 7.1 ± 0.4 | 8.3 ± 0.4 | 33.5 ± 1.2 | |
| Ni-TILL-2 | <1 | 3.1 ± 1.0 | 14.6 ± 1.6 | 5.8 ± 2.1 | 8.5 ± 0.9 | 33.3 ± 2.5 | 32 ± 3 |
| Ni-LKSD-4 ¹ | <1 | 10.2 ± 0.8 | 4.0 ± 1.0 | 4.8 ± 0.4 | 5.2 ± 1.3 | 30.6 ± 1.5 | 31 ± 5 |
| Co-TILL-2 | <1 | 4.3 ± 0.3 | 5.0 ± 0.1 | 2.0 ± 1.0 | 3.3 ± 0.3 | 14.7 ± 0.5 | |
| Co-TILL-2 | 1 ± 1 | 4.8 ± 0.5 | 4.8 ± 1.7 | 1.0 ± 1.0 | 3 ± 1 | 14.5 ± 1.4 | 15 ± 2 |
| Mn-TILL-2 | 92.4 ± 3.4 | 282 ± 5 | 124 ± 4 | 47.2 ± 2.1 | 155 ± 5 | 700 ± 7 | |
| Mn-TILL-2 | 86.8 ± 8.3 | 292 ± 11 | 125 ± 8 | 43.8 ± 4.0 | 145 ± 21 | 693 ± 40 | 780 ± 28 |
| Mn-LKSD-4 ¹ | 16.0 ± 2.0 | 56.0 ± 6.0 | 42.2 ± 3.3 | 11.2 ± 1.7 | 83.4 ± 1.9 | 460 ± 39 | 500 ± 30 |
| Fe-TILL-2 | 371 ± 11 | 9908 ± 122 | 14566 ± 213 | 4368 ± 112 | 6015 ± 152 | 35234 ± 266 | |
| Fe-TILL-2 | 403 ± 52 | 10190 ± 403 | 14866 ± 600 | 4131 ± 457 | 5821 ± 585 | 35403 ± 1036 | 37700 ± 1300 |
| Fe-LKSD-4 ¹ | 126 ± 20 | 4610 ± 580 | 7591 ± 620 | 5397 ± 278 | 4963 ± 354 | 26182 ± 142 | 28000 ± 200 |

¹ Pyrophosphate extraction had been carried out on LKSD-4 prior to this sequential leach. The total value includes this portion also.

² AEC = adsorbed/exchangeable/carbonate.

³ Recommended values for LKSD-4 from Lynch (1990) and for TILL-2 from J.J. Lynch (pers. comm., 1995).

Table 4. Sequential leach data for Zn in controls TILL-1, TILL-2, TILL-3, TILL-4, DS-A, and SB-B, with comparison to 'total' determination of Zn following HF-HClO₄-HNO₃-HCl digestion. Mean and standard

| Standard | PHASE | | | | | | |
|----------|------------------|-----------------------|------------|------------|------------|------------|-------------|
| | AEC ¹ | am Fe ox ² | cry Fe ox | sulphides | silicates | sum | total by HF |
| TILL-1 | 1.8 ± 0.2 | 26.8 ± 0.5 | 17.0 ± 0.5 | 9.0 ± 1.2 | 43.9 ± 1.1 | 97.8 ± 2.8 | 97.3 ± 2.3 |
| TILL-2 | 3.2 ± 0.4 | 38.2 ± 0.3 | 32.8 ± 0.3 | 18.2 ± 0.6 | 30.7 ± 0.4 | 123 ± 1.2 | 132 ± 0.0 |
| TILL-3 | 2.9 ± 0.3 | 15.8 ± 0.9 | 8.2 ± 0.6 | 4.2 ± 0.6 | 17.5 ± 0.2 | 48.6 ± 1.3 | 56.3 ± 2.3 |
| TILL-4 | 4.1 ± 0.3 | 18.7 ± 0.2 | 17.2 ± 0.3 | 13.5 ± 0.0 | 16.1 ± 0.1 | 69.5 ± 0.4 | 72.3 ± 2.3 |
| DS-A | 2.1 ± 0.2 | 84.1 ± 0.3 | 13.0 ± 0.0 | 32.3 ± 3.8 | 15.6 ± 0.7 | 147 ± 3.0 | 143 ± 2.3 |
| SB-B | 2.3 ± 0.3 | 15.7 ± 0.2 | 26.0 ± 0.0 | 19.3 ± 0.8 | 21.3 ± 1.9 | 84.4 ± 2.7 | 92 ± 0.0 |

¹ represents sum of three (not two) 6 h leaches

² represents sum of one 2 h and two (not one) 30 min leaches

Table 5. Sequential leach data for Cu in controls TILL-1, TILL-2, TILL-3, TILL-4, DS-A, and SB-B, with comparison to 'total' determination of Cu following HF-HClO₄-HNO₃-HCl digestion. Mean and standard deviation values in ppm; n = 3.

| Standard | PHASE | | | | | | |
|----------|------------------|-----------------------|------------|------------|------------|------------|-------------|
| | AEC ¹ | am Fe ox ² | cry Fe ox | sulphides | silicates | sum | total by HF |
| TILL-1 | 6.5 ± 0.5 | 18.9 ± 0.0 | 10.2 ± 0.3 | 7.7 ± 0.8 | 4.5 ± 0.3 | 47.8 ± 0.9 | 46.5 ± 0.5 |
| TILL-2 | 18.8 ± 0.2 | 51.9 ± 0.3 | 38.0 ± 0.9 | 14.0 ± 0.5 | 29.2 ± 0.7 | 152 ± 0.3 | 152 ± 1.7 |
| TILL-3 | 2.7 ± 0.0 | 7.2 ± 0.8 | 4.5 ± 0.0 | 6.3 ± 0.6 | 2.4 ± 0.1 | 23.1 ± 0.6 | 23.9 ± 1.8 |
| TILL-4 | 17.4 ± 0.3 | 66.8 ± 3.0 | 98.5 ± 0.5 | 24.5 ± 0.2 | 27.0 ± 0.4 | 234 ± 2.7 | 254 ± 10.6 |
| DS-A | <1 | 11.8 ± 0.2 | <1 | 1.5 ± 0.5 | <1 | 13.3 ± 0.5 | 19.7 ± 0.2 |
| SB-B | 9.4 ± 0.2 | 59.6 ± 0.2 | 51.5 ± 0.5 | 16.0 ± 0.5 | 29.0 ± 0.2 | 166 ± 0.7 | 175 ± 1.7 |

¹ represents sum of three (not two) 6 h leaches
² represents sum of one 2 h and two (not one) 30 min leaches

Table 6. Sequential leach data for Ni in controls TILL-1, TILL-2, TILL-3, TILL-4, DS-A, and SB-B, with comparison to 'total' determination of Ni following HF-HClO₄-HNO₃-HCl digestion. Mean and standard deviation values in ppm; n = 3.

| Standard | PHASE | | | | | | |
|----------|------------------|-----------------------|-----------|-----------|------------|------------|-------------|
| | AEC ¹ | am Fe ox ² | cry Fe ox | sulphides | silicates | sum | total by HF |
| TILL-1 | <1 | 2.0 ± 0.2 | 2.7 ± 0.6 | 4.8 ± 0.3 | 12.6 ± 0.2 | 22.1 ± 1.2 | 23.9 ± 0.6 |
| TILL-2 | <1 | 4.7 ± 0.7 | 7.3 ± 0.3 | 8.2 ± 0.6 | 11.3 ± 0.3 | 31.5 ± 1.0 | 32.9 ± 0.6 |
| TILL-3 | 0.4 ± 0.7 | 10.0 ± 0.8 | 5.8 ± 0.3 | 7.0 ± 0.5 | 18.9 ± 0.2 | 42.2 ± 0.9 | 43.5 ± 1.2 |
| TILL-4 | <1 | 1.6 ± 0.2 | 3.5 ± 0.1 | 2.7 ± 0.8 | 6.0 ± 0.2 | 13.8 ± 1.0 | 17.9 ± 1.0 |
| DS-A | 322 ± 2.5 | 1681 ± 17 | 401 ± 15 | 218 ± 21 | 284 ± 14 | 2906 ± 32 | 3178 ± 26 |
| SB-B | <1 | 0.4 ± 0.7 | 5.2 ± 0.3 | 4.5 ± 0.5 | 8.7 ± 0.3 | 18.7 ± 1.4 | 20.8 ± 0.4 |

¹ represents sum of three (not two) 6 h leaches
² represents sum of one 2 h and two (not one) 30 min leaches

Table 7. Sequential leach data for Co in controls TILL-1, TILL-2, TILL-3, TILL-4, DS-A, and SB-B, with comparison to 'total' determination of Co following HF-HClO₄-HNO₃-HCl digestion. Mean and standard deviation values in ppm; n = 3.

| Standard | PHASE | | | | | | |
|----------|------------------|-----------------------|------------|------------|------------|------------|-------------|
| | AEC ¹ | am Fe ox ² | cry Fe ox | sulphides | silicates | sum | total by HF |
| TILL-1 | 0.8 ± 0.7 | 4.6 ± 0.3 | 4.2 ± 0.3 | 3.3 ± 0.3 | 8.2 ± 0.2 | 21.1 ± 0.7 | 18.5 ± 0.2 |
| TILL-2 | <1 | 3.9 ± 0.1 | 5.0 ± 0.5 | 3.7 ± 0.8 | 4.5 ± 0.1 | 17.2 ± 0.3 | 15.9 ± 0.2 |
| TILL-3 | 2.9 ± 0.2 | 2.5 ± 0.2 | 4.3 ± 0.3 | 2.2 ± 0.8 | 6.0 ± 0.2 | 17.9 ± 0.9 | 15.9 ± 0.4 |
| TILL-4 | <1 | 1.9 ± 0.2 | 2.8 ± 0.3 | 1.1 ± 0.1 | 4.0 ± 0.2 | 9.7 ± 0.4 | 9.1 ± 0.5 |
| DS-A | 6.0 ± 0.5 | 41.3 ± 0.9 | 20.7 ± 0.3 | 30.8 ± 7.9 | 39.4 ± 6.0 | 138 ± 1 | 147 ± 2 |
| SB-B | <1 | 2.3 ± 0.6 | 5.0 ± 0.2 | 1.7 ± 0.8 | 4.5 ± 0.6 | 13.5 ± 1.6 | 12.3 ± 0.2 |

¹ represents sum of three (not two) 6 h leaches
² represents sum of one 2 h and two (not one) 30 min leaches

Replicate analyses for 18 soil, till, and humus samples from Snow Lake, Manitoba taken through the sequential procedure, are given in Tables 10-15 for Zn, Cu, Pb, Ni, Mn, and Fe. Also shown for all elements except Pb, which occurs at extremely low levels, are values for the average RSDs obtained for each phase. Replicate samples were purposely digested and analyzed in separate batches. The erratic data for humus sample 17 is atypical and suggests possible heterogeneity; this sample was collected in an area of mineralization and had a relatively low LOI of 35%. These tables show that precision for all elements is excellent, with RSDs in the range 3-10% and agreeing well with the precision obtained for the SRMs TILL-2 and LKSD-4 (Table 3). It should be borne in mind that most of these samples were simply sieved to <177 μm (80 mesh) and not ball-milled to pass 63-7 μm as the SRMs were prepared.

Data obtained by application of the sequential leach to the soils and tills collected from Snow Lake were used to examine the importance of carrying out the second extraction of the first three leaches. Plotted in Figures 2 to 4 are the elemental concentrations obtained in: (1) the sum of the two CH_3COONa leaches versus the first leach for Zn, Cu, Mn, and Fe; (2) the sum of the two 0.25 M $\text{NH}_2\text{OH}\cdot\text{HCl}$ (in HCl) leaches versus the first leach for Zn, Co, Cu, Ni, Mn, and Fe; and (3) the sum of the two 1.0 M $\text{NH}_2\text{OH}\cdot\text{HCl}$

(in CH_3COOH) leaches versus the first leach for Zn, Co, Cu, Ni, Mn, and Fe. Also indicated on the graphs are the values for n (number of data points), the correlation coefficient r^2 , the slope, and standard error of the slope for the line of best fit. The symbols differentiate soils and tills prepared by sieving to <80 mesh (177 μm) from their 2 μm component. The number of data points for Cu and Zn in Figure 2 for the CH_3COONa leach appears to be far fewer than 221 as many values were below the detection limit of 1 ppm. The second CH_3COONa leach dissolves about 35-40% more Zn, Cu, and Fe than the first but not as much Mn; in fact, the relationship between the first and second leach concentrations for Mn is much noisier ($r^2 = 0.75$ for Mn, cf. 0.99 for Zn and Cu). This different behaviour for Mn is evident again in Figure 3, examining the first and summed 0.25 M $\text{NH}_2\text{OH}\cdot\text{HCl}$ leaches for the 'am Fe ox' phase. Proportionately less Mn is extracted by the second leach (slope = 1.04) than the typical figure of 20-25% observed for Zn, Cu, Co, Ni, and Fe. All elements appear to behave similarly in the second 1.0 M $\text{NH}_2\text{OH}\cdot\text{HCl}$ leach designed to extract the 'cry Fe ox' phase (Fig. 4). About 15-20% more element is extracted by the second leach, though levels of Ni and Co are so low that confidence in these particular graphs is limited. Thus in progressing through the sequential scheme, the proportion of element extracted by the second application of the first three leaches diminishes, from about 35-40% to 20-25% and finally to 15-20%.

Table 8. Sequential leach data for Mn in controls TILL-1, TILL-2, TILL-3, TILL-4, DS-A, and SB-B, with comparison to 'total' determination of Mn following $\text{HF}\cdot\text{HClO}_4\text{-HNO}_3\text{-HCl}$ digestion. Mean and standard deviation values in ppm; n = 3.

| Standard | PHASE | | | | | | sum | | total by HF |
|----------|------------------|-----------------------|----------------|----------------|----------------|--|--------------|--|---------------|
| | AEC ¹ | am Fe ox ² | cry Fe ox | sulphides | silicates | | | | |
| TILL-1 | 226 \pm 3.5 | 663 \pm 8.3 | 60.0 \pm 0.9 | 18.0 \pm 0.9 | 410 \pm 12.2 | | 1377 \pm 9 | | 1433 \pm 12 |
| TILL-2 | 128 \pm 1 | 251 \pm 2.4 | 85.7 \pm 1.0 | 64.7 \pm 2.1 | 210 \pm 2 | | 739 \pm 3 | | 741 \pm 12 |
| TILL-3 | 123 \pm 2.1 | 65.1 \pm 0.3 | 35.8 \pm 1.4 | 19.5 \pm 1.3 | 233 \pm 2 | | 476 \pm 2 | | 501 \pm 5 |
| TILL-4 | 18.3 \pm 0.3 | 68.5 \pm 0.9 | 57.0 \pm 0.5 | 59.2 \pm 1.4 | 257 \pm 3 | | 460 \pm 3 | | 477 \pm 23 |
| DS-A | 123 \pm 0.3 | 453 \pm 3.5 | 168 \pm 2.0 | 132 \pm 26 | 369 \pm 21 | | 1245 \pm 4 | | 1349 \pm 10 |
| SB-B | 5.2 \pm 0.2 | 48.6 \pm 0.3 | 71.5 \pm 0.2 | 94.0 \pm 2.6 | 237 \pm 24 | | 457 \pm 27 | | 506 \pm 2.3 |

¹ represents sum of three (not two) 6 h leaches
² represents sum of one 2 h and two (not one) 30 min leaches

Table 9. Sequential leach data for Fe in controls TILL-1, TILL-2, TILL-3, TILL-4, DS-A, and SB-B, with comparison to 'total' determination of Fe following $\text{HF}\cdot\text{HClO}_4\text{-HNO}_3\text{-HCl}$ digestion. Mean and standard deviation values in ppm; n = 3.

| Standard | PHASE | | | | | | sum | | total by HF |
|----------|------------------|-----------------------|-----------------|-----------------|-----------------|--|------------------|--|------------------|
| | AEC ¹ | am Fe ox ² | cry Fe ox | sulphides | silicates | | | | |
| TILL-1 | 219 \pm 2 | 8565 \pm 96 | 12376 \pm 249 | 4515 \pm 200 | 21953 \pm 565 | | 47629 \pm 562 | | 47026 \pm 662 |
| TILL-2 | 701 \pm 4 | 9671 \pm 45 | 10670 \pm 343 | 7661 \pm 264 | 7813 \pm 115 | | 36516 \pm 430 | | 36613 \pm 283 |
| TILL-3 | 611 \pm 7 | 4807 \pm 47 | 8310 \pm 471 | 3528 \pm 411 | 10893 \pm 155 | | 28150 \pm 464 | | 27680 \pm 502 |
| TILL-4 | 939 \pm 12 | 10055 \pm 113 | 14705 \pm 45 | 6355 \pm 186 | 8107 \pm 83 | | 40160 \pm 136 | | 40120 \pm 223 |
| DS-A | 52 \pm 2 | 3789 \pm 54 | 5371 \pm 131 | 29008 \pm 941 | 35033 \pm 921 | | 73254 \pm 1031 | | 75706 \pm 1361 |
| SB-B | 77 \pm 1.8 | 4542 \pm 33 | 10311 \pm 121 | 7580 \pm 225 | 9733 \pm 181 | | 32244 \pm 361 | | 31626 \pm 83 |

¹ represents sum of three (not two) 6 h leaches
² represents sum of one 2 h and two (not one) 30 min leaches

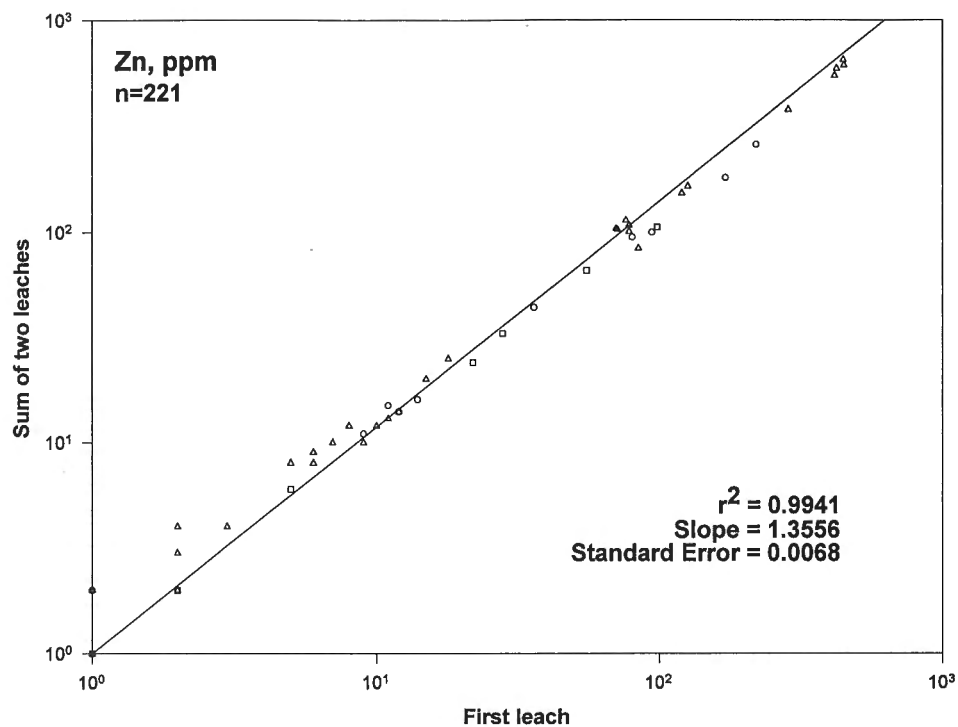


Figure 2a.

Figure 2.

Plot of sum of two CH_3COONa leaches versus first leach for a) Zn, b) Cu, c) Mn, and d) Fe, respectively. Designations are: o – soil (<177 μm); □ – till (<177 μm); Δ – <2 μm fraction of soils and tills.

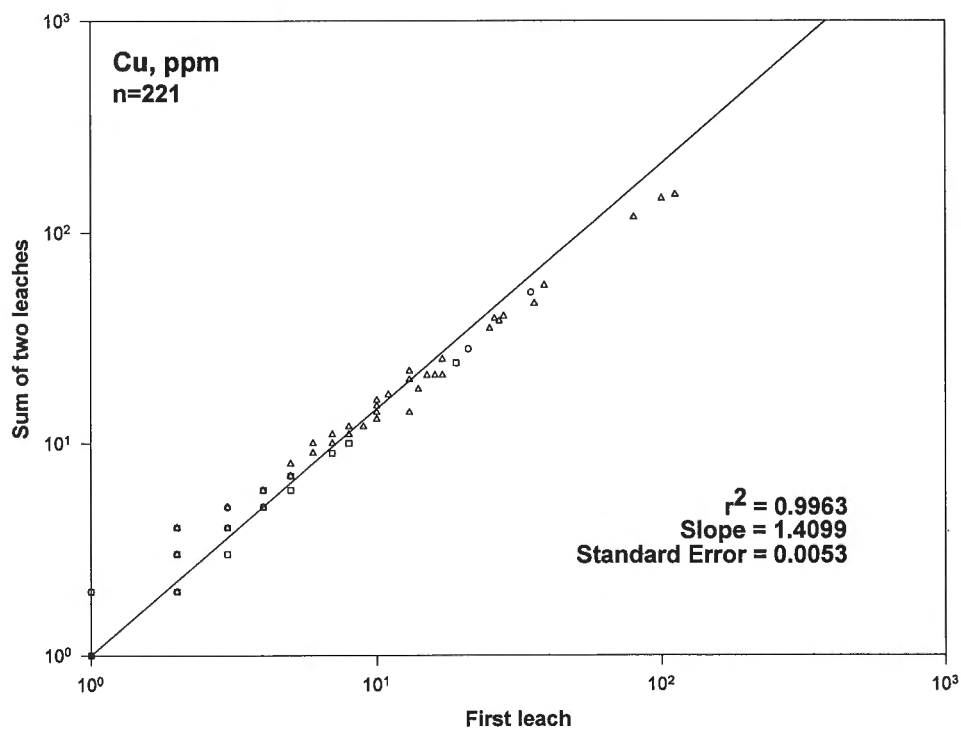


Figure 2b.

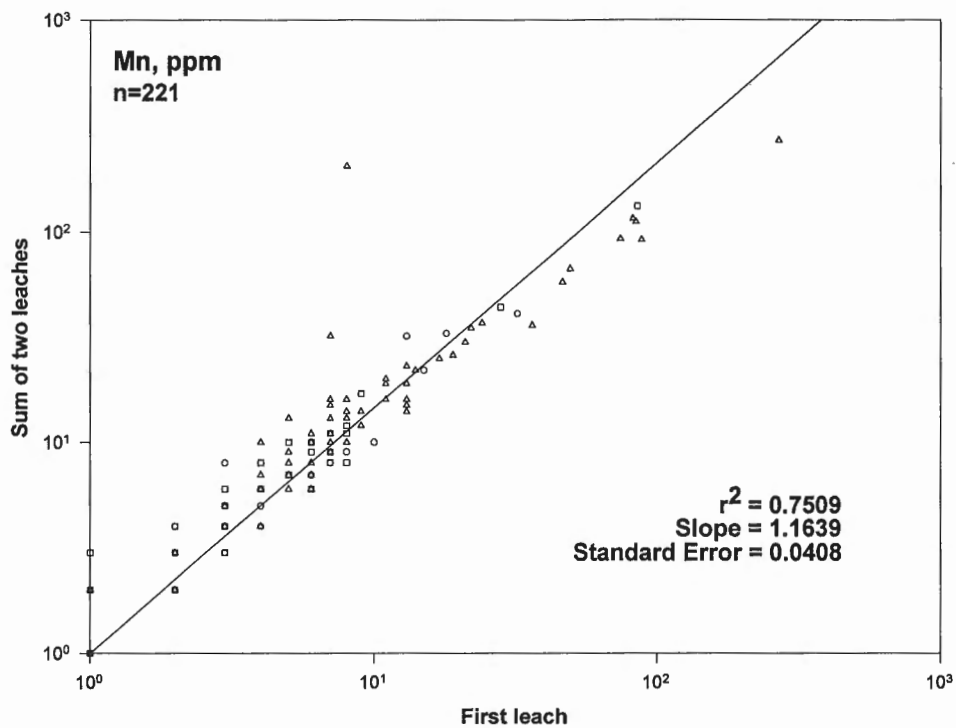
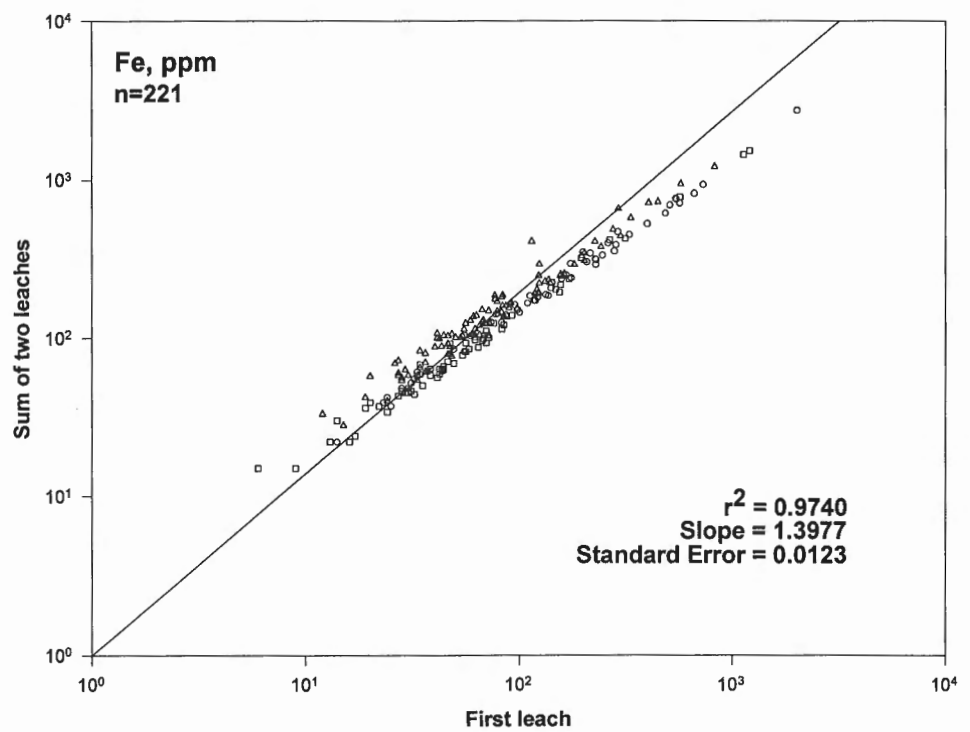


Figure 2c.

Figure 2d.



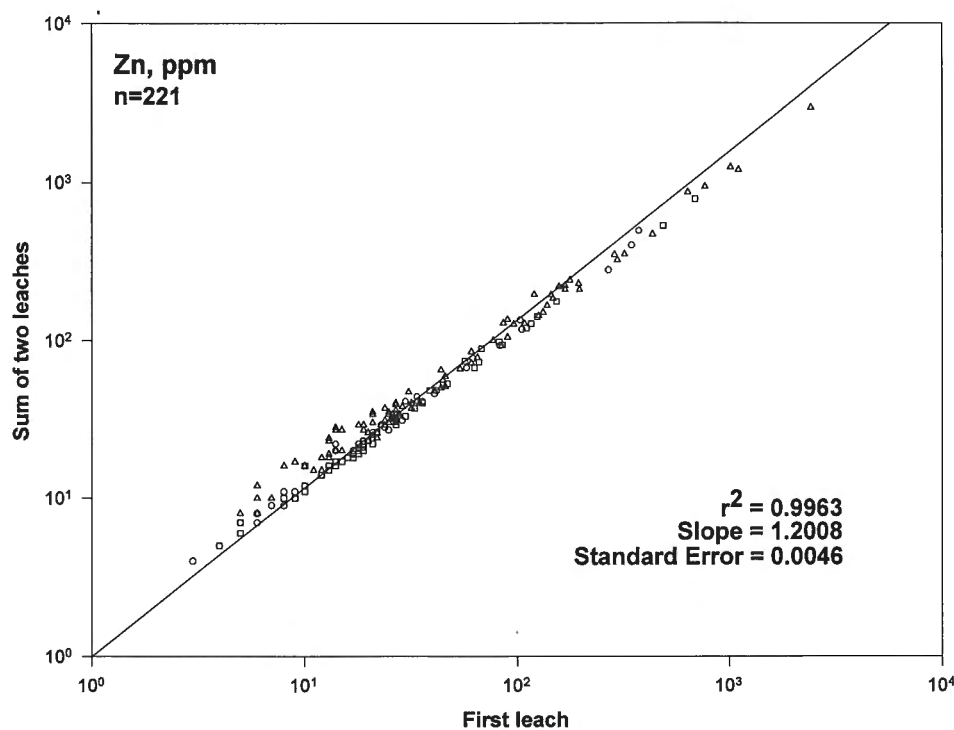


Figure 3a.

Figure 3.

Plot of sum of two 0.25 M $\text{NH}_2\text{OH}\cdot\text{HCl}$ (in 0.25 M HCl) leaches versus first leach for a) Zn, b) Cu, c) Co, d) Ni, e) Mn, and f) Fe, respectively. Designations are: o – soil (<177 μm); \square – till (<177 μm); Δ – <2 μm fraction of soils and tills.

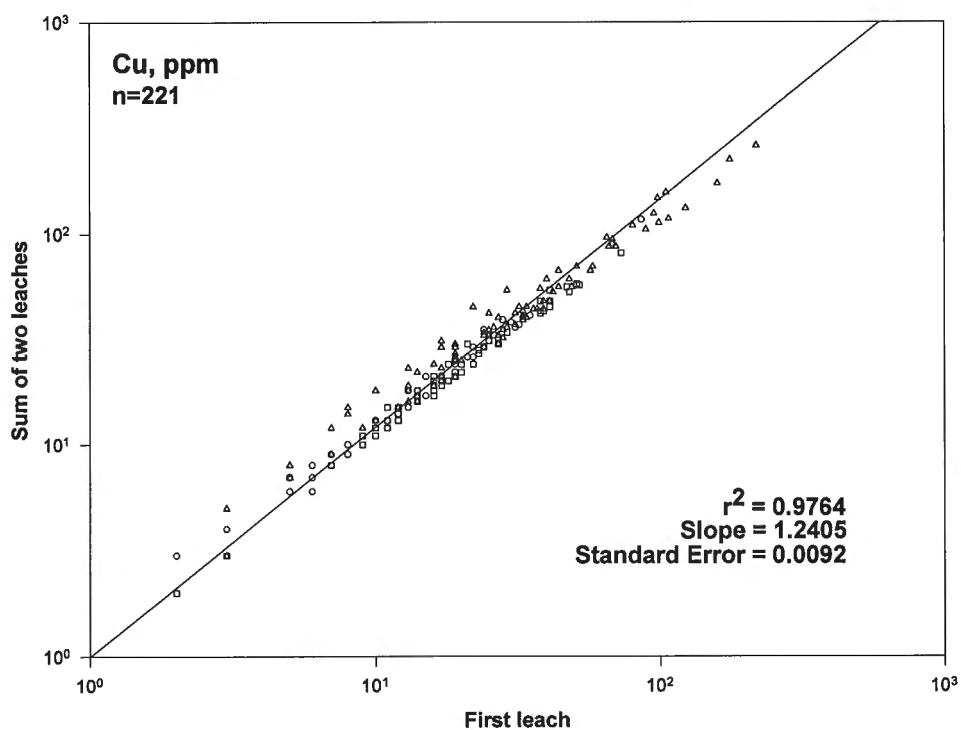


Figure 3b.

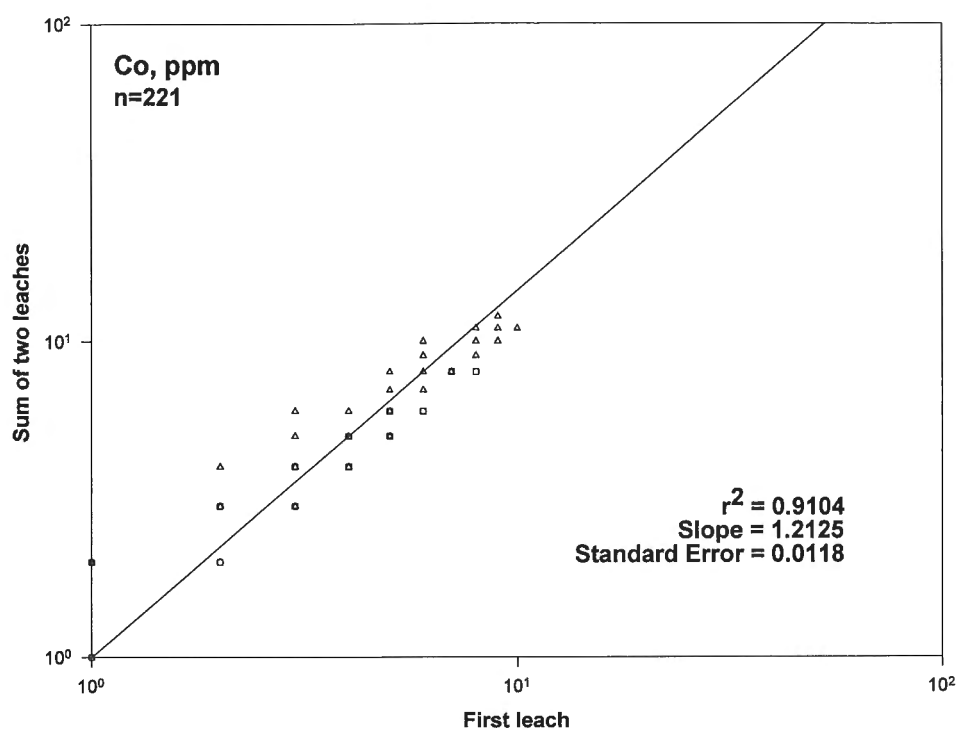
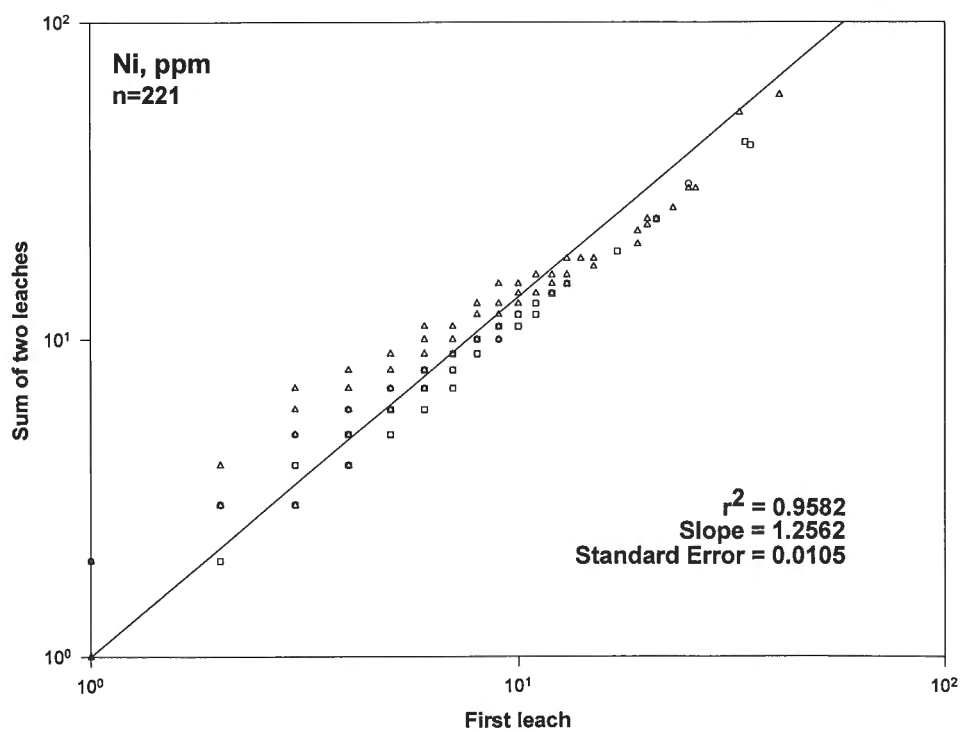


Figure 3c.

Figure 3d.



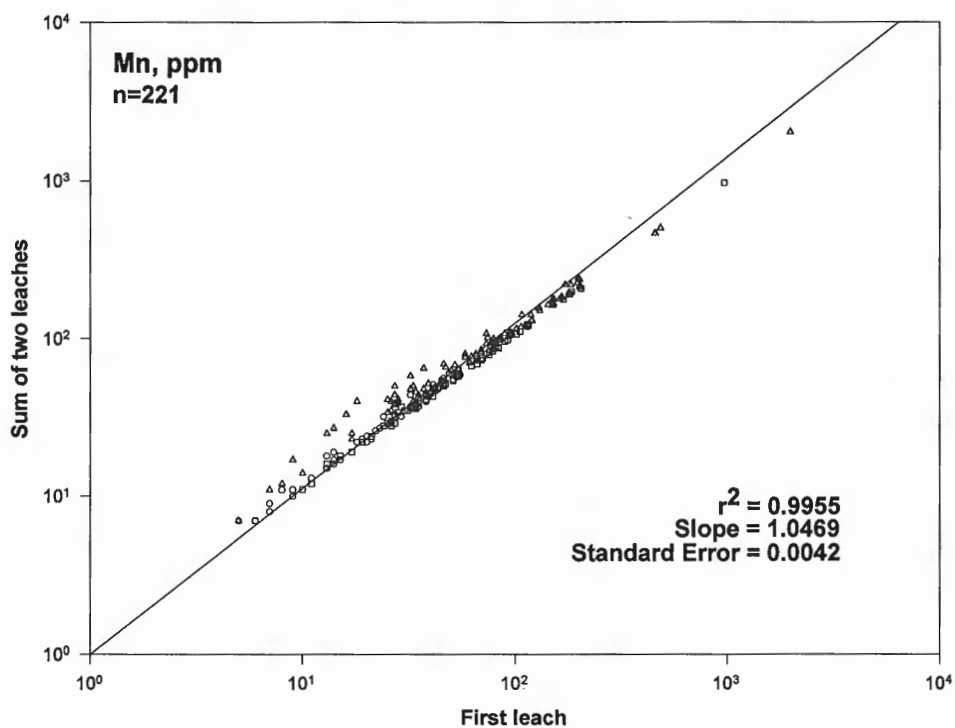


Figure 3e.

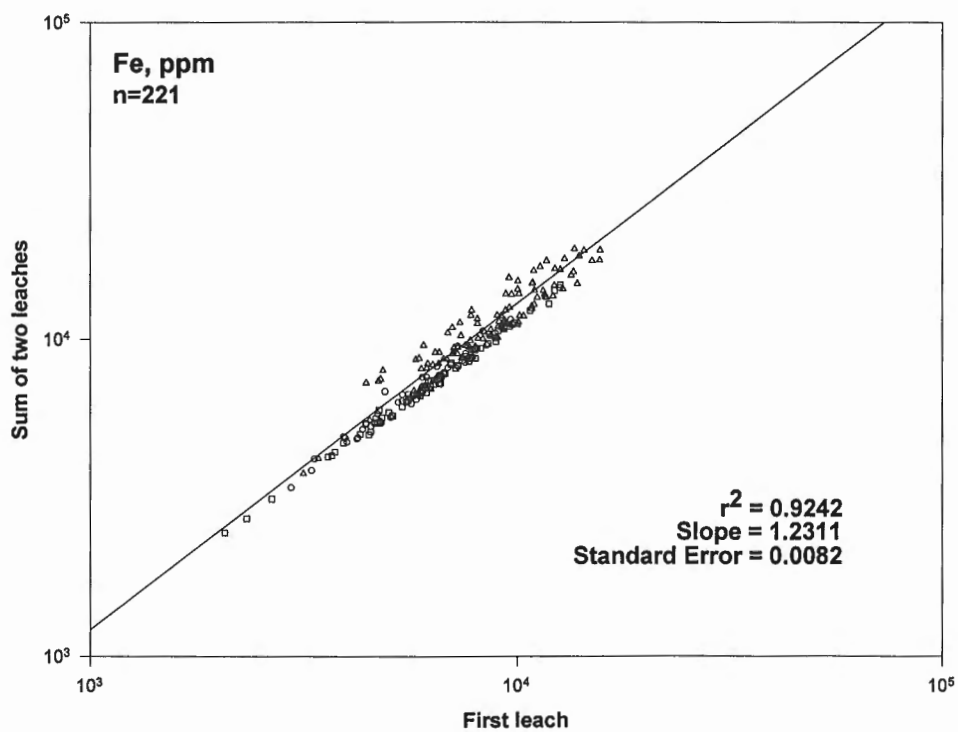


Figure 3f.

Table 10. Replicate analyses of soil, till, and humus samples from Snow Lake, Manitoba, for Zn through the sequential extraction scheme; values in ppm.

| Sample ¹ | AEC | am Fe ox | cry Fe ox | sulphides | silicates |
|--------------------------|--------|----------|-----------|------------|-----------|
| 4B, soil | 1, <1 | 7, 7 | 9, 10 | 3, 2 | 26, 26 |
| 27B, soil | <1, <1 | 14, 13 | 5, 6 | 4, 4 | 13, 15 |
| 37B, soil | <1, <1 | 44, 46 | 54, 56 | 12, 12 | 43, 43 |
| 48B, soil | 1, <1 | 5, 4 | 8, 9 | 2, 3 | 17, 19 |
| 16, till | <1, <1 | 23, 22 | 7, 7 | 3, 3 | 18, 18 |
| 54, till | <1, <1 | 15, 15 | 9, 9 | 5, 4 | 17, 17 |
| 60, till | <1, <1 | 18, 18 | 13, 12 | 7, 6 | 18, 16 |
| 48, till | <1, <1 | 7, 7 | 9, 9 | 4, 3 | 28, 28 |
| 31, till, 2 µm | <1, <1 | 33, 32 | 17, 22 | 42, 40 | 32, 32 |
| 41, till, 2 µm | <1, <1 | 19, 18 | 16, 16 | 28, 28 | 30, 28 |
| 8, humus | <1, 1 | 11, 9 | 4, 4 | 7, 5 | 28, 26 |
| 17, humus | 27, 17 | 98, 91 | 40, 37 | 2655, 2465 | 30, 128 |
| 23, humus | <1, 2 | 11, 19 | 5, 7 | 38, 166 | 14, 18 |
| 31, humus | <1, <1 | 12, 12 | 5, 5 | 4, 5 | 2, 12 |
| 42, humus | 2, <1 | 20, 20 | 6, 6 | 213, 214 | 37, 24 |
| 48, humus | 3, 3 | 28, 28 | 10, 10 | 350, 400 | 15, 18 |
| 56, humus | 6, 6 | 26, 25 | 13, 14 | 94, 97 | 31, 33 |
| 61, humus | 2, 1 | 32, 33 | 15, 14 | 14, 16 | 18, 17 |
| Average RSD ² | 4% | 5% | 6% | 3% | |

¹ Humus samples were leached with pyrophosphate prior to application of this sequential extraction scheme.

² Relative standard deviation, excluding two data points for humus 23 in the sulphide phase and humus 17 in the silicate phase.

Table 12. Replicate analyses of soil, till, and humus samples from Snow Lake, Manitoba, for Pb through the sequential extraction scheme; values in ppm.

| Sample ¹ | AEC | am Fe ox | cry Fe ox | sulphides | silicates |
|---------------------|--------|----------|-----------|-----------|-----------|
| 4B, soil | 2, 2 | 1, 1 | <1, <1 | 2, <1 | 10, 9 |
| 27B, soil | <1, <1 | 1, 2 | 3, 1 | 2, <1 | 12, 11 |
| 37B, soil | <1, 2 | <1, 3 | <1, <1 | 3, 1 | 7, 7 |
| 48B, soil | <1, <1 | 3, 4 | <1, 2 | 4, 1 | 7, 9 |
| 16, till | <1, 1 | 1, <1 | <1, <1 | <1, <1 | 8, 9 |
| 54, till | 2, <1 | 1, <1 | <1, 1 | <1, <1 | 11, 11 |
| 60, till | <1, <1 | <1, 1 | 1, <1 | <1, <1 | 10, 11 |
| 48, till | 5, <1 | 2, 1 | <1, <1 | 3, 1 | 10, 8 |
| 31, till, 2 µm | 2, 2 | 3, 5 | <1, 2 | 1, 1 | 8, 8 |
| 41, till, 2 µm | <1, 1 | 2, 3 | <1, <1 | <1, <1 | 3, 2 |
| 8, humus | 1, 1 | 4, 5 | 1, 1 | 3, <1 | 15, 5 |
| 17, humus | 5, 4 | 34, 31 | 87, 67 | 19, 18 | 6, 1051 |
| 23, humus | 2, 2 | 8, 9 | 1, 3 | <1, 1 | 4, 3 |
| 31, humus | 1, <1 | 3, 6 | <1, <1 | <1, <1 | 5, 4 |
| 42, humus | <1, <1 | 10, 13 | 9, 9 | 2, <1 | 2, 2 |
| 48, humus | 1, 1 | 10, 14 | 5, 6 | <1, <1 | 11, 4 |
| 56, humus | 3, 3 | 19, 18 | 4, 4 | <1, <1 | 16, 14 |
| 61, humus | <1, 1 | 11, 16 | 2, 2 | <1, <1 | 7, 5 |

¹ Humus samples were leached with pyrophosphate prior to application of this sequential extraction scheme.

Table 11. Replicate analyses of soil, till, and humus samples from Snow Lake, Manitoba, for Cu through the sequential extraction scheme; values in ppm.

| Sample ¹ | AEC | am Fe ox | cry Fe ox | sulphides | silicates |
|---------------------|--------|----------|-----------|-----------|-----------|
| 4B, soil | 1, 1 | 7, 8 | 11, 10 | 2, 1 | 4, 4 |
| 27B, soil | 1, 1 | 12, 12 | 8, 9 | 1, 1 | 2, 1 |
| 37B, soil | 3, 2 | 38, 39 | 47, 50 | 5, 5 | 9, 9 |
| 48B, soil | 5, 4 | 21, 21 | 11, 13 | 5, 5 | 9, 9 |
| 16, till | <1, <1 | 15, 15 | 7, 8 | 1, 1 | 1, 2 |
| 54, till | <1, <1 | 10, 10 | 5, 5 | 1, 1 | 3, 3 |
| 60, till | 3, 3 | 24, 24 | 14, 15 | 3, 3 | 2, 2 |
| 48, till | 7, 6 | 19, 18 | 8, 9 | 3, 3 | 9, 9 |
| 31, till, 2 µm | 3, 3 | 20, 21 | 11, 13 | 11, 13 | 8, 8 |
| 41, till, 2 µm | 7, 7 | 35, 35 | 38, 37 | 32, 34 | 38, 40 |
| 8, humus | <1, <1 | 9, 8 | 4, 4 | 4, 4 | 7, 8 |
| 17, humus | <1, <1 | 9, 5 | 10, 11 | 105, 95 | 3, 18 |
| 23, humus | <1, <1 | 4, 3 | 3, 4 | 9, 12 | 3, 3 |
| 31, humus | <1, <1 | 14, 15 | 15, 14 | 14, 17 | 10, 11 |
| 42, humus | <1, <1 | 13, 13 | 12, 11 | 23, 25 | 7, 7 |
| 48, humus | <1, <1 | 6, 7 | 7, 7 | 51, 60 | 3, 2 |
| 56, humus | <1, <1 | 10, 9 | 8, 7 | 17, 18 | 12, 12 |
| 61, humus | <1, <1 | 8, 8 | 12, 11 | 13, 16 | 7, 7 |
| Average RSD | | 3% | 5% | 5% | 10% |

¹ Humus samples were leached with pyrophosphate prior to application of this sequential extraction scheme.

Table 13. Replicate analyses of soil, till, and humus samples from Snow Lake, Manitoba, for Ni through the sequential extraction scheme; values in ppm.

| Sample ¹ | AEC | am Fe ox | cry Fe ox | sulphides | silicates |
|---------------------|--------|----------|-----------|-----------|-----------|
| 4B, soil | <1, <1 | 3, 3 | 4, 3 | 2, <1 | 7, 8 |
| 27B, soil | 1, <1 | 8, 7 | 6, 6 | 1, 2 | 12, 7 |
| 37B, soil | 1, <1 | 6, 6 | 9, 9 | 2, 3 | 14, 10 |
| 48B, soil | 2, 2 | 4, 5 | 7, 9 | 2, 3 | 13, 14 |
| 16, till | <1, 1 | 41, 42 | 19, 20 | 2, 4 | 28, 27 |
| 54, till | <1, 2 | 8, 9 | 6, 7 | 2, 3 | 8, 9 |
| 60, till | <1, <1 | 11, 11 | 8, 8 | 3, 4 | 8, 8 |
| 48, till | 1, <1 | 4, 4 | 9, 7 | 3, 3 | 12, 10 |
| 31, till, 2 µm | <1, <1 | 14, 14 | 9, 11 | 23, 22 | 20, 23 |
| 41, till, 2 µm | 1, <1 | 10, 9 | 7, 9 | 19, 19 | 23, 22 |
| 8, humus | <1, <1 | 2, 3 | 1, 1 | 1, 1 | 5, 5 |
| 17, humus | <1, <1 | 3, 4 | <1, <1 | <1, <1 | 3, 8 |
| 23, humus | <1, <1 | 2, 2 | <1, <1 | 1, <1 | 5, 4 |
| 31, humus | 2, <1 | 7, 7 | 1, 2 | 1, 1 | 3, 3 |
| 42, humus | <1, 1 | 2, 2 | <1, <1 | <1, 1 | 4, 3 |
| 48, humus | 1, <1 | 1, 2 | <1, <1 | <1, 1 | 1, 1 |
| 56, humus | <1, <1 | 2, 3 | <1, <1 | 1, 2 | 5, 5 |
| 61, humus | 1, <1 | 10, 10 | 3, 3 | 2, 2 | 3, 3 |
| Average RSD | | 7% | 5% | 10% | 9% |

¹ Humus samples were leached with pyrophosphate prior to application of this sequential extraction scheme.

Table 14. Replicate analyses of soil, till, and humus samples from Snow Lake, Manitoba, for Mn through the sequential extraction scheme; values in ppm.

| Sample ¹ | AEC | am Fe ox | cry Fe ox | sulphides | silicates |
|---------------------|--------|----------|-----------|-----------|-----------|
| 4B, soil | <1, <1 | 7, 8 | 10, 11 | 4, 4 | 275, 322 |
| 27B, soil | 5, 4 | 32, 31 | 18, 17 | 5, 5 | 270, 262 |
| 37B, soil | <1, 1 | 42, 41 | 32, 31 | 12, 13 | 495, 520 |
| 48B, soil | 2, 3 | 11, 10 | 23, 22 | 5, 5 | 180, 186 |
| 16, till | 1, 2 | 44, 45 | 20, 22 | 6, 6 | 328, 339 |
| 54, till | 1, 1 | 38, 39 | 24, 22 | 10, 9 | 242, 232 |
| 60, till | 10, 11 | 87, 88 | 28, 28 | 12, 12 | 274, 284 |
| 48, till | 3, 3 | 16, 16 | 23, 23 | 5, 5 | 286, 274 |
| 31, till, 2 µm | 3, 4 | 99, 96 | 49, 59 | 138, 135 | 103, 111 |
| 41, till, 2 µm | 1, 1 | 41, 39 | 32, 34 | 68, 70 | 55, 56 |
| 8, humus | <1, <1 | 5, 3 | <1, <1 | <1, <1 | 260, 264 |
| 17, humus | 2, 4 | 12, 12 | 9, 10 | 9, 8 | 133, 200 |
| 23, humus | 4, 5 | 6, 4 | 4, 4 | <1, <1 | 86, 61 |
| 31, humus | 1, 1 | 16, 17 | 10, 11 | 3, 1 | 44, 53 |
| 42, humus | 2, 2 | 6, 6 | 6, 6 | 5, 4 | 450, 434 |
| 48, humus | 10, 10 | 18, 18 | 7, 7 | 3, 2 | 66, 72 |
| 56, humus | 6, 6 | 10, 9 | 9, 9 | 3, 3 | 296, 306 |
| 61, humus | 60, 57 | 120, 123 | 31, 29 | 3, 4 | 63, 48 |
| Average RSD | 7% | 5% | 3% | 6% | 5% |

¹ Humus samples were leached with pyrophosphate prior to application of this sequential extraction scheme.

Table 15. Replicate analyses of soil, till, and humus samples from Snow Lake, Manitoba, for Fe through the sequential extraction scheme; values in ppm.

| Sample ¹ | AEC | am Fe ox | cry Fe ox | sulphides | silicates |
|--------------------------------|------------|------------------|------------------|------------------|------------------|
| 4B, soil | 236, 271 | 3839, 3864 | 6578, 6550 | 880, 885 | 15, 150, 17, 650 |
| 27B, soil | 39, 24 | 4865, 4700 | 5825, 5760 | 1355, 1230 | 14, 950, 14, 300 |
| 37B, soil | 313, 285 | 9263, 10145 | 15, 598, 15, 528 | 2500, 2450 | 30, 300, 31, 800 |
| 48B, soil | 2733, 2402 | 8763, 9254 | 7510, 7353 | 2345, 2075 | 15, 800, 16, 300 |
| 16, till | 111, 104 | 8292, 8397 | 5770, 5700 | 905, 905 | 16, 150, 15, 450 |
| 54, till | 82, 82 | 6897, 6869 | 5023, 4983 | 1860, 1830 | 13, 850, 13, 600 |
| 60, till | 45, 46 | 7604, 7740 | 6870, 6778 | 2940, 2905 | 15, 050, 15, 050 |
| 48, till | 1525, 1438 | 6577, 6710 | 7625, 7470 | 2165, 1905 | 18, 100, 17, 450 |
| 31, till, 2 µm | 58, 60 | 10, 218, 10, 020 | 6855, 7870 | 10, 100, 11, 000 | 14, 440, 14, 460 |
| 41, till, 2 µm | 165, 160 | 9888, 10047 | 8335, 8660 | 12, 300, 12, 500 | 20, 400, 21, 420 |
| 8, humus | 234, 193 | 1324, 1217 | 1721, 1657 | 490, 555 | 14, 840, 13, 720 |
| 17, humus | 214, 231 | 2114, 1934 | 2280, 2376 | 2855, 2420 | 5320, 10, 280 |
| 23, humus | 159, 138 | 514, 424 | 672, 761 | 239, 312 | 4700, 3420 |
| 31, humus | 31, 27 | 3600, 3655 | 2500, 2643 | 614, 591 | 3716, 4648 |
| 42, humus | 46, 47 | 1909, 1955 | 1100, 1094 | 584, 604 | 28, 500, 27, 040 |
| 48, humus | 146, 147 | 1783, 1788 | 850, 822 | 724, 813 | 2872, 3244 |
| 56, humus | 58, 44 | 5206, 4803 | 4051, 4288 | 899, 890 | 14, 932, 15, 076 |
| 61, humus | 71, 72 | 4136, 4177 | 3004, 2897 | 497, 574 | 4176, 3404 |
| Average RSD² | 6% | 2% | 2% | 4% | 5% |

¹ Humus samples were leached with pyrophosphate prior to application of this sequential extraction scheme.
² Relative standard deviation excluding the value for humus 17 in the silicate phase.

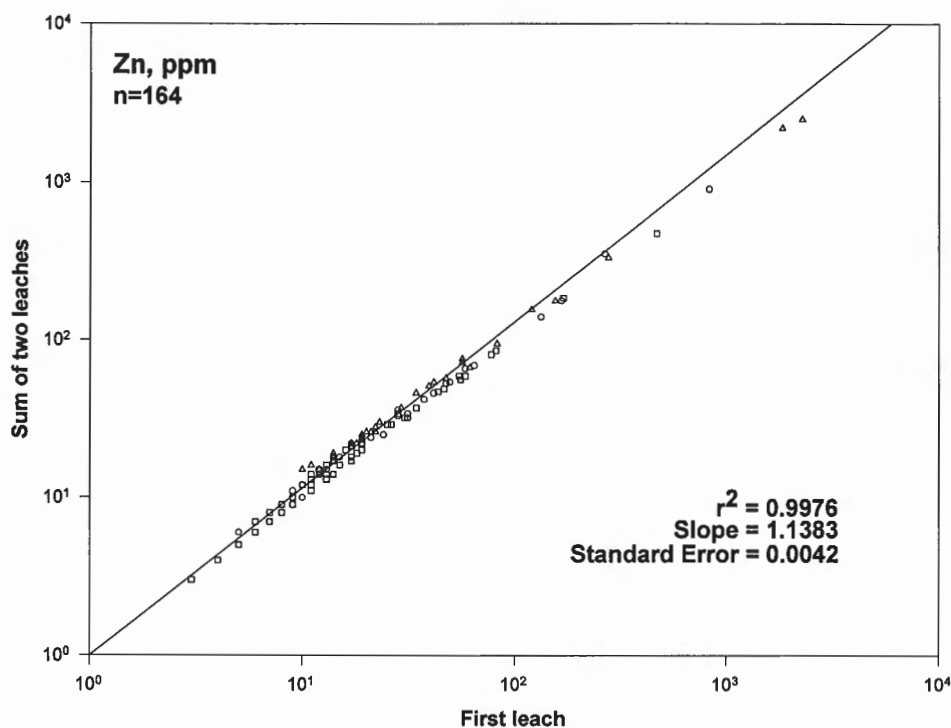
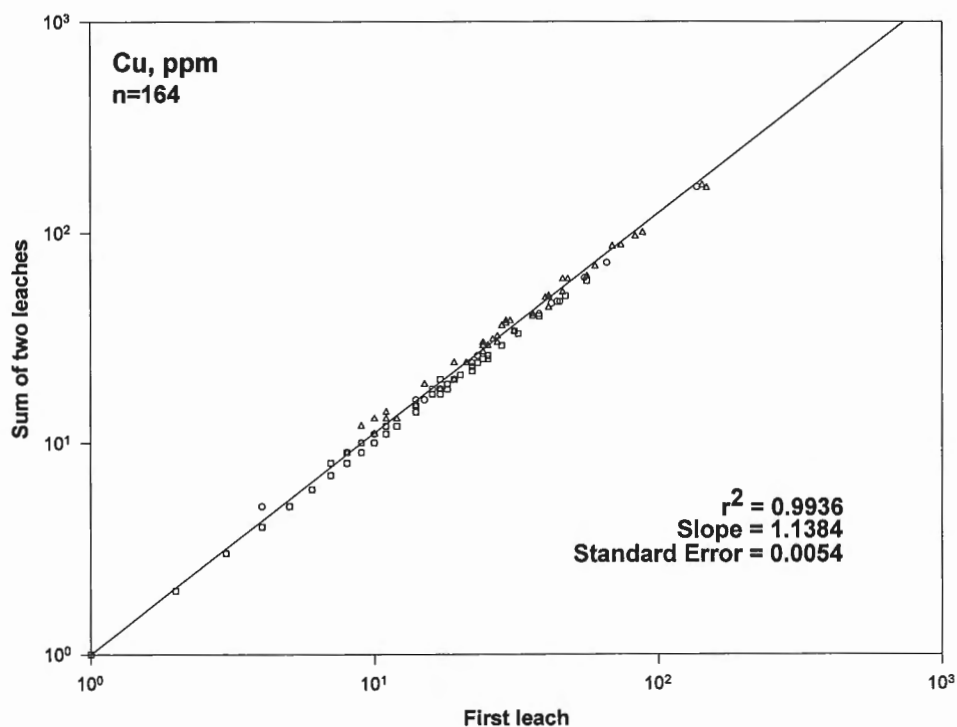


Figure 4a.

Figure 4.

Plot of sum of two 1 M $\text{NH}_2\text{OH}\cdot\text{HCl}$ (in 25% CH_3COOH) leaches versus first leach for a) Zn, b) Cu, c) Co, d) Ni, e) Mn, and f) Fe, respectively. Designations are: o – soil (<177 μm); \square – till (<177 μm); Δ – <2 μm fraction of soils and tills.

Figure 4b.



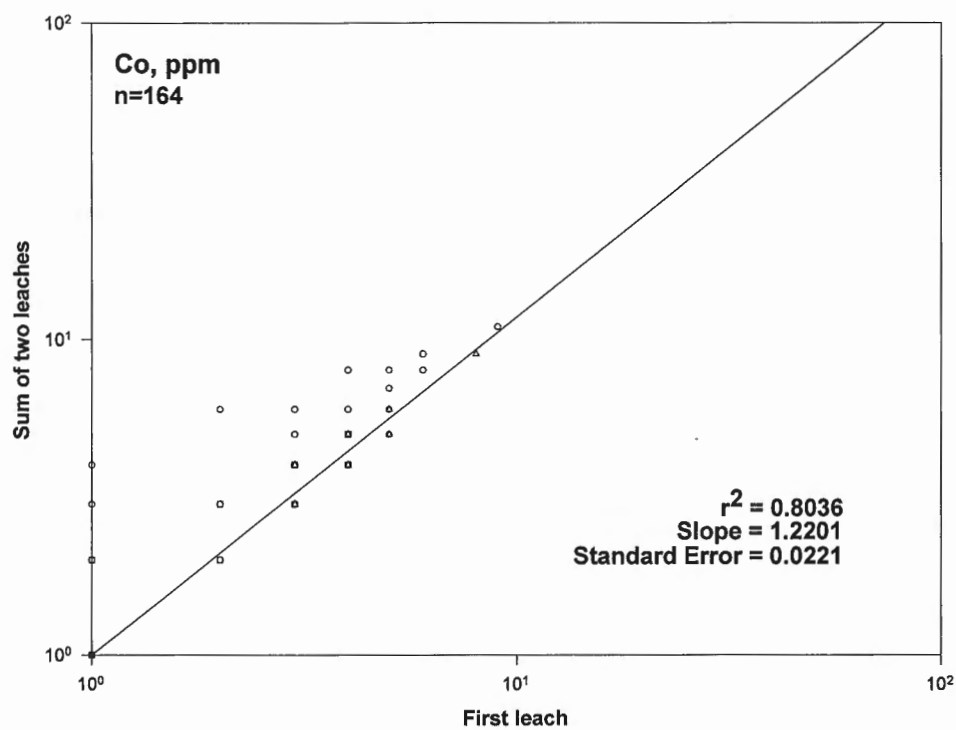


Figure 4c.

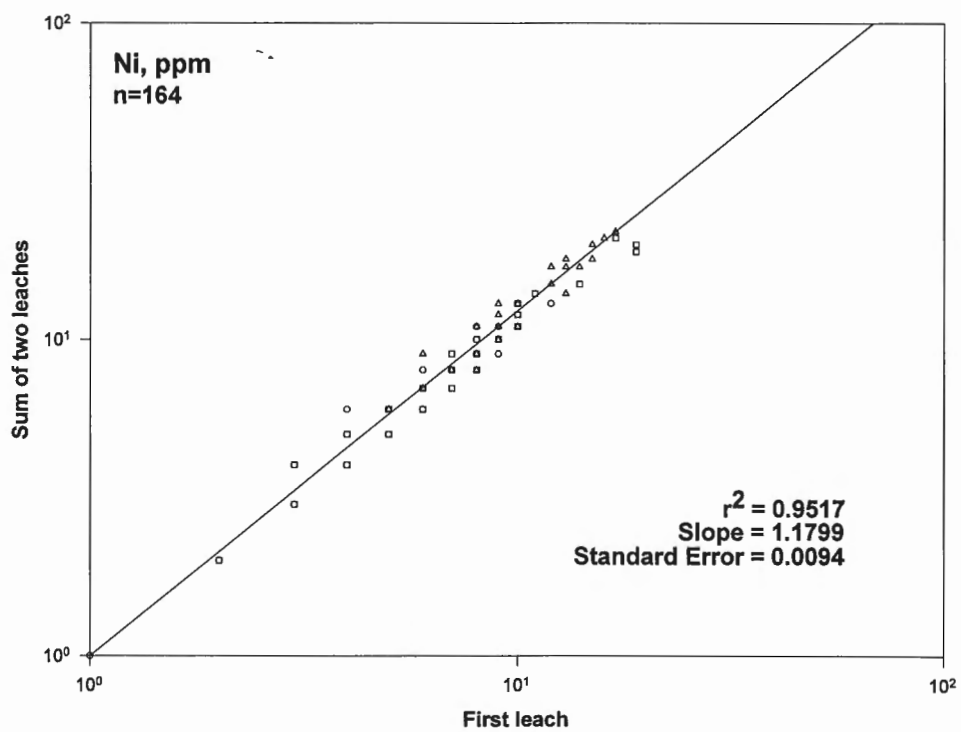


Figure 4d.

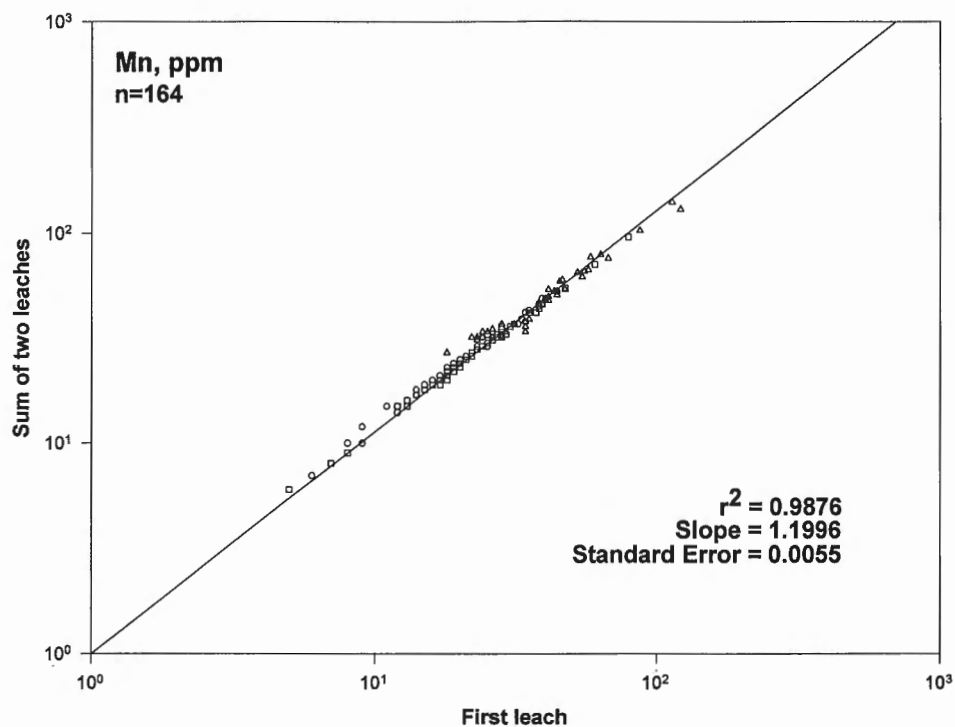


Figure 4e.

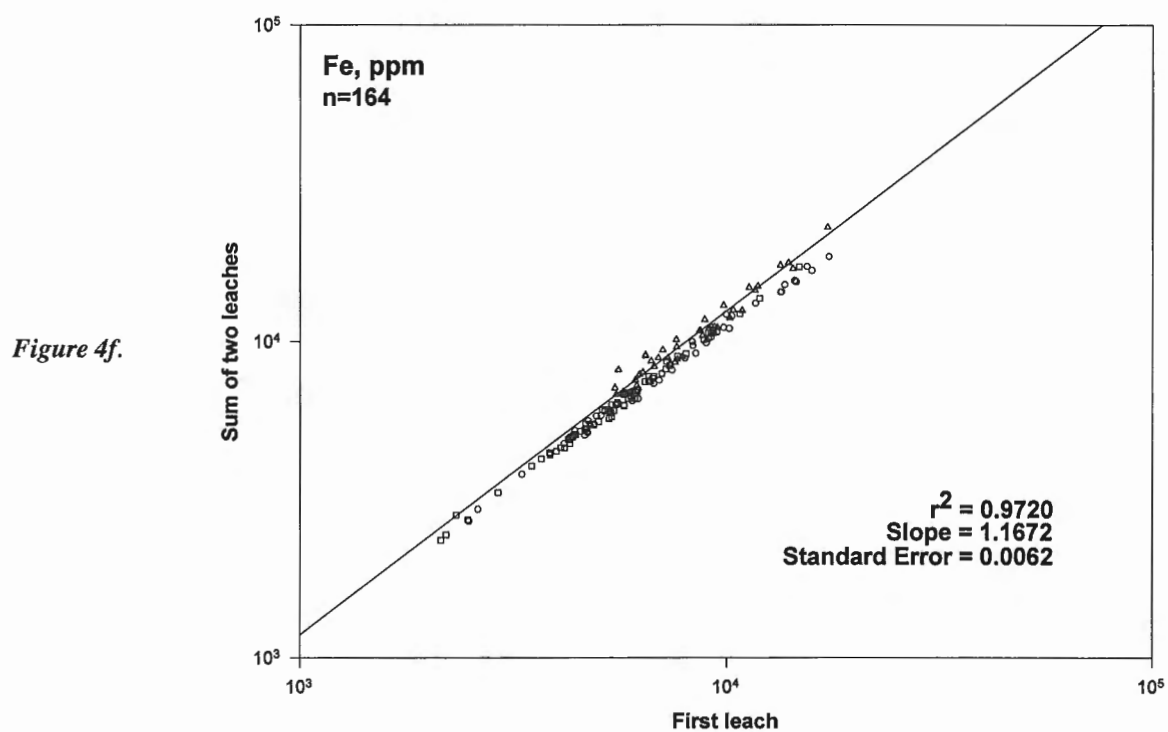


Figure 4f.

While the graphs of Figures 2 to 4 indicate that the portion of element extracted by the second application of the 0.25 and 1.0 M $\text{NH}_2\text{OH}\cdot\text{HCl}$ leaches may be insignificant, they do not provide information on the impact that their elimination would have on the value for the next leach in the sequence.

Randomly selected data for 29 samples were arranged as bar charts indicating the sequential leach results with and without incorporation of this second application of all three leaches, for Zn (Fig. 5a), Cu (Fig. 5b), and Fe (Fig. 5c). It was assumed that the amount of element which would have been extracted

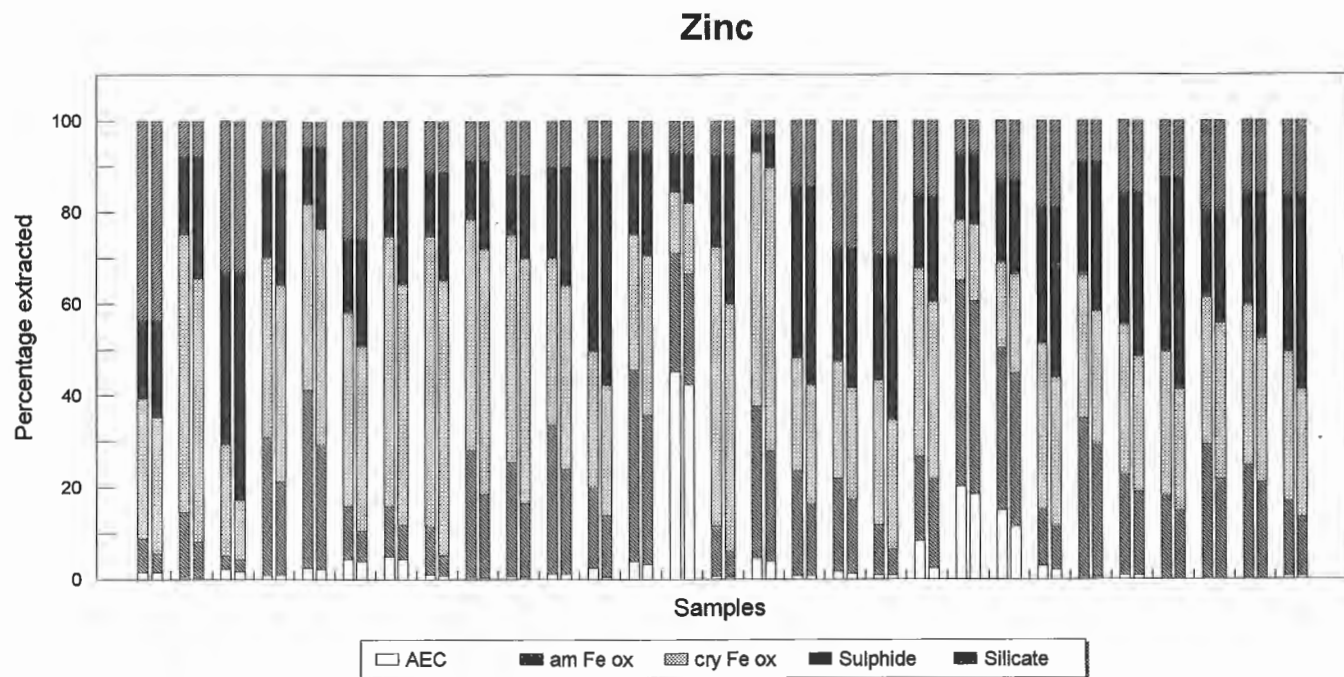


Figure 5. Bar charts showing results of sequential leach procedure for a) Zn, b) Cu, and c) Fe, respectively, in 29 samples from Snow Lake. First bar of each pair pertains to results with incorporation of second application of first three leaches and second pertains to projected data if second application was omitted.

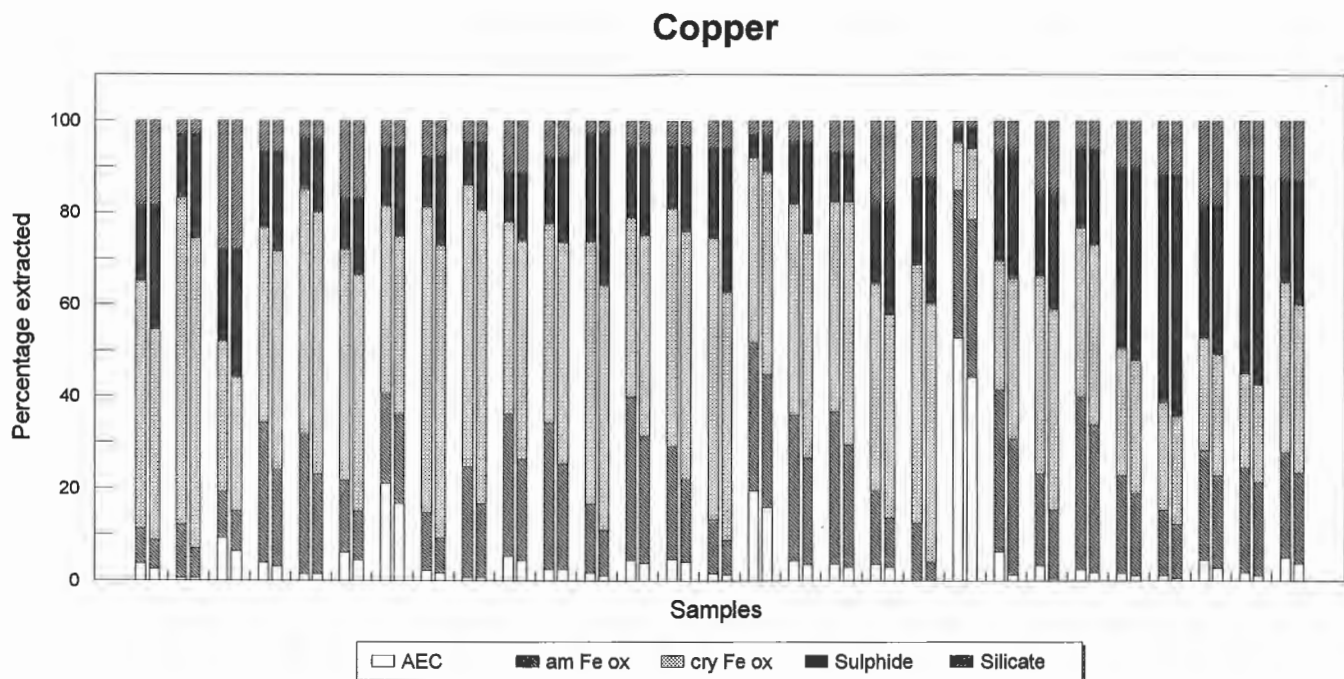


Figure 5b.

in the second application reported to the next leach in the series, an assumption which is justified by the chemistry involved and was borne out in trials. Generally the net effect of this cost-saving measure for these elements is: an overestimation of the sulphide phase concentration; not much change in the crystalline Fe oxide content; and a decrease in the amorphous Fe oxyhydroxide phase concentration. Whether these changes are of significance to the interpretation of the data depends upon the particular survey itself and its objectives. If a large number of samples are

involved, then a pilot study to examine the elimination of this second step and its effect for all relevant elements is warranted.

Amorphous Fe oxyhydroxide leach

Selectivity

The relatively high strength of HCl, at 0.25 M, recommended by Chao and Zhou (1983) in the 0.25 M $\text{NH}_2\text{OH}\cdot\text{HCl}$ leach of the amorphous Fe oxyhydroxide phase was tested for

Iron

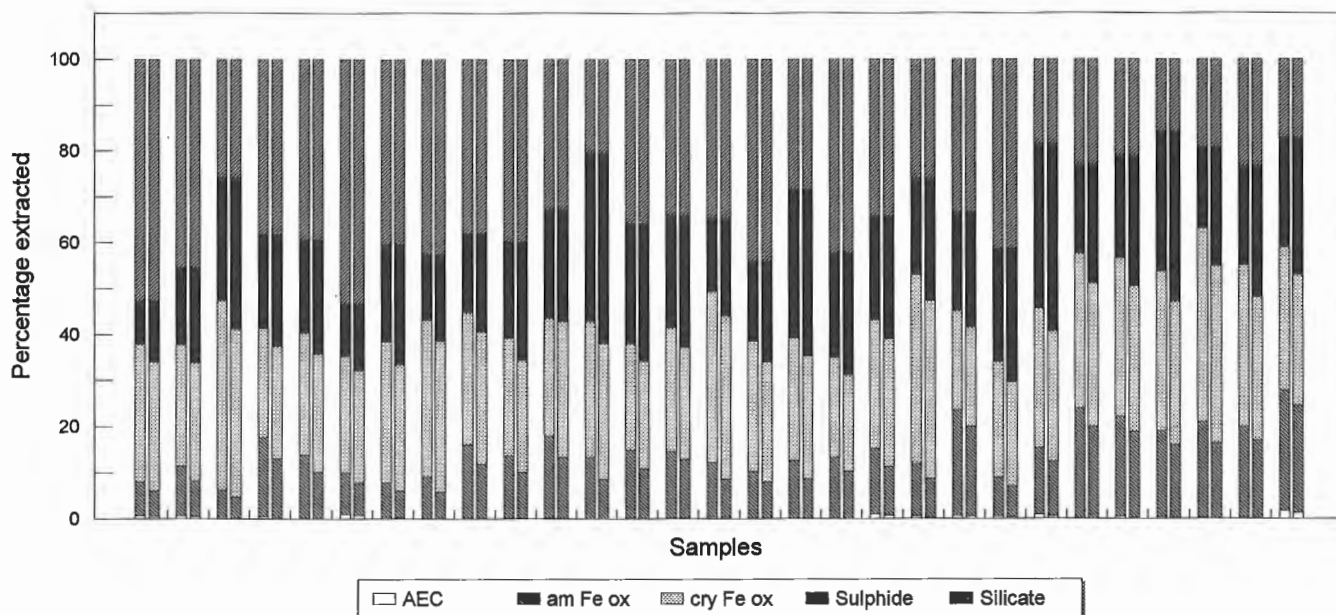


Figure 5c.

Table 16. Percentages of the major element extracted in the first and second applications of three selective leaches to 50 mg duplicates of control samples. First and second figures represent the per cent extracted by the first and second applications of each leach.

| | $\text{Na}_4\text{P}_2\text{O}_7$ leach | | CH_3COONa leach | | $\text{NH}_2\text{OH}\cdot\text{HCl}$ leach | |
|----------------------|---|-----------|---------------------------------|-----------|---|-----------|
| Sample | Dup1 | Dup 2 | Dup 1 | Dup 2 | Dup 1 | Dup 2 |
| CZn-1 | 4.92/0.61 | 5.02/0.61 | 5.48/0.70 | 5.21/0.74 | 6.00/1.75 | 6.03/1.59 |
| S-ZnS | 0.39/0.22 | 0.35/0.22 | 0.26/0.11 | 0.30/0.12 | 23.1/10.8 | 28.5/9.4 |
| CCu-1 | 2.80/0.34 | 2.81/0.32 | 2.48/0.51 | 2.82/0.54 | 2.02/0.90 | 2.13/1.03 |
| S-CuFeS ₂ | 1.04/0.30 | 1.20/0.23 | 0.42/0.40 | 0.41/0.34 | 2.04/0.80 | 1.97/1.04 |
| CPb-1 | 8.46/1.39 | 8.11/2.09 | 11.0/4.13 | 10.6/4.71 | 9.36/4.30 | 9.56/4.95 |
| S-PbS | 7.45/1.94 | 6.59/1.81 | 4.28/1.36 | 4.22/1.41 | 5.36/4.10 | 5.98/4.17 |
| SU-1 | 1.41/1.60 | 1.15/1.60 | 1.32/0.70 | 1.46/0.73 | 1.67/1.02 | 1.77/0.91 |
| S-FeS ₂ | 2.11/0.71 | 1.92/0.80 | 2.16/0.15 | 2.89/0.24 | 1.33/0.14 | 1.94/0.21 |

Table 17. Effect of HCl concentration on the 0.25 M $\text{NH}_2\text{OH}\cdot\text{HCl}$ dissolution of synthetic amorphous Fe oxyhydroxides containing analytes of interest. Concentrations are in per cent, calculated back to the solid phase.

| HCl | Fe/Zn oxide | | Fe/Cd oxide | | Fe/Cu oxide | | Fe/Co oxide | | Fe/Ni oxide | | Fe/Mn oxide | | Fe/Pb oxide | |
|--------|-------------|------|-------------|------|-------------|------|-------------|------|-------------|------|-------------|------|-------------|------|
| | Fe | Zn | Fe | Cd | Fe | Cu | Fe | Co | Fe | Ni | Fe | Mn | Fe | Pb |
| 0.00 M | 9.67 | 0.27 | 8.33 | 1.18 | 10.9 | 1.19 | 6.14 | 0.89 | 8.70 | 1.74 | 9.31 | 1.83 | 9.85 | 1.94 |
| 0.05 M | 40.7 | 0.84 | 30.5 | 2.03 | 38.6 | 1.78 | 31.8 | 2.50 | 25.2 | 2.32 | 38.0 | 3.73 | 33.0 | 5.20 |
| 0.10 M | 38.4 | 0.76 | 28.6 | 1.73 | 31.8 | 1.77 | 25.0 | 2.01 | 21.2 | 2.06 | 35.6 | 3.44 | 28.7 | 4.90 |
| 0.15 M | 42.4 | 0.83 | 30.6 | 1.89 | 40.2 | 1.71 | 30.6 | 2.37 | 24.0 | 2.33 | 33.3 | 2.78 | 30.6 | 4.97 |
| 0.20 M | 38.2 | 0.71 | 30.6 | 1.93 | 38.2 | 1.65 | 29.1 | 2.29 | 24.1 | 2.24 | 33.3 | 2.89 | 31.6 | 5.02 |
| 0.25 M | 44.1 | 0.86 | 31.2 | 2.09 | 37.4 | 1.64 | 31.4 | 2.44 | 26.1 | 2.33 | 33.0 | 3.24 | 34.3 | 5.45 |

dissolution of the various sulphide-rich samples mentioned earlier. Concentrations of the major elements in these samples were known from previous studies and from CCRMP certificates. Subsamples of 50 mg were taken in duplicate through the 0.25 M $\text{NH}_2\text{OH}\cdot\text{HCl}$ /0.25 M HCl leach (i.e. first 2 h and second 0.5 h, steps 5-8) and in addition, through the CH_3COONa leach (i.e. first and second 6 h, steps 1-4) and through the $\text{Na}_4\text{P}_2\text{O}_7$ leach to dissolve the 'soluble' organic phase (see Hall et al., 1996b). The results are shown in Table 16. Each pair of numbers represents first, the per cent of major element (e.g. Zn in CZn-1, Cu in S-CuFeS₂, and Ni in SU-1) extracted by the first application of the particular leach and second, the per cent extracted in the second application of that leach to the residue. At first glance, some of these percentages seem alarming. For example, all three leaches dissolve about 5-7.5% of the Zn held in CZn-1 and several per cent of Fe in S-FeS₂. All of these controls have oxidized to an extent over the years in storage and, moreover, the elements were not necessarily present originally at 100% as the sulphide mineral. The fact that the three leaches, quite different in their chemical attack and ranging in pH from <2 to 10, dissolve these elements approximately to the same degree suggests that there is a significant portion of them present in a very labile form. It is doubtful that, say, about 5% Zn exists in CZn-1 in the 'soluble' organic phase, another 5-6% in the adsorbed/exchangeable/carbonate phase, and yet another 6-7.5% Zn in the amorphous Fe oxyhydroxide phase. However, the amount of Pb dissolving from CPb-1 and S-PbS in the first and second applications of the 0.25 M $\text{NH}_2\text{OH}\cdot\text{HCl}$ leach is high, as is the amount of Zn dissolving from CZn-1 and S-ZnS. In fact, the odour of H₂S given off with the dissolution of S-ZnS was extremely powerful. These findings led to a study of the effect of both HCl and $\text{NH}_2\text{OH}\cdot\text{HCl}$ concentrations on the dissolution of these sulphides. Increasing the concentration of $\text{NH}_2\text{OH}\cdot\text{HCl}$ in increments of 0.05 M, from 0.00 to 0.25 M, did not have any significant effect on the concentration of the major element found. However, a repeat of this experiment varying the HCl concentration in the same manner (keeping the concentration of $\text{NH}_2\text{OH}\cdot\text{HCl}$ at 0.25 M) showed a steady increase from essentially zero to the values indicated in Table 16 for Zn in S-ZnS, Pb in S-PbS, and Cu in S-CuFeS₂. Thus improved selectivity of this extraction with minimization of sulphide (especially ZnS and PbS) dissolution would be gained by reducing the concentration of

HCl in the digestion. However, sufficient HCl must be present to ensure complete dissolution of the amorphous Fe oxyhydroxide.

Samples of synthetic hydrous Fe oxides, containing the analytes of interest, were prepared according to the method of Chao and Zhou (1983). Each element (Zn, Cd, Cu, Co, Ni, Mn, and Pb) in solution was added to a solution of 0.5 M $\text{Fe}(\text{NO}_3)_3$ to achieve a final strength of 0.05 M in that element. With constant stirring, 50 mL of 10% NaOH were then added to each mixture and the hydrous oxide so formed filtered off with Whatman #40 paper. Upon drying, each hardened precipitate was ground by hand with a pestle and mortar. A 50 mg portion was taken for aqua regia digestion and analysis for 'total' elemental concentration and another aliquot was taken through the 0.25 M $\text{NH}_2\text{OH}\cdot\text{HCl}$ leach after washing off any adsorbed elements with 1 M CH_3COONa solution, again varying the HCl concentration in increments of 0.05 M. The results of this experiment are shown in Table 17; concentrations given were calculated back to the precipitate. Clearly, a plateau is quickly reached at about 0.05 M HCl after which the concentration of Fe or other elements does not significantly increase. (The data are somewhat noisy as the precipitates are probably fairly heterogeneous.) It can be assumed then that this concentration of HCl is sufficient for complete dissolution of the amorphous Fe oxyhydroxide phase of a soil or sediment. At 0.05 M HCl, the amount of Cu, Pb, Ni, and Fe dissolved from the sulphides listed in Table 16 is well below 1% and the amount of Zn dissolved from sphalerite is below 2%. These figures then represent the maximum percentage of metal dissolved from its sulphide by 0.25 M $\text{NH}_2\text{OH}\cdot\text{HCl}$ in 0.05 M HCl as these samples evidently contain the element in a more labile, oxidized form also.

In order to observe the effect that changing the strength of HCl from 0.25 to 0.05 M in the amorphous Fe oxyhydroxide leach has on subsequent leaches, a batch of samples was taken through the sequential scheme using both approaches. Nineteen samples of soil and till were selected from the Snow Lake project, together with duplicates of three soil samples (from the National Institute of Standards and Technology, NIST, U.S.A.) and TILL-2. Their results are shown as bar charts in Figure 6a through Figure 6e, for Zn, Cu, Ni, Mn, and Fe, respectively. The last 8 bar charts on each figure represent the duplicate data obtained for the SRMs NIST 2709, 2710, 2711,

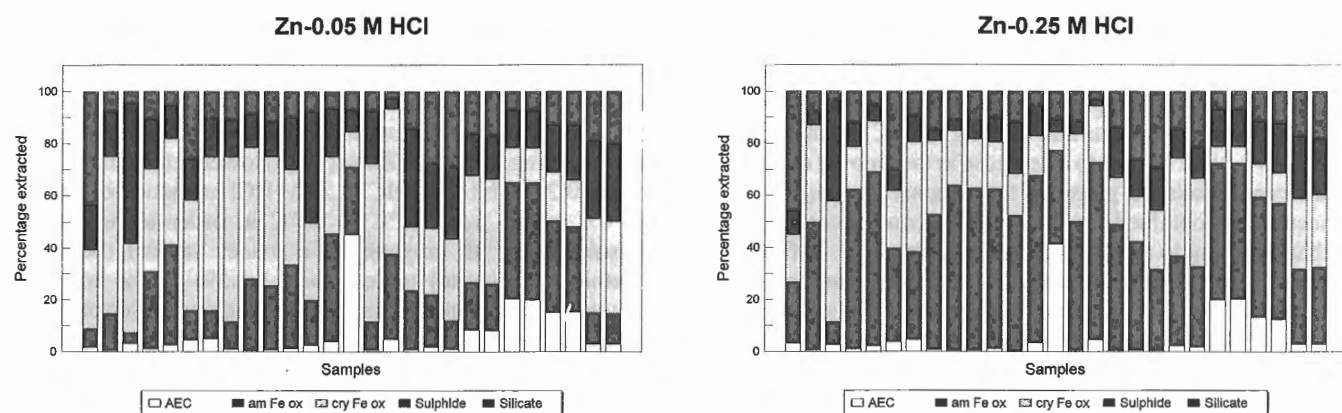


Figure 6a.

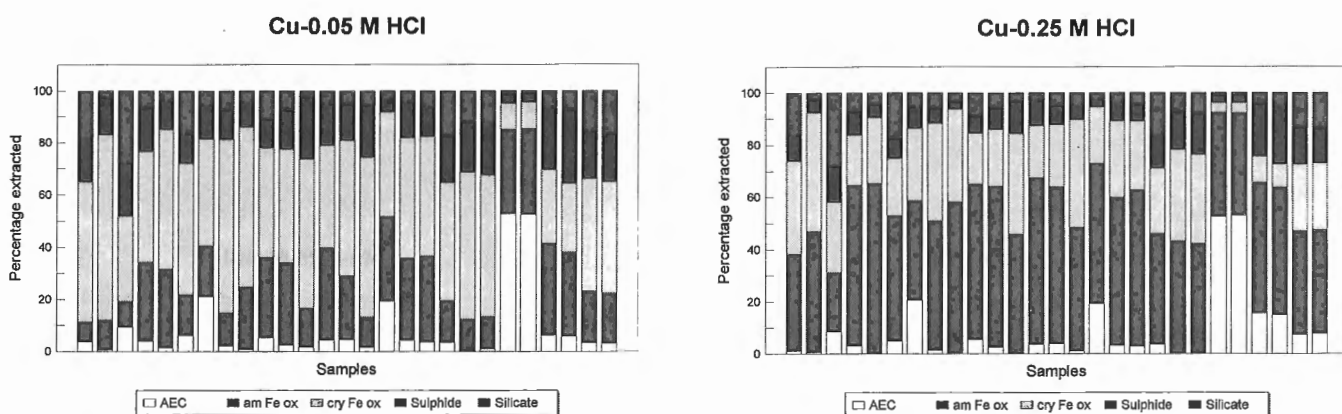


Figure 6b.

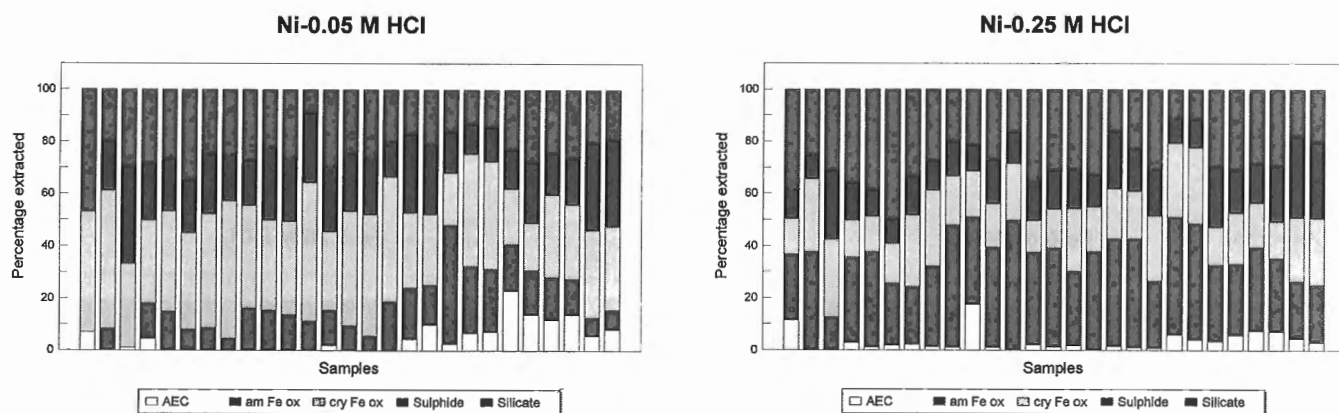


Figure 6c.

Figure 6. Bar charts showing results of sequential leach procedure for a) Zn, b) Cu, c) Ni, d) Mn, and e) Fe; respectively, for 19 samples from Snow Lake and duplicates of SRMs NIST 2709, 2710, 2711, and TILL-2. Two sets of results were obtained using 0.05 and 0.25 M HCl in the 0.25 M $\text{NH}_2\text{OH}\cdot\text{HCl}$ extraction of 'am Fe ox' phase.

and TILL-2, respectively. As conditions have not changed for the extraction of metals bound in the 'AEC' and silicate phases, their relevant percentages extracted remain constant, within the limits of sampling and analytical noise. However, for all elements, it is clear that altering the HCl strength from 0.25 M to 0.05 M has led to a decrease in the amount extracted in the amorphous Fe phase at the expense *not only* of the concentration obtained for the sulphide component *but also* of that reporting to the crystalline Fe oxide phase. In fact, the increase in element shown in the sulphide component, in changing to the 0.05 M strength, is generally of less significance than the increase in element reported to the 'cry Fe ox' phase. The degree to which this 'redistribution' amongst these three phases takes place is, naturally, sample dependent. The obvious questions are:

- Is the increase in elemental concentration in the 'cry Fe ox' phase due to inadequate dissolution of the earlier 'am Fe ox' phase (although the results shown in Table 17 contradict this)?
- Do the conditions of the 'am Fe ox' leach at the higher HCl concentration lead to premature dissolution of the 'cry Fe ox' phase?

The pH of the 'am Fe ox' extractant at the end of the leach period was measured for the suite of samples tested at the lower acid concentration of 0.05 M HCl. All values were well below 2, indicating that acidic conditions were maintained and loss of analytes through precipitation or hydrolysis was not occurring. Chao and Zhou (1983) lowered the temperature of this 0.25 M $\text{NH}_2\text{OH}\cdot\text{HCl}/0.25\text{ M HCl}$ extraction of the 'am Fe ox' phase from 70°C to 50°C in order to reduce the dissolution of all crystalline Fe oxides studied (hematite, goethite, magnetite) to less than 1-1.5% of the total Fe. However, the extent of dissolution of the crystalline oxides at the higher temperature was only slightly more, at 1-2% of the Fe. Therefore, extraction at an intermediate temperature of 60°C is not likely to be responsible for a significant positive error on the concentrations found in the 'am Fe ox' phase. Alternatively, the lower acid strength may not be adequate to dissolve completely all forms of amorphous Fe oxide. The two sets of results for the sequential extraction, at 0.05 and 0.25 M HCl in the 'am Fe ox' phase extraction, point to the 'fine line' in differentiating amorphous from crystalline Fe oxides. The transition from the amorphous Fe oxides through cryptocrystalline forms to the crystalline Fe oxides is by no means clearly defined and this is being reflected in these different results in chemical extractability. More research is

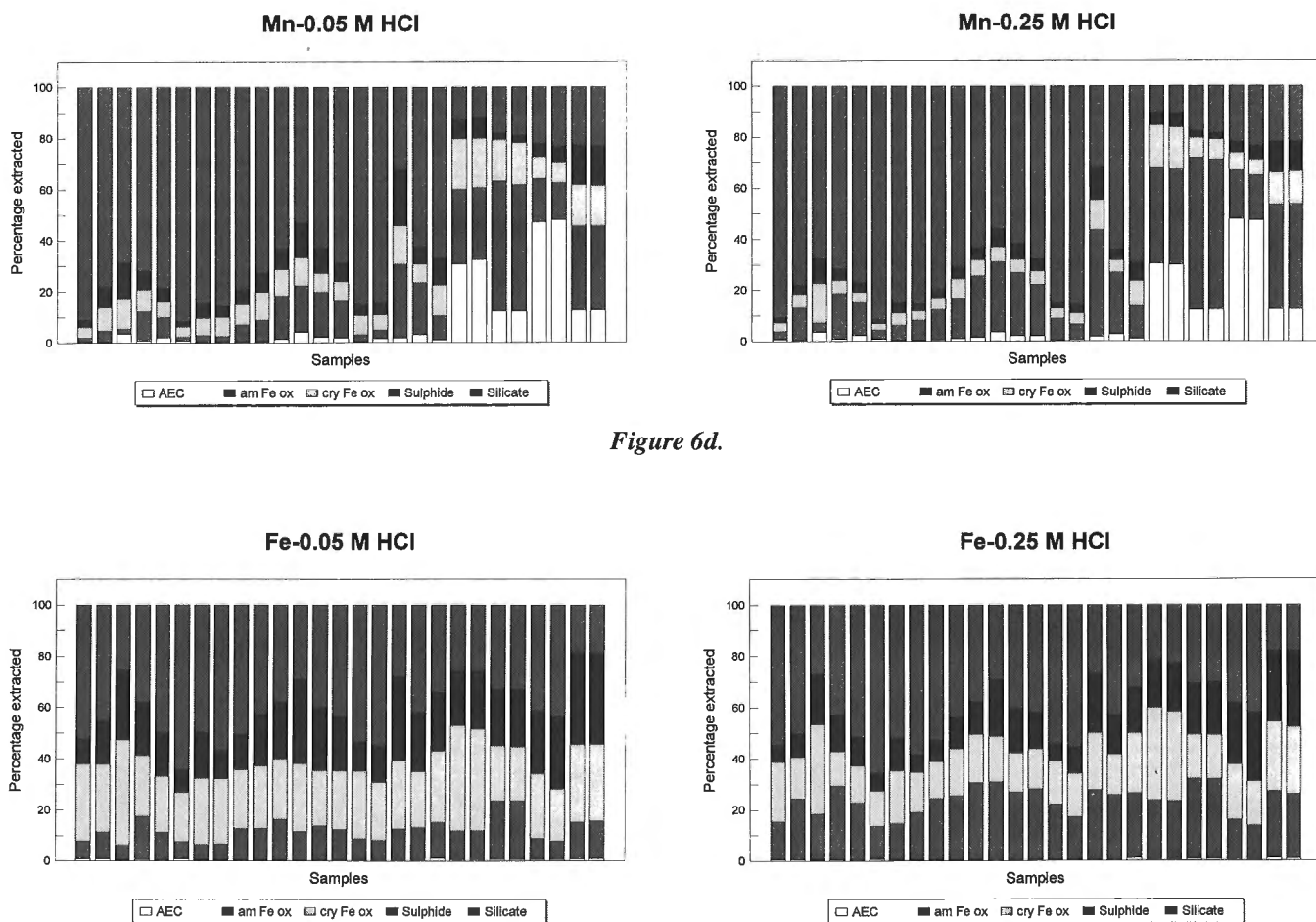


Figure 6d.

Figure 6e.

needed in this area to recommend extraction conditions in various circumstances. If sulphides, particularly sphalerite, are present in the matrix, then a compromise of 0.1 M HCl may be chosen. These results reaffirm the axiom that strict adherence to the experimental conditions selected is mandatory in the application of selective leaches in geochemical surveys. Merging of data from one survey with another where extraction conditions vary (though the phases supposedly dissolved are nominally the same) probably will introduce some degree of bias.

Another phase tested for possible dissolution in the 0.25 M $\text{NH}_2\text{OH}\cdot\text{HCl}$ extraction was the labile organic component, normally leached from the sample with 0.1 M $\text{Na}_4\text{P}_2\text{O}_7$ solution (see Hall et al., 1996b). The two 2 h and 30 min leaches were applied directly (without the previous CH_3COONa extraction) to soils collected in Manitoba in

addition to SRMs, LKSD-4, and TILL-2. The dissolved organic carbon content of the leachates was measured with a Shimadzu 5000 TOC instrument based on combustion at 680°C and nondispersive infra-red detection. Results are given in Table 18, together with concentrations of organic carbon soluble in two consecutive applications of a 1 h leach with 0.1 M $\text{Na}_4\text{P}_2\text{O}_7$ solution. Regardless of HCl concentration (0.05 or 0.25 M), an astonishing proportion of the labile organic component of these soils and sediment has been dissolved by the hydroxylamine reagent, up to 45% in the case of LKSD-4. Schemes such as those of Chao and Theobald (1976), Tessier et al. (1979), and Filipek and Theobald (1981), listed in Table 1, probably lead to overestimation of metals in the Fe oxyhydroxide phase due to release of those bound in the labile organic component. Although their original

Table 18. Comparison of the organic carbon leached by 0.25 M $\text{NH}_2\text{OH}\cdot\text{HCl}$ in 0.05 M HCl and that leached by 0.1 M $\text{Na}_4\text{P}_2\text{O}_7$ in soils and SRMs, TILL-2, and LKSD-4.

| Sample | Organic carbon (ppm) | | | |
|---------------------------|--|--------------------|---|-----------------|
| | 0.25 M $\text{NH}_2\text{OH}\cdot\text{HCl}$ | | 0.1 M $\text{Na}_4\text{P}_2\text{O}_7$ | |
| | 1st leach (2 h) | 2nd leach (0.5 h.) | 1st leach (1 h) | 2nd leach (1 h) |
| 93-HJB 2118 | 16 365 | 2913 | 49 040 | 12 536 |
| 93-HJB 2011H | 19 703 | 6121 | 46 220 | 9882 |
| 93-HJB 2011H ¹ | 19 672 | 6294 | | |
| 93-MOB 0205 | 6600 | 1227 | 15 988 | 3177 |
| 93-HJB 2023 | 5081 | 852 | 24 840 | 5244 |
| 93-HJB 1005H | 8053 | 1463 | 27 640 | 5800 |
| 93-JC 0080 | 5617 | 2046 | 34 160 | 4793 |
| TILL-2 | 5273 | 1263 | | |
| TILL-2 ² | 5472 | | 21 820 | |
| LKSD-4 | 14559 | 914 | 24 300 | 4479 |
| LKSD-4 ² | 15 525 | | 24 000 | |

¹ This is a separate 1 g subsample
² The HCl concentration was 0.25 M rather than 0.05 M in this case.

Table 19. Results for mean and standard deviation of elements extracted from till controls TC 3 and TC 4 by the 0.25 M $\text{NH}_2\text{OH}\cdot\text{HCl}$ leach Concentrations in ppm unless otherwise noted; values in parentheses are the RSDs in per cent.

| Sample | Al (%) | Ba | Co | Cr | Cu | Fe (%) | La | Mg (%) | Mn | Ni | Pb | Sr | V | Zn |
|-------------------|-----------------|-----------------|------------------|---------------|------------------|-----------------|---------------|-----------------|---------------|------------------|-----------------|---------------|------------------|-----------------|
| TC 3 ¹ | 1.28/19 (15) | 41/14 (34) | 12.4/1.2 (10) | 34/6 (17) | 19.6/2.5 (12) | 1.79/32 (18) | 9.9/8 (8) | 0.56/10 (17) | 392/28 (7) | 19.8/3.7 (18) | 9.8/1.3 (13) | 2.4/5 (21) | 37/5 (13) | 56/7 (12) |
| TC 3 ² | 1.12/12 (10) | 43/3 (7) | 10.9/8 (7) | 28/4 (14) | 17.3/1.5 (9) | 1.63/24 (14) | 9.6/7 (7) | 0.47/07 (14) | 353/21 (6) | 17.3/2.3 (13) | <2 (8) | 2.6/2 (8) | 33/3 (10) | 47/5 (10) |
| TC 4 ¹ | 1.25/05 (4) | 5.4/1.7 (31) | <1 (10) | 8.6/9 (10) | <0.5 (8) | 0.62/05 (8) | 2.0/3 (15) | 0.03/01 (33) | 19/3 (16) | 3.3/1.1 (33) | <2 (11) | 0.9/1 (11) | 10.6/1.1 (10) | 5.1/1.1 (21) |
| TC 4 ² | 1.30/04 (3) | 5.4/5 (9) | <1 (10) | 7.8/8 (10) | <0.5 (9) | 0.56/05 (9) | 2.0/1 (5) | 0.02/01 (50) | 19/2 (10) | 2.2/6 (27) | <2 (10) | 1.0/1 (10) | 10.0/7 (7) | 2.9/8 (27) |

¹ Result reflects the sum of the two extractions (after removing the AEC phase with CH_3COONa), n=21
² Result reflects the first $\text{NH}_2\text{OH}\cdot\text{HCl}$ extraction only (after removing the AEC phase with CH_3COONa), n=12

test work showed that organic carbon in the sediment was not diminished by the hydroxylamine leach, Tessier et al. (1979) did not rule out dissolution of metals held in a labile organic phase (as humates and fulvates). Clearly, for organic-rich soils and sediments, this component should be removed prior to the extraction for the amorphous Fe oxyhydroxide phase, by inserting the pyrophosphate leach immediately before it in the scheme (Fig. 1).

Precision

Long term precision data on results of the 'am Fe ox' phase have been obtained from the analyses of two till control samples, TC 3 and 4, collected and prepared (sieved to $<177\ \mu\text{m}$) under the Canada-Ontario Mineral Development Agreement (MDA) 1990-1995. These samples were used to monitor precision and bias in the application of this leach, under contract, by X-ray Assay Laboratories (XRAL) of Toronto over a 2 year period (1993-1995). The mean and standard deviation data, shown in Table 19, are separated into two groups for each control: the first row ($n = 21$, 1 g subsamples) represents the values obtained by carrying out the two $0.25\ \text{M}\ \text{NH}_2\text{OH}\cdot\text{HCl}/0.25\ \text{M}\ \text{HCl}$ leaches (2 h and 30 min) as suggested in the procedure (after removing the 'AEC' phase with CH_3COONa), whereas the second row ($n = 12$) represents the values obtained by only the first 2 h application. The analytical technique employed by XRAL was ICP-ES, providing the following detection limits: 0.5 ppm for Cu, La, Sr, and Zn; 1 ppm for Ba, Co, Cr, and Ni; 2 ppm for Mn, Pb, and V; and 0.01% for Al, Fe, and Mg. At concentrations a decade higher than detection limit, RSDs across these 14 elements average $12 \pm 6\%$, a figure which is certainly acceptable given the procedures involved, different operators, and time elapsed between batch submissions. The differences in element concentration between the two data sets (i.e. with/without the second leach) is not great, except for Pb where the only detectable value of 9.8 ppm for TC 3 is suspect.

Further evaluation of precision can be made using Thompson and Howarth (1978) control charts to view the 'blind' duplicate data for 75 soils and tills analyzed concurrently with TC 3 and 4 under the Ontario MDA. Blind duplicates are randomly selected samples split after preparation and their identity is unknown to the laboratory. These charts are shown in Figure 7 for 16 elements; different symbols have been used to differentiate on a yearly basis between soils (sieved to $<63\ \mu\text{m}$ and $177\ \mu\text{m}$), tills (sieved to $<63\ \mu\text{m}$ and $177\ \mu\text{m}$), and the clay-size fraction ($2\ \mu\text{m}$) of both media. On these log-log plots of absolute difference versus the mean are drawn two control lines at the 95th percentile for the selected precision (twice the RSD). The 95th percentile for a particular precision is an upper confidence line above which no more than 5% (in this case about 4) of the points should lie if that level of precision is to be accepted, and assuming that the errors are Gaussian. For comparison, the 95th percentile for another precision is also illustrated, as the 'sandwich' between the pair of lines assists a graphical appraisal. The lower (i.e. better precision) line on each graph is more representative of the majority of the samples where concentrations are above detection levels. The values for the

precision shown by these soils and tills are: 10% (i.e. $\pm 5\%$ RSD) for Al and Y; 15% for Ca, Cr, Fe, and Sr; 20% for Ba, Cu, La, V, and Zn; 25% for Mg, Mn, and Ni; and 30% for Co and Pb, elements being present at levels below about 10 ppm in this phase.

Sensitivity

With a dilution factor of 30, the detection limits achievable by FAAS or ICP-ES are generally not lower than 0.1-1 ppm which is inadequate for elements such as Cd and Pb. The more sensitive technique of ICP-MS does not tolerate direct analysis of the leachate solution because deposition on the sampler from this high salt solution causes rapid decrease in signal intensity and interference. Negation or minimization of such interferences by simple dilution was thought undesirable as it would ultimately reduce the overall detection capability and undermine the reasoning for turning to this technique. A considerable amount of research was carried out into separation from the leach matrix of the transition elements, rare-earth elements, Cd, and Pb by chelation using ion chromatography (as described in Hall et al., 1995). However, the results obtained did not justify the additional time and cost involved, particularly in view of the increased sensitivity of the newer ICP mass spectrometers recently on the market. Dilution of the leachate by a factor of 20 creates a solution which does not cause deterioration in the ICP-MS signal and ultimately provides detection limits in the ppb range. These results will be reported in a later paper.

CONCLUDING REMARKS

This work has shown that the precision associated with selective sequential leaches is excellent regardless of the number of manipulations involved. Where elements are present at levels above instrumental detection limits, long term RSDs shown by SRMs such as the TILL series and LKSD-4 are typically in the 5-12% range for all five leaches. It is the accuracy or specificity of selective leaches which requires further improvement. In particular, in support of exploration geochemistry techniques, the reducing hydroxylamine hydrochloride extraction of amorphous Fe oxyhydroxides should be further refined so that simultaneous dissolution of the labile organic component and monosulphides is minimized.

The use of selective leaches in both exploration and environmental geochemistry, regardless of their limitations, has now been widely recognized and several agencies have been active recently in establishing either certified SRMs or recommended protocols. NIST is providing an addendum to its certificates for the soils 2709-2711 where preliminary "leach" data are given. The leach employed by the participating laboratories is that specified in Method 3050 of the United States Environmental Protection Agency's recommended methods list and is based on $\text{HNO}_3\text{-H}_2\text{O}_2$, an oxidizing attack which is not very specific. The Measurements and Testing Program (formally known as the 'BCR') of the European Commission has launched the production of a sediment SRM

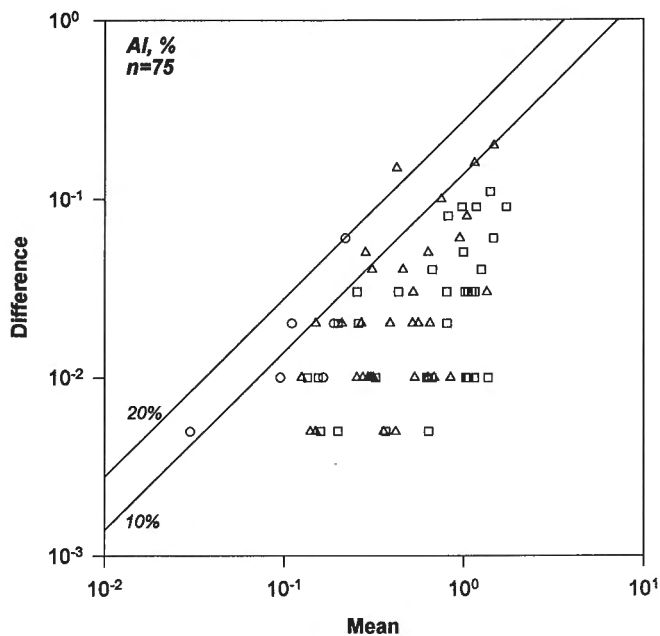


Figure 7a.

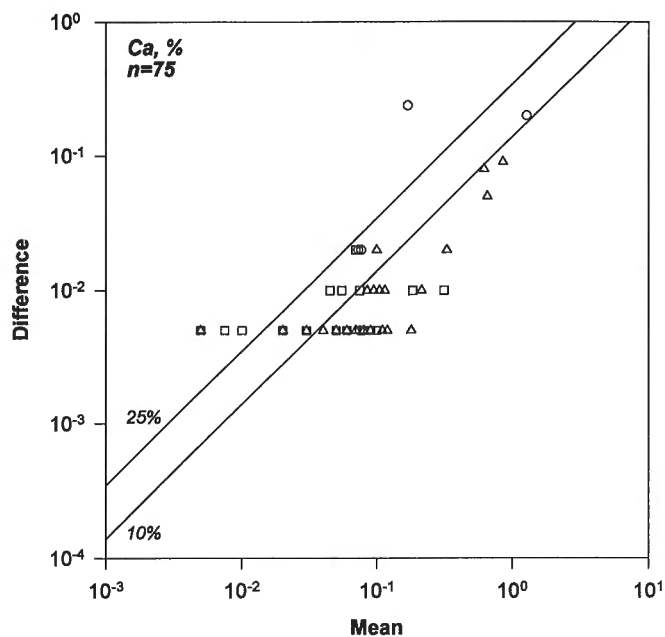


Figure 7c.

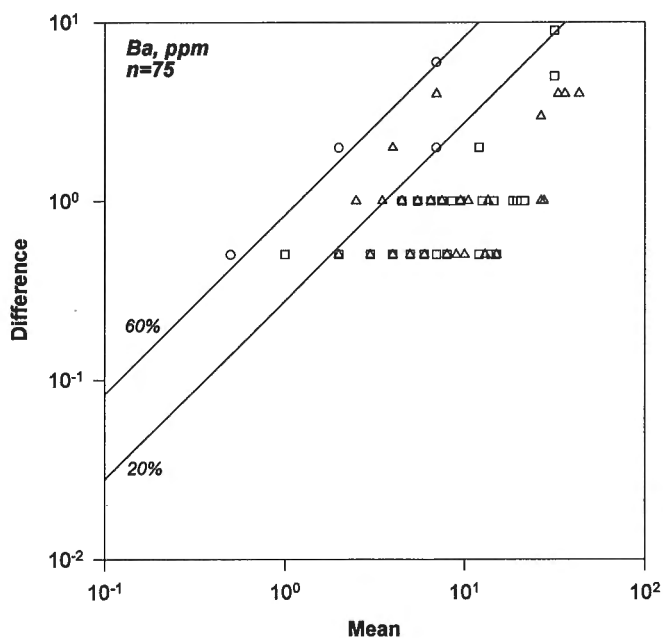


Figure 7b.

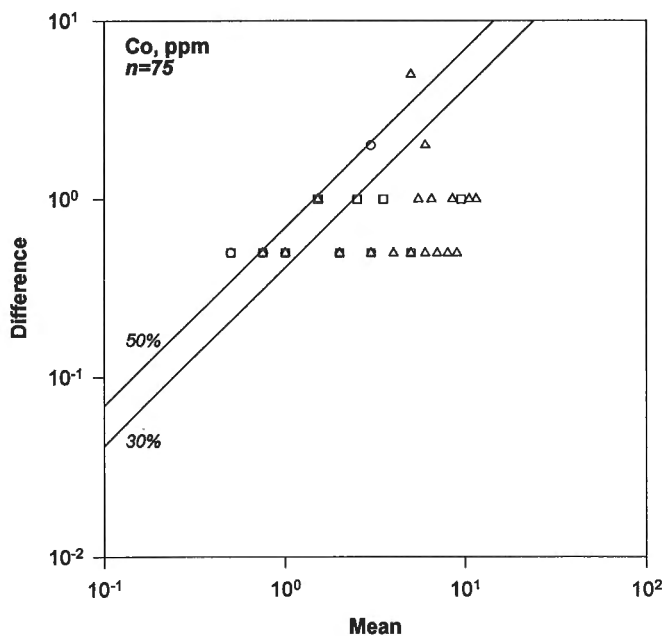


Figure 7d.

Figure 7. Thompson and Howarth (1978) plots of difference versus mean for a) Al, b) Ba, c) Ca, d) Co, e) Cr, f) Cu, g) Fe, h) La, i) Mg, j) Mn, k) Ni, l) Pb, m) Sr, n) V, o) Y, and p) Zn, respectively, in 75 duplicate samples from Ontario. Designations are: o – $<2\ \mu\text{m}$ fraction of soils and tills; \square – soil ($<177\ \mu\text{m}$ and $<63\ \mu\text{m}$); Δ – till ($<177\ \mu\text{m}$ and $<63\ \mu\text{m}$). Filled symbols indicate 92-93 collection and analyses; empty symbols indicate 93-94 collection and analyses.

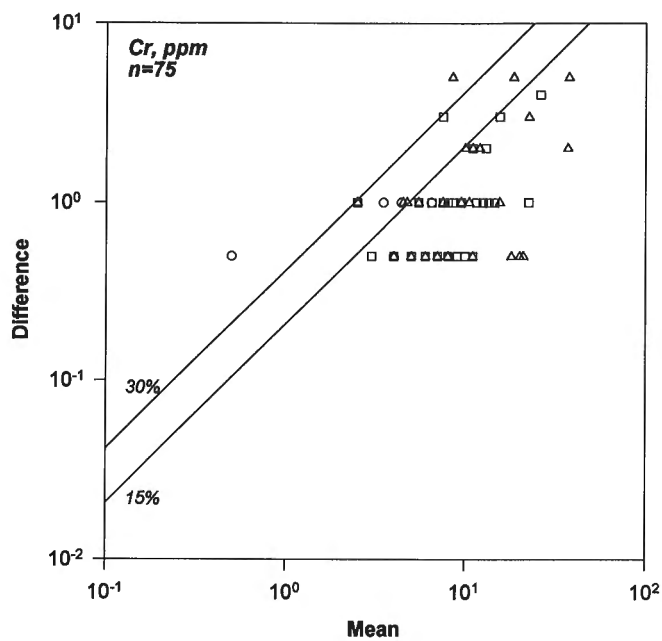


Figure 7e.

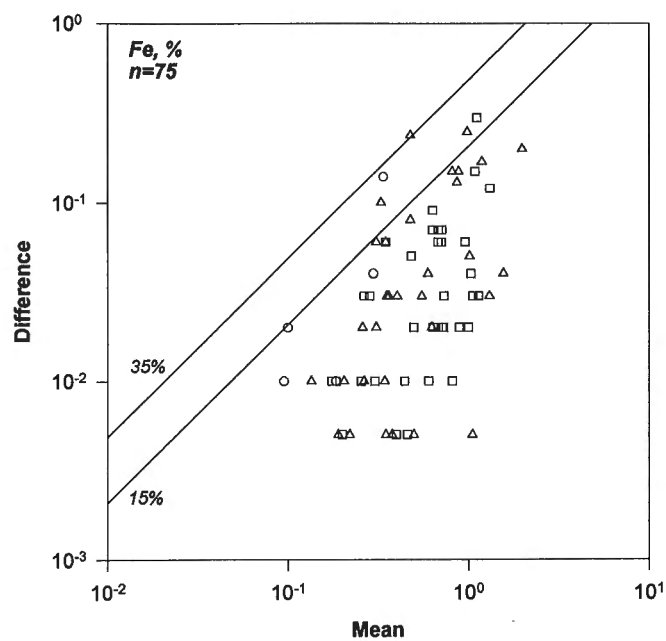


Figure 7g.

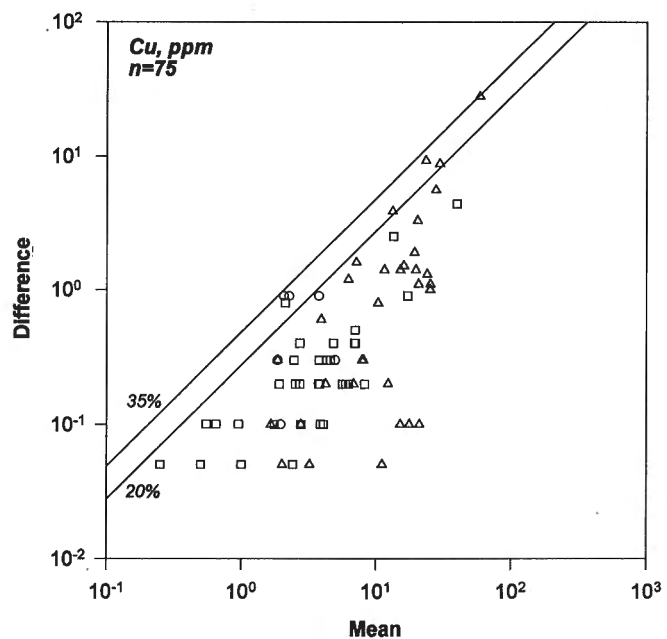


Figure 7f.

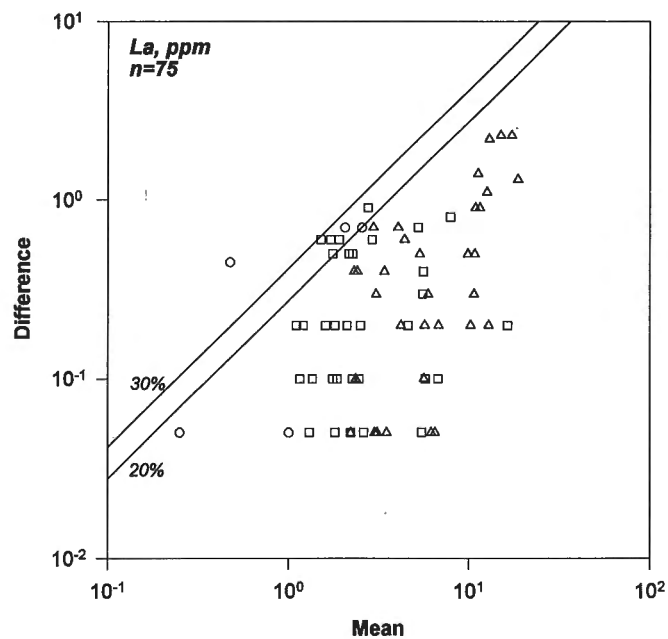


Figure 7h.

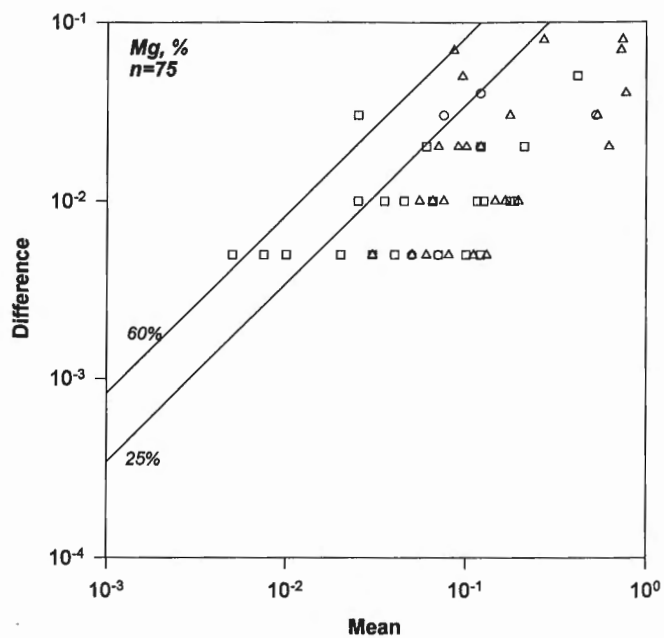


Figure 7i.

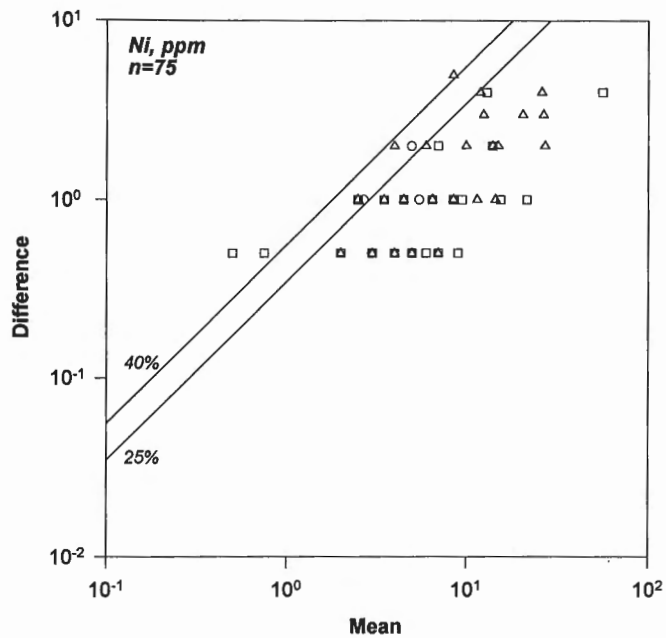


Figure 7k.

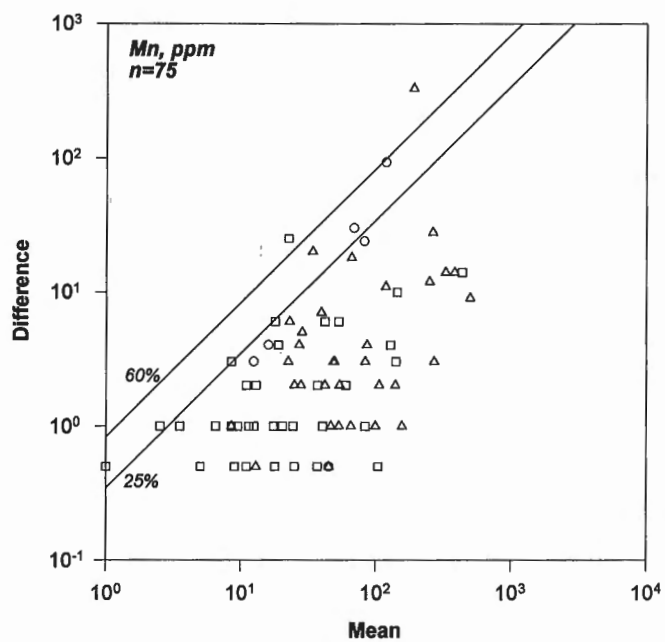


Figure 7j.

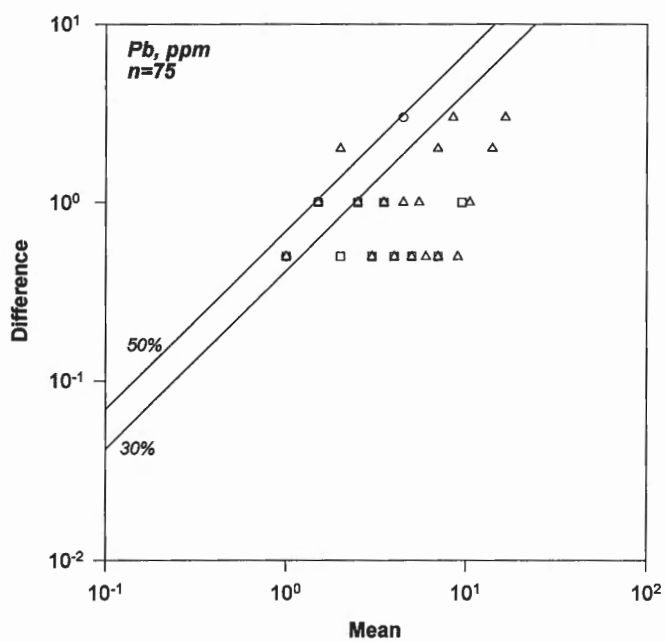


Figure 7l.

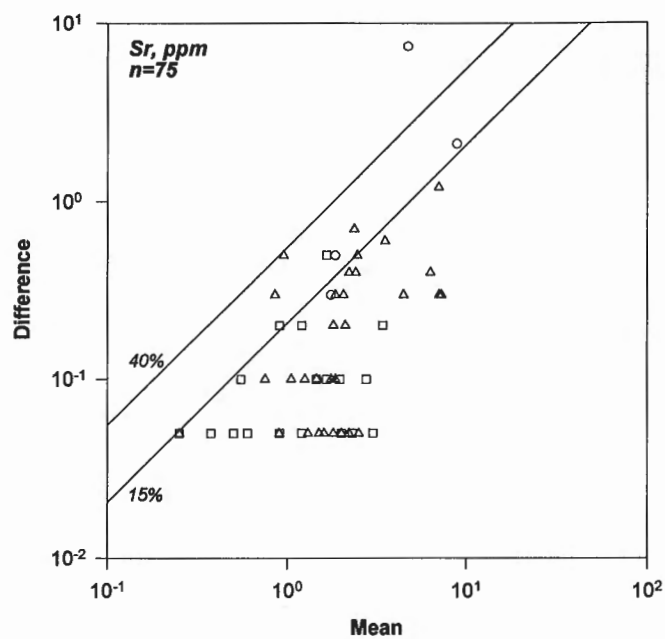


Figure 7m.

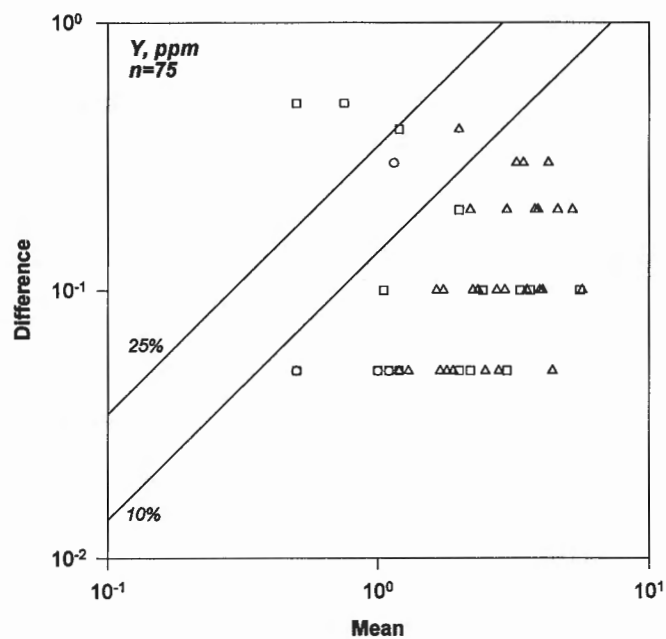


Figure 7o.

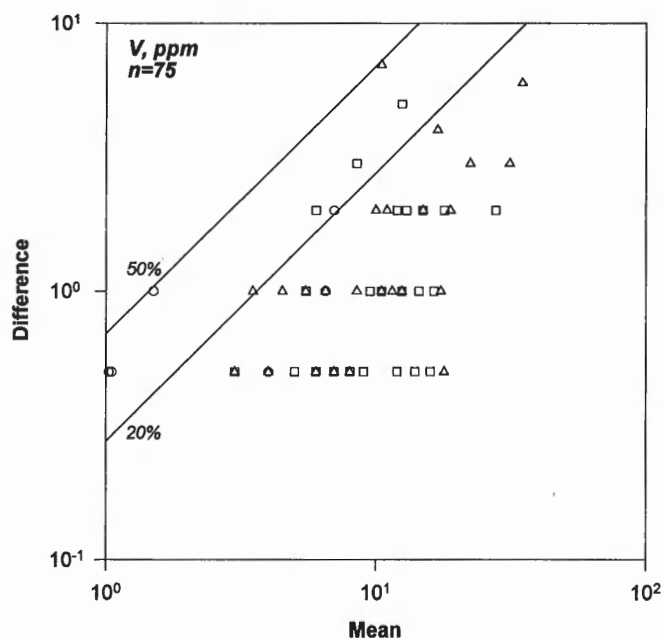


Figure 7n.

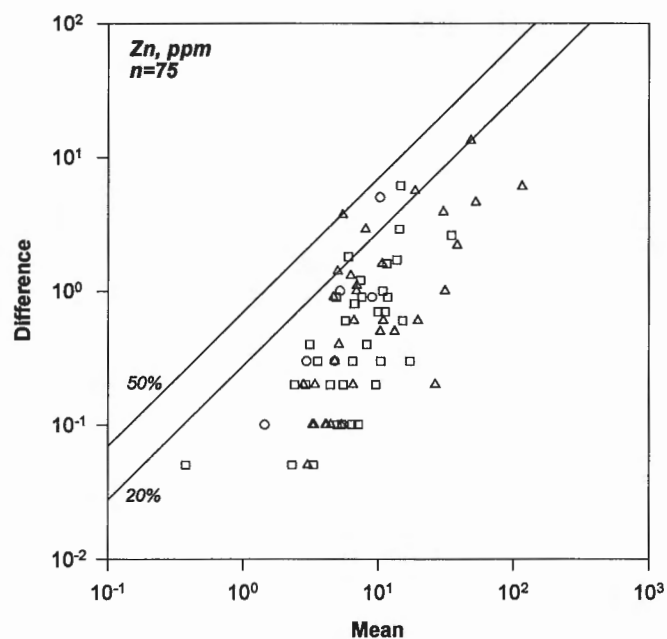


Figure 7p.

to be certified for elements extracted in a three-phase sequential scheme whose protocol is stipulated in detail (Quevauviller et al., 1994). The leaches comprise: acetic acid (16 h at room temperature) for the 'exchangeable' component; hydroxylamine hydrochloride (16 h at room temperature) for the 'reducible' phase; and hydrogen peroxide (at 85°C) for the 'oxidizable' phase. These terms of 'exchangeable', 'reducible' and 'oxidizable' are suitably vague, given the lack of specificity of these extractants. One could easily argue, for example that 0.1 M $\text{NH}_2\text{OH}\cdot\text{HCl}$ at 20°C is by no means effective for quantitative dissolution of Fe oxyhydroxides, species which should fall into the 'reducible' category. The recommendation to dry sediment samples at 105°C, thereby promoting a change of phase distribution for some elements, and the disregard for size fractionation prior to application of the scheme, are indeed curious. It should also be borne in mind that long term storage of SRMs in the absence of an inert atmosphere can lead to shifts in the partitioning of elements. Some assessment of accuracy and the associated tools (certified SRMs) to carry out the task are certainly required as data from the implementation of selective leaches are used increasingly worldwide. However, the danger with these approaches adopted by such bodies as the European Commission is that these schemes will become international standards, as is the intention, and will be implemented in projects whose objectives call for other chemistries and other phase separations. There is a tendency to overlook the deficiencies and lack of suitability of a protocol when it has been accepted by influential organizations and when service laboratories become 'certified' in its application. The results described in this paper suggest that further research is needed to improve the selectivity of these leaches and that concurrent mineralogical analyses of the residues would aid in their refinement. The final goal of such work is to provide an arsenal of thoroughly examined selective leaches, some or all of which would be used in a particular sequence to quantify the form(s) of an element for the objectives at hand.

REFERENCES

- Antropova, L.V., Goldberg, I.S., Voroshilov, N.A., and Ryss Ju.S.**
1992: New methods of regional exploration for blind mineralization: application in the USSR; *Journal of Geochemical Exploration*, v. 43, p. 157-166.
- Bogle, E.W. and Nichol, I.**
1981: Metal transfer, partition and fixation in drainage waters and sediments in carbonate terrain in southeastern Ontario; *Journal of Geochemical Exploration*, v. 15, p. 405-422.
- Cardoso Fonseca, E. and Martin, H.**
1986: The selective extraction of Pb and Zn in selected mineral and soil samples, application in geochemical exploration (Portugal); *Journal of Geochemical Exploration*, v. 26, p. 231-248.
- Chao, T.T.**
1984: Use of partial dissolution techniques in geochemical exploration; *Journal of Geochemical Exploration*, v. 20, p. 101-135.
- Chao, T.T. and Sanzalone, R.F.**
1977: Chemical dissolution of sulfide minerals; *Journal of Research, United States Geological Survey*, v. 5, p. 409-412.
- Chao, T.T. and Theobald, P.K.**
1976: The significance of iron and manganese oxides in geochemical exploration; *Economic Geology*, v. 71, p. 1560-1569.
- Chao, T.T. and Zhou, L.**
1983: Extraction techniques for selective dissolution of amorphous iron oxides from soils and sediments; *Journal of Soil Science Society, American Proceedings*, v. 47, p. 225-232.
- Chester, R. and Hughes, M.J.**
1967: A chemical technique for the separation of ferromanganese minerals, carbonate minerals and adsorbed trace elements for pelagic sediments; *Chemical Geology*, v. 2, p. 249-262.
- Filipek, L.H. and Theobald, P.K.**
1981: Sequential extraction techniques applied to a porphyry copper deposit in the basin and range province; *Journal of Geochemical Exploration*, v. 14, p. 155-174.
- Gatehouse, S., Russell, D.W., and Van Moort, J.C.**
1977: Sequential soil analysis in exploration geochemistry; *Journal of Geochemical Exploration*, v. 8, p. 483-494.
- Hall, G.E.M.**
1992: Inductively coupled plasma mass spectrometry in geoanalysis; *Journal of Geochemical Exploration*, v. 44, p. 201-249.
- Hall, G.E.M., MacLaurin, A.I., and Vaive, J.E.**
1996a: Readsorption of gold during the selective extraction of the 'soluble organic' phase of humus, soil, and sediment samples; in *EXTECH I: A Multidisciplinary Approach to Massive Sulphide Research in the Rusty Lake-Snow Lake Greenstone Belts, Manitoba*, (ed.) G.F. Bonham-Carter, A.G. Galley, and G.E.M. Hall; *Geological Survey of Canada, Bulletin* 426.
- Hall, G.E.M., Pelchat, J.C., and Loop, J.**
1988: Separation and recovery of various sulphur species in sedimentary rocks for stable sulphur isotopic determination; *Chemical Geology*, v. 67, p. 35-45.
- Hall, G.E.M., Vaive, J.E., MacLaurin, A.I., and Hoashi, M.**
1996b: Selective leaching of the labile organic component of humus and soils with sodium pyrophosphate solution; in *EXTECH I: A Multidisciplinary Approach to Massive Sulphide Research in the Rusty Lake-Snow Lake Greenstone Belts, Manitoba*, (ed.) G.F. Bonham-Carter, A.G. Galley, and G.E.M. Hall; *Geological Survey of Canada, Bulletin* 426.
- Hall, G.E.M., Vaive, J.E., and McConnell, J.W.**
1995: Development and application of a sensitive and rapid analytical method to determine the rare earth elements in surface waters; *Chemical Geology*, v. 120, p. 91-109.
- Hamilton, J.A., Royko, B., Burt, M., and Nichol, I.**
1992: Geochemical exploration applied to base metal and gold exploration in Ontario; *Department of Geological Sciences Report, Queen's University, Kingston, Ontario*.
- Hoffman, S.J. and Fletcher, W.K.**
1979: Selective sequential extraction of Cu, Zn, Fe, Mn, and Mo from soils and sediments; in *Geochemical Exploration 1978*, (ed.) J.R. Watterson and P.K. Theobald; *Association of Exploration Geochemists*, p. 289-299.
- Kersten, M. and Forstner, U.**
1989: Speciation of trace elements in sediments; in *Trace Element Speciation: Analytical Methods and Problems*, (ed.) G. Batley; *CRC Press*, p. 245-317.
- Lynch, J.J.**
1990: Provisional elemental values for eight new geochemical lake sediment and stream sediment reference materials LKSD-1, LKSD-2, LKSD-3, LKSD-4, STSD-1, STSD-2, STSD-3 and STSD-4; *Geostandards Newsletter*, v. 14, p. 153-167.
- Overstreet, W.C., Lowering, T.G., Rosenblum, K., Hubert, A.E., and Crenshaw, G.L.**
1978: Minor elements in magnetic concentrates from Alaska; *United States Geological Survey, Report USGS-GD-78-004*, 596 p.
- Quevauviller, P., Rauret, G., Muntau, H., Ure, A.M., Rubio, R., Lopez-Sanchez, J.F., Fiedler, H.D., and Griepink, B.**
1994: Evaluation of a sequential extraction procedure for the determination of extractable trace metal contents in sediments, *Fresenius Journal of Analytical Chemistry*, v. 349, p. 808-814.
- Ryss, J.S., Chermas, M.A., Goldberg, I.C., Voroshilov, N.A., Siegel, H.O., Kinrade, J., and Chance, P.**
1990: Final Report on the 1990 Geochemical Test Program Conducted by NPO Rudgeofizika and Scintrex Limited; unpublished report, 41 p.

Rose, A.W. and Suhr, N.H.

- 1971: Major element content as a means of allowing for background variation in stream-sediment geochemical exploration; in *Geochemical Exploration*, (ed.) R.W. Boyle; Canadian Institute of Mining and Metallurgy, Special Volume 11, p. 587-593.

Sondag, F.

- 1981: Selective extraction procedures applied to geochemical prospecting in an area of old mine workings; *Journal of Geochemical Exploration*, v. 15, p. 645-652.

Tessier, A., Campbell, P.G.C., and Bisson, M.

- 1979: Sequential extraction procedure for the speciation of particulate trace metals; *Analytical Chemistry*, v. 51, p. 844-850.

Thompson, M. and Howarth, R.J.

- 1978: A new approach to the estimation of analytical precision; *Journal of Geochemical Exploration*, v. 9, p. 23-30.

Viets, J.G. and O'Leary, R.M.

- 1992: The role of atomic absorption spectrometry in exploration geochemistry; *Journal of Geochemical Exploration*, v. 44, p. 107-138.

Contribution to the 1989-1994 Rusty Lake-Snow Lake Mining Camps, Canada-Manitoba Exploration Science and Technology Initiative (EXTECH I)

Selective leaching of the labile organic component of humus and soils with sodium pyrophosphate solution

G.E.M. Hall¹, J.E. Vaive¹, A.I. MacLaurin¹, and M. Hoashi

Hall, G.E.M., Vaive, J.E., MacLaurin, A.L., and Hoashi, M., 1996: Selective leaching of the labile organic component of humus and soils with sodium pyrophosphate solution; in EXTECH I: A Multidisciplinary Approach to Massive Sulphide Research in the Rusty Lake-Snow Lake Greenstone Belts, Manitoba, (ed.) G.F. Bonham-Carter, A.G. Galley, and G.E.M. Hall; Geological Survey of Canada, Bulletin 426, p. 201-213.

Abstract: The effectiveness of the 0.1 M $\text{Na}_4\text{P}_2\text{O}_7$ leach commonly used in soil science to extract humic and fulvic acid components was studied for application to humus samples collected in exploration geochemistry programs. A 1 h extraction of 1 g of sample by 100 mL of this reagent was found to leach about 80-90% of Co, Cu, Ni, Pb and Zn associated with this labile organic phase, with precision typically in the range 5-10% relative standard deviation. Longer extraction time led to readsorption of Ni onto the sample substrate and did not result in higher concentrations of other elements. A second 1 h extraction tended to release proportionately more Mn (and to a lesser degree, Fe) than other elements such as Cu and organic C. This probably reflects dispersion of colloidal Mn particles rather than dissolution of organically bound Mn and could be minimized by ultracentrifugation of the leachate prior to analysis.

Detection limits in the order of 1 ppm for these elements in the original sample by atomic absorption spectrometry would be improved by one to two orders of magnitude by flow injection inductively coupled plasma mass spectrometry. The latter technique requires dilution of the leachate by about 20-fold to obviate severe drift due to salt build-up on the sampling orifice, even with the use of flow injection.

Résumé : Une solution de lixiviation, le $\text{Na}_4\text{P}_2\text{O}_7$ (pyrophosphate de sodium) à 0,1 M, habituellement utilisée en sciences des sols pour l'extraction séquentielle des acides humique et fulvique, a fait l'objet d'une étude visant à vérifier son efficacité sur des échantillons d'humus recueillis dans le cadre de programmes d'exploration géochimique. Il a été constaté qu'une attaque d'une durée d'une heure sur un échantillon de 1 g avec 100 mL de ce réactif permettait de lixivier environ 80 % à 90 % du cobalt, du cuivre, du nickel, du plomb et du zinc associés à la phase organique labile, avec une précision de l'ordre de 5 % à 10 % (écart type relatif). Une attaque sur une plus grande période de temps s'est traduite par la réadsorption du nickel dans le substrat de l'échantillon; quant aux autres éléments, aucun n'a été plus concentré. Une deuxième attaque d'une heure a permis de dissoudre proportionnellement plus de manganèse (et dans une moindre mesure de fer) que des autres éléments comme le cuivre et le carbone organique. Cela reflète probablement la dispersion des particules colloïdales contenant du manganèse plutôt que la dissolution du manganèse lié dans la phase organique, et pourrait être atténué par ultracentrifugation du lixiviat avant analyse.

Les limites de détection de la spectrométrie d'absorption atomique, de l'ordre de 1 ppm dans le cas de ces éléments dans les échantillons originaux, pourrait être améliorée de 100 à 1 000 fois si la technique utilisée était la spectrométrie de masse à injection avec une source de plasma induit par haute fréquence. Cette dernière exige la dilution par un facteur d'environ vingt du lixiviat, pour éviter les écarts importants causés par l'accumulation de sel au niveau de l'orifice d'échantillonnage que le mécanisme d'injection n'empêche pas.

¹ Geological Survey of Canada, 601 Booth St., Ottawa, Ontario K1A 0E8

INTRODUCTION

Research at the Geological Survey of Canada into the optimum method by which to extract elements bound in the labile organic component of humus and soil samples was stimulated by the Canadian exploration community's interest in the Russian array of methods to discover deeply buried mineralization (Antropova et al., 1992). One such method, known commonly as 'MPF', is designed to measure and differentiate that portion of an element, bound to humic and fulvic complexes in humus or soil, from other forms which may include crystalline oxides, silicates, and sulphides. In this way, the signature reflecting ionic or gaseous mobility of the element is highlighted, the premise being that ore and pathfinder elements are transported by various mechanisms from the source to the surficial environment where they are held in relatively labile forms associated with reaction sites such as those present in humic and fulvic substances. The high scavenging capacity of these organic substances is usually attributed to their carboxylic acid functional groups, with contributions from other groups such as $-NH_2$ (amino) and $-SH$ (thiol). Interaction between metal ions and humic acids has been shown to yield both 1:1 species and 1:2 complexes. In the 1:1 forms, the metal ion is either retained through a salt-type linkage ($R\text{COO}^-M^{2+}$) or co-ordinated to suitably positioned pairs of functional groups as shown in Figure 1a. In the 1:2 complexes, the metal ion becomes fully co-ordinated to functional groups (Fig. 1b). Extended chains can develop owing to the polyfunctional nature of humic substances and thus various forms of binding can occur depending upon the conditions present during formation. This in part explains why different orders of stability for metal humate complexes are reported in the literature. In a study of 15 different extractants (acids, salt solutions, and chelating agents) applied to two metal-humate systems, Slavek et al. (1982) clearly demonstrated the greater affinity of humic

acids for Cu or Pb over Cd and Zn. For example, in one experiment a far smaller percentage of Cu and Pb was displaced by simple salt solutions than that of Cd and Zn.

In view of the fact that metals can be adsorbed, complexed, or chelated by these organic substances, finding a phase-specific reagent is challenging, if not impossible. Two approaches are available: destruction of the organic matter by oxidation with reagents such as H_2O_2 or $NaOCl$; or the use of an alkaline complexing agent such as $Na_4P_2O_7$, sodium pyrophosphate. We adopted the latter mechanism because of the following disadvantages associated with destructive oxidation:

1. H_2O_2 (and, to a lesser extent, $NaOCl$) also oxidizes sulphides (e.g., ZnS , Cu_2S , $CuFeS_2$) extensively and dissolves MnO_2 (Papp et al., 1991);
2. H_2O_2 reacts to form oxalic acid, leading to precipitation of insoluble oxalates (e.g., Ca , Pb);
3. H_2O_2 can dissolve silicates in poorly buffered organic-rich samples where pH rapidly decreases during extraction; and
4. $NaOCl$ leads to precipitation of metals, especially Fe , at the high pH used.

The non-oxidative approach with $Na_4P_2O_7$ appears to be the most specific, showing little attack on sulphides or amorphous or crystalline Fe oxyhydroxides at pH 10 (McKeague et al., 1971).

The effectiveness of $Na_4P_2O_7$ in removing the easily extractable organic matter has been attributed to its ability to chelate with Ca and trivalent metal ions. The removal of cations bound to flocculated humates results in the subsequent conversion of the polyanion to its soluble Na salts. The ratio of carbon in humic (C_h) to carbon in fulvic acid (C_f) in 0.1 M $Na_4P_2O_7$ extracts of soils has been used in differentiating certain A horizons from the associated B horizons, C_h/C_f

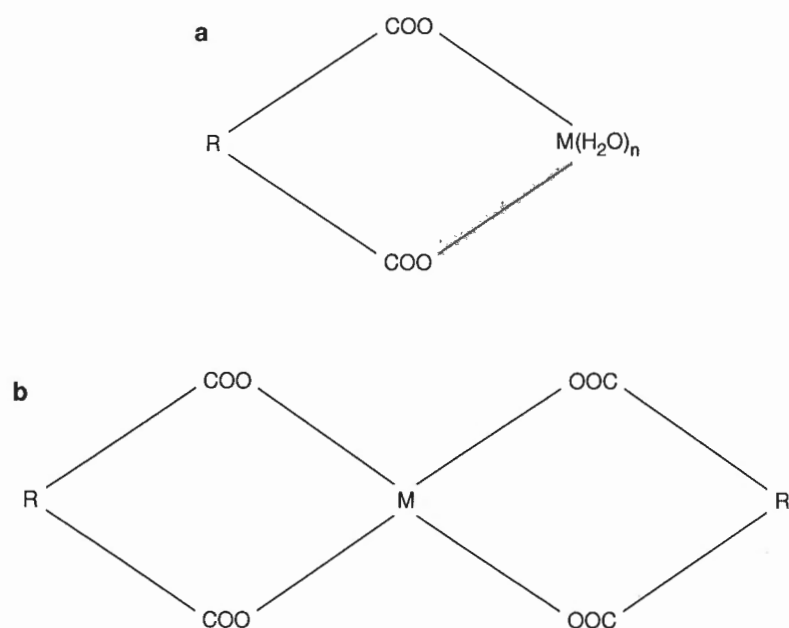


Figure 1.

a) 1:1 metal humate complex, b) 1:2 metal humate complex.

being <0.5 in nearly all A horizons (McKeague, 1968). Bascomb and Thanigasalam (1978) found pyrophosphate to be far superior to aqueous acetylacetone in selective extraction of organically-bound Fe from soils containing amorphous or poorly crystalline Fe oxyhydroxides (e.g., lepidocrocite, goethite, ferrihydrite). Solubility of these oxyhydroxides in 0.1 M $\text{Na}_4\text{P}_2\text{O}_7$ at pH 10 was extremely low, at less than 2% of the Fe in 40 h, even when their surface area was up to $300 \text{ m}^2\text{g}^{-1}$. Later work by Jeanroy and Guillet (1981) examined the forms of Fe extracted by $\text{Na}_4\text{P}_2\text{O}_7$ from some soil horizons. Iron could exist in one or more of the following forms: complexed with PO_4^{3-} ; complexed with extracted organic matter; and as solids in suspension. Electron micrographs of solids obtained by ultrafiltration and ultracentrifugation of the leach solution identified aggregates of non-crystalline spheroids less than 15 nm in diameter. The ratio of Fe/C in the solid phase was inconsistent with exclusive extraction of Fe complexed with organic matter. They concluded that, in addition to releasing Fe bound to organic matter, $\text{Na}_4\text{P}_2\text{O}_7$ serves to peptize and disperse finely divided ferruginous particles present in the soil. Thus, results by this leach could be erroneously high for Fe if these suspensates were not separated by ultracentrifugation or ultrafiltration. We considered this disadvantage of the $\text{Na}_4\text{P}_2\text{O}_7$ leach to be far less significant than those listed above associated with destructive oxidation of organic matter, particularly as our interest is focused much more on trace elements such as Zn and Cu than on Fe.

The normal procedure employed by soil scientists is that described by McKeague et al. (1971) where 1 g of sample is stirred for 16 h in 100 mL of 0.1 M $\text{Na}_4\text{P}_2\text{O}_7$ at room temperature. Berger et al. (1984) showed that the efficiency of this extraction increased with repetitive treatment. In their examination of suspended particles in the Gironde Estuary, they demonstrated that the ratio of extracted organic C to total particulate organic C was about 19% in the first 0.1 M $\text{Na}_4\text{P}_2\text{O}_7$ extraction, 11% in the second, and 5% in the third. Thus it appears that about 50% more is being extracted in the second leach, a significant amount which requires investigation. Our work focused on (1) testing and modifying the $\text{Na}_4\text{P}_2\text{O}_7$ procedure for cost-effective application in exploration geochemistry and (2) determining its performance for trace elements in humus samples collected in different geological environments. The analytical technique employed was atomic absorption spectrometry (AAS) which has the particular advantage of wide tolerance to solutions highly concentrated in dissolved salts, as the 0.1 M $\text{Na}_4\text{P}_2\text{O}_7$ leachate would be. However, a disadvantage of both AAS and inductively coupled plasma emission spectrometry (ICP-ES) is their relatively low sensitivity compared to ICP mass spectrometry (ICP-MS) and therefore the capabilities of this technique were examined.

EXPERIMENTAL

In the absence of an international humus standard, the development work was carried out on some lake sediment standard reference materials, specifically on LKSD-4 (loss-on-ignition, LOI, of 41%), previously described by Lynch

(1990). Two humus controls (LOIs of 71 and 66%) were collected in the Timmins camp under the Canada-Ontario Mineral Development Agreement and were used to assess long term precision and bias between batches. Humus samples from Sudbury and Timmins were sieved to <80 mesh (177 μm); LKSD-4 had been ballmilled to pass a 200 mesh (74 μm) screen. The pyrophosphate reagent (Baker Analysed Reagent grade) was made 0.1 M by dissolving 44.6 g in 1 L of distilled deionized water made up to pH 10.0 with HNO_3 . One gram of each sample was weighed into a test-tube and 100 mL of 0.1 M $\text{Na}_4\text{P}_2\text{O}_7$ solution added. The test-tubes were put on a horizontal shaker and mixed constantly for a specified time (1, 3, and 16 h). The sample was then centrifuged for 10-15 min at 2800 rpm and the supernatant decanted for analysis. A fresh 100 mL aliquot of 0.1 M $\text{Na}_4\text{P}_2\text{O}_7$ solution was added to the residue and the process repeated.

A Perkin-Elmer Model 3030 atomic absorption spectrometer was used to analyze the pyrophosphate solution directly, calibrating against standards made by spiking 0.1 M $\text{Na}_4\text{P}_2\text{O}_7$ with known quantities of analytes. The following absorption lines were used, with background correction: Co-240.7 nm; Cu-324.8 nm; Fe-248.8 nm; Mn-279.5 nm; Ni-232.0 nm; Pb-217.0 nm; and Zn-213.9 nm. For determination of organic C, the solution was diluted 20-fold and analyzed using the Shimadzu 5000 TOC instrument. This measurement is based on combustion at 680°C and nondispersive infra-red detection. The VG PlasmaQuad PQ2+ was used for ICP-MS analysis, employing for sample introduction both conventional pneumatic nebulization and flow injection with the VGS 100 system.

RESULTS

Method development

Early investigation of the 16 h and a 3 h leach applied to about 40 humus samples produced essentially identical results for Cu, Fe, Mn, Ni, Pb, Zn, and organic C; and therefore further work concentrated on examining a shorter leach period. The dependence of the amount of element extracted on length of time in the pyrophosphate solution is shown in Table 1 for control LKSD-4. Clearly, extending the leach duration from 1 h to 3 h does not result in a greater amount of element extracted for this sample. In fact, Ni shows a decrease in concentration, from 7.9 to 7.0 ppm over this period, which probably indicates readsorption back onto the sample substrate. It is interesting to note that, for all elements except Fe, a second 1 h leach (L2) extracts about 10% of that liberated in the first leach. The corresponding figure for Fe is about 30% and this may well reflect peptization of ferruginous particles, as demonstrated by Jeanroy and Guillet (1981). (An ultracentrifuge was not available in our laboratory to test for removal of this fraction). For LKSD-4 and others, a contact time of 0.5 h produced low and somewhat erratic results. These concentrations of elements associated with the labile organic component of LKSD-4 represent the following percentages of the total element present: Cu-30%; Fe-13%; Mn-48%; Ni-27%; Pb-68%; and Zn-38% (for total concentrations, see Lynch, 1990).

A more comprehensive examination of the effect of leach time is shown in Figure 2 (a)-(f) where results using 1 h and 3 h leaching times for 30 humus samples from Sudbury (Ontario) are compared for each element determined. Trend lines are plotted for: the sum of two 1 h leaches, the first 3 h leach, and the sum of two 3 h leaches against the concentration found in the first 1 h leach. The statistical data (r^2 and slope) associated with these lines of best fit are given in Table 2. As this test suite was not analyzed in full for organic C due to instrumental breakdown, data produced by the 1 h leaching procedure only of a larger suite ($n = 254$) of humus samples from this area near Sudbury are shown graphically in Figure 3. In comparing the data for the sum of the two 1 h leaches against the first 1 h (Fig. 2 and 3, Table 2), it is evident that correlation is excellent and that the second extraction generally amounts to about 10% of the first, with the notable exception of Mn (Fig. 2c) where this value is much higher, at 35%. The amount of organic C extracted in the second 1 h leach, for the larger data set, is generally about 17% that of the first (Fig. 3). Some deviation from linearity is evident at high carbon concentrations, indicating proportionately less organic carbon is extracted in the second leach. Given these amounts of organic carbon and trace elements extracted in the second application of the 0.1 M $\text{Na}_4\text{P}_2\text{O}_7$ leach, the relatively higher concentration of Mn extracted is suggestive of a colloidal suspension of its oxide rather than any organic association.

In examining the results for the first 3 h leach versus the first 1 h leach (Fig. 2), there appears to be little difference for Cu, Fe, and Zn, as was the case above for LKSD-4 (Table 1). However, much more Mn has been extracted in the 3 h leach (slope = 1.7, Table 2) and these data are quite erratic, again indicating Mn in suspension rather than true solution. This behaviour was also observed for a subsuite of the Timmins samples selected for the 1 h versus 3 h experiment. Though to a much lesser degree, results for Pb also show higher concentrations in the 3 h leach compared to the 1 h; this pattern has not been repeated in the Timmins suite or in others. Nickel is displaying quite different behaviour in that considerably less is being reported by the 3 h leach (Fig. 2d, slope = 0.82), indicative of readsorption as was shown previously by LKSD-4. The spread of points about the 'sum of 3 h' line for Fe or Mn (Fig. 2b and c) is much greater than that for say, Cu or Zn (Fig. 2a and f), which probably reinforces the argument that these data do not only represent the organically bound phase. Note that the slope of the line representing the sum of the 3 h leaches for Ni is still less than 1 (i.e. this concentration is less than that reported by one 1 h leach). Figure 4 compares summed 3 h versus single 3 h results for Fe, Mn, Zn, and organic C in 125 humus samples from several different geological terrains in the Timmins region. Similar percentages of element concentrations are being extracted here in the second 3 h leach as was evident in Figure 2, with Mn again showing a greater proportion than the others (30% cf. to 10-20%). These results differ from those reported by Berger et al. (1984) where the proportions of organic carbon released from river sediment by the second and third leaches were significantly higher. This difference may well be related to the compositions of the sample matrices involved in the two studies.

The data shown in Figures 2-4, together with those of other GSC projects, provide the justification in recommending the conventional $\text{Na}_4\text{P}_2\text{O}_7$ method used by soil scientists be shortened from 16 h to 1 h duration for its use in exploration geochemistry. This would benefit not only the efficiency of the procedure but also the results for Ni where readsorption would be minimized, and those for Fe and Mn which would otherwise reflect dispersion of fine grained inorganic colloidal material. The test suite of 30 humus samples was also extracted for 1 h at a ratio of 0.5 g to 100 mL of 0.1 M $\text{Na}_4\text{P}_2\text{O}_7$; results were identical to those for the 1 g to 100 mL ratio. The $\text{Na}_4\text{P}_2\text{O}_7$ leachates are stable in organic C over several months. Figure 5 shows two measurements of organic C made on randomly chosen solutions five months apart; there were essentially no differences in the determined organic C contents.

ICP-MS analysis for improved sensitivity of detection

Pyrophosphate leachates required dilution prior to analysis by conventional nebulization ICP-MS to prevent blockage of the sampler and skinner cones (see Hall, 1992). However, even at 20-fold dilution (creating an overall dilution factor of 2000), deposition of salts on the sampler orifice was encountered. Note in Figure 6a the sharp downward drift in sensitivity for about 0.2 ppb standard solutions of Mo, Cd, Sb, and Tl nebulized after every 10 sample leachates. Even with a dilution of 40-fold, an unacceptable decline in signal was observed (Fig. 6b). If flow injection (FI) is employed instead of nebulization, a discrete volume (typically 200 μL) of analyte solution is injected into a carrier stream, in this case 2% HNO_3 , and pumped to the nebulizer and then into the ICP. This mode of introduction facilitates the analysis of high salt solutions as most of the time it is the carrier solution which is being transported to the nebulizer and hence salt build-up on the sampler is minimized. Figure 6c illustrates the signals obtained when FI was employed for analysis of the same 20-fold diluted solutions of Figure 6a. The absence of steady downward drift indicates that plugging of the orifice was not occurring. However, the data are quite noisy and suggest that calibration every 10 samples is recommended. Internal standardization would likely obviate much of this noise. Though further research is necessary, these data indicate that detection limits by FI-ICP-MS would be in the order of 0.02-0.2 ppm in the original 1 g sample for most elements.

Precision for control samples

Results of the single and summed 1 h leaches for LKSD-4 and the two humus controls collected in Timmins are given in Table 3. These data were collected over 2 years and were produced by different analysts. For the trace elements, where concentrations are at least a decade higher than detection limit, the relative standard deviations (RSDs) are in the range 2-6%. Precision for organic C is excellent, at 2-7% RSD. Data for Humus-1 are generally noisier than those for the other two, with RSDs for Fe and Mn of 8-10% compared with 2-5%.

Table 1. Variability of elemental extraction amounts with shaking time for LKSD-4; all values in ppm.

| Time (h) | Cu | | Fe | | Mn | | Ni | | Pb | | Zn | |
|----------|-----|-----|------|-----|-----|----|-----|-----|----|-----|----|----|
| | L1 | L2 | L1 | L2 | L1 | L2 | L1 | L2 | L1 | L2 | L1 | L2 |
| 0.5 | 7.9 | 1.0 | 2502 | 921 | 198 | 27 | 8.1 | 1.0 | 56 | 7.9 | 69 | 3 |
| 1.0 | 8.2 | 1.0 | 2729 | 880 | 204 | 28 | 7.9 | 1.0 | 58 | 7.9 | 70 | 4 |
| 1.5 | 8.3 | 1.0 | 2740 | 789 | 210 | 25 | 7.7 | 1.0 | 54 | 6.9 | 68 | 2 |
| 2.0 | 8.1 | <1 | 2640 | 902 | 205 | 34 | 7.8 | <1 | 55 | 7.1 | 71 | 2 |
| 2.5 | 7.5 | 1.0 | 2793 | 775 | 220 | 31 | 7.4 | <1 | 55 | 6.9 | 72 | 3 |
| 3.0 | 8.0 | 1.0 | 2698 | 802 | 218 | 30 | 7.0 | <1 | 54 | 6.4 | 68 | 4 |

L1, L2: Sequential pyrophosphate leaches 1 and 2 (i.e. L2 refers to second leach, applied to residue remaining from L1).

Table 2. Statistical data for trend lines of plots (Fig. 2) against 1 h leach concentration results for: sum of two 1 h leaches; first 3 h leach; and sum of two 3 h leaches.

| Element | sum two 1 h | | first 3 h | | sum two 3 h | |
|---------|----------------|------------|----------------|------------|----------------|------------|
| | r ² | slope/SD | r ² | slope/SD | r ² | slope/SD |
| Cu | 0.998 | 1.098/.005 | 0.980 | 1.023/.017 | 0.978 | 1.108/.019 |
| Fe | 0.991 | 1.095/.008 | 0.929 | 0.960/.018 | 0.896 | 1.027/.024 |
| Mn | 0.982 | 1.347/.025 | 0.931 | 1.727/.067 | 0.907 | 2.010/.091 |
| Ni | 0.996 | 1.130/.006 | 0.980 | 0.823/.011 | 0.964 | 0.939/.016 |
| Pb | 0.999 | 1.099/.004 | 0.996 | 1.174/.011 | 0.996 | 1.251/.012 |
| Zn | 0.999 | 1.083/.004 | 0.989 | 1.023/.012 | 0.986 | 1.115/.015 |

SD : standard deviation of slope.

Table 3. Variability in results of 1 h pyrophosphate leach in controls LKSD-4, Humus-1, and Humus-2, over 2 year period.

| Control | Co (ppm) | Cu (ppm) | Fe (ppm) | Mn (ppm) | Ni (ppm) | Pb (ppm) | Zn (ppm) | Organic C (%) |
|-----------------------|-----------|-----------|------------|-----------|-----------|------------|------------|---------------|
| LKSD-4, 1h (8) | 2.0 ± 0.9 | 6.8 ± 1.3 | 2666 ± 141 | 207 ± 5 | 5.1 ± 0.9 | 54 ± 1 | 71 ± 2 | 2.53 ± 0.10 |
| LKSD-4, sum 1 h (20) | 2.0 ± 1.1 | 8.5 ± 0.7 | 3548 ± 154 | 235 ± 16 | 8.3 ± 1.9 | 65 ± 3 | 72 ± 3 | 2.75 ± 0.11 |
| Humus-1, 1 h (7) | 1.3 ± 0.5 | 6.0 ± 1.1 | 1432 ± 141 | 148 ± 12 | 6.0 ± 2.7 | 12.0 ± 1.7 | 10.1 ± 0.6 | 3.15 ± 0.22 |
| Humus-1, sum 1 h (13) | 1.8 ± 1.3 | 6.8 ± 1.9 | 1968 ± 194 | 192 ± 8 | 8.5 ± 3.2 | 14.2 ± 3.0 | 10.5 ± 0.8 | 3.73 ± 0.18 |
| Humus-2, 1 h (6) | 1.5 ± 0.8 | 3.5 ± 1.0 | 4808 ± 130 | 306 ± 15 | 2.8 ± 1.3 | 3.0 ± 0.5 | 26 ± 1 | 6.47 ± 0.15 |
| Humus-2, sum 1 h (12) | 1.6 ± 1.1 | 4.2 ± 1.4 | 6830 ± 447 | 850 ± 102 | 4.0 ± 1.7 | 3.3 ± 1.1 | 27 ± 2 | 7.32 ± 0.25 |

Brackets indicate number of separate analyses of 1 g subsamples

Figure 2a.

Plot of ○-sum of two 1 h leaches, □-first 3 h leach, and Δ-sum of two 3 h leaches against first 1 h leach for Cu in 30 humus samples from Sudbury.

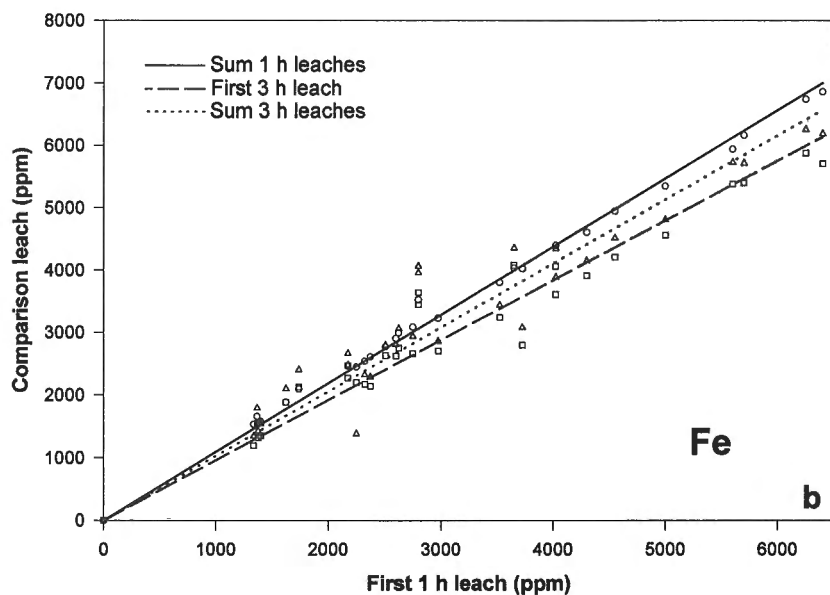
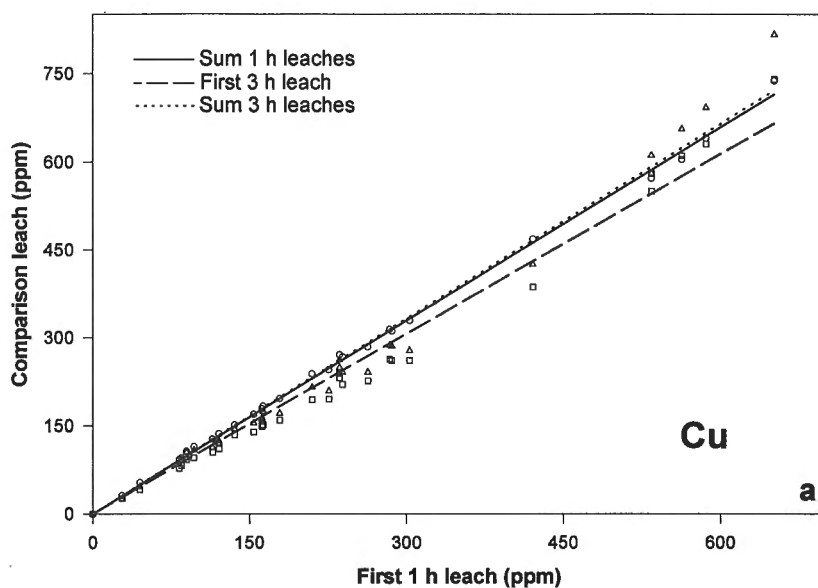


Figure 2b.

Plot of ○-sum of two 1 h leaches, □-first 3 h leach, and Δ-sum of two 3 h leaches against first 1 h leach for Fe in 30 humus samples from Sudbury.

Figure 2c.

Plot of ○-sum of two 1 h leaches, □-first 3 h leach, and Δ-sum of two 3 h leaches against first 1 h leach for Mn in 30 humus samples from Sudbury.

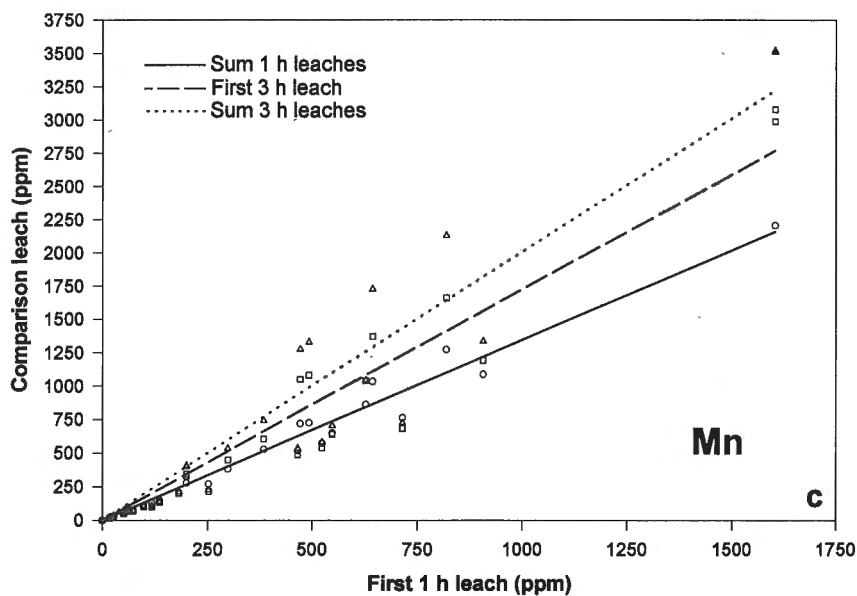


Figure 2d.

Plot of \bigcirc -sum of two 1 h leaches, \square -first 3 h leach, and Δ -sum of two 3 h leaches against first 1 h leach for Ni in 30 humus samples from Sudbury.

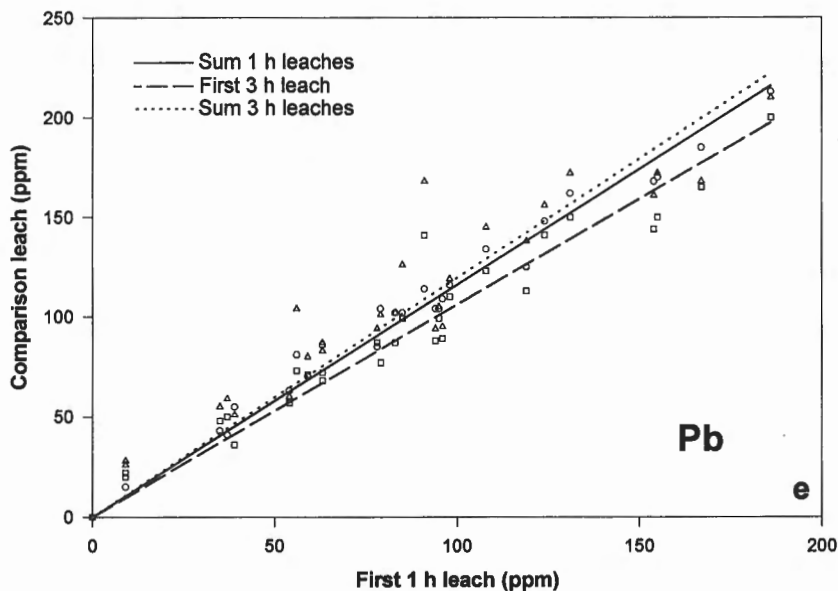
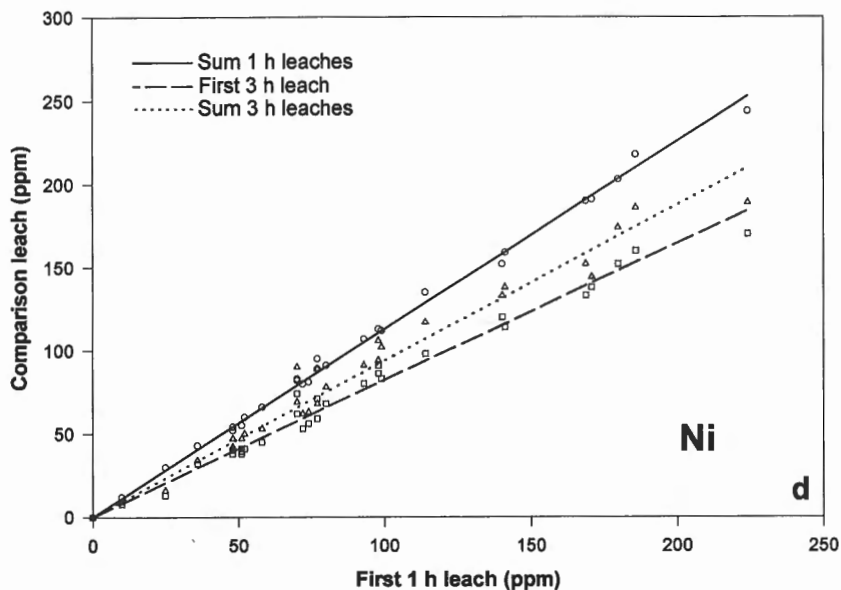
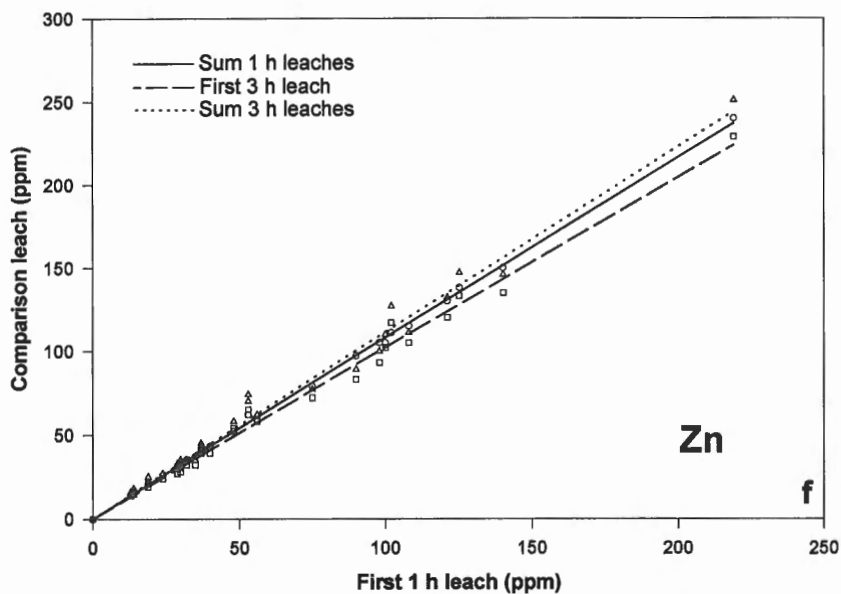


Figure 2e.

Plot of \bigcirc -sum of two 1 h leaches, \square -first 3 h leach, and Δ -sum of two 3 h leaches against first 1 h leach for Pb in 30 humus samples from Sudbury.

Figure 2f.

Plot of \bigcirc -sum of two 1 h leaches, \square -first 3 h leach, and Δ -sum of two 3 h leaches against first 1 h leach for Zn in 30 humus samples from Sudbury.



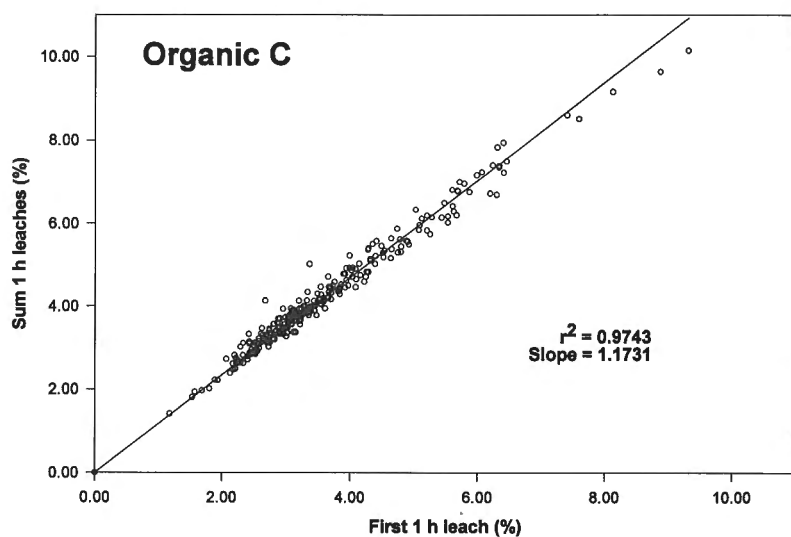


Figure 3.

Plot of sum of two 1 h leaches against first 1 h leach for organic C in 254 humus samples from Sudbury area.

Figure 4a.

Plot of sum of two 3 h leaches against first 3 h leach for Fe in 125 humus samples from Timmins area.

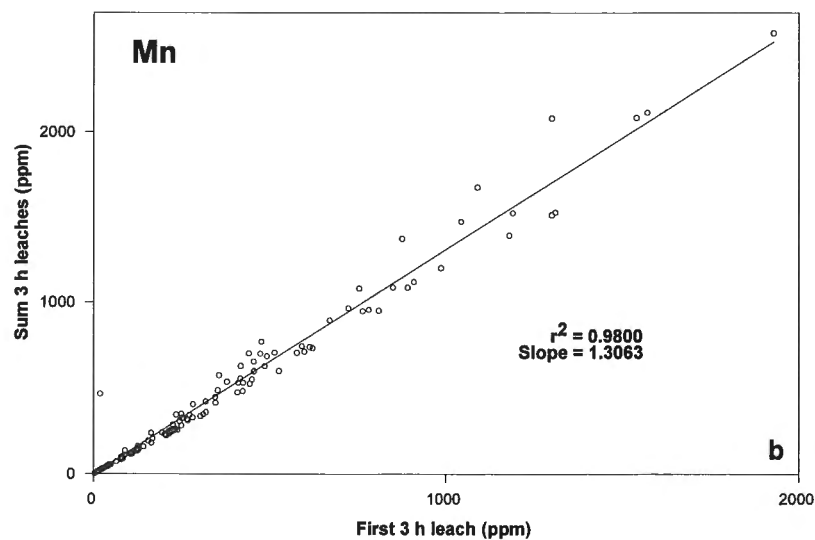
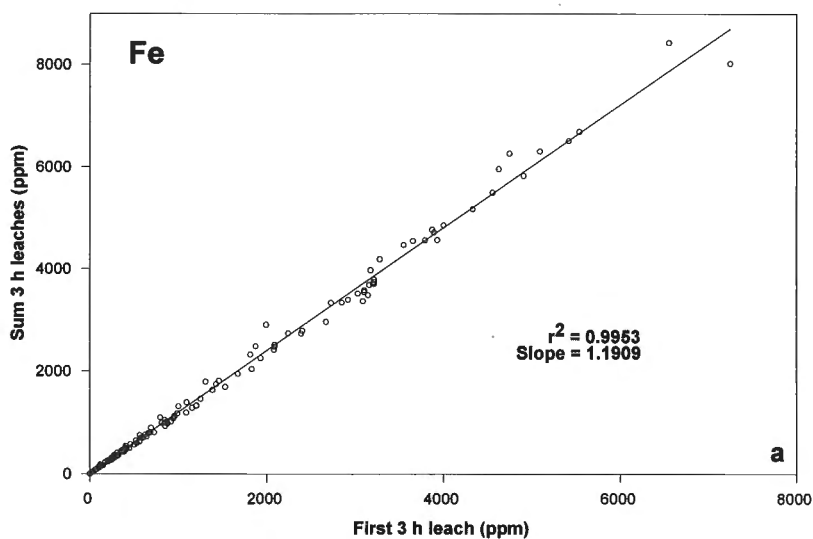


Figure 4b.

Plot of sum of two 3 h leaches against first 3 h leach for Mn in 125 humus samples from Timmins area.

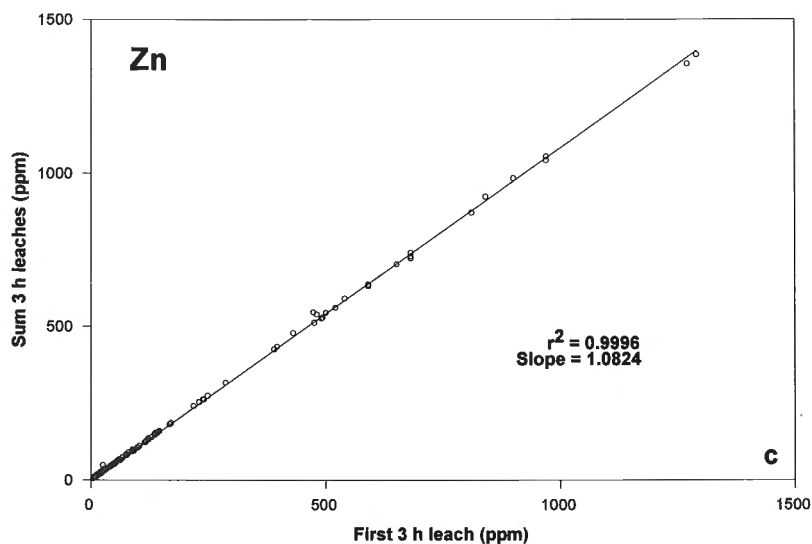


Figure 4c.

Plot of sum of two 3 h leaches against first 3 h leach for Zn in 125 humus samples from Timmins area.

Figure 4d.

Plot of sum of two 3 h leaches against first 3 h leach for organic C in 125 humus samples from Timmins area.

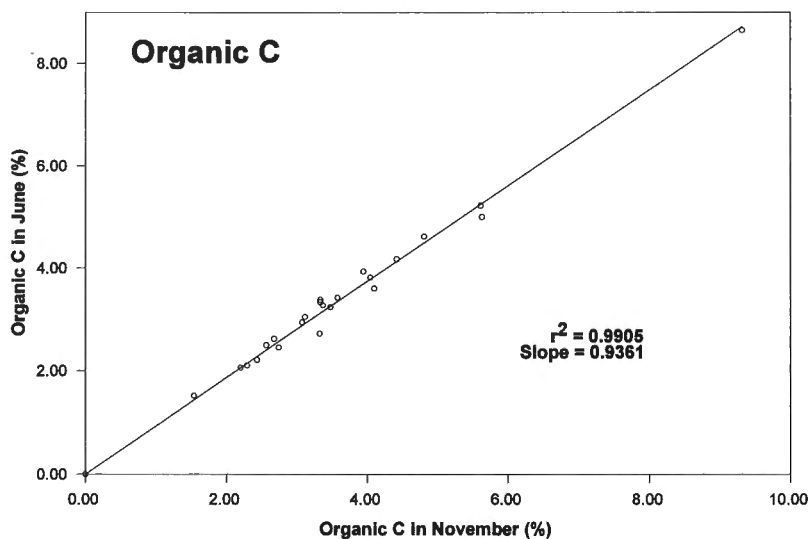
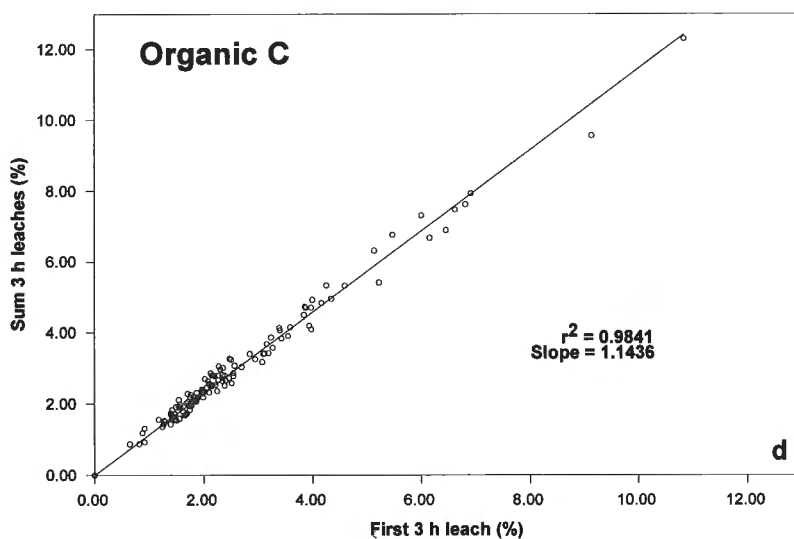


Figure 5.

Comparison of organic C results for 1 h leach of 23 humus samples measured in June versus November 1993.

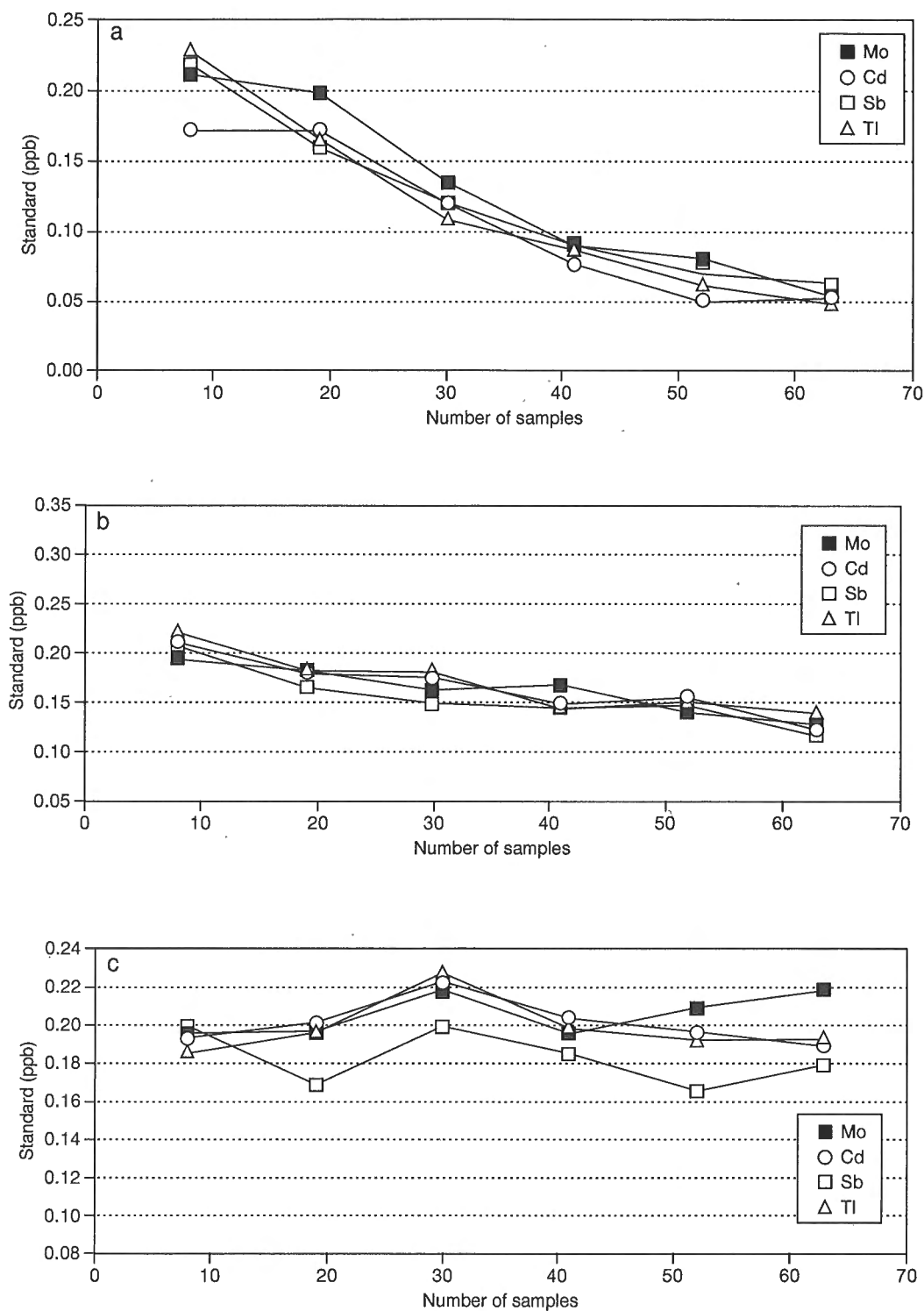


Figure 6. *a)* Drift in nebulization ICP-MS signal for standard solutions of Mo, Cd, Sb, and Tl when measured after every 10 humus sample leachates (diluted 20-fold). *b)* Drift in nebulization ICP-MS signal for standard solutions of Mo, Cd, Sb and Tl when measured after every 10 humus sample leachates (diluted 40-fold). *c)* Drift in FI-ICP-MS signal for standard solutions of Mo, Cd, Sb, and Tl when measured after every 10 humus sample leachates (diluted 20-fold).

Note the exaggerated increase in Mn extracted by the second 1 h leach from Humus-2, amounting to 64% of the total Mn whereas the equivalent figure for C is 12%. Apparently the action of the first leach has been to make Mn more available for extraction by fresh reagent.

Shown in Figures 7a-h are Thompson and Howarth (1978) log-log plots used to estimate precision based on replicate analyses of 37 humus samples collected in the Sudbury and Timmins areas in 1992 and 1993. These replicate digestions and analyses of 1 g samples were performed in separate batches several months apart. The differences between the

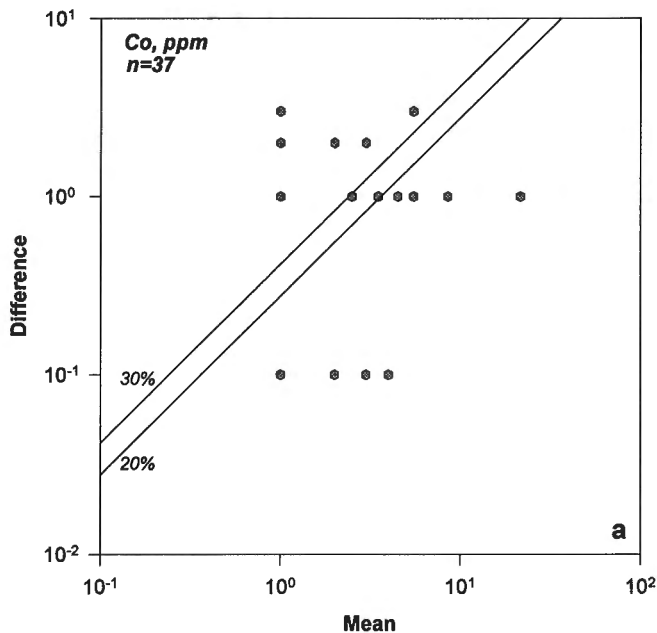


Figure 7a. Thompson and Howarth (1978) log-log plot of difference versus mean for replicate results of Co in 37 humus samples.

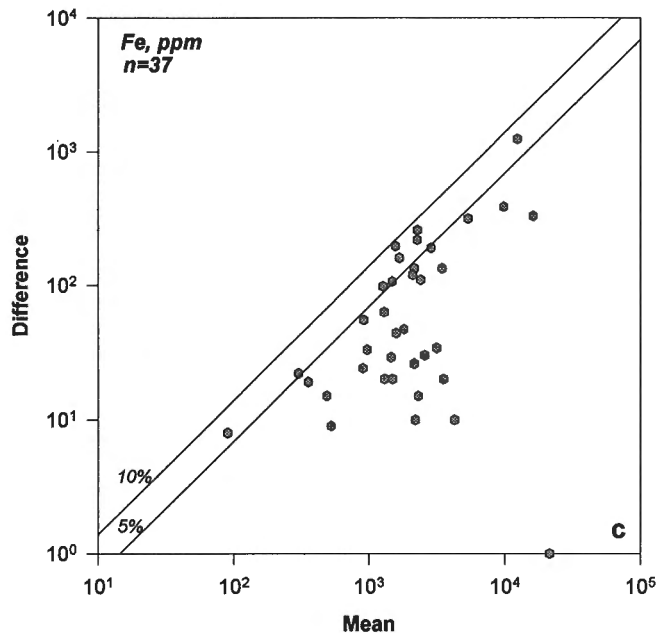


Figure 7c. Thompson and Howarth log-log plot of difference versus mean for replicate results of Fe in 37 humus samples.

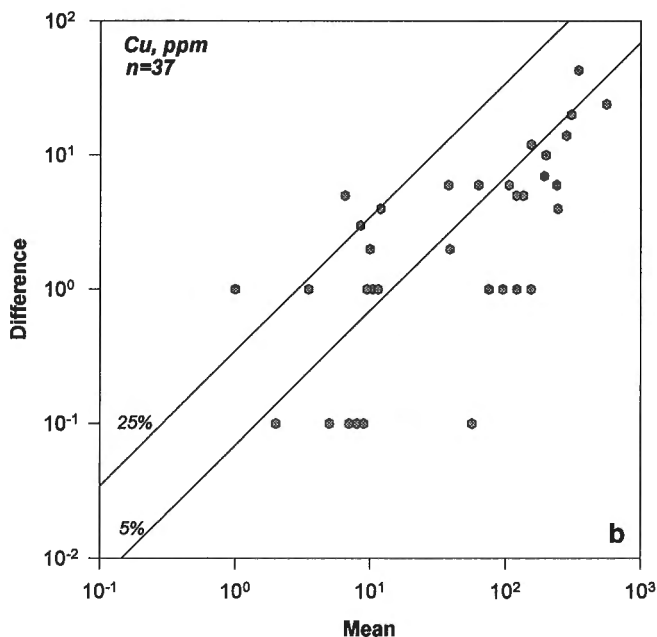


Figure 7b. Thompson and Howarth log-log plot of difference versus mean for replicate results of Cu in 37 humus samples.

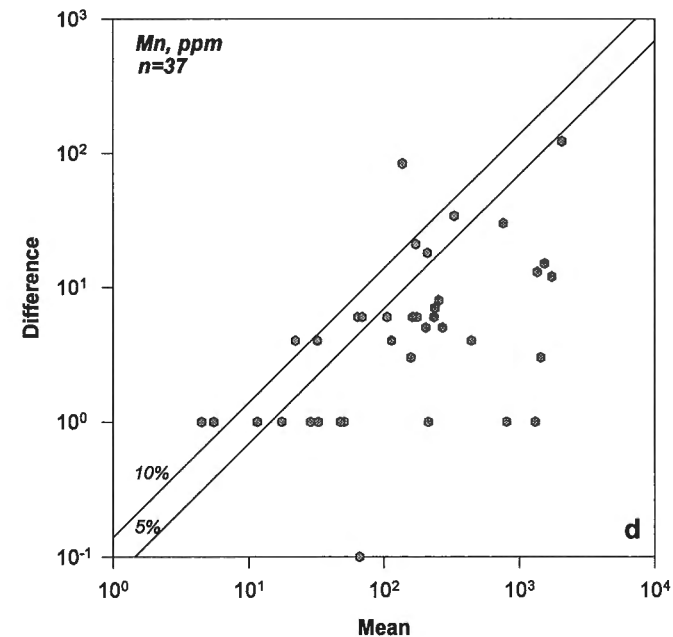


Figure 7d. Thompson and Howarth log-log plot of difference versus mean for replicate results of Mn in 37 humus samples.

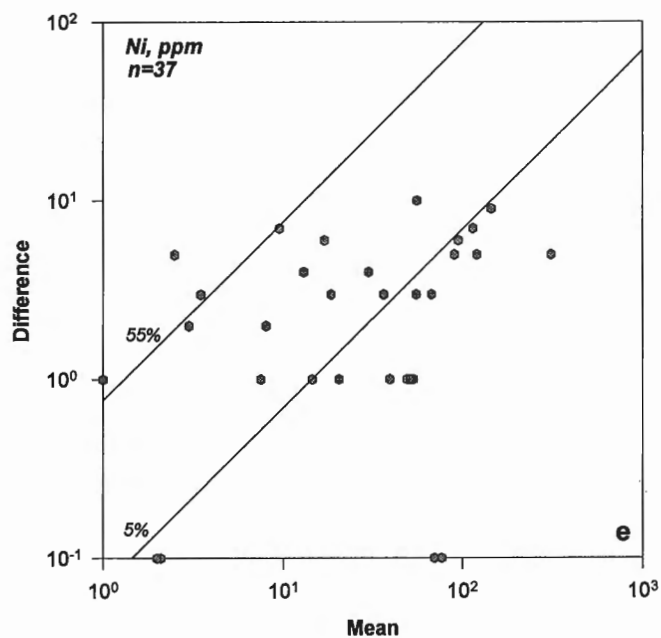


Figure 7e. Thompson and Howarth log-log plot of difference versus mean for replicate results of Ni in 37 humus samples.

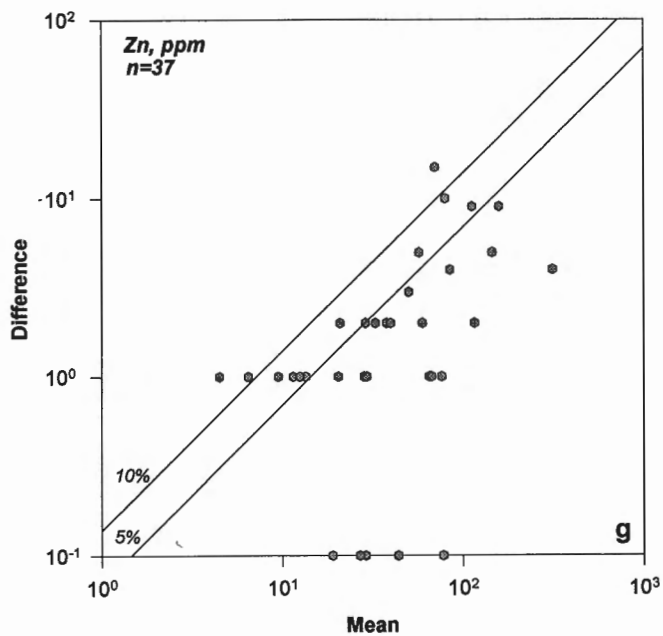


Figure 7g. Thompson and Howarth log-log plot of difference versus mean for replicate results of Zn in 37 humus samples.

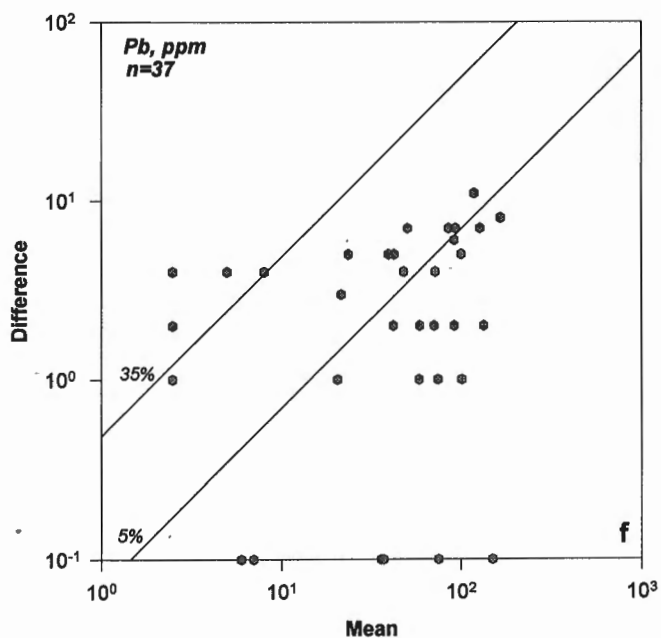


Figure 7f. Thompson and Howarth log-log plot of difference versus mean for replicate results of Pb in 37 humus samples.

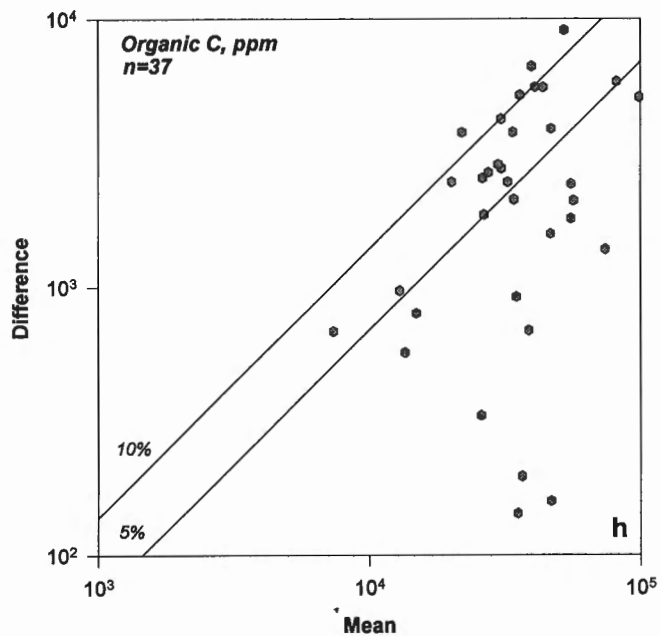


Figure 7h. Thompson and Howarth log-log plot of difference versus mean for replicate results of organic C in 37 humus samples.

replicate results are plotted against their means. The two data sets are shown separately; the shaded circles indicate results from one year and the open circles indicate the following year's results. The two control lines are drawn at the 95th percentile for the selected precision (twice the RSD). For these data, the uppermost precision line above which 2-3 points lie represents the worst-case precision to be expected over that concentration range. For example, precision for Cu is better than 25% for this suite of samples, but at concentrations greater than 10 ppm, improved precision of about 5% can be expected. Precision of 10% or better is indicated for Fe, Mn, Zn, and C; these data are well above detection levels. However, for the trace elements Co, Cu, Ni, and Pb, precision degrades drastically from 5-10% at high concentrations to worse than 30% at levels below 10 ppm. Clearly, precision of the analytical measurement itself is dominating that of sampling and the digestion procedure and substitution of FI-ICP-MS for the less sensitive AAS technique is required. Nevertheless, bearing in mind that these samples were merely sieved to <80 mesh (177 µm) and that they were not replicated within the same analytical batch, reproducibility of results is excellent.

SUMMARY

A 1 h 0.1 M Na₄P₂O₇ leach at a sample-to-volume ratio of 1:100 (g:mL) is recommended for extraction of the labile organic component of humus, soil, or sediment samples. Longer extraction time is deleterious for Ni which exhibits readsorption onto the sample substrate. Precision (twice the RSD) at 1 g sampling weight is typically in the range 5-10% at levels a decade above the analytical technique's detection limit. Proportionately less sample and leach solution could be used but reproducibility of sampling could become a controlling factor below 0.2-0.5 g. The use of FI-ICP-MS would substantially improve detection capabilities; for example, from about 0.5-1 ppm for Co, Cu, and Ni by AAS or ICP-ES to 0.02-0.2 ppm by ICP-MS.

A second 1 h leach extracts generally about 10-15% more organically bound element from the sample but proportionately more Mn (and sometimes Fe) is leached, reflecting dispersion of colloidal particles rather than an organic association. Ultracentrifugation would be beneficial in removing this inorganic component of Mn and Fe, but at the expense of productivity. Carrying out two 1 h leaches would be recommended if the sample residue was to be further characterized in a sequential leach scheme, thus ensuring majority removal of the humic and fulvic phase with its associated elements.

This leach does not require heat or evaporation, reagent cost is minimal, and it can be carried out rapidly in large sample batches. It would be much more cost-effective than

the aqua regia leach more commonly applied to humus samples in exploration geochemistry. Evaluation of its effectiveness in mapping labile, organically scavenged elements as opposed to their total concentration in humus is now required in different geological environments.

ACKNOWLEDGMENTS

We thank Pierre Pelchat for his enthusiastic production of many figures within this manuscript. Most of the sample data contained herein was produced under the Canada-Ontario Mineral Development Agreement 1991-1996.

REFERENCES

- Antropova, L.V., Goldberg, I.S., Voroshilov, N.A., and Ryss, Ju.S.
1992: New methods of regional exploration for blind mineralization: application in the USSR; *Journal of Geochemical Exploration*, v. 43, p. 157-166.
- Bascomb, C.L. and Thanigasalam, K.
1978: Comparison of aqueous acetylacetone and potassium pyrophosphate solution for selective extraction of organic-bound Fe from soils; *Journal of Soil Science*, v. 29, p. 382-387.
- Berger, P., Etcheber, H., Ewald, M., Lavaux, G., and Belin, C.
1984: Variation of organic matter extracted from particles along the Gironde Estuary (France); *Chemical Geology*, v. 45, p. 1-16.
- Jeanroy, E. and Guillet, B.
1981: The occurrence of suspended ferruginous particles in pyrophosphate extracts of some soil horizons; *Geoderma*, v. 26, p. 95-105.
- Hall, G.E.M.
1992: Inductively coupled plasma mass spectrometry in geoanalysis; *Journal of Geochemical Exploration*, v. 44, p. 201-249.
- Lynch, J.J.
1990: Provisional elemental values for eight new geochemical lake sediment and stream sediment reference materials LKSD-1, LKSD-2, LKSD-3, LKSD-4, STSD-1, STSD-2, STSD-3 and STSD-4; *Geostandards Newsletter*, v. 14, p. 153-167.
- McKeague, J.A.
1968: Humic-fulvic acid ratio, Al, Fe and C in pyrophosphate extracts as criteria of A and B horizons; *Canadian Journal of Soil Science*, v. 48, p. 27-35.
- McKeague, J.A., Brydon, J.E., and Miles, N.M.
1971: Differentiation of forms of extractable iron and aluminum in soils; *Soil Science Society of America, Proceedings*, v. 35, p. 33-38.
- Papp, C.S., Filipek, L.H., and Smith, K.S.
1991: Selectivity and effectiveness of extractants used to release metals associated with organic matter; *Applied Geochemistry*, v. 6, p. 349-353.
- Slavek, J., Wold, J., and Pickering, W.F.
1982: Selective extraction of metal ions associated with humic acids; *Talanta*, v. 29, p. 743-749.
- Thompson, M. and Howarth, R.J.
1978: A new approach to the estimation of analytical precision; *Journal of Geochemical Exploration*, v. 9, p. 23-30.

Contribution to the 1989-1994 Rusty Lake-Snow Lake Mining Camps, Canada-Manitoba Exploration Science and Technology Initiative (EXTECH I)

Readsorption of gold during the selective extraction of the 'soluble organic' phase of humus, soil, and sediment samples

G.E.M. Hall¹, A.I. MacLaurin¹, and J.E. Vaive¹

Hall, G.E.M., MacLaurin, A.I., and Vaive, J.E., 1996: Readsorption of gold during the selective extraction of the 'soluble organic' phase of humus, soil, and sediment samples; in EXTECH I: A Multidisciplinary Approach to Massive Sulphide Research in the Rusty Lake-Snow Lake Greenstone Belts, Manitoba, (ed.) G.F. Bonham-Carter, A.G. Galley, and G.E.M. Hall; Geological Survey of Canada, Bulletin 426, p. 215-224.

Abstract: Phase selective extractions are employed in the chemical analysis of geological materials to identify the *forms* in which the element is present and hence to elucidate the mechanisms by which the element has been transported and eventually accumulated in such media. Quantitation of Au bound to the 'soluble organic' phase of a humus or lake sediment sample would indicate hydromorphic dispersion, as distinct from mechanical dispersion suggested by Au in an inorganic or metallic form. Selective leaching of metals scavenged in the surficial environment by the humate and fulvate components of organic material has been successfully carried out for elements such as Zn, Cu, Co, and Pb using alkaline sodium pyrophosphate solution. This paper describes the problems encountered in application of this extraction to humus, soil, and sediment samples for Au.

The concentration of 'organically' bound Au in a lake sediment control is shown to be largely dependent upon the sample weight:leach volume ratio. This concentration is determined to be 128 ppb Au at 0.5 g subsampling and 59 ppb Au at 3 g subsampling. Thus, the larger the sample taken per unit volume, the lower the proportional amount of gold apparently extracted. Recovery of AuCl₃ spike added to 3 g of the control is less than 20%; 'lost' Au is shown to be present in the sample residue. Similar low recoveries were obtained for four humus samples and a gabbro control, WGB-1. Thus selective leaching for Au is severely hampered by the difficulty of maintaining Au in solution in the presence of the sample substrate.

Résumé : Les méthodes de lixiviation sélective des phases sont utilisées en analyse chimique des matériaux géologiques pour déterminer sous quelle(s) *forme(s)* un élément est présent dans un milieu et, ainsi, en élucider les mécanismes de transport et d'accumulation éventuelle. Le dosage de l'or lié à la phase «organique soluble» d'un échantillon d'humus ou de sédiments lacustres permet de déterminer la dispersion hydromorphe d'un élément, par opposition à la dispersion mécanique indiquée par la présence d'or lié à la phase inorganique ou métallique. La lixiviation sélective des métaux captés dans les milieux de surface par les composantes humiques et fulviques de la matière organique, à l'aide d'une solution alcaline de pyrophosphate de sodium, donne de bons résultats pour des éléments comme le zinc, le cuivre, le cobalt et le plomb. Le présent article fait état des problèmes que pose l'utilisation de cette méthode pour l'extraction de l'or dans des échantillons d'humus, de sol et de sédiments.

Il est démontré que la concentration d'or lié dans la phase organique d'un échantillon témoin de sédiments lacustres dépend étroitement du rapport du poids de l'échantillon sur le volume de la solution de lixiviation. Cette concentration a été établie à 128 ppb d'or pour un sous-échantillon de 0,5 g et à 59 ppb pour un sous-échantillon de 3 g. Ainsi, plus la taille de l'échantillon prélevé par unité de volume est grande, moins le volume proportionnel d'or apparemment extrait est important. La récupération d'une quantité connue de AuCl₃ ajoutée à 3 g de l'échantillon témoin n'a pas dépassé 20 %; on a observé que l'or «perdu» se retrouvait dans les résidus de l'échantillon. Les proportions d'or récupéré ont également été faibles dans le cas de quatre échantillons d'humus et d'un gabbro témoin (WGB-1). Il semble donc que la lixiviation sélective de l'or soit gravement limitée du fait qu'il est difficile de maintenir l'or en solution en présence du substrat de l'échantillon.

¹ Geological Survey of Canada, 601 Booth St., Ottawa, Ontario K1A 0E8

INTRODUCTION

Interest in 'selective leaching', referring here to the quantitation of elements bound in specific phases (e.g. in sulphides, organics, or crystalline oxides) of a geological sample, has been rekindled recently in exploration geochemistry programs. One stimulus has been the success reported by the Soviets in locating deeply buried gold and base metal mineralization employing, essentially, phase-selective analytical procedures (Antropova et al., 1992; Smith et al., 1993). Their reasoning is that ore and pathfinder elements are transported by various mechanisms from the source to the surficial environment where they are held in relatively labile forms associated with different reaction sites. Research indicates that organic matter and hydrous coatings of Fe and Mn are the most important surface-active phases, otherwise known as 'scavengers' in environments ranging from soils to seawater. Thus, geochemical exploration methods should be geared towards detecting these secondary forms of elements and differentiating them from the 'total' or near total signatures obtained by applying the more conventional aqua regia or perchloric/nitric acid digestions to soils, tills, humus, and sediments. Moreover, our understanding of processes taking place in the surficial environment will be greatly advanced by identifying the forms of an element present in such media and thereby elucidating its pathway toward deposition. The Analytical Method Development Section of the Geological Survey of Canada (GSC) has designed and applied both specific and sequential leach schemes to a host of different samples in both exploration and environmentally oriented projects (e.g. Hall et al., 1993; Mudroch et al., 1993). Probably the most cost-effective and straightforward medium to use in exploration would be humus material, if available with sufficient coverage in the survey area. Collection is simple and rapid, and preservation of sample integrity between time of collection and selective leaching of the so-called 'soluble organic' component is not problematic. (Samples taken from a reducing rather than oxidizing environment must be kept out of contact with air or oxygen to prevent phase transformation.) It must be appreciated that the results of a sequential or selective leaching experiment are 'operationally defined', that is, they are to some degree dependent upon the conditions employed (period of leaching, its chemistry, etc.) and a clean and absolute separation of elemental concentrations into their respective phase categories cannot be expected. However, experimental conditions can be designed to suit the objectives at hand and the sample matrices under investigation so that the degree of specificity is adequate.

Humic substances, complex heterogeneous polymers, can be classified into: humins (molecular weight $>10^6$, acid and alkali insoluble fraction); humic acid (molecular weight 10^4 - 10^6 , soluble in alkaline solutions only); and fulvic acid (molecular weight 10^3 - 10^5 , soluble in acid and alkaline solution.) The complexation capacity for trace metals of humic and fulvic acids combined is in the order of 200 to 600 $\mu\text{mol}\cdot\text{g}^{-1}$. Metals can be bound to organic matter by various mechanisms, namely chelation, complexation, or adsorption. This broad spectrum makes the goal of specificity in a reagent hard to achieve and also leads to difficulty in minimizing dissolution of this rather loosely described phase

by other extractants in a sequential scheme. Selective removal of the organic fraction is normally carried out either by oxidation (e.g. with acidified H_2O_2 or NaOCl) or by dissolution in an alkaline medium. We have chosen to avoid oxidative extraction which would, to varying degrees, also dissolve sulphides and would therefore be defeating the objectives of this research. Sodium pyrophosphate at pH 10, with or without added NaOH , has been widely used for extracting metal-organic complexes, particularly in the field of soil science (McKeague, 1968; Bascomb, 1968). The effectiveness of $\text{Na}_4\text{P}_2\text{O}_7$ in removing the easily extractable organic matter has been attributed to its ability to chelate with Ca and other trivalent metal ions. The removal of cations bound to flocculated humates results in the subsequent conversion of the polyanion to its soluble sodium salts. Bascomb (1968) demonstrated the effect of pH on the removal of different Fe oxides by this reagent. At an alkaline pH of 10, less than 1% of crystalline Fe oxides such as goethite and hematite was extracted over a 10 h period. However, 15% of freshly precipitated $\text{Fe}(\text{OH})_3$ was extracted under these conditions. Later work by Jeanroy and Guillet (1981) indicated that $\text{Na}_4\text{P}_2\text{O}_7$ not only extracted Fe complexed with organic matter but also peptized finely divided ferruginous particles so that they were dispersed and removed from the sample. Unless these were separated prior to analysis by, for example, ultracentrifugation or ultrafiltration their presence would lead to high Fe levels being attributed to the 'soluble organic' phase. Papp et al. (1991) have recently studied the selectivity and effectiveness of $\text{Na}_4\text{P}_2\text{O}_7$, H_2O_2 and NaOCl in releasing metals (specifically Zn, Cu, Mn, and Fe) associated with organic matter in peat samples. They recommended against the use of H_2O_2 if the samples contain sulphides or manganese oxides and found that NaOCl led to precipitation of metals from samples low in organic content. For our study, the lack of selectivity of $\text{Na}_4\text{P}_2\text{O}_7$ in that it partially brings into solution 'active' (rather than 'aged') hydrous oxides and associated metals is outweighed by the fact that it is not an oxidizing agent.

The pyrophosphate leach has now been applied, at the GSC and under contract commercially, to hundreds of humus and soil samples for the determination of transition elements. Usually 1 g of material, sieved to pass 80 mesh, is leached with 100 mL of 0.1 M $\text{Na}_4\text{P}_2\text{O}_7$ for a specified time (1 h to 5 h) and the residue subsequently centrifuged off. The leachate is analyzed directly for these metals by atomic absorption spectrometry (AAS), inductively coupled plasma emission spectrometry (ICP-ES), or ICP mass spectrometry (ICP-MS). The last technique normally requires dilution in order to reduce the high salt content for reduction of nonspectral interferences. Typical precision (twice the relative standard deviation, RSD) is in the range 10-20% for elements such as Zn, Cu, Ni, Co, and Pb, as has been demonstrated by analyses of control and duplicate samples in an earlier report (Hall et al., 1993). Detection limits are generally in the order of 0.1-1 ppm ($\mu\text{g}\cdot\text{g}^{-1}$). Application of this method to determine 'organically bound' Au, however, must address two concerns: (1) the requirement of a much lower detection limit of at least 1 ppb due to this element's lower natural abundance; and (2) maintaining Au in solution during the leach itself. In the absence of a complexing anion such as Cl^- or

CN⁻, Au can be lost readily from solution by various mechanisms such as adsorption onto container walls or solid material or reduction to the metallic state with subsequent precipitation (Chao et al., 1968). Adsorption of Au onto activated charcoal (Hall et al., 1986) or extraction of the chloride anion into methyl isobutyl ketone, MIBK (Hall and Bonham-Carter, 1988), serves two purposes: separation of Au from potential interferences in the analytical method and preconcentration from a relatively large volume of solution to attain improved detection capability. Solvent extraction with MIBK is used frequently in the commonly employed aqua regia (3 parts HCl, 1 part HNO₃) extraction of Au from geological materials. This leach can provide low results dependent upon sample matrix, as has been shown in an extensive comparison with data produced by direct instrumental neutron activation analysis, INAA (Hall et al., 1989).

This paper describes the limitations encountered in the conventional application of the Na₄P₂O₇ leach to humus, soil, and sediment samples for the specific determination of 'soluble organically bound' Au.

INSTRUMENTATION AND REAGENTS USED

Two analytical techniques were employed in this investigation: ICP-MS and graphite furnace AAS (GFAAS). The Perkin-Elmer/SCIEX Model 250 Elan was used for ICP-MS analysis of acid-based solutions; the 197 atomic mass unit was measured (Au is monoisotopic). Sample introduction was via conventional nebulization using a Gilson Minipuls 2 peristaltic pump for controlled uptake of solution. Operating conditions are shown in Table 1. The Perkin-Elmer Model 5000 spectrometer, equipped with the HGA-500 furnace was used for GFAAS analysis of MIBK extracts (Table 2). Palladium

Table 1. ICP-MS hardware and operating conditions.

| | |
|--|---|
| Inductively coupled plasma— | |
| R.f. generator | 2.5 kW, frequency 27.12 Mhz |
| Nebuliser | Meinhard C concentric glass |
| Spray chamber | Scott-type |
| Torch | Sciex, "long" |
| Distance from load coil to sampler orifice | 17 mm |
| R.f. power | 1.1 kW |
| Plasma Ar flow-rate | 12 L·min ⁻¹ |
| Auxiliary Ar flow-rate | 2.1 L·min ⁻¹ |
| Nebuliser flow rate | 1.0 L·min ⁻¹ |
| Solution uptake rate | 1.0 mL·min ⁻¹ |
| Mass spectrometer— | |
| Sampler | Nickel, 1.14-mm orifice |
| Skimmer | Nickel, 0.89-mm orifice |
| Ion lens settings | B = 50, EI = 51, P = 25, S2 = 17 |
| Resolution | High (0.6 a.m.u. at 10% peak height) |
| Data acquisition parameters | Measurement time = 1 s; dwell time = 50 ms in multichannel mode, 5 readings each solution |

Table 2. GFAAS hardware and operating conditions.

| | |
|------------------------|--|
| Instrumentation | |
| AA spectrometer | Perkin-Elmer Model 5000 with model HGA 500 graphite furnace and AS-1 autosampler |
| Graphite tubes | Pyrolytic-coated |
| Conditions | |
| Wavelength | 242.8 nm |
| Slit width | 0.7 nm |
| Calibration mode | Absorbance, peak height |
| Background correction | Deuterium arc |
| Argon flow rate | 300 mL·min ⁻¹ , interrupt at atomization stage |
| Sample volume | 30 µL |
| Pd modifier in MIBK | 5 µL |
| Dry stage | 120°C / 10 s |
| Char stage | 1150°C / 10 s |
| Atomize stage | 2400°C / 5 s |

is added as its iodo-complex in MIBK for matrix modification; this allows a much higher charring temperature and enhances sensitivity (Hall and Vaive, 1989).

All chemicals used were of analytical-reagent grade; deionized distilled water was employed throughout for dilutions and washing. The stock solution of Au, as AuCl₃ at 1000 ppm in 1.2 M HCl, was obtained from Aldrich Chemicals (Wisconsin, U.S.A.). This was serially diluted with water immediately prior to use. All glassware was washed in dilute aqua regia and thoroughly rinsed with water before use. Activated charcoal ('Darco G-60') was used as received from Matheson, Coleman and Bell (Ohio, U.S.A.); preliminary washing was not necessary for Au.

DETERMINATION OF Au BOUND IN THE 'SOLUBLE ORGANIC' PHASE

Development of the proposed method using Na₄P₂O₇ extraction

The weight of sample taken was increased from 1 g in the earlier method to 3 g in an attempt to bring more Au into solution and hence to improve detection capability. Once dissolved from the sample by Na₄P₂O₇ solution, Au is adsorbed onto activated charcoal in a similar manner to the procedure described for the analysis of waters (Hall et al., 1986). It is then redissolved from the ash of the activated charcoal with HCl and HNO₃, diluted and analyzed by ICP-MS. In the absence of ICP-MS instrumentation, the Au can be extracted from the acidified solution into MIBK and analyzed by GFAAS. Alternatively, the activated charcoal separation can be eliminated and replaced by extraction into MIBK following oxidative destruction of the organics in the Na₄P₂O₇ solution by acid evaporation. These procedures are detailed below.

Proposed procedure with activated charcoal separation (A)

1. Weigh 3 g of -80 mesh humus material into a flask or bottle and add 100 mL of 0.1 M $\text{Na}_4\text{P}_2\text{O}_7$ at pH 10. Mix continuously on a mechanical shaker for 5 h.
2. Filter off the residue with #41 Whatman paper at standard pressure. (Centrifuging prior to filtering can speed up the process). Add 10 mL of 16 M HNO_3 to the filtrate in a beaker and heat under reflux (simply cover with a watch-glass) for 1 h. With a 1.2 μm pore size filter paper (Millipore type HAWP) under vacuum, filter off the residue ('humic acid extract'), washing with deionized water, and place in a porcelain crucible.
3. To the filtrate from step (2) add 250 mg of activated charcoal and 10 mL of 12 M HCl and stir for 0.5 h. Filter off the residue ('fulvic acid extract') onto a 1.2 μm filter paper as before but wash with copious amounts of 1 M HCl . Add the residue and paper to the crucible.
4. Ash the contents (2 residues and filter papers) in a muffle furnace at 650°C for 3 h. To the residue add 2 mL of 12 M HCl and 2 drops of 16 M HNO_3 and warm to dissolve the Au. If the analytical technique to be employed is GFAAS, proceed to step (6).
5. *ICP-MS finish.* Evaporate to about 0.5 mL volume. Transfer the contents to a 5.0 mL calibrated test-tube (or use weight), adding deionized water rinses from the crucible and make up to the mark. Analyze the solution for Au by ICP-MS using calibration standards in 1 M HCl . Operating conditions are shown in Table 1. The dilution factor is 1.66 (5 mL/3 g).
6. *GFAAS finish.* Transfer the contents of the crucible to a separatory funnel and rinse it well with 4 M HCl , adding the rinses to the funnel to a final volume of about 15 mL. Add 3 mL of MIBK (previously saturated with 4 M HCl) and extract for 5 min on a shaker. Back-wash Fe from the MIBK layer by a second extraction with 10 mL of 0.1 M HCl . Analyze the MIBK layer for Au by GFAAS using the operating conditions shown in Table 2. Calibration standards are prepared by extracting known amounts of Au from 15 mL portions of 4 M HCl , in the same manner as the samples.

Alternative procedure for GFAAS finish only (B)

1. Weigh 3 g of -80 mesh humus material into a flask or bottle and add 100 mL of 0.1 M $\text{Na}_4\text{P}_2\text{O}_7$. Mix continuously on a mechanical shaker for 5 h.
2. Filter off the residue with #41 Whatman paper at standard pressure. Place 50 mL of filtrate in a beaker and add 20 mL of 16 M HNO_3 and 10 mL of 12 M HClO_4 . Heat to dense white fumes. Cool, add 4 mL of aqua regia and heat gently.
3. Transfer the contents of the beaker, with two 6 mL 12 M HCl rinses, to a graduated test-tube. When cool, make up to the 50.0 mL mark with deionized water (final HCl concentration is 4 M).

4. Extract Au from the 50 mL analyte solution into 3 mL of MIBK and back-extract the Fe with 0.1 M HCl (as in step 6 above). Calibrate against standards prepared by spiking known amounts of Au into the same acid mixture (i.e. 15 mL of HCl + 1 mL of HNO_3 + 34 mL of H_2O) and extracting them into MIBK.

During the development of this method (A), 10 mL of HCl were added together with the activated charcoal to the filtrate obtained from the pyrophosphate leach (after step 1). This combined step would serve to (a) precipitate Au in the humic fraction by addition of acid, and (b) adsorb Au in the soluble fulvic fraction onto activated charcoal. However, filtration of the residue at 1.2 μm was extremely slow (hours), even under vacuum. Attempts to hasten this process by filtering off the humic acid portion first by addition of HCl and then adding activated charcoal to the resultant filtrate proved fruitless. When refluxing with HNO_3 was introduced, both filtration procedures (steps 2 and 3) became very rapid. Typically a 'plug' of flocculant solid material is formed upon addition of HNO_3 to the pyrophosphate leachate; this then precipitates out clearly as discrete particles on refluxing. Washing these residues, particularly the activated charcoal with 1 M HCl , is critical in reducing the Na content of the final solution and thus producing an ideal matrix for ICP-MS analysis. Concentrations of Na in the final analyte solution from step 5 are typically below 10 ppm whereas they can be as high as 400 ppm in the absence of 1 M HCl washing.

Care must be taken in redissolution of the ashed residue (steps 4 and 5) in order to fully recover Au: evaporation must not proceed to dryness, to prevent volatilization of Au, and enough acid must be used to adequately wet the inner surface of the crucible.

Results for Au in the 'soluble organic' phase of humus, sediment, and soil samples

Application to GSC control samples

Despite the number of manipulations demanded by the proposed procedure, the recovery of Au in spiked synthetic samples analyzed in this manner was excellent. To develop the method, spiked additions of 50 and 100 ng of Au were added to 100 mL portions of (a) fresh 0.1 M $\text{Na}_4\text{P}_2\text{O}_7$ solution alone and (b) $\text{Na}_4\text{P}_2\text{O}_7$ solution which had been used to extract the soluble organic phase of a background humus control which was devoid of measurable Au. This second solution was prepared in bulk and filtered prior to use in recovery experiments. When the final protocols were fixed, recoveries of these spikes averaged $93 \pm 3\%$ ($n = 5$ each), regardless of the analytical technique used (ICP-MS or GFAAS) or which $\text{Na}_4\text{P}_2\text{O}_7$ solution was employed. Detection limit in solution is similar for both techniques by procedure A, equivalent to about 0.05 ppb of Au in the original sample.

The method was first applied to a selection of standard reference materials (SRM) for which there were available Au data. Results for Au in duplicate samples (two 3 g portions) of LKSD-1, STSD-1, STSD-3, TILL-1, and TILL-3 are compared in Table 3 with accepted 'total' Au data obtained by

INAA. The precision of the duplicate results seems reasonable in view of the low levels and the degree of homogeneity expected. Although LKSD-1 contains the least total Au at 5 ppb, it appears to have the highest percentage of organically bound Au, averaging 62%. This finding would be anticipated as this sample naturally has the highest concentration of organics (C = 12.3%). The concentration of C dissolved by the $\text{Na}_4\text{P}_2\text{O}_7$ leach typically ranges from the equivalent of 2 to 5% in the original sample (i.e. 600 to 1500 ppm C in the leachate itself).

The effect on the amount of Au leached by taking different sample weights and by altering the contact time between sample and $\text{Na}_4\text{P}_2\text{O}_7$ solution was investigated using an in-house lake sediment from Red Lake, near the Ontario-Manitoba border. This sediment was known to be remarkably homogeneous in its Au distribution, even at 1 g subsampling weights, and contains about 280 ppb total Au, confirmed by both INAA and aqua regia leach/GFAAS. Its organic content

is high, with an LOI (loss on ignition at 450°C) of 84%. The proposed procedure was applied in duplicate to Red Lake at 3 sample weights (0.5, 1.0, and 3.0 g) in a constant volume of 100 mL of 0.1 M $\text{Na}_4\text{P}_2\text{O}_7$ solution, and for 4 different contact times (0.5, 1.0, 3.0, and 5.0 h). Recoveries for a 250 ng Au spike (250 µL of stock 1.00 ppm Au solution) in the background humus leachate taken through these procedures, in duplicate as with the sample, averaged $92.7 \pm 3.6\%$ ($n = 8$). The data obtained for Red Lake is shown graphically in Figure 1. It is evident that there is indeed a dependency of the amount of Au recovered on the sample weight/leach volume ratio: the greater the amount of sample taken per unit volume, the smaller the percentage of Au recovered. For example, at a contact time of 3 h, 46% (128 ppb) of the total Au is extracted and recovered from a 0.5 g sample of Red Lake, whereas this figure is only 21% (59 ppb) for a 3.0 g sampling. This phenomenon is not present in $\text{Na}_4\text{P}_2\text{O}_7$ leaching experiments for base metals and organic carbon: in those cases, the more sample in contact with the leach, the more element is brought into solution. Thus the effect of increasing sample weight from the 1 g used for transition metals to 3 g in order to improve both representivity and detection capability for Au is being offset by this *apparent* reduction in extraction efficiency. The contact time between sample and leach solution appears to have little effect after about 1 h but is critical at shorter duration, particularly for the 0.5 g, and to a lesser extent the 1.0 g sample weight. These findings suggest that competing processes of dissolution of Au from the sample and readsorption back onto the sample surface during leaching are occurring. The actual mechanism of 'readsorption' is not identified in this study. This term is being used loosely to indicate loss from solution by any mechanism including precipitation, colloid aggregation, or sorption at exchange sites. It is interesting to observe the excellent precision of the duplicates at the 3 g sample weight in Figure 1, a reflection of improved representivity and/or reproducibility of the adsorption process. The organic carbon content of the $\text{Na}_4\text{P}_2\text{O}_7$ leach increases in an exponential manner, with the slope beginning to plateau after about the first hour; once separated from the residue these solutions are stable in organic content over at least 2-3 week period.

Table 3. Comparison of Au determined by $\text{Na}_4\text{P}_2\text{O}_7$ leach / ICP-MS and by INAA in SRMs LKSD-1, STSD-1, STSD-3, TILL-1, and TILL-3.

| Sample ^a | Au, ppb | |
|---------------------|--|-------------------|
| | $\text{Na}_4\text{P}_2\text{O}_7$ leach / ICP-MS | INAA ^b |
| LKSD-1 | 2.70, 3.47 | 5 |
| STSD-1 | 2.26, 1.26 | 8 |
| STSD-3 | 1.11, 1.52 | 7 |
| TILL-1 | 1.87, 1.37 | 11 |
| TILL-3 | 0.80, 1.62 | 6 |

^a SRMs offered by Canadian Certified Reference Materials Project (CCRMP), CANMET, Ottawa (see Lynch, 1990 for details)

^b Pers. comm.: J.J. Lynch ($n=39$ to 81 INAA determinations for each standard)

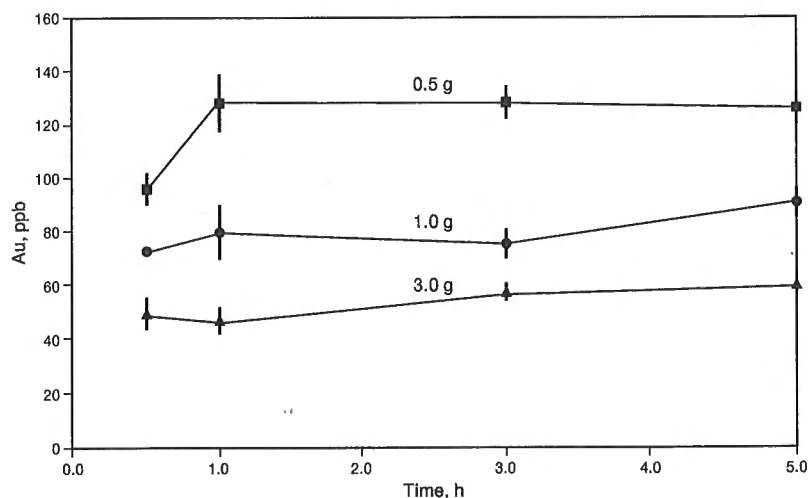


Figure 1.

Amount of Au recovered from different sample weights of Red Lake at varying contact time with leach solution, 0.1 M $\text{Na}_4\text{P}_2\text{O}_7$. Analysis by GFAAS. (Hall et al., 1995)

In order to demonstrate that the Au not recovered during the 5 h leach of the 3 g Red Lake sample remained fixed on the residue and was not lost elsewhere in the procedure, two 3 g subsamples were again processed. This time the alternative methodology B, using extraction into MIBK and analysis by GFAAS, was employed. The residues were then ashed in an oven at 650°C for 3 h and carried through a hot aqua regia leach as described by Hall et al. (1989), the final analysis also being by GFAAS following an MIBK extraction. The concentrations of Au found in these residues and those in the 0.1 M Na₄P₂O₇ leachates are given in Table 4. It is apparent that all the Au in these Red Lake samples is accounted for, by adding that remaining in the residue and that in solution following the 5 h 0.1 M Na₄P₂O₇ leach. These combined values of 271 and 272 ppb Au agree very well with the mean value of Au in Red Lake of 281 ± 12 ppb by aqua regia/GFAAS.

To test for readsorption, five 3 g samples of Red Lake were carried through the proposed procedure (i.e. 5 h contact time) and analyzed by ICP-MS after activated charcoal separation. Two samples were spiked with 250 ng of Au at the beginning of the leach in 0.1 M Na₄P₂O₇, two were spiked with 250 ng of Au at the end of the 5 h leach, and the fifth was analyzed as usual without a spike. The results are given in Table 5. The amount of organically bound Au recovered in the single unspiked sample of Red Lake is 51.5 ppb; taking this figure as the basis, full recovery of the 250 ng spike would be indicated by a concentration of 134.8 ppb Au (i.e. 51.5 ppb + 250 ng/3 g). By adding Au after the 5 h leach, spike recovery is reasonable at 89-93% but addition at the beginning of the leach results in only 10-19% recovery of Au, assuming that all the 51 ppb of organically bound Au in the sample is being recovered. Thus readsorption is clearly a problem and leads to incorrect data and therefore misleading interpretation. Initial Au spike recoveries during the development phase were good as there was no sample present, just the 0.1 M Na₄P₂O₇ solution itself. Another sample was selected, of contrasting matrix to the organic-rich Red Lake sediment, to ascertain whether this capacity for readsorption was limited to samples high in organic carbon content. Four 3 g subsamples of the Wellgreen gabbro, WGB-1, marketed under the CCRMP (CANMET) as a low-level PGE SRM, were processed in a similar manner to Red Lake above. Gold was determined both in the Na₄P₂O₇ leach and in the remaining residue (after aqua regia extraction) of two unspiked and two spiked WGB-1 samples. The certified value for Au in WGB-1 is 2.9 ± 1.1

Table 4. Concentration of Au leached by 0.1 M Na₄P₂O₇ (procedure B) and remaining in residue of 3 g samples of Red Lake.

| Sample | Au, ppb | | | |
|----------------|---|---------------|-------|---------------------|
| | By Na ₄ P ₂ O ₇ | In residue | Total | Total, by AR |
| Subsample 1 | 64 | 207 | 271 | 281 ± 12 (n = 9) |
| Subsample 2 | 51 | 221 | 272 | |
| AR: aqua regia | | | | |

ppb. The data in Table 6 indicate that readsorption of Au during the 5 h leach is indeed occurring for this organic-poor matrix, resulting in a recovery of only 23-25% for a 250 ng spike, just slightly higher than that for Red Lake.

Application to other humus and soil samples

Four humus samples, collected in a joint exploration program with Queen's University, were selected for application of the proposed procedure A to determine 'organically bound' Au. These were analyzed in duplicate for: (1) aqua regia leachable Au; (2) pyrophosphate leachable Au; and (3) pyrophosphate leachable Au after spiking with 250 ng of Au. The results are shown in Table 7, together with Au obtained by leaching for 5 h in 1 M HCl and applying steps 3 through 5 of procedure A. Although the 'total' (aqua regia leachable) Au contents of the humus samples varied from <2 to about 25 ppb, their 'organically bound' fractions were all similar, at 1-2 ppb. The spike recoveries of only 12 to 23% confirm the suspicion of Au readsorption. When a 250 ng spike of Au was added to sample 91-1048 after the 5 h shake in 0.1 M Na₄P₂O₇, values for Au of 85.2 and 80.1 ppb were obtained, indicating complete recovery. Readsorption also takes place in the 1 M

Table 5. Amount of Au in Red Lake at 3 g subsampling recovered by Na₄P₂O₇ leach / ICP-MS, unspiked and spiked with 250 ng of Au immediately before and after 5 h extraction. Spike recovery shown in brackets.

| Unspiked | Au, ppb | |
|----------|-------------------------------------|-----------------|
| | Spiked at equivalent of 83.3 ppb Au | |
| | Before 5 h leach | After 5 h leach |
| 51.5 | 67.8 | 125 |
| | (19.6%) | (93%) |
| | 60.1 | 120 |
| | (10.3%) | (89%) |

Table 6. Amount of Au in 3 g unspiked and spiked (with 250 ng of Au) subsamples of WGB-1 recovered by Na₄P₂O₇ leach / ICP-MS and remaining in residue. Spike recovery shown in brackets.

| Au, ppb | | | | |
|---|------------|--|------------|--------------------|
| WGB-1, unspiked | | WGB-1, spiked at equivalent of 83.3 ppb Au | | |
| By Na ₄ P ₂ O ₇ | In residue | By Na ₄ P ₂ O ₇ | In residue | Total |
| 1.2 | <2 | 19.3 | 59 | 78.3 |
| | | (23%) ^a | | (93%) ^a |
| 1.0 | <2 | 20.3 | 56 | 76.6 |
| | | (25%) ^a | | (91%) ^a |
| ^a Recovery assuming 1.1 ppb of 'organically bound' Au in WGB-1 | | | | |

HCl leach. Spikes equivalent to 83.3 ppb Au added in duplicate before and after the 5 h leach of sample 91-1048 gave 1.86 and 1.71 ppb, and 81.0 and 80.3 ppb, respectively. Further evidence of readsorption for these samples is provided in Table 8. Gold was determined in both the pyrophosphate leachates and their residues of these samples processed through procedure B; again half the suite was spiked with Au at the equivalent of 83.3 ppb (250 ng). Clearly the majority of the spike does not stay in the leach solution but rather is fixed with the remaining sample. Decreasing the time of extraction from 5 h to 2 h had negligible effect on the results for these four samples.

IMPLICATIONS FOR Au DETERMINATION IN OTHER SELECTIVE LEACHES

Having observed that readsorption was also occurring in a partial 1 M HCl leach, the phenomenon was further investigated in the application of another phase selective leach of interest in exploration geochemistry, namely hydroxylamine hydrochloride ($\text{NH}_2\text{OH}\cdot\text{HCl}$), used to preferentially dissolve amorphous Fe oxyhydroxide in soils (Chao and Zhou, 1983; Hall et al., 1993). In this method, 20 mL of 0.25 M $\text{NH}_2\text{OH}\cdot\text{HCl}$ in 0.25 M HCl are added to a 1 g sample in a test-tube. The mixture is loosely capped, heated in a water bath at 60°C for 2 h and periodically agitated on a vortex mixer to ensure adequate contact between solid and liquid phases. Following 10 minutes of centrifuging at 2800 rpm, the solution is decanted into another calibrated test-tube. The residue is rinsed with deionized water several times and the rinses after centrifuging are added to the original solution. After cooling, the solution is made up to the 30 mL mark with

Table 7. Concentrations of Au found in four 3 g humus samples by (1) aqua regia leach, (2) pyrophosphate leach with and without spiking (equivalent to 83.3 ppb Au), and (3) 1 M HCl leach. Analysis by ICP-MS following separation on activated charcoal.

| Sample | LOI, % | Au, ppb | | | |
|--|--------|------------|---|--------------------------------------|----------|
| | | AR leach | Na ₄ P ₂ O ₇ leach | | 1 M HCl |
| | | | Unspiked | Spiked | |
| 91-1036 | 47.5 | 23.1, 20.8 | 1.2, 1.1 | 10.3, 11.7 (12, 14%) ^a | 1.4, 1.0 |
| 91-1039 | 34.0 | <5, <5 | 2.0, 0.8 | 17.8, 19.1 (21, 23%) ^a | 1.4, 0.5 |
| 91-1048 | 51.6 | 5.4, 8.8 | 1.2, 1.2 | 17.4, 14.2 (21, 17%) ^a | 0.6, 0.6 |
| 91-1063 | 36.2 | 18.4, 27.6 | 1.6, 3.1 | 12.9, 11.2 (15, 13%) ^a | 3.2, 3.1 |
| ^a : recoveries of 83.3 ppb spike based on mean of unspiked sample LOI: loss on ignition at 450°C AR: aqua regia | | | | | |

Table 8. Analysis of four humus samples for Au in pyrophosphate leach and in respective residue with and without spiking at a level equivalent to 83.3 ppb Au prior to 5 h leach. Analysis by GFAAS following MIBK extraction.

| Sample | Au, ppb | | | | | |
|---------|---|---------|-------|---|---------|-------|
| | Unspiked leach | | | Spiked leach (at 83.3 ppb Au) | | |
| | Na ₄ P ₂ O ₇ | Residue | Total | Na ₄ P ₂ O ₇ | Residue | Total |
| 91-1036 | 1.1 | 15.8 | 16.9 | 14.4 | 87.6 | 102.0 |
| 91-1036 | 1.4 | 22.5 | 23.9 | 13.2 | 90.0 | 103.2 |
| 91-1039 | 3.0 | 3.1 | 6.1 | 19.1 | 71.2 | 90.3 |
| 91-1039 | 1.5 | 3.6 | 5.1 | 17.7 | 70.0 | 87.7 |
| 91-1048 | 0.8 | 5.4 | 6.2 | 13.2 | 77.6 | 90.8 |
| 91-1048 | 0.9 | 4.2 | 5.1 | 15.0 | 78.7 | 93.7 |
| 91-1063 | 1.0 | 21.7 | 22.7 | 10.9 | 101.1 | 112.0 |
| 91-1063 | 0.9 | 23.6 | 24.5 | 9.8 | 93.4 | 103.2 |

water and 250 mg of activated charcoal and 3 mL of 12 M HCl are added. Gold is determined by ICP-MS following steps 3 through 5 in procedure A.

This method was applied in duplicate to a suite of six B-horizon soil samples, three of which were collected in the joint project with Queen's University mentioned earlier and the remaining three (Blue Star, Genesis, and Vivian) were well characterized controls from Carlin, Nevada, ground to pass a 200-mesh screen. Table 9 presents the gold concentrations found in these samples, in the $\text{NH}_2\text{OH}\cdot\text{HCl}$ leach and in the remaining residue (extracted with aqua regia as before) with spiking at the 250 ppb (250 µL of 1.00 ppm stock) Au level just after addition of the leach solution. Clearly, adsorption is occurring to a great extent in the majority of these samples but recovery is dramatically improved for sample 1038. Perhaps it is not at all surprising that Au is being lost from the $\text{NH}_2\text{OH}\cdot\text{HCl}$ leach as its action on Fe oxyhydroxide is of a reducing nature and hence conversion to the stable elemental Au state is likely.

DISCUSSION

The work described here is solely of an empirical nature; we have not attempted to identify the way Au is bound in the Na₄P₂O₇ leach (complexed as humate and/or fulvate species, as a colloid?) or the mechanism of loss to the sample. Kinetics and the sample matrix obviously play critical roles in this partitioning. It can be argued that the Au added (as AuCl_4^-) in the spike is not the same form as that leached from the sample and that its behaviour may differ but ample evidence has been provided to document that significant loss (referred to as adsorption) does occur (Tables 5-10). Other research has demonstrated control of element concentrations in selective leaches by the process of readsorption for metals other than Au (e.g. Rendell et al., 1980). The importance of using natural

rather than synthetic samples and of spiking at reasonable rather than abnormally high concentrations of analyte has been stressed by Belzile et al. (1989) in their defence of the use of partial extractions and the information derived therefrom. Under these conditions, they found negligible readsorption of As, Cd, Cu, Ni, Pb, and Zn during application of a sequential scheme to oxic lake sediments. Our experiments confirm their findings for these elements; it is only the determination of Au and the precious metals where readsorption has been identified (Hall et al., 1993).

There is a growing number of reports in the geochemical literature concerning both the form(s) in which Au is mobilized and transported in the surficial environment (as humates, by Boyle et al., 1975 and Baker, 1978; as fulvate complexes, by Howell et al., 1993; as a chloride, by Mann, 1984; as the neutral monohydroxide, by Vlassopoulos and Wood, 1990) and the mechanisms by which it is precipitated from solution. The concentration of Au in organic-rich parts of tropical soil profiles (Friese, 1931; Ong and Swanson, 1969; Varshal et al., 1990; Howell et al., 1993) can be explained by reduction of Au-fulvate complexes or inorganic complexes by insoluble organic matter such as humic acid (pH <7) or humins. Gold (III) chloride and gold (I) thiosulphate adsorption by goethite has been thoroughly investigated by Machesky et al. (1991); they found adsorption of the chloride to increase with pH probably due to a shift in species to $\text{AuCl}(\text{OH})_3^-$ by hydrolysis. Steric properties (e.g. square planar vs. linear) of the individual species are thought to be responsible for the specific adsorption behaviour. Alkaline

Table 9. Analysis of 1 g samples of various soils for Au in a 0.25 M $\text{NH}_2\text{OH}\cdot\text{HCl}$ leach and in remaining residue, with spiking equivalent to 250 ppb Au just prior to leaching.

| Soil | Au, ppb | | | |
|-----------|---------------------|---------------------------------------|------------|-------|
| | Total by AR | Spiked at 250 ppb Au | | |
| | | $\text{NH}_2\text{OH}\cdot\text{HCl}$ | In residue | Total |
| Blue Star | 38 ± 2 ^a | 6.7 | 282 | 289 |
| Blue Star | | 6.3 | 278 | 284 |
| Genesis | 86 ± 6 ^a | 6.1 | 329 | 335 |
| Genesis | | 6.0 | 319 | 325 |
| Vivian | 33 ± 3 ^a | 1.5 | 284 | 286 |
| Vivian | | 2.2 | 286 | 288 |
| 91-1035 | 720, 600 | 0.3 | 888 | 888 |
| 91-1035 | | 0.2 | 940 | 940 |
| 91-1038 | 61.2, 65.2 | 100 | 221 | 321 |
| 91-1038 | | 120 | 218 | 338 |
| 91-1056 | 28.4, 15.6 | 4.9 | 254 | 259 |
| 91-1056 | | 5.2 | 270 | 275 |

AR: aqua regia
^a: Data from Hall et al. (1989)

Table 10. Effect of increasing contact time between a background humus control sample and a 0.1 M $\text{Na}_4\text{P}_2\text{O}_7$ solution containing 400 ppm of Au, Pt, and Pd. Results are concentrations of metals left in solution determined by ICP-MS.

| Contact time, min | Au, ppm | Pt, ppm | Pd, ppm |
|-------------------|---------|---------|---------|
| 0 (spiked sol'n) | 410 | 411 | 396 |
| 1 | 93 | 267 | 24 |
| 5 | 93 | 245 | 12 |
| 10 | 92 | 250 | 17 |
| 15 | 89 | 232 | 14 |
| 30 | 78 | 212 | 6 |

pH and low Cl^- concentration are likely conditions for adsorption onto goethite and other surfaces. Adsorption of Au species onto other mineral surfaces has also been studied, as reported by: Nechayev and Nikolenko (1986) and Fedoseyeva and Strel'tsova (1988) onto alumina, silica, and kaolin; Hyland and Bancroft (1989) onto sulphides; and Nechayev (1984) onto hematite.

These occurrences in nature are being reflected in the laboratory, under the various conditions of selective leaching. The degree to which they are proceeding is difficult to predict, given the complexity of the sample matrix and the competing processes at work. The repeatability of the results for individual samples suggests that equilibrium between adsorption and dissolution processes is attained, probably after the first hour (Fig. 1). The approach to adopt in pursuing selective leaching for Au is probably that of a flow-through system where the leachate does not remain in prolonged contact with the sample but the duration must be sufficient for adequate dissolution of that specific phase. A humus control sample was doped with Au by placing it in a spiked solution and stirring for several days; after washing with water and drying, it was found to contain 190 ± 12 ppb Au ($n = 3$, 2 g subsampling). Having formed the sample into a 1 g disc, 0.1 M $\text{Na}_4\text{P}_2\text{O}_7$ solution was automatically pumped through at the rate of $100 \text{ mL}\cdot\text{min}^{-1}$ and the first 20 mL of 'eluant' analyzed by ICP-MS. Duplicate results of the experiment are promising: 53.4 and 49.8 ppb Au were leached out of the sample. Clearly, parameters such as flow-rate and collection time remain to be optimized, while still ensuring even 'wetting' of the sample. The speed with which Au (and precious metals) is adsorbed from 0.1 M $\text{Na}_4\text{P}_2\text{O}_7$ solution is demonstrated by data shown in Table 10. The leach solution containing 400 ppm of Au (and Pt, Pd) was added to a 'background' humus control (of undetectable Au content) and sampled for analysis at intervals of 1, 5, 10, 15, and 30 min. Evidently, adsorption for Au (and Pd) takes place within the first minute and tails off thereafter. The experimental conditions chosen to maximize dissolution of the 'soluble organic' phase while minimizing adsorption of Au may well be significantly matrix dependent; this investigation is in progress.

SUMMARY AND CONCLUSION

Readsorption of Au onto the sample substrate has been demonstrated to occur to a high degree in the 0.1 M $\text{Na}_4\text{P}_2\text{O}_7$ leach for Au held in the 'soluble organic' phase of humus and soil samples. An equilibrium appears to be established between the competing processes of dissolution and adsorption dependent upon the sample weight:solution volume ratio, as evidenced by a control sediment, Red Lake. Recovery of a Au spike, added as the chloride at the 83 ppb level, is less than 20% during a 5 h leach of 3 g of Red Lake. Recovery is only slightly higher, at 23-25%, when this organic-rich matrix is substituted by a gabbro. Under similar conditions, such recoveries for four humus samples were in the range 12-21%, the 'missing' Au being proven to be in the sample residue.

Readsorption of Au was also observed in the $\text{NH}_2\text{OH}\cdot\text{HCl}$ leach designed to selectively dissolve amorphous Fe oxyhydroxides in soils. The degree of readsorption is dependent upon the sample matrix, leaching solution, and form(s) of Au dissolved. Further research in selective extraction for Au should be pursued using a flow-through system rather than batch mode of operation. These limitations encountered in applying selective leaches to soils and humus in order to quantify Au transported in a labile form and scavenged by such phases as humates and fulvates and amorphous Fe oxyhydroxides make the alternative approach of CHIM (Smith et al., 1993) more attractive. This in-situ technique uses a DC electrical current to move mobile cations into special fluid-filled cathodes (or conversely anodes for anions) placed in the ground. Parchment separates the collector and electrode from the sample itself and hence Au ions so mobilized do not remain in contact with the sample.

ACKNOWLEDGMENTS

We wish to thank Maki Hoashi for the flow-through leach studies carried out on the precious metals. We are grateful to Newmont Exploration Ltd. for continued use of their control material. Thanks also to John J. Lynch for his standard reference materials, data provided, and critical review of this paper.

REFERENCES

- Antropova, L.V., Goldberg, I.S., Voroshilov, N.A., and Ryss, Ju.S.
1992: New methods of regional exploration for blind mineralization: application in the USSR; *Journal of Geochemical Exploration*, v. 43, p. 157-166.
- Baker, W.E.
1978: The role of humic acid in the transport of gold; *Geochimica et Cosmochimica Acta*, v. 42, p. 645-649.
- Bascomb, C.L.
1968: Distribution of pyrophosphate-extractable iron and organic carbon in soils of various groups; *Journal of Soil Science*, v. 19, p. 251-268.
- Belzile, N., Lecomte, P., and Tessier, A.
1989: Testing readsorption of trace elements during partial chemical extractions of bottom sediments; *Environmental Science and Technology*, v. 23, p. 1015-1020.
- Bowell, R.J., Gize, A.P., and Foster, R.P.
1993: The role of fulvic acid in the supergene migration of gold in tropical rain forest soils; *Geochimica et Cosmochimica Acta*, v. 57, p. 4179-4190.
- Boyle, R.W., Alexander, W.M., and Aslin, G.E.M.
1975: Some observations on the solubility of gold; Geological Survey of Canada, Paper 75-24, p. 6.
- Chao, T.T. and Zhou, L.
1983: Extraction techniques for selective dissolution of amorphous iron oxides from soils and sediments; *Soil Science Society of America Journal*, v. 47, p. 225-232.
- Chao, T.T., Jenne, E.A., and Heppting, L.M.
1968: Prevention of adsorption of trace amounts of gold by containers; United States Geological Survey, Professional Paper 600-D, p. 16-19.
- Fedoseyeva, V.I. and Strel'tsova, O.A.
1988: Temperature effects in the adsorption of AuCl_4^- on Al_2O_3 ; *Geochemistry International*, v. 25, p. 112-115.
- Freise, F.W.
1931: The transportation of gold by organic underground solutions; *Economic Geology*, v. 26, p. 421-431.
- Hall, G.E.M. and Bonham-Carter, G.F.
1988: Review of methods to determine gold, platinum and palladium in production-oriented geochemical laboratories, with application of a statistical procedure to test for bias; *Journal of Geochemical Exploration*, v. 30, p. 255-286.
- Hall, G.E.M. and Vaive, J.E.
1989: Effect of palladium as a matrix modifier in the determination of gold by graphite furnace atomic absorption spectrometry; in *Current Research, Part F*; Geological Survey of Canada, Paper 89-1F, p. 27-30.
- Hall, G.E.M., MacLaurin, A.I., and Vaive, J.E.
1995: Readsorption of gold during the selective extraction of the 'soluble organic' phase of humus, soil and sediment samples; *Journal of Geochemical Exploration*, v. 54, p. 27-38.
- Hall, G.E.M., Vaive, J.E., and Ballantyne, S.B.
1986: Field and laboratory procedures for determining gold in natural waters: relative merits of preconcentration with activated charcoal; *Journal of Geochemical Exploration*, v. 26, p. 191-202.
- Hall, G.E.M., Vaive, J.E., Coope, J.A., and Welland, E.F.
1989: Bias in the analysis of geological materials for gold using current methods; *Journal of Geochemical Exploration*, v. 34, p. 157-171.
- Hall, G.E.M., Vaive, J.E. and Kaszycki, C.
1993: The diagnostic capabilities of selective leaching; *Explore (Association of Exploration Geochemists Newsletter)*, v. 80, p. 3-9.
- Hyland, M.M. and Bancroft, G.M.
1989: An XPS study of gold deposition at low temperatures on sulfide minerals: reducing agents; *Geochimica et Cosmochimica Acta*, v. 53, p. 367-372.
- Jeanroy, E. and Guillet, B.
1981: The occurrence of suspended ferruginous particles in pyrophosphate extracts of some soil horizons; *Geoderma*, v. 26, p. 95-105.
- Lynch, J.
1990: Provisional elemental values for eight new geochemical lake sediment and stream sediment reference materials LKSD-1, LKSD-2, LKSD-3, LKSD-4, STSD-1, STSD-2, STSD-3 and STSD-4; *Geostandards Newsletter*, v. 14, p. 153-167.
- Machesky, M.L., Andrade, W.O., and Rose, A.W.
1991: Adsorption of gold (III)-chloride and gold (I)-thiosulfate anions by goethite; *Geochimica et Cosmochimica Acta*, v. 55, p. 769-776.
- Mann, A.W.
1984: Mobility of gold and silver in lateritic weathering profiles: some observations from western Australia; *Economic Geology*, v. 79, p. 38-49.
- McKeague, J.A.
1968: Humic-fulvic acid ratio, Al, Fe and C in pyrophosphate extracts of criteria in A and B horizons; *Canadian Journal of Soil Science*, v. 48, p. 27-35.
- Mudroch, A., Hall, G.E.M., Azcue, J., Jackson, T., Reynoldson, T., and Rosa, F.
1993: Report on the effects of abandoned mine tailings at Wells, B.C., on the aquatic ecosystem of Jack of Clubs Lake; *National Water Research Contribution* 93-23.

Nechayev, Ye. A.

1984: The effects of solution composition on the adsorption of gold (III) complexes on hematite; *Geochemistry International*, v. 21, p. 87-93.

Nechayev, Ye.A. and Nikolenko, N.V.

1986: Adsorption of gold (III) chloride complexes on alumina, silica and kaolin; *Geochemistry International*, v. 23, p. 32-37.

Ong, H.L. and Swanson, V.E.

1969: Natural organic acids in the transportation, deposition and concentration of gold; *Quarterly Journal of the Colorado School of Mines*, v. 64, p. 395-425.

Papp, C.S.E., Filipek, L.H., and Smith, K.S.

1991: Selectivity and effectiveness of extractants used to release metals associated with organic matter; *Applied Geochemistry*, v. 6, p. 349-353.

Rendell, P.S., Batley, G.E., and Cameron, A.J.

1980: Adsorption as a control of metal concentrations in sediment extracts; *Environmental Science and Technology*, v. 14, p. 314-318.

Smith, D.B., Hoover, D.B., and Sanzalone, R.F.

1993: Preliminary studies of the CHIM electrogeochemical method at the Kokomo mine, Russell Gulch, Colorado; *Journal of Geochemical Exploration*, v. 46, p. 257-278.

Varshal, G.M., Velyukhanova, T.K. and Baranova, N.N.

1990: Geochemical and analytical aspects of the reaction of gold with humic substances in natural waters; *Geochemistry International*, v. 27, p. 10-19.

Vlassopoulos, D. and Wood, S.A.

1990: Gold speciation in natural waters: I. Solubility and hydrolysis reactions of gold in aqueous solution; *Geochimica et Cosmochimica Acta*, v. 54, p. 3-12.

Contribution to the 1989-1994 Rusty Lake-Snow Lake Mining Camps, Canada-Manitoba Exploration Science and Technology Initiative (EXTECH I)

The geochemistry of vegetation growing over the deeply buried Chisel North Zn-rich massive sulphide deposit, Snow Lake area

M.A.F. Fedikow¹ and C.E. Dunn²

Fedikow, M.A.F. and Dunn, C.E., 1996: The geochemistry of vegetation growing over the deeply buried Chisel North Zn-rich massive sulphide deposit, Snow Lake area; in EXTECH I: A Multidisciplinary Approach to Massive Sulphide Research in the Rusty Lake-Snow Lake Greenstone Belts, Manitoba, (ed.) G.F. Bonham-Carter, A.G. Galley, and G.E.M. Hall; Geological Survey of Canada, Bulletin 426, p. 225-255.

Abstract: The geochemistry of tissues from black spruce (*Picea mariana*), jack pine (*Pinus banksiana*), tamarack (*Larix laricina*), alder (*Alnus rugosa*), and dwarf birch (*Betula glandulosa*) was examined from an area directly over and up to 1.4 km away from Chisel North Zn-Cu massive sulphide deposit. Data obtained from neutron activation and inductively coupled plasma emission spectrometry (ICP-ES) analyses indicate that the outer bark and twigs represent the most effective tissues for establishing geochemical flux in the vegetation with proximity to the deposit. Black spruce twigs, outer bark, and needles record a 400 m by 300 m zone of multi-element enrichment over the western edge of the deposit. Based on twig geochemistry, the elements most useful for anomaly definition include the essential elements Zn, Cu, and P as well as the nonessential elements Au, Br, As, Sb, Pb, and Cd.

Airborne particulate contamination in the study area is reflected by the chemistry of the vegetation for a distance of approximately 50 m from Provincial Road 395, the major haulage route for Chisel North ore. Ash normalization of the data removes some of the effects of the particulates. Mobilization of metals from the deposit to near-surface vegetation root systems is attributed to multiple phases of deformation in the rocks, induced permeability and synmetamorphic fluid migration along brittle-ductile faults. Interaction between the skarn portions of Chisel North ore and groundwater represents a possible source of continuing gas streaming of reactants to surface. Complementary mechanisms assisting element migration include self-potential electrogeochemical effects, vegetation evapotranspiration, and hydraulic pumping.

Résumé : La géochimie des tissus de l'épinette noire (*Picea Mariana*), du pin gris (*Pinus banksiana*), du mélèze laricin (*Larix laricina*), de l'aulne rugueux (*Alnus rugosa*) et du bouleau glanduleux (*Betula glandulosa*) a été établie sur un territoire allant de la région directement au-dessus du gisement de sulfures massifs à Zn-Cu de Chisel North jusqu'à 1,4 km de ce dernier. Les données obtenues par activation neutronique et par spectrométrie d'émission avec une source de plasma induit par haute fréquence (SE/PIHF) indiquent que l'écorce externe et les brindilles représentent les tissus les plus révélateurs pour établir, à l'aide de la géochimie, le flux des éléments qui circulent dans la végétation à proximité du gisement. Les brindilles, l'écorce externe et les aiguilles d'épinette noire témoignent d'une zone de 400 m sur 300 m enrichie en plusieurs éléments sur la bordure ouest du gisement. Sur considération de la géochimie des brindilles, les éléments les plus utiles pour la définition des anomalies sont le zinc, le cuivre et le phosphore (éléments essentiels) ainsi que l'or, le brome, l'arsenic, l'étain, le plomb et le cadmium (éléments non essentiels).

¹ Manitoba Department of Energy and Mines, Geological Services Branch, 360-1395 Ellice Ave., Winnipeg, Manitoba R3G 3P2

² Geological Survey of Canada, 601 Booth St., Ottawa, Ontario K1A 0E8

Dans la zone à l'étude, la contamination par des particules aériennes est révélée par la chimie de la végétation sur une distance d'environ 50 m à partir de la route provinciale 395, principale route de transport du minerai de Chisel North. La normalisation de la cendre dans les données élimine certains effets dus aux particules. La migration des métaux du gisement vers les systèmes radicaux près de la surface est attribuée aux phases multiples de déformation des roches, à la perméabilité induite et à la migration synmétamorphique de fluides le long de failles cassantes et ductiles. L'interaction entre les secteurs à skarns du gisement de Chisel North et l'eau souterraine représente une source possible de réactifs gazeux s'échappant de façon continue vers la surface. Les mécanismes complémentaires de migration des éléments sont, entre autres, les effets électrogéochimiques spontanés, l'évapotranspiration de la végétation et le pompage hydraulique.

INTRODUCTION

The Chisel North base metal massive sulphide type deposit (Fig. 1) is located 5 km southeast of the town of Snow Lake in central Manitoba. The deposit contains in excess of 2.58 million tonnes of 8.9% Zn, 0.22% Cu, 0.4% Pb, 0.5 g/t Au, and 23.3 g/t Ag (Galley et al., 1993). It lies within a strongly deformed island arc volcanic assemblage of tholeiitic affinity 300 m down-plunge northeast of the Chisel Lake base metal massive sulphide deposit (5.06 million tonnes of 10.94% Zn and 0.60% Cu; Galley et al., 1993). Hudson Bay Mining and Smelting Co. Ltd. discovered the Chisel North deposit in 1987 using a combination of geological modelling, and data from geophysical and geochemical surveys.

Historically, mineral exploration in the Snow Lake mining camp has benefited from airborne and ground geophysical surveys followed by diamond drilling of conductors. Typical of this approach was the discovery of the Chisel Lake deposit, which was intersected by diamond drill testing of a weak airborne EM conductor. Until recently, geological mapping and geochemical surveys have played a relatively minor role in Snow Lake exploration. The discovery of the Lost Lake Cu-Zn deposit, however, is attributed to diamond drill testing of a structural geological interpretation of geological data collected from the Chisel Lake and Ghost Lake deposits.

Under the auspices of the Exploration Science and Technology Initiative (EXTECH), the Geological Survey of Canada and the Manitoba Geological Services Branch have assessed and developed new geophysical and geochemical techniques to evaluate new geological concepts for ore formation and discovery in the Snow Lake area. This integrated approach also includes spatial analysis of all data sets relevant to exploration for base and precious metals in the area.

As part of the EXTECH program a vegetation geochemical survey was undertaken to examine the chemistry of common species growing over the vertical projection of the blind and deeply buried Chisel North deposit. The development of geochemical techniques capable of detecting mineral deposits buried beneath overburden and/or bedrock will assist mineral exploration in the Snow Lake mining camp. The Chisel North deposit represents a formidable target for this survey since it occurs 600-625 m vertically below surface. A complicating factor is the potential masking of a mineralization-related vegetation geochemical signature by anthropogenic contamination. The sources of the contamination would be the Chisel Lake open pit/underground mining operations 1.3 km south-

east of the deposit and the haulage and access road between the mine and the concentrator (Provincial Road (PR) 395). Consequently, the potential for the addition of base and precious metal particulate to vegetation samples is considerable. Where particulate contamination was suspected in the samples, mostly by examination of vegetation ash contents, geochemical data were ash normalized using the method of Chukhrov et al. (1979) and interpreted in conjunction with nontransformed data.

PHYSIOGRAPHY AND VEGETATION

The survey area is characterized by outcrop ridges with intervening moderately to poorly drained, low-lying areas of overburden with variable thickness and composition. Outcrop is absent from the immediate area of the Chisel North deposit. Overburden, in general, consists of approximately 10-25 m of lacustrine clays topped by 1-3 m of till and peat. Hamilton et al. (1991, 1992) describe a typical profile of the sediments overlying the lacustrine clays, based on studies undertaken during a soil geochemical survey above the deposit. The profile is characterized by a 3 cm upper active layer of sphagnum and grass overlying 5-10 cm of humified sphagnum. This overlies up to 3 m of poorly to moderately decomposed sphagnum peat. The lower 20-25 cm of this interval is moderately to well decomposed and rests on lacustrine clay. Northwest of the deposit are ridges of basaltic rocks with intervening areas of poorly drained overburden.

Black spruce and jack pine are the predominant trees in the study area, with lesser coverage of tamarack. In the lower lying and more poorly drained areas, river alder and dwarf birch are present. Labrador tea is the dominant vascular plant. Drainage from Chisel Lake is southward from the study area (Fig. 2). Ghost Lake, 500 m east of the Chisel North deposit, is topographically confined and, accordingly, drainage from mining operations at the Lost Lake, Ghost Lake, and Chisel Lake Zn-Cu deposits does not affect the survey area. A drainage ditch has been dug from Chisel Lake eastward toward PR 395 and crosscuts the study area. Prevailing wind direction is to the southeast. Access to the study area, as well as to the Chisel Lake open pit and underground mining operations, is PR 395. This gravel road is used for ore haulage between the mine and the concentrator near the town of Snow Lake and is situated, in part, over the Chisel North deposit and adjacent to the study area.

GEOLOGY AND GEOCHEMISTRY OF THE CHISEL NORTH DEPOSIT

The Chisel North Zn-rich massive sulphide type deposit is situated within subaqueous Proterozoic volcanic, volcanoclastic, and chemical sedimentary rocks (Galley et al., 1993). These rocks form part of the highly metamorphosed and

strongly deformed tectonostratigraphic assemblage in the Snow Lake area (Fig. 1). Structure in the area of the Chisel Lake-Chisel North deposits is characterized by complex and intense deformation. Both deposits occur within the southern limb of the F₁ Chisel synform (Froese and Moore, 1980) and together comprise nine folded lenses of near solid to solid sulphide. The Chisel North deposit is an asymmetrically

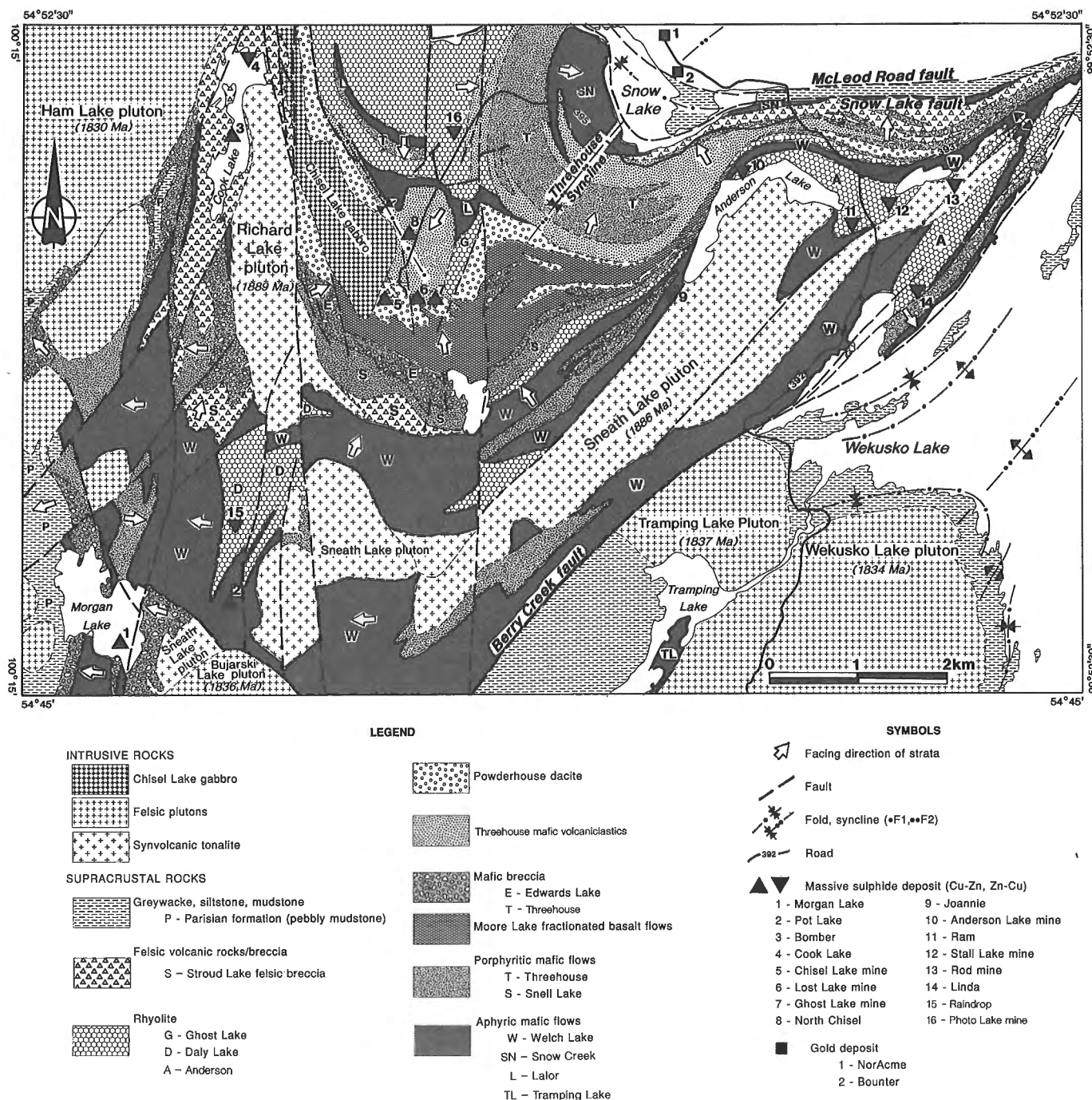


Figure 1. Geological setting of the Snow Lake mining camp with locations of massive sulphide type deposits and major gold deposits (modified from Bailes and Galley, 1991). Supracrustal rocks of the area are part of a distinctive tectonostratigraphic assemblage termed the Amisk Collage (Lucas et al., in press).

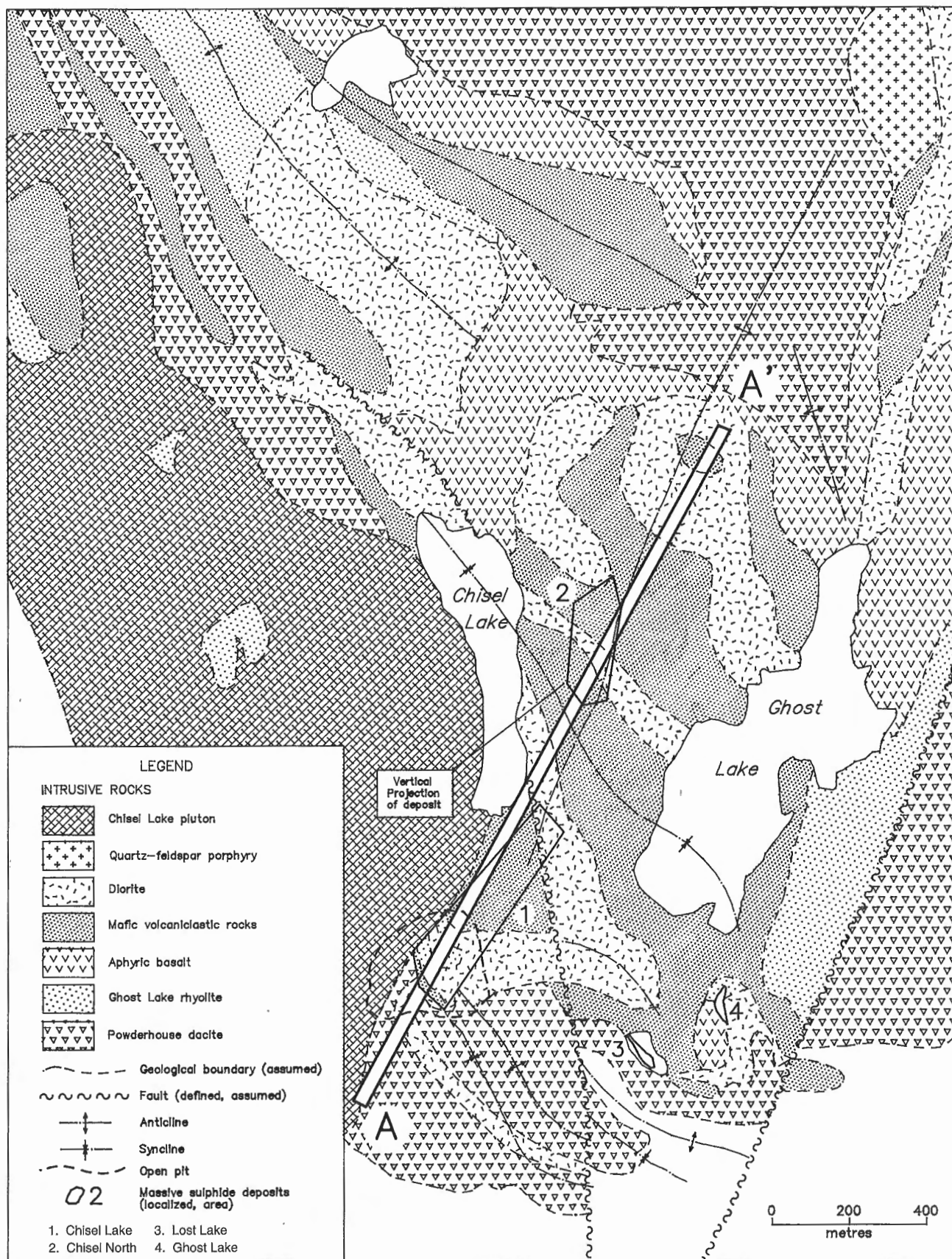


Figure 2. Geological setting and vertical surface projections of the Chisel North, Chisel Lake, Lost Lake, and Ghost Lake base metal massive sulphide type deposits (modified from Galley et al., 1993). A-A' represents the section line for the construction of Figure 3.

folded sulphide layer that plunges 10°-20° at 020°. Attenuation of this layer has produced two separate lenses of mineralization (Red zone and Green zone).

Multiple faults, fractures, and shears occur in immediate proximity to the Chisel North deposit. Early shallow-dipping faults, parallel to the D₁ axial planar foliation, border the deposit and offset an ore lens along an F₁ axial surface. Later, steeply dipping, north-striking brittle-ductile faults offset the footwall dacite contact and, at surface, crosscut late diorite dykes. Stratigraphically, the Red and Green zones occur at the contact between the 300 m thick feldspar-phyrlic Powderhouse dacite and hanging wall felsic volcanoclastic rocks, chert, heterolithological breccia, and mafic wacke. Hanging wall rocks are overlain by a 10-20 m thick unit of felsic breccia and well foliated chert with thin layers of biotite-pyrrhotite and chlorite-garnet-magnetite. These are overlain by mafic volcanoclastic rocks, sulphidic mudstones, felsic and mafic flows, and an upper mafic volcanoclastic unit. The succession has been intruded by aphyric to phyrlic (plagioclase±pyroxene) synvolcanic diorite. Outcrop in the area of the surface projection of the deposit consists of basaltic volcanoclastic rocks (Fig. 2). The Red zone lies 300 m down plunge from the Chisel Lake deposit and is, in part, overlain by the Green zone (Fig. 3). The Red zone occurs as an elongated polygon, 350 x 100 m; the Green zone is 150 m wide and has been traced down plunge for 500 m where it is open at depth. Both zones vary from 4-20 m thick and are characterized by solid to near solid pyrite sphalerite±chalcopyrite with thin layers of dolomite- or tremolite-rich material.

Footwall rocks are visibly altered for 250 m beneath the deposit in discordant zones of disseminated and stringer sulphide minerals and silicate mineral assemblages that typify lower amphibolite facies metamorphism. Sulphide veins occur to depths of 250 m below the deposit and contain chalcopyrite, sphalerite, galena, pyrite, arsenopyrite, and trace amounts of tetrahedrite, gold, electrum, and lead-silver tellurides. Quartz veins with sphalerite cores parallel to the F₂ axial planar schistosity are documented up to 50 m from the ore lenses. Precious metal-enriched (up to 1600 g/t Ag and 330 g/t Au) galena-chalcopyrite veins parallel to F₁ axial planar schistosity occur in hornblende-rich altered wall rocks adjacent to the deposit. Hanging wall alteration is characterized by patchy, areally restricted, pervasive or vein-controlled silicification and actinolite-biotite-garnet assemblages.

The geochemistry of representative samples of altered and mineralized host rock to the Chisel North deposit is summarized in Tables 1 and 2. Near solid sulphide sample 04918 contains high concentrations of numerous trace elements including Au, As, Cr, Hg, Sb, Se, Zn, Cd, Pb, Ag, and the highest Br (11 ppm) and Ge (4.3 ppm) levels observed in the samples. Sample 04919, characterized by near solid pyrite, pyrrhotite, and sphalerite, also contains high concentrations of As, Co, Hg, Se, Zn, and Cd. Samples 04916 and 04917 contain 5 and 15% iron sulphide minerals, respectively. Both samples are REE-enriched and generally contain lower concentrations of ore and ore-related elements but with high contents of Sc, U, Th, Sr, P, Ti, Y, and V relative to the sulphide-rich samples. Sample 04916 also contains higher Ba

than sulphide-rich samples 04918 and 04919. Further detailed information regarding the geological setting and geochemical alteration of the Chisel Lake and the Chisel North deposits is available in Galley and Kitzler (1990) and Galley et al. (1993) from which part of this background information has been derived.

SAMPLE COLLECTION, PREPARATION, AND ANALYSIS

Multi-species vegetation tissue samples were collected during a three day period in September, 1991, from an exploration grid that covers the vertical surface projection of the Chisel North deposit and the surrounding area (Fig. 4). Samples were collected on 25 m centres along one baseline (40 EBL) and three grid lines (L70N, L76N, and L84N). The area covered by 40 EBL, L70N, and L76N is predominantly sphagnum and black spruce bog virtually devoid of outcrop. Samples from L84N were collected, in part, from a basalt ridge and from intervening areas of poorly drained sphagnum bog. Twig, needle, and outer bark samples were collected from each of black spruce, jack pine, and tamarack. Black spruce twig samples comprised the most recent eight years of growth; tamarack and jack pine twigs were the most recent 40 cm of growth. Four branches were collected at chest height from around the periphery of an individual black spruce, jack pine, or tamarack tree at each sampling site. The four branches were combined to give a bulk sample thereby minimizing geochemical variability in the samples (Brooks, 1983; Fedikow, 1993). Twig samples from alder and dwarf birch comprised the most recent 40 cm of growth. Care was taken to collect twigs of similar diameter, age, and general appearance.

Samples of twigs, needles, and cones were collected from six black spruce crowns representing the top 35-40 cm of the trees. Four of these crown samples were collected over the deposit on 40 EBL and two samples away from the deposit on L76N. Geochemical partitioning was assessed using samples of trunk wood, inner bark, outer bark, twigs, and needles collected from single black spruce, jack pine, and tamarack trees at grid location L76N, 25W (Fig. 4). Additionally, cones from jack pine, and twigs, needles, and cones from the crown of the black spruce at this locality were collected to assess relative metal contents between "chest height" and crown tissues. The geochemical nature of particulates generated from traffic on PR 395 was examined in two dust samples collected from roadside vegetation. One sample of PR 395 road gravel was collected and the <2 µm size-fraction was analyzed.

Vegetation samples were air-dried and separated into tissue types. Dried samples were reduced to ash by controlled ignition at 470°C and encapsulated. Ashes were analyzed by instrumental neutron activation (INAA) at Activation Laboratories Ltd. (Ancaster, Ontario) and by inductively coupled plasma emission spectrometry (ICP-ES) by Barringer Laboratories Ltd. (Calgary, Alberta). This study is based on the interpretation of the concentrations of 38 elements determined by these two analytical methods. Ash yield was determined by gravimetric difference of the dry and ashed

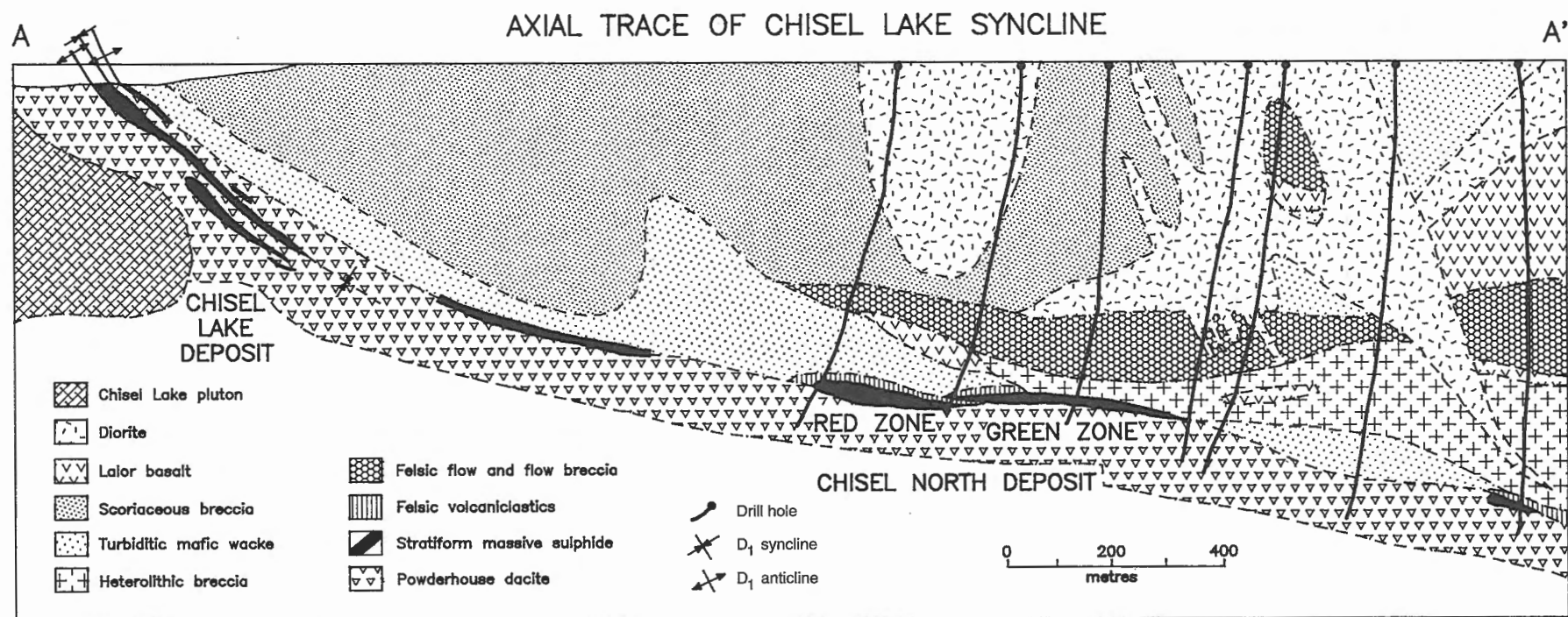


Figure 3. Geological cross-section through the Chisel North massive sulphide type deposit (modified from Galley et al., 1993). Location of cross-section plotted on Figure 2.

samples. Particulates from vegetation and the <2 µm fraction of the road gravel were analyzed by INAA. In this study the rare-earth elements (REE) La, Ce, Nd, Eu, Sm, Yb, and Lu were determined by INAA in ashed vegetation tissues. The sum of the concentrations of these 7 elements is referred to as ΣREE in the text and accompanying tables and should not be misinterpreted as the sum of all rare earth elements in the Periodic Table.

Table 1. The INAA data for representative altered and mineralized drill core samples from the Chisel North deposit. Mercury determined by hydride generation ICP-AA. Data in ppm unless otherwise indicated.

| Element | Sample | | | |
|----------|--------|----------|---------|---------|
| | 04916 | 04917 | 04918 | 04919 |
| Au (ppb) | 40 | 36 | 228 | <7 |
| As | 52 | 25 | 750 | 680 |
| Ba | 400 | <100 | <230 | <110 |
| Co | 24 | 51 | 25 | 53 |
| Cr | <10 | <10 | 55 | <10 |
| Fe(%) | 5.19 | 16.0 | 5.66 | 19.1 |
| Hf | 4.5 | 5.4 | <1 | <1 |
| Hg | 40 ppb | 2825 ppb | 140 ppm | 160 ppm |
| Sb | 9.6 | 1.0 | 1000 | 5.0 |
| Sc | 50 | 41 | 2.4 | 7.1 |
| Se | 12 | 57 | 52 | 175 |
| Th | 13 | 10 | 4.6 | 2.3 |
| U | 3.6 | 4.4 | <2.9 | <1.3 |
| W | 280 | 59 | 220 | 190 |
| Zn | 1720 | 18 700 | 446 000 | 215 000 |
| La | 120 | 64 | <1 | 19 |
| Ce | 240 | 130 | <6 | 33 |
| Nd | 93 | 49 | <11 | <5 |
| Sm | 17 | 8.6 | <0.1 | 2.0 |
| Eu | 4.8 | 1.8 | <1.3 | 1.6 |
| Tb | 1.3 | <0.5 | <0.7 | <0.5 |
| Yb | 3.67 | 4.3 | <0.58 | 1.44 |
| Lu | 0.71 | 0.81 | <0.11 | 0.25 |
| Cl | <0.01 | 0.10 | <0.01 | <0.01 |
| I | <0.05 | 0.9 | <0.05 | 1.6 |
| Br | <0.05 | <0.5 | 11.0 | <0.5 |

Sample 04916: DDH CH88-8 at 644.3 m (2114 ft.); sericite schist with 40-50% quartz, trace-2% fine grained (1 mm) biotite, trace -1% apatite as 1-2 mm crystals, 3-4% pyrite, and trace pyrrhotite.

Sample 04917: DDH CH88-6 at 619 m (2031 ft.); chlorite schist with 5% amphibole as fine elongate crystals up to 7 mm in length; trace to 2% kyanite, 8-10% pyrite, 2-3% pyrrhotite, and trace chalcopyrite.

Sample 04918: DDH CH88-8W2 at 627.9 m (2060 ft.); near solid sulphide consisting of 90%, granular, 2-3 mm sphalerite and trace galena; remainder is quartz with minor staurolite.

Sample 04919: DDH CH88-10 at 613 m (2011 ft.); disseminated pyrite (25-30%) and sphalerite (20-25%) in a sericite schist.

RESULTS

Vegetation geochemistry

Partitioning studies were undertaken to determine the relative abundances of metals in the various tissues of species available for sampling in the survey area. Table 3 provides comparative data for several trace elements in twigs and outer bark of the three conifers. A geochemical comparison of black spruce twigs from crown and from chest height is given in Table 4, and summary geochemical data for the partitioning studies are presented in Table 5. Analytical data of tissues from six black spruce crown samples are reproduced in Table 6.

Black spruce (*Picea mariana*)

Each of the black spruce tissue types sampled at chest height concentrate a specific group of elements (Tables 3 and 5); however, twigs and outer bark are the most effective for acquisition and storage of ore-related elements. Twigs contain higher concentrations than outer bark of Au, Sb, Cu, Pb, Zn, Cd, Ni, Cr, and Hf, although the differences in concentrations are small except for Zn (Table 3). Needles and trunk wood contain relatively high levels of Br; trunk wood concentrates Ag, Ba, and Rb (Table 5).

Table 2. Additional analytical data for samples described in Table 1. The Bi, and Te analyzed by hydride generation ICP-ES, F by specific ion electrode. All others by ICP-ES subsequent to 'total' acid digestion. Data in ppm unless otherwise indicated.

| Element | Sample | | | |
|---------|--------|-------|-------|-------|
| | 04916 | 04917 | 04918 | 04919 |
| Cu | 24 | 1394 | 251 | 358 |
| Pb | 1723 | 35 | 13840 | 62 |
| Ag | 10 | 6 | 76.9 | <0.4 |
| Ni | 3 | 4 | 5 | 3 |
| Mn | 143 | 3855 | 3309 | 981 |
| Sr | 46 | 30 | 5 | 19 |
| Cd | 2.6 | 46.1 | 951.2 | 368.2 |
| V | 105 | 69 | 6 | 21 |
| Ca(%) | 0.28 | 2.59 | 0.18 | 0.02 |
| P(%) | 0.101 | 0.058 | 0.002 | 0.005 |
| Mg(%) | 0.68 | 8.92 | 0.06 | 0.10 |
| Ti(%) | 0.17 | 0.32 | 0.01 | 0.03 |
| Al(%) | 10.24 | 8.13 | 0.31 | 2.27 |
| K(%) | 4.80 | 0.02 | 0.01 | 1.10 |
| Y | 16 | 22 | 2 | 2 |
| Bi | 0.4 | 0.3 | <1.0 | 0.2 |
| Te | 2.4 | 3.1 | 2.7 | <0.1 |
| F | 2100 | 1600 | 140 | 1000 |

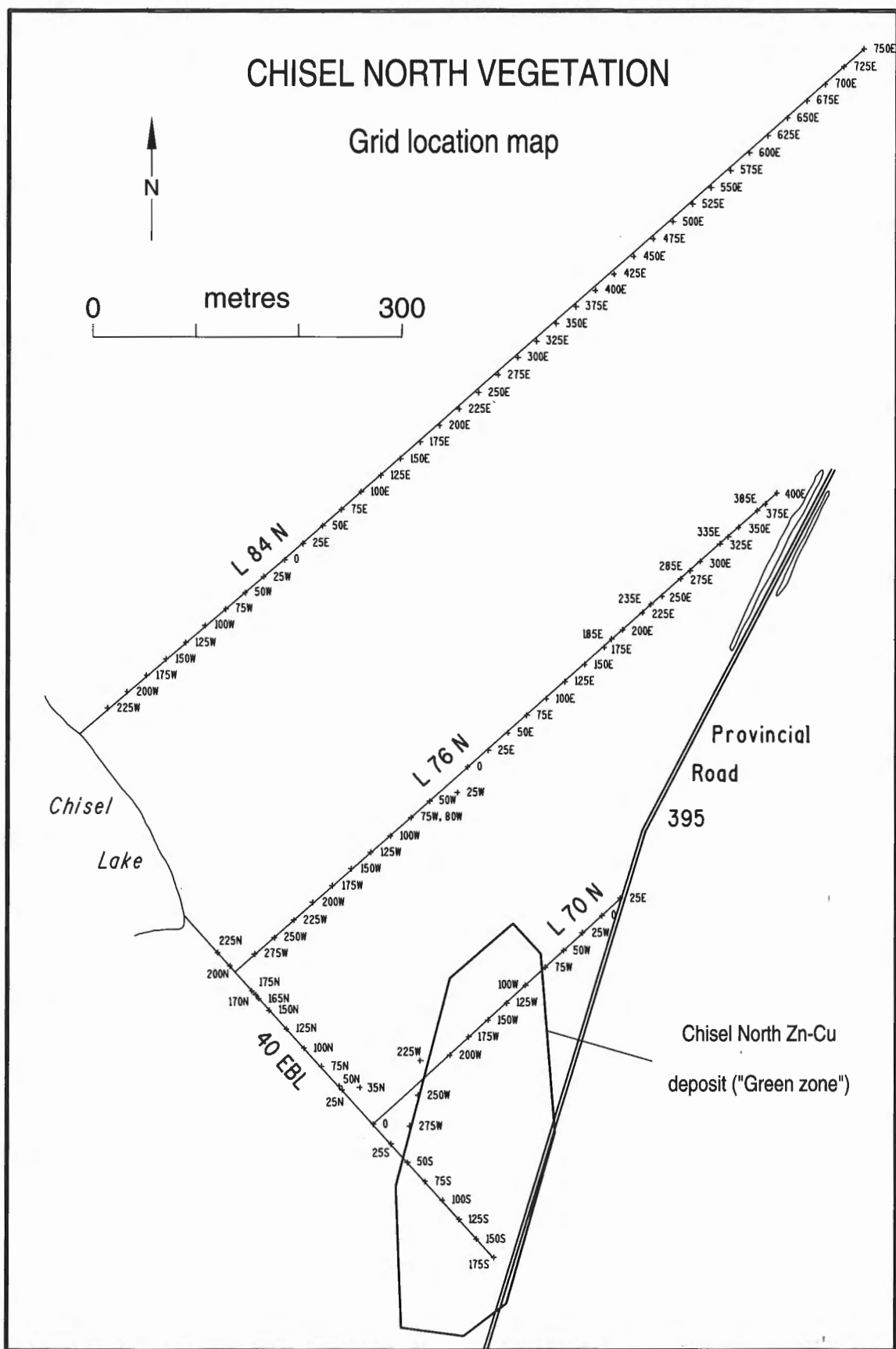


Figure 4. Vegetation geochemical sample locations in relation to the vertical surface projection of the Chisel North deposit.

Table 3. Comparison of ore-related element concentrations in ash of twigs and outer bark of black spruce (*Picea mariana*), jack pine (*Pinus banksiana*) and tamarack (*Larix laricina*). Σ REE represents the sum of the concentrations of seven rare-earth elements determined in this study. Samples collected at grid reference L76N, 25W. Blanks indicate insufficient sample for analysis.

| ELEMENTS | BLACK SPRUCE | | JACK PINE | | TAMARACK | |
|--------------------|--------------|------------|-----------|------------|----------|------------|
| | Twigs | Outer Bark | Twigs | Outer Bark | Twigs | Outer Bark |
| Au (ppb) | 91 | 60 | 128 | 75 | 55 | 86 |
| As (ppm) | 30 | 29 | 20 | 33 | 16 | 33 |
| Cr (ppm) | 24 | 19 | 20 | 24 | 14 | 21 |
| Hf (ppm) | 1.6 | 1.2 | 1.1 | 1.7 | <0.5 | 1.1 |
| Sb (ppm) | 4.4 | 3.9 | 4.0 | 5.7 | 2.7 | 4.4 |
| Sc (ppm) | 4.4 | 4.2 | 3.2 | 6.2 | 2.6 | 4.6 |
| Σ REE (ppm) | 36.84 | 43.93 | 45.05 | 69.51 | 31.99 | 53.52 |
| Zn (ppm) | 5800 | 3300 | 5500 | 5600 | 4000 | 4900 |
| Sc (ppm) | 17 | 10 | 21 | 20 | 11 | |
| Cu (ppm) | 346 | 296 | 359 | 409 | 219 | |
| Pb (ppm) | 568 | 344 | 643 | 550 | 315 | |
| Ni (ppm) | 34 | 24 | 37 | 22 | 16 | |
| Rb (ppm) | 49 | 26 | 120 | 57 | 100 | 54 |
| Cd (ppm) | 14 | 10 | 21 | 19 | 10 | 12 |
| Ash (%) | 3.6 | 5.3 | 1.9 | 3.8 | 2.4 | 4.6 |

Table 4. Comparison of trace element contents between crown tissues and tissues sampled at chest height in black spruce (*Picea mariana*) Σ REE represents the sum of the concentrations of seven rare-earth elements determined in this study. Sample collected at grid location L76N, 25W.

| ELEMENTS | CROWN | | | CHEST HEIGHT | |
|--------------------|-------|---------|-------|--------------|---------|
| | Twigs | Needles | Cones | Twigs | Needles |
| Au (ppb) | 168 | 47 | 135 | 91 | 16 |
| Ag (ppm) | 9 | <2 | 3 | <2 | 3 |
| As (ppm) | 44 | 7.6 | 45 | 30 | 3.8 |
| Cs (ppm) | 1.9 | 2.5 | 2.5 | <0.5 | 0.7 |
| Hf (ppm) | 2.1 | <0.5 | 1.7 | 1.6 | <0.5 |
| Rb (ppm) | 120 | 110 | 91 | 49 | 55 |
| Sb (ppm) | 7.7 | 1.4 | 8.0 | 4.4 | 0.8 |
| Zn (ppm) | 8150 | 2200 | 6500 | 5800 | 3550 |
| Σ REE (ppm) | 90.04 | 6.58 | 69.36 | 36.84 | 6.29 |
| Ash (%) | 3.4 | 2.6 | 1.1 | 3.6 | 3.5 |

A comparison of the trace element contents of chest height and crown tissues reveals significant chemical differences at this sampling site (Table 4). Crown twigs contain higher levels of Au, Ag, As, Cs, Hf, Rb, Sb, Zn, and Σ REE, and crown needles contain higher Au, As, Cs, and Rb, than their chest-height counterparts. Crown cones also contain more Au, As, Cs, Rb, Sb, Zn, and Σ REE than either chest-height twigs or needles.

Within crown tissues, twigs concentrate Au, As, Ba, Ca, Fe, Na, Sb, Sc, Th, Zn, and Σ REE. Higher contents of Ag and Hf are also present in the twigs but at concentrations close to the lower limit of determination (Table 5). Elements at or below the lower limit of determination by INAA in all crown tissues include Hg, Ir, Ni, Sn, Sr, Ta, U, W, and Mo. Crown

tissue data derived from six samples on 40 EBL and L76N generally conform to the partitioning characteristics exhibited by crown tissues from L76N, 25W. Crown twigs from these six localities concentrate Au, As, Ba, Cr, Fe, Na, Sb, Sc, Th, Zn, and most of the REEs. Crown cones concentrate Cs and Rb. These patterns of enrichment within the crown tissues are consistent, regardless of whether the sample was collected over the deposit or at a location presumed to represent background.

The four crown samples collected from 40 EBL at progressively increasing distances from PR 395 show no systematic change in ash percentages or trace element variation that would suggest particulate contamination. Ash content of the crown twigs is in general agreement with the observed median of 3.01% for black spruce twigs (Table 7). It should be noted, however, that this median level is higher than that commonly recorded for similar black spruce twig growth from elsewhere in Canada (Dunn, 1981: 1.9%, North Saskatchewan). Trace element analyses of the crown twigs indicate higher Ag, As, Cr, Fe, Sb, Sc, Th, Zn, La, and Ce and lower Cs and Rb in background samples compared to twigs from trees above the orebody.

Jack Pine (*Pinus banksiana*)

Jack pine twigs and outer bark concentrate a significantly greater number of elements of exploration interest than do the other tissue types. Table 3 presents comparative data based on 13 elements (plus Σ REE) for twigs and outer bark. These data indicate that twigs are relatively enriched in Au, Pb, Ni, and Rb whereas As, Cr, Hf, Sb, Sc, Zn, Cu, and Σ REE levels are higher in outer bark. Silver is more concentrated in trunk wood (Table 5).

Two types of cones were collected from jack pine for partitioning studies (Table 5). Green, closed cones collected from near the top of the tree ("apex cones") and open, brown cones found below the apex cones on the tree. Open, brown cones contain higher concentrations of the elements of interest to exploration: notably Au, As, Sb, and Zn. Apex cones contain the highest Cs (18 ppm) of all jack pine tissues.

Tamarack (*Larix laricina*)

Results for tamarack geochemical partitioning essentially mimic those for black spruce and jack pine. Tamarack outer bark and twigs represent the most effective concentrators of elements potentially useful for vegetation geochemical anomaly definition. The Au, As, Cr, Hf, Sb, Sc, Zn, and Σ REE are all higher in outer bark; Rb is significantly higher in twigs.

Table 5. Summary of analytical data for geochemical partitioning studies of element concentrations in ash of black spruce, jack pine, and tamarack. Samples collected from grid coordinate L76N, 25W. All data quoted in ppm unless otherwise designated. Blanks indicate insufficient sample for analysis by ICP-ES.

| SPECIES/TISSUE | INAA | | | | | | | | | | | | | | | | | |
|--|----------|----|------|------|-----|--------|----|----|------|------|------|-------|------|-----|------|-----|------|------|
| | Au (ppb) | Ag | As | Ba | Br | Ca (%) | Co | Cr | Cs | Fe | Hf | K (%) | Na | Rb | Sb | Sc | Sr | Th |
| Black spruce (<i>Picea mariana</i>) | | | | | | | | | | | | | | | | | | |
| Trunk wood | 10 | 30 | 1.8 | 1600 | 40 | 27.4 | 4 | 6 | 0.9 | 0.09 | <0.5 | 13.0 | 392 | 110 | <0.1 | 0.2 | <300 | <0.1 |
| Inner bark | 7 | <2 | 4 | 1200 | 12 | 27.6 | 2 | 5 | 0.5 | 0.17 | <0.5 | 6.5 | 561 | 65 | 0.5 | 0.5 | 430 | <0.1 |
| Outer bark | 60 | <2 | 29 | 760 | 13 | 21.2 | 6 | 19 | 1.2 | 1.34 | 1.2 | 1.5 | 3760 | 26 | 3.9 | 4.2 | <300 | 1.9 |
| Twigs | 91 | <2 | 30 | 810 | 17 | 19.3 | 8 | 24 | <0.5 | 1.55 | 1.6 | 5.3 | 4360 | 49 | 4.4 | 4.4 | <300 | 2.7 |
| Needles | 16 | 3 | 3.8 | 415 | 47 | 21.8 | 3 | 6 | 0.7 | 0.28 | <0.5 | 10.8 | 542 | 55 | 0.8 | 0.7 | <300 | 0.2 |
| Crown - cones | 135 | 3 | 45 | 330 | 44 | 16.1 | 11 | 34 | 2.5 | 1.88 | 1.7 | 5.57 | 4850 | 91 | 8 | 5.2 | <300 | 2.7 |
| - needles | 47 | <2 | 7.6 | 430 | 45 | 19.0 | 2 | 4 | 2.5 | 0.36 | <0.5 | 16.40 | 660 | 110 | 1.4 | 0.8 | <300 | 0.3 |
| - twigs | 168 | 9 | 44 | 1000 | 23 | 21.0 | 10 | 34 | 1.9 | 2.07 | 2.1 | 8.52 | 5450 | 120 | 7.7 | 5.7 | <300 | 3.3 |
| Jack pine (<i>Pinus banksiana</i>) | | | | | | | | | | | | | | | | | | |
| Trunk wood | 6 | 5 | 1.1 | 630 | 22 | 19.6 | 9 | 3 | 2.3 | 0.07 | <0.5 | 15.4 | 534 | 200 | 0.3 | 0.1 | 960 | <0.1 |
| Inner bark | 20 | <2 | 7.2 | 750 | 20 | 19.4 | 6 | 8 | 6.5 | 0.39 | <0.5 | 8.8 | 1120 | 160 | 1.1 | 1.0 | 910 | 0.4 |
| Outer bark | 75 | <2 | 33 | 520 | 20 | 18.5 | 10 | 24 | 1.7 | 1.89 | 1.7 | 1.9 | 5320 | 57 | 5.7 | 6.2 | <300 | 2.7 |
| Twigs | 128 | 3 | 20 | 390 | 35 | 15.6 | 10 | 20 | 1.8 | 1.19 | 1.1 | 11.1 | 3130 | 120 | 4.0 | 3.2 | <300 | 2.3 |
| Needles | 36 | <2 | 7.3 | 160 | 300 | 12.2 | 18 | 14 | 1.6 | 0.46 | <0.5 | 17.3 | 1040 | 160 | 1.5 | 1.2 | <300 | 0.7 |
| Cones ("apex") | | | | | | | | | | | | | | | | | | |
| - closed | 29 | <2 | 7.8 | <100 | 23 | 3.4 | 3 | 6 | 18 | 0.47 | <0.5 | 14.7 | 779 | 580 | 1.1 | 0.7 | <300 | 0.4 |
| - open | 80 | <2 | 25.0 | 130 | 20 | 9.1 | 7 | 14 | 10 | 1.18 | 0.8 | 9.4 | 3330 | 300 | 4.3 | 2.9 | <300 | 1.7 |
| Tamarack (<i>Larix laricina</i>) | | | | | | | | | | | | | | | | | | |
| Trunk wood | 11 | <2 | 3.0 | 4400 | 60 | 18.2 | 5 | 6 | 1.2 | 0.19 | <0.5 | 21.6 | 855 | 210 | 0.3 | 0.3 | 2900 | 0.2 |
| Inner bark | 8 | <2 | 4.5 | 3100 | 42 | 19.3 | 3 | 4 | 1.6 | 0.23 | <0.5 | 17.7 | 771 | 120 | 0.5 | 0.5 | 2100 | 0.2 |
| Outer bark | 86 | <2 | 33 | 630 | 15 | 19.2 | 7 | 21 | 1.7 | 1.55 | 1.1 | 3.9 | 3870 | 54 | 4.4 | 4.6 | <300 | 2.0 |
| Twigs | 55 | 4 | 16.0 | 1900 | 35 | 21.0 | 6 | 14 | <0.5 | 0.92 | <0.5 | 15.6 | 2590 | 100 | 2.7 | 2.6 | 2000 | 1.4 |
| Needles | 43 | <2 | 5.7 | 950 | 97 | 10.8 | 4 | 4 | 0.6 | 0.28 | <0.5 | 13.4 | 478 | 63 | 0.8 | 0.6 | 480 | 0.2 |

| | INAA | | | | | | | | | | | ICP-ES | | | | | | |
|---------------------------------------|------|------|------|----|----|------|-------|------|-------|-------|---------|--------|-----|--------|--------|----|-------|----|
| SPECIES/TISSUE | U | Zn | La | Ce | Nd | Sm | Eu | Tb | Yb | Lu | Ash (%) | Cu | Pb | Mg (%) | Mn | Ni | P (%) | Cd |
| Black spruce (<i>Picea mariana</i>) | | | | | | | | | | | | | | | | | | |
| Trunk wood | <0.1 | 4100 | 0.2 | <3 | <5 | <0.1 | <0.02 | <0.5 | <0.05 | <0.05 | 0.3 | 215 | 67 | 3.35 | 9217 | 7 | 0.68 | 5 |
| Inner bark | <0.1 | 3100 | 1.0 | <3 | <5 | 0.2 | <0.01 | <0.5 | 0.10 | <0.05 | 3.0 | 80 | 27 | 1.79 | 4819 | 5 | 0.92 | 1 |
| Outer bark | 0.7 | 3300 | 11.0 | 20 | 10 | 1.7 | 0.36 | <0.5 | 0.74 | 0.13 | 5.3 | 296 | 344 | 3.20 | 2166 | 24 | 0.40 | 10 |
| Twigs | 0.8 | 5800 | 16.0 | 17 | <5 | 2.3 | 0.51 | <0.5 | 0.86 | 0.17 | 3.6 | 346 | 568 | 3.04 | 3747 | 34 | 0.98 | 17 |
| Needles | <0.1 | 3550 | 1.8 | 4 | <5 | 0.3 | 0.10 | <0.5 | 0.09 | <0.05 | 3.5 | 70 | 85 | 2.87 | 9985 | 14 | 2.07 | 4 |
| Crown - cones | 1.1 | 6500 | 16 | 32 | 17 | 2.5 | 0.59 | <0.5 | 1.07 | 0.2 | 1.1 | | | | | | | |
| - needles | <0.1 | 2200 | 2.1 | 4 | <5 | 0.3 | <0.02 | <0.5 | 0.18 | <0.05 | | | | | | | | |
| - twigs | <0.1 | 8100 | 20 | 40 | 25 | 3 | 0.63 | <0.5 | 1.21 | 0.2 | | | | | | | | |
| Jack pine (<i>Pinus banksiana</i>) | | | | | | | | | | | | | | | | | | |
| Trunk wood | <0.1 | 3000 | 5.3 | 5 | <5 | 0.1 | <0.02 | <0.5 | <0.05 | <0.05 | 0.3 | | | | | | | |
| Inner bark | 0.5 | 3200 | 3.1 | 5 | <5 | 0.4 | <0.02 | <0.5 | <0.05 | <0.05 | 1.6 | 170 | 117 | 5.51 | 3203 | 8 | 2.34 | 16 |
| Outer bark | 1.0 | 5600 | 17.0 | 33 | 15 | 2.8 | 0.60 | <0.5 | 0.94 | 0.17 | 3.8 | 409 | 550 | 4.20 | 1166 | 22 | 0.41 | 20 |
| Twigs | 0.6 | 5500 | 12.0 | 21 | 9 | 1.9 | 0.38 | <0.5 | 0.65 | 0.12 | 1.9 | 359 | 643 | 4.88 | 2740 | 37 | 2.59 | 21 |
| Needles | <0.1 | 2600 | 3.7 | 6 | <5 | 0.6 | <0.03 | <0.5 | 0.30 | 0.08 | 2.2 | 160 | 279 | 5.55 | 8742 | 34 | 6.20 | 11 |
| Cones ("apex") | | | | | | | | | | | | | | | | | | |
| - closed | <0.1 | 3900 | 1.8 | 4 | <5 | 0.3 | <0.03 | <0.5 | <0.05 | <0.05 | 0.3 | | | | | | | |
| - open | 1.0 | 5000 | 11.0 | 20 | <5 | 1.7 | 0.32 | <0.5 | 0.52 | 0.11 | 0.5 | | | | | | | |
| Tamarack (<i>Larix laricina</i>) | | | | | | | | | | | | | | | | | | |
| Trunk wood | <0.1 | 2500 | 0.6 | <3 | <5 | <0.1 | <0.03 | <0.5 | <0.05 | <0.05 | 0.4 | 282 | 172 | 7.02 | 10 132 | 13 | 3.21 | 18 |
| Inner bark | <0.1 | 3200 | 1.3 | <3 | <5 | 0.2 | <0.02 | <0.5 | <0.05 | <0.05 | 2.2 | 157 | 82 | 4.29 | 8878 | 8 | 2.87 | 6 |
| Outer bark | 0.9 | 4900 | 1.3 | 25 | 12 | 2.1 | 0.51 | <0.5 | 0.77 | 0.14 | 4.6 | | | | | | | |
| Twigs | <0.1 | 4000 | 8.6 | 16 | 5 | 1.4 | 0.38 | <0.5 | 0.49 | 0.12 | 2.4 | 219 | 315 | 3.14 | 4622 | 16 | 2.60 | 11 |
| Needles | <0.1 | 990 | 1.6 | <3 | <5 | 0.3 | <0.02 | <0.5 | 0.18 | <0.05 | 4.3 | 91 | 109 | 4.84 | 1446 | 3 | 2.44 | 5 |

Table 6. Summary of analytical determinations by INAA for black spruce (*Picea mariana*) crown tissues, Chisel North survey area. All analyses in ppm unless otherwise indicated.

| ELEMENT | 40EBL, 50S | | | 40EBL, 125S | | | 40EBL, 150S | | | 40EBL, 175S | | | L176N, 25E | | | L176N, 25W | | |
|----------|------------|--------|---------|-------------|--------|---------|-------------|--------|---------|-------------|--------|---------|------------|--------|---------|------------|--------|---------|
| | Cones | Twigs | Needles | Cones | Twigs | Needles | Cones | Twigs | Needles | Cones | Twigs | Needles | Cones | Twigs | Needles | Cones | Twigs | Needles |
| Au (ppb) | 30 | 192 | 23 | 45 | 138 | 11 | 65 | 111 | 30 | 23 | 63 | 22 | 58 | 197 | 42 | 135 | 168 | 38 |
| Ag | <2 | <2 | <2 | <2 | <2 | 2 | 3 | 5 | <2 | 2 | 3 | <2 | <2 | 6 | <2 | 3 | 9 | <2 |
| As | 14 | 22 | 7 | 14 | 15 | 3.9 | 20 | 29 | 7.2 | 13 | 21 | 7.5 | 16 | 30 | 9.1 | 45 | 44 | 7.5 |
| Ba | 210 | 2100 | 1200 | 120 | 930 | 600 | 190 | 640 | 340 | 120 | 610 | 300 | 240 | 950 | 480 | 330 | 1000 | 430 |
| Br | 39 | 17 | 44 | 49 | 16 | 26 | 45 | 18 | 19 | 28 | 20 | 40 | 25 | 18 | 54 | 44 | 23 | 45 |
| Ca (%) | 3.8 | 18.3 | 19.7 | 5.7 | 20.6 | 18.2 | 8.6 | 22.1 | 22 | 4.7 | 21.1 | 17.2 | 5.8 | 20.4 | 16.1 | 16.1 | 21 | 19 |
| Co | 12 | 7 | 3 | 13 | 7 | 2 | 5 | 5 | 1 | 8 | 5 | 1 | 14 | 10 | 4 | 11 | 10 | 2 |
| Cr | <1 | 10 | 5 | <1 | 10 | <1 | 10 | 14 | 4 | 6 | 11 | 3 | 8 | 20 | 5 | 34 | 34 | 4 |
| Cs | 11 | 6.1 | 5.4 | 15 | 7.6 | 5.6 | 14 | 4.1 | 3.5 | 7.2 | 3.4 | 4.6 | 2.5 | 1.7 | 1.9 | 2.5 | 1.9 | 2.5 |
| Fe (%) | 0.4 | 0.98 | 0.31 | 0.46 | 0.65 | 0.18 | 0.69 | 1.3 | 0.31 | 0.41 | 0.89 | 0.38 | 0.6 | 1.47 | 0.4 | 1.88 | 2.07 | 0.37 |
| Hf | <0.5 | 1.6 | <0.5 | <0.5 | <0.5 | <0.5 | 1.3 | 1.4 | <0.5 | <0.5 | 0.6 | 0.8 | <0.5 | <0.5 | <0.5 | 1.7 | 2.1 | <0.5 |
| Hg (ppb) | <1 | <1 | <1 | <1 | <1 | <1 | <1 | <1 | <1 | <1 | <1 | <1 | <1 | <1 | <1 | <1 | <1 | <1 |
| Ir (ppb) | <3 | <2 | <2 | <4 | <2 | <2 | <3 | <2 | <2 | <2 | <2 | <2 | <2 | <2 | <2 | <2 | <2 | <2 |
| K (%) | 32.3 | 19.3 | 25.9 | 33.5 | 14.8 | 19.8 | 19.6 | 9.06 | 13.8 | 2.8 | 13.8 | 24 | 30.4 | 11.7 | 28.4 | 5.57 | 8.52 | 16.9 |
| Mo | 10 | <2 | <2 | <2 | <2 | <2 | <2 | <2 | <2 | 5 | 4 | <2 | <2 | <2 | <2 | 5 | 5 | 2 |
| Na | 690 | 2360 | 554 | 1050 | 1570 | 312 | 1460 | 3040 | 514 | 809 | 2310 | 749 | 1460 | 3530 | 805 | 4850 | 5450 | 732 |
| Ni | <50 | <50 | <50 | <50 | <50 | <50 | <50 | <50 | <50 | <50 | <50 | <50 | 71 | <50 | <50 | <50 | <50 | <50 |
| Rb | 660 | 390 | 320 | 680 | 330 | 270 | 310 | 110 | 120 | 460 | 230 | 320 | 450 | 190 | 240 | 91 | 120 | 110 |
| Sb | 0.8 | 3.7 | 0.9 | 1 | 2.4 | 0.7 | 2.7 | 4.7 | 1.3 | 0.8 | 3 | 1.3 | 2.8 | 5.8 | 1.8 | 8 | 7.7 | 1.4 |
| Sc | 0.6 | 2.3 | 0.6 | 0.9 | 1.7 | 0.4 | 1.5 | 3.2 | 0.8 | 0.7 | 2.4 | 0.9 | 1.3 | 3.7 | 0.9 | 5.2 | 5.7 | 0.8 |
| Se | <2 | <2 | <2 | <3 | <2 | <2 | <2 | <2 | <2 | <2 | <2 | <2 | 5 | 6 | <2 | 7 | <2 | 3 |
| Sn (%) | <0.011 | <0.009 | <0.007 | <0.018 | <0.009 | <0.007 | <0.014 | <0.008 | <0.007 | <0.01 | <0.008 | <0.007 | <0.009 | <0.009 | <0.008 | <0.009 | <0.009 | <0.007 |
| Sr | <300 | 920 | 700 | <300 | <300 | <300 | <300 | <300 | <300 | <300 | <300 | <300 | <300 | <300 | <300 | <300 | <300 | <300 |
| Ta | <0.5 | <0.5 | <0.5 | <0.5 | <0.5 | <0.5 | <0.5 | <0.5 | <0.5 | <0.5 | <0.5 | 0.5 | 0.8 | <0.5 | <0.5 | <0.5 | <0.5 | <0.5 |
| Th | <0.1 | 1.2 | <0.1 | <0.1 | 1 | 0.3 | 0.8 | 1.4 | 0.2 | 0.2 | 1.3 | 0.5 | 0.6 | 1.8 | 0.7 | 2.7 | 3.3 | 0.3 |
| U | <0.2 | <0.1 | <0.1 | <0.3 | <0.1 | <0.1 | <0.2 | 0.8 | <0.1 | 0.7 | <0.1 | <0.1 | <0.1 | 0.6 | <0.1 | 1.1 | <0.1 | <0.1 |
| W | <1 | <1 | <1 | <1 | <1 | <1 | <1 | <1 | <1 | <1 | <1 | 2 | <1 | <1 | <1 | <1 | <1 | <1 |
| Zn | 4300 | 5500 | 1400 | 3100 | 4100 | 1600 | 4300 | 5900 | 3100 | 3700 | 4500 | 1900 | 3700 | 6600 | 2200 | 6500 | 8100 | 2200 |
| La | 1.3 | 7.5 | 1.9 | 1.8 | 5.1 | 1 | 4.7 | 10 | 2 | 1.9 | 7.2 | 2.5 | 3.8 | 11 | 2.4 | 16 | 20 | 2.1 |
| Ce | 7 | 12 | 6 | 6 | 10 | <3 | 7 | 20 | <3 | <3 | 14 | 5 | 8 | 20 | 6 | 32 | 40 | 4 |
| Nd | <5 | 11 | <5 | <5 | <5 | <5 | <5 | 15 | <5 | <5 | <5 | <5 | 14 | <5 | <5 | 17 | 25 | <5 |
| Sm | 0.2 | 1.2 | 0.3 | 0.2 | 0.9 | <0.1 | 0.6 | 1.7 | 0.3 | 0.3 | 1.2 | 0.4 | 0.6 | 1.7 | 0.3 | 2.5 | 3 | 0.3 |
| Eu | <0.04 | 0.31 | <0.03 | <0.06 | 0.26 | <0.03 | <0.05 | 0.44 | <0.02 | <0.03 | 0.23 | 0.15 | <0.03 | 0.45 | <0.02 | 0.59 | 0.63 | <0.02 |
| Tb | <0.5 | <0.5 | <0.5 | <0.5 | <0.5 | <0.5 | <0.5 | <0.5 | <0.5 | <0.5 | <0.5 | <0.5 | <0.5 | <0.5 | <0.5 | <0.5 | <0.5 | <0.5 |
| Yb | <0.05 | 0.49 | <0.05 | <0.07 | 0.28 | <0.05 | <0.05 | 0.67 | <0.05 | 0.3 | 0.49 | 0.16 | 0.23 | 0.52 | 0.26 | 1.07 | 1.21 | 0.18 |
| Lu | <0.05 | 0.07 | <0.05 | <0.05 | <0.05 | <0.05 | <0.05 | 0.12 | <0.05 | <0.05 | 0.06 | <0.05 | 0.05 | 0.12 | <0.05 | 0.2 | 0.2 | <0.05 |
| Ash (%) | 1.09 | 3.39 | 2.86 | 0.74 | 2.45 | 2.56 | 0.76 | 1.97 | 2.56 | 0.83 | 2.22 | 2.68 | 0.68 | 2.91 | 2.92 | 0.61 | 2.54 | 2.47 |

Table 7. Summary and comparison of descriptive statistical parameters for selected analytical data from the twigs of species sampled for this study. 'A.Mean' is arithmetic mean. All data are ppm in ash unless otherwise indicated.

| SPECIES | | Au (ppb) | As | Br | Sb | Zn | Ni | Cu | Pb | Cd | P (%) | Ash (%) |
|--------------|--------|----------|---------|-------|---------|------------|-------|---------|----------|-------|-----------|-----------|
| Black spruce | | | | | | | | | | | | |
| (n=39) | Range | 36-325 | 12-49 | 11-32 | 2.4-8.0 | 3500-9300 | 13-49 | 285-565 | 315-1118 | 9-26 | 0.95-2.99 | 1.90-5.60 |
| | A.Mean | 105 | 29 | 21 | 4.5 | 6141 | 34 | 407 | 657 | 18 | 1.71 | 3.10 |
| | S.D. | 50 | 9 | 5 | 1.4 | 1394 | 8 | 85 | 225 | 4 | 0.58 | 0.76 |
| | Median | 91 | 28 | 20 | 4.2 | 6200 | 34 | 382 | 589 | 17 | 1.64 | 3.01 |
| Jack pine | | | | | | | | | | | | |
| (n=50) | Range | 52-1610 | 10-45 | 12-39 | 2.3-6.5 | 3200-7300 | 11-62 | 265-595 | 327-1030 | 17-35 | 0.76-4.45 | 1.30-5.10 |
| | A.Mean | 125 | 23 | 22 | 4.1 | 5318 | 32 | 378 | 651 | 24 | 2.13 | 2.39 |
| | S.D. | 216 | 9 | 6 | 1.2 | 856 | 9 | 78 | 207 | 4 | 0.73 | 0.82 |
| | Median | 93 | 20 | 20 | 3.9 | 5300 | 31 | 356 | 567 | 24 | 2.00 | 2.20 |
| Tamarack | | | | | | | | | | | | |
| (n=13) | Range | 55-115 | 13-39 | 17-48 | 2.6-4.8 | 3200-34000 | 14-31 | 219-426 | 315-681 | 10-19 | 1.81-6.24 | 2.1-5.3 |
| | A.Mean | 82 | 20 | 30 | 3.4 | 6454 | 22 | 341 | 514 | 14 | 3.91 | 2.86 |
| | S.D. | 20 | 8 | 10 | 0.8 | 83000 | 5 | 55 | 106 | 3 | 1.26 | 0.93 |
| | Median | 83 | 17 | 29 | 3.5 | 4100 | 23 | 356 | 546 | 14 | 3.83 | 2.40 |
| River alder | | | | | | | | | | | | |
| (n=22) | Range | 5-37 | 1.4-6.5 | 12-45 | 0.2-1.0 | 650-6700 | 12-44 | 157-583 | 48-160 | 1-6 | 2.07-5.76 | 1.4-2.2 |
| | A.Mean | 16 | 3.5 | 23 | 0.56 | 2994 | 22 | 335 | 111 | 4 | 3.95 | 1.85 |
| | S.D. | 10 | 1.3 | 9 | 0.22 | 1471 | 9 | 115 | 30 | 2 | 1.12 | 0.22 |
| | Median | 13 | 3.3 | 21 | 0.50 | 2800 | 19 | 317 | 110 | 4 | 3.79 | 1.90 |
| Dwarf birch | | | | | | | | | | | | |
| (n=5) | Range | 20-65 | 5.8-9.4 | 12-14 | 0.9-1.6 | 1100-13000 | 10-15 | 250-332 | 218-304 | 12-16 | 3.96-6.23 | 1.2-1.9 |
| | A.Mean | 41 | 7.8 | 13 | 1.2 | 8460 | 14 | 298 | 261 | 13 | 4.91 | 1.56 |
| | S.D. | 18 | 1.5 | 1 | 0.3 | 4427 | 2 | 32 | 38 | 2 | 0.88 | 0.27 |
| | Median | 35 | 7.6 | 13 | 1.2 | 9800 | 15 | 307 | 243 | 13 | 4.99 | 1.60 |

Trunk wood contains the highest Rb and Cd and only slightly lower Ni (13 ppm) than twigs (16 ppm). In comparisons of this type it is important to remember that the data are quoted on an ash basis. There is substantially lower ash yield from trunk wood and from crown cones (Table 5) than from other tree tissues, and therefore relative to other tissues the trunk wood is depleted in almost all trace elements when considered on a dry weight basis.

Comparative partitioning characteristics

Geochemical partitioning data for black spruce, jack pine, and tamarack tissues indicate the superiority of twigs and outer bark in acquiring and storing a wide range of elements useful for the definition of mineralization-related vegetation geochemical signatures. These elements occur at concentration levels that permit their determination by routine analytical procedures. The concentration levels of elements in twigs and outer bark from each of the three conifer trees examined are similar. Black spruce twigs contain higher concentrations of most elements, with the exception of Σ REE, compared to outer bark. Jack pine twigs contain higher Au, Pb, Ni, and Rb than outer bark but less As, Cr, Hf, Sb, Sc, Σ REE, Zn, and Cu. Tamarack outer bark contains higher levels of all elements except Rb, compared to tamarack twigs. Many of these chemical differences, however, are expressed by only a few ppm or ppb and may only reflect the chemical differences within a single tree at one grid location.

Of particular interest is the apparent acropetal tendency for the mobilization and concentration of Au, Ag, As, Cs, Rb, Sb, Zn, and Σ REE in crown twigs and, except for Ag, crown cones when compared to tissues sampled at chest height. The crown twigs contain the highest concentrations of Au, Ag, Rb, Zn, and Σ REE, as well as comparable concentrations of As, Cs, Hf, and Sb. The differences in concentration of these elements between crown and chest height twigs is generally in the order of a few tens of parts per billion (e.g., Au) or several hundred parts per million (e.g., Zn). The higher contents of many ore-related elements in the crown twigs indicates the potential for using this sample type for rapid, helicopter-supported regional-scale vegetation geochemical surveys (Dunn and Scagel, 1989). Lower, but significant element concentrations in chest height twigs provides a sampling medium for local- or property-scale evaluations.

The chemistry of twigs from the five species collected and analyzed for this study is compared in Table 7 with respect to 10 elements and ash yield. Medians for these elements indicate black spruce twigs contain the highest contents of As, Sb, Zn, Ni, Cu, Pb, and the lowest P of all the species sampled in this study. Medians for Au and Br, as well as many of the elements listed above, are similar for jack pine twigs. Some extreme values such as 34 000 ppm Zn in tamarack, 1610 ppb Au in jack pine, and the range in ash for black spruce (1.90-5.60%) suggest local contamination, and therefore comparisons should be made of median values rather than the maxima for each element.

Vegetation particulate geochemistry

Metal-contaminated dust resulting from ore haulage on gravel road PR 395 represents a potentially significant source of contamination in the study area. Visually, dust is restricted to within 25 m of the road, where it settles on the ground and on vegetation. Two particulate samples from vegetation at distances of 1 m and 7 m from the roadside and one sample of road fines (<2 μ m size fraction) were collected for geochemical analysis. Sufficient quantities of particulate for analysis could not be collected from vegetation further than 7 m from the road.

Data by INAA for these samples are given in Table 8. The results indicate enrichment in ore and ore-related elements in both the road fines and vegetation particulate samples. Concentrations of elements such as Fe, As, Cr, and Sb in the <2 μ m fraction of the road dust are probably related to fine grained sulphide and metals adsorbed on clays. Higher concentrations of Au, Br, Ca, Cr, Na, and Zn occur in the

Table 8. Neutron activation analyses of roadside (CHNP-3) and vegetation particulate samples. Ag, Hg, Ir, Ni, Sn, Sr, Ta, W, and Th contents are below the determination limits and are not listed. Data in ppm unless otherwise indicated.

| ELEMENT | CHNP-1:1m | SAMPLE CHNP-2:7 m | CHNP-3 |
|--------------|-----------|----------------------|--------|
| Au (ppb) | 128 | 125 | 16 |
| As | 64 | 40 | 150 |
| Ba | <60 | 110 | 414 |
| Br | 20 | 15 | <5 |
| Ca (%) | 20 | 19 | <1 |
| Co | 10 | 7 | 5 |
| Cr | 25 | 17 | 97 |
| Cs | <1 | <1 | 4 |
| Fe (%) | 3.34 | 2.12 | 7.84 |
| Hf | <1 | <1 | 19 |
| Mo | <3 | <1 | 9 |
| Na (%) | 0.70 | 0.41 | 0.38 |
| Rb | <15 | <15 | 86 |
| Sb | 5.6 | 3.9 | 17.0 |
| Sc | 6.4 | 4.1 | 11.0 |
| Se | <3 | 6 | <3 |
| Th | 3.5 | 1.6 | 23.0 |
| U | <0.5 | <0.5 | 7.0 |
| Zn | 8600 | 6500 | <50 |
| La | 14.0 | 8.6 | 54.0 |
| Ce | 21 | 17 | 110 |
| Nd | 8 | 8 | 24 |
| Sm | 2.2 | 1.5 | 4.5 |
| Eu | 0.8 | 0.3 | 1.2 |
| Yb | 0.8 | 0.5 | 2.6 |
| Lu | 0.15 | 0.12 | 0.19 |
| Σ REE | 46.95 | 36.02 | 196.49 |

Σ REE represents the total of the data obtained for seven rare-earth elements by this analytical method.
CHNP-1 and CHNP-2 were collected 1 m and 7 m, respectively, from PR 395;
CHNP-3 represents <2 μ fraction of sediment from PR 395.

vegetation particulates. There is a diminution of As, Ba, Cr, Cs, Fe, Hf, Mo, Rb, Sb, Sc, Th, U, and the REEs in the particulate sample at 7 m from the roadside as compared to both the road fines and the particulate from 1 m. Zn decreases from 8600 ppm to 6500 ppm between 1 m and 7 m from the road. Gold (125 ppb), Sb (3.9 ppm), and REEs remain almost as high in the particulate sample at 7 m as at 1 m and in the <2 µm fraction of the road gravel.

A systematic increase in the concentration of As, a non-essential element, with increased ash content in black spruce and jack pine twigs and outer bark is apparent (Fig. 5). This association is less apparent in needles of both species. As-rich particulate from PR 395 is interpreted as the cause for the As-ash association. The extent and magnitude of this contamination is difficult to quantify given the limited amount of particulate material available from vegetation at distances greater than 7 m from the road. The potential for base and precious metal particulate contamination from PR 395 that obscures mineralization-related vegetation geochemical signatures is exacerbated by the coarse nature of outer bark, in which dust can become lodged. Metal contents are similar in outer bark and twigs of black spruce, jack pine, and tamarack. Consequently, twigs were selected as an alternate tissue type for interpretation of geochemical data from the grid survey. A second precautionary step to avoid the effects of particulate contamination was to ash-normalize vegetation geochemical data from the grid survey. The wide range in ash content of tissues in this study makes this procedure helpful in interpreting the data (Chukhrov et al., 1979; Dunn, 1987).

Grid survey

Geochemical data from twig samples collected from the grid were examined and elements consistently close to or below the analytical determination limits were not included in the remainder of the study. Nontransformed geochemical data for twigs from the various species were ash-normalized using the procedure of Chukhrov et al. (1979) and plotted as percentiles on the sampling grid. These data were assessed for variations with proximity to the vertical surface projection of the deposit and to PR 395. Results are discussed with respect to individual species.

The ash normalization procedure proposed by Chukhrov et al. (1979) was used to more accurately assess element content in ashed vegetation samples by partially removing the chemical effects of particulate contamination. The method is based on transforming analyses by dividing element content in ash by the ash content of that sample. Care must be taken when using this normalization procedure since bona fide vegetation geochemical signatures can be subdued or eliminated depending on the composition of the particulates. Metal-poor silicate dust from road gravel will dilute the chemical signature of vegetation and the normalization procedure will then reduce a meaningful vegetation geochemical response, perhaps to the point of missing an anomaly. Ash normalization of the data is premised on anomalous metal concentrations in the particulates. The need for remedial ash

normalization of vegetation geochemical data in this study is demonstrated by analytical results for vegetation tissue samples collected adjacent to PR 395 at grid location 40 EBL, 150S. High coincident ash and metal contents in black spruce, jack pine, and tamarack tissues are evident at this site. Black spruce twigs (5.6% ash) and outer bark (10.4% ash) have elevated Fe, Cu, Au, and As; jack pine outer bark (11.3% ash) has high As. Tamarack twigs (5.3% ash) also contain elevated Au, As, and Zn.

Black spruce (*Picea mariana*) – twigs (n = 37: Fig. 6-11)

Ash yield (Fig. 6): 1.9-5.6%. Highest values of 5.6% and 4.6% occur within 40 m of PR 395 suggesting some contamination by airborne particulates.

Copper (Fig. 7): 285-565 ppm. A cluster of high values over and west of the deposit. Values of 446 and 449 ppm occur on L76N and a single high of 549 ppm occurs on 40 EBL. The significance of high Cu values directly over the deposit on L70N adjacent to PR 395 is reduced by ash normalization.

Lead (Fig. 7): 315-1118 ppm. Multi-sample anomaly with 716 to 1112 ppm coincides with Zn enrichment. Anomaly is unchanged by ash-normalization.

Zinc (Fig. 8): 3500-9300 ppm. Highest values (8000 to 9300 ppm) form a multi-sample anomaly, unaffected by ash normalization, directly over and up to 150 m west of the deposit.

Cadmium (Fig. 8): 9-26 ppm. Nontransformed data for Cd closely reflect the areal distribution of Zn and Pb results. Ash normalization of Cd values produces a less extensive, but well defined Cd anomaly northwest of the deposit.

Antimony (Fig. 9): 2.4-8 ppm. Highest values are clustered at the western edge of the deposit and up to 150 m north to L76N. Ash normalization reduces the areal extent of this anomaly, however, the zone of high values persists over the western edge of the deposit.

Arsenic (Fig. 9): 12-49 ppm. Highest values away from PR 395 occur directly over and up to 75 m west of the surface projection of the deposit.

Gold (Fig. 10): 36-325 ppb. Ash-normalized and non-transformed data identify a two-sample zone of Au enrichment (116 and 166 ppb) that partially covers the western portion of the deposit and extends westward for approximately 150 m. These results essentially mimic those for Zn, Pb, Cd, and Sb.

Bromine (Fig. 10): 11-32 ppm. A sample with 31 ppm Br occurs at the western edge of the deposit. Single sample highs also occur along L84N and L76N.

Phosphorus (Fig. 11): 0.95-2.99%. A three sample anomaly on L76N near the intersection with 40 EBL extends for 125 m from the western edge of the deposit. Two samples with high P (2.55% and 2.99%) occur 100 m east of Chisel Lake.

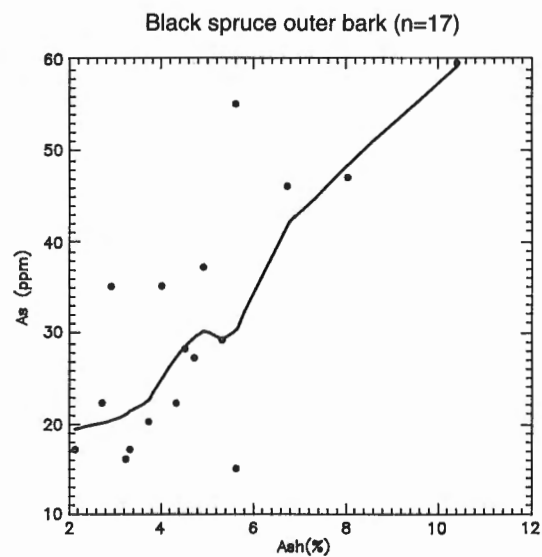
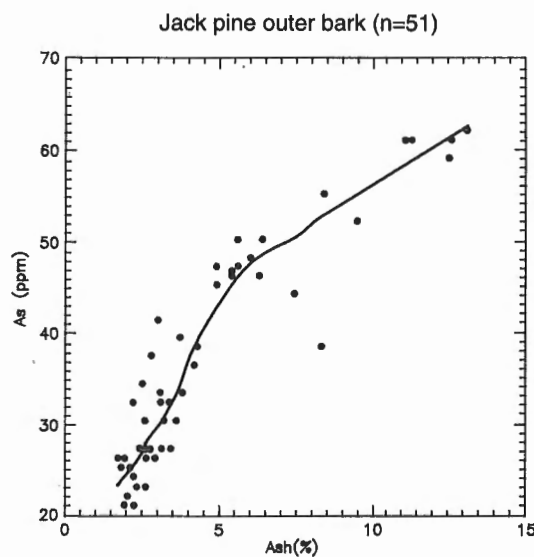
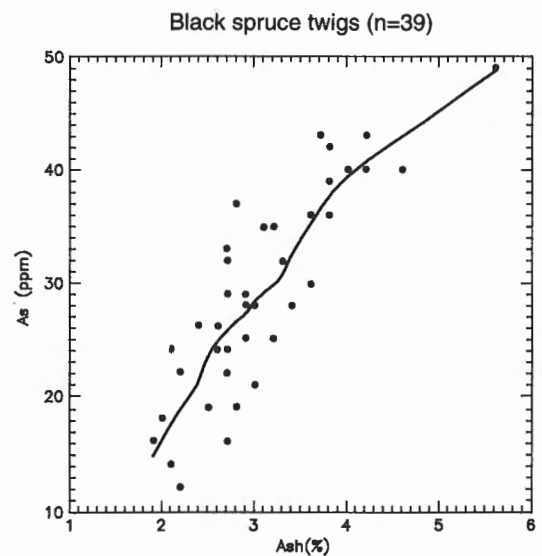
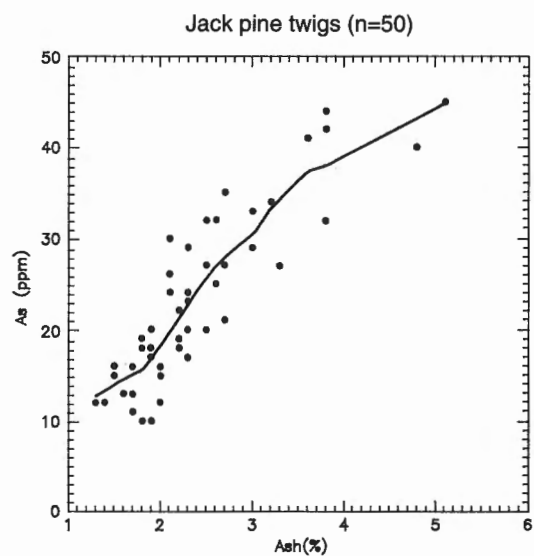
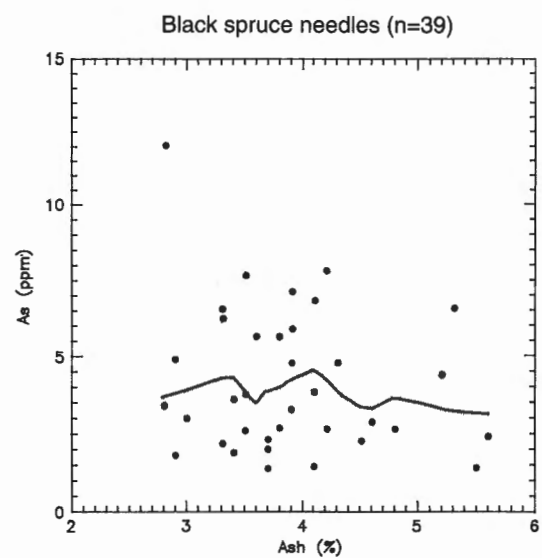
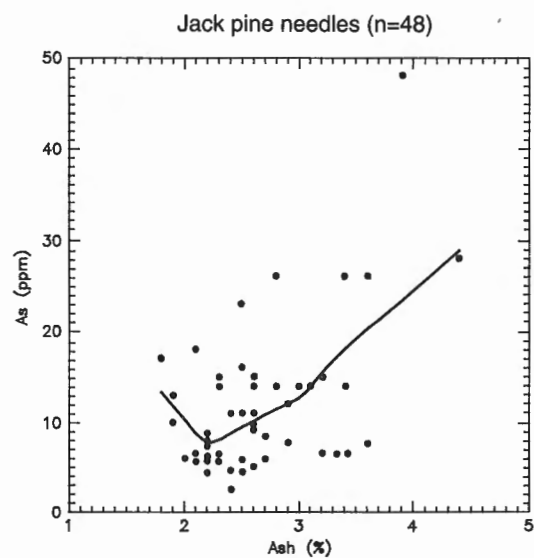


Figure 5. Plots of As versus ash for jack pine and black spruce tissues. Lines of best fit based on the procedure of Cleveland (1979, 1981).

An overlap of high concentrations of Zn, Pb, Au, As, and P, and to a lesser extent, Cu, Cd, Sb, and Br over and to the west of the deposit is apparent in the black spruce twig data. The dimensions of this anomalous zone are essentially unchanged by ash normalization although the areal distribution of anomalies for some elements, such as Cu, Sb, and Cd, are reduced subsequent to this transformation.

Jack pine (*Pinus banksiana*) – twigs (n = 48: Fig. 12-16)

Ash yield (Fig. 12): 1.3-5.1%. Particulate contamination is suspected for samples within 50 m of PR 395 based on ash contents of 3.8% and 5.1%.

Copper (Fig. 13): 265-595 ppm. Highest values (595 ppm Cu, 3.6% ash, and 548 ppm Cu, 3.8% ash) occur over the deposit but were negated by ash normalization.

Lead (Fig. 13): 327-1030 ppm. High values for Pb (1030 ppm Pb, 3.6% ash and 1003 ppm Pb, 2.5% ash) in single samples are localized over the deposit but within 40 m of PR 395. Anomalies were negated by ash-normalization.

The analysis of 1003 ppm Pb with 2.5% ash may represent an over-correction for particulate contamination using the Chukhrov et al. (1979) method.

Zinc (Fig. 14): 3200-7300 ppm. Single sample anomalies occur over the deposit (6600 ppm Zn, 2.3% ash) and west of the deposit near the intersection of L76N and 40 EBL (7300 ppm Zn, 2.2% ash). A four sample anomaly over the deposit and within 55 m of PR 395 (6200-6900 ppm Zn, 3.0-5.1% ash) and a 6600 ppm anomaly over the deposit were negated by ash normalization.

Cadmium (Fig. 14): 17-35 ppm. Highest values (29 ppm Cd, 2.5% ash and 35 ppm Cd, 2.1% ash) occur over the deposit but were negated by ash normalization. A series of high Cd values (26-29 ppm) with corresponding ash contents of 1.4-2.0% occur in samples collected along L84N.

Arsenic (Fig. 15): 10-45 ppm. Highest As on 40 EBL (45 ppm As, 5.1% ash and 44 ppm As, 3.8% ash), L70N (41 ppm As, 3.6% ash) and L76N (40 ppm As, 4.8% ash) are from samples within 40 m of the road. Particulate contamination in these samples is strongly suspected. Ash-normalized As data classified as 95th percentile occur over the deposit. These samples have less than 3.0% ash.

Antimony (Fig. 15): 2.3-6.5 ppm. High values of 5.7-6.5 ppm Sb with 3.2-5.1% ash are present in several samples collected west of the deposit near the intersection of L76N and 40 EBL. This multi-sample anomaly is unchanged by ash normalization.

Gold (Fig. 16): 52-1610 ppb. Ash-normalized and non-transformed Au data indicate scattered single sample anomalies near the deposit. Samples over the deposit on L70N contain 133 ppb Au (2.3% ash) and 105 ppb Au (2.1% ash), respectively. An exceptional analysis of 1610 ppb Au with 3.8% ash was obtained from a sample at 335E on L76N. A sample collected on L76N near the intersection with 40 EBL contained 144 ppb Au (2.2% ash).

Bromine (Fig. 16): 12-39 ppm. Highest value of 39 ppm is 1.3 km northwest of the deposit on L84N. These concentrations are all within the normal background range for Br in the ash of pine twigs.

Nickel (not plotted): 11-62 ppm. A single high value of 45 ppm Ni with 3.3% ash occurs over the deposit.

Phosphorus (not plotted): 0.76-4.45%. Highest values (3.07 to 3.96% P with 1.5 to 1.9% ash) occur along L84N approximately 1.3 km northwest of the deposit.

Tamarack (*Larix laricina*) – twigs (n = 11)

The small sample population for tamarack twigs precludes the use of percentiles to demonstrate changes in the geochemical data. Eight of 11 samples were collected from L70N along the western edge of the deposit. One sample collected within 25 m of PR 395 at grid location 40 EBL, 150S, with 5.3% ash and high concentrations of Zn, Pb, Cu, Sb, and As was probably contaminated by airborne particulates from PR 395.

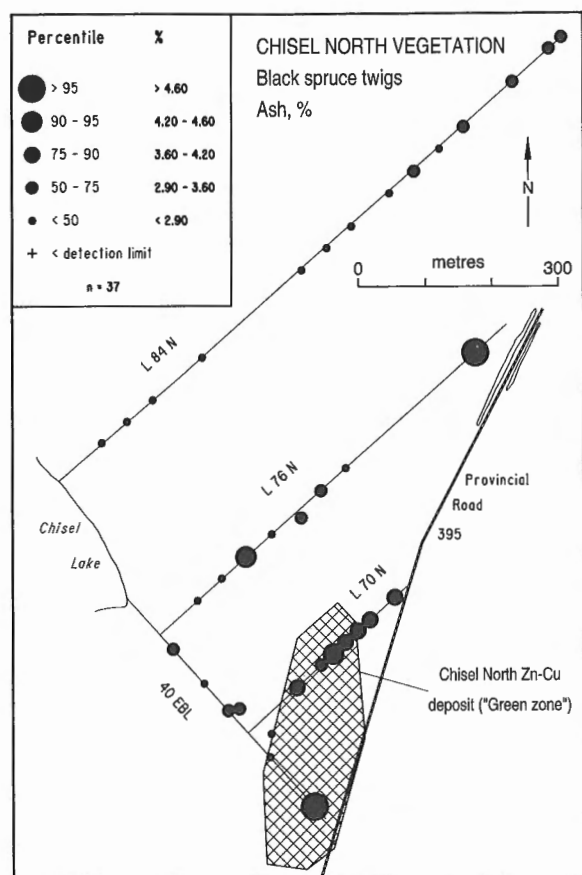


Figure 6. Variation in ash content in black spruce twigs, Chisel North deposit.

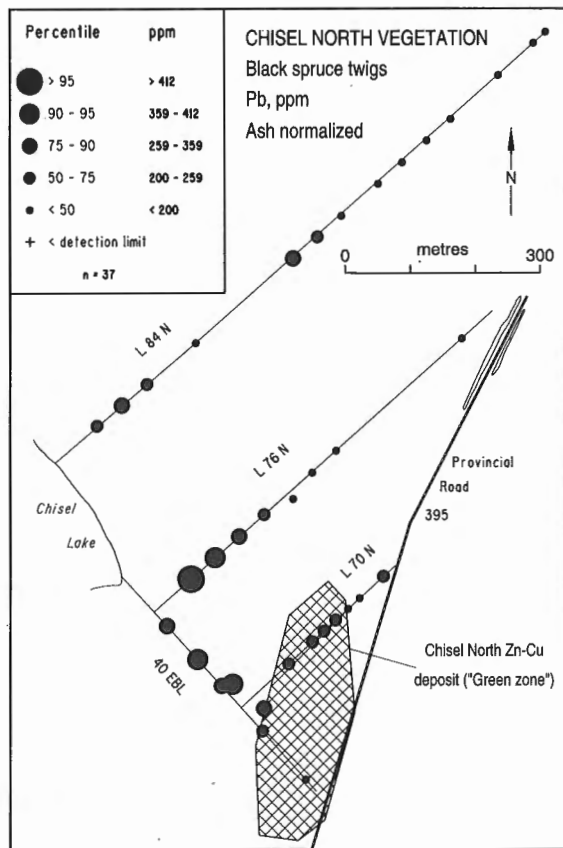
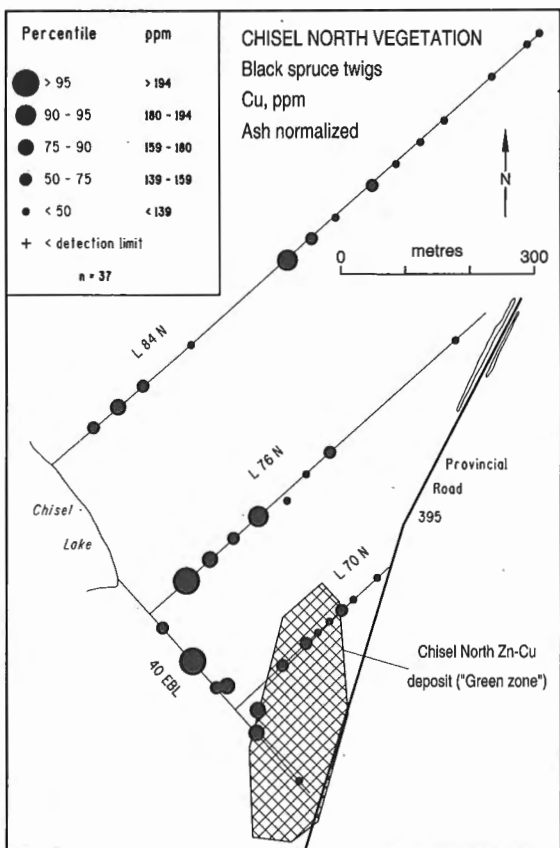
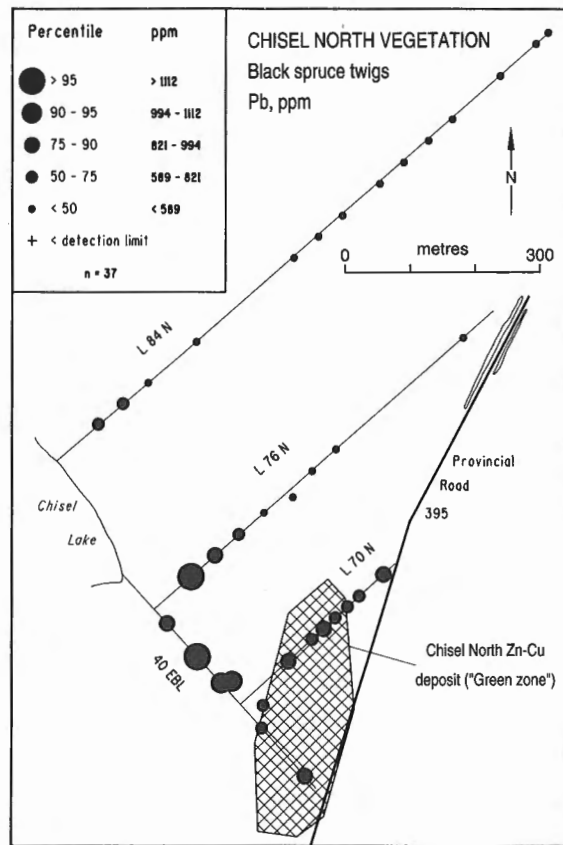
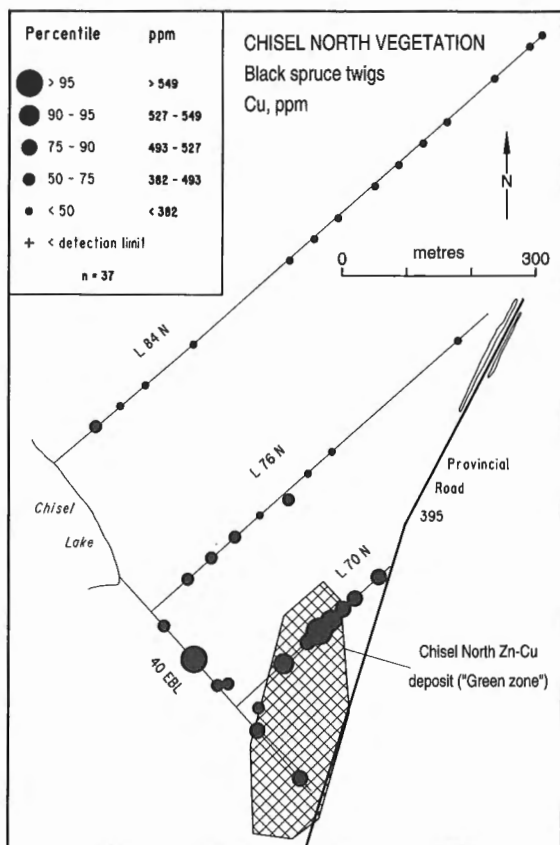


Figure 7. Variation in nontransformed and ash-normalized Cu and Pb contents, black spruce twigs, Chisel North deposit.

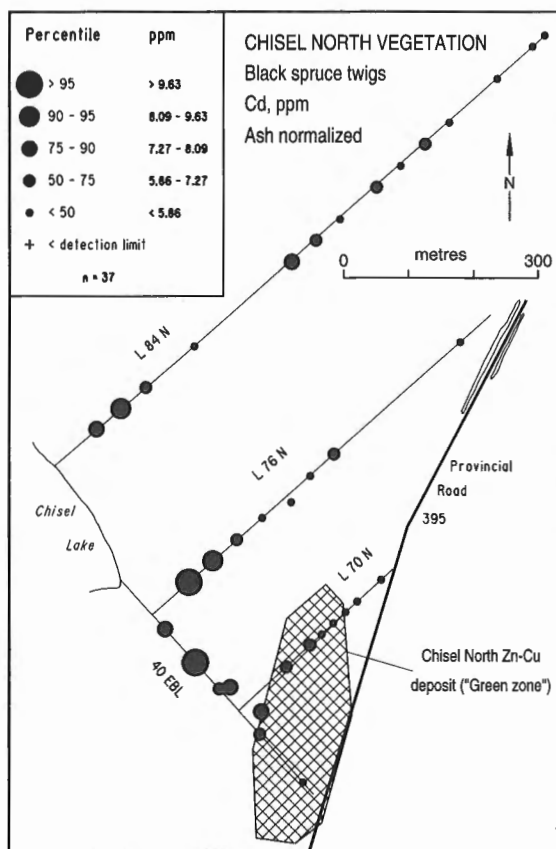
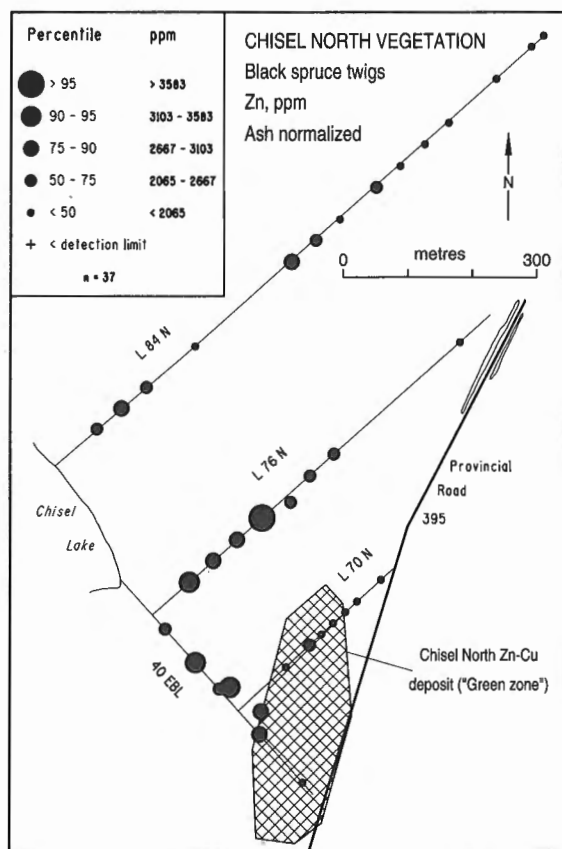
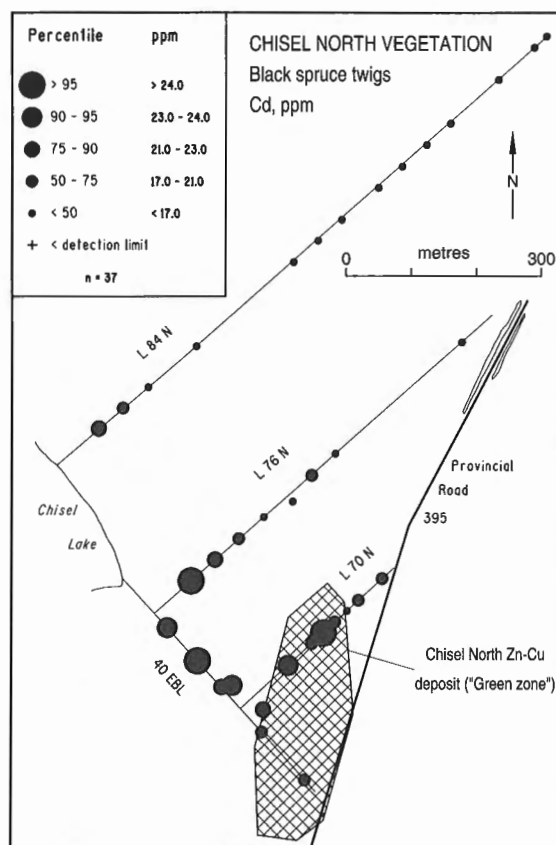
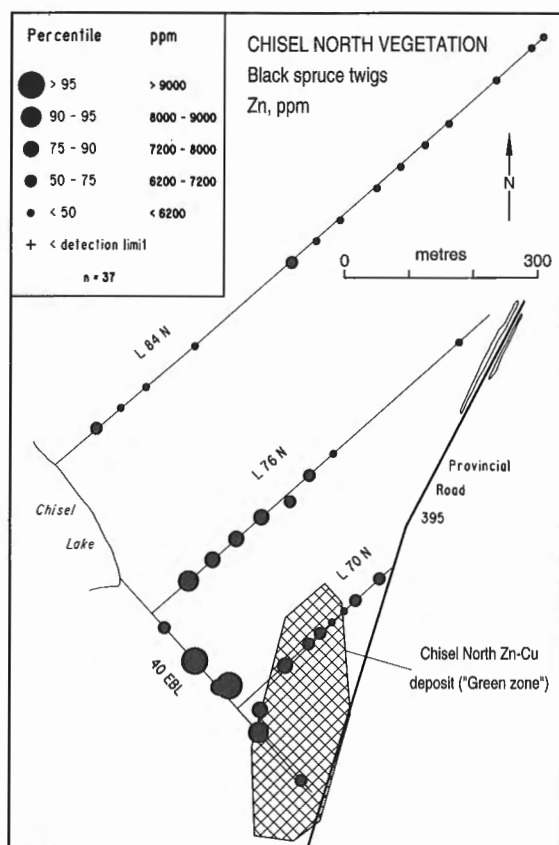


Figure 8. Variation in nontransformed and ash-normalized Zn and Cd contents, black spruce twigs, Chisel North deposit.

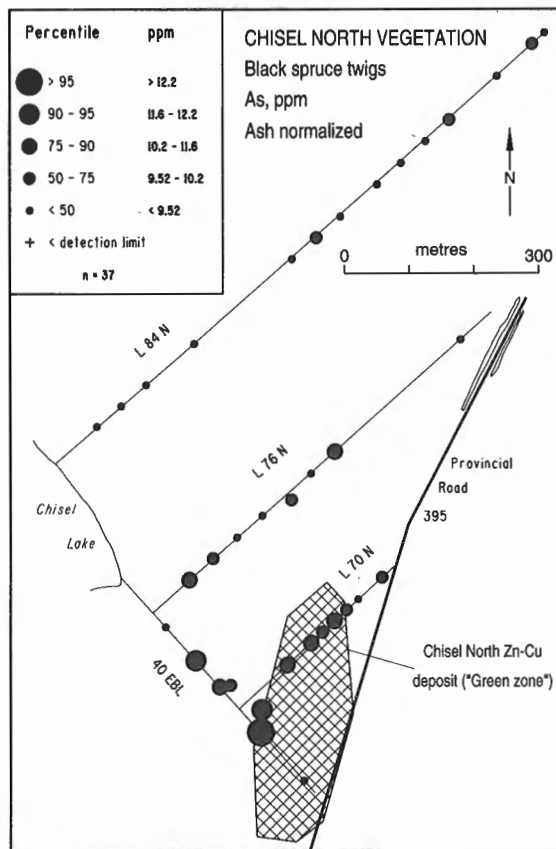
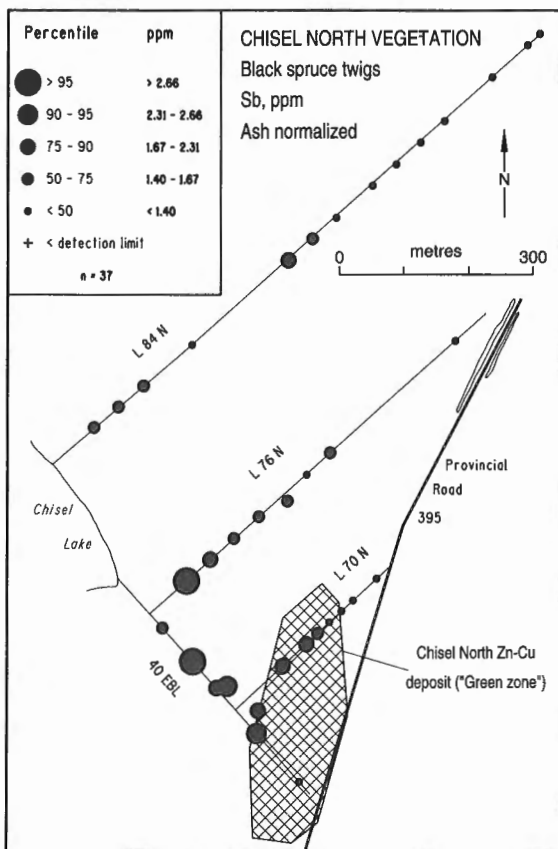
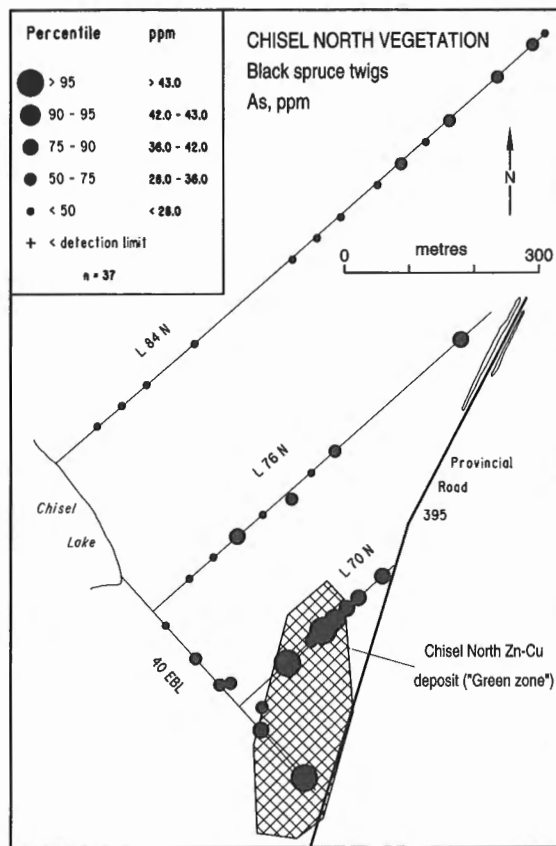
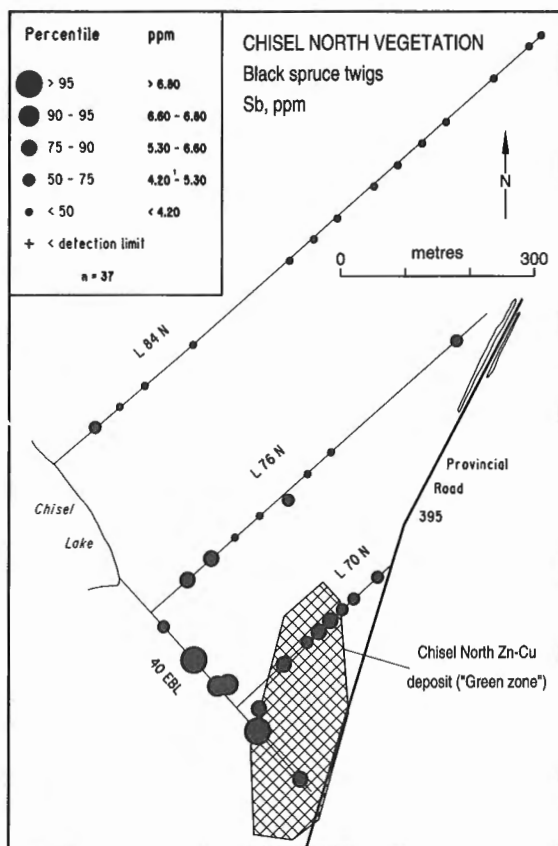


Figure 9. Variation in nontransformed and ash-normalized Sb and As contents, black spruce twigs, Chisel North deposit.

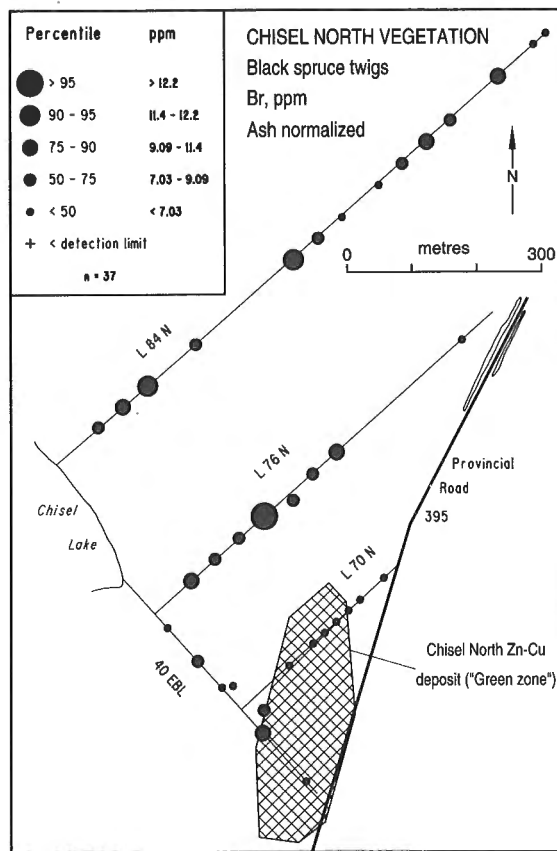
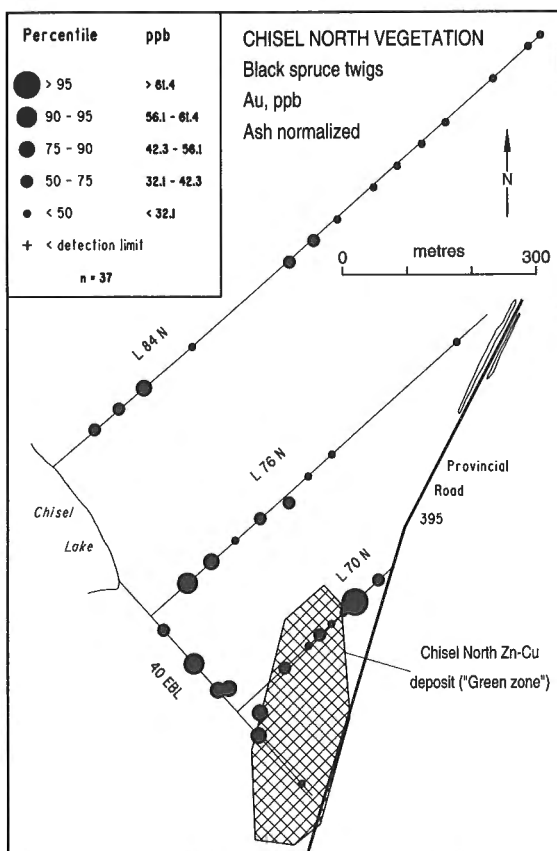
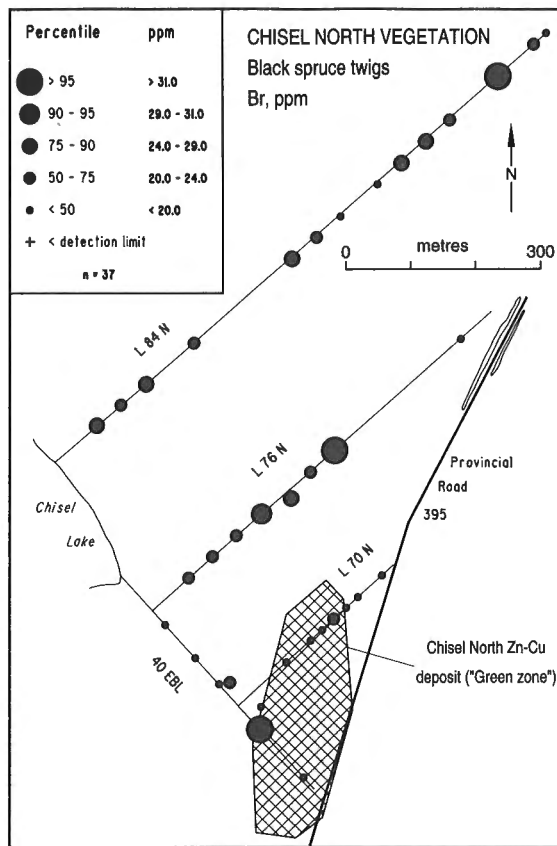
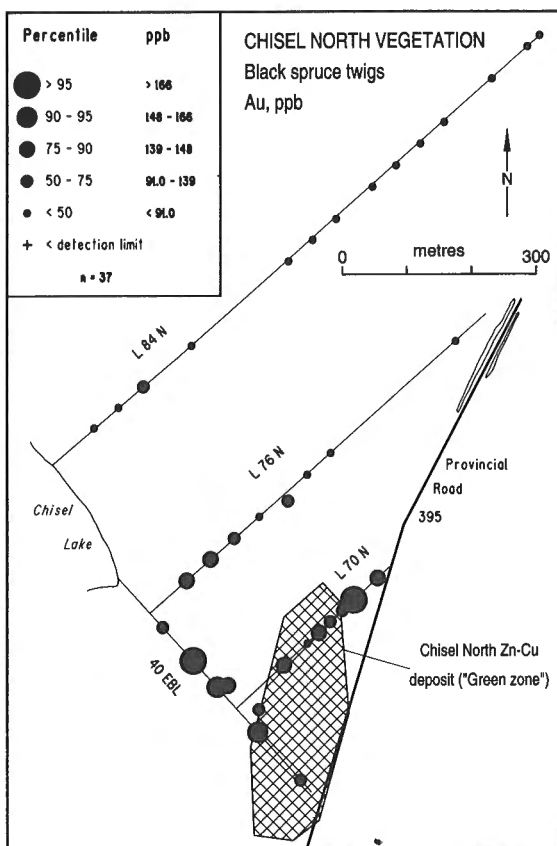


Figure 10. Variation in nontransformed and ash-normalized Au and Br contents, black spruce twigs, Chisel North deposit.

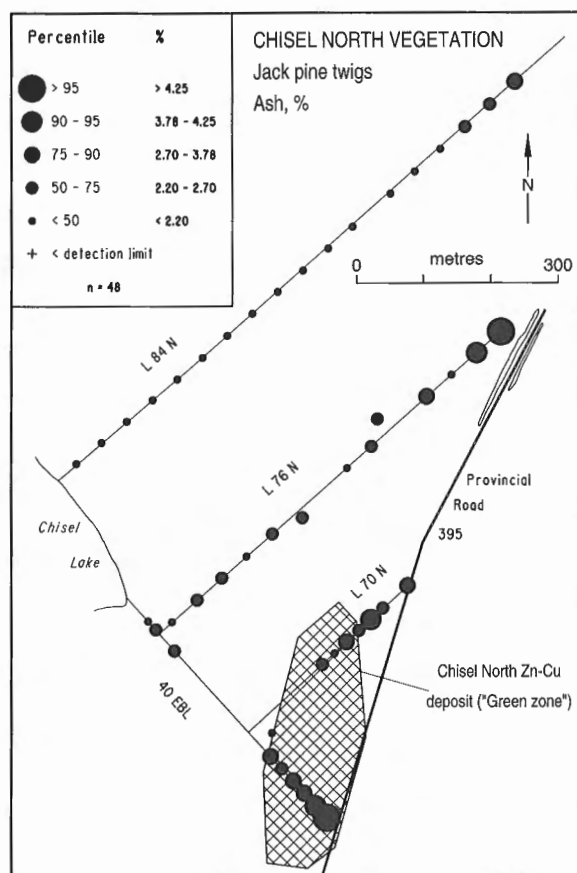
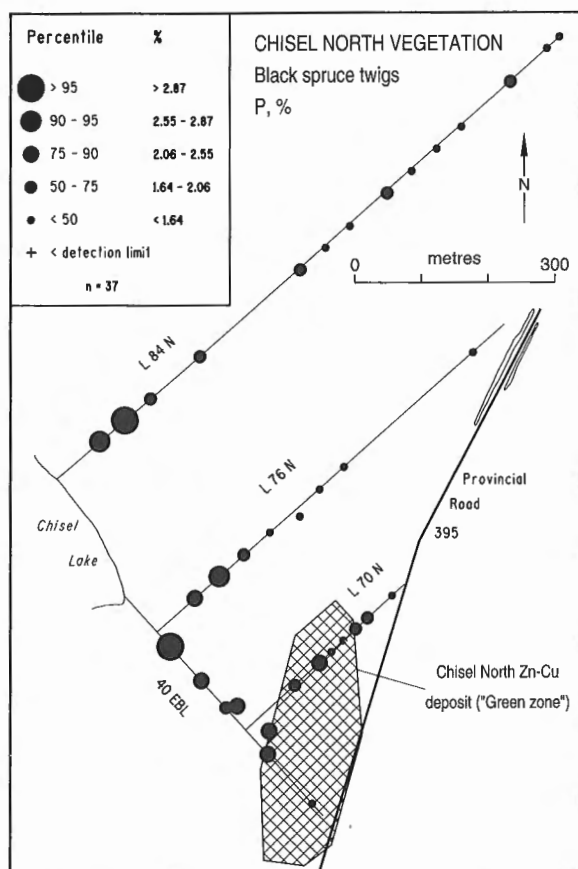


Figure 12. Variation in ash content in jack pine twigs, Chisel North deposit.

The ash yield for tamarack twigs varies from 2.1 to 5.3%, with two samples collected at the western edge of the deposit yielding 3.6 and 3.8% ash. Individual elements of interest were ash normalized.

High geochemical responses are situated over the vertical projection as well as to the west of the deposit. High P (6.24% P, 2.1% ash, and 6.05% P, 2.1% ash) and Br (48 ppm, 2.1% ash) occur directly over the deposit. The highest values for Cu (401 ppm), As (30 and 25 ppm), Sb (4.3 and 4.1 ppm), and Au (115 ppb) occur over the western edge of the deposit. An extraordinary analysis of 34 000 ppm Zn (2.3% ash), associated with high contents of REEs, Sr, Th, U, and W was obtained from a sample collected at grid location L84N, 400E. The tree was gnarled and twisted, suggesting metal stress. One sample with 5000 ppm Zn occurs 35 m west of the deposit on 40 EBL. A sample collected approximately 150 m north of the deposit has 96 ppb Au and corresponds to a relatively high analysis of 46 ppm Br.

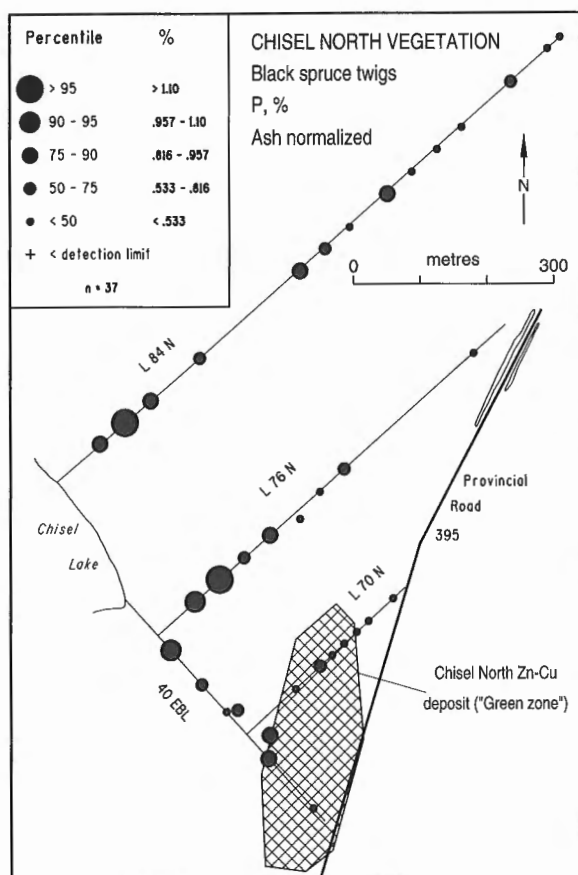


Figure 11. Variation in nontransformed and ash-normalized P in black spruce twigs, Chisel North deposit.

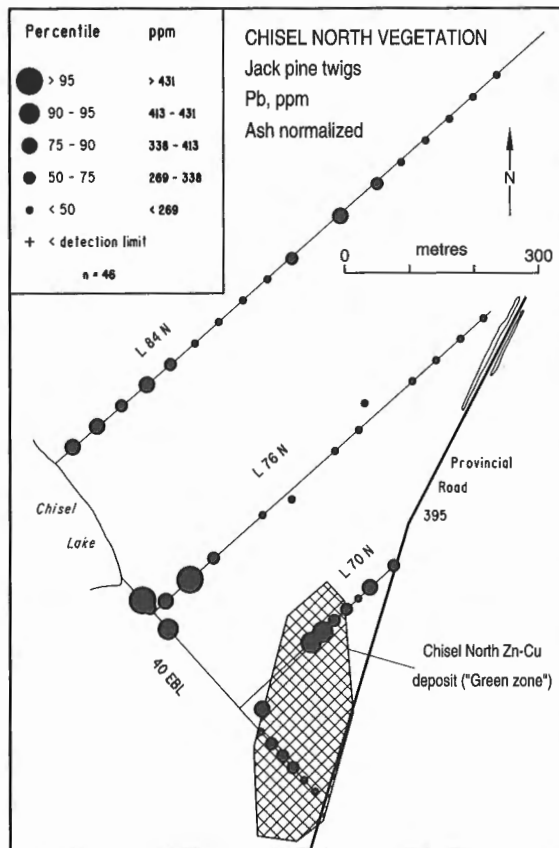
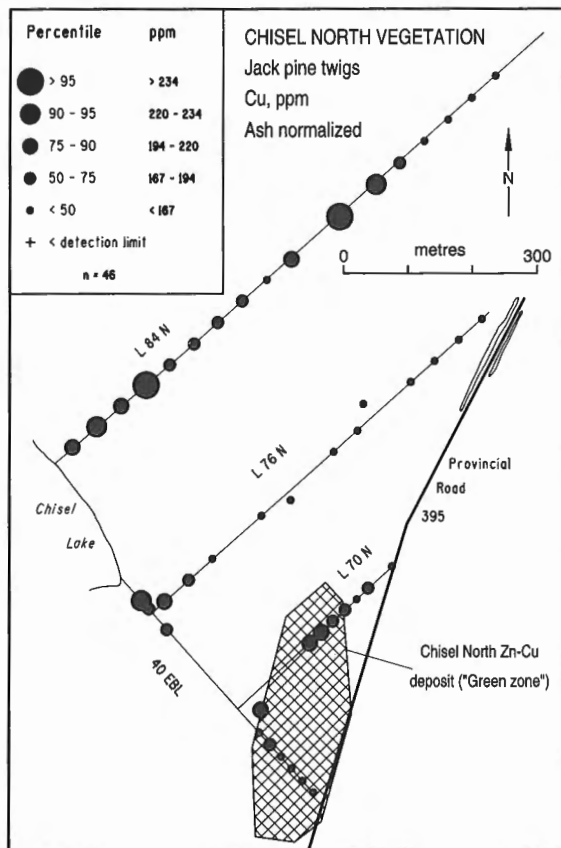
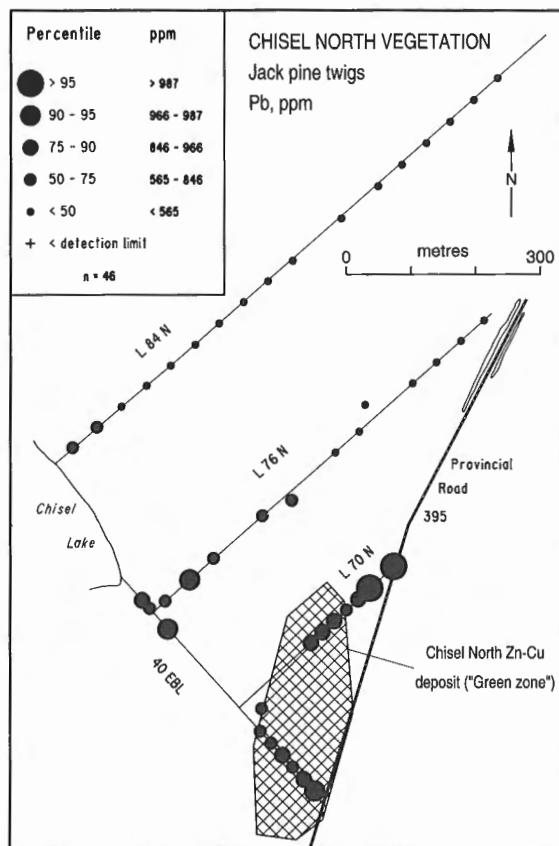
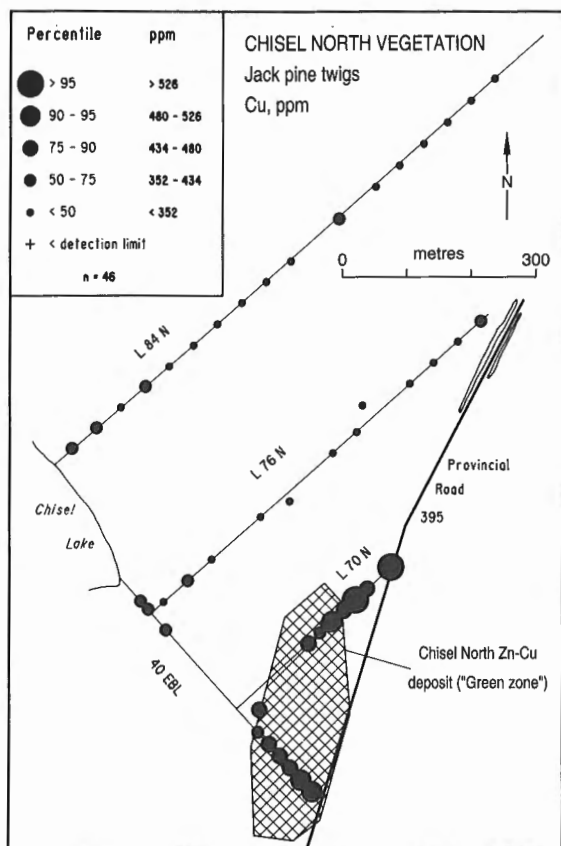


Figure 13. Variation in nontransformed and ash-normalized Cu and Pb contents, jack pine twigs, Chisel North deposit.

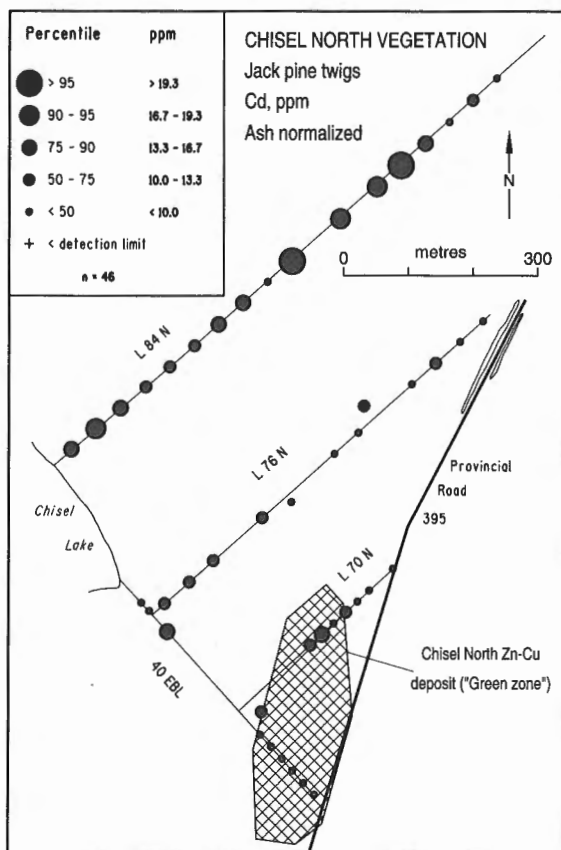
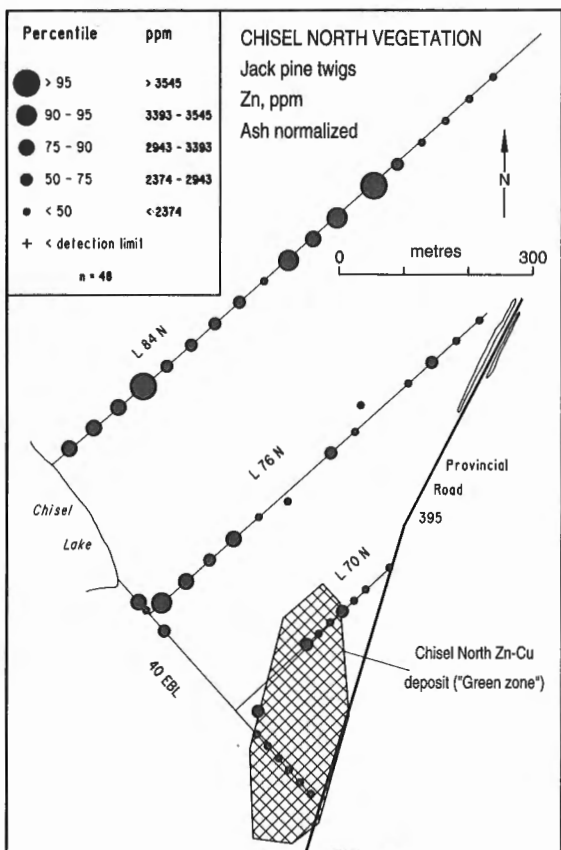
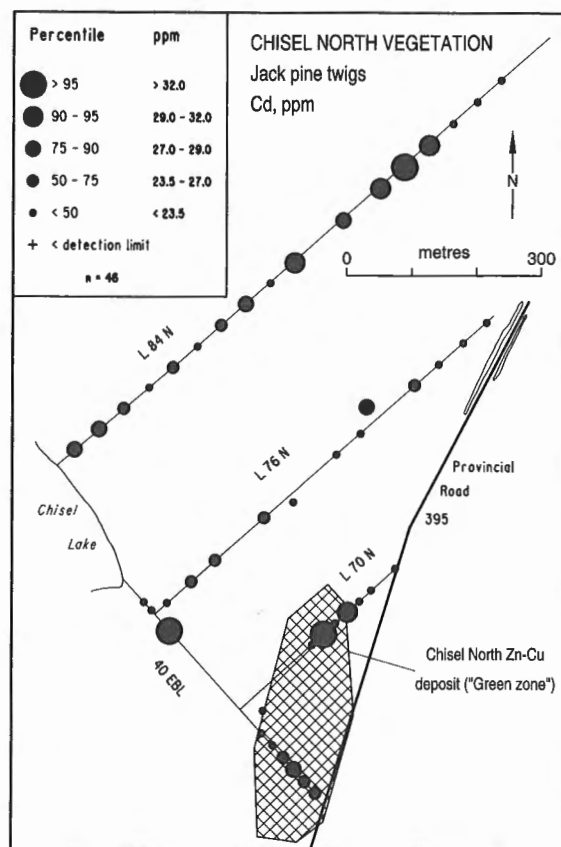
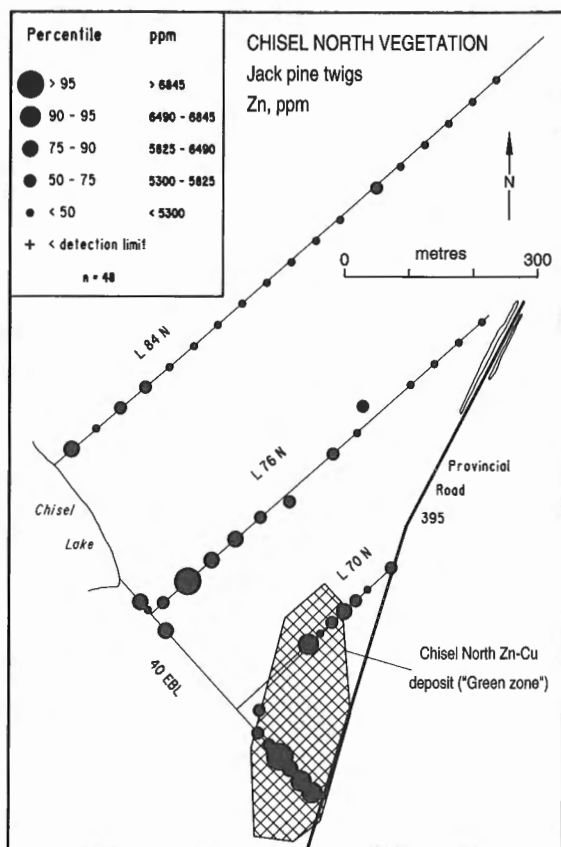


Figure 14. Variation in nontransformed and ash-normalized Zn and Cd contents, jack pine twigs, Chisel North deposit.

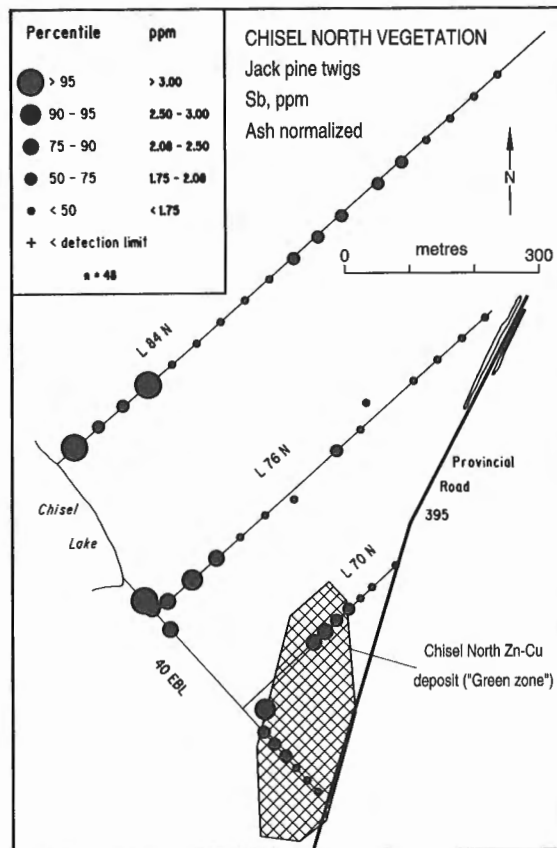
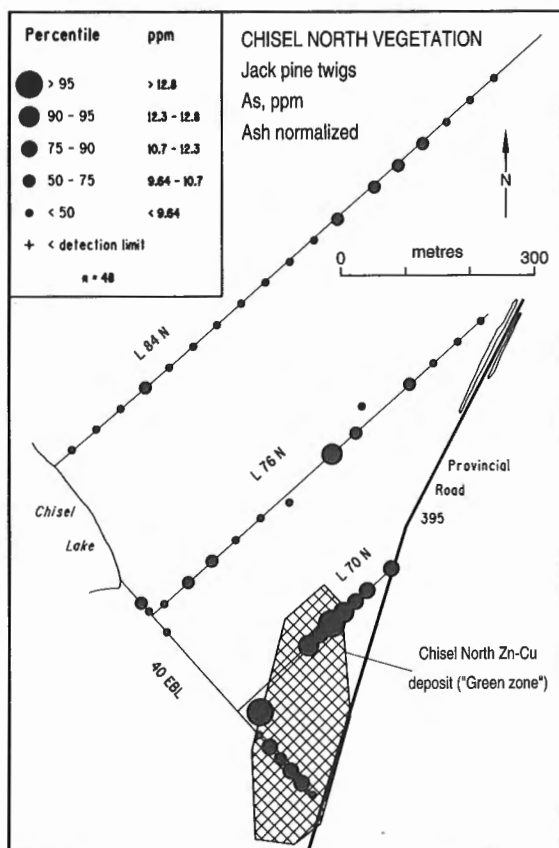
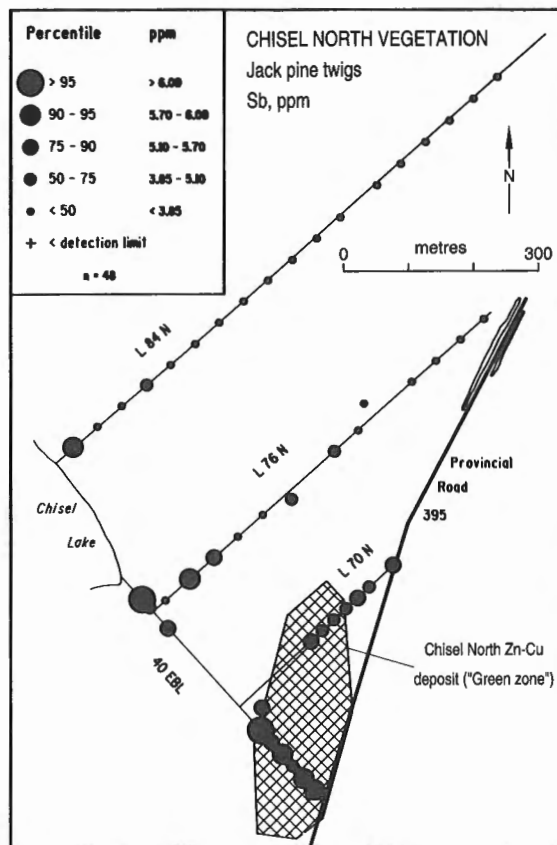
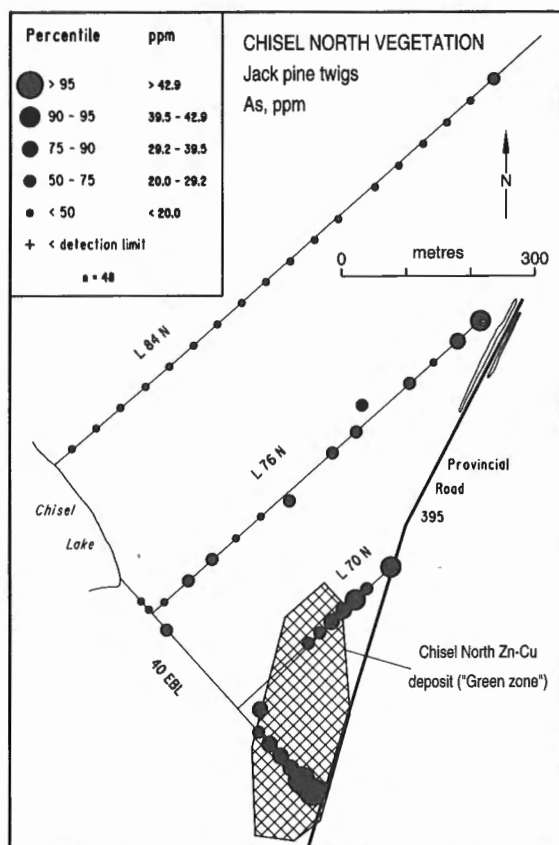


Figure 15. Variation in nontransformed and ash-normalized As and Sb contents, jack pine twigs, Chisel North deposit.

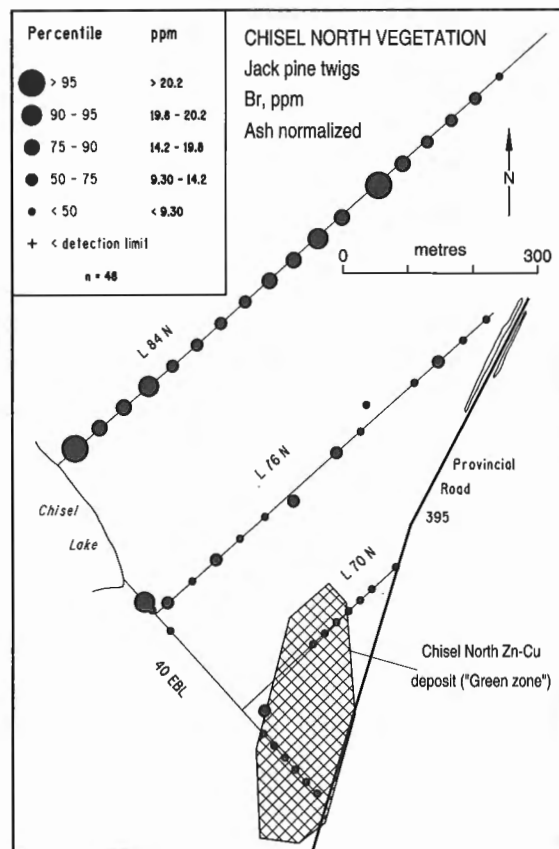
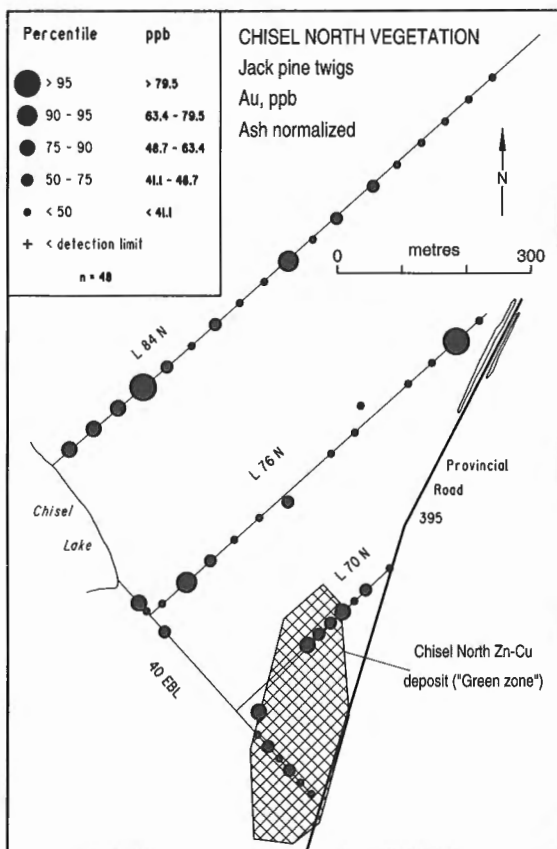
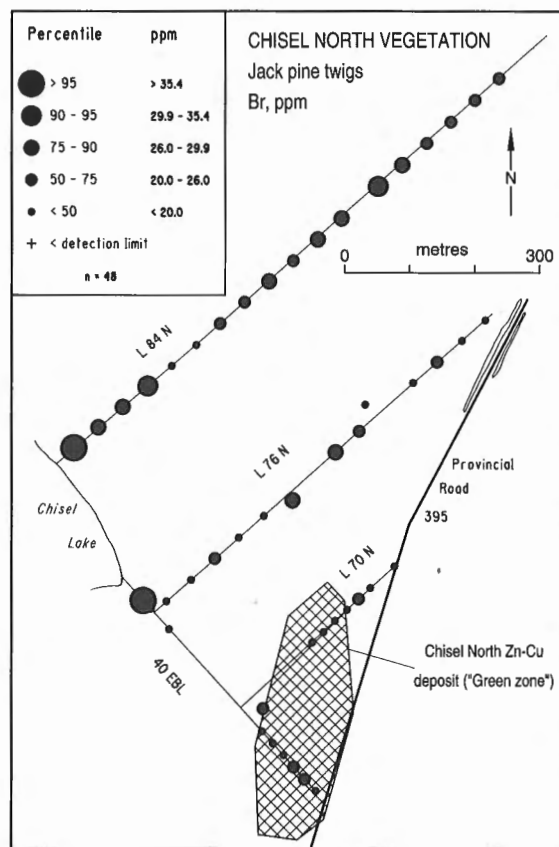
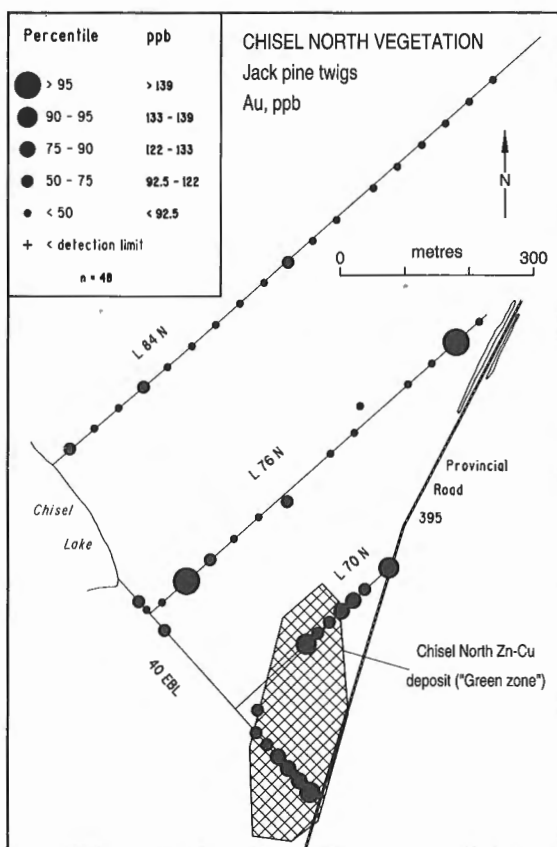


Figure 16. Variation in nontransformed and ash-normalized Au and Br contents, jack pine twigs, Chisel North deposit.

Tamarack twig geochemistry is characterized by relatively low contrast in variability for individual elements of exploration interest. The 34 000 ppm Zn (2.3% ash) analysis from a gnarled tree growing in an undisturbed area is an obvious exception.

River alder (*Alnus rugosa*) – twigs (n = 22: Fig. 17 and 18)

Alder twig data are based upon the analysis of 22 irregularly spaced samples (Fig. 17 and 18). Geochemical data are characterized by restricted ranges of element concentration including ash contents of 1.4-2.2%. The limited range of low ash content was interpreted to represent the relative absence of particulate contamination and, accordingly, ash normalization was not undertaken.

Phosphorus (Fig. 17): 2.07-5.76%. A five-sample cluster of high P occurs along L70N and 40 EBL at the western edge of the deposit. Within this zone P ranges from 4.72 to 5.76% versus 2.07-4.50% away from the deposit. This anomaly coincides with the results for Cu.

Copper (Fig. 18): 157-583 ppm. A five-sample cluster of high Cu occurs along L70N and 40 EBL at the western edge of the deposit. Within this zone Cu varies from 455 to 583 ppm. Away from the deposit Cu ranges from 157 to 404 ppm.

Lead (Fig. 18): 48-160 ppm. Highest value of 160 ppm (1.6% ash) occurs approximately 450 m northeast of the deposit.

Gold (Fig. 18): <5-37 ppb. Highest value of 37 ppb Au corresponds to 157 ppm Pb near the intersection of 40 EBL and L76N, approximately 150 m west of the deposit.

Bromine (Fig. 18): 12-45 ppm. Highest value of 45 ppm occurs 140 m north of the deposit on L76N and corresponds to a high Co analysis of 38 ppm.

Dwarf birch (*Betula glandulosa*) – twigs (n = 5)

The dwarf birch twig database is limited to five samples collected over and adjacent to the deposit. Although it is difficult to relate the geochemical response of the dwarf birch twigs to the mineralization because of a lack of samples, some

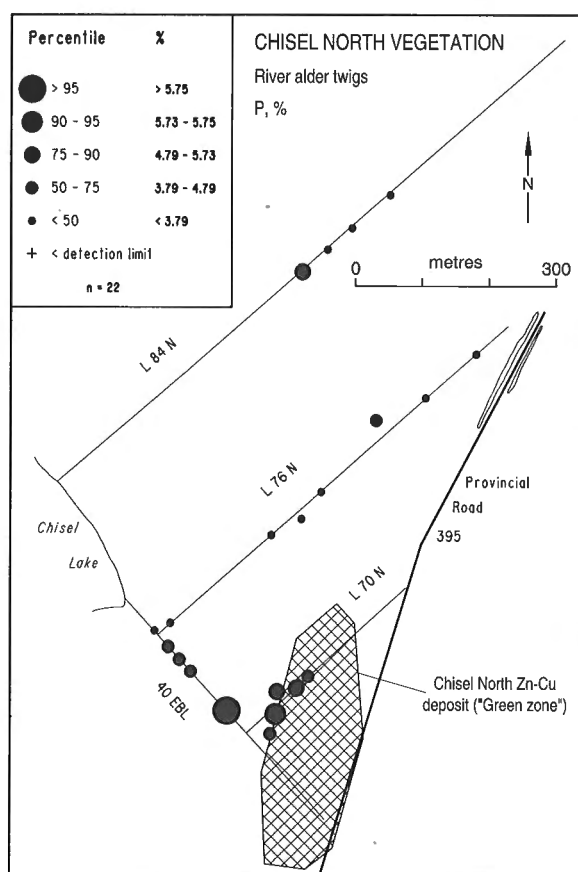
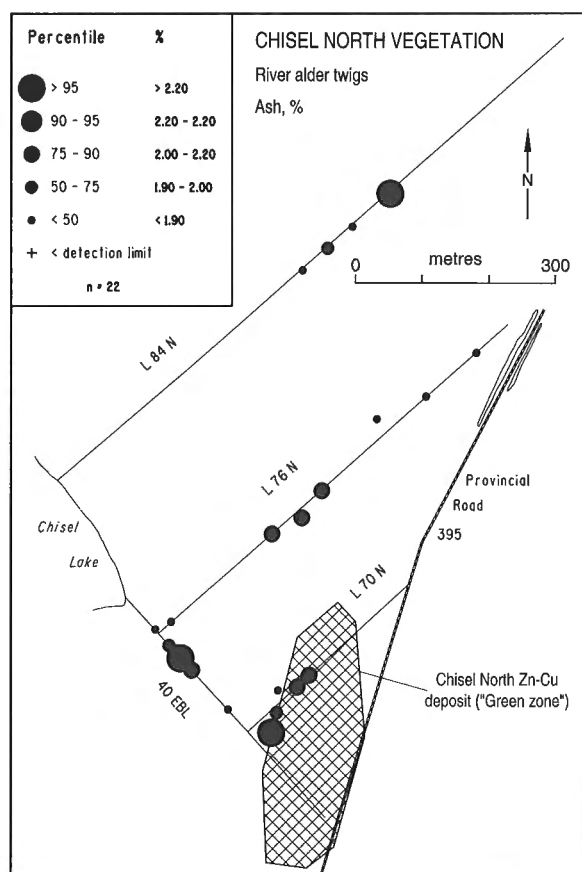


Figure 17. Variation in ash contents and nontransformed and ash-normalized P contents, alder twigs, Chisel North deposit.

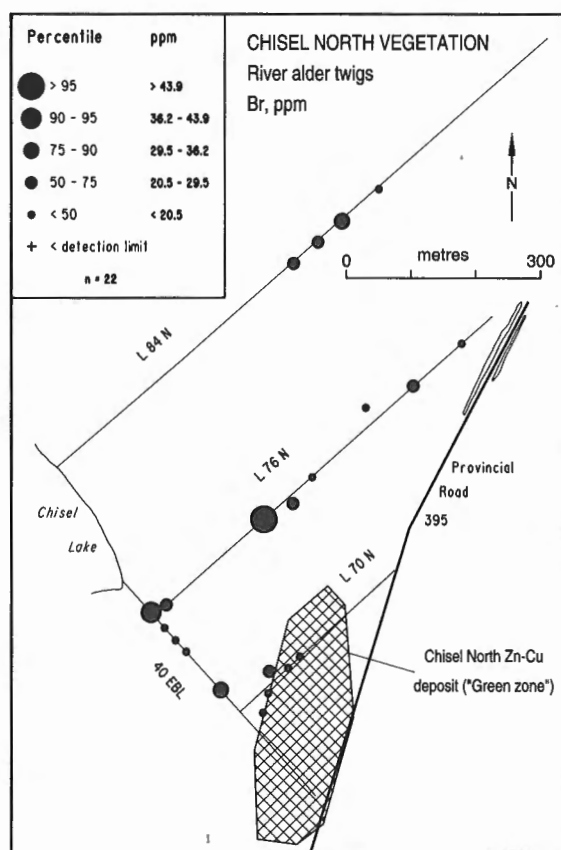
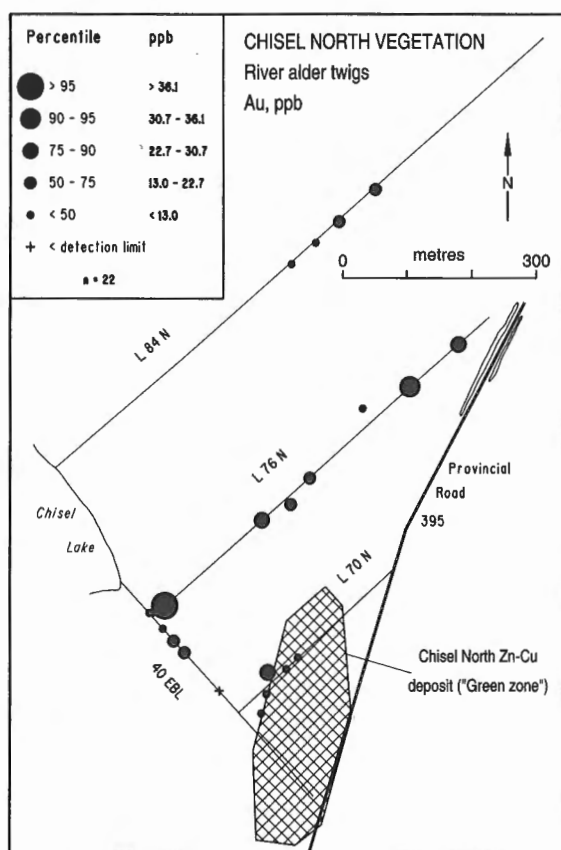
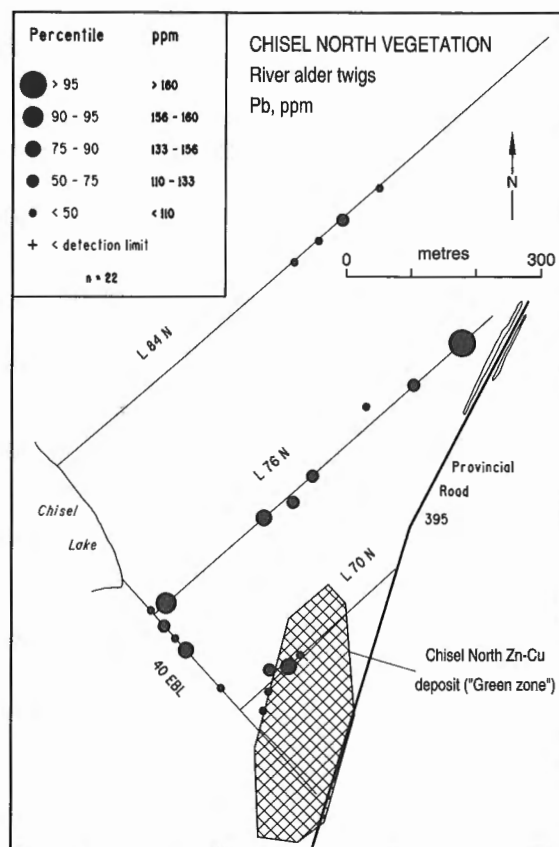
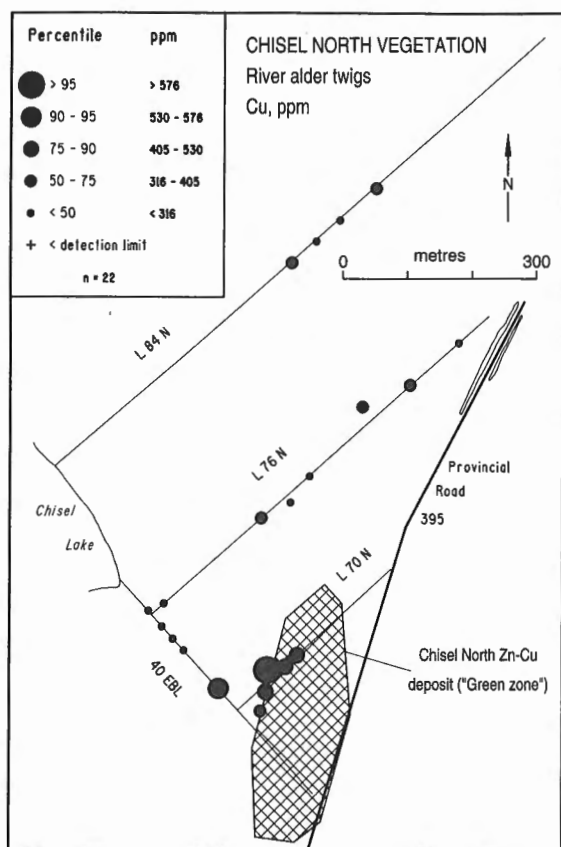


Figure 18. Variation in nontransformed Cu, Pb, Au, and Br contents, alder twigs, Chisel North deposit.

observations can be made about the relative abundances of metals. Median values are higher and ranges in concentration greater for dwarf birch twigs than alder twigs for Au, As, Sb, Zn, Pb, Cd, and P (Table 7). A sample of dwarf birch twig records the highest median for Zn (9800 ppm) in the study. A single analysis of 13 000 ppm Zn (1.4% ash) was obtained from a sample collected at 40 EBL, 150S. Table 7 illustrates generally lower metal values for dwarf birch twigs when compared to black spruce, jack pine, and tamarack twigs.

Composite vegetation geochemical anomalies

The areal distribution of samples classified in the 90th and 95th percentiles for nontransformed geochemical data representing black spruce, jack pine, and tamarack twigs, needles, and outer bark were combined to give "composite" anomalies (Fig. 19). These anomalies are interpreted to represent the variation in vegetation chemistry attributable to proximity to the vertical projection of the Chisel North deposit. Alder twig and tamarack needle, twig, and outer bark data are also summarized in Figure 19. The location of these composite anomalies is significantly different from those that occur adjacent to PR 395, which are characterized by high ash contents in combination with Cu, Pb, Zn, Fe, Sb, Au, and As for black spruce, jack pine, and tamarack tissues. In the black spruce composite data, "ash-only" anomalies are documented adjacent to PR 395 and are considered to represent the absence of base and precious metals in dust originating from the gravel road.

Composite anomalies for all species occur consistently over, and for approximately 200 m to the west of the western edge of the deposit. The largest of these is the areally extensive zone of multi-element enrichment in black spruce tissues, which measures approximately 400 m in length and 300 m in width.

DISCUSSION

The assessment of vegetation geochemical exploration methods for base metal massive sulphide type deposits in temperate boreal forest has not been extensively documented. Erdman and Motooka (1983) assessed the biogeochemical response of the Late Triassic Greens Creek Zn-Pb-Cu-Ag-Ba massive sulphide type deposit (Admiralty Island, Alaska) on the basis of single stems of the crowns of Sitka spruce (*Picea sitchensis*) collected from helicopter. Geochemical flux, with proximity to the deposit, was characterized as low for Cu and Zn but up to an order of magnitude higher than background levels for As, Ba, Cd, Mo, Ni, and Pb. A depletion anomaly, consisting of low Ba, Al, and Ni in cones and low As, B, Al, Ni, and P in stems, was delineated at the gossanous surface expression of the deposit. The response of crown vegetation geochemical sampling for this type of deposit was considered inconclusive by the authors. The study indicated that elements concentrated as ore in the deposit may be less indicative of mineralization than associated minor elements.

Fedikow (1983, 1984, 1985, 1986) documented the vegetation geochemical signature of the base metal-enriched MacLellan, Nisku, and Rainbow Au±Ag deposits near Lynn Lake, Manitoba. Low contrast anomalies in unashed samples of black spruce twigs and needles were defined for Cu, Pb, Zn, Fe, Au, and As. The anomalies successfully delineated a target greater in areal distribution than the mineralization. The vegetation geochemical response was attributed, in part, to a metal-enriched substrate at the deposit (Nielsen and Fedikow, 1987; Fedikow and Amor, 1990). Similarly, DiLabio et al. (1982) geochemically mapped a metalliferous glacial dispersion zone down-ice from a marble-hosted Zn occurrence in the Grenville Province of southeastern Ontario using the Zn content of conifers and grasses. In each of these studies, the deposits subcrop and are associated with a significant glacially dispersed metal-enriched substrate.

Soil and till geochemical surveys

Metal-enriched portions of soil located at the surface projection of the Chisel North deposit have been documented in samples collected from the same grid used for this vegetation geochemical study. Hamilton et al. (1991, 1992) define a three to four sample anomaly for Cu, Pb, and Zn just west of the deposit in B-horizon soils. Partial extraction-based analyses define a Cu, Pb, and Zn anomaly characterized by a three-sample grouping between 25 m and 75 m north on 40 EBL. These anomalies are of low contrast, as exemplified by results for Pb, which has a range of 5-10 ppm against a background of <1-4 ppm. Additionally, the low contrast anomalies are defined by distinctive patterns of variation in concentration. Three- to four-sample groupings of higher Cu, Pb, and Zn differ significantly from single sample peaks and highs separated by low values along the remainder of 40 EBL.

This soil geochemical anomaly coincides spatially with high Au, Cu, Pb, Zn, P, Cd, and Sb in black spruce twigs; Zn, Cd, P, Au, and possibly Pb and Sb in tamarack twigs; and high P and Cu and slightly elevated Br in alder twigs. Inasmuch as the B horizon may act as a long term integrator of vegetation geochemical signatures this covariance in sampling media is not unexpected. Ash contents in these twigs in the area of this anomaly fall within an expected range for each species and do not appear to indicate particulate contamination. In a separate study, Kaszycki and Hall (1996), on the basis of sequential dissolutions, define a C-horizon till anomaly containing 150-300 ppm Zn approximately 200 m southwest of the Chisel North deposit.

Surface contamination

Kaszycki and Hall (1996) document surface contamination anomalies in their overburden geochemical survey of the Chisel Lake-Chisel North area. Their work is based upon sequential dissolutions that differentiate between high metal contents in overburden resulting from a variety of dispersal mechanisms, including airborne particulates. Samples for their study were not collected directly over the Chisel North deposit, however, results indicate surface contamination approximately 200 m south of the deposit and within 75 m of

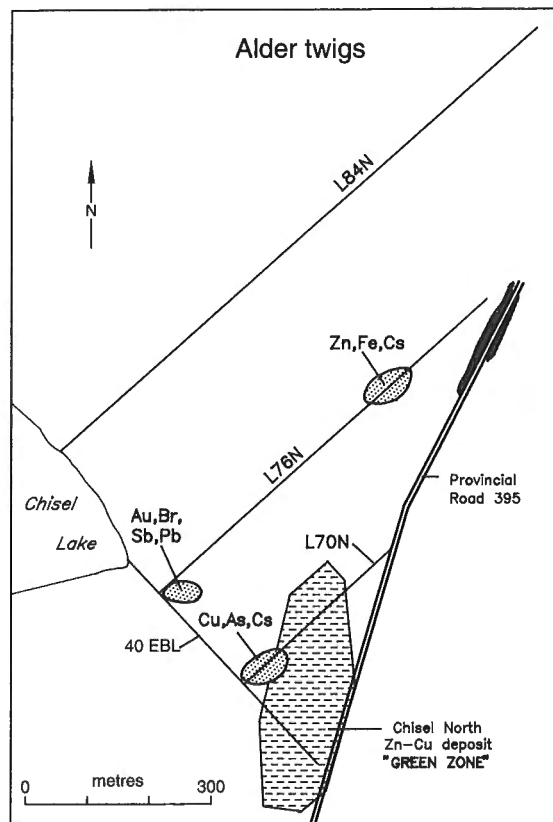
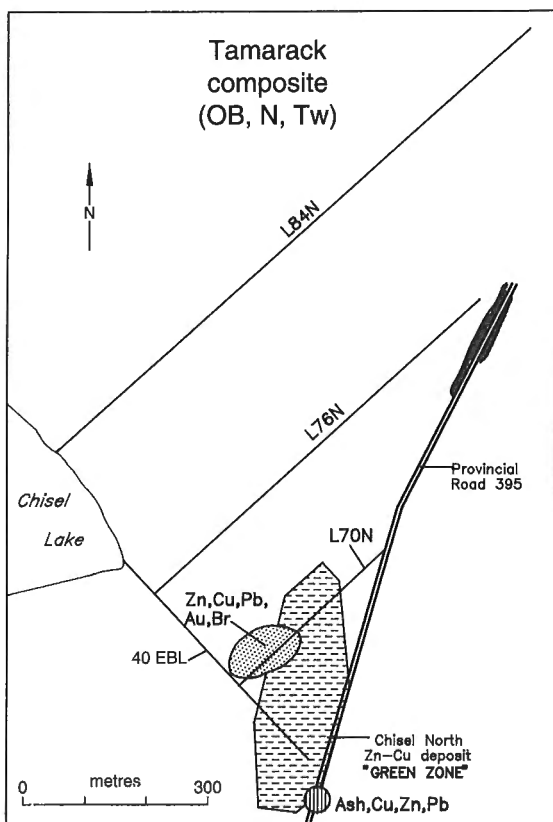
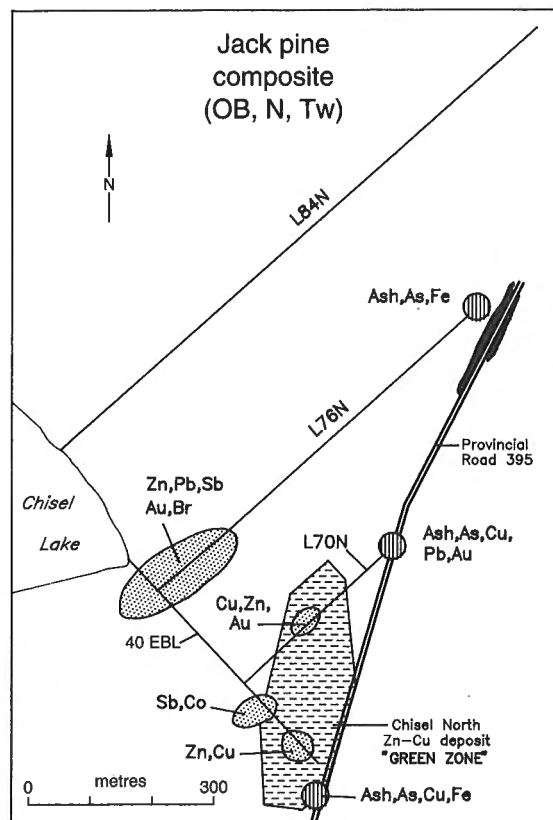
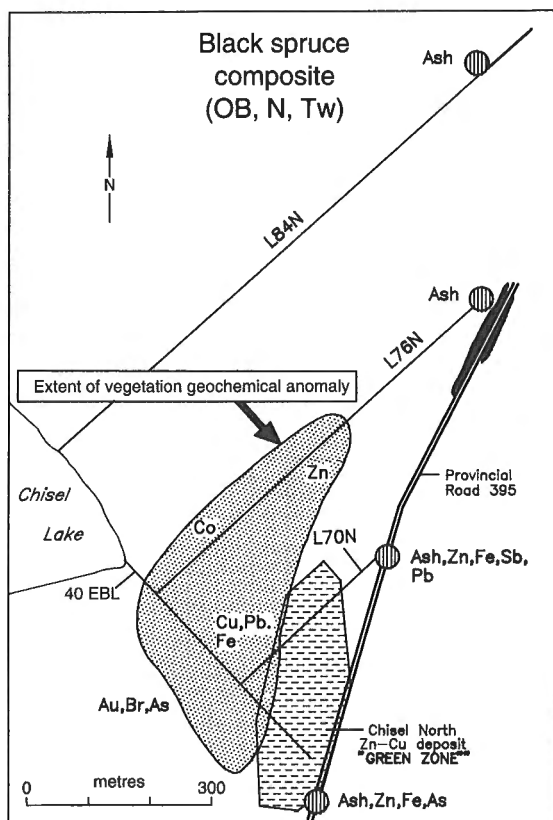


Figure 19. Areal distribution of composite vegetation geochemical anomalies for black spruce, jack pine, tamarack, and alder tissues, Chisel North deposit; OB – outer bark, N – needles, Tw – twigs.

PR 395 on the west and 350 m on the east side of the road. The broader areal dispersion of contamination anomalies to the east is attributed to prevailing southeast winds that redistribute metal-enriched particulate from PR 395. The delineation of airborne particulate soil geochemical anomalies in these areas is consistent with the results of this study. These include the recognition and definition of particulate vegetation geochemical anomalies in samples collected within 50 m of PR 395 and high metal concentrations in both the vegetation particulate and road fines. Ash normalization of the vegetation geochemical data was moderately successful in removing the effects of airborne particulates and "seeing through" the contamination.

Metal mobilization

Mechanisms for the mobilization of metals to surface from deeply buried and blind mineral deposits are controversial. However, there appears to be a hierarchical combination of geological and geochemical processes, exploration observations, and research, that provide an explanation for the observed vegetation geochemical results at the Chisel North deposit. Mineral explorationists and other workers in the Snow Lake mining camp have observed that base- and precious-metal enriched quartz veins are common near base metal massive sulphide type deposits. These veins are interpreted as products of deformation, metamorphism, and metal mobilization from the massive sulphide deposits and their host rocks. Harrison (1949) and Fedikow et al. (1989) describe a 1 m thick quartz vein with high Au concentrations associated with pyrite, chalcopyrite, galena, and possibly tennantite exposed in a trench near the recently discovered Photo Lake Cu-Zn-Au deposit. Fedikow et al. (1989, 1993) document similar base and precious metal-enriched quartz vein type deposits near other massive sulphide type deposits in the Snow Lake mining camp. These include the Morgan Lake Zn-Cu deposit, Rod Cu deposit, and the Ruby Zn-Pb-Ag deposits. Galley et al. (1986) postulate that zones with high Au content in the deformed portions of the Chisel Lake deposit may have been deposited coevally with the base metals and then mobilized and concentrated in the massive sulphide subsequent to middle amphibolite facies metamorphism. Galley et al. (1993) describe precious- and base-metal enriched quartz veins, parallel to the F_2 schistosity, up to 50 m from the massive sulphide mineralization as well as late faults that crosscut the deposit and offset late dykes in surface outcrop. Interestingly, a litho-geochemical Hg anomaly in the immediate area of the deposit was delineated by Hudson Bay Mining and Smelting Co. Ltd. during routine exploration in the area. The anomaly was based on the analysis of fracture coatings in outcrop. Galley et al. (1993) postulate that metamorphism and deformation are responsible for the mobilization of Hg into the structural hanging wall. The development of this Hg anomaly may be related to significant element redistribution in the deposit and altered wall rocks during synmetamorphic fluid migration along late brittle-ductile faults (Galley et al., 1990).

Skarns, comprising silicate- and dolomite-rich material interlayered with sulphide minerals at the Chisel North deposit theoretically provide a source for the formation and

continued evolution of sulphur-based gaseous compounds from the deposit. Oxidation reactions between groundwater and carbonate and sulphide minerals might be expected to produce a variety of sulphur and trace element gaseous compounds. Hale (1993) compiled research that documents soil geochemical anomalies produced by oxidation reactions associated with reducing groundwater and sulphide-bearing mineral deposits. Chalcogen and unspecified Se, Te, As, and Sb gases liberated during oxidation reactions are adsorbed onto active surfaces in soils developed over a variety of mineral deposit types.

The development of multi-element soil geochemical anomalies and the mobilization or electrogeochemical migration of metals as a function of self potential from the vicinity of massive sulphide type deposits has previously been demonstrated by Govett (1973, 1976) at the White Lake Cu-Zn deposit and by Ferreira and Fedikow (1990) at the Rod Cu deposit in the Flin Flon-Snow Lake greenstone belt.

SUMMARY

Multi-element/multi-species vegetation geochemical anomalies occur near the Chisel North deposit. These anomalies are variable in contrast, areally extensive in the case of black spruce tissues, and are characterized by a suite of elements that are enriched in the deposit and its alteration zones. This relatively small group of elements is a combination of essential and nonessential elements. Gold, Br, Sb, Pb, and Cd are nonessential elements for vegetation physiological processes; they reside in the tissues of the species sampled for this study as a byproduct of nutrient acquisition. Essential elements include: As, which may be utilized for carbohydrate metabolism; Zn, which assists carbohydrate and protein metabolism; and Cu, which aids photosynthesis, respiration, and protein metabolism. Subtle differences in the concentrations of these metals may reflect the general health of the plant, whereas major concentration differences, such as those documented in this study, are more likely to reflect chemical variation in the soil. It is noteworthy that the majority of the indicator elements determined in this study are not ore-forming elements; rather, they are associated minor constituents of the ore and are nonessential in terms of plant nutrition. Future applications of vegetation geochemistry to massive sulphide type deposit exploration should, therefore, include minor and trace element contents. This argues for multi-element approaches, particularly in the orientation stages of a program.

Acquisition of these metals by root systems of the species studied ultimately involves movement of metals from the deposit through significant amounts of post-ore rock and overburden. The mechanism for delivering these metals from a deeply buried source to the root systems of vegetation is necessarily speculative: however, a significant amount of evidence has been established. Element migration initiated during deposit formation was subsequently enhanced by deformation and metamorphism with accompanying redistribution of metals during synmetamorphic fluid migration along late brittle-ductile faults. Precious- and base-metal enriched quartz veins exposed near the Chisel North deposit

may be products of this redistribution of metals from source. The offset of the ore lenses by late faults, the recognition of these faults in surface outcrop, and the delineation of Hg lithogeochemical anomalies associated with the faults argues for large-scale element migration to surface. Gas streaming of the products of sulphide oxidation and related volatile metal halides and chalcogenides for metals such as Cu, Zn, Pb, As, and Sb represents an mechanism for continued metal delivery to surficial material and ultimately, vegetation.

Self potential mechanisms would enhance ion movement through the barren hanging wall and overburden. Thick lacustrine clays, traditionally considered to represent serious barriers to electrochemical migration (Smee, 1983), may have vertical properties, such as cracks, root channels, or soil biopores that can significantly enhance water and gas movement. Vegetation evapotranspiration or hydraulic pumping would complete the processes of mobilization of metals to vegetation root systems.

Geochemical signatures disguised by particulate contamination related to current or past exploration and/or production activity may be partially ameliorated by ash normalization. As a consequence, vegetation geochemical surveys in this environment can provide another source of information in exploration for base metal massive sulphide type deposits.

ACKNOWLEDGMENTS

We acknowledge Hudson Bay Mining and Smelting Co. Ltd. for permission to undertake this study and for assistance with grids, the surface projection of the deposit, and for the representative samples of Chisel North deposit mineralization. Don Birak and Jerry Kitzler of Hudson Bay Mining and Smelting Co. Ltd. are thanked for their constructive criticisms of an earlier version of this manuscript. L. Chackowsky is thanked for assistance in producing computer generated plots. E. Truman and G. Corbeil assisted with AutoCAD diagram preparation. K. Dunn and G. Conley assembled the tables. Comments and editorial reviews by K.J. Ferreira, I. Hosain, D. Baldwin, and W.D. McRitchie of Manitoba Department of Energy and Mines and Bill Coker and Gwendy Hall of the Geological Survey of Canada improved the manuscript.

REFERENCES

- Bailes, A.H. and Galley, A. H.
1991: Geological setting of base metal mineralization in the Anderson Lake area; in Report of Field Activities, Manitoba Department of Energy and Mines, Minerals Division, p. 8-13.
- Brooks, R.R.
1983: Biological Methods of Prospecting for Minerals; John Wiley, New York, 322 p.
- Chukhrov, F.V., Churikov, V.S., Ermilova, L.P., and Kalentchuk, G.E.
1979: Background levels of copper and zinc in common plants from various regions of the Soviet Union; Journal of Geochemical Exploration, v. 12, p. 79-86.
- Cleveland, W.S.
1979: Robust locally weight regression and smoothing scatterplots; Journal of the American Statistical Association, v. 74, p. 829-836.
- 1981: LOWESS: a program for smoothing scatterplots by robust locally weighted regression; The American Statistician, v. 35, p. 54.
- DiLabio, R.N.W., Rencz, A.N., and Egginton, P.A.
1982: Biogeochemical expression of a classic dispersal train of metalliferous till near Hopetown, Ontario; Canadian Journal of Earth Sciences, v. 19, p. 2297-2305.
- Dunn, C.E.
1981: The biogeochemical expression of deeply buried uranium mineralization in Saskatchewan, Canada; Journal of Geochemical Exploration, v. 15, p. 437-452.
- 1987: Developments in biogeochemical exploration; in Proceedings of Exploration '87, Third Decennial International Conference On Geophysical and Geochemical Exploration For Minerals and Groundwater, (ed.) G.D. Garland; Ontario Geological Survey, Special Volume 3, p. 417-438.
- Dunn, C.E. and Scagel, R.K.
1989: Tree-top sampling from a helicopter – a new approach to gold exploration; Journal of Geochemical Exploration, v. 34, p. 255-270.
- Erdman, J.A. and Motooka, J.M.
1983: Biogeochemical response at the Greens Creek massive sulphide deposit, Admiralty Island; in United States Geological Survey in Alaska: Accomplishments During 1983; United States Geological Survey, Circular 0945, p. 88-91.
- Fedikow, M.A.F.
1983: Geological and geochemical studies at the Agassiz Au-Ag deposit, Lynn Lake, Manitoba; in Report of Field Activities, Manitoba Department of Energy and Mines, Mineral Resources Division, p. 94-97.
- 1984: Preliminary results of biogeochemical studies in the Lynn Lake area; Manitoba Mineral Resources Division, Open File Report OF84-1, 104 p.
- 1985: The vegetation geochemical signature of the Agassiz stratabound Au-Ag deposit, Lynn Lake, Manitoba; Manitoba Mineral Resources Division, Open File Report OF85-6, 94 p.
- 1986: Detection of gold mineralization and lithologic mapping within the Agassiz Metaltect (Lynn Lake area) utilizing black spruce (*Picea mariana*) bark; Manitoba Mineral Resources Division, Open File Report OF86-6, 61 p.
- Fedikow, M.A.F. and Amor, S.D.
1990: Evaluation of a mercury-vapour detection system in base- and precious metal exploration, northern Manitoba; Journal of Geochemical Exploration, v. 38, no. 3, p. 351-374.
- Fedikow, M.A.F., Athayde, P., and Galley, A.G.
1993: Mineral deposits and occurrences in the Wekusko Lake area, NTS 63J/13; Manitoba Energy and Mines, Mineral Deposit Series Report No. 14, 437 p., including Mineral Deposit Series Map No. 14, scale 1:50 000.
- Fedikow, M.A.F., Ostry, G., Ferreira, K.J., and Galley, A.G.
1989: Mineral deposits and occurrences in the File Lake area, NTS 63K/16; Manitoba Energy and Mines, Mineral Deposit Series Report No. 5, 277 p., including Mineral Deposit Series map No. 5, scale 1:50 000.
- Ferreira, K.J. and Fedikow, M.A.F.
1990: Specific conductance and hydrogen ion concentration as indicators of trace-element geochemical response in humus: Rod Cu-Zn and Big Island Zn-Cu-Au deposits, Manitoba (Canada); Journal of Geochemical Exploration, v. 37, p. 185-203.
- Froese, E. and Moore, J.M.
1980: Metamorphism in the Snow Lake area, Manitoba; Geological Survey of Canada Paper 78-27, 16 p.
- Galley, A.G. and Kitzler, G.H.
1990: Geology and structural setting of the Chisel North deposit (NTS 63K/16); in Report of Activities, Manitoba Department of Energy and Mines, Minerals Division, p. 170-177.
- Galley, A.G., Bailes, A.H., and Kitzler, G.H.
1993: Geological setting and hydrothermal evolution of the Chisel Lake and North Chisel Zn-Pb-Cu-Ag-Au massive sulphide deposits, Snow Lake, Manitoba; Exploration and Mining Geology v. 2, no. 4, p. 271-295.
- Galley, A.G., Bailes, A.H., Syme, E.C., Bleeker, W., Macek, J.J., and Gordon, T.M.
1990: Geology and mineral deposits of the Flin Flon and Thompson Belts, Manitoba. IAGOD Field Trip Guidebook #10, Geological Survey of Canada, Open File 2165, 136 p.

Galley, A.G., Ziehlke, D.V., Franklin, J.M., Ames, D.E., and Gordon, T.M.

- 1986: Gold mineralization in the Snow Lake-Wekusko Lake region, Manitoba; in *Gold In The Western Shield*, (ed.) L.A. Clark; Canadian Institute of Mining and Metallurgy, Special Volume 38, p. 379-398.

Govett, G.J.S.

- 1973: Differential secondary dispersion in transported soils and post-mineralization rocks: an electrochemical interpretation; in *Geochemical Exploration 1972*, (ed.), M.J. Jones; Institute of Mining and Metallurgy, London, p. 81-91.
- 1976: Detection of deeply buried and blind sulphide deposits by measurement of H⁺ and conductivity of closely spaced surface soil samples; *Journal of Geochemical Exploration*, v. 6, p. 359-382.

Hale, M.

- 1993: Mineral deposits and chalcogen gases; *Mineralogical Magazine*, v. 57, p. 599-606.

Hamilton, J.A., Royko, B., Burt, M., and Nichol, I.

- 1991: Geochemical exploration applied to base metal and gold exploration in Ontario; Progress Report for the Period July 1st-December 31st, 1991, Department of Geological Sciences, Queen's University, Kingston, Ontario.
- 1992: Geochemical exploration applied to base metal and gold exploration in Ontario; Final Report, June, 1992, Department of Geological Sciences, Queen's University, Kingston, Ontario, p. C95-C107.

Harrison, J.M.

- 1949: Geology and mineral deposits of File-Tramping Lakes area, Manitoba; Geological Survey of Canada, Memoir 250, 92 p.

Kaszycki, C.A. and Hall, G.E.M.

- 1996: Application of phase-selective and sequential-extraction methodologies in surficial geochemistry; in *EXTECH I: A Multidisciplinary Approach to Massive Sulphide Research in the Rusty Lake-Snow Lake Greenstone Belts, Manitoba*, (ed.) G.F. Bonham-Carter, A.G. Galley, and G.E.M. Hall; Geological Survey of Canada, Bulletin 426.

Lucas, S.B., Stern, R.A., and Syme, E.C.

- in press: Flin Flon greenstone belt: intraoceanic tectonics and the development of continental crust (1.92-1.84 Ga); *Geological Society of America Bulletin*.

Nielsen, E. and Fedikow, M.A.F.

- 1987: Glacial dispersion of trace elements in Wisconsinan till in the Dot Lake-MacLellan Mine area, Lynn Lake, Manitoba; Manitoba Mineral Resources Division, Open File Report OF87-2, 45 p.

Smee, B.W.

- 1983: Laboratory and field evidence in support of the electro-geochemically enhanced migration of ions through glaciolacustrine sediment; *Journal of Geochemical Exploration*, v. 19, p. 277-304.

Contribution to the 1989-1994 Rusty Lake-Snow Lake Mining Camps, Canada-Manitoba Exploration Science and Technology Initiative (EXTECH I)

Results of a detailed infill lake-sediment survey in the Snow Lake area: evaluation and comparison of grab sample and short core data

P.W.B. Friske¹ and M.W. McCurdy¹

Friske, P.W.B. and McCurdy, M.W., 1996: Results of a detailed infill lake-sediment survey in the Snow Lake area: evaluation and comparison of grab sample and short core data; in EXTECH I: A Multidisciplinary Approach to Massive Sulphide Research in the Rusty Lake-Snow Lake Greenstone Belts, Manitoba, (ed.) G.F. Bonham-Carter, A.G. Galley, and G.E.M. Hall; Geological Survey of Canada, Bulletin 426, p. 257-277.

Abstract: As part of the Exploration Science and Technology Initiative (EXTECH) program a detailed infill lake-sediment and water survey was undertaken in the Snow Lake area during the fall of 1991. This involved the collection of 346 lake sediment grab samples and concomitant waters. In 1993, additional work was undertaken involving the collection of 23 short cores from selected grab sample sites. The primary objectives of the infill survey and short core work were to: 1) evaluate the effectiveness of lake sediment geochemistry in detecting known mineralization in the Snow Lake area; 2) evaluate and develop new approaches in the use of lake sediment geochemistry; and, 3) define, if possible, new exploration targets.

At most sites, data from the cores verify the original grab sample results. However, at a few sites the original anomalous grab sample results are interpreted as being related to contamination as opposed to naturally elevated levels. An unusually thick sequence of contaminated surface sediments with extremely high concentrations of trace metals is a likely contributing factor, a condition which is restricted to lakes in the immediate vicinity of local anthropogenic activity. Collection of lake cores provides a useful new approach to the follow-up of grab sample data and to the application of lake sediment geochemistry, particularly in areas with significant local contamination.

Much of the known mineralization in the area is clearly reflected by the lake sediment data. Character of the anomalies mirror the composition of the nearby mineralization. The lake sediment data also identify a number of areas that warrant further investigation, several of which are discussed.

Résumé : Dans le cadre du Programme de science et technologie de l'exploration (EXTECH), on a entrepris, au cours de l'automne de 1991, un levé détaillé des sédiments et des eaux lacustres dans la région de Snow Lake. On a ainsi prélevé à la benne 346 échantillons de sédiments lacustres et des eaux concomitantes. En 1993, on a en outre prélevé 23 carottes courtes à des sites d'échantillonnage choisis. Les principaux objectifs du levé et du carottage étaient les suivants : 1) évaluer l'efficacité de la géochimie des sédiments lacustres à détecter la minéralisation connue dans la région de Snow Lake; 2) évaluer et élaborer de nouvelles méthodes d'application de la géochimie des sédiments lacustres; et 3) définir, si possible, de nouvelles cibles d'exploration.

¹ Geological Survey of Canada, 601 Booth St., Ottawa, Ontario K1A 0E8

À la plupart des sites, les données sur les carottes ont servi à vérifier les résultats d'analyse des échantillons recueillis à la benne. Cependant, à certains sites, les concentrations anormales établies dans les échantillons prélevés à la benne sont considérées comme liées à une contamination et non comme étant naturellement élevées. Une séquence inhabituellement épaisse de sédiments superficiels contaminés dont les concentrations en métaux traces sont très élevées est probablement un facteur expliquant ce phénomène, qui se limite aux lacs des environs immédiats de l'activité anthropique locale. La collecte de carottes lacustres représente une nouvelle méthode utile pour corroborer les résultats obtenus par échantillonnage à la benne et constitue une autre façon d'établir la géochimie des sédiments lacustres, en particulier dans les zones qui sont par endroits significativement contaminées.

La presque totalité de la minéralisation connue dans la région ressort nettement des données sur les sédiments lacustres. Le caractère des anomalies reflète la composition de la minéralisation voisine. Les données sur les sédiments lacustres permettent en outre d'identifier un certain nombre de zones qui justifient une recherche plus approfondie; plusieurs d'entre elles sont identifiées dans le présent article.

INTRODUCTION

The Geological Survey of Canada (GSC) and provincial geological surveys have collected lake sediment samples from over 190 000 sites throughout Canada under the auspices of the National Geochemical Reconnaissance (NGR) program (Fig. 1). The surveys were initially undertaken to assist mineral exploration by mapping regional geochemical patterns and anomalous element concentrations potentially related to economic mineral deposits (Friske and Hornbrook, 1991). Recently, the data have been used in environmental studies providing valuable information on the natural distribution and baseline levels for upwards of 35 elements (e.g. Friske et al., 1994; Friske and Coker, 1995).

To better understand the processes that control element distribution in the surficial environment, orientation and follow-up studies are being undertaken on particular aspects of lake and stream sediment geochemistry. Information obtained from these directed studies are used to enhance interpretative techniques for the voluminous NGR database. To this end, a detailed lake sediment and water survey around Snow Lake, Manitoba was completed during late September and early October 1991, as part of the Exploration Science and Technology Initiative (EXTECH). Part of the survey area, which covers all of sheet 63K/16 and the west half of 63J/13, had been previously surveyed in 1985 and the data released as part of GSC Open File 1212 (Geological Survey of Canada, 1986) (see Fig. 2). Resampling of sheet 63K/16 was undertaken during the 1991 survey primarily to increase the sample density, which was 1 sample per 13 km² in the original reconnaissance survey and 1 sample per 3.9 km² in the 1991 infill survey. All results of the 1991 infill survey have been released as GSC Open File 3015 (Friske et al., 1995).

In November 1993, 23 lake sediment short-cores were taken from selected sites in the Snow Lake area. Site selection was guided by results of the 1991 infill lake-sediment survey. The primary objectives of the infill survey and short core work were to: 1) evaluate the effectiveness of lake sediment geochemistry in detecting known mineralization in the Snow Lake area; 2) evaluate and develop new approaches in the use of lake sediment geochemistry; and, 3) define, if possible, new exploration targets.

STUDY AREA

Bedrock geology

The Snow Lake area occurs at the eastern end of the Flin Flon-Snow Lake volcanic belt. The general geology of the study area has been variously described by Armstrong (1941), Harrison (1949), Price (1977), Bailes (1980), Froese and Moore (1980), Walford and Franklin (1982), and Bailes and Galley (1991). Two distinct sequences of supracrustal rocks have been identified (Fig. 3). The Amisk Group, a metamorphosed island-arc assemblage of volcanic and sedimentary rocks dated at 1892 Ma (Machado and David, 1992), is the oldest of the two and is host to all of the significant volcanic-hosted massive sulphide (VHMS) deposits in the area. The metasediments predominate in the upper portion of the over 5000 m thick sequence, which is intruded by numerous synvolcanic intrusions including the Sneath Lake and Richard Lake plutons (Galley et al., 1993). The Missi Group unconformably overlies Amisk Group rocks and is made up of fluvial-alluvial sandstones and conglomerates.

The northern edge of the study area is bounded by high-grade sedimentary and igneous rocks of the Kisseynew Gneiss Belt which are separated from the rocks to the south by faults, changes in the dominant rock type, or rapid increases in the metamorphic grade (Connors and Ansdell, 1994). South of the survey area, Ordovician dolomitic limestone and dolomite of the Red River Formation overlie the Proterozoic basement.

Mineralization

The area around Snow Lake was first prospected for gold, and the town of Snow Lake was built around the Nor-Acme mine which produced 19 million grams of gold from 1948 to 1959 (Walford and Franklin, 1982). The deposit, at the north end of Snow Lake, occurs as a fault-controlled replacement deposit along east-trending faults – the McLeod Road Fault and the Snow Lake Fault. The ore zones are silicified and carbonatized. Highest gold values are in quartz veins. The mineral assemblage includes arsenopyrite, pyrrhotite,

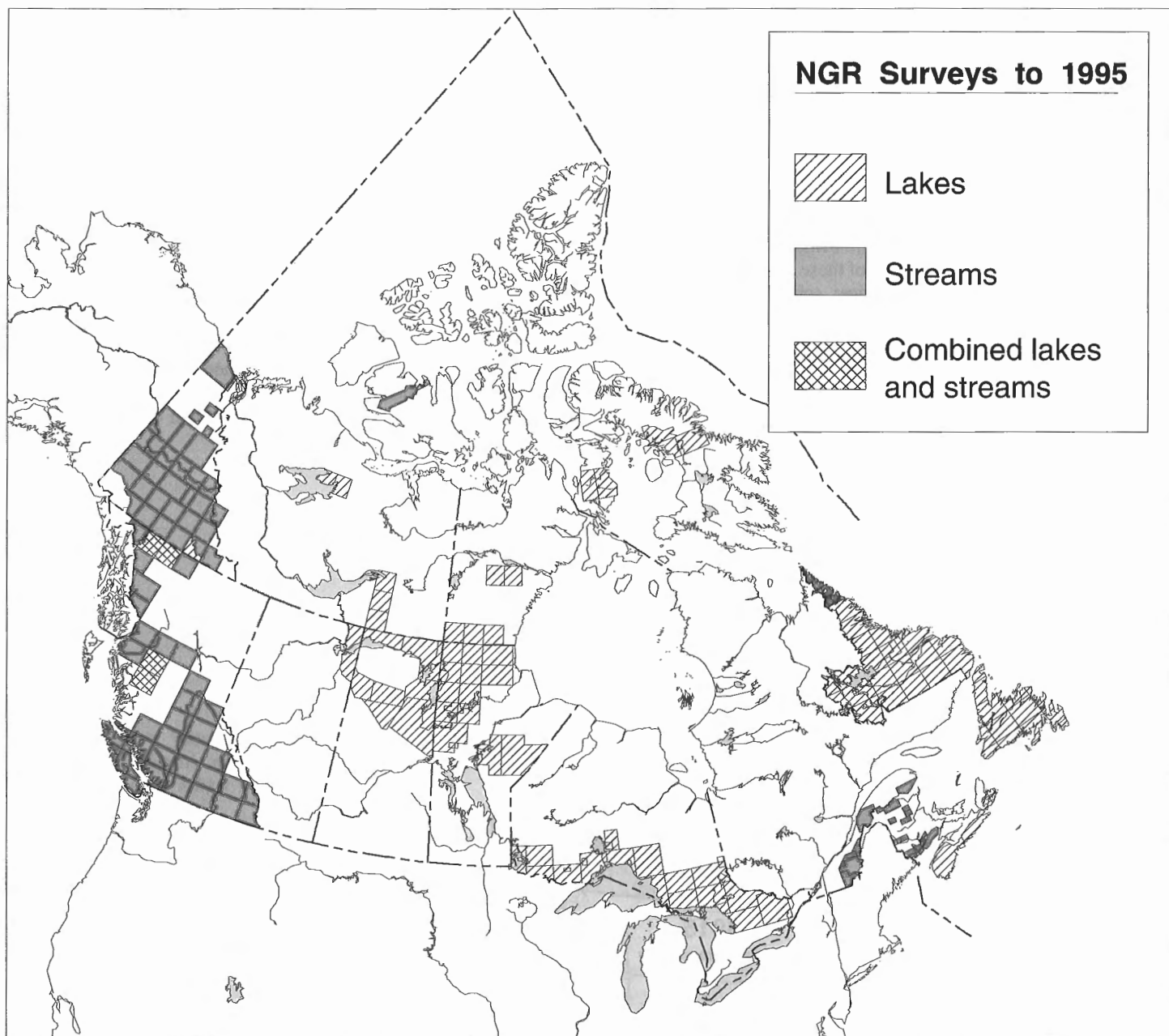


Figure 1. National Geochemical Reconnaissance (NGR) coverage in Canada to 1995.

pyrite, chalcopyrite, native Au, with tourmaline and axinite. Mineralization follows faults cutting basaltic to andesitic tuffs, gabbro, and dacitic to rhyolitic tuffs (Ziehlke, 1983).

More recently, base metal volcanic-hosted massive sulphide deposits have provided the economic mainstay of the area. The first massive sulphide deposit to open was the Chisel Lake open pit in 1960, and at present there are more than a dozen known volcanic-hosted massive sulphide deposits within the Amisk Group. Galley et al. (1993), have recognized three distinct sulphide-rich intervals within this package of supracrustal rocks. The lowest mineralized horizon is characterized by Cu-rich volcanic-hosted massive sulphide deposits, i.e., the Anderson, Stall, and Rod deposits. For example, the Anderson mine is a single elongated lens composed primarily of pyrite, chalcopyrite, and pyrrhotite with minor sphalerite that produced 3.2 million tonnes grading 3.44% Cu and 0.1% Zn. (Walford and Franklin, 1982).

The second mineralized interval is marked by an uneconomic thin sulphide-chert-tuff unit that extends for 15 km. The third and stratigraphically youngest horizon, is characterized by Zn-rich deposits (e.g. Chisel Lake, North Chisel, Ghost Lake, and Lost Lake) as opposed to the Cu-rich deposits formed during the earlier event. Principal sulphides in the Chisel Lake orebody, the largest of these Zn-rich deposits, are in order of decreasing abundance: sphalerite, pyrite, pyrrhotite, chalcopyrite, galena, and arsenopyrite (Williams, 1966). The average grade of the 7.3 million tonne deposit was 10.9% Zn and 0.6% Cu.

For a detailed description of these and more than 150 other mineral deposits and occurrences within the study area the reader is referred to Fedikow et al. (1989) and Fedikow et al. (1993).

Physiography and surficial deposits

Klassen (1986) named the physiographic region within which the survey area falls the Southern Indian bedrock plateau. Vegetation consists mainly of thin stands of conifers, mostly black spruce, and burned over areas are common. Relief changes with the underlying bedrock, with the highest elevations in areas of intrusive rocks and relatively moderate relief over metasedimentary and metavolcanic rocks. Relief within individual catchment basins does not exceed 50 m. Drainage is to the northeast into Hudson Bay.

Till deposits were left by the Keewatin ice lobe, centered north and west of the survey area, during the Late Wisconsin glacialation. Ice flow was south to southwest, towards 210° (Mihychuk, 1988a, b). Based on striations, similar ice flow directions have been noted along the southeast shore of Wekusko Lake just outside the study area (McMartin, 1994) and in the immediate vicinity of Snow Lake (Clark, 1989). Exposed till is rare, some lodgment till and diamicton are found on the lee sides of bedrock knolls. Isolated deposits of glaciofluvial sands and gravels are noted in a few areas.

Glaciolacustrine silts and clays related to glacial Lake Agassiz overlie much of the area, and areally extensive bogs and swamps have formed over grey or brown clay between

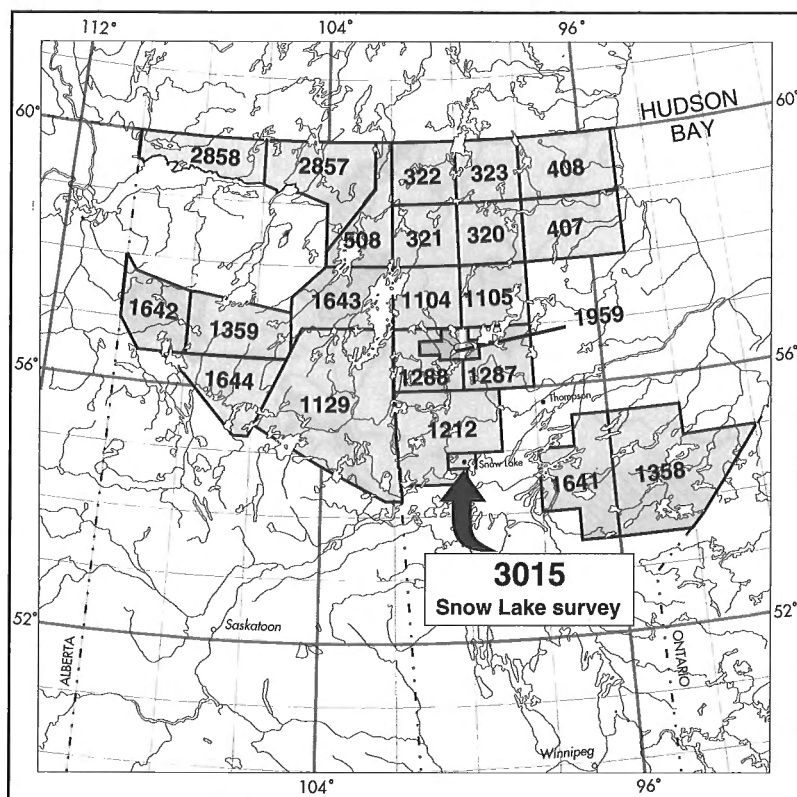


Figure 2.

NGR lake sediment and water coverage in Manitoba and Saskatchewan. Numbers refer to GSC Open Files through which such data are made publicly available.

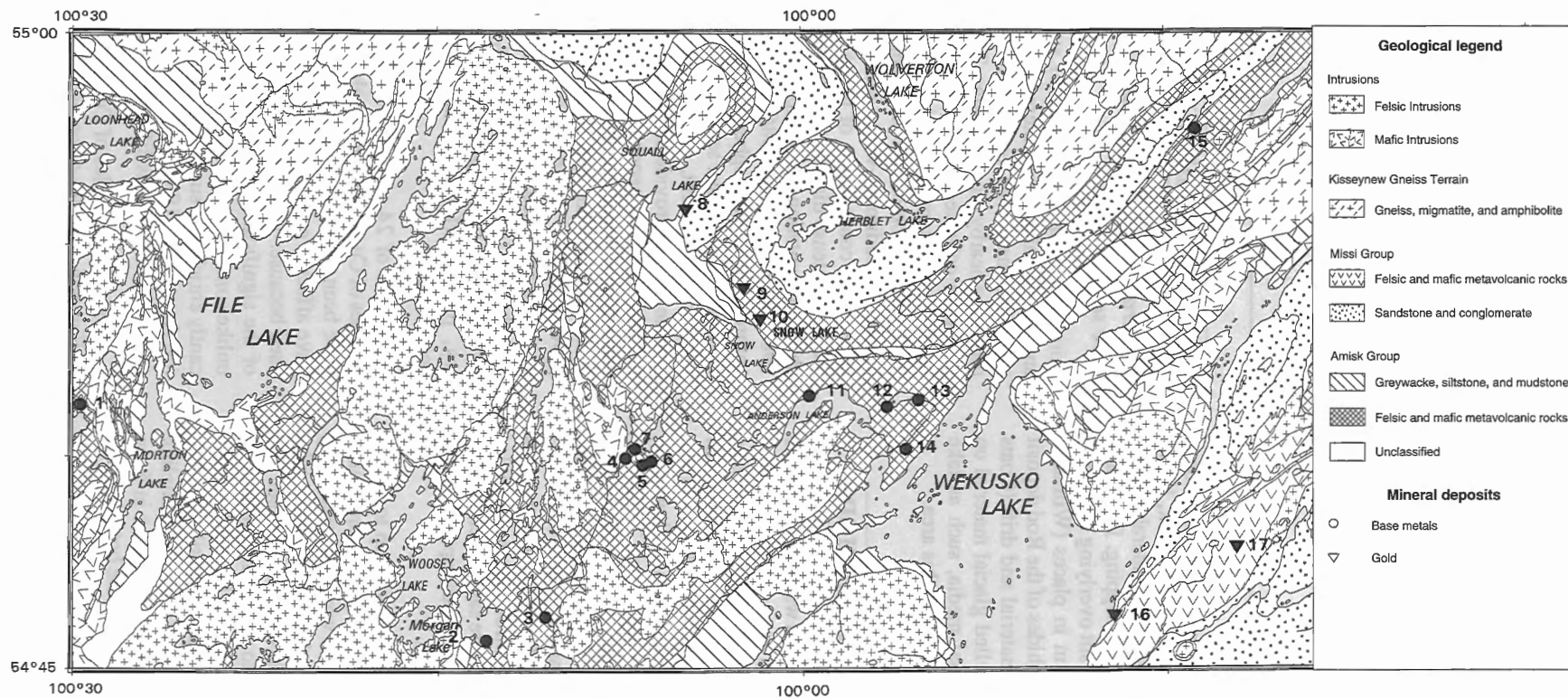


Figure 3. Bedrock geology and selected mineral deposits of Snow Lake survey area (modified after Fedikow et al., 1989 and Fedikow et al., 1993). Mineral deposits: 1 – Dickstone; 2 – Morgan Lake; 3 – Pot Lake; 4 – Chisel Lake; 5 – Lost Lake; 6 – Ghost Lake; 7 – Chisel North; 8 – Squall Lake; 9 – Snow Lake mines; 10 – Nor-Acme; 11 – Anderson Lake; 12 – Stall Lake; 13 – Rod; 14 – Linda; 15 – Osborne Lake; 16 – Rex-Laguna 17 – Ferro.

Table 1. Variables determined and methods used for Snow Lake lake sediment and water samples.

| LAKE SEDIMENT | LAKE WATER |
|---|---|
| Ag, Cd, Co, Cu, Fe, Mn, Mo, Ni, Pb, V, Zn (atomic absorption spectrometry) | pH (glass calomel electrode and pH meter) |
| F (ion selective electrode) | F (ion selective electrode) |
| As, Au, Ba, Br, Ce, Co, Cr, Cs, Eu, Fe, Hf, La, Lu, Mo, Na, Ni, Rb, Sb, Sc, Sm, Ta, Tb, Th, U, W, Yb (instrumental neutron activation analysis) | U (laser-induced fluorescence) |
| Hg (cold vapour extraction-atomic absorption spectrometry) | |
| LOI (gravimetry) | |

higher areas of exposed rock. In some areas, nearshore deposits of sand and gravel have been mapped (Clark, 1989). Exploration programs have encountered considerable overburden thicknesses during drilling and stripping. For example, till and glaciolacustrine clay and silt overlying the Chisel Lake deposit were in excess of 50 m in places (Williams, 1966), and surface expression of sulphides of the Rod deposit was buried under 17 m of organic material and drift (Coats et al., 1970). The effects of far travelled glacial material on the geochemical response in surficial media, such as lake sediment, therefore need to be considered in this area.

SAMPLING AND ANALYTICAL METHODS

During the fall of 1991, lake sediment and water samples were collected from 346 sites covering an area of approximately 1340 km² (NTS 63K/16 and 63J/13W/2) (see Fig. 4). These were collected using standard NGR methodology, details of which are given in Friske and Hornbrook (1991) and Friske (1991). Lake sediments were taken with a hollow-pipe, bottom-valve sampler from a float-equipped Bell 206B helicopter. Sediment and water samples were analyzed for a wide range of variables by a number of different techniques, summarized in Table 1. Quality of the analytical data was monitored and controlled using a sampling design that incorporates field duplicate, blind duplicate, and control reference samples at a frequency of 5% throughout the entire sample set. All data have been published along with detailed descriptions of the survey procedures (Friske et al., 1995).

In November of 1993 lake sediment cores, up to 1 m in length, were collected from selected sites (Fig. 4) previously sampled during the 1991 survey. These were collected using a modified Kajak-Brinkhurst corer. A 1.1 m long acrylic tube (inside diameter 7.0 cm) was attached to the sampler and slowly lowered into the sediment to avoid disturbance of material at the sediment-water interface. After retrieval the core tubes were sealed and carried upright until extruded. Subsectioning was completed within 24 hours. Sampling intervals were 0 to 2 cm, 2 to 5 cm, and 5 to 20 cm in 5 cm intervals, and then generally from 20 cm to the bottom of the core in 10 cm intervals. In the laboratory the samples were freeze dried and then passed through an 80 mesh sieve to disaggregate the sample and remove larger fragments. Samples were then analyzed for the same suite of variables determined in the 1991 survey samples (Table 1).

RESULTS AND DISCUSSION

General discussion and comparison of grab and core sample data

Initial interpretation of the 1991 survey data suggested that anomalous values encountered at some sites could be related to contamination as opposed to naturally elevated levels reflecting nearby mineralization. The original 1991 grab samples were collected using a Hornbrook sampler. In general lake sediment samples obtained using this device represent a 30-35 cm section of lake sediment from at least 10 to 20 cm below the sediment-water interface (Friske, 1991). This reflects the composition of the relatively stable zone below the most intense diagenetic activity and, assuming a reasonable sedimentation rate of up to 2.5 mm·a⁻¹ (cf. Wong et al., 1984; Johnson et al., 1986; Fortescue, 1988), predates any anthropogenic atmospheric component. Therefore it was decided to collect lake sediment cores to: 1) determine if, and if so to what extent, contamination has affected the grab sample data; 2) provide additional information to characterize the lake sediment geochemical dispersion pattern related to known mineralization; and 3) evaluate the ability of lake sediment cores to "see through" local contamination and provide data on "natural" element concentrations which pre-date contamination. If lake sediment coring can be used to "see through" local contamination, it would provide a useful new approach to the application of lake sediment geochemistry, particularly in areas that have been extensively contaminated.

A total of 24 cores were collected (Fig. 5). Down core profiles of Cu and Zn were evaluated to determine which sites have been contaminated, and as a result were most likely to have affected grab sample results. These two elements were used because: 1) one or both are major constituents of most of the significant mineralization in the area; 2) Cu and Zn, unlike some elements such as As, are not likely to be significantly enriched in surface sediments due to diagenetic cycling (cf. Azcue et al., 1994; Friske, 1995); and, 3) the data are very reproducible, which is difficult for some elements such as Au.

Down core profiles of Cu and Zn from 4 cores are shown in Figure 6. Profiles of cores K/01 and J/02 (Fig. 6a, b) are typical of contaminated sites, displaying a marked increase in Cu and/or Zn in the upper portion that decreases down section until a relatively constant background value is

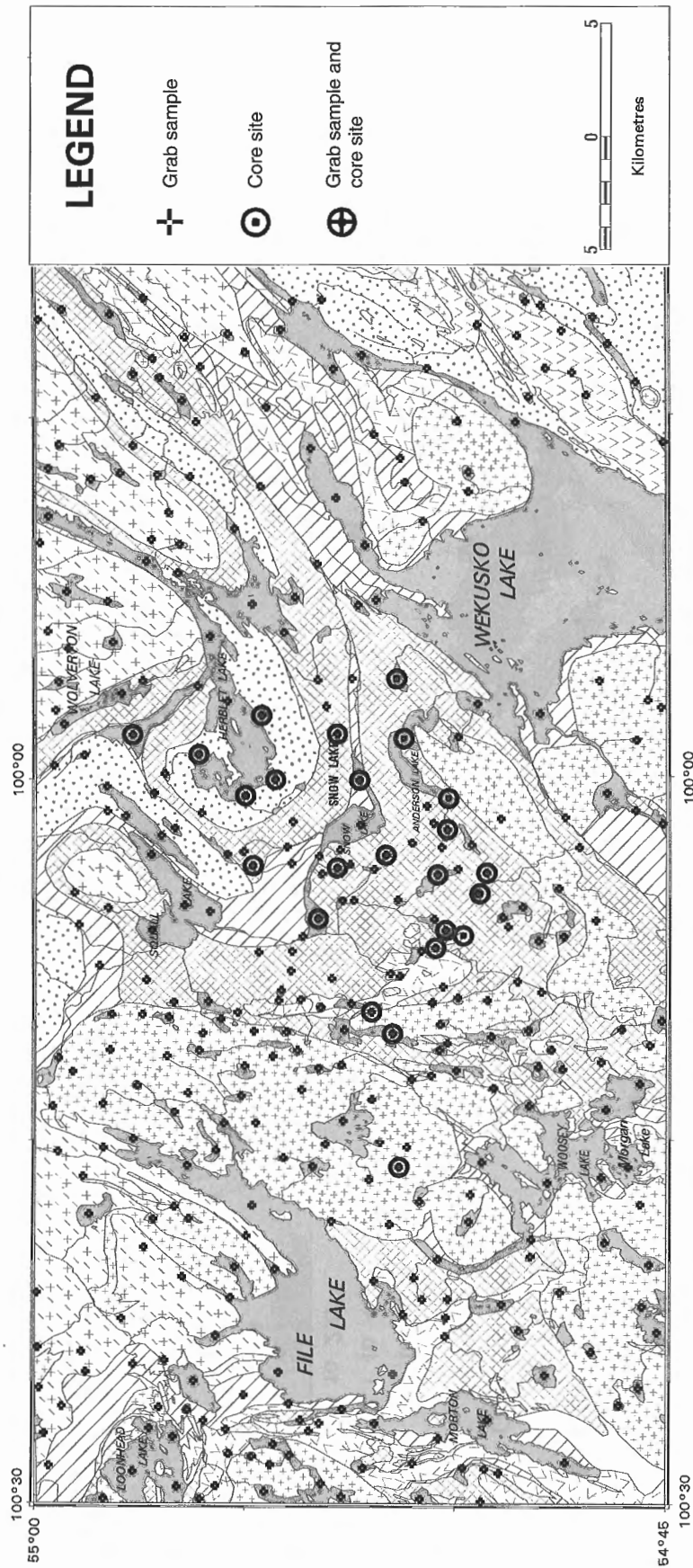


Figure 4. Location of lake sediment grab samples and core sites.

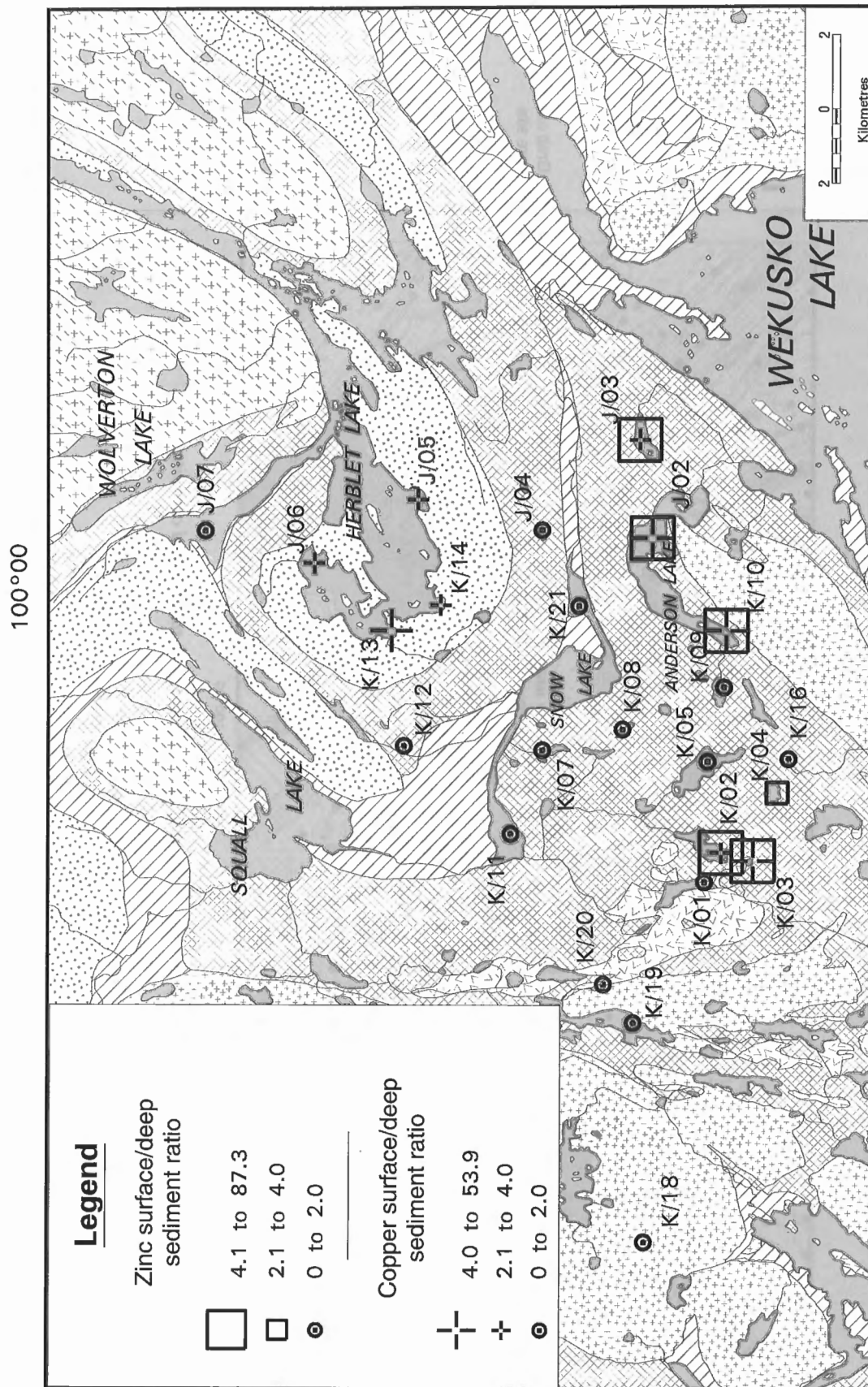


Figure 5. Core locations and surface to deep sediment ratio for Cu and Zn (ppm) at each site.

reached. Similar trends often also occur for one or more elements including As, Pb, Hg, Ag, Cd, and Au. The change from elevated levels to relatively constant background values is variable, occurring as shallow as the 5 to 10 cm interval or as deep as the 20 to 30 cm interval. Cores J/04 and K/20 (Fig. 6c, d (location on Fig. 5)) illustrate the down-core profiles encountered at sites unaffected by local contamination, that is, the concentrations of Cu and Zn are essentially constant throughout the length of the core.

Based on these and the other lake sediment profiles, "background" or "deep" sediment values, referred to in the following discussions, represent the average concentration of all samples extending from 30 cm to the bottom of the core at a given site. This is considered to be analogous to the "natural" concentration levels that predate any possible local anthropogenic input. In contrast, "surface" sediments refer to the upper 15 cm of the core.

Table 2 and Figure 7 summarize the ratio of surface to deep sediment values for Cu and Zn at all coring sites. Values less than two are considered to represent uncontaminated sites whereas values greater than two reflect varying degrees of contamination of the surface sediments. These data show that the surface sediments of lakes in the immediate vicinity of the major mining activity in the Chisel Lake and Anderson Lake areas are contaminated to varying degrees in both Cu and Zn (e.g. Anderson Lake, Ghost Lake, Potten Lake, and Stall Lake).

Four sites in the southwestern end of Herblet Lake show enrichment of Cu (but not Zn) in the surface sediments (Fig. 5). This likely reflects a migration of material from two small tailing ponds just northeast of Snow Lake, which have an outflow that enters Herblet Lake in the vicinity of coring site K/13 (Fig. 5). Two factors supporting this are 1) similar

geochemical signature to the contamination (i.e., highly enriched in Cu relative to Zn) of two grab samples taken from the tailings pond; and, 2) the highest ratio of surface to background Cu occurs at the coring site (K/13) closest to the inflow from the tailings ponds.

Figure 5 also shows that most of the other lakes in the area are not significantly contaminated, indicating that there has been no widespread airborne contamination. Significant contamination appears only to occur in lakes in the immediate vicinity of mining activity (i.e. roads, pits, etc.) or lakes linked to tailings ponds.

To evaluate the effects of contamination on the original grab sample results, the grab sample data for Cu and Zn is compared to the average surface (0-15 cm) and deep (>30 cm) sediment values (Table 2 and Fig. 7). At most sites the surface sediment, deep sediment, and grab sample values are comparable. The largest differences occur at sites which have the greatest level of contamination as indicated by high levels of Cu and Zn in the surface sediment. For example, grab sample values from sites 63J/02, 63K/03, and 63K/10 are considerably higher than the corresponding deep sediment values (Fig. 7). This suggests that the grab samples, in these cases, have a component of the surface sediment.

Using the average surface and deep sediment composition determined for these sites (Table 2), the relative proportion of each required to produce the observed grab sample value, was calculated (Table 3). The most notable feature of these data is that they indicate that the surface sediment component within the grab samples is relatively small, averaging 3% based on the Cu data and 6% based on the Zn data. The difference in the calculated value between the two elements likely reflects sampling and analytical variability and highlight the inexact nature of these calculations.

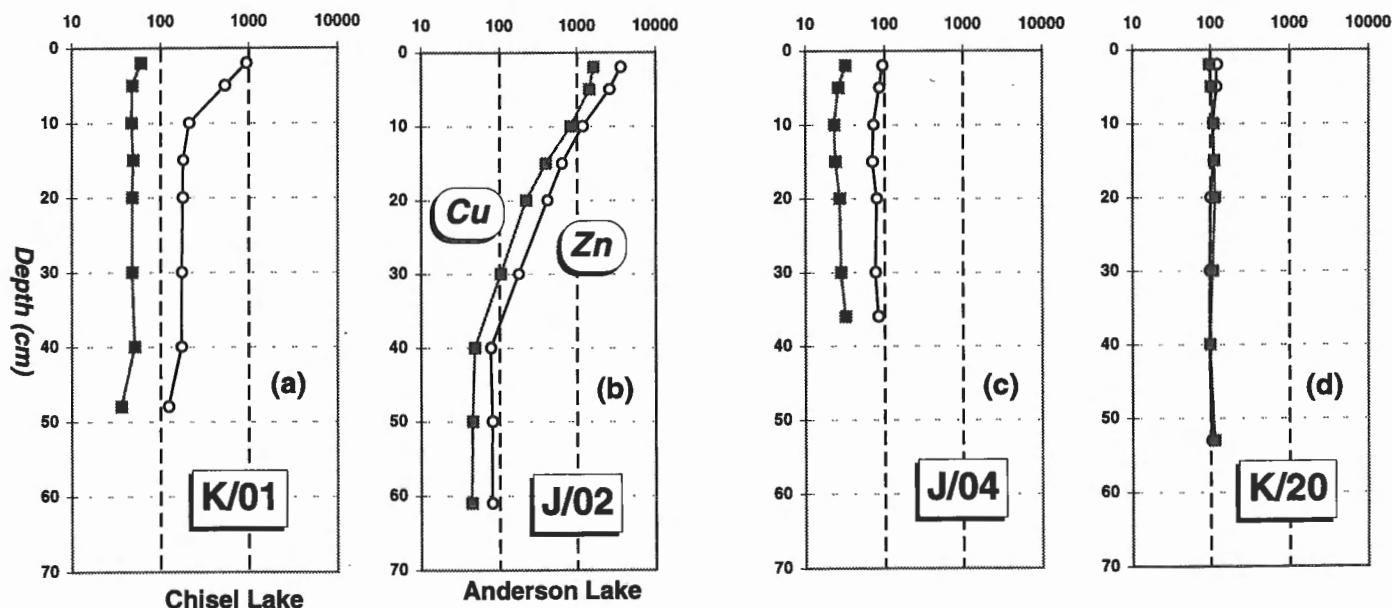


Figure 6. Down core profiles of Cu and Zn in selected cores.

Table 2. Average surface and deep sediment concentration and ratio of the two for Cu and Zn. Also shown are data for the grab samples collected at these sites during the 1991 infill survey.

| Core | Cu (ppm) | | | | Zn (ppm) | | | |
|--------|-------------|------------------|---------------|-----------|-------------|------------------|---------------|-----------|
| | Grab sample | Surface sediment | Deep sediment | S/D ratio | Grab sample | Surface sediment | Deep sediment | S/D ratio |
| 63J/02 | 75* | 1065 | 51 | 20.9 | 191* | 1993 | 79 | 25.2 |
| 63J/03 | 120* | 159 | 55 | 2.9 | 1200* | 1558 | 102 | 15.3 |
| 63J/04 | 25 | 26 | 32 | 0.8 | 89 | 80 | 83 | 1.0 |
| 63J/05 | 50 | 92 | 31 | 3.0 | 132 | 93 | 80 | 1.2 |
| 63J/06 | 34 | 257 | 36 | 7.1 | 124 | 146 | 106 | 1.4 |
| 63J/07 | 58 | 72 | 64 | 1.1 | 141 | 110 | 112 | 1.0 |
| 63K/01 | 36 | 51 | 44 | 1.2 | 245 | 465 | 148 | 3.1 |
| 63K/02 | 30 | 68 | 33 | 2.1 | 138 | 1111 | 81 | 13.7 |
| 63K/03 | 103* | 1282 | 47 | 27.3 | 2200* | 23,753 | 272 | 87.3 |
| 63K/04 | 15 | 44 | 22 | 2.0 | 152 | 434 | 113 | 3.8 |
| 63K/05 | 20 | 24 | 25 | 1.0 | 155 | 157 | 109 | 1.4 |
| 63K/07 | 46 | 42 | 58 | 0.7 | 105 | 141 | 75 | 1.9 |
| 63K/08 | 24 | 35 | 25 | 1.4 | 94 | 114 | 81 | 1.4 |
| 63K/09 | 34 | 43 | 42 | 1.0 | 136 | 105 | 78 | 1.3 |
| 63K/10 | 140* | 3125 | 58 | 53.9 | 272* | 5408 | 118 | 45.8 |
| 63K/11 | 35 | 46 | 46 | 1.0 | 120 | 123 | 109 | 1.1 |
| 63K/12 | 137 | 139 | 138 | 1.0 | 102 | 73 | 63 | 1.2 |
| 63K/13 | 101 | 673 | 56 | 12.0 | 120 | 115 | 91 | 1.3 |
| 63K/14 | 37 | 107 | 34 | 3.1 | 108 | 87 | 86 | 1.0 |
| 63K/16 | 8 | 19 | 11 | 1.7 | 293 | 255 | 180 | 1.4 |
| 63K/18 | 19 | 23 | 31 | 0.7 | 380 | 45 | 290 | 0.2 |
| 63K/19 | 52 | 51 | 59 | 0.9 | 146 | 120 | 108 | 1.1 |
| 63K/20 | 103 | 104 | 106 | 1.0 | 128 | 114 | 100 | 1.1 |
| 63K/21 | 51 | 70 | 53 | 1.3 | 94 | 144 | 77 | 1.9 |

Surface-to-deep sediment ratio >2.0
 * Data not published in Open File 3015

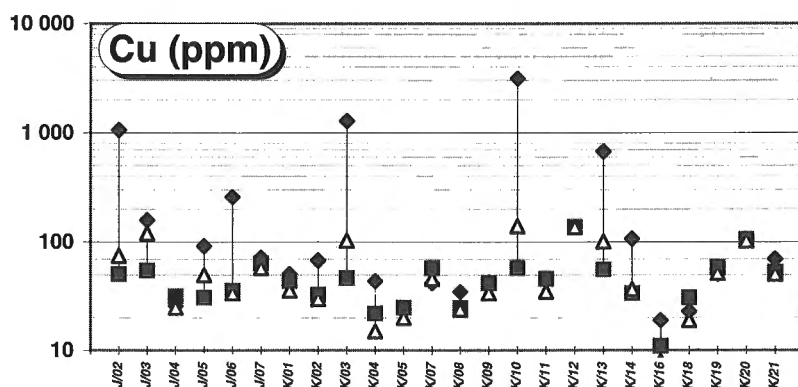
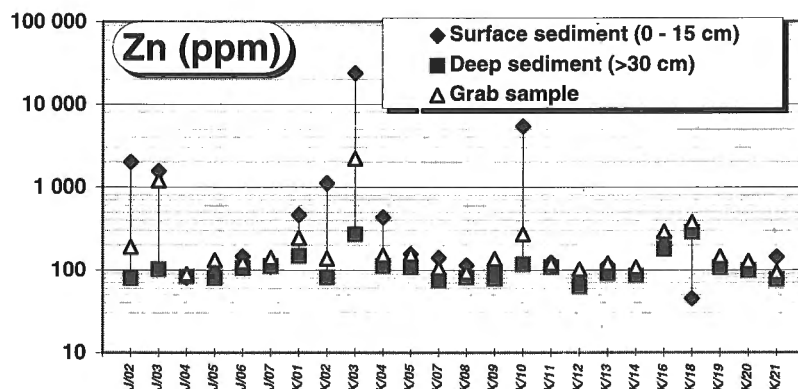


Figure 7.

Comparison of Cu and Zn data for surface sediment, deep sediment and grab samples at all coring sites.



The elevated levels encountered in the grab samples at these three sites are therefore not so much related to a large incorporation of contaminated surface material but rather inclusion of a small amount of highly contaminated material. For example, if more typical levels of contamination existed at the three sites (2 or 3 times the deep sediment values), the concentration of Cu and Zn in the original grab sample would not have been significantly different from that of the deep sediment as illustrated in Figure 8. Inclusion of a small amount of surface material with the deep sediment may have occurred as the sampler passed through the surface sediments during its drop and/or retrieval.

Table 3. Calculated proportions of surface and deep sediment required to produce the observed grab sample values.

| Core | Cu (ppm) | | | | |
|------|------------------|---------------|-------------|------------------|---------------|
| | Surface sediment | Deep sediment | Grab sample | Per cent surface | Per cent deep |
| J/02 | 1065 | 51 | 75 | 3% | 97% |
| K/03 | 1282 | 49 | 103 | 4% | 96% |
| K/10 | 3125 | 58 | 140 | 3% | 97% |
| Core | Zn (ppm) | | | | |
| | Surface sediment | Deep sediment | Grab sample | Per cent surface | Per cent deep |
| J/02 | 1993 | 79 | 191 | 6% | 94% |
| K/03 | 23 753 | 272 | 2 200 | 8% | 92% |
| K/10 | 5408 | 118 | 272 | 3% | 97% |

It is also possible that the elevated levels encountered in the three grab samples are to some extent a consequence of the considerable thickness of contaminated surface sediments at some sites. As noted previously, contaminated sediments extend to a depth of about 30 cm. In this situation, penetration of the Hornbrook sampler to 20 cm, as designed, would still result in the incorporation of contaminated sediment in the grab sample.

In summary, it would appear that some of the anomalous values encountered in 1991 survey data are related to contamination as opposed to naturally elevated levels. Unusually thick surface sediments with extremely elevated concentrations of trace metals are likely contributing factors. However since there is no widespread airborne contamination of the lakes in the area, these conditions are likely only to be encountered within lakes in the immediate vicinity of significant local anthropogenic activity (i.e. roads, railways, mining pits, tailings ponds, etc.).

Characterization of lake sediment response to known mineralization

Table 4 lists summary statistics for the 1991 Snow Lake infill survey data, and regional data from over 31 000 NGR sites throughout Manitoba and Saskatchewan (Fig. 2). It is evident that, for some elements, there are significant differences between the two data sets. For example, the median As value of 5.3 ppm for the Snow Lake data is more than twice that of the regional value of 2.3 ppm. Threshold levels (herein somewhat arbitrarily defined as the value separating background

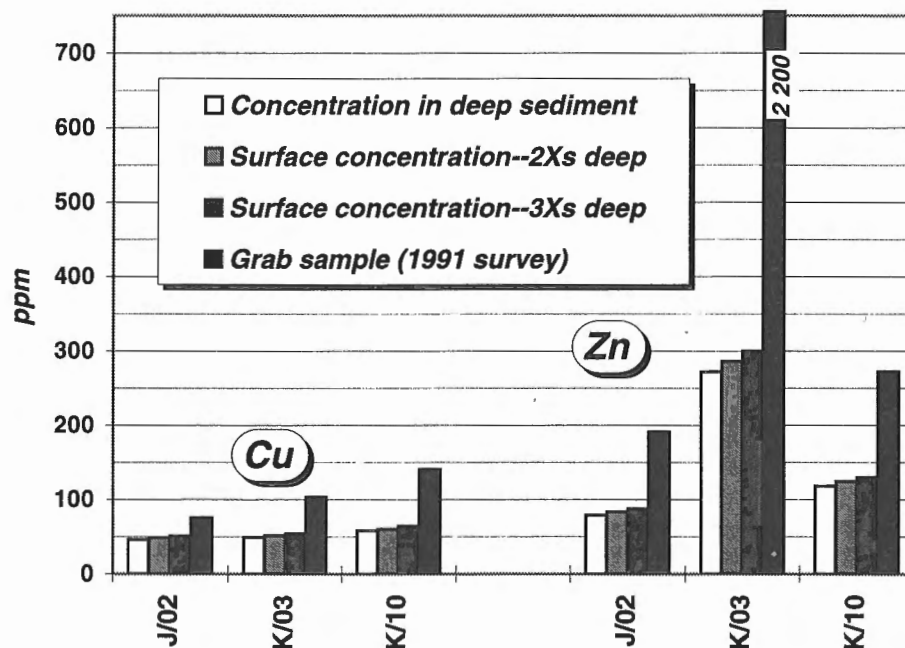


Figure 8. Calculated composition of grab samples assuming incorporation of 5% surface and 95% deep sediment. Calculations based on concentrations within the surface sediment that are either 2 or 3 times that of the deep sediment. Deep sediment and original grab sample values are also shown.

Table 4. Summary statistics for the Snow Lake infill survey, and regional data from over 31 000 NGR sites throughout Manitoba and Saskatchewan.

| | Ag | | As | | Au | | Br | | Cd | | Cu | | Hg | | Pb | | Sb | | Zn | |
|-----------------------|--------|-------|------|------|--------|------|------|------|--------|------|--------|------|--------|--------|--------|------|-------|-------|--------|---------|
| | R | SL | R | SL | R | SL | R | SL | R | SL | R | SL | R | SL | R | SL | R | SL | R | SL |
| Number of values | 31 006 | 338 | 6041 | 338 | 10 201 | 338 | 6041 | 338 | 17 336 | 338 | 31 006 | 338 | 30 036 | 338 | 31 005 | 338 | 6041 | 338 | 31 005 | 338 |
| Detection limit | 0.2 | 0.2 | 0.5 | 0.5 | 2 | 2 | 0.5 | 0.5 | 0.2 | 0.2 | 2 | 2 | 10 | 10 | 2 | 2 | 0.1 | 0.1 | 2 | 2 |
| Units | ppm | ppm | ppm | ppm | ppb | ppb | ppm | ppm | ppm | ppm | ppm | ppm | ppb | ppb | ppm | ppm | ppm | ppm | ppm | ppm |
| Analytical method | AAS | AAS | INA | INA | INA | INA | INA | INA | AAS | AAS | AAS | AAS | CV-AAS | CV-AAS | AAS | AAS | INA | INA | AAS | AAS |
| Mean | <0.2 | <0.2 | 3.3 | 9.4 | <2 | 2.1 | 45 | 45 | 0.13 | 0.22 | 22.6 | 30.6 | 54 | 51 | 3.6 | 5.3 | 0.08 | 0.13 | 102 | 153 |
| Std error of the mean | 0.001 | 0.01 | 0.05 | 1.5 | 0.06 | 1.25 | 0.38 | 1.23 | 0.006 | 0.35 | 0.39 | 1.08 | 0.19 | 1.04 | 0.04 | 0.24 | 0.002 | 0.011 | 0.85 | 19.2 |
| Std deviation | 0.22 | 0.18 | 3.9 | 26.7 | 4.63 | 22.9 | 29.2 | 22.5 | 0.84 | 0.65 | 68.9 | 19.9 | 33 | 19.1 | 7.1 | 4.4 | 0.19 | 0.196 | 150.4 | 352 |
| Variance | 0.047 | 0.34 | 15.3 | 715 | 21.4 | 528 | 853 | 507 | 0.7 | 0.42 | 4742 | 396 | 1090 | 363 | 50.8 | 19 | 0.035 | 0.039 | 22 630 | 124 119 |
| Median | <0.2 | <0.2 | 2.3 | 5.3 | <2 | <2 | 40 | 45 | 0.2 | 0.2 | 18 | 28 | 50 | 50 | 3 | 4 | 0.1 | 0.15 | 96 | 128 |
| Mode | <0.2 | <0.2 | 1.7 | 13 | <2 | <2 | 37 | 47 | <0.2 | 0.3 | 12 | 37 | 40 | 60 | <2.0 | 2 | <0.1 | 0.2 | 120 | 126 |
| Skewness | 25 | 0.97 | 6.3 | 15.2 | 35.5 | 13.1 | 3.7 | 1.05 | 56.4 | 14.1 | 154 | 3.9 | 9.5 | 1.6 | 24.8 | 1.2 | 9.8 | 2.6 | 99 | 17.5 |
| Kurtosis | 1739 | -1.01 | 67 | 257 | 2037 | 194 | 35.4 | 4 | 4169 | 237 | 25 779 | 28 | 298 | 9 | 1413 | 4.7 | 277 | 20.3 | 11 781 | 315 |
| Minimum value | <0.2 | <0.2 | <0.5 | 1.3 | <2 | <2 | <0.5 | 1.8 | <0.2 | <0.2 | <2 | 6 | <10 | <10 | <2.0 | <2.0 | <0.1 | <0.1 | <2 | 27 |
| 5th percentile | <0.2 | <0.2 | 1 | 2.1 | <2 | <2 | 11 | 7.8 | <0.2 | <0.2 | 6 | 10 | 20 | 20 | <2.0 | <2.0 | <0.1 | <0.1 | 38 | 73 |
| 10th percentile | <0.2 | <0.2 | 1.2 | 2.5 | <2 | <2 | 18 | 18 | <0.2 | <0.2 | 8 | 12 | 25 | 30 | <2.0 | 2 | <0.1 | <0.1 | 50 | 85 |
| 25th percentile | <0.2 | <0.2 | 1.6 | 3.5 | <2 | <2 | 29 | 33 | <0.2 | <0.2 | 12 | 18 | 36 | 40 | <2.0 | 2 | <0.1 | <0.1 | 72 | 106 |
| 50th percentile | <0.2 | <0.2 | 2.3 | 5.3 | <2 | <2 | 40 | 45 | 0.2 | 0.2 | 18 | 28 | 50 | 50 | 3 | 4 | 0.1 | 0.15 | 96 | 128 |
| 75th percentile | <0.2 | 0.2 | 3.4 | 8.9 | <2 | 2 | 55 | 57 | 0.4 | 0.3 | 28 | 37 | 65 | 60 | 6 | 8 | 0.2 | 0.2 | 123 | 150 |
| 90th percentile | 0.2 | 0.2 | 5.8 | 16 | 4 | 4 | 76 | 67 | 0.6 | 0.4 | 40 | 48 | 88 | 70 | 10 | 11 | 0.2 | 0.3 | 150 | 181 |
| 95th percentile | 0.2 | 0.2 | 8.8 | 21 | 5 | 12 | 92 | 81 | 0.7 | 0.5 | 49 | 55 | 102 | 81 | 12 | 13 | 0.3 | 0.4 | 170 | 201 |
| 98th percentile | 0.4 | 0.2 | 16 | 37 | 7 | 27.6 | 120 | 109 | 0.8 | 0.8 | 69 | 87 | 130 | 100 | 15 | 14 | 0.4 | 0.5 | 200 | 259 |
| 99th percentile | 0.5 | 0.3 | 21 | 66 | 8 | 65.4 | 148 | 128 | 1 | 1.1 | 85 | 123 | 150 | 100 | 17 | 16 | 0.5 | 0.7 | 230 | 366 |
| Maximum value | 17.8 | 0.4 | 82.3 | 467 | 273 | 365 | 533 | 163 | 72 | 11.1 | 11 600 | 218 | 1560 | 180 | 510 | 34 | 6 | 1.9 | 20 000 | 6500 |

R = Regional data SL = Snow Lake

from anomalous), often estimated using the 95th percentile value, also differ significantly: 21 ppm As for the Snow Lake data and 8.8 ppm As for the regional data set. These differences in As levels likely reflect the large number of deposits, mineral occurrences, and mineralized exhalite horizons in the Snow Lake area with which As is almost universally associated. Owing to the relatively small size of the Snow lake data set ($N = 338$) the effect has been to increase dramatically the threshold level for As and, to a lesser extent for other elements, such as Au and Zn. For the Snow Lake data a threshold value of 21 ppm for As translates into 19 anomalous sites, whereas based on a regional threshold value of 8.8 ppm, 89 sites are anomalous. Therefore when evaluating the Snow Lake data, threshold levels based on the regional data set (Table 4) are used.

Chisel Lake area

Four Zn-rich volcanic hosted deposits (Chisel Lake, Chisel North, Lost Lake, and Ghost Lake; Galley et al., 1993) occur in the Chisel Lake area. Figure 9a summarizes the grab and core sample data in the vicinity of these deposits. As described above, core data represent the average value of the deep sediment at each site.

Figure 10 shows the down-core profiles for As, Cu, and Zn from the Lost Lake core (K/03). The high levels encountered in the upper 20 cm reflect local anthropogenic input which overprints the natural background levels. However, for a number of elements these background levels are anomalous compared to the regional threshold level as defined by the 95th percentile value. For example, the average Zn concentration of 272 ppm in the deep sediments is greater than the 99th percentile value of 230 ppm for the regional data. In addition to Zn, the deep sediments from Lost Lake are anomalous in As, Cd, Ag, and Br.

The presence of a strong Zn response and absence of anomalous Cu reflects the composition of the deposits which are notably Zn-rich relative to Cu. Total reserves plus past production for Chisel Lake, the largest deposit in the area, were 7.5 million tonnes averaging 10.9% Zn and 0.5% Cu (as of December 31, 1984; Fedikow et al., 1989).

Of the four grab samples and two cores collected from Chisel and Ghost lakes, only the two grab samples from Chisel Lake are anomalous in Zn. Grab samples K/1098 and K/1099 returned values of 171 ppm and 245 ppm, respectively. The regional threshold value (95th percentile) for Zn is 170 ppm (Table 4). However, the average concentration for the deep sediment in core K/01 (Fig. 10), taken at the same site as grab sample K/1099, is 148 ppm. The grab sample data at this site therefore likely reflects incorporation of contaminated surface material and not a naturally elevated background level. The surface sediments of core K/01 contain up to 935 ppm Zn.

It is also noteworthy that although the surface sediments of Ghost Lake are highly enriched in Zn and other elements (Fig. 10), the grab samples have not been adversely affected. Grab sample K/1071 has a Zn concentration of 131 ppm even though certain intervals of the surface sediments at the site have Zn levels ranging up to 1620 ppm.

The lack of a geochemical response for Zn in the lake sediments of Chisel and Ghost lakes is largely a function of the spatial distribution of the mineralization in the Chisel Lake area. Figure 9a shows the surface trace of the Chisel-Lost-Ghost mine horizon, as delineated by Syme et al. (1982). It occurs approximately 0.5 to 1.0 km south of Ghost Lake and Chisel Lake, passing through Lost Lake. Glacial direction is to the southwest and therefore any dispersal train would be away from Chisel and Ghost lakes. Unfortunately there is a paucity of lakes in the immediate area to the south and southwest (down ice) of the ore horizon.

Another factor complicating any response in the lakes of this area is the fact that although the favorable horizon outcrops, there is no significant mineralization associated with the contact at surface. For example, the Ghost Lake orebody tops at 60 m below surface (Stephansson, 1975) and its surface expression is gossaned material containing only 400 to 600 ppm Cu and Zn (Syme et al., 1982). The response in Lost Lake is likely related to low-grade lateral equivalents of the ore zones.

Although there is no base metal response in Ghost and Chisel lakes, there are anomalous As levels at all four sites within these two lakes, as well as many other lakes in the area. Figure 11 shows the distribution of anomalous As values in

the Snow Lake area. Particularly striking is the strong spatial correlation with the Amisk volcanics in the vicinity of Snow Lake. Although many of the anomalous As values are likely related to mineralization, the extent and pervasive nature to the distribution suggests that they also reflect other features associated with these volcanics. It is possible that some of the metasomatically altered rocks and/or exhalite horizons, both of which are extensive in the area, are enriched in As. If this is the case, then extensive As anomalies should be of some interest when evaluating regional lake sediment data, because they may distinguish between mineralized and barren regions within volcanic belts.

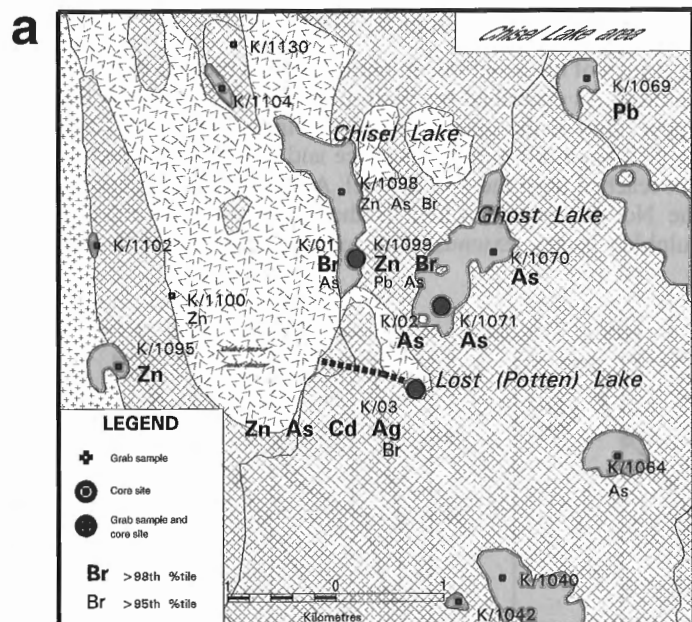
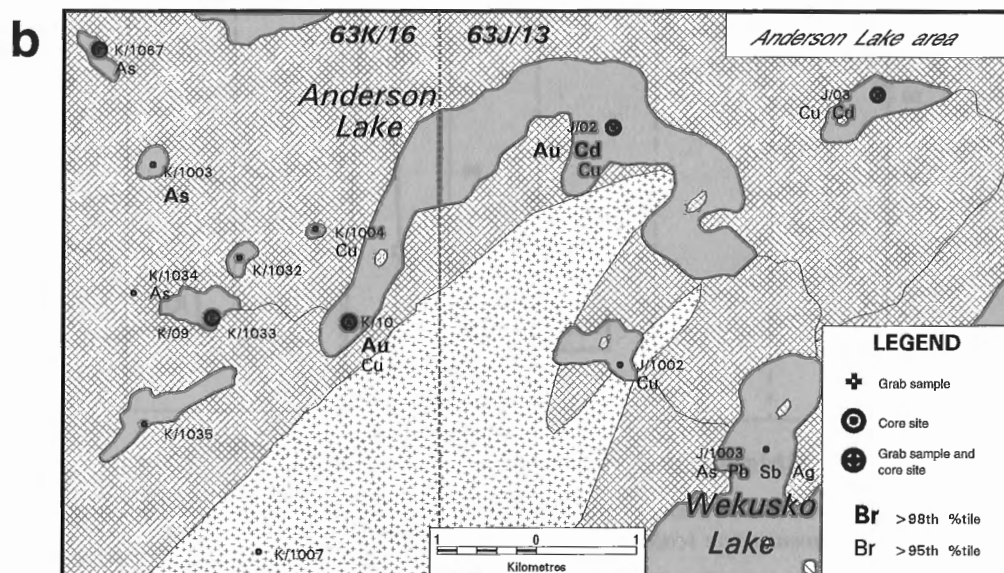


Figure 9.

Summary of grab and core sample data in the **a)** Chisel Lake and **b)** Anderson Lake areas.



Two other sites (K/1095 and K/1100, Fig. 9a) located west of the Chisel Lake gabbro are anomalous in Zn. These are not considered to be related to the *known* mineralization and are discussed separately below.

Anderson Lake area

Original grab samples collected from Anderson and Stall lakes clearly contain a portion of contaminated surface sediment and subsequently were not published (Friske et al., 1995) and are not used to evaluate lake sediment response in the Anderson Lake area. This feature is a function of the thickness of the contaminated surface sediment and/or the extremely high concentrations of Cu, Zn, and other elements in these sediments as described above. Another factor is the silty character of these surface sediments that impedes the normal penetration of the Hornbrook sampler. An attempt to collect a core from the central portion of Anderson Lake was unsuccessful because the sulphide-rich sludge encountered limited the penetration of the KB corer to only 15 cm.

Figure 9b shows the distribution of grab and core sites in the area. Anomalous Cu values characterize the lake sediment response in the area. The deep sediments in the two cores from Anderson Lake as well as the core from Stall Lake J (03) are anomalous in Cu, as are the two grab samples south and west

of Anderson Lake (site K/1002 and J/1004). In addition to Cu, the deep sediments from Anderson Lake are highly anomalous in Au. The average deep sediment Au content of core J/02 is 11 ppb and 17 ppb in core K/10. Both are greater than the 99th percentile value of 8 ppb based on the regional data (Table 4).

As is the case for the lake sediment samples from the Chisel Lake area, response of the Anderson Lake area lake sediments mirror the composition of the local mineralization. The volcanic-hosted massive sulphide deposits of this area are relatively Cu-rich and Zn-poor (Walford and Franklin, 1982). The anomalous Au response in Anderson Lake and lack thereof in the Chisel Lake area may also be related to compositional differences between the two types of deposits. A small sulphide lens associated with the No. 1 orebody of the Stall Lake deposit, which outcrops at surface, has an extremely high Au content with some assays approaching 1 oz/ton (Studer, 1982; approx. 30 g/t).

Much of the economic mineralization in the area does not outcrop. As described by Walford and Franklin (1982), the upper edge of the massive sulphides in the Anderson Lake deposit begin 90 m below surface and economic grades are not reached until the 185 m level. At the Stall Lake deposit, the No. 4 orebody, which is the largest of four massive sulphide lenses, extends along plunge from the 1500-foot

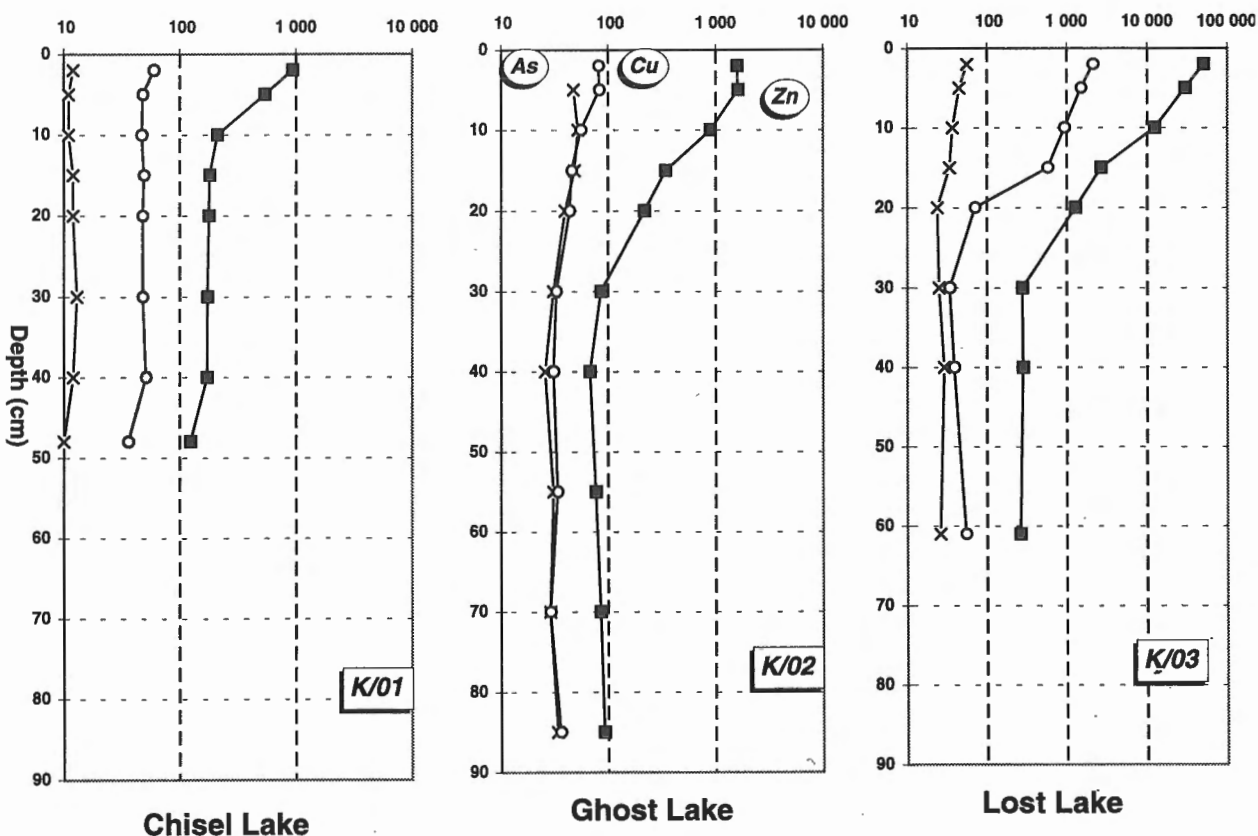


Figure 10. Down core profiles for Cu, Zn, and As in three lakes cored in Chisel Lake area. Note change of concentration scale for Lost Lake core (K/03).

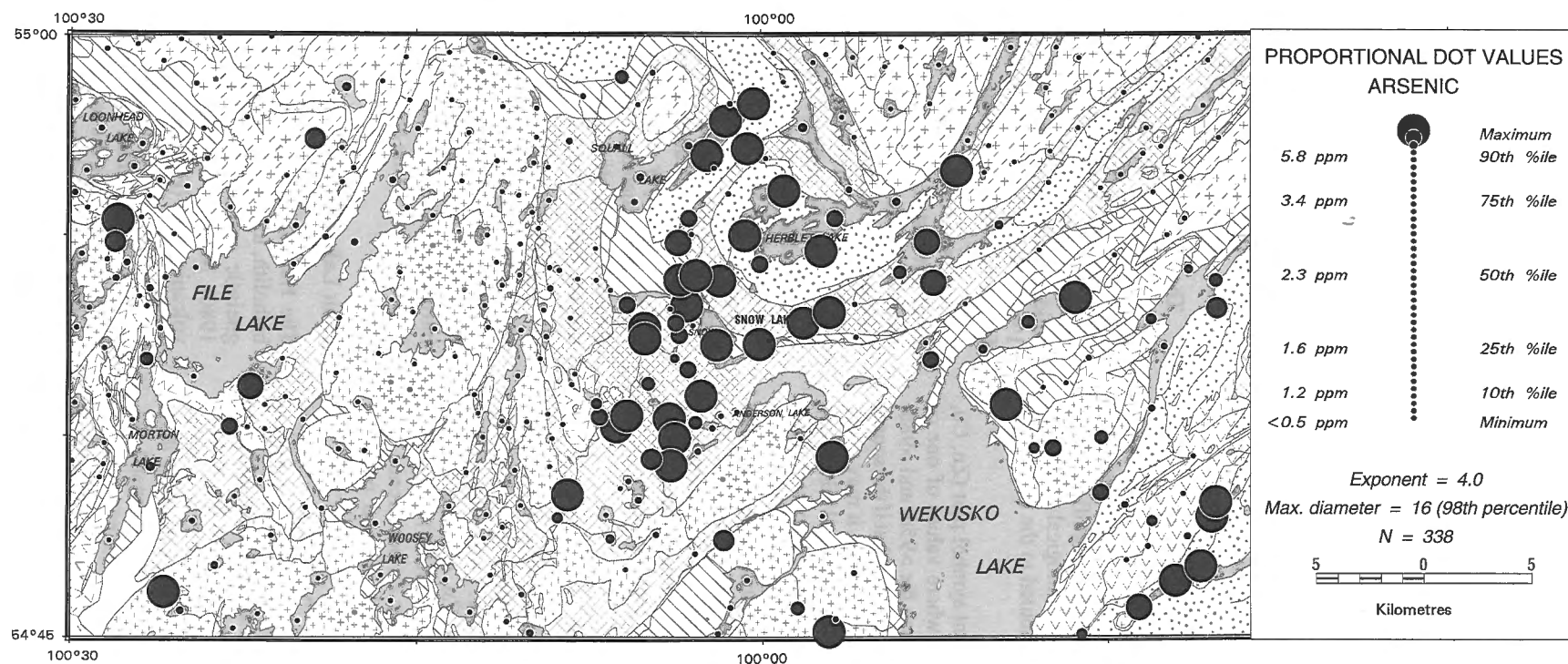


Figure 11. Distribution of As in lake sediments of Snow Lake area.

level to the 4600-foot level (Studer, 1982). Most likely the lake sediments are reflecting relatively weaker and less significant surface expressions of the much more extensive subcropping massive sulphides. These would include the alteration pipe associated with the Anderson Lake deposit and/or the No. 1 zones of the Stall and Rod deposits. The Anderson Lake alteration pipe outcrops along the north shore of Anderson Lake and is characterized by a central chlorite-biotite-kyanite zone containing chalcopyrite, as well as pyrite and pyrrhotite (Walford and Franklin, 1982).

Areas of interest for further investigation

The lake sediment survey has identified a number of areas that warrant further investigation, a few of which are discussed in the following section. In general, follow-up of any geochemical data should commence with a resampling of the original site along with more detailed sampling, to confirm the anomaly and better evaluate its cause. In addition, the collection of short cores would be useful in areas where significant local anthropogenic input and/or unique limnological conditions are suspected which may have contributed to the anomalous lake sediment response.

As a starting point, a three element symbol plot (Zn, Cu, and Au) was created showing sites where values of one or more of these elements are greater than the >95th and >98th percentile values (Fig. 12). It should be noted that if the source of these anomalies is related to mineralization, it may occur within the immediate vicinity of the lake or several kilometres away if the lake is sampling a glacial dispersal train (cf. McConnell and Batterson, 1987; Chapman et al. 1990). Therefore anomalous sites do not define drill targets but rather areas that warrant further detailed investigation. It is also important to keep in mind that the following discussion is by no means exhaustive. In theory each anomalous site may be related to mineralization and warrants consideration.

Chisel Lake-Morgan Lake corridor

There are several lake sediment anomalies (Fig. 12) within a southwest-trending corridor that stretches approximately 13 km from Chisel Lake to Morgan Lake. Two samples taken from Morgan Lake are anomalous in Zn, and likely reflect known mineralization, particularly site K/1017 (Fig. 12) which is just south of the Morgan Lake Zn occurrence. The main mineralization consists of sphalerite and pyrite in sericite schist, with estimated reserves of 272 000 t grading 15% Zn and 3.42 g/t Au (Fedikow et al., 1989).

Of greater interest are sites K/1074, K/1027, and K/1073 (Fig. 12). These are all multi-element anomalies, notably site K/1027 which is anomalous in As, Au, Cd, Cu, Sb, and Zn. All three sites are, however, in close proximity to a set of Canadian National (CN) railway tracks and a drainage ditch that flows from the south end of Chisel Lake to Morgan Lake. Both of these features may have affected the composition of the lake sediments at these sites. Therefore the first step in evaluating these anomalies should be the collection of short cores to verify the significance of the anomalies. A core was

collected by the authors from site K/1027, but the sediment was contaminated during the extrusion process and not kept for chemical analysis.

Cook Lake area

Figure 13 summarizes the data associated with eight grab samples and two cores collected from the Cook Lake area. The two core samples confirm the original grab sample results. The absence of anomalous Hg in the grab samples and presence in the cores is not related to a major difference in concentrations but rather to proximity to the threshold value of 102 ppb. For example, Hg content of grab sample K/1129 is 90 ppb (background) while that of the deep sediment from the corresponding core (K/20) is 110 ppb (anomalous).

There are two known occurrences in the immediate vicinity of Cook Lake. Both are described as stratabound massive sulphide-type mineralization in altered felsic volcanic rocks of the Amisk Group (Fedikow et al., 1989). The occurrence at the north end of Cook Lake consists of a series of stacked solid sulphide lenses, sections of which contain greater than 1% Cu. These two occurrences likely account to some extent for the lake-sediment anomalies encountered in Cook Lake.

A reason for the strong Cu and Au response in the small pond just east of Cook Lake (site K/1129) and the weaker Cu anomaly in Maw Lake (site K/1137) is not evident. There is no known mineralization in the immediate catchment basins or up-ice direction of both sites. The pond occurs over a small wedge of mafic intrusive rocks bounded immediately to the west by felsic intrusives of the Richard Lake pluton and to the east by Amisk Group volcanic rocks. The close proximity of the pond to several different lithologies implies that several types of mineralization may have been the source of the anomaly (e.g., volcanic-hosted massive sulphide mineralization, Cu-porphyry mineralization, or vein mineralization). Minor disseminated mineralization has been noted within the Richard Lake pluton approximately 6 km to the south (location 69, Fedikow et al., 1989).

The influence of elevated Cu levels in the mafic intrusive rocks relative to other lithologies also needs to be considered when assessing these anomalies, particularly in the case of Maw Lake because of: 1) the large proportion of mafic intrusive rocks within its catchment basin; 2) the weaker Cu response; and, 3) the absence of other anomalous elements.

Ham Lake pluton

The Ham Lake pluton is a 18 km long and 6.5 km wide batholith, located east of File Lake, composed of massive to gneissic granodiorite, leucotonalite, and tonalite (Bailes, 1980). Much of the pluton is surrounded by Amisk Group volcanic rocks (Fig. 3). Thirteen of the 45 samples collected from over the pluton (Fig. 12) are anomalous in Zn, concentrations ranging from 173 ppm to 380 ppm. The sites are concentrated along the eastern flank and southern third of the pluton. No other element is consistently anomalous in these samples. Anomalous Cd and Sb are encountered only in two samples. Core K/18 was collected at grab sample site K/1088

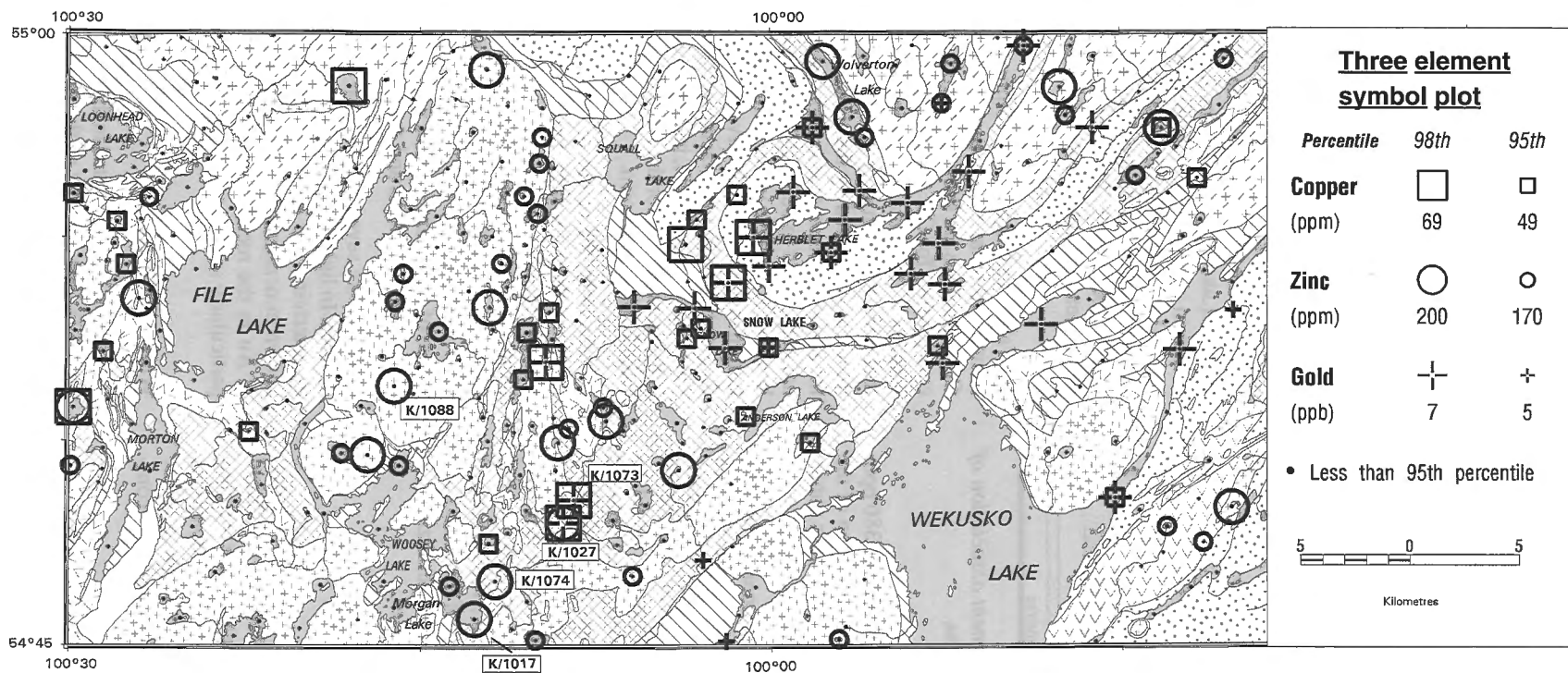


Figure 12. Three-element symbol plot showing distribution of anomalous Cu, Zn, and Au in Snow Lake area.

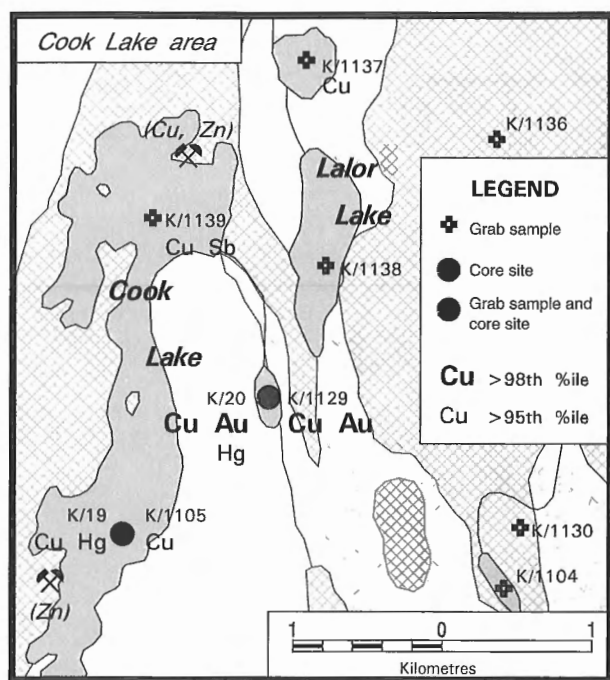


Figure 13. Location and anomalous element association of grab samples and cores in Cook Lake area.

(Fig. 12), which has the highest Zn concentration of 380 ppm and an anomalous Cd value of 1.3 ppm. Composition of the deep sediments from this core confirm the anomalous nature of this site (Zn = 290 ppm, Cd = 1.1 ppm),

The possible cause of these anomalies is considered to be Zn-rich volcanic-hosted massive sulphide mineralization that occurs within the volcanics that flank the pluton and/or rafts of this type of mineralization within the pluton itself. In the first case the anomalous lake sediment response would be related to a dispersal train that has been transported onto the granite terrain. Rafts of sedimentary gneiss and associated mineralization have been noted within the pluton at an occurrence located 1.3 km southeast of Ham Lake. One drill hole intersected a 67 m graphitic section that contained 10-15% pyrite and 10% chalcopyrite (Fedikow et al., 1989). Several other occurrences are known in the vicinity of the Ham Lake pluton but, overall, it would appear that this mineralization is insufficient to explain the observed anomalies.

Snell Lake

Snell Lake is located approximately 1.5 km west of Chisel Lake within a wedge of Amisk volcanics between the Chisel Lake gabbro and Richard Lake pluton. Of interest are two sites (K/1095 and K/1100, Fig. 9a) both of which have anomalous Zn concentrations. There are no known occurrences in the area according to the mineral deposits and occurrences compilation of Fedikow et al. (1989).

Assuming that the glacial direction in this area is to the south and southwest, it is unlikely that these anomalies reflect glacial dispersal from the known mineralization around

Chisel Lake because they occur almost due west of the surface trace of these deposits (Fig. 9a). As described by Martin (1966), the western end of the Chisel Lake deposit is truncated by the Chisel Lake gabbro. It is possible that these two sites, which occur within or near Amisk Group volcanics, reflect mineralization related to the continuation of the Chisel-Lost-Ghost mine horizon west of the Chisel Lake gabbro. Alternatively they may reflect volcanic-hosted massive sulphide mineralization totally unrelated to that of the Chisel Lake deposits.

Snow Lake-Herblet Lake area

The vast majority of Au anomalies encountered in the lake sediment data are located in the vicinity of Snow Lake and Herblet Lake (Fig. 12). Anomalous As and/or Cu values are common associations. Extensive mining activity in this region has contaminated the surface sediments of some lakes in the area, notably the southwestern portion of Herblet Lake as described above. To assist in the evaluation of these gold anomalies a number of the original grab sample sites were cored.

Table 5 compares the composition of the original grab sample with that of the deep sediment taken at the same site. Core locations are shown in Figure 5. Figure 14 shows down core profiles for Cu, Au, and As for three of the sites. Several features of this data are particularly noteworthy. The first is that contamination may be more extensive in Herblet Lake than was suggested by the distribution of Zn and Cu data in the surface sediments as outlined above. Core J/07 which was not considered to be significantly contaminated has elevated levels of As and Au in the surface sediments. The Au concentration in the 0 to 2 cm interval is 255 ppb. The extent to which diagenetic cycling is a factor in this enrichment, particularly for As (cf. Friske, 1995), is unclear. Whether or not the source is the same as that for the other contaminated sites in Herblet Lake is also not known.

Secondly, the results of the coring indicate that some of the anomalous Au sites, based on the grab sample data, are related to contamination and not naturally elevated Au values. Of the seven sites tested with anomalous Au values, the deep sediment from three have background concentrations (cores K/11, J/05, and K/14, Table 5). However, the anomalous nature of the other four sites were confirmed, all of which are also anomalous in As and three of the four in Cu.

There are several significant deposits and occurrences in the area. In light of the coring results, further work is required to determine the extent to which these anomalies reflect known mineralization, contamination, regional enhancement of Au in the rocks, or new areas of mineralization. This is particularly so for samples from Herblet Lake.

Wolverton Lake

Wolverton Lake is located in the northwest quadrant of 63J/13 (Fig. 12). The geology of the area is characterized by felsic pyroclastic and volcanoclastic rocks of the Amisk Group bounded to the east by granitoid gneiss and to the west by

Missi and Amisk sedimentary rocks (Bailes, 1975). Three lake sediment samples were collected from the lake, all of which returned anomalous values for Zn, ranging from 192 to 212 ppm. None of the other nine elements evaluated (Table 4) are anomalous in these samples.

Three occurrences are known in the immediate vicinity of the lake (Fedikow et al., 1993). Two occur along the west shore and are classed as vein type mineralization neither of which have significant Zn content. The third consists of disseminated and veinlet (5%) pyrite and chalcopyrite in altered volcanics that occur at several localities along the

southeastern shore. Only one of several grab samples returned any significant values; site 3 contained 44 ppb Au and 1410 ppm Zn (Fedikow et al., 1993).

Rusty weathered rhyolites extend for approximately 8 km from Wolverton Lake to the Wim deposit to the northwest. Drill-indicated graphite-iron and base metal sulphide layers also suggest the presence of a regionally active mineralizing system (Fedikow and Ziprick, 1991) and mineral potential for the area. These features along with a lack of known significant mineralization in the Wolverton Lake area, particularly at the northern end, suggests that the lake sediment response may be reflecting something more substantial than is presently known.

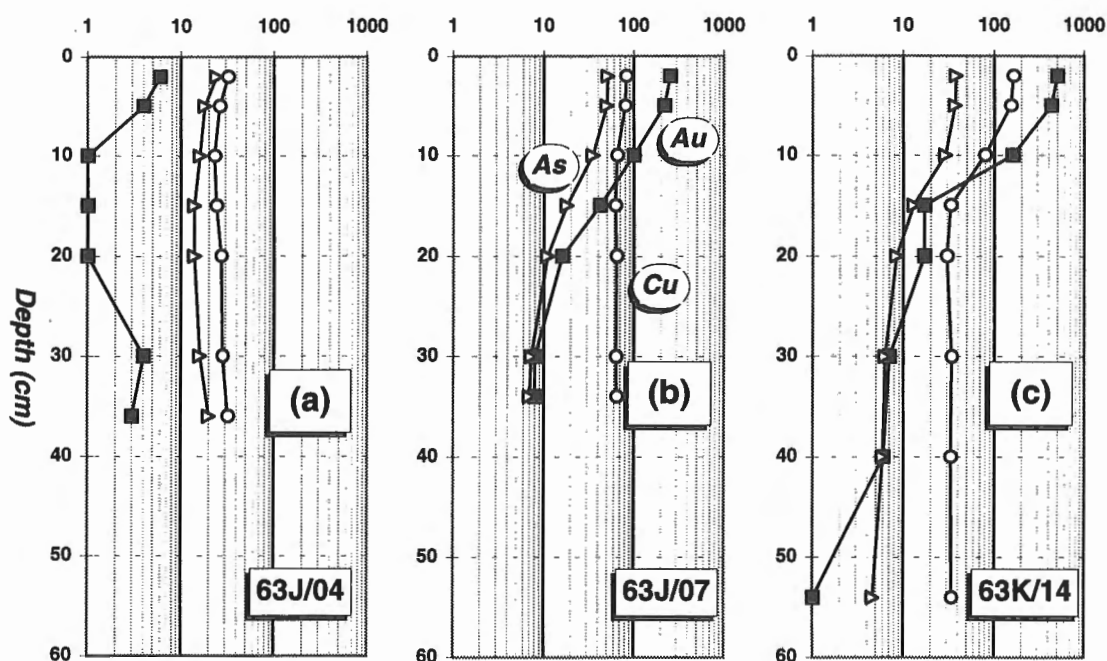


Figure 14. Down-core profiles for Cu, Au, and As from lakes in Snow Lake-Herblet Lake area.

Table 5. Comparison of concentration levels for selected elements in grab samples and deep sediment core samples taken at the same site.

| Core site ID | Original grab sample ID | Contam.* Site | Au (ppb) | | Cu (ppm) | | As (ppm) | | Zn (ppm) | |
|--------------|-------------------------|---------------|----------|------|----------|------|----------|------|----------|------|
| | | | Dp Sed | Grab | Dp Sed | Grab | Dp Sed | Grab | Dp Sed | Grab |
| J/04 | 063J 911028 | No | 3 | 2 | 32 | 25 | 20 | 17 | 83 | 89 |
| J/07 | 063J 911115 | No | 6 | 17 | 64 | 58 | 9 | 10 | 112 | 141 |
| K/11 | 063K 911165 | No | <2 | 9 | 46 | 35 | 9 | 13 | 109 | 120 |
| K/12 | 063K 911239 | No | 4 | 3 | 138 | 137 | 14 | 15 | 63 | 102 |
| K/21 | 063K 911291 | No | 7 | 6 | 53 | 51 | 11 | 23 | 77 | 94 |
| J/05 | 063J 911062 | Yes | 3.5 | 79 | 31 | 50 | 8 | 28 | 80 | 132 |
| J/06 | 063J 911087 | Yes | 19 | 43 | 36 | 34 | 9 | 18 | 106 | 124 |
| K/13 | 063K 911285 | Yes | 55 | 170 | 56 | 101 | 15 | 39 | 91 | 120 |
| K/14 | 063K 911286 | Yes | 3.5 | 30 | 34 | 37 | 5 | 13 | 86 | 108 |

values >95th percentile

*Based on enhanced levels of Cu and/or Zn in the surface sediments.

SUMMARY

Results of this study clearly demonstrate the effectiveness of lake sediment geochemistry in detecting known mineralization within the Snow Lake area. This is based on data from grab samples and short cores. Characteristics of the anomalies typically mirror the composition of the nearby mineralization. For example, the lake sediment response related to Zn-rich volcanic-hosted massive sulphide deposits of the Chisel Lake area is characterized by anomalous Zn values and background Cu levels. In contrast, lake sediments from the Anderson Lake area (Cu-rich volcanic-hosted massive sulphide mineralization) have anomalous Cu and background Zn levels.

Comparison of data from grab samples and cores collected at the same site indicates that some of the anomalous values encountered in the 1991 grab sample survey are related to contamination as opposed to naturally elevated levels. Unusually thick sequences of contaminated surface sediments with extremely high concentrations of trace metals are a contributing factor. These conditions are restricted to lakes (e.g., Anderson Lake, Chisel Lake, Ghost Lake, and Herblet Lake) in the immediate vicinity of significant local anthropogenic activity and are not widespread throughout the area. Collection of lake cores provides a useful new approach to the follow-up of grab sample data and to the application of lake sediment geochemistry, particularly in areas with significant local contamination. This is because data from lake sediment cores have the ability to "see through" local contamination and provide data on background element concentrations that predate the contamination.

The lake sediment survey has identified a number of areas that warrant further investigation. In general, follow-up of any geochemical data should commence with a resampling of the original site along with more detailed sampling, to confirm the anomaly and better evaluate its cause. In addition, the collection of short cores would be useful in areas where significant anthropogenic input and/or unique limnological conditions are suspected that may have contributed to the anomalous lake sediment response.

ACKNOWLEDGMENTS

The authors wish to thank Steve Day and Chris Durham, of the GSC, for their assistance with logistics and collection during the 1991 infill survey. Steve Day's assistance during the collection of the short cores in November 1993 under particularly adverse conditions is also greatly appreciated. Thanks are also expressed to Bill Coker and Graeme Bonham-Carter of the GSC for helpful recommendations on the manuscript.

REFERENCES

- Armstrong, J.E.**
1941: Wekusko, Manitoba; Geological Survey of Canada, Map 665A, scale 1:50 000.
- Azcue, J.M., Mudroch, A., Rosa, F., and Hall, G.E.M.**
1994: Effects of abandoned gold mine tailings on the arsenic concentrations in water and sediments of Jack of Clubs Lake, B.C.; *Environmental Technology*, v. 15, p. 669-678.
- Bailes, A.H.**
1975: Geology of the Guay-Wimapedi Lakes area; Manitoba Mines, Resource and Environmental Management, Mineral Resources Division, Publication 75-2, 104 p.
1980: Geology of the File Lake area; Manitoba Department of Energy and Mines Mineral Resources Division, Geological Report 78-1, 134 p.
- Bailes, A.H. and Galley, A.G.**
1991: Geological setting of base metal mineralization in the Anderson Lake area (NTS 63K/16SE and 63J/13SW); in *Report of Activities, 1991*, Manitoba Energy and Mines, Minerals Division, p. 8-13.
- Chapman, R., Curry, G., and Sopuck, V.**
1990: Bakos Deposit discovery—a case history; in *Modern Exploration Techniques*, (ed.) L.S. Beck and C.T. Harper; Special Publication Number 10, Saskatchewan Geological Society, p. 195-212.
- Clark, M.D.**
1989: Surficial geology, Cormorant Lake, Manitoba-Saskatchewan; Geological Survey of Canada, Map 1699A, scale 1:250 000.
- Coats, C.J.A., Clark, L.A., Buchan, R., and Brummer, J.J.**
1970: Geology of the copper-zinc deposits of the Stall Lake Mines Ltd., Snow Lake area, N. Manitoba; *Economic Geology*, v. 65, no. 8, p. 970-984.
- Connors, K.A. and Ansdell, K.M.**
1994: Transition between the Flin Flon and Kiseynew domains of the Trans-Hudson Orogen, File Lake-Limestone Point area, northern Manitoba; in *Current Research 1994C*; Geological Survey of Canada, p. 183-192.
- Fedikow, M.A.F. and Ziprick, D.**
1991: The geological setting of the Wim massive sulphide type Cu deposit, Snow Lake area (NTS 63N/1); in *Report of Activities, 1991*, Manitoba Energy and Mines, Minerals Division, p. 41-42.
- Fedikow, M.A.F., Athayde, P., and Galley, A.G.**
1993: Mineral deposits and occurrences in the Wekusko Lake area, NTS 63J/13; Manitoba Energy and Mines, Geological Services, Mineral Deposit Series, Report No. 14, 460 p.
- Fedikow, M.A.F., Ostry, G., Ferreira, K.J., and Galley, A.G.**
1989: Mineral deposits and occurrences in the File Lake area, NTS 63K/16; Manitoba Energy and Mines Geological Services, Mineral Deposit Series, Report No. 5, 277 p.
- Fortescue, J.A.C.**
1988: The use of the geochemistry of long lake sediment cores for verification of regional geochemical results: Goudreau Lake area, District of Algoma; in *Summary of Field Work and Other Activities, 1988*; Ontario Geological Survey, Miscellaneous Paper 141, p. 482-488.
- Friske, P.W.B.**
1991: The application of lake sediment geochemistry in mineral exploration; Geological Survey of Canada, Open File 2390, Paper #4, p. 4-1 to 4-20.
1995: Effects of limnological variation on element distribution in lake sediments from Tatin Lake, central British Columbia—implications for the use of lake sediment data in exploration and environmental studies; in *Current Research 1995-E*; Geological Survey of Canada, p. 59-67.
- Friske, P.W.B. and Coker, W.B.**
1995: The importance of geological controls on the natural distribution of mercury in lake and stream sediments across Canada; *Water, Air, and Soil Pollution*, v. 80, p. 1047-1051.
- Friske, P.W.B. and Hornbrook, E.H.W.**
1991: Canada's National Geochemical Reconnaissance programme; *Transactions of the Institution of Mining and Metallurgy*, Section B; v. 100, p. 47-56.
- Friske, P.W.B., McCurdy, M.W., Day, S.J., and Adcock, S.W.**
1994: National Geochemical Reconnaissance—Ontario compilation: distribution of copper in 17 934 lake sediment samples; Geological Survey of Canada, Open File 2959a; 1 map, scale 1:1 500 000.
- Friske, P.W.B., McCurdy, M.W., Day, S.J., Gross, H., Lynch, J.J., and Durham, C.C.**
1995: Lake sediment and water infill survey data, Snow Lake area, Manitoba (NTS 63J/13 west and 63K/16); Geological Survey of Canada, Open File 3015, 42 maps, 86 p.

Froese, E. and Moore, J.M.

1980: Metamorphism in the Snow Lake area, Manitoba; Geological Survey of Canada, Paper 78-27, 16 p.

Galley, A.G., Bailes, H.B., and Kitzler, G.

1993: Geological setting and hydrothermal evolution of the Chisel Lake and North Chisel Zn-Pb-Cu-Ag-Au massive sulphide deposits, Snow Lake, Manitoba; *Exploration Mining Geology*, v. 2, no. 4, p. 271-295.

Geological Survey of Canada

1986: Regional lake sediment and water geochemical reconnaissance data, Province of Manitoba (parts of NTS 63K, 63N, and 63O); Geological Survey of Canada, Open File 1212; 22 maps, 84 p.

Harrison, J.M.

1949: Geology and mineral deposits of the File-Tramping Lakes area, Manitoba; Geological Survey of Canada, Memoir 250, 92 p.

Johnson, M.G., Culp, L.R., and George, S.E.

1986: Temporal and spatial trends in metal loadings to sediments of the Turkey Lakes, Ontario; *Canadian Journal of Fisheries and Aquatic Sciences*, v. 43, p. 754-762.

Klassen, R.W.

1986: Surficial geology of north-central Manitoba; Geological Survey of Canada, Memoir 419.

Machado, N. and David, J.

1992: Geochronology of the Reindeer-Superior transition zone and of the Snow Lake area: preliminary results; in *Lithoprobe Trans-Hudson Orogen Transect Workshop No. 2, Report No. 26*, p. 40-42.

Martin, P.L.

1966: Structural analysis of the Chisel Lake orebody; *Canadian Mining and Metallurgical Bulletin*, p. 630-636.

McConnell, J.W. and Batterson, M.J.

1987: The Strange Lake Zr-Y-Nb-Be-REE deposit, Labrador: a geochemical profile in till, lake and stream sediment, and water; *Journal of Geochemical Exploration*, v. 29, p. 105-127.

McMartin, I.

1994: Surficial geology of the Mitishto River area, Manitoba (NTS 63J11, J12, J14); Geological Survey of Canada, Open File 2835, 1 sheet, scale 1:100 000.

Mihychuk, M.

1988a: Surficial geology and aggregate of the Snow Lake area; in *Report of Field Activities 1988*, Manitoba Energy and Mines Minerals Division, p. 193-195.

Mihychuk, M. (cont.)

1988b: Surficial geology and aggregate resources of Herb Lake (63J/13), File Lake (63K/16), Tramping Lake (63K/9), and Buzz Lake (63J/12); Manitoba Energy and Mines, *Aggregate Resources, Preliminary Maps 1988SL-1.2.3 and 4*.

Price, D.P.

1977: Geology and economic potential of the Flin Flon-Snow Lake area; University of Manitoba Centre for Precambrian Studies, 1977 Annual Report, p. 52-83.

Stephansson, A.E.

1975: Development and production at Hudson Bay's Ghost Lake mine; *The Canadian Institute of Mining and Metallurgy*, v. LXXVIII, p. 7-12.

Studer, R.D.

1982: Geology of the Stall Lake copper deposit, Snow Lake, Manitoba; *Canadian Mining and Metallurgical Bulletin*, v. 75, no. 837, p. 66-72.

Syme, E.C., Bailes, A.H., Price, D.P., and Ziehlke, D.V.

1982: Flin Flon volcanic belt: geology and ore deposits at Flin Flon and Snow Lake, Manitoba; Geological Association of Canada and Mineralogical Association of Canada, *Field Trip Guidebook, Trip Number 6*.

Walford, P.C. and Franklin, J.M.

1982: The Anderson Lake Mine, Snow Lake, Manitoba; in *Precambrian Sulphide Deposits*, (ed.) R.W. Hutchinson, C.D. Spence and J.M. Franklin; Geological Association of Canada, Special Paper 15, p. 481-523.

Williams, H.

1966: Geology and mineral deposits of the Chisel Lake map-area, Manitoba; Geological Survey of Canada, Memoir 342, 38 p.

Wong, H.K.T., Nriagu, J.O., and Coker, R.D.

1984: Atmospheric input of heavy metals chronicled in lake sediments of the Algonquin Provincial Park, Ontario, Canada; in *Geochronology of Recent Deposits*, (ed.) J.A. Roberts; *Chemical Geology*, v. 44, p. 187-201.

Ziehlke, D.V.

1983: The Nor-Acme gold deposit, Manitoba; *Canadian Institute of Mining Bulletin*, v. 76, no. 851 p. 80.

Contribution to the 1989-1994 Rusty Lake-Snow Lake Mining Camps, Canada-Manitoba Exploration Science and Technology Initiative (EXTECH I)

Application of airborne multiparameter geophysical data (gamma ray, magnetometer, VLF-EM) to mapping and exploration in the Rusty Lake and Snow Lake areas

R.B.K. Shives¹

Shives, R.B.K., 1996: Application of airborne multiparameter geophysical data (gamma ray, magnetometer, VLF-EM) to mapping and exploration in the Rusty Lake and Snow Lake areas; in EXTECH I: A Multidisciplinary Approach to Massive Sulphide Research in the Rusty Lake-Snow Lake Greenstone Belts, Manitoba, (ed.) G.F. Bonham-Carter, A.G. Galley, and G.E.M. Hall; Geological Survey of Canada, Bulletin 426, p. 279-297, 382-386.

Abstract: Airborne gamma ray spectrometric-magnetic-VLF-EM surveys in the Rusty Lake and Snow Lake areas, Manitoba, aid geological mapping and mineral exploration for volcanic-associated massive sulphide (VMS) deposits.

In general, the radiometric and magnetic patterns are complementary, reflecting magmatic differentiation processes: radioelement highs delineate low-magnetic felsic units; magnetic highs are associated with mafic to ultramafic rocks exhibiting low radioelement patterns.

Airborne spectrometry in the Eden Lake-Rusty Lake area delineates granite-hosted REE mineralization in the Eden Lake intrusive suite, but extensive clay and organic surficial deposits throughout much of the survey generally inhibit definition of bedrock signatures. Ground spectrometry over the northeast extension of the Ruttan Cu-Zn deposit effectively maps microcline alteration and subdivides the supracrustal Ruttan Group.

The airborne data do not directly target volcanic-associated massive sulphide mineralization. However, at Snow Lake, airborne radioelement (K, eU, eTh) and magnetic patterns map important variations between and within two chemically different subvolcanic intrusions and distinguishes them from late kinematic plutons. Ground spectrometric and magnetic susceptibility results refine the airborne patterns and provide strong support for previously established chemostratigraphic relationships. Thorium concentrations are low in the Sneath Lake tonalite and the related, felsic extrusive complex (Anderson Rhyolite) which hosts the Cu-rich Anderson Lake, Stall Lake, and Rod 1, 2 volcanic-associated massive sulphide deposits. Consistently higher Th and magnetic signatures are evident in the Richard Lake tonalite, related felsic dykes, and Powderhouse dacite, which hosts the Chisel Lake, Chisel North, Lost Lake, and Ghost Lake Zn-rich massive sulphide deposits.

Results clearly demonstrate the benefit of including multiparameter geophysical surveys in an integrated approach to exploration for volcanic-associated massive sulphide deposits.

¹ Geological Survey of Canada, 601 Booth St., Ottawa, Ontario K1A 0E8

Résumé : Les levés géophysiques aéroportés (spectrométrie gamma, magnétisme, VLF-EM) effectués dans les régions de Rusty Lake et de Snow Lake (Manitoba) facilitent la cartographie géologique et l'exploration minière visant à découvrir des gisements de sulfures massifs volcanogènes (SMV).

En général, les configurations radiométriques et magnétiques sont complémentaires, reflétant les processus de différenciation magmatique. En effet, l'abondance de radioéléments correspond aux creux magnétiques associés aux unités felsiques et, à l'inverse, les radioéléments peu nombreux correspondent aux crêtes magnétiques associées aux roches mafiques à ultramafiques.

Un levé spectrométrique aéroporté de la région des lacs Eden et Rusty a permis de délimiter une minéralisation en ÉTR encaissée dans du granite dans la suite intrusive d'Eden Lake, mais les vastes dépôts superficiels argileux et organiques dans presque toute la région visée empêchent généralement de définir les signatures du substratum rocheux. Un levé spectrométrique au sol dans la région englobant le prolongement nord-est du gisement de Cu-Zn de Ruttan a permis d'identifier l'altération en microcline et de subdiviser le Groupe de Ruttan (roches supracrustales).

Les levés aéroportés ne donnent pas la possibilité de cibler directement les minéralisations en SMV. Cependant, à Snow Lake, les cartes radiométriques (K, eU, eTh) et magnétiques découlant des levés aéroportés font ressortir d'importantes variations entre deux intrusions hypovolcaniques chimiquement différentes et au sein de celles-ci, en plus de les distinguer des plutons tardi-cinématiques. Les résultats des levés au sol de spectrométrie et de susceptibilité magnétique permettent d'affiner les configurations établies à partir des levés aéroportés et appuient les relations chemostratigraphiques déterminées antérieurement. Les teneurs en thorium sont faibles dans la tonalite de Sneath Lake et le complexe extrusif felsique apparenté (rhyolite d'Anderson), dans lequel sont encaissés les gisements de SMV riches en cuivre d'Anderson Lake, de Stall Lake et de Rod. Les signatures magnétiques et les teneurs en thorium sont uniformément plus élevées dans la tonalite de Richard Lake, les dykes felsiques apparentés et la dacite de Powderhouse, laquelle renferme les sulfures massifs zincifères de Chisel Lake, de Chisel North, de Lost Lake et de Ghost Lake.

Les résultats montrent clairement les avantages à inclure des levés géophysiques multiparamétriques pour en arriver à une approche intégrée d'exploration des gisements de SMV.

INTRODUCTION

Airborne multiparameter geophysical surveys were flown in 1990 in the Rusty Lake and Snow Lake areas of Manitoba under the Exploration Science and Technology Initiative, 1989-1994 (EXTECH). The purpose of these surveys was to provide new, regionally coherent gamma-ray spectrometric, magnetic, and VLF-EM data to aid regional, mining camp, and deposit scale geological mapping and mineral exploration for base metal deposits. The surveys cover portions of green-schist to lower amphibolite grade volcano-plutonic rocks within the Flin Flon, Lynn Lake, and Rusty Lake belts, the adjacent higher metamorphic grade rocks of the Kisseynew Gneiss Terrane and the large, granite-granodiorite composite Baldock batholith (Fig. 1).

The airborne results were compiled in 1990 and published in 1991 as digital data and colour maps for the Rusty Lake-Ruttan Lake area and the Snow Lake area (Geological Survey of Canada, 1991a, b, respectively). The reader should consult these publications for detailed, colour map views of the airborne results not presented here.

Ground radiometric studies were conducted within both surveys, in truck or boat accessible areas, and were selected in consultation with D. Ames and A. Galley (GSC), and

A. Bailes (Manitoba Geological Services Branch), to relate airborne radioelement patterns to bedrock and surficial lithologies. Ground investigation in the Ruttan area in 1991 was conducted over the northeastern extension of the mine horizon. In the Snow Lake area, emphasis in 1991 was on radioelement characterization of subvolcanic and regional, syn- to late kinematic intrusives. In 1992, detailed transects were completed through stratigraphic sections hosting the Chisel Lake-Lost Lake-Ghost Lake and Anderson Lake-Stall Lake-Rod 1, 2 deposits, and across the Richard Lake subvolcanic intrusive complex. All results were presented in several posters and talks (R.B.K. Shives, GSC Minerals Colloquium, Ottawa, 1992 (abstract); R.B.K. Shives, GSC Minerals Colloquium, Ottawa, 1994 (abstract)) and are summarized in this paper. All ground station results, including location co-ordinates, field notes, radiometric and magnetic susceptibility measurements, and selected rock, sand and clay sample geochemical results are tabulated in Open File 3231 (Shives, in press). Complete bedrock and surficial geological descriptions of the survey areas are provided by Ames (1996), Bailes and Galley (1996), Kaszycki et al. (1996). In 1993 the digital airborne data was incorporated into a GIS by Bonham-Carter and Wright for further analysis (D.F. Wright, G.F. Bonham-Carter, A.H. Bailes, and A.G. Galley, GSC Current Activities Forum, January 1993, Ottawa, Ontario, (abstract); Wright and Bonham-Carter, 1996).

As no detailed interpretation of the regional aeromagnetic or airborne VLF-EM results has been undertaken, these data are mentioned only briefly where appropriate. Ground magnetic, VLF-EM, and electromagnetic studies conducted over selected sulphide deposits in the Snow Lake area are summarized by Sinha and Palacky (1996). Although application of the radiometric data was focused on volcanic-associated massive sulphide deposit exploration during EXTECH I, it should be emphasized that the airborne patterns can also be applied to exploration for Au, Cu, Mo, U, and other commodities known to occur in a variety of geological settings within the surveyed areas.

Airborne survey parameters

The GSC Skyvan fixed-wing aircraft was flown at a mean terrain clearance of 120 m. The system included a 256 channel high resolution gamma-ray spectrometer with 50 L of NaI detectors, a Geometrics model G-803 proton precession magnetometer and a Herz Totem 2A VLF-EM receiver. All data were sampled at 1 second intervals, roughly equivalent to a sample every 50 m at an average ground speed of 190 km·h⁻¹.

Gamma-ray spectrometric data

The energies of gamma rays produced by radioactive decay are characteristic of the decaying nuclide (International Atomic Energy Agency, 1991). Gamma-ray spectrometers

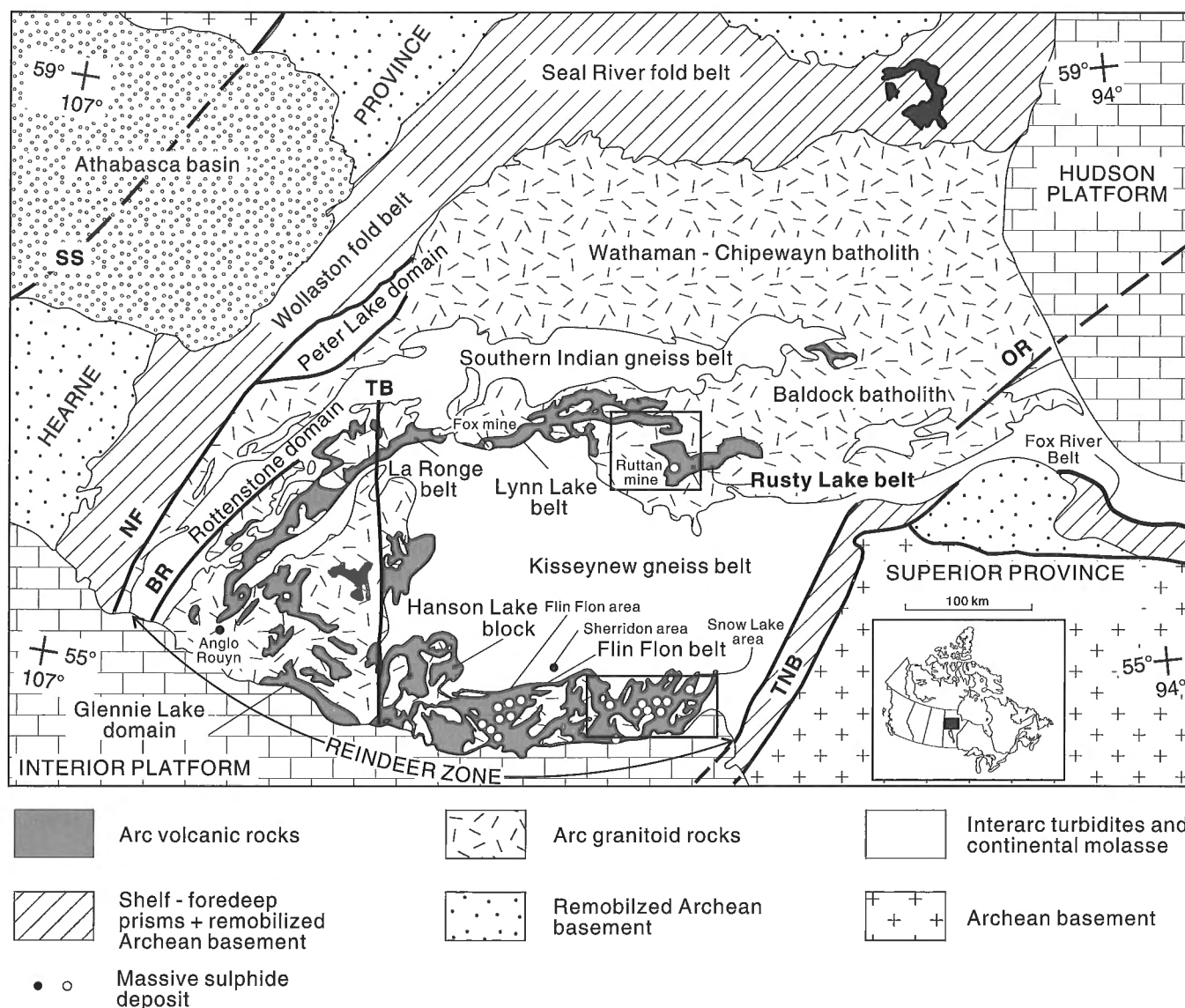


Figure 1. Location (boxes) of 1991 airborne gamma ray spectrometer-magnetometer-VLF surveys, Rusty Lake and Snow Lake areas, within the Trans-Hudson Orogen, Manitoba (after Ames, 1996). OR – Owl River shear zone; TNB – Thompson Nickel Belt; BR – Beech Rapids shear zone; NF – Needle Falls shear zone; TB – Tabbornor Fault; SS – Snowbird shear zone.

measure intensities and energies of gamma rays and hence the abundance of particular radioactive nuclides. There are many naturally occurring radioactive elements, but only three are sufficiently abundant for accurate determination by gamma-ray spectrometry. These are ^{40}K (0.0118% of total K) and daughter nuclides in each of the ^{238}U and ^{232}Th decay series. The abundance and chemical attributes of these three radioelements provide powerful geological mapping tools, as K is a major constituent of most rocks, U and Th are respectively, mobile and relatively immobile trace elements. Furthermore, where lithological radioelement signatures are altered by hydrothermal processes, radioelement enrichment or depletion offer direct exploration guides.

The airborne data represent an average surface radioelement concentration which is influenced by varying amounts of outcrop, overburden, vegetation, soil moisture, and surface water. In general, zones of increased total radioactivity correspond to areas with greater bedrock exposure, whereas lakes and wet, swampy areas are low in radioactivity. For each 1 second reading, most of the measured counts emanate from a ground surface area roughly the size of a football field. This concept of field-of-view becomes particularly important where, as for parts of the Ruttan survey, small, moderately radioactive bedrock exposures are scattered between relatively "hotter" Quaternary clays, making it difficult to measure the bedrock concentrations. The concept of depth penetration does not apply to gamma-ray spectrometry, as the signal emanates from the top few tens of centimetres only.

Very Low Frequency (VLF) electromagnetic data

The VLF receiving coils were tuned to Station NLK in Seattle, Washington, during these surveys, operating at a frequency of 24.8 kHz. When Station NLK was not operating, Station NAA in Cutler, Maine, which transmits at 24.0 kHz, was used. The primary electromagnetic field generated by the VLF stations induces eddy currents in geological or man-made conductors, creating secondary electromagnetic fields. These secondary fields cause local distortions in the primary field, producing anomalies. VLF total field values, the vector

sum of horizontal and vertical components, are expressed as positive anomalies. The VLF quadrature, out-of-phase, component produces cross-over responses. These data can be used to define conductivity contrasts and discrete lithological or structurally controlled conductive zones, such as graphitic pelite beds or clay alteration along faults. Although VLF stands for "very low frequency" with respect to communications frequencies, for exploration purposes the operating frequency is very high. As a result, only near-surface conductivity is measured.

Total field magnetic data

The magnetic total field data were collected using an instrument with 1 nT sensitivity. Data were corrected for spikes, heading effects, and diurnal variations. No magnetic control lines were flown.

RUTTAN LAKE REGION

Eden Lake-Rusty Lake-Ruttan Lake regional airborne survey

The 1000 m flight line spacing used for this survey provides regional coverage centered over NTS 64 B/12, including portions of 64 B/5, 6, 11, 13, 14 and 64 C/8, 9, 16 (Fig. 2A). A detail survey block, using 500 m line spacing, was included over the Ruttan mine area. Flight lines were oriented north-south for both regional and detailed blocks.

The regional survey covers portions of the Lynn Lake and Rusty Lake greenstone belts and the intervening granitoids within the calc-alkaline, late-orogenic Baldock batholith (Fig. 1). With exceptions, the airborne spectrometric patterns (Fig. 3, [see colour section](#)) generally show only moderate correlation with mapped bedrock lithologies due to extensive surficial cover and relatively low radioactivity contrasts between the various plutonic phases. The metavolcanic belts are predominantly mafic, and exhibit uniformly low radioactivity. Total field magnetic trends clearly define the regional

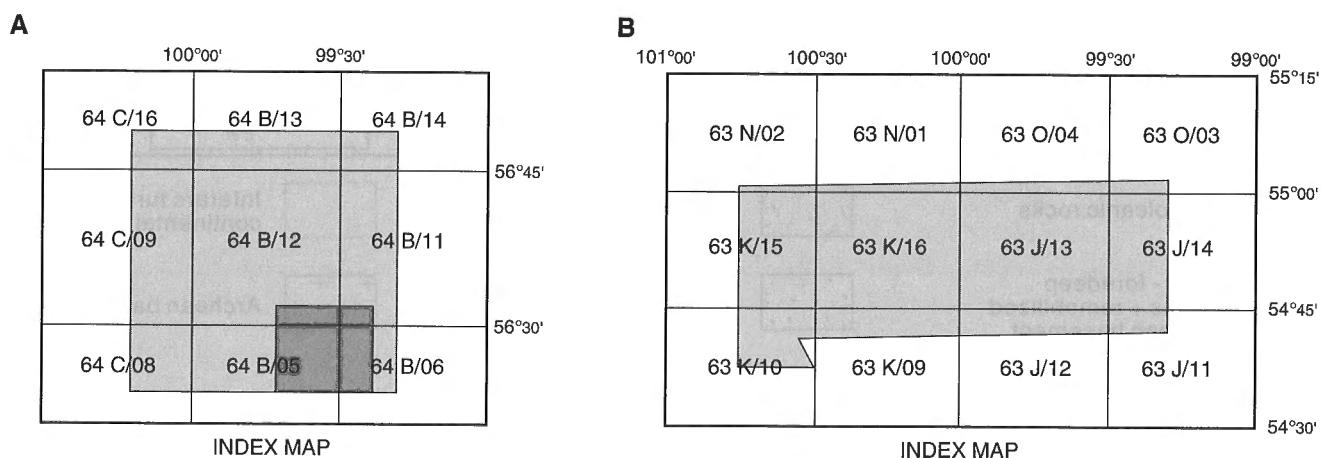


Figure 2. NTS coverage, 1991 airborne geophysical surveys, Manitoba: **A)** Rusty Lake regional and Ruttan Lake detail; **B)** Snow Lake.

fabric as linears along the volcanic belts, circular features within felsic plutonic domains, or strong highs over gabbroic intrusions. Several mapped and unmapped northwest-trending Mackenzie diabase dykes are also apparent. The combined magnetic and radiometric patterns define intrusive phases within the synkinematic plutons (i.e. west and north of Issett Lake, midway between Leaf Rapids and the Ruttan mine).

Airborne radioelement patterns in the northern part of the survey area are dominated by a broad 40 km by 20 km area of coincident K, eU, and eTh highs. The 1 km line-spacing provides significantly better resolution than an earlier 5 km line spaced airborne spectrometric survey (Geological Survey of Canada, 1977) and defines a number of discrete anomalies. These radiometrically anomalous areas also contain high U and F in lake waters, and U and Sn in lake sediments. McRitchie (1989) conducted ground scintillometer surveys over the anomalies using the 5 km survey as a guide. Additional scintillometer and spectrometer ground surveys were conducted over three anomalies in the Eden Lake area defined by the 1 km spaced airborne survey (McRitchie, 1990; Young and McRitchie, 1990) (Fig. 3E, F). These anomalies outlined concentrations within an alkalic intrusive complex of REE-enriched allanite, fracture-controlled pyrite±magnetite in aegirine-augite-bearing monzonite, pyroxene lenses, fluorite-bearing pegmatites, and Ce-bearing allanite and britholite. Samples contained up to 45 900 ppm Ce, 22 900 ppm Nd, and 17 000 ppm La, but the zones are discontinuous and presently uneconomic. Aplite, fine grained granite, biotite monzogranite, and K-feldspar megacrystic phases are also generally more radioactive. No ground investigations were carried out in the Eden Lake intrusive complex under the current study.

Lower amplitude U and eU/eTh ratio anomalies are associated with similar intrusions located along the boundary between the Leaf Rapids and Lynn Lake domains (Manitoba Energy and Mines, 1986a, b) along the west shore of Opachuanau Lake. This area also has high U and F in lake waters. (Schmitt et al., 1989). South of Leaf Rapids, southwest of Turnbull Lake, strong U and eU/eTh ratio anomalies occur within greywackes and calc-silicate-rich sedimentary strata.

Extensive surficial deposits throughout the northern and eastern parts of the survey are effectively mapped by high eTh/K ratio patterns. These areas correspond to organic deposits (bogs, swamps) and clays formed by glacial Lake Agassiz. Identical responses are evident over similar deposits along the eastern margin of the Snow Lake survey area. A string of linear K highs extends north and south from the town of Leaf Rapids, tracing the course of Highway 391 (Fig. 3C). These anomalies relate to well drained, discontinuous ridges of bedded beach sands and gravels within the Leaf Rapids interlobate moraine (Kaszycki and DiLabio, 1986) formed at the confluence of the Hudson and Keewatin ice sheets. The eskers separate carbonate-rich Hudson ice lobe till to the east from non calcareous, shield-derived Keewatin lobe till on the west. Although the eskers yield well defined K anomalies, there is no radioelement contrast between the two till types.

Ruttan detailed airborne survey

The 500 m line spaced portion of the survey provides increased resolution of all geophysical patterns (Fig. 3). The Ruttan mine site exhibits a subtle increase in eU (which creates a high eU/eTh ratio anomaly) and K (giving a moderate eTh/K ratio low) and relatively flat aeromagnetic response. These patterns continue very weakly to the northeast over the along-strike continuation of the mine horizon (Ames and Scoates, 1992). Strong radioelement lows near the mine occur over Ruttan Lake and the adjacent tailings pond. High eTh and eTh/K ratio patterns associated with extensive surficial deposits coincides with bogs and swamps. In general, correlation with bedrock geology is limited to the few better exposures of granite, quartz monzonite, and rhyolitic flows (Baldwin, 1988) well east and south of the mine area.

Ground spectrometry results: northeast Ruttan

Ground spectrometry traverses (stations 91-086 to 91-131) were conducted, in consultation with D. Ames, in three areas along the northeastern extension of the Ruttan mine strata. Station locations are shown in Figure 4, and field results are summarized in GSC Open File 3231 (Shives, in press). Geological map units and descriptions below are as shown in Figure 2 of Ames (1996) included in the back of this volume.

Plots of eTh versus K and eU versus eTh (Fig. 5A, B) show that several units within the oceanic arc tholeiite formations of the Ruttan Group can be segregated radiometrically. Petrological evolution of the footwall stratigraphy is indicated by increasing radioelement concentrations, from the lower footwall pyroxene-phyric basalt (unit 2) through aphyric basaltic-andesite (unit 5), plagioclase-phyric andesite (unit 6) and microcline-rich rhyolite (unit 4) up to the upper felsic volcanoclastic (unit 7a). A similar pattern of radioelement enrichment is apparent in the postvolcanic intrusions, from diorite (unit 11) through quartz-plagioclase porphyry (unit 13) to feldspar porphyry (unit 12). The intrusive phases define separate, distinct fields on the eTh versus K plot. The fine grained, unaltered mafic epiclastic units (8b) of the Powderhouse Magazine formation contain less than 0.25% K. In the altered parts of the formation (measured at station 91-114), the eTh value remains constant (just over 2 ppm eTh) but K increases six-fold to 1.4% K.

A fine grained mafic dyke crosscuts pyroxene-phyric basalt (unit 2) at station 91-098 (Fig. 4). This dyke plots within the diorite (unit 11) field (Fig. 5A), demonstrating the use of ground spectrometry to correlate dykes with the larger, probably parental intrusions.

Similar radioelement signatures (eTh vs. K plot) of intermediate volcanoclastic rocks (unit 3), intrusive feldspar porphyry (unit 12), and quartz-plagioclase porphyry suggest they have similar chemical compositions. Ames and Scoates (1992) note that feldspar porphyry sill in the Ruttan deposit footwall, previously mapped as unit 3 intermediate volcanoclastic rock, has identical whole rock, trace element, and REE profiles as the unit 12 feldspar porphyry dyke in the northeast part of the map sheet.

Attempts to extend the microcline-rich rhyolite (unit 4) and the Mine Sequence rhyolite tuff into unexposed, clay-covered areas were not successful, as the inherently higher radioactivity of the Agassiz clays effectively masks the bed-rock signals. Chemical analyses show the clay at station 91-124 contains 3 ppm U, 25 ppm Th and 3.2% K, similar to Agassiz clay samples from the Snow Lake area, and consistent with the elevated eTh and K airborne concentrations.

Stations 91-117, 91-117A, and 91-118 were taken along a north-trending traverse across the Vol Fault, along an high eU/eTh airborne anomaly extending northeasterly from the Ruttan mine (Fig. 3, 4). These outcrop stations plot in the intermediate, andesite field on the radioelement plots, suggesting at least some of the relatively poorly exposed units in the Vol Fault area may be higher in the stratigraphy, or the

basalts are altered. Bleaching and pyritic hairline fractures were noted in tan to cream units here, supporting the latter. North of the assumed position of the Vol Fault, a clay sample collected at station 91-119 contains elevated concentrations of U, Zn, Cu, and Ni (Shives, in press).

SNOW LAKE REGION

Regional airborne survey results

The Snow Lake survey covers NTS 63J/13, 14W; K/15E, 16, 15W and small portions of adjacent sheets (Fig. 2B). Flight lines for the entire Snow Lake survey were oriented east-west at 500 m line spacing. This configuration was chosen to:

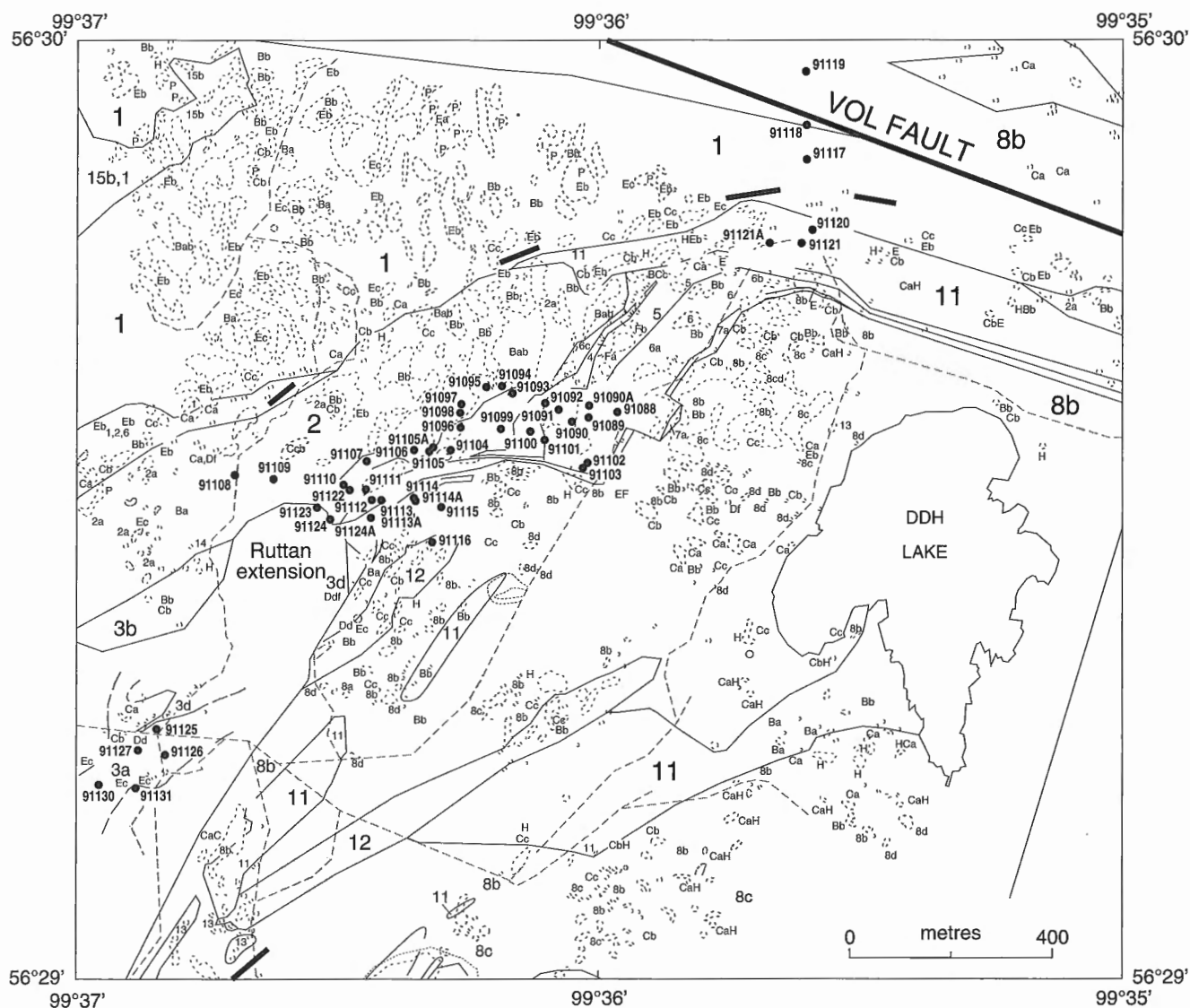


Figure 4. Geology, ground radiometric stations, Ruttan northeast area. (See Fig. 2 Ames, 1996 in pocket).

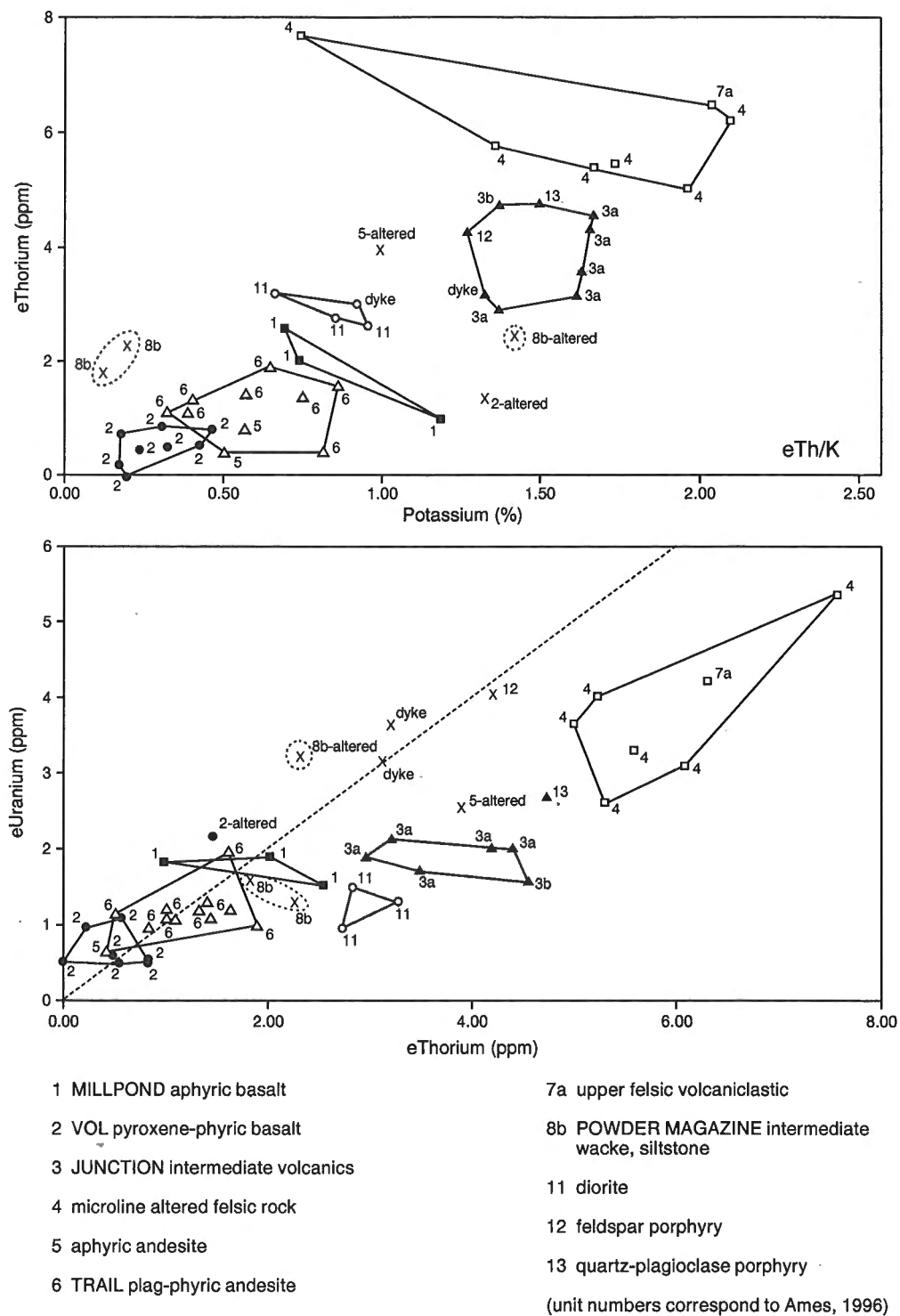


Figure 5. Ground spectrometric results, Rutan northeast traverses. Geological unit numbers correspond to those in Figure 4. See text for explanation.

1. provide regional airborne geophysical/geochemical information to aid ongoing and future, bedrock and surficial geological mapping and exploration programs within the eastern portion of the Paleoproterozoic Flin Flon greenstone belt;
2. characterize airborne radioelement, magnetic, and VLF-electromagnetic patterns within the Chisel Lake-Lost Lake-Ghost Lake and Anderson Lake-Stall Lake-Rod 1, 2 massive sulphide-hosting supracrustal sequences to aid mining camp-scale bedrock mapping and volcanic-associated massive sulphide deposit exploration;
3. determine if anomalous airborne radioelement/magnetic/VLF survey responses over known deposits can be distinguished. Radiometrically, this goal was considered to be improbable, due to the low radioelement content of the juvenile, tholeiitic island-arc supracrustal host rocks and the associated hydrothermal alteration zones.

The regional gamma-ray spectrometric and magnetic patterns (Fig. 6, *see* colour section) show significant correlation, and many important contrasts, with the regional bedrock geology. Radiometric and magnetic patterns are generally complementary, reflecting compositional differences between the plutonic and volcanic formations. Radioelement highs delineate flat- or low-magnetic felsic units and magnetic highs are associated with mafic to ultramafic rocks exhibiting low radioelement patterns.

Ground spectrometry surveys and lithogeochemical sampling were conducted in several areas (white X's in Fig. 6) to explain some of the airborne radioelement and magnetic patterns. The airborne patterns and results of ground investigations are described below for each area. Specific radioelement anomalies relating to Au-bearing structures (such as K highs) or Li-, Sn-, U-, and REE-bearing pegmatites (U and eU/eTh ratio highs) are evident, but were not investigated under the present study.

Radioelement patterns relating to surficial deposits

Within the Snow Lake survey area, airborne radioelement anomalies coincide with surficial deposits in several areas. In general, well drained, sandy units produce high K (1.7 to 2.5%), relatively low eU (less than 2 ppm) airborne responses, whereas clay deposits have elevated levels of both radioelements, with U values in the 2 to 4 ppm eU range.

A broad, K anomaly north of Reed Lake (Fig. 6B) crosses mapped bedrock lithologies, delineating horizontally bedded beach sands and gravels within the Reed Lake moraine. Clarke (1989) reports that the broad, flat-topped nature of the moraine and localized pockets of dark brown to grey lacustrine clay indicate extensive reworking of this ice contact deposit by glacial Lake Agassiz. Five of the six ground stations (91-031 to 91-036) on the moraine produced radioelement concentrations (2% K, 2.5 ppm eU, 3 ppm eTh) consistent with the airborne values. At station 91-034 total radioactivity was approximately twice that of the other stations, over sand with abundant small pebbles, a few cobbles, and a larger (35 cm diameter) gneissic boulder. An unsorted sample of this material, excluding the cobble/boulder sized

clasts, contains elevated concentrations of several elements including Au (110 ppb), As (65.7 ppm), Ni, Cr, V, Cu, Pb, Zn, Ce, La, Sm, and high U (26 ppm), Th (140 ppm), and W (25 ppm). This interesting anomaly likely relates to heavy mineral concentrations within the sandy gravels of Reed Lake moraine.

Additional sand deposits extend discontinuously to the north, along the eastern shore of Morton Lake, south and north of File Lake (Bailes, 1980) with identical high K, low eU responses. The Reed Lake moraine is reported to be the southward extension of the Leaf Rapids interlobate moraine (Kaszycki and DiLabio, 1986) where similar high K, low U signatures are apparent (*see* Eden Lake-Rusty Lake-Ruttan Lake regional airborne survey, *above*).

Smaller deposits of well sorted, nearshore, glaciolacustrine beach sand and gravel located northeast of Reed Lake also produce distinct K anomalies (Fig. 6B). The airborne patterns suggest the presence of at least two additional, unmapped, sand deposits in the area.

A broad, high K, high U anomaly extending west and south of the Chisel pit (shown by letter "c" in Fig. 9C, D in colour section) crosses bedrock lithological contacts, coincident with a large flat deposit of Lake Agassiz clay and silt excavated from the Chisel open pit. Ground spectrometry at stations 001 to 91-003A (2.3% K, 3.7 ppm eU, 7 ppm eTh) and several other sites within the Ruttan and Snow Lake areas, confirms the elevated eU and eTh signature of the clays relative to sand deposits (Fig. 7A, B).

Snow Lake regional ground traverses of syn-kinematic intrusions

Labell Lake-Little Lake area (stations 91-020 to 91-030)

This traverse crossed the southwestern edge of a large, oval, total-field magnetic high, coincident with low radioactivity (Fig. 6). The anomaly relates to the mafic members of the bimodal Little Swan Lake pluton (LSLP) (Morrison and Whalen, 1995) which intrudes the large, north-south elongated Gants Lake Batholith (Whalen, 1993). Where traversed, the magnetic mafic intrusive phases (stations 91-022, 027, 028, 029) are black, fine- to medium-grained, equigranular, massive hornblende gabbro to quartz-diorite. The nonmagnetic intermediate (stations 91-023, 024, 026) to felsic (stations 91-020 and 021) intrusive phases are pink, foliated to crudely banded, medium- to coarse-grained, hornblende-biotite granodiorite and granite. They contain numerous mafic xenoliths and discontinuous mafic dykes which subparallel and crosscut foliation. Both mafic and felsic phases are cut by irregular pink aplite and quartz veins.

Radioelement contrasts (Fig. 8) reflect strong magmatic differentiation, with mafic Little Swan Lake Pluton units having low K (0.4-0.8%), low eU (0.7-1.4 ppm), and low eTh (0.1-1.3 ppm) relative to the intermediate and felsic rocks, which contain 2.5-3.9% K, 2.0-4.7 ppm eU, and 3.2-8.3 ppm eTh. In Figure 8, the eU/eTh and eTh/K fields for the Little Swan Lake pluton felsic phases coincide with those of the more evolved portions of the Ham Lake, Barron Lake, and

Wekusko Lake plutons. In the Little Swan Lake pluton intermediate phases, the presence of mafic inclusions and the radioelement signatures, suggest they are the product of mixing of the end-member mafic and felsic magmas. The litho-geochemical contrasts are equally distinct (Shives, in press), reflecting appropriate mafic-felsic whole rock and trace element chemical differences. Elevated levels of base metals, Co, Ni, Cr, and V suggest these late (the comagmatic granodiorite yielded a U-Pb titanite age of $1826 \pm 7/-6$ Ma; Whalen and Hunt, 1994) mafic intrusions offer exploration potential for nickel and PGEs.

Ham lake pluton (stations 91-037 to 91-039A)

The western margin of the 1.34 Ga synkinematic Ham Lake pluton is distinguished from the remainder of the intrusive suites by a linear magnetic low coincident with radioelement highs. Northeast of the northwest arm of Woosey Lake, large, well exposed outcrops of pink, medium grained, weakly foliated, equigranular biotite granite-granodiorite suggest the anomalies relate to slightly more evolved border phases of the pluton, where ground radioelement concentrations averaged 2.9% K, 4 ppm eU, and 6 ppm eTh.

Barron Lake pluton (stations 91-040 to 91-045)

This small, circular pluton is composed of tan to white, fine- to medium-grained, massive nonfoliated, biotite-microcline porphyritic granite characterized by very high airborne K, eU, and eTh anomalies and a uniformly flat, low magnetic signature. Ground radiometric values average 3.8% K, 8 ppm eU, and 8 ppm eTh. These U levels represent the highest of all late kinematic intrusive rocks measured, and are accompanied by increased concentrations of F and Mo. The west and southern margin of the pluton has an irregular contact containing abundant rafts, or pendants, of grey garnetiferous biotite gneisses of the File Lake Formation due to lit-par-lit style intrusion of the pluton into the metasediments. Bailes (1980) shows separate, smaller Barron Lake dykes intruding the Ham Lake pluton to the northeast. The radioelement and trace element chemistry and contact relationships support Bailes' suggestion that this pluton is one of the youngest of the late kinematic intrusions in the Snow Lake area.

Reed Lake pluton (Stations 91-1.9, 91-2.51, 91-047 to 91-051, 91-055)

Strong, curvilinear aeromagnetic highs along the margins and within the mapped boundaries of the Reed Lake pluton correlate with previously mapped gabbro-dioritic intrusions

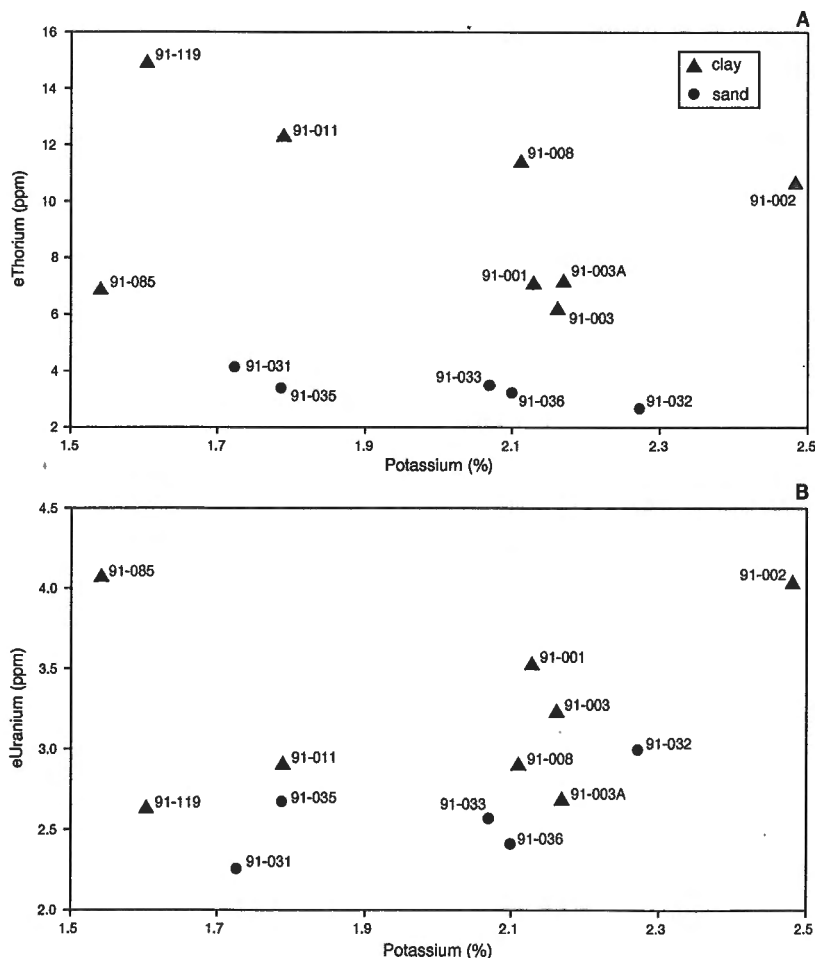


Figure 7.

Ground spectrometric results, overburden, Snow Lake and Ruttan Lake areas. Clay and sand deposits are both potassic but can be distinguished by consistently higher eU and eTh in the clays.

(stations 91-1.9, -2.51, -047, -047A) or mafic volcanic enclaves and pendants (stations 91-048, -055). Radioelement concentrations over these areas are low, and corresponding lithochemical results (Shives, in press) reflect the mafic character of these units.

Wekusko and Tramping Lake Plutons (Stations 91-012 to 91-019A, 91-056 to 91-065A)

These plutons have uniformly low aeromagnetic signatures, with the exception of a small circular magnetic high located just east of old Highway 393 (Fig. 6). Both plutons contain granitic phases which are enriched in radioelements, with the Tramping Lake pluton yielding the highest K (4.2-5.0% K) and Th (8-10 ppm eTh) values of all late kinematic intrusions measured (Fig. 8). In addition, whole rock analyses of

Tramping Lake pluton samples show higher SiO_2 (75%), K_2O (>5%), and Na_2O (3.1%) and significantly lower CaO (0.45-0.99%) than the Wekusko Lake intrusion and all other plutons sampled. These results indicate a high degree of magmatic differentiation within these two plutons. Whalen and Hunt (1994) suggest that the Wekusko Lake pluton represents one of the few late (1834 \pm 6 Ma; Gordon et al., 1990) high-K postcollisional granites in the Paleoproterozoic Trans-Hudson Orogen. Based on radioelement and chemical similarities, the Tramping Lake pluton should be included in the high-K category.

Where sampled, the Tramping Lake pluton is typically pink, medium grained, equigranular, and massive to weakly foliated near its margins. Elevated As (up to 274 ppm), Sb (2.7 ppm), and Au (44 ppb) are associated with strong bleaching, hematization, and sulphide

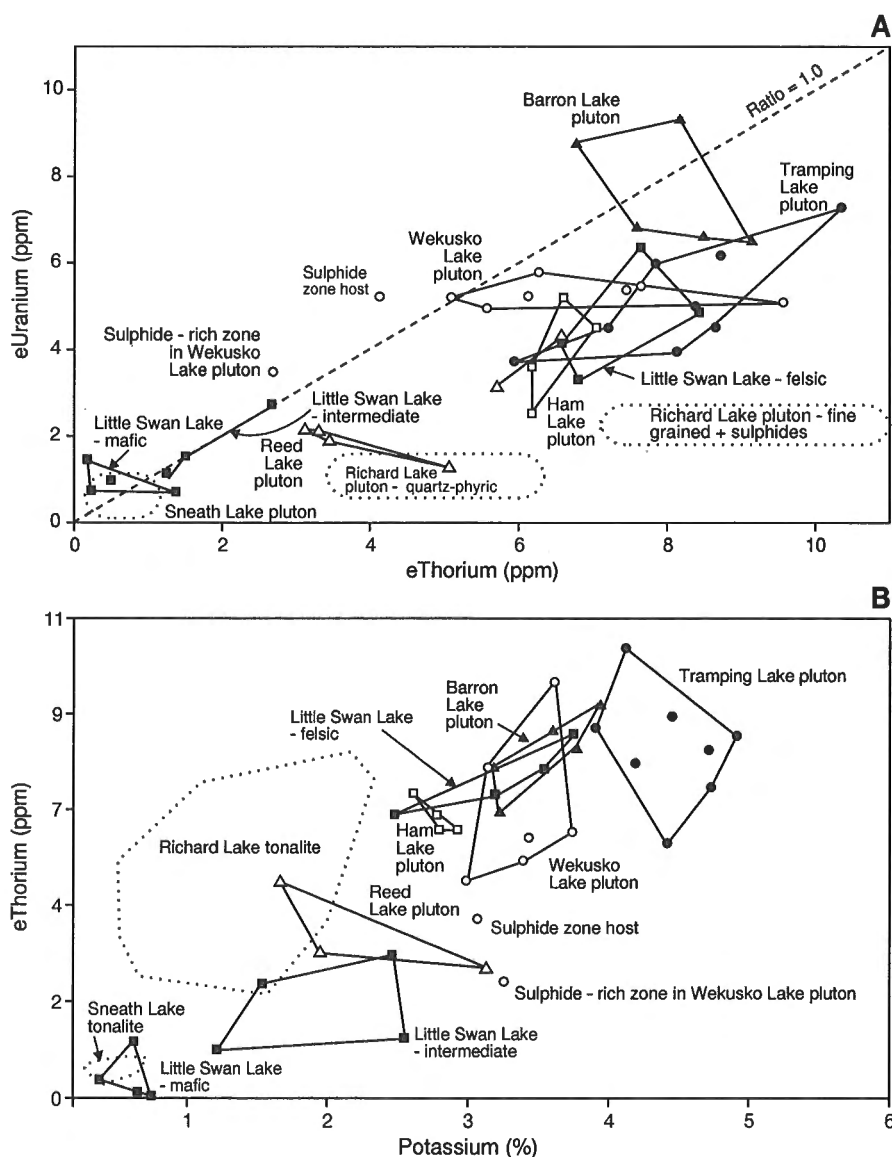


Figure 8. Ground spectrometric results, Snow Lake area, subvolcanic and synkinematic intrusives. See text for explanation.

mineralization (stations 91-019A, 91-012) near contacts with Amisk mafic volcanics. The Wekusko Lake pluton contains pink, massive, nonfoliated, fine grained, porphyritic hornblende granite to granodiorite phases. Weakly anomalous Au and Sb (stations 91-065, 91-065A) are associated with a wide (>100 m) bleached, rusty, east-trending brittle fracture zone containing fine-grained mafic dykes. Decreasing radioelement concentrations within the intrusive, towards the rusty sulphide-rich ($S = 1.15\%$) zone, are reflected in the airborne radioelement patterns, offering potential exploration vectoring (R.B.K. Shives, GSC Minerals Colloquium, Ottawa, 1992 abstract). These results indicate good potential for granite-hosted gold mineralization, along fractures, shears or quartz veins within these relatively unexplored plutons. As exemplified by several economic discoveries made in the LaRonge gold belt, Saskatchewan during the 1980s (Saskatchewan Energy and Mines, 1984), epigenetic gold deposits may not be limited to the more thoroughly prospected supracrustal units in the area.

Ground spectrometry measurements of subvolcanic intrusive complexes

Sneath Lake tonalite (stations 91-066 to 91-084)

These stations cross the north end of the subvolcanic, multi-phase Sneath Lake tonalitic intrusion (Fig. 9, *see* colour section; *see* Fig. 12). Bailes and Galley (1993) have subdivided the pluton into four separate intrusive phases: equigranular fine grained tonalite, quartz-phyric fine grained leucotonalite, quartz megacrystic tonalite, and quartz megacrystic mesotonalite. Although amplitudes are much lower than over the younger, synkinematic intrusions, subtle variations in the airborne radioelement and magnetic patterns over the pluton crudely reflect the distribution of these phases (Fig. 9). Ground spectrometry differentiates the intrusive phases into porphyritic and equigranular types through their K and U contents (Fig. 10). Lower average radioelement concentrations in the equigranular units (0.4% K, 0.3 ppm eU, 0.6 ppm eTh) suggest they may be earlier, and slightly less fractionated relative to quartz-phyric and quartz-megacrystic phases (0.7% K, 0.6 ppm eU, 0.8 ppm eTh). This supports the theory that the phenocryst content of a magma is evidence for a period of crustal residence during which cooling towards subsolidus temperatures takes place, usually accompanied by some degree of differentiation.

Richard Lake tonalite (stations 92-155 to 92-189)

This subvolcanic intrusive complex also contains quartz porphyritic and equigranular tonalite and leucotonalite phases, but has measurable differences in geophysical signature, and REE and trace-element concentrations with megascopically similar phases within the Sneath Lake pluton (Fig. 9, 10). Geochemical differences include higher U, Th, and light to middle REEs (La, Ce, Nd, Sm) in the Richard Lake pluton (Bailes, 1988). The differences can be related to the fact that the Richard Lake complex is younger than the Sneath Lake complex, and chemically similar to the evolved arc magmas of the phase 3 volcanic sequence that contains the Chisel

Lake-Lost Lake-Ghost Lake volcanic-associated massive sulphide deposits (Bailes and Galley, 1996). The Sneath Lake complex, on the other hand, is chemically similar to the older, primitive arc lavas that host the Anderson Lake-Stall Lake-Rod 1, 2 volcanic-associated massive sulphide deposits.

Ground radiometric results (Fig. 11) support these contrasts as radioelement concentrations in the Richard Lake complex are significantly higher than the Sneath Lake complex. Quartz-phyric phases average 1.5% K, 4.5 ppm eTh, and 1.2 ppm eU. Equigranular phases average 1.7% K, 2 ppm eU, and 8 ppm eTh. The Richard Lake pluton is also markedly more magnetic than the Sneath Lake pluton (Fig. 9B). It is interesting to note that the highest eU and eTh values in the intrusive complex are from samples of hydrothermally altered and sulphide mineralized samples (Fig. 11). There may well be a correlation between the concentrations of phyllosilicate and aluminosilicate in these alteration zones and positive shift in radioelement concentrations. The low K, and generally lower eTh, values can be used to differentiate this subvolcanic intrusive complex from the synkinematic intrusions to the west and southeast.

Ground spectrometry measurements for the Chisel Lake and Anderson Lake stratigraphic sections (stations 92-001 to 92-145)

Detailed transects (Fig. 12, 13, 14) through the strata forming the footwall and hanging wall volcanic sequences to the Chisel Lake-Lost Lake-Ghost Lake and Anderson Lake-Stall Lake-Rod 1, 2 deposits were conducted in 1992 to establish radioelement signatures of the host supracrustal rocks. Despite the low radioelement concentrations typical of oceanic island arc assemblages, spectrometric variations are discernible. As shown in Figure 15, the eTh and K compositions determined by ground spectrometry clearly distinguish two separate fields defining the primitive and evolved volcano-plutonic arc assemblages decreed by Bailes and Galley (1996).

The eTh/K and eU/K ratios indicate a close litho-geochemical relationship between the Sneath Lake subvolcanic intrusive complex and the rhyolite extrusive complex that hosts the Anderson Lake-Stall Lake-Rod 1, 2 volcanic-associated massive sulphide deposits (Fig. 15). This includes the Anderson rhyolite, which Bailes and Galley (1996) have grouped into the phase 2 volcanic sequence. The generally higher K concentrations of the rhyolite may be due to low temperature hydrothermal alteration that occurred after emplacement of the felsic flows (Galley et al., 1993).

The second grouping includes the Richard Lake intrusive complex, the dacite sill/dyke swarm that intrudes the phase 2 and 3 volcanic rocks, the phase 3 Powderhouse formation volcanoclastic dacite, and the Photo Lake rhyolite. Textural, mineralogical, and geochemical similarities between the intrusive dacite and Powderhouse formation established by Bailes (1988) indicate that these rock types are cogenetic. The positive K value shift of the Powderhouse dacite may be again due to extensive hydrothermal alteration of this formation (Galley et al., 1990; Galley et al., 1993). The overlap of fields between the Photo Lake rhyolite and the Richard Lake

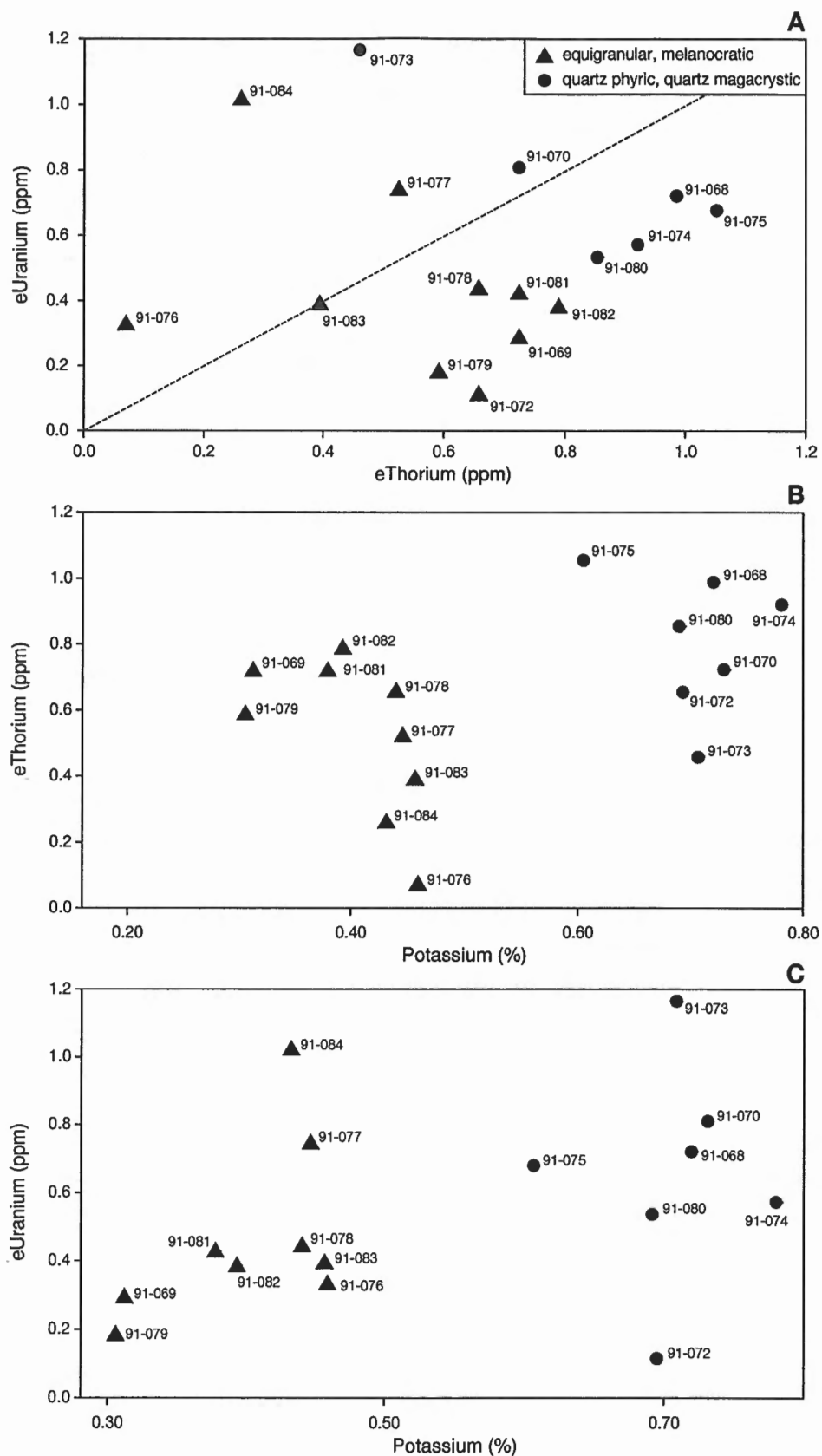


Figure 10. Ground spectrometric results, Sneath Lake subvolcanic tonalite. A phyric and phyric phases form clearly distinct fields.

intrusive complex may be genetic, but this is difficult to assess as the two rock types are separated by a late fault (Varnson Lake Fault). It suffices to note the strong correlation between the signature of the Richard Lake complex and the extrusive units belonging to the evolved arc sequence that contains the Chisel Lake-Lost Lake-Ghost Lake deposits. The similarities are enough for Bailes (1988) to hypothesize that the intrusive complex may have been the heat source responsible for the generation of the Chisel Lake-Lost Lake-Ghost Lake hydrothermal system.

The two remaining fields (high and low magnetic susceptibility quartz-phyric rhyolite) belong to two rhyolite units within the phase 4 volcanic assemblage sampled north of the Anderson Lake-Stall Lake-Rod 1, 2 deposits. Both units are relatively unaltered, and so the strong separation of the fields indicates separate magma sources. This is not surprising, considering the heterogeneity of units within this depositional cycle (Bailes and Galley, 1994).

SUMMARY AND CONCLUSIONS

The objective of this study was to evaluate the use of airborne, multiparameter geophysical surveys in defining potential volcanic-associated massive sulphide environments in the Rusty Lake and Snow Lake mining camps. Where similar surveys have been flown over Kuroko style volcanic-associated massive sulphide deposits in Newfoundland, the airborne potassium patterns successfully targeted sericitic hydrothermal alteration directly associated with the mineralization (Ford, 1993).

In the primitive, tholeiitic arc terranes of the Rusty Lake and Snow Lake areas, alteration is dominated by silicification and iron-magnesium metasomatism (garnet-chlorite-biotite-staurolite-actinolite) and less extensive sericitic zones. Low radioelement (K, U, Th) abundances are associated with these assemblages. The 500 m line-spacing used to collect the airborne data was found to be too coarse to detect the narrow

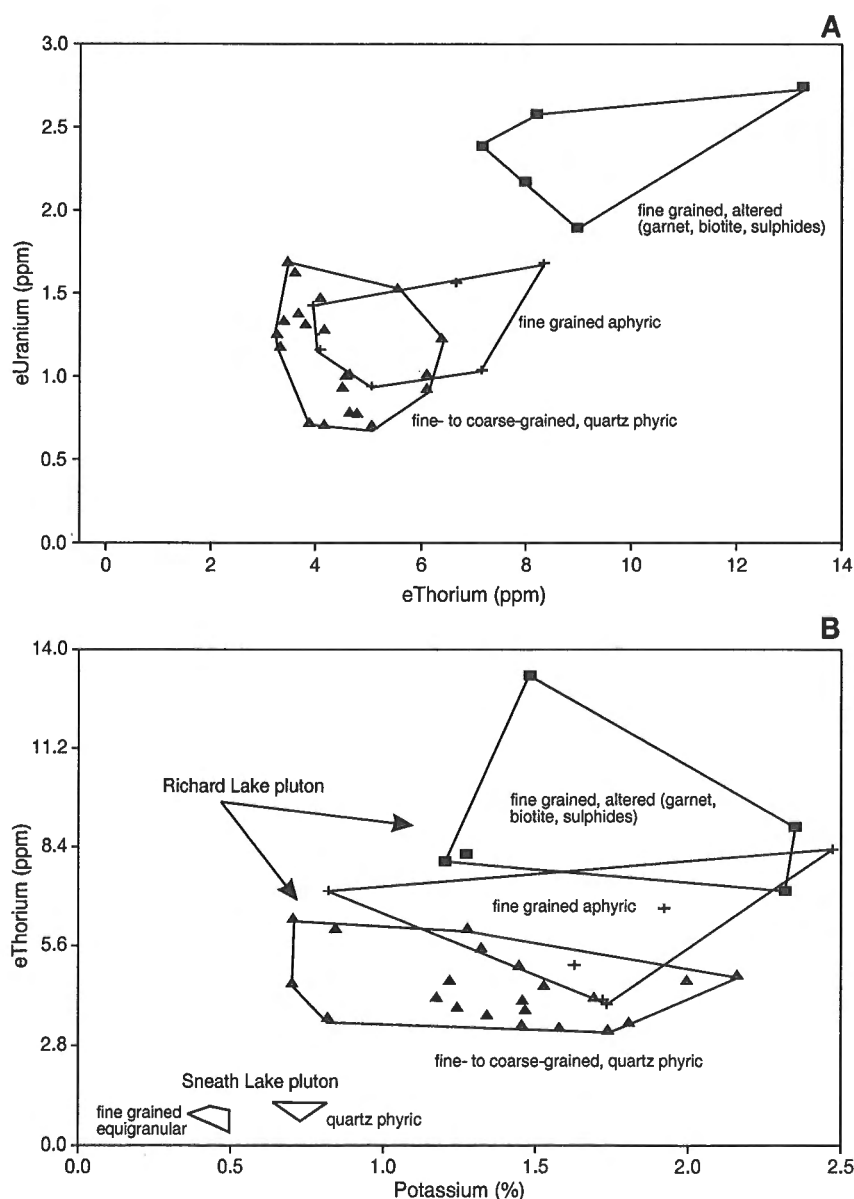
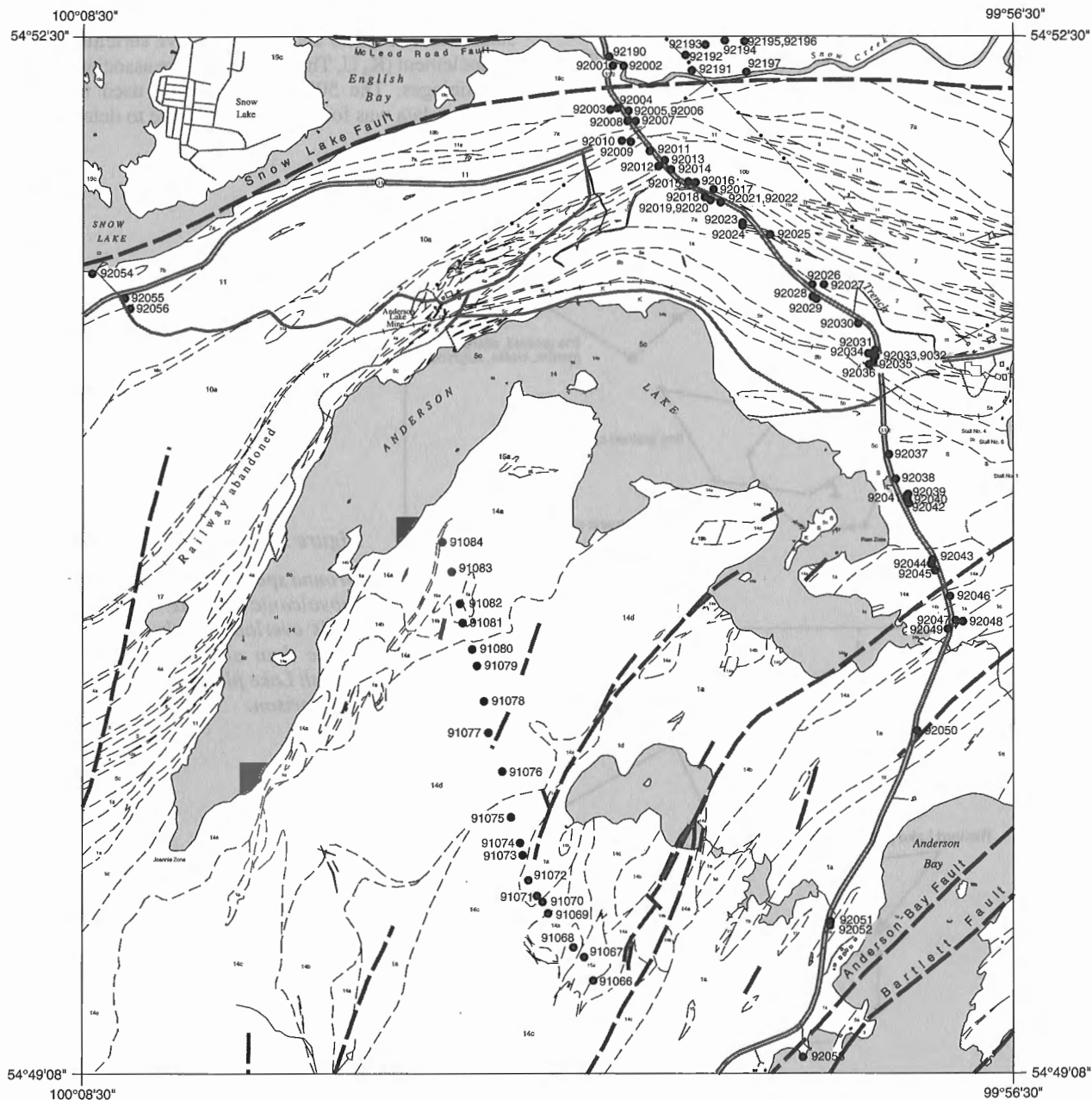


Figure 11.

Ground spectrometric results, Richard Lake subvolcanic tonalite. Aphyric and phyric fields overlap slightly and are less radioactive than altered phases. In Figure B, Sneath Lake pluton fields are indicated, for comparison.

sericitic alteration zones associated with individual volcanic-associated massive sulphide deposits. However, radiometric distinction of larger geological features can be used to direct explorationists towards terranes with volcanic-associated massive sulphide potential. These include the discrimination between synvolcanic and synkinematic intrusions, the latter being commonly spatially associated with clusters of massive sulphide deposits. It is hypothesized that the emplacement of these subvolcanic intrusive complexes causes the generation of seawater convection systems in the overlying volcanic pile. The formation of metal-rich hydrothermal fluids through fluid-rock interaction, and their subsequent focused discharge

on the seafloor results in the formation of massive sulphide deposits (Cathles, 1983). The fact that in the Precambrian subvolcanic intrusions commonly associated with volcanic-associated massive sulphide camps are I-type bodies with low radioelement concentrations typical of tholeiitic oceanic island arc environments makes it relatively easy to differentiate them from more evolved, K-U-Th-enriched synkinematic plutons. The fact that low K, I-type intrusions associated with successor arc volcanism are present in the Flin Flon Belt (Whalen and Hunt, 1994), and are younger and unrelated to the volcanic-hosted massive sulphide-hosting volcanic strata must also be taken into consideration. The use



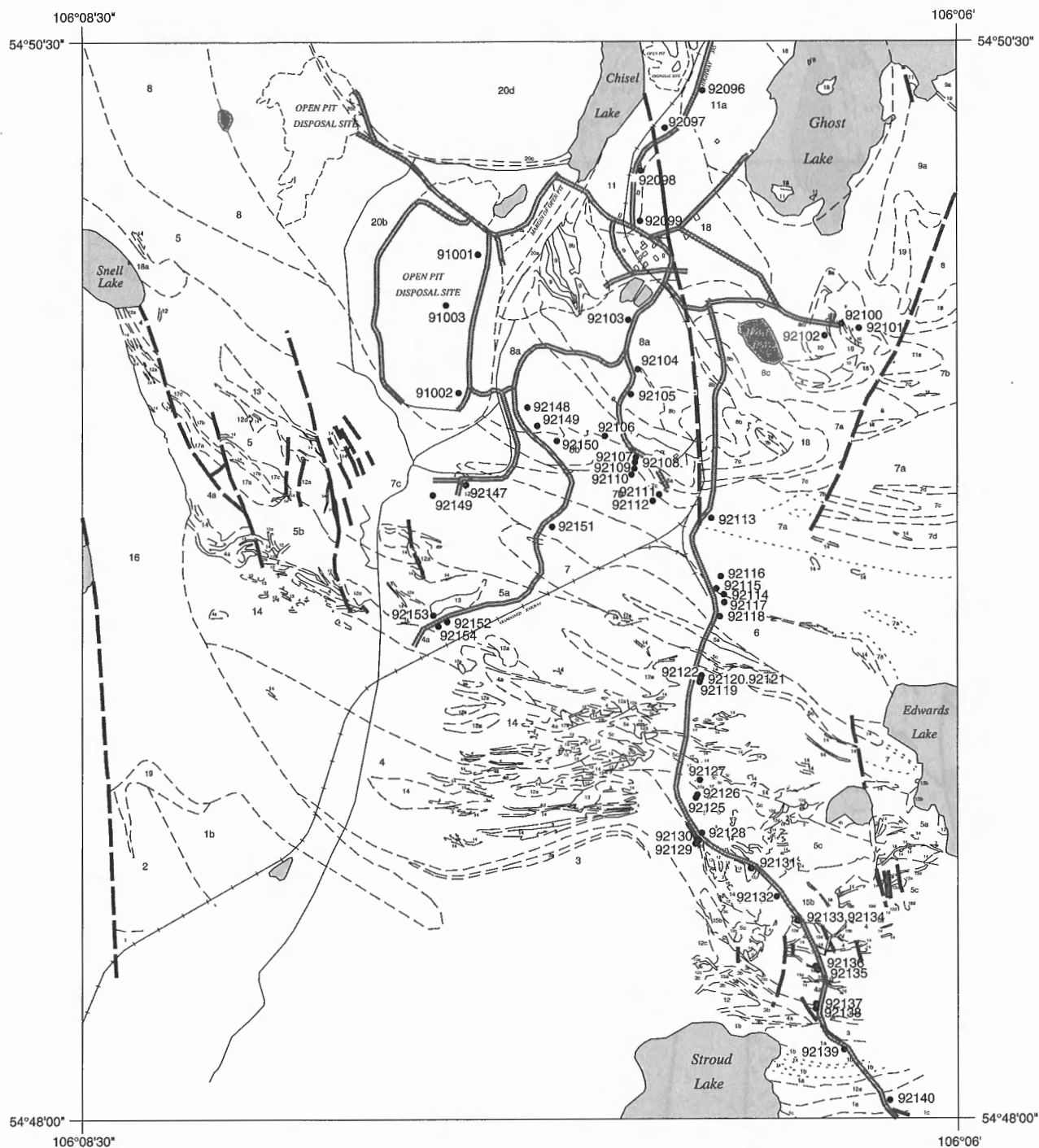


Figure 14. Geology, ground radiometric stations, Chisel Lake section detail traverses (geology from Galley, 1996).

of airborne spectrometric data must therefore be considered a "first-pass" tool, in which most synkinematic intrusions are recognized. Unfortunately, total field airborne magnetic data is not a good discriminant between synvolcanic and synkinematic intrusions, even when used in conjunction with radiometric data. For example, the synvolcanic Sneath Lake pluton in the Snow Lake mining camp has a very low magnetic signature, whereas certain intrusive phases of the Richard Lake pluton have enhanced magnetic signatures.

The ground spectrometric data collected in the Snow Lake area supported the airborne radiometric data in differentiating not only synvolcanic from synkinematic plutons, but also demonstrated chemical similarities between the two

subvolcanic intrusive complexes and spatially related rhyolite extrusive complexes that host volcanic-associated massive sulphide deposits. This is important, in that ground spectrometry can be used for on-site lithogeochemical fingerprinting and identification of cogenetic felsic intrusive-extrusive suites, an important guide to isolating rhyolite centres with the greatest potential for base-metal mineralization (Campbell et al., 1981; Cathles, 1983; Galley, 1995). In a broader context ground spectrometric data on volcanic strata and smaller intrusive dykes and sills can help bedrock mappers to correlate and differentiate the various rock units. This is particularly useful in highly deformed terranes where it is difficult to reconstruct original stratigraphy.

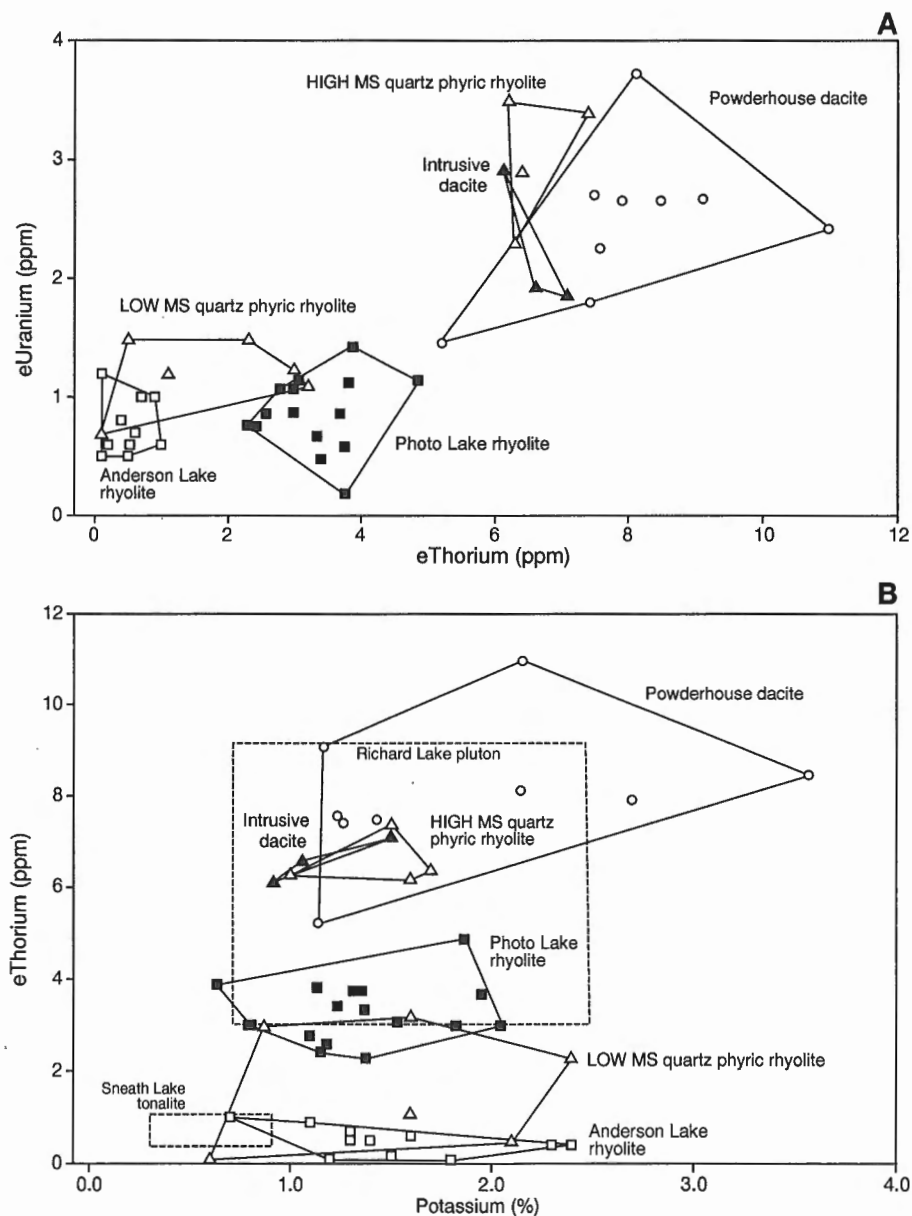


Figure 15. Ground spectrometric results, Chisel Lake and Anderson Lake area traverses. MS – magnetic susceptibility.

In the Rusty Lake belt spectrometry was less useful in targeting the host strata to the Ruttan deposit, as much of the volcanic sequence, and any associated subvolcanic intrusions, were displaced, or ingested, by synkinematic intrusions. Much of the volcanic rocks remaining are covered by surficial deposits which effectively mask the bedrock radiometric signature. Detailed ground spectrometry did identify the different intrusive suites present, and the occurrence of alteration in the basal basalt. The most significant uses for spectrometry in this region was the identification of REE-rich zones within the late kinematic Eden Lake alkalic intrusive complex, and delineation and differentiation between sand/gravel and clay deposits, useful criteria for Quaternary geology mappers.

In conclusion the results of this EXTECH project demonstrate that airborne and ground radiometric and magnetic measurements can be used to aid regional and local geological mapping. As a practical aid to volcanic-associated massive sulphide deposit exploration, these techniques can be used to identify and correlate volcanic stratigraphy (chemostratigraphy); to distinguish and subdivide subvolcanic intrusions acting as hydrothermal system heat engines and correlate them with specific volcanic cycles; and to identify felsic eruptive centres.

ACKNOWLEDGMENTS

The airborne data were collected by P. B. Holman and compiled by J.R. Hetu. A. Galley, A. Bailes, and D. Ames provided useful discussion regarding preliminary interpretation and ground follow-up targeting. D. Kurfurst, G. Labell, R. Lacroix, and J.R. Hetu are thanked for digitization and plotting of figures. J. Kitzler of Hudson Bay Exploration and Development kindly granted property access and accommodation in Snow Lake. Field assistance in 1991 was given by B. Maracle and in 1992 by L. Rebollo. Comments by A. Galley greatly improved the original manuscript.

REFERENCES

Ames, D.E.

- 1996: Stratigraphic and tectonic setting of the Paleoproterozoic Ruttan Cu-Zn VHMS deposit, Rusty Lake belt, Trans-Hudson orogen; in EXTECH I: A Multidisciplinary Approach to Massive Sulphide Research in the Rusty Lake-Snow Lake Greenstone Belts, Manitoba, (ed.) G.F. Bonham-Carter, A.G. Galley, and G.E.M. Hall; Geological Survey of Canada, Bulletin 426.

Ames, D.E. and Scoates, J.S.

- 1992: Geology, preliminary map of the geological setting of the Ruttan Cu-Zn deposit, Rusty Lake Belt, Manitoba; Geological Survey of Canada, Open File 2571, scale 1:5000.

Bailes, A.H.

- 1980: Geology of the File Lake area, Manitoba; Manitoba Department of Energy and Mines, Mineral Resources Division, Geological Report 78-1, 134 p.
- 1987: Silicification, Fe-Mg metasomatism and synvolcanic plutonism, Snow Lake, Manitoba; Geological Association of Canada-Mineralogical Association of Canada, Joint Annual Meeting, Saskatoon, Saskatchewan, Program with Abstracts, v. 12, p. 22.
- 1988: GS-8 Chisel-Morgan Lakes project; in Manitoba Department of Energy and Mines, Mineral Resources Division, Geological Report 88-1, p. 53-61.

Bailes, A.H. (cont.)

- 1993: Geology of the Anderson-Stall volcanic-hosted massive sulphide area, Snow Lake, Manitoba; Geological Survey of Canada, Open File 2776, scale 1:10 000.
- 1994: Geology of the Anderson-Stall volcanic-hosted massive sulphide area, Snow Lake, Manitoba; Geological Survey of Canada, Open File 2772, map with marginal notes, scale 1:10 000.

Bailes, A.H. and Galley, A.G.

- 1996: Setting of Paleoproterozoic volcanic-hosted massive base metal sulphide deposits, Snow Lake in EXTECH I: A Multidisciplinary Approach to Massive Sulphide Research in the Rusty Lake-Snow Lake Greenstone Belts, Manitoba, (ed.) G.F. Bonham-Carter, A.G. Galley, and G.E.M. Hall; Geological Survey of Canada, Bulletin 426.

Baldwin, D.A.

- 1988: Geology of the southern part of the Rusty Lake Volcanic Belt; Manitoba Energy and Mines, Geological Report GR86-1, 90 p.

Campbell, I.H., Franklin, J.M., Gorton, M.P., Hart, T.R., and Scott, S.D.

- 1981: The role of subvolcanic sills in the generation of massive sulphide deposits; *Economic Geology*, v. 76, p. 2248-2253.

Cathles, L.M.

- 1983: An analysis of the hydrothermal system responsible for massive sulphide deposition in the Hokuroku basin of Japan; *Economic Geology*, Monograph 5, p. 439-487.

Clarke, M.D.

- 1989: Surficial geology, Cormorant Lake, Manitoba-Saskatchewan; Geological Survey of Canada, Map 1699A, scale 1:250 000.

Ford, K.L.

- 1993: Application of gamma-ray spectrometry to the exploration for VMS deposits in the Robert's Arm Group and Tulk's volcanic belt, central Newfoundland; in Report of Activities 1993, Newfoundland Department of Mines and Energy, p. 12-13.

Galley, A.G.

- 1995: Target vectoring using lithogeochemistry: applications to the exploration for volcanic-hosted massive sulphide deposits; *Canadian Institute of Mining and Metallurgy*, v. 88, no. 990, p. 15-27.

Galley, A.G., Bailes, A.H., Syme, E.C., Bleeker, W., Macek, J.J., and Gordon, T.M.

- 1990: Geology and mineral deposits of the Flin Flon and Thompson belts, Manitoba; field trip guidebook No. 10, 8th International Association on the Genesis of Ore Deposits Symposium, Geological Survey of Canada, Open File 2165.

Galley, A.G., Bailes, A.H., and Kitzler, G.

- 1993: Geological setting and hydrothermal evolution of the Chisel Lake and North Chisel Zn-Pb-Ag-Au massive sulphide deposit, Snow Lake, Manitoba; *Exploration and Mining Geology*, v. 2, p. 271-295.

Geological Survey of Canada

- 1977: Geophysical series (airborne gamma ray spectrometric), map 35364G (NTS 64B, Uhlman Lake, Manitoba) and map 35364 (64C, Granville Lake, Manitoba); U Reconnaissance Program, Geological Survey of Canada, scale 1:250 000.

- 1991a: Airborne geophysical survey of the Snow Lake area, Manitoba; Geological Survey of Canada, Open File 2300, scale 1:250 000.

- 1991b: Airborne geophysical survey of the Ruttan area, Manitoba; Geological Survey of Canada, Open File 2301, scale 1:250 000.

Gordon, T.M., Hunt, P.A., Bailes, A.H., and Syme, E.C.

- 1990: U-Pb ages from the Flin-Flon and Kiseeweenaw belts, Manitoba: chronology of crust formation at an Early Proterozoic accretionary margin; in The Early Proterozoic Trans-Hudson Orogen of North America, Geological Association of Canada, Special Paper 37, p. 177-200.

International Atomic Energy Agency

- 1991: Airborne gamma ray spectrometer surveying; Technical Report Series No. 323, IAEA Vienna, 97 p.

Kaszycki, C.A. and DiLabio, R.N.W.

- 1986: Surficial geology and till geochemistry, Lynn Lake-Leaf Rapids region, Manitoba; in Current Research, Part B; Geological Survey of Canada, Paper 86-1B, p. 245-256.

Kaszycki, C.A., Neilsen, E., and Gobert, G.

- 1996: Surficial geochemistry and response to volcanic-hosted massive sulphide mineralization in the Snow Lake region; in EXTECH I: A Multidisciplinary Approach to Massive Sulphide Research in the Rusty Lake-Snow Lake Greenstone Belts, Manitoba, (ed.) G.F. Bonham-Carter, A.G. Galley, and G.E.M. Hall; Geological Survey of Canada, Bulletin 426.

Manitoba Energy and Mines

- 1986a: Bedrock geology compilation map series, NTS 64B – Uhlman Lake; Manitoba Energy and Mines, scale 1:250 000.
1986b: Bedrock geology compilation map series, NTS 64C – Granville Lake; Manitoba Energy and Mines, scale 1:250 000.

McRitchie, W.D.

- 1989: Ground scintillometer reconnaissance of the Eden Lake aegirine-augite monzonite; in Report of Field Activities 1989, Manitoba Energy and Mines, Minerals Division, p. 7-12.
1990: Ground scintillometer reconnaissance of the Eden Lake aegirine-augite monzonite; in Report of Field Activities 1989, Manitoba Energy and Mines, Minerals Division, p. 7-12.

Morrison, D.W. and Whalen, J.B.

- 1995: Granitoid plutons and major structures in the Iskwasum Lake sheet, Manitoba: a portion of the Flin Flon Domain of the Trans-Hudson Orogen; in Current Research 1995-C; Geological Survey of Canada, p. 225-234.

Saskatchewan Energy and Mines

- 1984: Gold in Saskatchewan; Saskatchewan Geological Survey Open File 84-1, 134 p.

Schmitt, H.R., Hornbrook, E.H., and Friske, P.W.B.

- 1989: Geochemical results and interpretations of a lake sediment and water survey in the Lynn Lake-Leaf Rapids region, northern Manitoba; Geological Survey of Canada, Open File 1959, 147 p.

Shives, R.B.K.

- in press: Results of in situ gamma-ray spectrometry and lithogeochemical analyses of selected samples, Snow Lake and Ruttan Lake areas, Manitoba; Geological Survey of Canada, Open File 3231.

Sinha, A.K. and Palacky, G.J.

- 1996: Ground electromagnetic, magnetic, and VLF-EM surveys at four sites near Snow Lake; in EXTECH I: A Multidisciplinary Approach to Massive Sulphide Research in the Rusty Lake-Snow Lake Greenstone Belts, Manitoba, (ed.) G.F. Bonham-Carter, A.G. Galley, and G.E.M. Hall; Geological Survey of Canada, Bulletin 426.

Whalen, J.B.

- 1993: Geology, Elbow Lake, Manitoba; Geological Survey of Canada, Open File 2709, scale 1:50 000.

Whalen, J.B. and Hunt, P.A.

- 1994: Geochronological study of granitoid rocks in the Elbow Lake map area, Manitoba: a portion of the Flin Flon Domain of the Trans Hudson Orogen; in Radiogenic Age and Isotopic Studies: Report 8; Geological Survey of Canada, Current Research 1994-F, p. 87-96.

Wright, D.F. and Bonham-Carter, G.F.

- 1996: VHMS favourability mapping with GIS-based integration models, Chisel Lake-Anderson Lake area; in EXTECH I: A Multidisciplinary Approach to Massive Sulphide Research in the Rusty Lake-Snow Lake Greenstone Belts, Manitoba, (ed.) G.F. Bonham-Carter, A.G. Galley, and G.E.M. Hall; Geological Survey of Canada, Bulletin 426.

Young, J. and McRitchie, W.D.

- 1990: REE investigations, Eden Lake intrusive suite (NTS 64C/9); in Report of Field Activities 1990, Manitoba Energy and Mines, Minerals Division, p. 9-19.

Contribution to the 1989-1994 Rusty Lake-Snow Lake Mining Camps, Canada-Manitoba Exploration Science and Technology Initiative (EXTECH I)

Ground electromagnetic, magnetic, and VLF-EM surveys at four sites near Snow Lake

A.K. Sinha¹ and G.J. Palacky²

Sinha, A.K. and Palacky, G.J., 1996: Ground electromagnetic, magnetic, and VLF-EM surveys at four sites near Snow Lake; in EXTECH I: A Multidisciplinary Approach to Massive Sulphide Research in the Rusty Lake-Snow Lake Greenstone Belts, Manitoba, (ed.) G.F. Bonham-Carter, A.G. Galley, and G.E.M. Hall; Geological Survey of Canada, Bulletin 426, p. 299-317.

Abstract: Ground electromagnetic (EM) and magnetic surveys were conducted over four major volcanogenic massive sulphide occurrences in the Snow Lake greenstone belt, Manitoba, as part of the EXTECH I Project. The purpose of the survey was to measure typical EM and magnetic signatures over these deposits, interpret the results in terms of the electrical and magnetic properties of the sulphides and the host rock, and compare the results with rock properties of drill core and hand specimen samples of sulphides in the laboratory. A multifrequency, multiseparation horizontal-loop EM survey was used at three sites, and the ground VLF-EM method was used at the fourth site to determine the conductivity characteristics of the sulphide bodies and the host rocks. Magnetic characteristics of the deposits were obtained by interpreting total field and vertical magnetic gradient survey data.

Despite differences in geological setting and mineralogical compositions, the investigation showed that all four sulphide deposits are poorly conductive (conductances from 0.1 to 2 S). Some conductors are distinctively magnetic, while others have little magnetic association. Such characteristics are unlike those observed in other Precambrian greenstone belts, where sulphide deposits are highly conductive and usually have some association with magnetic minerals. The results of this study could have important significance for future mineral exploration in the Snow Lake area.

Résumé : Dans le cadre du projet EXTECH I, on a procédé à des levés électromagnétiques et magnétiques au sol au-dessus de quatre gisements de sulfures massifs volcanogènes de la ceinture de roches vertes de Snow Lake, au Manitoba. On voulait ainsi mesurer les signatures électromagnétiques et magnétiques typiques de ces gisements, interpréter les résultats en termes de propriétés électriques et magnétiques des sulfures et des encaissants, mais aussi comparer les résultats obtenus aux propriétés déterminées en laboratoire de carottes et d'échantillons de sulfures. À trois des sites choisis, on a utilisé les levés électromagnétiques à boucle horizontale (plusieurs fréquences et plusieurs intervalles de séparation de l'émetteur et du récepteur); au quatrième site, on a fait appel aux levés VLF-EM au sol pour déterminer les caractéristiques de conductivité des corps minéralisés en sulfures et des encaissants. Les caractéristiques magnétiques des gisements ont été établies grâce à l'interprétation des données du champ total et du gradient magnétique vertical.

Malgré les différences en ce qui a trait au contexte géologique et à la composition minéralogique, les analyses ont démontré que les quatre gisements de sulfures sont peu conducteurs (conductance variant de 0,1 à 2 S). Certains conducteurs sont clairement magnétiques tandis que d'autres le sont peu. Ces résultats diffèrent de ceux obtenus dans d'autres ceintures de roches vertes, où les gisements de sulfures sont très conducteurs et sont habituellement liés d'une quelconque façon à des minéraux magnétiques. Les résultats de la présente étude pourraient avoir d'importantes répercussions sur les futurs travaux d'exploration minière dans la région de Snow Lake.

¹ 835 Acadian Gardens, Gloucester, Ontario K1C 2V7

² Geological Survey of Canada, 601 Booth St. HFSE, Ottawa, Ontario K1A 0E8

INTRODUCTION

The Geological Survey of Canada initiated the Exploration Science and Technology (EXTECH) program in 1989 for multi-disciplinary integrated research on volcanogenic massive sulphide (VMS) deposits at two base metal mining camps located at Snow Lake and Leaf Rapids (Ruttan mine) in Manitoba. The aim of the five year (1989-1994) project was to develop and improve existing exploration technology and to generate new exploration ideas and approaches to explore for volcanogenic massive sulphide deposits in the two areas. It was believed that the enhanced regional databases for airborne and ground geophysics, regional lake sediment and water geochemistry, bedrock geology, till geochemistry, and Quaternary geology would result in integrated deposit modelling and development of a regional mineral potential model through a geographic information system (GIS). The sharing and integration of the information from a wide range of sources was expected to lead to true *synergism*, in other words, knowledge and information from one discipline could be used to improve the conceptual model derived from other disciplines.

The Snow Lake and the Leaf Rapids areas were selected as sites for the EXTECH program mainly because they were established mining camps with an abundance of developed Cu-Zn-rich massive sulphide deposits and numerous sub-economic base metal occurrences. The project also benefited from relatively easy access to much of the area and co-operation of the provincial geological survey and private mining and exploration companies operating in the area.

Geophysical investigations formed an essential part of the multidisciplinary EXTECH investigations. A study of previous activities in the Snow Lake area indicated that ground electromagnetic (EM) methods, such as multifrequency horizontal-loop EM (HLEM), Turam, AFMAG, and time-domain EM had been used by contractors and exploration companies. The Turam and AFMAG systems respond best to long, linear conductors and have been most successful in detecting geological contacts, shear zones, and thin, long sulphide bands. Time-domain EM systems (Crone DEEPEM) and HLEM systems, such as the MaxMin and the Geonics EM-17, have been more successful in detecting massive sulphide ore bodies. Airborne EM (AEM) systems, such as the multifrequency, multicoil Dighem II helicopter EM and time-domain INPUT systems, have also been flown over the area.

Discussions with geologists from mining companies operating in the Snow Lake area indicated that the MaxMin HLEM system had fairly good success in detecting shallow (less than 100 m deep) conductors in the area. However, most of these contract surveys used only one or two frequencies, and generally one transmitter-receiver separation, for fast conductor detection. The lack of determination of the electrical characteristics of the conductors made it difficult for the interpreter to decide which were appropriate for drilling.

The purpose of the present investigation was to conduct ground EM and magnetic surveys over a number of known subeconomic (and therefore undeveloped) volcanogenic

massive sulphide deposits using state-of-the art HLEM, very low frequency (VLF) EM and ground magnetic gradiometer instruments to obtain data about electrical conductivity and magnetic susceptibility of the deposits. The latest MaxMin system, MaxMin I, used in this investigation, can operate at 8 frequencies and up to 8 coil separations between the transmitter and the receiver, and offers more flexibility for detecting conductors of varying conductance and depth. Furthermore, sulphide samples from several Snow Lake deposits were tested for their electrical properties (Katsube et al., 1996). Such information would be an essential component of the geophysical database on the volcanogenic massive sulphide deposits of the area and would be useful in exploration for additional ore bodies in the Snow Lake camp.

Since EM measurements are adversely affected by the presence of man-made structures, surveys near operating mines were not considered. The ideal targets for our surveys would be undeveloped sulphide occurrences with which there is extensive geological information and drilling data. But in the Snow Lake area, the amount of geological information on subeconomic deposits is limited and access to some of them is difficult. After extensive consultations with EXTECH project geologists and mining companies, four occurrences near Snow Lake were selected. During the winter of 1990, EM and magnetic surveys were conducted over three sites (Linda 2, Joannie, and Cook Lake north), and the fourth site (Copperman) was surveyed during the summer of 1990.

GEOLOGICAL SETTING AT THE FOUR SURVEY AREAS

The Snow Lake area is situated in north-central Manitoba within the eastern half of the Paleoproterozoic Flin Flon-Snow Lake greenstone belt, which is 250 km long in an east-west direction, and is up to 60 km wide. The belt consists of a series of variably metamorphosed 1.89 to 1.95 Ga subaqueous volcano-sedimentary domains representing several accreted oceanic arc segments that are intruded by 1.75 to 1.34 Ga synkinematic batholiths. The youngest intrusions are contemporaneous with 1.45 to 1.32 Ga subaerial sedimentation and minor volcanism. These rocks have undergone complex folding and faulting, and have been affected by increasing grades of metamorphism from south to north, where the greenstone belt grades into the Kiseynew Sedimentary Gneiss terrane. All of the massive base-metal sulphide deposits in the belt are hosted within the 1.89 to 1.95 Ga volcanic suites. The massive sulphide deposits of the Snow Lake area are hosted within a bimodal suite of volcanic rocks that represent various stages of oceanic island-arc evolution. The known massive sulphide deposits contain a total of 35 million tonnes of massive sulphide, and are divided into Cu- and Zn-rich types. For a more comprehensive overview of the tectonics and metallogeny of the belt, and the setting and character of the Snow Lake massive sulphide deposits, refer to Bailes and Galley (1996).

In common with most of Manitoba, the area has been subjected to recent glaciation, the last glacial retreat having occurred about 10 000 BP. The glacial scouring flattened the

surface, so that the present topographical relief ranges from 20 to 70 m (Jackson, 1983). The area has many low ridges, trending north, separated by lakes or low-lying areas containing muskeg. The amount of outcrop exposure is almost nil in the low ground, but good along some of the ridges. The locations of the four sulphide deposits investigated in this study are shown in Figure 1. Descriptions of the geological settings at the four survey areas are given below.

Linda 2 deposit

The Linda 2 deposit was extensively drilled by Falconbridge Ltd. during 1978-1981 and consists of 13 million tonnes grading 0.3% Cu and 0.79% Zn (Bailes and Galley, 1996). The deposit is hosted by the Anderson felsic extrusive complex on the overturned limb of the Anderson Bay anticline (Zaleski and Halden, 1988). The deposit consists of a large massive sulphide lens underlain by two smaller lenses, all encapsulated by sericite-rich alteration facies. Minor amounts of stratiform graphite is present, possibly along fault surfaces.

The deposit is a massive to semimassive sulphide body, which occurs as a concordant thick lens with a maximum thickness of about 50 m, associated with quartz porphyry. Medium- to coarse-grained, granular pyrite is intergrown with abundant calcite or quartz. Pyrrhotite, sphalerite, and chalcopryrite are present in minor amounts sporadically through the deposit. Several smaller, less extensive sulphide lenses are associated with stringer and disseminated mineralization underlying the main sulphide body. These lenses vary from dominantly pyrite-calcite, to pyrite with minor pyrrhotite-sphalerite-chalcopryrite and silicate alteration minerals. According to Falconbridge Ltd. geologists, the shallowest depth of the deposit is about 30 m at the western end, and it plunges to more than 700 m at the eastern end. The host strata generally strike 040 to 070° and dip 55 to 70° northwest.

In the immediate vicinity of the Linda 2 deposit, exposure is generally poor and neither the deposit nor its associated alteration outcrops on the surface. The definition of both surface and subsurface stratigraphy and morphology has depended mainly on the interpretation and projection of drill core data.

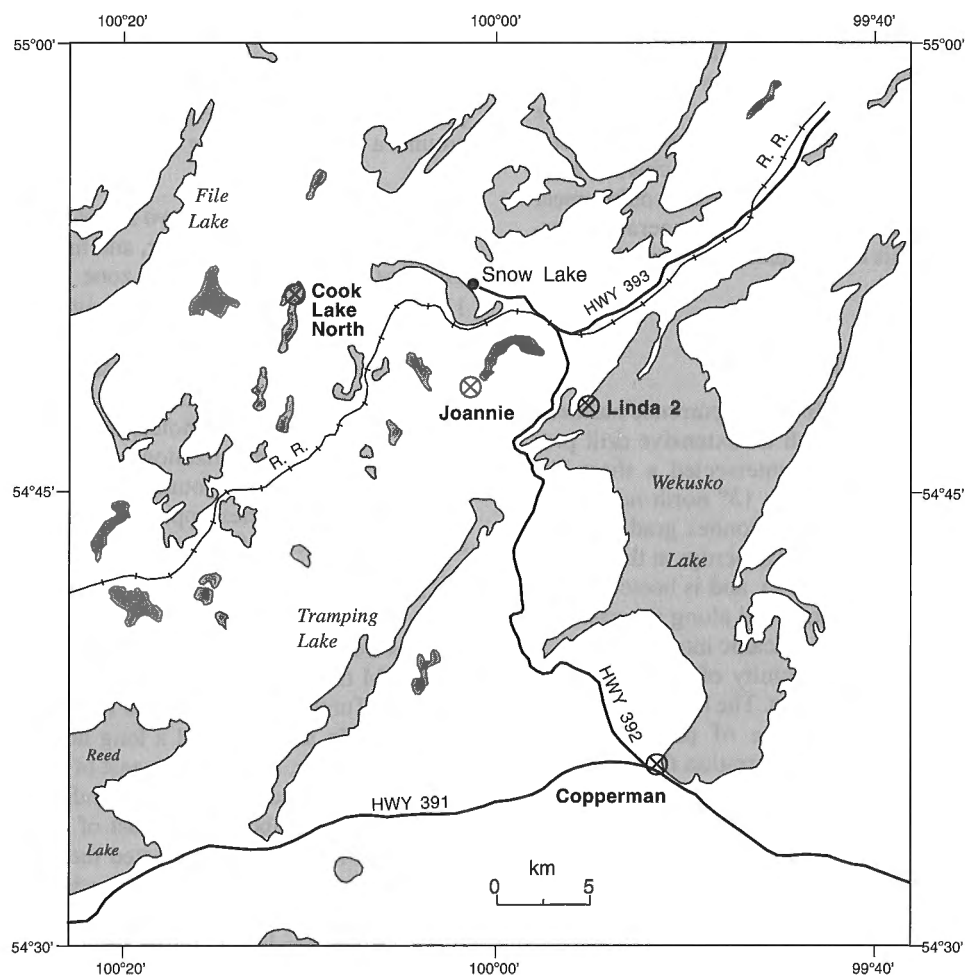


Figure 1. Location of four survey areas near Snow Lake, Manitoba.

Joannie occurrence

The Joannie occurrence, also called Occurrence 20, was first recorded as a claim in 1943, and occurs just west of the termination of the Anderson rhyolite, a large extrusive complex that hosts three of the areas Cu-rich massive sulphide deposits (Fig. 1). The occurrence is hosted within a sequence of mafic flows of the Welch Formation. The flows are truncated several hundred metres to the south by the north margin of the Sneath Lake subvolcanic intrusive complex, and the immediate area of the occurrence is crosscut by several dykes from the complex. Eccles and Fedikow (1985) describe eight discontinuous units of mafic and intermediate volcanic flows and fragmental rocks. A chlorite-garnet-biotite schist, produced as a result of mineralization-related alteration of fragmental hornblende andesite, forms one of the eight units. The chlorite-garnet-biotite schist is crosscut by quartz veins that contain vestiges of assimilated wall rock and very minor disseminated sulphides. The remaining strata are affected by moderate to strong amphibole alteration (Bailes and Galley, 1996, in pocket).

The Joannie occurrence consists of a Cu-rich discordant vein stockwork zone representing epigenetic vein mineralization that commonly underlies volcanic-hosted massive sulphide deposits (Eccles and Fedikow, 1985). Drill intersections contained up to 5 m of 3.16% Cu as pyrrhotite-chalcopryrite veins and disseminations in a chlorite-garnet-biotite-rich alteration envelope. Drilling has failed to locate an associated stratiform massive sulphide lens, although there is a thin, extensive unit of sulphidic exhalite present several tens of metres into the hanging wall of the stockwork zone (Foot-Mud horizon; Bailes and Galley, 1996). It would appear that either the hydrothermal system failed to generate a massive sulphide lens above this fluid channelway, or it has been subsequently eroded.

Cook Lake north occurrence

The Cook Lake north massive sulphide occurrence has been tested by Falconbridge Ltd. through an extensive drill program. Twelve diamond-drill holes intersected a sheet-like body of rather complex shape dipping 13° north-northwest, consisting of approximately 4 million tonnes grading 0.4% Cu. (Edwards, 1990). The occurrence subcrops at the bottom of the north end of Cook Lake (Fig. 1), and is hosted within a felsic rhyolite complex that is intruded along the east side of the lake by the Richard Lake subvolcanic intrusion (Bailes, 1988). The volcanic units in the vicinity of the occurrence strike north, dipping steeply to the west. The lake morphology is controlled by an extensive zone of phyllosilicate-amphibole-aluminosilicate-sulphide alteration that was preferentially eroded by glacial action (Jackson, 1983). A series of late, brittle, north-trending faults crosscut the host stratigraphy several hundred metres east of the occurrence.

The top of the conductor appears to be about 150 m deep. The sulphide horizon is characterized by massive pyrrhotite, pyrite, and chalcopryrite. The pyrite occurs both as coarse

(2 cm) pyrite euhedra and fine grained pyrite (0.1 mm). The average copper grades range from 0.23% to 0.99% with less than 0.04% zinc which does not make the deposit economic. Exploration strategy of Falconbridge Ltd. was based on drilling anomalies detected by ground time-domain EM surveys, but the approach resulted in investigating many graphitic conductors.

Copperman occurrence

The Copperman occurrence is located near the southwest corner of the Wekusko Lake, about 27 km southeast of Snow Lake, and is hosted within a series of mafic volcanoclastic strata and minor extrusive flows intruded by quartz diorite. Outcrops northeast of the surface expression of the deposit consist of massive, very fine grained basalt flows. A series of fragmental basalts, lapilli tuffs with 5% intercalated fine grained, green, massive flows are located south and east of the deposit (Trembath and Fedikow, 1990). The access to the site is good, since Highway 391 runs across the property. The deposit, first drilled in 1928, was described by Wright (1931) as a northeasterly striking mineralized outcrop, 160 by 30 m in size near the southern tip of Wekusko Lake, and consisting of greyish green quartz, chlorite, and sericite schists cut by quartz veins up to 45 cm wide. The veins and the portions of the schists contain pyrite, sphalerite, and chalcopryrite. Earlier drilling in the area indicated that the richest sulphide zones were located at 30 to 90 m depth. The Cu-Zn showing presently consists of several old trenches and pits in and around a gossan showing extensive hematite and limonite stains.

The deposit consists of two zones of high-grade mineralization containing zinc, copper, and minor amounts of silver. The first zone, called the "A" zone is estimated to contain 170 000 tons ($\approx 188\ 000\ t$) of ore averaging 3.13% Cu and 4.17% Zn to a vertical depth of 245 m. A second zone, called the "B" zone, is estimated to contain 74 200 tons ($\approx 82\ 300\ t$) of ore averaging 1.49% Cu and 3.19% Zn to a vertical depth of 170 m. Several deep holes, drilled in late 1960s found copper and zinc mineralization below depths of 305 m, comparable in grade to that found in earlier drilling at shallower depths. The two zones appear to consist of narrow lenses, stringers, and pods of a massive sulphide body.

The area has been surveyed earlier by various companies using different ground and airborne geophysical methods, such as Turam, vertical loop EM, resistivity, magnetics, IP, DEEPEM time-domain EM, and Dighem II helicopter EM. A recent Turam survey detected two short conductors south of the Cu-Zn showing and a long northeast-southwest graphitic conductor, about 500 m east of it. A ground DEEPEM survey also located the graphitic conductor along with a short strike conductor about 50 m east of the Cu-Zn showing. A Dighem II AEM survey detected the graphitic horizon, but recorded only a weak response over the showing. An induced polarization and frequency-domain EM survey with a McPhar P-660 system produced similar results.

GEOPHYSICAL INSTRUMENTS AND SURVEY PROCEDURES

Surveys at Cook Lake north, Linda 2, and Joannie were conducted using the multifrequency, multiseparation MaxMin I HLEM system and EDA Omni IV magnetic gradiometer; the latter measures the total magnetic field and the vertical gradient of the field. At the Copperman site, VLF-EM measurements were taken using two or three frequencies simultaneously as well as the magnetic gradiometer and total field measurements. The two systems were integrated in the Omni-Plus system originally designed by EDA Instruments of Toronto, and now built by Scintrex Ltd. of Toronto. Brief descriptions of the geophysical instruments used and the survey procedures are outlined below.

Multifrequency Horizontal Loop Electromagnetic surveys

The MaxMin I is a multifrequency HLEM system designed and built by APEX Parametrics Ltd. of Uxbridge, Ontario. Surveys with the system can be carried out in five different coil configurations. In this study, only the Max I (horizontal coplanar) mode, which has the largest depth of investigation, was used. The distance between the transmitter and the receiver is maintained constant for all stations on a survey line. Increasing the coil separation results in greater depth penetration, but lower horizontal resolution of targets. The coil separation is restricted to one of the eight values (from 12.5 to 400 m) fixed by the manufacturer. Often, a line is resurveyed with more than one coil separation to resolve shallow and deep conductors. The system is designed such that the primary field from the transmitter is cancelled at the receiver for a given coil separation. If the actual coil separation during a survey differs from the intended value due to survey or human errors, the measured quadrature and especially the in-phase component will be in error. In fact, in rough terrain, topographic corrections are needed to account for changes in coil separation. The outputs consist of the in-phase and the quadrature components of the secondary magnetic field which are expressed as percentages of the primary EM field. The plotting point for the survey data is the mid-point between the transmitter and the receiver. The instrument can operate at eight preset frequencies from 110 to 14 080 Hz in multiples of two, and readings can be taken at any or all frequencies at the operator's discretion. In normal mineral exploration programs, the in-phase and quadrature components are measured at 2 or 3 frequencies and the results are plotted with in-phase and quadrature data on separate graphs for each frequency. Quantitative interpretation to determine the conductance (product of conductivity and thickness) and depth of the conductor requires the magnitude of the in-phase and quadrature response values at one frequency. When interpretation is done at several frequencies, the dispersion of conductance values with frequency indicates how individual interpretations were affected by the presence of conductive host rock and overburden in the area (Frischknecht et al., 1991).

The survey procedure consisted of operating the system with a fixed coil separation over the entire survey grid using as many frequencies as possible. If the survey area is not flat, topographic corrections are applied to the raw data (Apex Parametric, 1988). All field data were recorded using an APEX Parametrics MMC data logger and transferred to a portable computer periodically for examination and plotting. The acquired data were edited in the field office to conform to the "xyz" file format, which is the one used by the EMIX-MM Plus interpretation software (Interpex Limited, 1989) for the quantitative interpretation of the data.

Total field magnetic and gradiometer surveys

Magnetic surveys involving the measurement of the total field and its vertical gradient were carried out using an EDA Omni IV magnetic gradiometer built by EDA Instruments of Toronto. The magnetometer-gradiometer unit consists of two identical proton precession magnetometers mounted vertically at the end of a rigid fibreglass pole. The distance between the magnetometers is 0.5 m in the standard configuration. An identical unit served as the base station, which was set up in a magnetically quiet area near the survey grid. The field data were corrected for diurnal variations using software provided by the manufacturer.

The survey procedure consisted of recording the total field and the gradiometer readings at every station, generally every 25 m. In addition to the measured parameters, the LCD display also shows the statistical error of the measurement, based on several measured values, thereby giving an indication of the confidence level in the data. In case of a large statistical error, which could be caused by atmospheric noise and/or magnetic storms, the operator can reject the current measured values and repeat the sequence of measurements until a valid set of measurements are recorded.

Each survey line forms a new file in which the line number, station number, date and time of measurement, errors in the data, diurnal drift, magnetic intensity, magnetic gradient, and data quality factors are indicated. The magnetic surveys were considered as secondary to EM investigations during this survey. The main purpose of the magnetic survey was to determine if there were any correlation between bed-rock conductors detected by EM surveys and magnetic features.

Very low frequency electromagnetic surveys

The VLF-EM surveys were carried out using an OMNI-PLUS system, built by Scintrex Ltd., Toronto. It is a portable, microprocessor-based system capable of measuring contrasts in the physical properties by two different types of geophysical sensors: magnetic and EM. Thus, the OMNI-PLUS is a combined magnetometer and VLF system capable of recording either the magnetometer, VLF, or both data sets depending on the user's requirement. The system is capable of measuring and recording the VLF response at up to 3 frequencies simultaneously. The total time for acquiring three VLF and magnetic data sets at a station can be as little as 4 seconds.

The VLF sensor consists of three orthogonal coils, two horizontal and one vertical, mounted in a cylindrical housing on a back-pack frame. The OMNI-PLUS normally records the magnetic field components and their derived parameters such as the tilt angle at three frequencies. As the VLF primary field is a plane wave field, conductors oriented parallel to the direction to the station get preferential excitation. Therefore, the presence of two VLF stations with orthogonal or near orthogonal azimuths to the OMNI-PLUS receiver permits a complete mapping of all conductors in a survey area. In the system with the resistivity option, the instrument also measures the horizontal electric fields using three probes connected to the module. The system automatically calculates the apparent resistivity of the ground and the phase angle at three frequencies. The output of the instrument is the vertical in-phase, vertical quadrature, total VLF field intensity, dip angle, direction of the primary VLF field, signal/noise ratio which indicates the quality of the data, apparent resistivity of the ground, and the phase angle.

In normal ground VLF measurements, a uniform survey direction is maintained while taking readings in order to maintain consistent signs on all in-phase, quadrature, and tilt angle values. Since OMNI-PLUS has no orientation system, a convention is followed that north and east are positive. Hence, profiles plotted looking east (i.e., south to north) or north (i.e., west to east) will have the proper crossover sign. If a VLF station goes off the air during the survey, the operator can continue the survey with an alternative VLF station without losing any of the previously recorded data. A standard OMNI-PLUS can store the data for up to 1300 stations.

The digital data from the OMNI-PLUS is transferred to a personal computer from time to time. The first stage of processing consists of correcting the total field value by using a ground VLF monitor or some comparable method. In rugged terrain, a terrain correction is applied to the data. The corrected field parameters are then plotted in stacked profile form for the vertical in-phase, vertical quadrature, tilt angle, and total field values to locate linear conductive features in the survey area. The apparent resistivity values are contoured to show the variation of resistivity values measured at three VLF frequencies.

SURVEY RESULTS AND DATA INTERPRETATION

For the analysis of horizontal-loop EM (HLEM) data, two models were used for quantitative interpretation: a dipping half-plane and a horizontally-layered medium. The first model approximates bedrock conductors. If the shape of the conductor differs significantly from that of a plate, which is often the case, the interpreted parameters (conductance and depth to the top) may not be good estimates of the true values. The second model is used in situations where the HLEM response is presumably due to horizontally layered media (Quaternary overburden, sedimentary formations).

Identification and interpretation of bedrock conductors was done in three steps. First, trough-like anomalies with widths equal to or larger than the coil separation were identified on in-phase and quadrature plots of HLEM data. In theory, such anomalies are caused by vertical or dipping plate-like conductors. In practice, such response is often associated with bedrock conductors. Second, conductance and depth of conductors were determined with the aid of the EMIX-MM Plus program (Interpex Limited, 1989) at frequencies selected by the interpreter. The procedure was repeated for all coil separations. Finally, conductor locations were plotted on a map and the anomaly identification procedure was repeated on parallel lines to determine the strike direction and the extent of the conductor. At this stage, HLEM data were examined along the projected strike so that poorly resolved features, which were not apparent during the initial interpretation, were not omitted.

Horizontal-layer interpretation was carried out with the aid of the EMIX-MM program (Interpex Limited, 1988). At each survey location, in-phase and quadrature readings at 6 frequencies (from 440 to 14 080 Hz) were used in the inversion, which produced estimates of layer thicknesses and resistivities. In the first three survey areas, the HLEM data obtained at the two lowest frequencies (110 and 220 Hz) were too noisy to be useful. In Linda 2 and Joannie survey areas, the model consisted of two layers – poorly conductive glacial overburden and resistive bedrock. Because of the lack of a consistent pattern, the inversion results were not plotted in map form. In the Cook Lake north grid, the model consisted of three layers – resistive lake water, moderately conductive lake-bottom clays, and highly resistive bedrock. The results were compiled as a schematic map of resistivity.

The magnetic methods were used in the area to determine the magnetic characteristics of the sulphide bodies. As the presence of pyrrhotite is fairly common at the Snow Lake deposits, a coincident magnetic and HLEM anomaly would be indicative of the presence of sulphide conductors. Qualitative interpretation of total-field and vertical gradient data concentrated on anomalies coincident with HLEM responses.

The third geophysical technique used at one site (Copperman) is ground VLF. The OMNI-PLUS system is capable of measuring several parameters at three VLF frequencies simultaneously, which may be interpreted quantitatively using the model of two-dimensional conductor in a host rock of finite resistivity (Sinha, 1990). The presence of a conductor is indicated by a maximum on the total-field data and/or a crossover in the in-phase, quadrature, and the tilt angle response, if the survey line is normal to the azimuth to the transmitter station and the conductor strike. By measuring orthogonal components of the horizontal electric and magnetic fields, the method also provides apparent resistivity of the ground. If VLF anomalies are caused by conductors which cannot be approximated by two-dimensional models, quantitative interpretation will be in error.

The following sections describe the survey results and interpretations at each site.

Linda 2 deposit

The Linda 2 survey grid is depicted in Figure 2. Line 120S from a previous survey by Falconbridge Ltd. was selected as the base line for the new survey grid. Line 168W from the previous grid was similarly chosen as line 0 for the present survey. As Figure 2 shows, the angle between the base line and the Linda 2 deposit is approximately 30°. The spacing of the survey lines (parallel to line 0) was 50 m in the central part of the grid (between lines 150W and 100E). Two lines spaced 100 m apart were surveyed to the east and west of this core grid. Survey lines in the central area were 1200 m long (450S to 750N), while those near the edges were 1 km long (350S to 650N). The entire grid was surveyed using two coil spacings, 150 and 200 m. An interpretation report and digital geophysical data were released as a GSC Open File (Sinha and Palacky, 1992).

An HLEM anomaly most likely associated with the Linda 2 deposit was detected between lines 250W and 200E. An example of magnetic and HLEM response on line 100W is given in Figure 3. At the top of the figure are traces for total field and vertical gradient magnetic data. They are followed by in-phase and quadrature HLEM data (both are shown for a coil separation of 200 m and 7 frequencies, from 220 to 14 080 Hz). The trough-like HLEM anomaly centred at 85S is typical of bedrock conductors. For the in-phase response, the anomaly becomes visible at 880 Hz, but the trough disappears on the 14 080 Hz data, when the effect of moderately conductive overburden becomes prominent. For the quadrature response, negative readings associated with the anomaly are evident even at 220 Hz. There is a definite amplitude reversal at the highest frequency (14 080 Hz), which is typical

of bedrock conductors covered by overburden. Using 440 Hz data at 85S, interpretation with the EMIX-MM Plus program yielded a conductor with conductance of 1.2 S, depth 140 m, width 20 m, and a subvertical dip. On line 150W, the conductor was located at 100S and the conductance estimate was 0.9 S, while the remaining parameters were unchanged. On line 250W, the conductor was identified at 90S with interpreted conductance of 0.6 S, depth 150 m, width 20 m, and subvertical dip. Along the strike, HLEM amplitudes decrease rapidly in the northeasterly direction. Therefore, quantitative interpretation could not be reliably carried out east of line 100W, and only the locations of conductor positions are indicated. This finding is not surprising; geological mapping has indicated that the cigar-shaped body plunges rather steeply to the north-northeast, where it is known from drilling to be about 300 m deep at 300E. Such a depth is beyond the penetration capabilities of the APEX MaxMin I system. In fact, even on the lines to the west of 100W, quantitative interpretation was somewhat difficult and possibly not very reliable. The Linda 2 conductor (marked A in Fig. 4) has an associated magnetic high, about 50 nT in amplitude, which indicates that the deposit is weakly magnetic.

In addition to the Linda 2 deposit, three conductive trends were detected in the course of the HLEM survey and indicated as conductors B, C, and D in Figure 4. Conductor B extends from 350W-400N to 100W-300N. Its depth has been estimated between 130 and 200 m, comparable to the Linda 2 deposit. Conductance estimates on four lines, where it was detected, range from 0.2 to 1.6 S. There is a magnetic anomaly of over 100 nT associated with the conductor on lines 350W to 100W. Conductor C has a strike length of about 150 m (from 100W-575N to 50E-615N). A fairly strong magnetic

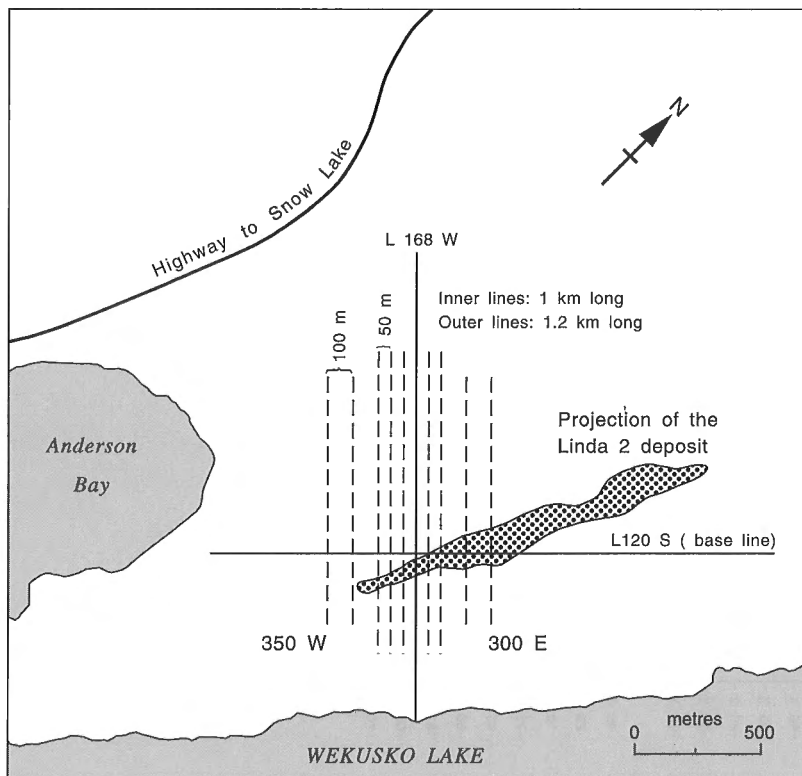


Figure 2.

Geophysical survey grid at Linda 2 and projection of deposit on surface.

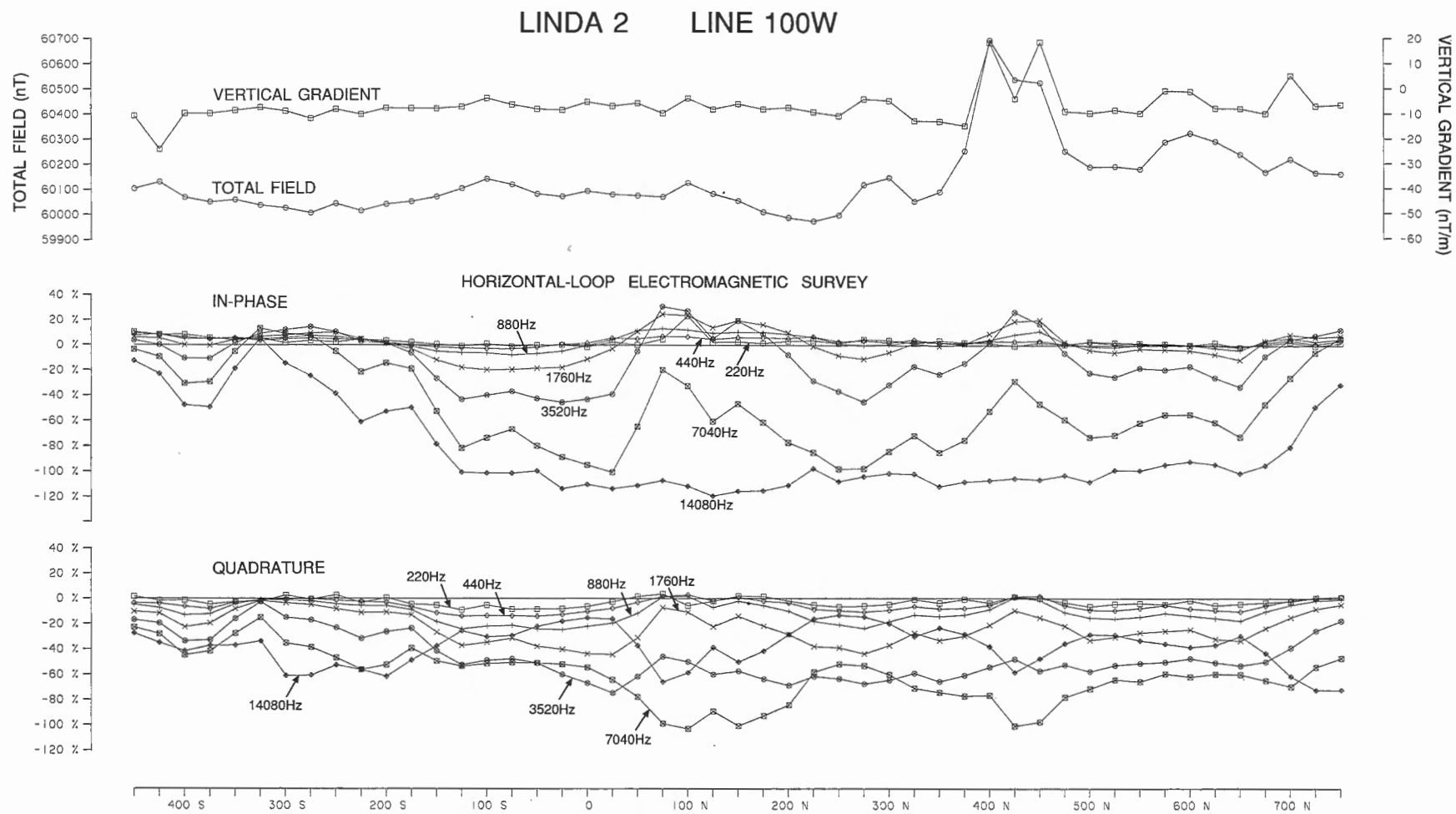


Figure 3. Magnetic and HLEM data acquired on line 100W at Linda 2. Coil separation was 200 m for HLEM survey.

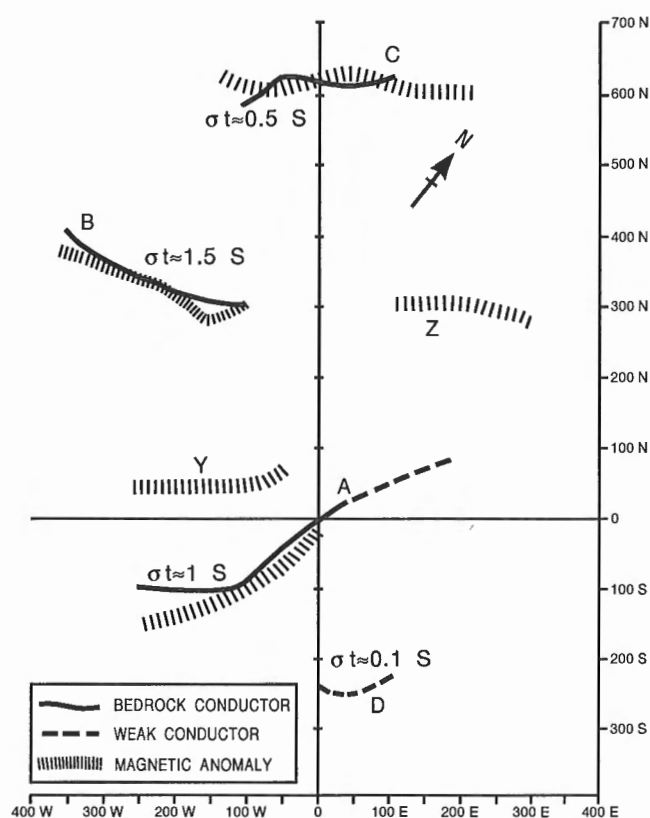


Figure 4. Map indicating interpreted locations of EM conductors and magnetic anomalies at Linda 2.

anomaly (over 100 nT) from 150W to 200E is associated with the short conductor. Depth estimates range from 80 to 160 m and conductances from 0.2 to 1 S.

Another conductor (D) is located to the southeast of Linda 2 deposit. It was identified on three survey lines (0-235S, 50E-240E, and 100E-220S) and only using the short coil separation (150 m). The fact that no clear response could be identified on data obtained with a 200 m coil separation, suggests that the anomaly is likely of surficial origin. The conductance estimates are very low (0.1 S) and no magnetic association was detected. Hence, the anomaly probably does not constitute a mineral exploration target.

There are two magnetic trends in the survey area not associated with conductors. Trend Y is very weak, with a maximum total-field anomaly of about 50 nT, extending from 350W-50N to 50W-100N. Trend Z, along which the total-field anomaly reaches 600 nT on line 100E (station 300N), extends east to the last survey line (300E).

To summarize our interpretation, the Linda 2 deposit (conductor A) is a poorly conductive and weakly magnetic target. Because of the rather unusual shape of the deposit (cigar-like), the use of a half-plane model for interpretation was not very appropriate. However, in HLEM interpretation there are no other models available to approximate a three-dimensional body. One can nevertheless conclude that the body has a very low conductance (1 S was the average of values obtained on several lines). This conclusion is

supported by laboratory resistivity measurements on four core samples from the deposit, which yielded a mean resistivity of 152 $\Omega \cdot m$, a rather high value for massive sulphides (Katsube et al., 1996). If a body with this resistivity was homogeneous with a thickness of 20 m, its conductance would be 0.12 S. These results indicate that a body like Linda 2 would be a difficult target for airborne EM surveys. Because of its considerable depth, such a deposit would not be easily detectable by helicopter EM surveys. Time-domain AEM systems, which have deeper penetration, but limited capability to discriminate low conductance targets, would probably fare no better in picking possible targets.

In the survey area, two conductors (B and C) have similar characteristics to the Linda 2 deposit: low conductance (around 1 S), depth at the detection limit of APEX MaxMin I system with a coil separation of 200 m (average depth 150 m), and some magnetic association. Because of the similarities, both might be considered exploration targets. However, they appear even more limited in size than the subeconomic Linda 2 deposit.

Joannie occurrence

The grid surveyed at Joannie covers an area of 1 km² and the base line is oriented northeast-southwest. The Joannie deposit lies approximately parallel to the base line, at around 350N. The survey lines (from 500W to 500E) are spaced 100 m apart, but fill-in lines at 50 m spacing were surveyed between 100W and 200E (Fig. 5). The lines extend 300 m southeast of the base line (to 300S) and 700 m northwest (to 700N). The grid was surveyed with HLEM using a 150 m coil spacing; the central lines were also surveyed with a 200 m coil spacing. The digital survey data and a geophysical interpretation report on the area were released as a GSC Open File (Palacky and Sinha, 1992b).

The Joannie deposit causes a strong magnetic anomaly from 100W-325N to 300E-415N. The total-field amplitudes reach the largest values at the ends of the conductor (over 1000 nT on line 100W and 900 nT on line 100E) dropping to about 400 nT on lines 0 and 50E and 300 nT on line 300E. An example of total-field and vertical-gradient magnetic data is depicted in Figure 6 for line 50E. The strong magnetic anomaly is consistent with the description of the deposit as being rich in pyrrhotite.

Well defined HLEM anomalies were detected on five central lines, from 100W to 100E, which were surveyed with two coil separations. Clear trough-like responses were detected in all ten cases. A sample of the HLEM response on line 50E (coil separation 150 m) is shown in Figure 6 below the magnetic profile. The in-phase anomaly is well defined only on the two highest frequencies, while the quadrature response is clear on six frequencies. The shape of the anomaly is asymmetrical, indicating a dip of about 15° to the south, which is consistent with the known geology. From the HLEM response, there is no evidence of even moderately conductive overburden (no reversals of high-frequency quadrature data). Quantitative interpretation was made with the EMIX-MM Plus program. Fairly consistent conductance estimates were obtained with both coil separations on all five lines; they

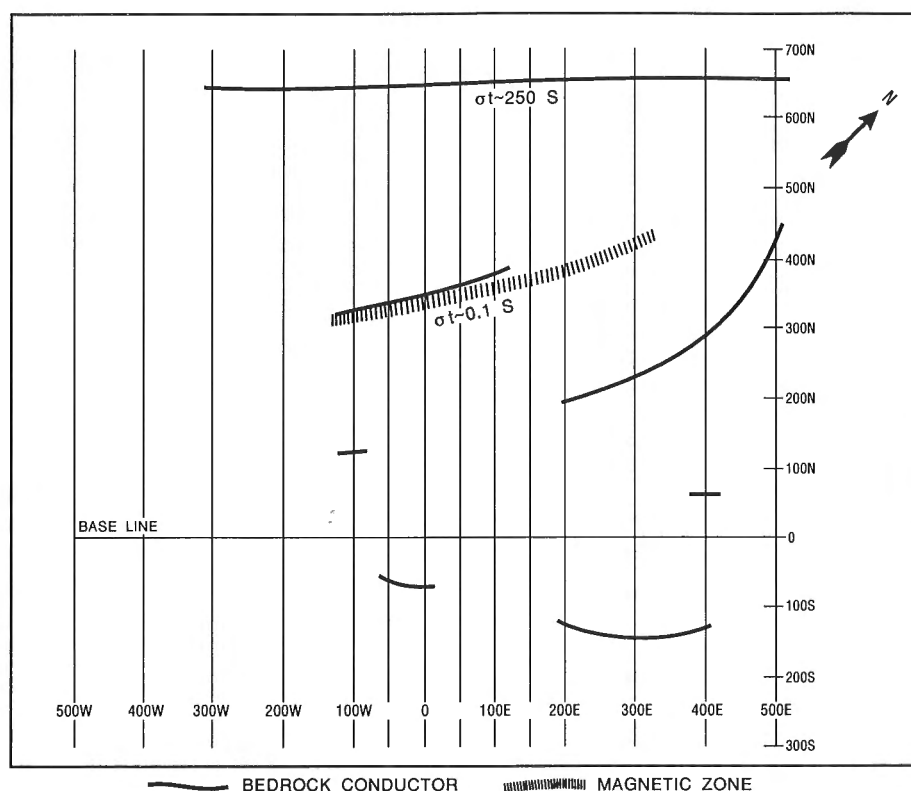


Figure 5. Geophysical survey grid at Joannie and interpreted locations of HLEM conductors and magnetic anomalies.

ranged from 0.07 to 0.25 S. Conductance values appeared to be slightly higher on the three middle lines, but the pattern was not conclusive. There was a significant discrepancy between depth estimates obtained with the two coil separations. With a 200 m coil separation, the depth to the top ranged from 40 m on line 0 to 120 m on lines 100W, 50W, 50E, and 100E. With the 150 m coil spacing, shallower depth values were obtained: 15 m in the centre and 40 m on the flanks. At present, there is no satisfactory explanation for this discrepancy.

The most prominent conductor detected in the survey area lies close to its northern edge (at approximately 650N), between lines 300W and 500E. On most lines, less than half of the anomaly (characteristic trough) was outlined, and hence no reliable quantitative interpretation was possible. An estimate of conductance on line 200W yielded a value of 250 S, which is consistent with the known nature of the conductor from drilling – a zone of massive graphite. As expected, there was no associated magnetic response. Since the existence of this graphitic conductor, which does not have any economic importance, was known before this survey, no attempt was made to outline it completely by extending measurements beyond the specified area.

Several other conductors were detected during the survey (Fig. 5). Their HLEM responses were weak with little associated magnetic response, thus suggesting clay-filled shear zones or local accumulations of conductive Quaternary sediments. Some of the broad HLEM anomalies were also

interpreted with the horizontal-layer program, but the results were not sufficiently consistent to produce a map of apparent resistivity of the overburden. The glacial sediments in the area are generally thin and poorly conductive.

In conclusion, one can state that the main target, Joannie deposit, is strongly magnetic and very poorly conductive. Conductance estimates are about 10 times less than those obtained over the Linda 2 deposit. No core samples from the Joannie deposit were available for laboratory investigations. The total-field magnetic response measured over the Joannie deposit is about 20 times larger than that observed over the deeper Linda 2 deposit. In regional reconnaissance surveys, targets such as Joannie could be identified on the airborne magnetic data, but would be barely detectable from their airborne EM response. But, in greenstone belts, it is not viable to identify possible volcanogenic massive sulphide targets on the basis of high magnetic response only.

Cook Lake north occurrence

The Cook Lake north survey block is depicted in Figure 7. The deposit, known from drilling information to be 100 to 150 m deep, strikes east-northeast and intersects line 0 at around 60N. The survey lines were oriented north-south and were 1000 m long (500 m north and south from the base line). All lines from 350W to 300E were surveyed with a 200 m coil separation while the middle lines (between 150W and 100E) were also surveyed with a 150 m coil separation. The line

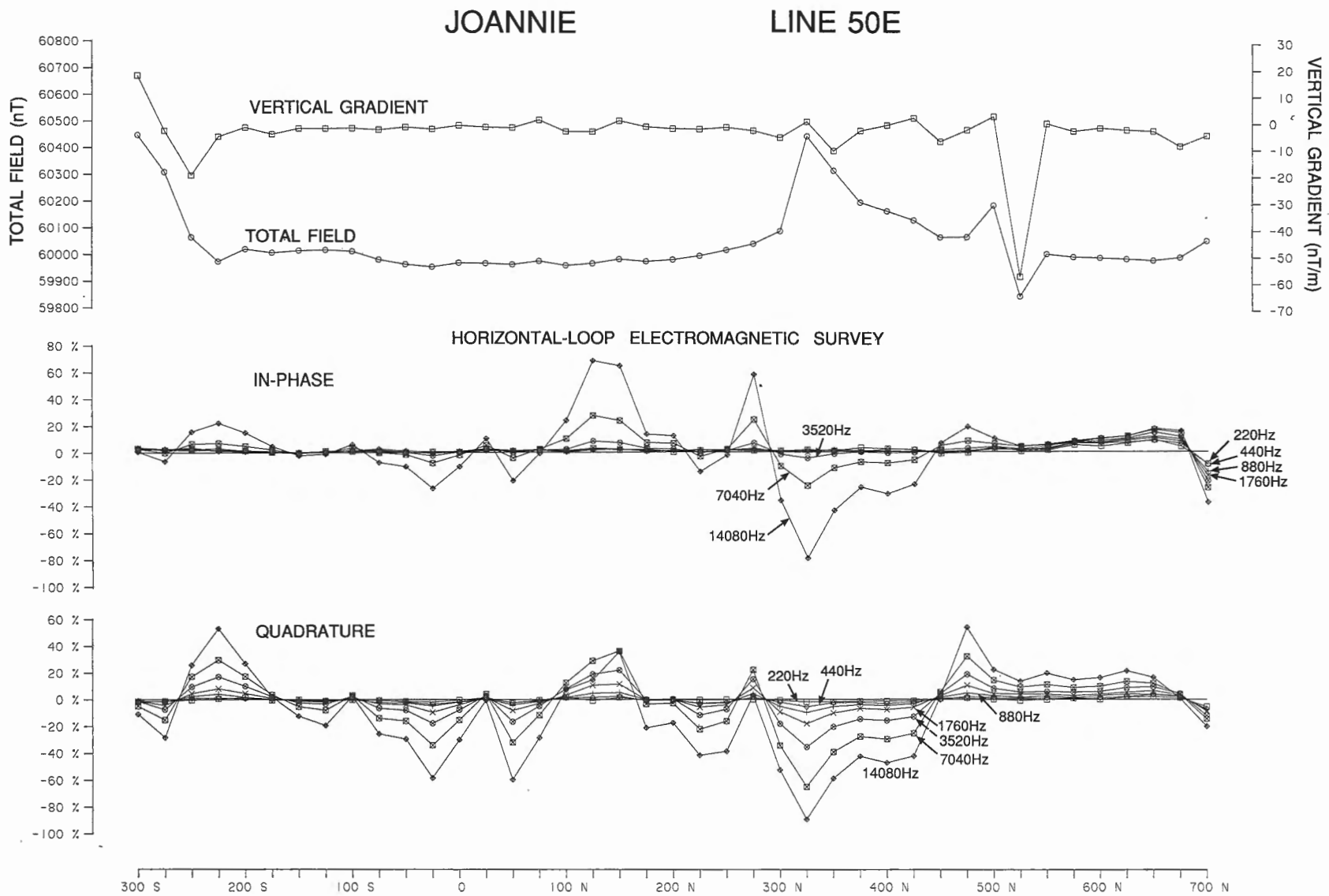


Figure 6. Magnetic and HLEM data acquired on line 50E at Joannie. The coil separation was 150 m for HLEM survey.

spacing in the central part of the grid (150W to 100E) was 50 m, while the lines west of 150W and east of 100E were spaced 100 m apart. The digital survey data and a geophysical interpretation report were released as a GSC Open File (Palacký and Sinha, 1992a).

A sample of the survey data from line 50E (with 150 m coil separation) is shown in Figure 8. A well defined magnetic anomaly of about 200 nT was observed on total-field magnetic data at around 60N. The magnetic anomaly is centred around 50N on line 0 and at 100N on line 100E. A weaker magnetic anomaly (about 100 nT) was detected along the same trend to the west (lines 150W to 350W). Thus the magnetic anomaly is most likely caused by the complex geological structure of the Cook Lake north deposit. An HLEM anomaly, which appears to be of bedrock origin, but displaced about 95 to 175 m to the south of the magnetic anomaly was detected on lines 50E, 100E, and 200E (Fig. 7). On line 50E, a weak HLEM response was observed on data obtained with both coil separations, but there was a discrepancy of about 40 m between the positions of the anomaly centre: 75S on data measured with the 200 m coil separation and 35S with the 150 m coil separation. This shift in the conductor location raises doubts as to whether the response is

really due to a bedrock conductor. The main reason for its interpretation as a bedrock conductor is the strong amplitude reversal on high-frequency quadrature data. Unlike Joannie and Linda 2 surveys, the effect of conductive overburden on the EM response is strong, making quantitative interpretation difficult. Relatively thick lake-bottom clays are present in the area (W. Shilts, pers. comm., 1991). Also, the presumed bedrock conductor is close to the northern limit of the conductive lake-bottom clays, which produced another characteristic anomaly. Using the EMIX-MM Plus program, the conductance of the conductor was estimated at 0.3 S on line 50E and 0.75 S on lines 100E and 200E. There seems to be a progressive decrease in depth to the top from west to east (130 m on line 50E to 70 m on line 200E). There are indications on lines 0 and 50W that the body extends to the west, but the response is so weak that no quantitative interpretation was possible. Therefore, one can conclude that the conductor is plunging to the west. The dip of the conductor appeared subvertical on all three lines. While magnetic anomalies were detected at the expected location of the Cook Lake north deposit, which from drill hole information appeared to have a east-northeast strike, dip 13° north, and cross line 0 at around 60N, the HLEM anomalies were shifted by as much

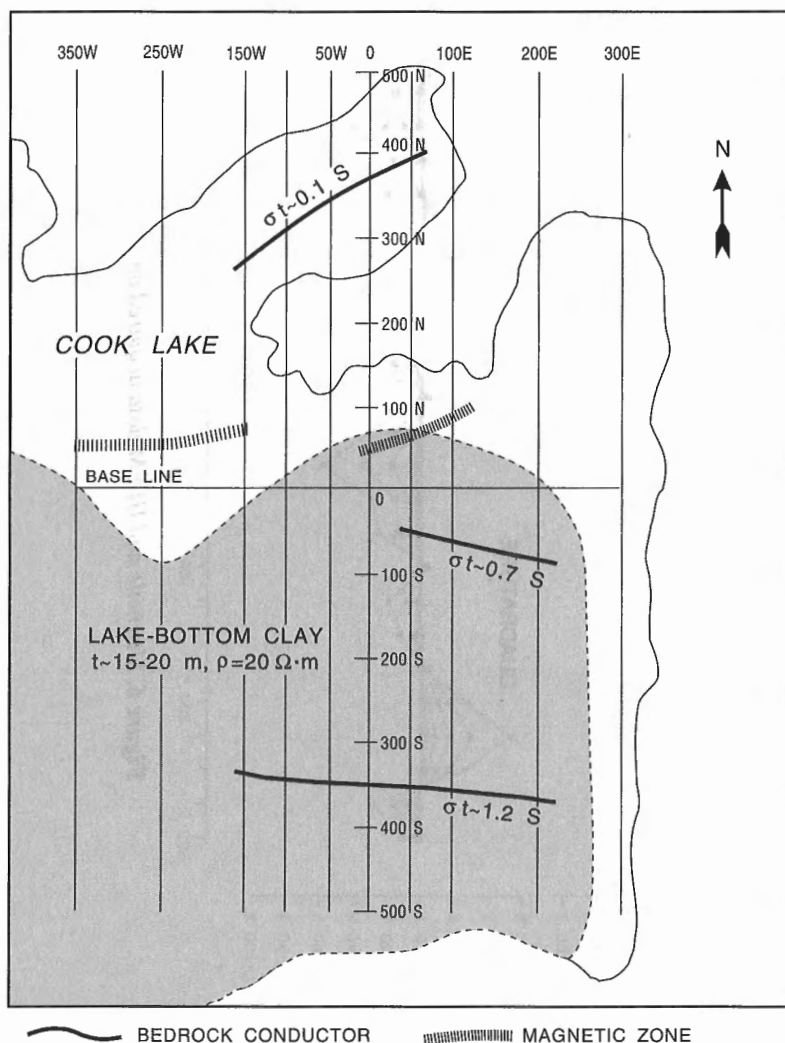


Figure 7.

Geophysical survey grid over the Cook Lake north deposit showing outline of lake, and interpreted locations of EM conductors, magnetic anomalies, and lake-bottom clay in area.

COOK LAKE NORTH LINE 50E

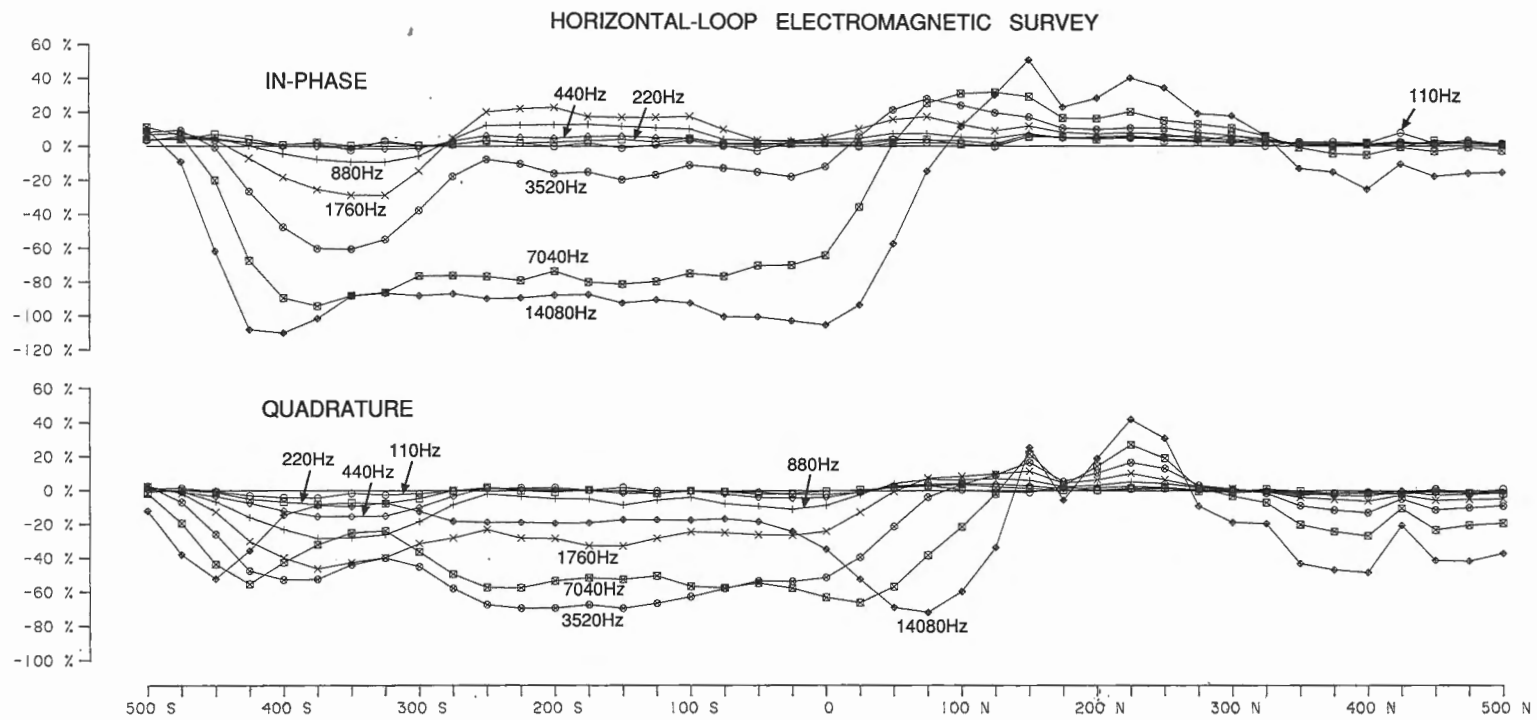
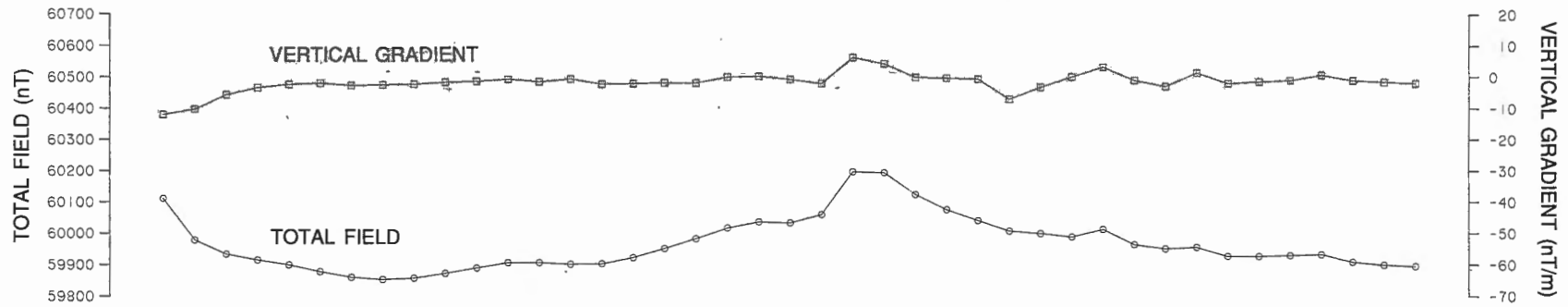


Figure 8. Magnetic and HLEM data acquired on line 50E at Cook Lake north grid. Coil separation was 150 m for HLEM survey.

as 175 m to the south and had a different strike direction. Hence, the observed HLEM anomaly is probably not associated with the deposit.

Another significant conductor detected in the survey area has an east-west trend at approximately 350S, extending from line 150W to 200E (Fig. 7). Its response can be seen clearly on line 50E (centre and bottom of Fig. 8). On the three highest frequencies (3520, 7040, and 14 080 Hz), there is a reversal of the quadrature response, which is characteristic of a bedrock conductor overlain by moderately conductive overburden (lake-bottom clays). Conductance estimates, made with the EMIX-MM Plus program for both coil separations, varied along the conductive trend, but the depth estimates were fairly consistent at about 60 m. The average conductance was 1.2 S, marginally higher than that estimated for the conductor close to the Cook Lake north deposit. The interpreted values are not very reliable because of the effect of conductive lake-bottom clays. There was no magnetic anomaly associated with the conductor. Its geological nature is unknown, as no drilling has been carried out in this area. Because of the highly variable geophysical signatures of sulphide deposits in the Snow Lake area, this conductor may be worth following up as a mineral exploration target.

The third bedrock conductor detected in the Cook Lake north survey area is located under the northern inlet of the lake (Fig. 7). Its conductance varies along the strike, but on average it is very low (0.1 S) and there is no associated magnetic anomaly. The geophysical signature of this conductive feature and its topographic location along an arm of the Cook Lake suggests that it could be a clay-filled shear zone. A magnetic anomaly was detected at approximately 50N between lines 350W and 150W, but no HLEM anomalies could be identified at this location.

In the Cook Lake north area, HLEM data were also interpreted using the layered earth model. In-phase and quadrature readings taken at six frequencies (110 and 220 Hz were too noisy) were inverted at all stations where data were not affected by lateral inhomogeneities (e.g., bedrock conductors). Based on the results of inversion, the survey area was divided into two environments: a) conductive lake-bottom sediments (dark shading in Fig. 7), where resistivity and thickness of individual layers (water, lake-bottom clay, bedrock) could be determined; b) resistive areas, where such determinations were impossible or unreliable because measurable HLEM responses were recorded only at high frequencies making inversions difficult due to insufficient data points.

A conductive zone underlies the southern half of the survey grid. Its northern boundary is irregular, running roughly parallel to the base line. The eastern boundary is most likely located between lines 200E and 300E (conductive response on 200E, but not on 300E). To the south and west, the conductive area extends beyond the survey grid. Estimates of layer thicknesses and resistivities were fairly consistent in all inversions made with two coil separations at over 300 stations. The average resistivity of the first layer (water) was 500 $\Omega\cdot\text{m}$, the second layer (overburden) 20 $\Omega\cdot\text{m}$, and in excess of 5000 $\Omega\cdot\text{m}$ for the third layer (bedrock).

Geologically, only the second-layer resistivity is meaningful because estimates based on HLEM measurements are unreliable for highly resistive rocks. The average resistivity of overburden (20 $\Omega\cdot\text{m}$) is typical of water-saturated lake-bottom clays. The interpreted overburden thickness varies only slightly, between 15 and 20 m, and this has been confirmed by overburden drilling (W. Shilts, pers. comm., 1991). The extent of conductive clays does not coincide with the present outline of the lake. The clays are absent or very thin near the northern end of Cook Lake.

The geophysical results at Cook Lake north are the most ambiguous of the three surveys discussed so far. It is likely that the HLEM anomalies detected close to the centre of the survey grid are not due to the Cook Lake north deposit, which was studied by drilling. The anomalies neither match its expected location, nor its strike direction. The MaxMin I instrument with a coil separation of 150 or 200 m also would not have the penetration to detect conductors at depths in excess of 100 m under a conductive clay layer. Time-domain EM methods would be more successful, if the target were highly conductive. Drill core samples were not available from the deposit for laboratory investigations; its electrical properties remain unknown.

Copperman occurrence

The location of the Copperman survey area at the southwestern edge of the Wekusko Lake is shown in Figure 9. As indicated earlier, this area has been surveyed previously by several ground and airborne geophysical methods.

A recent single-frequency ground VLF survey over four lines passing near the Cu-Zn showing (R. Band, pers. comm., 1990) indicated measurable tilt angle response on two lines and detected a short-strike conductor about 50 m east of the Cu-Zn showing (indicated by "X" on Fig. 9). In view of the positive results with the VLF survey and the fact that all previous surveys had indicated that the conductance of the conductor is low, a more extensive ground VLF survey using a modern system capable of operating at three frequencies simultaneously was planned in the area. The OMNI-PLUS system, which measures several geophysical parameters such as the total field and the tilt angle which help in locating the position of long conductors, can also measure the apparent resistivity of the ground. A follow-up total field and vertical gradient ground magnetic survey was also planned to supplement the VLF results.

A forest fire in 1989 burnt down most of the trees and the wooden picket posts used in previous geophysical surveys. The northeast-trending base line (oriented at 54°E) was located with the help of Falconbridge Ltd. geologists, along with one of the survey lines (line 400N) from the previous imperial grid. A new metric grid was established using this line as line 0 as shown in Figure 9. Seven lines, at 50 m spacing were cut and surveyed, which varied in length from 750 to 1100 m. The VLF and magnetic digital data sets and preliminary interpretation were released as a GSC Open File (Sinha, 1992).

The OMNI-PLUS system is designed to record data simultaneously at three VLF frequencies selected to be those that had the strongest signals in the area, with significantly different azimuths to the transmitters so that conductors of different orientations are mapped. These were NAA transmitting from Cutler, Maine (24.0 kHz), NSS transmitting from Annapolis, Maryland (21.4 kHz), and NLK transmitting from Jim Creek, Washington (24.8 kHz). The OMNI-PLUS system also recorded the magnetic total field and vertical magnetic gradient. The station spacing was 25 m for both VLF and magnetic measurements.

Figure 10 shows a sample of the VLF total field and the vertical quadrature components recorded on line 50S using all three frequencies. Similar plots are made for the in-phase components and the tilt or the dip angle measurements. The figure shows that the VLF response is moderate in the area and presence of several conductors can be inferred from the total field and quadrature responses. A long linear conductor is usually indicated by a maximum in the total VLF field and crossover anomaly in the in-phase, quadrature, and the tilt angle response. But in the case of weak conductors, one or more of the above parameters may not be clearly evident. Conductors were detected at approximately 380W, 250W, 25E, 175E, and at 275E on this line. The first, second, fourth, and fifth anomalies are stronger than the third anomaly, specially in the quadrature response, although the third anomaly at 25E is clearly evident in the total field response from station NLK. In general, all VLF anomalies in the area are of moderate amplitude and irregular in shape, presumably due to limited strike length and low conductances of the conductors. The total field anomalies were generally stronger and more diagnostic than the tilt angle anomalies, since the total

field produces a peak response over a conductor irrespective of the azimuth of the VLF field, while the other parameters produce the maximum anomaly only when the strike of the conductor is parallel to the azimuth. Conductor locations were also derived from the crossover responses of the tilt angle and in-phase response.

Although the conductor positions obtained by using different VLF parameters yielded similar results, there were discrepancies of up to 40 m in the conductor location in some cases. Such discrepancies can occur when the conductors are not long, two-dimensional bodies, but rather made up of three-dimensional lenses, stringers, and pods which would produce a more complex response. In most places, the plotted positions of conductors reflect the average of values obtained by using different parameters, although in certain cases more weight was given to the values from total field measurements than from the others.

The magnetic responses in the area show only slight variations in both the total field and vertical gradient. Several spiky and single point anomalies were observed near old drill hole collars, and are considered cultural in origin. The total magnetic field and vertical gradient values were contoured to locate zones of interest for further studies. Figure 11 shows a map of the interpreted locations of the VLF conductors in the area derived from total field response and also magnetic anomalies. Two conductors west of the base line (A and B) and one just east of it (C) are clearly mapped as are two somewhat weaker conductors (D and E) east of the base line. A short strike conductor (F) was detected in the southwest corner of the grid. Anomaly (A) splits into two conductors north of line 50S. Due to a malfunction during the transfer of

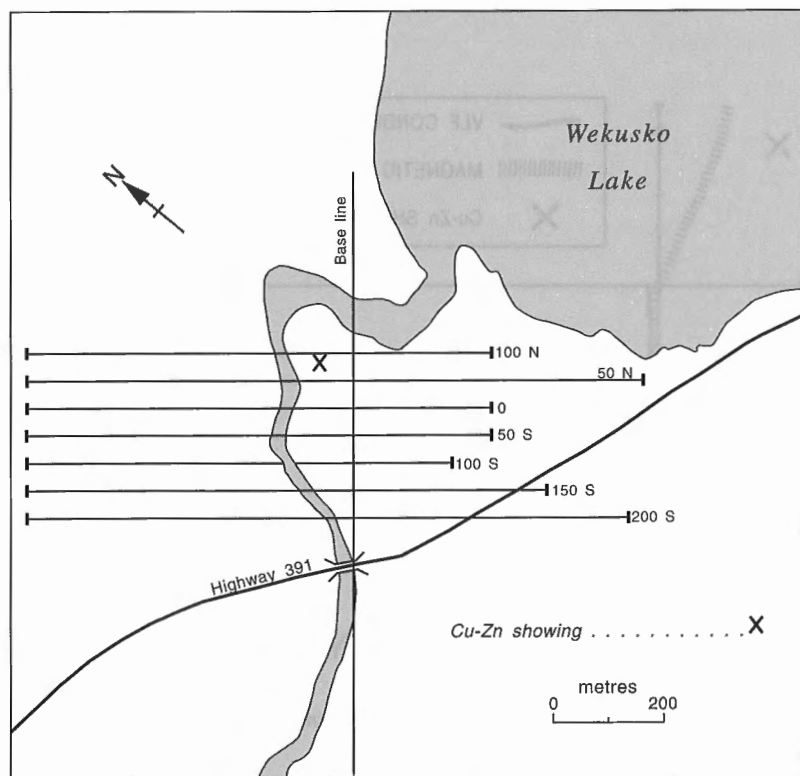


Figure 9.
Location of geophysical survey grid at Copperman. Position of Cu-Zn showing is indicated by X.

data from the OMNI-PLUS memory to the computer hard disk, the VLF data sets over the two northernmost lines were lost and VLF conductors were not mapped north of line 0.

The magnetic anomalies, generally, do not coincide with VLF anomalies. The only exception is conductor C which has a coincident magnetic anomaly. Several magnetic trends,

more or less parallel to the VLF anomalies, were mapped as shown in Figure 11. The magnetic anomaly associated with conductor C passes just east of the Cu-Zn showing (Fig. 11). Since no VLF data exists north of line 0, it is not possible to say if conductor C would have passed through or near the Cu-Zn showing.

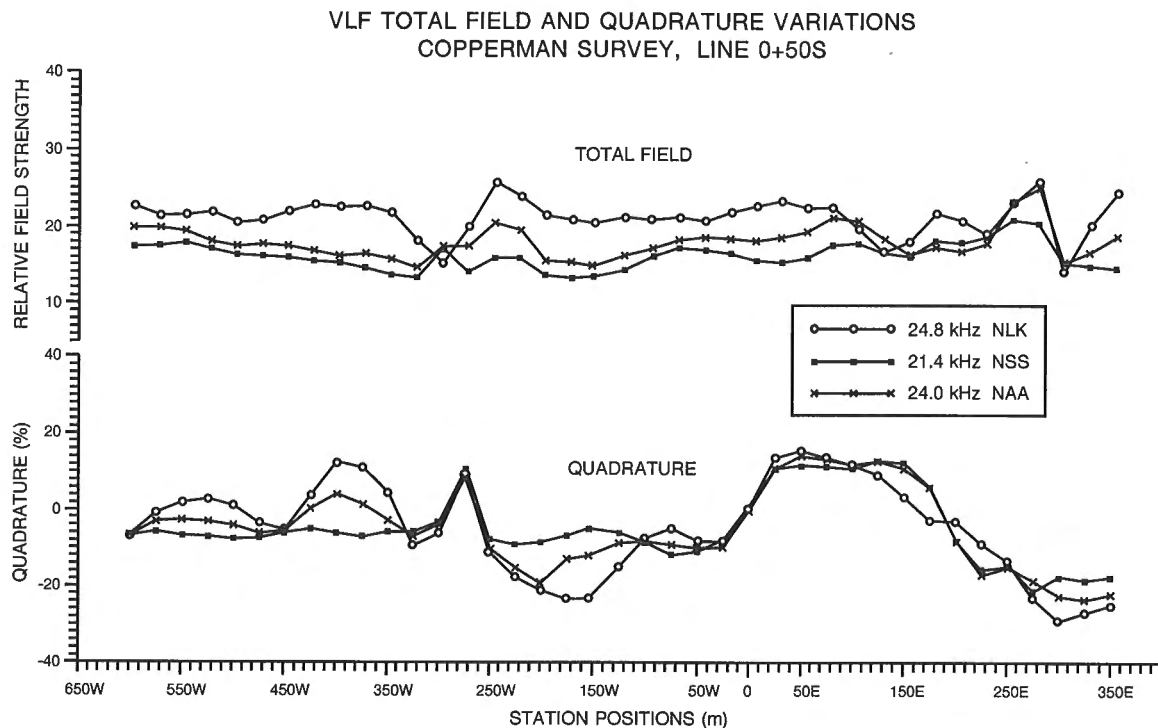


Figure 10. VLF total field and vertical quadrature field variations on line 50S at Copperman at three frequencies.

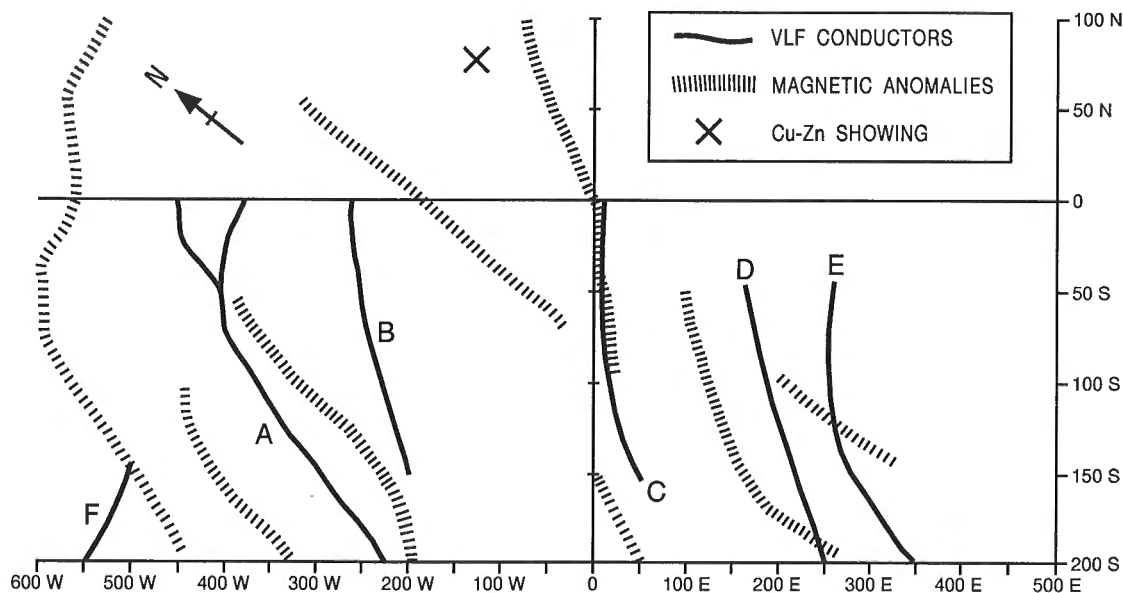


Figure 11. Map of interpreted VLF conductors and magnetic anomalies at Copperman. Location of Cu-Zn showing is shown by X.

Figure 12 illustrates the contoured apparent resistivity values in the grid using data from the VLF station NAA (24.0 kHz). The low resistivity values in the southwest part of the grid are due to extensive soil and moss cover, which has produced fairly thick vegetation in that area. Several high resistivity zones were mapped in the area where the bedrock or dolerite dykes were exposed. Since the VLF conductors in the area appear to have low conductance, their presence do not seem to affect the overall apparent ground resistivity values of the survey area significantly.

Figures 13 and 14 show contour maps of the total field and the vertical magnetic gradient values, respectively. In Figure 13, a regional magnetic field of 60 000 nT has been subtracted from the measured values. The total field data show a magnetic high (about 575 nT), about 125 m south of the Cu-Zn showing. A sharp anomaly of over 1500 nT is

observed at 0-50N, which decreases rapidly to east and west. This location, about 50 m southeast of the showing also produced a large vertical magnetic gradient response (Fig. 14). The source of this anomaly is unknown, but it was repeated in a later recording and there were no obvious magnetic sources like drill hole collars in the neighbourhood. Another large magnetic high is observed at the northwest end of line 100N (Fig. 13). Unfortunately, the lack of VLF data in this area makes any attempt to interpret this anomaly difficult. Figure 14 shows large vertical gradient anomalies at the same two locations near line 0 in the central part of the survey area. Actually, a zone of large negative gradient was mapped east of the large high centred at 0-50N. A large gradient anomaly is observed at the northwestern edge of the area at the same location where a large total field anomaly was observed in Figure 13. A swarm of dolerite dykes is present in that area and are the likely cause of the magnetic

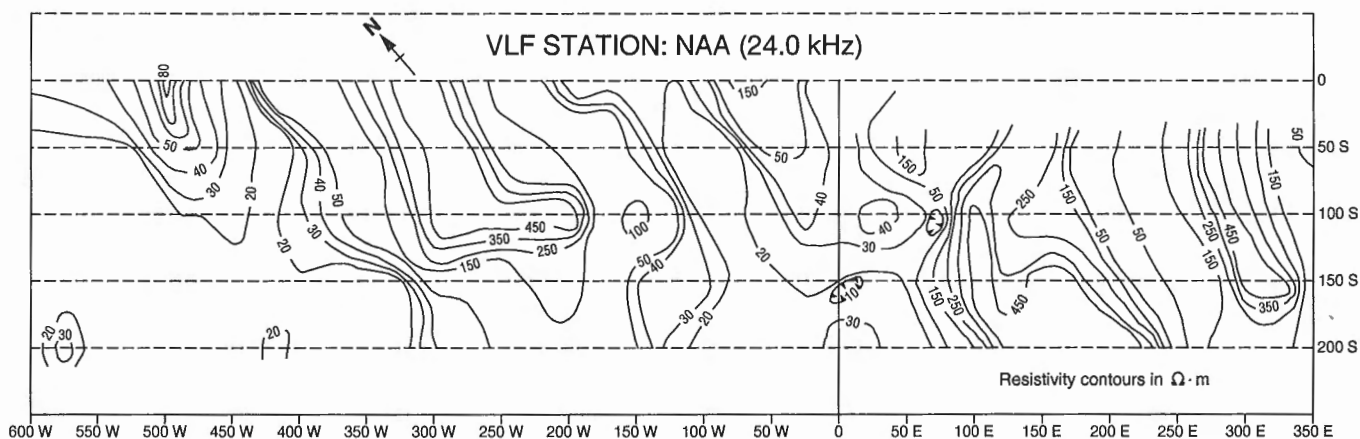


Figure 12. Contour map of apparent resistivity at Copperman grid in $\Omega \cdot m$ using VLF station NAA (24 kHz).

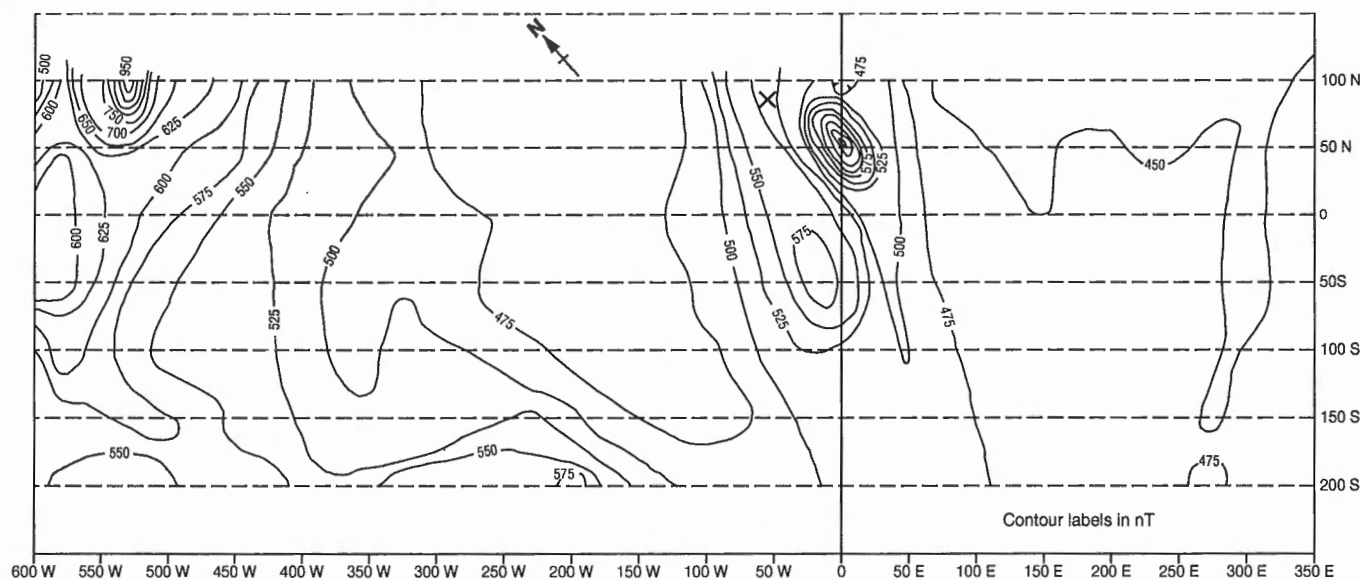


Figure 13. Contour map of magnetic total field anomalies in nT at Copperman. Subtracted regional field was assumed to be 60,000 nT in area. Location of Cu-Zn showing is indicated by X.

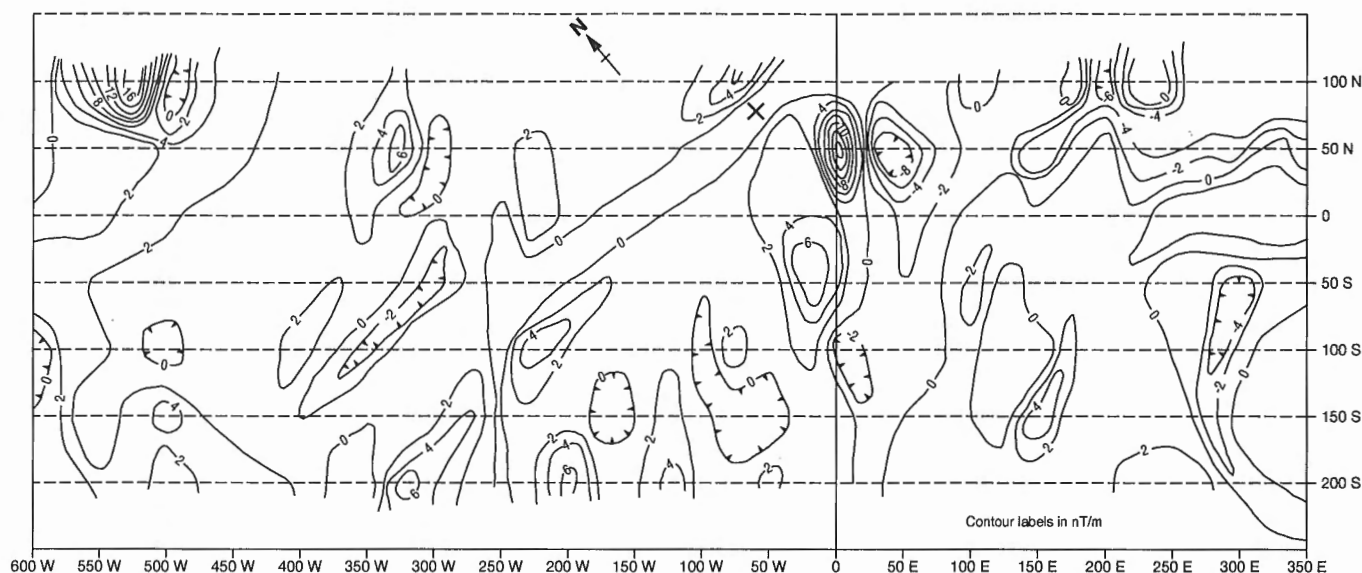


Figure 14. Contour map of vertical magnetic gradient values in nT/m at Copperman grid. Location of Cu-Zn showing is indicated by X.

anomaly in that area. Several additional zones with high magnetic gradient were also mapped, in the area as shown in Figure 14.

To summarize, both VLF and magnetic surveys produced EM and magnetic anomalies in the area. But the results did not indicate the presence of highly conductive shallow targets in the survey zone. The VLF anomalies were low to moderate in amplitude and irregular in shape, which did not permit quantitative interpretation of the data. The low amplitude and irregular nature of the VLF anomalies is likely caused by the presence of three-dimensional, possibly en échelon low conductance targets in the area. This agrees with results of geological mapping which indicated that the mineralized zones at Copperman consist of narrow lenses and stringers. The implied low conductance of the conductors here agrees with the results of the HLEM surveys over three deposits at the Snow Lake area. An accidental loss of VLF data on the two northern lines close to the Cu-Zn showing made the interpretation of the ground VLF data somewhat incomplete. The magnetic total field and vertical gradient results, on the other hand, showed that they can be useful in mapping sulphide conductors if the conductor is associated with magnetic minerals such as magnetite or pyrrhotite.

CONCLUSIONS

The main purpose of the ground geophysical surveys was to investigate in situ the electrical and magnetic properties of selected volcanogenic massive sulphide deposits, typical of the Snow Lake mineralization style. Four deposits were studied, and while their individual responses were different, all of them had very low conductivity. This finding is important for evaluating the effectiveness of previous EM surveys in the Snow Lake greenstone belt and for planning future exploration strategies. Between 1955 and 1984, at least 26 airborne

EM and magnetic surveys were carried in the Flin Flon-Snow Lake greenstone belt by various mining companies (Hosain, 1988), with only limited success at finding orebodies. AEM surveys are considered a standard tool of mineral exploration in many environments. They were particularly successful in the Abitibi greenstone belt in Ontario and Quebec, the Bathurst camp in New Brunswick, and the Rusty Lake area (Ruttan mine) in Manitoba, where volcanogenic massive sulphide deposits are highly conductive and often magnetic. Although over 750 ground EM investigations have been conducted in the Snow Lake area (Hosain, 1988), the rate of success has been low. Our investigations provide an explanation for the failure – the deposits have extremely low conductivities and exploration criteria used in other mining camps in Canada cannot be applied in the Snow Lake greenstone belt. The low conductivity of exploration targets will have to be considered while planning future AEM surveys. So far, all highly conductive bands in the Snow Lake area were caused by graphitic formations. Advanced multifrequency EM systems operating at high frequencies will be required in prospecting for near-surface sulphide deposits in the Snow Lake area. The magnetic method is useful for geological mapping and a coincident magnetic-EM response definitely enhances the likelihood of the target being a volcanogenic massive sulphide.

Ground EM surveys conducted in the frequency domain (APEX MaxMin) should always use several frequencies, particularly those at the high end (over 3 kHz), to be of any use for detection of volcanogenic massive sulphide targets in the Flin Flon-Snow Lake greenstone belt. However, in the past, the MaxMin measurements were often limited to two or three frequencies in the medium range (440 to 1760 Hz). Because of the large depth of some targets, wide-band time-domain surveys may be considered, but previous experience with existing instruments has shown that they are not very effective in detecting poorly conductive targets. The ground

VLF technique, which responds well to poorly conductive targets, may be effective in situations where massive sulphides are continuous and at shallow depths. However, its drawback is poor anomaly discrimination, as many VLF responses could be due to surficial inhomogeneities. As a result of our investigations, several previously unknown conductive targets were identified at all four survey areas, and some of them may be of exploration interest.

ACKNOWLEDGMENTS

The authors would like to acknowledge the help of Mr. Ray Band and Mr. Daryl Hodges of Falconbridge Ltd., Winnipeg, and Mr. Jerry Kitzler and Mr. Ted Baumgartner of Hudson Bay Exploration Limited at Flin Flon and Snow Lake respectively in obtaining geological and logistical information about the four survey areas. Funding from the Manitoba EXTECH project is gratefully acknowledged.

REFERENCES

- Apex Parametrics Limited**
1988: Operating Manual for the MaxMin 1 system; APEX Parametrics Limited, Uxbridge, Ontario.
- Bailes, A.H.**
1988: Chisel-Morgan Lakes Project; in Report of Field Activities, Manitoba Energy and Mines, Minerals Division, p. 53-61.
- Bailes, A.H. and Galley, A.G.**
1996: Setting of Paleoproterozoic volcanic-hosted massive base metal sulphide deposits, Snow Lake; in EXTECH I: A Multidisciplinary Approach to Massive Sulphide Research in the Rusty Lake-Snow Lake Greenstone Belts, Manitoba, (ed.) G.F. Bonham-Carter, A.G. Galley, and G.E.M. Hall, Geological Survey of Canada, Bulletin 426.
- Eccles, D.R. and Fedikow, M.A.F.**
1985: Mineral occurrence documentation and alteration zone mapping, Snow Lake Area; in Report of Field Activities, Manitoba Energy and Mines, p. 82-99.
- Edwards, M.D.**
1990: Petrology and geochemistry of the alteration zone at the North Cook Lake massive sulphide deposit, Snow Lake, Manitoba; BSc. thesis, Department of Geology, University of Regina, Regina, Saskatchewan, 41 p.
- Frischknecht, F.C., Labson, V.F., Spies, B.R., and Anderson, W.L.**
1991: Profiling methods using small sources; in Electromagnetic Methods in Applied Geophysics – Volume 2, Applications, Part A, (ed.) M.N. Nabighian; Society of Exploration Geophysicists, p. 105-270.
- Hosain, I.T.**
1988: An update summary and evaluation of geophysical data from open assessment files of the Flin Flon-Snow Lake greenstone belt (NTS Sheets 63K (N1/2) and 63J/12, 13); Manitoba Energy and Mines, Mines Branch, Open File Report OF87-11.
- Interpex Limited**
1988: EMIX-MM – User's Manual; Interpex Limited, Golden, Colorado.
1989: EMIX-MM PLUS – User's Manual; Interpex Limited, Golden, Colorado.
- Jackson, A.R.N.**
1983: Volcanism and genesis of the Cu-Zn mineralization at Cook Lake, Snow Lake greenstone belt, Manitoba; MSc. thesis, University of Western Ontario, London, Ontario, 154 p.
- Katsube, T.J., Palacky, G.J., Sangster, D.F., Galley, A.G., and Scromeda, N.**
1996: Electrical properties of disseminated sulphide ore samples from Snow Lake; in EXTECH I: A Multidisciplinary Approach to Massive Sulphide Research in the Rusty Lake-Snow Lake Greenstone Belts, Manitoba, (ed.) G.F. Bonham-Carter, A.G. Galley, and G.E.M. Hall, Geological Survey of Canada, Bulletin 426.
- Palacky, G.J. and Sinha, A.K.**
1992a: Results of ground magnetic and electromagnetic (multifrequency, horizontal-loop) measurements in the Cook Lake north area, Snow Lake, Manitoba; Geological Survey of Canada, Open File 2463.
1992b: Results of ground magnetic and electromagnetic (multifrequency, horizontal-loop) measurements at Joannie Options, Snow Lake, Manitoba; Geological Survey of Canada, Open File 2464.
- Sinha, A.K.**
1990: Interpretation of ground VLF-EM data in terms of inclined sheet-like conductor models; Pure and Applied Geophysics, v. 132, no. 4, p. 733-756.
1992: Ground very low frequency (VLF) and magnetic survey results at the Copperman site, near-Snow Lake, Manitoba; Geological Survey of Canada, Open File 2458.
- Sinha, A.K. and Palacky, G.J.**
1992: Ground electromagnetic (multifrequency, horizontal-loop) and magnetic survey results over the Linda-2 deposit, Snow Lake, Manitoba; Geological Survey of Canada, Open File 2462.
- Trembath, G.D. and Fedikow, M.A.F.**
1990: Geological setting of the Copperman base metal deposit; in Report of Activities, Manitoba Energy and Mines, Minerals Division, p. 84-86.
- Wright, J.F.**
1931: Geology and mineral deposits of part of northwest Manitoba; Geological Survey of Canada, Summary Report, Part C, p. 1-124.
- Zaleski, E. and Halden, N.M.**
1988: Reconstruction of synvolcanic alteration associated with the Linda massive sulphide deposit; Geological Survey of Canada, Paper 88-1C, p. 73-81.

Contribution to the 1989-1994 Rusty Lake-Snow Lake Mining Camps, Canada-Manitoba Exploration Science and Technology Initiative (EXTECH I)

Electrical properties of disseminated sulphide ore samples from Snow Lake

T.J. Katsube¹, G.J. Palacky¹, D.F. Sangster¹, A.G. Galley¹,
and N. Scromeda¹

Katsube, T.J., Palacky, G.J., Sangster, D.F., Galley, A.G., and Scromeda, N., 1996: Electrical properties of disseminated sulphide ore samples from Snow Lake; in EXTECH I: A Multidisciplinary Approach to Massive Sulphide Research in the Rusty Lake-Snow Lake Greenstone Belts, Manitoba, (ed.) G.F. Bonham-Carter, A.G. Galley, and G.E.M. Hall; Geological Survey of Canada, Bulletin 426, p. 319-329.

Abstract: Electrical characteristics (resistivity and formation factor) of seven samples (15 specimens), representing various sulphide mineralization types in the Flin Flon-Snow Lake volcanic belt, have been investigated. The purpose of the study was to seek an explanation for the weaker than expected electromagnetic (EM) responses of the sulphide bodies in this region.

Results indicate that resistivities of many of the samples are 10-2,100 $\Omega\cdot\text{m}$, much higher than the typical range of massive sulphide bodies (0.01-1 $\Omega\cdot\text{m}$), and above the conventional detection limit (10 $\Omega\cdot\text{m}$) of surface EM survey systems. In addition, surprisingly strong resistivity anisotropy (high as 45:1 to 70:1) has been observed in some of the samples, resulting in one of the directions displaying resistivities (2 $\Omega\cdot\text{m}$) within the conventional EM survey system detection limit, but other directions (40-100 $\Omega\cdot\text{m}$) displaying values well above those limits. These results may explain the reason for the limited success of some past EM surveys, and indicate that they were poorly designed for anisotropic low-resistivity targets. It is suggested that either broadband systems with at least one coil pair operating in the 30 to 60 kHz range, or time domain EM systems with an in-pulse channel may offer greater success in detecting these anisotropic conductors.

Résumé : Dans le cadre de la présente étude, on a déterminé les caractéristiques électriques (résistivité et facteur de formation) de sept échantillons (15 spécimens), représentant divers types de minéralisation en sulfures de la ceinture volcanique de Flin Flon-Snow Lake. Ces travaux avaient pour objectif d'expliquer les réponses électromagnétiques (EM) plus faibles que prévues des corps minéralisés en sulfures de cette région.

Les résultats indiquent que la résistivité de nombreux échantillons est comprises entre 10 et 2 100 $\Omega\cdot\text{m}$, intervalle dont les valeurs sont beaucoup plus élevées que l'intervalle obtenu habituellement dans le cas des amas de sulfures massifs (0,01 à 1 $\Omega\cdot\text{m}$) et au-dessus de la limite de détection (10 $\Omega\cdot\text{m}$) des appareils classiques de levés EM en surface. De plus, on a observé une anisotropie de résistivité étonnamment prononcée (entre 45:1 et 70:1) dans certains échantillons; ainsi, dans une des directions de mesure de la résistivité, la valeur obtenue se chiffrait à 2 $\Omega\cdot\text{m}$, ce qui est dans les limites de détection des appareils classiques de levés EM. Dans d'autres directions cependant, les valeurs atteignaient 40 à 100 $\Omega\cdot\text{m}$, ce qui dépasse les limites de détection. Ces résultats peuvent expliquer le succès limité de certains levés EM antérieurs et indiquent qu'ils n'étaient pas bien conçus pour les cibles anisotropes de faible résistivité. Pour mieux réussir à détecter ces conducteurs anisotropes, on propose des appareils à large bande dotés d'au moins une paire de bobines fonctionnant dans l'intervalle de 30 à 60 kHz, ou des appareils de levés EM fonctionnant dans le domaine temporel dotés d'un canal *in-pulse*.

¹ Geological Survey of Canada, 601 Booth St., Ottawa, Ontario, Canada K1A 0E8

INTRODUCTION

The Flin Flon-Snow Lake volcanic belt has been the target of mineral exploration for several decades, with Flin Flon being one of the most important base metal mines in Canada. Although airborne and ground electromagnetic (EM) methods are generally effective prospecting tools for massive-sulphide deposits, with these techniques having been successful in the discovery of more than 50 deposits in many other mining camps in Canada, they have not been as successful in this area as might be expected. Therefore, laboratory electrical property measurements on a suite of samples with varying degrees of sulphide mineralization were carried out as an initial investigation of the electrical characteristics of the sulphide bodies of this volcanic belt.

Airborne EM methods have been used in the Flin Flon-Snow Lake volcanic belt since 1955 and, by 1984, at least 26 surveys were carried out by various mining companies (Hosain, 1988). A variety of airborne EM systems were used, such as two-frequency quadrature, towed-bird systems of various designs, the time-domain INPUT system at various stages of development, and the multicoil helicopter systems.

A survey, commissioned by Sheritt Gordon in 1973-1974, covered most of the volcanic belt, using a two-frequency quadrature system. However, no mineral discoveries resulted from the survey and the known Centennial orebody did not show a measurable EM response. In addition, ground EM methods were extensively used in this belt, but with varying degrees of success. Hosain (1988), for example, listed 750 such surveys.

A re-evaluation of the effectiveness of EM techniques in the Snow Lake volcanic belt has been part of the EXTECH program. An important question asked was whether new-generation EM techniques could be more successful for mineral exploration in this environment. For example, are the known orebodies nonconductive or poorly conductive, or could have improvements and design changes been made in the original surveys? The GSC EXTECH team investigated this problem by taking two separate approaches: in one, field surveys were carried out on four selected targets using an advanced ground EM system, and in the other, laboratory electrical measurements were carried out on samples collected from several sulphide deposits in the belt. In principle, both field and laboratory studies should have been carried out

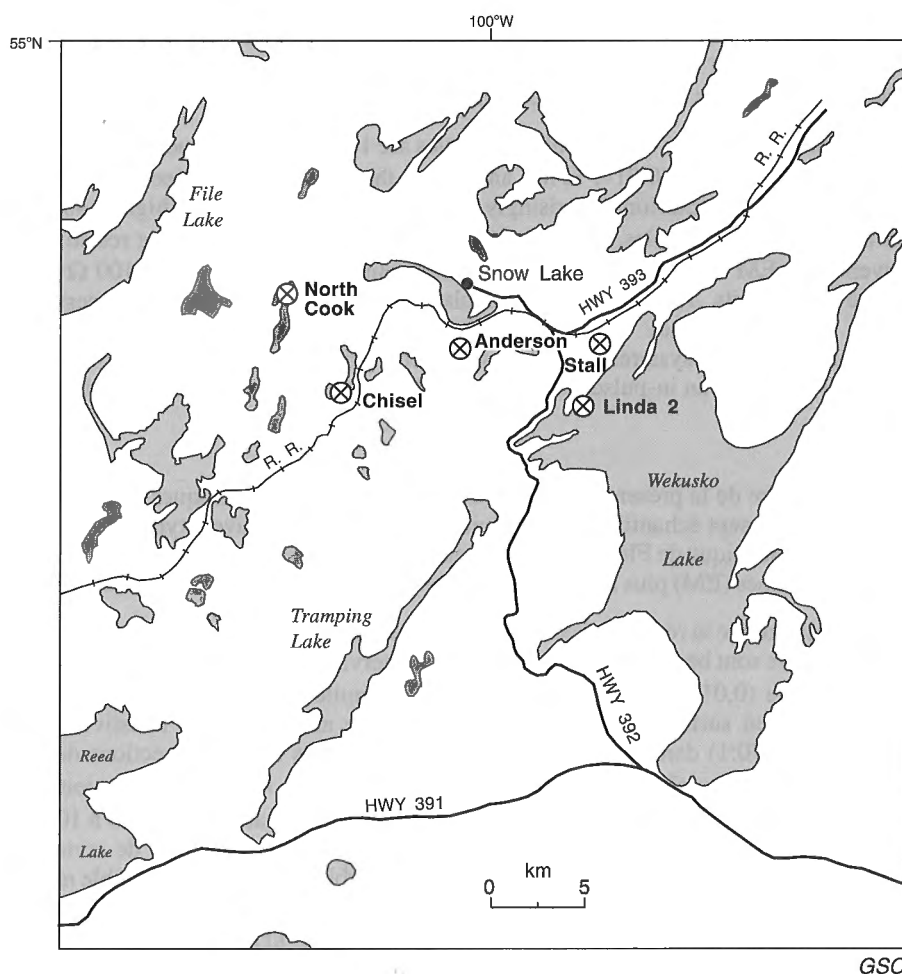


Figure 1. Map of deposits and occurrences in Snow Lake volcanic belt, with sample locations.

on the same sulphide bodies. However, logistical problems prevented this, since fieldwork could not be carried out over operating mines where rock samples would have been available. The results of the field surveys and interpretation are described in Sinha and Palacky (1996), and the results of the laboratory study are the subject of this paper.

Laboratory electrical measurements (bulk resistivity and formation factor) have been carried out on samples from five deposits and occurrences in the Snow Lake volcanic belt (Fig. 1). Measurements have been made in three-directions, whenever possible. The prime consideration was to obtain measurements on samples representative of various mineralization styles in the Snow Lake mining camp. While sampling from known economic orebodies (Chisel, Stall, Anderson) has been emphasized in this study, consideration has also been given to the inclusion of sites where ground EM investigations have been carried out as part of the EXTECH program. Suitable drill core samples were available from only two of the five deposits and occurrences (Linda 2 and North Cook).

GEOLOGY

Snow Lake sulphide deposits

The Snow Lake massive sulphide deposits are located within two of the five volcanic cycles recognized in the Amisk Group south of Snow Lake (Bailes and Galley, 1996). The copper-rich massive sulphide deposits, which include Anderson, Stall, and Linda 2, are hosted by a large rhyolite flow complex within the cycle 1 volcanics. The zinc-rich Chisel, Lost Lake and Ghost Lake deposits are located at the contact between felsic rocks of cycle 3 and the overlying mafic volcanic rocks of cycle 4. The copper-rich deposits have many of the characteristics of proximal, volcanic-hosted massive sulphide deposits (Franklin et al., 1981), but the Chisel deposit is a more extensive, sediment-hosted deposit (Galley et al., 1993).

All of the massive sulphide deposits have been strongly deformed and metamorphosed to lower amphibolite grade. This has resulted in re-orientation of the massive sulphide lenses into linear, pencil-shaped bodies, with remobilization and coarsening of the sulphide mineral assemblages.

Chisel deposit

The Chisel Lake Zn-Pb-Cu-Ag-Au massive sulphide deposit was discovered in 1956 and contained 7.167 million tonnes grading approximately 11% Zn, 1.4% Pb, 0.4% Cu, 54 g/t Ag, and 2.2 g/t Au (Galley et al., 1993). The deposit is hosted within a thin, carbonate-rich sedimentary exhalative unit that rests over the top of the Chisel rhyolite and underlying Powderhouse dacite. The ore consists of sphalerite and pyrite, with minor chalcopryrite, pyrrhotite, galena, and arsenopyrite. Gangue minerals include dolomite, quartz, microcline, sericite, biotite, and aluminosilicates. Two samples (SN-C1 and SN-C2 in Table 1) were collected from this deposit for our study, one (SN-C1) contains 15-20% sulphides

Table 1. Sample numbers, their field identification number (I.D.), rock type (including sulphide content), and name of sulphide body within Snow Lake area, Manitoba.

| Sample number | Sample I.D. | Rock type | Sulphide deposit |
|------------------------------|-------------|--|------------------|
| SN-A1 | SP-1195 | Sph (mainly Cp) >15% | Anderson |
| SN-A2 | SP-1199 | Sph (mainly Cp) >80% | Anderson |
| SN-C1 | SP-1176 | Sph (Py) = 15 - 20% | Chisel |
| SN-C2 | SP-1181 | Sph (Sph, Py, Cp) = 80% (Py and Cp imbedded in Sph) | Chisel |
| SN-S1 | SP-1152 | Sph = 10% (Chl = Sph = 5%, Pyr <1%) | Stall |
| SN-L2 | | Low grade layered Py | Linda |
| SN-CL | | Sph>80% | Cook Lake |
| Sph = Total sulphide content | | Py = Pyrite | |
| Sph = Sphalerite | | Cp = Chalcopryrite | |
| | | Pyr = Pyrrhotite | |

(mainly pyrite). The second (SN-C2), typical of the ore from this deposit, contains 80% sulphides with pyrite and chalcopryrite imbedded in sphalerite.

Anderson deposit

The Anderson deposit was discovered in 1963 and mined out in 1988. It consists of two sulphide lenses, 350 m apart, both hosted by the Anderson rhyolite complex. Only the eastern body was mined, and contained 3.2 million tonnes grading 3.41% Cu and 0.10% Zn (Walford and Franklin, 1982). It is composed largely of pyrite, chalcopryrite, and pyrrhotite, with minor sphalerite. The hanging wall to the sulphide lens consists of 4 m of muscovite schist followed by 5 m of partly altered felsic rocks overlain by the Foot-Mud unit, which is a narrow unit of thin-laminated, cherty pyrite-bearing "tuffite". Below the 807 m (2650 ft.) level of the mine, the hanging wall felsic unit consists of quartz porphyritic rhyolite. The footwall consists of up to 50 m of sparsely quartz porphyritic altered rhyolite followed down section by 300 m of aphyric rhyolite. Two samples (SN-A1 and SN-A2 in Table 1) from this deposit were collected for our study. One (SN-A2), rich in sulphides (>80%), contains mainly chalcopryrite. The other (SN-A1) contains more than 15% sulphides, also mainly chalcopryrite.

Stall deposit

The Stall deposit, discovered in 1963, is the largest Cu-rich ore body in the Snow Lake area at 7 million tonnes, grading 4.39% Cu and 0.5% Zn. It is described in considerable detail by Studer (1982). The orebody consists of four large and a number of smaller massive sulphide lenses hosted by the Anderson rhyolite. The main lenses occur at the contact between the lower aphyric and middle quartz phyrlic members of the Anderson rhyolite. The main massive sulphide lenses consist of coarse grained pyrrhotite with lesser pyrite and chalcopryrite, chlorite, and quartz. Massive pyrrhotite zones locally contain pyrite porphyroblasts up to 30 cm across. The sample (SN-S1 in Table 1) collected for this study contains

5% chalcopyrite and 5% sphalerite with a minor amount of pyrrhotite (<1%). This is not necessary typical of the orebody, but contains some of its major sulphide minerals.

Linda 2 deposit

The Linda 2 massive sulphide occurrence lies on the western shore of Lake Wekusko, about 9 km southwest of the town of Snow Lake (NTS sheet 63J/13). The mineralization which is hosted by felsic volcanic rocks consists of medium- to coarse-grained granular pyrite intergrown with calcite and quartz. Pyrrhotite, sphalerite, and chalcopyrite occur sporadically (Zaleski, 1986). The sample (SN-L2) analyzed in this study contained layered, low-grade pyrite. An extensive drilling program was carried out, from 1978 to 1981, at the occurrence. In March 1990, multifrequency horizontal-loop EM surveys were carried out in the Linda 2 target area by Geotrex Limited for the EXTECH program. The deposit was detected by EM surveys as a steeply dipping conductor of short strike length, with low conductance (between 0.5 and 1.5 S). The results of magnetic and EM surveys are discussed in Sinha and Palacky (1992). A detailed description of the surveys is included in this volume (Sinha and Palacky, 1996).

North Cook deposit

Several massive sulphide occurrences were found under North Cook by Falconbridge Limited, as a result of airborne and ground EM surveys. The lake is located about 10 km west of the town of Snow Lake (NTS sheet 63K/16). In 1983, drilling carried out at the northern end of Cook Lake intersected a 10 m wide sulphide zone at a depth of 150 m (R.B. Band, pers. comm., 1990). The sample (SN-CL in Table 1) collected for this study was rich in sulphides (>80%). Ground EM measurements with the APEX MaxMin I multifrequency horizontal-loop system were conducted at the North Cook property in March 1990. It was hoped that detailed geophysical studies would define the geophysical signature of the body. However, the EM method used could not detect this deep massive sulphide body because of insufficient coil separation (200 m) and strong effect of lake-bottom clays. There was a well defined magnetic anomaly associated with the deposit. The results of EXTECH-funded magnetic and EM surveys are described in Palacky and Sinha (1992). Sinha and Palacky (1996) provide details of the surveys and data interpretation.

METHOD OF INVESTIGATION

Samples and sample preparation

Seven samples were collected from the five orebodies. Two of the samples were from split cores (SN-L2 and SN-CL in Table 1), and the rest are hand samples collected during underground visits. One to three rectangular specimens were cut from each of the hand samples, and partial-disk specimens were cut out of the split core samples, as illustrated in Figure 2

(excludes SN-CL series specimens in Table 1). A total of 15 specimens were cut from the 7 samples. Illustrations of the approximate shape and distribution of the conductive sulphide grains are given in the same figure. The sample numbers, sampling locations (sulphide deposit), and identification numbers are listed in Table 1. Results of visual examination of the mineral content for these samples are also listed in this table.

The specimens are identified by the letters a, b, and c, following the sample numbers (e.g., SN-A1a, SN-C2b), as shown in Table 2a and 2b. When a specimen is measured in three directions, these directions are identified by α , β , and λ . Therefore, a number (see Table 2a) such as "SN-C1b/ β " represents direction β for specimen b of sample SN-C1.

The geometric characteristics of the specimens are listed in Table 2a for the rectangular specimens, their dimensions of the order of (1.4-2.3) x (1.6-2.3) cm for the cross-section and 0.6-2.3 cm for thicknesses, and in Table 2b for the partial-disk specimens, their dimensions being 3.6 cm in diameter and 1.3-2.2 cm in thickness. Electrical measurements were made in the three directions for six out of the 11 rectangular specimens. The orientations of the specimens described above are shown in detail in Figure 2. The geometric factor, K_G (with the units 10^{-2} m), required for calculating resistivity, is defined as

$$K_G = A/\ell \quad (1)$$

where A (cm^2) is the cross-section area and ℓ (cm) is the thickness, was determined for all specimens prior to measurement.

Complex resistivity and formation factor measurements

The objective of the laboratory measurements was to determine the electrical characteristics of the specimens in terms of their resistivity and formation factor parameters. The techniques used here have been described elsewhere (e.g., Katsube and Walsh, 1987; Katsube et al., 1991; Katsube and Salisbury, 1991).

Resistivity measurements were made on specimens saturated in distilled water for 24-48 hours. Each specimen is placed in a sample holder connected to an electrical impedance system. The in-phase and out-of-phase components of the impedance are measured at frequencies in the range 1.0-10⁶ Hz. Resistivity is then expressed as a complex variable, ρ^* , (Katsube 1975) consisting of a real part (the real resistivity, ρ_R) and an imaginary part (the imaginary resistivity, ρ_I):

$$\rho^* = \rho_R + i\rho_I \quad (2)$$

where i is the square root of minus one. ρ^* is derived from the impedance measurements by

$$\rho^* = K_G Z \quad (3)$$

where Z is the impedance, and K_G is the geometric factor introduced previously. The bulk rock resistivity, ρ_r , is then determined from plots of ρ_I versus ρ_R , as described by Katsube and Walsh (1987), Katsube et al. (1991), and Katsube and Salisbury (1991).

The formation factor, F , is derived by measuring the bulk resistivity, ρ_m , of the rock saturated with solutions of different salinities (NaCl: 0.02, 0.05, 0.10, 0.20, and 0.50 N). The

apparent formation factor, F_a , is first calculated from the ratio ρ_m/ρ_w , where ρ_w is the pore fluid resistivity. The Patnode and Wyllie equation (Patnode and Wyllie, 1950) is then fitted to the results for each specimen to obtain estimates of F and the bulk surface resistivity, ρ_c :

$$\frac{1}{P_m} = \frac{1}{(FP_w)} + \frac{1}{P_c} \quad (4)$$

where ρ_w is the pore fluid resistivity. Further details of these procedures and calculations are described in the papers cited at the beginning of this section.

These measurements were made at room temperature conditions. The errors for ρ_r and F are estimated to be in the ranges of 10-20% and 20-40%, respectively (Katsube, 1981; Wadden and Katsube, 1982; Katsube and Scromeda, 1993) for ρ_r or ρ_m values above 10 $\Omega \cdot m$. For measurements of ρ_r and ρ_m values below 10 $\Omega \cdot m$, larger errors are expected, and the measurement limitation of this high resistivity measuring system is considered to be 1 $\Omega \cdot m$.

EXPERIMENTAL RESULTS

Two sets of complex resistivity measurements were carried out on each of the 15 specimens. The results are listed in Table 3. Typical examples of complex resistivity (ρ^*) plots (ρ^* as a function of frequency, f , and ρ_I as a function of ρ_R) used to determine the bulk resistivity (ρ_r) values are shown in Figures 3 to 6. In these figures, various complex resistivity arc patterns are displayed: a normal arc (Fig. 3) usually seen in high resistivity rocks, a suppressed arc (Fig. 4) with strong electrode polarization normally seen in intermediate resistivity rocks with sulphide dissemination, and an extensively suppressed arc (Fig. 5) with strong electrode polarization normally seen in low resistivity rocks with sulphide dissemination. An example of an extensively suppressed arc with strong electrode polarization, probably due to sulphide minerals, is displayed in Figure 6. This is an example of a situation where difficulty was experienced in determining ρ_r .

Results of bulk resistivity (ρ_m) measurements used for formation factor (F) determination by equation (4) are listed in Table 4. Only nine formation factor (F) values were determined, for 6 specimens, representing 4 samples (SN-A1, SN-C1, SN-C2, and SN-S1), with only one specimen (SN-C1b) having measurements in all three directions. The bulk resistivity (ρ_m) values were generally too small to be measured accurately for the other specimens. Typical examples of the $1/\rho_m$ versus $1/\rho_w$ relationship (equation 4) observed when determining formation factor (F) and surface resistivity (ρ_c) are shown in Figure 7. This figure displays a good linear relationship between $1/\rho_m$ and $1/\rho_w$ (Fig. 7a) which results in small errors for both F and ρ_c , and a rather poor linear relationship (Fig. 7b) resulting in larger errors for the two parameters. The solid line in this figure is the reduced major axis (Davis, 1986; Katsube and Agterberg, 1990), and the broken lines are the two normal regression lines.

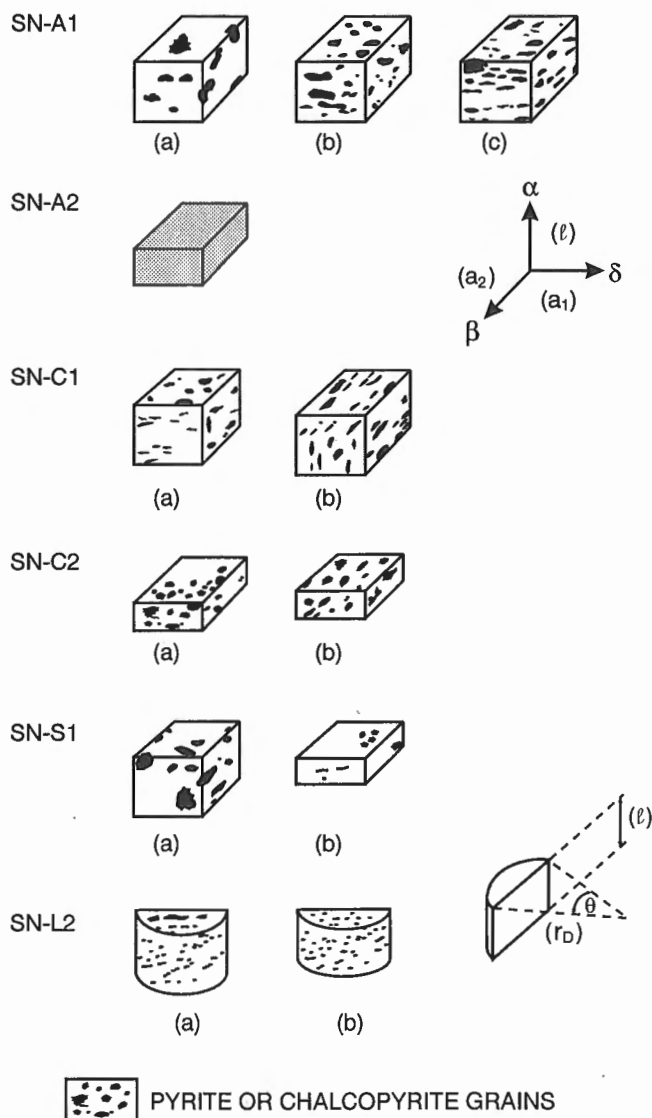


Figure 2. Block diagram of specimens used for complex resistivity and formation factor measurements. Three directions are α , β , and γ for rectangular specimens. Specimens for Sample SN-L2 are part of discs with r_D , θ , and l being diameter, separation angle, and thickness, respectively (sample SN-CL is not included). In sample SN-C2, pyrite and chalcopyrite grains are imbedded in sphalerite; for other samples, sulphide grains are imbedded in silicates.

Table 2a. Dimensions of specimens cut out from the samples for electrical measurements.

| Sample | a_1 (cm) | a_2 (cm) | ℓ (cm) | W (g) | K_a (10^{-2} m) | δ_E (g/mL) |
|--|---------------|---------------|----------------|----------|-------------------------|----------------------|
| SN-A1a/ α | 2.295 | 2.057 | 1.697 | 25.4319 | 2.78 | 3.18 |
| SN-A1a/ β | 1.697 | 2.295 | 2.057 | 25.4319 | 1.89 | 3.18 |
| SN-A1a/ γ | 1.697 | 2.057 | 2.295 | 25.4319 | 1.52 | 3.18 |
| SN-A1b/ α | 2.050 | 2.315 | 1.698 | 27.2618 | 2.80 | 3.39 |
| SN-A1b/ β | 1.698 | 2.315 | 2.050 | 27.2618 | 1.92 | 3.39 |
| SN-A1b/ γ | 1.698 | 2.050 | 2.315 | 27.2618 | 1.50 | 3.39 |
| SN-A1c/ α | 2.324 | 2.017 | 1.611 | 24.1720 | 2.91 | 3.21 |
| SN-A1c/ β | 1.611 | 2.324 | 2.017 | 24.1720 | 1.86 | 3.21 |
| SN-A1c/ γ | 1.611 | 2.017 | 2.324 | 24.1720 | 1.40 | 3.21 |
| SN-A2 | 1.979 | 1.812 | 1.097 | 17.4773 | 3.27 | 4.44 |
| SN-C1a/ α | 2.147 | 1.678 | 1.467 | 17.9574 | 2.46 | 3.43 |
| SN-C1a/ β | 1.467 | 2.147 | 1.678 | 17.9574 | 1.88 | 3.43 |
| SN-C1a/ γ | 1.467 | 1.678 | 2.147 | 17.9574 | 1.15 | 3.43 |
| SN-C1b/ α | 2.125 | 2.250 | 1.599 | 25.8609 | 2.99 | 3.40 |
| SN-C1b/ β | 1.599 | 2.250 | 2.125 | 25.8609 | 1.69 | 3.40 |
| SN-C1b/ γ | 1.599 | 2.125 | 2.250 | 25.8609 | 1.51 | 3.40 |
| SN-C2a | 2.063 | 2.235 | 1.008 | 19.3344 | 4.57 | 4.16 |
| SN-C2b | 1.409 | 1.984 | 0.847 | 10.1145 | 3.30 | 4.27 |
| SN-S1a/ α | 2.157 | 1.625 | 1.555 | 16.6114 | 2.25 | 3.06 |
| SN-S1a/ β | 1.555 | 2.157 | 1.625 | 16.6114 | 2.06 | 3.06 |
| SN-S1a/ γ | 1.555 | 1.625 | 2.157 | 16.6114 | 1.17 | 3.06 |
| SN-S1b | 1.491 | 2.170 | 0.848 | 9.5487 | 3.82 | 3.48 |
| SN-L2c | 1.983 | 2.252 | 0.574 | 8.5648 | 7.78 | 3.34 |
| a_1, a_2 = Length of the two sides of the rectangular specimen ℓ = Thickness of specimen W = Weight of specimen under room dry conditions K_a = Geometric factor δ_E = Bulk density XX-XX = Sample numbers a,b,c = Specimen numbers α, β, γ = Direction of measurement (see Fig. 2) | | | | | | |

Table 2b. Dimensions of partial disc specimens cut out from the split core samples.

| Samples | r_D (cm) | θ ($^\circ$) | A (cm ²) | ℓ (cm) | W (g) | K_g (10 ⁻² m) | δ (g/cm ³) |
|--|---------------|--------------------------|-------------------------|---|----------|-------------------------------|----------------------------------|
| SN-L2a | 3.61 | 145 | 3.19 | 2.182 | 23.4930 | 1.46 | 3.38 |
| SN-L2b | 3.61 | 167 | 4.38 | 1.340 | 19.2978 | 3.27 | 3.29 |
| SN-CLa | 3.61 | 161 | 4.06 | 1.306 | 26.6610 | 3.11 | 5.07 |
| SN-CLb | 3.60 | 162 | 4.08 | 1.292 | 25.2272 | 3.15 | 4.82 |
| r_D = diameter θ = separation angle (Fig. 2) A = area ℓ = thickness | | | | W = weight K_g = geometric factor δ = bulk density | | | |

DISCUSSION AND CONCLUSIONS

The bulk resistivities (ρ_r) of these samples range from less than 1.0 to 2100 $\Omega\cdot\text{m}$. Considering the fact that resistivities of naturally occurring pyrites and chalcopyrites are normally in the range of 10^{-5} to 1.0 $\Omega\cdot\text{m}$ (Keller, 1982) and those of tight crystalline rocks commonly exceed $10^4 \Omega\cdot\text{m}$ (Katsube and Mareschal, 1993), it is not surprising that these samples, which contain variable dissemination of these two sulphide minerals, display ρ_r values within these two extremes. The sample (SN-C2) from Chisel deposit with conductive sulphides imbedded in a sphalerite matrix displays ρ_r values of 3-6 $\Omega\cdot\text{m}$, values also within the range of published values of 3×10^{-3} to $1.2 \times 10^4 \Omega\cdot\text{m}$ for sphalerite (Keller, 1982).

The complex resistivity (ρ^*) plot for sample SN-S1 (from Stall deposit) in Figure 3 displays a normal pattern for a high resistivity rock (e.g., Katsube, 1975, 1977; Katsube et al., 1992).

Table 3. Results of the bulk resistivity (ρ_r) measurements.

| Sample | Mes. #1 | ρ_r ($\Omega\cdot\text{m}$) Mes. #2 | Mean |
|------------------|---------|---|------|
| SN-A1a/ α | 37 | 43 | 40 |
| SN-A1a/ β | 116 | 68 | 92 |
| SN-A1a/ γ | 2.1 | 1.8 | 2.0 |
| SN-A1b/ α | 1.8 | 2.4 | 2.1 |
| SN-A1b/ β | *** | *** | *** |
| SN-A1b/ γ | *** | *** | *** |
| SN-A1c/ α | 1.5 | 3.8 | 2.7 |
| SN-A1c/ β | *** | *** | *** |
| SN-A1c/ γ | *** | *** | *** |
| SN-A2 | *** | *** | *** |
| SN-C1a/ α | 148 | 185 | 167 |
| SN-C1a/ β | 137 | 264 | 200 |
| SN-C1a/ γ | 46 | 44 | 45 |
| SN-C1b/ α | 199 | 218 | 208 |
| SN-C1b/ β | 93 | 80 | 86 |
| SN-C1b/ γ | 449 | 482 | 466 |
| SN-C2a | - | 2.7 | 2.7 |
| SN-C2b | 5.9 | 6.0 | 5.9 |
| SN-S1a/ α | 21 | 38 | 29 |
| SN-S1a/ β | 2293 | 1910 | 2102 |
| SN-S1a/ γ | 21 | 49 | 35 |
| SN-S1b | 271 | 235 | 253 |
| SN-L2a | 185 | 164 | 174 |
| SN-L2b | 146 | 117 | 131 |
| SN-L2c | 287 | 247 | 267 |
| SN-CLa | *** | *** | *** |
| SN-CLb | *** | *** | *** |

ρ_r = Bulk Electrical Resistivity.
 Mes. #1 = Measurement after 24 hours of saturation.
 Mes. #2 = Measurement after 48 hours of saturation.
 *** = Bulk resistivity (ρ_r) values below 1.0 $\Omega\cdot\text{m}$.
 - = Data not available.

The complex resistivity plots for the rest of the samples (Fig. 4-6) also display patterns previously observed (Katsube, 1975, 1977). The existence of the high resistivity value (β direction) of the ore sample from Stall (sample SN-S1) is surprising, because pyrite- and pyrrhotite-rich sulphides, such as those from Stall, are usually highly conductive. Additional studies are recommended to investigate how representative this sample is of the Stall deposit.

Also surprising are the extreme differences in ρ_r values for different directions (anisotropy) in the same sample or specimen. For example, sample SN-S1a shows a ρ_r value of 2100 $\Omega\cdot\text{m}$ in the β direction and 29-35 $\Omega\cdot\text{m}$ in the other two

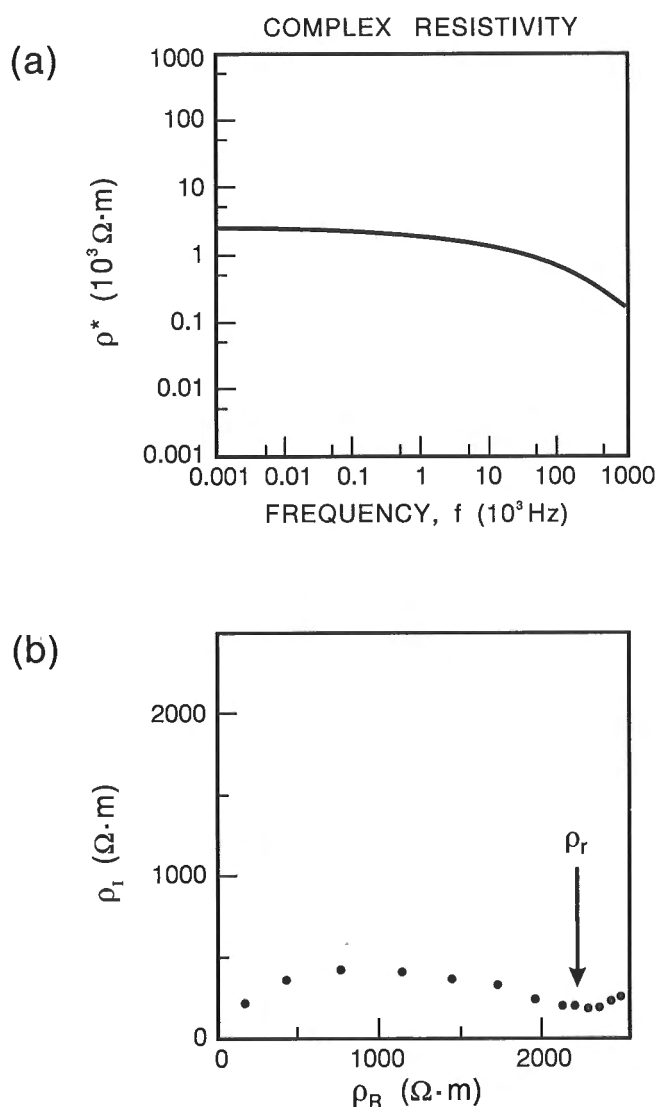


Figure 3. Typical examples of complex resistivity (ρ^*) plots used to determine bulk resistivity (ρ_r) for sample/specimen SN-S1a/ β (I.D. = SP-1152). **a)** Complex resistivity (ρ^*) as function of frequency (f), and **b)** imaginary resistivity (ρ_i) as function of real resistivity (ρ_R) displaying normal arc; such patterns are usually seen in highly resistive rocks.

directions, a difference of about 70 times. Similarly, differences of 4 (sample SN-C1a) to 45 times (sample SN-A1a) in the same specimen are seen in the rest of the samples, as shown in Table 3. It is highly desirable that a systematic investigation on this subject of anisotropy be conducted on samples representing various mineralized zones, in addition to barren zones. Such studies may be useful for planning future exploration programs.

Five of the seven samples (11 of the 15 specimens) have resistivities greater than $1 \Omega \cdot m$, several of them exceeding $100 \Omega \cdot m$. Laboratory resistivity values less than $1 \Omega \cdot m$ cannot be accurately determined by the methods employed. The typical resistivity range of massive sulphides is 0.01 to $1 \Omega \cdot m$ (Palacky, 1988). A conductive zone 10 m wide with a resistivity of $10 \Omega \cdot m$ has a conductance of 1 S, which would be detectable only by EM systems operating on high frequencies.

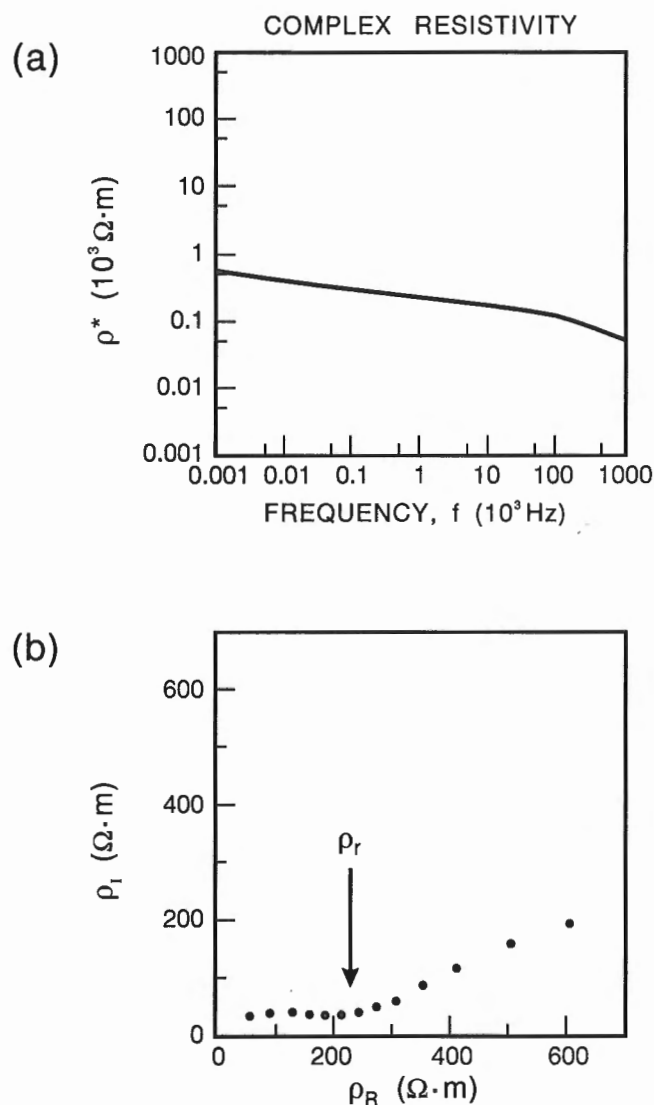


Figure 4. Typical examples of complex resistivity (ρ^*) plots used to determine bulk resistivity (ρ_r) for sample/specimen SN-C1a/ α (I.D. = 79-1176). **a)** Complex resistivity (ρ^*) as function of frequency (f), and **b)** imaginary resistivity (ρ_i) as function of real resistivity (ρ_R) displaying suppressed arc with strong electrode polarization shown on right-hand side, probably due to sulphide minerals. Such patterns are normally seen in intermediate resistivity rocks containing disseminated sulphides.

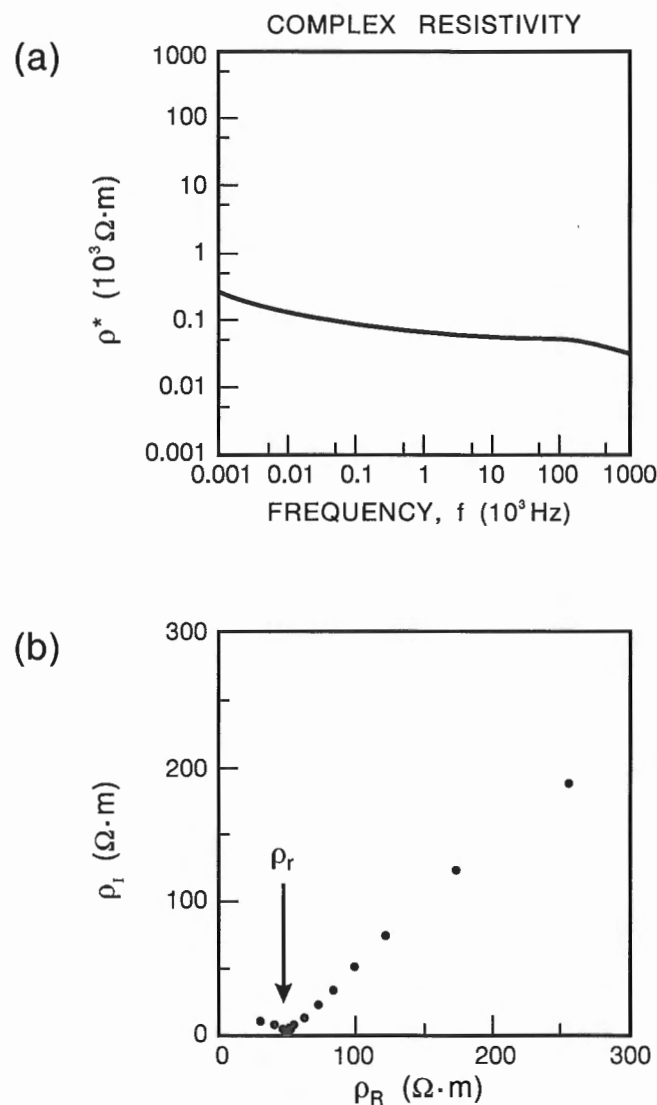


Figure 5. Typical examples of complex resistivity (ρ^*) plots used to determine bulk resistivity (ρ_r) for sample/specimen SN-S1a/ γ (I.D. = SP-1152). **a)** Complex resistivity (ρ^*) as function of frequency (f), and **b)** imaginary resistivity (ρ_i) as function of real resistivity (ρ_R) displaying extensively suppressed arc with strong electrode polarization shown on the right hand side, probably due to both sulphide minerals and the electrodes. Such patterns are normally seen in poorly conductive rocks with sulphide dissemination.

The results of this laboratory study are consistent with empirical findings made during almost 40 years of EM surveys in the Snow Lake volcanic belt. Even known deposits could not be reliably detected with the narrow-band two-frequency quadrature airborne EM systems or the time-domain INPUT system, which were extensively flown in the volcanic belt (Hosain, 1988). Such systems are not effective in detecting poorly conductive targets such as those in our study. Therefore, it is suggested that future airborne EM

surveys in the area would be more effective if carried out with broadband systems, having at least one coil pair operating in the high-frequency range (30 to 60 kHz), or with time-domain systems which use an in-pulse channel (Palacky and West, 1991).

The most significant findings of this study are the existence of the unexpectedly high resistivity values for most of the ore samples that were investigated, and their strong directional effects. Most of these resistivity values are well above

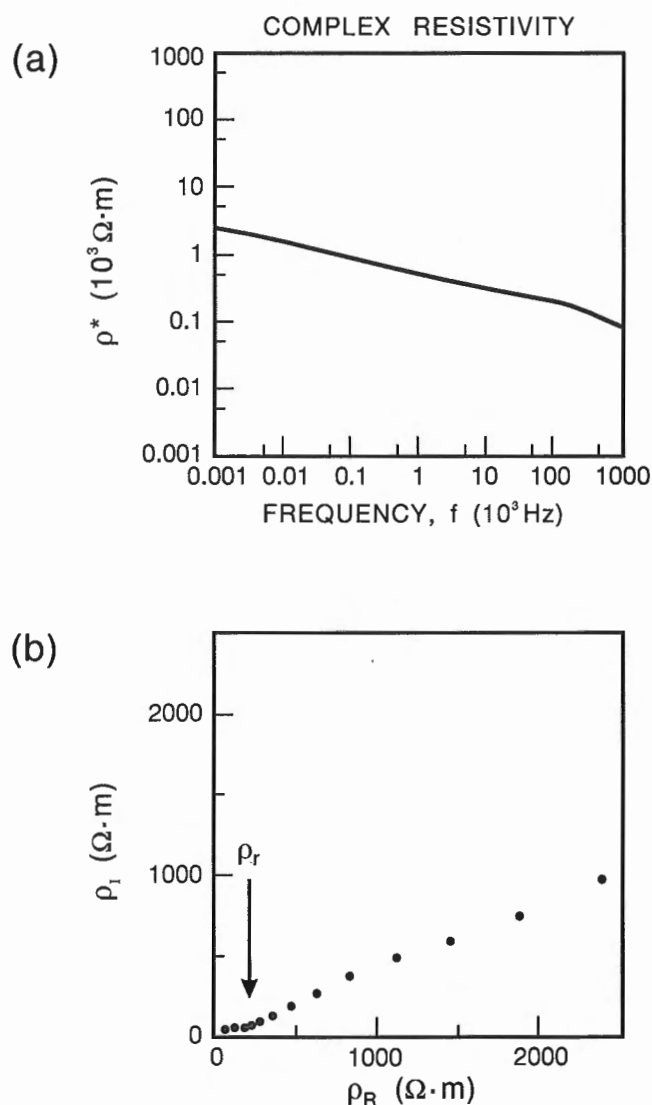


Figure 6. Typical examples of complex resistivity (ρ^*) plots used to determine bulk resistivity (ρ_r) for sample/specimen SN-S1b/ α (I.D. = SP-1152). **a)** Complex resistivity (ρ^*) as function of frequency (f), and **b)** imaginary resistivity (ρ_i) as function of real resistivity (ρ_R) displaying extensively suppressed arc with strong electrode polarization shown on right hand side, probably due to sulphide minerals. Example of measurements where difficulty was experienced in determining ρ_r .

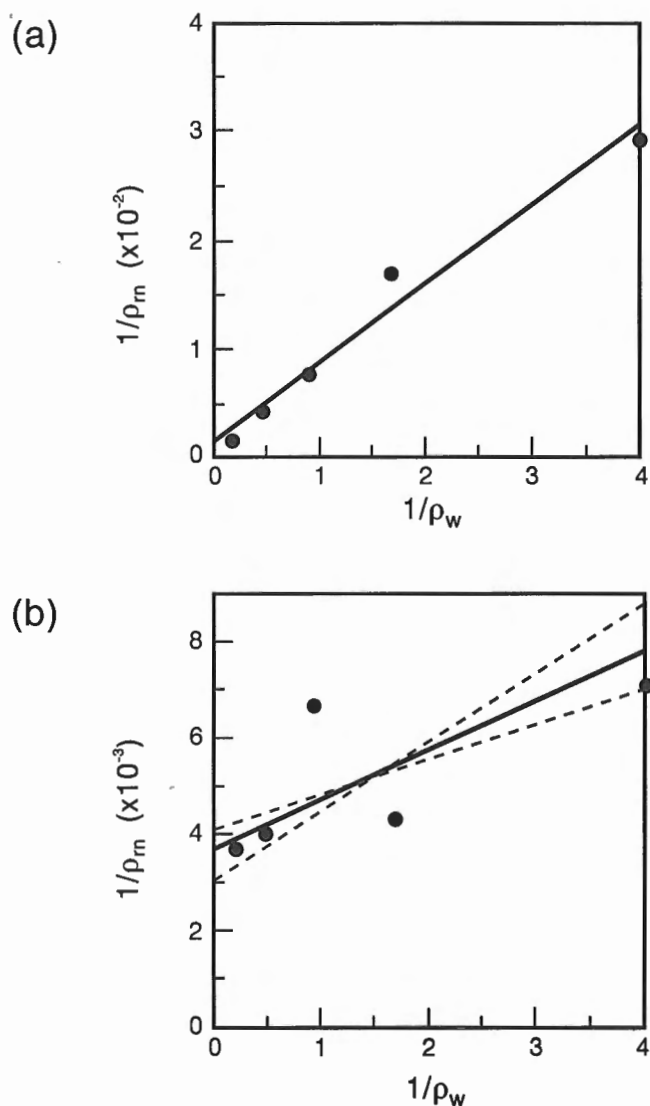


Figure 7. Typical examples of $(1/\rho_m)$ versus $(1/\rho_w)$ relationship observed when determining formation factor (F) and surface resistivity (ρ_c), **a)** for sample SN-S1a/ β displaying normal results with small errors for both parameters, and **b)** for sample SN-C1a/ α displaying some scatter resulting in a certain degree of uncertainty for both parameters. Solid lines are the reduced major axis, and the broken lines are the two normal regression lines. Parameters ρ_w and ρ_m are pore fluid resistivity and bulk resistivity, respectively, of rock specimens saturated with solutions of different salinities.

Table 4. Formation-factor (F), surface resistivity (ρ_c) and bulk resistivities (ρ_m) for different NaCl solutions for the samples.

| Sample | ρ_m ($\Omega \cdot m$) | | | | | F \pm % | $\rho_c \pm$ % ($\Omega \cdot m$) |
|---|----------------------------------|---------------------|---------------------|---------------------|--------------------|--------------------|--|
| | ρ_w ($\Omega \cdot m$) | 0.25 ± 0.001 | 0.59 ± 0.002 | 1.09 ± 0.003 | 2.11 ± 0.01 | 5.33 ± 0.03 | |
| | NaCl (N) | 0.5 | 0.2 | 0.1 | 0.05 | 0.02 | |
| SN-A1a/ β | 43 | 42 | 46 | 56 | 59 | 488 \pm 35 | 56.5 \pm 6 |
| SN-C1a/ α | 140 | 230 | 150 | 250 | 270 | 952 \pm 40 | 274 \pm 20 |
| SN-C1a/ β | 81 | 120 | 87 | 100 | 170 | 592 \pm 60 | 140 \pm 25 |
| SN-C1b/ α | 180 | 380 | 250 | 290 | 310 | 1379 \pm 32 | 368 \pm 14 |
| SN-C1b/ β | 51 | 72 | 83 | 71 | 74 | 529 \pm 12 | 84 \pm 3 |
| SN-C1b/ γ | 160 | 380 | 400 | 470 | 500 | 862 \pm 3 | 709 \pm 4 |
| SN-C2a | 5.0 | 6.7 | 6.1 | 6.5 | 5.8 | 76.3 \pm 41 | 6.71 \pm 6 |
| SN-S1a/ β | 34 | 59 | 130 | 230 | 650 | 135 \pm 1 | 820 \pm 13 |
| SN-S1b | 28 | 46 | 78 | 140 | 480 | 155 \pm 2 | 302 \pm 9 |
| ρ_w = pore fluid resistivity ρ_m = bulk resistivity of the rock for solutions of different salinities F = formation-factor ρ_c = surface resistivity X = data points used for formation factor determination | | | | | | | |

the conventional detection limits ($10 \Omega \cdot m$) of the surface EM survey systems, and many have resistivity values greater than $100 \Omega \cdot m$. One sample (SN-A1) that displayed a resistivity value of $2 \Omega \cdot m$ in one direction, a value normally expected for such an ore sample and within the conventional detection limit of EM survey systems, produced values of 40 – $100 \Omega \cdot m$ in the other directions which were above the normal EM detection limits. Samples with anisotropic textural characteristics, such as SN-A1c (Fig. 2), are expected to show some degree of directional effects in their electrical characteristics. The chalcopyrite grains tend to be aligned along the β and γ directions for this sample/specimen. Therefore, it is expected that these directions would show lower resistivities, and indeed the measurements of $2.7 \Omega \cdot m$ in the α direction, and values below $1.0 \Omega \cdot m$ in the β and γ directions (Table 3) bear this out. However, it is surprising that some samples/specimens display considerable resistivity anisotropy *without* any such trends observed in the texture; thus what is expected to be the more conductive direction from the texture is actually more resistive. For example, samples SN-A1a and SN-S1a give some indication, from their textural characteristics, that the β direction may be less resistive than the others. However, that direction actually displays the greatest resistivity values for these samples, with SN-A1a and SN-S1a displaying $92 \Omega \cdot m$ and $2100 \Omega \cdot m$ in those directions, respectively, 30–100 times the resistivity values of the other directions. A preliminary examination of these sample/specimens suggest the existence of shearing in directions approximately normal to that of β . Shearing could break any good electrical connectivity that may have existed, and could be the main cause of the strong resistivity anisotropy that exists.

It should be emphasized that these laboratory measurements were carried out on a limited suite of samples. In order to characterize the electrical properties of the Snow Lake sulphide bodies fully, many more samples would be required to provide representivity. Thus although the results explain the limited EM response of the Snow Lake deposits, future work should be directed towards a more comprehensive set of samples, in order to understand the spatial variability of resistivity and its relationship to rock texture.

ACKNOWLEDGMENTS

The authors are thankful to A.K. Sinha (Geological Survey of Canada) for making arrangements for the supplying of some of the samples used in this study. The authors thank K.A. Richardson (Geological Survey of Canada) for providing advice and directions to this study, and for critically reviewing this paper. The authors also thank M. Hannington (Geological Survey of Canada) for his comments.

REFERENCES

- Bailes, A.H. and Galley, A.G.
1996: Setting of Paleoproterozoic volcanic-hosted massive base metal sulphide deposits, Snow Lake; in EXTECH I: A Multidisciplinary Approach to Massive Sulphide Research in the Rusty Lake-Snow Lake Greenstone Belts, Manitoba, (ed.) G.F. Bonham-Carter, A.G. Galley, and G.E.M. Hall; Geological Survey of Canada, Bulletin 426.
Davis, J.C.
1986: Statistics and Data Analysis in Geology; John Wiley & Sons, 646 p.

Franklin, J.M., Lydon, J.W., and Sangster, D.F.

- 1981: Volcanic-associated massive sulphide deposits; in *Economic Geology, Seventy-fifth Anniversary Volume*, (ed.) B.J. Skinner; p. 485-627.

Galley, A.G., Bailes, A.H., and Kitzler, G.

- 1993: Geological setting and hydrothermal evolution of the Chisel Lake and North Chisel Zn-Pb-Ag-Au massive sulphide deposit, Snow Lake, Manitoba; *Exploration and Mining Geology*, v. 2, p. 271-296.

Hosain, I.T.

- 1988: An update summary and evaluation of geophysical data from open assessment files of the Flin Flon-Snow Lake greenstone belt (NTS sheets 63K(N1/2) and 63J/12, 13); Manitoba Energy and Mines, Mines Branch, Open File Report OF87-11, 101 p. and 18 maps.

Katsube, T.J.

- 1975: The electrical polarization mechanism model for moist rocks; in *Report of Activities, Part C*; Geological Survey of Canada, Paper 75-1C, p. 353-360.
- 1977: Electrical properties of rocks; in *Induced Polarization for Exploration Geologists and Geophysicists*; Short Course Presented by the University of Arizona, Tucson, March 14-16, p. 15-44.
- 1981: Pore structure and pore parameters that control the radionuclide transport in crystalline rocks; *Proceedings of the Technical Program, International Powder and Bulk Solids Handling and Processing*, Rosemont, Illinois, p. 394-409.

Katsube, T.J. and Agterberg, F.P.

- 1990: Use of statistical methods to extract significant information from scattered data in petrophysics; in *Statistical Applications in the Earth Sciences*, (ed.) F.P. Agterberg and G.F. Bonham-Carter; Geological Survey of Canada, Paper 89-9, p. 263-270.

Katsube, T.J. and Mareschal, M.

- 1993: Petrophysical model of deep electrical conductors; graphite lining as a source and its disconnection due to uplift; *Journal of Geophysical Research*, v. 98, no. B5, p. 8019-8030.

Katsube, T.J., Best, M.E., and Mudford, B.S.

- 1991: Petrophysical characteristics of shales from the Scotian shelf; *Geophysics*, v. 56, p. 1681-1689.

Katsube, T.J. and Salisbury, M.

- 1991: Petrophysical characteristics of surface core samples from the Sudbury structure; in *Current Research, Part E*; Geological Survey of Canada, Paper 91-E, p. 265-271.

Katsube, T.J. and Scromeda, N.

- 1993: Formation factor determination procedure for shale sample V-3; in *Current Research, Part E*; Geological Survey of Canada, Paper 93-1E, p. 321-330.

Katsube, T.J., Scromeda, N., Mareschal, M., and Bailey, R.C.

- 1992: Electrical resistivity and porosity of crystalline rock samples from the Kapuskasing Structural Zone; in *Current Research, Part E*; Geological Survey of Canada, Paper 92-E, p. 225-236.

Katsube, T.J. and Walsh, J.B.

- 1987: Effective aperture for fluid flow in microcracks; *International Journal of Rock Mechanics and Mining Sciences and Geomechanics Abstracts*, v. 24, p. 175-183.

Keller, G.V.

- 1982: Electrical properties of rocks and minerals; in *Handbook of Physical Properties of Rocks, Volume I*, (ed.) R.S. Carmichael; CRC Press, Inc., Florida, p. 217-293.

Palacky, G.J.

- 1988: Resistivity characteristics of geologic targets; in *Electromagnetic Methods in Applied Geophysics, Volume 1 - Theory*, (ed.) M.N. Nabighian; *Investigations in Geophysics 3*, Society of Exploration Geophysicists, p. 52-129.

Palacky, G.J. and Sinha, A.K.

- 1992: Results of ground magnetic and electromagnetic (multifrequency, horizontal-loop) measurements at Cook Lake North, Snow Lake, Manitoba; Geological Survey of Canada, Open File 2463, 19 p. and diskette.

Palacky, G.J. and West, G.F.

- 1991: Airborne electromagnetic methods; in *Electromagnetic Methods in Applied Geophysics, Volume 2 - Applications, Part B*, (ed.) M.N. Nabighian; *Investigations in Geophysics 3*, Society of Exploration Geophysicists, p. 811-877.

Patnode, H.W. and Wyllie, M.R.J.

- 1950: The presence of conductive solids in reservoir rocks as a factor in electric log interpretation; *Transactions of the American Institute of Mining, Metallurgical and Petroleum Engineers*, v. 189, p. 47-52.

Sinha, A.K. and Palacky, G.J.

- 1992: Results of ground magnetic and electromagnetic (multifrequency, horizontal-loop) measurements at Linda 2, Snow Lake, Manitoba; Geological Survey of Canada, Open File 2462, 15 p. and diskette.
- 1996: Ground electromagnetic, magnetic, and VLF-EM surveys at four sites near Snow Lake; in *EXTech I: A Multidisciplinary Approach to Massive Sulphide Research in the Rusty Lake-Snow Lake Greenstone Belts, Manitoba*, (ed.) G.F. Bonham-Carter, A.G. Galley, and G.E.M. Hall; Geological Survey of Canada, Bulletin 426.

Studer, R.D.

- 1982: Geology of the Stall Lake copper deposit, Snow Lake, Manitoba; *Canadian Institute of Mining and Metallurgy Bulletin*, v. 75, p. 66-72.

Wadden, M.M. and Katsube, T.J.

- 1982: Radionuclide diffusion rates in crystalline rocks; *Chemical Geology*, v. 36, p. 191-214.

Walford, P.C. and Franklin, J.M.

- 1982: The Anderson Lake mine, Snow Lake, Manitoba; in *Precambrian Sulphide Deposits*, (ed.) R.W. Hutchison, C.D. Spence, and J.M. Franklin; Geological Association of Canada, Special Paper 25, p. 481-523.

Zaleski, E.

- 1986: Geology of Linda volcanogenic massive sulphide deposit, Snow Lake, Manitoba; in *Current Research, Part A*; Geological Survey of Canada, Paper 86-1A, p. 15-20.

Contribution to the 1989-1994 Rusty Lake-Snow Lake Mining Camps, Canada-Manitoba Exploration Science and Technology Initiative (EXTech I)

Development of a borehole surveying probe using 3-component fluxgate magnetometers

P.G. Killeen¹, C.J. Mwenifumbo¹, and G.R. Bernius¹

Killeen, P.G., Mwenifumbo, C.J., and Bernius, G.R., 1996: Development of a borehole surveying probe using 3-component fluxgate magnetometers; in EXTECH I: A Multidisciplinary Approach to Massive Sulphide Research in the Rusty Lake-Snow Lake Greenstone Belts, Manitoba, (ed.) G.F. Bonham-Carter, A.G. Galley, and G.E.M. Hall; Geological Survey of Canada, Bulletin 426, p. 331-338.

Abstract: The location of a geophysical measurement in a borehole is just as important as the measurement itself. A co-operative effort between Geological Survey of Canada and industry in the EXTECH project has resulted in the development of a new borehole surveying tool which combines a three-component fluxgate magnetometer with solid-state tiltmeters. The device produces a continuous record of the dip and azimuth of the borehole and does a vector magnetic survey.

The tiltmeters track the dip of the hole and rotation of the probe. The hole azimuth is determined from the total field computed from the three magnetic components. Logging at 6 m/min with measurements every 0.5 seconds yields a data set at 5 cm intervals. This high data density makes it possible to separate the slow changes in the magnetic azimuth of the hole from anomalies caused by magnetic bodies in the vicinity of the hole. These magnetic bodies are themselves of geological interest. The path of the hole may be visualized as a 3-D plot in a wire grid box, as projections on vertical planes in north-south or east-west directions, or in a plan view. Vector displays of the data plotted along the borehole path in these planes can help to visualize the location of a magnetic body. Both borehole orientation and magnetic surveys have been successfully carried out in several mining areas. The probe is now commercially available and has been used extensively world-wide.

Résumé : La localisation d'une mesure géophysique dans un trou de sondage est tout aussi importante que la diagraphie elle-même. Dans le cadre du projet EXTECH, un travail de collaboration entre la Commission géologique du Canada et l'industrie s'est traduit par la mise au point d'un nouvel instrument de diagraphie dans les sondages qui combine, d'une part, un magnétomètre électronique à sursaturation («fluxgate») à trois composantes et, d'autre part, des inclinomètres à semi-conducteurs. L'appareil produit un enregistrement continu du pendage et de l'azimut du trou de sondage et réalise un levé magnétique vectoriel.

Les inclinomètres enregistrent le pendage du trou et la rotation de la sonde. L'azimut du trou est basé sur le champ total calculé à partir des trois composantes magnétiques. La diagraphie se fait à une vitesse de 6 m/min avec une mesure à chaque demi-seconde, ce qui permet d'obtenir une donnée à tous les 5 centimètres. Cette forte densité des mesures permet de séparer les variations lentes de l'azimut magnétique du trou des anomalies causées par les massifs magnétiques à proximité du trou, lesquels sont d'intérêt en géologie. Le tracé du trou peut être visualisé sur un diagramme tridimensionnel (boîte grillagée) selon trois plans, en l'occurrence les plans verticaux nord-sud et est-ouest ou la vue de dessus. Les représentations vectorielles des données recueillies le long du trou de sondage dans ces plans peuvent faciliter la visualisation de l'emplacement du massif magnétique. Dans plusieurs régions minières, les diagraphies de l'orientation du trou et du champ magnétique ont été concluantes. La sonde est maintenant commercialisée et utilisée abondamment dans le monde entier.

¹ Geological Survey of Canada, 601 Booth St., Ottawa, Ontario K1A 0E8

INTRODUCTION

Boreholes are drilled to obtain information in the third dimension, i.e. at some depth below the Earth's surface. The path of the borehole does not necessarily continue at the dip and azimuth of the collar of the borehole due to the vagaries of the drilling operation. The problem of determining the borehole position or orientation at any given depth is not simple. The problem of determining position on the surface of the Earth has been the subject of intensive investigation and improvement since the days of Marco Polo, and can today be considered to be "solved" with the advent of the Global Positioning System (GPS) based on triangulation with satellites at known points in orbit in space. Geophysical surveys now utilize GPS to locate the position of each geophysical measurement.

Unfortunately GPS cannot be used to locate the position of borehole-geophysical instruments beneath the Earth's surface, where the satellite transmissions will not penetrate.

Numerous ingenious methods have been tried in order to produce an accurate survey of borehole orientation. These have been based on surveying tools containing, for example: (1) a level bubble and a magnetic compass which is photographed sequentially inside the probe as it moves in the hole; (2) clockwork mechanisms which lock a pendulum and compass in place, at a given time, and which can then be retrieved from the hole to be read; (3) gyroscopic mechanisms which, due to the size constraints of the hole, must spin at such a high rate that their jewelled bearings have a short lifespan; and (4) devices based on light beams aimed at the centre of a target in a long probe, which move off-centre as the probe bends with the curvature of the hole (one version photographs the target and a level bubble; another records electronically with light sensitive detectors on the target). Other variations of borehole orientation devices have been tried with the advent of new technology, but often the new hardware is only adaptable to surveying the large diameter holes drilled in petroleum exploration (e.g. laser gyroscopes that use cruise missile navigation technology), and is not small enough to run in the 60 to 75 mm diameter holes drilled in mineral exploration. In many of the methods, the number of determinations of orientation information in the hole is relatively small. The clockwork mechanism mentioned previously, for example, usually results in only a single measurement every few hundred metres, due to the length of time it takes to travel down and up the hole to obtain each reading. This produces significant errors if any reading is erroneous, due to local magnetic effects adjacent to the hole when the reading is taken, such as those caused by the presence of magnetite. In some of the methods, such as the gyroscope method, the cost is high, and in addition there is significant instrumental drift.

An attempt was made to improve borehole surveying technology within the EXTECH project, by utilizing a new generation of "ring-core" fluxgate magnetometers combined with solid state tiltmeters to provide detailed borehole azimuth and dip information.

Today, as mineral exploration boreholes are often drilled to depths of 1000 m or greater, it has become more and more important to survey the path of the hole, as the orientation errors become larger with depth. Probably one of the most important areas of application is in estimating the size and tonnage of a new deposit based on the intersection of numerous boreholes. Deviations in the borehole path can result in the difference between the deposit becoming an 'ore body' or just an 'occurrence'.

NEW BOREHOLE ORIENTATION PROBE

The new orientation probe was designed to operate on the basis of sensing changes in the Earth's gravity and magnetic fields as the probe moved along a borehole. Working with the Borehole Geophysics Section of the Geological Survey of Canada, two Ontario-based firms, Morris Magnetics Inc. of Lucan, and IFG Corporation of Brampton, developed the hardware and software, and a prototype was field tested under a joint venture arrangement. The probe was designed to:

1. obtain real-time continuous borehole orientation measurements which may be monitored and sampled as often as desired,
2. operate in an AQ size hole (46 mm),
3. recognize and possibly correct for anomalous magnetic fields, and
4. provide an error assessment.

The magnetic method was chosen because it was amenable to the above considerations. The other advantages were that the probes:

1. are relatively inexpensive,
2. require little service or maintenance, and
3. have no moving parts and are relatively shock-proof.

Probe limitations include the inability to operate inside steel casing, or in areas of high remanent magnetization in the hole. However, these usually affect the measurements along only short sections of the hole and recovery outside these sections is possible.

The magnetic sensors in the probe consist of a set of three orthogonal ring-core fluxgate magnetometers originally developed for use with NASA's MAGSAT program. Each fluxgate sensor consists of a 12 mm ring core around which is wound the driving coil. The ring core and the driving coil are encased in a plastic holder around which is wound the sensing coil. The total package is 32 mm x 24 mm x 12 mm. One fluxgate, (Mz), is oriented along the axis of the probe and the other two fluxgates, (Mx and My), are orientated orthogonal to each other, and in a plane perpendicular to the probe axis.

The solid state tiltmeters, Tx and Ty, are oriented in the same directions as Mx and My, respectively. The tiltmeters consist of an electrolyte which half fills the space between

two conductors on opposite sides of a disc-shaped glass container. As the container rotates (tilts), the electrolyte moves, changing the resistance between the conductors on opposite sides, which is calibrated in terms of the degree of tilt (Balch and Blohm, 1991).

A diagram of the orientation probe with the configuration of the main components is shown in Figure 1. The probe housing is 40 mm diameter, and is made of a nonmagnetic, nonconductive material which is pressure rated to 2000 m water depth. The housing is divided into 3 sections: (1) a microprocessor section, (2) an electronics section, and (3) the sensor section.

The five sensors, (M_x , M_y , M_z , T_x , and T_y), are mounted in a rigid holder near the bottom of the probe. The electronics section digitizes each analog signal from the five sensors into values with 24 bit resolution twice per second. The magnetic field components are measured with a resolution of 0.1 nT and the tilt components resolution is 0.1° . The microprocessor section transmits each set of readings along the logging cable to the surface console in a digital format. Data acquisition is time based.

DIP AND AZIMUTH MEASUREMENT OF A BOREHOLE

As the orientation probe is lowered in a borehole, the output of the tiltmeters, T_x and T_y , will change as the dip of the hole changes. The measured dip angles from T_x and T_y are apparent

dip angles oriented at 90° from each other. The dip angle of the hole is computed from these two tilt measurements. The computed dip angle is still only an absolute dip and can be in any direction as shown in Figure 2. The true dip (which includes the azimuth) lies somewhere on the cone of equal dip shown in the figure. The azimuth is determined from the M_x and M_y fluxgate measurements which give the direction of the Earth's field at that measurement point in the borehole.

However, to complicate the measurements, the probe can also rotate in the hole while it moves up or down. If a borehole had a constant azimuth, then the probe rotation would cause the output of the fluxgates and the tiltmeters to vary sinusoidally. The sine wave output of the rotating fluxgates would have the same period as the rotating tiltmeters, and the phase difference would remain constant. If the dip of the hole changed, the maximum amplitude of the sine wave variation in the output signal of both the tiltmeters and the fluxgates would also change. However, if the azimuth of the hole changed, the phase difference between the sine wave output of the fluxgates and tiltmeters would also change. This change in the phase angle between tiltmeter and fluxgate data can be converted into the desired azimuthal information thereby eliminating the effect of the probe rotation on the magnetometer data. A typical plot of raw data from the five sensors, (M_x , M_y , M_z , T_x , and T_y) as well as the dip and total field which are computed by the microprocessor in the probe, is shown in Figure 3. In practice, vertical holes are the most difficult to survey, but in mining, inclined holes are the rule rather than the exception. In that case the friction of the probe on the borehole walls tends to keep probe rotation to a minimum.

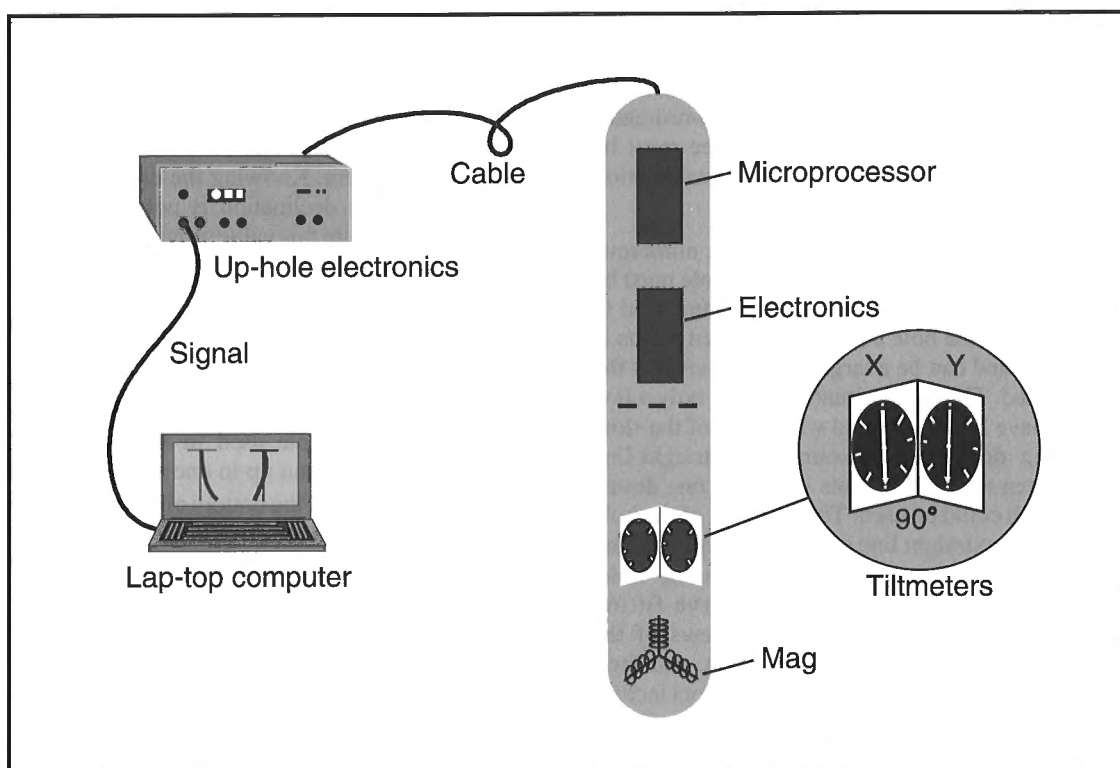


Figure 1. Diagram of orientation probe showing configuration of main components.

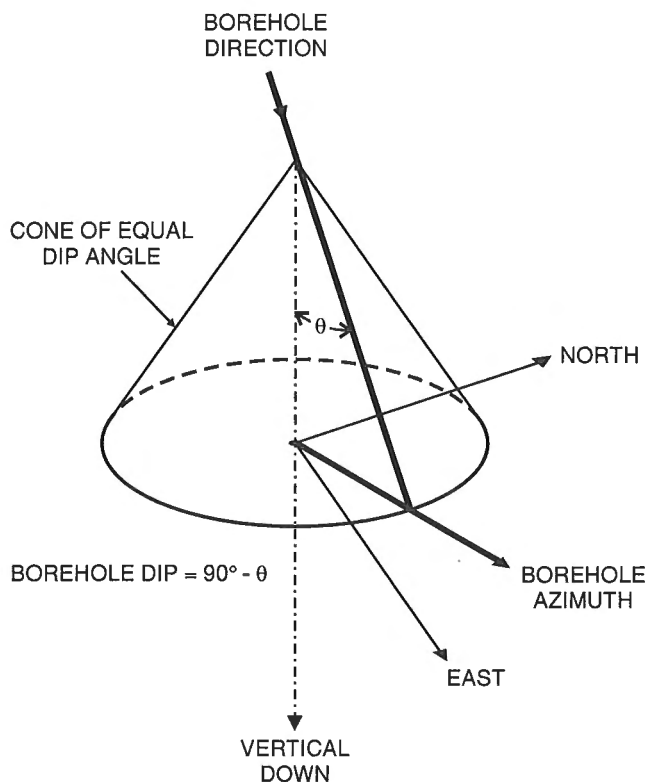


Figure 2. Cone of measured dip (from tiltmeters) for all possible azimuths around measurement point. Correct azimuth of borehole is determined from fluxgate magnetometer measurement at that point.

GEOMETRY OF THE BOREHOLE

Having determined the dip and azimuth of a borehole at many different depths in the hole (e.g. every 5 cm), the co-ordinates of the path of the hole in three-dimensional space must be computed. This is referred to as the desurveying calculation (Howson and Sides, 1986).

Although the dip and azimuth are known at numerous locations along the borehole, the true path of the hole must be computed between the measured points. The method used to compute the position of the hole between measured points is extremely important and can be a large source of error if the wrong method is used. This is the situation where only a few points in the hole have been measured with some of the slow borehole surveying devices. For example, a straight-line interpolation between measured points would be one desurveying method which could be used. The true path of the hole does not usually follow straight line segments, only changing dip and azimuth at the measurement points in the hole. Various computation methods involving curve-fitting between points have also been proposed. Reviews of the various methods of computing borehole position, and their possible errors have been presented by several authors including Walstrom et al. (1969), Harvey et al. (1971), Truex (1971), Walstrom et al. (1972), and Wolff and deWardt

(1981). These methods include the angle averaging method, balanced tangential method, radius of curvature method, and minimum curvature method, details of which are beyond the scope of this paper.

The new orientation probe makes measurements continuously, and these are sampled every half-second. At a logging speed of 6 m/min, measurements of dip and azimuth are made every 5 cm along the path of the hole. This data interval is much smaller than the length of the orientation probe itself. Because the interval between readings is so small, the borehole desurveying method used to compute the position co-ordinates of the hole will have very little effect on the results. Therefore, the simplest method which assumes a straight path between measurements was chosen. If the logging speed is increased, the sample interval will also increase because the sampling rate (twice per second) is constant. The effect of increasing the sample interval was investigated by Balch and Blohm (1991). They presented an example of a survey of a 600 m deep borehole using the new orientation probe. By using only part of the measured data, thus simulating measurements at larger intervals, they recomputed the position of the bottom of the hole. In their worst example with an average sample interval of up to 10 m, the position of the bottom of the hole varied by about ± 4 m. They also compared logging continuously at 9 m/min with logging in an incremental mode, stopping every 5 m in the hole. They found the error in computing the position of the bottom of the hole was within ± 2 m, between the continuous and incremental mode.

The desired final computed co-ordinate positions of the borehole are with respect to the geographical coordinate system. Every point along the path of the hole has a northing, easting, and vertical depth. However, the actual measurements are made with respect to the geomagnetic field. The computed azimuth is a magnetic azimuth until it has been converted to a geographic azimuth. It is necessary to know the declination of the local field, in order that the borehole magnetic co-ordinates can be rotated into the geographical co-ordinate system. Knowing the correct value to apply for the geomagnetic declination is not a trivial problem. It is possible to measure this value provided that proper equipment is used and the area has been gridded accurately. One compromise is to take the value for the geomagnetic declination from a regional geomagnetic declination and inclination map. This is the method most commonly employed. Balch and Blohm (1991) considered this problem by repeating the computations with the wrong geomagnetic declination, for the 600 m depth borehole used in their other field tests. By varying the declination up to one degree west (from 346° to 345°), the position of the bottom of the hole varied up to ± 5 m. They concluded that the error in the position of the bottom of the hole is more sensitive to errors in the value of the geomagnetic declination used in the computations, than the errors that might arise from the orientation probe measurements in the borehole.

The geographical path of the borehole may be displayed in several different ways. The projection of the path of the hole in a north-south vertical section, in an east-west vertical

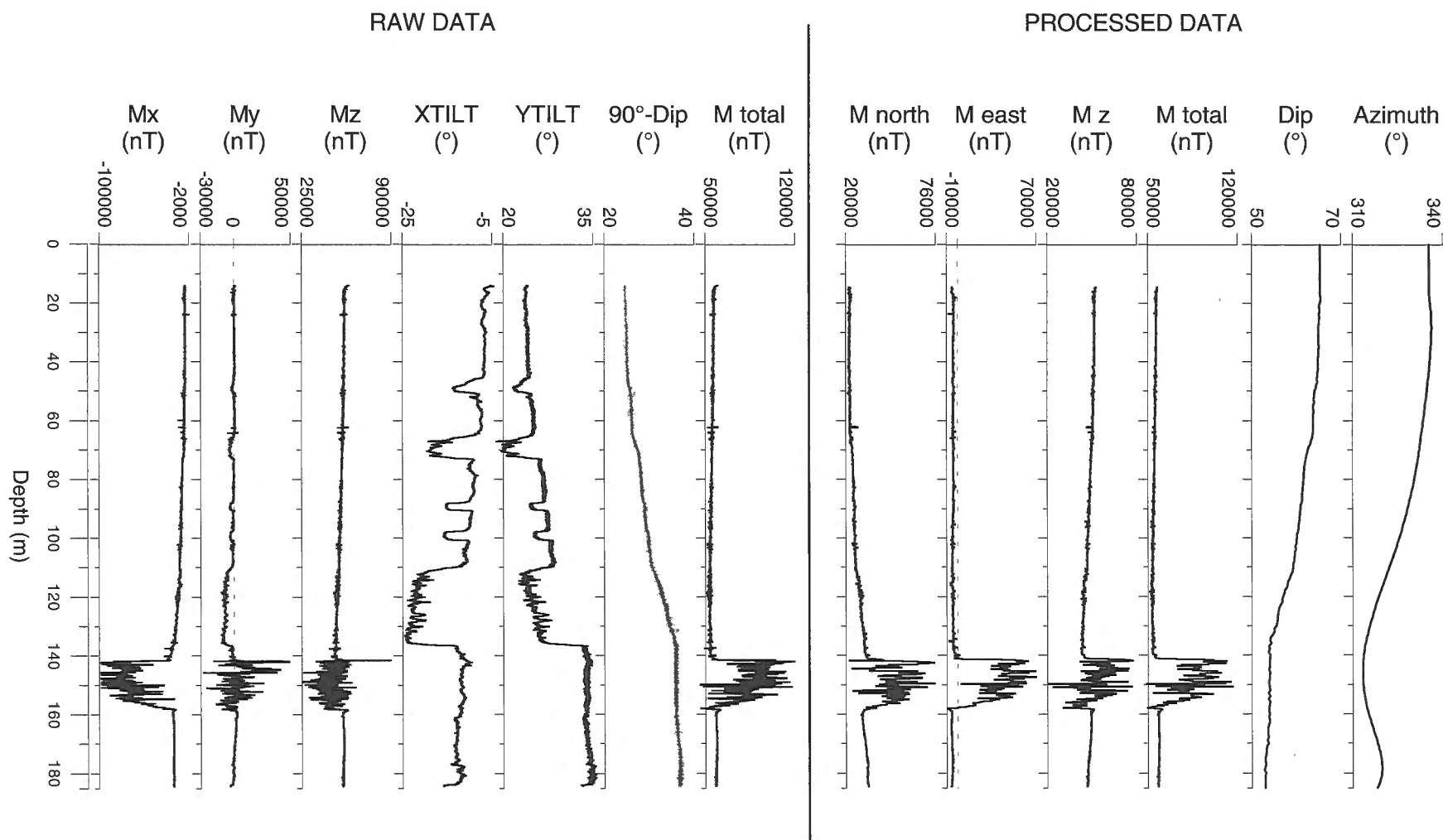


Figure 3. Left: example of raw data from Mx, My, Mz, Tx, Ty, sensors, and microprocessor-computed dip and total field transmitted to surface from probe. Right: preliminary processed data with rotation effects removed and true dip and magnetic azimuth computed.

section, or in plan view, are all possible as shown in Figure 4. Several versions of the plan view are also possible. Figure 5 shows a combination of all of the above views in a wire grid box showing the path in “3-D”.

SOURCES OF POSSIBLE ERROR

With any geophysical instrument there are numerous sources of possible error related to the construction and use of the instrument. Proper calibration of the orientation probe is necessary to eliminate or correct for these possible errors. During the development and testing of the new probe, corrections were developed as the sources of error were recognized. These are summarized below (Balch and Blohm, 1991):

1. **Zero offset errors** occur in the form of a base line shift when the negative to positive peak values of a sensor are not equal. Measurement of the peak-to-peak response of a sensor is achieved by rotating the sensor about its sensitive axis through 180°, repeated for four directions of orientation, north, south, east, and west.
2. **Gain adjustment** must be applied in two ways. First, in the magnetometer, the peak to peak response for all three components must be equal for a rotation about their sensitive axes. Second, in the tilt sensor, the measured tilt must be as close to the absolute value as possible. Calibration of the tilt sensors is accomplished using a rotation wheel which is calibrated to within 0.1° of the absolute tilt angle. This is the limit of accuracy of the tilt sensor.
3. **Orthogonality errors** are created when the sensors are not aligned at right angles to one another. These errors are minimized by rotating each component mathematically through its non-orthogonality error angle, which is determined through a least-squares analysis of data generated by no less than three complete rotations about the long axis of the probe.
4. **Linearity errors** require using some form of absolute calibration against which the sensor output can be compared. The relationship between the sensor output and the actual output can be nonlinear, which makes the correction algorithm more complicated. Linearity corrections are applied to the tilt sensors. The magnetic components have been found to be linear over their operating ranges.
5. **Temperature drift** can be present as a long term gradual change in the output of a sensor. Calibration of the sensors in a temperature bath can quantify temperature effects and

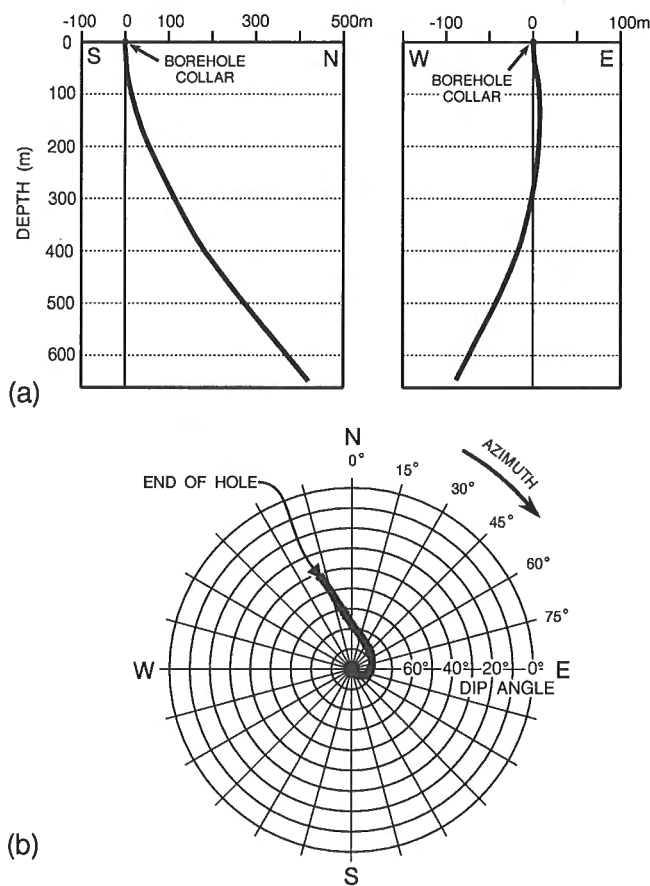


Figure 4. a) Projections of computed path of borehole in north-south vertical section, east-west vertical section, and b) plan view with stereonet-like co-ordinates.

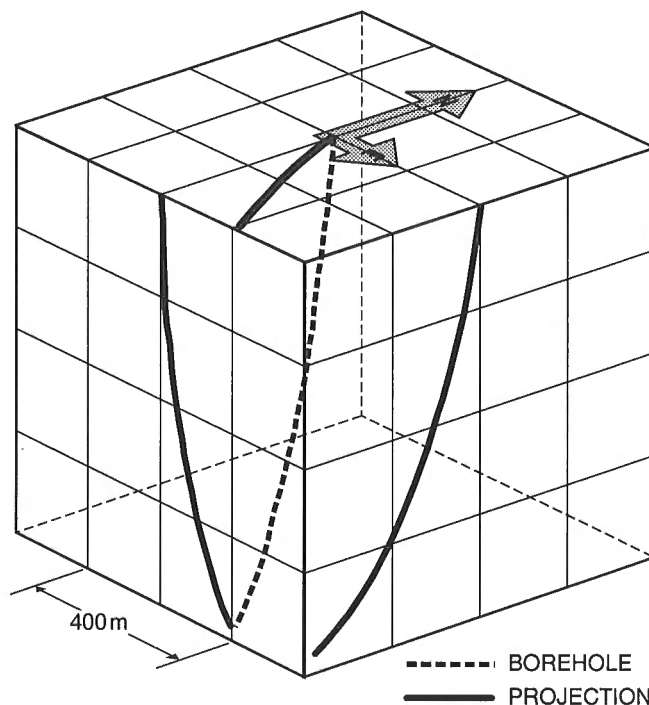


Figure 5. Three-dimensional view of borehole path combining vertical projections with rectangular grid plan view projection. In centre of wire grid box, path of hole in 3-D is also shown.

is set for the temperature operating range of the probe. It is helpful to obtain temperature logs of any borehole being surveyed to identify any possible temperature effects. The tilt sensors were found to show temperature-related drift, but the amount was less than 1% over a temperature change of 20°C and was not considered significant.

A postprocessing algorithm is used to apply calibration values for the above types of errors and thereby improve the accuracy of the orientation measurements. Although the calibration values can be obtained by performing a series of rotations of the probe about its long axis, it was found that logging in a vertical borehole in nonmagnetic rock, was better. For this purpose the GSC Borehole Geophysics test area at Bells Corners was used (Killeen, 1986; Schock et al., 1991). At the test area, a set of six vertical NQ holes (dip is approximately 89°) are drilled through about 60 m of 'non-magnetic' sedimentary rocks (mainly sandstone) and into the more magnetic underlying Precambrian rocks. Measurements were made below the casing and above the Precambrian at depths from about 17 to 30 m. The recorded data were processed by the calibration software. The calibration software uses three separate criteria to produce the best overall fit of the measured data to the known borehole geometry. These are the total magnetic field, the vector sum of M_x and M_y , and the vector sum of T_x and T_y . Since the dip of the hole is constant, these logs should be a straight line. Typically the maximum error is ± 70 nT per fluxgate and $\pm 0.1^\circ$ per tilt component. Based on the above error, the magnetometer will

contribute $\pm 0.3^\circ$ of uncertainty to the position of the probe in the hole. This represents the best level of accuracy that currently can be achieved in measuring the hole azimuth assuming no other sources of error are present.

Another possible external source of error is the presence of anomalous magnetic fields caused by magnetite or other magnetic minerals intersected by the hole. This has been investigated in some mining areas including Timmins. In summary, good results have been obtained when using the new orientation probe in boreholes where strongly magnetic units are present. This success is attributed to the high sensitivity of the probe and to the high sample rate which provides closely spaced measurements. Most of the error introduced by the magnetic units is randomly distributed. If enough readings are taken, the error tends to cancel out.

DETECTION OF OFF-HOLE MAGNETIC BODIES

Although the orientation probe uses the 3-component magnetometers to survey the borehole, plotting the magnetic vectors resulting from each measurement can be useful for determining the direction to the source of anomalous magnetic fields. A theoretical example is shown in Figure 6 which illustrates the magnetic vectors plotted along the path of two inclined holes which have a spherical magnetic body between them. It is easy to see from this example how the magnetic

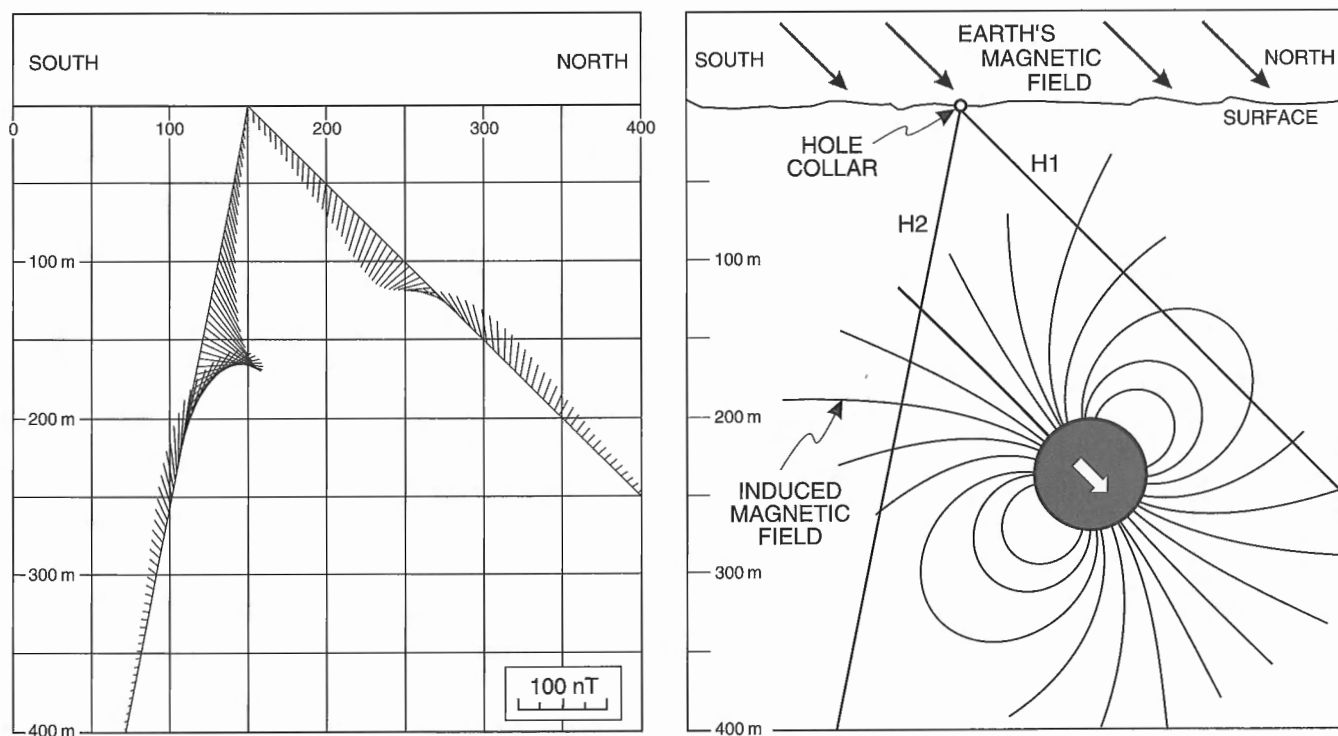


Figure 6. Left: north-south projection of theoretical magnetic vectors for two inclined holes located to south and north of spherical body, (right), which has induced magnetic field. This shows how amplitude and direction of vectors change, as the probe moves past a magnetized sphere.

information can be used. IFG Corporation, which now markets and sells the new orientation/magnetometer probe, is actively developing interpretation methods for the vector magnetometer data.

ACKNOWLEDGMENTS

The authors would like to acknowledge the contributions to this development by Detlef Blohm and Steve Balch of IFG Corporation, Bill Morris of Morris Magnetics Inc., and Quentin Bristow, Bill Hyatt, and Barbara Elliott of the GSC, who contributed to the development considerations in the electronics, field tests, and software respectively. Funding from the Manitoba EXTECH project is also gratefully acknowledged, as well as the contribution of numerous mining companies who provided test holes. In particular we thank Yves Rougerie of Aur Resources, Val d'Or; Ken Robertson of Noranda Exploration; and Barry Krause and Alan King of INCO Exploration and Technical Services.

REFERENCES

Balch, S.J. and Blohm, D.

- 1991: Development of a new borehole orientation probe; in *Proceedings of the 4th International Minerals and Geotechnical Logging Society – Canadian Exploration Geophysical Society Symposium on Borehole Geophysics for Minerals, Geotechnical and Groundwater Applications*; Toronto, 18-22 August 1991, p. 9-20.

Harvey, R.P., Walstrom, J.E., and Eddy, H.D.

- 1971: A mathematical analysis of errors in directional survey calculations; *Journal of Petroleum Technology*, v. 23, p. 1368-1374.

Howson, M. and Sides, E.J.

- 1986: Borehole desurvey calculations; *Computers & Geosciences*, v. 12, no. 1, p. 97-104.

Killeen, P.G.

- 1986: A system of deep test holes and calibration facilities for developing and testing new borehole geophysical techniques; in *Borehole Geophysics for Mining and Geotechnical Applications*, Geological Survey of Canada, Paper 85-27, p. 29-46.

Schock, L.D., Killeen, P.G., Elliott, B.E., and Bernius, G.R.

- 1991: A review of Canadian calibration facilities for borehole geophysical measurements; in *Proceedings of the 4th International Minerals and Geotechnical Logging Society – Canadian Exploration Geophysical Society Symposium on Borehole Geophysics for Minerals, Geotechnical and Groundwater Applications*; Toronto, 18-22 August 1991, p. 191-202.

Truex, J.N.

- 1971: Directional survey problems, east Wilmington Oil Field, California; *Bulletin AAPG*, v. 55, no. 4, p. 621-628.

Walstrom, J.E., Brown, A.A., and Harvey, R.P.

- 1969: An analysis of uncertainty in directional surveying; *Journal of Petroleum Technology*, v. 21, p. 515-523.

Walstrom, J.E., Harvey, R.P., and Eddy, H.D.

- 1972: A comparison of various directional survey models and an approach to model error analysis; *Journal of Petroleum Technology*, v. 24, p. 935-943.

Wolff, C.J.M. and deWardt, J.P.

- 1981: Borehole position uncertainty – analysis of measuring methods and derivation of systematic error model; *Journal of Petroleum Technology*, v. 33, p. 2339-2350.

Contribution to the 1989-1994 Rusty Lake-Snow Lake Mining Camps, Canada-Manitoba Exploration Science and Technology Initiative (EXTECH I)

VHMS favourability mapping with GIS-based integration models, Chisel Lake-Anderson Lake area

D.F. Wright¹ and G.F. Bonham-Carter¹

Wright, D.F. and Bonham-Carter, G.F., 1996: VHMS favourability mapping with GIS-based integration models, Chisel Lake-Anderson Lake area; in EXTECH I: A Multidisciplinary Approach to Massive Sulphide Research in the Rusty Lake-Snow Lake Greenstone Belts, Manitoba, (ed.) G.F. Bonham-Carter, A.G. Galley, and G.E.M. Hall; Geological Survey of Canada, Bulletin 426, p. 339-376, 387-401.

Abstract: Maps showing spatial variation of volcanic-hosted massive sulphide (VHMS) potential in the Snow Lake area have been generated by combining digital data from a variety of sources. An exploration model, based on a volcanic-hosted massive sulphide deposit model, but expanded to include regional exploration data sets, provides a conceptual framework for the extraction of predictive evidence from the raw data sources. The evidence is divided into five factors: stratigraphic evidence, evidence related to available heat, alteration evidence, geophysical evidence, and geochemical evidence.

Three approaches have been applied for combining spatial evidence to predict mineral potential. (1) The weights of evidence method (data-driven) is used to characterize the spatial associations between the known deposits, and to calculate weights for each predictive map layer. (2) In the fuzzy logic method, evidence is expressed in terms of fuzzy membership functions, subjectively assigned by an expert, for each predictor map. (3) Dempster-Shafer belief theory is more flexible than fuzzy logic for representing uncertainty in the data, but is somewhat restricted in the expressiveness of the combination rules.

The resulting favourability maps from each method have similar patterns that show all the known deposits in highly favourable zones and a number of prospective areas that have the right combination of factors but no known deposits. The new volcanic-hosted massive sulphide discovery at Photo Lake made during summer 1994 is in a favourable zone as predicted by these models.

Résumé : Des cartes figurant la variation spatiale du potentiel en sulfures massifs volcanogènes (SMV) dans la région de Snow Lake ont été dressées en combinant des données numériques de diverses sources. Un modèle d'exploration, dont le fondement est un modèle de gisement de SMV sauf qu'il inclut des ensembles de données d'exploration dans la région, offre un cadre conceptuel pour faire ressortir les facteurs importants dans la prédiction d'un potentiel à partir des données brutes. Cinq facteurs ont été mis en évidence; ce sont le cadre stratigraphique, la chaleur disponible, l'altération, le caractère géophysique et le caractère géochimique.

Trois méthodes ont été appliquées pour combiner les preuves spatiales de façon à prédire le potentiel minéral. 1) La méthode du poids de la preuve (articulée autour des données) sert à caractériser les associations spatiales entre les gisements connus et à calculer les poids de chaque couche cartographique de prédiction. 2) Selon la méthode de la logique floue, la preuve s'exprime en termes de fonctions

¹ Geological Survey of Canada, 601 Booth St., Ottawa, Ontario K1A 0E8

d'appartenance floues, subjectivement établies par un expert pour chaque carte de prédiction. 3) Quant à la théorie de la croyance de Dempster-Shafer, elle est plus souple que la logique floue en ce qui concerne la représentation de l'incertitude dans les données, mais est quelque peu limitée dans l'expression des règles de combinaison.

Les cartes des «chances» de découvrir un gisement qui résultent de chacune des méthodes donnent des configurations semblables qui indiquent non seulement tous les gisements connus dans des zones très favorables, mais aussi un certain nombre de secteurs prometteurs présentant la bonne combinaison de facteurs mais où aucun gisement n'a été découvert. Le nouveau gisement de SMV de Photo Lake, découvert au cours de l'été 1994, est situé dans une zone favorable identifiée à l'aide de ces modèles.

INTRODUCTION

Mineral exploration is a task that involves the collection, analysis, and integration of data from a variety of sources, generally beginning at a small scale over sizeable areas and progressing to large scales over relatively small areas, with the objective of defining targets for mineral deposits.

Traditionally, the integration of exploration data sets to investigate overlap relationships between anomalies was done manually with the aid of a light table. This process was highly subjective, labour-intensive, and almost impossible to repeat without getting different results. Recently, with the availability of relatively inexpensive, high-powered computing workstations and Geographic Information Systems (GIS), the efficiency with which this process can be carried out has improved dramatically. Computer-based mineral potential mapping allows the geologist to make the evaluation process more thorough, analytical, less subjective, and more repeatable than strictly manual methods. Furthermore, improvements in statistical and expert-system methods applied for integrating data sets allow computer-generated analyses to mimic and in some cases improve upon the performance of experienced exploration geologists. This paper describes the GIS-based analysis of exploration data sets for the Snow Lake area, during the EXTECH program.

The Exploration Science and Technology Initiative (EXTECH), a co-operative effort between the Geological Survey of Canada, the Manitoba Department of Mines and Energy, and the mining industry, began in 1989. One of the principal goals of EXTECH was to improve the concepts and technologies applicable to exploration for volcanic-hosted massive sulphide deposits through the development of *integrated* regional- and deposit-scale models, using the Snow Lake camp as a study area. The GIS study focused on the quantitative integration of regional data sets, drawing on the extensive sources of data collected during the program, the improved understanding of a mineral deposit model appropriate for the volcanic-hosted massive sulphide deposits in the area, and the recent developments in integration methodology. The program provided a rather complete collection of

exploration data sets (with some notable deficiencies such as EM data), and an excellent opportunity to try out the GIS-based mineral potential approach.

The objectives of the GIS project were to:

- establish a digital, geographically-registered database of the exploration data sets available for the Snow Lake area,
- develop and apply quantitative methods for characterizing each data set, for studying their inter-relationships, and for combining them to estimate mineral potential, and
- generate maps showing areas favourable for volcanic-hosted massive sulphide type deposits for the Snow Lake area, using a variety of assumptions and integration models, and to investigate the sources of uncertainty in these maps.

Pilot GIS studies were carried out at the start of the EXTECH project, before the main EXTECH data were available. These initial studies used data from 1:50 000 scale mapping, covering the western half of the region described in the present paper, and the next adjacent sheet to the east. The data consisted of regionally-compiled geological maps and broad-scale regional geophysical and geochemical coverage available before the EXTECH project began. Volcanic-hosted massive sulphide potential was evaluated using statistical methods, including Bayesian weights of evidence (Reddy et al., 1990), decision tree (classification and regression tree) analysis (Reddy and Bonham-Carter, 1991), and area-weighted logistic regression analysis (Reddy et al., 1991). Potential was also estimated using an expert-system approach, with a Prospector-type model modified for regional data sets, applied to the western half only of the study area used in this paper (Reddy et al., 1992; Bonham-Carter et al., 1994). The work described in the present report benefited from the earlier pilot studies, taking advantage of the new data sets collected during EXTECH, the improved understanding of the mineral deposit model developed during EXTECH, and from some new approaches for expert-system models, notably the fuzzy logic and Dempster-Shafer methods studied by Ping An for his PhD. at the University of Manitoba (An, 1992;

An et al., 1991, 1992, 1994a, b). An's work was applied mainly to geophysical data from the region to the east of the present study.

Location of study area

The EXTECH study area covers two 1:50 000 scale NTS map sheets, 63J/13 and 63K/16, bounded by the intervals 54°45'-55°N and 90°30'-100°30' (see Fig. 1). The results presented in this paper are restricted to a part of this area that contains 15 past and non-producing deposits of volcanic-hosted massive sulphide type. This subarea is approximately 20 km by 15 km, extending from Wekusko Lake in the east to Ham Lake in the west, and from Snow Lake in the north to Morgan Lake in the south. We refer to this subarea as the Chisel Lake-Anderson Lake map area (Fig. 2).

Lake in the south. We refer to this subarea as the Chisel Lake-Anderson Lake map area (Fig. 2).

Framework for methodology

The process for producing mineral favourability maps using GIS can be considered in four main steps:

1. establish a conceptual model,
2. build a spatial database,
3. process the data, and
4. apply integration modelling to generate favourability maps.

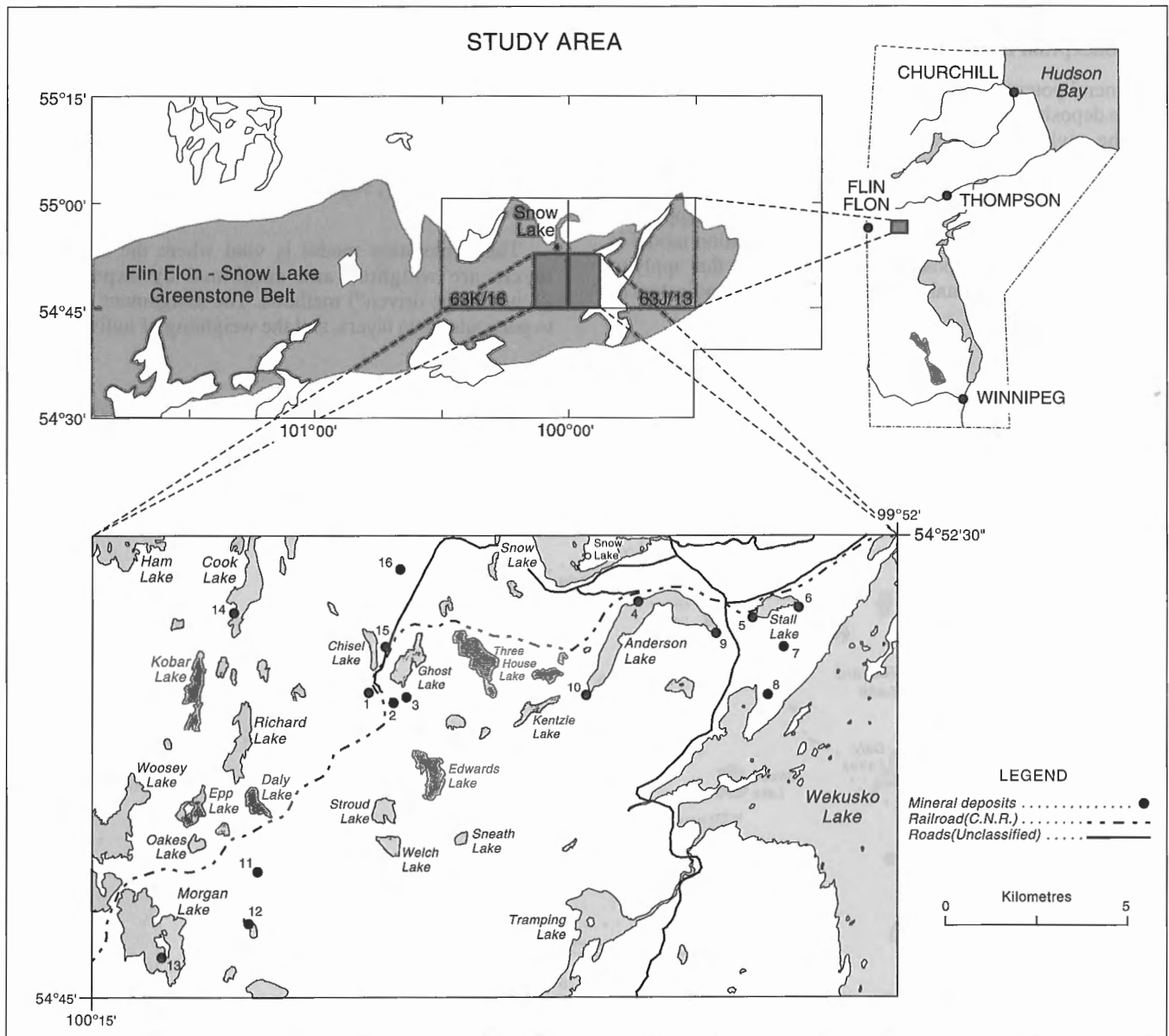


Figure 1. Location of study area. Data has been collected for area covering NTS sheets 63K/16 and 63J/13. Results discussed in this paper are for area highlighted in centre of two map sheets and shown in bottom half of figure. The key to the VHMS deposits, labelled 1 to 16 on the map, is found in Table 1.

The conceptual model, even if not explicitly stated, guides many of the decisions throughout the study. The spatial database in a GIS is an organized collection of individual data sets, incorporating a variety of data structures (raster, vector, relational, for example). The data processing step involves many operations to extract and enhance critical predictive information from each of the "raw" data layers. Integration modelling, as used here, refers to the methods for combining predictive data layers into favourability maps, by statistical or expert-system methods. Favourability mapping does not attempt to estimate the number and size of mineral deposits, as in the United States Geological Survey three-step resource appraisal methodology, (see Singer, 1993 for a recent review), although the output from favourability mapping could be used as input for the USGS method.

(1) Conceptual model

In mineral potential mapping, the conceptual model is based on the deposit model applicable to the deposit type of interest and the environment in which the deposits occur. However, because the deposit model usually focuses on the characteristics of deposits seen at, or near to, the deposits themselves, the conceptual model for favourability mapping is closer to the "exploration" model. The exploration model is composed of all the deposit model components that apply to exploration from regional data sets, plus deposit indicators as

seen on regional geophysical and geochemical surveys, satellite images, and other data sources used by exploration companies.

The exploration model guides the choice of data sets, the operations employed to extract useful information for mineral prediction, and, where expert-system methods are used for data combination, for ranking or weighting of data layers. For this study, some data layers such as airborne radiometrics, Landsat TM, and surficial geology, although available and incorporated in the database, were not employed directly as evidence for volcanic-hosted massive sulphide deposits, and they do not appear in the exploration model. Of course, some of these data layers were thoroughly examined in the GIS to determine whether they could have exploration utility before being rejected.

The methods used to extract evidence from raw data depend on the deposit type. For example, proximity to contacts between selected lithologies may be important for volcanic-hosted massive sulphide deposits, but without predictive value for placer gold deposits. Similarly, enhancements to geochemical, geophysical, and satellite data depend on the mineralogy, structure, and size of the deposit type of interest.

The exploration model is vital where the critical data layers are weighted and combined by expert-system ("knowledge-driven") methods. The assignment of weights to particular data layers, and the weighting of individual map

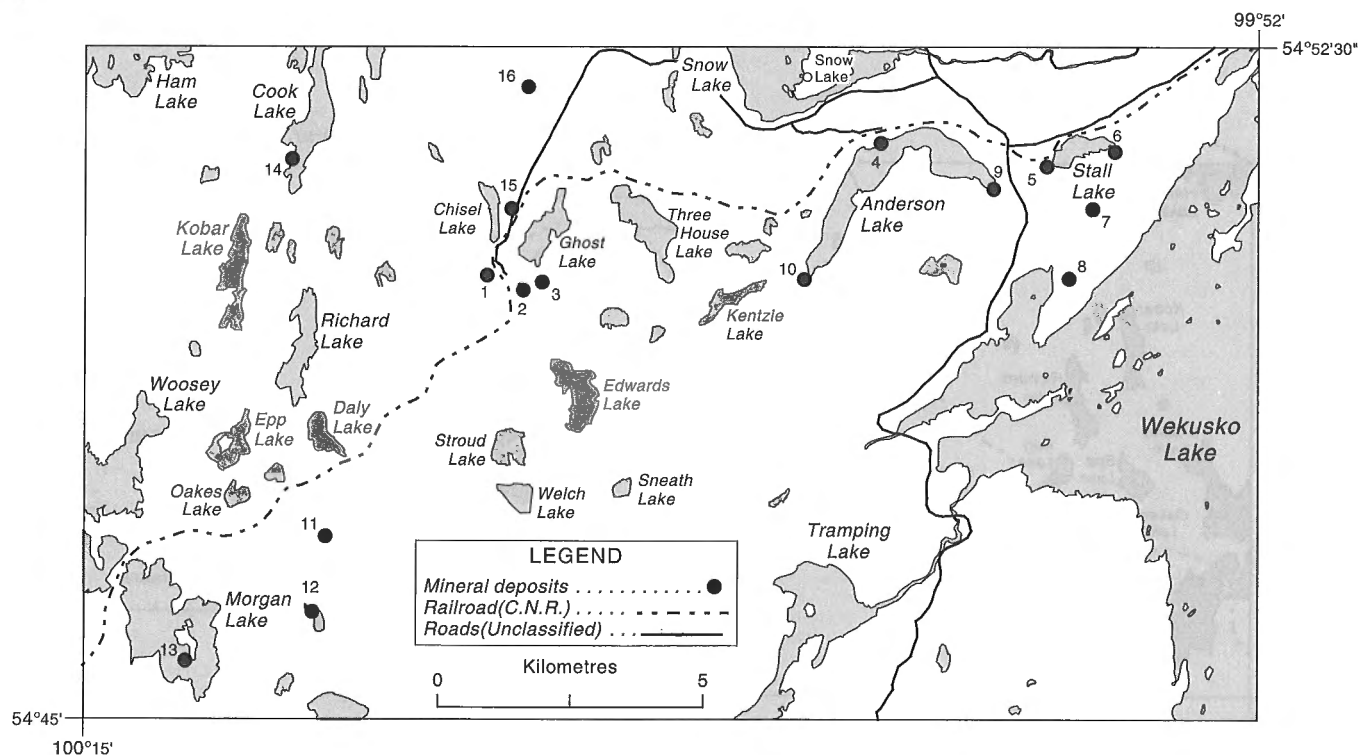


Figure 2. Selected area showing volcanic-hosted massive sulphide deposits and key geographical features of region. Selected area is approximately 15 by 20 km. Names of numbered deposits on figure are found in Table 1.

classes within a layer, requires expert opinion as expressed by the exploration model. The construction of an inference network with a mix of combination rules depending on the type of decision process being modelled, is also guided by the exploration model. Even where statistical methods of data combination are employed, as in regression, weights of evidence or neural network approaches, for which the weighting is determined automatically using the locations of known mineral deposits for training, the exploration model still comes into play for deposit selection. For example, if the exploration model dictates that the deposits should be classified by geological characteristic or by size, different sets of weighting must be calculated for each deposit class; see for example the study on the effects of deposit size as studied by Knox-Johnson (1994).

(2) Building the database

Building the database is the most time-consuming phase of most GIS projects. Data sets come in many shapes and sizes, according to a variety of data models, data structures, and data formats. Data such as the bedrock geology, surficial geology, alteration, and catchment basin maps usually require manual digitizing, unless they have already been digitized previously. Geochemical data, including till geochemistry and lake-sediment geochemistry are available as point data sets, in the form of ASCII tables containing geographical co-ordinates, geochemical values, and other information. In order to be treated as layers of area data, with values known everywhere on the map, as is needed for multiple map combination, geochemical data must be transformed into gridded maps by surface interpolation methods (we have used kriging in this study), or represented as discontinuous "stepped" surfaces, using catchment basins as the zones of influence around sample points. Where geophysical data and satellite images are available as digital grids, already levelled and calibrated in a pre-processing stage, only a format conversion is required to bring them into the GIS. Sometimes mineral deposit records, and other information, are available as digital files, otherwise they require manual data entry.

(3) Data processing

The third step involves processing the original "raw" data sets to extract evidence critical for the prediction of volcanic-hosted massive sulphide deposits. Some examples are:

- The original geological map units are usually too numerous and should be grouped together (map "reclassification") for the purposes of favourability mapping;
- the contacts between felsic flow units and volcanoclastic units are extracted from the reclassified geological map as vectors, and converted to a new map showing proximity to this contact by a line dilation process ("buffering" in GIS terminology);

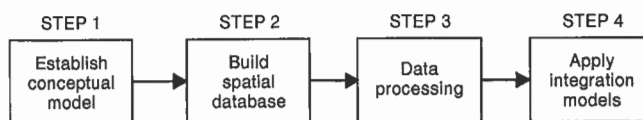


Figure 3. Steps followed in this study to produce mineral potential map.

- principal component analysis is applied to the lake-sediment geochemical data in order to compress the multi-element distributions into a smaller number of element combinations ("principal components") that are easier to manage and interpret;
- filters of various kinds are applied to geophysical and satellite images to enhance characteristics known to be indicative of volcanic-hosted massive sulphide deposits, such as a filter to localize inflection points in the VLF quadrature image, sometimes caused by buried sulphide bodies.

(4) Map combination

The final step consists of combining the various derived maps that provide evidence for volcanic-hosted massive sulphide type deposits into one or more mineral favourability maps, in some cases with maps showing the uncertainty of the favourability estimates. The combination process involves the weighting and union of evidence. Many favourability maps can be generated from the same database, depending on the combination method employed, on the choice of data layers used for prediction, and on the weighting schemes applied to the data layers. Combination methods can be classed either as data-driven or knowledge-driven methods, depending whether they use statistical or expert-system principles, respectively. In this study, three methods were applied to the same predictive data layers: weights of evidence, a method that is data-driven in the sense that the weighting is determined by the spatial associations of each layer with the known deposits; and two knowledge-driven methods, using fuzzy logic theory and Dempster-Shafer belief theory, where the weighting and combination of data layers is determined by a mineral deposit expert, as expressed in the conceptual exploration model.

This four-step favourability mapping approach is summarized in Figure 3. We now turn to the geological setting and exploration model used for the EXTECH study.

EXPLORATION MODEL FOR VHMS DEPOSITS IN THE SNOW LAKE CAMP

Geological setting

The geological characteristics of the Snow Lake volcanic-hosted massive sulphide deposits are described in detail by Bailes (1990a, b), Bailes and Galley (1991), Galley et al. (1993), and Bailes and Galley (1996). The deposits of the Snow Lake camp occur in the eastern part of the Early

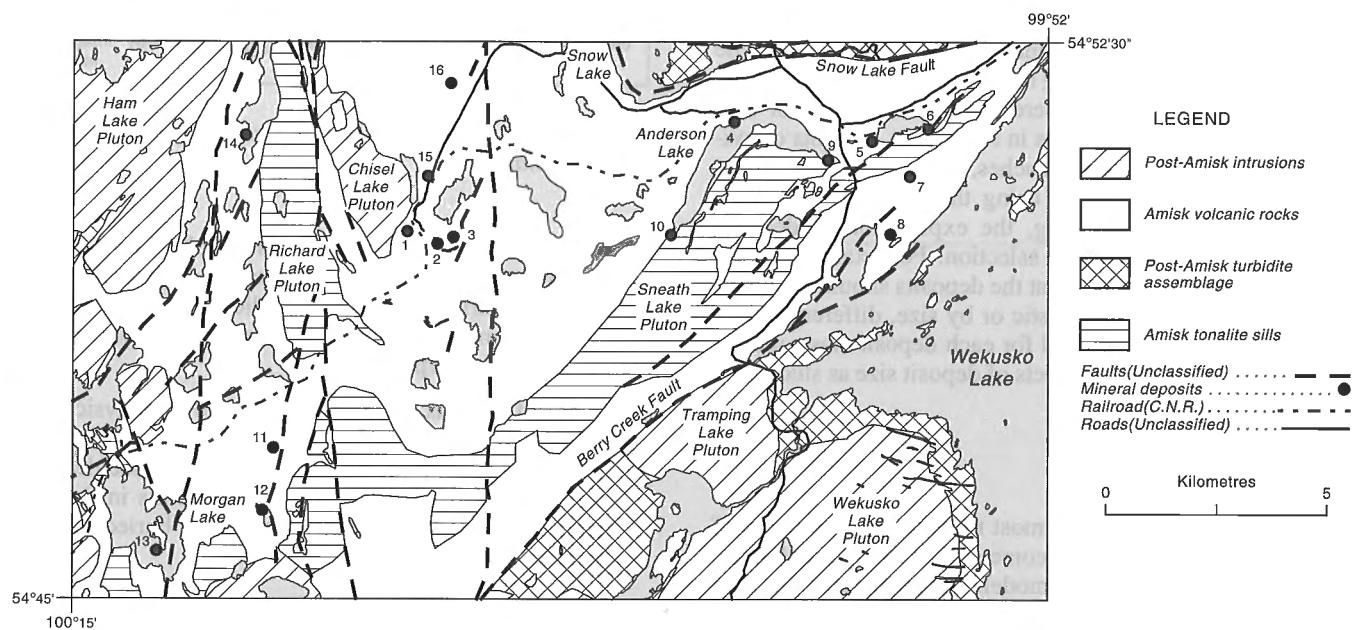


Figure 4. Locations of volcanic-hosted massive sulphide deposits and generalized geological features in Chisel Lake-Anderson Lake map area. Deposits are keyed to Table 1.

Table 1. Volcanic-hosted massive sulphide deposit names and characteristics for Chisel Lake-Anderson Lake study area (see Fig. 1 and Fig. 4). *Sources: Fedikow et al. (1988), Fedikow et al. (1993), Syme and Bailes (1993), Bailes and Galley (1996).

| Map No. | Name | *Tonnage (t) (reserves and production) | Grades Cu (%), Zn (%), Au (g/t), Ag(g/t) | Past or present producer |
|---------|-------------------------------------|---|---|--------------------------|
| 1 | Chisel Lake Chisel Lake open pit | 7 299 816 1 000 000 | 0.60 Cu, 10.94 Zn 0.25 Cu, 8.5 Zn, 2.74 Au, 54.86 Ag | Past |
| 2 | Lost Lake | 590 233 | 1.3 Cu, 8.5 Zn, 32.6 Au, 3.8 Ag | Past |
| 3 | Ghost Lake | | | |
| 4 | Anderson Lake | 3 189 601 | 3.41 Cu, 0.10 Zn | Past |
| 5 | Stall Lake | 6 263 779 | 4.29 Cu, 0.57 Zn | Past |
| 6 | Rod 1 Rod 2 | 22 675 810 440 | 4.5 Cu, 0.74 Zn 6.6 Cu, 2.9 Zn | Past |
| 7 | Linda 1 | N/A | N/A | Occurrence |
| 8 | Linda 2 | 13 000 000 | 0.30 Cu, 0.79 Zn | Nonproducer |
| 9 | Ram zone | N/A | N/A | Occurrence |
| 10 | Joannie | N/A | N/A | Occurrence |
| 11 | Rain Drop | N/A | N/A | Occurrence |
| 12 | Pot Lake | 123 000 | 1.43 Cu, 4.5 Zn, 0.4 Au, 18 Ag | Nonproducer |
| 13 | Morgan Lake | N/A | N/A | Occurrence |
| 14 | Bomber zone | N/A | 0.4 Cu, 1.0 Zn, 0.1 Au, 8.6 Ag | Occurrence |
| 15 | North Chisel | 2 580 000 | 0.22 Cu, 8.9 Zn, 2.54 Au, 23.3 Ag | Nonproducer |
| 16 | Photo Lake | 1 000 000 (approx.) | discovered in the summer of 1994 | |

Proterozoic Flin Flon volcano-sedimentary belt. There are at least fifteen known volcanic-hosted massive sulphide deposits hosted in 1.4 Ga submarine volcanics within the Chisel Lake-Anderson Lake map area. A sixteenth deposit, Photo Lake, was discovered following the completion of this study. (Fig. 4 and Table 1). The volcanics are an island-arc tholeiitic succession of lavas and volcanoclastic rocks of varying composition, that is divided into at least five eruptive cycles. The stratigraphic associations indicate that massive sulphide generation usually occurred at the end of an eruptive cycle that involved seismic activity (as suggested by debris flows) and explosive volcanism. Intruded into this succession are two, multiphase, tonalitic, subvolcanic intrusive complexes known as the Sneath Lake Pluton and Richard Lake Pluton, and synvolcanic dykes of diverse composition, (see Fig. 5 in colour section). The volcanic strata are affected by broad zones of semiconformable alteration that are up to 700 m thick and extend along strike up to 15 km (see Fig. 6 in colour section). Alteration consists of semiconformable silicification and epidotization, and semi- to disconformable Fe-Mg and Fe-Mg-Ca metasomatism and pyritization.

Deposit characteristics and interpretation

In general, the principal characteristics of the deposits for the Snow Lake area, pertinent to an exploration model, can be summarized as follows.

- Deposits occur within thick sequences of submarine volcanic rocks and deposits are spatially associated with felsic flows. A number of the deposits are close to the contact between felsic flows and overlying epiclastic strata, marking the termination of eruptive cycles.
- Most of the known deposits occur within 3 km stratigraphically above tonalitic intrusions (Sneath Lake and Richard Lake plutons). The intrusions are hypothesized to be the source of heat that triggered hydrothermal convection cells. Evolved seawater circulated through the volcanic rocks leaching metals and redepositing them at or near the seafloor.
- There is a strong spatial association of deposits with proximity to dykes. It is likely that vent areas were fed from vertical fractures that cut through the volcanic rocks, localizing the upward flow of hydrothermal fluids, and that dykes were also intruded along a similar fracture set. The cooling dykes assisted in focusing zones of thermal upwelling.
- The deposits are characterized by extensive zones of footwall alteration. These include semiconformable zones of silicification, chloritization, and amphibole alteration and chlorite-aluminosilicate alteration. These zones were produced by discordant rock-seawater interaction, the hydrothermal fluids reacting with volcanic rocks to produce alteration minerals. The variation in metamorphosed hydrothermal mineral assemblages and whole rock chemistry define a series of chemical gradients.
- Deposits are sometimes overlain by elevated levels of trace metals in drainage sediments and till. This is caused by weathering and erosion of deposits that produces a dispersion halo that can be picked up in surficial materials.
- Deposits are associated with magnetic, electrical, and gravity anomalies, due to the physical characteristics of buried sulphide bodies.

Exploration model

The characteristics outlined above must be recognizable on regional data sets for them to be useful for mapping regional favourability. For the EXTECH area, the geological and alteration mapping at 1:20 000 scale allows the following types of evidence to be derived as *layers of evidence*.

The first three layers are related to what might be termed *stratigraphic evidence* for volcanic-hosted massive sulphide deposits.

- A layer showing geological map units, classified as shown in Figure 5. Each map unit varies in importance as a potential host for volcanic-hosted massive sulphide deposits: felsic flows are the most important, other volcanic units are moderately important; nonvolcanic lithologies are least important.
- Layers representing proximity to the surface trace of the contact between felsic units with mafic volcanoclastic units or felsic volcanoclastic units, with proximal being most important and distal being least important. Proximity to other contacts between volcanic lithologies may also be predictive.

The next two layers also have a stratigraphic origin, but are related to the source of heat for driving the hydrothermal circulation. Here we call them the *heat evidence*.

- A layer representing the proximity to the surface trace of the contact between the tonalitic intrusions and the submarine volcanic units. Close proximity indicates a greater probability of an active hydrothermal circulation, and therefore greater favourability of a volcanic-hosted massive sulphide deposit, whereas far proximity suggests a lower favourability.
- A layer showing proximity to synvolcanic dykes, with close proximity being more favourable than far proximity. A layer showing proximity to vertical fractures would be useful, but synvolcanic fractures can generally not be recognized, except by inference from the stratigraphy.

The next layers are related to evidence of hydrothermal alteration, that in turn may indicate the activity and intensity of mineralization processes. Such evidence can be obtained from mapping of alteration patterns of various types, and here we have called the *alteration evidence*.

- A layer showing presence and proximity to zones of silicification, with higher favourability assigned to presence or close proximity than zones with no evidence of silicification.

- Other layers of showing presence and proximity to alteration zones of other types: chlorite-alumosilicate, epidote, and Fe-Mg metasomatism.

Other evidence comes from regional surficial geochemical surveys, and from geophysical surveys. The *geochemical evidence* is based on a combination of indicators from till and from lake sediments. In general, one would expect that sulphide deposits occurring at the surface would be detectable in lake sediment samples, and in till samples. Hydromorphic dispersion of metals in groundwater may also occur around buried deposits, with reprecipitation in lakes or streams depending on local Eh-pH conditions.

- Lake sediment geochemical layers for Zn, Pb, Cu, and other metallic trace elements.
- Till geochemical layers for a similar suite of elements.

Geophysical evidence is used widely by exploration companies for finding volcanic-hosted massive sulphide targets, but has not been emphasized in this study. Electromagnetic anomalies are particularly important for detecting buried sulphide bodies, due to their electrical, magnetic, and density properties. No consistent regional EM survey was available for the EXTECH study, although a number of site-specific EM studies were carried out, (Sinha and Palacky, 1996). The radiometric, magnetic, and VLF surveys flown by GSC proved of marginal value as direct evidence of volcanic-hosted massive sulphide mineralization, due to the relatively wide line-spacing compared with the size of volcanic-hosted massive sulphide targets. At the scale of this study, the regional geophysical data were valuable in some cases for geological mapping, interpretation of compositional trends in intrusive rocks, for recognizing gradients due to geophysical contrasts across contacts, and locally were used for recognizing alteration effects (Shives, 1996). Given closely spaced geophysical data (EM, magnetics, and gravity in particular), the exploration evidence would have played a more important role in the exploration model. As used here the *geophysical evidence* was derived from:

- Airborne magnetics layers (total field and vertical gradient). In general volcanic-hosted massive sulphide deposits are associated with magnetic anomalies, due to the presence of magnetic sulphide minerals.
- Gravity layers (free air, Bouguer, and vertical gradient). In general buried sulphide deposits are associated with gravity highs, due to the high density of buried sulphide deposits.
- VLF layers (total field and quadrature). Volcanic-hosted massive sulphide deposits are often associated with VLF anomalies, due to their electrical properties.

A number of factors for volcanic-hosted massive sulphide exploration that have been used elsewhere are not considered here. Litho-geochemical evidence was not used, because the available data were too sparse, and unsuitable for interpolation to quasi-continuous geochemical surfaces required for this style of integrated modelling. Information on the details of the volcanic cycles was not included, because even at the detailed scale of the field mapping, there was too much

uncertainty in tracing individual units over the map area. Satellite imagery was not used, because the spectral information was dominated by vegetation as opposed to lithological effects, and the structural information visible on satellite images failed to reveal lineaments that could be related to synvolcanic faults. A number of faults are clearly visible on the TM and radar images, confirmed by ground mapping, but they postdate the mineralization. Radiometric uranium, thorium, and potassium show interesting patterns, but the volcanic-hosted massive sulphide deposits do not appear to be directly related to radiometric signatures. The radiometric data yields information about the composition of rock units, but at the scale of the present study are not directly usable for predicting volcanic-hosted massive sulphide deposits.

BUILDING THE SPATIAL DATABASE

One of the objectives of this project was to build a digital database that would be useful, not only for this study, but also for future mineral potential or other geoscience-related studies. Therefore, a full range of data sets were included in the database, even though not all of them were applied to volcanic-hosted massive sulphide deposit prediction, as suggested by the exploration model. For example, airborne radar data, proven elsewhere for identifying structural features, such as lineaments, and Landsat data, which have been used for mapping applications, were included in the database, but were not applied directly for modelling volcanic-hosted massive sulphide deposit favourability.

The database comprises “raw” data, and a series of “derived” data sets, obtained by processing the raw data into a form suitable for mineral prediction. The processing and production of derived data sets is discussed in a following section. The raw data sets are summarized in Table 2 and discussed briefly below with respect to source, data structure, and data format.

Bedrock geology

Geological maps of the bedrock were available at two scales, 1:50 000 and 1:20 000. The 1:50 000 scale maps were manually digitized as topological vector data from a compilation of the sheets for NTS 63K/16 (Fedikow et al., 1988b) and NTS 63J/13 (Fedikow et al., 1993b) using the TYDIG digitizing package. These data were imported into the GIS (SPANS GIS was used throughout this study) and converted to a quadtree raster format with a digital spatial resolution (size of smallest quad or pixel) of approximately 10 m. The 1:20 000 scale map (Bailes and Galley, 1992a, b), generated as the result of mapping during the course of EXTECH, was also digitized manually and imported into the GIS (see Table A1, Appendix).

Alteration map

Six main types of alteration were mapped at 1:20 000 scale by Bailes and Galley (1992a, b). They identified the following alteration types: (1) silicification, (2) Fe/Fe-Mg

metasomatism, (3) pyritization, (4) epidote/hematite, (5) amphibole, and (6) alteration pipes, and mapped them as mutually exclusive zones (Fig. 6).

Lake sediment geochemistry

A lake sediment geochemical survey was conducted over the whole of NTS sheet 63K/16, and over the western two-thirds of 63J/13. A total of 346 samples were collected at a sample density of approximately 1 per 6 km². Samples were analyzed

for 42 elements using atomic absorption spectrometry (AAS) and instrumental neutron activation (INAA). The atomic absorption method determined values for Zn, Cu, Pb, Ni, Co, Ag, Mn, As, Mo, Fe, Hg, LOI, U, F, V, Cd, and Sb. Acceptable values from INAA included Au, As, Ba, Br, Co, Cr, Cs, Fe, Hf, Na, Rb, Sb, Sc, Ta, Th, U, W, La, Ce, N, Sm, Eu, Tb, Yb, and Lu. The data were input into the GIS as point attribute tables, with a record for each sample containing geographic co-ordinates followed by element concentrations (see Friske et al., 1995; Friske and McCurdy, 1996).

Table 2. Summary of digital data sets.

| Data type | Description |
|--|---|
| GEOLOGY | Geology from field mapping at scales of 1:50 000, 1:20 000, and 1:5000 |
| ALTERATION | Alteration was mapped based on mineral assemblages 1)qtz-ep-plag, 2)chl-bio-amp, 3)ep-hem for 1:20000 only |
| GEOCHEMISTRY -till -lake sediments -drainage basins -whole rock | A total of 346 lake sediment samples were analyzed for 32 different elements using AAS and INAA. Regional tills were collected and analysis of 240 samples, 32 elements done for <2 µm and <63 µm. Whole rock data has not been used for this study |
| RADIOMETRICS -U, Th, K -U/Th, U/K, K/Th | Collected by GSC Skyvan using 256 ch gamma ray spectrometer at 500 m line spacing east-west. GSC Open File 2300 |
| GRAVITY -Bouger -Free air -Vertical gradient | GSC Geophysical Data Centre, National Gravity Bank, 2 km resolution resampled to 200 m. |
| MAGNETICS - Total field - Vertical gradient - Horizontal gradient | GSC Geophysical Data Centre, Regional Coverage, 800 m spacing resampled to 200 m |
| VLF | Collected by GSC Skyvan using Hertz Totem VLF unit at 500 m east-west line spacing. GSC Open file 2300. |
| RADAR | Collected by CCRS, Data Acquisition Division, C band (HH), 15 m ground resolution. |
| LANDSAT TM - Bands 1- 7 | Landsat TM acquired from CCRS at 30 m resolution |
| DIGITAL ELEVATION | Digital Terrain Elevation Data from Defense Mapping Agency, 1:250 000 coverage |
| MINERAL DEPOSITS | Compiled from 1:50 000 maps (Fedikow et al. 1988a,b, 1993a,b) |
| Note: qtz-ep-plag; quartz-epidote-plagioclase chl-bio-amp; chlorite-biotite-amphibole ep-hem; epidote-hematite | |

Catchment basin map

A map of the lake catchment basins was prepared with the use of 1:50 000 scale topographic sheets and digital plots of the sample locations. Basins were constructed by manually tracing the drainage divides defined by the contour lines on the topographic map so that there was one basin for each sample. The basin outlines were manually digitized, input to the GIS as vectors in arc-node format and then rasterized. The catchment basin map was then linked to the geochemical attribute table allowing map construction for any variable in the table.

Till geochemistry

Both regional and detailed till sampling surveys were carried out in the study area (Gobert and Nielsen, 1991 and Kaszycki et al., 1996). C-horizon till and humus were sampled at 254 sites for the regional survey and C horizon, B horizon, and an organic rich fraction were sampled at 86 sites (around Chisel Lake, Chisel North, and Linda 2 deposits) for the detailed study. The <2 µm size fraction of all till samples has been analyzed by AAS for Ag, As, Cd, Co, Cr, Cu, Fe, Hg, Mn, Ni, Pb, and Zn. The <63 µm size fraction of all till samples has been analyzed by INAA using a standard "Au-plus 34 element" package. The heavy mineral fraction for all C-horizon till samples was extracted and analyzed for visible gold. These multivariate point data were input to the GIS as point attribute tables with geographic co-ordinates and geochemical variables.

Radiometric data

Airborne radiometric data were collected for the Snow Lake area (63J/13 and 63K/16) using the standard 256-channel gamma-ray spectrometer aboard the GSC Skyvan (Hetu, 1991). All data were sampled at one-second intervals on a survey grid flown with an east-west flight line direction and 500 m line spacing. Potassium was measured directly from gamma-ray photons emitted by ⁴⁰K, while uranium was monitored by measuring ²¹⁴Bi and thorium from measuring ²⁰⁸Tl. Airborne measurements were converted to ground concentrations using standard processing methods and published as a GSC Open File (Hetu, 1991).

The raster files were imported directly into the GIS as georeferenced rasters resampled to 100 m pixels. Radiometric data included eU (ppm), eTh (ppm), K (%), and the ratios eU/eTh, eU/K, and eTh/K.

VLF

Included as part of the airborne radiometric survey was a VLF electromagnetic survey using a Totem 1A VLF unit (Hetu, 1991). Georeferenced digital raster files of Total Field VLF and Quadrature (out-of-phase component) VLF, resampled to 100 m pixels, were imported directly into the GIS. The data are published in a GSC Open File (Hetu, 1991).

Gravity

Gravity data from the national gravity mapping database, with samples collected at an average station spacing of approximately 8 km (Goodacre et al., 1987), were obtained as a georeferenced digital raster file resampled to 2 km.

Magnetics

Airborne magnetic data from the national coverage (Geophysical Data Centre, Geological Survey of Canada), with flight lines spaced at 800 m, were obtained as raster files georeferenced and resampled to 200 m pixels.

Radar

Radar images were provided for sheets 63J/13 and 63K/16 by the Canadian Centre for Remote Sensing (CCRS) Data Acquisition Centre. The data were collected by an airborne, wide-swath, Synthetic Aperture Radar system by CCRS. Microwavelengths of 5.66 cm (Band C), transmitted and received horizontally polarized (HH) were used to generate the image. The swath width is 64 km, and angle of incidence from horizontal varies from 45° in the near range to 5° in the far range and has a 15 m ground resolution. The images were supplied as georeferenced raster files resampled to 30 m pixels.

Landsat data

Landsat V Thematic Mapper (TM) bands 1-7 were obtained through the CCRS Data Acquisition Centre. The data are from Path 34/Row 22, Quadrant 8, collected on June 8, 1988. The image was georeferenced by CCRS.

Digital elevation

Digital elevation data in raster format were obtained from the Surveys, Mapping and Remote Sensing Sector. The data were originally collected for the United States Defense Mapping Agency (Defense Mapping Agency, 1981) for military purposes. The information content is roughly equivalent to that of 1:250 000 scale contour maps.

Mineral deposits

Mineral deposit data for map sheets 63J/13 and 63K/16 were derived from Fedikow et al. (1988a, 1993) and were digitized as point attribute tables with information on location, name, mineral occurrence classification, size, and principal commodities.

DATA PROCESSING

Having compiled the spatial database, the next step was to process the data to extract evidence critical to the prediction of volcanic-hosted massive sulphide deposits, bearing in mind the guidelines imposed by the exploration model. Five principal approaches were used to process the data, prior to data combination: (1) map reclassification, to simplify the geological map to a small number of units suitable for modelling; (2) generation of proximity maps showing distance to linear features such as formation contacts; (3) multivariate statistical analysis of geochemical data to reduce the number of variables by principal components analysis; (4) spatial interpolation of geochemical point data by kriging; and (5) filtering operations on geophysical data. Spatial evidence is grouped according to five major factors, as explained in the exploration model, namely: stratigraphic factor, heat factor, alteration factor, geochemical factor, and geophysical factor.

Stratigraphic factor

Detailed mapping at the 1:20 000 scale has improved the understanding of the relationship between the stratigraphy and mineralization. Volcanic-hosted massive sulphide deposits are commonly affiliated with rhyolites that occur near the termination of a volcanic cycle, and sometimes in rhyolitic tuffs and breccias. Deposits can also occur in more mafic lavas, and associated with mafic and mixed mafic-felsic tuffs and breccias. They are most prominent in the stratigraphic hanging wall to such volcanic sequences. Proximity to volcanic breccias, particularly near contacts with felsic, and sometimes mafic flows, appears to be a favourable condition.

To facilitate modelling, without losing critical information, the units on the 1:20 000 scale geological map have been reduced to the following: (1) felsic extrusive rocks, (2) mafic extrusive rocks, (3) felsic volcanoclastic rocks, (4) mafic volcanoclastic rocks, (5) heterolithic volcanoclastic rocks, (6) subvolcanic tonalite intrusions (sills), (7) synvolcanic dykes of mixed composition that crosscut the subaqueous volcanic units (1-5), (8) Post-Amisk sediments, and (9) Post-Amisk intrusive rocks. This reclassification was achieved using a lookup table that links each original map unit to a new class. The simplified map is shown in Figure 5 and the lookup is defined in Table A1 (Appendix).

What has been lost in this process is the potentially valuable information about individual volcanic cycles, and the knowledge that certain stratigraphic horizons are better candidates for deposits than others. If it were possible to trace the detailed stratigraphy with confidence throughout the map, this would be valuable for defining the relative stratigraphic position of each point on the map (significant for mapping direction of heat flow), as well as pinpointing critical stratigraphic horizons. Unfortunately, the attempt to provide this level of detail was abandoned, due to the inability to provide systematic and complete coverage (A.H. Bailes, pers. comm., 1993).

Nevertheless, the key information about contacts between the classified volcanic units, that occur at several stratigraphic levels in the volcanic package can readily be extracted from the digital map. These lines were then buffered at intervals of 250 m, to generate the three proximity maps shown in Figure 7 (see colour section).

The stratigraphic evidence was thus broken down into four layers, the simplified lithological units on one, and the three others being proximity to felsic flows, proximity to felsic volcanoclastics, and proximity to mafic volcanoclastics.

Heat factor

A source of heat is necessary to convect fluids through the volcanic pile, setting up a hydrothermal circulation that draws seawater downwards through the volcanic strata, with upward flow along fractures to be discharged as hot springs on the seafloor. The fluids leach metals from the volcanic rocks, transporting them upwards to the sea where they precipitate to form deposits. Two pieces of mappable evidence can be used to predict favourable thermal conditions: (1) proximity to the large subvolcanic intrusions, and (2) proximity to synvolcanic dyke swarms that are often associated with the subvolcanic intrusions. Like the maps generated for the stratigraphic evidence, the heat evidence is derived directly from the geological map.

The tonalite polygons on the map were extracted and buffered, as shown in Figure 8a, and the synvolcanic intrusions were likewise transformed, as shown in Figure 8b (see colour section). Clearly this involves an assumption that the contacts are vertical, which is untrue, although in this area many of the lithological contacts are steeply dipping. The combination of these two proximity maps is used to model the probable variation in heat intensity.

Alteration factor

Recognizing alteration zones in the volcanic stratigraphy is critical to exploring for volcanic-hosted massive sulphide deposits. Alteration zones have been mapped by Bailes and Galley (1989, 1992a, b) and discussed in relation to other volcanic-hosted massive sulphide deposits in Galley (1993). The presence of Si-rich semiconformable alteration zones define a paleoseafloor on which there is a high potential for sulphide precipitation. Semiconformable zones of silicification and crosscutting zones of Fe-Mg metasomatized rocks are typical of deep, mature volcanic-hosted massive sulphide-producing hydrothermal cells. Proximity to zones of silicification or Fe-Mg metasomatism is considered a favourable indicator for the occurrence of volcanic-hosted massive sulphide deposits. Though not commonly identified on regional-scale maps, the presence of crosscutting alteration pipes, discharge conduits that are often Fe-Mg rich and Na-depleted, is also a most important indicator of volcanic-hosted massive sulphide deposits.

Based on the locations of patches of alteration, as seen in Figure 6, a series of proximity maps were generated showing both the presence and distance to the various kinds of

alteration, as shown in Figure 9 (see colour section). These various kinds of alterations are weighted and combined to create the alteration factor.

Geochemical factor

Lake sediment geochemistry

Out of the 346 lake sediment samples collected in the Snow Lake area, 79 fell within the Chisel Lake-Anderson Lake study region. A map of the lake catchment basins was prepared by plotting sample sites on 1:50 000 topographic map sheets and manually digitizing the catchment basins so that there was one catchment basin per sample. Each basin was treated as a spatial entity containing a geochemical sample, and was linked to the corresponding record of the geochemical attribute table. In this manner, the catchment basin map could be readily classified according to any field in the attribute table, to produce maps of the metallic trace elements.

Since each sample had been analyzed for 32 elements, principal component analysis (PCA) was applied to simplify the data by searching for meaningful multi-element associations, and thereby reduce the number of geochemical variables to a manageable number. Table 3 lists the varimax-rotated principal component loadings for the elements analyzed by INAA. The first four components explain over 80% of the total variance. Component scores were added as new fields to the attribute table, and component maps for PC-1 to PC-3 are shown in Figure 10 (see colour section).

The first component, PC-1, is a combination of Fe, V, F, Ni, Co, Pb, Sb, Mn, and Cu and explains 52.1% of the total variance. Significantly, the Cu-rich deposits (Anderson Lake, Stall Lake, and Rod 1, 2) are associated with elevated PC-1 scores, indicated by the red coloured basins in the northwest part of the study area. PC-2 is a combination of Zn and Cd and explains 14.7% of the total variance. The Zn-rich deposits (Chisel Lake, Lost Lake, and Ghost Lake) in the centre of the

Table 3. Principal component loadings for first four axes on elements analyzed for by INAA methods. The data were log transformed.

| Variables | PC - 1 | PC - 2 | PC - 3 | PC - 4 |
|-------------------|--------|--------|---------|--------|
| Fe | 0.945* | -0.064 | 0.109 | -0.042 |
| V | 0.918* | -0.122 | 0.001 | -0.043 |
| F | 0.907* | -0.160 | 0.182 | -0.069 |
| Ni | 0.904* | -0.160 | 0.041 | 0.003 |
| Co | 0.888* | 0.198 | 0.070 | -0.028 |
| Pb | 0.860* | 0.143 | 0.052 | 0.249 |
| Sb | 0.787* | 0.155 | -0.286 | 0.201 |
| Mn | 0.786* | -0.065 | 0.224 | -0.064 |
| Cu | 0.693* | 0.154 | -0.380 | 0.266 |
| Zn | 0.204 | 0.917* | -0.015 | 0.200 |
| Cd | -0.272 | 0.874* | -0.193 | 0.175 |
| Mo | -0.139 | 0.118 | -0.911* | 0.041 |
| Hg | 0.020 | 0.331 | -0.066 | 0.918* |
| Per cent of Total | 52.110 | 14.694 | 9.244 | 8.469 |

* Multi-element grouping for each principal component.

study area, are generally associated with higher PC-2 scores, although the Stall deposit is also associated with high PC-2 scores. Molybdenum depletion stands out on its own in PC-3 and shows an association with both the Zn-rich and Cu-rich volcanic-hosted massive sulphide deposits. The distinct behaviour of Cu and Zn is consistent with the notion of Cu- and Zn-rich horizons in the subaqueous volcanics, but the sample density is inadequate to resolve the spatial variation that one might expect given the details of the volcanic cycles in the stratigraphy.

Till geochemistry

Preliminary results indicate that both B-horizon and C-horizon samples produce similar geochemical trends. For this study the C-horizon analyses for the <63 μm were used to represent the till geochemical component. There were 80 till samples out of the total of 254 that fell within the study region.

Principal component analysis was tried on the till data, but produced no clearly interpretable results. We do not see the same associations in the till data as were observed in the lake sediment data. Therefore, the spatial distributions of Cu, Pb, and Zn were studied individually, because of their likely value as volcanic-hosted massive sulphide predictors. Kriging was used for spatial interpolation (see Fig. 11, colour section). A summary of the variogram model parameters used to generate the three maps are summarized in Table 4.

The variograms (Fig. 12) show that autocorrelation is present to a distance of 1 to 1.5 km. The Pb has the shortest range, and Cu the longest range, suggesting that Pb is less mobile than Cu and Zn. The kriging variance was used to screen out areas where the estimated element value is relatively uncertain.

Stall and Rod are associated with elevated levels of Cu and Zn. Lead and copper appear to be enriched in a large zone north of the Chisel Lake-Lost Lake-Ghost Lake deposits. The till patterns are quite different from the lake sediment patterns, and again, the till samples are too widely spaced to resolve the spatial variability that one would expect from the stratigraphy.

In summary, six maps were derived from the geochemical data to be used as volcanic-hosted massive sulphide predictors: lake sediment PC-1 to PC-3 (dominated by Zn, Cu, and Mo depletion, respectively) and till Zn, Cu, and Pb. The combination of these six maps is used as the *geochemical factor*.

Table 4. Variogram model parameters used for kriging till geochemistry.

| Element | Model Type | Nugget Eff. | Sill | Range (m) | Direction |
|---------|------------|-------------|------|-----------|-----------|
| ln Cu | Spherical | 0.025 | 0.3 | 1500 | 0.0 |
| ln Pb | Spherical | 0.45 | 0.4 | 1000 | 0.0 |
| ln Zn | Gaussian | 0.01 | 0.11 | 1300 | 0.45 |

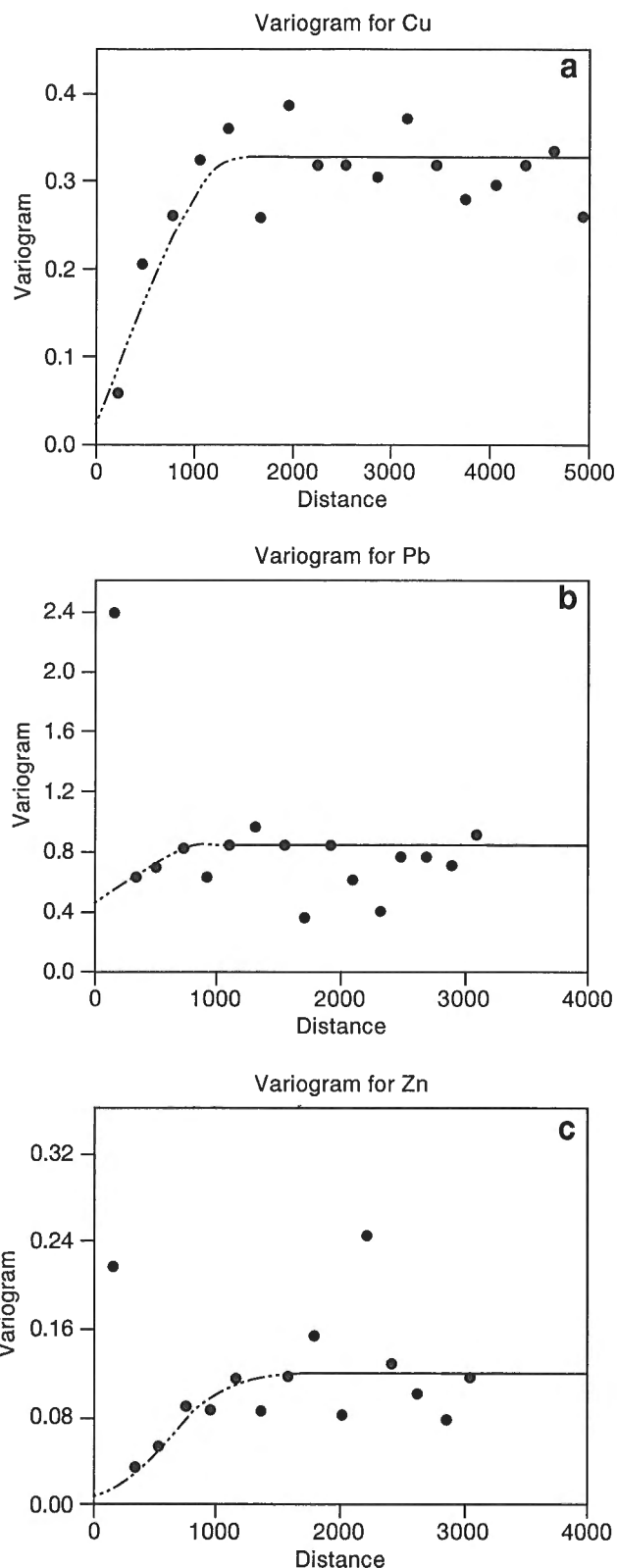


Figure 12. Experimental variograms for a). ln Cu, b). ln Pb, and c). ln Zn. Fitted model parameters are shown in Table 4.

Geophysical factor

In general, volcanic-hosted massive sulphide deposit areas are characterized by relatively high conductivity, moderate magnetic response, and moderate to high gravitational response. Radiometric data is useful for eliminating areas of younger postmineralization lithologies or for identifying low K intrusions that are potential subvolcanic heat sources.

Conductivity

Good conductivity is typically characteristic of Cu-Zn volcanic-hosted massive sulphide deposits (Rod 1, 2, Stall Lake, Anderson Lake). Total field VLF is a measure of conductivity but can respond to changes in elevation, permeability, and other factors besides conductivity. The quadrature component tends to be less affected by other factors and gives a more reliable indication of conductivity. Significant VLF conductors can be identified where elevated total field and quadrature signals coincide. Because raw quadrature data tends to show conductors where a "cross-over" occurs (Fig. 13) it is useful to filter the raw quadrature data to enhance zones of conductivity.

The following expression was used to filter the quadrature data:

$$V_i = (V_{i+1} + V_{i+2}) - (V_{i-1} + V_{i-2})$$

This emphasizes points of inflection, as shown in Figure 13. The processed quadrature and total field are shown in Figure 14a and b ([see colour section](#)).

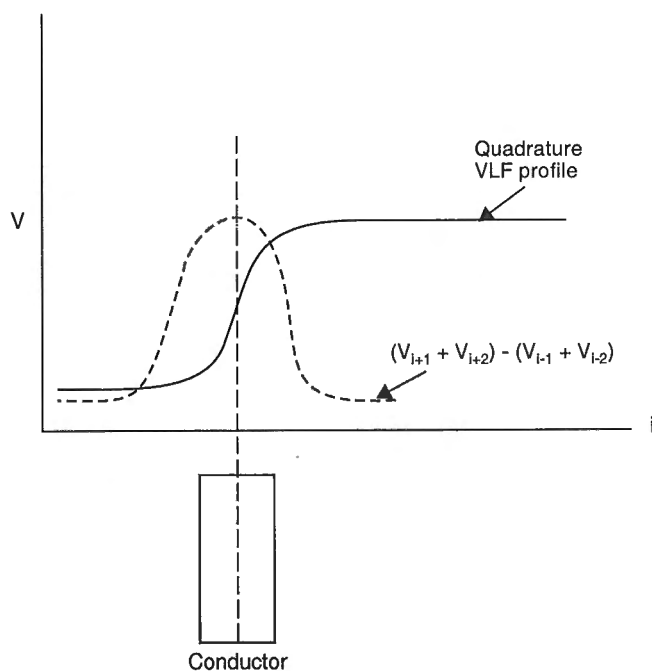


Figure 13. Method for processing quadrature VLF data to isolate crossover points.

Magnetic signature

Volcanic-hosted massive sulphide deposits are expected to have a relatively strong magnetic signature due to the presence of magnetite (e.g. Sinha and Palacky, 1996). However, there are several formations in the study area that show a relatively strong magnetic response, yet are unrelated to the volcanic-hosted massive sulphide horizons. For example, some of the intrusive bodies, such as the Chisel Lake pluton (post-Amisk) shows as a magnetic high on the map. Anomalies obtained by a simple threshold of the total field data are clearly inadequate to identify zones related to mineralization, but a more useful map is produced by a combination with vertical gradient data. Figure 14c shows that there are broad regional trends in the total field, and local features on the vertical gradient (Figure 14d). The most reliable signatures are where TF and VG highs coincide.

Gravity

Gravity signatures can be an effective tool for identifying volcanic-hosted massive sulphide targets, but because of the wide spacing between sample stations and relatively small size of the deposits, gravity data were useful only for broad-scale lithological information. For example, felsic intrusions have a low gravitational response (relatively low-density minerals and large vertical extent) and are not potential volcanic-hosted massive sulphide targets, so Bouguer anomaly lows are likely to be areas of low volcanic-hosted massive sulphide potential. In the present study we found that the calculated vertical gradient of gravity ([see Fig. 14e](#)) was moderately useful as evidence.

Radiometrics

Volcanic-hosted massive sulphide deposits tend to be associated with more evolved igneous and volcanics suites, which in turn tend to have relatively low radiometric signatures. A map of the airborne uranium survey is shown in Figure 15 ([see colour section](#)). It is noted that elevated radiometric signatures are associated primarily with the Ham Lake pluton in the northwest, the Wekusko Lake pluton in the southeast and the Missi sediments in the northeast. These are all younger postvolcanic units and have no associations with volcanic-hosted massive sulphide deposits. The potassium and thorium maps show similar patterns.

Radiometric surveys can be effective for helping to map lithological units on a regional scale, as indicated by the broad correlations between radiometric patterns and the geology, seen in Figure 15. However, in the present study, detailed field mapping provided more reliable geological evidence than broad-scale airborne radiometric data, so the radiometric data were not used as a source of evidence for volcanic-hosted massive sulphide mineralization. In the absence of detailed geological mapping, however, radiometric data could have been used in conjunction with gravity and magnetic data as a proxy for the geological map.

In summary, the mapped geophysical factor was composed of a combination of five evidence maps: total field VLF, processed quadrature VLF, total field magnetics, vertical gradient magnetics, and vertical gradient gravity.

INTEGRATION MODELLING

The last step in the process consists of combining, or integrating, the various map layers of evidence to estimate mineral potential. The combination process involves weighting and 'fusing' of evidence and can be carried out in a number of different ways. Fuzzy logic, an expert system type approach, was employed as one of the mechanisms for knowledge representation and to integrate the evidence from input maps, via intermediate factor maps as described below.

Fuzzy logic

The fuzzy logic approach is appealing, because it is straightforward to understand and implement. It can be used with data from any measurement scale and the weighting of evidence is controlled entirely by the deposit expert. This is in contrast to the data-driven approaches such as weights of evidence or logistic regression that use the locations of known deposits to estimate weights or coefficients (see below).

The idea is to consider the spatial objects on a map as members of a set. For example, the spatial objects could be areas on a map and the set defined as "areas containing a volcanic-hosted massive sulphide deposit". In classical set theory, an object is a member of a set if it has a membership value of 1, or not a member if it has a membership value of 0. In fuzzy set theory, membership can take on any value between 0 and 1 reflecting the degree of certainty of membership. Fuzzy set theory employs the idea of a membership function, that expresses the degree of membership with respect to some attribute of interest. With maps, generally the attribute of interest is measured over discrete intervals (whatever the measurement scale), and the membership function can be expressed as a table relating map classes to membership values. Fuzzy membership can also be thought of in terms of support for a proposition or hypothesis. In this study, the goal is to identify ground favourable for volcanic-hosted massive sulphide deposits. The maps to be used as evidence to support or refute the proposition are all expressed on a common information metric – namely fuzzy membership on the [0, 1] scale.

Membership functions are established for each of the map layers that are to be combined. Thus we might have membership functions for aeromagnetic data, for lithological units, for geochemical data, and so on. Maps are combined by using fuzzy operators on the membership functions. All of the Boolean operators have fuzzy counterparts, and many others have been proposed. The final result is an output map showing the combined membership function, after applying a classification to create discrete classes for display.

Table 5. Hypothetical example showing membership values expressed as table.

| Aeromagnetic intensity, x | Class number | Membership ($\mu_A(x)$) |
|---------------------------|--------------|---------------------------|
| >3000 | 1 | 0.35 |
| 500 - 3000 | 2 | 0.20 |
| <500 | 3 | 0.25 |

A fuzzy set can be defined as follows. If $X = \{x\}$ denotes a "space" of objects, then the fuzzy set A in X is the set of ordered pairs

$$A = \{x, \mu(x)\} \text{ where } x \in X$$

and $\mu_A(x)$ is the membership function. Suppose that A is the set of pixels containing volcanic-hosted massive sulphide deposits, and $X = \{x\}$ is a "space" of objects reflecting aeromagnetic intensity values, then the membership function for A with respect to aeromagnetic intensity might be represented as shown in Table 5.

This implies that given the aeromagnetic data alone, the possibility that a particular location on the map contains a volcanic-hosted massive sulphide deposit is given by the set of values from the membership function. Although membership values lie in the range [0, 1], the membership function is not the same as a probability density function. For example, the aeromagnetic intensity >3000 implies that the possibility of a volcanic-hosted massive sulphide deposit at that location is 0.35. However, the possibility that a map polygon is favourable for volcanic-hosted massive sulphide deposits is not a probability, so one minus the possibility does not imply improbability, nor is there an implication of probability of a deposit per unit area, as in probabilistic approaches such as weights of evidence. The membership scale is therefore a ranking and magnitude of membership and is treated on a relative basis (An et al., 1991; Bonham-Carter, 1994a). The word favourability or potential is thus used instead of the more formal term, probability.

Choosing membership function values is a subjective and often difficult task. Nevertheless it does permit an unambiguous and quantitative expression of expert judgement.

Fuzzy operators are used to combine fuzzy sets. For example, if a particular location on the map has a possibility of being a volcanic-hosted massive sulphide deposit of 0.35 from magnetic evidence and 0.05 from ground EM, fuzzy combination of these two numbers could take on a variety of values in the range [0,1] depending on the operator. Fuzzy operators can be applied to any number of input maps or layers of evidence.

The different fuzzy operators and the effect that they have on combining membership functions are summarized in Figure 16, and further explained in An et al. (1991), Bonham-Carter (1994a), and Wright (1996).

For this study the gamma operator and the fuzzy "OR" and the fuzzy "AND" were employed. On output, the fuzzy OR results in taking the maximum value of the 2 or more input

membership values, whereas the fuzzy AND results in the minimum of the input values. Thus the OR is an optimistic operator, and the AND is a conservative operator. In some situations, it is desirable that the combination of two favourable pieces of evidence is more favourable than either one taken individually, an “increasive” effect. The fuzzy gamma operator allows the degree of AND and OR to be parameterized, even permitting an “increasive” effect for large values of gamma, as illustrated in Figure 16. The advantage of the gamma operator is that when evidence is conflicting (one or more data sets indicating strong possibilities and others very weak possibilities), the resulting aggregation can produce possibilities somewhere between the extremes, with the degree of compensation controlled by the magnitude of the gamma parameter. This variability in choosing the type of fuzzy operator allows the modeller to mimic the decision-making processes typical of an exploration geologist.

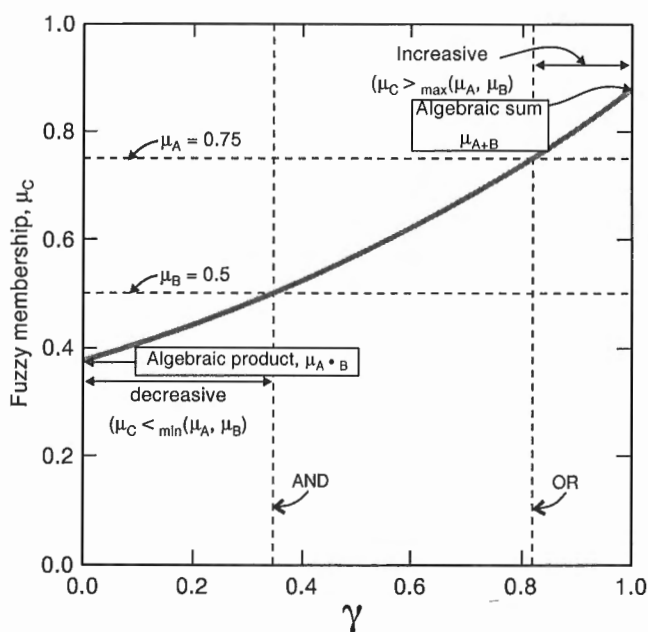
Weighting the evidence

The original data were processed to generate 23 layers of evidence that are relevant to the exploration model. These evidence maps are summarized in Table 6, and grouped into the five factors discussed for the model. A membership function was assigned to each map so that each class on the

map has a value between 0 and 1. The values are subjective and based on “expert” opinion. In practice, membership functions are represented as fields in the GIS map attribute tables. These tables can be edited, allowing the modeller to experiment with different assumptions. Membership functions are summarized in Table A2 (Appendix), along with the belief functions used for the Dempster-Shafer method.

Table 6. Summary of maps used as evidence.

| Factor | Evidence map |
|---------------|--|
| Stratigraphic | Bedrock geology Proximity to felsic volcanoclastics Proximity to mafic volcanoclastics Proximity to felsic flows (rhyolites) |
| Heat | Proximity to subvolcanic intrusions (tonalite sills) Proximity to synvolcanic dykes |
| Geochemical | Lake sediment chemistry - Principal Component 1 Lake sediment chemistry - Principal Component 2 Lake sediment chemistry - Principal Component 3 Till chemistry - Krige In Cu (C horizon) Till chemistry - Krige In Pb (C horizon) Till chemistry - Krige In Zn (C horizon) |
| Alteration | Presence and proximity to silica alteration Presence and proximity to Fe-Mg metasomatism Presence and proximity to alteration pipes Presence and proximity to amphibole alteration Presence and proximity to epidote-hematite alteration Presence and proximity to pyritic alteration |
| Geophysical | Total field VLF (measured) Processed quadrature VLF (calculated) Total field magnetics (measured) Vertical gradient magnetics (calculated) Vertical gradient gravity (calculated) |
| Total | 23 evidence maps |



fuzzy AND

$$\mu_{\text{COMB}} = \min(\mu_A, \mu_B, \mu_C \dots)$$

fuzzy OR

$$\mu_{\text{COMB}} = \max(\mu_A, \mu_B, \mu_C \dots)$$

fuzzy GAMMA OPERATOR

$$\mu_{\text{COMB}} = (\text{FUZZY ALGEBRAIC SUM})^\gamma * (\text{FUZZY ALGEBRAIC PRODUCT})^{1-\gamma}$$

fuzzy ALGEBRAIC PRODUCT

$$\mu_{\text{COMB}} = \prod_{i=1}^n \mu_i$$

fuzzy ALGEBRAIC SUM

$$\mu_{\text{COMB}} = 1 - \prod_{i=1}^n (1 - \mu_i)$$

Table 7. Membership function for proximity to synvolcanic dykes map, shown as map attribute table. The actual membership values are in the second field of the records following “DATA” line.

| | |
|---------|---|
| ID | zdykcon |
| TITLE | Fuzzy memberships for dyke contacts |
| MAPID | dykebuf1 |
| WINDOW | nc 5808 7704 142208 12080 |
| TABTYPE | 1 |
| NRECORD | 10 |
| 1 | 4 5.00 Class Map class value |
| 2 | 0 6.20 Zheat Fuzzy membership for distance from dykes |
| 3 | 35 15.0 Leg Legend on map |
| DATA | |
| 1 | 0.80 'On Dyke' |
| 2 | 0.95 '0.00 - 0.25 km' |
| 3 | 0.75 '0.25 - 0.50 km' |
| 4 | 0.65 '0.50 - 0.75 km' |
| 5 | 0.55 '0.75 - 1.00 km' |
| 6 | 0.50 '1.00 - 1.25 km' |
| 7 | 0.45 '1.25 - 1.50 km' |
| 8 | 0.40 '1.50 - 1.75 km' |
| 9 | 0.35 '1.75 - 2.00 km' |
| 10 | 0.10 '> 2.00 km' |

Figure 16. Fuzzy operators and their effects as combination operators. Using different operators can allow evidence maps to be combined in a way that reflects expert decisions.

An example of the actual attribute table associated with the proximity to synvolcanic dykes is shown in Table 7. The table consists of 10 header records describing the file to the GIS system followed by 10 data records, one for each class on the map. The table has three attribute fields. The first is the keyfield, linking the record to the map class, the second is the membership function, and the third is a descriptive text field. Class 1 on the map – regions actually where a dyke is present – have been assigned a fuzzy membership of 0.8, reflecting the importance of such regions with respect to the heat conditions favourable for volcanic-hosted massive sulphide deposits. The region just off a dyke, but within 250 m of the contact are assigned an even more favourable value, 0.95. Then with increasing distance from the contact, the membership value decreases, and beyond 2 km the value is set to 0.1. It should be noted that the input maps are assigned memberships with respect to a series of intermediate propositions. For example, the membership function for proximity to synvolcanic dykes is with respect to the proposition “area with heat factor favourable for volcanic-hosted massive sulphide”. The heat factor then becomes evidence for the proposition

“area favourable for volcanic-hosted massive sulphide deposits”. In this way the evidence is structured hierarchically, and can be represented by an inference network.

Map classes where the variable in question is ‘unknown’ were assigned a fuzzy membership value corresponding to the 50th percentile, to minimize the bias introduced in areas of missing data; see for example the membership functions for Zn, Cu, and Pb in till in Table A2 (Appendix).

Integration – intermediate maps

After each evidence layer has been weighted by assigning membership functions, the input maps are combined in stages. This not only solves the problem of being limited to “stacking” a maximum of 15 maps in a single pass (in the SPANS GIS used for the study), but also emphasizes the spatial patterns in the intermediate maps, facilitating the interpretation of results. The inference network that summarizes the combination process is shown in Figure 17.

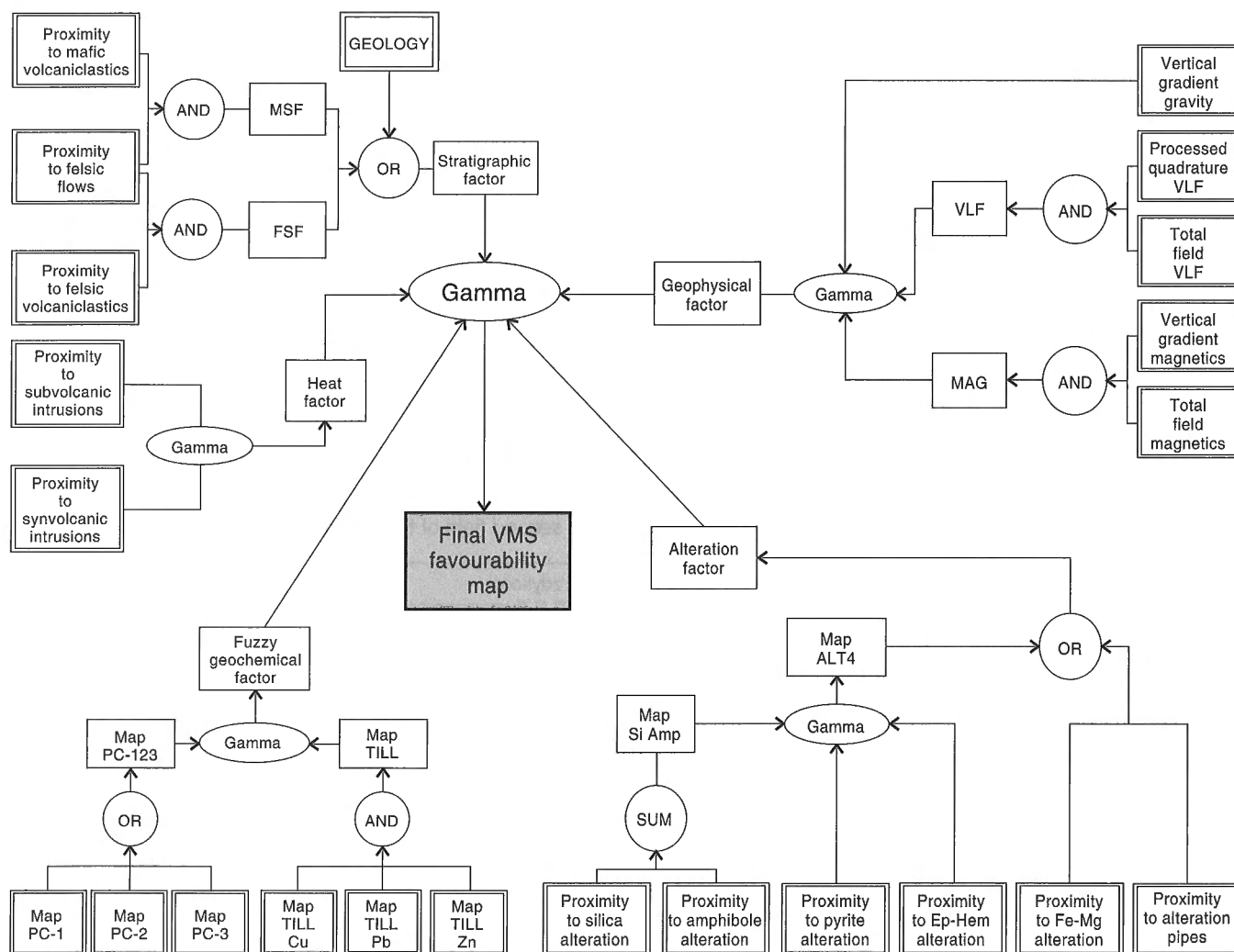


Figure 17. Inference net summarizing how 23 evidence from maps, described in Table 6, were combined to arrive at final favourability map using various fuzzy operators; Ep-hem = epidote-hematite.

Geochemical factor

Figure 18 shows the portion of the inference net defining how the geochemical evidence was combined to create the fuzzy geochemical factor map, which expresses the spatial variation in overall geochemical evidence favourable for volcanic-hosted massive sulphide deposits. Since PC-1 (lake sediments) was explained as being related to Cu-rich deposits, PC-2 related to Zn-rich deposits, and PC-3 as being related to both types, it was unnecessary for all three components to be coincident for favourable volcanic-hosted massive sulphide conditions. Following this reasoning the three PC maps were combined using a fuzzy OR, resulting in a new combined PC map, consisting of the maximum fuzzy membership value from PC-1, PC-2, or PC-3. Thus if any one of the PC maps is favourable, the result is also favourable.

Areas with anomalous concentrations of Cu and Pb and Zn in the till were considered to be the best till geochemical targets. To represent this situation, the till geochemical maps were combined using a fuzzy AND. An intermediate map, labelled TILL in Figure 18, was created that took the minimum membership value of the three maps at each spatial location. On this map, elevated membership function values occur only where all three elements are anomalous. It is noted that this decision rule could easily be modified to a fuzzy OR. Fuzzy AND is much more restrictive and conservative, fuzzy OR is more generous and optimistic.

Finally, if both favourable lake sediment chemistry and favourable till chemistry are coincident, these areas would be considered more favourable than if only one of these two conditions existed. This strategy was executed by combining the intermediate maps PC-123 and TILL using the gamma operator, with $\gamma = 0.95$. The resulting fuzzy geochemical factor is shown in Figure 19 (see colour section).

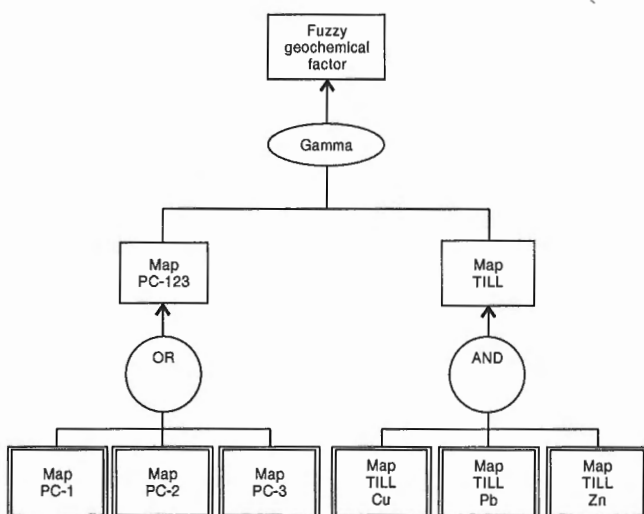


Figure 18. A portion of inference shown in Figure 17 detailing how geochemical evidence was combined.

Stratigraphic factor

The inference net related to the stratigraphy is shown in Figure 20. To model areas that are close to both felsic flows and volcaniclastic units a fuzzy AND was used. This results in intermediate map, labelled FSF in the figure, which assigns a high membership value to areas that are close to both felsic flows and felsic volcaniclastics. MSF in Figure 20 is a map showing favourable proximity to both felsic flows and mafic volcaniclastics. Maps MSF and FSF are then combined with GEOL (fuzzy memberships for presence of individual lithologies) using a fuzzy OR. The stratigraphic factor map (Fig. 21, see colour section), is thus assigned the highest membership values to areas close to the contact between volcaniclastics and felsic flows, followed by areas close to, or within, a felsic flow.

Heat factor

The heat factor map is really an extension of the stratigraphic factor, but focuses on the geological constraints on the source of heat driving the hydrothermal system. The maps of proximity to subvolcanic intrusions and synvolcanic dykes were combined using the gamma operator (Fig. 22; and Fig. 23, see colour section). Because a high value of the gamma parameter was used ($\gamma = 0.95$), areas that are close to both subvolcanic intrusions and synvolcanic dykes can have combined membership values larger than either one taken individually, an increase effect.

Alteration factor

The six evidence maps showing proximity to the various types of alteration are combined as shown by the inference net in Figure 24. The fuzzy SUM operator was used to combine the Si and amphibole evidence maps to ensure that areas in close

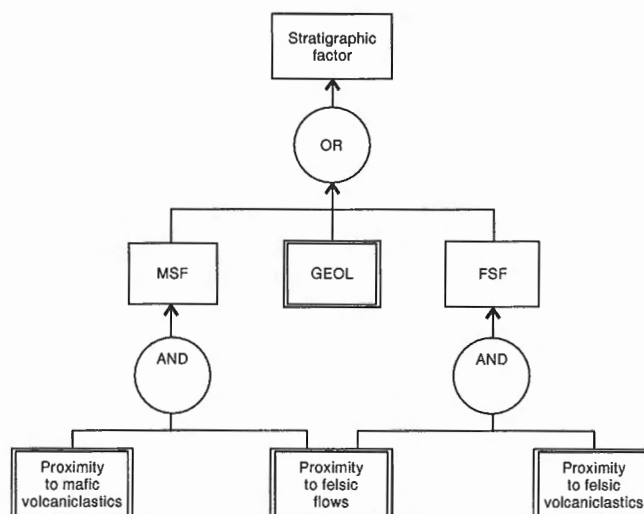


Figure 20. Inference net for stratigraphic factor combines information so that highest membership values are assigned to areas close to contact between volcaniclastics and felsic flows, followed by areas close to, or within, a felsic flow.

proximity to both types of alteration, had a resulting membership value that was higher than either of the two input maps. The resulting map (SIAMP) was then combined with the pyrite and epidote-hematite evidence map using the gamma operator to produce an intermediate map that has high membership values where there are coincident zones of alteration (ALT4). Because the Fe-Mg metasomatism map and the Alteration Pipe map are important evidence independent of the others, a fuzzy OR was used to combine these maps with ALT4 to retain the high membership values assigned to them, as shown in the resulting alteration factor map in Figure 25 (see colour section).

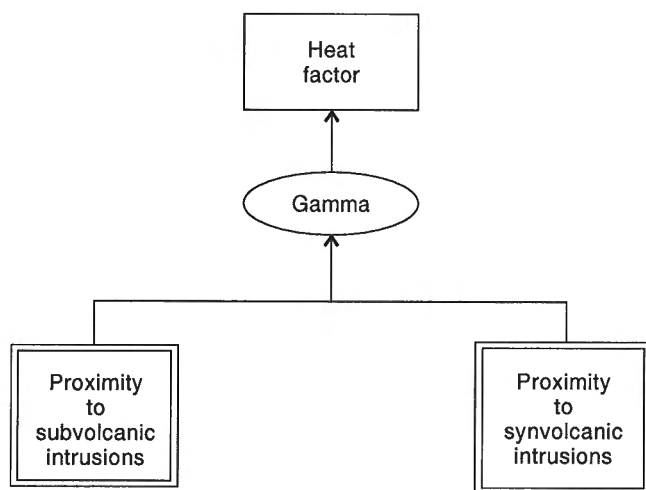


Figure 22. Inference net for combining heat source evidence. A high gamma parameter ($\gamma = 0.95$) forces combined membership value to be larger than membership value for either of two evidence maps taken individually.

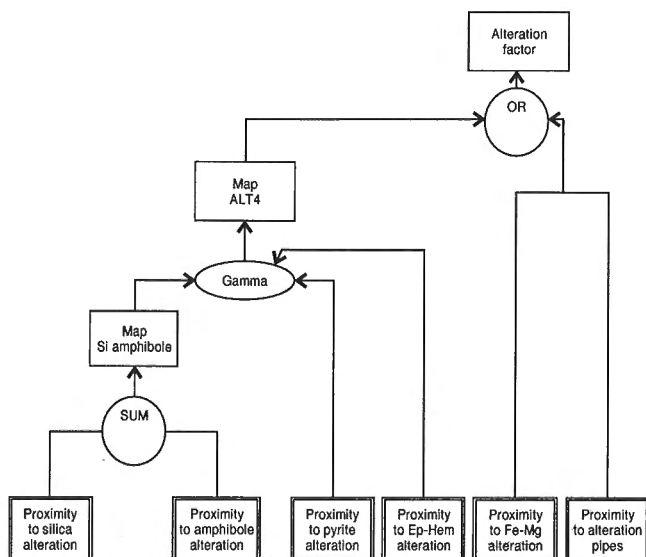


Figure 24. Six evidence maps showing proximity to various types of alteration are combined as indicated by inference net; Ep-hem = epidote-hematite.

Geophysics factor

Geophysical evidence was combined using the scheme in Figure 26. The total field and quadrature VLF maps were combined using a fuzzy AND resulting in the map 'VLF', with elevated memberships only where both total field and quadrature anomalies occur together. Similarly the total field magnetic response and vertical gradient magnetic response were combined using a fuzzy AND. Since the highest membership values were assigned to the moderate magnetic responses in the two magnetic evidence maps, the resulting intermediate map (MAG) shows the highest membership values where the intermediate magnetic responses are coincident.

Finally VLF, MAG, and the vertical gradient of gravity were combined using the gamma operator (see Fig. 27, colour section). On this map, zones with high conductivity, moderate magnetic response and a regionally high gravity response are the most favourable.

Final favourability map for volcanic-hosted massive sulphide

The five intermediate factor maps – heat, alteration, stratigraphic, geophysical, and geochemical factors – were combined to generate the final favourability map, as shown in Figures 28 and 29 (see colour section). It is noted that an additional “weighting factor” in the range [0,1] was used as a multiplier to modify the membership values of each intermediate map and provide a flexible method of changing the influence of each of the component factors. This is an overall weighting to express the expert’s opinion as to the relative importance of each factor, that enables the modeller to make changes interactively with the GIS modelling language. To a certain degree, these weights also reflect the confidence the expert has in the data. For example, the low weighting factor assigned to the geochemical factor reflects the fact that there is incomplete coverage in the till survey and that the lake

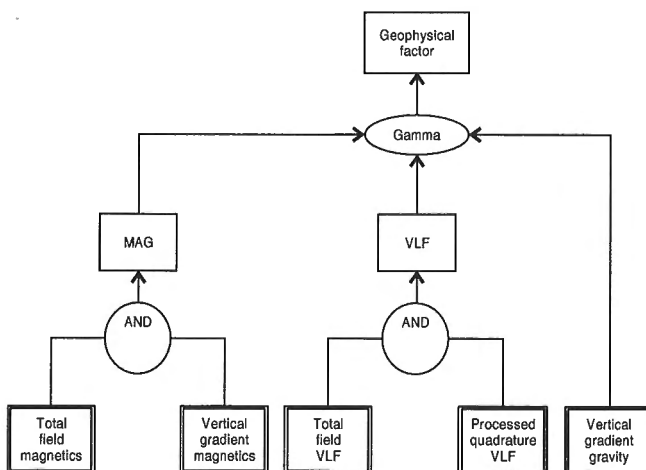


Figure 26. Inference net for combining five geophysical evidence maps to produce intermediate geophysical factor map.

sediment samples were collected at a low density. Similarly the relatively low weighting factor for the geophysical data reflects that the data was collected at regional rather than local scales. The stratigraphic factor has a relatively high weighting factor reflecting the detail and information content expressed in the 1:20 000 bedrock geology map.

The final favourability map is shown in Figure 29. The legend shows the membership function values for the areas identified by the corresponding colour. The breakpoints were determined by dividing the membership function into 20 quantile classes.

Of the 15 volcanic-hosted massive sulphide deposits known before the modelling, seven deposits have membership values in the top 20th percentile and all of the deposits are within the top 30th percentile with the exception of the North Chisel deposit (Table 8). The new discovery at Photo Lake falls in the 80th percentile class (top 20th percentile).

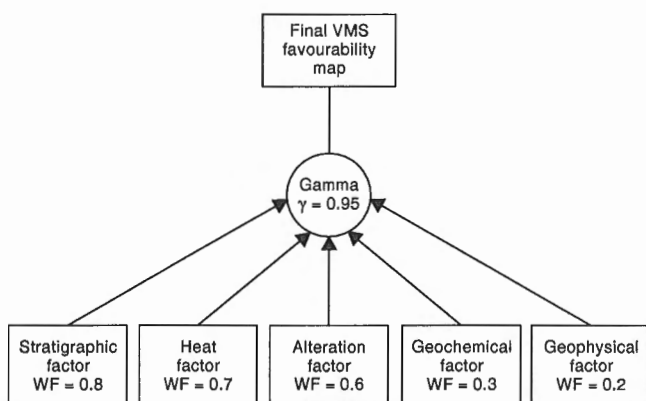


Figure 28. Inference net showing how five “factor maps” were combined to produce final favourability map for volcanic-hosted massive sulphide deposits using fuzzy logic method.

Within the GIS there is the ability to make interactive spatial queries of the data and results. This tool is useful to help understand the results at particular locations. The results of querying the membership values of the five factor maps for each of the 16 volcanic-hosted massive sulphide deposit locations is summarized in Table 8. The low membership value on the final favourability map associated with the North Chisel deposit can be explained due to low membership values for the stratigraphic factor and alteration factor at that location.

Weights of evidence approach

The fuzzy logic method described above is considered an expert approach as the predictor maps were weighted and combined using the subjective opinion of an expert. The weights of evidence method is data-driven in the sense that statistical calculations are used to estimate the weights, based on the measured associations between locations of known deposits and predictor map patterns. A preliminary study employing the weights of evidence method, but using a partial data set for the western half of this study area, is found in Reddy et al. (1992), and Bonham-Carter et al. (1994).

A detailed discussion of weights of evidence modelling for integrating geoscience data sets to predict mineral potential may be found in Bonham-Carter et al. (1988, 1989), Agterberg (1989), Bonham-Carter and Agterberg (1990), and Bonham-Carter (1994a, b). The following is a brief summary from these publications.

Each mineral deposit or occurrence within the study area is assigned to a small unit cell of area $u \text{ km}^2$. The total number of unit cells containing a deposit is represented by $N(D)$, where $N()$ is the count of unit cells and D refers to the presence of deposits. Cells either contain a deposit or not; there is no provision for modelling deposit size. The total area of the region being studied is $t \text{ km}^2$, or $N(T) = t/u$ unit cells. The average density of known deposits in the area is then $N(D)/N(T)$. This ratio is taken as the prior probability of a cell

Table 8. Fuzzy membership values estimated at locations of volcanic-hosted massive sulphide deposits. Values have been calculated as percentiles so that evidence can be compared directly.

| Deposit | Heat factor | Stratigraphic factor | Geochemical factor | Alteration factor | Geophysical factor | Overall |
|---------------|-------------|----------------------|--------------------|-------------------|--------------------|---------|
| Morgan Lake | 55 | 30 | No data | 25 | 85 | 60 |
| Bomber zone | 75 | 75 | 40 | 85 | 80 | 90 |
| Rain Drop | 45 | 75 | 60 | 90 | 65 | 80 |
| Pot Lake | 50 | 75 | 70 | 85 | 85 | 75 |
| North Chisel | 30 | 40 | 85 | 25 | 70 | 45 |
| Chisel Lake | 40 | 95 | 85 | 95 | 80 | 90 |
| Lost Lake | 60 | 95 | 90 | 90 | 80 | 90 |
| Ghost Lake | 30 | 95 | No data | 85 | 85 | 85 |
| Joannie | 15 | 25 | 70 | 90 | 5 | 10 |
| Anderson Lake | 75 | 75 | 30 | 90 | 80 | 90 |
| Stall Lake | 70 | 75 | 90 | 95 | 90 | 90 |
| Rod | 75 | 75 | 90 | 65 | 80 | 90 |
| Ram zone | 15 | 15 | 85 | 95 | 5 | 10 |
| Linda 1 | 70 | 75 | 80 | 85 | 85 | 90 |
| Linda 2 | 30 | 75 | 80 | 95 | 25 | 90 |
| Photo Lake | 45 | 85 | 65 | 85 | 90 | 80 |

containing a deposit, $P(D)$. The goal is to estimate the posterior probability, given the presence or absence evidence, which may be larger or smaller than the prior, depending on the favourability of the evidence.

The predictor (evidence) maps are commonly reduced to binary form in order to obtain robust estimates of the weights. Each binary predictor map has an area that is more favourable for deposits (pattern present) and an area less favourable for deposits (pattern absent). For the j -th binary predictor map, B_j , the area with the pattern present is denoted as $N(B_j)$ unit cells, and $N(\bar{B}_j) = N(T) - N(B_j)$ is the area with the pattern absent (except in the case of missing data).

If the prior probability that a unit cell contains a deposit is assumed to be constant over the whole study region, then from Bayes' Rule the posterior probability that a cell contains a deposit, given the presence of the j -th binary pattern is:

$$P(D|B_j) = \frac{P(B_j|D)P(D)}{P(B_j|D)P(D) + P(B_j|\bar{D})P(\bar{D})} \quad (1)$$

where the bar over the D refers to absence of deposits. Similarly, the posterior probability that a cell contains a deposit given the absence of pattern B_j is

$$P(D|\bar{B}_j) = \frac{P(\bar{B}_j|D)P(D)}{P(\bar{B}_j|D)P(D) + P(\bar{B}_j|\bar{D})P(\bar{D})} \quad (2)$$

Recasting these equations in loglinear form results in the following expressions for the posterior logit (posterior log odds) of a cell containing a deposit, given the presence/absence of the j -th binary pattern:

$$\text{posterior logit}(D|B_j) = \text{prior logit}(D) + W_j^+ \quad (3)$$

and

$$\text{posterior logit}(D|\bar{B}_j) = \text{prior logit}(D) + W_j^- \quad (4)$$

where the positive weight of evidence is defined as

$$W_j^+ = \ln \frac{P(B_j|D)}{P(B_j|\bar{D})} \quad (5)$$

and the negative weight of evidence as

$$W_j^- = \ln \frac{P(\bar{B}_j|D)}{P(\bar{B}_j|\bar{D})} \quad (6)$$

The contrast, C , for the j -th map is an overall measure of spatial association between the deposits and the binary pattern:

$$C_j = |W_j^+ - W_j^-| \quad (7)$$

It is assumed that there are only two mutually exclusive hypotheses, either that a cell contains a deposit, or does not contain a deposit, so that

$$P(D|B_j) + P(\bar{D}|B_j) = 1 \quad (8)$$

If n binary predictor maps are used as evidence, a general expression for the posterior logit can be written as

$$\text{posterior logit}(D|B_1^{k(1)} \cap B_2^{k(2)} \dots \cap B_N^{k(n)}) = \text{prior logit}(D) + \sum_{j=1}^n W_j^{k(j)} \quad (9)$$

where the superscript $k(j)$ is $+$ for presence or $-$ for absence of the j -th binary pattern. The logits are usually transformed to probability for mapping, but they can also be left in logit units because the transformation does not affect the rank order of values.

Equation (9) assumes that the binary predictor maps are conditionally independent (CI) with respect to the deposits. If the assumption is violated, the posterior probability will be either over- or under-estimated. In practice this assumption is commonly violated to some degree, particularly if a large number of maps is being combined. The CI value can be checked using statistical tests to show how serious the violation is and to identify which maps are the worst culprits.

The simplest check is make an overall test on the final favourability map, to determine whether the total number of predicted deposits is equal to the total observed number, as should be the situation under CI (Bonham-Carter, 1994a). The predicted number of deposits is determined by adding together the product of the area in unit cells times the posterior probability, over all the polygons on the map. Assuming that the prior was calculated as the average density of known deposits, then the predicted total number of deposits should equal the observed number of deposits. In our experience, the predicted number is always larger, indicating that, on average, the posterior probabilities are overestimated. If the overestimation is more than 10-15%, pairwise tests of independence can be carried out, to reveal whether particular map pairs are in serious violation.

The pairwise test involves using a chi-squared or G^2 test of CI between all possible pairings of the binary predictor maps. This test is explained in detail in Bonham-Carter (1994a). Maps that are in serious violation can be rejected from the posterior probability calculations, or combined. In practice, it appears that even where CI is violated, the rank order of the polygons by posterior probability is not greatly affected, but each application should be evaluated for this independently.

The variance of the posterior probability values is given by the expression

$$s_{(P_{post})}^2 = \frac{1}{N(D)} + \sum_{j=1}^N s^2(W_j^{k(j)}) P_{post}^2 \quad (10)$$

where $s^2(W_j^{k(j)})$ is the variance of the weight for the j -th map, and $k(j) = +$ for presence and $-$ for absence of the binary pattern, as before. The variances of the weights become large for cases with a small number of deposits. The variance formulas are

$$s^2(W_j^+) = \frac{1}{N(B_j \cap D)} + \frac{1}{N(B_j \cap \bar{D})} \quad (11)$$

$$s^2(W_j^-) = \frac{1}{N(B_j \cap D)} + \frac{1}{N(B_j \cap \bar{D})} \quad (12)$$

where $N(B_j \cap D)$ is the number of unit cells where both deposits and the j -th binary pattern are present, and the other terms are defined similarly.

If one or more of the binary maps being used as evidence is incomplete, Agterberg et al. (1990) show how a variance component can be calculated in areas of missing data.

Generating binary predictor maps

The predictor maps used in the weights of evidence approach are the same as the ones used for fuzzy logic, summarized in Table 6. However, each multiclass map was reclassified to binary form. Multiclass weights of evidence can be carried out (see Goodacre et al., 1993; Bonham-Carter, 1994b, for example), but with only a small number of known deposits the weight estimates are unstable, and their variances are large. Transformation to binary maps, besides improving the robustness of the estimated weights, is also advantageous for facilitating interpretation. The weight calculations are invaluable for determining optimal thresholds objectively between 'anomaly' and 'background' that maximize the spatial association between the deposits and each predictor pattern.

For maps with an ordinal, interval, or ratio level of measurement, weights are calculated at successive class cutoffs, using cumulative areas, with each cutoff as the threshold between pattern present and pattern absent. This process is illustrated using proximity to felsic flows as an example.

The evidence map showing the distances from felsic flows is shown in Figure 7b. There are 10 buffers, or corridors, each 250 m wide, extending out from the felsic flow contacts. By superimposing the deposit locations on this buffer map, and appending the distance buffer class as an attribute to the deposit attribute table (a straightforward operation in GIS), the distance distribution of the deposits can be summarized by counting the number of deposits in each class. Visual inspection clearly indicates that a major proportion of the

deposits are situated close to the felsic flows. The question is whether there are more than would be expected due to chance. To quantify this relationship, weights are calculated using Equations 5 and 6 for cumulative distances, as shown in Table 9. Figure 30 is a plot of the contrast against distance, and reveals a maximum contrast at 0.5 km (see second row in Table 9). At this distance 12 of the 15 deposits are present and the area of the region lying within 0.5 km is only 56 km² out of a total study area of 268 km². If the deposits are located at random and independent of the flows, the weights and contrast values are zero, or negligibly small. This result shows that there is a strong spatial association of deposits with proximity to felsic flows. For the first buffer zone, W^+ is positive (nearly 2.3) because 7 out of the 18 cells in this buffer zone contain a deposit, far more than would be expected due to chance. Similarly W^- is -0.58, because the buffer zones

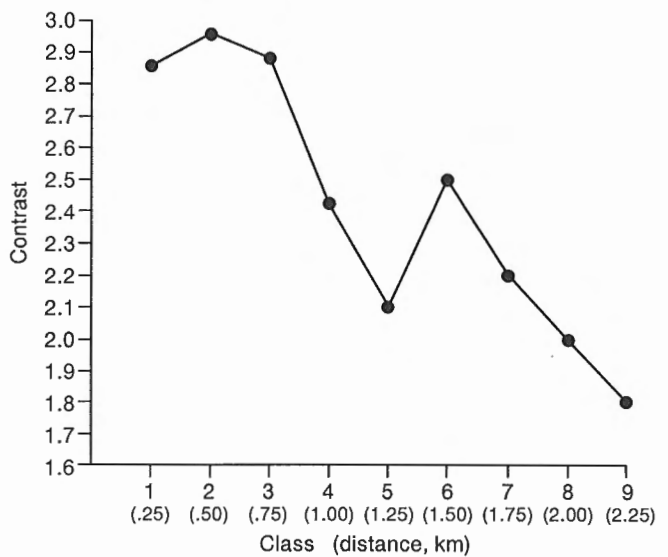


Figure 30. Graph of contrast versus distance from felsic flows. Cutoff between binary classes is set at 500 m, where contrast is maximum.

Table 9. Summary of weights for cumulative distances from felsic flow contacts using a unit cell of 1 km². Note that Contrast, C, has a maximum at class 2 (<0.5 km). Areas are in unit cells.

| Class | Distance | Area | Deposits | W+ | s(W+) | W- | s(W-) | C |
|-------|----------|------|----------|--------|--------|---------|--------|--------|
| 1 | 0.25 km | 18 | 7 | 2.2995 | 0.4764 | -0.5807 | 0.3593 | 2.8802 |
| 2 | 0.50 km | 56 | 12 | 1.5122 | 0.3251 | -1.4154 | 0.5815 | 2.9277 |
| 3 | 0.75 km | 81 | 13 | 1.1602 | 0.3024 | -1.6979 | 0.7109 | 2.8581 |
| 4 | 1.00 km | 104 | 13 | 0.8727 | 0.2963 | -1.5653 | 0.7115 | 2.4380 |
| 5 | 1.25 km | 125 | 13 | 0.6683 | 0.2929 | -1.4275 | 0.7121 | 2.0958 |
| 6 | 1.50 km | 145 | 14 | 0.5852 | 0.2811 | -1.9744 | 1.0041 | 2.5596 |
| 7 | 1.75 km | 163 | 14 | 0.4578 | 0.2795 | -1.8152 | 1.0048 | 2.2730 |
| 8 | 2.00 km | 177 | 14 | 0.3693 | 0.2784 | -1.6721 | 1.0055 | 2.0414 |
| 9 | 2.25 km | 167 | 14 | 0.3116 | 0.2778 | -1.5578 | 1.0062 | 1.8693 |

greater than 250 m from the flows contain fewer deposits than expected due to chance. The contrast = $2.2995 - (-0.5807) = 2.8802$ for the first zone is a measure of this association. However, notice that the contrast is greater in buffer zone 2 (the cumulative area of buffer zones 1 and 2), and then decreases with increasing distance away from the flow contact. Of course this calculation could be refined by using a smaller interval than 250 m, but in general the result would be similar; and because this calculation makes a simplifying 2-D assumption about the flow contacts being vertical, the more accurate distance measurements are not justified.

It is noted that there is not always a simple maximum and that some subjective judgement must be used in interpreting these contrast relationships. The variances of the weights and contrasts are also helpful for determining the optimum cutoff level for binary conversion. The variance of C is the sum of the variances of the weights. When the ratio of C to its standard deviation (square root of variance) is large, say greater than about 1.5, the contrast value is relatively reliable. Note that the variance of the weights depends on the cell size. It can be seen that both $N(B \cap \bar{D}) \Rightarrow \infty$ and $N(\bar{B} \cap \bar{D}) \Rightarrow \infty$, hence as unit cell

size $\Rightarrow 0$, $s^2(w_j^+) \Rightarrow 1/N(B \cap D)$ and $s^2(w_j^-) \Rightarrow 1/N(\bar{B} \cap D)$, see Equations (11) and (12). Bonham-Carter et al. (1989) discuss this and other aspects of the variances of weights and contrast in detail.

Weights and contrasts were calculated for all the proximity, geochemical, and geophysical input maps using the cumulative form as described above. The weights and contrasts for the geological map, a categorical scale map, was calculated using a noncumulative form. Two units, the felsic flows, hosting 7 of the 15 deposits, and the synvolcanic dykes, hosting 4 of the 15 deposits, showed the strongest spatial association to the deposits. The generalized geological map that was used as an input map for the fuzzy logic approach was replaced by two binary maps representing these two units. It is also noted that no statistical correlation was found between the deposits and proximity to zones mapped as pyrite alteration, so this map was omitted from the weights of evidence study.

In Table 10, the maps are ordered from largest to smallest contrast values. In general, the maps derived from the geological and alteration map tend to have the greatest contrast

Table 10. Summary of weights of evidence determined for evidence maps that define optimal association between known mineral deposits and map pattern. They are sequenced according to decreasing values of contrast, C.

| Map | W+ | s(W+) | W- | s(W-) | C | C/s(C) | Description of evidence map |
|-----|--------|--------|---------|--------|--------|--------|---|
| M1 | 3.3787 | 0.7393 | -0.394 | 0.3225 | 3.7728 | 0.8066 | Areas mapped as alteration pipes with 10 buffers 0.25 km wide surrounding areas |
| M2 | 2.2995 | 0.4764 | -0.5807 | 0.3593 | 2.8802 | 4.8263 | Areas mapped as felsic flows only |
| M3 | 1.1602 | 0.3024 | -1.6979 | 0.7109 | 2.8581 | 3.6996 | Areas mapped as felsic flows with 10 buffers 0.25 km wide extending from contacts |
| M4 | 0.6202 | 0.2816 | -2.0109 | 1.0039 | 2.6311 | 2.5234 | Areas mapped as mafic volcanoclastic rocks with 10 buffers 0.25 km wide extending from contacts |
| M5 | 1.275 | 0.3319 | -1.0925 | 0.5049 | 2.3675 | 3.9183 | Areas mapped as Fe alteration with 10 buffers 0.25 km wide extending from contacts |
| M6 | 0.4897 | 0.2798 | -1.8596 | 1.0046 | 2.3493 | 2.2528 | Areas mapped as Si alteration with 10 buffers 0.25 km wide extending from contacts |
| M7 | 0.3873 | 0.2786 | -1.7039 | 1.0054 | 2.0911 | 2.0044 | Areas mapped as synvolcanic dykes with 10 buffers 0.25 km wide extending from contacts |
| M8 | 1.7937 | 0.5821 | -0.2648 | 0.3083 | 2.0585 | 3.1252 | Kriged In concentrations of Zn in C horizon tills (<63 μ m size fraction) |
| M9 | 1.5525 | 0.4617 | -0.4223 | 0.3397 | 1.9749 | 3.4451 | Areas mapped as amphibole alteration with 10 buffers 0.25 km wide extending from contacts |
| M10 | 1.6182 | 0.5095 | -0.3371 | 0.3228 | 1.9553 | 3.2416 | Principal Component 1 scores mapped on catchment basin map |
| M11 | 1.447 | 0.4566 | -0.412 | 0.3398 | 1.859 | 3.266 | Areas mapped as epidote alteration with 10 buffers 0.25 km wide extending from contacts |
| M12 | 1.0052 | 0.3408 | -0.8189 | 0.453 | 1.8241 | 3.2177 | Kriged In concentrations of Cu in C horizon tills (<63 μ m size fraction) |
| M13 | 0.6853 | 0.3051 | -1.0934 | 0.583 | 1.7797 | 2.7029 | Areas mapped as felsic volcanoclastics with 10 buffers 0.25 km wide extending from contacts |
| M14 | 1.4897 | 0.5617 | -0.2482 | 0.3084 | 1.7379 | 2.7121 | Principal Component 2 scores mapped on catchment basin map |
| M15 | 1.3791 | 0.5556 | -0.2406 | 0.3084 | 1.6198 | 2.549 | Areas mapped as synvolcanic dykes |
| M16 | 1.3692 | 0.555 | -0.2399 | 0.3084 | 1.6091 | 2.534 | Kriged In concentrations of Pb in C horizon tills (< 63 μ m size fraction) |
| M17 | 0.9573 | 0.3798 | -0.533 | 0.3845 | 1.4903 | 2.7577 | Principal Component 3 scores mapped on catchment basin map |
| M18 | 0.6814 | 0.3342 | -0.6872 | 0.4538 | 1.3686 | 2.4284 | Vertical gradient gravity map |
| M19 | 1.2595 | 0.7772 | -0.1045 | 0.2846 | 1.364 | 1.6479 | Processed quadrature VLF data map |
| M20 | 0.5102 | 0.316 | -0.7415 | 0.507 | 1.2517 | 2.0953 | Total field magnetics |
| M21 | 0.5169 | 0.3315 | -0.5918 | 0.4545 | 1.1087 | 1.9709 | Vertical gradient magnetics |
| M22 | 0.3596 | 0.314 | -0.6047 | 0.508 | 0.9643 | 1.6147 | Total field VLF |
| M23 | 0.1598 | 0.327 | -0.2588 | 0.4573 | 0.4187 | 0.5622 | Areas mapped as subvolcanic sills with 10 buffers 0.50 km wide extending from contacts |

values, indicating that they are the best predictors of the known deposits, whereas the geophysical predictor maps have the least predictive capability. Note that the map showing proximity to the subvolcanic intrusions, a strongly weighted input map for the fuzzy logic method, has only a low contrast value. This is because four of the major deposits (Chisel Lake, Chisel North, Lost Lake, and Ghost Lake) are not very close to the sill contact.

Pairwise conditional independence tests, summarized in Table 11, show that there are no χ^2 values greater than 5.4 meaning that for a probability level of 98%, there is no reason to reject the hypothesis that conditional independence exists for any of the pairs of maps. At least on a pairwise basis, there are no serious problems introduced by conditional dependence.

The weighted binary maps are now combined to create a posterior probability map by applying Equation (9). This process is readily carried out with the built-in GIS modelling language. For regions of maps where no data are available, such as areas outside the catchment basins in the lake sediment geochemical maps, the weight is assigned the value 0. The final probability map is shown in Figure 31 (see colour section). The posterior probabilities were classified by percentiles so that the 20 categories in the legend represent the 5th, 10th, 15th ... >95th percentiles. The prior probability using a unit cell area of 1 km² is 0.0560. All areas that show posterior probabilities greater than the prior are characterized by combined evidence that is favourable for deposits, whereas values less than the prior are relatively unfavourable. The ranking of regions by posterior probability produces a favourability map that is based on a statistical model and assumes that the known deposits are an adequate sample of deposits (known and undiscovered) in the region.

The overall CI test (sum of probability x area, over all polygons) predicts 32 deposits, more than double the number of observed deposits. Thus although there are no serious pairwise violations, the multiple interactions of such a large number of predictor maps results in a failure of the overall test. This is not unexpected, because many of the maps carry somewhat similar information. For example, the lake sediment chemistry and the till chemistry both reflect concentrations of Cu, Pb, and Zn. Although the posterior probabilities are too large, we believe that the ranking of areas by favourability is little affected by the violation of CI. This has been confirmed by carrying out a logistic regression analysis (Wright, 1996), involving no assumption of CI, which shows a closely similar favourability map to that obtained with weights of evidence.

Figure 32 (see colour section) is a map of the posterior probability divided by its standard deviation due to uncertainties in the weights and due to missing data. This map shows regions where the favourability estimates are relatively uncertain.

Dempster-Shafer model

Dempster-Shafer belief theory is an alternative mechanism for knowledge representation and map combination. It is a knowledge-driven approach, with some advantages and

disadvantages as compared with fuzzy logic. With the fuzzy logic approach, each evidence map is associated with a membership function that expresses the importance of the evidence on a scale between 0 and 1. For the Dempster-Shafer approach, each evidence map is associated with two independent "belief" functions that represent the information content of evidence, also on a scale from 0 to 1. The upper belief function (known as the "plausibility") can be considered as an optimistic assessment that the evidence supports a proposition, whereas the lower belief function (known as the "support") is a conservative estimate. The interval between the plausibility function and the support function is the uncertainty or ignorance. Disbelief is defined as one minus the plausibility. These relationships are summarized in Figure 33.

The advantage of this approach is that it allows the user to represent uncertainty in the knowledge representation, because the interval between support and plausibility (also known as the "evidential interval") can be considered as a confidence band. Furthermore, missing data can be modelled by defining the plausibility as 1, the support as 0, so the uncertainty is 1. Evidence from two or more maps is combined using Dempster's rule of combination. The combined support, plausibility, disbelief, and uncertainty can each be separately mapped, although only two of these quantities are independent. This contrasts with the fuzzy logic output, consisting only of a single map, the combined fuzzy membership.

The Dempster-Shafer method has been discussed in a mineral exploration context using a hypothetical data set by Chung and Moon (1991) and Chung and Fabbri (1993). An (1992), An et al. (1994a, b) applied the method to combine

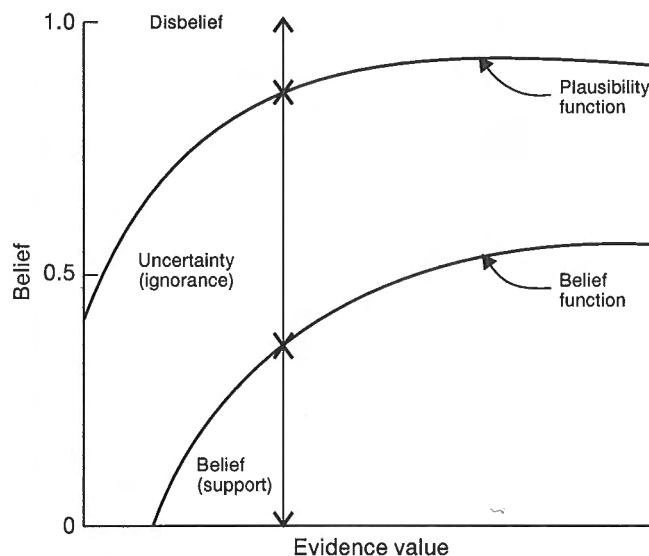


Figure 33. Idealized diagram of belief functions. Note that when plausibility and support are equal, uncertainty is zero and support plus disbelief equals 1, as in probability approach.

a variety of geophysical data sets to predict base metal and iron-formation deposits in an area north and west of this present study area.

Belief function theory

A detailed theoretical exposition and a formalization of the belief function approach can be found in Dempster (1968) and Shafer (1976). The discussion here is simplified and informal. A simple numerical example is given to illustrate Dempster's rule of combination.

Each map to be used as evidence to evaluate a proposition (e.g. "this cell contains a volcanic-hosted massive sulphide deposit") is associated with a pair of belief functions, the support function and the plausibility function. In practice, these functions are usually held in map attribute tables, where each class on the map is associated with a support value and a plausibility value. Suppose we have map A, we will simply denote the value of the support due to A as Sup_A , and the plausibility due to A as Pls_A , where these are functions that vary with the value (map class) of A, and therefore can be mapped in their own right as lookup operations from map A. For a given value of map A, the ignorance or uncertainty is denoted as Unc_A , calculated as $Pls_A - Sup_A$, and the disbelief, Dis_A is $1 - Pls_A$. Thus the sum $Sup_A + Unc_A + Dis_A = 1$. The disbelief is the belief that the proposition is false, i.e. that a cell does not contain a volcanic-hosted massive sulphide deposit. Note that plausibility is greater than or equal to support. Where plausibility and support are equal, the uncertainty is zero, and $Sup + Dis = 1$, as in the probability approach. These relationships are illustrated graphically on Figure 33.

For each map used as evidence, two independent functions must be estimated, usually either the support and disbelief, or the support and plausibility, but in some cases the uncertainty may be chosen with one of the other values. An et al. (1994a) and Chung and Fabbri (1993) discuss the estimation procedure.

Given two maps A and B, with the support and disbelief functions for each, Dempster's rule of combination for estimating the combined support and disbelief (and therefore uncertainty) is

$$Spt_c = \frac{Spt_A Spt_B + Spt_A Unc_B + Spt_B Unc_A}{\beta} \quad (13)$$

$$Dis_c = \frac{Dis_A Dis_B + Dis_A Unc_B + Dis_B Unc_A}{\beta} \quad (14)$$

$$Unc_c = \frac{Unc_A Unc_B}{\beta} \quad (15)$$

where the denominator for all three equations

$$\beta = 1 - Spt_A Dis_B - Dis_A Spt_B \quad (16)$$

is a normalizing factor that ensures that $Spt + Dis + Unc = 1$.

Table 12. Example of applying Dempster's combination rule. At one pixel, support and disbelief values for maps A and B are supplied (bold). Map C is combination of maps A and B. Values in italics are calculated.

| | Support | Disbelief | Uncertainty | Plausibility |
|-------|---------------|---------------|---------------|---------------|
| Map A | 0.0500 | 0.3500 | <i>0.6000</i> | <i>0.6500</i> |
| Map B | 0.1000 | 0.4000 | <i>0.5000</i> | <i>0.6000</i> |
| Map C | <i>0.0952</i> | <i>0.5873</i> | <i>0.3175</i> | <i>0.4127</i> |

Consider an example of using these equations to combine two maps A and B at a location for which the support and disbelief values are given, see Table 12. The objective is to create a new map C. For each location the first step is to calculate the uncertainty (and plausibility if desired) values for A and B. Then applying Equations (13-16) we obtain

$$\beta = 1 - 0.02 - 0.035 = 0.9450,$$

$$Spt_C = ((0.05 \times 0.10) + (0.05 \times 0.50) + (0.10 \times 0.60)) / 0.945 = 0.0952,$$

$$Dis_C = ((0.35 \times 0.40) + (0.35 \times 0.50) + (0.40 \times 0.60)) / 0.945 = 0.5873,$$

$$Unc_C = (0.60 \times 0.50) / 0.945 = 0.3175,$$

$$\text{and the } Pls_C = 1 - 0.5873 = 0.4127.$$

Dempster's rule is applied recursively, so that the combination map C can now be combined with other maps in pairwise fashion.

Assigning belief function values

The same 23 input maps used in the fuzzy logic and weights of evidence approaches were combined using the Dempster-Shafer method. The assignment of the belief function values was made subjectively for each input map. In practice, two problems are encountered at this stage. The first difficulty is the conceptualization of belief and disbelief. There is a tendency to think of disbelief as one minus the belief. It is often difficult to quantify an opinion indicating the difference between disbelief and uncertainty. The second problem, more on the pragmatic side, is that if two maps being combined both have large support values, the combined support becomes close to 1. Further combination with other maps with high support values results in values even closer to 1 (and disbelief and uncertainty approaching zero), making the results difficult to interpret.

In the present application, we have information about the locations of known deposits. It was decided, therefore, to use this information to guide the estimation of belief functions, using an ad hoc approach. Because the number of deposits is relatively small, the estimates are over-ridden by subjective opinion, using the exploration model. For the i-th class of input map A, the probability that a small unit area (pixel)

contains a deposit, $P(D|A_i)$, is estimated by the ratio of the number of pixels containing a deposit by the total number of pixels:

$$P(D|A_i) = \frac{N(D \cap A_i)}{N(A_i)} \quad (17)$$

This calculated probability (labelled CP in Fig. 34) is considered to represent an “average” belief, somewhere between the support and plausibility. The lower belief function (support) value for the i -th map class is then calculated by multiplying the probability by a constant, α_S , in the range [0, 1]:

$$Spt_{A_i} = \alpha_S P(D|A_i) \quad (18)$$

The magnitude of α_S is dependent on the certainty the expert associates with the calculated probability. The larger the constant the smaller the uncertainty. The disbelief, which is related to the upper belief function (plausibility) by $Dis = 1 - Pls$, is calculated by multiplying one minus the probability by a second constant, α_D , also in the range [0, 1].

$$Dis_{A_i} = \alpha_D (1 - P(D|A_i)) \quad (19)$$

Again, the larger the constant, the smaller the uncertainty. This approach is illustrated in Figure 34.

In practice, the constants α_S and α_D were kept relatively small, in the order of 0.01-0.001, to avoid the problem of obtaining combined belief functions that approach unity. The same values were used for all maps. The calculated probabilities (see Table A2 of the Appendix) for maps of continuous variables have been manually smoothed to show a

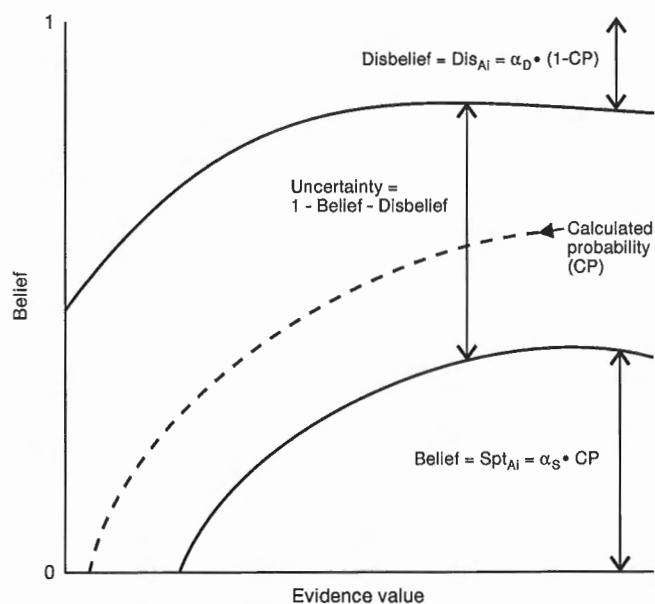


Figure 34. Estimating belief functions is generally a subjective process. In this study generating belief functions was guided by probabilities calculated using weights of evidence method (see text for a detailed explanation).

continuous function assuming that gaps in found in the distribution are caused by the small number of known deposits. The belief function values are also listed in Table A2.

Maps of combined belief functions

The 23 input maps were combined using equations 13-16 and the values in Table A2 held as map attribute tables. The output consists of four maps, showing the combined support, disbelief, plausibility, and uncertainty associated with the proposition “favourable location for volcanic-hosted massive sulphide deposits” (see Fig. 35-38, in colour section).

Figure 35 shows the spatial distribution of support. Elevated support is found associated with known deposits in the area. Of particular interest are the areas that show strong support but are not associated with known deposits. The zones showing uniform values of weak support in the southeast, northwest, and northeast are underlain by geological units that are post-Amisk in age and considered unsuitable for volcanic-hosted massive sulphide deposits. All post-Amisk rocks were assigned a constant high disbelief, low belief, and low uncertainty, effectively masking out this region.

In general, disbelief (Fig. 36) is low for areas showing high support. The spatial distribution of uncertainty is shown in Figure 37. As expected, areas of high support and low disbelief also have low uncertainty values. A northeast-trending area of high uncertainty located north of the Wekusko Lake pluton is due mainly to missing data on the lake sediment maps and till maps. The plausibility map (Fig. 38), which can be considered the most optimistic assessment that an area will contain a deposit, is in general correlated with support, as might be expected from our method of estimating the belief functions. Two areas of elevated plausibility (but modest support) are situated on the northwest flank of the Wekusko Lake pluton. These two areas, seen distinctly as zones of strong disbelief (Fig. 36), result from the combination of elevated uncertainty with moderate support.

Comparison of favourability maps

A cursory visual inspection of the final potential maps by the three methods, fuzzy logic, weights of evidence, and Dempster-Shafer, shows a broad similarity between the results. In general, areas with known mineral deposits are associated with moderate to very high potential. Areas geologically unrelated to volcanic-hosted massive sulphide deposits have a relatively low potential by all three methods. However, there are some areas where the maps differ, and the next section describes the results of inter-map comparisons. To determine an overall measure of the correlation between the potential maps, pairwise comparisons were made using an area-weighted Spearman's rank correlation coefficient, and to identify specific areas of difference, a matrix overlay was performed.

Spearman's rank correlation coefficients

Each of the four potential maps (using the support and plausibility maps from Dempster-Shafer) were classified using 5% quantiles, thereby normalizing each map to a uniform

distribution with 20 classes. The resulting map classes were then treated as ordinal-scale numbers, and Spearman's rank correlation coefficient calculated as a global measure of similarity. Because the maps were in a vector polygon structure, an area-weighted Spearman's rank correlation coefficient was calculated using the following expression

$$r_s = \frac{\sum_{i=1}^n T_i (R_x - \bar{R}_x)(R_y - \bar{R}_y)}{\sqrt{\sum_{i=1}^n T_i (R_x - \bar{R}_x)^2 \sum_{i=1}^n T_i (R_y - \bar{R}_y)^2}} \quad (20)$$

where R_x and R_y are the area-weighted ranks of map x and map y respectively and T_i is the area of the i -th polygon. The bar indicates the mean value of the ranks which is the middle value, an integer if n is odd, a half integer if n is even (see Bonham-Carter, 1994a, chapter 8).

The resulting coefficients (see Table 13), indicate that the strongest correlation is between the weights of evidence posterior probability map and the Dempster-Shafer support map. This is presumably because the belief functions were estimated using guidelines from probability calculations, and WOE is also based on similar calculations. However, it is still perhaps surprising that the two maps agree so well when one considers that the WOE input maps are binary, whereas the DS input maps are multiclass. The second largest coefficient is between DS support and DS plausibility. Again, this is to be expected, due to the method of estimating the belief functions. The two lowest coefficients are between DS plausibility, FL, and WOE. This is not unexpected as some of the favourable zones on the plausibility map are also associated with a high level of uncertainty.

Matrix overlay

To see where the actual differences and similarities between maps occur, a matrix overlay operation was performed between each pair of potential maps. A matrix overlay operation is carried out by assigning the classes of the output map in a matrix (Fig. 39), with the rows being the classes of input map 1, and the columns being the classes of input map 2. Where the classes (ranks) are the same for both input maps,

the output is assigned to class value 10 (see diagonal in Fig. 39). Note that output classes less than 10 are used if the class of input map 1 is less than the class of input map 2, but output classes greater than 10 are used for the converse situation. The result is to show the location and extent of differences in favourability between the input maps. The resulting comparative maps are shown in Figure 40 (see colour section).

Discussion and summary

Three methods for combining spatial data have been developed for use with geoscience data and successfully implemented in a GIS environment during this study. The fuzzy logic method and Dempster-Shafer belief theory can be described as "knowledge-driven" approaches and the weights of evidence method as "data-driven". Some distinct advantages and disadvantages are associated with each method.

Because the weights of evidence approach uses statistical measures to characterize the spatial associations between known deposits and map patterns to establish a weight for the evidence layer, a training site with known deposits is required to implement this method. The Snow Lake study area has a total of 15 known volcanic-hosted massive sulphide type deposits or a density of approximately 1 per 18 km², which is marginal for a suitable sample. The advantage is that the weights assigned to the evidence layers are not biased towards the experts' opinions.

The fuzzy logic approach tends to be much more flexible in representing the experts' thought processes assisted with the use of inference nets constructed with fuzzy operators. It has the advantage of being able to evaluate the influence of different types of evidence by constructing intermediate maps. In this study, the geochemical, stratigraphic, heat, alteration, and geophysical factor maps are such intermediate maps. The concept of a fuzzy membership function used to express the varying importance of each layer of evidence is intuitively simple for the expert, generally not familiar with numerical methods, to work with.

The Dempster-Shafer belief theory is more flexible than fuzzy logic for representing uncertainty in the data, but is more restrictive in the expressiveness of the combination

Table 13. Spearman's rank correlation coefficients for comparing favourability maps generated using different combination rules. The same evidence was used for all methods.

| | Fuzzy logic | Weights of evidence | Dempster-Shafer support | Dempster-Shafer plausibility |
|------------------------------|-------------|---------------------|-------------------------|------------------------------|
| Fuzzy logic | 1 | 0.677 | 0.667 | 0.498 |
| Weights of evidence | | 1 | 0.811 | 0.557 |
| Dempster-Shafer support | | | 1 | 0.757 |
| Dempster-Shafer plausibility | | | | 1 |

| | | Map 1 | | | | | | | | | | | | LEGEND | | |
|-------------------------|----|-------|----|----|----|----|----|----|----|----|----|----|----|--------|---------------------------|---------------------------|
| Map 2 value rankings | | 1 | 2 | 3 | 4 | 5 | 6 | 7 | 8 | 9 | 10 | 11 | 12 | ... | 1 | Map 1 ≥ Map 2 by 18 ranks |
| | 1 | 10 | 11 | 11 | 12 | 12 | 13 | 13 | 14 | 14 | 15 | 15 | 16 | | 2 | Map 1 ≥ Map 2 by 16 ranks |
| | 2 | 9 | 10 | 11 | 11 | 12 | 12 | 13 | 13 | 14 | 14 | 15 | 15 | | 3 | Map 1 ≥ Map 2 by 14 ranks |
| | 3 | 9 | 9 | 10 | 11 | 11 | 12 | 12 | 13 | 13 | 14 | 14 | 15 | | 4 | Map 1 ≥ Map 2 by 12 ranks |
| | 4 | 8 | 9 | 9 | 10 | 11 | 11 | 12 | 12 | 13 | 13 | 14 | 14 | | 5 | Map 1 ≥ Map 2 by 10 ranks |
| | 5 | 8 | 8 | 9 | 9 | 10 | 11 | 11 | 12 | 12 | 13 | 13 | 14 | | 6 | Map 1 ≥ Map 2 by 8 ranks |
| | 6 | 7 | 8 | 8 | 9 | 9 | 10 | 11 | 11 | 12 | 12 | 13 | 13 | | 7 | Map 1 ≥ Map 2 by 6 ranks |
| | 7 | 7 | 7 | 8 | 8 | 9 | 9 | 10 | 11 | 11 | 12 | 12 | 13 | | 8 | Map 1 ≥ Map 2 by 4 ranks |
| | 8 | 6 | 7 | 7 | 8 | 8 | 9 | 9 | 10 | 11 | 11 | 12 | 12 | | 9 | Map 1 ≥ Map 2 by 2 ranks |
| | 9 | 6 | 6 | 7 | 7 | 8 | 8 | 9 | 9 | 10 | 11 | 11 | 12 | | 10 | Map 1 = Map 2 |
| | 10 | 5 | 6 | 6 | 7 | 7 | 8 | 8 | 9 | 9 | 10 | 11 | 11 | | 11 | Map 1 ≤ Map 2 by 2 ranks |
| | 11 | 5 | 5 | 6 | 6 | 6 | 7 | 8 | 8 | 9 | 9 | 10 | 11 | | 12 | Map 1 ≤ Map 2 by 4 ranks |
| | 12 | 4 | 5 | 5 | 6 | 6 | 7 | 7 | 8 | 8 | 9 | 9 | 10 | | 13 | Map 1 ≤ Map 2 by 6 ranks |
| ... | | | | | | | | | | | | | | 14 | Map 1 ≤ Map 2 by 8 ranks | |
| | | | | | | | | | | | | | | 15 | Map 1 ≤ Map 2 by 10 ranks | |
| | | | | | | | | | | | | | | 16 | Map 1 ≤ Map 2 by 12 ranks | |
| | | | | | | | | | | | | | | 17 | Map 1 ≤ Map 2 by 14 ranks | |
| | | | | | | | | | | | | | | 18 | Map 1 ≤ Map 2 by 16 ranks | |
| | | | | | | | | | | | | | | 19 | Map 1 ≤ Map 2 by 18 ranks | |
| | | | | | | | | | | | | | | 20 | Map 1 ≤ Map 2 by 20 ranks | |

Figure 39. Overlay matrix for intermap comparison. The numbers represent the classes on the output map. Maps were compared by ranks, not absolute values. Resulting maps show actual location and extent of differences in favourability between favourability maps produced by three different methods.

rules. The Dempster-Shafer method produces outputs that include a conservative estimate of the favourability (support), an optimistic estimate of favourability (plausibility), and related uncertainties (ignorance). Conceptually this approach is more difficult with some confusion arising when assigning support and disbelief function values.

Exploration targets versus drill targets

It is important to keep in mind that the mineral favourability maps generated in this study are not intended to be used for defining drill targets but rather to define specific areas that warrant further detailed exploration. The source data used in this study included airborne geophysics flown with 500 m line spacings or more, lake sediment geochemical survey at densities of 1 sample per 6 km², and geological mapping at 1:20 000 scale, which do not provide sufficient detail to define a drill target. However these data can be used effectively for excluding areas that lack the general geological and geophysical characteristics determined from the exploration model, and to identify favourable zones with no known deposits.

The “best” method

All three of the methods have successfully identified areas containing known deposits as having high potential. Table 14 shows how deposits are linked with areas of favourability for the three different methods. There are 10 out

of the 15 deposits known at the time of the analysis within areas that have been identified by the fuzzy logic and weights of evidence method as being in the top 10% of area with respect to favourability for volcanic-hosted massive sulphide mineralization. For the Dempster-Shafer method there are 11 deposits in areas in the top 16% of area. The Photo Lake deposit (number 16), discovered following the analysis, is also shown in Table 14.

Deciding which approach is best is really a subjective decision and depends largely on how comfortable the users are with the conceptual aspects of each method. However, some general guidelines should be considered. As mentioned above, if no suitable training site is available, a data-driven approach is not possible. On the other hand if a clearly defined exploration model is not developed a knowledge-driven approach may not be appropriate. Two other criteria may also be used to evaluate the effectiveness of each method; the number of known deposits predicted to be in favourable areas and the size of the area predicted to be favourable. Given a specific deposit type and a large geological environment to explore for it, one of the initial goals for an exploration project is to reduce the amount of area to a reasonable size for a more detailed study. If a method for assigning potential to areas for exploration does not restrict the amount of area defined as favourable to a reasonable amount, it could be considered less effective. Similarly if a method fails to predict areas as favourable where known deposits exist it also could be considered less effective.

Table 14. Summary of areas predicted to be favourable for each method and the number of known deposits found in these areas. Deposit 16, Photo Lake, was discovered after the

| Fuzzy logic | | Weights of evidence | | | | Dempster-Shafer | |
|------------------------------|---------|---------------------|--|------------------------------|---------|-----------------|---------|
| Cum. area (km ²) | | Deposits* | | Cum. area (km ²) | | Deposits* | |
| 0 | | | | 6.8 | (2.54%) | 10.2 | (3.8%) |
| 6.7 | (2.5%) | 1,2,4,7,5,6,14 | | 12.8 | (4.7%) | 20.8 | (7.7%) |
| 17.3 | (6.4%) | 3 | | 19.9 | (7.4%) | 31.8 | (11.8%) |
| 26.5 | (9.8%) | 11,16 | | 26.9 | (10.0%) | 43.0 | (16.0%) |
| 37.9 | (14.1%) | 12 | | 32.4 | (12.0%) | 54.5 | (20.3%) |
| 47.1 | (17.5%) | | | 38.4 | (14.3%) | 66.2 | (24.6%) |
| 58.5 | (21.7%) | | | 44.2 | (16.4%) | 78.4 | (29.2%) |
| 69.1 | (25.7%) | 13 | | 50.8 | (18.9%) | 91.3 | (33.9%) |
| 79.4 | (29.5%) | | | 61.2 | (22.8%) | 103.6 | (38.5%) |
| 91.6 | (34.1%) | | | 69.8 | (25.9%) | 117.0 | (43.5%) |
| 102.5 | (38.1%) | 15 | | 79.2 | (29.4%) | 132.4 | (49.2%) |
| 115.1 | (42.8%) | | | 93.9 | (34.9%) | 142.8 | (53.1%) |
| 119.3 | (44.4%) | | | 102.3 | (38.1%) | 156.5 | (58.2%) |
| 122.8 | (53.7%) | | | 123.6 | (45.9%) | 173.0 | (64.3%) |
| 268.8 | (100%) | 9,10 | | 268.8 | (100%) | 268.8 | (100%) |

* See Table 1 for deposit names. Cum. area = cumulative area.

Also included in the top 10% of area are the four largest deposits (Chisel Lake, Stall Lake, Anderson Lake, and Linda 2). Though the fuzzy logic approach does slightly better at limiting the amount of favourable area it does not represent a significant benefit.

Based on the results from this study, it initially appears that what is used for evidence is more critical than the actual spatial combination rule used. This implies that even for data-driven models, careful consideration should be given at the beginning of the project to understanding the deposit model and identifying critical evidence.

GIS versus light table

Much effort and time has been spent on creating a digital georeferenced spatial database, learning a GIS, and developing methods for combining spatial data sets. It is difficult to evaluate whether the results produced through this study are better or worse than what could have been produced using traditional methods, as the real test would be whether more deposits were found. Although the newly discovered Photo Lake deposit is in a zone predicted as favourable by these methods, the analysis reported here was not used by the exploration company who discovered it. However, some very distinct advantages have become apparent as a result of using GIS and integration models.

- Having all the available data as a georeferenced digital database allowed easy updating of information, such as geological maps, as new data were collected. Problems associated with trying to overlay maps at different scales and projections were eliminated. The digital database was also a very effective filing system, allowing the data be organized and accessible.

- Processing the data to generate derived information such as kriging geochemical data or extracting important geological units was quick and made modifications easy to incorporate in a new model.
- Accommodating modifications in the integration model to generate new favourability maps could also be done very quickly.
- Querying several layers of evidence at a location within the study area allowed better understanding of the results.
- Perhaps the single biggest advantage in the process described in this study was developing the exploration model, representing it as evidence maps, and constructing inference nets to combine the evidence. This forces the user to become intimate with the geological characteristics associated with the deposits and become familiar with their interrelationships and how they affect the results. This, of course, could be done without a GIS, but the GIS facilitates this process.

Predictor maps

One of the most critical steps in this project was establishing what criteria would be used as evidence for the presence of volcanic-hosted massive sulphide type deposits and generating representative “evidence” maps. Results will undoubtedly be affected if different types of evidence are used. It is important to note that the 23 evidence maps used in this study, listed in Table 10, were selected based on one possible exploration model. It is emphasized that a large range of results can be obtained depending on how the exploration model is defined and what is selected as evidence. The results obtained in this study should not be interpreted as the only possibility. One of the advantages of using a GIS as a tool for implementing integration methods is that different inputs can be used to reflect different models and results generated relatively quickly.

This study had the advantage of having access to bedrock mapping at a 1:20 000 scale. The availability of lithological information at this level of detail is exhibited by the presence of six predictor maps related to stratigraphic data; four for the stratigraphic factor and two for the heat factor. Typically, areas being selected for regional exploration programs do not have bedrock coverage at this level of detail. This may necessitate alternative means to obtain the required stratigraphic information, such as using radiometric data to identify younger from older intrusive bodies. It may also demand that certain evidence not be included. For example, in this study the presence of rhyolite flows was an important piece of evidence that was mapped on the 1:20 000 scale map but was grouped into a general "felsic volcanic" unit on the 1:50 000 compilation map. If only the 1:50 000 compilation map was available this evidence could not be used.

The detail of data may also influence the importance the expert assigns to a certain piece of evidence. In this study the geophysical data were collected at a moderately detailed level, 800 m line spacing for magnetic data, 500 m line spacing for VLF data, and a 2 km grid for gravity. Though geophysical data are important in the exploration for volcanic-hosted massive sulphide deposits the resolution of the data available in this study was not sufficient to identify well defined anomalies. This resulted in less emphasis being put on the geophysical data.

The evidence maps listed in Table 10 are ranked with respect to the calculated contrast values ($C = W^+ - W^-$). The contrast value defines the strength of the association between known mineral deposits and a map pattern. In general stratigraphic evidence is ranked highest followed by alteration evidence, geochemical evidence, heat source evidence, and finally geophysical evidence. It may seem surprising that the geophysical data appears to have the least significance. The explanation may be related to the resolution of the data. The rather coarse resolution of the data allows broad anomaly patterns to be defined and there will be a much smaller points-per-pattern area ratio. On the other hand tight, well defined buffer zones around selected contacts defining stratigraphic evidence, results in a much larger points-per-area ratio. How the evidence is ranked for the fuzzy logic approach is very dependent on the inference network and fuzzy operators used. In this study the overall weights for the five evidence factors generally defines the general order of significance. An overall weighting factor of 0.8 was assigned to the stratigraphic factor, 0.7 to the heat factor, 0.6 to the alteration factor, 0.3 to the geochemical factor, and 0.2 to the geophysical factor. It can be seen that the experts' ranking is similar to the empirically derived ranking from the weights of evidence method. This ranking also reflected the experts' general confidence in the data.

Areas of interest for exploration

In general, selecting areas for further detailed exploration is simply a matter of identifying areas that have a high favourability but no known deposits. However, the selection

process can be approached in different ways and influenced by several factors. Each favourability map can be examined independently and targets selected on the merit of each method, or the maps can be combined to form a "composite" picture. Depending on the exploration geologist's confidence in the different methods, one or more methods can be ignored. Whether the top 5th percentile, 10th percentile of the area, or a lower value is selected as the level that defines the "most" favourable regions will depend largely on budget restrictions.

Figure 41 (see colour section) summarizes the volcanic-hosted massive sulphide potential predicted by the three integration methods. Virtually all the coloured regions are potentially interesting but of particular interest are those areas that prove to have high potential by two or more methods.

In order to discuss particular zones of high potential, some regions have been outlined and numbered, as seen in Figure 41. This is to facilitate discussion but it must be emphasized that any of the coloured areas on Figure 41 is worthy of examination. Area 4 and area 6 already contain known deposits, however, they are discussed here because it is useful to recognize the evidence associated with these known deposits and because the favourable areas seem to be extensive enough to warrant the possibility of finding further deposits. The characteristics associated with these seven selected areas are discussed below. It is of interest to mention that the GIS was an invaluable tool for investigating these areas. It allows the user to interactively select locations on the target map and obtain a summary of the inputs from the evidence maps and the modelling results. These areas are not ranked in order of importance.

Area 1

This is a narrow north-trending zone 1-3 km south of Cook Lake on the west side of the Richard Lake pluton.

The stratigraphy for this area is of particular significance. The primary lithology is a felsic flow unit which has been recognized by Bailes (1987) as being a facies equivalent to part of the intact sequence of Amisk Group metavolcanic rock underlying the Chisel Lake, Lost Lake and Ghost Lake deposits. These rocks have been separated from the Chisel Lake area by Richard Lake pluton and the north-trending Varnson Lake fault and are complexly folded. Its proximity to the Richard Lake pluton, less than 0.5 km, allows for a favourable heat environment. It is noted that this area is also adjacent to synvolcanic dykes; however, it is a fault contact making it difficult to determine how close the felsic flow unit was to the dykes before the faulting. This illustrates a general weakness in the modelling approach used here. Generating buffers around contacts to determine proximity to different features, does not take into account faults, unconformities, the presence of late intrusions, dip of contacts, or other features that could alter the interpretation of the distance. The alteration factor is beneficial due to the presence of strong to weak Fe-Mg metasomatism. There is a strong magnetic and total field VLF signature for this area. Geochemical evidence is weak as no till samples were collected in this area and the lake sediment geochemical signature was not substantial.

Area 2

This area is located 0.5 km east of Cook Lake, in a small wedge between Richard Lake pluton and Chisel Lake pluton.

The presence of felsic flows, also recognized as possibly being part of the volcanic stratigraphy underlying the Chisel Lake, Lost Lake, and Ghost Lake deposits (Bailes, 1987) make this a favourable zone stratigraphically. The felsic units are immediately adjacent to the Richard Lake Pluton and synvolcanic dykes potential heat sources, however, as with area 1, they are fault contacts so the true distance is not known and the heat factor may not be as significant as modelled. Strong Fe-Mg alteration is present and again no till samples were taken in this area while the lake sediment geochemistry has background levels. The geophysical signature showed strong magnetic responses and moderate VLF and gravity responses.

Area 3

This region is located at the northern limit of the study area centred between Snow Lake and Cook Lake.

An abundance of felsic flows and felsic volcaniclastic units make this a stratigraphically interesting area. Though it is rather distant from a subvolcanic tonalite, a moderately favourable potential with respect to a heat source is indicated by proximal synvolcanic dykes. Alteration in this area is characterized by strong and extensive Fe-Mg metasomatism. Till geochemistry shows anomalies in Pb and Cu and lake sediment geochemistry resulted in high PC-1 scores (Cu) for this zone. The geophysical factor is typified by high magnetic responses, low VLF responses, and high gravity responses.

Photo Lake. Photo Lake is a massive sulphide deposit in the order of 800 000 t, discovered in 1994 by Hudson Bay Mining after drilling an airborne EM anomaly. Details of the deposit are being withheld on request of Hudson Bay Mining. (A.H. Bailes, pers. comm., 1994).

It is of interest to note that the favourability modelling for this project and the selection of target areas, including area 3 which includes the Photo Lake deposit, was completed and presented at the Geological Survey of Canada's Forum in January, 1994. The new discovery at Photo Lake was unknown to the authors until September, 1994, after preparing the first draft of this paper.

Area 4

This is a large area covering approximately 25 km² (7% of study area) to the north and west of Anderson Lake. It includes the past producing Anderson Lake, Stall Lake, and Rod 1, 2 mines as well as the large (13 Mt) subeconomic Linda 2 deposit. Despite this high density of deposits this whole area is generally characterized by favourable evidence and contains relatively large zones of favourability with no known deposits which are indicated on Figure 41 and summarized below.

The area labelled 4a is at the south end of Anderson Lake just north of the Joannie deposit. This area contains felsic flows and is close to both felsic and mafic volcaniclastic

lithologies favourable for volcanic-hosted massive sulphide deposits. Tonalite sills and synvolcanic dykes are within 0.75 km providing good potential for heat sources. Till geochemistry indicates background levels of Pb and Zn, however, lake sediment geochemistry gives PC-1 (Cu) and PC-2 (Zn) scores above the 90th percentile. This zone is also proximal to Fe-Mg and Si alteration. High magnetic and gravity responses characterize this area.

The area labelled 4b is 2 km due north of the Joannie deposit on the south shore of Snow Lake. Units of fragmental rhyolite flows and proximal mafic volcaniclastics comprise a favourable stratigraphic environment. Potential heat sources are within 2 km (tonalite sills) and 1 km (synvolcanic dykes). Till geochemistry indicates anomalous Cu and Pb concentrations above the 90th percentile and lake sediment geochemistry does not indicate any anomaly. Alteration is present in the form of Fe-Mg metasomatism. The geophysical factor is represented by a high magnetic response and high gravity response.

The area marked 4c is a continuous zone of high favourability extending for over 2 km between the Anderson Lake deposit and the Stall Lake deposit north of Anderson Lake. The lithology in this area is dominated by an abundance of felsic flows (Anderson Rhyolites). These rocks are stratigraphically close to both the tonalite sills and synvolcanic dykes making them favourable with respect to being close to a heat source. Alteration is ubiquitous, dominated by chlorite-biotite-rich rocks. Completely altered rocks characteristic of alteration pipes are also present. Geochemical responses are variable with the lake sediment PC-1 (Cu) being the most favourable indicator. Generally, magnetic responses are high while VLF and gravity responses are moderate.

The subarea 4d is located to the northeast of Stall Lake. Units of rhyolite flows proximal to mafic volcaniclastic units and within 2 km of potential heat sources make the stratigraphy favourable. Iron-magnesium and Si alteration has been mapped in this area. PC-1 (Cu) scores above the 90th percentile range are present and Zn concentrations in the till are present above the 80th percentile. Geophysical responses are variable but are generally high for magnetics and moderate for VLF and gravity.

The area labelled 4e is located 2 km south of Stall Lake between the Linda 1 and Linda 2 deposits. The area is underlain predominately by an aphyric phase of the Anderson Rhyolite proximal to heat sources. A number of alteration pipes characterized by pervasive staurolite/sericite/biotite alteration have been mapped. Small amounts of Fe-Mg alteration have also been mapped. Till geochemistry is not favourable, however, lake sediment geochemistry shows a moderately high PC-2 (Zn) signature. The geophysical factor is typified by a high magnetic response and low VLF and gravity response.

Area 5

Area 5 is located north of Sneath Lake in the south central part of the study area. The presence of rhyolite flows and proximity to heat sources make this area stratigraphically favourable.

Iron-magnesium alteration has been mapped in the area and Si alteration 1.5 km to the northeast. No till samples were taken in the area and lake sediment geochemistry shows a moderately strong PC-2 (Zn) signature for the area. The magnetic signature is high and both VLF and gravity show moderately high responses.

Area 6

Area 6 is a large region to the northeast of Morgan Lake extending for approximately 5 km between Hirst Lake in the south to Daly Lake in the north. This zone contains the Pot Lake and Tear Drop occurrences.

The general wedge shape of this area reflects the underlying rhyolites (Daly Lake Rhyolites). Small amounts of felsic volcanoclastic units are also present. Tonalite sills and synvolcanic dykes are both within 1 km of the area. Alteration is present in the form of Fe-Mg metasomatism and is proximal to Si alteration mapped to the west. No till samples were collected in the area and lake sediment geochemistry generally showed background values though PC-3 had a moderately strong signature. The magnetic response for the area was generally high while the VLF and gravity responses were variable.

Area 7

Area 7 is located to the northeast of Daly Lake. This is a favourable stratigraphic zone, underlain by felsic flows mapped and close to a possible heat source. It is proximal to Si and Fe-Mg alteration. Till geochemistry showed background concentrations of Cu, Pb, and Zn and the lake sediment geochemistry showed a strong PC-1 (Cu) signature for this area. Regional geophysical data indicated high magnetic responses and moderately high VLF and gravity responses.

REFERENCES

- Agterberg, F.P.**
1989: Systematic approach to dealing with uncertainty of geoscience information in mineral exploration; in *Proceedings 21st Symposium on the Application of Computers in the Mineral Industries*, Las Vegas, March 1989, p. 165-178.
- Agterberg, F.P., Bonham-Carter, G.F., and Wright, D.F.**
1990: Statistical pattern integration for mineral exploration; in *Computer Applications in Resource Estimation Prediction and Assessment for Metals and Petroleum*, (ed.) G. Gaal and D.F. Merriam; Pergamon Press, Oxford-New York, p. 1-21.
- An, P.**
1992: Spatial reasoning techniques and integration of geophysical and geological information for resource exploration; PhD. dissertation, The University of Manitoba, Winnipeg, Manitoba, 162 p.
- An, P., Moon, W.M., and Bonham-Carter, G.F.**
1992: On a knowledge-based approach of integrating remote-sensing, geophysical and geological information; *Proceedings International Geoscience and Remote Sensing Symposium*, Houston, Texas, May 26, 1992, p. 34-38.
- 1994a: Uncertainty management in integration of exploration data using the belief function; *Nonrenewable Resources*, v. 3, no. 1, p. 60-71.
- 1994b: An object-oriented knowledge representation structure for exploration data integration; *Nonrenewable Resources*, v. 3, no. 2, p. 132-145.
- An, P., Moon, W.M., and Rencz, A.**
1991: Application of fuzzy set theory for integration of geological, geophysical and remote sensing data; *Canadian Journal of Exploration Geophysics*, v. 27, p. 1-11.
- Bailes, A.H.**
1987: GS-12 Chisel-Morgan Lakes Project; in *Report of Activities 1987*, Manitoba Energy and Mines, Minerals Division, p. 70-78.
- 1990a: Chisel-Anderson Project (NTS 63K/16SE); in *Report of Activities 1990*, Manitoba Energy and Mines, Mineral Division, p. 43-48.
- 1990b: Geology of the Chisel-Morgan-Anderson Lake area; Manitoba Energy and Mines, Minerals Division, Preliminary Map 1990S-1, scale 1:20 000.
- Bailes, A.H. and Galley, A.G.**
1989: Geological setting of and hydrothermal alteration below the Chisel Lake massive Zn-Cu sulphide deposit; in *Report of Field Activities 1989*, Manitoba Energy and Mines, Minerals Division, Report of Field Activities, p. 31-37.
- 1991: Geological setting of base metal mineralization in Anderson area; in *Report of Activities 1991*, Manitoba Energy and Mines, Minerals Division, p. 8-13.
- 1992a: Chisel-Anderson-Morgan Lakes; Manitoba Energy and Mines, Preliminary Map 1992 S-1, scale 1:20 000.
- 1992b: Wekusko Lake (North); Manitoba Energy and Mines, Preliminary Map 1992 S-2, scale 1:20 000.
- 1996: Setting of Paleoproterozoic volcanic-hosted massive base metal sulphide deposits, Snow Lake; in *EXTECH I: A Multidisciplinary Approach to Massive Sulphide Research in the Rusty Lake-Snow Lake Greenstone Belts*, (ed.) G.F. Bonham-Carter, A.G. Galley, and G.E.M. Hall; Geological Survey of Canada, Bulletin 426.
- Bonham-Carter, G.F.**
1994a: *Geographic Systems for Geoscientists: Modelling with GIS*; Pergamon Press, Oxford, 398 p.
- 1994b: When to use the weights of evidence method for map data; in *Proceedings of Workshop on Spatial Modelling*, Macaulay Land Research Institute, Aberdeen Scotland, September 1-2, 1994.
- Bonham-Carter, G.F. and Agterberg, F.P.**
1990: Application of a microcomputer-based geographic information system to mineral potential mapping; in *Microcomputers in Geology*, Volume 2, (ed.) T. Hanley and D.F. Merriam; Pergamon Press, Oxford, p. 49-74.
- Bonham-Carter, G.F., Agterberg, F.P., and Wright, D.F.**
1988: Integration of geological datasets for gold exploration in Nova Scotia; *Photogrammetry and Remote Sensing*, v. 54, no. 11, p. 1585-1592.
- 1989: Weights of evidence modelling: a new approach to mapping mineral potential; in *Statistical Applications in the Earth Sciences*, (ed.) F.P. Agterberg and G.F. Bonham-Carter; Geological Survey of Canada, Paper 89-9, p. 171-183.
- Bonham-Carter, G.F., Reddy, R.K.T., and Galley, A.G.**
1994: Knowledge-driven modeling of volcanogenic massive sulphide potential with a geographic information system; in *Mineral Deposit Modeling*, (ed.) R.V. Kirkham, W.D. Sinclair, R.I. Thorpe, and J.M. Duke; Geological Association of Canada, Special Paper 40, p. 735-749.
- Chung, C.F. and Fabbri, A.G.**
1993: The representation of geoscience information for data integration; *Nonrenewable Resources*, v. 2, no. 2, p. 122-139.
- Chung, C.F. and Moon, W.M.**
1991: Combination rules of spatial geoscience data for mineral exploration; *Geoinformatics*, v. 2, no. 2, p. 159-169.
- Defense Mapping Agency**
1981: Product specifications for digital terrain elevation data (DTED); Defense Mapping Agency, Aerospace Center, St. Louis Air Force Station, Missouri., Stock No. SPECXDTED, 23 p.
- Dempster, A.P.**
1968: A generalization of Bayesian inference; *Journal Royal Statistical Society*, ser. B, v. 30, p. 205-247.
- Fedikow, M.A., Athayde, P., and Galley, A.G.**
1993a: Mineral deposits and occurrences in the Wekusko Lake area, NTS 63J/13; Manitoba Energy and Mines, Mineral Deposit Series Report No. 14, 460 p.
- 1993b: MDS Map 14, Mineral Deposits and Occurrences in the File Lake area, Manitoba (NTS 63J/13); Manitoba Department of Mines and Energy, Mineral Deposits Series, MDS map 14, scale 1:50 000.

- Fedikow, M.A., Ostry, G., Ferreira, K.J., and Galley, A.G.**
1988a: Mineral deposits and occurrences in the File Lake area, NTS 63K/16; Manitoba Energy and Mines, Mineral Deposit Series, Report No. 5, 277 p., Mineral Deposit Series, Map No. 5, scale 1:50 000.
1988b: Mineral deposits and occurrences in the File Lake area, NTS 63K/16; Manitoba Department of Mines and Energy, Mineral Deposit Series, Map 5, scale 1:50 000.
- Friske, P.W. and McCurdy, M.W.**
1996: Results of a detailed infill lake-sediment survey in the Snow Lake area: evaluation and comparison of grab sample and short core data; in EXTECH I: A Multidisciplinary Approach to Massive Sulphide Research in the Rusty Lake-Snow Lake Greenstone Belts, Manitoba, (ed.) G.F. Bonham-Carter, A.G. Galley, and G.E.M. Hall; Geological Survey of Canada, Bulletin 426.
- Friske, P.F., McCurdy, M.W., Day, S.J.A., Gross, H., Lynch, J.J., and Durham, C.C.**
1995: National Geochemical Reconnaissance lake sediment and water data, Snow Lake area, Manitoba (NTS 63J/13W and 63K/16E); Geological Survey of Canada, Open File 3015.
- Galley, A.G.**
1993: Characteristics of semi-conformable alteration zones associated with volcanic massive sulphide districts; *Journal of Geochemical Exploration*, v. 48, p. 175-200.
- Galley, A.G., Bales, A.H., and Kistler, G.**
1993: Geological setting and hydrothermal evolution for the Chisel Lake and North Chisel Zn-Pb-Ag-Au massive sulphide deposit, Snow Lake, Manitoba; *Exploration and Mining Geology*, v. 2, p. 271-295.
- Gobert, G. and Nielsen, E.**
1991: Till geochemistry of the Snow Lake File Lake area (NTS 63K/16 and 63J/13); in Report of Activities 1991, Manitoba Energy and Mines, Mineral Division, p. 47-48.
- Goodacre, A., Bonham-Carter, G.F., Agterberg, F.P., and Wright, D.F.**
1993: A statistical analysis of spatial associations of seismicity with drainage patterns and magnetic anomalies in western Quebec; *Tectonophysics*, v. 217, p. 205-305.
- Goodacre, A.K., Grieve, R.A.F., and Halpeny, J.F.**
1987: Observed gravity values of Canada; Geological Survey of Canada, Canadian Geophysical Atlas, Map 1, scale 1:10 000 000.
- Hetu, R.**
1991: Airborne Geophysical Survey of the Snow Lake area, Manitoba; Geological Survey of Canada, Open File 2300.
- Kaszycki, C.A., Neilsen, E., and Gobert, G.**
1996: Surficial geochemistry and response to volcanic-hosted massive sulphide mineralization in the Snow Lake region; in EXTECH I: A Multidisciplinary Approach to Massive Sulphide Research in the Rusty Lake-Snow Lake Greenstone Belts, Manitoba, (ed.) G.F. Bonham-Carter, A.G. Galley, and G.E.M. Hall; Geological Survey of Canada, Bulletin 426.
- Knox-Robinson, C.M.**
1994: Archean lode gold mineralisation potential of portion of the Yilgarn Block Western Australia: Development and implementation of methodology for the creation of the regional-scale prospectivity maps using conventional geological map data and a geographic information system (GIS); PhD. dissertation, University of Western Australia, Perth, Australia, 178 p.
- Reddy, R.K.T. and Bonham-Carter, G.F.**
1991: A decision-tree approach to mineral potential mapping in Snow Lake area, Manitoba; *Canadian Journal of Remote Sensing*, v. 17, p. 191-200.
- Reddy, R.K.T., Agterberg, F.P., and Bonham-Carter, G.F.**
1991: Application of GIS-based logistic models to base-metal potential mapping in Snow Lake area, Manitoba; in Proceedings Canadian Conference on GIS, Ottawa, Canada, March 18-22, 1991, p. 607-618.
- Reddy, R.K.T., Bonham-Carter, G.F., and Galley, A.G.**
1992: Developing a geographic expert system for regional mapping of volcanogenic massive sulfide (VHMS) deposit potential; *Nonrenewable Resources*, v. 1, no. 2, p. 112-124.
- Reddy, R.K.T., Bonham-Carter, G.F., and Wright, D.F.**
1990: GIS for mapping mineral resource potential: preliminary results of a base-metal study, Snow Lake area, Manitoba; in Proceedings of GIS for the 1990s Conference, Ottawa, Canada Ontario, March 5-9, 1990, p. 384-400.
- Shafer, G.**
1976: *A Mathematical Theory of Evidence*; Princeton University Press, New Jersey, 297 p.
- Shives, R.B.K.**
1996: Application of multiparameter geophysical data (gamma ray, magnetics, VLF-EM) to mapping and exploration in Snow Lake and Rusty Lake areas, Manitoba; in EXTECH I: A Multidisciplinary Approach to Massive Sulphide Research in the Rusty Lake-Snow Lake Greenstone Belts, Manitoba, (ed.) G.F. Bonham-Carter, A.G. Galley, and G.E.M. Hall; Geological Survey of Canada, Bulletin 426.
- Singer, D.A.**
1993: Basic concepts in three-part quantitative assessments of undiscovered mineral resources; *Nonrenewable Resources*, v. 2, no. 2, p. 69-81.
- Sinha, A.K. and Palacky, G.J.**
1996: Ground electro-magnetic, magnetic and VLF-EM surveys at 4 sites near Snow Lake, Manitoba; in EXTECH I: A Multidisciplinary Approach to Massive Sulphide Research in the Rusty Lake-Snow Lake Greenstone Belts, Manitoba, (ed.) G.F. Bonham-Carter, A.G. Galley, and G.E.M. Hall; Geological Survey of Canada, Bulletin 426.
- Syme, E.C. and Bales, A.H.**
1993: Stratigraphic and tectonic setting of Early Proterozoic volcanogenic massive sulfide deposits, Flin Flon, Manitoba; *Economic Geology*, v. 88, p. 566-589.
- Wright, D.F.**
1996: Evaluating Volcanic-Hosted Massive Sulphide Favourability using GIS-based spatial data integration models, Snow Lake area, Manitoba; PhD. dissertation, University of Ottawa, Ottawa, Canada, 338 p.

Contribution to the 1989-1994 Rusty Lake-Snow Lake Mining Camps, Canada-Manitoba Exploration Science and Technology Initiative (EXTECH I)

Table A1. Lookup table relating classes on 1:20 000 geological map to smaller set of simplified geological units, used in favourability mapping.

| Chisel Lake-Morgan Lake-Anderson Lake analog map legend (1:20 000) | Code | Digital Map Code | Simplified Digital Map Legend | Code |
|---|------|---------------------|-------------------------------|------|
| PROTEROZOIC | | | | |
| Post-Amisk intrusive rocks | | | | |
| Ham Lake Pluton | 30 | 1 | Post-Amisk intrusive rocks | 1 |
| a) up to 30% xenoliths | 30a | 2 | | 1 |
| Hornblende-phyric quartz diorite | 29 | 3 | | 1 |
| Granodiorite, tonalite | 28 | 4 | | 1 |
| a) equigranular, granodiorite | 28a | 5 | | 1 |
| b) hornblende-phyric tonalite | 28b | 6 | | 1 |
| c) hornblende-phyric tonalite with abundant xenoliths | 28c | 7 | | 1 |
| Pyroxenite, metagabbro | 27 | 8 | | 1 |
| Mafic intrusive complex: gabbro, diorite, quartz diorite | 26 | 9 | | 1 |
| a) intrusion breccia | 26a | 10 | | 1 |
| b) dyke complex | 26b | 11 | | 1 |
| Chisel Lake Intrusion | 25 | 12 | | 1 |
| a) lower and upper peridotite | 25a | 13 | | 1 |
| b) pyroxenite | 25b | 14 | | 1 |
| c) lower gabbro | 25c | 15 | | 1 |
| d) middle gabbro | 25d | 16 | | 1 |
| e) upper gabbro | 25e | 17 | | 1 |
| f) gabbro pyroxenite | 25f | 18 | | 1 |
| Amisk intrusive rocks | | | | |
| Quartz-phyric tonalite, tonalite | 24 | 19 | | 8 |
| a) quartz-phyric (3-8 mm phenocrysts) | 24a | 20 | Subvolcanic tonalite sills | 8 |
| b) quartz-phyric (10-20 mm phenocrysts) | 24b | 21 | | 8 |
| c) quartz-plagioclase-phyric | 24c | 22 | | 8 |
| d) equigranular | 24d | 23 | | 8 |
| e) fine grained (1 mm and less) | 24e | 24 | | 8 |
| f) abundant xenoliths | 24f | 25 | | 8 |
| g) intrusion breccia | 24g | 26 | | 8 |
| Fine grained tonalite/felsic intrusions | 23 | 27 | | 8 |
| a) equigranular | 23a | 28 | | 8 |
| b) plagioclase-phyric | 23b | 29 | | 8 |
| Quartz porphyry, quartz-plagioclase porphyry | 22 | 30 | Synvolcanic intrusive rocks | 9 |
| a) phenocrysts smaller than 5 mm | 22a | 31 | | 9 |
| b) phenocrysts greater than 5 mm | 22b | 32 | | 9 |
| c) dyke complex | 22c | 33 | | 9 |
| d) breccia | 22d | 34 | | 9 |
| e) mesocratic, portions pyroxene-phyric | 22e | 35 | | 9 |
| Dacite intrusions | 21 | 36 | | 9 |
| a) plagioclase-phyric | 21a | 37 | | 9 |
| b) dyke complex | 21b | 38 | | 9 |
| Pyroxene and pyroxene-plagioclase-phyric diorite | 20 | 39 | | 9 |
| a) pyroxene-plagioclase-quartz-phyric quartz diorite | 20a | 40 | | 9 |
| b) intrusion breccia | 20b | 41 | | 9 |
| Gabbro, diorite, quartz diorite | 19 | 42 | | 9 |
| a) fine- to medium-grained | 19a | 43 | | 9 |
| b) medium grained | 19b | 44 | | 9 |
| c) coarse grained | 19c | 45 | | 9 |
| d) plagioclase-phyric | 19d | 46 | | 9 |
| e) pyroxene-phyric, pyroxene-plagioclase-phyric | 19e | 47 | | 9 |
| f) quartz diorite, melatonalite, tonalite | 19f | 48 | | 9 |
| g) magnetiferous diorite, quartz diorite, tonalite | 19g | 49 | | 9 |
| AMISK GROUP | | | | |
| Sedimentary rocks | | | | |
| Parisian Formation: Paraconglomerate, minor greywacke | 18 | 50 | Missi turbidite assemblage | 7 |
| a) greywacke, mudstone | 18a | 51 | | 7 |
| Greywacke, siltstone, mudstone | 17 | 52 | | 7 |

Table A1. (cont.)

| Chisel Lake-Morgan Lake-Anderson Lake analog map legend (1:20 000) | Code | Digital Map Code | Simplified Digital Map Legend | Code |
|---|------|---------------------|-------------------------------|------|
| Heterolithic volcanic breccia | | | | |
| Mixed mafic and felsic heterolithic volcanic breccia | 16 | 53 | Mixed volcaniclastic rocks | 6 |
| a) mainly mafic fragments | 16a | 54 | | 6 |
| b) mainly felsic fragments | 16b | 55 | | 6 |
| Heterolithic mafic volcanic breccia | 15 | 56 | | 6 |
| Felsic volcaniclastic rocks | | | | |
| Felsic volcanic breccia and minor wacke | 14 | 57 | Felsic volcaniclastic rocks | 4 |
| a) contains 10-50% mafic volcanic breccia and wacke | 14a | 58 | | 4 |
| b) related volcanic wacke and mudstone | 14b | 59 | | 4 |
| Dacite tuff, lapilli tuff | 13 | 60 | | 4 |
| Mafic volcaniclastic rocks | | | | |
| Mafic volcanic wacke | 12 | 61 | Mafic volcaniclastic rocks | 5 |
| a) mainly porphyritic fragments | 12a | 62 | | 5 |
| Mafic monolithic volcanic breccia | 11 | 63 | | 5 |
| a) aphyric | 11a | 64 | | 5 |
| b) plagioclase-phyric | 11b | 65 | | 5 |
| c) pyroxene-phyric, pyroxene-plagioclase-phyric | 11c | 66 | | 5 |
| Mafic tuff, lapilli tuff, tuff breccia, wacke | 10 | 67 | | 5 |
| Felsic flows | | | | |
| Fine grained quartz-feldspathic metamorphic rocks | 9 | 68 | Felsic flows | 2 |
| a) quartz-phyric | 9a | 69 | | 2 |
| b) fragmental | 9b | 70 | | 2 |
| c) plagioclase-phyric | 9c | 71 | | 2 |
| d) large quartz amygdales | 9d | 72 | | 2 |
| Massive quartz-phyric rhyolite | 8 | 73 | | 2 |
| Massive rhyolite lobes enveloped by breccia | 7 | 74 | | 2 |
| a) quartz-phyric | 7a | 75 | | 2 |
| b) quartz-plagioclase-phyric | 7b | 76 | | 2 |
| Mafic flows | | | | |
| Fine grained mafic metamorphic rocks | 6 | 77 | Mafic flows | 3 |
| a) porphyritic | 6a | 78 | | 3 |
| b) fragmental | 6b | 79 | | 3 |
| Pillow fragment breccia | 5 | 80 | | 3 |
| a) aphyric | 5a | 81 | | 3 |
| b) porphyritic | 5b | 82 | | 3 |
| Pyroxene-phyric flows, pyroxene-plagioclase-phyric flows | 4 | 83 | | 3 |
| a) pillow fragment breccia | 4a | 84 | | 3 |
| b) amoeboid pillow breccia, thin pillowed flows | 4b | 85 | | 3 |
| Plagioclase-phyric flows | 3 | 86 | | 3 |
| a) pillow fragment breccia | 3a | 87 | | 3 |
| b) amoeboid pillow breccia, thin pillowed flows | 3b | 88 | | 3 |
| Sparsely pyroxene-phyric flows, aphyric flows | 2 | 89 | | 3 |
| a) pillow fragment breccia | 2a | 90 | | 3 |
| b) amoeboid pillow breccia, thin pillowed flows | 2b | 91 | | 3 |
| Aphyric flows | 1 | 92 | | 3 |
| a) pillow fragment breccia | 1a | 93 | | 3 |
| b) amoeboid pillow breccia, thin pillowed flows | 1b | 94 | | 3 |

Table A2. Fuzzy membership and Dempster-Shafer functions for each map used as evidence.

| Data set | $\mu_A(x)^1$ | SCP ² | Spt _A ³ | Dis _A ⁴ | Unc _A ⁵ | Data set | $\mu_A(x)^1$ | SCP ² | Spt _A ³ | Dis _A ⁴ | Unc _A ⁵ |
|--|--------------|------------------|-------------------------------|-------------------------------|-------------------------------|---------------------------------|--------------|------------------|-------------------------------|-------------------------------|-------------------------------|
| Fe-Mg alteration buffers | | | | | | Alteration pipes | | | | | |
| ON Alteration | 0.75 | 0.4 | 0.0040 | 0.0008 | 0.9954 | ON alteration | 0.90 | 0.80 | 0.0080 | 0.0002 | 0.9918 |
| 0.00 - 0.25 km | 0.75 | 0.2 | 0.0020 | 0.0008 | 0.9972 | 0.00 - 0.25 km | 0.90 | 0.80 | 0.0080 | 0.0002 | 0.9918 |
| 0.25 - 0.50 km | 0.60 | 0.1 | 0.0010 | 0.0009 | 0.9981 | 0.25 - 0.50 km | 0.70 | 0.50 | 0.0050 | 0.0005 | 0.9945 |
| 0.50 - 0.75 km | 0.60 | 0.1 | 0.0010 | 0.0009 | 0.9981 | 0.50 - 0.75 km | 0.70 | 0.30 | 0.0030 | 0.0007 | 0.9963 |
| 0.75 - 1.00 km | 0.55 | 0.07 | 0.0007 | 0.0009 | 0.9983 | 0.75 - 1.00 km | 0.65 | 0.50 | 0.0050 | 0.0005 | 0.9945 |
| 1.00 - 1.25 km | 0.50 | 0.07 | 0.0007 | 0.0009 | 0.9983 | 1.00 - 1.25 km | 0.60 | 0.30 | 0.0030 | 0.0007 | 0.9963 |
| 1.25 - 1.50 km | 0.45 | 0.05 | 0.0005 | 0.0009 | 0.9985 | 1.25 - 1.50 km | 0.55 | 0.20 | 0.0020 | 0.0008 | 0.9972 |
| 1.50 - 1.75 km | 0.40 | 0.05 | 0.0005 | 0.0009 | 0.9985 | 1.50 - 1.75 km | 0.40 | 0.10 | 0.0010 | 0.0009 | 0.9981 |
| 1.75 - 2.00 km | 0.35 | 0.02 | 0.0002 | 0.0009 | 0.9988 | 1.75 - 2.00 km | 0.35 | 0.10 | 0.0010 | 0.0009 | 0.9981 |
| > 2.00 km | 0.10 | 0.01 | 0.0001 | 0.0010 | 0.9989 | > 2.00 km | 0.10 | 0.05 | 0.0005 | 0.0009 | 0.9985 |
| Silica alteration buffers | | | | | | Pb in tills | | | | | |
| ON Alteration | 0.70 | 0.20 | 0.0020 | 0.0008 | 0.9972 | > 98th percentile | 0.80 | 0.50 | 0.0050 | 0.0005 | 0.9945 |
| 0.00 - 0.25 km | 0.70 | 0.20 | 0.0020 | 0.0008 | 0.9972 | > 95th percentile | 0.76 | 0.30 | 0.0030 | 0.0007 | 0.9963 |
| 0.25 - 0.50 km | 0.65 | 0.15 | 0.0015 | 0.0008 | 0.9976 | > 90th percentile | 0.73 | 0.20 | 0.0020 | 0.0008 | 0.9972 |
| 0.50 - 0.75 km | 0.60 | 0.15 | 0.0015 | 0.0008 | 0.9976 | > 80th percentile | 0.70 | 0.06 | 0.0006 | 0.0009 | 0.9984 |
| 0.75 - 1.00 km | 0.50 | 0.10 | 0.0010 | 0.0009 | 0.9981 | > 70th percentile | 0.67 | 0.05 | 0.0005 | 0.0009 | 0.9985 |
| 1.00 - 1.25 km | 0.50 | 0.10 | 0.0010 | 0.0009 | 0.9981 | > 50th percentile | 0.65 | 0.04 | 0.0004 | 0.0009 | 0.9986 |
| 1.25 - 1.50 km | 0.45 | 0.08 | 0.0008 | 0.0009 | 0.9982 | < 50th percentile | 0.10 | 0.02 | 0.0002 | 0.0008 | 0.9988 |
| 1.50 - 1.75 km | 0.40 | 0.05 | 0.0005 | 0.0009 | 0.9985 | NO DATA | 0.65 | 0.00 | 0.0000 | 0.0000 | 1.0000 |
| 1.75 - 2.00 km | 0.35 | 0.02 | 0.0002 | 0.0009 | 0.9988 | | | | | | |
| > 2.00 km | 0.10 | 0.01 | 0.0001 | 0.0010 | 0.9989 | | | | | | |
| Amphibole alteration buffers | | | | | | Zn in tills | | | | | |
| ON alteration | 0.70 | 0.10 | 0.0010 | 0.0009 | 0.9981 | > 98th percentile | 0.80 | 0.20 | 0.0020 | 0.0008 | 0.9972 |
| 0.00 - 0.25 km | 0.70 | 0.20 | 0.0020 | 0.0008 | 0.9972 | > 95th percentile | 0.76 | 0.20 | 0.0020 | 0.0008 | 0.9972 |
| 0.25 - 0.50 km | 0.65 | 0.20 | 0.0020 | 0.0008 | 0.9972 | > 90th percentile | 0.73 | 0.15 | 0.0015 | 0.0008 | 0.9976 |
| 0.50 - 0.75 km | 0.65 | 0.15 | 0.0015 | 0.0008 | 0.9976 | > 80th percentile | 0.70 | 0.10 | 0.0010 | 0.0009 | 0.9981 |
| 0.75 - 1.00 km | 0.55 | 0.15 | 0.0015 | 0.0008 | 0.9976 | > 70th percentile | 0.67 | 0.08 | 0.0008 | 0.0009 | 0.9982 |
| 1.00 - 1.25 km | 0.50 | 0.10 | 0.0010 | 0.0009 | 0.9981 | > 50th percentile | 0.65 | 0.07 | 0.0007 | 0.0009 | 0.9983 |
| 1.25 - 1.50 km | 0.45 | 0.10 | 0.0010 | 0.0009 | 0.9981 | < 50th percentile | 0.10 | 0.05 | 0.0005 | 0.0009 | 0.9985 |
| 1.50 - 1.75 km | 0.40 | 0.05 | 0.0005 | 0.0009 | 0.9985 | NO DATA | 0.65 | 0.00 | 0.0000 | 0.0000 | 1.0000 |
| 1.75 - 2.00 km | 0.35 | 0.05 | 0.0005 | 0.0009 | 0.9985 | | | | | | |
| > 2.00 km | 0.10 | 0.01 | 0.0001 | 0.0010 | 0.9989 | | | | | | |
| Epidote-hematite alteration buffers | | | | | | Cu in tills | | | | | |
| ON Alteration | 0.65 | 0.10 | 0.0001 | 0.0009 | 0.9981 | > 98th percentile | 0.80 | 0.30 | 0.0030 | 0.0007 | 0.9963 |
| 0.00 - 0.25 km | 0.65 | 0.20 | 0.0020 | 0.0008 | 0.9972 | > 95th percentile | 0.76 | 0.20 | 0.0020 | 0.0008 | 0.9972 |
| 0.25 - 0.50 km | 0.55 | 0.30 | 0.0030 | 0.0007 | 0.9963 | > 90th percentile | 0.73 | 0.10 | 0.0010 | 0.0009 | 0.9981 |
| 0.50 - 0.75 km | 0.55 | 0.20 | 0.0020 | 0.0008 | 0.9972 | > 80th percentile | 0.70 | 0.05 | 0.0005 | 0.0009 | 0.9985 |
| 0.75 - 1.00 km | 0.55 | 0.20 | 0.0020 | 0.0008 | 0.9972 | > 70th percentile | 0.67 | 0.04 | 0.0004 | 0.0009 | 0.9986 |
| 1.00 - 1.25 km | 0.50 | 0.15 | 0.0015 | 0.0008 | 0.9976 | > 50th percentile | 0.65 | 0.02 | 0.0002 | 0.0008 | 0.9988 |
| 1.25 - 1.50 km | 0.35 | 0.15 | 0.0015 | 0.0008 | 0.9976 | < 50th percentile | 0.10 | 0.01 | 0.0001 | 0.0009 | 0.9989 |
| 1.50 - 1.75 km | 0.30 | 0.10 | 0.0010 | 0.0009 | 0.9981 | NO DATA | 0.65 | 0.00 | 0.0000 | 0.0000 | 1.0000 |
| 1.75 - 2.00 km | 0.30 | 0.10 | 0.0010 | 0.0009 | 0.9981 | | | | | | |
| > 2.00 km | 0.10 | 0.05 | 0.0005 | 0.0009 | 0.9985 | | | | | | |
| Generalized geology | | | | | | Lake sediment geochemistry PC-1 | | | | | |
| Post-Amisk lithologies | 0.00 | -0.00 | 0.0000 | 1.0000 | 0.0000 | No Data | 0.50 | 0.00 | 0.000 | 0.000 | 1.000 |
| Felsic flows | 0.80 | 0.40 | 0.0040 | 0.0006 | 0.9954 | > 98th Percentile | 0.73 | 0.30 | 0.003 | 0.0009 | 0.9987 |
| Mafic flows | 0.60 | 0.05 | 0.0005 | 0.0009 | 0.9985 | > 95th Percentile | 0.70 | 0.20 | 0.002 | 0.0008 | 0.9972 |
| Felsic volcanoclastic rocks | 0.20 | 0.15 | 0.0015 | 0.0008 | 0.9976 | > 90th Percentile | 0.67 | 0.05 | 0.0005 | 0.0009 | 0.9985 |
| Mafic volcanoclastic rocks | 0.30 | 0.10 | 0.0010 | 0.0009 | 0.9981 | > 80th Percentile | 0.60 | 0.04 | 0.0004 | 0.0009 | 0.9986 |
| Heterolithic volcanoclastic rocks | 0.10 | 0.10 | 0.0010 | 0.0009 | 0.9981 | > 70th Percentile | 0.50 | 0.03 | 0.0003 | 0.0009 | 0.9987 |
| Other sedimentary rocks | 0.01 | 0.01 | 0.0001 | 0.0010 | 0.9989 | > 50th Percentile | 0.30 | 0.02 | 0.0002 | 0.0009 | 0.9988 |
| Subvolcanic intrusions | 0.00 | 0.005 | 0.0001 | 0.0009 | 0.9990 | < 50th Percentile | 0.10 | 0.02 | 0.0002 | 0.0009 | 0.9988 |
| Synvolcanic intrusions | 0.40 | 0.20 | 0.0020 | 0.0008 | 0.9972 | | | | | | |
| Unmapped | 0.00 | 0.00 | 0.0000 | 0.0000 | 1.0000 | | | | | | |
| ¹ $\mu(x)$ = fuzzy membership function ² SCP = smoothed calculated probability ³ Spt _A = support or belief function ⁴ Dis _A = disbelief function ⁵ Unc _A = uncertainty = 1 - Spt _A - Dis _A | | | | | | | | | | | |

Table A2 (cont.)

| Data set | $\mu_A(x)^1$ | SCP ² | Spt _A ³ | Dis _A ⁴ | Unc _A ⁵ | Data set | $\mu_A(x)^1$ | SCP ² | Spt _A ³ | Dis _A ⁴ | Unc _A ⁵ |
|-------------------------------|--------------|------------------|-------------------------------|-------------------------------|-------------------------------|----------------------|--------------|------------------|-------------------------------|-------------------------------|-------------------------------|
| Proximity to felsic flows | | | | | | Lake sediment | | | | | |
| ON flow | 0.20 | 0.40 | 0.0040 | 0.0006 | 0.9954 | geochemistry PC-2 | 0.50 | 0.00 | 0.0000 | 0.0000 | 1.0000 |
| 0.00 - 0.25 km | 0.90 | 0.25 | 0.0025 | 0.0007 | 0.9967 | No Data | 0.73 | 0.30 | 0.0030 | 0.0009 | 0.9987 |
| 0.25 - 0.50 km | 0.85 | 0.10 | 0.0020 | 0.0009 | 0.9981 | > 98th Percentile | 0.70 | 0.10 | 0.0020 | 0.0009 | 0.9981 |
| 0.50 - 0.75 km | 0.80 | 0.05 | 0.0005 | 0.0009 | 0.9985 | > 95th Percentile | 0.67 | 0.10 | 0.0020 | 0.0009 | 0.9981 |
| 0.75 - 1.00 km | 0.70 | 0.045 | 0.0004 | 0.0009 | 0.9985 | > 90th Percentile | 0.60 | 0.05 | 0.0005 | 0.0009 | 0.9985 |
| 1.00 - 1.25 km | 0.60 | 0.04 | 0.0004 | 0.0009 | 0.9986 | > 80th Percentile | 0.40 | 0.05 | 0.0005 | 0.0009 | 0.9985 |
| 1.25 - 1.50 km | 0.40 | 0.03 | 0.0003 | 0.0009 | 0.9987 | > 70th Percentile | 0.30 | 0.02 | 0.0002 | 0.0009 | 0.9988 |
| 1.50 - 1.75 km | 0.30 | 0.02 | 0.0002 | 0.0009 | 0.9988 | > 50th Percentile | 0.10 | 0.01 | 0.0001 | 0.0010 | 0.9989 |
| 1.75 - 2.00 km | 0.20 | 0.01 | 0.0001 | 0.0010 | 0.9989 | < 50th Percentile | | | | | |
| > 2.00 km | 0.01 | 0.01 | 0.0001 | 0.0010 | 0.9989 | | | | | | |
| Proximity to mafic volcanics | | | | | | Lake sediment | | | | | |
| ON Unit | 0.20 | 0.20 | 0.0020 | 0.0008 | 0.9972 | geochemistry PC-3 | | | | | |
| 0.00 - 0.25 km | 0.90 | 0.20 | 0.0020 | 0.0008 | 0.9972 | No Data | 0.50 | 0.00 | 0.0000 | 0.0000 | 1.0000 |
| 0.25 - 0.50 km | 0.85 | 0.20 | 0.0020 | 0.0008 | 0.9972 | > 98th Percentile | 0.73 | 0.15 | 0.0010 | 0.0008 | 0.9976 |
| 0.50 - 0.75 km | 0.80 | 0.20 | 0.0020 | 0.0008 | 0.9972 | > 95th Percentile | 0.70 | 0.13 | 0.0010 | 0.0008 | 0.9978 |
| 0.75 - 1.00 km | 0.70 | 0.20 | 0.0020 | 0.0008 | 0.9972 | > 90th Percentile | 0.67 | 0.08 | 0.0008 | 0.0009 | 0.9982 |
| 1.00 - 1.25 km | 0.60 | 0.20 | 0.0020 | 0.0008 | 0.9972 | > 80th Percentile | 0.60 | 0.06 | 0.0006 | 0.0009 | 0.9984 |
| 1.25 - 1.50 km | 0.40 | 0.20 | 0.0020 | 0.0008 | 0.9972 | > 70th Percentile | 0.40 | 0.05 | 0.0005 | 0.0009 | 0.9985 |
| 1.50 - 1.75 km | 0.30 | 0.20 | 0.0020 | 0.0008 | 0.9972 | > 50th Percentile | 0.30 | 0.03 | 0.0003 | 0.0009 | 0.9987 |
| 1.75 - 2.00 km | 0.20 | 0.10 | 0.0010 | 0.0009 | 0.9981 | < 50th Percentile | 0.10 | 0.01 | 0.0001 | 0.0010 | 0.9989 |
| > 2.00 km | 0.01 | 0.01 | 0.0001 | 0.0010 | 0.9989 | | | | | | |
| Proximity to felsic volcanics | | | | | | | | | | | |
| ON alteration | 0.20 | 0.25 | 0.0020 | 0.0007 | 0.9967 | | | | | | |
| 0.00 - 0.25 km | 0.90 | 0.25 | 0.0020 | 0.0007 | 0.9967 | | | | | | |
| 0.25 - 0.50 km | 0.85 | 0.15 | 0.0010 | 0.0008 | 0.9976 | | | | | | |
| 0.50 - 0.75 km | 0.80 | 0.10 | 0.0010 | 0.0009 | 0.9981 | | | | | | |
| 0.75 - 1.00 km | 0.70 | 0.05 | 0.0005 | 0.0009 | 0.9985 | | | | | | |
| 1.00 - 1.25 km | 0.60 | 0.02 | 0.0002 | 0.0009 | 0.9988 | | | | | | |
| 1.25 - 1.50 km | 0.40 | 0.02 | 0.0002 | 0.0009 | 0.9988 | | | | | | |
| 1.50 - 1.75 km | 0.30 | 0.015 | 0.0001 | 0.0009 | 0.9988 | | | | | | |
| 1.75 - 2.00 km | 0.20 | 0.010 | 0.0001 | 0.0009 | 0.9989 | | | | | | |
| > 2.00 km | 0.01 | 0.005 | 0.0001 | 0.0009 | 0.9989 | | | | | | |
| Total Field VLF (%) | | | | | | Airborne total field | | | | | |
| | | | | | | magnetics | | | | | |
| 1 -16.5461 - -3.5122 | 0.20 | 0.01 | 0.0001 | 0.00099 | 0.99891 | 1 Low | 0.20 | 0.005 | 0.00005 | 0.00099 | 0.9989 |
| 2 -3.5122 - -2.7688 | 0.20 | 0.01 | 0.0001 | 0.00099 | 0.99891 | 2 | 0.20 | 0.01 | 0.0001 | 0.0009 | 0.9989 |
| 3 -2.7688 - -2.2215 | 0.20 | 0.02 | 0.0002 | 0.00098 | 0.99882 | 3 | 0.20 | 0.01 | 0.0001 | 0.0009 | 0.9989 |
| 4 -2.2215 - -1.7850 | 0.20 | 0.02 | 0.0002 | 0.00098 | 0.99882 | 4 | 0.20 | 0.010 | 0.0001 | 0.0009 | 0.9989 |
| 5 -1.7850 - -1.4185 | 0.20 | 0.02 | 0.0002 | 0.00098 | 0.99882 | 5 | 0.20 | 0.015 | 0.0015 | 0.00085 | 0.99886 |
| 6 -1.4185 - -1.1041 | 0.20 | 0.03 | 0.0003 | 0.00097 | 0.99873 | 6 | 0.20 | 0.015 | 0.0015 | 0.00085 | 0.99886 |
| 7 -1.1041 - -0.8426 | 0.20 | 0.03 | 0.0003 | 0.00097 | 0.99873 | 7 | 0.20 | 0.015 | 0.0015 | 0.00085 | 0.99886 |
| 8 -0.8426 - -0.6273 | 0.20 | 0.03 | 0.0003 | 0.00097 | 0.99873 | 8 | 0.20 | 0.02 | 0.0002 | 0.0009 | 0.99882 |
| 9 -0.6273 - -0.4409 | 0.20 | 0.04 | 0.0004 | 0.00096 | 0.99864 | 9 | 0.20 | 0.02 | 0.0002 | 0.0009 | 0.99882 |
| 10 -0.4409 - -0.2795 | 0.20 | 0.04 | 0.0004 | 0.00096 | 0.99864 | 10 | 0.20 | 0.02 | 0.0002 | 0.0009 | 0.99882 |
| 11 -0.2795 - -0.1269 | 0.20 | 0.04 | 0.0004 | 0.00096 | 0.99864 | 11 | 0.20 | 0.025 | 0.00025 | 0.00097 | 0.9987 |
| 12 -0.1269 - 0.0192 | 0.20 | 0.05 | 0.0005 | 0.00095 | 0.99855 | 12 | 0.20 | 0.025 | 0.00025 | 0.00097 | 0.9987 |
| 13 0.0192 - 0.1675 | 0.20 | 0.05 | 0.0005 | 0.00095 | 0.99855 | 13 | 0.20 | 0.025 | 0.00025 | 0.00097 | 0.9987 |
| 14 0.1675 - 0.3207 | 0.20 | 0.05 | 0.0005 | 0.00095 | 0.99855 | 14 | 0.20 | 0.030 | 0.0003 | 0.0009 | 0.9987 |
| 15 0.3207 - 0.4898 | 0.20 | 0.05 | 0.0005 | 0.00095 | 0.99855 | 15 | 0.20 | 0.030 | 0.0003 | 0.0009 | 0.9987 |
| 16 0.4898 - 0.6815 | 0.20 | 0.05 | 0.0005 | 0.00095 | 0.99855 | 16 | 0.20 | 0.030 | 0.0003 | 0.0009 | 0.9987 |
| 17 0.6815 - 0.9071 | 0.20 | 0.10 | 0.0010 | 0.00090 | 0.99810 | 17 | 0.20 | 0.030 | 0.0003 | 0.0009 | 0.9987 |
| 18 0.9071 - 1.1799 | 0.20 | 0.10 | 0.0010 | 0.00090 | 0.99810 | 18 | 0.20 | 0.030 | 0.0003 | 0.0009 | 0.9987 |
| 19 1.1799 - 1.5076 | 0.20 | 0.10 | 0.0010 | 0.00090 | 0.99810 | 19 | 0.20 | 0.04 | 0.0004 | 0.0009 | 0.9986 |
| 20 1.5076 - 1.9076 | 0.20 | 0.10 | 0.0010 | 0.00090 | 0.99810 | 20 | 0.20 | 0.05 | 0.0005 | 0.0009 | 0.9985 |
| 21 1.9076 - 2.4073 | 0.20 | 0.10 | 0.0010 | 0.00090 | 0.99810 | 21 | 0.70 | 0.10 | 0.0010 | 0.0009 | 0.9981 |
| 22 2.4073 - 3.0723 | 0.20 | 0.20 | 0.0020 | 0.0008 | 0.9972 | 22 | 0.70 | 0.15 | 0.0015 | 0.00085 | 0.9976 |
| 23 3.0723 - 4.0246 | 0.20 | 0.20 | 0.0020 | 0.0008 | 0.9972 | 23 | 0.70 | 0.15 | 0.0015 | 0.00085 | 0.9976 |
| 24 4.0246 - 5.9972 | 0.20 | 0.20 | 0.0020 | 0.0008 | 0.9972 | 24 | 0.20 | 0.2 | 0.0020 | 0.0008 | 0.9972 |
| 25 5.9972 - 24.6247 | 0.85 | 0.20 | 0.0020 | 0.0008 | 0.9972 | 25 High | 0.20 | 0.2 | 0.0020 | 0.0008 | 0.9972 |

Table A2 (cont.)

| Data set | $\mu_A(x)^1$ | SCP ² | Spt _A ³ | Dis _A ⁴ | Unc _A ⁵ | Data set | $\mu_A(x)^1$ | SCP ² | Spt _A ³ | Dis _A ⁴ | Unc _A ⁵ |
|--|--------------|------------------|-------------------------------|-------------------------------|-------------------------------|--------------------------------------|--------------|------------------|-------------------------------|-------------------------------|-------------------------------|
| Processed VLF | | | | | | Airborne vertical gradient magnetics | | | | | |
| 1 Low | | | | | | 1 Low | | | | | |
| 2 | | | | | | 2 | 0.20 | 0.01 | 0.00010 | 0.00099 | 0.99891 |
| 3 | 0.20 | 0.02 | 0.0002 | 0.000980 | 0.99882 | 3 | 0.20 | 0.01 | 0.00010 | 0.00099 | 0.99891 |
| 4 | 0.20 | 0.02 | 0.0002 | 0.000980 | 0.99882 | 4 | 0.20 | 0.02 | 0.00020 | 0.00098 | 0.99882 |
| 5 | 0.20 | 0.02 | 0.0002 | 0.000980 | 0.99882 | 5 | 0.20 | 0.02 | 0.00020 | 0.00098 | 0.99882 |
| 6 | 0.20 | 0.02 | 0.0002 | 0.000980 | 0.99882 | 6 | 0.20 | 0.02 | 0.00020 | 0.00098 | 0.99882 |
| 7 | 0.20 | 0.02 | 0.0002 | 0.000980 | 0.99882 | 7 | 0.20 | 0.02 | 0.00020 | 0.00098 | 0.99882 |
| 8 | 0.20 | 0.02 | 0.0002 | 0.000980 | 0.99882 | 8 | 0.20 | 0.02 | 0.00020 | 0.00098 | 0.99882 |
| 9 | 0.20 | 0.02 | 0.0002 | 0.000980 | 0.99882 | 9 | 0.20 | 0.03 | 0.00030 | 0.00097 | 0.99873 |
| 10 | 0.20 | 0.05 | 0.0005 | 0.000950 | 0.99855 | 10 | 0.20 | 0.03 | 0.00030 | 0.00097 | 0.99873 |
| 11 | 0.20 | 0.05 | 0.0005 | 0.000950 | 0.99855 | 11 | 0.20 | 0.03 | 0.00030 | 0.00097 | 0.99873 |
| 12 | 0.20 | 0.05 | 0.0005 | 0.000950 | 0.99855 | 12 | 0.20 | 0.03 | 0.00030 | 0.00097 | 0.99873 |
| 13 | 0.20 | 0.05 | 0.0005 | 0.000950 | 0.99855 | 13 | 0.20 | 0.03 | 0.00030 | 0.00097 | 0.99873 |
| 14 | 0.20 | 0.05 | 0.0005 | 0.000950 | 0.99855 | 14 | 0.20 | 0.04 | 0.00040 | 0.00096 | 0.99864 |
| 15 | 0.20 | 0.05 | 0.0005 | 0.000950 | 0.99855 | 15 | 0.20 | 0.04 | 0.00040 | 0.00096 | 0.99864 |
| 16 | 0.20 | 0.10 | 0.0010 | 0.00090 | 0.99810 | 16 | 0.20 | 0.04 | 0.00040 | 0.00096 | 0.99864 |
| 17 | 0.20 | 0.10 | 0.0010 | 0.00090 | 0.99810 | 17 | 0.20 | 0.04 | 0.00040 | 0.00096 | 0.99864 |
| 18 | 0.20 | 0.10 | 0.0010 | 0.00090 | 0.99810 | 18 | 0.20 | 0.05 | 0.00050 | 0.00095 | 0.99855 |
| 19 | 0.20 | 0.10 | 0.0010 | 0.00090 | 0.99810 | 19 | 0.02 | 0.05 | 0.00050 | 0.00095 | 0.99855 |
| 20 | 0.20 | 0.10 | 0.0010 | 0.00090 | 0.99810 | 20 | 0.20 | 0.05 | 0.00050 | 0.00095 | 0.99855 |
| 21 | 0.20 | 0.10 | 0.0010 | 0.00090 | 0.99810 | 21 | 0.20 | 0.10 | 0.0010 | 0.00090 | 0.99810 |
| 22 | 0.20 | 0.10 | 0.0010 | 0.00090 | 0.99810 | 22 | 0.90 | 0.10 | 0.0010 | 0.00090 | 0.99810 |
| 23 | 0.90 | 0.15 | 0.0015 | 0.00085 | 0.99765 | 23 | 0.90 | 0.10 | 0.0010 | 0.00090 | 0.99810 |
| 24 | 0.90 | 0.15 | 0.0015 | 0.00085 | 0.99765 | 24 | 0.90 | 0.15 | 0.0015 | 0.00085 | 0.99765 |
| 25 High | 0.90 | 0.20 | 0.0020 | 0.00080 | 0.99720 | 25 High | 0.20 | 0.15 | 0.0015 | 0.00085 | 0.99765 |
| | 0.90 | 0.25 | 0.0025 | 0.00075 | 0.99675 | | 0.20 | 0.15 | 0.0015 | 0.00085 | 0.99765 |
| | 0.90 | 0.30 | 0.0030 | 0.00070 | 0.99630 | | | | | | |
| Airborne vertical gradient gravity | 0.30 | 0.001 | 0.00001 | 0.00099 | 0.99899 | Proximity to subvolcanic sills | 0.00 | 0.001 | 0.00001 | 0.00099 | 0.99899 |
| 1 Low | 0.30 | 0.01 | 0.00010 | 0.00099 | 0.99899 | ON sill | 0.95 | 0.05 | 0.00050 | 0.00095 | 0.99855 |
| 2 | 0.30 | 0.01 | 0.00010 | 0.00099 | 0.99899 | 0.00 - 0.50 km | 0.80 | 0.05 | 0.00050 | 0.00095 | 0.99855 |
| 3 | 0.30 | 0.01 | 0.00010 | 0.00099 | 0.99899 | 0.50 - 1.00 km | 0.60 | 0.04 | 0.00040 | 0.00096 | 0.99864 |
| 4 | 0.30 | 0.01 | 0.00010 | 0.00099 | 0.99899 | 1.00 - 1.50 km | 0.60 | 0.04 | 0.00040 | 0.00096 | 0.99864 |
| 5 | 0.30 | 0.02 | 0.00020 | 0.00098 | 0.99882 | 1.50 - 2.00 km | 0.55 | 0.03 | 0.00030 | 0.00097 | 0.99873 |
| 6 | 0.30 | 0.02 | 0.00020 | 0.00098 | 0.99882 | 2.00 - 2.50 km | 0.50 | 0.03 | 0.00030 | 0.00097 | 0.99873 |
| 7 | 0.30 | 0.02 | 0.00020 | 0.00098 | 0.99882 | 2.50 - 3.00 km | 0.45 | 0.03 | 0.00030 | 0.00097 | 0.99873 |
| 8 | 0.30 | 0.02 | 0.00020 | 0.00098 | 0.99882 | 3.00 - 3.50 km | 0.30 | 0.02 | 0.00020 | 0.00098 | 0.99882 |
| 9 | 0.30 | 0.02 | 0.00020 | 0.00098 | 0.99882 | 3.50 - 4.00 km | 0.10 | 0.001 | 0.00001 | 0.00099 | 0.99899 |
| 10 | 0.30 | 0.03 | 0.00030 | 0.00097 | 0.99873 | > 4.00 km | | | | | |
| 11 | 0.30 | 0.03 | 0.00030 | 0.00097 | 0.99873 | Proximity to synvolcanic | | | | | |
| 12 | 0.30 | 0.03 | 0.00030 | 0.00097 | 0.99873 | dykes ON Dyke | 0.80 | 0.2 | 0.0020 | 0.0008 | 0.99720 |
| 13 | 0.30 | 0.03 | 0.00030 | 0.00097 | 0.99873 | 0.00 - 0.50 km | 0.95 | 0.2 | 0.0020 | 0.0008 | 0.99720 |
| 14 | 0.30 | 0.03 | 0.00030 | 0.00097 | 0.99873 | 0.50 - 1.00 km | 0.75 | 0.15 | 0.0015 | 0.00095 | 0.99765 |
| 15 | 0.90 | 0.03 | 0.00030 | 0.00097 | 0.99873 | 1.00 - 1.50 km | 0.65 | 0.15 | 0.0015 | 0.00095 | 0.99765 |
| 16 | 0.90 | 0.03 | 0.00030 | 0.00097 | 0.99873 | 1.50 - 2.00 km | 0.55 | 0.10 | 0.0010 | 0.00090 | 0.99810 |
| 17 | 0.90 | 0.05 | 0.00050 | 0.00095 | 0.99855 | 2.00 - 2.50 km | 0.50 | 0.10 | 0.0010 | 0.00090 | 0.99810 |
| 18 | 0.90 | 0.05 | 0.00050 | 0.00095 | 0.99855 | 2.50 - 3.00 km | 0.45 | 0.05 | 0.00050 | 0.00095 | 0.99855 |
| 19 | 0.30 | 0.1 | 0.0010 | 0.00090 | 0.99810 | 3.00 - 3.50 km | 0.40 | 0.05 | 0.00050 | 0.00095 | 0.99855 |
| 20 | 0.30 | 0.1 | 0.0010 | 0.00090 | 0.99810 | 3.50 - 4.00 km | 0.35 | 0.02 | 0.00020 | 0.00098 | 0.99882 |
| 21 | 0.30 | 0.15 | 0.0015 | 0.00095 | 0.99765 | > 4.00 km | 0.10 | 0.001 | 0.00001 | 0.00099 | 0.99899 |
| 22 | 0.30 | 0.15 | 0.0015 | 0.00095 | 0.99765 | | | | | | |
| 23 | 0.30 | 0.20 | 0.0020 | 0.00080 | 0.99720 | | | | | | |
| 24 | 0.30 | 0.20 | 0.0020 | 0.00080 | 0.99720 | | | | | | |
| 25 High | | | | | | | | | | | |
| ¹ $\mu(x)$ = fuzzy membership function ² SCP = smoothed calculated probability ³ Spt _A = support or belief function ⁴ Dis _A = disbelief function ⁵ Unc _A = uncertainty = 1 - Spt _A - Dis _A | | | | | | | | | | | |

LIST OF OTHER EXTECH I PUBLICATIONS

Does not include abstracts of oral and poster presentations.

Ames, D.E.

1991: The Ruttan Cu-Zn deposit and depositional environment: an update (NTS 64B/5); *in* Report of Activities, 1991; Manitoba Energy and Mines, Minerals Division, p. 106-107.

Ames, D.E. and Scoates, J.S.

1992: Preliminary map of the geological setting of the Ruttan Cu-Zn deposit, Rusty Lake Belt, Manitoba (part of NTS 64B/5); Geological Survey of Canada, Open File 2571, 2 maps, scale 1:5000.

Ames, D.E., Scoates, J.S., and Franklin, J.M.

1990: Preliminary report on the geological setting of the Ruttan base metal deposit and associated hydrothermal alteration, Rusty Lake volcanic belt, Manitoba (NTS 64B/5); *in* Report of Activities, 1990; Manitoba Energy and Mines, Minerals Division, p. 178-186.

An, P., Moon, W.M., and Bonham-Carter, G.F.

1992: On a knowledge-based approach of integrating remote-sensing, geophysical and geological information; Proceedings IGARSS'92, International Geoscience and Remote Sensing Symposium, p. 34-38.

1994: Uncertainty management in integration of exploration data using the belief function; *Nonrenewable Resources*, v. 3, no. 1, p. 60-71.

1994: An object-oriented knowledge representation structure for exploration data integration; *Nonrenewable Resources*, v. 3, no. 2, p. 132-145.

Armstrong, M. and Coker, W.B.

1991: EXTECH; *Geos*, v. 21, no. 1, p. 28-29.

Bailes, A.H. and Galley, A.G.

1991: Wekusko Lake (N.T.S. 63K/16SE); Manitoba Energy and Mines, Minerals Division, preliminary geological map 1991S-6, scale 1:20 000.

Bailes, A.H. and Galley, A.G. (cont.)

1992: Stall-Kormans Lake; Preliminary 1:5000 scale geological map, distributed with Manitoba Report of Field Activities 1992.

1993: Geology of the Anderson-Stall volcanic-hosted massive sulphide area, Snow Lake, Manitoba; Geological Survey of Canada, Open File 2776, 1 map, scale 1:10 000.

Bailes, A.H., Galley, A.G., Skirrow, R.G., and Young, J.
in press: Geology of the Chisel volcanic-hosted massive sulphide area, Snow Lake, Manitoba (part of 63K/16SE); Geological Survey of Canada, Open File, scale 1:5000.

Bonham-Carter, G.F.

1990: Mapping mineral potential with a geographic information system; *in* Proceedings of Computer Treatment of Exploration and Mining Data: Do's and Don'ts, Computer Applications in Mining Exploration, Toronto, March 9-10, 1990, p. 121-130.

1994: Methods of spatial data integration for mineral potential mapping; *in* Proceedings 7th Australasian Remote Sensing Conference, Melbourne, March 1-4, 1994, p. 61-67.

1994: Geographic Information Systems for Geoscientists: Modelling with GIS; Pergamon, Oxford, 398 p.

Bonham-Carter, G.F., Reddy, R.K.T., and Galley, A.G.

1993: Knowledge-driven modeling of volcanogenic massive sulphide potential with a geographic information system; *in* Mineral Deposit Modeling, (ed.) R.V. Kirkham, W.D. Sinclair, R.I. Thorpe and J.M. Duke; Geological Association of Canada, Special Paper 40, p. 735-749.

Coker, W.B.

1993: The Exploration Science and Technology Initiative (EXTECH), Snow Lake and Ruttan mine areas, Manitoba: an overview; *in* Report of Activities 1993, Manitoba Energy and Mines, Minerals Divisions, p. 13-16.

Friske, P.W.B., McCurdy, M.W., Day, S.J., Gross, H., Lynch, J.J., and Durham, C.C.

1995: Lake sediment and water infill survey data, Snow Lake area, Manitoba (NTS 63J/13 west and 63K/16); Geological Survey of Canada, Open File 3015, 42 maps, 86 p.

Galley, A.G.

1993: Characteristics of semi-conformable alteration zones associated with volcanogenic massive sulfide deposits; *Journal of Geochemical Exploration*, v. 48, p. 175-200.

Galley, A.G. and Scoates, J.S.

1990: Relationship of synvolcanic dykes to hydrothermal alteration in the Edwards Lake formation, Chisel Lake area (NTS 63K/16); *in* Report of Activities 1990, Manitoba Energy and Mines, Minerals Division, p. 170-177.

Geological Survey of Canada

1986: Regional lake sediment and water geochemical reconnaissance data, Province of Manitoba (parts of NTS 63K, 63N, and 63O); Geological Survey of Canada, Open File 1212, 22 maps, 84 p.

1991: Airborne geophysical survey of the Snow Lake area, Manitoba; Geological Survey of Canada, Open File 2300, scale 1:250 000.

1991: Airborne geophysical survey of the Ruttan area, Manitoba; Geological Survey of Canada, Open File 2301, scale 1:250 000.

Hall, G.E.M. and Vaive, J.E.

1992: Application of a field portable anodic stripping voltameter to the analysis of sulphide selective leaches and waters; *Chemical Geology*, v. 97, p. 295-306.

Hall, G.E.M., MacLaurin, A.I., and Vaive, J.E.

1995: Readsorption of gold during the selective extraction of the 'soluble organic' phase of humus, soil and sediment samples; *Journal of Geochemical Exploration*, v. 54, no. 1, p. 27-38.

Hall, G.E.M., Vaive, J.E., Beer, R., and Hoashi, M.

in press: Selective leaches revisited with emphasis on amorphous iron hydroxide phase extraction; *Journal of Geochemical Exploration*.

Hall, G.E.M., Vaive, J.E., and Kaszycki, C.

1993: Diagnostic capabilities of selective leaches in exploration and environmental geochemistry; *in* EXPLORE (Association of Exploration Geochemists Newsletter), no. 80, p. 3-9.

Hall, G.E.M., Vaive, J.E., and MacLaurin, A.I.

in press: Analytical aspects of the application of sodium pyrophosphate reagent in the specific extraction of the labile organic component of humus in soils; *Journal of Geochemical Exploration*.

Palacky, G.J. and Sinha, A.K.

1992: Results of ground magnetic and electromagnetic (multifrequency, horizontal-loop) measurements in the Cook Lake North area, Snow Lake, Manitoba; Geological Survey of Canada, Open File 2463, 19 p. + diskette.

1992: Results of ground magnetic and electromagnetic (multifrequency, horizontal loop) measurements at Joannie Options, Snow Lake, Manitoba; Geological Survey of Canada, Open File 2464, 17 p. + diskette.

Reddy, R.K.T., Agterberg, F.P., and Bonham-Carter, G.F.

1991: Application of GIS-based logistic models to base-metal potential mapping in Snow Lake area, Manitoba; *in* Proceedings Canadian Conference on GIS, March 18-22, 1991, p. 607-618.

Reddy, R.K.T. and Bonham-Carter, G.F.

1991: A decision-tree approach to mineral potential mapping in Snow Lake area, Manitoba; *Canadian Journal of Remote Sensing*, v. 17, no. 2, p. 191-200.

Reddy, R.K., Bonham-Carter, G.F., and Galley, A.G.

1992: Developing a geographic expert system for regional mapping of Volcanogenic Massive Sulphide (VMS) deposit potential; *Nonrenewable Resources*, v. 1, no. 2, p. 112-124.

Reddy, R.K.T., Bonham-Carter, G.F., and Wright, D.F.

1990: GIS for mapping mineral resource potential: preliminary results of base-metal study, Snow Lake Area, Manitoba; *in* Proceedings Canadian Conference on GIS- "GIS for the 1990s", March 5-8, 1990, p. 384-400.

1994: Application of GIS for integration of geoscientific datasets for base-metal evaluation in Manitoba; *in* Proceedings GEOINFO IV, June 24-29, 1990, Geological Survey of Canada, Open File 2315, p. 57-68.

Sinha, A.K.

1992: Ground very low frequency (VLF) and magnetic survey results at the Copperman site, near Snow Lake, Manitoba; Geological Survey of Canada, Open File 2458, 25 p.

Sinha, A.K. and Palacky, G.J.

1992: Results of ground magnetic and electromagnetic (multifrequency, horizontal-loop) measurements over the Linda-2 deposit, Snow Lake, Manitoba; Geological Survey of Canada, Open File 2462, 15 p. + diskette.

Wright, D.F. and Bonham-Carter, G.F.

1996: Evaluating volcanic hosted massive sulphide favourability using GIS-based spatial data integration models, Snow Lake area, Manitoba; Ph.D. thesis, University of Ottawa, Ottawa, Ontario, 338 p.

This section contains colour figures for two reports:

Application of airborne multiparameter geophysical data (gamma ray, magnetometer, VLF-EM) to mapping and exploration in the Rusty Lake and Snow Lake areas

R.B.K. Shives

Figures 3, 6, and 9

VHMS favourability mapping with GIS-based integration models, Chisel Lake-Anderson Lake area

D.F. Wright and G.F. Bonham-Carter

Figures 5, 6, 7, 8, 9, 10, 11, 14, 15, 19, 21, 23, 25, 27, 29, 31, 32, 35, 36, 37, 38, 40, and 41

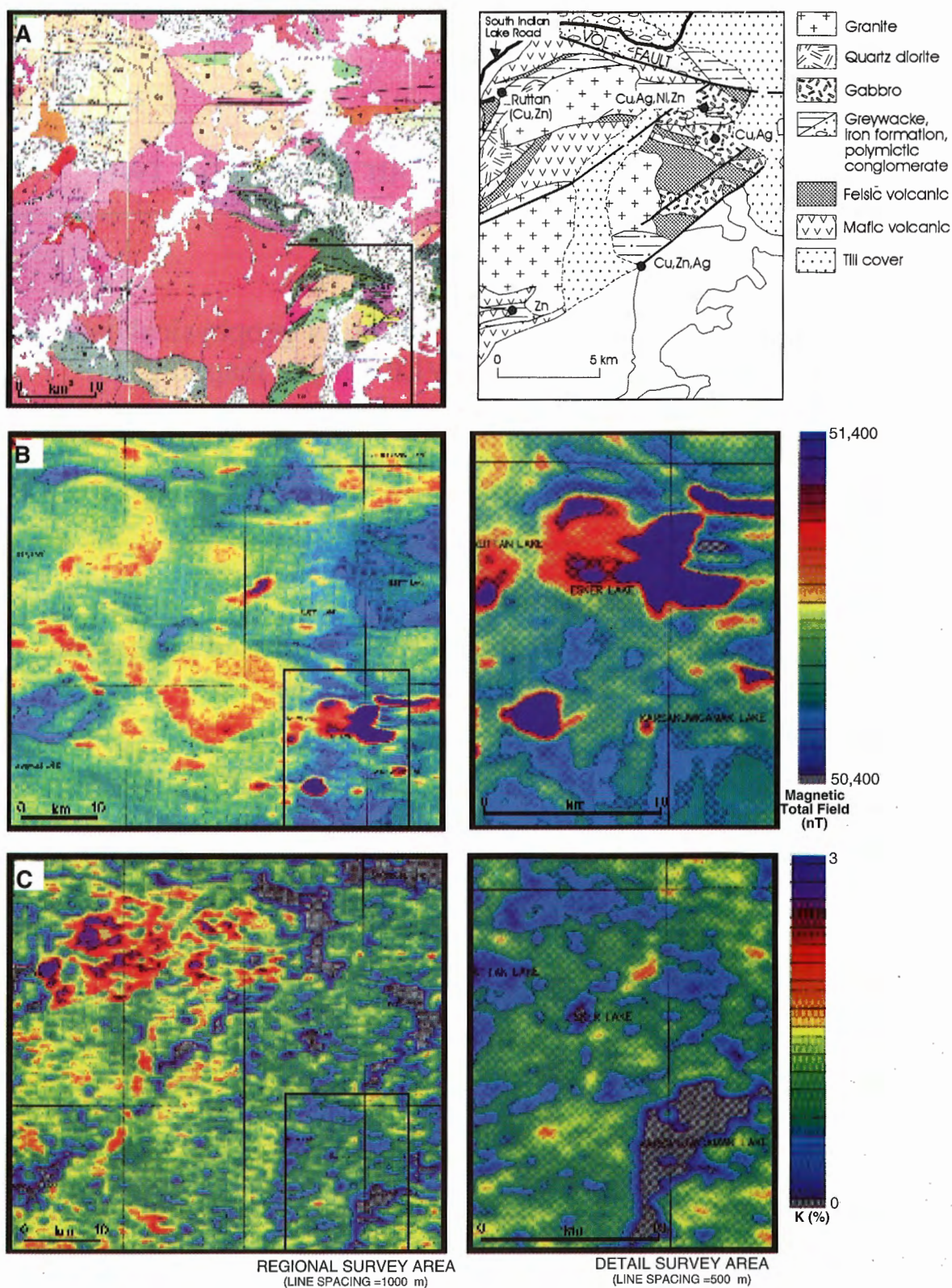


Figure 3. Geology, selected airborne geophysical patterns, Rusty Lake regional and Ruttan detail areas. (Geology from Baldwin, 1988, and Manitoba Energy and Mines, 1986a, b).

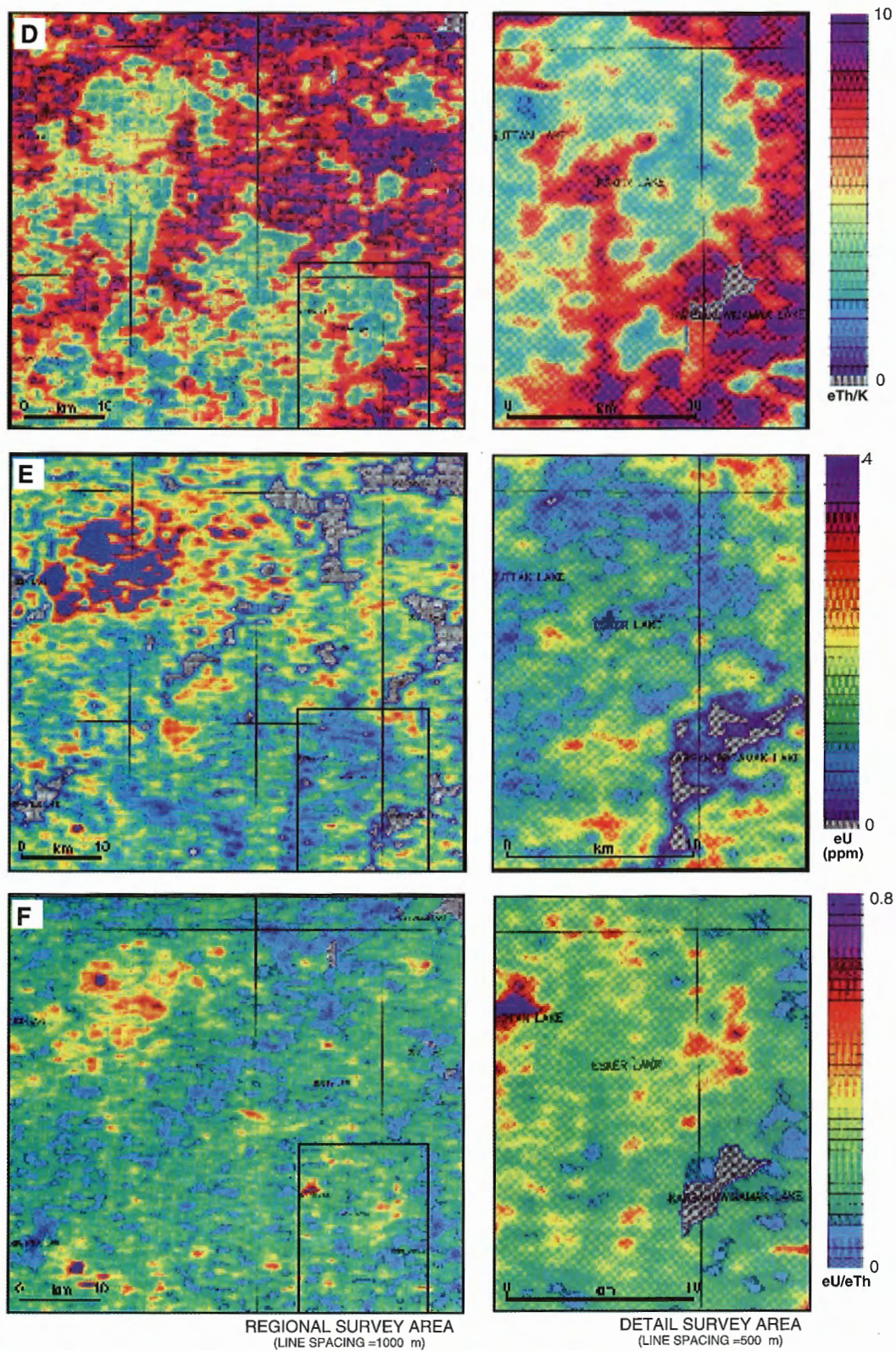


Figure 3. (cont.)

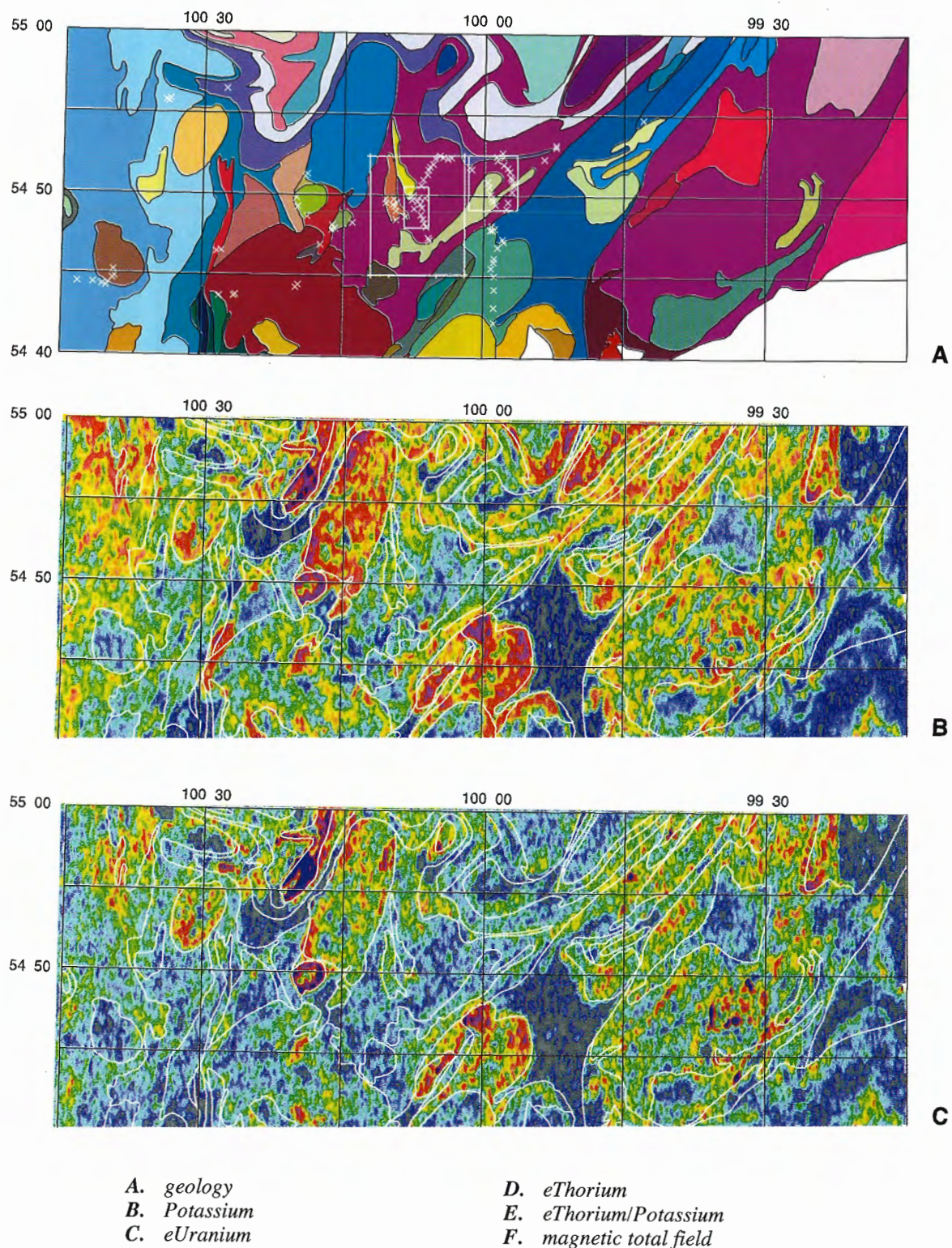


Figure 6. Geology, selected airborne geophysical patterns, Snow Lake survey. White X's indicate traverses. Areas within white boxes are shown in detail in Figures 12, 13, 14. (Digital geology courtesy S. Lucas GSC)

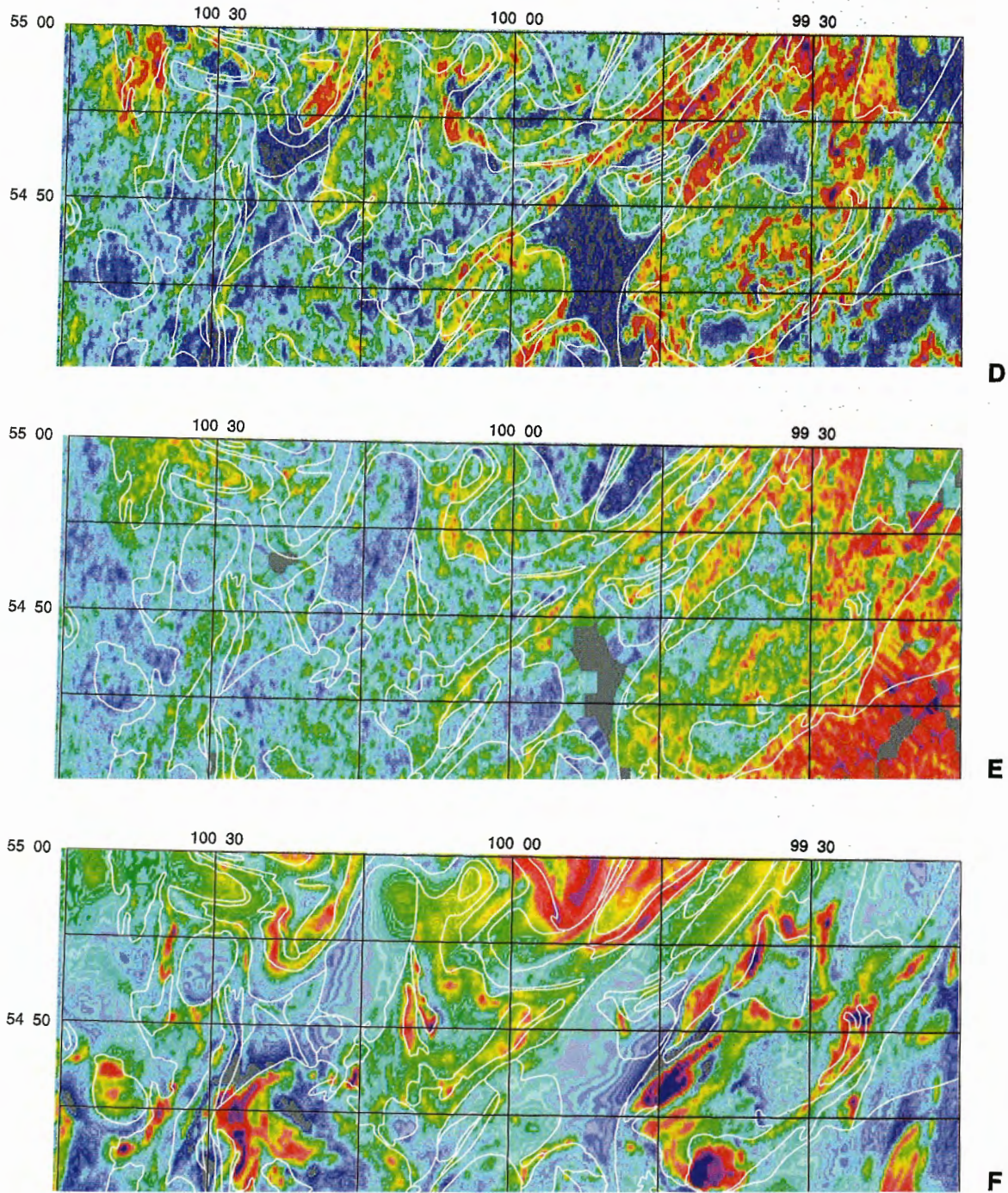


Figure 6. (cont.)

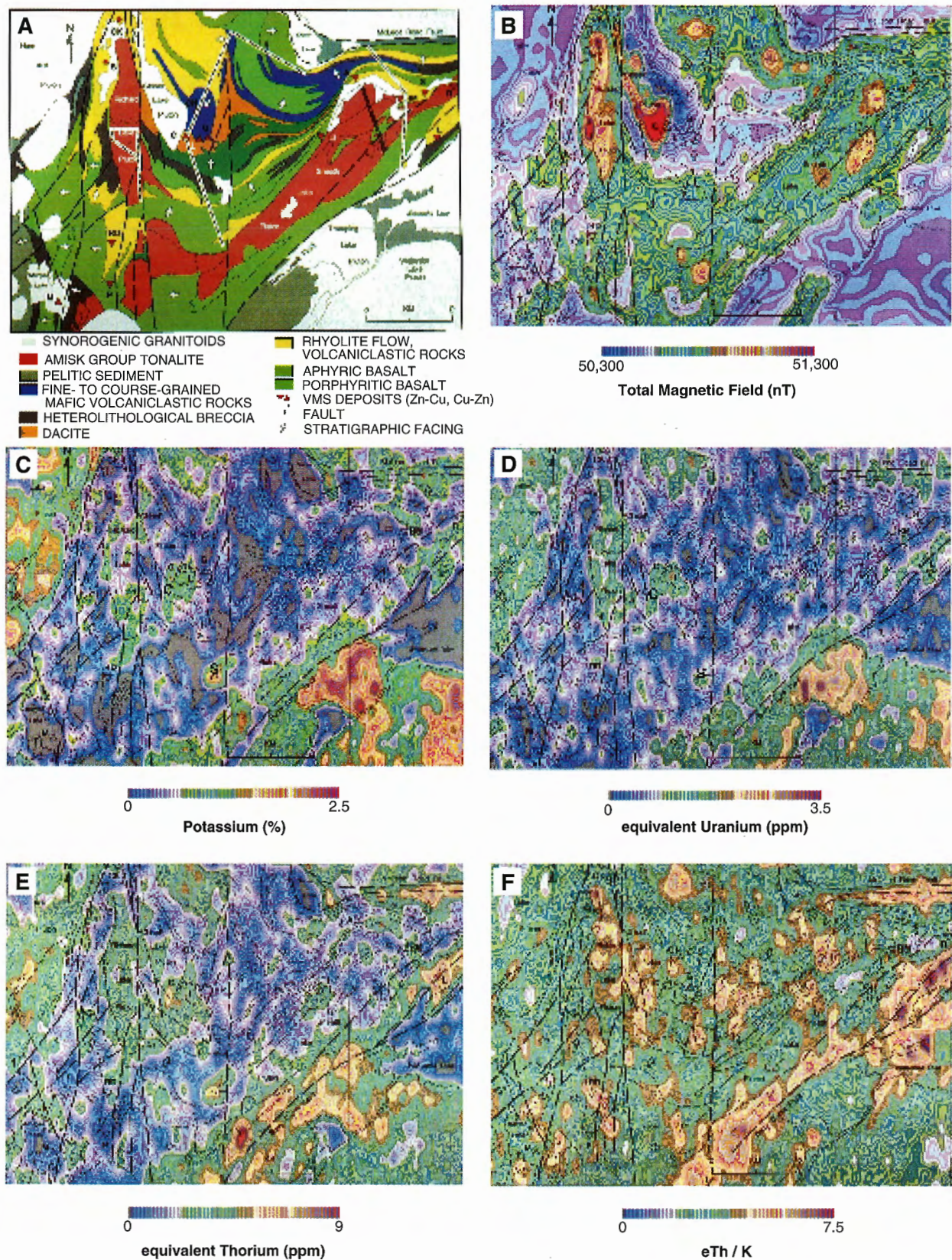


Figure 9. Geology, selected airborne geophysical patterns, Chisel-Anderson basins. (Geology courtesy A. Galley, GSC)

Bedrock geology - Snow Lake area

(and simplified geological model)

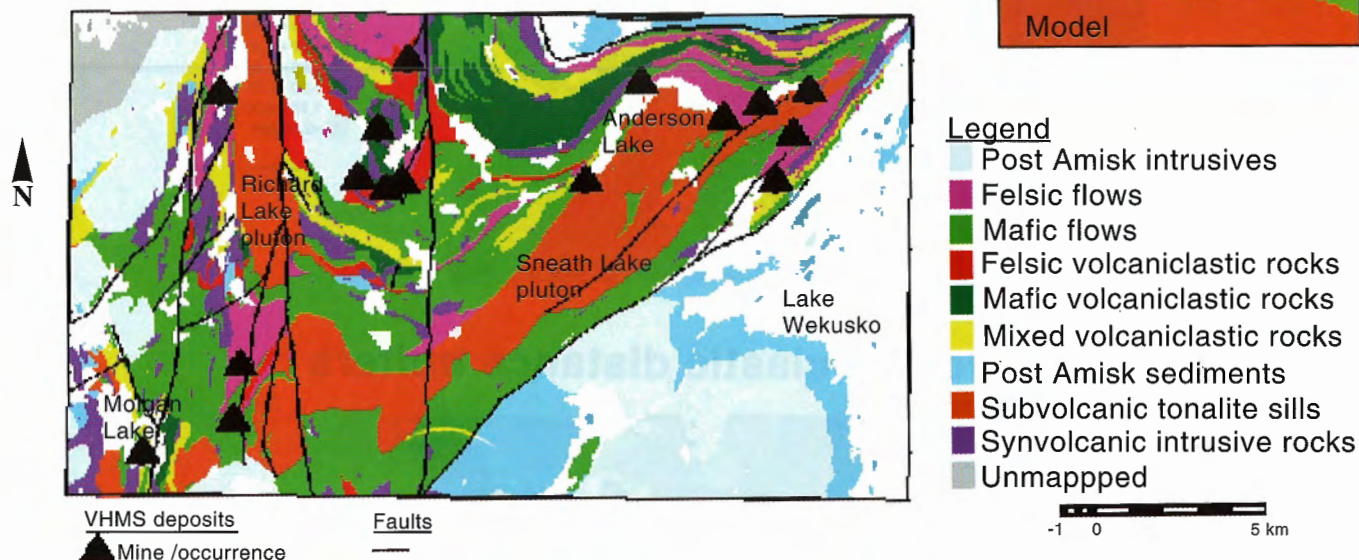


Figure 5. Geological setting for Chisel-Anderson area, with simplified model for VHMS deposits.

Alteration types - Snow Lake area

(and simplified model)

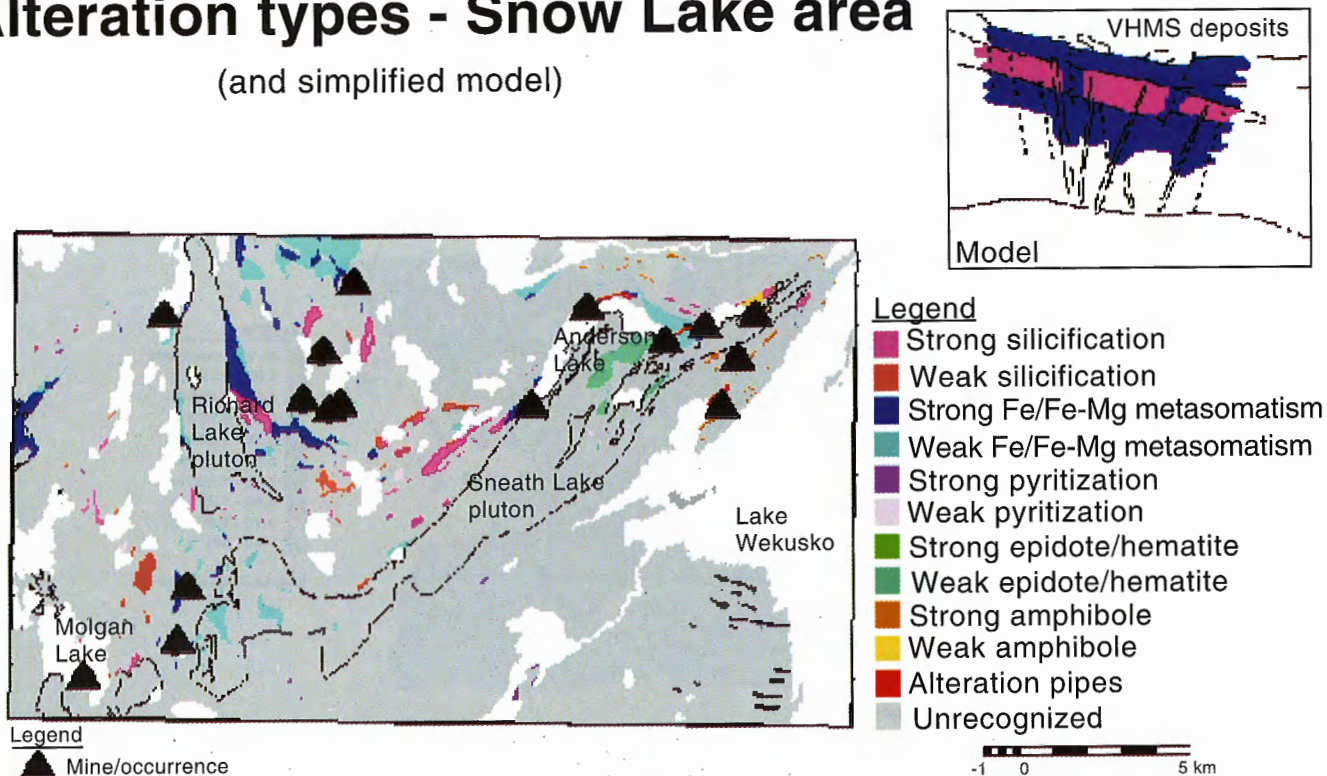
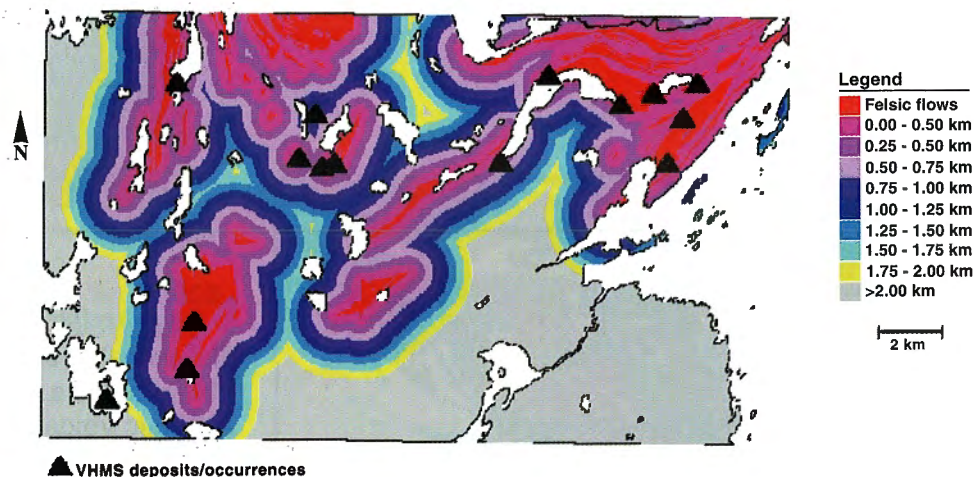
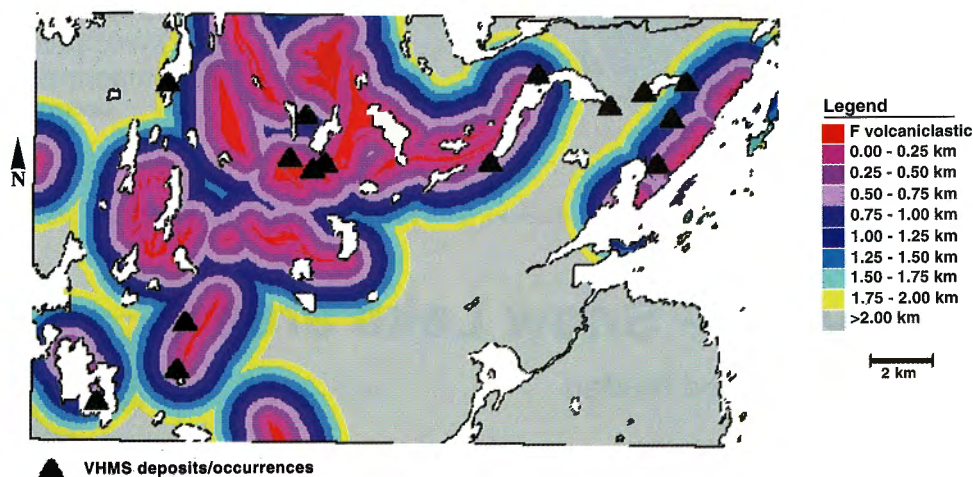


Figure 6. Mapped alteration based on mineral assemblages. Typical regional alteration associated with VHMS deposits is shown in cartoon to upper right.

Felsic flows distance buffers



Felsic volcaniclastic distance buffers



Mafic volcaniclastic distance buffers

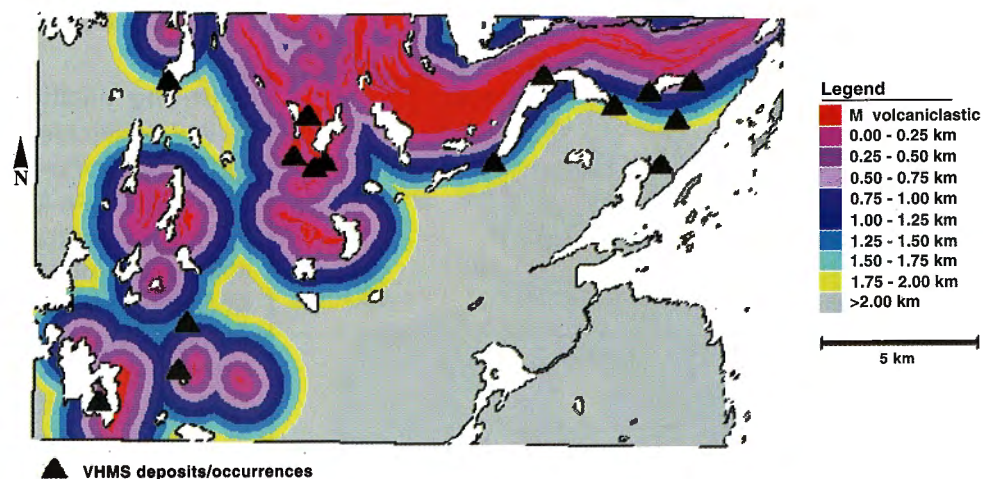
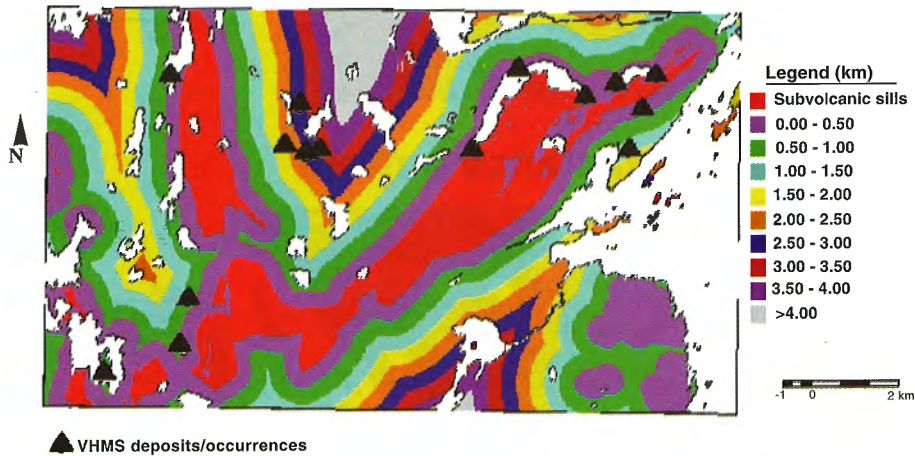


Figure 7. Proximity maps used in stratigraphic factor. A) Proximity to felsic flows, B) proximity felsic volcaniclastics, and C) proximity to mafic volcaniclastics.

Distance buffers for tonalite sills



Synvolcanic dykes and buffers

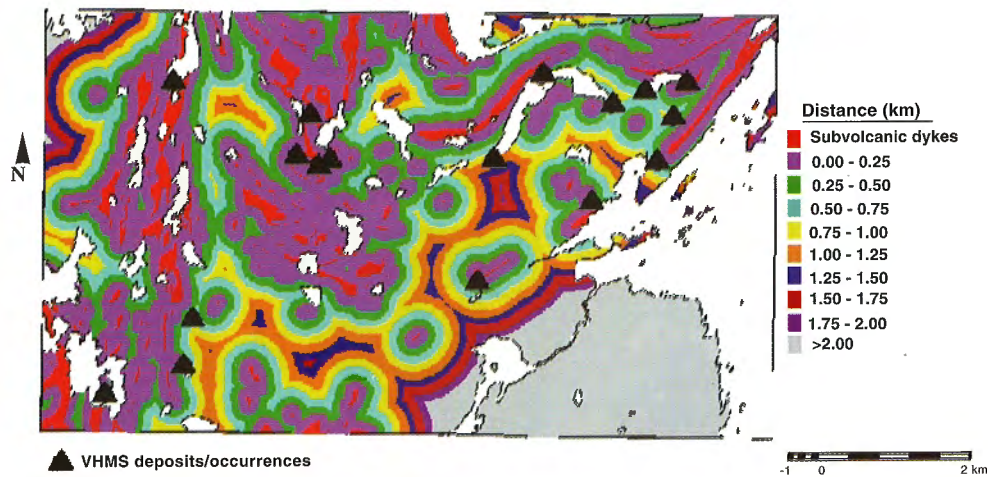
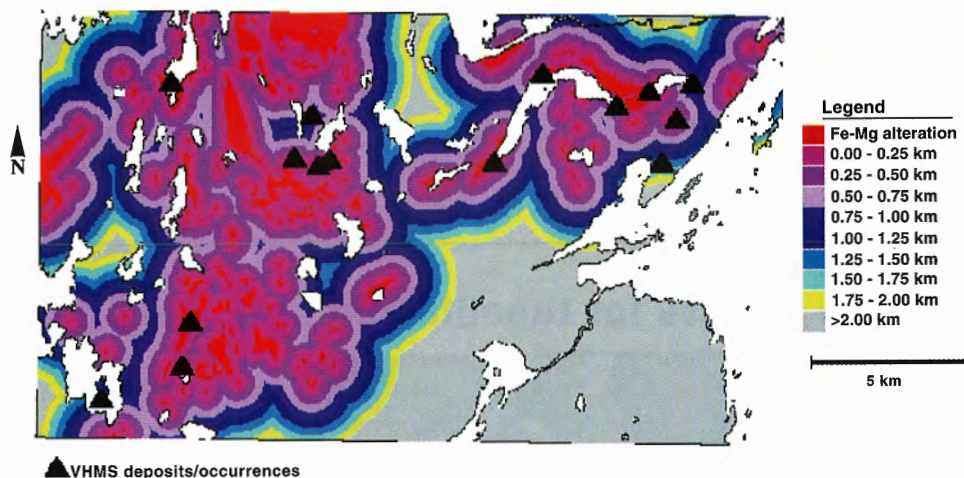
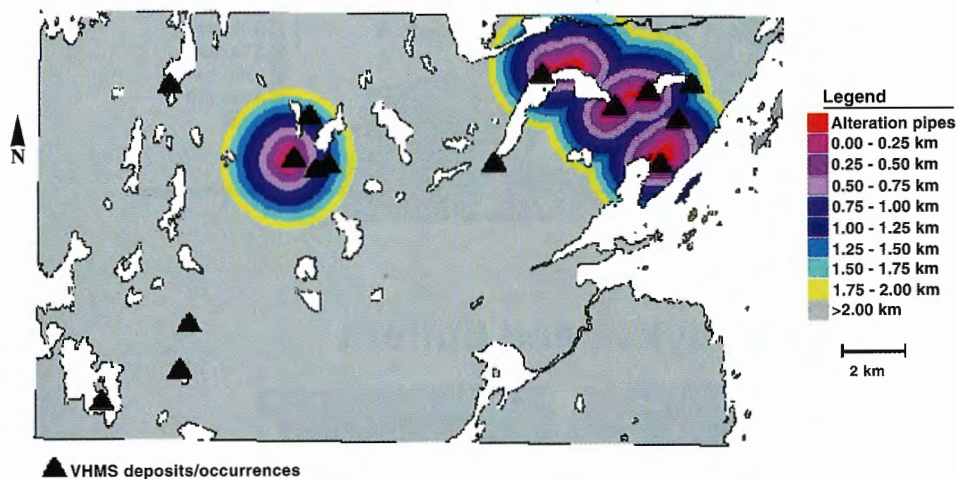


Figure 8. Proximity maps used for heat factor. Buffers generated round A) subvolcanic tonalite sills, and B) synvolcanic dykes.

Fe/Mg alteration distance buffers



Alteration pipes distance buffers



Pyrite alteration distance buffers

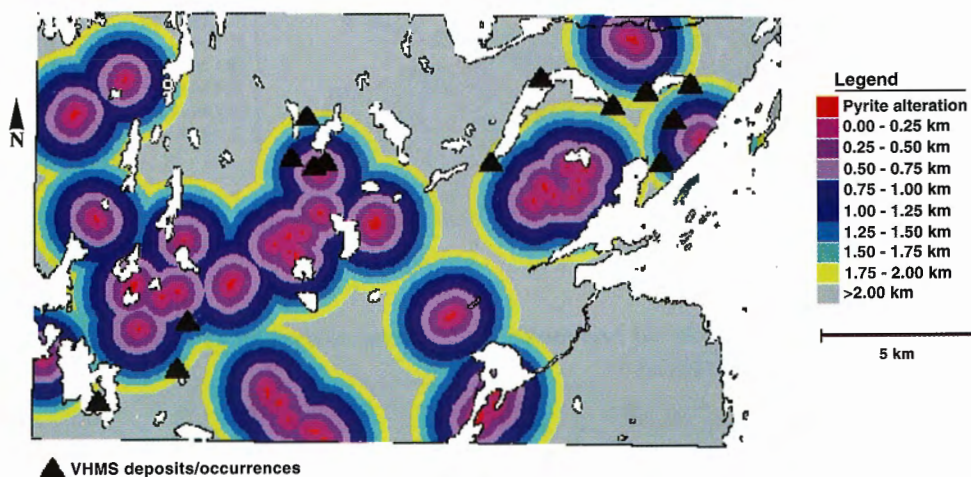
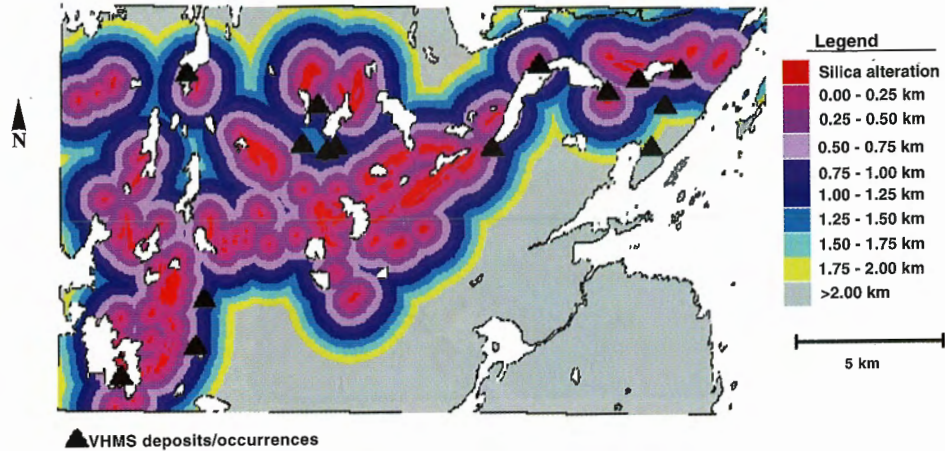
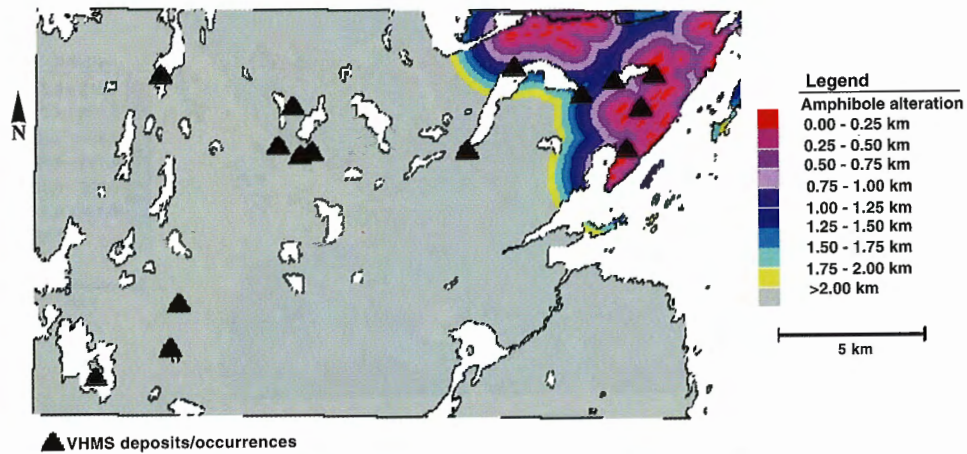


Figure 9. Proximity maps for alteration zones. *A) Fe-Mg metasomatism, B) alteration pipes, C) pyrite alteration, D) silicification, E) amphibole alteration and F) epidote-hematite.*

Silica alteration distance buffers



Amphibole alteration distance buffers



Ep-hem alteration distance buffers

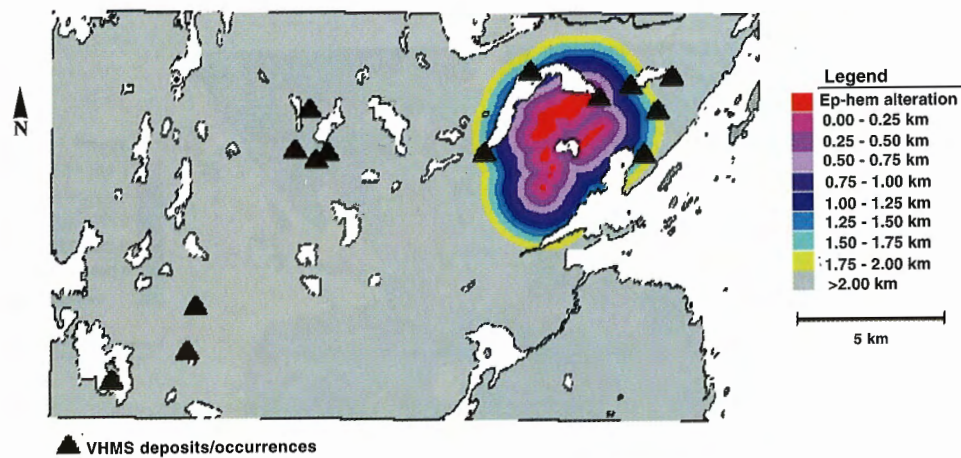
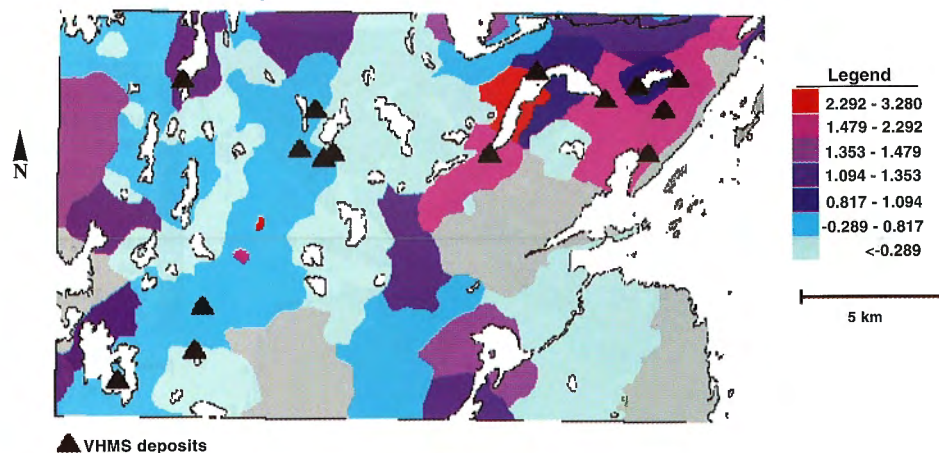
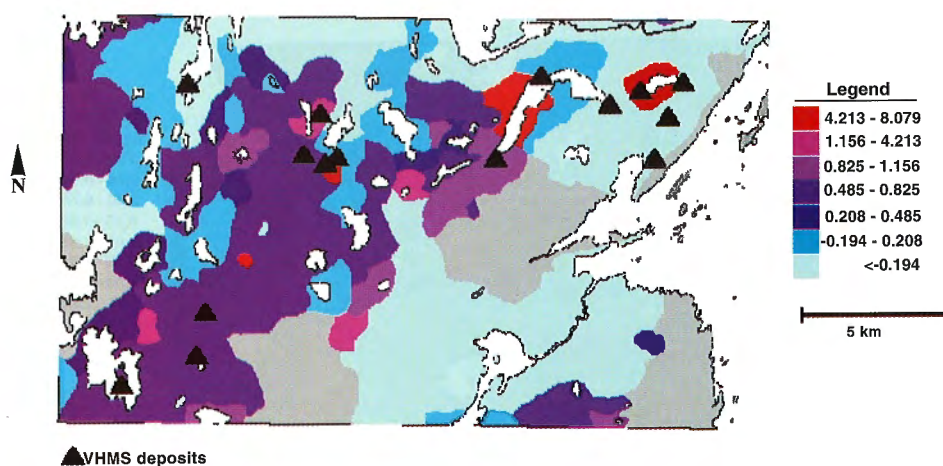


Figure 9. (cont.)

Principal component 1



Principal component 2



Principal component 3

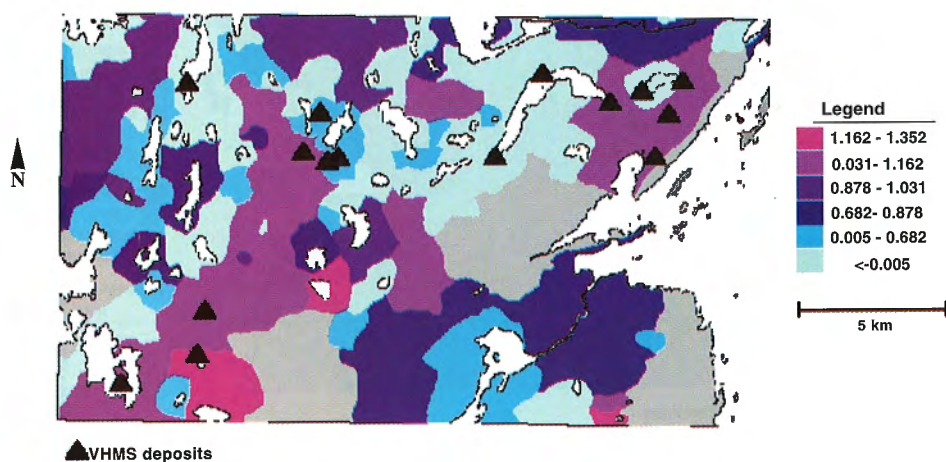
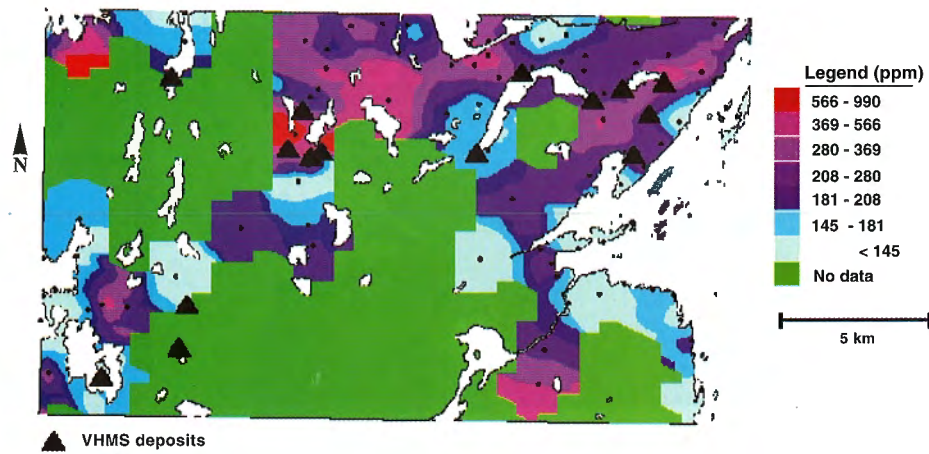
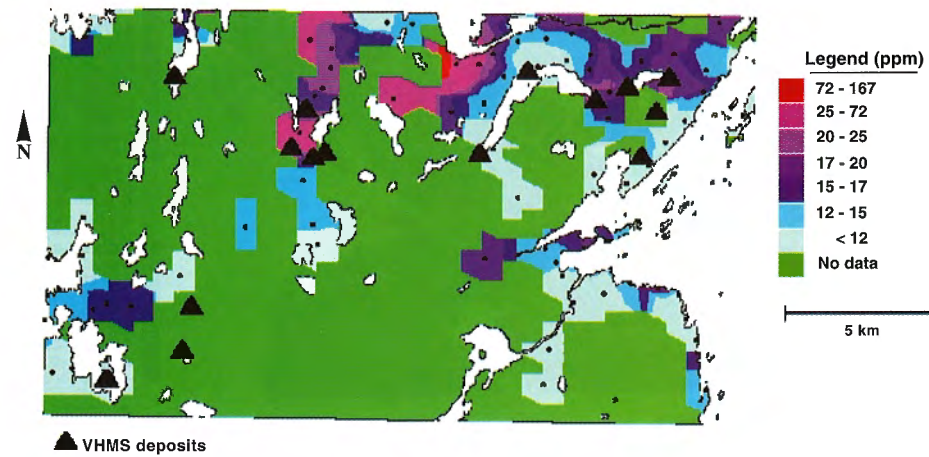


Figure 10. Principal component maps for lake-sediment geochemistry. Catchment basin maps have been coloured to reflect PC scores. A) PC-1 having an association of Cu, Pb, Fe, Ni, V, F, and Co. B) PC-2 having an association of Zn and Cd. C) PC-3 Mo.

Kriged Cu



Kriged Pb



Kriged Zn

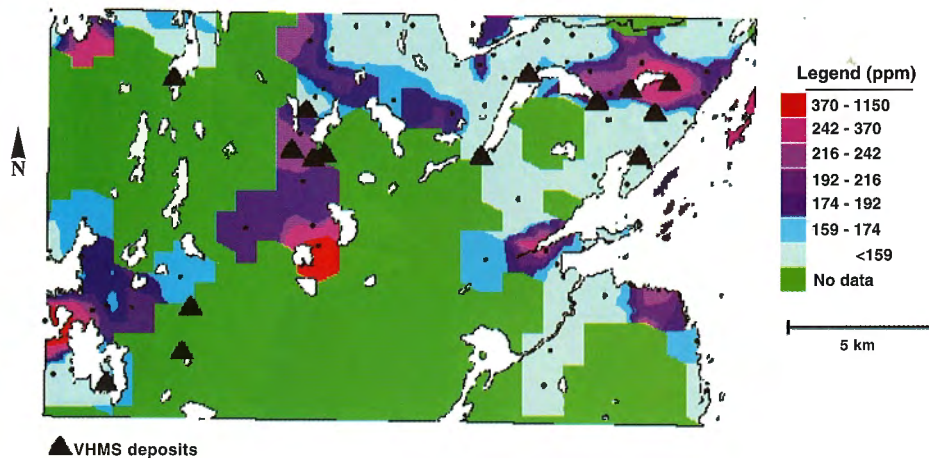
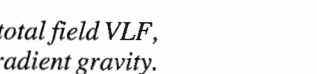
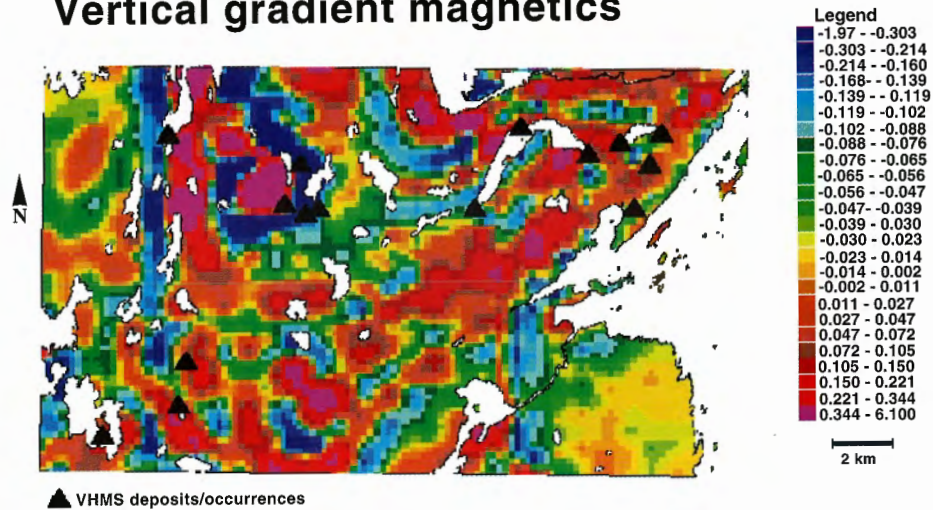


Figure 11. Kriged log concentrations of A) Cu, B) Pb, and C) Zn. Areas with high kriging variance are classed as 'no data'.



Vertical gradient magnetics



Vertical gradient gravity

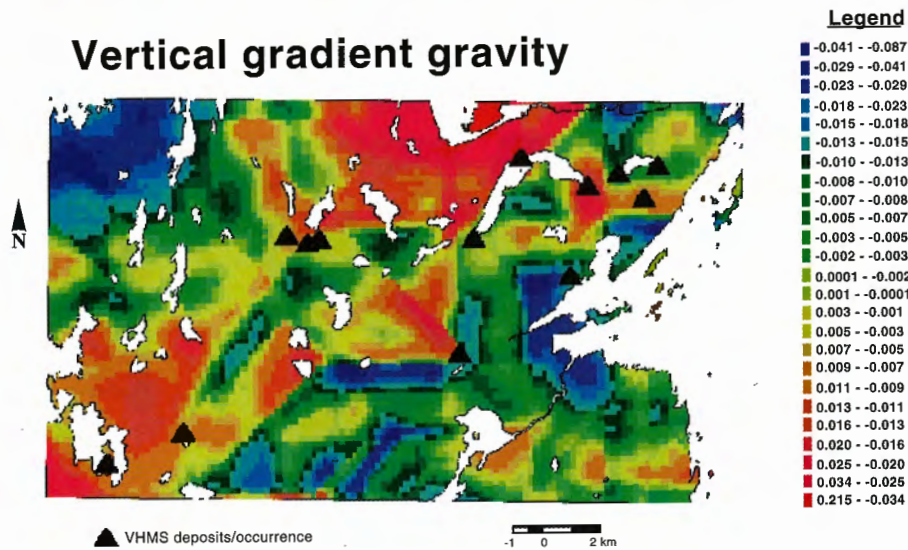


Figure 14. (cont.)

Airborn potassium (%K)

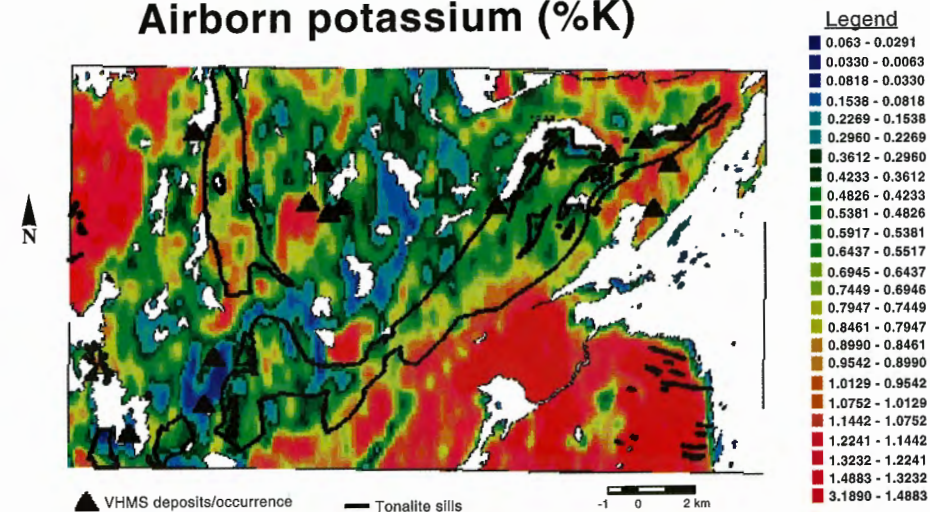


Figure 15. Airborne %K with contacts of tonalite sills overlain. Elevated responses in northwest and southeast are correlated with Ham Lake and Wekusko Lake plutons interpreted to be younger than Sneath Lake Pluton.

Fuzzy geochemical factor

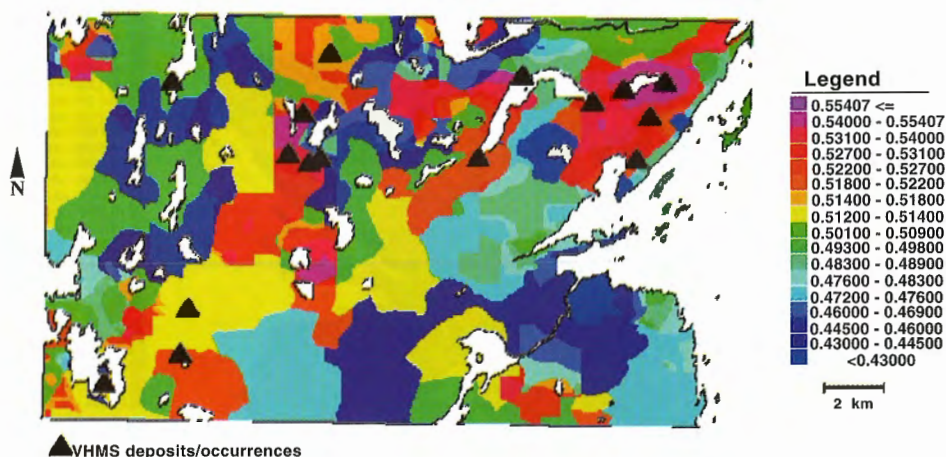


Figure 19. Fuzzy geochemical factor map resulting from combination of six geochemical evidence maps using inference net shown in Figure 18.

Fuzzy stratigraphic factor

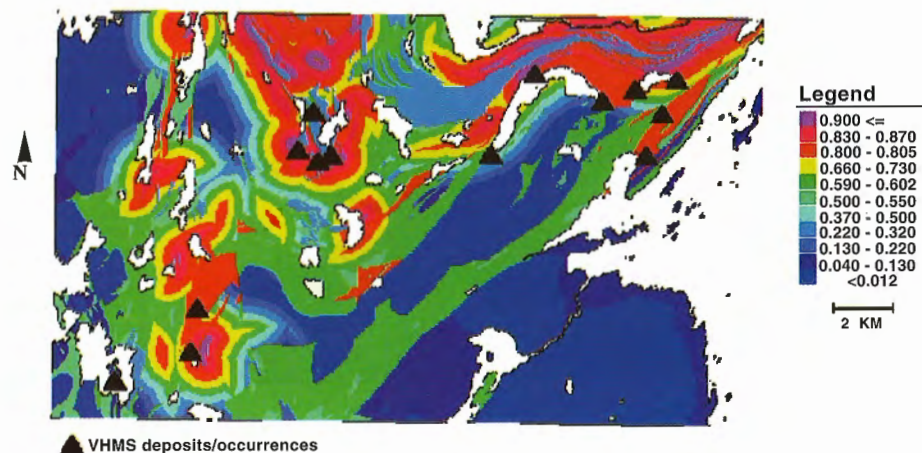


Figure 21. Fuzzy stratigraphic factor map resulting from combination of four stratigraphic evidence maps using inference net shown in Figure 20.

Fuzzy heat source factor

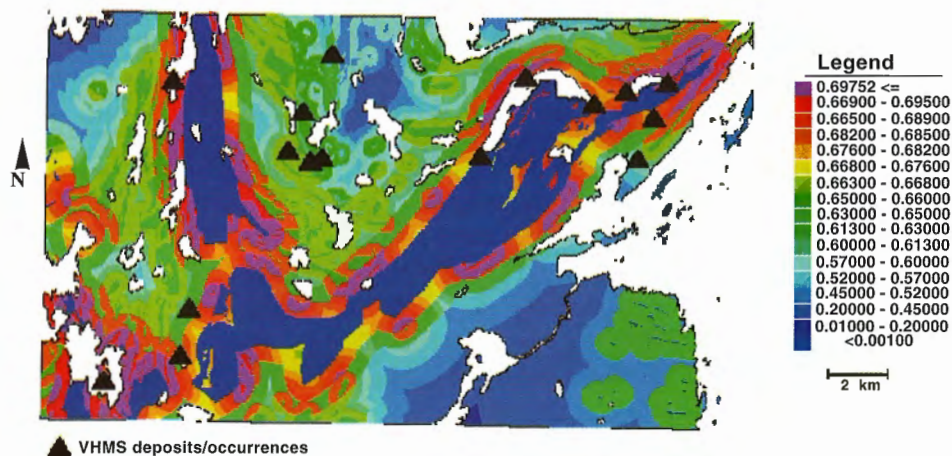


Figure 23. Fuzzy heat source factor map resulting from combination of two evidence maps related to heat sources using inference net shown in Figure 22.

Fuzzy alteration factor

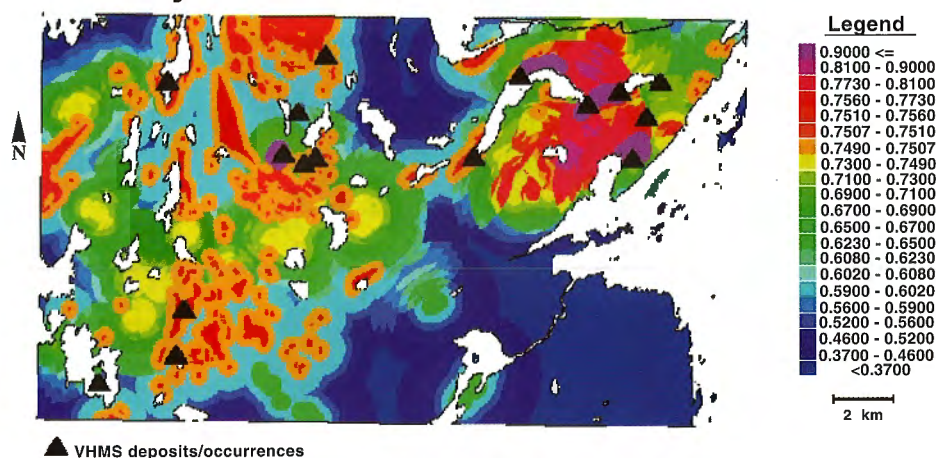


Figure 25. Fuzzy alteration factor map resulting from combination of six evidence maps showing proximity to various types of alteration using inference net shown in Figure 24.

Fuzzy geophysical factor

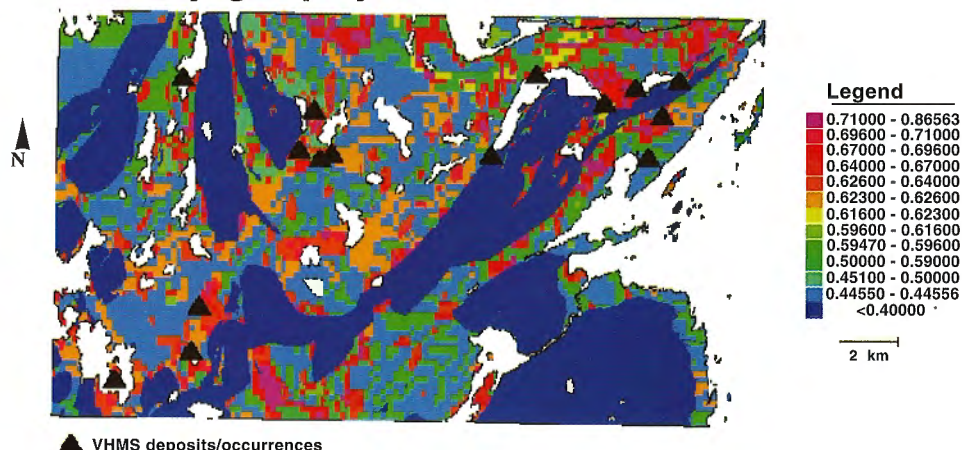


Figure 27. Fuzzy geophysical factor map resulting from combination of five geophysical evidence maps.

VHMS potential - fuzzy logic approach

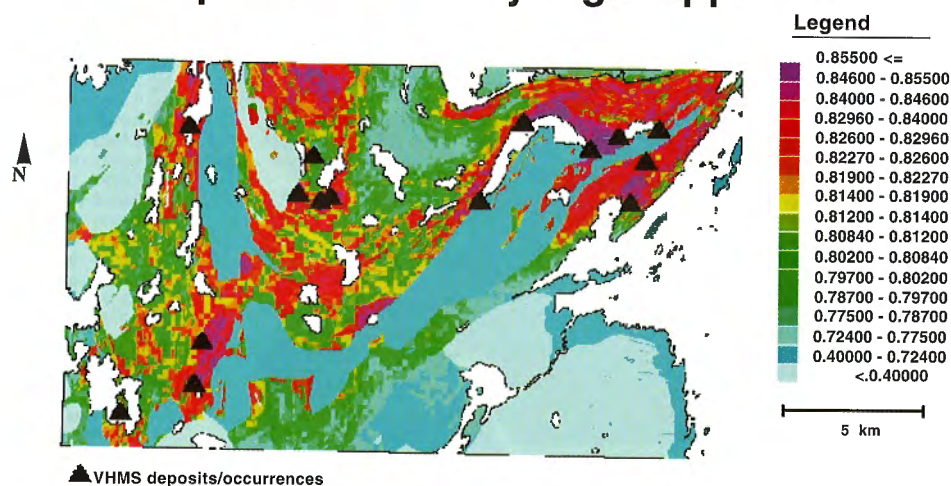


Figure 29. Favourability map for VHMS deposits, generated using fuzzy logic.

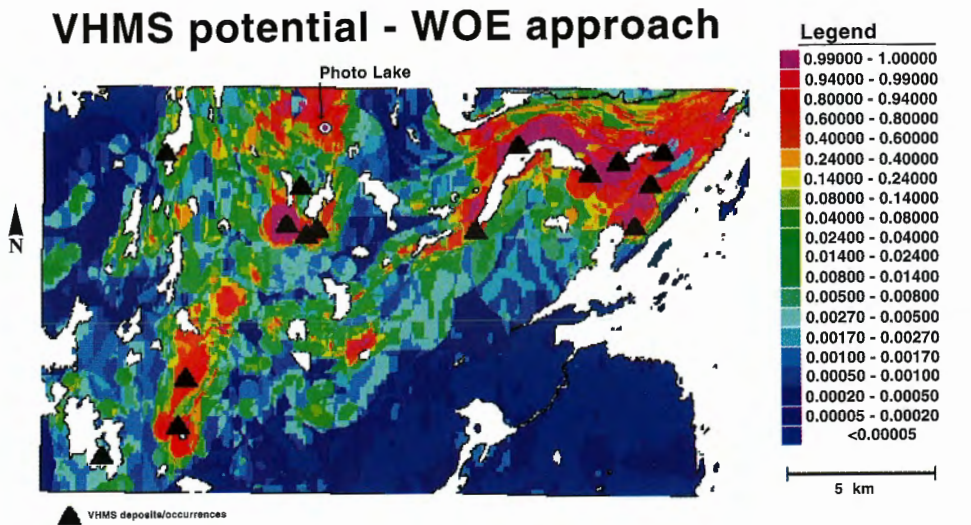


Figure 31. Posterior probability map for VHMS deposits generated by weights of evidence method.

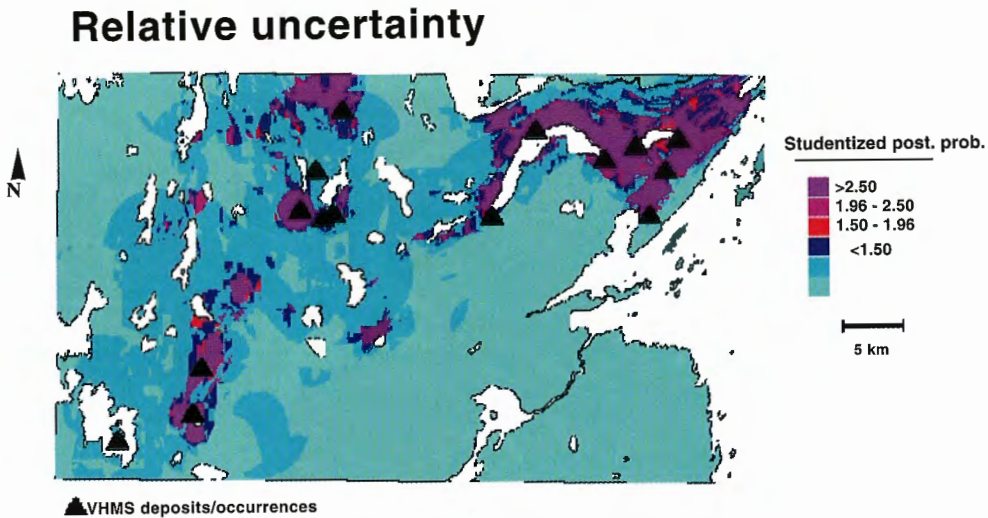


Figure 32. Relative uncertainty calculated by dividing posterior probability by its standard deviation. Values greater than 1.645 indicate that corresponding posterior probability is greater than 0 with a probability of 95%.

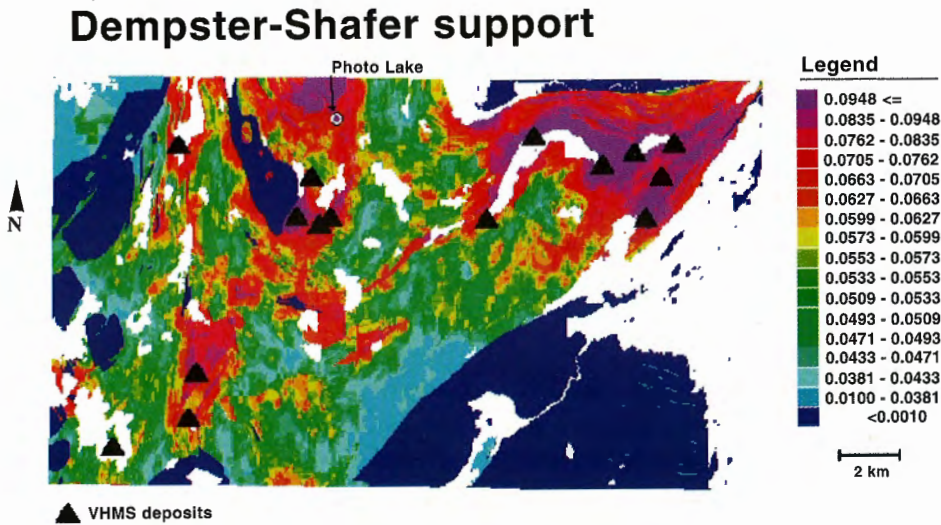


Figure 35. Map of Dempster-Shafer support, a conservative assessment that evidence supports proposition that deposit is present.

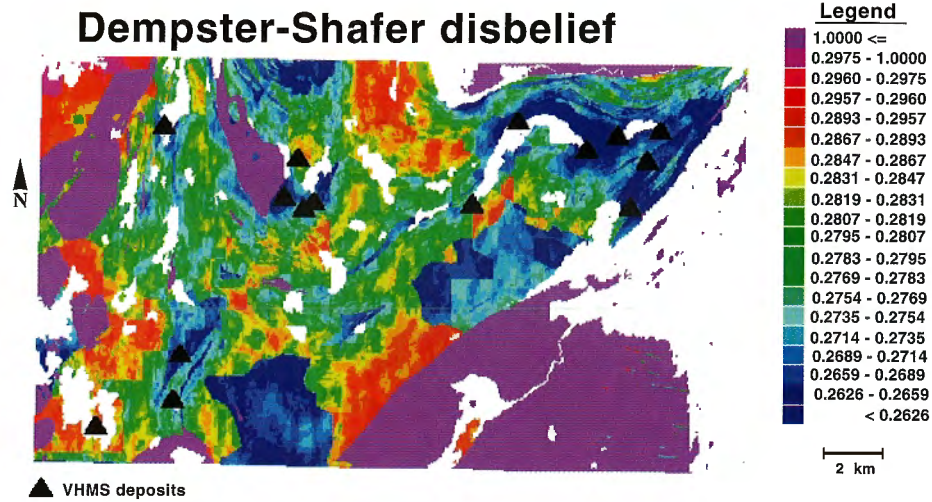


Figure 36. Map of Dempster-Shafer disbelief. Disbelief function is belief that proposition that there is a deposit present is false.

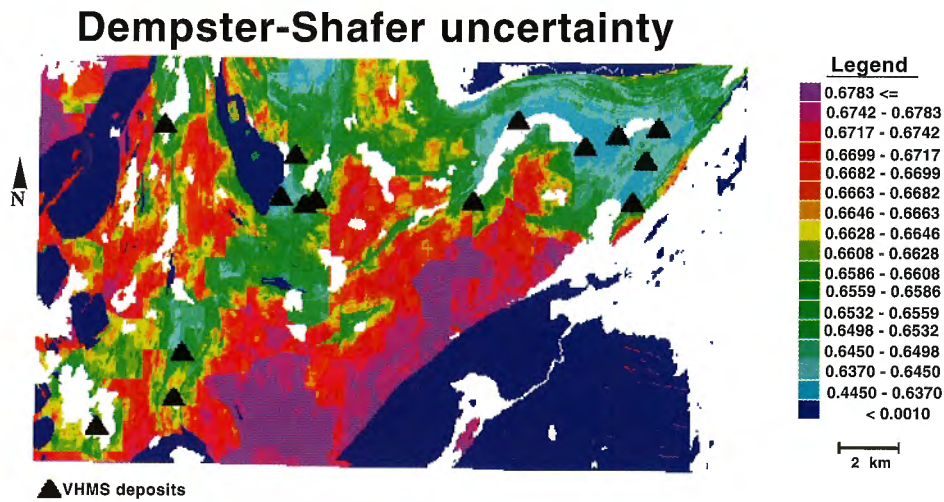


Figure 37. Map of Dempster-Shafer uncertainty where uncertainty is calculated as difference between support (conservative belief) and plausibility (optimistic belief).

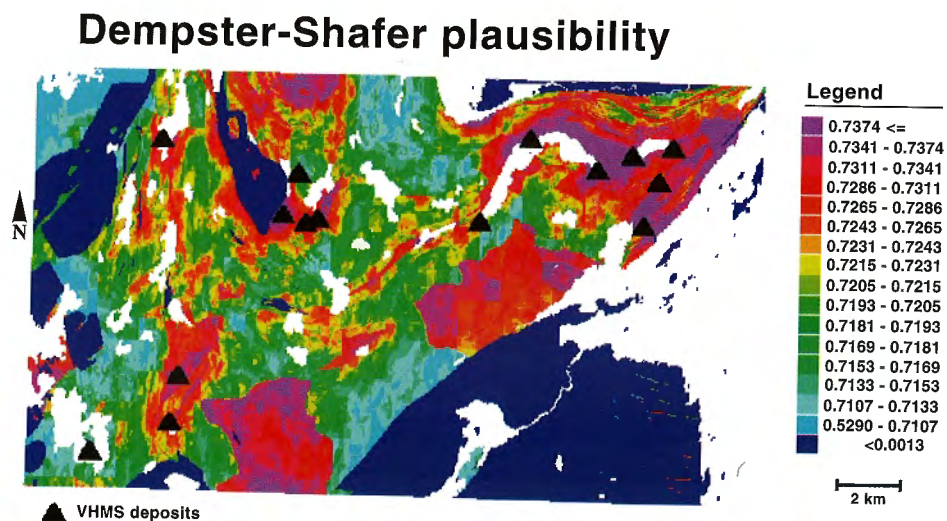
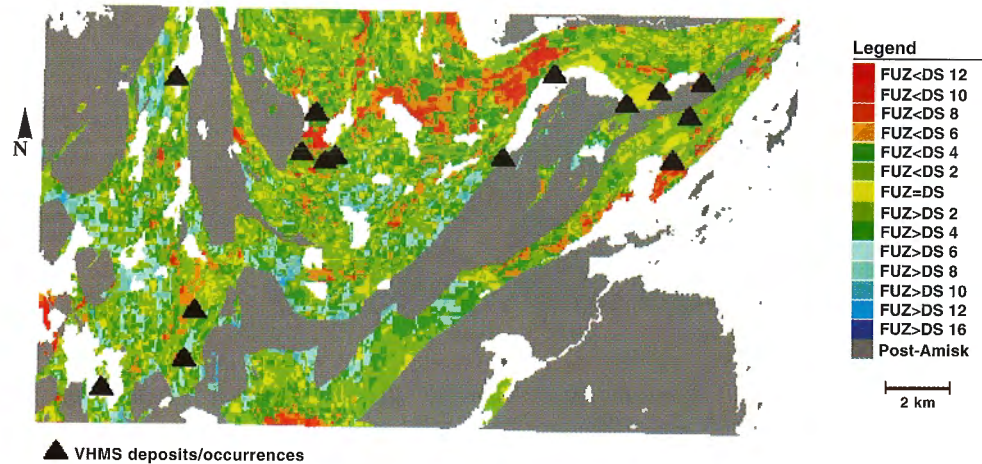
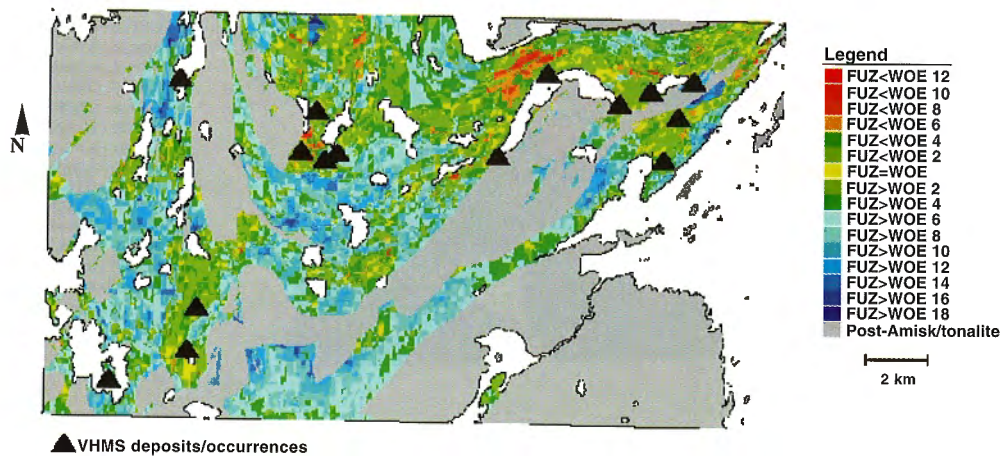


Figure 38. Map of Dempster-Shafer plausibility, an optimistic assessment that evidence supports proposition that a deposit is present.

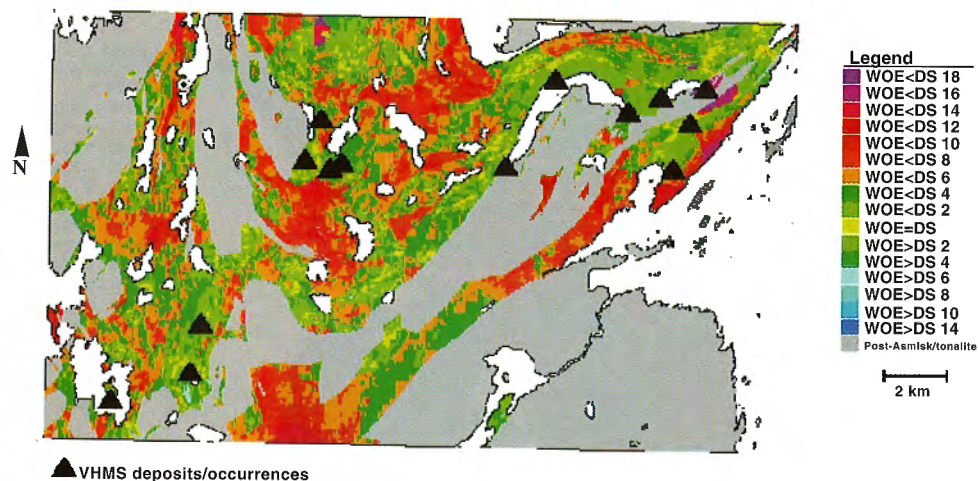
Difference between FL and DS support



Difference between FL and WOE



Difference between WOE and DS support



Target areas for exploration

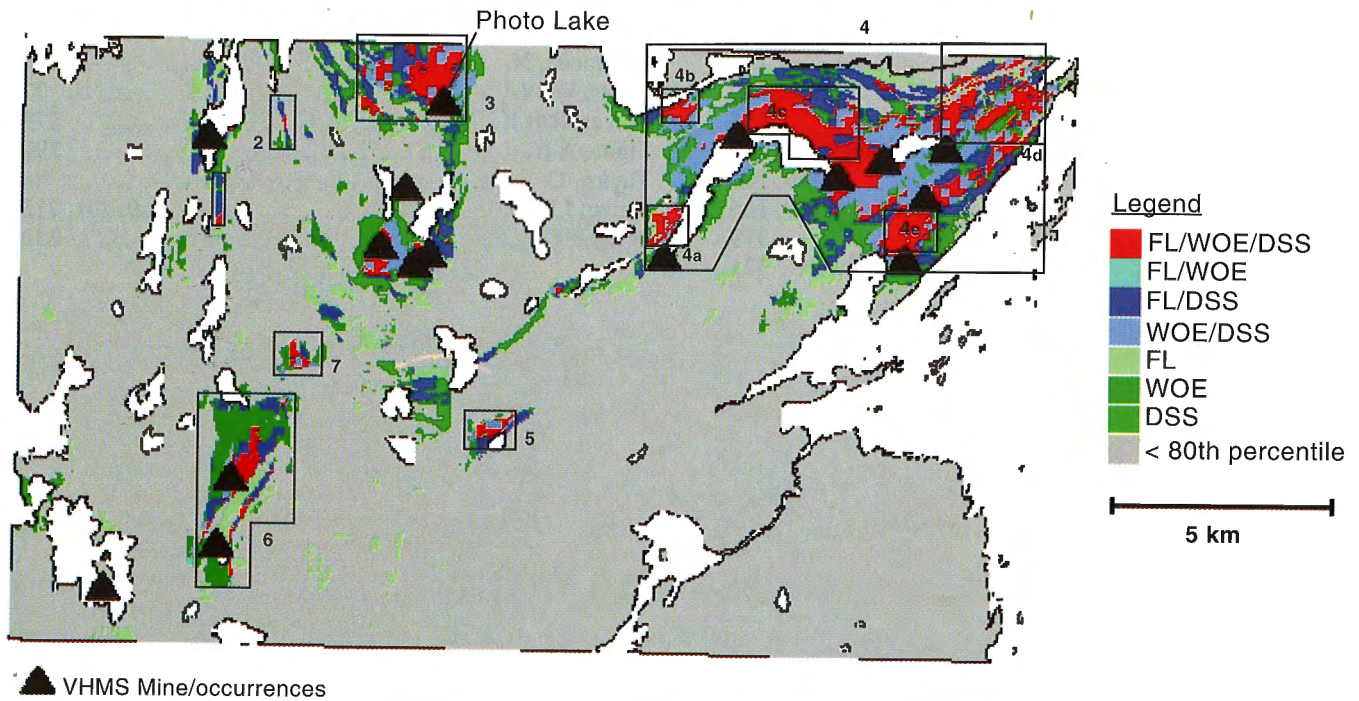


Figure 41. Map showing areas of particular interest for VHMS favourability. These areas were selected using results from all three methods, and were displayed at Geological Survey of Canada's Forum in January 1994. New discovery at Photo Lake by EM was unknown to authors until September 1994, after preparing first draft of paper.

Figure 40. Map comparisons. A) Fuzzy logic and Dempster-Shafer support. B) Fuzzy logic and weights of evidence. C) Weights of evidence and Dempster-Shafer support.

AUTHOR INDEX

| | | | |
|-----------------------------|--------------------|--------------------------|---------------|
| Ames, D.E. | 15, 45 | MacDonald, A.M. | 77 |
| Bailes, A.H. | 105 | MacLaurin, A.I. | 201, 215 |
| Beer, R. | 169 | McMurdy, M.W. | 257 |
| Bernius, G.R. | 331 | Moashi, M. | 169 |
| Bonham-Carter, G.F. | 339 | Mwenifumbo, C.J. | 331 |
| Coker, W.B. | 3, 77 | Nielsen, E. | 139 |
| Dunn, C.E. | 225 | Palacky, G.J. | 299, 319 |
| Fedikow, M.A.F. | 225 | Sangster, D.F. | 319 |
| Friske, P.W.B. | 257 | Scromeda, N. | 319 |
| Galley, A.G. | 3, 105, 319 | Shilts, W.W. | 77 |
| Gobert, G. | 139 | Shives, R.B.K. | 279 |
| Hall, G.E.M. | 155, 169, 201, 215 | Sinha, A.K. | 299 |
| Hoashi, M. | 169, 201 | Taylor, C. | 45 |
| Kaszycki, C.A. | 139, 155 | Vaive, J.E. | 169, 201, 215 |
| Katsube, T.J. | 319 | Wright, D.F. | 339 |
| Killeen, P.G. | 331 | | |